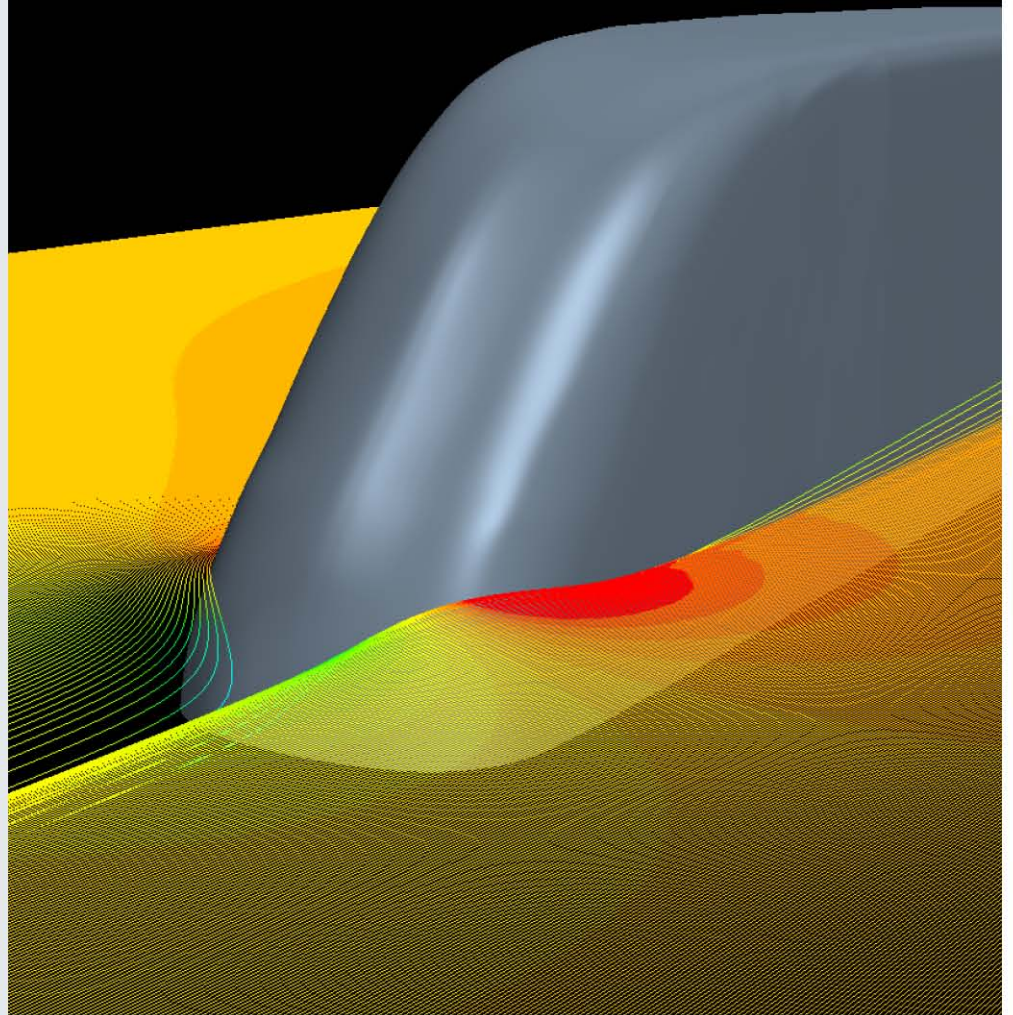


Vehicle Systems

2015 Annual Report

Vehicle Technologies Office



Front Cover Picture : The radically new and highly aerodynamic LLNL design for the shape of the next generation of heavy duty tractor trailers can significantly lower drag and improve fuel economy.

Credit: Lawrence Livermore National Laboratory

Disclaimer

This report was prepared as an account of work sponsored by an agency of the United States government. Neither the uNited States government nor any agency thereof, nor any of their employees, makes any warranty, express or implied, or assumes any legal liability or responsibility for the accuracy, completeness, or usefulness of any information, apparatus, product, or process disclosed or represents that its use would not infringe privately owned rights. reference herein to any specific commercial product, process, or service by trade name, trademark, manufacturer, or otherwise does not necessarily constitute or imply its endorsement, recommendation, or favoring by the United States government or any agency thereof. The views and opinions of authors expressed herein do not necessarily state or reflect those of the United States government or any agency thereof.

Table of Contents

Acronyms and Abbreviations	xxiii
I. Introduction	1
I.1. Mission and Objectives.....	1
I.2. Accomplishments	3
I.3. Approach and Organization of Activities	8
I.4. Future Directions for VS	14
II. Industry Awards.....	15
ADVANCED VEHICLE TESTING & EVALUATION (AVTE).....	15
II.1. Advanced Vehicle Testing & Evaluation [DE-EE0005501]	15
WIRELESS POWER TRANSFER	25
II.2. Wireless Charging for Electric Vehicles [M612006444]	25
II.3. High Efficiency, Low EMI and Positioning Tolerant Wireless Charging of EVs [DE-EE0005963]	35
THERMAL LOAD REDUCTION.....	41
II.4. Design and Implementation of a Thermal Load Reduction System for a Hyundai Sonata PHEV for Improved Range	41
II.5. Electric Phase Change Material Assisted Thermal Heating System (ePATHS) [DE-EE0006444]	51
II.6. Advanced Climate Control and Vehicle Preconditioning [DE-EE0006445].....	61
II.7. Unitary Thermal Energy Management for Propulsion Range Augmentation [DE-EE0006840]	68
POWERTRAIN.....	76
II.8. Multi-Speed Transmission for Commercial Delivery Medium Duty PEDVs [DE-EE0006843]	76
II.9. Integrated Boosting and Hybridization for Extreme Fuel Economy and Downsizing [DE-EE0006844]	83
FRICTION AND WEAR	89
II.10. Methods to Measure, Predict and Relate Friction, Wear and Fuel Economy [DE-EE0006793]	89
SUPERTRUCK.....	96
II.11. Development & Demonstration of a Fuel Efficient Class 8 Tractor & Trailer [DE-EE0003303]	96
II.12. Systems Level Technology Development and Integration for Efficient Class 8 Trucks [arravt080]	100
II.13. Volvo SuperTruck [DE-EE0004232]	104
TIRES	108
II.14. A System for automatically Maintaining Pressure in a Commercial Truck Tire [DE-EE0005447]	108
II.15. Advanced Truck and Bus Radial Materials for Fuel Efficiency [DE-EE0006794].....	115

ZERO EMISSION CARGO TRANSPORT.....	122
II.16. San Pedro Bay Ports Hybrid & Fuel Cell Electric Vehicle Project [DE-EE0006874]	122
II.17. Hydrogen Fuel-Cell Electric Hybrid Truck Demonstration [DE-EE0005978] and Houston Zero Emission Delivery Vehicle Deployment [DE-E0005979]	127
II.18. Zero Emission Drayage Trucks Demonstration [DE-EE0005961].....	134
III. Vehicle Technology Evaluations	142
III.1. Advanced Technology Vehicle Lab Benchmarking (L1&L2)	142
III.2. Advanced Vehicle Testing Activity.....	179
III.3. Electric Drive Vehicle Climate Control Load Reduction – FY 2014.....	188
III.4. Electric Drive Vehicle Climate Control Load Reduction – FY 2015	205
III.5. Increasing EDV Range through Intelligent Cabin Air Handling Strategies	216
III.6. Integrated Vehicle Thermal Management – Combining Fluid Loops on Electric Drive Vehicles	226
III.7. In-Vehicle Test Platform Evaluation of Lower-Energy Energy Storage System (LEESS) Devices	244
III.8. Medium-Duty Electric Vehicle Data Collection and Performance Assessment.....	256
III.9. Electric Bus Facility and Grid Integration.....	273
III.10. Fleet DNA.....	282
III.11. Fleet DNA Database Development and Support	294
III.12. Medium- and Heavy-Duty Field Testing.....	306
III.13. Commercial EV Battery Degradation Field Evaluation	332
III.14. Truck Platooning Follow-on Study.....	338
IV. Modeling and Simulation.....	342
IV.1. Autonomie Maintenance and Model Based System Engineering (MBSE) Enhancements	342
IV.2. VTO Baseline and Scenario (BaSce).....	353
IV.3. VSATT, TSDC and Miscellaneous Support.....	363
IV.4. Long-Haul Truck Idle Climate Control Load Reduction.....	370
IV.5. VTCab, Rapid Vehicle HVAC Load Estimation Tool	379
IV.6. ACEC Technology Analysis and Evaluation.....	391
IV.7. Technology Requirements and Evaluations for High Power Applications of Wireless Power Transfer	399
IV.8. Vehicle Thermal System Model Development in Simulink	409
IV.9. Advanced Transmission Selection to Provide Accurate VTO Benefits	419
IV.10. Benefits of Connected Route-Based Energy Management for Light-Duty Electrified Vehicles	426
IV.11. Honda PHEV Thermal Model Validation	435
IV.12. EcoCAR3 Support	442
IV.13. Evaluation of Benefits of DOE Vehicle Technology Research on Real-World Driving.....	444
IV.14. Analyzing Real-World Light-Duty Vehicle Efficiency Benefits.....	449
IV.15. Thermal Impact of Energy Consumption on Real-World Drive Cycles.....	462

V. Codes and Standards	467
V.1. Green Racing Technical Support.....	467
V.2. Test Standards Development for EV, PHEV and HEVs	477
V.3. SAE Standards Development Support.....	489
V.4. Codes and Standards and Technical Team Activities.....	493
V.5. PEV-Grid Connectivity	500
VI. Vehicle Systems Efficiency Improvements.....	524
VI.1. DOE’s Effort to Improve Heavy Vehicle Fuel Efficiency through Improved Aerodynamics.....	524
VI.2. DOE/DOD Parasitic Energy Loss Collaboration.....	532
VI.3. Thermal Control through Airside Evaporative Heat Removal	540
VI.4. Aerodynamics and Underhood Thermal Analysis of Truck Platooning.....	554
VI.5. Experimental Investigation of Coolant Boiling in a Half-Heated Circular Tube – CRADA with PACCAR.....	567
VI.6. Cummins MD&HD Accessory Hybridization CRADA.....	583
VI.7. Powertrain Controls Optimization for HD Hybrid Line Haul Trucks	592
VI.8. Thermal Control of Power Electronics of Electric Vehicles with Small Channel Coolant Boiling	608
VI.9. DC Fast Charging Study.....	622
VI.10. Wireless and Conductive Charger Evaluation and Onroad 12-V Auxiliary Load Evaluation.....	628
VI.11. Wireless Power Transfer Grid Integration.....	644
VI.12. INTEGRATE - Electric Vehicle Grid Integration R&D	655
VI.13. EVSE Data Collection.....	664

List of Figures

Figure I-1: VS outcome objectives and mission	1
Figure I-2: VS primary processes, project objectives, and outcome objectives.....	2
Figure I-3: VS activities integration – Arrows represent information flow between activity focus areas that enhances effectiveness of individual activities.	8
Figure I-4: VS activities providing estimates of national benefits and impacts of advanced technologies.	9
Figure II-1: AVTE fleet vehicles at Intertek for DOE review in February 2015.....	20
Figure II-2: 2014 Tesla Model S 85 that underwent baseline testing	21
Figure II-3: EZ Messenger Phoenix fleet location charging infrastructure with AVTE vehicles.....	23
Figure II-4: Ford Focus Electric participating in SAE J2953 interoperability testing at the Intertek Plymouth site.....	23
Figure II-5: Grid side unit operational block diagram with Evatran control module and ORNL DSP controller.	28
Figure II-6: Operational block diagram of the wireless J1772 integration.	28
Figure II-7: Operational block diagram for the direct battery or CHAdeMO connection of vehicle side WPT equipment.	28
Figure II-8: Scion iQ pretests and efficiency measurement and power analyzer hardware.....	30

Figure II-9: Wireless charging of a Plug-in Prius 30

Figure II-10: Toyota RAV4 EV test results: Power flow and efficiency across 5 power conversion stages..... 31

Figure II-11: Electrical test results across all power conversion stages as well as the primary coil and tuning capacitor voltages..... 31

Figure II-12: Operational waveforms for high frequency elements (inverter, transformer, coupling coils)..... 32

Figure II-13: Operational waveforms for low frequency elements (AC grid input, DC link, vehicle battery). 32

Figure II-14: Wireless Charging System Topology 36

Figure II-15: Coil Placement Under Kia Soul EV 36

Figure II-16: Coil Design..... 37

Figure II-17: DC-DC Efficiency 38

Figure II-18: Efficiency Data..... 38

Figure II-19: Magnetic and Electric Field Emissions at Front Bumper..... 39

Figure II-20: Vehicle Experimental setup at NREL's Vehicle Testing and Integration Facility 44

Figure II-21: Select baseline vehicle thermal soak data collected over a continuous three-day interval..... 47

Figure II-22: Sample results for HVAC system demonstration for summer AC system pull-down followed by automatic control to cabin air temperature..... 48

Figure II-23: Mechanized ePATHS System Design 54

Figure II-24: Operating Modes: a. PCM Charging, b. PCM Discharging, c. Energy Recovery, d. PTC Heating..... 54

Figure II-25: PCM Heat Exchanger Design..... 56

Figure II-26: PCM Heat Exchanger without Insulation 56

Figure II-27: PCM Filling System 57

Figure II-28: ePATHS System Simulation 57

Figure II-29: ePATHS System Control Design 58

Figure II-30: Operation Mode Control 58

Figure II-31: Integrated PCM and Traction Battery Charging System..... 59

Figure II-32: PCM Charging Surface Heater Power Control..... 59

Figure II-33: ePATHS System Test Bench..... 60

Figure II-34: Schematic Showing What Baseline Data was Used to Validate 63

Figure II-35: Predicted and Actual Cabin Temperatures 63

Figure II-36: Predicted and Actual Sensation and Comfort..... 64

Figure II-37: Schematic of Refrigerant and Glycol Systems 64

Figure II-38: Vehicle Test Showing Benefit of WCC with Thermal Storage..... 65

Figure II-39: Predicted Power Consumption during Heat Pump Operation at 5°C and -18°C..... 66

Figure II-40: Range Extension Predictions..... 66

Figure II-41: Schematic of a sample configuration of the UTEMPRA refrigerant loop 70

Figure II-42: Thermal management of the Fiat 500e..... 71

Figure II-43: UTEMPRA Coolant loop architecture 71

Figure II-44: Under-hood location of the UTEMPRA components 72

Figure II-45: CD25 and HTRWU trends of the breath and vent temperatures 73

Figure II-46: CD25 and HTRWU trends of the breath and vent temperatures 73

Figure II-47: MMFC design - hot and cold halves 74

Figure II-48: Component designs of the UTEMPRA System 74

Figure II-49: Autonomie representation of battery electric medium duty truck architecture 79

Figure II-50: Wide open throttle acceleration to max speed..... 80

Figure II-51: The Acceleration Performance and Top Speed Results 81

Figure II-52: Simulink Controls and GTP co-simulation framework 85

Figure II-53: Simulink Controls and GTP co-simulation framework 86

Figure II-54: GTP Model Screenshot 86

Figure II-55: Expander Dynamometer Setup..... 87

Figure II-56: Ring-on-Liner Test Configuration; radial and diametrical tension definition in RINGPAK..... 91

Figure II-57: Results from ROL RINGPAK simulation using Isuzu geometries, typical material properties, and generic 15w40 oil properties. 92

Figure II-58: Comparison of Hand-Calculated, ROL Simulation, and Engine Simulation Stribeck numbers. 93

Figure II-59: AART test rig used to evaluate friction and wear properties of candidate ring and liner configurations..... 94

Figure II-60: Candidate oils with different friction modifiers for: (a) CI oils and (b) SI oils..... 95

Figure II-61: Project Engine Progress..... 97

Figure II-62: Navistar SuperTruck Freight Efficiency Plan 98

Figure II-63: Final Demonstration Fuel Economy Results: SuperTruck vs 2009 Baseline Cascadia..... 102

Figure II-64: Tread rubbers surface energy at different temperatures 117

Figure II-65: Functional diagram of battery electric truck with H2 fuel cell range extender 124

Figure II-66: Transpower truck subsystems..... 124

Figure II-67: U.S. Hybrid battery electric trucks with H2 fuel cell generator 125

Figure II-68: Hybrid Electric Truck with CNG range extender..... 125

Figure II-69: Parallel PHEV truck 126

Figure II-70: TransPower BEV System..... 136

Figure II-71: US Hybrid BEV System..... 137

Figure II-72: TransPower CNG PHEV System 137

Figure II-73: US Hybrid LNG PHEV System 138

Figure II-74: TransPower EDD Trucks 139

Figure II-75: Fuel Economy Comparison: EDD2 vs Conventional Diesel Trucks..... 140

Figure II-76: US Hybrid Fully Integrated BET 140

Figure III-1: Advanced Vehicle Testing Activity process. 144

Figure III-2: Illustration of testing at 95°F with sun emulation (left) and at 20°F cold ambient temperature (right). 145

Figure III-3: Data dissemination and project partners 146

Figure III-4: Map of Downloadable Dynamometer Database content..... 146

Figure III-5: NOx concentration before and after exhaust after treatment system, UDDS hot start and cold start 72F..... 148

Figure III-6: 2014 Chevrolet Cruze diesel fuel economy (uncorrected)..... 148

Figure III-7: Alternator and capacitor operation during a highway cycle at 72F..... 150

Figure III-8: 2014 Smart Electric energy consumption 152

Figure III-9: Range extending engine power and battery power for a steady state speed test at 72F (in charge sustaining mode)..... 154

Figure III-10: Range extender power and battery power for a steady state speed 6% grade test at 72F (charge sustaining mode). 154

Figure III-11: BMW i3 Rex fuel economy during charge sustaining operation (uncorrected)..... 155

Figure III-12: 2014 BMW i3 BEV energy consumption at varying temperatures..... 157

Figure III-13: Temperature effect on UDDS hot and cold start energy consumption..... 157

Figure III-14: BMW i3 BEV high voltage component energy use at cold temperatures..... 158

Figure III-15: Kia Soul EV Energy Consumption. 159

Figure III-16: Percent of energy consumption by component on the 20F UDDS CS cycle 160

Figure III-17: Kia Soul BEV energy consumption at varying speeds and grade 160

Figure III-18: Comparison of HEV and PHEV battery power during high power demand 162

Figure III-19: 2015 Chevrolet Spark EV energy consumption. 164

Figure III-20: Energy use over the comparing preconditioning over the MCT 165

Figure III-21: Components Consumption for Hot and Cold Starts UDDS Cycles. 165

Figure III-22: Fuel Economy of the 2012 VW Passat EcoFuel TSI 167

Figure III-23: 2014 BMW i3 REx mounted in APRF for evaluation. 168

Figure III-24: Vehicle high voltage and low voltage bus description..... 170

Figure III-25: BMW i3 REx Level 2 cooling system instrumentation 171

Figure III-26: Exhaust system instrumentation..... 172

Figure III-27: Interior cabin and vent temperature instrumentation 172

Figure III-28: Three phase voltage taps routed internal to the drive unit..... 173

Figure III-29: Shielding current over UDDS CS on the 2014 BMW i3 Rex 174

Figure III-30: General specifications of the 3 PHEV's under comparison..... 175

Figure III-31: Comparison of electric-only acceleration and maximum speed..... 175

Figure III-32: UDDS operation of the Prius PHEV, Accord PHEV, and Fusion PHEV (in order)..... 176

Figure III-33: US06 operation of the Prius PHEV, Accord PHEV, and Fusion PHEV (in order)..... 176

Figure III-34: Depletion summary of HV battery energy depletion 177

Figure III-35: Battery performance data are shown for a 2012 Chevrolet Volt. The data shown are from tests performed at 4,000; 14,000; and 60,000 miles. Two additional tests will be performed prior to completion of testing to characterize battery performance through the life of the battery. The Volt battery exceeded the United States Advanced Battery Consortium (USABC) power goal for a PHEV-40 for all tests. 183

Figure III-36: A 2014 BMW i3 electric vehicle fitted with testing and measurement equipment for track testing. 184

Figure III-37: Electrical energy consumption data are shown for a 2014 BMW i3 electric vehicle. The data shown are from on-road operations logged over several thousand miles. 184

Figure III-38: Final report's executive summary about federal agency PEV suitability, which explains the economic, energy, and emissions reductions possible through replacement of conventional vehicles with PEV equivalents. 185

Figure III-39: The range and mean of EVSE port utilization is shown by region. 186

Figure III-40: Overhead Vent Incorporated into Focus BEV Model 190

Figure III-41: Overhead Vent and Duct Geometry Incorporated into Focus BEV Model..... 191

Figure III-42: Thermal Sensation and Comfort Results, Overhead A/C Case Compared to Baseline..... 191

Figure III-43: Comparison of Baseline to Insulated Headliner Soak Temperatures 192

Figure III-44: Interior Surface Temperature Difference with Insulated Headliner during a Cool-down Simulation 192

Figure III-45: Comparison of Glass Temperatures during Cool-down, Stationary vs. Moving Vehicle 192

Figure III-46: Comparison of Breath Temperatures during Cool-down, Stationary vs. Moving Vehicle 193

Figure III-47: Defrost and Frogleg Ducts 193

Figure III-48: Comparison of Cold-Soak Temperatures..... 194

Figure III-49: Comparison of Simulation Data to Test Data for a Baseline Warm-up Test, Breath Air Temperatures..... 194

Figure III-50: Comparison of Simulation Data to Test Data for a Baseline Warm-up Test, Interior Surface Temperatures..... 195

Figure III-51: Ford Focus Electric Vehicles at NREL's VTIF..... 195

Figure III-52: Shading Canopy Test Configuration..... 196

Figure III-53: Soak Temperature Reduction and Cool-down Energy Savings for Warm Weather Thermal Load Reduction Test Cases 197

Figure III-54: Driver Air Temperatures and Cumulative Energy Savings after 20-minute Cool-down for Zonal Cooling Configurations..... 198

Figure III-55: Results of a Thermoelectrically-cooled Seat on Driver Thermal Sensation and HVAC Energy Consumption..... 198

Figure III-56: Time to Neutral Thermal Sensation and Cumulative Energy Savings after 20 Minutes for Zonal Heating Tests..... 200

Figure III-57: Energy Savings from Exterior Insulation for Steady-state Heating 200

Figure III-58: Climate Control Power vs. Time..... 201

Figure III-59: Zonal heating test configurations 208

Figure III-60: Zonal heating test results..... 209

Figure III-61: Comparison of simulated cabin air temperature to experimental data for baseline warm-up 210

Figure III-62: Predicted thermal sensation for baseline and zonal heating 210

Figure III-63: Focus Electric test vehicle and CoolCalc model; results of model validation to test data for summer and winter days..... 211

Figure III-64: Results of CoolCalc analysis of polycarbonate glazing 212

Figure III-65: Calculated driving range for no heating, baseline heating, and zonal heating 213

Figure III-66: Reduction in range due to cabin heating by state; fraction of the national EDV fleet per state 213

Figure III-67: Ford Motor Company patent drawings for proposed "suction surface" locations 217

Figure III-68: Recirculation return and exhauster locations in Ford Focus CAD cabin model 218

Figure III-69: Left - Cabin inlet vent CAD geometry; Right - Human passenger CAD models in four seating locations within cabin 219

Figure III-70: Cabin air velocity field of split flow case with rear split flow recirculation return ducts and exhausters at 63% recirculation..... 220

Figure III-71: Front windshield interior surface temperatures of the fractional recirculation control case..... 220

Figure III-72: Windshield RH of fractional recirculation control (left) and split flow (right) at 63% recirculation fraction 221

Figure III-73: Windshield RH of fractional recirculation control (left) and split flow (right) at highest recirculation fractions before fogging point..... 221

Figure III-74: Vehicle glass surface RH of fractional recirculation control at 75% recirculation (top); split flow at 84.5% recirculation (middle); and split flow with OEM exhausters at 84.5% recirculation (bottom)..... 222

Figure III-75: Vehicle glass surface RH at 63% recirculation for fractional recirculation control (top); split flow with OEM recirculation ducts and exhausters (middle); and split flow with rear recirculation ducts and OEM exhausters (bottom)..... 223

Figure III-76: Air RH at center plane along length of vehicle of fractional recirculation control at 63% recirculation (top) and split flow with OEM exhausters at 63% recirculation (bottom)..... 224

Figure III-77: Basic schematic of CFL bench test apparatus..... 229

Figure III-78: CFL bench test apparatus 229

Figure III-79: Delphi prototype refrigerant system components 230

Figure III-80: Schematic of full experimental CFL system 230

Figure III-81: Schematic of experimental CFL system cooling mode 231

Figure III-82: Delphi prototype refrigerant system components 231

Figure III-83: Delphi prototype refrigerant system components 231

Figure III-84: Schematic of full experimental CFL system 232

Figure III-85: Schematic of experimental CFL system cooling mode 232

Figure III-86: Schematic of experimental CFL system heating mode 233

Figure III-87: Drive cycle profiles for UDDS and double HWFET 235

Figure III-88: Component temperatures for cooling mode, double HWFET cycle, $T_{amb} = 38^{\circ}\text{C}$, no soak, PEEM and ESS cooling case 236

Figure III-89: Cabin temperatures for cooling mode, double HWFET cycle, $T_{amb} = 38^{\circ}\text{C}$, no soak, PEEM and ESS cooling case 236

Figure III-90: Summary of combined drive cycle cooling results for vehicle range 237

Figure III-91: Component temperatures for heating mode, UDDS cycle, $T_{amb} = -2^{\circ}\text{C}$, PEEM and ESS conditioning case 238

Figure III-92: Cabin temperatures for heating mode, UDDS cycle, $T_{amb} = -2^{\circ}\text{C}$, PEEM and ESS conditioning case 238

Figure III-93: Supplemental PTC heating power and compressor speed for heating mode, UDDS cycle, $T_{amb} = -2^{\circ}\text{C}$, PEEM and ESS conditioning case 239

Figure III-94: Summary of combined drive cycle heating results for vehicle range 239

Figure III-95: National vehicle use weighting for ambient temperature 240

Figure III-96: CFL versus baseline system for combined drive cycle vehicle range 241

Figure III-97: Fusion Hybrid's HVTB and associated components 246

Figure III-98: Schematic of connections between replacement components and the vehicle 246

Figure III-99: ANL-provided ESS power trace over the US06 test cycle 247

Figure III-100: Passing and 0-60 mph acceleration distances for NiMH compared with unrestricted LIC and EDLC configurations (top) and compared with restricted-energy EDLC configurations (bottom) 249

Figure III-101: Performance comparison of the production battery and the lowest restricted-energy LIC configuration over the US06 cycle 250

Figure III-102: US06 fuel consumption vs. energy window for multiple vehicle configurations 250

Figure III-103: UDDS fuel consumption vs. energy window for LIC and NiMH configurations 251

Figure III-104: NiMH and EDLC configuration power limits during cold start city cycle testing at -10°F 252

Figure III-105: Highway Fuel Economy Test showing similar fuel consumption for widely varying energy windows between the production NiMH and the lowest-energy LIC configurations 253

Figure III-106: Engine stop/start cycling and fuel consumption comparison between the production NiMH and a restricted-energy LIC configuration over the 95°F SC03 cycle 253

Figure III-107: Project framework schematic 257

Figure III-108: Data flow from vehicle to final reporting 258

Figure III-109: Data processing and analysis 259

Figure III-110: Smith Newton delivery vehicle 260

Figure III-111: Home locations of Smith Vehicles: Gen1 (orange), Gen2 (green) 261

Figure III-112: Distribution of Smith Gen 1 data by state 261

Figure III-113: Distribution of Smith Gen 2 data by state 261

Figure III-114: Average daily driving duration for Gen 1 Smith EVs 261

Figure III-115: Average daily driving distance for Gen 1 Smith EVs 262

Figure III-116: Gen 1 Smith EV representative custom drive cycle..... 262

Figure III-117: Navistar eStar, Battery Electric Delivery Vehicle..... 263

Figure III-118: Navistar driving duration – 3 sigma distribution 264

Figure III-119: Navistar driving distance – 3 sigma distribution..... 264

Figure III-120: Stops per kilometer vs. average acceleration 265

Figure III-121: Navistar eStar custom representative drive cycle..... 265

Figure III-122: Map showing energy consumption by ARRA site and PADD regions through February 2015..... 266

Figure III-123: Shorepower seasonal utilization..... 267

Figure III-124: Shorepower weekly utilization..... 267

Figure III-125: Hours booked per plug-in event..... 267

Figure III-126: Odyne Parallel Hybrid Architecture schematic..... 268

Figure III-127: Odyne Parallel Hybrid Architecture graphic model with system components shown in color 268

Figure III-128: Vocational vehicle configured with aerial bucket and the Odyne PHEV system 269

Figure III-129: Digger vocational vehicle the Odyne PHEV system..... 269

Figure III-130: Completed Odyne vehicle file transfers 270

Figure III-131: Distribution of ARRA funded vehicle types 270

Figure III-132: Typical daily vehicle usage profile for a bucket truck 271

Figure III-133: Example summary report 272

Figure III-134: Foothill Transit Line 291 route map 276

Figure III-135: Foothill Transit route 291 shown with GPS data 276

Figure III-136: Fast charger location on Foothill Transit’s line 291..... 277

Figure III-137: Kinetic intensity shown as a function of average driving speed for all Foothill Transit data (purple) and all Fleet DNA mass transit data (blue) compared to select standard chassis dynamometer test cycles..... 278

Figure III-138: Kinetic intensity as a function of daily average stops per mile for both the Fleet DNA mass transit database and the Foothill Transit BEBs 278

Figure III-139: Vehicle speed, distance, and battery pack SOC shown for one full "loop" on line 291..... 279

Figure III-140: Average battery pack SOC for all vehicles sampled at 2 Hz while vehicle was logging data..... 279

Figure III-141: Auxiliary load analysis example showing the power impact of the resistive element heater during stationary use 280

Figure III-142: Heat map showing the distribution of battery power as a function of vehicle speed (positive power indicates energy into the pack)..... 280

Figure III-143: Illustration of data fusion in Fleet DNA with multiple data layers 284

Figure III-144: Historical growth of Fleet DNA project..... 285

Figure III-145: Current geographic coverage of Fleet DNA data..... 285

Figure III-146: U.S. major highway corridors, color coded by vehicle miles traveled..... 286

Figure III-147: Example beverage delivery truck..... 288

Figure III-148: Effects of aerodynamic drag and rolling resistance on fuel consumption..... 289

Figure III-149: Overall simulated road grade fuel economy penalty..... 290

Figure III-150: Effect of grade on fuel economy penalty 290

Figure III-151: Effect of vehicle payload on fuel economy over range of road grade conditions 291

Figure III-152: Fleet DNA website interface..... 292

Figure III-153: Fleet DNA DC Extraction Tool - Parameters 296

Figure III-154: Fleet DNA DC Selection Criteria 297

Figure III-155: Fleet DNA DC Selection Criteria and Search Results 298

Figure III-156: User Selected DC 299

Figure III-157: Distribution of DCs by Distance Traveled 300

Figure III-158: Distribution of DCs by Percent Stop Time 301

Figure III-159: Distribution of DCs by Distance Traveled on Freeways 301

Figure III-160: Distribution of DCs by Distance Traveled in Urban Areas 302

Figure III-161: Distribution of DCs by Maximum Speed 302

Figure III-162: Distribution of DCs by Average Speed 303

Figure III-163: Distribution of DCs by Maximum Deceleration (Logarithmic Scale) 303

Figure III-164: Distribution of DCs by Maximum Acceleration (Logarithmic Scale) 304

Figure III-165: Distribution of DCs by Distance Traveled and Percentage of Stop Time 304

Figure III-166: Fuel economy comparison of diesels and EVs 310

Figure III-167: Energy consumption as a function of distance traveled for the Smith EVs 311

Figure III-168: Subset of data from Chateau Energy management system January 4–10, 2015 shown 311

Figure III-169: Average and peak power delivered by each EVSE while charging 312

Figure III-170: Time of day when vehicles are charging during the diesel comparison period (April–
May 2014) 312

Figure III-171: Fleet depot utility bill monthly peak demand 312

Figure III-172: Comparison of Federal Way facility power consumption and EVSE usage (data from
01/10/2015) 313

Figure III-173: Campus base load and EV charging contribution 313

Figure III-174: Charge management schemes developed by NREL could save FLNA in peak demand
charges 314

Figure III-175: Modeled 100-kW AC system located at FLNA Federal Way facility average hourly
output based on array orientation 314

Figure III-176: Miami-Dade County’s first generation (MY2013) hydraulic hybrid refuse trucks at the
PWWMD facility 316

Figure III-177: Miami-Dade County, first generation (MY2013) Hydraulic Hybrid Refuse Truck on
route 316

Figure III-178: Parker Hydraulic Hybrid schematic 317

Figure III-179: Several vehicle routes shown in Miami-Dade County with the locations of the Covanta
Waste to Energy (WTE) facility and main terminal indicated 319

Figure III-180: Neighborhood detail showing GPS vehicle routes 319

Figure III-181: Kinetic intensity vs. average driving speed for first-generation HHVs and conventional
vehicles 320

Figure III-182: Kinetic Intensity vs. average stops per mile for first-generation HHVs and
conventional vehicles 320

Figure III-183: Average fuel economy vs. kinetic intensity 321

Figure III-184: Average fuel economy vs. average acceleration 321

Figure III-185: School bus distance driven daily 323

Figure III-186: School bus average speed driven 323

Figure III-187: School bus distance travelled by time of day 324

Figure III-188: School bus stops per mile vs. kinetic intensity 324

Figure III-189: UPS package car (left) and day cab tractor (right) 325

Figure III-190: UPS vehicle activity map 326

Figure III-191: Kinetic intensity vs. speed 327

Figure III-192: Standard drive cycles 328

Figure III-193: Fuel distillation profile..... 329

Figure III-194: Fuel consumption..... 330

Figure III-195: Fuel economy..... 330

Figure III-196: Relative difference 331

Figure III-197: Intended data collection—collecting several points over a period of years will help to validate life models 334

Figure III-198: Schematic of load bank and data acquisition set-up..... 335

Figure III-199: Load test conducted at Casa Grande, AZ..... 336

Figure III-200: Example of sample drive cycle data from the ARRA Smith data collection project (top) used to generate models fit to a root-mean-square error of less than 6% open circuit voltage (bottom)..... 337

Figure III-201: Truck Platooning Air Flow 340

Figure III-202: Trucks in Platoon Formation during Testing 340

Figure IV-1: Import Functionality—Converting Models to Improved Autonomie Metadata 343

Figure IV-2: Vehicle Tree View—Browsing the New Vehicle Tree View 344

Figure IV-3: Multi-Option Vehicle Study—Embarking on a New Way to Define and Launch Large-Scale Studies 345

Figure IV-4: Multiple Instances of Simulink—Benefiting from Running Simulations in Parallel 345

Figure IV-5: A Vehicle Simulation Workflow—Getting to the Point, Increasing a User's Productivity 346

Figure IV-6: A Visual Studio Project is Provided—Simplifying the Integration 346

Figure IV-7: Database Tool—Managing Datasets Produced by Large-Scale Simulations 347

Figure IV-8: New Dataset Report—Reviewing and Understanding the Results from a Large-Scale Simulation 347

Figure IV-9: SAE Configuration—Applying the SAE J3409 Standard 348

Figure IV-10: Automated Testing Setup—Illustrating the Testing Workflow and Manage Unit and Integration Tests..... 349

Figure IV-11: Building Options Control—Reducing the Simulation Time..... 349

Figure IV-12: Simple Projects—Reusing Features to Provide a Rudimentary Notion of Projects..... 350

Figure IV-13: Documentation Index—Finding Help on Functions in the Auto-Generated API Documentation 350

Figure IV-14: Study process for running and analyzing large-scale simulation 354

Figure IV-15: Vehicle classes, timeframes, configurations, and fuels considered 355

Figure IV-16: Engine peak efficiency for conventional vehicle 356

Figure IV-17: Fuel-cell system efficiency 356

Figure IV-18: Battery energy density for high energy application PHEV 357

Figure IV-19: Glider mass reduction for all vehicle classes 357

Figure IV-20: Ratio of fuel consumption gasoline equivalent (unadjusted) for HEV to that of conventional Gasoline vehicle of same year and case 358

Figure IV-21: Vehicle cost ratio for HEVs compared to gasoline conventional vehicle of the same year and case 358

Figure IV-22: Ratio of fuel consumption gasoline equivalent (unadjusted) for HEV to that of fuel cell HEV of same year and case 359

Figure IV-23: Fuel consumption evolution for HEV, PHEVs, gasoline engine vehicle for midsize class 359

Figure IV-24: Manufacturing cost of PHEVs for gasoline engine..... 360

Figure IV-25: Incremental manufacturing cost (in comparison with the reference conventional gasoline vehicle manufacturing cost) as a function of fuel consumption for midsize HEVs..... 360

Figure IV-26: Incremental manufacturing cost (in comparison with the reference conventional gasoline vehicle manufacturing cost) as a function of fuel consumption for fuel-cell vehicles 361

Figure IV-27: Examples of the Types of Datasets Discussed in Data Inventory Presentations to the Derivative Workgroup from VSATT on "Quantifying Vehicle Usage Parameters Based on Existing Data" 365

Figure IV-28: Trends in TSDC User Growth for the Two Data Access Environments..... 366

Figure IV-29: Heat Plot of Travel Estimates for Individual Roads, Available for Use in Combination with TSDC Data..... 367

Figure IV-30: NREL-Simulated Fuel Penalty due to Grade over a Subset of Trips with Net Elevation Gain Close to Zero 368

Figure IV-31: A (left), Stock Insulation; B (center), Advanced Insulation; C (right), Additional Layer with Reflective Barrier..... 372

Figure IV-32: A (left), NREL's Vehicle Testing and Integration Facility; B (right), UA Test Heater in Sleeper..... 373

Figure IV-33: (A) Cab and (B) Sleeper Thermocouple Locations. Dimensions: A = 12", B = 6", C = 18". Blue: TMC standard [8]; red: NREL added 374

Figure IV-34: UA Calibration Results for: A. Sleeper with Standard Sleeper Curtain and Shades, B. Sleeper with Window Shades Only and No Curtain 375

Figure IV-35: VTCab interface: A. Standard rendering, B. Imported light-duty model, C. Zone assignment tool with exploded view 382

Figure IV-36: Relationship between the rest-period climate control fuel use estimation process and energy conversion 383

Figure IV-37: A (left), VMT per weather station; B (right), Cumulative total of VMT by weather station..... 384

Figure IV-38: Map of weather station locations for A) all stations, and B) remaining top 200 stations 384

Figure IV-39: A. Process diagram for the internal resistance battery model used for the fuel use estimation process, B. Alternator efficiency as a function of speed and current for the fuel use estimation process..... 386

Figure IV-40: Auxiliary A/C system battery pack recharge process sequence for fuel use estimation. A (left), beginning of a recharge event; B (right), end of a recharge event (right). 387

Figure IV-41: A (left), daily maximum 10-hr window A/C electric loads (left) B (right), daily peak cooling power for combined cooling loads of 200 US locations 389

Figure IV-42: Example of steady-state engine maps for the GM 1.9L engine with the RCCI-enabled zone highlighted (a) and for the 1.6L GTDI stoichiometric engine, (b) the pink marks in Figure IV-42(a) indicate measured RCCI operating conditions..... 394

Figure IV-43: Example comparison of the simulated and measured DOC oxidation efficiencies of CO emissions in the CDC and RCCI exhaust stream as a function of exhaust temperature. 395

Figure IV-44: Comparison of fuel economies and engine efficiencies between CDC and different RCCI fueling strategies in the simulated vehicles over a UDDS drive cycle. 395

Figure IV-45: Effect of the proactively RCCI control strategy on cumulative engine-out CO/HC emissions as a function of exhaust temperature in the hybrid vehicles over the cold-start FTP cycle. The RCCI fueling strategy is a combination of conventional diesel and gasoline. 396

Figure IV-46: Effect of the proactive RCCI control strategy on engine efficiency and cumulative CO/HC emissions in hybrid vehicles with DOC, over the cold-start FTP cycle. The RCCI fueling strategy is a combination of conventional diesel and gasoline. 397

Figure IV-47: Examples of infrastructure powering transit systems by wires..... 401

Figure IV-48: Power semiconductor devices power and frequency relationship. 402

Figure IV-49: Circular coil. 404

Figure IV-50: Flat pickup coil. 404

Figure IV-51: E-pickup coil..... 404

Figure IV-52: U-pickup coil. 404

Table IV-40: Tuning configuration comparisons..... 404

Figure IV-53: Eddy current model of coupling coils for frequency domain analysis..... 405

Figure IV-54: B-vector in the cross-sectional plane. 405

Figure IV-55: B-field magnitude of the flux guiding ferrite plates..... 405

Figure IV-56: ORNL power electronics approach utilizing three inverters and an integrated magnetic structure..... 406

Figure IV-57: Preliminary simulation results based on ~122kW power transfer. 407

Figure IV-58: Cabin warm-up simulation results vs. data 415

Figure IV-59: Cabin cool-down simulation results vs. data 415

Figure IV-60: Schematic of NREL's CFL system 416

Figure IV-61: NREL's CFL test bench 416

Figure IV-62: Simulated and measured capacities of coolant-to-air heat exchangers 416

Figure IV-63: Simulated and measured system temperatures..... 416

Figure IV-64: ORNL heavy-duty A/C system scheme..... 417

Figure IV-65: Top level of the ORNL A/C system developed using the CoolSim framework. Red color - high pressure components. Blue color - low pressure components. 417

Figure IV-66: Study process for developing advanced transmission models and optimization processes 421

Figure IV-67: Shifting curves and parameters selected for optimization 421

Figure IV-68: Fuel consumption as a function of the trajectory of the optimization algorithm 422

Figure IV-69: Comparison of fuel economy benefits with and without the use of optimization..... 423

Figure IV-70: Schematic of the input-split type 423

Figure IV-71: Comparison of fuel economy benefits with and without the use of optimization..... 424

Figure IV-72: Route-based energy management concept..... 427

Figure IV-73: Evolution of queue length as a function of average speed for various speed limits (30, 40 and 50 km/h) for a 4-way stop intersection 429

Figure IV-74: Probability of approach scenario as a function of the volume for an intersection with traffic lights 430

Figure IV-75: Example of Speed profile at intersection with stop signs: four-way stop (left), two-way stop (left) 431

Figure IV-76: Example of Speed profile at intersection with traffic light; one stop scenario (left), two stop scenario (right) 431

Figure IV-77: Unadjusted and SOC-adjusted fuel savings of PMP as a function of EQF (left); Total fuel energy and total battery energy for various EQF values (right)..... 432

Figure IV-78: SOC-adjusted fuel savings of the PMP controller with optimal EQF for all μ -VTPs 432

Figure IV-79: Series-parallel configuration of the Accord PHEV..... 436

Figure IV-80: Engine fuel rate map (left) and Battery internal resistance (right), with temperature as a variable..... 437

Figure IV-81: Wheel output power at engine starts as a function of vehicle speed (left) and battery SOC (right)..... 437

Figure IV-82: Clutch locking patterns - wheel output power at clutch lock and unlock 438

Figure IV-83: Steady-state (blue points) engine operating points in series (left) and parallel (right) mode..... 438

Figure IV-84: Comparison of tested and simulated signals for UDDS cycle in cold ambient conditions..... 439

Figure IV-85: Generation of daily driving events from real-world drive cycles from NREL 445

Figure IV-86: Generation of sets of daily driving trips to meet the NHTS distribution 446

Figure IV-87: Ratio of electric to total miles across different daily driving distances 447

Figure IV-88: Good agreement was achieved between the simplified powertrain model's fuel consumption estimates and fuel consumption measurements from laboratory chassis dynamometer testing 452

Figure IV-89: Good agreement was achieved between the simplified powertrain model's thermal predictions and measured temperatures from the laboratory chassis dynamometer testing (shown here for engine oil as an example)..... 452

Figure IV-90: Model snapshot: 50 minutes 453

Figure IV-91: Model snapshot: 13 hours 453

Figure IV-92: Model snapshot: 7 days..... 454

Figure IV-93: FHWA HPMS road classifications in California 454

Figure IV-94: Operational mapping results: Simulated real-world fuel economy relative to urban/rural designation, HPMS functional class, and average ambient temperature (solar load impacts also captured but not illustrated on the plot) 455

Figure IV-95: National FHWA VMT data disaggregated to cities and overlaid with typical climate data 456

Figure IV-96: Example calculation results over the course of a year in Chicago 457

Figure IV-97: City-level fuel economy estimates plotted relative to the percentage of highway driving and the annual average temperature in each city. The size of each circle is proportional to that city's relative VMT contribution to the national total. 458

Figure IV-98: Wheel torque losses as a function of temperature for the Ford Fusion 464

Figure IV-99: Comparison of test and simulation signals (Urban Dynamometer Driving Schedule [UDDS], cold start, normal ambient temperature) 464

Figure IV-100: Impact of thermal conditions on UDDS and RWDCs for a conventional vehicle..... 464

Figure IV-101: Impact of thermal conditions on UDDS and RWDCs for a hybrid vehicle 465

Figure IV-102: Impact of thermal conditions on the UDDS, Highway Fuel Economy Test (HWFET), and RWDCs for a BEV 465

Figure V-1: Typical Formula 1 Hybrid Power Unit: two motor generator units (MGU) are used: 1 by the kinetic energy of the car (MGU-K) connected to the engine flywheel, and 2, driven by waste heat from a common shaft on the turbocharger (MGU-H; produces electricity fed to the energy storage and/or the MGU-K). The energy storage is limited to 4 MJ that is available for propulsion each lap. The 1.5 L V-6 engine's revs are capped at 15,000 rpm; the entire power unit weighs 145 kg (340 lbs.) and produces over 600 hp. 469

Figure V-2: 2014-15 Formula E car: note the batteries behind the driver with power electronics above and electric motor behind attached to five-speed transaxle..... 470

Figure V-3: Porsche 919 HEVs took first and second place in the 2015 24 Hours of Le Mans (left) and in cutaway to show electric front drive, energy storage in the center of the car, and 2 liter V4 engine with energy recovery and electric transaxle in rear (right). 472

Figure V-4: The DeltaWing showed more pace in 2015, leading several races. Note the absence of traditional wings and highly aerodynamic design; most of the downforce is developed under the side pods. It has a remarkable drag/lift ratio, together with its light weight allowing it to be competitive with about 60% of the engine power of its rivals. 473

Figure V-5: DEKRA Green Challenge Awards were given in all ten TUSC races in 2015 474

Figure V-6: Mazda Skyactiv-Diesel production-based race engine competed in all ten TUDOR United Sportscar Championship races using 100% renewable synthetic diesel fuel. 475

Figure V-7: Fans and professional racing drivers alike try their hand at the GRS. Tommy Milner of Corvette Racing puts the simulated E85/Hybrid Corvette to the test..... 475

Figure V-8: Dynamometer Equipment Used in Experiments 479

Figure V-9: Experimental Vehicles Used for Developing System Power Rating Test..... 479

Figure V-10: Description of Forces during Tests to Determine Road Load (Force of drag)..... 480

Figure V-11: Power Test Options Invented/Explored During Testing Program..... 481

Figure V-12: Three Fundamental Ways to Determine "Net Power" from a Test 482

Figure V-13: All Three Methods Applied to a Parallel HEV during Max Power..... 483

Figure V-14: All Three Methods Applied to a PHEV in Series Mode during Max Power 483

Figure V-15: Chevy Volt Road Load Testing (vehicle has mechanically disengaged neutral gear) 483

Figure V-16: Ford Focus BEV Road Load Testing (motor is always mechanically engaged)..... 484

Figure V-17: Ford Focus BEV On-Dyno Motor Load Testing..... 485

Figure V-18: A comparison of Ford Focus BEV Road Load Curves 485

Figure V-19: Several Runs of a Simple Pull Test to Determine Low-Speed Road Force 486

Figure V-20: PEV Charging Power vs. Time 491

Figure V-21: San Francisco NHTS versus EV Project - Weekday..... 491

Figure V-22: 3.3kW PEV impact on typical San Francisco distribution feeder 491

Figure V-23: Bench test setup for wireless charging for SAE J2954. 495

Figure V-24: Vehicle test setup for wireless charging for SAE J2954. 495

Figure V-25: Charging efficiency of onboard charger vs. alternating current (A) for several production PEVs. 497

Figure V-26: Power factor of onboard charger vs. alternating current (A) for several production PEVs. 498

Figure V-27: Total harmonic distortion in current of onboard charger vs. alternating current (A) for several production PEVs. 498

Figure V-28: Standards Definition Organizations and Standards Related to PEV-Grid Integration 504

Figure V-29: DC charging interoperability testing with PEVs, EVSE and communication modules at the ANL IOC-hosted testing festival ('Festival') in November 2014..... 507

Figure V-30: Mechanization of the Smart Energy Plaza 508

Figure V-31: Example of Solar Power Generation and Loads in the ANL IOC Smart Energy Plaza 508

Figure V-32: Proof-of-concept Sub-metering/Load Control Adaptor (SLCA) 509

Figure V-33: Multiple EVSE hardware studies; Quad EVSE and EVSE building block..... 509

Figure V-34: Example coil topologies similar to proposed reference coils 511

Figure V-35: Wireless Charging test system DAQ Graphic User Input screens from left to right; vehicle/coil positioning, data and probe positioning 511

Figure V-36: ANL Wireless test system with field probe/coil positioners-DAQ; custom international shipping crates..... 512

Figure V-37: Commissioning wireless test fixture in the RF chamber and outdoors (above) and for component/vehicle level alignment assessment using Evatran system (below)..... 512

Figure V-38: ANL EUMD design (versions 1-3) on left; Preliminary 2" x 2" board layout and potential commercial packaging formats; CAD rendering of the EUMD design to replace a standard circuit breaker 513

Figure V-39: DFGM sensors and sensor pair on EUMD bus bar; analog signal conditioning circuit with PSoC; comparison of previous and PSoC-based designs..... 514

Figure V-40: Output current signal from DFGM; drive versus EMF signal symmetry; magnetic sense field modeling 514

Figure V-41: Design of DFGM-based current sensor in DIN rail mounted case/wire guide..... 515

Figure V-42: Smart Load DAQ© internal construction, system components and in a field trial 515

Figure V-43: Interoperability Center Activities Supporting Global Harmonization 518

Figure VI-1: GSF1 1/8 scale wind tunnel model in the NASA Ames 7x10 wind tunnel. 525

Figure VI-2: Drag coefficient as a function of yaw angle for the streamlined heavy vehicle in Figure VI-1 a) without and b) with skirts. 526

Figure VI-3: Streamlined heavy vehicle geometry at 15 degrees yaw with a a) 42" and b) 138" boattail. c-d) Corresponding velocity magnitude contours. 526

Figure VI-4: Drag coefficient as a function of boattail angle for a streamlined heavy vehicle at 15 degrees yaw..... 527

Figure VI-5: Heavy vehicle model (1/8th scale) in the NASA Ames 7x10 wind tunnel..... 527

Figure VI-6: Experimental setup for the PIV system in the NASA Ames 7x10 wind tunnel..... 528

Figure VI-7: Locations of the horizontal PIV imaging planes in the heavy vehicle wake. 528

Figure VI-8 Time-averaged velocity magnitude at the mid-height of the trailer at 0 deg (top) and 6 deg (bottom) yaw. 529

Figure VI-9: Time-averaged velocity streamlines in the trailer wake at 6 deg yaw. 530

Figure VI-10: Model heavy vehicle platoon (1/50th scale) and splitter plate design. 531

Figure VI-11: Internal details of the 1/50th scale platoon model. 531

Figure VI-12: Location of eight load and/or speed locations used in the simulations 535

Figure VI-13: Calculated FMEP for the skirt and/or liner interface of a large diesel engine as a function of viscosity for different operating modes (Speed/Load) 536

Figure VI-14: FCSF maps for a 20 WT, 0% BFR (yellow) and 20 WT, 90% BFR (black mesh) oil relative to a baseline oil (40 WT, 0% BFR) 537

Figure VI-15: Predicted change in fuel consumption for a large diesel engine as functions of oil viscosity and asperity friction reduction 538

Figure VI-16: Hybrid Radiator System..... 541

Figure VI-17: Top View of a Section of the Hybrid Radiator 542

Figure VI-18: Increased Radiator Heat Transfer 542

Figure VI-19: Reduced Radiator Size 543

Figure VI-20: Droplet Movement..... 544

Figure VI-21: Droplet Evaporation..... 544

Figure VI-22: Air Flow Effect 545

Figure VI-23: Droplet Evaporation with Air Flow Effect 545

Figure VI-24: Experimental Test System Overview 546

Figure VI-25: Experimental Test Strip Assembly 547

Figure VI-26: Heating Wire and Thermocouples 548

Figure VI-27: Droplet Dispersing Head Assembly..... 549

Figure VI-28: Surface Temperature Effect on Droplet Movement and Evaporation..... 551

Figure VI-29: Surface Temperature Effect on Droplet Movement and Evaporation (Close-Up View) 551

Figure VI-30: Droplet Size Effect on Droplet Movement and Evaporation..... 552

Figure VI-31: Leading Vehicle (LV) and Trailing Vehicle (TV) configuration in single-lane traffic 557

Figure VI-32: Comparison of fuel savings in single-lane traffic vehicles at different vehicle separation distances [averaged values of three different yaw angles 0°, -6°, and 6°]. 557

Figure VI-33: Static pressure distribution in 0° yaw angle (i) no-traffic, (ii) 60 ft, and (iii) 150 ft..... 558

Figure VI-34: Leading Vehicle (LV) and Trailing Vehicle (TV) configuration in two-lane traffic 558

Figure VI-35: Comparison of fuel savings in one-way two-lane traffic vehicles at different vehicle separation distances [averaged values of three different yaw angles 0°, -6°, and 6°]. 559

Figure VI-36: Velocity fields in 6° yaw angle (i) 30 ft, (ii) 60 ft, and (iii) 90 ft 559

Figure VI-37: Velocity fields in 30ft vehicle separation distance at different yaw angles (i) 0°, (ii) 6°, and (iii) -6° 560

Figure VI-38: Two vehicles in side-by-side positions in multi-lane traffic 560

Figure VI-39: Comparison of fuel consumption for each of vehicle in one-way two-lane traffic [averaged values of three different yaw angles 0°, -6°, and 6°]. 560

Figure VI-40: Static pressure distribution in 6° Yaw angle (i) no-traffic and (ii) two-vehicles 561

Figure VI-41: Three vehicles in side-by-side positions in multi-lane traffic 561

Figure VI-42: Comparison of fuel consumption for each of vehicle in one-way three side-by-side vehicles [averaged values of three different yaw angles 0°, -6°, and 6°]. 561

Figure VI-43: Three vehicle configuration; two leading vehicles are in side-by-side position and one trailing vehicle behind one of the leading vehicles. 562

Figure VI-44: Comparison of fuel consumption for each of vehicle in one-way two-lane traffic at 30 ft vehicle separation distance [averaged values of three different yaw angles 0°, -6°, and 6°]. 562

Figure VI-45: Velocity fields in 0° Yaw angle (i) one-leading vehicle and (ii) two-leading vehicles 563

Figure VI-46: Vehicle underhood components; (i) top view and (ii) cooling package 563

Figure VI-47: Averaged temperature rise in heat exchangers of trailing vehicle at constant fan speed [averaged values of three different yaw angles 0°, -6°, and 6°]. 564

Figure VI-48: Temperature distribution in 0° Yaw angle at 30ft vehicle separation distance [horizontal plane at fan center position]. 564

Figure VI-49: Averaged temperature rise in heat exchangers of trailing vehicle at constant fan speed [averaged values of three different yaw angles 0°, -6°, and 6°]. 565

Figure VI-50: Temperature distribution in 0° Yaw angle at 30ft vehicle separation distance [horizontal plane at fan center position]. 565

Figure VI-51: Schematic of Heat Transfer Facility 569

Figure VI-52: Test Section Heating Wire Arrangement 569

Figure VI-53: Heat Transfer Facility Overview 570

Figure VI-54: Heat Loss Calibration 571

Figure VI-55: Turbulent Heat Transfer Coefficient Comparison 572

Figure VI-56: Laminar Heat Transfer Coefficient Comparison 572

Figure VI-57: Water Turbulent Flow Boiling Curves..... 574

Figure VI-58: 40/60 EG/W Mixture Turbulent Flow Boiling Curves 575

Figure VI-59: 50/50 EG/W Mixture Turbulent Flow Boiling Curves 576

Figure VI-60: EG/W Mixture Laminar Flow Boiling Curves 577

Figure VI-61: Boiling Heat Transfer Coefficients 577

Figure VI-62: Correlation of Boiling Number Term 578

Figure VI-63: Heat Transfer Coefficient Comparison 578

Figure VI-64: Correlation of Boiling Number Term for All Data 579

Figure VI-65: Heat Transfer Coefficient Comparison for All Data 579

Figure VI-66: Wall Temperature Comparison 580

Figure VI-67: Pressurizing System 580

Figure VI-68: Surface Rust Effects 581

Figure VI-69: System Pressure Effects 582

Figure VI-70: Original Autonomie “lumped” mechanical accessory model. 585

Figure VI-71: Separated accessory models. (cooling fan, air compressor, power steering, air conditioning, and electrical accessories) 586

Figure VI-72: HD class 8 line haul sleeper cab based on a chassis tested Kenworth T700..... 586

Figure VI-73: First component test cell setup. Conventional sleeper cab setup with electrified condenser fan. 587

Figure VI-74: Second component test cell setup. Electrified compressor with electrified condenser fan..... 588

Figure VI-75: ORNL's VSI Component test cell. Open configuration. 589

Figure VI-76: ORNL's VSI Component test cell with insulated environmental box..... 590

Figure VI-77: NREL's CoolSim model and the structure it will take inside our Autonomie model when validated. 590

Figure VI-78: Project focus areas. 594

Figure VI-79: Engine dynamometer configuration..... 595

Figure VI-80: Updated fuel consumption and emissions maps. 596

Figure VI-81: ORNL transient engine model and associated aftertreatment models. 597

Figure VI-82: Aftertreatment model validation data. 598

Figure VI-83: HD truck HESS simulation model..... 599

Figure VI-84: HD HESS load current profile: +/-100A; +/-80A. 599

Figure VI-85: HD HESS modified for high-Z state of buck/boost cConverter. 600

Figure VI-86: HD HESS buck/boost voltage mode control logic (initial power management strategy architecture). 600

Figure VI-87: HD truck propulsion power, P(V), (fully loaded trailer case)..... 601

Figure VI-88: HD truck motoring power with filtered PICE..... 601

Figure VI-89: HD truck regeneration power (fully loaded trailer case). 602

Figure VI-90: HD truck dynamic power (fully loaded trailer case)..... 602

Figure VI-91: HD truck dynamic load current (fully loaded trailer case)..... 603

Figure VI-92: PSIM simulation of the HD truck HESS: Initial $SOC_b=0.8$, $SOC_{uc}=0.697$, $U_{d0}=680V_{dc}$ 603

Figure VI-93: PSIM simulation of the HD truck HESS: Initial $SOC_b=0.8$, $SOC_{uc}=0.54$, $U_{d0}=680V_{dc}$ 604

Figure VI-94: PSIM simulation of the HD truck HESS: Initial $SOC_b=0.8$, $SOC_{uc}=0.54$, $U_{d0}=700V_{dc}$ 604

Figure VI-95: PSIM model of the HD truck HESS: Initial $SOC_b=0.8$, $SOC_{uc}=0.54$, $U_{d0}=700V_{dc}$ 605

Figure VI-96: PSIM model mode control logic 605

Figure VI-97: PSIM simulation of the HD truck HESS: Initial $SOC_b=0.8$, $SOC_{uc}=0.54$, $U_{d0}=700V_{dc}$ 606

Figure VI-98: PSIM simulation of the HD truck HESS: dc-dc converter output and LIB currents. 606

Figure VI-99: PSIM simulation of the HD truck HESS: dc-link voltage, U_d , and UC voltage, U_{in} 606

Figure VI-100: PSIM simulation of the HD truck HESS: dc-dc Converter Duty Ratio, $dT(t)$ 607

Figure VI-101: Concept of Subcooled Flow Boiling System 609

Figure VI-102: Vehicle Power Electronic Package 610

Figure VI-103: Side View of Vehicle Power Electronic Package 610

Figure VI-104: Fin Structure 611

Figure VI-105: Mesh Structure (All Units in Meter)..... 611

Figure VI-106: TIM Thermal Conductivity Effects 612

Figure VI-107: Junction Temperatures 613

Figure VI-108: Coolant Flow Velocity Effects..... 613

Figure VI-109: Fluid Inlet Temperature Effects 614

Figure VI-110: Heat Flux Effects 615

Figure VI-111: High Heat Flux Applications 615

Figure VI-112: Experimental Test Module..... 617

Figure VI-113: Experimental Test Module Overview 617

Figure VI-114: Convective Heat Transfer Simulation Results 618

Figure VI-115: Subcooled Boiling Heat Transfer Simulation Results 618

Figure VI-116: Heat Loss Calibration Results..... 619

Figure VI-117: Fin Effect on Subcooled Boiling..... 619

Figure VI-118: Wall Temperature as a Function of Subcooled Boiling Length..... 620

Figure VI-119: Distribution of battery pack temperature for each charge condition group. These data represent 50,000 miles of driving, charging, and parking over more than 500 days of the

onroad study. The DCFC packs show a shift of a few degrees Celsius higher temperature than the two AC 2 charged packs..... 624

Figure VI-120: Battery capacity remaining, as a percent of baseline, THAT IS averaged among the onroad vehicles of each charge condition group. 624

Figure VI-121: Constant-speed average range achieved at three different speeds for each test group after 50,000 miles of onroad operation. 625

Figure VI-122: Constant-speed average range at 45 mph for each test group when new and after 50,000 miles of onroad operation..... 625

Figure VI-123: Battery capacity measured or inferred by three methods: (1) laboratory capacity testing, (2) track constant-speed range testing, and (3) onroad energy usage during daily driving. 626

Figure VI-124: The percent of energy retained versus miles (or miles equivalent) driven or cycled is shown for the onroad and laboratory-cycled packs. 626

Figure VI-125: Eaton smart grid-enabled EVSE. 632

Figure VI-126: Delta smart grid EVSE. 633

Figure VI-127: Delta smart grid EVSE energy meter test results..... 634

Figure VI-128: Siemens smart grid EVSE..... 635

Figure VI-129: Siemens smart grid EVSE energy meter test results. 636

Figure VI-130: Vehicle testing of the production Evatran PLUGLESS wireless charger on a 2012 Chevrolet Volt..... 637

Figure VI-131: Bench testing of the production Evatran PLUGLESS wireless charger. 637

Figure VI-132: Bench test efficiency results of the production PLUGLESS wireless charger. 638

Figure VI-133: Vehicle test (i.e., Chevy Volt) efficiency results of the production PLUGLESS wireless charger..... 639

Figure VI-134: Bench test electromagnetic field scan results of the production PLUGLESS wireless charger..... 639

Figure VI-135: Vehicle test electromagnetic field scan results of the production PLUGLESS wireless charger..... 640

Figure VI-136: Individual auxiliary load characterization..... 641

Figure VI-137: Quarterly average onroad vehicle auxiliary loads..... 642

Figure VI-138: Ambient temperature impact on auxiliary loads (Jetta TDI). 642

Figure VI-139: Hourly Distribution of Vehicle Miles Travelled on Selected Roadways for a "Typical" Week of Travel..... 646

Figure VI-140: Comparison of Previous Analysis Roadway (Green) to Selected Roadway from 2013 HPMS (Black) with the 2010 Census CSA Boundary (blue Dashed) and 2013 CSA Boundary (Orange) 646

Figure VI-141: Electrified Roadway Grid Load for a "Typical" Week as a Percentage of Light-Duty VMT on the Designated Roads 648

Figure VI-142: Electrified Roadway Scenarios Added to Typical Winter Grid Load. The numbers in colored text indicate the percent load growth over the baseline at the new seasonal average load peak resulting from each fractional VMT electrification scenario..... 649

Figure VI-143: Electrified Roadway Scenarios Added to Typical Spring Grid Load. The numbers in colored text indicate the percent load growth over the baseline at the new seasonal average load peak resulting from each fractional VMT electrification scenario..... 649

Figure VI-144: Electrified Roadway Scenarios Added to Typical Summer Grid Load. The numbers in colored text indicate the percent load growth over the baseline at the new seasonal average load peak resulting from each fractional VMT electrification scenario..... 650

Figure VI-145: Electrified Roadway Scenarios Added to Typical Fall Grid Load. The numbers in colored text indicate the percent load growth over the baseline at the new seasonal average load peak resulting from each fractional VMT electrification scenario..... 650

Figure VI-146: Electrified Roadway Scenarios Added to the Highest Yearly Grid Load Week. The numbers in colored text indicate the percent load growth over the baseline at the new seasonal average load peak resulting from each fractional VMT electrification scenario. 651

Figure VI-147: Absolute and Incremental Percentage Load Impacts from the 5% of Light-Duty VMT Electrified Roadway Scenario Added to the Baseline Highest Yearly Grid Load Week..... 652

Figure VI-148: Historical Non-coincident Peak Load (All-Interconnects) with Linear and Polynomial Fits and Non-coincident Peak Load for the Summer Period for All Interconnection on the Grid from 1986 until 2011. 653

Figure VI-149: Approach to Conduct Research for Electric Vehicle Grid Integration 657

Figure VI-150: Characterization of A Mini-E with Bi-directional Power Flow through Aggregation Software Tools was completed in ESIF 658

Figure VI-151: Testing Power Interface Functions of PG&E Utility Truck with V2G capability was conducted at NREL's ESIF 658

Figure VI-152: NREL Demonstrates Interface between Vehicle and Building Energy Management Systems at NREL Parking Garage 659

Figure VI-153: Testing Communications Architecture for PEV control..... 659

Figure VI-154: V2G Simulation Functions were built as an Extension to the BLAST-V tool..... 660

Figure VI-155: Simulations Show Opportunity to Provide V2G Functions can be Optimized Based on Driving Profile 661

Figure VI-156: Daily and Seasonal Grid Variability will Impact PEV Value Proposition 661

Figure VI-157: Sample summary pages of charge data 667

Figure VI-158: ORNL Solar-Assisted Charging Summary Report 668

Figure VI-159: Knoxville Market Square Data 669

List of Tables

Table I-1 FY 2015 Accomplishment Highlights..... 3

Table II-1: AVTE Vehicles Tested During FY2015..... 19

Table II-2: Summary of vehicle integration specifications..... 29

Table II-3: Conventional and color-matched near-infrared reflective paint sample solar reflectance values 46

Table II-4: Advanced glass package composition and expected properties for Phase I evaluation..... 46

Table II-5: Vehicle cabin insulation product selection for phase I evaluation..... 47

Table II-6: Properties of Candidate Phase Change Materials 55

Table II-7: Performance targets 76

Table II-8: Energy efficiency for single speed vehicle. (mpgde stands for mile per gallon diesel equivalent and does not include the on-board charger efficiency)..... 79

Table II-9: Acceleration times for 10T baseline vehicle..... 80

Table II-10: Comparison of gradeability performance of baseline vehicle with singles speed gearbox and vehicle with 3 speed transmission. 81

Table I-II-11: Lab-Scale and RINGPAK Test Conditions and Equivalent Loads/Ring Tensions..... 92

Table I-II-12: Peak values of the Str number for lab-scale tests and a typical fired engine 94

Table II-13: Project Status 111

Table II-14: Silica prototypes surface energy 117

Table II-15: NR/BR compound data..... 118

Table II-16: NR/SSBR compound data 119

Table II-17: 2012 Zero Emission Drayage Truck Demonstration Portfolio 135

Table III-1: 2014 Chevrolet Cruze Diesel specifications..... 147

Table III-2: 2014 Chevrolet Cruze diesel fuel consumption penalty at varying temperatures 149

Table III-3: 2014 Mazda 3 Skyactive i-ELOOP specifications 149

Table III-4: 2014 Smart Fortwo Electric drive specifications 151

Table III-5: 2014 BMW i3 REx specifications 153

Table III-6: 2014 BMW i3 BEV Specifications 156

Table III-7: 2015 Kia Soul BEV Specifications 158

Table III-8: 20F UDDS CS energy use by component for varying BEV's 160

Table III-9: 2015 Honda Accord Hybrid Specifications..... 161

Table III-10: 2015 Chevrolet Spark EV Specifications 163

Table III-11: 2012 VW Passat Ecofuel TSI Specifications 166

Table III-12: VW Passat Ecofuel TSI emissions of the standard US drive cycles 167

Table III-13: Predicted Focus Electric Range (miles)..... 201

Table III-14: Predicted Range Improvement over Baseline A/C..... 202

Table III-15: Test configuration descriptions 219

Table III-16: Steady-state energy savings summary 224

Table III-17: Selection of basic model inputs 228

Table III-18: Control parameters 233

Table III-19: CFL versus baseline configurations 241

Table III-20: Baseline ESS Device Comparisons 248

Table III-21: Smith Newton Vehicle Specifications 260

Table III-22: Navistar eStar Vehicle Specifications 263

Table III-23: Utilization summary 266

Table III-24: Foothill Transit daily drive cycle statistics 277

Table III-25: Information on the Conventional Diesel Truck Model..... 287

Table III-26: Predictive Results of FASTSim and MARS Approaches..... 287

Table III-27: Vehicle Specifications 288

Table III-28: Identified DCs - Selected Parameter Information 300

Table III-29: Federal Way vehicles monitored in second logger deployment 309

Table III-30: Hybrid Propulsion-Related Systems..... 317

Table III-31: Vehicle summary statistics 327

Table III-32: Standard Test Cycle Summary Statistics..... 328

Table III-33: Fuel Properties..... 329

Table III-34: Smith EV subjects of battery degradation testing 334

Table I-35: Thermal Load Reduction with Advanced Insulation 375

Table I-36: Thermal Load Reduction with Advanced Insulation 376

Table I-37: Thermal Load Reduction with Sleeper Curtains Open 376

Table IV-38: A/C national-level fuel use simulation result summary 388

Table IV-39: Battery sizing impacts of TLRP..... 389

Table IV-40: Tuning configuration comparisons..... 404

Table IV-41: Preliminary system design parameters..... 406

Table IV-42: Validation results (Urban/UDDS)..... 439

Table IV-43: Validation results (Highway) 440

Table IV-44: Impact of VTO Technology Benefits for Conventional Powertrain (Real-World and Standard Procedure)..... 447

Table IV-45: Impact of VTO Technology Benefits for Hybrid Powertrain (Real-World and Standard Procedure).....	447
Table IV-46: Impact of VTO Technology Benefits for an Electric Powertrain (Real-World and Standard Procedure).....	448
Table IV-47: Impact of VTO Technology Benefits for an Electric Powertrain (Real-World and Standard Procedure) for two sets of Daily Driving Schedules.....	448
Table IV-48: Estimates for hypothetical window glazing technology.....	458
Table IV-15: Estimates for hypothetical accessory load reduction technology.....	459
Table IV-50: Estimates for hypothetical thermal retention technology.....	459
Table V-1: Focus BEV Load Curve Summary	486
Table V-2: Status of Key Standards and Committee Participation.....	505
Table VI-1: Components modeled, code, friction model, and baseline friction coefficients used in calculations [4].....	534
Table VI-2: Lubricant viscosity and asperity friction coefficients used in calculations [5]	534
Table VI-3: Radiator Fan Speed Effect on Droplet	549
Table VI-4: Operating conditions for aerodynamic drag simulations.....	556
Table VI-5: Heat exchanger porous body modeling.....	563
Table VI.6: Accessory Entitlements for the Cummins Proprietary Cycle (HD Class 8 Line Haul Sleeper Cabin).....	588
Table VI-7: Materials and Dimensions of Each Layer	611
Table VI-8: Comparison of Convection and Subcooled Boiling	616
Table VI-9: Eaton smart grid EVSE efficiency.	632
Table VI-10: Eaton EVSE standby power (watts).	632
Table VI-11. Delta smart grid EVSE efficiency.	633
Table VI-12: Delta EVSE standby power (watts).....	634
Table VI-13: Siemens smart grid EVSE efficiency.	635
Table VI-14: Siemens EVSE standby power (watts).....	636
Table VI-15: Test results from the PLUGLESS wireless charger at nominal conditions.....	638
Table VI-16: Power quality test results from the PLUGLESS wireless charger.	639

Acronyms and Abbreviations

A

AC	Alternating Current
accel	Acceleration
ACE	Advanced Combustion Engine
ACEC	Advanced Combustion and Emission Control
ACFL	Advanced Combined Fluid Loop
AD	Automotive Dialog
AER	All-electric range
AFV	Alternative Fuel Vehicle
ALMS	American Le Mans Series
AMI	Advanced Metering Infrastructure
ANL	Argonne National Laboratory
ANN	Artificial Neural Network
AOI	Areas of Interest
APEC	Asia Pacific Economic Council
APRF	Advanced Powertrain Research Facility
ARRA	American Recovery and Reinvestment Act
AVTA	Advanced Vehicle Testing Activity
AVTE	Advanced Vehicle Testing and Evaluation

B

BaSc	Baseline and Scenario
Batt	Battery
BEB	Battery Next-Generation Electric Transit Bus
BEC	Bussed Electrical Center
BECM	Battery Energy Control Module
BEMS	Building Energy Management System
BET	Battery Electric Truck
BETO	Bioenergies Technologies Office
BEV	Battery Electric Vehicle
BMW	Bayerische Motoren Werke AG
BOL	Beginning of Life
BR	Butadiene Rubber
BSFC	Brake Specific Fuel Consumption
BTE	Brake Thermal Efficiency

C

CAC	Charge Air Cooler
CAE	Computer-Aided Engineering
CAFE	Corporate Average Fuel Economy

CAN	Controller Area Network
CARB	California Air Resources Board
CCGI	Car Charging Group Inc.
CCS	Combined Charging System
CD	Charge-Depleting
CDC	Conventional Diesel Combustion
CERV	Conference on Electric Roads and Vehicles
CFD	Computational Fluid Dynamics
CFDC	Commercial Fleet Data Center
CFL	Combined Fluid Loop
CH4	Methane
CHTS	California Household Travel Survey
CI	Diesel Compression Ignition
CILCC	City, Composite International Truck Local and Commuter
CIP	Common Integration Platform
CLEERS	Cross-Cut Lean Exhaust Emissions Reduction Simulations
Cm3	Cubic
CNG	Compressed Natural Gas
CO	Carbon monoxide
CO2	Carbon Dioxide
Conv	Conventional Vehicle
COP	Coefficient of Performance
CRADA	Cooperative Research and Development Agreement
CS	Charge Sustaining
Cs	Cold start
CSA	Combined Statistical Area
CSHVC	City Suburban Heavy Vehicle Cycle
CSS	Cascade Sierra Solutions
csv	comma-separated values
CT	Current Transformer
CV	Conventional vehicle
CVS	Constant Volume Sample
CVT	Continuously variable transmission
D	
D3	Downloadable Dynamometer Database
DC	Direct current
DCFC	Direct Current Fast Charge
DCT	Dual-clutch transmission
decel	Deceleration
DFGM	Digital Flux Gate Magnetometer
DFMEA	Design of Failure Modes Analysis

DI	Direct injection
DIST	Devices and Integrated Systems Testing
DOC	Diesel oxidation catalyst
DOE	U.S. Department of Energy
DOHC	Dual over head cam
DPF	diesel particulate filter
DRIVE	Drive-Cycle Rapid Investigation, Visualization, and Evaluation Analysis Tool
DSC	Differential Scanning Calorimeter
DSP	Digital Signal Processor
dt	Change in time
DTS	Dynamic Thermal Sensation
dv	Change in velocity
Dyno	Dynamometer

E

E85	Ethanol fuel blend of 85% ethanol and 15% gasoline by volume
EAVS	Electrically Assisted Variable Speed
EC	European Commission
ECMS	Equivalent Consumption Minimization Strategy
ECVT	Electronically Controlled Continuously Variable Transmission
EDV	Electric Drive Vehicle
EERE	Energy Efficiency and Renewable Energy
EEV	Electronic Expansion Valve
EGR	Exhaust Gas Recirculation
EMM	Electricity Market Module
EOL	End of life
EPA	Environmental Protection Agency
EPCU	Electric Powertrain Control Unit
ePTO	Electric Power Take-Off
EQF	Equivalence Factor
EREV	Extended-Range Electric Vehicles
ERGIS	Eastern Renewable Generation Integration Study
ESIF	Energy Systems Integration Facility
ESS	Energy Storage System
ETT	Electric Transportation Technologies
EUMD	End-Use Measurement Device
EV	Electric Vehicle
EV2G	Electric Vehicle-to-Grid
EVSE	Electric Vehicle Service Equipment
EVT	Infinitely variable transmission

F

F	Force
FASTSim	Future Automotive Systems Technology Simulator
FC	Fuel cell
FC	Fast charge
FCons	Fuel consumption
FCSF	Fuel Consumption Scaling Factor
FE	Fuel Economy
FE	Formula E
FEX	Front-end Heat Exchanger
FHWA	Federal Highway Administration
FIA	Federation Internationale de l'Automobile
FLNA	Frito-Lay North America
FLT	Fuel and lubricant technologies
FMEP	Friction Mean Effective Pressure
FMI	Functional Mockup Interface
FOA	Funding Opportunity Announcement
FTP	Federal Test Procedure
FWD	Four wheel drive
FY	Fiscal year

G

g	gram
GA	Ground Assembly
GCEDV	Grid Connected Electrical Drive Vehicles
GEM	Gas Emissions Model
GHG	Greenhouse Gas
GMLC	Grid Modernization Lab Consortium
GPRA	Government Performance and Results Act
GPS	Global Positioning System
GREET	Greenhouse gases, Regulated Emissions, and Energy use in Transportation
GRI	Green Racing Initiative
GRS	Green Racing Simulator
GSF1	Generic Speed Form 1
GSU	Grid side unit
GTLM	GT Le Mans
GTO	Gate turn-off
GUI	Graphic User Interface
GVW	Gross Vehicle Weight

H

h-APU	hybrid Auxiliary Power Unit
HATCI	Hyundai America Technical Center, Inc.
HC	Unburned hydrocarbons
HD	Heavy Duty
HDDE	Heavy Duty Diesel Engine
HDS	Highly Dispersible Silicas
HEV	Hybrid-Electric Vehicle
H-GAC	Houston-Galveston Area Council
HHDDT	Heavy Heavy-Duty Diesel Truck
HHV	Hydraulic Hybrid Vehicle
HIL	Hardware-In-the-Loop
HP	Heat Pump
Hp	Horsepower
HTUF4	Hybrid Truck Users Forum Parcel Delivery Class
HTML	HyperText Markup Language
HV	High Voltage
HTDC	Heavy Truck Duty Cycle
HVAC	Heating Ventilating and Air Conditioning
HWFET	Highway Fuel Economy Test
HPMS	Highway Performance Monitoring System
HVTB	High Voltage Traction Battery
HWY	Highway Program or Highway Fuel Economy Test Cycle
HPC	High Performance Computing
Hz	Hertz

I

I	Inertia
IC	Internal Combustion
ICD	Iterim Component Durability
ICDV	Internal Combustion Drive Vehicles
ICE	Internal Combustion Engine
ICTF	Intermodal Container Transfer Facility
ICU	Inverter-Charger Unit
IEB	Information Exchange Bus
IEC	International Electrotechnical Commission
IGBT	Insulated Gate Bipolar Transistors
IHX	Internal Heat Exchanger
IMSA	International Motor Sport Association
INL	Idaho National Laboratory
INTEGRATE	Intetrated Network Testbed for Energy Grid Research and Technology
IR	Infrared Radiation
ISO	International Organization for Standardization

ITEC15	IEEE Transportatino Electrification Conference & Expo
ITS	Intelligent Transportation Systems
i-VTEC	Intelligent -Variable Valve Timing and Lift Electronic Control

J

JARI	Japan Automobile Research Institute
JIT	Just-in-Time
JRC-IET	Joint Research Center- Insitute for Energy & Transport

K

kg	Kilogram
km	Kilometer
kW	Kilowatt
kWh	Kilowatt hour

L

L	litre
L1	Level 1 benchmark
L2	Level 2 benchmark
Lbf	Pounds force
LCC	Liquid-Cooled Condenser
LD	Light-duty
LEESS	Lower-Energy Energy Storage System
LH	line haul
Li	Lithium
LIB	Lithium ion battery
LIC	Lithium-Ion Capacitor
LLNL	Lawrence Livermore National Laboratory
LMP1	Le Mans Prototype
LTC	Lockport Technical Center
LV	Leading Vehicle

M

M	Mass
MABx	MicroAutoBox
MARS	Multivariate Adaptive Regression Splines
MAP	Manifold air pressure
MBSE	Model Based System Engineering
M2M	Machine-to-Machine
MC	Electric Motor & Control
MD	Medium Duty
MGU	Motor generator unit
mpg	Miles per gallon

MMTCE	Million Metric Tons of Carbon Equivalent
MIIT	Ministry of Industry and Information Technology
mi	Mile
MJ	Megajoules
MOSFET	Metal-Oxide Semiconductor Field-Effect Transistor
mph	Miles per hour
MPGe	Miles per gallon equivalent
MTDC	Medium Truck Duty Cycle
MOVES	Motor Vehicle Emission Simulator
MRF	Moving Reference Frame
MY	Model year
M-VTP	Macroscopic vehicle trip profile
M2	Meters squared
μ-VTP	Microscopic vehicle trip profile

N

NATC	Nevada Automotive Test Center
NDA	Non-Disclosure Agreement
NETL	National Energy Tehcnology Laboratory
NHTS	National Household Travel Survey
NHTSA	National Highway Transportation Safety Administration
NiMH	Nickel-Metal-Hydride
NM	Newton meters
NOx	Nitrogen oxides
NR	Natural Rubber
NREL	National Renewable Energy Laboratory
NRT	National Retail Trucking
NSRDB	National Solar Radiation Database
NTSDC	National Transportation Secure Data Center
NVH	Noise, vibration, and harshness
NVUSD	Napa Valley Unified School District
NYCC	New York Composite Cycle
NYSERDA	New York State Energy Research Development Authority

O

OBC	On-board charger
OCBC	Orange County Bus Cycle
OEM	Original Equipment Manufacturer
OneSAF	One Semi-Automated Forces
ORNL	Oak Ridge National Laboratories

P

P	Active Power
PADD	Petroleum Administration for Defense District
PC	Polycarbonate
PCM	Phase-Change Material
PCU	Power Control Unit
PCU	Powertrain Control Unit
PEEM	Power Electronics and Electric Motor
PFC	Power factor correction
PFI	Port fuel injection
PGW	Pittsburgh Glass Works
PHEV	Plug-in Hybrid Electric Vehicle
PHEV##	Plug-in hybrid electric vehicle with ## miles of all-electric range
PM	Permanent Magnet
PM	Particulate Matter
PMP	Pontryagin Minimum Principle
PMV	Predicted Mean Vote
PNN	Polynomial Neural Network
PPD	Predicted Percentage Dissatisfied
ppm	Parts per Million
PSoC	Programmable System-on-Chip
PTC	Positive Temperature Coefficient
PTO	Power Take-Off
PWM	Pulse Width Modulation
PWWMD	Public Works and Waste Management Department
λ	Power Factor
φ	Power Angle

Q

Q	Reactive power
QA	Quality assurance
QC	Quality control

R

R ²	Coefficient of Determination
RCCI	Reactivity controlled compression ignition
REx	Range Extending Engine
RFS	Renewable Fuel Standard
RH	Relative Humidity
RMS	Root Mean Square
ROL	Ring-On-Liner
rpm	Revolutions Per Minute

RTOS	Real-Time Operating System
RWDC	Real-World Drive-Cycle
RWDC	Real-World Design Challenge

S

S	Apparent power
SAE	Society of Automotive Engineers
SC03	SC03 Supplemental Federal Test Procedure
SCAG	Southern California Association of Governments
SCAQMD	South Coast Air Quality Management District
SCIG	Southern California International Gateway
SCR	Silicon Controlled Rectifier
SCR	Selective Catalytic Reduction
SDO	Standards Definition Organizations
SEP2	Smart Energy Profile 2.0
SI	Système International d'Unités
SI	Gasoline Spark Ignition
SLCA	Sub-metering/Load Control Adaptor
SOC	State of Charge
SR	Speed Ratio
SS	Steady State
SSR	Solid State Relay
StAR	Storage-Assisted Recharging
STEM	Science, Technology, Engineering, and Mathematics

T

T	Torque
TARDEC	Tank Automotive Research Development and Engineering Center
TBR	Truck and Bus Radial
TE	Thermoelectric
TES	Thermal Energy Storage
TESPT	Triethoxy-silypropyl Tetrasulfide
TEV	Thermostatic Expansion Valve
TEVAC	Tennessee Electric Vehicle Advisory Council
Tgt	Target
THC	Total hydrocarbon emissions
TIM	Thermal Interface Materials
TLRP	Thermal Load Reduction Package
TOU	Time-Of-Use
TSDC	Transportation Secure Data Center
TSI	Turbocharged stratified injection
TUSC	TUDOR United Sportscar Championship
TUSD	Torrance Unified School District

TV	Trailing Vehicle
TXVs	Thermal Expansion Valves

U

U.S. DRIVE	U.S. Driving Research and Innovation for Vehicle Efficiency and Energy Sustainability
UA	Transfer Coefficient
UC	Ultra-capacitor
UCR	University of California, Riverside
UDDS	Urban Dynamometer Driving Schedule
ULSD	Ultra-low sulfur diesel
UN ECE	United Nations Economic Council for Europe
UPS	United Parcel Service
URL	Uniform Resource Locator
US06	Environmental Protection Agency US06 or Supplemental Federal Test Procedure
USABC	United States Advanced Battery Consortium
USCAR	U.S. Council for Automotive Research
Util	Battery capacity utilization

V

V	Voltage
V2G	Vehicle-to-Grid
VAr	Volt-Amp-reactive
VGI	Vehicle-Grid Integration
VIP	Vacuum Insulated Panels
VMT	Vehicle Miles Traveled
VS	Vehicle Systems
VSATT	Vehicle Systems Analysis Technical Team
VSI	Vehicle Systems Integration
VSST	Vehicle Systems Simulation and Testing
VPC	Vehicle Supervisory Controller
VTCab	Vehicle Thermal Cab Simulator
VTIF	Vehicle Testing and Integration Facility
VTO	Vehicle Technologies Office
VTP	Vehicle Travel Profile
VTs	Vehicle technical specifications

W

dw	Change in Angle W
WCC	Water Cooler Condenser
WEC	World Endurance Championship
WEG	Water/Ethylene Glycol
Wh	Watt hour

WPT	Wireless Power Transfer
WTW	Well-to-Wheels
WVU	West Virginia University

X

Y

Z

I. Introduction

On behalf of the Vehicle Technologies Office (VTO) of the U.S. Department of Energy (DOE), we are pleased to submit the Annual Progress Report for Fiscal Year (FY) 2015 for the Vehicle Systems (VS) program activities.

I.1. Mission and Objectives

VS is concerned with advancing light-, medium-, and heavy-duty (HD) vehicle systems to support DOE’s goals of reducing petroleum consumption, and reducing greenhouse gas (GHG) emissions in the U.S. transportation sector. To help reach those goals, VTO conducts research and development (R&D) programs implementing strategies to help maximize the number of electric vehicle miles driven, and increase the energy efficiency of transportation vehicles.

VS’s mission is to accelerate the market introduction and penetration of advanced vehicles and systems with R&D that have a significant impact on petroleum displacement, GHG reduction, and DOE electrification goals. Figure I-1 below outlines the outcome objectives that VS has identified as important to fulfilling its mission. Figure I-2 lists the primary processes and examples of tangible R&D project objectives that contribute to one or more VS outcome objectives.

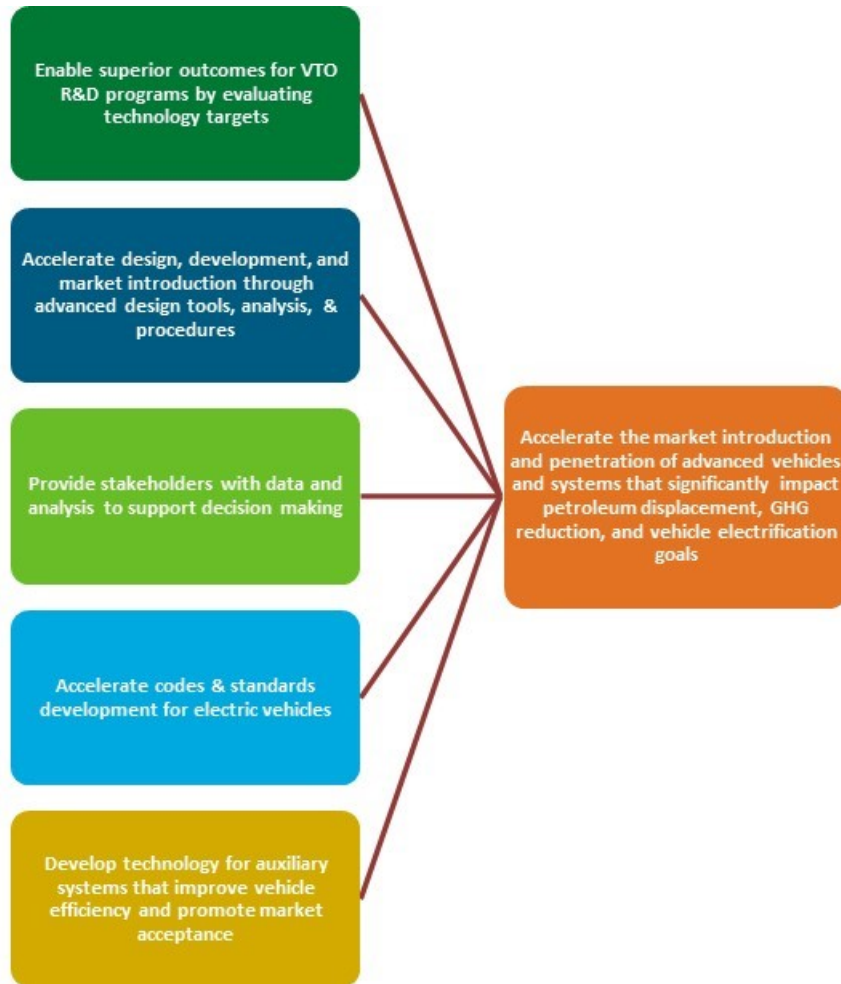


Figure I-1: VS outcome objectives and mission

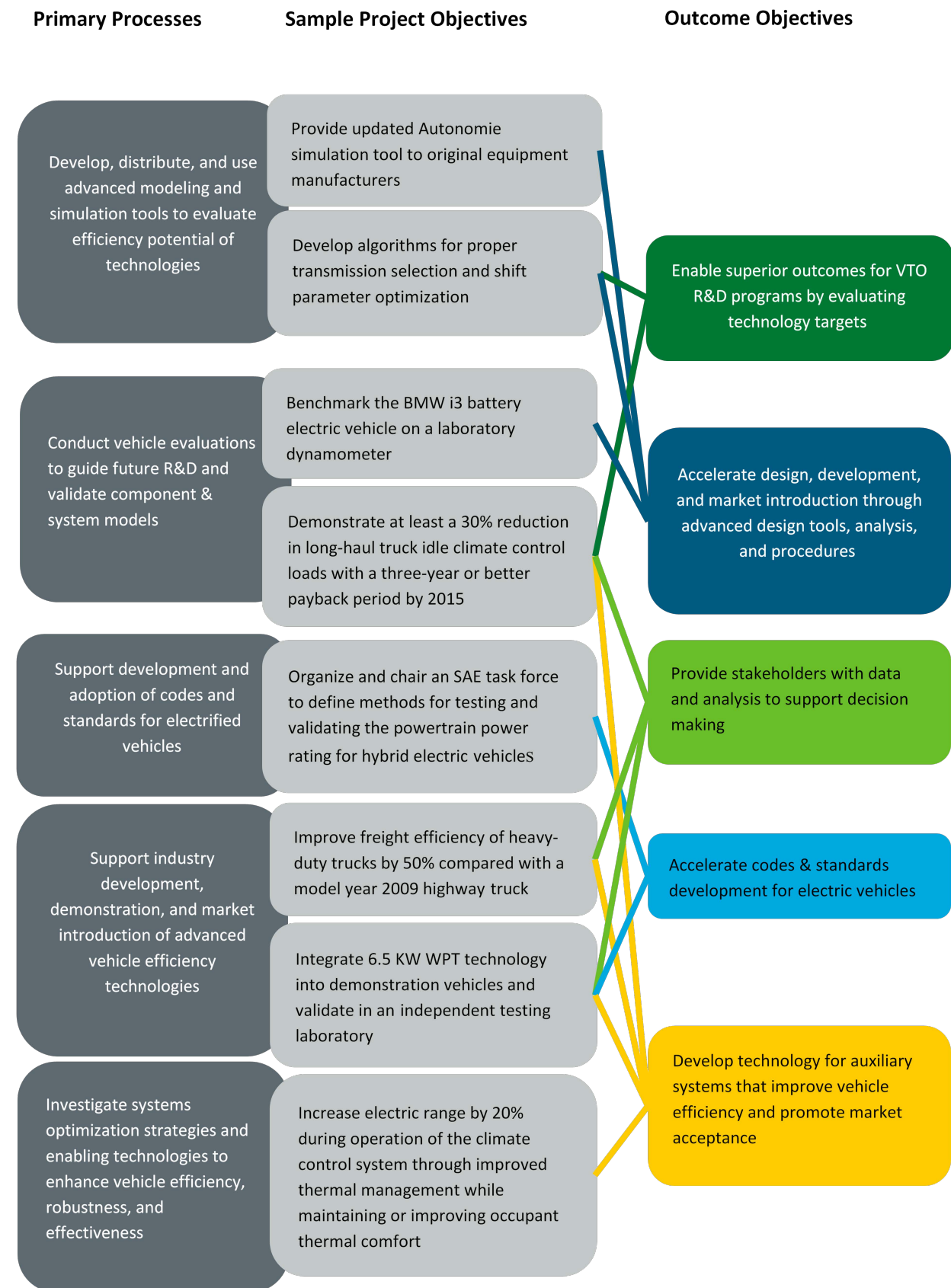


Figure I-2: VS primary processes, project objectives, and outcome objectives

I.2. Accomplishments

A snapshot of VS project highlight accomplishments for FY 2015 are provided in Table I-1. These accomplishments are intermediate steps to realizing the potential real world benefits of advanced vehicle systems technologies. As an example of end-goal real world benefits that VS is working toward, the section below describes the benefits accruing from market adoption of aero-reduction retro-fit technologies that were developed from 2001-2013 as part of VS's project on Heavy Vehicle Aerodynamic Drag.

Class 8 Aero Drag Reduction Project Real World Fuel Savings

Real world petroleum reduction benefits are accruing from commercial fleet adoption of trailer skirt and box-tail technologies developed by phase one of DOE's Project on Heavy Vehicle Aerodynamic Drag. The on-going real world benefits to the U.S. economy given below are the successful outcome of the VS sustained R&D project from 2001-2013 which was led by Dr. Kambiz Salari at Lawrence Livermore National Laboratory (LLNL) and featured collaborative technology development with component manufacturers and commercial fleet managers. A 2014 study by the North American Council for Freight Efficiency (NACFE) documented commercial fleet adoption of Class 8 trailer skirts and box-tail drag reduction devices. Rapid adoption has been accomplished in the absence of additional regulatory mandates because commercial fleet operators receive an attractive return on their investment in these fuel saving devices. Using NACFE's fleet adoption numbers we estimate the following benefits from trailer skirt and box-tail retrofits:

- The devices reduced diesel fuel consumption by U.S commercial truck fleets by 1.1 billion gallons annually in 2014 and 2015. The 1.1 billion gallon reduction of diesel consumption also reduced CO2 production by 11 million metric tons annually.
- U.S. commercial fleet adoption of the project's trailer skirt and box-tail retro-fit technologies are on-track to deliver the following cumulative real world benefits by 2030
 - 25 billion gallon reduction in diesel fuel consumption
 - 252 million metric tons reduction in CO2 production
 - \$75 billion in freight transportation fuel savings

Table I-1 FY 2015 Accomplishment Highlights

Accomplishment	Significance	R&D Organization	Links to Details
SuperTruck project team demonstrated 115% improvement in vehicle freight efficiency (12.2 mpg average).	Far exceeded the SuperTruck Project's goal to improve freight efficiency by 50%.	Daimler Trucks North America	Systems Level Technology Development and Integration for Efficient Class 8 Trucks [arravt080]
Published Plug-in Electric Vehicle and Infrastructure Analysis Report addressing driving and charging behaviors throughout the United States, and findings of five multi-year demonstrations of plug-in electric vehicles and charging infrastructure.	The report provides analysis of the largest PEV and charging infrastructure demonstrations ever conducted. The projects were active from 2010-2015. The results are used by DOE, vehicle manufacturers, researchers, policy decision makers, and charging infrastructure purchasers to site future charging infrastructure and inform policy making decisions.	Idaho National Laboratory (INL)	avt.inel.gov/summaryreport.shtml (external link)
Completed an on-road study that measures the impact of frequent fast	This is believed to be the first study to publish real-world battery degradation due to fast charging. The results contradict the previously	INL	DC Fast Charging Study

Accomplishment	Significance	R&D Organization	Links to Details
charging on battery capacity degradation in battery electric vehicles.	accepted tenet that fast charging significantly increases the rate of battery capacity degradation.		
Completed first-of-a-kind benchmark testing on the efficiency and power quality of plug-in electric vehicle charging systems.	Test results will help industry accelerate vehicle and charging equipment product development and understand potential negative impacts of vehicle/grid power quality interaction.	INL	Codes and Standards and Technical Team Activities
Completed efficiency, functionality, and cybersecurity testing of the General Electric, Eaton, Siemens, and Delta smart grid-capable EVSE.	DOE's Office of Electricity Delivery and Energy Reliability funded development of smart-grid capable EVSE. The test results were provided to DOE to support contract assurance and to the manufacturers to support product development.	INL	Wireless and Conductive Charger Evaluation and Onroad 12-V Auxiliary Load Evaluation
Performed independent testing of a wide assortment of advanced technology light-duty passenger vehicles to determine suitability for deployment, lifetime performance, and life-cycle costs of new technology components and vehicle systems.	Published test reports benefit industry, regulators, researchers, and consumers by quantifying vehicle performance, energy efficiency, battery performance degradation, maintenance and repairs, and overall cost of ownership for the vehicles. Tests provided data on parasitic thermal loads during fast charging.	Intertek, INL	Advanced Vehicle Testing Activity, Advanced Vehicle Testing & Evaluation [DE-EE0005501]
Completed testing of the first commercially available system for wirelessly charging plug-in electric vehicle batteries (Evatran's PLUGLESS system).	Test results of multiple design iterations were provided to Evatran and made available to industry to accelerate the development and commercialization of this new technology.	INL	Wireless and Conductive Charger Evaluation and Onroad 12-V Auxiliary Load Evaluation
Prototyped a novel big data analytical methodology that estimates fuel savings of 'off-cycle' technologies.	This accomplishment facilitates adoption of fuel and CO2 reduction technologies. Corporate Average Fuel Economy (CAFÉ) credits play a major role in determining the technologies that vehicle OEMs will include in LD vehicle models for the U.S. market. When it comes to emerging 'off-cycle' technologies, there is a scarcity of valid test methodologies and data that objectively demonstrate the reduced CO2 output required to claim a new credit. This scarcity is impeding the transition of emerging 'off-cycle' technologies into the commercial market. This methodology provides a way to objectively quantify the aggregate benefit of off-cycle technologies to inform claims for new earned 'off-cycle' credits.	National Renewable Energy Laboratory (NREL)	Analyzing Real-World Light-Duty Vehicle Efficiency Benefits
Completed testing of a zonal cabin heating	If driver zonal air flow with heated surfaces is implemented, we calculated that it would	NREL	Electric Drive Vehicle Climate

Accomplishment	Significance	R&D Organization	Links to Details
strategy that demonstrates potential for 28.5% drop in EV heating energy use while maintaining driver thermal comfort during warm-up.	result in a nationally weighted 7.1% improvement in EV range over the baseline heating strategy which is a 33% reduction in range penalty due to heating.		Control Load Reduction – FY 2015
Developed a thermal load reduction package to reduce climate control energy consumption by long-haul trucks during rest periods.	National-level fuel use analysis determined that 774 gallons are saved annually per truck for cooling using a battery electric air conditioning (A/C) system with advanced thermal load reduction technologies. If 20% of the long haul truck population featured the battery electric A/C and thermal load reduction package it would reduce U.S. long-haul truck consumption of diesel by 100 million gallons annually.	NREL	Long-Haul Truck Idle Climate Control Load Reduction
Vehicle chassis dynamometer testing of ten advanced technology vehicles ranging from alternative fuel vehicles to hybrid and plug-in hybrid vehicles. This year also included five battery electric vehicles.	Technology analysis with focus on heat pumps, pre-conditioning during charging, ranger extender capabilities, CAFÉ off cycle credits, and energy losses across the powertrain and other components. Analysis contrasting the PHEV operation and range of three deeply instrumented vehicles based on battery sizing and available power.	Argonne National Laboratory (ANL)	Advanced Technology Vehicle Lab Benchmarking (L1&L2)
Conducted vehicle road load investigation which showed differences between an electric-drive vehicle with a mechanically disconnected neutral gear and another vehicle that had the powertrain always connected to the wheel.	Informed improvements of setup procedures for chassis dynamometers which is the most significant input to the fuel and energy consumption testing.	ANL	Test Standards Development for EV, PHEV and HEVs
Invented several test method approaches for finding the maximum powertrain power using a wide variety of vehicle configurations. Organized and chaired by SAE Vehicle Powertrain Power Rating Standard working group.	Developed public and independent data to support the SAE Vehicle Powertrain Power Rating Standard.	ANL	Test Standards Development for EV, PHEV and HEVs
Developed and demonstrated a Common Integration Platform (CIP), a universal electronic module with embedded open source software to connect EVSE and other devices to the grid.	The CIP is an enabling technology to support grid integration studies. The studies will demonstrate it as a common interface for communication between and integrated control of grid-connected devices. The CIP uses a suite of open source software that is available to anyone. The open source software has the potential to make it easier for industry	ANL	PEV-Grid Connectivity

Accomplishment	Significance	R&D Organization	Links to Details
	to integrate grid-connected devices without having to license proprietary software. Argonne is developing open source software modules and making them available for commercial use.		
Development of the test tool for measuring electric fuel delivery of a L2 AC EVSE according to the requirements of NIST Handbook 44; for NIST Weights & Measures.	Implementation of test tools compliant with NIST measurement standards for EVSE increases the utility of VS Codes and Standards projects and helps to advance the nation's technology infrastructure because it facilitates technology characterization and improvement.	ANL	PEV-Grid Connectivity
Quantified the impact of VTO technologies on vehicle energy consumption and cost for a wide range of vehicle classes, technologies and timeframes.	Improved the outcomes of VTO component R&D activities by evaluating the energy consumption impacts of advanced technologies. Evaluations simulated performance using standard and real world driving cycles across a range of thermal conditions.	ANL	VTO Baseline and Scenario (BaSce), Evaluation of Benefits of DOE Vehicle Technology Research on Real-World Driving
Released two versions of Autonomie.	The Autonomie modeling and simulation tool accelerates the development of advanced technologies via Model Based System Engineering (MBSE). Autonomie is licensed to more than 175 companies and research organizations worldwide. It allows researchers to rigorously evaluate the impact of VTO technologies on fuel displacement and the costs of advanced vehicles.	ANL	Autonomie Maintenance and Model Based System Engineering (MBSE) Enhancements
Analyzed aerodynamics and under hood thermal characteristics of truck platooning.	The study provided new insights into under hood thermal impacts of truck platooning. A significant drop in cold mass flow rates (temperature rise) were observed in the cooling package of trailing vehicle due to a vortex (low velocity region) that impacts the cooling system performances. The study findings also validated results from a previous study by NREL showing that significant fuel savings were observed in both leading and trailing vehicles during single-lane truck platooning.	ANL	Aerodynamics and Underhood Thermal Analysis of Truck Platooning
Demonstrated 6.6kW wireless power transfer to Toyota Scion iQ EV with >85% end-to-end efficiency while meeting the electric and electromagnetic field limits. Also successfully demonstrated the wireless charging operation of the	Wireless charging of electric vehicles (EVs) has the potential to eclipse conductive chargers because of its flexibility and convenience to the customer. Use of private and secure radio communications, especially vehicle to infrastructure (V2I), and standardization means that any vehicle would be able to charge at any location. Through this project, Oak Ridge National Laboratory (ORNL) and partners developed a deep	ORNL	Wireless Charging for Electric Vehicles [M612006444]

Accomplishment	Significance	R&D Organization	Links to Details
<p>Toyota Prius Plug-in and Scion iQ EVs including the wireless communications, alignment system, charging initiation and ramping, full charging, and orderly and emergency shut down procedures.</p>	<p>understanding of wireless power transfer (WPT), real vehicle implementations, control system design and communications for closed loop regulation of power transfer, and the design improvements for higher performance and cost effectiveness.</p>		
<p>Designed and tested a hybrid Auxiliary Power Unit (h-APU) architecture that would allow for hybridization for the air conditioning, electrification of the condenser fans, and energy storage for other electrical hotel loads of MD/HD trucks. This allows for the truck to eliminate or greatly reduce all over night idling by providing hotel loads from a battery pack that uses regenerative braking for charging.</p>	<p>This architecture allows for the truck to eliminate or greatly reduce all over night idling by providing hotel loads from a battery pack that uses regenerative braking for charging. The project uses a two-part approach for developing fuel saving auxiliary load components that includes selecting the best component technology, and/or architecture, and optimized controls that are vehicle focused. The approach addresses idle reduction and optimized component strategies.</p>	<p>ORNL</p>	<p>Cummins MD&HD Accessory Hybridization CRADA</p>
<p>All of the full-season GT Le Mans (GTLM)-class cars racing with the TUDOR United Sportscar Championship (TUSC) used E85R fuel with cellulosic ethanol sourced from INEOS, a DOE grant recipient. This fuel reduced oil consumption by over 62% and provided more than 65% reduction in greenhouse gas (GHG) emissions compared to conventional racing fuels with no renewable content. The conventional racing fuel used for the comparison corresponds to the 2005 International Motor Sport Association (IMSA) baseline.</p>	<p>Motorsports are the only professional sport that can directly help attain national energy and environmental objectives relating to transportation. The rapid developmental cycles in racing, the focused development of advanced technologies and alternative fuels, and the search for more efficient and capable vehicles inherent in racing, all tie directly with our national transportation goals.</p>	<p>ORNL</p>	<p>Green Racing Technical Support</p>
<p>Designed a new heavy vehicle body shape for the Next Generation of highly aerodynamic and integrated Class 8 tractor-trailers – Generic Speed Form 1 (GSF1).</p>	<p>Tractor-trailer trucks consume roughly 11-12% of the total United States petroleum usage. The wind tunnel test data from the GSF1 design adds to the database that is used to provide guidance to industry to improve the fuel economy of class 8 tractor-trailer through the use of aerodynamics.</p>	<p>LLNL</p>	<p>DOE’s Effort to Improve Heavy Vehicle Fuel Efficiency through Improved Aerodynamics</p>

I.3. Approach and Organization of Activities

VS groups its projects into focus area activity categories that implement its primary processes (see Figure I-2). In FY 2015, these focus areas were Vehicle Modeling and Simulation (M&S), Vehicle Technology Evaluations (VTE), Codes and Standards (C&S), Industry Projects, and Vehicle Systems Efficiency Improvements (VSEI).

Projects within each focus area typically produce outputs in one or more of the following forms: data, analysis, reports, tools, specifications, and procedures. The outputs from one project are often used as the inputs for one or more projects in other focus areas. The integration of computer modeling and simulation, laboratory and field vehicle evaluations, and codes and standards development and validation for vehicle classes from LD to HD is critical to the success of the VS program. Information exchange between focus area activities enhances the effectiveness of each activity (illustrated in Figure I-3).



Figure I-3: VS activities integration – Arrows represent information flow between activity focus areas that enhances effectiveness of individual activities.

An example of beneficial data exchange is the increased accuracy of predictive simulation models for advanced technology vehicles made possible by empirical test data that characterize a vehicle’s real-world performance. (In the example case, VTE activities feed information to the M&S activity). Laboratory and field technology evaluation studies provides data that informs support of Codes and Standards. Test data from VTE activities are also used to identify requirements for new more efficient technologies and validate those technologies that are developed under VSEI.

VS provides an overarching vehicle systems perspective in support of the technology R&D activities of DOE’s VTO and Hydrogen Fuel Cells Technologies Program (HFCTP). VS uses analytical and empirical tools to model and simulate potential vehicle systems, validate component performance in a systems context, verify and benchmark emerging technologies, and validate computer models. HIL testing allows components to be controlled in an emulated vehicle environment. Laboratory testing then provides measurement of progress toward VTO technical goals and eventual validation of DOE-sponsored technologies at ANL’s Advanced Powertrain Research Facility (APRF) for light- and medium-duty vehicles and at NREL’s Renewable Fuels and Lubricants (ReFUEL) facility for HD vehicles. For this program to be successful, extensive collaboration with the technology development activities within the VTO and HFCTP is required for both analysis and

testing. Analytical results of this sub-program are used to estimate national benefits and/or impacts of DOE-sponsored technology development (illustrated in Figure I-4).

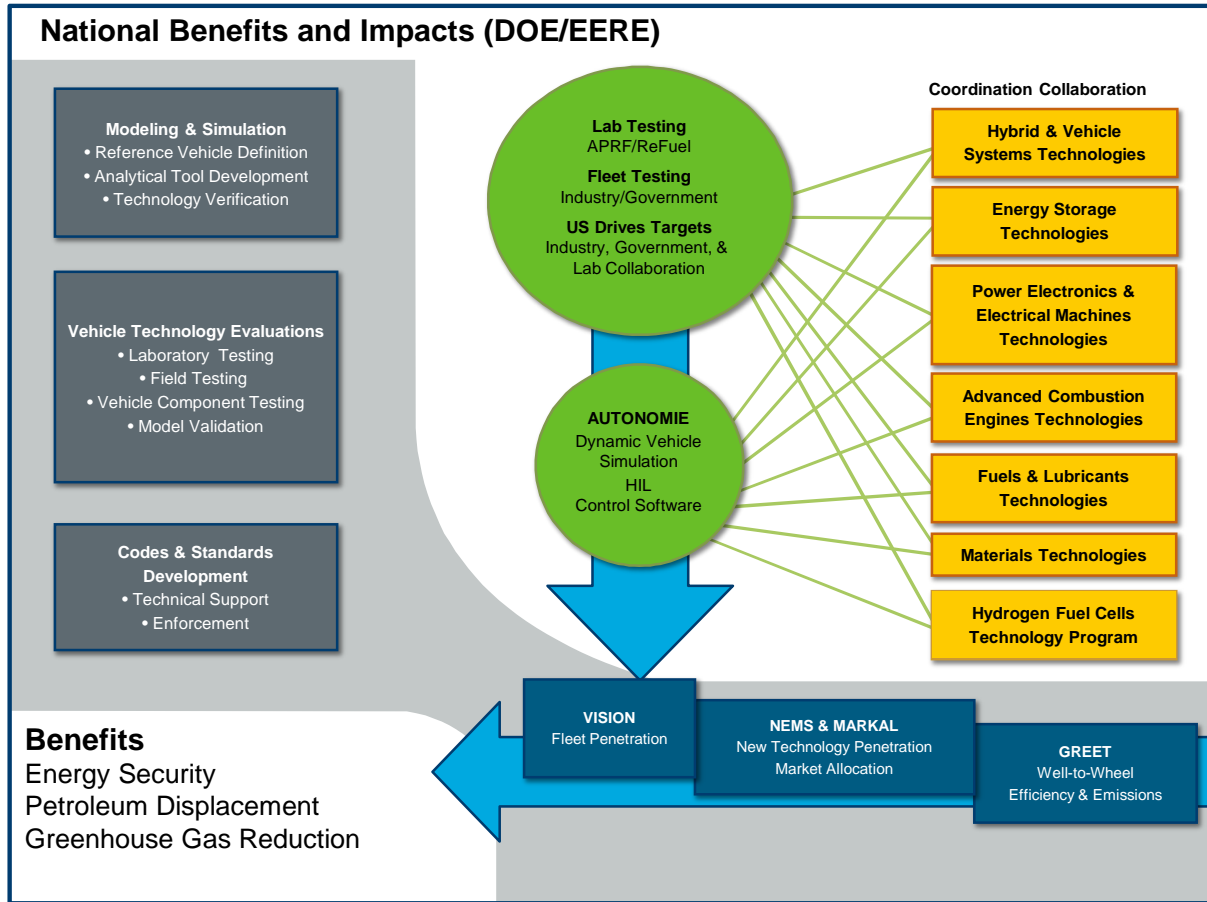


Figure I-4: VS activities providing estimates of national benefits and impacts of advanced technologies.

VS R&D activities are performed by the national laboratories and industry. National laboratory R&D activities are organized into the four focus areas. A brief description of each focus area and its major accomplishments for FY 2015 are outlined below.

Modeling and Simulation

DOE has developed and maintains software tools that support VTO research. VISION, NEMS, MARKAL, and GREET are used to forecast national-level energy, environmental, and economic parameters, including oil use, market impacts, and GHG contributions of new technologies. These forecasts are based on VTO vehicle-level simulations that predict fuel economy and emissions using VS’s Autonomie modeling tool. Autonomie’s simulation capabilities allow for accelerated development and introduction of advanced technologies through computer modeling rather than through expensive and time-consuming hardware building. Modeling and laboratory and field testing are closely coordinated to enhance and validate models as well as ensure that laboratory and field test procedures and protocols comprehend the needs of new technologies that may eventually be commercialized.

Autonomie is a MATLAB-based software environment and framework for automotive control system design, simulation, and analysis. This platform enables dynamic analysis of vehicle performance and efficiency to support detailed design, hardware development, and validation. Autonomie was developed under a CRADA with General Motors and included substantial input from other OEMs, and replaces its predecessor, the Powertrain Systems Analysis Toolkit (PSAT). One of the primary benefits of Autonomie is its plug-and-play foundation, which allows integration of models of various degrees of fidelity and abstraction from multiple

engineering software environments. This single powerful tool can be used throughout all the phases of model-based design of the vehicle development process (VDP).

HIL simulation provides a novel and cost-effective approach to isolate and evaluate advanced automotive component and subsystem technologies while maintaining the rest of the system as a control. HIL allows actual hardware components to be tested in the laboratory at a full vehicle level without the extensive cost and lead time of building a complete prototype vehicle. This approach integrates modeling and simulation with hardware in the laboratory to develop and evaluate propulsion subsystems in a full vehicle-level context. The propulsion system hardware components—batteries, inverters, electric motors, and controllers—are further validated in simulated vehicle environments to ensure that they meet the vehicle performance targets established by the government–industry technical teams.

Vehicle Technology Evaluations

This section describes the activities related to laboratory validation and fleet testing of advanced propulsion subsystem technologies and advanced vehicles. In laboratory benchmarking, the objective is to extensively test production vehicle and component technology to ensure that VTO-developed technologies represent significant advances over technologies that have been developed by industry. Technology validation involves the testing of DOE-developed components or subsystems to evaluate the technology in the proper systems context. Validation helps to guide future VTO research and facilitates the setting of performance targets.

The facilities that perform laboratory and field testing activities include the APRF, INL’s transportation testing facilities, NREL’s ReFUEL and thermal test facilities, and ORNL’s Vehicle Systems Integration (VSI) laboratory.

The APRF is equipped with dynamometers (for testing integrated components such as engines, electric motors, and powertrains), and a thermal chamber (for testing battery electric vehicles, hybrid electric vehicles, and plug-in hybrids in temperatures from as low as 20°F to as high as 95°F).

INL’s transportation testing facilities encompass the Advanced Vehicle Test and Evaluation Activity (AVTE) facility for LD vehicles, the Heavy Duty Transportation Test Facility, and the Energy Storage Technologies Laboratory. AVTE’s capability to securely collect, analyze, and disseminate data from multiple field tests located throughout the United States is critical to VS laboratory and field activities.

NREL’s ReFUEL facility is equipped with dynamometers for testing medium-duty vehicles and components. NREL’s thermal test facilities have capabilities for LD vehicle cabin thermal studies and outdoor HD vehicle cabin studies. NREL also has facilities for testing subsystems (such as energy storage systems and EVSE) and functions as the VS data collection and evaluation hub for medium-duty and HD vehicle fleet tests.

ORNL’s facilities for integrated testing include advanced engine technologies (e.g., advanced combustion modes, fuels, thermal energy recovery, and emissions after-treatment), advanced power electronics and electric machines (e.g., motor drives, components, power electronics devices, and advanced converter topologies), and vehicle testing and evaluation (e.g., chassis and component dynamometers, integrated powertrain stands, test track evaluations, and field operational testing).

The AVTE, working with industry partners, conducts field and fleet testing to accurately measure real-world performance of advanced technology vehicles via a testing regime based on test procedures developed with input from industry and other stakeholders. The performance and capabilities of advanced technologies are benchmarked to support the development of industry and DOE technology targets. The testing results provide data for validating component, subsystem, and vehicle simulation models and hardware-in-the-loop testing. Fleet managers and the public use the test results for advanced technology vehicle acquisition decisions. INL conducts LD testing activities. In FY 2015, INL continued its partnership with an industry group led by Intertek. Accelerated reliability testing provides reliable benchmark data of the fuel economy, operations and maintenance requirements, general vehicle performance, engine and component (such as energy storage system) life, and life cycle costs. These tests are described below.

Baseline Performance Testing

The objective of baseline performance testing is to provide a highly accurate snapshot of a vehicle's performance in a controlled testing environment. The testing is designed to be highly repeatable. Hence it is conducted on closed tracks and dynamometers, providing comparative testing results that allow “apples-to-apples” comparisons within respective vehicle technology classes. The APRF at ANL is used for the dynamometer testing of the vehicles.

Fleet Testing

Fleet testing provides a real-world balance to highly controlled baseline performance testing. Some fleet managers prefer fleet testing results to the more controlled baseline performance or the accelerated reliability testing.

During fleet testing, a vehicle or group of vehicles is operated in normal fleet (field) applications. Operating parameters such as fuel use, operations and maintenance, costs/expenses, and all vehicle problems are documented. Fleet testing usually lasts one to three years and, depending on the vehicle and energy storage technology, between 5,000 and 12,000 miles are accumulated on each vehicle.

For some vehicle technologies, fleet testing may be the only viable test method. Neighborhood electric vehicles are a good example. Their manufacturer-recommended charging practices often require up to 10 hours per charge cycle, while they operate at low speeds (<26 mph). This makes it impractical to perform accelerated reliability testing on such vehicles.

Accelerated Reliability Testing

The objective of accelerated reliability testing is to quickly accumulate several years or an entire vehicle-life's worth of mileage on each test vehicle. The tests are generally conducted on public roads and highways, and testing usually lasts for up to 36 months per vehicle. The miles to be accumulated and time required depend heavily on the vehicle technology being tested. For instance, the accelerated reliability testing goal for plug-in hybrid electric vehicles and battery electric vehicles is to accumulate 12,000 miles per vehicle in one year, while the testing goal for hybrid electric vehicles is to accumulate 160,000 miles per vehicle within three years. This is several times greater than most hybrids will be driven in three years, but it is required to provide meaningful vehicle-life data within a useful time frame. Generally, two vehicles of each model are tested to ensure accuracy. Ideally, a larger sample size would be tested, but funding tradeoffs necessitate testing only two of each model.

Depending on the vehicle technology, a vehicle report is completed for each vehicle model for both fleet and accelerated reliability testing. However, because of the significant volume of data collected for hybrid electric vehicles, the test results are published in the form of summary fleet testing fact sheets (including accelerated reliability testing) and maintenance sheets.

Codes and Standards Development

A comprehensive and consistent set of codes and standards addressing grid-connected vehicles and infrastructure is essential for the successful market introduction of electric drive vehicles. The VTO is active in driving the development of these standards through committee involvement and technical support by the national laboratories. Codes and Standards work performed by the National Laboratories emphasized grid modernization during FY 2015. These activities also supported the U.S. DRIVE's Grid Interaction Tech Team (GITT), a government/industry partnership aimed at ensuring a smooth transition for vehicle electrification by closing technology gaps that exist in connecting vehicles to the electric grid.

The consumer markets for electric vehicles transcend national boundaries. ANL was employed in international cooperative initiatives to adopt international electric drive vehicle standards and promote market penetration of grid-connected vehicles. Many new technologies require adaptations and more careful attention to specific procedures. ANL supported development of interoperability validation procedures and operated the SmartGrid Joint Interoperability Center as the U.S. base for international cooperative work between the European Union and U.S. energy R&D laboratories.

Vehicle Systems Efficiency Improvements

This focus area involves R&D on a variety of mechanisms to improve the energy efficiency of LD, medium-duty, and HD vehicles. Projects in this focus area involve reducing the aerodynamic drag of vehicles, thermal management approaches to increase the engine thermal efficiency and reduce parasitic energy losses, the development of advanced technologies to improve the fuel efficiency of critical engine and driveline components by characterizing the fundamental friction and wear mechanisms, and fast and wireless charging technology development.

Aerodynamic Drag Reduction

The primary goal of this focus area is improving the freight efficiency of vehicles. Aerodynamic drag reduction, thermal management, and friction and wear are the main focuses of this area. Reduction of aerodynamic drag in Class 8 tractor-trailers can result in a significant improvement on fuel economy while satisfying regulatory and industry operational constraints. An important part of this effort is to expand and coordinate industry collaborations with DOE. Industry collaboration CRADAs establish buy-in through and accelerate the introduction of proven aerodynamic drag reduction devices into new vehicle offerings.

The project's approach seeks to reduce drag through design features that control the flow of air around the vehicle. These 'flow field control' design features include geometry modifications, integration, and flow conditioning. Phase 1 of this project focused on development and design of retrofit devices from 2001-2013. Phase 2 of this project began in 2014 and focuses on developing and designing the next generation of aerodynamically integrated tractor-trailers.

Thermal Management

Thermal management of vehicle engines and support systems is a technology area that addresses reduction in energy usage through improvements in engine thermal efficiency and reductions in parasitic energy uses and losses. Fuel consumption is directly related to the thermal efficiency of engines and support systems. New methods to reduce heat-related losses are investigated and developed under this program.

FY 2015 thermal management R&D focused on exploring:

- The possibilities of repositioning the Class 8 tractor radiator and modifying the frontal area of the tractor to reduce aerodynamic drag
- The possibilities of using evaporative cooling under extreme conditions of temperature and engine load
- Engine coolant subcooled boiling heat transfer phenomena in heavy-duty vehicles
- Small channel coolant boiling for thermal control for power electronics
- Underhood thermal analysis of truck platooning

Friction and Wear

Parasitic engine and driveline energy losses arising from boundary friction and viscous losses consume 10% to 15% of fuel used in transportation. Thus engines and driveline components are being redesigned to incorporate low-friction technologies to increase fuel efficiency of passenger and HD vehicles. Research to improve the fuel efficiency and reliability of critical engine and driveline components included:

- Developing a web-based tool kit based on friction mean effective pressure (FMEP) maps to predict the impact of key tribological engine parameters on vehicle fuel economy.

On the highway, heavy trucks spend 32% of their usable propulsion energy to overcome rolling resistance. Research to improve the fuel efficiency by reducing rolling resistance of heavy trucks included:

- Goodyear Tire and Rubber Company's project to develop a system for automatically maintaining pressure in a commercial truck tire

- PPG Industries, Inc. and Bridgestone Americas Tire Operations project to develop a novel surface-modified silica technology and demonstrate 4-6% improved fuel efficiency.

Fast and Wireless Charging

Electrification of the transportation sector will be enabled by adoption of vehicle charging technologies that minimize costs in terms of time and money while maximizing energy throughput, battery life, safety, and convenience.

Industry Awards

Industry projects for FY 2015 include the categories of transportation electrification, SuperTruck, wireless charging, zero-emissions cargo transport (ZECT), and energy load reduction and management. In FY 2015, the following new projects were added to the VS portfolio:

- Connected and Autonomous Vehicle Systems Project awarded under VTO Incubator [DE-FOA-1213, Awardee: University of Michigan]
- Medium and Heavy Duty Vehicle Powertrain Electrification and Dual Fuel Fleet Demonstration [DE-FOA-1349, Selection notification April 2016]

The new technology development and demonstration projects listed above were awarded through DOE's competitive solicitation process and involve resource matching by DOE and industry.

This report describes major projects conducted by the national laboratories and industry partners in support of these areas in FY 2015. The reports describe the approaches, accomplishments and future directions for the projects. For further information on an individual project, please contact the DOE project leader.

I.4. Future Directions for VS

Near-term solutions for reducing the nation's dependence on imported oil, such as plug-in hybrid electric vehicles, will require the development, integration, and control of vehicle components, subsystems, and support systems. These solutions will require exploration of high-capacity energy storage and propulsion system combinations to get the most out of hybrid propulsion. Analysis and testing procedures at the national laboratories will be enhanced to study these advanced powertrains with simulation tools, component/subsystem integration, and hardware-in-the-loop testing. DOE-sponsored hardware developments will be validated at the vehicle level, using a combination of testing and simulation procedures.

In FY 2016, the VS will continue activities in the area of vehicle M&S and vehicle technology evaluations, including further baseline performance testing of conversion and OEM electric drive vehicles. Field and laboratory testing will continue to be integrated with M&S activities, including validation of simulation models for advanced vehicles tested in the APRF. Fleet evaluation of plug-in vehicles will continue, with continued emphasis on evaluation fleets of OEM production vehicles.

In addition to the hybrid electric vehicle and plug-in hybrid electric vehicle activities, a full range of simulation and evaluation activities will be conducted on battery electric vehicles as they are brought to market by OEMs. Because electric vehicles are dependent on a robust charging infrastructure for their operation and ultimate consumer acceptance, VS will continue efforts to address issues related to electric vehicle codes and standards, charging infrastructure, and vehicle/grid integration.

VS will pursue the objective of using less energy for cabin climate control of LD and HD vehicles. This work will contribute to progress on reaching the DOE EV Everywhere Grand Challenge Blueprint's Efficient Climate Control Technologies Objective and the VS target objective to increase freight efficiency of HD vehicles by 50% through system-level innovations.

In support of the EV Everywhere Initiative, VS will continue to develop objective information for stakeholders to help them increase their readiness for EVs and pave the way to electrified transportation. These efforts include supporting an online hub for electric vehicles information designed to allow visitors to search according to topic of interest and stakeholder type including: states and municipalities, employers, fleets, electrical contractors and inspectors, and utilities. VS will develop data and analysis that quantify technology performance issues, real world drive cycles, petroleum displacement, and GHG reduction benefits of EVs.

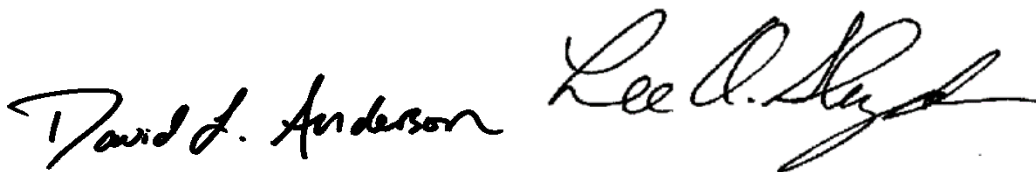
VS will fund grid modernization projects at several National Laboratories to address VTO program specific activities. VS will also analyze the impact of concentrations of electric drive vehicles on the electricity grid.

Vehicle systems efficiency improvement work in the areas of aerodynamics, thermal management, grid integration, transportation electrification, and friction & wear will continue. The focus of these activities will revolve around cooperative projects with industry partners with the goal of bringing developed technologies to market quickly.

VS plans to award the following new projects during FY16:

- Grid Modernization VTO Program Specific Activities (to be performed by awardees at DOE National Laboratories).
- SuperTruck 2

Inquiries regarding the VS activities may be directed to the undersigned.



David L. Anderson and Lee Slezak
Technology Managers

II. Industry Awards

ADVANCED VEHICLE TESTING & EVALUATION (AVTE)

II.1. Advanced Vehicle Testing & Evaluation [DE-EE0005501]

Richard Jacobson, Principal Investigator

Intertek Testing Services NA, Inc.
430 S. 2nd Avenue
Phoenix, AZ 85003
Phone: (480) 525-5871
E-mail: richard.jacobson@intertek.com

Lee Slezak, DOE Program Manager

U.S. Department of Energy
Phone: (208) 586-2335
E-mail: lee.slezak@ee.doe.gov

Start Date: October 1, 2011
End Date: September 30, 2018

II.1.A. Abstract

Objectives

- Test and evaluate advanced vehicle technologies that reduce petroleum consumption.
- Produce lifecycle cost data for vehicles that are utilizing these advanced technologies.
- Provide fleet operations data to the Idaho National Laboratory (INL) database in order to disseminate the results of vehicle and infrastructure testing & analysis.
- Provide benchmark data for advanced technology vehicles and their associated fueling infrastructure.

Accomplishments

- Acquired 27 advanced technology vehicles during FY2015 for a total of 95 vehicles tested throughout the year.
- Completed baseline testing information on 33 vehicles consisting of 9 vehicle models.
- A total of 49 vehicle component durability tests were completed on 45 different vehicles.
- One vehicle met its final mileage target and completed end of life testing.
- The new Intertek California test location added the capability to acquire advanced technology vehicles that are only available in California.
- Updated advanced technology vehicle mileage targets and component testing intervals for all vehicles.
- Continued collaboration between Intertek and Department of Energy (DOE) National Laboratories in baseline vehicle and interim component durability report creation.
- Level 2 AC Interoperability testing between Original Equipment Manufacturers (OEMs) and Electric Vehicle Supply Equipment (EVSE) completed.

Future Achievements

- Collaborate with INL and the National Renewable Energy Laboratory (NREL) to engage original equipment manufacturers in future AVTE vehicle testing.
- Continue acquisition and rapid mileage accumulation of vehicles for testing based on their advanced technologies and market availability.
- Accelerated reliability testing of a Toyota Mirai fuel cell vehicle.
- Implement a Storage-Assisted Recharging (StAR) unit at a fleet test location to facilitate opportunity charging of AVTE fast charge capable vehicles.
- Conduct DC Fast Charging Interoperability testing between OEM vehicles and fast charge units utilizing the CHAdeMO and SAE Combined Charging System (CCS) standards.
- Additional heavy-duty truck platooning testing with NREL utilizing optimized aero designs from Lawrence Livermore Laboratory.



II.1.B. Technical Discussion

Background

The Advanced Vehicle Testing & Evaluation (AVTE) project incorporates the conduct of advanced technology vehicle and infrastructure testing in DOE's Advanced Vehicle Testing Activity (AVTA). The AVTA is the only activity tasked by DOE to conduct field evaluations of vehicle technologies that use advanced technology systems and subsystems in vehicles to reduce petroleum consumption. The results are available through publically available reports published on the AVTA website at avt.inel.gov/. The website provides insight into advanced vehicle technology long-term performance, durability, maintenance and life-cycle costs that cannot be found through media outlets. The site is a resource for the public to gain knowledge on advanced technology vehicle progress and innovation.

INL has responsibility for the technical direction of the overall project, along with data collection, analysis, and test reporting of light-duty vehicles in coordination with Intertek Testing Services NA, Inc. (Intertek). Medium and heavy-duty truck data collection, analysis, and test reporting is coordinated between Intertek and NREL. The AVTA is contractually administered by DOE's National Energy Technology Laboratory. All of DOE's Laboratories participating in the AVTA coordinate with Intertek in order to determine project scope and direction within the AVTE for dynamometer testing as well as other component testing activities.

The objective of the AVTE project is to conduct unbiased laboratory and field evaluations of advanced technology vehicles and their associated fueling infrastructures, and the development of new test procedures and/or modifications of existing test procedures necessary to accomplish these performance evaluations. The scope of the work included baseline performance, accelerated reliability, and fleet testing of state-of-the-art light-, medium-, and heavy-duty advanced technology vehicles and the required vehicle-to-infrastructure interface required for fueling/charging vehicles.

Introduction

The AVTE project focuses on testing and evaluating commercially-available, early production, and pre-production light-, medium-, and heavy-duty advanced technology vehicles using internal combustion engine powertrains burning advanced fuels (such as hydrogen and compressed natural gas (CNG) fuels); and electric (EV), extended range electric (EREV), hybrid electric (HEV), plug-in hybrid electric (PHEV), or fuel cell (FCV) vehicle propulsion technologies. Components and subsystems such as advanced energy storage technologies (such as batteries, ultra-capacitors, and hydrogen storage tanks), advanced drivetrains, and the necessary infrastructure required to fuel and/or charge (EV, PHEV) advanced technology vehicles are candidates for testing. This includes the interaction between infrastructure, vehicles, and the electric grid. The

evaluation data collected through the AVTE project are used to validate the results of research, modeling, and simulation activities using laboratory and field benchmarking results.

Approach

The AVTE project is managed into separate tasks to accomplish testing of advanced technology vehicles and their respective infrastructure. The tasks are as follows:

Project Management

This task includes the activities necessary to provide management of AVTE activities, including budget and schedule control, fleet coordination, procurement, status reporting, presentations of activity results and status to DOE and industry, preparation of the Project Management Plan, and quarterly updates of the Project Management Plan. Work under this task also includes management of test results reports and/or data sheets for each task.

Vehicle Specification and Test Procedure Development

Specifications for vehicles, components and infrastructure are prepared to define specific design and performance requirements. Test procedures are developed that will evaluate requirements stated in the specification.

New testing procedures incorporate industry standard test procedures as applicable. Vehicle tests typically include on-track testing of performance and operating characteristics as well as DOE Laboratory chassis dynamometer testing. Special tests for components and infrastructure are developed along with test facilities uniquely to validate specification requirements.

Existing procedures for accelerated and fleet testing are revised, as necessary, to include the unique aspects of each class of the anticipated subject vehicles and to keep them current with new industry standards and requirements. Procedures incorporate mission-based requirements (i.e., simulating actual fleet operating practices). Data collection techniques are developed to measure and record the data necessary to provide the information required for each class of vehicle.

Baseline Performance Testing

Baseline performance testing includes, but is not limited to, testing of acceleration, maximum speed at fixed distances, gradeability, braking distance, time to recharge, charging efficiency (for grid-connected vehicles), energy storage capacity, and fuel efficiency during closed track and dynamometer testing that includes several test cycles, and various operating modes and ambient conditions. Baseline performance test procedures are in place for all of these testing regimes and additional procedures are developed, as required, for vehicles with unique operational characteristics.

Baseline track testing is normally performed at a limited access test track in the greater Phoenix area, which allows year round testing. Light-duty vehicle chassis dynamometer testing is conducted at Argonne National Laboratory (ANL). Dynamometer testing of vehicle technologies with unique operational characteristics (transit, agricultural, military, etc.) is provided as required. As part of baseline testing, Beginning-of-Test battery testing is performed on all vehicles with traction battery energy storage. Vehicles will be purchased, leased, or rented unless provided by DOE or vehicle manufacturers. All vehicles are insured, operated, and maintained in accordance with manufacturer's recommendations.

Accelerated Vehicle Testing

During accelerated testing, at least one vehicle is tested under supervised and semi-controlled conditions in order to evaluate one or more characteristics of the vehicle's performance or operational characteristics, in an accelerated time frame, while evaluating vehicle reliability, maintenance requirements, long-term performance, energy efficiency, and lifecycle costs. Vehicles are placed in accelerated testing when the vehicle is unlikely or too expensive to operate in a long-term fleet application due to technical and manufacturing robustness. This can also include vehicle testing that requires special data collection or operating conditions.

The accelerated testing duration is based the testing objectives for the particular subject vehicle. Testing typically achieves 6,000 miles on a subject vehicle, but may reach higher mileage as documented in the Project Management Plan. Vehicles are purchased, leased, or rented unless provided by another program. All vehicles are insured, operated and maintained in accordance with manufacturer's recommendations. Fueling infrastructure is provided, as required, to conduct testing and evaluation.

Fleet Testing

Fleet testing includes high-mileage testing of two to four production vehicles of the same make and model in an operating fleet to determine vehicle reliability, maintenance requirements, long-term performance, life-cycle costs, and user acceptance. Vehicles are driven on-road to achieve a target mileage suitable for the advanced technology that is being studied during a three year minimum exposure to fleet operations. HEV and ICE vehicles are targeted to achieve 195,000 miles in fleet testing. PHEVs are targeted to achieve 160,000 miles in fleet testing due to the requirement to start daily operations in charge-depleting mode. BEVs are targeted to achieve 36,000 miles in fleet testing due to the limited range achievable per charge. Vehicles are purchased, leased, or rented unless provided by another organization. All vehicles are insured and maintained in accordance with manufacturer's recommendations. Fueling infrastructure is provided, as required, to conduct testing and evaluation.

Data collection systems necessary to collect operating data as required per test procedures are installed on all fleet vehicles. Repair and maintenance costs are collected manually. The fleet operator maintains logs of fuel dispensed (including electricity on plug-in electric vehicles) and mileage. Operating data, repair and maintenance costs are maintained current on a monthly basis. Quality checks and trend analysis are performed to ensure that the data are accurate and that the vehicles are performing properly.

Interim Component Testing

This task includes testing of vehicle components during accelerated or fleet testing. Interim component durability (ICD) tests for traction-battery equipped vehicles are capacity and performance related between baseline and end-of-testing. For vehicles utilizing CNG as a fuel, compression testing is conducted to verify the engine performance over the life of the vehicle. Other advanced vehicle technology component testing specifications and procedures are developed as other technologies and components are tested. Raw data from the testing is provided to the AVTA at the INL for analysis and verification.

End-of-Test Vehicle and Component Testing

This task consists of vehicle and component testing at the completion of fleet or accelerated testing including, but not limited to, vehicle performance, mechanical components, batteries, and other energy storage devices. Tests are performed as required by the Project Management Plan and are conducted in accordance with procedures developed under Test Procedure Development. Raw data from the testing is provided to the AVTA at the INL for analysis and verification.

Infrastructure Test and Evaluation

This task consists of testing vehicle and infrastructure interfaces, operations, and reliability. For grid-connected electric-drive vehicles, the testing includes charger efficiency, vehicle-to-grid communication, and bi-directional power flow (if applicable). The evaluation collects data on the installation, operation, energy, and maintenance costs of the infrastructure and track user feedback related to the overall interface and operations of the infrastructure. Deliverables include test result data sheets and a report on the cost, safety, operations, maintenance, and reliability of the infrastructure.

Additional Procedure Development, Testing or Test Support

This task consists of various additional procedure developments, testing, and test support activities that may be determined necessary. The activities are detailed in the Project Management Plan, and the work is reviewed and approved by DOE.

Results

Vehicle Testing

Vehicles under test during the fiscal year are summarized in Table II-1. A total of 95 vehicles were tested during FY2015, which accumulated an estimated 2,923,988 miles. Due to the timing of this report, the final vehicle mileage for September 2015 was estimated based on previous monthly average mileage. There were 4 Chevrolet Impala CNG Bi-Fuel vehicles acquired late in the fiscal year that were undergoing the addition of data loggers prior to fleet testing and they are not included in the total.

Table II-1: AVTE Vehicles Tested During FY2015

Qty	Year	Make	Model	Type	Vehicle Testing Focus	Estimated Mileage
1	2011	Nissan	Leaf	BEV	Energy Storage System (ESS)	2,778
2	2011	Chevrolet	Volt	PHEV	ESS	66,408
4	2013	Volkswagen	Jetta TDI	ICE	12 V Acc. Loads	215,102
4	2012	Honda	Civic CNG	ICE	Compression Testing	131,320
4	2013	Chevrolet	Malibu ECO	HEV	ESS / 12 V Acc. Loads	180,742
4	2013	Chevrolet	Volt	PHEV	ESS	173,333
4	2013	Honda	Civic Hybrid	HEV	ESS	265,993
4	2013	Toyota	Prius Plug-In	PHEV	ESS	251,136
4	2013	Volkswagen	Jetta Hybrid	HEV	ESS	228,762
2	2012	Mitsubishi	i-MiEV	BEV	ESS	11,347
4	2013	Nissan	Leaf	BEV	ESS	33,364
4	2013	Ford	C-Max Energi	PHEV	ESS	170,821
4	2013	Ford	C-Max Hybrid	HEV	ESS	260,504
4	2013	Ford	Fusion Energi	PHEV	ESS	234,607
4	2013	Ford	Focus Electric	BEV	ESS	36,944
1	2013	Ram	1500 w/ Start/Stop	ICE	CNG/Gas Fuel Efficiency	19,407
4	2014	Smart	ED	BEV	ESS	27,163
4	2014	Mazda	Mazda3 i-ELOOP	ICE	Capacitor	169,915
4	2014	Chevrolet	Cruze Turbo Diesel	ICE	12 V Acc. Loads	144,416
4	2014	BMW	i3 Range Extender	PHEV	ESS	53,556
4	2014	BMW	i3	BEV	ESS	34,158
4	2015	Kia	Soul	BEV	ESS	34,485
4	2015	Chevrolet	Spark EV	BEV	ESS	21,826
4	2015	Honda	Accord Hybrid	HEV	ESS	129,829

Qty	Year	Make	Model	Type	Vehicle Testing Focus	Estimated Mileage
4	2015	Volkswagen	e-Golf	BEV	ESS	16,964
1	2014	Tesla	Model S 85	BEV	Track Performance Only	904
4	2015	Mercedes	B-Class Electric	BEV	ESS	8,215
95	TOTAL	TESTED	VEHICLES		FY2015 ESTIMATED MILES:	2,923,998

There were three vehicles remaining that were transferred from a previous test project (DE-FC26-05NT42486) to AVTE on March 22, 2013 to continue mileage accumulation and component testing. A 2011 Nissan Leaf (0178) continued with mileage accumulation until it reached 36,000 miles. The vehicle achieved its mileage target, but the indicated high voltage battery capacity was below the Nissan manufacturer warranty specifications. The high voltage battery was replaced in the vehicle and it will be utilized for another AVTA project. The remaining vehicles, consisting of two 2011 Chevrolet Volts, continue to accumulate mileage and perform component testing to reach their goal of 160,000 miles each.

Prior to the start of FY2015, there were 67 vehicles operating and accumulating whole-vehicle test data and advanced component testing data. New vehicles for FY2015 were vetted with DOE and the project management plan was updated. These vehicles include the remaining three 2014 BMW i3 Range Extender vehicles (PHEV), four 2014 BMW i3 EVs (BEV), four 2015 Kia Soul EVs (BEV), four 2015 Chevrolet Spark EVs (BEV), four 2015 Honda Accord Hybrids (HEV), four 2015 Volkswagen e-Golfs (BEV), four 2015 Mercedes B-Class Electrics (BEV), and four 2015 Chevrolet Impala Bi-Fuels (ICE). A large selection of these vehicles is pictured in Figure II-1.



Figure II-1: AVTE fleet vehicles at Intertek for DOE review in February 2015
Intertek

The 2014 BMW i3 with Range Extender is a BEV with a 1.9 gallon fuel tank for the range-extending two-cylinder engine. While this vehicle is classified as a PHEV by the EPA, for component testing, the high voltage battery will be tested at mileage intervals for BEVs. The 2014 BMW i3 EV is the same architecture as the Range Extender but it also includes the SAE Combined Charging System (CCS) for fast charging. The 2015 Kia Soul EV is unique for the inclusion of CHAdeMO fast charging, which is the first non-Japan based manufacturer to utilize the CHAdeMO standard. The 2015 Chevrolet Spark EV utilizes the SAE CCS fast charging system. The 2015 Honda Accord Hybrid is a replacement to the planned 2014 Honda Accord PHEV. The Accord PHEV had been confirmed as no longer available for sale. With the same dual-motor propulsion technology being available in the 2015 Honda Accord Hybrid with a different battery pack size, the Hybrid models were acquired in place of the PHEV. Of the four Volkswagen e-Golfs, two include a heat pump for more efficient heating, while the remaining two are base models without the heat pump. Of the four Mercedes B-Class Electrics, two include an adjustable regenerative braking feature and can also vary their regenerative

braking automatically with cruise control engaged. The remaining two Mercedes B-Class Electrics are base models without the adjustable regenerative braking. The four Chevrolet Impala Bi-Fuels were acquired near the end of FY2015 and are beginning the process of adding data loggers to the vehicles.

A 2013 Ram 1500 with stop-start capability conducted accelerated reliability testing after being converted to operate on both gasoline and CNG. A set route was utilized to accumulate mileage in CNG-only and gasoline-only modes on certain days of operation. The stop-start capability was also varied to study the effects of this fuel saving feature. The vehicle completed its testing and has been removed from the fleet.

A 2014 Tesla Model S 85 kWh vehicle was rented to obtain baseline data. Over a period of two weeks, the vehicle was outfitted with a pre-programmed data logger and tested to the baseline testing protocol for BEVs to obtain performance and charge-depleting range information. ESS testing was not conducted on this vehicle. The Tesla Model S 85 is pictured in Figure II-2.



Figure II-2: 2014 Tesla Model S 85 that underwent baseline testing

Intertek

An additional 27 advanced technology vehicles were acquired for testing during FY2015. Of the vehicles acquired and under test in FY2015, 33 vehicles completed baseline testing consisting of 9 different models. A total of 49 vehicle component durability tests were completed on 44 different vehicles in FY2015. At the end of FY2015, 89 vehicles were in fleet operation. The remaining vehicles that did not continue from the 95 vehicles that were tested include the accelerated reliability 2013 Ram 1500, a rented Tesla Model S 85, a 2011 Nissan Leaf BEV. The 2011 Nissan Leaf BEV had reached its target of 36,000 miles and completed final component testing. A 2013 Ford C-Max Energi, a 2014 Mazda Mazda3 i-ELOOP, and a 2013 Honda Civic Hybrid were totaled in accidents during fleet testing. The testing of four similar make and model vehicles not only provides greater statistical accuracy to the testing results but also ensures that advanced vehicle technologies can be evaluated at their final target mileage.

Vehicle Testing Intervals

After discussion with DOE during FY2015, it was agreed that the vehicle mileage targets should be updated to reflect actual mileage accumulation that was observed during current fleet testing. With a minimum of three years of fleet testing for each vehicle and a minimum mileage target, the fleet and interim component durability testing will have historical AVTA test results for comparison. The adjusted mileage targets also require adjustment to the component testing mileage intervals. The adjusted mileage target for ICE vehicles and HEVs is a minimum of three years and 195,000 miles of fleet testing. For PHEVs, the minimum is three years and 160,000 miles of fleet testing. For BEVs, the minimum is three years and 36,000 miles of fleet testing.

Component testing for each vehicle adjusts based on the new mileage targets. For ICE vehicles and HEVs, the baseline testing occurs at approximately 4,000 miles, and then ICD testing occurs at approximately 50,000, 105,000, and 160,000 miles, with a final test at approximately 195,000 miles. For BEVs, the initial baseline component testing occurs at approximately 400 miles, and then ICD testing occurs at approximately 4,000, 12,000, and 24,000 miles, with a final test at approximately 36,000 miles. For PHEVs, due to their capability to drive in charge-sustaining mode after the energy storage device is depleted in charge-depleting mode from an overnight charge, their testing is based on time intervals in the fleet after the initial baseline testing at 4,000 miles. The ICD testing occurs at approximately 6 months, 1.5 years, and 2.5 years of fleet testing, and with a final test at approximately 3 years of fleet testing with a minimum of 160,000 miles obtained during this period.

Collaboration between Intertek and DOE's National Laboratories

The deliverables for the AVTE project consist of vehicle baseline reports, interim component durability reports, and end-of life component reports that are posted to the INL AVTA website. INL provides the technical direction for the project along with direction on the data required from the vehicles and infrastructure projects, and analysis of the data collected. When putting together the initial vehicle baseline report, data is compiled from literature review, track testing at a proving ground, vehicle inspection, and dynamometer testing. As previously mentioned, the dynamometer testing for fuel economy occurs at ANL, and the vehicle cycle testing is conducted at multiple ambient temperatures for inclusion into the baseline report. The multiple ambient temperatures provide background on the function of the propulsion systems and the effects secondary heating and cooling systems have on fuel economy, which is not evident from the EPA fuel economy ratings for the different vehicle models. ANL also conducts additional testing that is requested for Autonomie simulations with the AVTE vehicles and provides public access to all obtained data through their Downloadable Dynamometer Database website.

NREL conducts similar testing to AVTE with medium and heavy-duty trucks. Intertek has been collaborating with the NREL team to explore possible fleets to implement XL Hybrid conversions during FY2016. Future work is planned for heavy-duty truck platooning and other medium- and heavy-duty trucks planned for AVTE in FY2016.

Fleet Locations

EZ Messenger, a courier and legal document delivery service, operates a majority of the AVTE fleet vehicles in multiple fleet locations. With the installation of 24 EVSE units at the EZ Messenger location in Phoenix, a majority of the AVTE plug-in vehicles recharge here. See Figure II-3 for the charging infrastructure in place at this location. EZ Messenger also operates vehicles out of their Tucson, Houston, Dallas, Austin, and Oklahoma City locations, with plans to expand to other locations in cooler climates. Based on the need for obtaining vehicle data in cooler climates, the vehicles can be moved as needed, but fueling infrastructure will need to be in place to allow the AVTE vehicles to obtain their target mileages. For example, the 2012 Honda Civic CNG vehicles are based out of Oklahoma City and Texas due to the large network of CNG filling stations in the area. The Chevrolet Impala Bi-Fuel vehicles that can operate on both gasoline and CNG are also planned for fleet operation in this area.



Figure II-3: EZ Messenger Phoenix fleet location charging infrastructure with AVTE vehicles

Intertek

AC Conductive Charging Interoperability between Vehicles and EVSE

AC Conductive Charging Interoperability testing between OEM vehicles and EVSE manufacturers, per the proposed SAE J2953 standard, was completed in FY2015. The testing consisted of 11 OEMs that provided 14 vehicles and 11 EVSE manufacturers. Testing was conducted at Intertek's Plymouth, Michigan laboratory in a round-robin fashion between the vehicles and EVSE units with project management from Phoenix. A Ford Focus Electric and some of the charging infrastructure that participated in the testing are shown in Figure II-4.

The final test results were disseminated to the OEMs and EVSE manufacturers during FY2015. Anonymous results were provided to SAE for all participants and a final report created from the anonymous results was posted to the AVTA website.



Figure II-4: Ford Focus Electric participating in SAE J2953 interoperability testing at the Intertek Plymouth site

Intertek

Storage-Assisted Vehicle Recharging

A Storage-Assisted Vehicle Recharging (StAR) unit is planned for the Phoenix EZ Messenger fleet location. The site infrastructure construction has been completed in preparation for the StAR unit installation. Discussions with potential project partner VLI-EV revealed that their StAR unit is the only one that meets all of the project requirements, which includes having both the CCS and the CHAdeMO connectors required for connection to all of the fast-charge capable vehicles in the AVTE fleet. The VLI-EV StAR unit also includes

an Energy Storage System (ESS) designed into the unit. Competitors were researched throughout FY2015 and reviewed for selection of the most qualified StAR unit. The unit is on order with a planned installation during FY2016.

Conclusions

The AVTE project provides real-world testing of production vehicles, their energy storage systems, and their associated infrastructure that was not always publically available. The selection of advanced technology vehicles improved in FY2015 with the ability to acquire vehicles sold only in California. While the public may be limited on vehicle availability, a large majority of affordable advanced technology vehicles are included within AVTE to provide a full data set for those that are considering purchasing or leasing advanced technology vehicles.

Data and reports from vehicle testing are available for further study by DOE's National Laboratories and are disseminated to the general public. This valuable unbiased information provides performance data that cannot be found in media outlets, such as the performance of the ESS over the life of the vehicle, maintenance cost per mile, fuel economy over the life of the vehicle, and charging economy, all available through the AVTA website.

II.1.C. Products

Presentations/Publications/Patents

1. "Baseline Performance Testing, Series of Reports," Idaho National Laboratory, Intertek Testing Services NA, 2014-2015.
2. "Battery Testing Results, Series of Reports," Idaho National Laboratory, 2014-2015.
3. Wishart, J., "AVTE Interoperability Project, Phase 1: AC Conductive Charging," Intertek Testing Services NA, June 2015.

All listed reports can be found on the AVTA website. Vehicle specific reports are organized by vehicle type. Access: avt.inel.gov/hev.shtml for HEVs, avt.inel.gov/phev.shtml for PHEVs and EREVs, avt.inel.gov/ice.shtml for advanced ICE vehicles, and avt.inel.gov/fsev.shtml for BEVs.

WIRELESS POWER TRANSFER

II.2. Wireless Charging for Electric Vehicles [M612006444]

Omer C. Onar, Principal Investigator and Perry T. Jones, Project Manager

Oak Ridge National Laboratory
 Power Electronics and Electric Machinery Group,
 National Transportation Research Center
 2360 Cherahala Boulevard
 Knoxville, TN 37932
 Phone: (865) 946-1351 and (865) 946-1772; Fax: (865) 946-1262 and (865) 946-1568
 E-mail: onaroc@ornl.gov and jonespt@ornl.gov

Lee Slezak, DOE Program Manager

Vehicle Systems Program, Vehicle Technologies Office
 Phone: (202) 586-2335
 E-mail: Lee.Slezak@ee.doe.gov

Start Date: October 2014

End Date: October 2015

II.2.A. Abstract

Wireless power transfer (WPT) is a paradigm shift in electric-vehicle (EV) charging that offers the consumer an autonomous, safe, and convenient option to conductive charging and its attendant need for cables. WPT can be fully autonomous due to the vehicle and grid side radio communication systems, and is non-contacting; therefore issues with leakage currents, ground faults, and touch potentials do not exist. It also eliminates the need for touching the heavy, bulky, dirty cables and plugs. It eliminates the fear of forgetting to plug-in and running out of charge the following day and eliminates the tripping hazards in public parking lots and in highly populated areas such as malls, recreational areas, etc. Furthermore, the high-frequency magnetic fields employed in power transfer across a large air gap are focused and shielded, so that fringe fields (i.e., magnetic leakage fields) attenuate rapidly over a transition region to levels well below limits set by international standards for the public zone (which starts at the perimeter of the vehicle and includes the passenger cabin). The convenience of WPT cannot be overstated. Oak Ridge National Laboratory's (ORNL's) approach to WPT charging places strong emphasis on radio communications in the power regulation feedback channel augmented with software control algorithms. The over-arching goal for WPT is minimization of vehicle on-board complexity by keeping the secondary side content confined to coil tuning, rectification, filtering, and interfacing to the regenerative energy-storage system (RESS). This report summarizes program work performed during the second phase of the project.

Objectives

- Coordinate multi-party team for the cost optimization and fabrication of the WPT grid side unit (GSU) and WPT coils and getting prepared for the end of phase #2 demonstrations. ORNL is the leading entity and coordinates the following responsibilities with the partners:
 - Evatran is the commercialization partner and under ORNL guidance works on cost and component optimization and fabrication of GSUs and also the primary and secondary coils. Evatran is also working on vehicle integrations in coordination with ORNL and other partners.
 - Clemson University's International Center for Automotive Research (ICAR) Center is the demonstration site for phase #2 deliverables and phase #3 field evaluation for the project. They are also supporting the radio communications developments and radio integrations to the vehicles and the WPT equipment on the vehicles.
 Toyota Motor Corporation is the vehicle original equipment manufacturer (OEM) partner providing the vehicles and support on the vehicle integrations.

- The overall program goal is to integrate ORNL developed WPT technology into demonstration vehicles and validate in an independent testing laboratory and to provide a facility for continued field testing of this technology which will assist in standards development.
- There are six main objectives of the project:
 - Complete building the coils and GSUs for the phase #2 demonstrations and phase #3 field tests.
 - Complete vehicle integrations for the Toyota Prius Plug-in, Scion IQ, Toyota RAV4, and the Chevy Volt.
 - Build a single GSU/single coil setup and associated integrated vehicle hardware for evaluation.
 - Build a single GSU/dual coil setup.
 - Validate full wireless operation including vehicle integration and system regulation at program efficiencies and power level.
 - Integrate two RAV4 vehicles with wireless charging capability for in-motion wireless power transfer demonstration and data collection.

Accomplishments

- Coordinated hardware and software updates, technology developments, as well as project strategies with partners.
- During the phase #2 of the project, team achieved:
 - Integrated Toyota Prius Plug-in, Scion iQ EV, and Toyota RAV4 EV vehicles with wireless charging capability.
 - Completed two GSUs.
 - Demonstrated 6.6kW power transfer to Scion iQ EV with >85% end-to-end efficiency while meeting the electric and electromagnetic field limits indicated in International Commission on Non-Ionizing Radiation Protection (ICNIRP); i.e., <6.25 μ T and <83 V/m.
 - Successfully demonstrated the wireless charging operation of both the Toyota Prius Plug-in and Scion iQ EV including the wireless communications, alignment system, charging initiation and ramping, full charging, and orderly and emergency shut down procedures.
- ORNL designed and built a switch box system that will serve as a power routing interface between the GSU and two primary coils in order to energize them depending on different vehicles parking on the coils and time sequencing of the coils if two vehicles parked on two coils.
- Hardware and software developments completed and system is designed to be interoperable with five different vehicles with different charging protocols, target voltage, current, power levels, ramp rates, and response times. A single hardware is built to be interoperable with software changes for each different vehicle.
- ORNL also outfitted two Toyota RAV4 EVs with WPT hardware. The first vehicle is tested in the lab and test results collected meeting the efficiency and fringe field targets. The second RAV4 with a GSU were shipped to Idaho National Laboratory (INL) for independent testing and evaluation and also characterization of the system with different battery state-of-charge (SOC) levels, misalignment, and power transfer levels.
- The second RAV4 integration is also completed and getting ready for the dynamic wireless charging deployment and testing.
- Site preparation completed at the Clemson University ICAR facilities for stationary charging demonstration. Site preparation is almost completed for the dynamic WPT tests with an electrified road track of 60 feet with a 480V 3-phase disconnect switch.

Future Achievements

- Complete two more GSUs with direct current (DC) power supply connection for the dynamic WPT demonstration.

- Complete site preparation at the Clemson University ICAR facilities including the acquisition of a high power DC power supply to power the GSUs.
- Deploy two Toyota RAV4 vehicles for dynamic WPT demonstrations.



II.2.B. Technical Discussion

Background

Wireless charging of electric vehicles (EVs) has the potential to eclipse conductive chargers because of its flexibility and convenience to the customer. Use of private and secure radio communications, especially vehicle to infrastructure (V2I), and standardization means that any vehicle would be able to charge at any location. The wireless charging process can be totally transparent to the customer, which would increase the use of opportunity charging with the appropriate infrastructure. The goals and accomplishments of this project during this year cover several advancements and integrations in areas including coils, control systems, vehicle integrations, and the site preparations performed for phase #2 demonstrations. Through this project, Oak Ridge National Laboratory (ORNL) and partners developed a deep understanding of wireless power transfer (WPT), real vehicle implementations, control system design and communications for closed loop regulation of power transfer, and the design improvements for higher performance and cost effectiveness.

Introduction

During the phase #2 of the Funding Opportunity Announcement (FOA) #667 project, the team improved the overall operation of the active front-end rectifier with power factor correction, high-frequency power inverter, high-frequency isolation transformer, and the efficiency of the primary and secondary electromagnetic induction resonance coupling coils. Hardware and software developments are completed and the system is designed to be interoperable with five different vehicles with different charging protocols, target voltage, current, power levels, ramp rates, and response times. A single hardware is built to be interoperable with software changes for each different vehicle.

Approach

The approach followed for achieving the goals of the phase #2 is summarized in following subsections.

Grid Side Unit (GSU) Operation: The function of the primary system is to take the alternating current (AC) power from a 208/240V AC supply and generate high frequency current to the primary coil for electromagnetic field generation. During this operation, the power factor correction (PFC) gets the AC voltage from the grid, rectifies it while boosting and provides a regulated voltage to the inverter input. Inverter uses the input voltage provided by PFC and generates high frequency AC voltage to the primary coil. Evatran controller handles the alignment of the secondary coil to the primary coil and communicates to the vehicle side through the radios and commands to the slave digital signal processor (DSP) unit. The operation and normal or emergency shut down commands, reference secondary power or voltage commands are all communicated to the DSP through the Evatran control module. This operation is illustrated in Figure II-5.

For the Prius Plug-in electric vehicle, the team needs to utilize the vehicle on-board charger (OBC). Based on the OBC restrictions, a secondary inverter will be connected at the output of the vehicle side rectifier in order to generate AC voltage again for the OBC. The selected inverter has a wide input range and its output voltage is regulated. In this mode of operation for the Prius, the control system utilizes a voltage regulation feedback control loop. The reference DC link voltage at the vehicle side is communicated to the DSP controller and the DSP controller regulates the PFC output voltage at the grid side to accommodate this need. The block diagram of this operation is featured in Figure II-6.

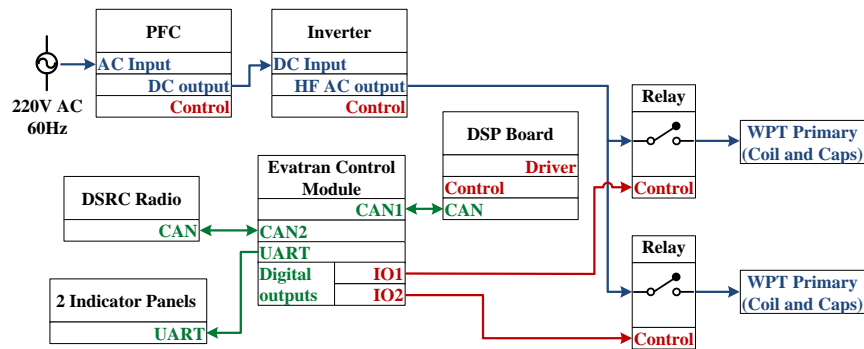


Figure II-5: Grid side unit operational block diagram with Evatran control module and ORNL DSP controller.

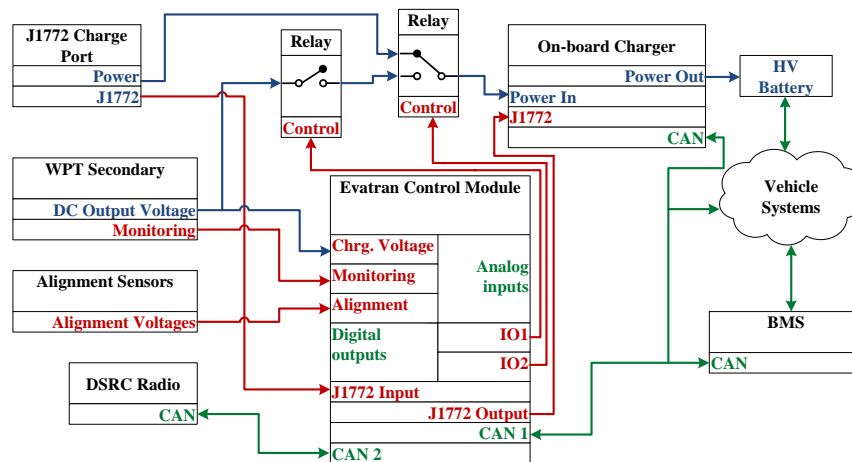


Figure II-6: Operational block diagram of the wireless J1772 integration.

For the direct battery connection, which is featured for the add-on battery system of the modified Toyota Rav4 EV vehicle, a reference current is applied to the battery in current regulation mode while monitoring the battery maximum voltage limit. This mode of operation is illustrated in Figure II-7.

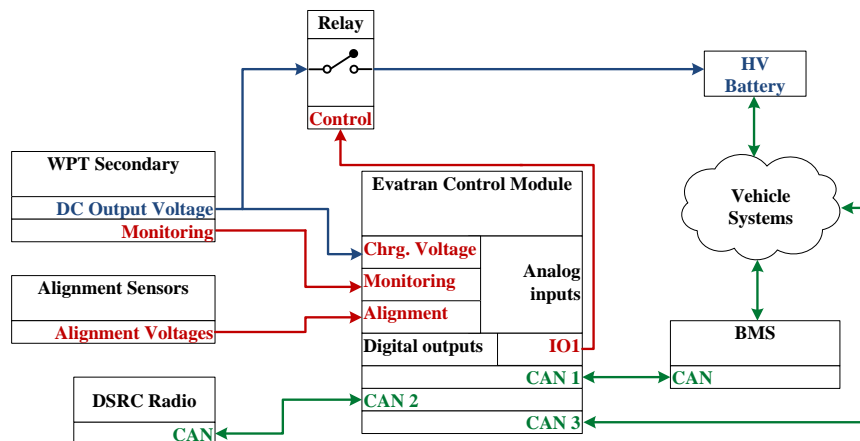


Figure II-7: Operational block diagram for the direct battery or CHAdeMO connection of vehicle side WPT equipment.

The vehicle integration challenges are outlined below.

- **Toyota Prius Plug-in:** This vehicle requires integration through the vehicle side on-board charger (OBC). The Prius Plug-in OBC only works with regulated 208-240 Vrms AC voltage input with 50-60 Hz frequency. The nominal power rating of the Prius Plug-in OBC is 2.1 kW with a maximum of 2.5 kW.
- **Scion iQ EV:** Nominal battery voltage of this vehicle is 277 Vdc. This vehicle requires integration through CHAdeMO charging protocol with a predefined response time, current ramp rate, maximum current ripples, and the reference current tracking. For instance, once the charge request is received, the WPT system should respond in 1 second with a 10 A/s ramp rate. Power transferred is up to 6.6 kW.
- **Toyota RAV4 EV:** This vehicle is equipped with 392.5 V (maximum), 11kWh add-on battery pack for WPT integration. Power rating is 6.6kW.
- **Chevy Volt:** This vehicle also requires through the OBC integration with an optional direct current (DC) (185-265 V) or AC input. The nominal power rating is 3.3 kW.

These vehicle integration specifications are summarized in Table II-2.

Table II-2: Summary of vehicle integration specifications.

				
Charging protocol	J1772 OBC	J1772 OBC	CHAdeMO	Direct to battery
Vehicle input side requirement	DC or AC input	No DC, only AC 50/60Hz	DC reference current tracking with very fast, specific current ramp rates and response times	N/A
Vehicle input voltage (DC)	185-265 Vdc	N/A	Vdc>277V	Vdc>350V
Vehicle input voltage (AC)	208/220/240 Vac	208/220/240 Vac	N/A	N/A
Rated power	3.3 kW	2.1 kW	6.6kW to a nominal 277V battery	6.6kW to nominal 350V battery

Phase #2 demonstrations:

In preparation for the day’s events Grid-side Unit #1 (GSU#1) and the Toyota supplied Scion iQ, with the WPT system integrated by Evatran, were setup with appropriate power meters and sensors to provide measurements of the system’s charging efficiency and power transfer rate as shown in Figure II-8.



Figure II-8: Scion iQ pretests and efficiency measurement and power analyzer hardware.

During the morning’s testing, the system was able to charge the Scion iQ at 6.9 kW across a 165 mm air gap and obtain a 85.49% power transfer efficiency, as seen in Figure II-8. This exceeds the gateway power, efficiency and air gap requirements for the program. However, during this testing some other system parameters were recognized as possible impact parameters for the efficiency of the system.

Furthermore, a Toyota Plug-in Prius was added to the vehicle test fleet to show how the system might interact with a J1772 interface. For this project, Toyota required the WPT system to pass through the vehicle’s original equipment manufacturer (OEM) OBC which meant the power transfer rate was 2.1 kW nominal and 2.5kW maximum, depending on the vehicle request. Additional power electronics were also required to enable the OBC of the Prius to function with a wireless setup. ORNL provided final integration components and met the challenge of repairing Grid-Side unit #2 (GSU#2) in time for the demonstration. Prius Plug-in being wirelessly charged is shown in Figure II-9.



Figure II-9: Wireless charging of a Plug-in Prius.

Results

This subsection presents the Toyota RAV4 wireless charging test results as example. At 162 mm airgap with 220V AC input voltage, the power flow and efficiency across 5 power conversion stages with 6 input and output voltage and current pairs are presented in Figure II-10. According to these results, active front-end rectifier with power factor correction, high frequency inverter, high frequency isolation transformer, primary and secondary coupling coils, and the vehicle side rectifier and filter efficiency recorded 97.41%, 97.94%, 97.05%, 94.17%, and 97.70%. End-to-end efficiency of the system is recorded 85.18% whereas dc-to-dc

efficiency from inverter input to the vehicle battery terminals resulted in 89.51%. In order to deliver 6.6kW power to the vehicle battery, 7.76kW power is drawn from the utility grid. Voltage, current, active power (P), reactive power (Q), apparent power (S), power factor (λ), and the power angle (ϕ) for all power conversions strategies, in addition to the primary coil voltage and the primary side tuning capacitor voltage are presented in Figure II-11. Operational waveforms with expanded views for the high frequency elements (inverter, transformer, and the coils) are presented in Figure II-12 whereas Figure II-13 shows the operational waveforms for low frequency items (grid side AC input, DC link, and vehicle battery voltage and current).

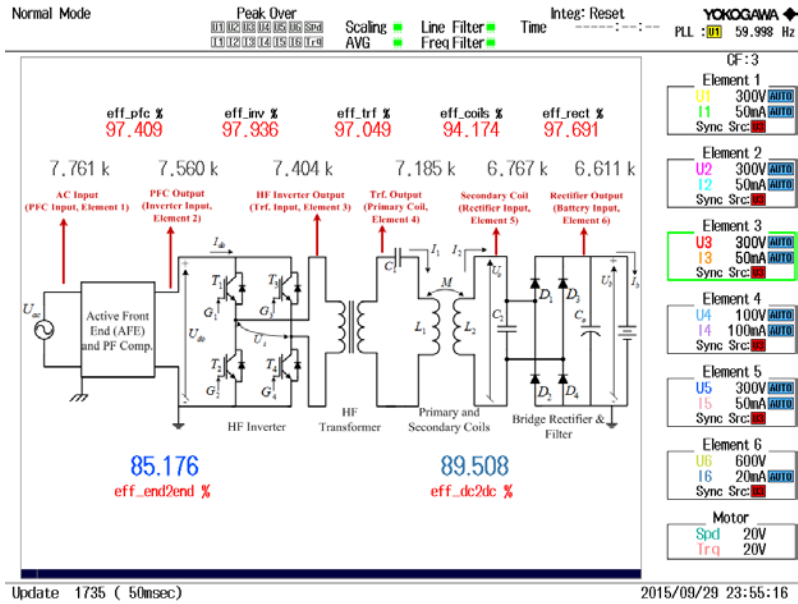


Figure II-10: Toyota RAV4 EV test results: Power flow and efficiency across 5 power conversion stages.

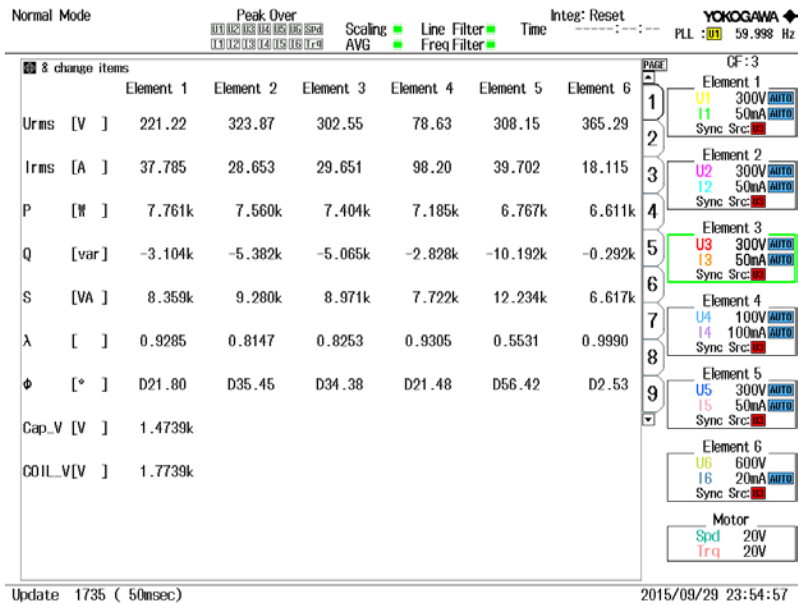


Figure II-11: Electrical test results across all power conversion stages as well as the primary coil and tuning capacitor voltages.

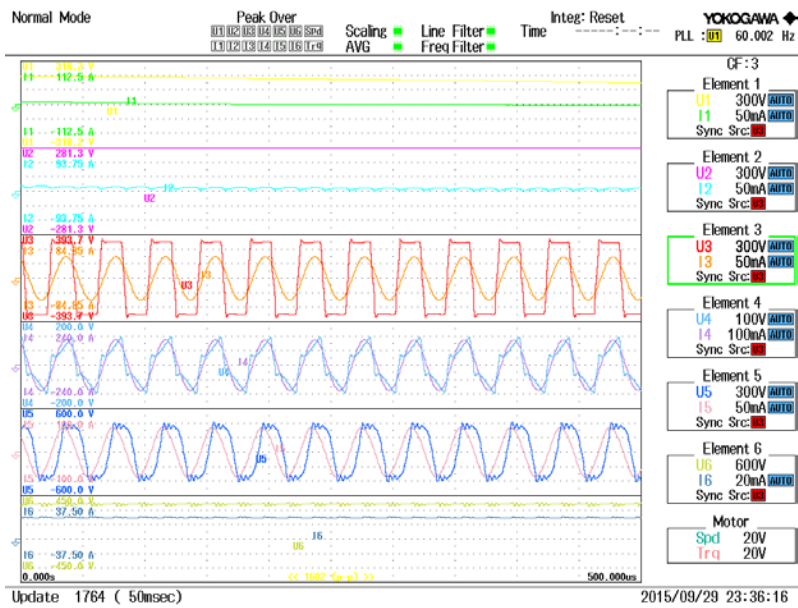


Figure II-12: Operational waveforms for high frequency elements (inverter, transformer, coupling coils).

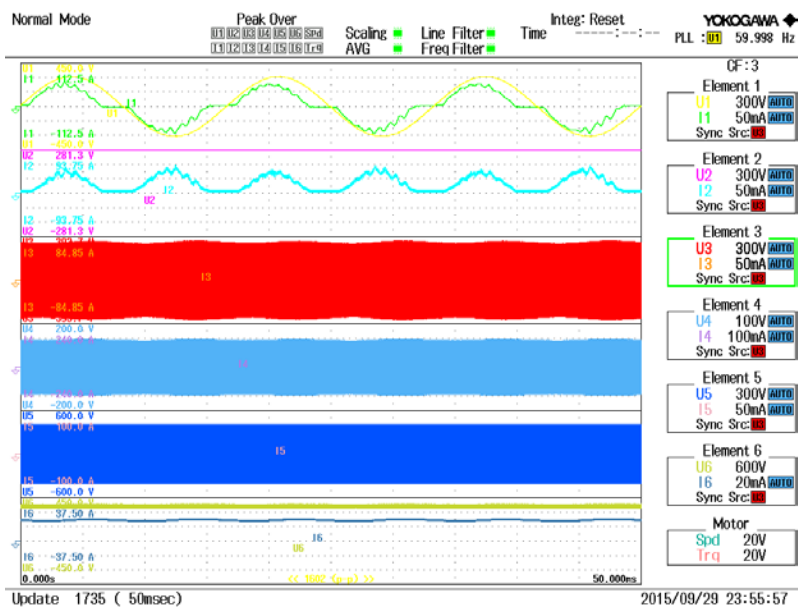


Figure II-13: Operational waveforms for low frequency elements (AC grid input, DC link, vehicle battery).

Conclusions

This report summarizes significant progress, deep insights, and promotion of wireless charging system design technology led by ORNL. The team has demonstrated cost savings for the WPT power electronics equipment and also improved coil-to-coil efficiency and the overall end-to-end efficiency. Vehicle integrations for the phase #2 demonstrations have been completed and demonstrated in July 2015. ORNL demonstrated that a single grid side unit can be interoperable for all different vehicles with different energy storage systems and charging protocols.

ORNL worked closely with our program partners, especially for commercialization and shared with them specifics of the WPT system design, schematics, bill of materials (BOM), and test data.

II.2.C. Products

Presentations/Publications/Patents

1. Journal publications:
 - a. J. M. Miller, O. C. Onar, and M. Chinthavali, "Primary side power flow control of wireless power transfer for electric vehicle charging," *IEEE Journal of Emerging and Selected Topics in Power Electronics – Special Issue on Wireless Power Transfer*, vol. 3, no. 1, pp. 147-162, December 2014.
 - b. J. M. Miller, P. T. Jones, J. –M. Li, and O. C. Onar, "ORNL experience and challenges facing dynamic wireless power charging of EVs," *IEEE Circuits and Systems Magazine*, May vol. 15, no. 2, pp. 40-53, May 2015.
 - c. K. Colak, E. Asam M. Bojarski, D. Czarkowski, and O. C. Onar, "A novel phase shift control of semi-bridgeless active rectifier for wireless power transfer," *IEEE Transactions on Power Electronics – Special Issue on Wireless Power Transfer*, vol. 30, no. 11, pp. 6288-6297, May 2015.
2. Conference papers/presentations:
 - a. M. Chinthavali, O. C. Onar, S. L. Campbell, and L. M. Tolbert, "All-SiC inductively coupled charger with integrated plug-in and boost functionalities for PEV applications," *IEEE Applied Power Electronics Conference and Exposition (APEC)*, accepted for presentation, March 2016, Long Beach, CA.
 - b. M. Chinthavali, O. C. Onar, S. L. Campbell, and L. M. Tolbert, "Isolated wired and wireless battery charger with integrated boost converter for PEV applications," *IEEE Energy Conversion Congress and Exposition (ECCE)*, September 2015, Montreal, Canada.
 - c. M. Chinthavali, O. C. Onar, S. Campbell, and L. M. Tolbert, "Integrated charger with wireless charging and boost function for PHEV and EV applications," in *Proc., IEEE Transportation Electrification Conference and Expo (ITEC)*, June 2015, Dearborn, MI.
 - d. P. T. Jones and O. C. Onar, "Wireless power transfer developments and the potential impact on transportation," in *Proc., Conference on Electric Roads and Vehicles (CERV)*, February 2015, Park City, UT.
 - e. O. C. Onar, S. L. Campbell, C. P. White, C. Coomer, L. E. Seiber, M. Chinthavali, Paul Chambon, P. T. Jones, and J. M. Miller, "ORNL dynamic wireless power transfer system demonstration with electrochemical energy buffers," in *Proc., Conference on Electric Roads and Vehicles (CERV)*, February 2015, Park City, UT.
 - f. O. C. Onar and P. T. Jones, "System parameters, modeling, design, and simulations of high power wireless charging for heavy duty vehicles," in *Proc., SAE Hybrid & Electric Vehicle Technologies Symposium*, February 2015, Los Angeles, CA.
 - g. P. T. Jones and O. C. Onar, "Impact of wireless power transfer in transportation: Future transportation enabler, or near term distraction," in *Proc., IEEE International Electric Vehicle Conference (IEVC)*, December 2014, Florence, Italy.
 - h. J. –M. Li, P. T. Jones, O. Onar, and M. Starke, "Coupling electric vehicles and power grid through charging-in-motion and connected vehicle technology," in *Proc., IEEE International Electric Vehicle Conference (IEVC)*, December 2014, Florence, Italy.
3. Technical report:
 - a. P. T. Jones and O. C. Onar, "Summary of WPT FOA Phase II Demonstration Performed on July 21, 2015," ORNL/TM-2015/421, August 2015.

4. Invited talks and panels:

- a. O. C. Onar, "Recent Advances in Wireless Power Transfer Systems," IEEE Applied Power Electronics Conference and Exposition, Industry Special Session on Recent Development in Wireless Power Transfer, March 2015, Charlotte, NC.
- b. J. M. Miller (Moderator), Ted Bohn, O. C. Onar, J. Taiber, and M. de Rooji, "Wireless Power Transfer: Facts and Fictions," RAP Session at the IEEE Applied Power Electronics Conference and Exposition, March 2015, Charlotte, NC.
- c. O. C. Onar, "Electric Vehicles without Plugging-In," Presentation at the University of Tennessee Science Forum, November 2014, Knoxville, TN.
- d. O. C. Onar, "Electric Vehicles without Plugging-In," Presentation to the Technical Society of Knoxville, November 2014, Knoxville, TN.

5. Patents:

- a. O. C. Onar and J. M. Miller, "Buffering energy storage systems for reduced grid and vehicle battery stress for in-motion wireless power transfer systems," International patent application: PCT/US2013/027578, Pub. No: WO2014130046 A1.
- b. C. P. White, O. C. Onar, J. M. Miller, L. Tang, P. Chambon, and P. T. Jones, "Overvoltage protection systems for wireless power transfer systems," U.S. Patent Application, #14/631,903, 02/26/2015.

II.3. High Efficiency, Low EMI and Positioning Tolerant Wireless Charging of EVs [DE-EE0005963]

Rakan Chabaan, Principal Investigator

Hyundai America Technical Center, Inc.
6800 Geddes Road
Superior Township, MI 48198
Phone: (734) 337-2305; Fax: (734) 629-0690
E-mail: rchabaan@hatci.com

Lee Slezak, DOE Program Manager

Vehicle Technologies Program
Phone: (202) 586-2335
E-mail: Lee.Slezak@ee.doe.gov

Start Date: October, 2012
End Date: September, 2016

II.3.A. Abstract

Objectives

- The objective of this project is to develop, implement, and demonstrate a wireless power transfer system that is capable of the following metrics.
- Total system efficiencies of more than 85% with minimum 20_cm coil-to-coil gap.
- System output power at least 6.6 kW; but design system up to 19 kW for future higher power study.
- Maximum lateral positioning tolerance that can be achieved while meeting regulatory emission guidelines.

Accomplishments in Phase II and 1st quarter of Phase III

- Built third generation wireless charging system which has smaller coil design, and improved power electronics.
- Total system (grid to DC output) efficiency: 93% at 6.6kW output.
- Custom AC/DC front end with 98% efficiency, tested up to 10kW.
- Robust controller software with real-time operating system (RTOS) and closed loop power regulation between transmitter and receiver modules.
- New resonant inverter board design with improvement in performance, cost, and safety features such as high-side low-side dead-time insertion.

Future Goals

- Finish fourth generation (final) system with improved power electronics and control software.
- Continue development of charger-to-vehicle communications over CHAdeMO protocol for successful battery charging.
- Perform vehicle-level as well as module-level tests to evaluate prototype system.
 - Maximum power output.
 - Efficiency at various misalignment conditions.
 - Foreign object effect.
 - Emission levels at vehicle boundary.
- Build fleet of five wireless-charge enabled vehicles (Kia Soul EV) and chargers.



II.3.B. Technical Discussion

Background

Wireless charging for electric vehicles is an alternative to plug-in conductive chargers. The main advantage of wireless charging is automation because the user does not have to plug in the charger or even exit the vehicle. This offers increased convenience and safety but also opens the door to wireless chargers integrated into the infrastructure for semi-dynamic and dynamic charging.

Introduction

This project is a joint effort between Hyundai America Technical Center and Mojo Mobility. We are currently in phase 3 of 3. The activities for phase 3 include revising system to address problems found at end of phase 2, performing tests to evaluate system performance, delivering vehicle to Idaho National Labs for testing, and building a 5-vehicle fleet of wireless-charging enabled vehicles and chargers.

In last year's report, we presented results from the second generation wireless charging system. This year we are presenting a revised and improved third generation system, while we are currently redesigning to produce the fourth and final generation system.

Approach

Our system topology, in terms of power flow is shown below in Figure II-14.

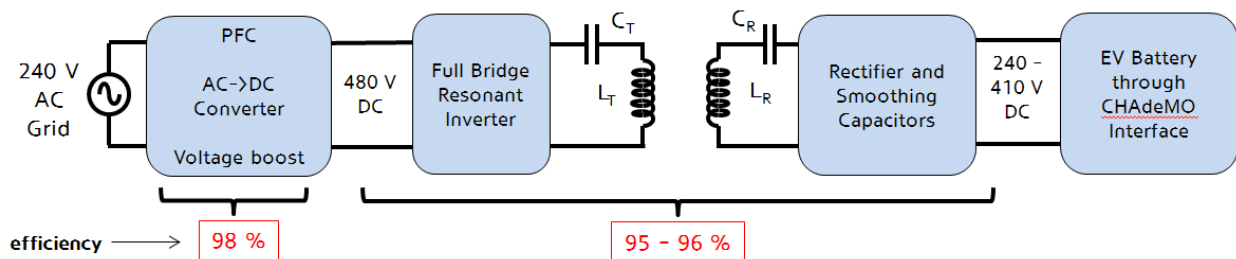


Figure II-14: Wireless Charging System Topology

Input power is 240VAC single phase which is converted and boosted to about 480VDC. This becomes input for Resonant Inverter which feeds 85 kHz current into resonance circuit. After receiver resonant circuit, there is passive rectifier and smoothing capacitors which feed into the DC high voltage bus on the vehicle. Our system does not have any filters after the Resonant Inverter at this point. More discussion regarding efficiency is in Results section.

Based on preliminary packaging study, the vehicle-side coil assembly is designed to be placed just in front of the front axle of the Kia Soul EV, as shown in Figure II-15.



Figure II-15: Coil Placement under Kia Soul EV

The location chosen for the vehicle-side coil assembly shown in figure.

The new coil design for the third generation system is described in Figure II-16. In this report, the x-axis is defined to be along the length of the vehicle; and the y-axis is along the width of the vehicle.

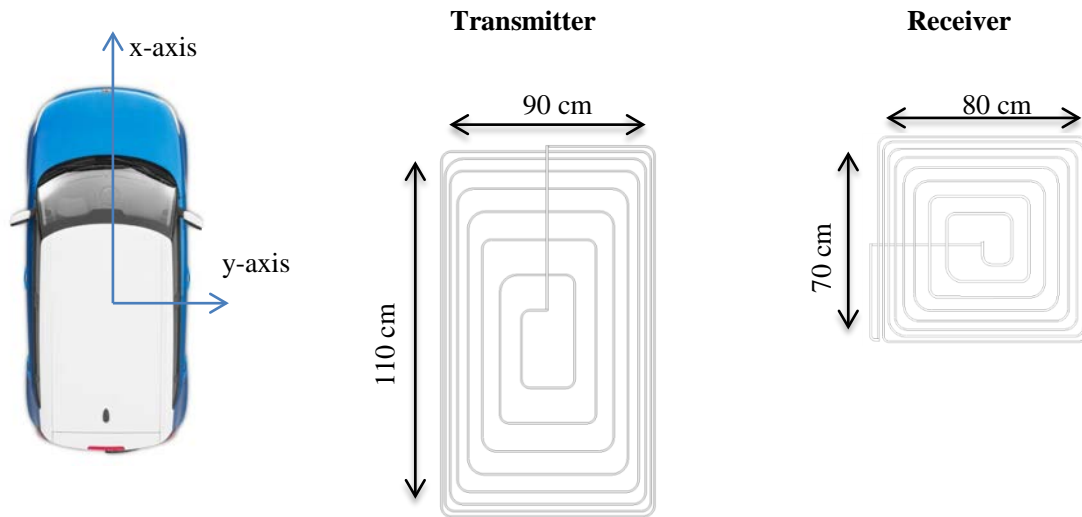


Figure II-16: Coil Design

The coil design and dimensions. Dimensions include ferrite pad extending beyond coil. [1]

The ferrite in our design completely covers the coil without any empty regions in the middle. Hyundai and Mojo are using TDK N95 material with 100x100x2mm tiles.

The AC/DC converter and Resonant Inverter boards are actively air-cooled. Besides that, there is no cooling device for the coils or receiver-side electronics. At power levels above 6.6kW, however, thermal issues will become more important.

Results

The system was built according to above description of coil, ferrite, and circuit. All our results so far are from bench testing, without shielding; however, next steps include vehicle-integration testing.

The custom-built AC/DC converter measured about 98% efficiency from 5-10kW.

Below (Figure II-17) is a measurement of our system efficiency excluding AC/DC front end (thus DC→DC efficiency).

Third Generation Wireless Charging System DC-DC Efficiency

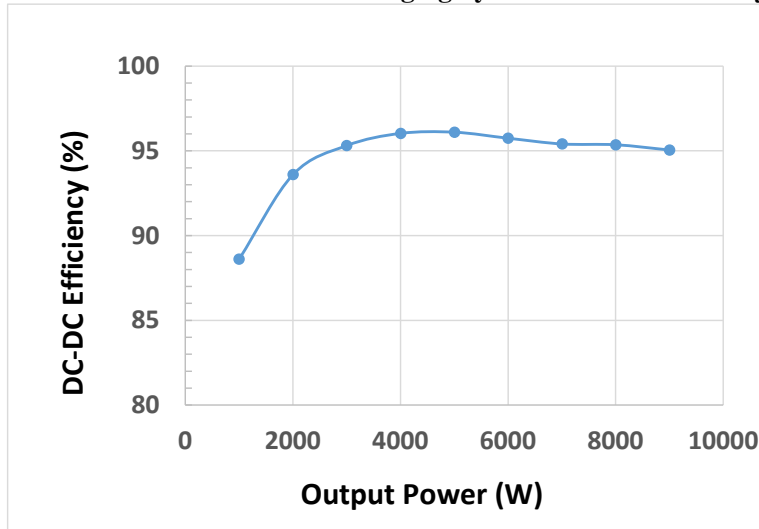


Figure II-17: DC-DC Efficiency

Test Condition: 20 cm z-gap; no misalignment (test lab at Mojo Mobility).

The lab at Mojo Mobility has a custom-built XY stage for doing misalignment testing. The results for misalignment tolerance are relatively good compared with current standardization trends.

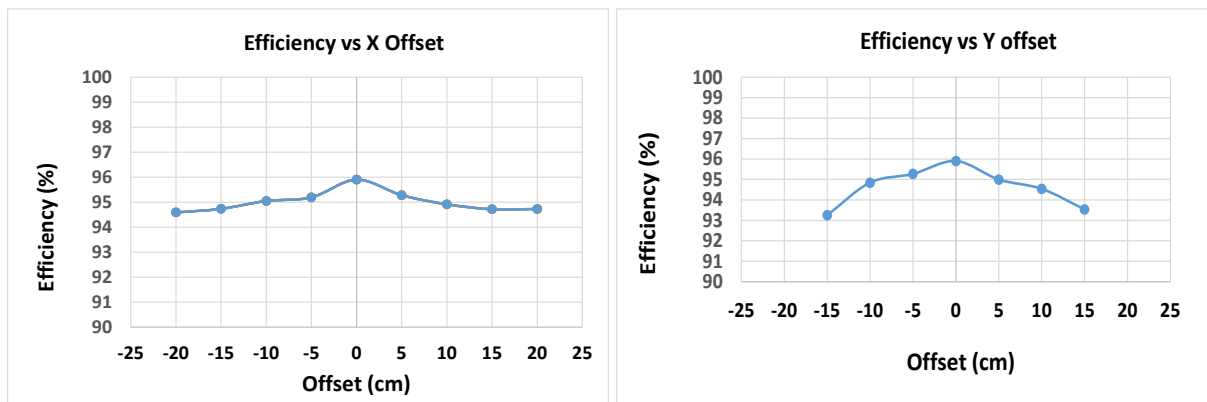


Figure II-18: Efficiency Data

Test Condition: 6.6kW output power; 20 cm z-gap (test lab at Mojo Mobility).

Even with high efficiency and high power, a practical consideration for wireless charging systems is electromagnetic emissions. This includes human safety from 85 kHz (and harmonics) electric and magnetic fields, as well as FCC compliance in regards to radiated emissions. Figure II-19 below shows some results for evaluating human safety.

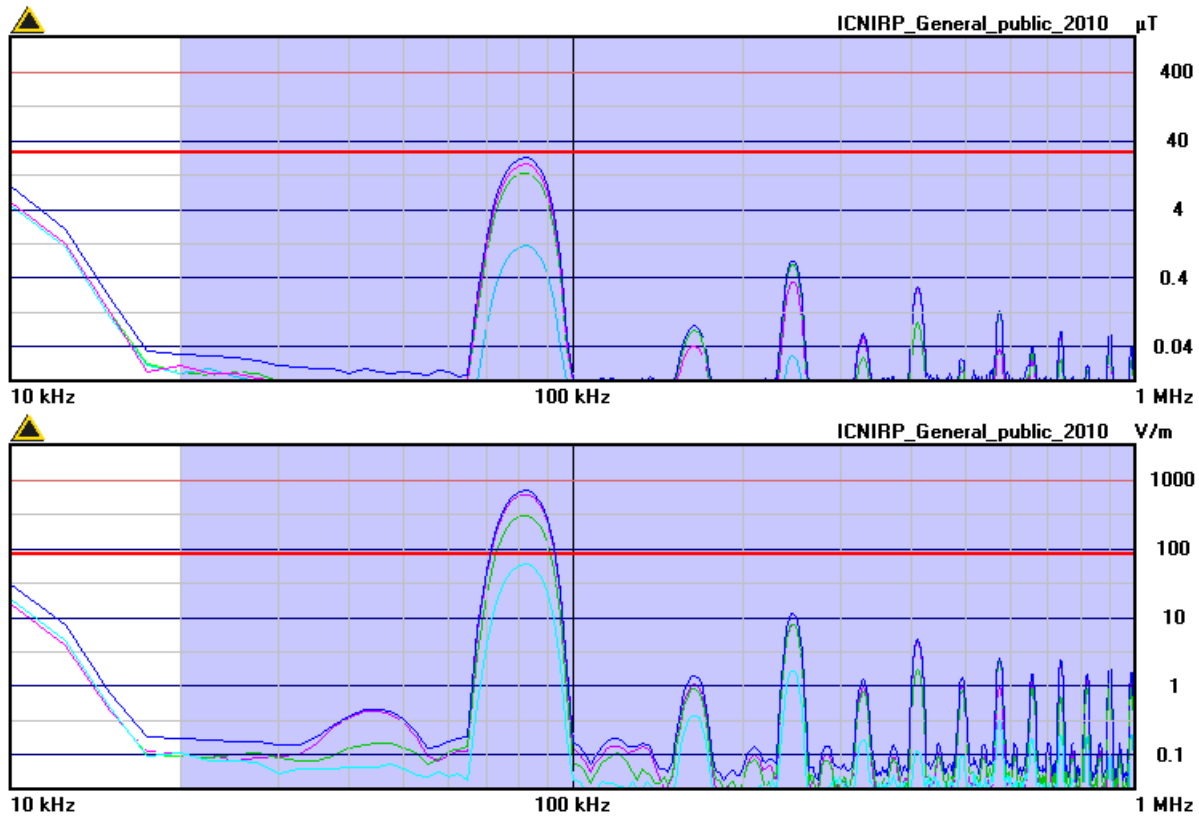


Figure II-19: Magnetic and Electric Field Emissions at Front Bumper.

Test conditions: 6.6kW output power; 20 cm z-gap; no misalignment; probe was 10cm above ground, and 32cm in front of the front edge of the Rx coil assembly, this represents the location of the front edge of the Kia Soul EV. From lab at Mojo Mobility.

The thick red line marks the field level limit according to 2010 ICNIRP general public guidelines. Note that this is a bench test and we expect with vehicle integration, the vehicle will shield some of the fields with the conductive underbody.

Conclusions

The results shown here demonstrate the success of our system’s power electronics, coil, and magnetic designs up to about 10kW with about 93% system efficiency. The next steps are focused more on output regulation control algorithm, vehicle-communication development, and further software development for automation.

II.3.C. Products

Presentations/Publications/Patents

1. Partovi, Afshin. Wireless Power Summit. December 2013. Austin, TX.
2. Partovi, Afshin. Wireless Power World; October 2014; Shanghai, China.
3. Partovi, Afshin. Autotech Council Meeting; July 2014; Sunnyvale, CA.
4. Partovi, Afshin. Autotech Council Meeting; May 2013; Santa Clara, CA.
5. Partovi, Afshin. Sustain Summit; February 2015; Newport Beach, CA.
6. Partovi, Afshin. KPMG’s Automotive Executive Share Forum during NAIAS; January 2015; Detroit, MI.
7. Partovi, Afshin. Wireless Power World Keynote Talk and Panel; September 2015; Beijing, China.
8. Partovi, Afshin. IDTechEx (planned); November 2015; Santa Clara, CA.

9. PR Newswire. "[Hyundai-Kia America Technical Center, Inc. And Mojo Mobility, Inc. Collaborate On Wireless Electric Vehicle Charging System](#)".
10. USA Today. "[More automakers test wireless electric car charging](#)".
11. Auto blog. "[Kia, Hyundai working on wireless charging with Mojo Mobility](#)".

II.3.D. References

1. Kia Soul EV top view: Electric Cars 2016. "2016 Kia Soul EV Review and Price".

THERMAL LOAD REDUCTION

II.4. Design and Implementation of a Thermal Load Reduction System for a Hyundai Sonata PHEV for Improved Range

Cory Kreutzer, Principal Investigator

National Renewable Energy Laboratory
 Transportation and Hydrogen Systems Center
 15013 Denver West Parkway, MS 1633
 Golden, CO 80401
 Phone: (303) 275-3772
 E-mail: Cory.Kreutzer@nrel.gov

John P. Rugh, Task Leader

Phone: (303) 275-4413
 E-mail: John.Rugh@nrel.gov

David Anderson, DOE Program Manager

Vehicle Technologies Office
 Phone: (202) 586-2335
 E-mail: David.Anderson@ee.doe.gov

Start Date: October 1, 2015
 End Date: September 30, 2017

II.4.A. Abstract

Objectives

- Increase grid-connected electric drive vehicle (EDV) range by 20% during operation of the climate control system by reducing thermal loads
- Implement a thermal load reduction system on a production vehicle and quantify performance of the system over the combined city/highway drive cycle at peak heating and cooling conditions
- Maintain occupant thermal comfort, verified through modeling and experimental evaluations.

Accomplishments

- Completed subcontract awards to project partners:
 - Hyundai America Technical Center, Inc. (HATCI)
 - Pittsburgh Glass Works (PGW)
 - PPG Industries (PPG)
 - Sekisui S-LEC America
- Selected technologies, selected vehicle testing platform, fabricated technologies, and delivered technologies for Phase I summer experimental evaluation
- Instrumented and performed preliminary baseline quantification of test vehicles, including measurement of vehicle infiltration rate, solar soak performance, and paint property analysis
- Developed preliminary vehicle heating, ventilating, and air conditioning (HVAC) system model with the CoolSim modeling software subsequent operational demonstration.

Future Achievements

- Complete Phase I summer and winter evaluation of technologies and identify technologies as Go/No-Go for Phase II implementation
- Complete construction of vehicle cabin model in CoolCalc, HVAC system model in CoolSim, and vehicle model and estimate national level range improvements of thermal load reduction system
- Integrate technologies into Phase II vehicle platform and quantify the vehicle's performance during operation of the climate control system for the combined city/highway drive cycle.



II.4.B. Technical Discussion

Background

The EV Everywhere Grand Challenge identified major opportunity areas to increase the adoption of plug-in hybrid and electric vehicles that address the hurdles associated with vehicle market penetration. These opportunity areas are vehicle lightweighting, reducing battery cost per unit of energy delivered, reducing the cost of electric drive systems, improved charging infrastructure, and improved climate control efficiency [1]. Operation of the climate control system has been shown to significantly impact the range of EDVs due to the need for the traction battery to supply power to not only the air conditioning (AC) system, but also the heating system because there is no waste heat available from an internal combustion engine. As an example, a Ford Focus Electric vehicle tested at Argonne National Laboratory's Advanced Powertrain Research Facility measured degradation in vehicle range of 53.7% due to operation of the AC system and a 59.3% degradation in range due to operation of the cabin heating system [2]. By minimizing the amount of energy needed to perform climate control, more energy is available for vehicle propulsion, thereby increasing the range of the vehicle.

Climate control efficiency is determined by the efficiency of the HVAC components, the effectiveness of conditioned air being delivered to the occupant, control strategy, and the thermal energy exchange between the surroundings and the occupied space. Reduction of thermal energy exchange between the surroundings and the occupied space is commonly referred to as thermal load reduction. Placing emphasis on thermal load reduction for plug-in hybrid and electric vehicles is expected to lead to battery sizing and cost reductions, reduced climate control equipment capacities, as well as enabling advanced HVAC system components and control strategies. In addition, thermal load reduction and advanced climate control design can positively impact occupant comfort. The quantification of a number of individual thermal load reduction strategies have been performed for both heating and cooling at the proof-of-concept level. For instance, an infrared reflective windshield combined with pre-ventilation demonstrated on a pre-production electric vehicle reduced the transient 20-minute AC cool-down energy consumption in summer conditions by 44.2% [3]. Similarly, a combination of driver-only panel air ventilation in combination with heated seating, steering wheel, and floor mat demonstrated on the pre-production electric vehicle reduced the 20-minute transient heating energy consumption in winter conditions by 28.5% [4]. In addition, the potential impact of improved vehicle cabin insulation on steady-state heating performance was quantified on the pre-production electric vehicle, with a 3.3% reduction in energy consumption [5]. Finally, the potential impact of solar reflective coatings on the exterior opaque surfaces of the vehicle was measured by applying a solar-reflective film on the roof of a light-duty vehicle during summer daytime conditions, obtaining a 6.7°C reduction in exterior surface temperature of the vehicle roof, demonstrating its ability to positively impact vehicle thermal performance [6].

While the impact of thermal load reduction strategies have been demonstrated under various conditions, their performance is dependent on manufacturing constraints, and the need remains to quantify individual technologies at a production-ready stage rather than the proof-of-concept stage. In addition, it is expected that the performance of some thermal load reduction technologies are dependent on one another. Therefore, a need exists to implement and quantify an entire thermal load reduction system as a whole.

Introduction

The National Renewable Energy Laboratory (NREL), in partnership with HATCI, PGW, PPG, Hanon Systems, Sekisui S-LEC America, Gentherm, and 3M, is focusing on development and subsequent integration of a complete thermal load reduction system for a light-duty electric vehicle. The project scope was developed in response to the FY14 Vehicle Technologies Office-wide funding opportunity announcement solicitation for the Advanced Climate Control Auxiliary Load Reduction area of interest. The overall goal of the project is to provide technology solutions that help reduce range anxiety, improve customer acceptance of EDVs, and increase the penetration of these vehicles into the national fleet. To achieve the project goals, the project objective is to increase grid-connected EDV range by 20% at peak heating and cooling conditions over the combined city/highway drive cycle. The objective is expected to be met by decreasing thermal loads during all modes of vehicle operation, including thermal soak, cool-down and warm-up transients, steady-state operation, and thermal preconditioning while connected to the grid. The project is a three-year project that is divided into an individual technology development and assessment phase (Phase I) followed by a technology integration and performance evaluation phase (Phase II). The project will be completed by providing vehicle performance results obtained through estimation of national-level range improvements based on validated models as well as standardized original equipment manufacturer experimental testing performed at HATCI's test facilities.

Approach

To perform an evaluation of thermal load reduction technologies both independently and as an entire system, the project is divided into two phases. During Phase I, the project team is focusing on identification of candidate thermal load reduction technologies, determination of the design specifications for the technologies, implementation on a pre-production vehicle, and individual evaluation through both testing and modeling approaches. In addition, analysis tools are constructed during Phase I, including a vehicle cabin thermal model, HVAC system model, overall vehicle model, and computer-aided engineering thermal and human comfort models. Phase I will conclude with a go/no-go decision point for the integration of candidate thermal load reduction technologies into the Phase II vehicle. Phase II will be initiated by enhancement and integration of technologies into a drivable vehicle, including determination of feature control integration where necessary. Analysis tools will be validated with Phase I experimental results and leveraged to provide a national scale estimation of the impact of the thermal load reduction system on vehicle range. Once the thermal load reduction system is fully integrated into the drivable vehicle, its performance will be evaluated experimentally through outdoor cold and hot weather testing in addition to environmental chamber testing. Phase II will conclude with a demonstration and summary presentation of the vehicle to key U.S. Department of Energy personnel.

The project relies heavily on collaboration between NREL and project partners to complete all components of the project work plan. HATCI provides the vehicle platform, modeling data, and technology interfacing requirements for Phase I evaluation of technologies. Thereafter, HATCI will lead Phase II of the project, with integration of technologies into the Hyundai vehicle platform in addition to standardized original equipment manufacturer testing at HATCI facilities to characterize the performance of the vehicle. In addition to HATCI's contributions, the project relies heavily on select tier one and tier two supplier research teams to develop, manufacture, aid in testing and analysis tasks, and provide general direction for the project. PGW is providing automotive glass manufacturing capabilities for the project in addition to advanced glass technologies for evaluation. Sekisui is providing advanced materials and integration expertise for candidate thermal load reducing glass technologies, collaborating with PGW for manufacturing. 3M is providing advanced materials and integration techniques for both candidate thermal load reducing glass technologies and vehicle cabin insulation. PPG Industries is developing and providing baseline and solar reflective paint formulations for the vehicles in addition to their thermal property characterization. Gentherm is interfacing directly with both NREL and HATCI to develop and provide active seating, door glass defogging, and individual heated surface technologies. Finally, Hanon Systems is performing experimental characterization of the vehicle HVAC system and model inputs for the construction and validation of the HVAC system model, in addition to expertise in HVAC system control.

Experimental Setup

For Phase I summer testing, two pre-production 2016 Hyundai Sonata plug-in hybrid electric vehicles (PHEVs) were provided by HATCI and instrumented at NREL's Vehicle Integration and Testing Facility, as shown in Figure II-20. The facility is located in Golden, Colorado, at an elevation of 5,997 feet and latitude 39.7 N and longitude 105.1 W. The two vehicles are oriented to face south for maximum solar irradiation into the air volume surrounding the driver. The vehicles are separated to minimize shadowing effects. Each vehicle is instrumented with a total of 48 k-type thermocouples installed on the exterior glass and opaque surfaces, interior glass and trim surfaces, and front occupant seating, as well as a range of internal air temperature measurements, including driver's breath and footwell locations and HVAC vent outlet locations. Air temperature sensors are equipped with a double concentric cylindrical radiation shield to prevent errors due to direct solar radiation exposure. A National Instruments cDAQ-9188 equipped with multiple NI-9214 thermocouple cards is used for data acquisition. All thermocouples are calibrated using a five-point calibration protocol, achieving a U95 uncertainty of less than 0.11 °C for each measurement in accordance with American Society of Mechanical Engineers standards [7].



Figure II-20: Vehicle Experimental setup at NREL's Vehicle Testing and Integration Facility

Image Source: Cory Kreuzer, National Renewable Energy Laboratory

Summer Testing Methodologies

To fully evaluate the performance of technologies and obtain experimental information for analysis validation, Phase I summer testing methods included thermal soak testing, infiltration rate testing, and AC testing. The purposes of each test method and measurements obtained are provided below:

- Thermal Soak Testing:** Thermal soak testing was completed by collecting surface and air temperatures while the vehicles were irradiated in a high solar environment. The primary purpose of this testing is collection of experimental vehicle temperature data for model adjustments and validation. In addition, thermal soak testing provides a means of quantifying the impact of technologies during vehicle-off scenarios. Critical measurements are the vehicle mean interior air temperature, interior and exterior surface temperatures, and environmental conditions.
- Infiltration Rate Testing:** Infiltration rate tests provide experimental vehicle air exchange rate information valuable for vehicle cabin modeling and analysis. Tests were completed by following the concentration decay test methods for tracer gas according to ASTM standard [8]. For the tests, sulfur hexafluoride gas was injected into the vehicle, and a Bruel and Kjer 1303 photoacoustic spectrometer was used to quantify the concentration of tracer gas.

- *Air Conditioning Testing:* The primary purpose of AC testing is to quantify the impact of a thermal load reduction technology on AC system energy consumption. Critical measurements for AC testing are system energy consumption, vehicle cabin air and surface temperatures, and environmental conditions. Due to the limited time for summer testing in 2015, AC tests were not performed. Additional information on the test approach and results will be provided in future reports.

Modeling and Analysis

A number of modeling and analysis tasks are defined for the project. Each analysis component is described below:

- *Vehicle Cabin Thermal Modeling:* A cabin vehicle model for the test platform is in construction and is being developed using the CoolCalc HVAC rapid load estimation tool [9, 10]. Once completed, the cabin vehicle model will be used to perform vehicle thermal load analyses of technologies for both heating and cooling applications. The CoolCalc platform allows the use of both local weather data from NREL's Vehicle Testing and Integration Facility and Solar Radiation Research Laboratory weather stations in addition to Typical Meteorological Year (TMY) weather data provided from locations throughout the United States [11].
- *HVAC System Modeling:* An HVAC system model for the 2016 Hyundai Sonata is being developed using the CoolSim A/C system "Quasi-transient" model framework in the MATLAB/Simulink environment [12]. Once completed, the system model will be used to create HVAC system performance maps as a function of input variables such as ambient temperature and cabin thermal load. The performance maps will then be used to convert cabin thermal loads into HVAC system loads for input into a full vehicle model.
- *CAE Human Comfort and Cabin Thermal Analysis:* Human comfort and cabin thermal analysis tools are in development that include a virtual human model for estimating the impact of technologies on occupant comfort and sensation. Once completed, the analysis tools will also be used for evaluations that are impractical to perform experimentally, such as the measurement of external vehicle surface convection coefficients. The impact of technologies on occupant comfort and sensation will be used to aid in the selection of technologies for Phase II integration.
- *Vehicle-Level Modeling:* A vehicle model of the 2016 Hyundai Sonata is planned to be constructed on the project. The vehicle model will be used to evaluate the impact of varying HVAC accessory loads on vehicle range for prescribed conditions and drive cycles. The impact of technologies on vehicle range with the model will be used as an input to the estimation of national-level range improvement.
- *National-Level Analysis:* A national-scale estimation of the impact of the thermal load reduction system is expected to be constructed. This construction will be completed by combining vehicle cabin thermal modeling, HVAC system performance analysis, and vehicle performance analysis with additional data-processing algorithms.

Results

Technology Selection for Phase I Summer Testing

Candidate thermal load reduction technologies for Phase I summer experimental evaluation were selected based on expected impact, previous studies, and commercial readiness. For advanced paint, PPG identified two red, two blue, and a black paint color formulations that were expected to be good candidates for conversion to a paint with increased solar reflectivity. Small samples of both conventional and near-infrared (NIR) reflective versions of the five paint colors were prepared and applied to standard substrates. PPG then evaluated the properties of the paint samples, quantifying their total solar reflectivity (TSR), and verifying color match performance. The total solar reflectance values for the samples are provided in Table II-3. Solar reflectivity was measured using infrared-visible-near infrared spectroscopy. The dark red color was selected for experimental evaluation for Phase I due to the strong improvement in TSR for dark red combined with its NIR reflective TSR being approximately midway between that of conventional white and black paint based on previous studies [13].

Table II-3: Conventional and color-matched near-infrared reflective paint sample solar reflectance values

Measured Total Solar Reflectance, [%]					
	Red	Dark Red	Blue	Dark Blue	Black
Conventional	12.63	6.62	5.87	5.44	3.71
NIR Reflective	40.84	38.11	21.54	22.58	34.19
Difference	28.21	31.49	15.67	17.14	30.48

In addition to the NIR reflective paint color selection for Phase I evaluation, three advanced glass packages were manufactured by PGW with material and technical support by Sekisui. The three glass package compositions and select estimated performance properties for each are provided in Table II-4. For the three packages, all glass contains a laminate middle layer (interlayer) and includes the windshield, driver door window, passenger door window, rear driver side door window, and rear passenger side door window. The three packages were selected for varying design tradeoffs: Package #1 contained a combination of PGW and Sekisui technologies, Package #2 focused on Sekisui’s advanced interlayer technology and maximization of radio frequency signal transmission, and Package #3 focused on maximization of outer layer reflectivity and total solar energy rejection.

Table II-4: Advanced glass package composition and expected properties for Phase I evaluation

	Package #1	Package #2	Package #3
Outer Glass Layer	2.1-mm Clear with Double Silver IR Reflective Coating	2.1-mm Clear	2.0-mm Ultraclear with Triple Silver IR Reflective Coating
Middle layer (Interlayer)	Sekisui IR Absorbing	Sekisui IR Reflecting & Absorbing	0.76-mm Polyvinyl Butyral
Inner Glass Layer	1.8-mm Solex	2.1-mm Green	2.1-mm Clear
Visible Light Transmission (L _{ta})	71.3%	73.4%	71.7%
T _{sae} ^a	33.4%	34.7%	33.4%
R _{sae} ^b	30.5%	19.7%	48.3%
Total Solar Factor (T _{ts})	43.3%	47.2%	38.4%

^a T_{sae} – Transmission of radiation from 300 – 2,500 nm

^b R_{sae} – Reflection of radiation from 300 – 2,500 nm

Vehicle cabin insulation was selected for Phase I evaluation by collaboration between NREL and 3M. For Phase I evaluation, three different insulation materials were provided by 3M and were selected based on thermal performance while minimizing the amount of mass added to the vehicle. The products, application, and select properties of the three insulation materials are provided in Table II-5 and were used to form one complete insulation package for evaluation.

Table II-5: Vehicle cabin insulation product selection for phase I evaluation

Product	Application	Nominal Thickness [mm]	Thermal Conductivity [W/m-K]	Density [kg/m ³]
TC1803	Walls, pillars	21	2.3	9.05
TC2203	Walls, pillars	26	1.9	9.15
TH4320-1	Flooring	16	2.5	15.69

Phase I Baseline Results

The infiltration rate of the test and control vehicles in the baseline south-facing configuration were measured as described in the Approach section of this report. The infiltration rates for the test vehicle were measured to be 0.51 air volume exchanges per hour while that for the control vehicle was 0.56. The infiltration rate measured for both vehicles was very similar, indicating similar sealing characteristics. In addition, the results indicate that infiltration rate differences between the two vehicles are not expected to contribute significantly to variations in HVAC system performance. The evaluation of thermal load reduction technologies is not expected to impact the infiltration rate of the vehicle; therefore, no additional infiltration rate testing will be performed.

In addition to infiltration rate testing, baseline thermal soak performance data were collected for the Phase I vehicles. Vehicle thermal soak data were collected over a continuous three-day period containing two days of clear skies until late afternoon followed by one partially cloudy day. The mean interior air temperatures of the vehicles are provided in Figure II-21. The mean interior air temperature for each vehicle was obtained from an arithmetic average of the front and rear passenger and driver-side breath level and footwell air temperature measurements. Over the three-day period, the mean interior air temperature difference between the two vehicles varied by an average of 0.03°C with a maximum value of 0.81°C. The baseline soak performance of the test and control vehicles verifies their similarity, and the results obtained will be used for future testing and analysis purposes.

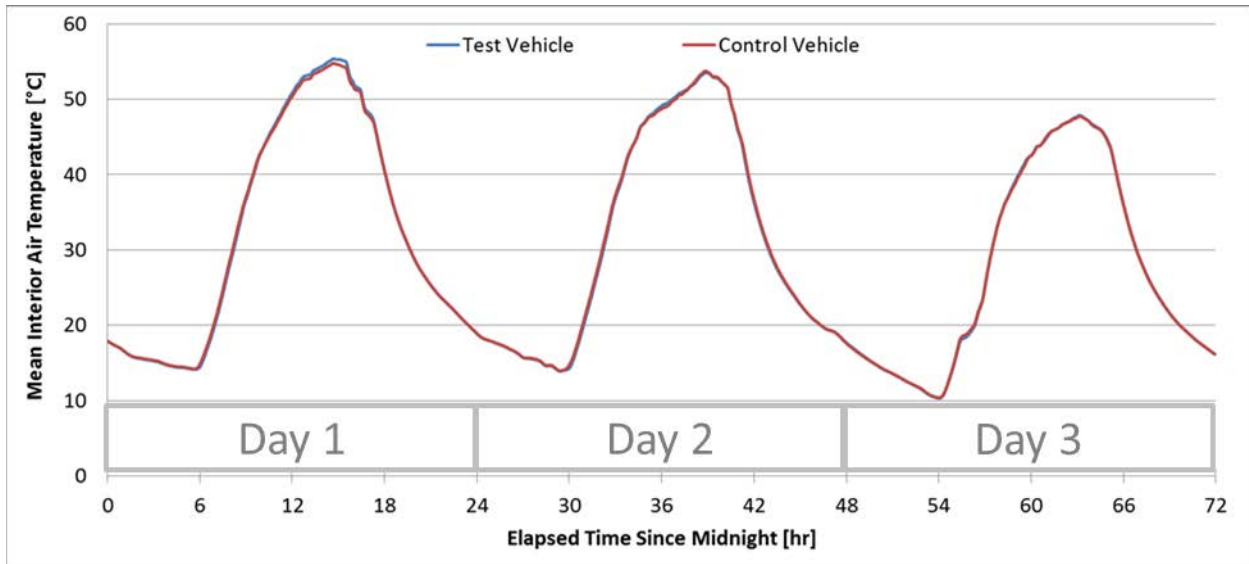


Figure II-21: Select baseline vehicle thermal soak data collected over a continuous three-day interval

Preliminary HVAC System Model

A quasi-transient variable compressor speed electrical HVAC system model was developed as described in the Approach section with component information obtained through engineering estimates. The demonstration model represents a complete HVAC system and will be updated with 2016 Hyundai Sonata vehicle-specific

information through upcoming collaboration with Hanon Systems and NREL. Model functionality was demonstrated by performing a transient cool-down at maximum capacity followed by an automatic control phase with cabin air temperature as the control variable. For the model, summer boundary conditions were implemented, with solar heat load to the exterior surfaces of the vehicle's cabin model fixed at $1,000 \text{ W/m}^2$ and 300 W/m^2 entering the vehicle interior. Ambient temperature was fixed at 30°C and 20% relative humidity, and the initial cabin air temperature was set at 60°C to represent soak conditions. The drive cycle implemented for the system was the SC03 cycle followed by idle conditions for the remainder of the simulation. Select example results are provided in Figure II-22. The system demonstrates control functionality for both the transient cool-down and automatic control phases.

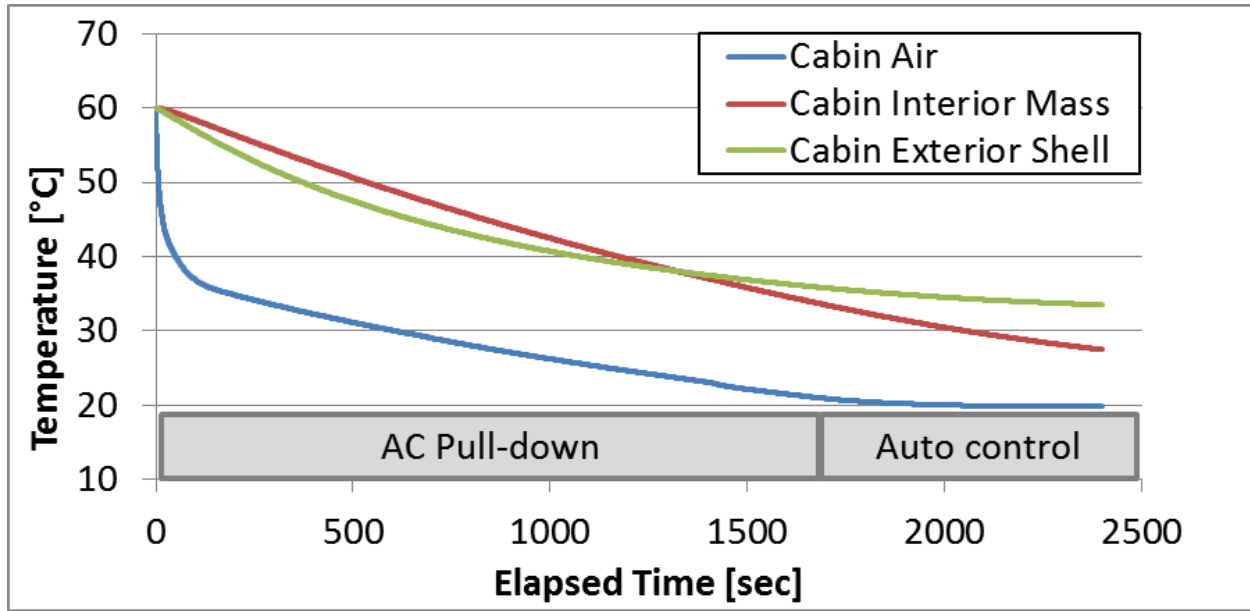


Figure II-22: Sample results for HVAC system demonstration for summer AC system pull-down followed by automatic control to cabin air temperature

Conclusions

Through collaboration between NREL and the project partners, individual thermal load reduction technologies for summer testing were identified. The test vehicle platform for the project was selected by HATCI to be the 2016 Hyundai Sonata PHEV, and two pre-production vehicles were delivered to NREL test facilities for Phase I evaluation. The two vehicles were instrumented in preparation for testing, and paint color was selected from a group of color-matched conventional and NIR reflective paint samples provide by PPG. A dark red exterior paint color was selected, and both vehicles were painted with the conventional formulation for baseline evaluation. In addition to paint color, three advanced glass packages were identified by PGW and Sekisui for individual evaluation. The glass packages were manufactured by PGW with support by Sekisui and delivered to NREL for future performance testing. In addition, vehicle cabin insulation materials were selected by NREL and 3M and base materials provided by 3M. The insulation materials will be combined to provide an advanced insulation package for both winter and summer Phase I evaluations.

Preliminary Phase I summer testing was completed with vehicle performance data obtained for infiltration rate and thermal soak test methods. The infiltration rates of the two vehicles were determined to be 0.55 and 0.51 air volume exchanges per hour, indicating very similar sealing characteristics. A three-day thermal soak test was also performed for the baseline vehicle configuration with significant agreement between vehicles for interior mean air temperatures, measuring an average difference of 0.03°C and maximum instantaneous difference of 0.81°C for the three day duration. The close agreement between the two vehicles indicates that they are expected to have near-identical performance for the evaluation of individual load reduction technologies. In addition to vehicle characterization, infiltration rate results will be integrated into the vehicle cabin thermal model and thermal soak performance used to validate the model. The completion of Phase I summer and winter testing of technologies is scheduled to be completed in FY16.

Progress in the development of the Phase I analysis tool was made during FY15 with emphasis on collection of information for modeling and construction of a preliminary variable-speed electric compressor-based HVAC system model. The HVAC system model functionality was demonstrated by performing a transient cool-down at maximum capacity followed by an automatic control phase with cabin air temperature as the control variable. The system maintained control functionality for both phases of the simulation and will be updated with 2016 Hyundai Sonata PHEV vehicle-specific parameters in FY16.

With continued collaboration between NREL, HATCI, PGW, Hanon Systems, Sekisui, PPG Industries, Gentherm, and 3M, the project aims to complete Phase I of the project in FY16, concluding with Go/No-Go decisions for the integration of each technology into a thermal load reduction system. Thereafter, integration and system performance quantification will be led by HATCI in FY17, culminating in the vehicle demonstration marking the end of the project.

II.4.C. Products

Presentations/Publications/Patents

1. Kreutzer, C., Rugh, J. "Design and Implementation of a Thermal Load Reduction System in a Hyundai PHEV," poster presentation at U.S. Department of Energy Vehicle Systems Simulation, Integration and Testing Annual Merit Review, Arlington, VA., June 9, 2015.

II.4.D. References

1. United States Department of Energy. 2013. EV Everywhere Grand Challenge Blueprint (January 31, 2013). Published by Argonne National Laboratory.
2. Rask, Eric. Argonne National Laboratory Advanced Powertrain Research Facility data, Vehicle Systems Analysis Technical Team (VSATT) meeting presentation, April 2, 2014.
3. Jeffers, M., Chaney, L., Rugh, J. "Climate Control Load Reduction Strategies for Electric Drive Vehicles in Warm Weather." SAE Technical Paper 2015-01-0355, 2015, doi: 10.4271/2015-01-0355.
4. Jeffers, M., Rugh, J. "Electric Drive Vehicle Climate Control Load Reduction." Presentation at 2015 Department of Energy Vehicle Technologies Office Annual Merit Review, June 9, 2015, Arlington, VA.
5. Rugh, J. 2014. "Electric Drive Vehicle Climate Control Load Reduction." Vehicle and Systems Simulation and Testing 2014 Annual Progress Report.
6. Rugh, J., Chaney, L., Lustbader, J., Meyer, J., Rustagi, M., Olson, K., Kogler, R. "Reduction in Vehicle Temperatures and Fuel Use from Cabin Ventilation, Solar-Reflective Paint, and a New Solar-Reflective Glazing." Presented at the 2007 SAE World Congress, April 16-19, 2007, Detroit, MI. SAE Paper 2007-01-1194.
7. Dieck, R.H., Steele, W.G., Osolobe, G. Test Uncertainty. ASME PTC 19.1-2005. New York, NY: American Society of Mechanical Engineers. 2005.
8. ASTM Standard E 741-00, 2006. "Standard Test Method for Determining Air Change in a Single Zone by Means of a Tracer Gas Dilution." ASTM International, West Conshohocken, PA, 2006.
9. Lustbader, J., Rugh, J., Rister, B., Venson, T. 2011. "CoolCalc: A Long-Haul Truck Thermal Load Estimation Tool." presented at 2011 SAE World Congress & Exhibition, April 12, 2011, Detroit, MI. NREL Report No. CP-5400-52452.
10. Lustbader, J. 2013. "CoolCalc HVAC Tool." In Vehicle Systems Simulation and Testing 2012 Annual Progress Report, pp. 292-298.
11. National Solar Radiation Data Base for Typical Meteorological Year 3 Data. redc.nrel.gov/solar/old_data/nsrdb/1991-2005/tmy3/
12. Kiss, T., Lustbader, J., "Comparison of the Accuracy and Speed of Transient Mobil A/C system Simulation Models." SAE Int. J. Passeng. Cars - Mech. Syst. 7(2):739-754, 2014, doi: 10.4271/2014-01-0669.

13. Lustbader, J., Kreutzer, C., Jeffers, M., Adelman, S. et al. "Impact of Paint Color on Rest Period Climate Control Loads in Long-Haul Trucks." SAE Technical Paper 2014-01-0680, 2014, doi: 10.4271/2014-01-0680.

II.5. Electric Phase Change Material Assisted Thermal Heating System (ePATHS) [DE-EE0006444]

Dr. Mingyu Wang, Principal Investigator

MAHLE Behr Troy Inc.
350 Upper Mountain Road
Lockport, NY 14094
Phone: (716) 531-2579
E-mail: mingyu.wang@us.mahle.com

Lee Slezak, DOE Program Manager

Vehicle Technologies Program
Phone: (202) 586-2335
E-mail: Lee.Slezak@ee.doe.gov

Start Date: 10/01/2013

End Date: 1/01/2017

II.5.A. Abstract

Objectives

- Thermal Energy Storage (TES) system can store sufficient thermal energy to heat the Electric Vehicle (EV) cabin for an extended period of time. Depending on the sizing of such a system, the TES can provide up to 100% of the thermal energy necessary to heat the cabin during typical commuter driving. Using the TES system for heating can increase the electric drive range more than 20% in cold ambient conditions. For this project, the goal is to design and develop a prototype TES system through analysis and testing that can be quickly commercialized. The project scope includes the development of an advanced PCM (phase change material) along with the component and system architecture for integration into a Grid Connected Electric Drive Vehicle (GCEDV) environment to provide heating comfort. The system performance will be demonstrated at both a bench and vehicle level.
- In operation, the TES system will incorporate a high temperature PCM that will be housed in a standalone container and will seamlessly integrate with the existing charge control architecture. Energy from the electric grid will provide the charging energy to heat the TES system while the EV is being charged at home or at an EV charge station. The TES will be heated via an electrical resistance heater during the plug-in charging cycle. An intelligent TES charge control algorithm will be implemented.
- The basis of the TES is a Phase Change Material (PCM) storage unit. Innovative to this storage unit is that it incorporates a PCM that has up to 50% more latent heat during phase change in comparison with PCMs on the market today. Further, the storage unit will be insulated to minimize parasitic energy loss while the vehicle is parked.

Accomplishments

- System and Components Specifications:
 - The vehicle and sub-system specification for the ePATHS system was revised and released for the initial development of the system. In this version of the specification, a significant change to the system architecture was made as compared to that of the original project proposal to improve energy recovery. An innovative heat exchanger CapHX was incorporated into the system architecture to allow efficient use of thermal energy stored in the PCM heat exchanger. Further update to the system architecture included a proportional control bypass valve for coolant temperature control during thermal discharge, and an operating state control valve to allow the PCM heat exchanger to operate in either charging mode or discharging mode.

- Component specifications for the PCM heat exchanger, PCM, insulation, pumps, valves and hoses, etc., were completed. Based on the specifications, a Gen I PCM heat exchanger was designed and other required components were sourced. As part of the component specifications, a system controls specification was established for the hardware and software required for the intelligent control of the TES system. The controls specification requires an integrated traction battery and thermal battery charging system using a common power plug.
- System, Components Design and Development:
 - A MATLAB Simulink model was developed for the ePATHS system. A system simulation model of the full ePATHS system was completed by ORNL that integrates the previously developed parametric PCM HX model and the latest system layout. System simulations with the model confirmed that the design-intent TES should provide the heating capacity and heat discharge rate necessary for a typical US daily commute.
 - A method was developed to monitor vehicle CAN bus communication. This involves identifying the key messages from the bus and developing a “bridge” to relay the messages to the ePATHS controller as well as the data logging system. The information is required for data analysis during vehicle testing.
 - Testing of two potential PCM charging (heating) technologies was completed and resulted in the selection of surface heating technology as the mainstream design.
 - A PCM filling apparatus was designed and fabricated. A concept ¼ width PCM heat exchanger fabricated in the prior reporting period was successfully filled using the apparatus.
 - A prototype insulation container for the PCM heat exchanger was evaluated on the ¼ width unit. The heat loss was measured in a cold chamber with a thermally fully charged PCM heat exchanger containing DPT-68 to establish the effective thermal resistance. Based on the work, an improved insulation design for the full sized PCM heat exchanger was completed. It is being built and will be evaluated in the fourth Quarter of 2015.
 - Entropy Solutions has completed the development of DPT68 PCM with a latent heat of 350 J/g and a melting temperature of 68 °C. Pilot scale production process has been developed and validated. Concept development of a second PCM, DPT83, with a latent heat of 340 J/g and a melting temperature of 83 °C was completed. Process development for medium scale production is in progress.
 - New direction was approved to use the Ford Fusion Energi PHEV as the final demonstration vehicle for the ePATHS project. The BP-1 Ford Focus BEV will be used as a mule vehicle for initial system and component testing. Packaging studies were completed for both the Focus BEV and the Fusion Energi.
 - A unique cabin heater, CapHX, was designed and built. Dissipation tests have been performed to gauge its performance. Tests indicate that it meets the specification requirements.
- Program management:
 - Milestones for BP-1 were met. DOE authorized continuation into budget period 2.
 - ePATHS was presented at 2015 Annual Merit Review.
 - DOE site visit to Lockport, NY was completed.

Future Achievements

- The specifications for the demonstration vehicle will be revised based on ePATHS system bench and mule vehicle testing.
- New components, if needed to meet the revised specifications, will be designed, built and tested.
- System control and charging subsystems will be improved to meet vehicle requirements.
- Ford Fusion PHEV will be integrated with the ePATHS system for climatic tunnel testing and road evaluation
- Range extension analysis will be completed based on climatic tunnel and road testing.



II.5.B. Technical Discussion

Background

Climate control poses a severe challenge for battery electric vehicles (BEVs), plug-in hybrid electric vehicles (PHEVs), extended range electric vehicles (EREVs), and even hybrid electric vehicles (HEVs). Cabin heating, depending on the size of the vehicle and the environmental conditions, typically requires 3.2 to 6.5 kW of battery power at the ambient of -10°C to meet transient and steady state comfort requirements. For the larger sized electric vehicles of various genres (xEV), the required battery power may be even greater. The battery power used to generate the heating, either through a heat pump or direct resistive heating, leads to dramatic decrease in the driving range of xEVs. It is estimated that the range of a BEV can be reduced by 20-40%, depending on the drive cycle. It is essential, therefore, to develop a reliable, cost-competitive, and more energy efficient occupant heating system that can help reduce traction battery load and increase the vehicle electrical driving range while still ensuring occupant comfort.

Introduction

The term “Phase Change Material” (PCM) is used to describe materials that use phase changes (e.g., melting) to absorb or release relatively large amount of latent heat at essentially constant temperature. In general, when the temperature becomes warmer than the freeze point, PCMs liquefy and absorb and store heat. Conversely, when the temperature decreases, the material will solidify and give off heat to warm a medium for productive use.

The MAHLE team is working with its project partner Entropy Solutions, a leading PCM material supplier in the industry, to custom-develop an advanced PCM material with a latent heat value equal to or greater than 350 J/g and a phase transition temperature near 85 °C (as compared with the latent heat of 334 J/g melting at 100°C for water), and integrate the PCM material into an innovative, self-contained system to provide charging and discharging of heat to support BEV climatic heating for passenger comfort. The ePATHS project aims to develop a light-weight, compact, and scalable TES system to meet a wide range of grid connected vehicles’ heating needs. MAHLE is working with its OEM partner, Ford Motor Company, to integrate the ePATHS system into a Ford Focus electric vehicle and a Ford Fusion plug-in hybrid vehicle to demonstrate its capability and commercial viability. The development of the ePATHS system is also be supported by the analysis and testing capabilities from Oak Ridge National Laboratory (ORNL) to achieve optimization in performance, packaging, weight and other key metrics.

Approach

System Architecture Development

The ePATHS system was designed to store heat using power from the electric grid and release heat to warm up vehicle cabin during driving in low temperature ambient conditions. The objective was to facilitate range extension for Battery Electric Vehicles (BEV). The PCM heat exchanger is the core of the ePATHS system. It contains the PCM heat storage medium and internal heat transfer surfaces that allow heat to be added to the PCM material using electric heaters, or removed from the PCM material by circulating a low temperature coolant stream. A pump is used to provide the pressure head for coolant circulation. Figure II-23 shows a system that also incorporates a configurable CapHX for deep heat recovery from the PCM heat exchanger. This is an improved system design over the original proposed architecture.

The system of Figure II-23 has been mechanized to achieve three modes of heating: PCM discharging, energy recovery, and PTC heating, along with a fourth mode of PCM charging. An actuated configuration valve was prototyped to allow the CapHX function as a single-parallel heat exchanger attached to either the PCM loop or the PTC loop of the BEV, allowing PCM heating or PTC heating. The valve can also allow the CapHX to function as two separate heat exchangers, with the front half attached to the PCM loop to preheat the incoming cold air, and the rear half in the PTC loop to allow final heating of the airstream to fulfill the requirements of cabin heating. This is known as the energy recovery mode of operation.

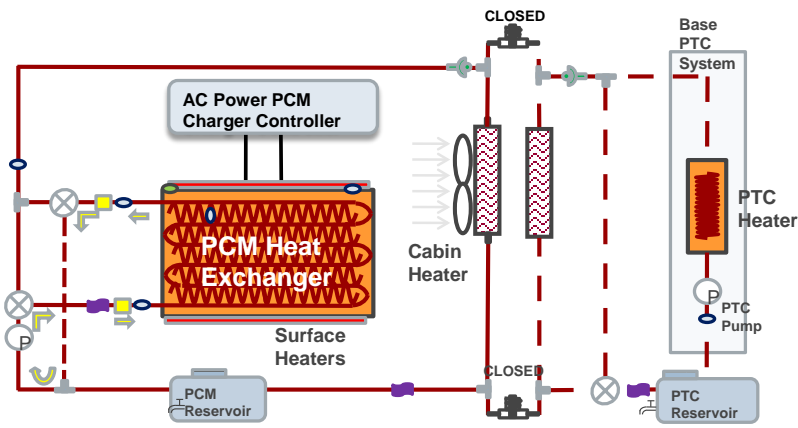


Figure II-23: Mechanized ePATHS System Design

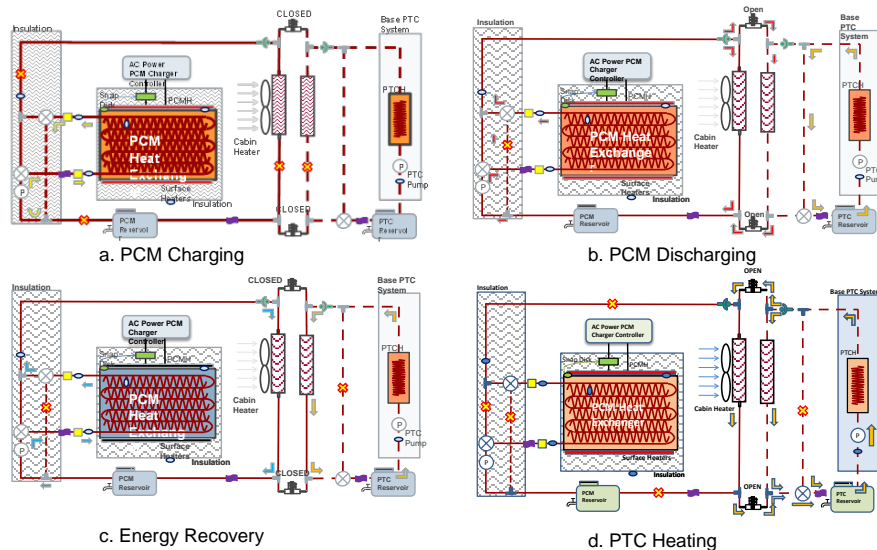


Figure II-24: Operating Modes: a. PCM Charging, b. PCM Discharging, c. Energy Recovery, and d. PTC Heating

All four operating modes are depicted in Figure II-24. Figure II-24.a shows the system operating in the PCM charging mode. The operating state valve at the exit of the PCM heat exchanger is positioned to return coolant to the inlet of the pump. The coolant bypass valve at the inlet of the PCM heat exchanger is positioned to route all the coolant through the PCM heat exchanger. The pump may be operated from 0% to 100% duty cycle, pending further optimization of the charging process. When the pump operates to circulate coolant through the PCM heat exchanger in the figure-8 routing, it is expected that the PCM heat exchanger internal temperature distribution will be more uniform. When the pump is shut off, heat loss may be minimized during the charging process, but higher temperature non-uniformity is expected inside the PCM heat exchanger.

Figure II-24.b shows the ePATHS system in PCM discharging mode. The operating state valve is placed to route the coolant stream from the PCM heat exchanger left to the Tee joint, where a non-heated stream directly from the pump is mixed with the heated stream to regulate the coolant temperature going to the cabin heat exchanger CapHX. The proportion of the non-heated stream is determined by the coolant bypass valve downstream of the pump. Linear control or ON-OFF control may be implemented to control the cabin heater inlet coolant temperature using the inlet thermistor as feedback.

Figure II-24.c illustrates the ePATHS system operating in the "energy recovery" mode. As the PCM heating mode continues to the point where even 100% coolant flow going through the PCM heat exchanger fails to provide the required air discharge temperature at the cabin heater outlet, the PCM heat exchanger is considered "exhausted", since it alone is unable to provide sufficient cabin heating. However, at the ambient temperature of -10°C or lower, there is still quite a bit of thermal energy left in the PCM heat exchanger that can be used to

pre-heat the incoming cold air. The energy recovery mode allows the two halves of the CapHX to function separately in the PCM loop and the PTC loop, with the first half providing pre-heating of cold air using PCM heat and "final" heating using PTC power. It is expected that PCM energy extraction is possible in cabin air recirculation mode when the PCM temperature is above 20 °C. In the outside air mode of the climate control system, further extraction down to 0°C should be possible.

Finally, PCM heat exchanger is truly exhausted by energy recovery extraction such that it is meaningless to continue circulate coolant in the PCM loop. At this point, the two halves of the CapHX can be reconfigured to the PTC heating loop to let the PTC heater provide all the heat needed. This mode of operation is shown in Figure II-24.d.

Phase Change Material Development

Entropy Solutions synthesized five families of PCM materials to screen for potential candidates. The PCM development process starts with synthesizing a chemical compound in sufficient amount of PCM for characterization of its melting temperature and latent heat of solidification. Upon synthesis, the sample is purified as required for characterization. Differential Scanning Calorimeter (DSC) was used to measure the melt temperature and the latent heat. If a candidate PCM meets the phase change temperature and latent heat targets, the sample is then cycled thermally to establish the temperature stability of the PCM.

Table II-6: Properties of Candidate Phase Change Materials

PCM	Melting Point (°C)	Latent Heat (J/g)	Latent Heat Ratio over Water
DPT-12	-12	267	0.80
DPT-14	14	298	0.89
DPT-23	23	335	1.00
DPT-38	38	320	0.96
DPT-50	50	343	1.03
DPT-68	68	342	1.02
DPT-83	83	348	1.04
DPT-86	86	321	0.96

As shown in Table II-6, DPT-83 and DPT-68 demonstrate acceptable latent heat and melt temperature. DPT-68 can be adequately applied to BEV vehicles with supplemental PTC heating for extremely cold ambient temperatures. Cold soak in a parking lot under very low ambient temperatures is likely to require high coolant temperature near 85 °C. DPT-68 based thermal storage would have used up the high temperature sensible heat in the first commute trip to work, leaving the PCM material at 68 °C, which might be insufficient to meet the transient heating needs as the car leaves the parking lot. Low power supplemental heating with the PTC heater may be needed to ensure cabin comfort.

DPT-83, on the other hand, has a phase change temperature of 83 °C, which practically meets the current BEV coolant temperature specification of 85 °C. Therefore, it should be able to provide heating under all ambient conditions equivalent to that provided by the PTC heater for as long as there is still energy left in the PCM thermal storage.

Both PCM materials should be able to provide heating to PHEV. A slightly different engine restarting condition needs to be defined to accommodate the differences in melting temperature.

For both DPT-83 and DPT-68, it has been recognized that isolation from air and moisture is required for thermal stability. This imposes special requirements during shipping and during filling into the thermal storage system.

Preliminary indications show that DPT-83 and DPT-68 are materially compatible with aluminum. Additional compatibility studies are being carried out.

PCM Heat Exchanger Development

The PCM thermal storage heat exchanger is a key component of the ePATHS system. Figure II-25 shows the construction of the full sized PCM heat exchanger. The design includes 2 PCM filling ports, 18 internal PCM temperature measurement thermocouples for development, one PCM temperature thermistor, one heating surface temperature thermistor, coolant tubes, PCM fins, tanks, and coolant inlet and outlet connectors. The heat exchanger core composed of coolant tubes, fins and headers, once brazed, is disposed in a prismatic shell container to provide storage space for PCM material between the shell and the fin-tube surfaces. On the coolant side, the heat exchanger has a two-pass design. The coolant stream enters from the inlet, traverses the first pass of the heat exchanger tubes, and then turns around in the return tank to flow through the second pass of the heat exchanger. The coolant exits the heat exchanger through the outlet connector. As the coolant flows through the PCM heat exchanger, it is heated up by extracting heat from the PCM material. Figure II-26 shows the aluminum heat exchanger built in MAHLE's Lockport Technical Center (LTC) model shop.

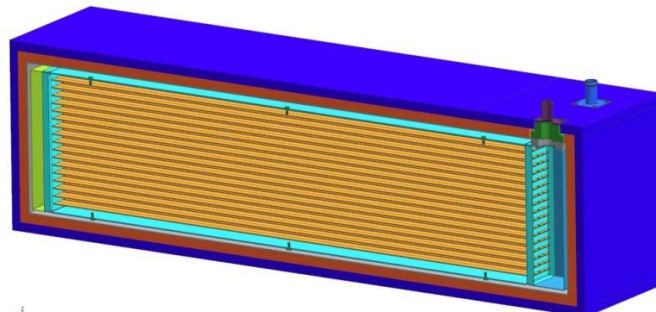


Figure II-25: PCM Heat Exchanger Design

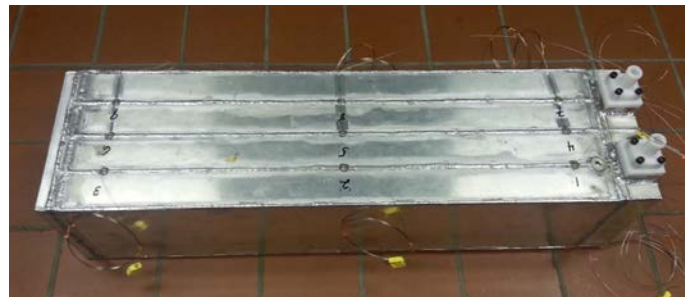


Figure II-26: PCM Heat Exchanger without Insulation

Six surface electric heaters of two different sizes provide the heating for the PCM material. These surface heaters are epoxied to the axial surfaces of the containing shell. The surface with the input and output couplers and the opposite surface have two smaller surface heaters each, while the adjacent surfaces to the aforementioned surfaces have one long surface heater each. The selection of the surface heating technology and the surface heaters themselves were based on BP-1 testing studies.

The PCM heat exchanger requires an insulation system that can keep 90% of the stored heat and lose only 10% of it over an 8 hour period in the parking lot. Vacuum Insulated Panels (VIP) was deemed as the primary candidate technology to meet the heat loss specification. The insulation development went through 3 prototype phases. Most recently in the Phase 3 development, a full-sized VIP insulation system was designed built and initially tested. Final evaluation is to occur in 3Q2015 on an ePATHS system bench.

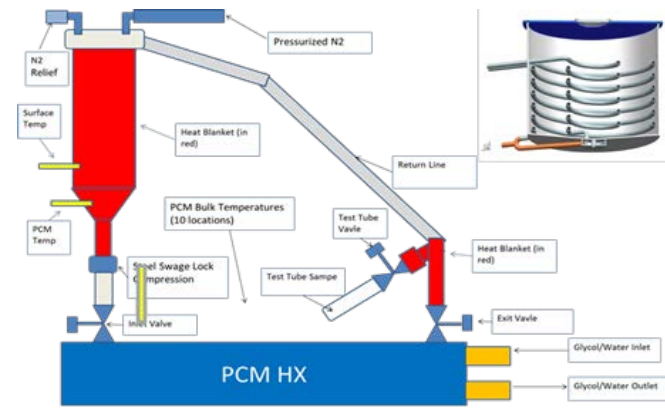


Figure II-27: PCM Filling System

The PCM material for thermal storage is in a solid state under normal ambient temperatures. In order to fill the material into the PCM heat exchanger, it is necessary to preheat the PCM into a liquid for it to flow into the heat exchanger freely. Also, due to the tendency for DPT-68 and DPT-83 to react with air and moisture, isolation must be provided during the filling process. Figure II-27 shows a custom designed filling system that accommodates both of the requirements. Nitrogen is used to pre-purge the PCM heat exchanger and provide isolation during filling. The PCM holding tank uses hot coolant to melt the PCM inside.

ePATHS System Math Modeling

An ePATHS system model was developed and implemented in MATLAB Simulink (Figure II-28). It simulates the heat transfer and fluid flow conditions that are present in the ePATHS system as the PCM heat exchanger is charged and discharged. With the model, the PCM heat storage system’s performance can be more realistically evaluated and its design better optimized.

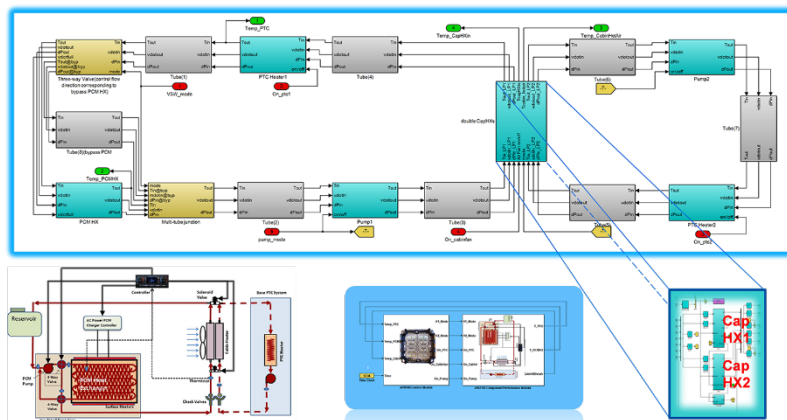


Figure II-28: ePATHS System Simulation

ORNL continued its development and refinement of the ePATHS system model and has completed analysis of the ePATHS using the full system model for various system design configurations under consideration. The sub-model for the PCM heat exchanger that is included in the system model was modified to implement a two-node model for the sensible heat transfer so that the extraction of thermal energy from the PCM is properly accounted for during the periods of heat removal from the initially superheated liquid and subsequently when sub-cooled solid is present in the PCM after freezing is complete. The two-node model enables a rapid solution of the sensible heat transfer that takes place before and after the primary heat transfer process associated with the phase change. In addition, ORNL implemented multiple control strategies in the system model that allow the air temperature discharged to the cabin to be adjusted according to cabin demand. Flow control algorithms were implemented for bypassing a portion of the flow around either the cabin heat exchanger or the PCM heat exchanger in order to deliver the heat transfer rate into the vehicle cabin as needed.

System Controls Development

The MAHLE HVAC development controller is used to control ePATHS system operations. It is an automotive grade controller meeting validation requirements for automotive applications. The controller is equipped with a 7 inch color touch screen interface for displaying and inputting system data and control values. It can communicate with the vehicle CAN bus through a bridging module. A laptop PC may be used to directly communicate with the controller for calibration and data logging. Sufficient input and out channels, both digital and analog, are available to allow the ePATHS system to be controlled effectively.

As shown in Figure II-29, the MAHLE controller is interfaced to the vehicle OBD-II port by using neoVI Fire as a bridging device. The controller communicates with neoVI Fire using LIN bus. The neoVI Fire unit communicates with the vehicle using CAN protocol. A message forwarding script is used inside the neoVI Fire unit to allow two-way communication.

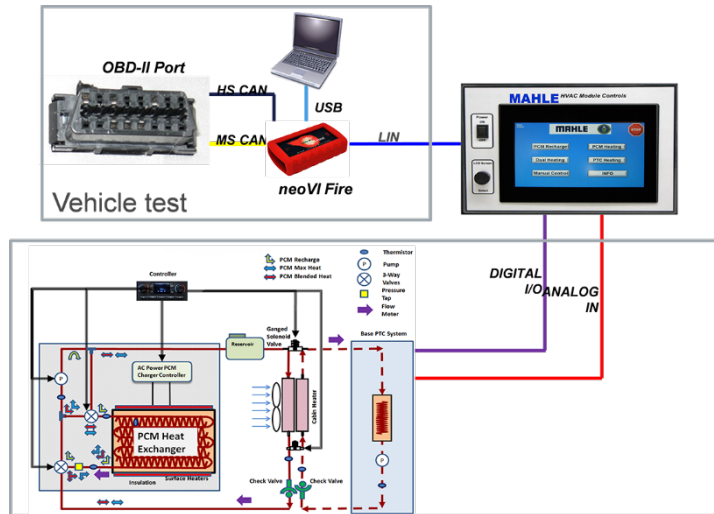


Figure II-29: ePATHS System Control Design

On the ePATHS side, the MAHLE controller controls the valves, pumps, and the HVAC blower to accomplish various modes of operation. Mainly, there are four modes of operation: PCM charging, PCM heating, PTC heating, and energy recovery (dual heating). As shown in Figure II-30, these modes of operation can be selected using the touch screen display. There is an additional manual mode of operation that allows direct control of any individual component in the system.



Figure II-30: Operation Mode Control

Figure II-31 shows the integrated charging system design that allows the vehicle traction battery and the ePATHS TES to be charged using the same EVSE (charger), power cable, and plug. A relay added to the

vehicle switches the 220V or 120V power either to charge the vehicle or to charge the PCM storage system, under the control of the MAHLE controller. When charging the PCM thermal storage, proper pilot signal is provided to the EVSE to enable power flow.

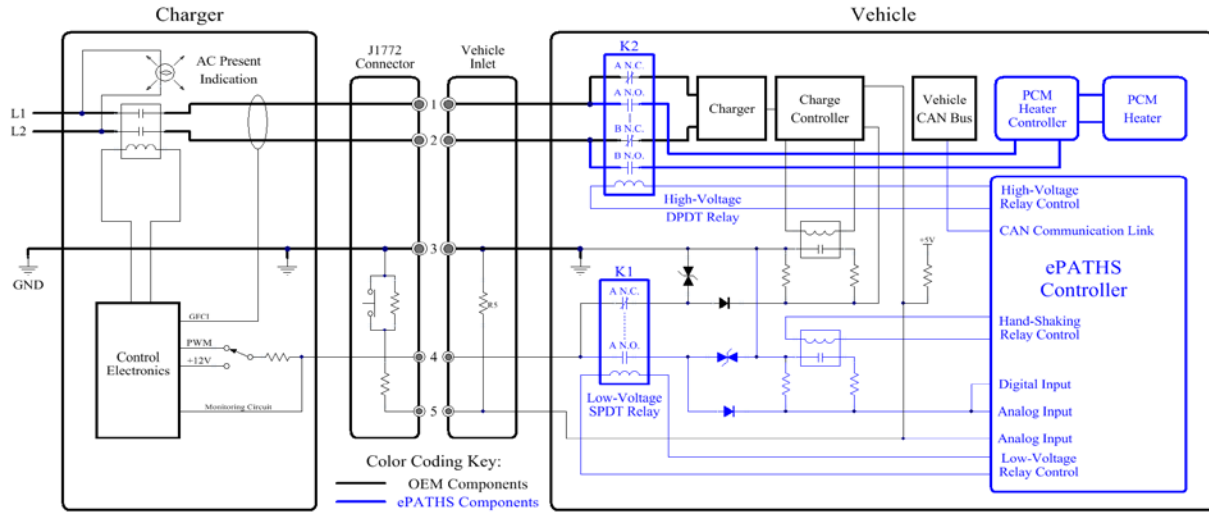


Figure II-31: Integrated PCM and Traction Battery Charging System

The electric power to the surface heaters are controlled by a Solid State Relay (SCR) controller (Figure II-32). The MAHLE controller output a Pulse Width Modulation (PWM) signal which is subsequently converted to a 4~20mA control signal for the SCR controller. The electric power to the surface heaters can be varied from 0 to 3 kW, based on availability and need. The electric power is measured and communicated to the controller for status monitoring.

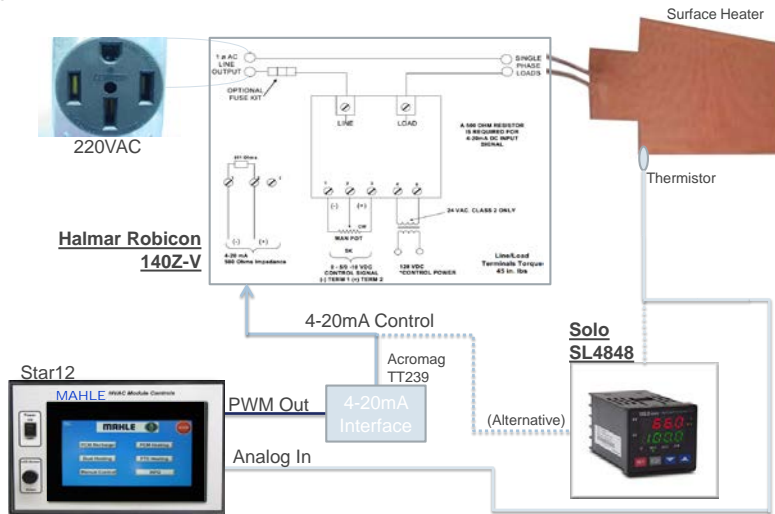


Figure II-32: PCM Charging Surface Heater Power Control

Bench Build

The ePATHS system has been integrated on a bench (Figure II-33) to support system functionality and performance testing. The test bench system uses a Ford Focus Electric HVAC module for air handling. The OEM heater in the module has been replaced with the MAHLE CapHX to support energy recovery operation. The coolant loop with pumps and valves has been instrumented with thermocouples, flow meters, and pressure transducers, with the pressure transducers intended for both safety monitoring and for pressure drop measurement. The MAHLE controller has been programmed with custom designed software to support various modes of testing. As part of the controller software, a State of Charge (SOC) calculation routine has been established with DPT-100 and will be updated for DPT-68. Initial debugging of the control software using a

quarter-sized PCM heat exchanger filled with a surrogate PCM material DPT-100 has been completed. A full sized PCM heat exchanger with DPT-68 will be used for final bench testing.

Test program has been established to investigate three areas of concern of the ePATHS system. The first is to confirm the time it takes to thermally charge the PCM heat exchanger, thereby confirming the heat transfer capability of the heat exchanger. Secondly, the bench will be tested to evaluate the VIP insulation's effectiveness in maintaining a low energy loss of less than 10% over an 8-hour period. Lastly, the discharging of the PCM heat exchanger to evaluate the amount of heat actually stored therein.



Figure II-33: ePATHS System Test Bench

Conclusions

Significant progress has been made by the MAHLE team on the ePATHS project since the 2014 annual progress report. The project has made the transition from establishing system and component specifications to prototyping components and integrating them into a system on the bench. Particularly noteworthy are the progresses in the following areas:

1. System architecture has been enhanced using CapHX to achieve deep energy recovery.
2. MATLAB Simulink component and system model has been established to provide analysis for PCM heat exchanger and ePATHS system optimization.
3. PCM synthesis and characterization yielding two promising candidates, DPT-68 and DPT-83 that demonstrates good melting temperature and high latent heat.
4. Full sized PCM heat exchanger design and build that contains PCM material and allows heat to be exchanged with a coolant stream. Initial testing indicates that the energy storage capacity is within specification and the heat transfer capability exceeds specification requirements.
5. System controls hardware and software has been developed to coordinate the operation of the ePATHS system.
6. Integrated PCM and traction battery charging system has been designed. PCM charging has been demonstrated on the bench with quarter-sized PCM heat exchanger.

The final system bench is expected to be completed in October. Detailed performance data will be collected and evaluated to lay the foundation for vehicle development in the year 2016.

II.5.C. Products

Presentations/Publications/Patents

1. MATLAB Simulink model for PCM heat exchanger
2. MATHLAB Simulink model for ePATHS system

II.5.D. References

N/A

II.6. Advanced Climate Control and Vehicle Preconditioning [DE-EE0006445]

John Meyer, Principal Investigator

Hanon Systems
One Village Center Drive
Van Buren Twp., MI 48111
Phone: (734) 710-5420
E-mail: jmeyer8@hvccglobal.com

Lee Slezak, DOE Program Manager

Phone: (202) 586-2335
E-mail: Lee.Slezak@ee.doe.gov

Start Date: October 2013

End Date: January 2017

II.6.A. Abstract

Objectives

- Increase the range of light duty electric drive vehicles through climate system load-reducing technologies
- Maintain occupant comfort
- Validate energy efficient technologies through the use of computer aided engineering (CAE) models
- Develop a commercial pathway toward utilizing the load-reducing technologies in light duty electric vehicles
- Integrate and validate technologies in a vehicle.

Accomplishments (FY 2015)

- Completion of system evaluation on bench
 - Both air-conditioning and heat pump operation tested
- Model Validation
 - 1-D system and 3-D cabin models fully validated
- Cold weather evaluation of early concepts on vehicle
- System architecture defined
- Hot weather testing of new concepts
- Enhanced components designed and fabricated
- Range extension prediction updated.

Future Achievements

- Evaluate new technologies on vehicle
- Budget Period 2 go/no-go presentation
- Vehicle integration, validation, and demonstration of final technologies
- Final range calculations.



II.6.B. Technical Discussion

Background

The transportation sector is an industry segment that must contribute to reducing petroleum dependence in the United States, as well as greenhouse gas emissions. One area with a high potential to decrease oil consumption and emissions is the electric drive vehicle. However, a barrier to its widespread acceptance is consumer “driving range anxiety.” Can an electric vehicle take me the distance I need to go? Increasing the range of electric vehicles is a key factor in achieving its mass market adoption. Since the climate system is the largest auxiliary load on electric drive vehicles, it is a prime candidate for onboard load reduction, which in turn increases vehicle range and, positively impacts consumer acceptance of electric vehicles. This is especially true in extreme hot and cold climates where range is significantly diminished by the climate system load.

Introduction

This project is exploring a technical approach to reducing the power required to operate the climate control system on a grid-connected electric drive vehicle, while still maintaining occupant comfort. It focuses on three main technology areas for climate system load reduction in an electric drive vehicle: thermal energy storage with preconditioning, refrigerant system performance and zonal cabin comfort.

Providing occupant thermal comfort can consume as much as 40 percent of the energy stored in GCEDV batteries, and thus improving the way comfort is achieved will result in extending the range of these vehicles. Achievements in electric vehicle climate load reduction has the opportunity to improve the current electric vehicle market, as well as open the market to climate zones previously unable to utilize these vehicles.

Approach

A three phase approach is being taken to define, design and demonstrate climate power reduction technologies. This method ensures positive progress and results of shorter term objectives, which are vital to overall project success, before moving between phases. During phase 1, the major project metrics were defined. These metrics will be used throughout the project to guide and measure the success of the technologies introduced. In addition, the computer aided engineering (CAE) models were built and correlated to data from baseline vehicle and system level testing. These validated models were then used to support trade studies that assess various technology alternatives. This phase ended with a decision on the most favorable technologies to be applied to the baseline vehicle architecture to improve range. In phase 2, the componentry necessary for each of the technology areas are designed, fabricated and verified through bench testing. Finally the vehicle is integrated with the new technology in phase 3 and the vehicle level impacts confirmed. The project is currently in phase 2.

Results

Highlights of FY2014 accomplishments include choosing to develop a system for the 2015 electric Kia Soul, defining the test conditions, wind tunnel testing the baseline vehicle, developing initial range improvement targets, initiating bench testing, and developing models for the thermal performance of the refrigerant system and the cabin.

The first major accomplishment of FY2015 was the completion of system evaluation, both air conditioning (A/C) and heat pump, on the bench. An extensive test matrix, spanning simulated ambient temperatures from 25°C to 50°C and 2,000 to 7,000 compressor RPM, was obtained for A/C operation. An even more extensive matrix, covering temperatures from +15°C to -10°C and compressor speeds of 1,500 to 5,000 RPM was obtained for heat pump operation. This data, along with wind tunnel data, was used to fully validate the 1-D system and cabin, 3-D cabin and comfort models. This is depicted in Figure II-34. The models were used to predict HVAC performance and passenger comfort. A comparison of the 1-D (lumped sum) transient cabin

model and vehicle data from a 43°C wind tunnel test is shown in Figure II-35. The predicted 3-D temperatures from the cabin model were then used as inputs to NREL's sensation and comfort models. The outcome for the 5°C warm up is shown in Figure II-36.

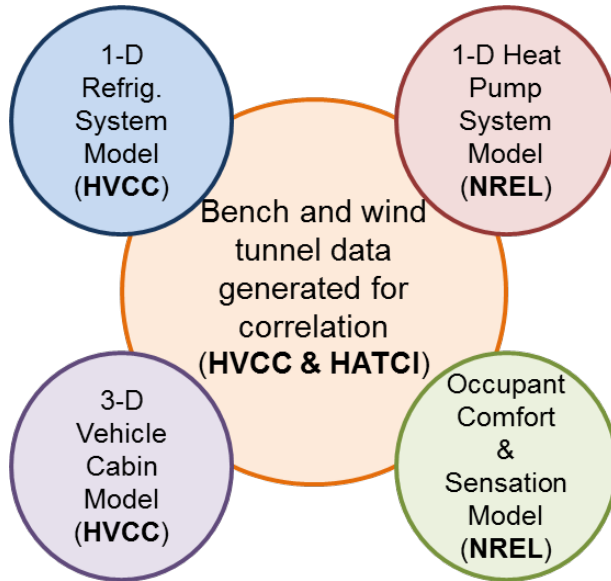


Figure II-34: Schematic Showing What Baseline Data was used to Validate

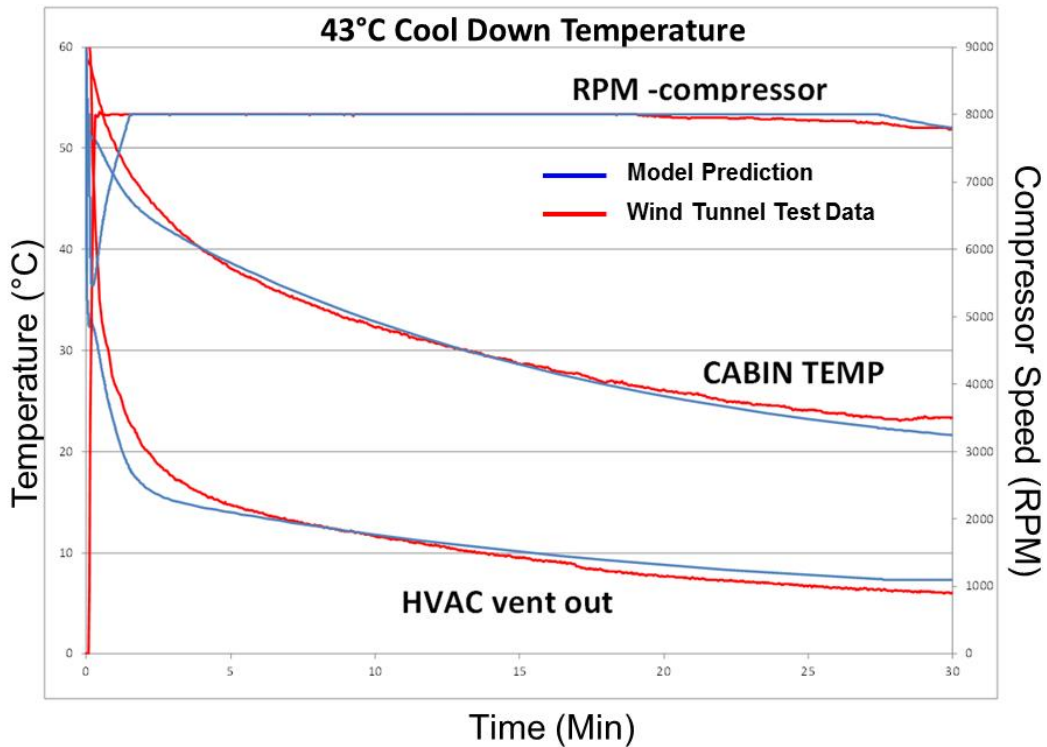


Figure II-35: Predicted and Actual Cabin Temperatures

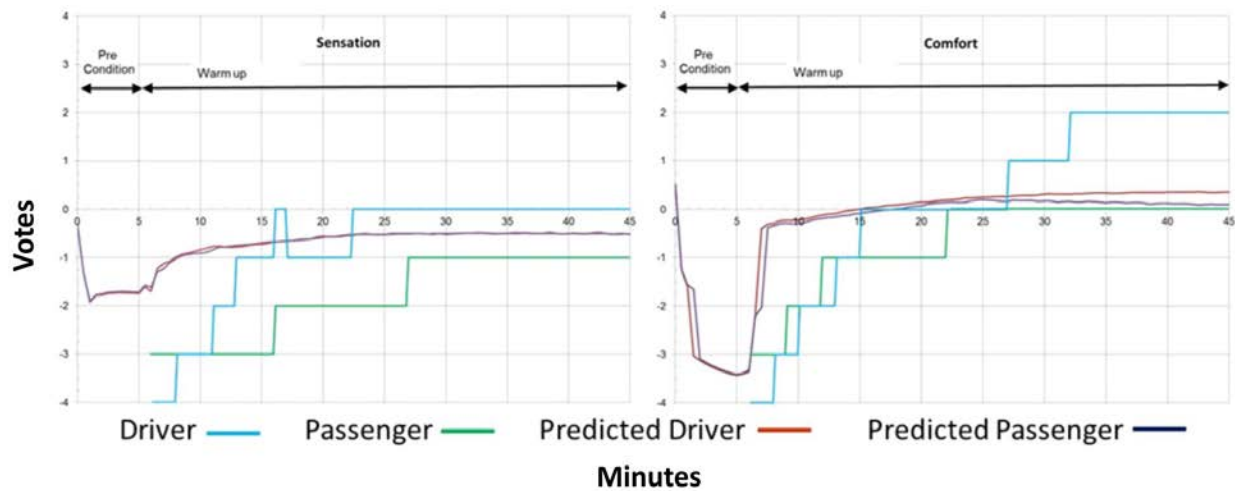


Figure II-36: Predicted and Actual Sensation and Comfort

Once the models were fully validated they were used to predict the impact of various technologies. From these predictions the individual technologies for the enhanced system were chosen. However, after some full system modeling it became clear that further enhancement was possible. After some additional system evaluation, architectures for both the refrigerant and glycol system emerged. These are shown in Figure II-37.

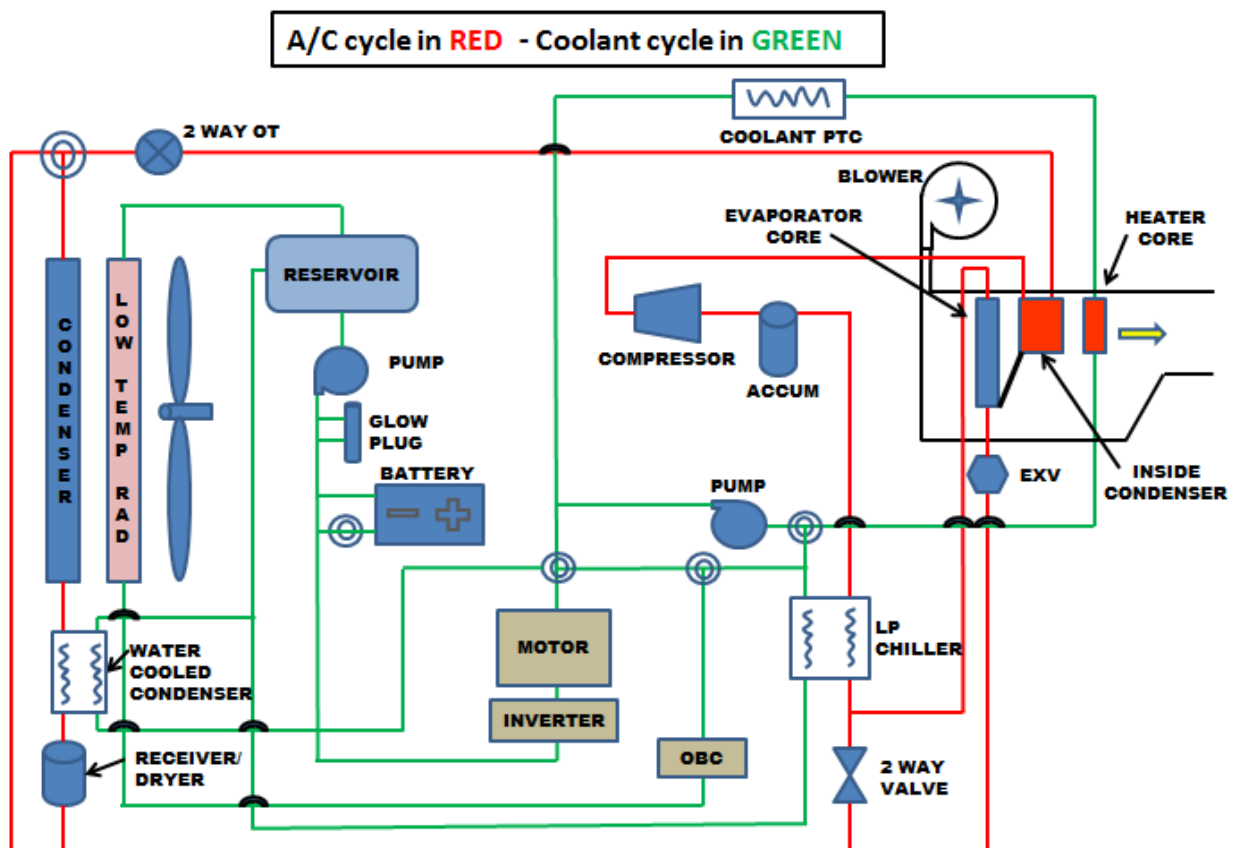


Figure II-37: Schematic of Refrigerant and Glycol Systems

The significant changes to the refrigerant system include increasing the effectiveness of the internal heat exchanger (IHX) and adapting the controls to take full advantage of the new hardware, removing the receiver/dryer (R/D) from the condenser, adding a water cooled condenser (WCC) before the external R/D (referred to as the modified liquid line), and increasing the effectiveness of the condenser and evaporator.

The modifications to the glycol loop include adding a heater core to the HVAC case, repositioning the chiller so it can be used to both harvest heat and store cold, adding a heater for thermal storage of heat, and introducing a control strategy that delivers the required amount of heat to the cabin while using minimal battery energy.

During the summer months of CY2015 the vehicle was modified so the concepts of an inside condenser bypass and the modified liquid line could be tested. Although the inside condenser bypass resulted in significantly cooler temperatures within the HVAC case, the impact on system capacity and power consumption was minimal. For this reason the concept of the hot refrigerant bypassing the inside condenser in AC mode was not pursued further. When cool glycol is available, the WCC in the modified liquid line allows for a drastic reduction in compressor power consumption.

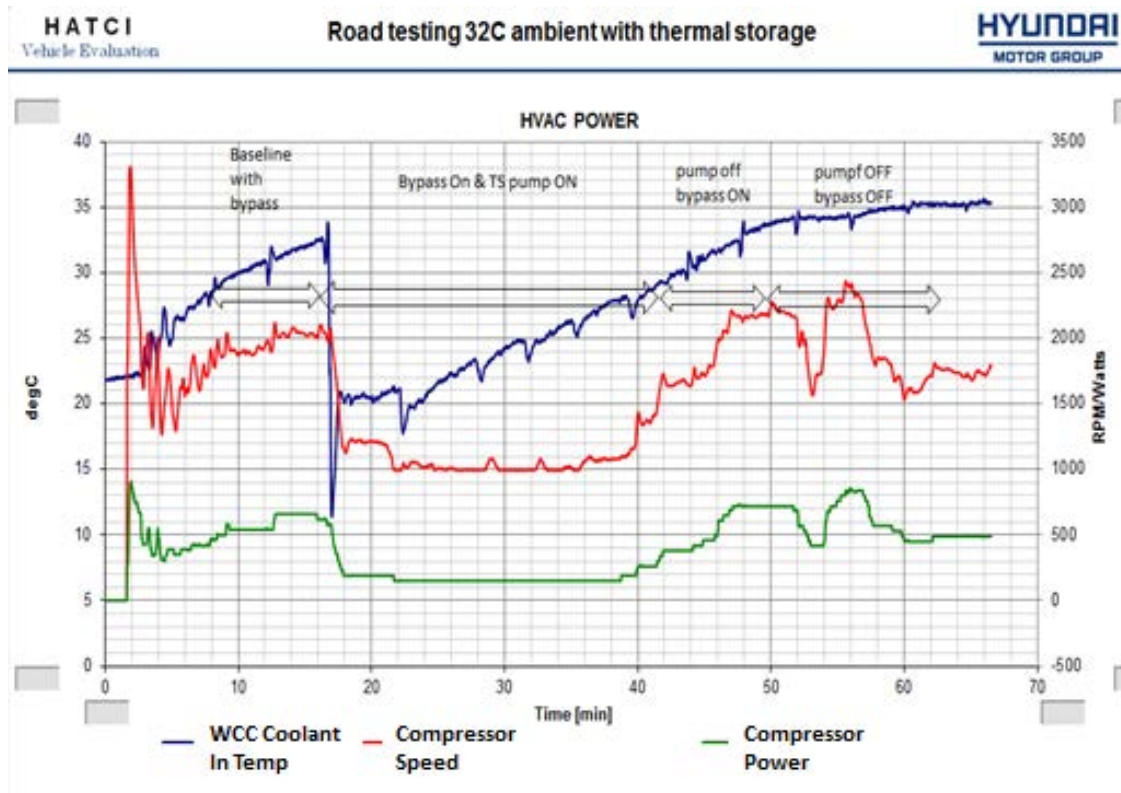


Figure II-38: Vehicle Test Showing Benefit of WCC with Thermal Storage

Figure II-38 shows the system response of passing cool glycol through the WCC. The initial glycol temperature is approximately 20°C, and that results in a compressor speed reduction from 2,000 to 1,000 RPM (light green line) and a power reduction from about 600W to about 200W (red line). The blue line shows the increase in glycol temperature entering the WCC as the thermal reservoir warms up.

While Hanon Systems and HATCI ran warm weather tests of air conditioning concepts, NREL was further developing their comfort model and running a heat pump model to evaluate cold weather options. The heat pump model includes four modes of operation. Mode one simply uses a small pump to circulate glycol through the warm thermal mass and deposits the heat in the cabin via the newly installed heater core. As the thermal mass cools, it will eventually no longer be warm enough to provide sufficient heat to the cabin. At this point the PTC comes on to ensure adequate heat. As the thermal mass cools further, mode three commences. In this mode the warm glycol is routed to the chiller and become the source for heat in heat pump operation. The PTC can be turned off. If the heat pump cannot provide sufficient heat to the cabin, the PTC also is used. Figure II-39 shows power consumption for providing cabin heat at 5°C and -18°C. For both cases the initial temperature of the thermal mass was 60°C. At 5°C, on the left, sufficient heat can be provided to the cab for approximately 20 minutes. The PTC comes on briefly before the compressor comes on in mode three. At -

18°C, neither mode one or mode two can provide adequate heat to the cabin. The controls will go directly to mode three.

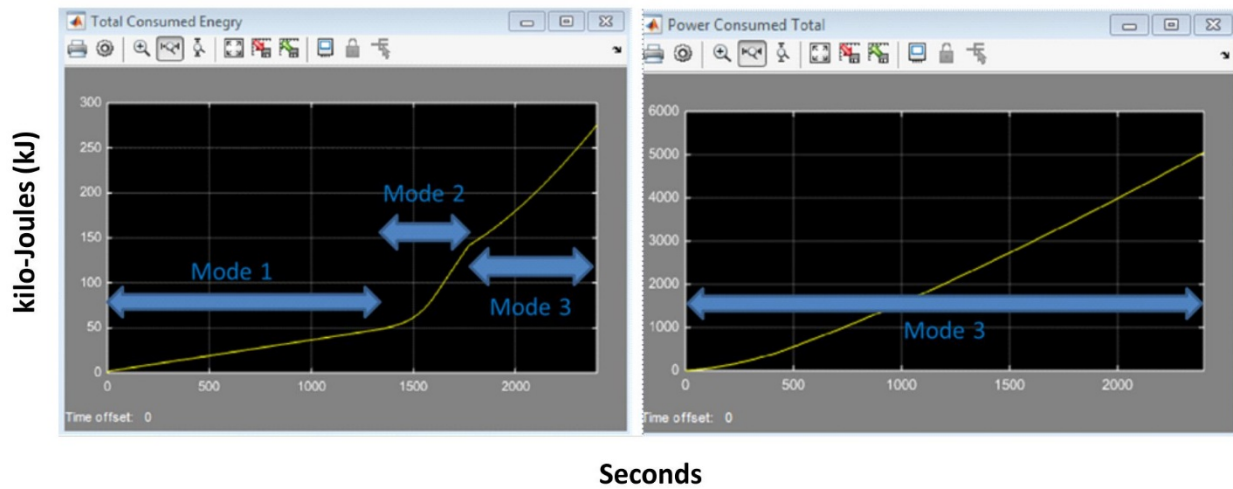


Figure II-39: Predicted Power Consumption during Heat Pump Operation at 5°C and -18°C

After summer evaluations are completed the vehicle will be retrofitted with "final" hardware. Testing during 4Q15 and 1Q16 will show us if the hardware needs further modifications before final testing. Based on both modeling and limited test data, updated range extension calculations were made. The output, shown in Figure II-40, reaches a high of 26% at -18°C and the remaining ambient conditions are all close to 10%.

Test Condition	August 2015 Assessment (%)
Cold 3 (-18°C)	26%
Cold 2 (-5°C)	8%
Cold 1 (5°C)	9%
Hot 1 (28°C)	8%
Hot 2 (32°C)	9%
Hot 3 (43°C)	12%

Figure II-40: Range Extension Predictions

Conclusions

In CY2015, the test bench matrix was completed for both A/C and heat pump, the data, along with vehicle data, was used to validate 1-D system and cabin models, a full 3-D cabin model, and the sensation and comfort models. The models were used to assess component contributions to range extension and system performance. Areas for additional enhancements were identified and strategies were developed to further increase vehicle efficiency. Two range-extending A/C concepts were evaluated in-vehicle, while NREL refined the heat pump model. The final technologies are currently being installed in the vehicle for testing this winter.

II.6.C. Products

Presentations/Publications/Patents

1. J. Meyer & J. Schneider, "Advanced Climate Systems for EV Extended Range." 2014 Department of Energy Annual Merit Review Conference, Washington DC, June 19, 2014.
2. HR Shim, T. Vespa, SH Kang, & J. Meyer, "Production Heat Pump System for a Battery Electric Vehicle." 2014 SAE Thermal Management Systems Symposium, Denver, CO, September 23, 2014.
3. J. Meyer & H. Crandall, "Advanced Climate Systems for EV Extended Range." 2015 Department of Energy Annual Merit Review Conference, Arlington, VA., June 10, 2015.

II.7. Unitary Thermal Energy Management for Propulsion Range Augmentation [DE-EE0006840]

Sourav Chowdhury, Principal Investigator

MAHLE Behr Troy Inc.
350 Upper Mountain Road
Lockport, NY 14094
Phone: (716) 439-2799; Fax: (716) 439-3168
E-mail: sourav.chowdhury@us.mahle.com

Mark Zima, Manager

Phone: (716) 438-4924
E-mail: mark.zima@us.mahle.com

David Anderson, DOE Program Manager

Vehicle Technologies Office
Phone: (202) 586-2335
E-mail: David.Anderson@ee.doe.gov

Start Date: October 1, 2014
End Date: October 31, 2015

II.7.A. Abstract

Objectives

- To design a unified, flexible, robust and efficient thermal management system which reduces the load on the vehicle traction battery, and therefore, increases the electric propulsion range of a state-of-the-art EV in -10°C ambient by 15% after meeting all thermal needs in the vehicle.
- To positively impact the environment by lowering refrigerant usage by about 50%.
- To design the system comprehending the packaging restrictions, long-term durability and manufacturing requirements already established in the automotive industry.

Accomplishments

- The Program Management baseline timeline was established. Also, sub-recipient contracts with Fiat Chrysler Automobiles (FCA), Norgren and NREL.
- The technical specification for the thermal systems including power electronics, battery management, and cabin climate control were established via a combination of written requirements from FCA and climatic tunnel tests of the vehicle conducted in Lockport, NY during February and March 2015.
- R-134a is in the production vehicle. However, R-1234yf was selected as the refrigerant of choice after consultation with FCA as this is the industry-wide refrigerant choice for future vehicles.
- The MAHLE electric compressor has been demonstrated to have capacity.
- Preliminary packaging of the UTEMPRA system was established under-hood by moving the 12V battery to the vehicle trunk.
- FCA has provided a Fiat 500e vehicle which was instrumented and 19 separate tests were conducted in the MAHLE climatic test tunnels in hot and cold ambients ranging from -10C to 43C.
- The first version of the component specifications were written based on the test results and performance requirements. The coolant system architecture was established through the teamwork of Norgren, NREL and MAHLE.

- The designs of 5 heat exchangers comprising the UTEMPRA system were established with CAD model generation. The final sizing of the heat exchangers will occur after the NREL model is executed in the remainder of Budget Period.
- NREL established a baseline vehicle system model and also initiated a UTEMPRA system model. The baseline system vehicle model is currently being validated against vehicle climatic test data. This model has calibrated component sub-models.
- The manifold proof-of-concept design and valve selection are key achievements in the development of the MMFC. The material system and subcomponents have been selected. Pressure drop tests of valves and the system are in progress.
- A very detailed specification for prototyping braze furnace was established. Key design features were identified to establish the special low oxygen environment necessary for flux-less brazing and to accommodate tall plate-type heat exchangers. Purchase order was issued to vendor.

Future Achievements

- Completion of a UTEMPRA simulation models by NREL
- Final sizing of heat exchangers following NREL simulation
- Completion of MMFC design and build and test of proof-of-concept part
- Laboratory evaluation of flux-less braze materials and selection of best material
- Continuation of braze furnace equipment build



II.7.B. Technical Discussion

Background

Grid Connected Electrical Drive Vehicles (GCEDV) are finding their limited and weather-dependent drive range, higher cost and limited battery life as the key hurdles to achieving wide consumer acceptance. There is a strong need to reduce the significant energy drain and resultant drive range loss due to auxiliary electrical loads of which the climate control is the predominant one. Studies show that thermal sub-systems together can reduce the drive range by as much as 40% under cold ambients such as below -10C. Currently, this heat is generated purely using resistive heating. Regaining a part of this range would significantly improve the attractiveness of electric vehicles (EVs) among consumers. This project develops a unifying strategy that satisfies diverse thermal and design needs of the auxiliary loads in EVs. This strategy will address the issues related to long term durability, robustness and mass manufacturing and cost.

Introduction

The UTEMPRA system comprises a semi-hermetic refrigeration loop and a coolant network for thermal energy distribution and waste energy harvesting. The refrigeration loop, shown schematically in Figure II-41 consists of an electric Compressor, a TXV, a Liquid-Cooled Condenser (LCC) and a Chiller, latter two have the same function as the condenser and the evaporator in a traditional refrigeration loop. Instead of exchanging heat with air, these heat exchangers exchange heat with coolant and, therefore, act as sources of hot and cold coolant streams.

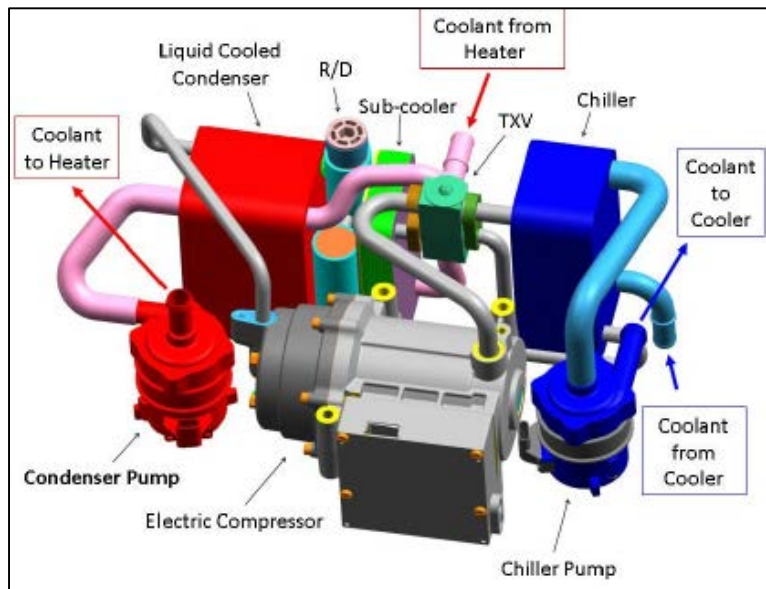


Figure II-41: Schematic of a sample configuration of the UTEMPRA refrigerant loop

The coolant network utilizes two coolant pumps and valve arrangements that help distribute the energy to the vehicle HVAC system to and other thermal loads (ESS, PEEM etc.). In the Cooling Mode, the cold coolant is conveyed from the chiller to the HVAC Cooler for cabin cooling and dehumidification. When needed, after the Cooler, this same coolant stream can be directed to cool the ESS. A Front-end Heat Exchanger (FEX) rejects the heat from the hot coolant coming from LCC to the ambient. In the Heating Mode, the hot coolant from LCC is directed to an HVAC Heater for cabin heating. Downstream of the HVAC Heater, this coolant can be directed to the ESS to maintain its temperature at normal levels.

Further, since PEEM produces waste heat, the coolant from LCC can pick-up this heat on its way to the HVAC heater thereby re-using the waste energy and improving the EV range. Also, in this mode, the cold coolant stream is directed to the FEX to absorb energy from the ambient. Therefore, the Cooling Mode is akin to the standard A/C operation while the Heating Mode is the Heat Pump (HP) mode. The heat exchangers, pumps and compressor will be sized to meet the full thermal needs of the vehicle.

With its unique flexibility in design and integration of the coolant architecture, the UTEMPRA system significantly simplifies and unifies the thermal management system in the EVs. It replaces the separate Condenser and a low temperature Radiator in the vehicle front-end with a single heat exchanger, thereby increasing its capacity and effectiveness due to higher available air pressure head. Further, it eliminates the need for separate refrigeration and/or coolant loop for the ESS and PEEM cooling and thereby significantly reduces the total refrigerant charge, pumping power, and overall system mass and cost. In summary, the UTEMPRA system serves as a thermal ‘platform’ within the EV architecture as it enables other future thermal & electrical load management strategies such as vehicle idle-stop energy savings, phase-change material (PCM) -based thermal storage, etc.

Approach

The GCEDV identified for this study is Fiat 500e all-electric vehicle. There are three thermal loops present in this vehicle that need to be combined into the UTEMPRA system: (a) Cabin air conditioning loop (b) Battery heating/cooling loop (c) Power electronics and electric motor cooling loop. This vehicle has a dual-purpose refrigerant vapor compression loop for cabin air cooling and providing active cooling to traction battery via a refrigerant-to-coolant heat exchanger (Battery Chiller). The vapor compression loop runs R-134a refrigerant and has an electric compressor, a standard refrigerant-to-air evaporator and standard thermal expansion valves (TXVs). Heating of the cabin air is achieved using a 5kW PTC-based electric air heater located in the HVAC module. In addition to being actively cooled by the Battery Chiller, the battery is also actively cooled by coolant circulating in a loop between the battery and a front-end battery radiator receiving forced ambient air flow across it. Figure II-42 below is a schematic of the thermal loops in this vehicle.

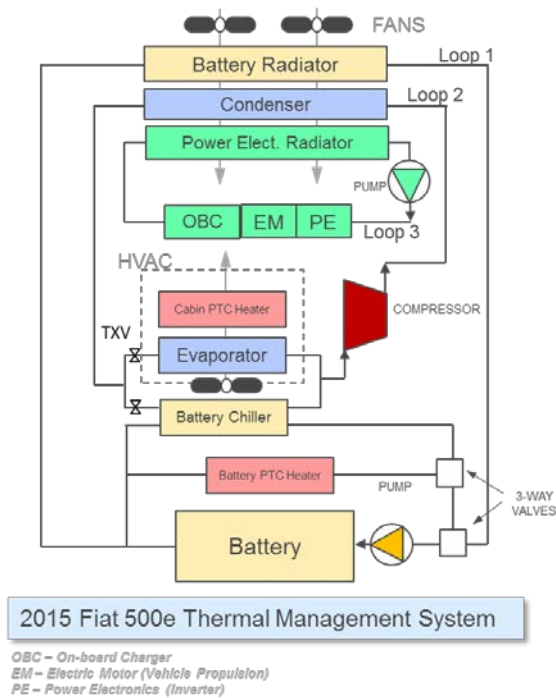


Figure II-42: Thermal management of the Fiat 500e.

Based on prior experience in heat pump loop design, vehicle requirements review and initial component flow versus pressure drop testing, the full coolant and refrigerant flow loop was created (Figure II-43).

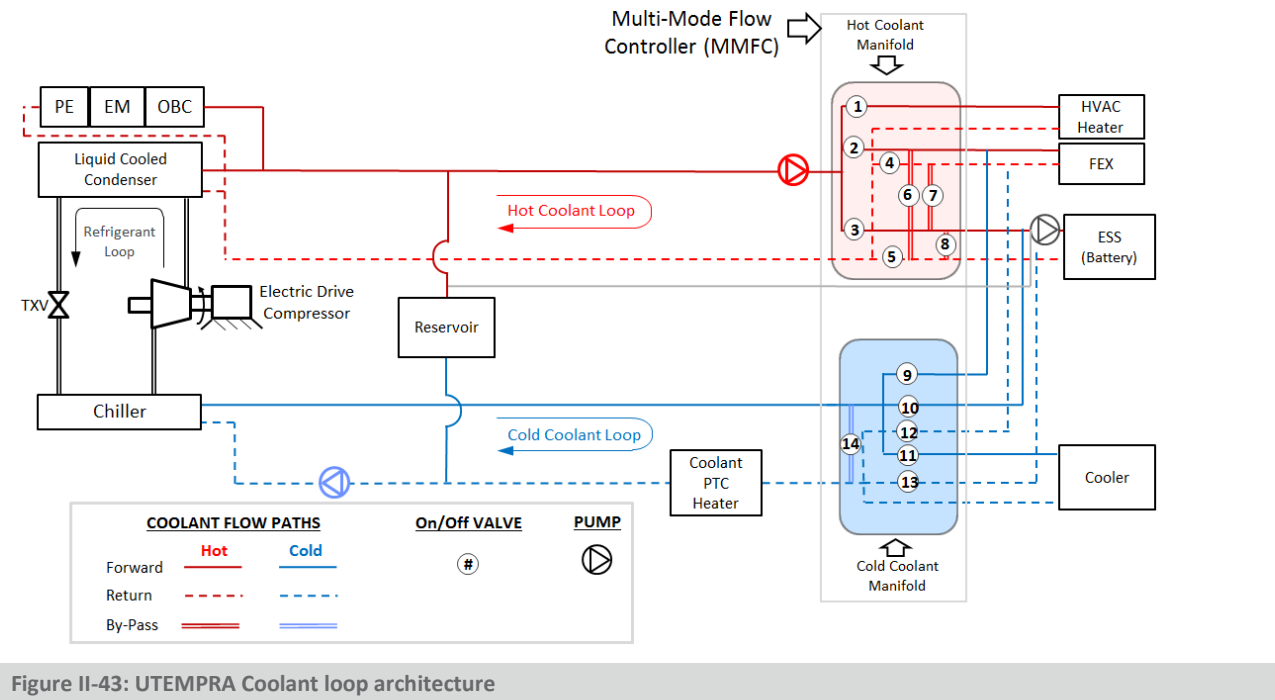


Figure II-43: UTEMPRA Coolant loop architecture

One part of the circuit is the refrigeration unit with a liquid-cooled condenser, chiller, and Thermostatic expansion valve (TXV) and electric-drive compressor. The coolant flowing through the liquid-cooled condenser is always hot (50 to 65C) while that through the chiller is always cold (5 to -15C). The Multi-Mode Flow Controller (MMFC) which is a fluid manifold with integrated "on-off" valves is located in the coolant network such that the refrigerant-to-coolant heat exchangers reside on its upstream side and the components which will receive the coolant flows from them are on its downstream side.

A PTC coolant heater which contains a temperature-controlled resistive heating element is required as, in extreme cold ambients (below -12C), the heat generated from heat pump mode may be insufficient or the heat pump may even be inoperable. In that case the PTC heater will be turned on to provide supplemental heat. This heat combined with the heat absorbed from the ambient by the FEX, if any available, will be ‘pumped’ up using the refrigeration unit to the hot-coolant circuit wherefrom it will be distributed to the destination components.

Results

At the beginning of the project a rough packaging of the UTEMPRA system components was designed in CAD to ensure that the different parts of the loop can be accommodated in the very tight under-hood space in the Fiat 500e. Figure II-44 indicates an approximate location of the UTEMPRA refrigeration unit. To accommodate it, the 12 Volt battery will be re-located to the rear of the vehicle with appropriate low electrical resistance extension cables.

To generate the performance heating and cooling targets for this vehicle, an important task in the Budget Period I was to complete baseline vehicle testing in MAHLE climatic wind tunnel. A test matrix (-10C to 43.3C) was jointly determined by MAHLE and FCA, our OEM partner, for the UTEMPRA performance targets. Tests specifically to determine baseline vehicle range will be conducted later in the project by FCA at their facility per their established procedures.

As an example of the performance data analysis, Figure II-45 and Figure II-46 show breath and vent temperature trends of a soaked vehicle under 43.3C (CD25) and -10C (HTRWU) ambient. UTEMPRA components are designed to meet these heating and cooling targets.

Based on the requirements outlined in the MMFC Specification document, the packaging constraints and the coolant system architecture, Norgren has generated a compact design of MMFC with separate hot and cold halves. This design has experienced two iterations, Gen I and II. Figure II-47 illustrates the Gen II design of the hot and cold halves of the MMFC proof-of-concept (POC) modules. At present, the MMFC-POC part is being machined and assembled at Norgren following which, preliminary tests to be conducted in MAHLE at the end of the BP-I.

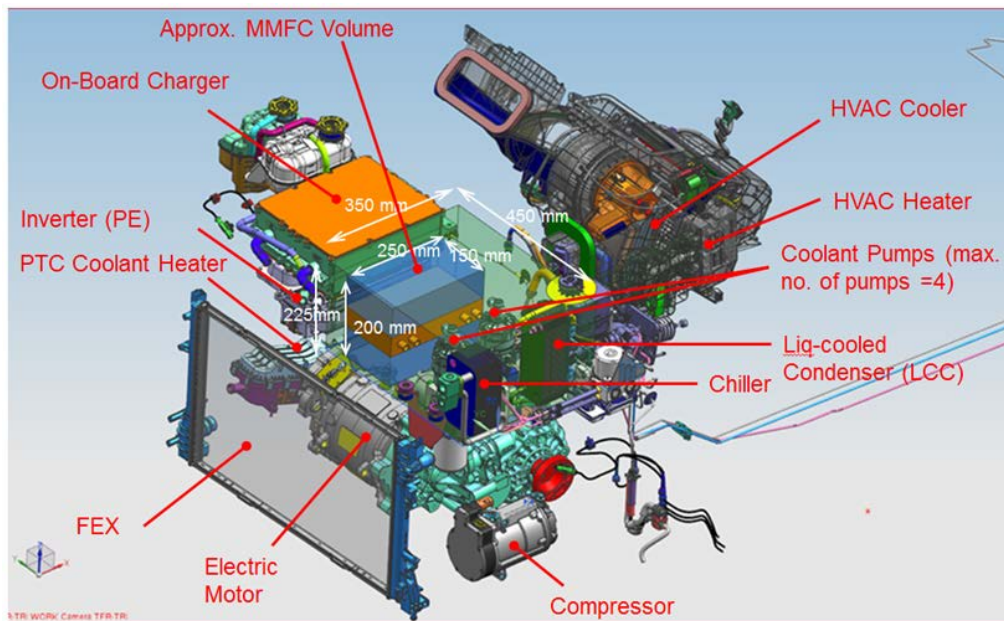


Figure II-44: Under-hood location of the UTEMPRA components

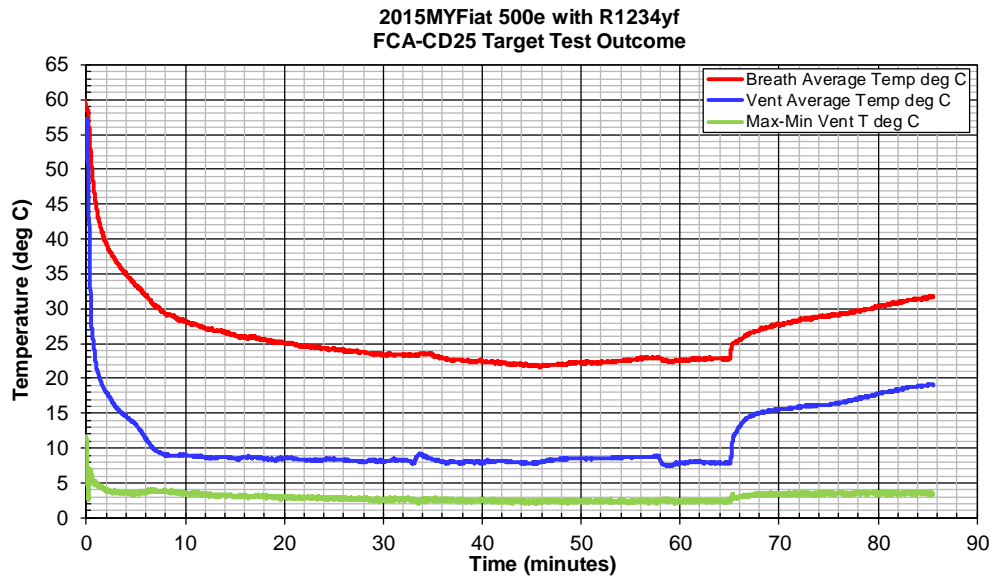


Figure II-45: CD25 trends of the breath and vent temperatures

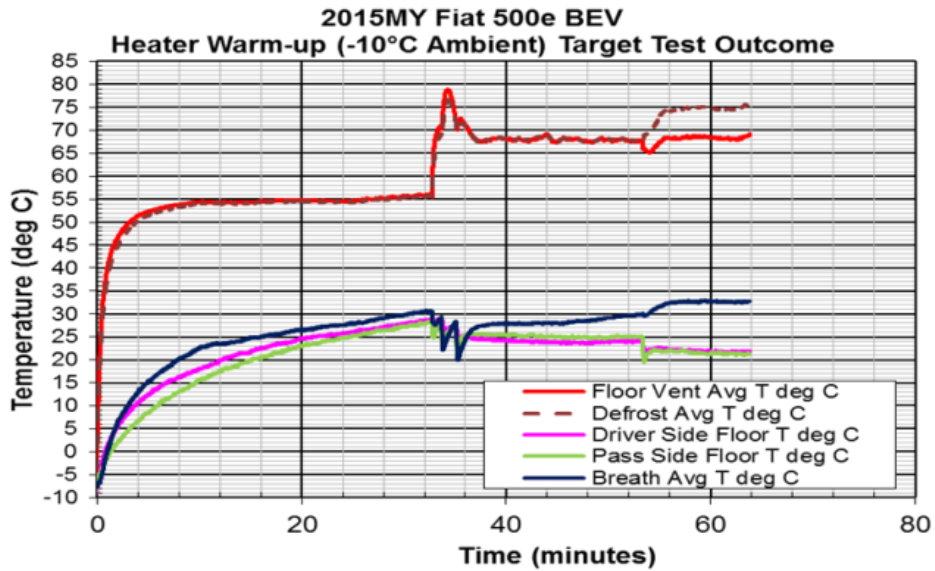


Figure II-46: HTRWU trends of the breath and vent temperatures

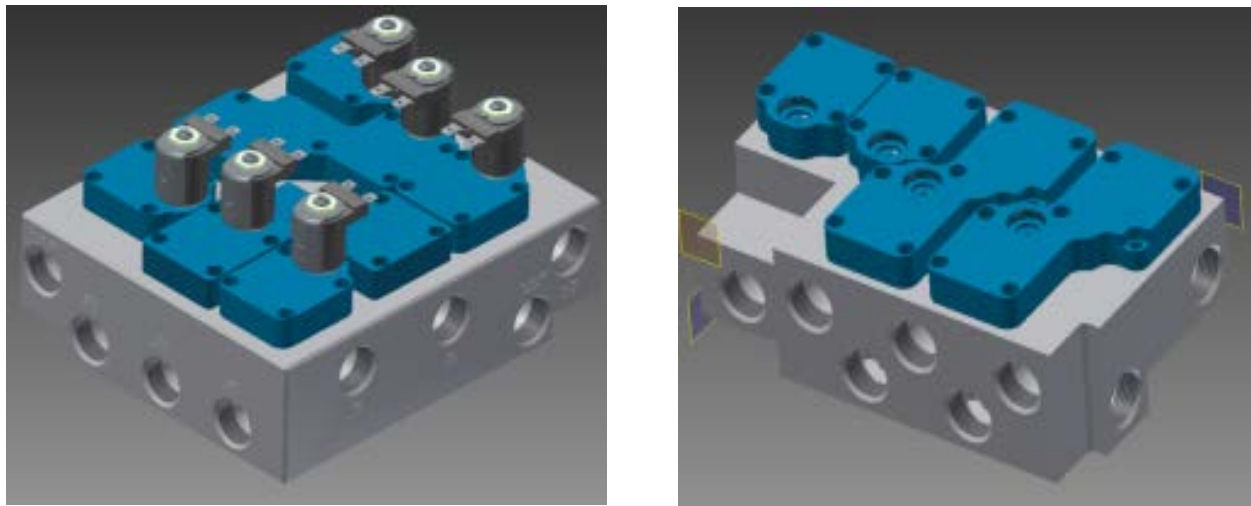


Figure II-47: MMFC design - hot and cold halves

Figure II-48 indicates the component designs completed in the BP-1 for the UTEMPRA system. NREL has completed the baseline vehicle simulation model in CoolSim program which was validated with baseline wind tunnel test data. NREL is currently creating a UTEMPRA simulation model to understand the coolant loop behavior and also to optimize the sizes of the heat exchangers.

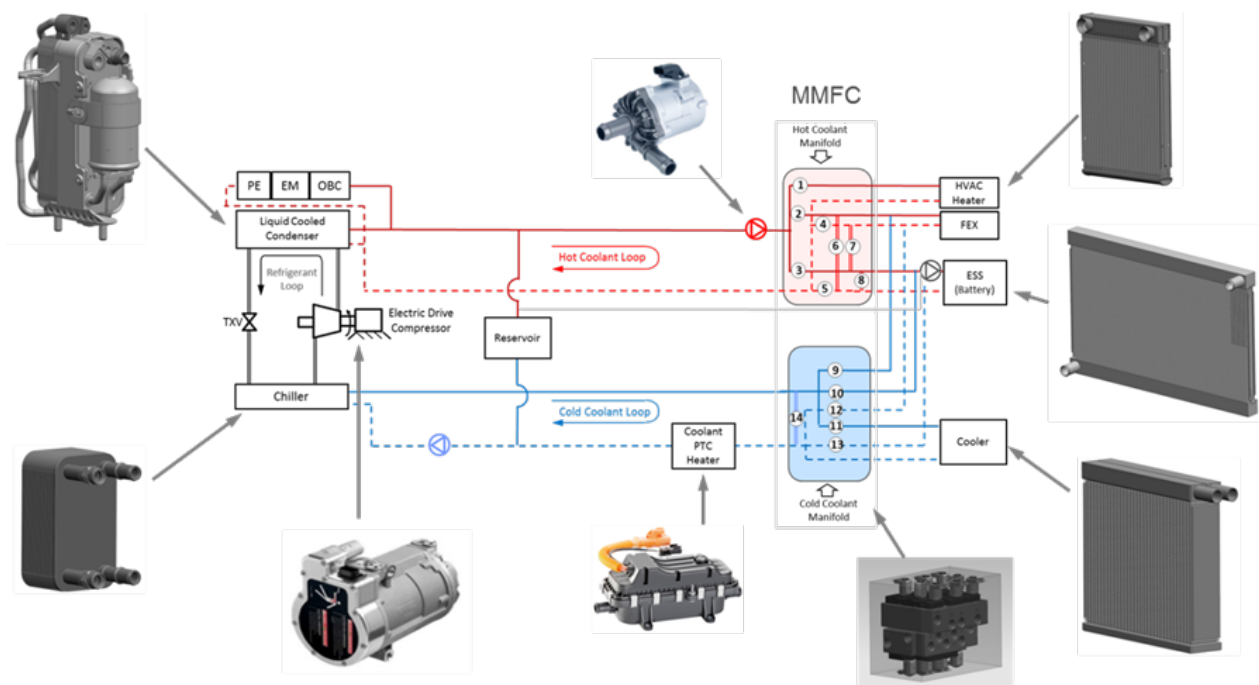


Figure II-48: Component designs of the UTEMPRA System

Conclusions

1. The UTEMPRA components can be packaged in the existing compact space of the Fiat 500e.
2. The total thermal load of the heating/cooling of the cabin, traction battery and power electronics/motor can be integrated into one system.

3. Initial engineering guidance cost estimate indicates the UTEMPRA system to be the same cost as the existing production thermal system on vehicle.
4. MMFC is a component of significant size and incorporating commonized valves will reduce power consumption and component cost.
5. The braze furnace design addresses the need for a well-controlled low oxygen environment capable of brazing stacked plate heat exchange.

II.7.C. Products

UTEMPRA System components will be the products that are the outcome at the end of the project:

(a) Heat Exchangers (Five types) (b) Compressor (c) Flow Controller (d) Control Algorithm and Software

Presentations/Publications/Patents

None

II.7.D. References

None.

POWERTRAIN

II.8. Multi-Speed Transmission for Commercial Delivery Medium Duty PEDVs [DE-EE0006843]

Bulent Chavdar, Principal Investigator

Eaton Corporation
 W126N7250 Flint Drive
 Menomonee Falls, WI 53051-4404
 E-mail: BulentChavdar@Eaton.com

Jason Conley, DOE Program Manager

U.S. Department of Energy's (DOE)
 National Energy Technology Laboratory (NETL)
 Phone: (304) 285-2023
 E-mail: John.Conley@NETL.doe.gov

Start Date: October 1, 2014
 End Date: December 31, 2017

II.8.A. Abstract

Objectives

- The objective of this project is to develop a multi-speed transmission for medium duty electric vehicles to expand the vehicle operating performance and range. The project addresses the following technical barriers:
 - The public acceptance of electric vehicles will be increased with a transmission
 - The performance gap between Electric Vehicles (EVs) and Internal Combustion Drive Vehicles (ICDVs) will be reduced with a transmission
 - The concept transmission will be reliable, affordable, scalable and low weight
- The proposed multi-speed transmission will narrow motor operation to the peak efficiency region thereby increasing the electric powertrain efficiency. Further, it will enhance customer satisfaction by improving vehicle acceleration, top speed and gradeability over the baseline as listed in Table II-7.

Table II-7: Performance targets

Characteristic	Units	Smith Baseline 10t GVW with SS gearbox	Current Project Targets with MS transmission
Top speed (on flat)	mph	54.5	59
Energy efficiency/range	mpge	30.3 on UDDS 41.8 on CILCC	33.9 on UDDS 44.7 on CILCC
Acceleration (0-30 mph)	s	18.7	18
Acceleration (30-50 mph)	s	69.1	43
Gradeability (top speed on 2% grade)	mph	38.8	41.3
Startability (Maximum grade upon which vehicle launching from rest allows motor reaches maximum power in 3 seconds)	% grade	9.8%	20%

Accomplishments (BP1, Q1-Q3)

- Vehicle performance requirements defined based on operational data and analysis.
- Market segments, potential volume projections, scalability, and cost targets for penetration are identified.
- Baseline vehicle model development was completed. Component and vehicle models were integrated and validated for the baseline vehicle.
- Breadboard transmission platform selection was completed.

Future Achievements (BP1-Q4, BP2)

- Complete preliminary transmission design. Prototype gearbox design and configuration to meet performance requirements.
- Complete breadboard transmission gearbox design. Assess and modify the gearbox housing and assemblies for procurement and build.
- Complete prototype transmission build.
- Complete transmission and controller shakedown testing at Eaton.
- Complete integrated powertrain hardware-in-the-loop testing at Oak Ridge National Laboratory. Tuning and validation of shift strategy. Complete steady-state and transient HIL tests. Improve deficiencies.

II.8.B. Technical Discussion

Background

The EV Everywhere Grand Challenge aims at realizing PEDVs that meet or exceed the performance of ICDVs on the basis of cost, convenience, and consumer satisfaction. The average range of a PEDV is approximately one-third the range of an ICDV. The Eaton team proposed to develop a multi-speed transmission that will help close the range gap by increasing the electric powertrain efficiency. Customer satisfaction will also improve when vehicle acceleration, the top speed, and the gradeability improve significantly over the baseline vehicle.

Successful completion of the project will set a course for improving quality of life in three areas by overcoming key challenges in the gearbox for commercial-delivery, medium-duty, plug-in electric drive vehicles: It will reduce US dependency on foreign oil through the use of electric driven propulsion instead of fuel driven. It will reduce health risks by replacing tailpipe emissions in densely populated city centers. Finally, it will improve the performance-cost basis to meet or exceed the expectations of the targeted medium duty vehicle fleet owners and the independent customers.

Introduction

The project will develop a new multi-speed gearbox to match the performance characteristics of an electric motor. The gear ratios, shift strategy, cost, and weight will be optimized to provide a commercially feasible solution to meet medium duty electric vehicle requirements for starting torque, top speed, acceleration, and efficiency.

Eaton has assembled the appropriate team to develop a multi-speed transmission for medium duty (MD) PEDVs. The team includes the leading transmission developer for MD and heavy duty (HD) vehicles (Eaton), the leader in MD PEDVs (Smith Electric), and two critical testing laboratories (ORNL and NREL). Eaton will design transmission hardware and controller, integrate the transmission with power electronics, conduct motor drive optimization study, prepare manufacturing plan and provide a breadboard transmission. ORNL will perform vehicle level simulations, powertrain loop integration, component testing and HIL testing. NREL will conduct duty cycle analysis, and vehicle integration and testing.

Approach

The project will be conducted in three budget periods:

Budget Period 1: Technology Development: The high-level vehicle powertrain models will be used to optimize candidate transmission architectures and ratios along with a variety of traction motor characteristics for concept selection. The detailed driveline design and component dynamics will be chosen to meet medium duty electric vehicle requirements. The optimized solution will include a multi-speed transmission, a permanent magnet motor, and an integrated bidirectional shift strategy.

Budget Period 2: Technology Development and Prototype Demonstration: The prototype transmission and the controller will be built and tested in a laboratory to meet project requirements.

Budget Period 3: Technology Integration, Testing, and Demonstration: The transmission will be fully integrated into a demonstration vehicle. The vehicle will be tested and compared with the baseline vehicle performance. Transmission development will continue with the vehicle testing to further refine the transmission.

Results

Baseline vehicle and drive cycle information

Smith provided the simulation parameter requirements document to Eaton. The full information set included: Weight parameters, driveline parameters, wheel parameters, vehicle drag parameters, motor parameters, battery parameters, drive system overview and powertrain interface schematic, drive controller power limiting description, baseline vehicle acceleration test data at various gross vehicle weights, sample high resolution drive cycle with a mix of urban and highway driving to serve as source for model calibration.

NREL's Drive Cycle Rapid Investigation Visualization and Evaluation (DRIVE) tool and database of Smith EV drive cycle data were leveraged to identify appropriate standard chassis dynamometer test cycles for evaluating the performance of both the baseline and project vehicles. As part of the DRIVE analysis, NREL performed three additional exploratory analyses to examine individual subsets of data and compare them to the overall vehicle population. First, a drive cycle analysis was performed on the entirety of the Smith vehicle data contained within NREL's Fleet DNA database. Next, a comparative analysis of different generations of Smith technology was performed, to explore whether or not there are any identifiable differences in vehicle operation between the first and second generation Smith EV platforms. In addition to performing a comparative analysis of technology vintages, an additional comparative analysis was performed to examine operating differences within the Smith dataset based on final vehicle chassis configuration. In this case, the analysis was to compare the operation of step vans with cab body builds. Finally, to explore whether or not the Smith EV data was representative of Step Vans and cab trucks on a whole, the results of the previous three analyses were compared to past NREL Fleet evaluation projects and the standard chassis test cycles that were identified and tested.

Baseline vehicle model development

The vehicle system modeling tool Autonomie® was used to create the vehicle model architecture of a battery electric medium duty truck (shown in Figure II-49).



Figure II-49: Autonomie representation of battery electric medium duty truck architecture

Each component model was parameterized based on data provided by Smith Electric. Component models and parameters were integrated in the vehicle architecture.

A generic Autonomie Vehicle Supervisory Controller (VPC) was also implemented and calibrated to coordinate the vehicle electric propulsion drive. Specific features were added such as current limitation set to 240A for traction purposes and power limitation during regeneration set to 50kW.

The baseline vehicle also includes a generic Autonomie driver model capable of following speed profiles. Its speed controller parameters were tuned for the medium duty truck.

Proper operation of the vehicle was verified by operating the vehicle on standard drive cycles such as a Hybrid Truck Users Forum Parcel Delivery Class 4 (HTUF4) and Orange County Bus Cycle (OCBC) cycles to make sure that it can follow those speed profiles.

Baseline model validation

NREL provided standard drive cycles, Smith representative drive cycles and on-route drive cycles with grade information (#10000 and #10028). The efficiency of baseline vehicle with single speed gearbox was evaluated for all of these drive cycles and summarized in Table II-8. Furthermore Smith Electric provided experimental test data to validate the baseline model. The experimental data yielded a good match with the model while re-using component specifications and coast down parameters provided by Smith Electric. Acceleration tests were simulated on a 10T baseline vehicle. Results are listed in Table II-9. Top speed is 54.5mph after 190sec as shown on Figure II-50.

Table II-8: Energy efficiency for single speed vehicle. (mpgde stands for mile per gallon diesel equivalent and does not include the on-board charger efficiency)

	Single speed vehicle efficiency [Wh/mile]	Single speed vehicle efficiency [mpgde]
UDDS Truck cycle (10T)	1249	30.1
CILC cycle (10T)	889	42.3
Smith Representative Box Truck Cycle (10T)	1146	32.8
Smith Representative Step Van Cycle (10T)	1129	33.3
Smith Overall Representative Cycle (10T)	1147	32.8
NREL Cycle #10000	1045	36.0
NREL Cycle #10028	997	37.7

Table II-9: Acceleration times for 10T baseline vehicle

Speed Intervals	Time [s]
0-30mph time	18.8
0-40mph time	38.1
0-50mph time	88
30-40mph time	19.3
30-50mph time	69.2

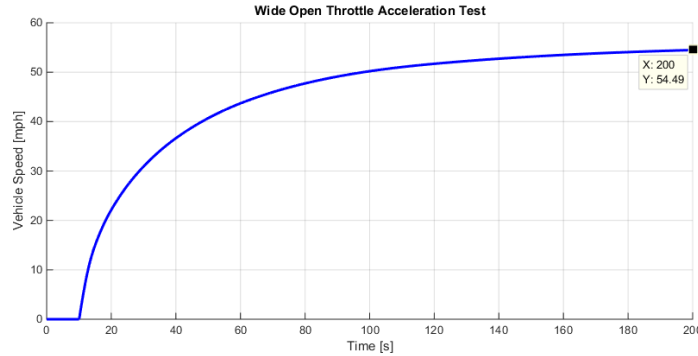


Figure II-50: Wide open throttle acceleration to max speed.

Gearbox Model Development

A gearbox model is developed that replaces single gear reduction of the base-line model. The first gearbox model is based on Automated Manual Transmission (AMT) technology. The efficiency of gears is the same as single speed gearbox used for the baseline except for the direct drive (1:1 ratio) which is 99.5% efficient. The goal of gearbox optimization is to find the number of gears and ratios in the gearbox as well as appropriate Final Drive (FD) gear ratio. The following results are based on a 3-speed transmission. Gear 1 has high ratio and is engaged only at grades higher than 15%. In lower grades the vehicle is launched at the second gear. Gear 3 is direct drive that is 1:1 ratio.

The acceleration performance and top speed results are shown in Figure II-51. The 0-50 mph acceleration is not sensitive to final drive ratio but improves as the gear-2 total ratio increases. With high gear 2 ratio, the shift to gear 3 happens quickly and since gear 3 is more efficient than gear 2, this means higher power to wheels and better acceleration. The top speed is close to 60 mph with final drive ratio 6.9. The improvement of acceleration and top speed over the base line is achieved by down speeding the motor and driveline which results in lower losses in the motor and gear.

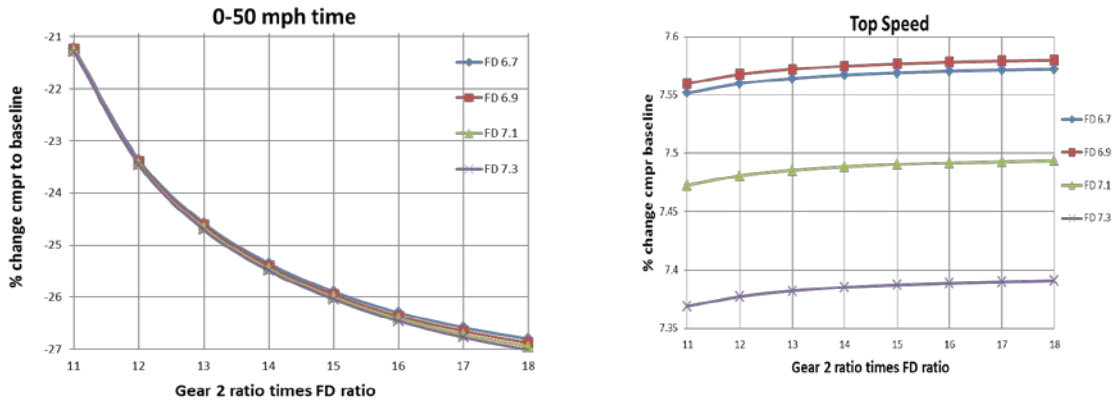


Figure II-51: The Acceleration Performance and Top Speed Results

These figures show acceleration performance and top speed of the Smith vehicle with 3-speed transmission for different FD and gear 2 ratio values (gear 1 is used for high grade launch). The x-axes are the total gear 2 ratio (gear 2 ratio multiplied by final drive). The y-axes show the percent change of acceleration performance and top speed of Smith vehicle with 3-speed transmission compared with the baseline vehicle.

Next we chose gear 1 ratio based on the startability (launch acceleration) performance on a high grade road. We observed that with decrease of gear 1 ratio, the vehicle acceleration becomes more sluggish because the torque to the wheel is lower. For acceptable startability any ratio greater than 3.5 is acceptable. With gear ratio 4.3 the vehicle is capable of launching with acceptable acceleration on grades up to 22.5% while the baseline capability is limited to 9.8%.

The vehicle with 3-speed transmission has improved gradeability that is higher top speed from 0 to 3% grades as compared to the baseline vehicle as shown in Table II-10. Multi speed transmission does not have any impact on the top speed beyond 3% grades since the electric motor does not operate at high rpm lower efficiency region beyond 3% grade on baseline vehicle.

Table II-10: Comparison of gradeability performance of baseline vehicle with singles speed gearbox and vehicle with 3 speed transmission.

Grade %	Baseline Vehicle with single speed gearbox Top speed (mph)	Vehicle with 3-speed transmission Top speed (mph)
1	46.6	50.4
2	38.8	41.3
3	32.6	32.7

Conclusions

- Project is on schedule. All required project milestones have been met to date.
- Baseline vehicle model development was completed.
- Baseline vehicle model was created and correlated at ORNL and Eaton.
- Model was validated with on-route data of 10t Smith although not a perfect match.
- Transmission concept development is in progress

- VoCs and CWNs of MD-EV were identified and ranked. Discussions on the functional requirements of transmission continue.
- Optimization studies with 2 and 3 speed automated gearbox completed. 4-speed optimization studies with automated and automatic gearboxes continue.

II.8.C. Products

Presentations/Publications/Patents

1. 2015-DOE-AMR PowerPoint Presentation at Arlington, Washington, on June 11, 2015. Project ID-vss161, Multi-Speed Transmission for Commercial Delivery Medium Duty Plug-In Electric Drive Vehicles.

II.8.D. References

1. No references.

II.9. Integrated Boosting and Hybridization for Extreme Fuel Economy and Downsizing [DE-EE0006844]

Vasilios Tsourapas, Principal Investigator

Eaton Corporation
 W126N7250 Flint Drive
 Menomonee Falls, WI 53051-4404
 Phone: (248) 226-7114
 E-mail: VasiliosTsourapas@Eaton.com

Jason Conley, DOE Program Manager

U.S. Department of Energy's (DOE)
 National Energy Technology Laboratory (NETL)
 Phone: (304) 285-2023
 E-mail: John.Conley@NETL.doe.gov

Start Date: October 1, 2014
 End Date: December 31, 2017

II.9.A. Abstract

Objectives

- The objective of this project is to develop, demonstrate, and evaluate commercialization of a highly efficient downsized engine by electrification of the air delivery and waste heat recovery system and optimizing energy usage to achieve a 20% fuel economy improvement at a commercially viable cost.

Accomplishments

- Developed and tested a roots based expander for diesel engines at rated temperature and showed that the system operated efficiently with no failure
 - Thermal analysis completed
 - Stress analysis completed
 - CFD analysis for porting completed
 - System designed, built and tested
 - Preliminary dyno testing completed
- Model based analysis of the EAVS/WHR System completed and identified right application for the proposed technology
 - GT power system level model completed
 - Model based analysis for varying applications (passenger and commercial) and engines (gasoline and diesel of varying displacements)
 - Identifying best application for EAVS/WHR combination
 - Developed preliminary control strategies for the system

Future Achievements

Next steps include:

- Setting up target diesel engine on dyno
- Baseline vehicle testing
- Design, integration and testing of EAVS/WHR hardware on new engine



II.9.B. Technical Discussion

Background

Improvement in fuel economy in the automotive market is driven both by regulations (EPA, CAFÉ, EURO etc.) as well as the increasing gas prices. Consumers demand cost effective solutions that can reduce vehicle fuel consumption and which, at the same time, meet their performance (vehicle acceleration) requirements. A primary solution to reduced fuel consumption is engine downsizing and downspeeding; a smaller and slower engine will exhibit fewer friction losses and higher operating efficiency since it will be forced, for the same vehicle mass, to operate at a relative higher percentage of load.

Introduction

The project will develop, build and test a highly efficient and fully controllable technology for optimizing engine energy usage. Through energy usage and breathing optimization of a downsized and downsped engine a fuel economy (FE) improvement of more than 20% will be targeted over an already turbocharged and downsized engine while maintaining or improving performance, at an industry accepted cost point. Recovering both brake and exhaust energy and using it in a variable ratio boosting system (rather than a traction system) offers cost-effective, high impact hybridization independent of the drive cycle.

Approach

The project shall be conducted in three budget periods:

Budget Period 1: Model-based System Analysis and Individual Technology Risk Mitigation

The activities will focus on evaluating integration of the two technologies in a model-based environment where the architecture and the component sizes will be optimized. Multiple integration schemes will be examined that combine Electrically Assisted Variable Speed (EAVS) supercharger and Waste Heat Recovery (WHR) in different ways in a model environment. The sizes of the motor, generator, and battery will be optimized. The component risks will be addressed, such as WHR high temperature durability, by designing and testing WHR hardware on an engine.

Budget Period 2: Design and Engine Dynamometer Testing of System and Optimize Controls

The second budget period will focus on designing and integrating the two technologies on a full engine dynamometer. The engine with EAVS and WHR will be designed and tested in preparation for transferring and installing the system in a demonstration vehicle. The engine with the EAVS/WHR system will be calibrated on the dynamometer for emissions, performance and fuel economy. In parallel, the vehicle-level supervisory controls will be optimized and ready for transfer to the demonstration vehicle.

Budget Period 3: Vehicle Demonstration and Testing; Commercialization Analysis

The third budget period will focus on integrating and testing the demonstration vehicle against the fuel economy, emissions, performance, and cost targets. The engine developed in budget period 2 will be transferred to the demonstration vehicle. The vehicle will be finalized and calibrated on a chassis dynamometer and tested. The cost estimate, commercialization, and manufacturing readiness will be analyzed and the next steps to production will be finalized.

Results

Tasks 1.1

The vehicle platform and engine selected was the Chevy Cruze with the 1.4L turbo engine and a 1.2L engine for the EAVS/WHR technology demonstration. The vehicle has been purchased and is undergoing instrumentation for baseline testing. The vehicle is being outfitted with pressure and temperature sensors as

well as a data acquisition system. Once instrumentation is complete, the baseline vehicle will be tested at a chassis dyno in order to establish baseline performance and fuel economy. Once baseline testing is complete, the engine will be removed from the vehicle and modified to a 1.2L and outfitted with EAVS/WHR by the end of the year.

Furthermore the vehicle is being used in order to design the mounting hardware and piping between the engine and the EAVS/WHR components.

Task 1.2.1

The vehicle model is in place (model parameterization depending on the final vehicle selection) and the EAVS model has been developed for an R410 TVS supercharger. To develop the expander (WHR) model, we are performing analytical work to evaluate the pulse energy that can be recovered via a roots expander. This work will feed into an expander model that will be integrated with the overall vehicle level model.

Furthermore, the integration of preliminary control algorithms is in progress where the system operating modes are defined and conditions for mode switching are evaluated. The controls are being developed in Matlab Simulink while the vehicle model will be in GT Power and the two will be co-simulated. A preliminary interface between the controls and the system model has been defined as shown in Figure II-52. The goal is that the model based controls that are developed under this task will eventually be utilized for the demonstrator engine and vehicle via auto-code generation in Phases 2 and 3.

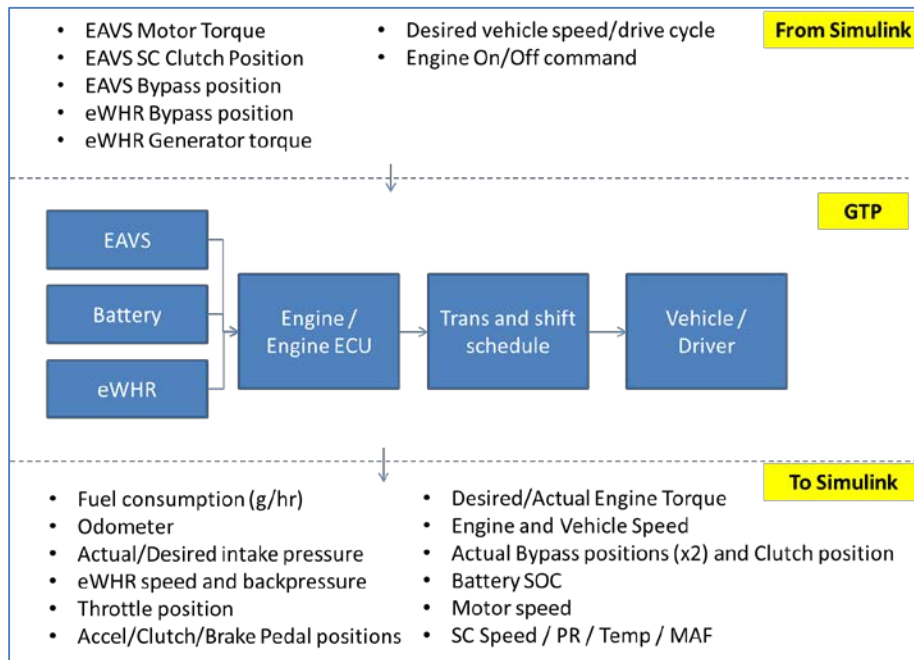


Figure II-52: Simulink Controls and GTP co-simulation framework

The system modeling effort is on track and initial modeling simulations have been completed. The framework is now completed with the system controls in Matlab Simulink being co-simulated with the GT power plant model. A screenshot of the actual model is shown in Figure II-53.

Next steps in the modeling process involve controls optimization for fuel economy and energy management and model based fuel economy evaluation for the EPA test cycles.

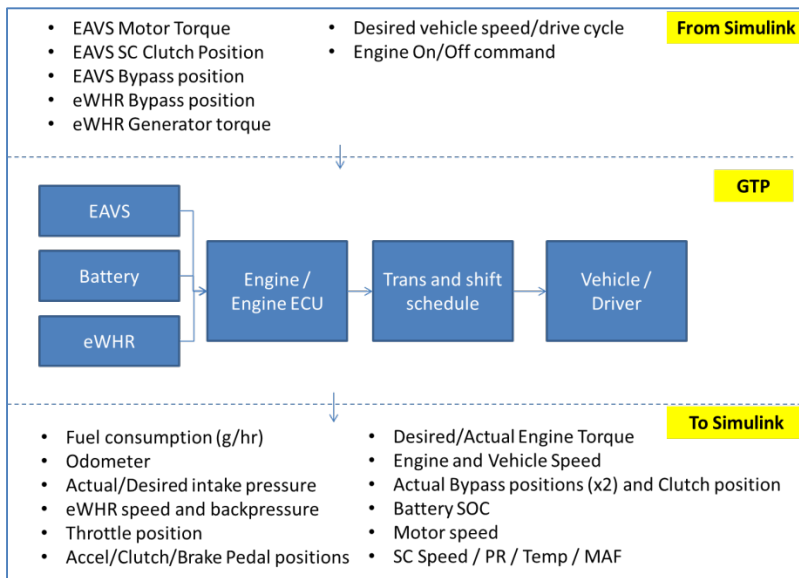


Figure II-53: Simulink Controls and GTP co-simulation framework

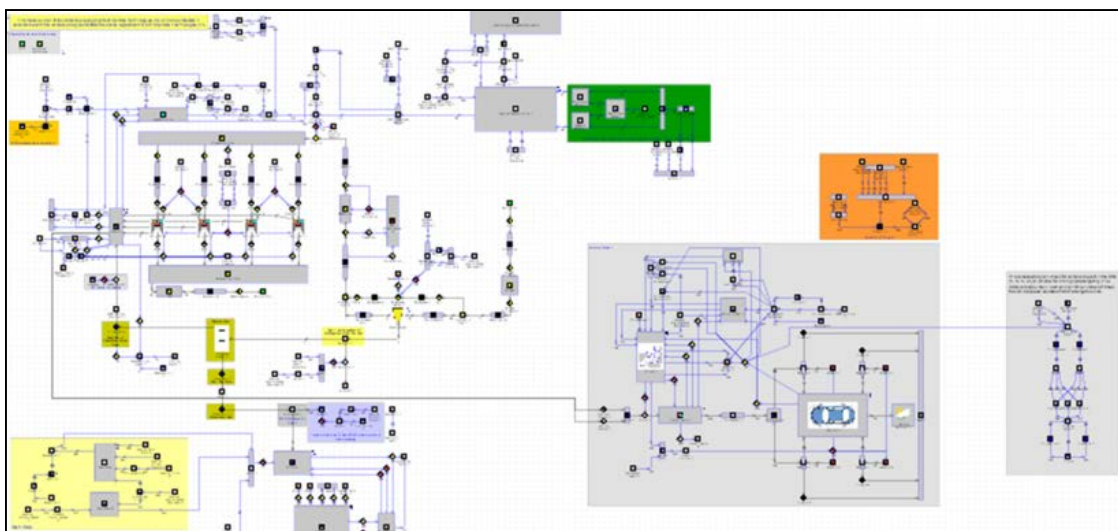


Figure II-54: GTP Model Screenshot

A complete high fidelity model was developed including a vehicle model, EAVS/WHR modules, gasoline and diesel engine models as well as a driver in the loop model to allow simulation of regulation duty cycles. The model was utilized in analyzing the benefits of each proposed technology and also in identifying the right architecture and control strategies. Key outcome of this early investigation was that the gasoline application due to its low volumetric flow rates (due to throttling), is not a suitable application for the WHR technology. Instead diesel seems to be a better fit due to the un-throttled operation and in turn the high volumetric flow rates even at low operating loads.

Task 1.3.1

To date outputs from the analytical activities have resulted in the following design optimizations with a preliminary design.

1. Housing structure
2. Housing outlet port geometry

3. Bearing plate and rotor material selection
4. Rotor coating that will abrade and handle operating environment
5. Front and rear bearings
6. Static flange seals and bolt patterns at all mating surfaces

Eaton has engaged suppliers to develop the rotor coating, bearings, static flange seals and generator. Packaging of a readily available generator onto the expander has been completed with fixture procurement in progress to enable investigation into conversion efficiency of mechanical to electrical power. This design is using an available generator for the dyno operation but since the generator is oversized for this application, further optimization needs to be done before implementation on the vehicle.

The following analytical activities have been completed and updating of the expander design with the required optimizations identified from the studies is 90% complete.

1. CFD studies on porting and rotor geometry
2. Combination of thermal CFD and structural analysis on expander assembly
3. Thermal expander assembly stack ups at worst case tolerances

Supplier engagement to finalize specifications for rotor coating, static seals and the generator are in progress.

Analytical activities are in progress to identify an optimal exhaust manifold design to maximize the expander output shaft torque generation from the blow down energy pulse that results when the exhaust valve opens.

Available packaging space within the engine compartment of the procured 1.4L Cruze has been established for the initial proof of concept expander coupled with a generator. Further optimization of the expander displacement, generator and exhaust manifold is required but sufficient space is present to package the waste heat recovery technology.

Task 1.3

Simulations have shown that the direct waste heat roots expander technology is not a fit for gasoline engines. The low mass flow rates due to part throttle operation lead to low levels of power generation which provides negligible fuel economy improvement. Preliminary testing of a 2.4L diesel off road engine with a direct waste heat roots expander and R410 electrically driven supercharger has been completed with positive results. Further testing and simulation activities are required but the direct waste heat roots expander appears to be a viable option for diesel applications due to no throttle and higher volumetric flow rates.

Figure II-55, shows the dyno setup that has been completed with a full instrumented WHR expander attached to a torque and speed sensor in order to measure the amount of power generated as well as flow measurements, exhaust/intake pressures and temperatures.



Figure II-55: Expander Dynamometer Setup

The direct waste heat roots expander design has been updated with the results from the analytical investigations. Finalization of the expander design is on hold based on the project scope change. Supplier engagement to develop a specification and design for an optimized generator for the direct waste heat roots expander is in progress.

Development of an optimal exhaust manifold design through CFD has progressed well with various design iterations investigated. Additional manifold designs and points of engine operation are under investigation but to date an increase in output shaft torque of approximately 8 to 12% has been predicted.

Finally, testing was conducted in order to identify the effects of backpressure to the engine. Since WHR energy recovery is proportional to backpressure and flow rate, we need to understand the effects of backpressure on the engine.

Conclusions

Based on testing and model based analysis to-date the EAVS and WHR technologies show promising results for diesel engine applications. The WHR system was tested at the target operating temperature and shown to operate efficiently. Significant amount of power was recovered from the exhaust. The team will continue to optimize the system using the target engine in BP2 and work with the team members to ensure that the target engine is ready to be installed in the demonstration vehicle in BP3.

II.9.C. Products

Presentations/Publications/Patents

1. 2015-DOE-AMR PowerPoint Presentation at Arlington, Washington, on June 11, 2015. Project ID-vss162, Integrated Boosting and Hybridization for Extreme Fuel Economy and Downsizing.

II.9.D. References

1. No References

FRICITION AND WEAR

II.10. Methods to Measure, Predict and Relate Friction, Wear and Fuel Economy [DE-EE0006793]

Steve P. Gravante, Principal Investigator

Ricardo, Inc.
40000 Ricardo Drive
VanBuren Township, MI 48111
USA
Phone: 1 (630) 468-8712; Fax: 1 (630) 789-0127
Email: steve.gravante@ricardo.com

Nick D'Amico, DOE Program Manager

US Dept of Energy / NETL
PO Box 10940
626 Cochrans Mill Road
Pittsburgh, PA 15236-0940
USA
Phone: (412) 386-7301; Fax: (412) 386-5835
Email: nicholas.damico@netl.doe.gov

Start Date: 15 December 2014

End Date: 15 December 2017

II.10.A. Abstract

Objectives

- To develop characterizations of friction and wear mechanisms in internal combustion engines and methods to predict the impact of such mechanisms on engine fuel consumption or vehicle fuel economy respectively. The methods of prediction will be both empirically and analytically based.
 - Empirical correlations will be established that allows for estimating changes in engine friction mean effective pressure (FMEP) or brake specific fuel consumption (BSFC) based only on the engine power and tribological parameters such as oil viscosity and coefficient of friction which can be determined a priori in lab-scale tests.
 - In parallel, the same parameters will be used as input to advanced computational aided engineering (CAE) methods to predict changes in friction torque.

Accomplishments

- Successful creation of a RINGPAK model which simulates the lab-scale test rig at Argonne National Lab (ANL)
- Mapping of friction regimes of the lab-scale test rig and a typical engine has been initiated
- Identified the low viscosity oil with friction modifier to be used in subsequent engine dyno tests
- De-greening of the Isuzu engine and base (uncoated parts) for future thermal survey work and motored and fired friction measurements has initiated

Future Achievements

- Complete de-greening process of all parts (coated)
- Complete Stribeck mapping

- Complete lab-scale friction testing of base and coated parts
- Validate the RINGPAK model of lab-scale rig through the correlation of Stribeck number at which transition between friction regimes occurs
- Conduct thermal survey of engine



II.10.B. Technical Discussion

Background

A Funding Opportunity Announcement (FOA) was issued on January 24th, 2014 (DE-FOA-0000991). This FOA is supported by the Vehicle Technologies Office (VTO) in the Department of Energy (DOE) with the following objectives:

- Reduce the usage of highway petroleum by 1.4 million barrels per day by 2020
- Develop cost-effective technologies to improve vehicle fuel efficiency and achieve or exceed corporate average fuel economy (CAFE) standards of 144 gCO₂/mile (61.6 miles per gallon) for cars and 203 gCO₂/mile (43.7 miles per gallon) for light trucks by 2025

Fourteen (14) Areas of Interest (AOI) that focus on advanced light-weighting, advanced battery development, power electronics, advanced heating, ventilation, air conditions systems and fuels and lubricants make up the scope of the FOA. Ricardo along with Argonne National Lab requested funding under AOI 11B.

Introduction

AOI 11 is concerned with powertrain friction and wear reduction. According to the FOA, parasitic losses within vehicle powertrains (engine and transmission) account for approximately two million barrels of oil consumption per day in the US.

Under topic 11 there are two subtopics: 11A and 11B. Subtopic 11A is concerned with the development and demonstration of friction and wear reduction technologies for light-, medium- and heavy-duty vehicles.

Subtopic 11B, for which this grant has been issued, is concerned with the identification and quantification of friction losses along with methods to measure and predict fuel economy gains in full engines and/or vehicles.

- Ricardo's objective is to develop empirical characterizations of friction and wear mechanisms in internal combustion engines and methods to predict the impact of such mechanisms of engine fuel consumption and/or vehicle fuel economy. This work will include advanced analytical methods as well.
- The value of such predictive schemes whether empirical or analytical is that if one knows how a particular friction reduction technology changes oil viscosity and/or friction coefficient then the fuel consumption or economy impacts can be estimated without the excessive cost of motored or fired engine tests realizing that it is more cost effective to measure oil properties and friction coefficients in a lab-scale test.

Approach

Ricardo's technical approach begins with acquiring a detailed and high fidelity dataset of the friction and wear characteristics of typical power cylinder components, e.g., piston ring, liner and piston skirt. The friction and wear characteristics will be measured for different configurations of ring on liner and piston skirt on liner in combination with typical friction and/or wear reduction technologies such as a low viscosity oil, friction modifying oil additives and coatings.

The dataset will be obtained by using the same components and friction/wear reduction technologies through a progression of control tests each with its own pros and cons for quantifying friction and wear. These include lab-scale bench tests using a reciprocating test rig (Adjustable Angle Reciprocating Tester or AART), motored dyno tests and fired engine tests.

The data obtained will be used as follows:

- To establish a correlation between the lab-scale friction measurements and the measurements of motored friction torque and fired engine FMEP
- To establish wear rate coefficients for the prediction of wear
- To provide necessary inputs to simulations of the engine power cylinder for friction and wear prediction
- To provide data for validation of CAE methods used for the prediction friction and wear

Results

The results for Task 1 are summarized in this report. This task consists of three subtasks:

1. Create a RINGPAK model of the lab-scale ring-on-liner (ROL) reciprocating test rig (AART) used to measure friction (i.e., asperity friction coefficient).
2. Map and compare lubrication regimes realized in lab-scale and fired engine tests through the calculation and comparison of Stribeck parameters ($\eta \bullet S/L$) as a function of crank angle for typical lab-scale and engine conditions.
3. Measure friction and wear properties of different hardware (coated and uncoated power cylinder components) and lubricant combinations (low and high viscosity fluids with and without friction modifiers) for different loads, speeds, and temperatures.

Task 1.1 – RINGPAK Model of Lab-Scale Measurements

A RINGPAK model was developed to simulate the reciprocating motion of the AART. Figure II-56 shows a schematic of the lab-scale ROL test configuration:



Figure II-56: Ring-on-Liner Test Configuration; radial and diametrical tension definition in RINGPAK

The ROL RINGPAK model simulates the applied normal load (L) by controlling the ring tension, F_d . To replicate the sinusoidal motion of the ROL test rig within RINGPAK, a long crank coupled with a short crank throw is imposed on the RINGPAK model to provide a stroke comparable to ROL test rig (i.e., 20 mm). Typical operating conditions and the corresponding simulation boundary conditions for the ROL test rig and ROL RINGPAK simulation are given in Table I-1.

Table I-II-11: Lab-Scale and RINGPAK Test Conditions and Equivalent Loads/Ring Tensions.

	ROL Test				ROL RINGPAK			
Rotational Speed	0 – 300 rpm				0 to 3600 rpm			
Load (N)	15	50	100	250	-	-	-	-
Load (N/mm) for a 15 mm contact path	1	3.3	6.7	16.7	-	-	-	-
Equivalent Radial Force, Fr (N)	358	1194	2388	5969	358	1194	2388	5969
Equivalent Ring Tension, Fd (N)	-	-	-	-	117	390	779	1948

The ROL RINGPAK model simulates the ROL test conditions through the appropriate selection of the ring tension, Fd. Experimentally, the ROL rig uses (normal) loads ranging from 15 N to 250 N (with loads up to 2000N possible) and a contact region of 10 to 15 mm wide (typical). This results in a load per unit width of 1 to 17 N/mm. For a 115 mm bore, this load range would be equivalent to total radial force from 358 to 5969 N. Equivalent diametric ring tensions used in the RINGPAK simulations were calculated using the following relationship:

$$F_r = 2\pi F_d / 2.05$$

Although the equivalent ring tensions in Table I-II-11 are high compared to typical HDD rings (Fd = 25 to 50 N), gas pressure during the combustion cycle can increase the radial force dramatically to produce unit loadings near 50 N/mm (i.e., Fr in excess of 15kN).

The ROL RINGPAK model includes all of the essential engine geometries and typical material properties of the Isuzu engine that will be used in subsequent motored and fired dyno tests. Simulation results show similar behavior as the ROL tests (see Figure II-57). Further development will include fine-tuning material surface properties, updating the analysis with new oil properties, and determination of ideal lubrication model and film thickness.

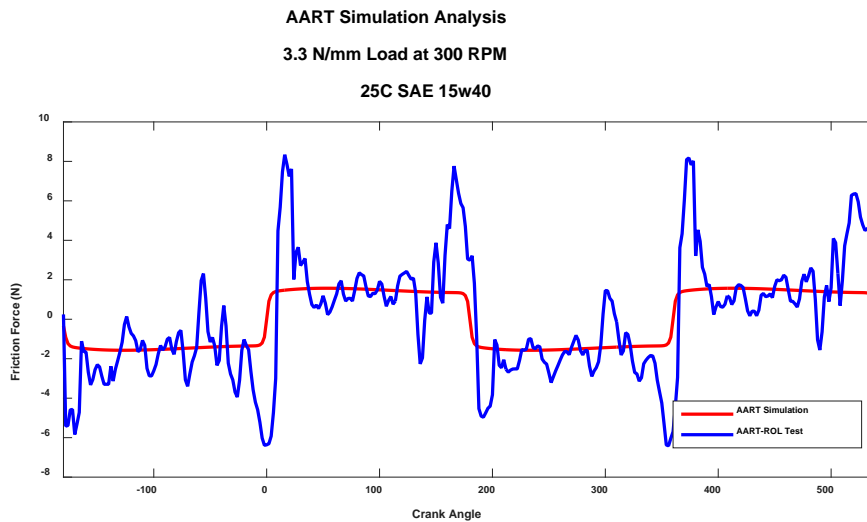


Figure II-57: Results from ROL RINGPAK simulation using Isuzu geometries, typical material properties, and generic 15w40 oil properties.

Task 1.2: Engine Stribeck Map

This subtask entails assessing how closely the reciprocating ROL rig can overlap the lubrication regimes experienced at the ring/liner interface in a typical engine. This is assessed by comparing the range of the Stribeck parameter present in a lab-scale rig against the range of Stribeck parameter present in a typical fired engine. For the purpose of these comparisons, the Stribeck parameter, S_{tr} , is defined as:

$$S_{tr} = \eta S / L$$

where η is the dynamic viscosity (Pa-s), S is the speed (m/s), and L is the load (N/m). The Stribeck parameter was calculated as a function of crank angle, CA, for the following scenarios:

- Spreadsheet calculation of S_{tr} of a ROL test under the following conditions: a 20 mm stroke, 300 rpm, 15W/40 oil @ 20 and 100 C, and a normal load range of 1 to 16.7 N/mm normal load, and
- ROL RINGPAK simulation of the high load/high viscosity ROL test case (using a ring tension, F_d , of 1948 N (equivalent to 16.7 N/mm)), and
- RINGPAK simulation of a fired diesel engine at 1200 rpm peak torque condition (including ring tension and 180 bar combustion chamber loading)

The high load/high viscosity results of the S_{tr} calculations are shown in Figure II-58 with all cases summarized in Table I-2. The ROL spreadsheet calculations and the ROL Ringpak simulations (based on a specified ring tension) are in agreement. Peak S_{tr} numbers range from 0.24×10^{-6} for 16.7 N/mm @ 100 C (high load/low viscosity) to 81×10^{-6} for 1 N/mm @ 20 C (low load/high viscosity). The Ringpak simulation of the fired engine which operates at a greater speed, larger stroke, and higher loads shows peak S_{tr} parameters ranging from 14×10^{-6} to 66×10^{-6} during the combustion cycle. The engine and ROL simulations show an important overlap near TDC during the compression/combustion phases of the cycle. At this point, asperity friction is expected to dominate hydrodynamic friction and be a major contributor to engine wear.

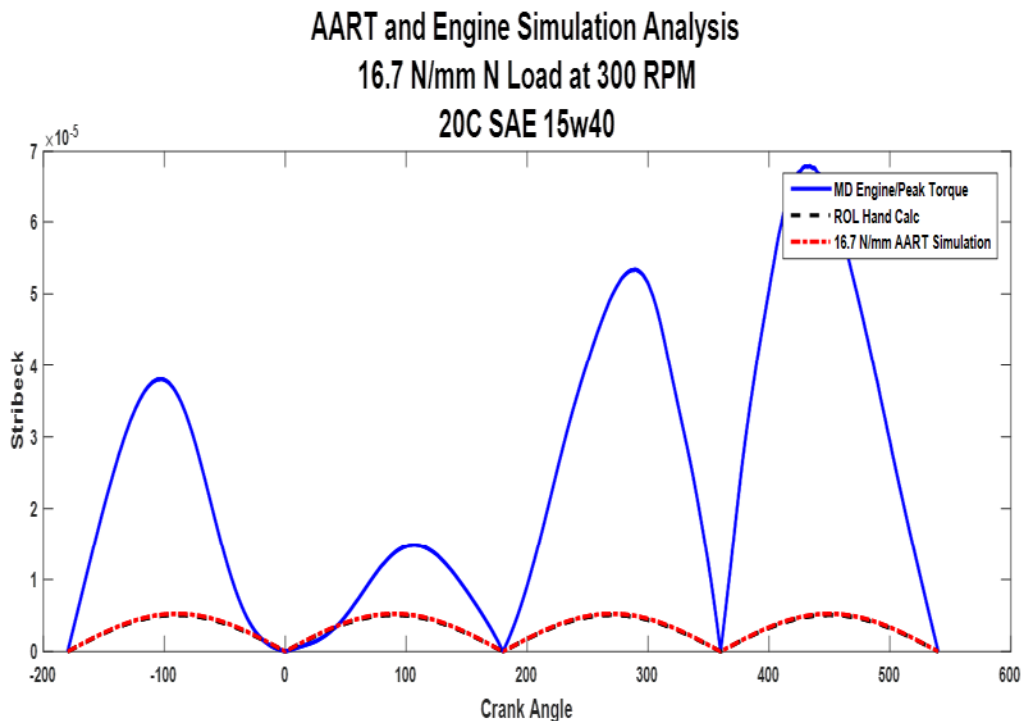


Figure II-58: Comparison of Hand-Calculated, ROL Simulation, and Engine Simulation Stribeck numbers.

Table I-II-12: Peak values of the Str number for lab-scale tests and a typical fired engine

ROL @ 300 rpm					Fired Diesel				
	Load (N/mm)					Load (IMEP)			
	1	3.3	6.7	16.7		180 bar			
Temperature	Str (x 10 ⁻⁶)				Speed (rpm)	Str (x 10 ⁻⁶)			
20 C	81.7	24.8	12.2	4.9	1200	comp	comb	exh	int
100 C	3.9	1.2	0.6	0.2		38	14	53	66

From Table I-2 the results indicate that ROL test rig is capable of matching the Str parameters present in a fired engine; however, it must be noted that the lab-scale rigs are not intended to accurately replicate the higher end of the Str regime where hydrodynamic lubrication dominates.

Task 1.3: Lab-Scale Friction and Wear Measurements

Subtask 1.3 consists of using the AART rig to generate the initial friction and wear properties of candidate materials, coatings, and lubricants that will also be tested in a motored and fired engine. Figure II-59 shows a schematic of the AART test rig and two of the configurations used in this project: ball-on-flat, and ring-on-liner. The system can accurately measure friction and contact resistance continuously. Tests will be performed at different temperatures (70, 100, and 130 C) and loads (25, 100, and 250 N). Material combinations will include both as-received, and coated rings, pistons and liners.

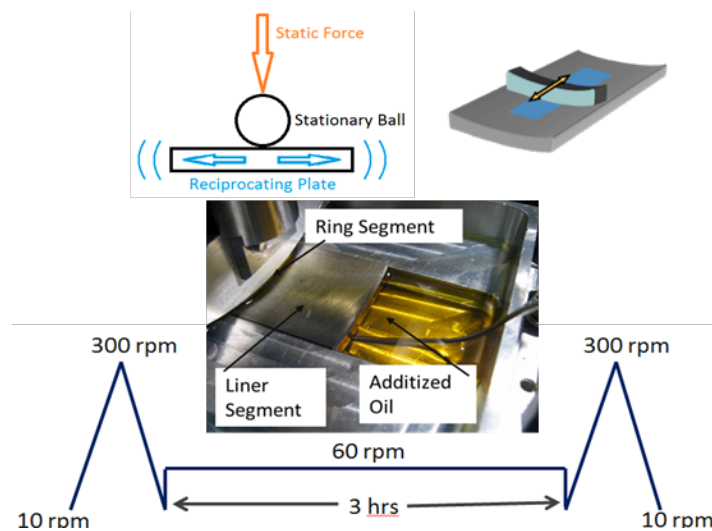


Figure II-59: AART test rig used to evaluate friction and wear properties of candidate ring and liner configurations

During the initial phase of this task, the AART was used to assess different candidate oil formulations for the purpose of identifying the best oil to be used in subsequent engine dyno tests at Ricardo. Twelve candidate oils have been studied: (2) high viscosity 15W/40 oils – with and without a FM (friction modifier), and 10 low-viscosity oils – with different FMs and treat rates.

Figure II-60 shows results from a series of tests using 8 of the 12 candidate oils. These oils fall into two categories; the first category included CI oils while the second included SI oils. As seen in this figure, Oil 3 (SI) exhibited the lowest coefficient of friction and was selected for further optimization. Two additional variations of this oil were produced and tested. However, they exhibited very similar performance. Therefore, the project will move forward with Oil 3 (SI) as the low viscosity, friction-modified, candidate for subsequent engine tests.

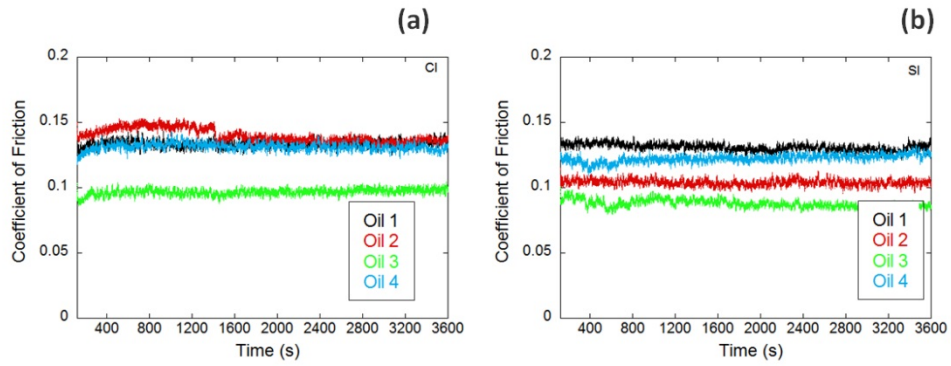


Figure II-60: Candidate oils with different friction modifiers for: (a) CI oils and (b) SI oils.

Conclusions

Adequate progress has been made in achieving the goals set forth for this project of which the key deliverable of identifying the low viscosity oil with friction modifier to be used in subsequent engine tests has been achieved.

II.10.C. Products

Presentations/Publications/Patents

1. NA

II.10.D. References

1. NA

SUPERTRUCK

II.11. Development & Demonstration of a Fuel Efficient Class 8 Tractor & Trailer [DE-EE0003303]

Russ Zukouski, Principal Investigator

Navistar, Inc.
2601 Navistar Drive
Lisle, IL 60531
Phone: (331) 332-2908
E-mail: russ.zukouski@navistar.com

Roland Gravel, DOE Program Manager

Phone: (202) 586-9263
E-mail: Roland.Gravel@ee.doe.gov

Start Date: October 2010
End Date: September 2016

II.11.A. Abstract

Objectives

- Demonstrate 50% improvement in vehicle Freight Efficiency vs. a 2009 base vehicle by developing leading edge technologies resulting in the design and build of a prototype tractor / trailer configuration
- Demonstrate 50% engine Brake Thermal Efficiency (BTE) on an engine dynamometer
- Model a path to 55% engine brake thermal efficiency.

Accomplishments

- Achieved 48.5% BTE with additional technologies still to be utilized
- Development vehicle (T3) was built and tested
- Ride and Drive event was conducted with the DOE at the Navistar Proving Grounds in New Carlisle, Ind. This development vehicle (T3) was compared to the 2009 baseline Prostar on a flat oval proving grounds and demonstrated a significant fuel consumption improvement.
- Development vehicle (T3) was then tested on one of the 3 Navistar cycles that will be used to gauge the total vehicle freight efficiency improvement (Illinois Flatlands Cycle). Initial results indicate a significant improvement in freight efficiency vs. the 2009 baseline Prostar.

Future Achievements

- Build the final demonstration vehicle (T4)
- Conduct a final fuel economy test that will be combination of three routes:
 - Illinois Flatlands (Highway)
 - City
 - Kentucky hill
- Demonstrate 50% BTE on engine dynamometer
- Model a pathway to 55% BTE

II.11.B. Technical Discussion

Background

The objective of this research and development project is to develop and demonstrate a 50% improvement in overall freight efficiency on a heavy-duty Class 8 tractor-trailer measured in ton-miles per gallon, relative to our 2009 baseline Prostar. This objective will include the development of an engine capable of achieving 50% brake thermal efficiency. A secondary objective is to identify, through modeling and analysis, key pathways to achieving long-term goal of developing a 55% efficient heavy-duty diesel engine. The overall timing of the project has five phases of development and includes the following milestones:

- 10/01/2010 – Awarded DOE contract start
- 8/2012 – Completed Phase 1
- 9/2012 through 02/2014 – Entered into pause period
- 10/31/14 – Authorized to restart
- 1/30/15 – Completed Phase 2
- 6/2015 – Completed Phase 3

Introduction

In late 2014, Navistar came out of a “pause” period and re-started the SuperTruck program. In accelerated timing, it has gone through Phase 2 & 3 in a five phase development program. In phase 3, a development vehicle (T3) showed very optimistic results. Further technology additions and enhancements are planned for the final demonstration truck that should exceed the results shown on the (T3) vehicle. We are on track to achieve the 50% BTE and showing a pathway to 55% BTE.

Approach

The Navistar approach is to do development (simulation & testing) work on evolving technologies while gathering data & experimenting on mule vehicles that have more mature technologies. Since Navistar manufactures engines as well as vehicles, the following summarizes the efforts in these areas over the past year.

Engine

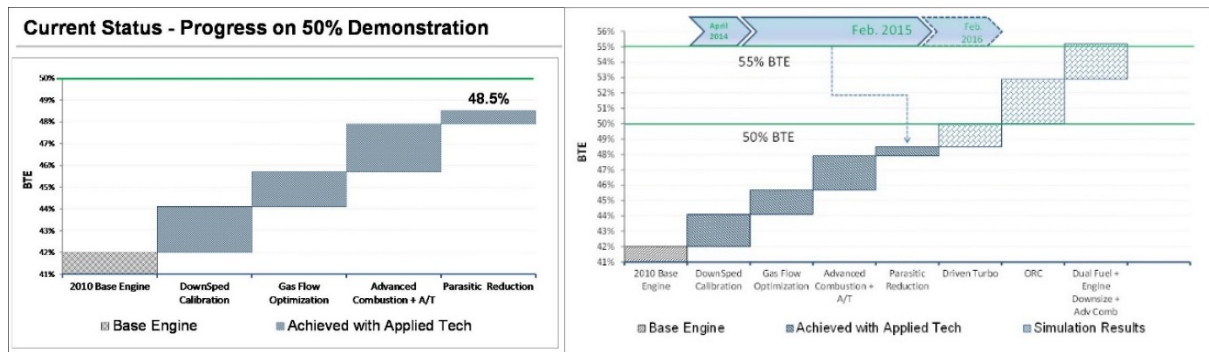


Figure II-61: Project Engine Progress

We are currently at 48.5% BTE with several technologies still to be analyzed. Over the past year, several evolving technologies have been examined and some are being implemented. They include: downsizing / downsizing, high efficiency turbos, techniques to reduce parasitic losses, combustion simulation, in-cylinder thermal management, driven turbo, and waste heat recovery. Additionally, Argonne National Labs is one of our partners analyzing dual fuel technologies. Test results show a 1% BTE gain over conventional diesel; however this technology is not mature and needs further investigation.

Vehicle

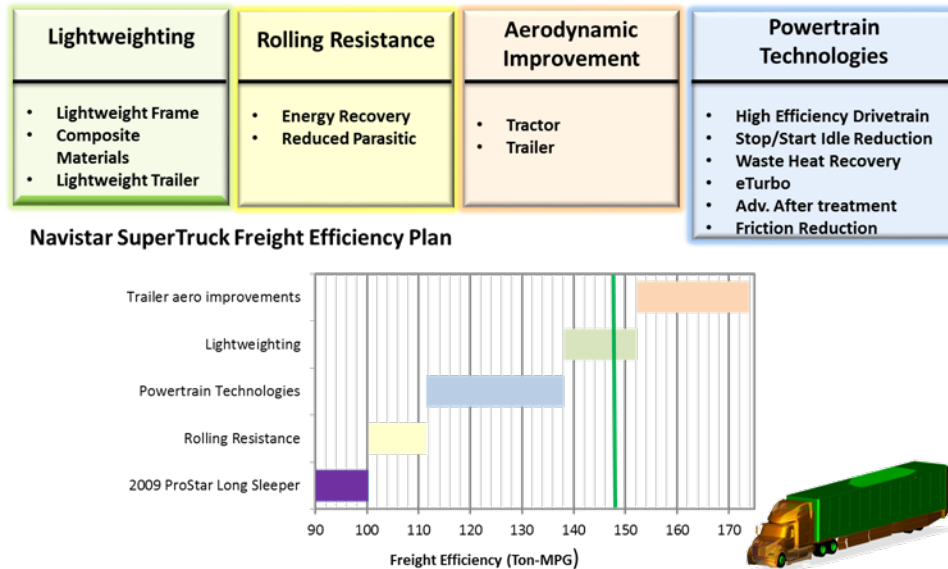


Figure II-62: Navistar SuperTruck Freight Efficiency Plan

Extensive wind tunnel testing has resulted in a tractor / trailer speedform with >55% reduced drag as compared to a 2009 baseline Prostar. Engine and truck efficiency improvements have reduced coolant flow requirements to such an extent that a simplified FEAD will be implemented. In addition, heat exchangers have been redesigned for high temp cooling. As a result of this, grille designs have been changed and optimized.

One of the technologies that was simulated and then utilized in the mules is regenerative braking with high efficiency electrical charging. Tests were run over the various duty cycles and different battery types for an optimum solution.

Development Vehicles

A mule vehicle (T2) was outfitted with lightweight suspension and axles. It was outfitted with an air biasing system between drive axles / a lift axle, and a ride height control system. Testing validated the drag reduction and fuel economy estimates from previous wind tunnel simulation.

Another mule vehicle (T3) was built that had the same technologies as T2 but also smart / high temp cooling, high temp / recuperative charging for 48V HVAC, and a lightweight trailer fitted with photovoltaic panels, additional aero devices, and air fairings. This vehicle was then demonstrated at the Ride and Drive event with the DOE that was driven on a flat oval track and showed a significant fuel consumption reduction.

A (T4) final demonstrator vehicle has been designed with its vehicle architecture defined based on mule vehicle experiences. Material ordering is currently being conducted with the build scheduled to start later this year.

Results

Two development mules (T2 & T3) were designed and built to test and validate various technologies that were targeted to go into the final demonstrator vehicle (T4). Vehicle technologies included: lightweight suspensions, load biasing between the drive axles, pneumatic height control, modified engine, lightweight trailer with aero devices and efficient transmission. They were run on test tracks as well as various duty cycles. T2 results fed into the build of T3, which had more technologies added to it. This culminated in flat track testing and initial Illinois Flatlands testing that resulted in significant improvements toward achieving 50% freight efficiency. This reinforces our technology direction for implementing and optimizing these technologies into the final (T4) demonstrator vehicle / trailer.

Conclusions

The Navistar SuperTruck team has completed three of the five phases of this research and development project. With the conclusion of Phase 3, we have achieved:

Significant freight efficiency improvements have been demonstrated on one of the 3 Navistar test cycles. This is a strong indication that we are on track for meeting or exceeding our goal of 50% freight fuel efficiency across all three duty cycles. The final demonstrator vehicle will have more finalized and optimized technologies that should further exceed the 50% target.

We continue to show slow and steady increases to our current engine BTE of 48.5%, with additional technologies and enhancements still to be added.

Work will continue finalizing / optimizing technologies on mule vehicles as well as designing and ordering material for the final demonstrator (T4).

II.11.C. Products

Presentations/Publications/Patents

N/A

II.11.D. References

N/A

II.12. Systems Level Technology Development and Integration for Efficient Class 8 Trucks [arravt080]

Derek Rotz, Principal Investigator

Daimler Trucks North America
4747 North Channel Avenue
Portland, OR 97217
Phone: (503) 745-6303
E-mail: derek.rotz@daimler.com

Roland Gravel, DOE Program Manager

Phone: (301) 938-3347
E-mail: roland.gravel@ee.doe.gov

Start Date: April 1st, 2010
End Date: April 30th, 2015

II.12.A. Abstract

Objectives

- Demonstration of a 50% total increase in vehicle freight efficiency measured in ton-miles per gallon (at least 20% improvement through the development of a heavy-duty diesel engine)
- Development of a heavy-duty diesel engine capable of achieving 50% brake thermal efficiency on a dynamometer under a load representative of road load
- Identify key pathways through modeling and analysis to achieving a 55% brake thermal efficient heavy-duty diesel engine.

Accomplishments

- Completion of final demonstration test of SuperTruck vs. the 2009 baseline Cascadia tractor over three drive cycles and two idle cycle test
 - 115% improvement in vehicle freight efficiency measured
 - 12.2 mpg average over five days of testing on San Antonio - Dallas route at 65,000 Gross Vehicle Weight and at 65 mph.

Future Achievements

- Program ends April 30th, 2015 with no future achievements planned.



II.12.B. Technical Discussion

Background

SuperTruck is a 5 year research and development program with a focus on improving diesel engine and vehicle efficiencies. The objective is to develop and demonstrate a class 8, long haul tractor-trailer which achieves a 50% vehicle freight efficiency improvement (measured in ton-miles per gallon) over a best-in-class 2009 baseline vehicle. The engine for the SuperTruck program will deliver 50% brake thermal efficiency. Daimler's SuperTruck Program consisted of 5 phases of development which explained below.

Introduction

Phase 1 of the program has primarily centered on system analysis through the use of modeling and simulation, bench testing and on-road vehicle tests. Vehicle efficiency simulation software, Autonomie, was used for determining the optimal engine, powertrain and drivetrain specification, including engine rating, transmission/axle gear ratio sets, driveline efficiencies and rolling resistance. External aerodynamics and vehicle cooling systems have been analyzed through the use of 1D thermodynamics and 3D fluid dynamic modeling in addition to the use of scale model wind tunnel testing. Finite element analysis software has been used in the design of a load optimized chassis with lightweight materials with subsequent testing both in bench tests and on-vehicle.

Phase 2 encompassed the detailed design, installation and testing of technologies on a system level by conducting on-highway fuel economy tests. In this phase the program target of experimentally demonstrating 25% vehicle freight efficiency was successfully reached. In parallel the engine target of 46% brake thermal efficiency was reached by means of dynamometer tests. Installation of vehicle systems occurred on two 'Tinker' Trucks, from which basic functionality, performance and fuel economy tests were conducted. One truck is equipped with an A-sample hybrid electric powertrain and high voltage electric HVAC system. The second truck has installed powertrain/drivetrain systems along with auxiliary systems which were optimized for efficiency. Several SAE Fuel Economy tests were conducted on numerous systems, spanning powertrain drivetrain, auxiliary components, idle reduction, and control systems. Furthermore aerodynamics testing was accomplished via scale model wind tunnel testing and Computational Fluid Dynamics. Lastly prototype lightweight chassis component were built and tested for strength and stiffness.

In Phase 3, the program target of experimentally demonstrating 50% vehicle freight efficiency was successfully reached through continued development and improvement of external aerodynamics, powertrain components and hybrid testing.

Research on aerodynamics in phase 3 encompasses additional improvements in both tractor and trailer systems. The methods employed in quantifying these improvements entail a combination of scale model wind tunnel testing and computational fluid dynamics. In this phase, a total drag reduction has been measured and correlated, through refinement of the basic shape concepts. On the tractor roughly half drag reduction was achieved through refinements of aero systems such as side extenders, bumper and chassis fairing/wheel cover enhancements. On the trailer side, the remaining drag reduction was reached through refinements of side skirt, boat tail and tractor trailer gap minimization approaches.

Powertrain improvements in phase 3 centered on the further development of axle, tire and hybrid technologies. Incremental efficiency gains in axle technology improvements were achieved through testing and measurement of gear ratios and lubrication to identify an optimum. On-highway testing of rear axle ratios was conducted to evaluate engine operating points and shifting. In parallel, axle dynamometer testing was completed, which evaluated the impact of gear oil formulations, levels and temperatures on efficiencies. Low rolling resistance tires were evaluated, with an emphasis on non-driven, wide based singles on the trailer, in collaboration with our tire partner Michelin. Additional freight efficiency gains were achieved through decreasing resistance forces and through weight reduction on the tire, wheel and hub design.

Lastly, a fuel economy test of the A-sample parallel electric hybrid powertrain was conducted in 2013, which demonstrated positive fuel savings. The hybrid system consists of a Daimler proprietary eMotor and inverter in a parallel configuration and an A123 Li-Ion battery pack. The test data confirmed the base regeneration functionality traveling across hilly terrain as designed. However the control interfaces between the hybrid controller, engine controller and ABS controller were not optimized, causing an unexpected limit on available regeneration torque. Improved calibration is needed to optimize the system to maximize the amount of recuperated energy.

This test provided input for further optimization of the hardware components and software for the final SuperTruck hybrid system.

Phase 4 entailed the buildup of the A-Sample SuperTruck. The purpose is to integrate multiple technologies onto a single chassis in order to design and test thermal and high voltage interfaces and to complete a series of

functional and performance tests of multiple systems on one vehicle. Given the complexities of each system individually in addition to vehicle integration complexities which were not well understood, the buildup was deemed necessary. The scope of the A-sample build includes the target SuperTruck engine and aftertreatment system, waste heat recovery, an updated hybrid electric system and an automated manual transmission with updated controls. A 6x2 axle with custom rear axle ratio, electric HVAC system, a custom cooling package with variable speed fan drive were also incorporated. Lastly a custom hood, bumper and grille were fabricated and installed. The buildup and commissioning occurred in four stages to achieve a fully integrated functional vehicle.

Once these systems were functionally integrated, including optimization and tuning of relevant controls systems, the A-Sample vehicle was tested against the 2009 baseline Cascadia tractor, using the TMC Type IV test method for competitive benchmarking. Testing was conducted on two highway routes; Interstate 5 in Oregon and Interstate 35 in Texas. The test results measured a 52% fuel economy improvement on the Oregon route and a 61% improvement on the Texas route. The combined A-Sample tractor/trailer weighed in at 1500 lbs less than the baseline, further improving freight efficiency.

Approach

Phase 5 activities focuses on the buildup and testing of the final demonstrator SuperTruck. This vehicle incorporates all SuperTruck technologies onto a single vehicle to conduct the complete final demonstration test. These technologies include everything from the A-sample vehicle, plus several more. These include a 50% BTE engine and waste heat recovery system, full tractor and trailer aerodynamics, lightweight truck exterior and frame, a 6x2 axle configuration with active oil management among others. Daimler's SuperTruck Program has completed this final phase on April 30th, 2015. The deliverables for the period include completion of the final demonstration testing by measuring a 50% improvement in vehicle freight efficiency.

Five cycles were specified and conducted as part of final demonstrating testing, including Interstate 5 between Portland and Canyonville Oregon at 55 mph, Interstate 35 between San Antonio and Dallas at 65 mph, Portland city cycle and parked tests in both summer mode and winter mode at ambient temperatures of 100°F and 0°F respectively.

Results

Figure II-63 illustrates the composite fuel economy results.

Route	Oregon		Texas		City		Winter		Summer		Total		% Improvement
Actual Distance (Mi)	408.3		438.3		44.6		-		-		891.2		
Weighted Distance (Mi)	206.0		523.0		19.8		-		-		748.8		
Weighted Time (Hr)	3.9		9.0		1.1		5.0		5.0		24		
Truck*	ST	BL	ST	BL	ST	BL	ST	BL	ST	BL	ST	BL	
Fuel Consumed (gal)	17.3	31.1	42.8	86.0	3.7	5.0	1.3	3.0	0.1	3.6	65.2	128.7	
Fuel Efficiency (mpg)	11.9	6.6	12.2	6.1	5.4	4.0					11.5	5.8	97.4%
Freight Efficiency** (Ton · MPG)	201.5	102.6	206.3	94.2	91.5	61.8					194.1	90.3	115.2%

Figure II-63: Final Demonstration Fuel Economy Results: SuperTruck vs 2009 Baseline Cascadia

Source: Daimler Trucks North America

Reduction of the tare weight of the tractor and trailer also contributes to freight efficiency in that additional payload can be added while maintaining 65,000 lbs Gross Vehicle Weight (GVW). The baseline 2009 Cascadia tractor contained 15.5 short tons of freight. The SuperTruck in contrast with additional lightweighting technologies both on the chassis of the tractor as well as the trailer was able to haul 16.9 short tons of freight, while maintaining the same GVW.

Conclusions

Daimler's SuperTruck comfortably exceeded the program targets by achieving an overall 115% improvement in freight efficiency. This was achieved by developing and demonstrating a range of technologies on the tractor, engine and trailer and effectively integrating the technologies together onto a single vehicle.

The fuel efficiency contribution of the technologies is fairly even split between Engine and Vehicle systems developed by Daimler and technologies developed by our trailer and tire partners. This underlines the notion that several companies across the trucking supply chain have a role to play in improving efficiencies, not just an OEM. Secondly, a fairly even split can be observed across shorter and longer term technologies, with perhaps a slightly higher bias towards the shorter term. One takeaway from this observation is that a mix of technologies, both short and long term, were deployed in SuperTruck. It indicates some degree of success in transferring technologies to production. It also shows further research is needed on more experimental, high risk-high reward technologies that did yield fuel economy savings by revealing significant challenges that remain with respect to system maturity and costs. In this case SuperTruck succeeds in bringing clarity to barriers of commercialization and identifying further areas of needed research.

Moving forward, a greater emphasis on future research should be placed on overcoming economic and maturity hurdles in order to mature the longer term technologies discovered in SuperTruck as well as to identify new technologies for further fuel savings.

II.12.C. Products

Presentations/Publications/Patents

1. Singh, Sandeep: "Super Truck Program: Engine Project Review Recovery Act –Class 8 Truck Freight Efficiency Improvement Project", Project ID:ACE058, DoE Annual Merit Review, June 12, 2015
2. Rotz, Derek: "Super Truck Program: Vehicle Project Review Recovery Act –Class 8 Truck Freight Efficiency Improvement Project", Project ID ARRAVT080, DoE Annual Merit Review, June 11, 2015

II.13. Volvo SuperTruck [DE-EE0004232]

Pascal Amar, Principal Investigator

Volvo Technology of America

7825 National Service Road

Greensboro, NC 27409

Phone: (336) 291-5842

E-mail: pascal.amar@volvo.com

Roland Gravel, DOE Program Manager

VTO

Phone: (202) 586-9263

E-mail: Roland.Gravel@ee.doe.gov

Start Date: June 2011

End Date: June 2016

II.13.A. Abstract

Objectives

- Demonstrate 50% increase in freight efficiency [ton-mi/Gal] compared with a 'best in class' MY 2009 highway truck.
- Demonstrate 50% brake thermal efficiency.
- FY2015 Objectives
 - Complete integration of technologies into demonstration vehicle.
 - Fully develop aerodynamic solutions identified during concept selection (Phase I).
 - Apply lessons learned to current products and bring improvements to market.

Accomplishments

- Demonstrator build completed in time to begin road testing in FY2015.
- Developed and commercialized practical trailer aerodynamic devices.
- Commercialized tractor aerodynamic improvements.

Future Achievements

- Demonstrate complete vehicle efficiency improvements through on-road testing.
- Demonstrate 50% brake thermal efficiency of powertrain.



II.13.B. Technical Discussion

Background

SuperTruck is a 5-year research and demonstration program with the objective to identify technologies that could significantly reduce fuel use by Class 8, long haul trucks. The program focuses equally on diesel engine efficiency and vehicle efficiency.

Introduction

Volvo's SuperTruck project is divided into two main phases, as shown on right: the first phase utilized a mule vehicle to evaluate concepts and technologies during FY 2013; the second phase will deliver the SuperTruck demonstrator comprising the technologies selected to achieve the program objectives.

The Volvo SuperTruck project team has completed all activities planned for Fiscal Year 2015 according to the original schedule. An overview of the main achievements is presented in this report.

Approach

The SuperTruck project develops multiple concepts simultaneously in order to achieve significant freight efficiency and thermal efficiency improvements. The Volvo team uses its complete vehicle simulation tools to gain quantitative insight into potential trade-offs or synergies between the new technologies, thereby developing a completely integrated vehicle. This simulation platform was used to analyze the energy usage of the baseline truck which helped set engineering targets for the technologies addressing each of the areas.

Complete Vehicle Aerodynamics

Since aerodynamic drag is the primary contributor to fuel use of a highway vehicle the team targets to reduce it by 40% using an integrated design approach between tractor and trailer. The new designs are optimized using a combination of complete vehicle computational fluid dynamics (CFD) simulations and wind tunnel scale testing to design and optimize geometries, then verified through track and on-road testing to confirm aerodynamic performance and fuel savings. This project is committed to making the improved aerodynamic designs practical from an operational perspective in order to deliver commercially viable solutions.

Advanced Materials and Structures

Even though long haul trucks are typically not limited in weight carrying capacity, it is important to offset the curb weight increase brought by new technologies in order to maintain the payload capacity of the vehicle. One key challenge is to identify advanced materials which could become cost effective for the highway truck operating environment. The team is therefore evaluating new structure concepts as well as recycled materials in order to reduce weight with a minimal cost increase.

A study of new chassis concepts was started in early FY 2013 with the goal to reduce the weight of the frame rails and mounting brackets by 40% compared with the baseline vehicle. After several iterations of virtual design and verification a full scale prototype frame was delivered in FY 2014, which was the starting point for the assembly of the demonstrator truck that was completed this year.

Parasitic Losses

Efficient LED lights are used for both interior and exterior lighting in order to reduce energy usage, which can already save hundreds of gallons of diesel fuel saved per vehicle per year in current trucks. The trailers' exterior lights also use Grote's LightForm lightweight and low profile technology. Several technical solutions are being investigated to reduce the amount of energy used to cool or heat the cabin.

Idle Reduction

A bank of light-weight energy optimized batteries is used to power 'hotel loads' during driver rest time, including a 2-zone fully electric air conditioning system. The combination of solar power and improved thermal insulation allows for downsized climate unit and energy storage. The batteries are recharged during driving periods using kinetic energy recovery and are compatible with electrified truck stops.

Intelligent Energy Management

The Volvo team utilizes predictive algorithms to minimize the amount of fuel used to power the truck along its route as well as run auxiliary devices. This information is also used to assist the driver.

Results

During this reporting period the Volvo team continued to make significant progress towards its goals of integrating selected concepts into the demonstrator and bringing mature technologies to market. The key achievements for each area of the project are described below.

Complete Vehicle Aerodynamics

The SuperTruck cab components designed and optimized during the past reporting periods were fabricated in preparation for assembly of the demonstrator. Once the cab components were assembled they were scanned to confirm that the final shape of the truck matched the optimized aerodynamic shape. The trailer was equipped with updated gap, side and tail fairings which are designed to deliver approximately 15% fuel economy improvement in combination with the new tractor geometry.

During the SuperTruck concept selection phase Volvo had identified potential aerodynamic enhancements for highway tractors. A parallel investigation was launched to further refine and test new design ideas, which resulted in the market launch of a new sleeper roof fairing, front bumper, and new flared chassis fairings during this fiscal year. Ridge/Freight Wing also focused its efforts on preparing for the commercialization of the aerodynamic trailer devices that have been developed in the project. Fuel economy testing was conducted in accordance with EPA protocols and several packages received SmartWay certification in the new 'Elite' category for devices with fuel savings in excess of 9% at 65 mph. Following extensive operational and durability testing these products were also launched to the market during the reporting period.

Advanced Materials and Structures

A full scale prototype of the new chassis concept, nearly 45% lighter than the baseline assembly, was built in FY 2014 and became the starting point for the assembly of the demonstrator truck that was completed this year. A second vehicle was built for endurance track evaluation and data collection. Detailed comparison of the baseline and the advanced frame confirmed that the significant weight reduction did not impact performance.

Parasitic Losses

The team is deploying a combination of commercial and experimental technologies to reduce the energy usage of the truck. These include efficient LED lights to reduce electricity consumption, roof-mounted photovoltaics to harvest solar energy, as well as advanced bearings and lubricants to minimize rolling resistance.

Leveraging previous work performed together with the National Renewable Energy Laboratory (NREL) under the CoolCab project, the Volvo team has improved the thermal insulation of the cabin. Combined with a more precise climate control strategy and improved air circulation, the energy usage of the cabin heating and cooling system is greatly reduced.

Idle Reduction

The new electrified climate control system and batteries were installed on the demonstrator vehicle and are ready for testing. The energy storage system is sized to run 'hotel loads' during a full rest period under heavy usage e.g. hot and humid. The batteries are recharged using high-efficiency alternators which are able to capture kinetic energy when the truck is moving, hence eliminating the need to idle the engine during rest periods without compromising on driver comfort or productivity.

Intelligent Energy Management

Volvo has designed an intelligent energy management concept which minimizes the amount of fuel required to operate the complete vehicle using map data and predictive algorithms. Some of the features that will be demonstrated include predictive cruise control, kinetic energy recovery, predictive free-rolling, etc.

Conclusions

During this fiscal year the team focused on the integration of selected technologies into the demonstrator (Phase II). Assembly of the complete vehicle was completed on schedule and key-on activities have begun. Development and testing of the advanced 50% BTE powertrain system continues simultaneously through engine dynamometer testing.

Next fiscal year will be dedicated to testing and validation of the final vehicle and powertrain configurations as well as demonstration of the Volvo SuperTruck prototype.

II.13.C. Products

Presentations/Publications/Patents

1. No publications

II.13.D. References

1. No references.

TIRES

II.14. A System for automatically Maintaining Pressure in a Commercial Truck Tire [DE-EE0005447]

John Maloney, Principal Investigator

The Goodyear Tire and Rubber Company
200 Innovation Way
Akron, OH 44316-0001
Phone: (330) 796-5146
Email: john.maloney@goodyear.com

David Ollett, DOE Program Manager

Office of Energy Project Management, National Energy Technology Laboratory (NETL)
626 Cochran Mill Road
Pittsburgh, PA 15236-0940
Phone: (412) 386-7339
Email: David.Ollett@netl.doe.gov

Start Date: October 1, 2011
End Date: September 30, 2016*

*No-cost extensions have changed the original end-date of this project from September 30, 2014

II.14.A. Abstract

Objectives

- Increase overall commercial fleet fuel efficiency
- Improve tire wear and service life
- Decrease fleet tire maintenance cost and compliance with federal safety regulations.

Accomplishments

Overall

- Over road trials were carried out. Various combinations of AMT tires, from as-molded without system components to system pumping tires, were placed on the truck before the full system tires with functioning regulators became available in mid-August. The docks are not of the latest design iteration, but the decision was made to go forward and begin on vehicle testing in order to gain experience with the regulators
- The tire design for the fleet evaluation was finalized
- System component selection for the large volume fleet evaluation was completed
- An improved (second generation) manufacturing system for AMT system component installation was designed, procured, and installed. This system is used to manufacture prototype tires for the fleet evaluation
- The AMT manufacturing process and system installation equipment was relocated, installed, and is fully functional
- Process optimization efforts are ongoing
- The regulator docks are not of the latest design iteration, but the decision was made to go forward and begin on vehicle testing in order to gain experience with the regulators
- Full system tires will be available for placement on the truck by mid-November.

Components

- Pump
 - AMT system component installation and curing process was further optimized to provide consistent pumping performance across a broad range of vehicle loads
 - Pumping variation and repeatability trials were conducted in an effort to understand process variations and rim and mounting potential effects.
- System
 - A removable system dock cap was built to take the place of the regulator and permit functional pumping (minus regulation). This cap was debugged and optimized. Replacement of the cap with a functioning regulator will enable a direct comparison and provide regulator performance characterization.
- Passage
 - Passage tubes were obtained and underwent testing for release to use in the fleet evaluation
 - Modelling was done to understand the effect that material modulus has on pumping performance
 - Passage tube modelling has been done to understand the effect that material modulus has on pumping performance.
- Pump tube
 - Acceptance criteria for pump tubes were defined
 - Pump tube to passage tube connections continue to be critically evaluated for robustness after a number of leaking connections were identified in tires designated for dynamometer testing
 - Bench tests were developed to evaluate connection integrity without the need to assemble into a full AMT system tire.
- Filter
 - Various methods to retain the filter housing in the tire during operation were developed by the vendor and have been evaluated in lab testing. This is a temporary solution that can be used with both the truck testing and if necessary, in the larger volume fleet trial
 - The performance of the temporary solution to affix the filter is acceptable. A permanent solution for filter attachment has not been tested or implemented.
- Regulator & Dock
 - Iterations of regulators were received and bench tested
 - Goodyear created a new functional performance specification to simplify the bench testing procedure for regulator acceptance criteria
 - A joint workshop between Eaton and Goodyear was held to identify opportunities and plans to improve the regulator functionality. A reduced performance specification for the regulator was agreed to temporarily in Q1 of FY15 in order to expedite the delivery of some quantity of regulators to advance testing of the regulator in full assembly in the tire
 - The temporary reduction of performance specification for the regulators agreed to in the December workshop allowed delivery of twenty functioning regulators in February/March. Bench testing discrepancies between Goodyear and Eaton led to plans to upgrade the Goodyear test system as well as documentation on test procedures
 - Air leakage was also found between the dock and the regulator leading to a partial fix implemented by Eaton. A workshop was held to address the problem of air leakage between the dock and the regulator
 - The result of the workshop (via PUGH matrix analysis) was an agreement to redesign the dock with regulator design unchanged. In the current design, where the sealing mechanism is integral (over-molded) to the dock, the loss or lack of sealing necessitated scrapping the AMT tire. In the new design, the dock to regulator interface will now utilize a replaceable sealing mechanism that will enable replacement of this part if sealing is inadequate or compromised. A replaceable seal also provides the ability to evaluate multiple seal designs or materials more efficiently. This dock design iteration has not yet been implemented or tested. Delivery of small lots of new docks, seals, and regulators is targeted for 10/07/2015.

- Regulator attachment
 - Dock design changes were implemented and will continue to be incorporated. This resolved high speed attachment issues
 - Further Eaton dock design changes were identified to improve high speed attachment and wear issues. This requires dock over-mold tooling modifications. Eaton has confirmed these changes and timing with over-mold supplier.

Process

- Manufacturing
 - Development and optimization of a second generation assembly process continues with the goals of delivering better process control and larger volumes. This process will be used to produce fleet trial tires
- The quick pump system test for QC check of full system tires was proven to perform successfully.

Fleet Evaluation

- The fleet evaluation plan was defined to include several fleets and a range of service conditions
- In service tire monitoring procedures were defined
- Fleet evaluation will not be initiated until successful vehicle evaluation on the Goodyear tractor trailer has been confirmed.

Future Achievements

Overall

- Redesign dock to provide sealed interface with regulator
- Evaluate permanent filter retention options
- Continue on road vehicle tests
- Lab test tires for product release requirements
- Prep for the large volume fleet evaluation development tire build
- Quality test next iterations of regulators
- Test next generation docks
- Continue to optimize AMT generation 2 system installation equipment.



II.14.B. Technical Discussion

Background

Pressurized air in the tire cavity naturally escapes by diffusion through the tire and wheel, leaks in tire seating, and through the filler valve and its seating. As a result, tires require constant maintenance to replenish lost air. Since manual tire inflation maintenance is both labor intensive and time consuming, it is frequently overlooked or ignored. By automating the maintenance of optimal tire pressure, the tire's contribution to the vehicle's overall fuel economy can be maximized.

Introduction

Under-inflated tires significantly reduce a vehicle's fuel efficiency by increasing rolling resistance (drag force). The Air Maintenance Technology system developed through this project replenishes lost air and maintains optimal tire cavity pressure whenever the tire is rolling in service, thus improving overall fuel

economy by reducing the tire’s rolling resistance. The system consists of an inlet air filter, an air pump driven by tire deformation during rotation, an air passage through the tire and a pressure regulating device.

Approach

The work is divided into three phases. The objectives of first phase, Planning and Initial Design, will result in an effective project plan and to create a baseline design. The objectives for the second phase, Design and Process Optimization, are: to identify finalized design for the pump, regulator and filter components; identify a process to build prototype tires; assemble prototype tires; test prototype tires and document results. The objectives of Phase 3, Design Release and Industrialization, are to finalize system tire assembly, perform full release testing and industrialize the assembly process.

Results

Table II-13: Project Status

Milestone	Phase 1: Planning and Initial Design (Concept Scoping)	Month	Date	
M01	Revised work plan & budget accepted by DOE & Goodyear	01	31-Oct-11	✓
M02	Initial system, component & process specifications complete	06	31-Mar-12	✓
Milestone	Phase 2: Design and Process Optimization (Prototype Development)	Month	Date	
Iteration 1				
M03	Initial simulation and modeling complete	09	30-Jun-12	✓
M04	First iteration system assemblies complete	11	31-Aug-12	✓
M05	Evaluation of first design complete	12	30-Sep-12	✓
Iteration 2				
M06	Second iteration system assemblies complete	17	28-Feb-13	✓
M07	Go/No go decision based on evaluation of refined design	18	31-Mar-13	✓
Iteration 3				
M08	Third iteration system assemblies complete	23	31-Aug-13	✓
M09	Go/No decision for on-vehicle trial	24	30-Sep-13	✓
M10	On-vehicle trial initiated – San Angelo (a)	27	31-Dec-13	✓
Iteration 4				
M11	Fourth iteration system assemblies complete - Eaton 1	31	21-Apr-14	✓
M12	Go/No go decision based on evaluation of refined design	32	19-May-14	✓
Iteration 5				
M13	Fifth iteration system assemblies complete - Eaton 2	33	16-Jun-14	✓
M14	Go/No go decision based on evaluation of refined design	34	7-Jul-14	✓
M15	Delivery of latest iteration of Eaton regulator/filter components (b, e)	41	24-Feb-15	✓
Milestone	Phase 3: Design Validation	Month	Date	New Date
M16	Delivery of Eaton regulator/filter components begins for fleet testing assembly (b, d, c)	48	16 Jun 15	22-Sep-15
M17	Assembly of fleet evaluation tires commences (e)	40	17 Jun 15	1-Oct-15
M18	Qualification testing completed prior to fleet (customer) evaluation	50	22 Sep 15	15-Nov-15
M19	Go/No go decision for fleet trial based on qualification testing	50	23 Sep 15	16-Nov-15
M20	Fleet evaluation tire shipments begin (f)	51	1 Oct 15	1-Dec-15
M21	DOE project completed. Approximately 5 months fleet evaluation completed	57	30-Jun-16	30-Jun-16

(a) Check valve test - non-functioning regulator. Continuous test. Tires with functioning regulators will be deployed (see M15)
 (b) Functioning regulators
 (c) Goodyear Akron / San Angelo qualification testing, ~13 weeks, leading to M19 (Go/No go)
 (d) Approx. 100 / week (delivery to begin prior to M19 to be ready for fleet trial - some risk involved)
 (e) Approx. 40 / week (assembly to begin prior to M19 to be ready for fleet trial - some risk involved)
 (f) 1st group of tires to be assembled and ready to ship per M19 decision. Deployment to accounts Oct 2015 - Dec 2015. Expected duration 18 mos.
 Note: If M19 decision is a 'No go', additional iterations would be needed. Additional iterations could consume an additional 7-17 weeks (1.5-4.0 mos)

Conclusions

The AMT team focused efforts on in two major areas this period - AMT component issues identified in lab and road testing, and manufacturing readiness for test and fleet tire assembly.

Critical areas of the docks and regulators have been identified, which contributed to leaking issues in lab and field testing, using Root Cause Analysis. The mold manufacturer has reworked the dock and regulator molds to provide a finished surface of SPI-A2, in these critical areas. Mold part alignment and registration has been improved to reduce molding flash. Two different types of seal materials, with different durometer specifications, were tested to optimize sealing and durability requirements. The validation process has been improved to inspect these critical areas. All components are now validated using an agreed upon Product Validation Process and reporting process to ensure component quality and consistency. We have updated our vibration specification using actual data acquired from an instrumented truck, fitted with an AMT Tire, driving on Interstate 77 South of Akron. The final filter design and been agreed to and under way. Discussions have been initiated with manufactures, to redesign tooling to incorporate the new specifications.

The AMT Assembly Manufacturing Cell is fully operational and equipped to assemble AMT Products. We are in the process of hiring and training technicians to assemble AMT products for fleet testing. Standard work procedures, AMT assembly processes, and component validation criteria, are nearing completion. A component and product traceability recording process is being developed to support Root Cause analysis efforts for any AMT Product issues observed in fleet testing. Fleets testing AMT Products will be equipment with Tire Pressure Monitoring Systems where AMT tire performance can be tracked real time on all fleet vehicles. Any AMT Product issues can be identified and addressed as they are observed and the team will have all the data leading up to the issue.

The AMT team is now in the position to assemble AMT products for internal lab and road testing. After this initial phase of internal testing, the team will assemble AMT products for fleet testing.

II.14.C. Products

Presentations/Publications/Patents

II.14.D. Presentations

N/A

II.14.E. Publications

N/A

II.14.F. Patents

Goodyear currently has thirty four (34) US Patents involving Air Maintenance Technology (AMT). Twelve (12) patents were granted during FY15. We have additional patent applications filed with the US Patent office.

20th Patent issued: US 8,851,132 - Issued 10/07/2014

Abstract: A tire has an elongate profiled sidewall groove extending into a first tire sidewall from an outward first sidewall surface. An elongate air tube is positioned within the elongate sidewall groove in contact with the groove sidewalls, the air tube having an external surface configuration corresponding with and seating within the internal sidewall configuration defining the sidewall groove. The air tube when subject to outward originating impinging force collapses from an expanded unstressed configuration into a collapsed configuration to allow the tube to insert through the groove entry opening and expand outwardly once within the sidewall groove to its unstressed configuration. The configuration of the groove sidewalls capture the air tube within the groove in its expanded unstressed configuration to prevent separation of the tube from the tire during use.

21st Patent issued: US 8,857,484 - Issued 10/14/2014

Abstract: A self-inflating tire assembly includes an air tube connected to a tire and defining an air passageway, the air tube being composed of a flexible material operative to allow an air tube segment opposite a tire footprint to flatten, closing the passageway, and resiliently unflatten into an original configuration. The air tube is sequentially flattened by the tire footprint in a direction opposite to a tire direction of rotation to pump air along the passageway to an inlet device for exhaust from the passageway or to an outlet device for direction into the tire cavity. The inlet device is positioned within the annular passageway 180 degrees opposite the outlet device such that sequential flattening of the air tube by the tire footprint effects pumping of air along the air passageway with the tire rotating in either a forward or reverse direction of rotation. The invention further includes an inlet device for regulating the inlet flow of the air tube pump.

22nd Patent issued: US 8,875,762 - Issued 11/04/2014

Abstract: An air maintenance tire and connector system includes a tire carcass having an elongate integral air passageway contained within a flexible tire component of the tire carcass between an air inlet and an air outlet cavity and a connector assembly inserted within an outlet one of the cavities. The connector assembly includes a hollow right angled elbow-shaped body fitting within the outlet cavity. The elbow-shaped body's second housing segment has an axial length sufficient to project axially inward from the first housing segment through a tire wall thickness to a tire central cavity. A valve device attaches to a remote end of the second housing segment within the tire cavity, the valve device operative to regulate air flow between the elbow-shaped body central chamber and the tire cavity.

23rd Patent issued: US 8,915,277 - Issued 12/23/2014

Abstract: An air maintenance tire and connector system includes a tire carcass having an elongate integral air passageway contained within a flexible tire component of the tire carcass between an air inlet and an air outlet cavity and a connector assembly inserted within one or both of the cavities. A coupling post having an axial bore extends from the hollow body through a tire wall thickness to a tire central cavity. A remote end of the coupling post is operative for sequential alternative attachment to a punch device for penetrating in a pre-cure procedure through the tire wall thickness to the tire central cavity.

27th Patent issued: US 8,960,249 - Issued 2/24/15

Abstract: A self-inflating tire assembly includes an air tube connected to a tire and defining an air passageway, the air tube being composed of a flexible material operative to allow an air tube segment opposite a tire footprint to flatten, closing the passageway, and resiliently unflatten into an original configuration. The air tube is sequentially flattened by the tire footprint in a direction opposite to a tire direction of rotation to pump air along the passageway to an inlet device for exhaust from the passageway or to an outlet device for direction into the tire cavity.

28th Patent issued: US 8,985,171 - Issued 3/24/2015

Abstract: A connector system and tire assembly includes an elongate integral air passageway contained within a flexible tire component of a tire carcass, the air passageway extending between an air inlet cavity and an air outlet cavity in the flexible tire component, and the air passageway extending at least a partial circumferential path around the tire carcass. A hollow dome-shaped inlet nut seats within the inlet cavity and a hollow dome-shaped outlet nut seats within the outlet cavity. The inlet nut couples to an air inlet device for conducting air external to the tire carcass into the inlet nut central chamber; and the outlet nut outward body side couples to a valve device positioned within the tire cavity.

29th Patent issued: US 8,991,456 - Issued 3/31/2015

Abstract: An air maintenance tire and pump assembly includes an elongate annular air passageway enclosed within a bending region of a tire, the air passageway operatively closing and opening segment by segment as the bending region of the tire passes through a rolling tire footprint to pump air along the air passageway. A pair of inline valves are positioned on respective opposite sides of an inlet junction and

direct a flow of inlet air in opposite directions into the air passageway; and a pair of outlet valves are positioned at a downstream side of a respective inline valve and direct a flow of the inlet air from the downstream side of a respective inline valve toward the tire cavity. The valves are selectively opened by a direction of air flow within the air passageway which, in turn, is directionally determined by the direction in which the tire rotates.

30th Patent issued: US 9,045,005 - Issued 6/02/15

Abstract: A tire assembly includes a tire having a pneumatic cavity, first and second sidewalls, a sidewall groove, an air passageway, and a pressure regulator mounted to an inner surface of the pneumatic tire cavity. The pressure regulator controls air pressure within the pneumatic tire cavity. The first and second sidewalls extend respectively from first and second tire bead regions to a tire tread region. The first sidewall has at least one bending region operatively bending when circumferentially within a rolling tire footprint. The sidewall groove defining groove sidewalls positioned within the bending region of the first tire sidewall. The groove and air passageway deform segment by segment between a non-deformed state and a deformed, constricted state in response to the bending of the first sidewall bending region circumferentially within the rolling tire footprint.

31st Patent issued: US 9,050,858 - Issued 6/09/2015

Abstract: The invention relates generally to air maintenance tires and, more specifically, to a pump mechanism for supplying air into such tires.

32nd Patent issued: US 9,056,435 - Issued 6/16/2015

Abstract: A pneumatic tire assembly includes a pneumatic tire having an inner cavity and an inner surface at least partially defining the inner cavity, a rigid structure for facilitating operation of the tire assembly, and a docking base for securing the rigid structure to the inner surface of the inner cavity. The docking base has been integrally bonded to the inner surface during curing of the pneumatic tire. The docking base has a shape formed by a mold attached to the inner surface of the inner cavity during curing of the pneumatic tire. The mold subsequently is removed thereby resulting in the docking base integrally secured to the inner surface.

33rd Patent issued: US 9,056,533 - Issued 6/16/2015

Abstract: An elongate air tube is positioned within a tire sidewall cavity in contacting internal engagement with the tire sidewall to form an assembly. The air tube includes an internal elongate air passageway and wing projections projecting in opposite directions at an axially inward body portion. The wing projections seat within cavity pockets to retain the air tube within the cavity. The air tube body operatively compresses responsive to impinging stress forces from the tire sidewall against the air tube body, whereby the air tube body reconfiguring from an expanded unstressed configuration into a compressed configuration to constrict the air passageway. The air tube body decompresses into the expanded configuration upon reduction of the impinging stress forces against the air tube body.

34th Patent issued: US 9,061,556 Issued 6/23/2015

Abstract: The present invention is directed to a pneumatic tire with an elongate substantially annular air passageway enclosed within a bending region of the tire and extending substantially in a circumferential direction, wherein upon rolling of the tire air is pressed through the air passageway and a valve assembly in air flow communication with the tire cavity, the annular air passageway and the exterior of the tire and having an air inlet for allowing air to enter the valve assembly from the exterior of the tire as well as an air outlet for allowing air to enter the tire cavity.

II.15. Advanced Truck and Bus Radial Materials for Fuel Efficiency [DE-EE0006794]

Lucas Dos Santos, Senior R&D Engineer

PPG Industries, Inc.
440 College Park Drive
Monroeville, PA 15146
Phone: (724) 325-5381; Fax: (724) 325-5313
E-mail: dossantosfreire@ppg.com

Brian Kornish, Program Manager, Government Contracts

PPG Industries, Inc.
Phone: (412) 492-5165
E-mail: kornish@ppg.com

David Anderson, DOE Program Manager

Vehicle Technologies Office
Phone: (202) 586-2335
E-mail: David.Anderson@ee.doe.gov

Start Date: 10/01/2014

End Date: 09/30/2017

II.15.A. Abstract

Objectives

- PPG Industries, Inc. and Bridgestone Americas Tire Operations propose to develop a novel surface-modified silica technology and demonstrate 4-6% improved fuel efficiency of truck and bus radial (TBR) tires built from the technology. The proposed fuel efficiency increase will be achieved while maintaining or improving tear strength and tread wear compared to carbon black filled treads.

Accomplishments

- Synthesized and characterized silica samples with different surface energies.
 - Obtained initial compound data on said silicas in NR, NR/BR and NR/SSBR based compounds.
 - Concluded that untreated and treated silica samples behave differently in polymer blends.

Future Achievements

- Obtain direct evidence of silica distribution in different polymer phases.
 - Establish optimum treated silica/polymer blend compound to achieve fuel efficiency goal.



II.15.B. Technical Discussion

Background

Precipitated silica is an amorphous particle produced commercially by the acid neutralization of a sodium silicate solution. Highly dispersible silicas (HDS) are used as the main reinforcing filler in passenger treads. In conventional HDS/in situ silane systems, HDS and coupling agents such as 3,3'-bis(triethoxy-silylpropyl)tetrasulfide (TESPT) are co-reacted during the tire compounding process to create a strong interaction between the HDS and the rubber polymers to deliver better tire performance. In recent years, to

overcome the VOCs and other issues associated with the HDS/in situ silane process, Agilon® 400 Performance Silica came into the market. In the Agilon process, silane coupling agents, as well as other compatibilizers, are pre-reacted onto the silica surface so that tire manufacturers don't need to control this reaction during compounding. For passenger tires, which are synthetic rubber based, Agilon products can reduce rubber mixing time by 36%, increase batch sizes by 18-27%, eliminate VOCs, and further improve the "magic triangle" of treadwear, traction, and rolling resistance.

When tires are predominantly comprised of natural rubber (NR), as in the case of TBR tires, silicas no longer provide the same benefits as in passenger tires. NR provides the chip and tear resistance essential for TBR applications, but NR contains proteins, organic matter, and metal ion contaminants. These contaminants are believed to interfere with the in situ coupling reaction required to effectively disperse silica in non-polar rubber yielding poor filler dispersion, tire performance, and processing properties. Recently, a high surface area Agilon® that was able to be dispersed in NR has been developed, which provided dramatic improvements in rolling resistance compared to carbon black.^{1,2,3,4} This performance is obtained due to the ability of Agilon® to overcome the NR contaminants problem, since the silane coupling reaction is already completed before mixing the silica with rubber.

Introduction

Bridgestone Americas Tire Operations (Bridgestone) evaluated commercial Agilon® materials in actual TBR formulas. They identified that further improvements need to be made before Agilon® would be truly impactful to the TBR segment of the tire industry. The state of the art TBR compounds are carbon black-reinforced NR/butadiene rubber (BR) blends. The Agilon® materials tested, preferentially dispersed into synthetic rubbers and this non-uniform dispersion creates performance issues for NR/synthetic rubber blends. It is hypothesized that if the Agilon® process could be used to control silica surface energy and morphology to more uniformly disperse across blends of natural and synthetic rubbers, not only will TBR tires experience a potential 20-30% reduction in rolling resistance yielding a 4-6% increase in fuel efficiency, but also a greater range of rubber blends will be possible. This will enable TBR tires with an optimum balance of fuel efficiency, traction and tread wear, as well as tear strength.

Approach

To achieve the goal of this project, we will systematically and thoroughly investigate the properties that enable uniform dispersion of silica in both natural and synthetic rubbers. This knowledge will be used to drive the development of new silica surface treatments and rubber formulations to control the phase distribution and/or enhance the dispersion of fillers throughout the TBR tread compound. By the end of the program, we expect to identify:

- a methodology to controllably and uniformly disperse silica fillers into the various phases of the rubber formula,
- a new surface modified silica technology that reduces the rolling resistance of a TBR tread compound by at least 60% in laboratory testing relative to carbon black technology, and
- a new rubber blend for TBR compounds containing surface modified silica, optimized for on-tire rolling resistance, tear strength, and tread wear performance.

Results

The first stage of this project is to understand how different silica surface chemistries and surface areas are linked to dispersion performance in different rubber phases including both natural and synthetic rubbers. It was hypothesized that by measuring the individual dispersive and polar component of the overall rubber surface energy as well as the filler dispersive and polar component, a prediction can be made as to which fillers will have the best compatibility with a given rubber system. To determine this, surface energy measurements were performed. The surface energy of the rubbers was measured at different temperatures, since tires are used at room temperature, but mixing with silica is performed at higher temperatures (150-170°C). Measurements were performed using polar and non-polar liquids, and the polar and dispersive components of the surface

energy were determined. The surface polarity measured for different rubbers, commonly used in truck tires, is shown in Figure I-1. Rubber are hydrocarbon based, and significantly non-polar. The surface polarity for all rubber tested is between 13% and 26%. The surface polarity is in the order, from lowest polarity to higher polarity: polybutadienes, oil-extended SSBR, oil-extended polybutadienes and, with the highest polarity, natural rubber samples. Also, it can be observed in the Figure that surface polarity slightly decreases with increasing temperature.

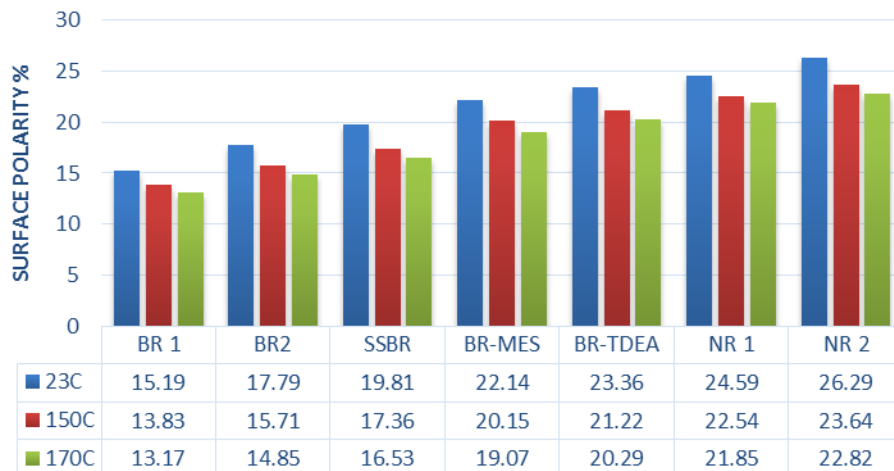


Figure II-64: Tread rubbers surface energy at different temperatures

Silica, by its nature, has a very polar surface. It was hypothesized that surface treatment could cover part of the surface by hydrophobic groups, and reduce the surface energy. Surface polarity of pretreated silicas, prepared for this project with different functional groups, was measured. The measurement of surface energy was performed using the Washburn technique and the Fowkes surface energy theory. Half gram packs of each silica in a standard Kruss FL12 powder cell were tested for wettability with water and diiodomethane, and hexane as the material constant determination liquid. When the Fowkes theory was applied to the contact angle data, the surface energy data shown in Table II-14 was determined. Samples JM0316-18 and JM0316-14, which have the highest surface energy, do not have any surface treatment. The rest of the samples contain different proprietary treatments. The silicas are all higher in surface energy and surface polarity than any of the rubbers, so interfacial tensions are significant in most cases. The samples with the lowest interfacial tension (JM0359-1 and JM0359-4) were scaled up and used for compounding.

Table II-14: Silica prototypes surface energy

Silica	Overall Surface Energy (mJ/m ²)	Polar Component (mJ/m ²)	Dispersive Component (mJ/m ²)	Surface Polarity (%)	Interfacial tension with NR (mN/m)
JM0316-18	66.2	31.1	35.1	46.9	8.2
JM0316-14	65.0	30.1	34.9	46.3	7.7
JM0316-13	59.5	26.0	33.5	43.7	5.6
JM0316-17	58.2	25.3	32.9	43.5	5.2
JM0317-8	56.7	24.2	32.5	42.6	4.7
JM0317-7	53.2	21.7	31.5	40.8	3.6
JM0359-3	52.5	21.4	31.1	40.7	3.4
JM0316-12	50.2	19.6	30.6	39.1	2.7

JMO359-4	48.9	18.7	30.2	38.2	2.4
JMO359-1	44.2	15.0	29.2	33.8	1.2

Initial compounding work with selected silicas was performed on NR/BR and NR/SSBR (styrene-butadiene rubber) blends with NR content between 70 and 100 phr. Table II-15 shows data for a non-treated control silica (Hi-Sil 190G) and a silica treated with a blend of compatibilizer agent and silane coupler (JM0359-4). The compounds with Hi-Sil 190G contain also TESPT, while the compounds with treated silica do not have this silane coupler. When comparing the samples with only natural rubber, it can be seen that the treated sample has a higher uncured Mooney, lower cure level (S' max), slower cure (higher T90), with higher elongation and lower tensile strength. Rheological data indicates that the compound with the treated silica sample provides a lower G' at low strain, known to be an indicator of better silica dispersion, with higher tan δ at room temperature and 60°C. An interesting observation can be made when looking at the data change with increasing polybutadiene content. While G' remains more or less constant, and tan δ increases for the untreated silica, G' almost doubles, tan δ decreases 55-60%, and DIN abrasion (treadwear indicator) improves 22% for the treated sample when increasing the polybutadiene content to only 20%. This happens without any other significant difference in processing behavior, cure and tensile indicators. This shows that treated silicas have a different behavior than untreated silicas in polymer blends.

Table II-15: NR/BR compound data

BR (%)	0	10	20	0	10	20	30
Silica	Hi-Sil 190 G	Hi-Sil 190 G	Hi-Sil 190 G	JM0359-4	JM0359-4	JM0359-4	JM0359-4
Uncured ML(1+4)	48	52	54	62	65	61	65
S' Max	27.7	29.6	31	22.3	21.8	27.5	26.9
S' Min	2.6	2.8	3.1	3.8	3.9	4	4.5
MH-ML	25.1	26.7	27.9	18.5	17.8	23.4	22.4
T90	5.8	5.8	7.1	6.8	6.9	10.6	12.3
Tensile, MPa	30.4	26	25.4	19.6	23.8	26.3	21.2
Elongation, %	483	495	471	646	652	573	568
Modulus @ 100%, MPa	3.4	3.1	3.3	1.6	1.8	2.5	2.4
Modulus @ 300%, MPa	16.3	14.9	14.6	6.4	7	9.8	9.1
300/100 % Modulus ratio	4.74	4.76	4.4	3.92	3.83	3.91	3.75
Hardness @ 23 °C	65	68	69	57	61	63	65
Hardness @ 100 °C	63	67	68	49	56	61	64
Rebound @ 23 °C, %	64	68	67	53	55	65	67
Rebound @ 100 °C, %	77	79	79	63	66	76	77

BR (%)	0	10	20	0	10	20	30
Silica	Hi-Sil 190 G	Hi-Sil 190 G	Hi-Sil 190 G	JM0359-4	JM0359-4	JM0359-4	JM0359-4
G' @ 60 °C, MPa	2.49	2.44	2.64	1.33	1.44	2	2.38
tan (δ) @ 60 °C	0.046	0.053	0.062	0.114	0.082	0.053	0.05
tan (δ) @ 0 °C	0.085	0.089	0.098	0.156	0.137	0.098	0.095
G' @ 1 %, 30 °C, MPa	2.82	2.78	3.04	1.95	2.05	2.13	2.52
G' @ 16 %, 30 °C, MPa	1.9	1.78	1.86	1.28	1.33	1.51	1.79
Δ G', 1.0 % - 16 %	0.92	1.00	1.18	0.67	0.65	0.62	0.73
tan (δ) @ 1.0 %	0.042	0.048	0.052	0.133	0.098	0.057	0.054
tan (δ) @ 16 %	0.078	0.088	0.094	0.153	0.103	0.078	0.074
DIN Abrasion Index	100	106	105	90	92	99	110
Streblor Tear (N/mm)	42.7	44.9	41.8	46.3	41.3	45.4	42.4

Table II-16 shows lab compound data for samples with the same silica samples from the previous Table, but for NR/SSBR blends. In this case, different trends to those observed in the NR/BR blends are observed. While G' and tan δ slightly decrease for the untreated silica, G' marginally increase and tan δ remains more or less constant for the treated silica. These results indicate again that the untreated and treated silicas react different to the incorporation of synthetic rubber in the compound.

Table II-16: NR/SSBR compound data

SSBR (%)	0	10	20	0	10	20	30
Silica	Hi-Sil 190 G	Hi-Sil 190 G	Hi-Sil 190 G	JM0359-4	JM0359-4	JM0359-4	JM0359-4
Uncured ML(1+4)	47	47	51	61	58	61	65
S' Max	25.1	26.1	28.7	24.2	13.1	22.8	22.8
S' Min	2.5	2.5	2.6	3.1	4.1	4.2	4.1
MH-ML	22.6	23.6	26.0	21.1	9.0	18.6	18.7
T90	3.9	4.7	7.1	6.5	8.9	7.6	8.7
Tensile, MPa	28.8	27.5	30.8	24.3	21.1	23.1	23.2
Elongation, %	515	494	492	644	622	590	581

SSBR (%)	0	10	20	0	10	20	30
Silica	Hi-Sil 190 G	Hi-Sil 190 G	Hi-Sil 190 G	JM0359-4	JM0359-4	JM0359-4	JM0359-4
Modulus @ 100%, MPa	3.1	3.0	3.3	1.7	2.0	2.1	2.4
Modulus @ 300%, MPa	15.1	14.9	15.8	7.2	7.9	8.4	9.0
300/100 % Modulus ratio	4.86	4.95	4.73	4.14	3.90	3.91	3.72
Hardness @ 23 °C	62	62	64	63	57	65	65
Hardness @ 100 °C	61	61	61	57	45	56	58
Rebound @ 23 °C, %	59	59	64	55	51	50	51
Rebound @ 100 °C, %	75	75	80	67	55	66	67
G' @ 60 °C, MPa	1.96	1.92	1.82	1.41	1.55	1.84	1.65
tan (δ) @ 60 °C	0.044	0.036	0.035	0.094	0.090	0.059	0.089
tan (δ) @ 0 °C	0.091	0.086	0.089	0.147	0.142	0.124	0.143
G' @ 1 %, 30 °C, MPa	2.18	2.00	1.92	2.20	2.30	2.33	2.53
G' @ 16 %, 30 °C, MPa	1.59	1.54	1.54	1.42	1.52	1.61	1.79
Δ G', 1.0 % - 16 %	0.59	0.46	0.38	0.78	0.78	0.72	0.74
tan (δ) @ 1.0 %	0.049	0.044	0.043	0.111	0.102	0.072	0.107
tan (δ) @ 16 %	0.073	0.066	0.059	0.132	0.125	0.094	0.123
DIN Abrasion Index	100	101	100	93	75	86	87
Streblor Tear (N/mm)	56.6	56.3	44.9	42.0	45.5	47.1	40.3

Conclusions

The surface energy of prototype silica samples treated with a proprietary PPG process and different functional groups were determined. It was found that treatment reduces the surface energy, thus reducing the interfacial tension with natural rubber and synthetic rubbers. The reduction in surface energy was dependent on the specific treatment agents used. Silica samples with the lowest surface energy obtained were compounded in NR/BR and NR/SSBR based compounds. It was observed that the untreated and treated silica samples have a different behavior when a small amount of NR is replaced by synthetic rubber in the compounds. It is believed that this difference in behavior is due to different dispersion of the silica samples in the different rubber phases.

II.15.C. References

1. T. Okel and J. Martin “Innovating the silica surface for Improved NR truck tire vulcanisates” Tire Technology International 2/2014.
2. T. Okel and J. Martin “Functionalized silicas for improved NR truck tire vulcanizates” Rubber World (2014) 249(2), 19-24.
3. T. Okel and J. Martin “Bringing Innovation to the Surface: Functionalized Silicas for Improved Natural Rubber Truck Tire Vulcanizates” 184th Technical Meeting of the American Chemical Society Rubber Division, October 2013, paper #33.
4. T. Okel, R. Kollah and J. Martin “Agilon Performance Silicas in Natural Rubber Truck Tire Tread Compounds” 180th Technical Meeting of the American Chemical Society Rubber Division October 2011, paper #70.

ZERO EMISSION CARGO TRANSPORT

II.16. San Pedro Bay Ports Hybrid & Fuel Cell Electric Vehicle Project [DE-EE0006874]

Joseph Impullitti, Program Supervisor

South Coast Air Quality Management District
21865 Copley Drive
Diamond Bar, CA 91765
Phone: (909) 396-2025; Fax: (909) 396-3252
Email: jimpullitti@aqmd.gov

Adrienne Riggi, Program Manager

NETL
Phone: (304) 285-5223
Email: Adrienne.Riggi@netl.doe.gov

Start Date: October 1, 2014
End Date: September 30, 2019

II.16.A. Abstract

Objectives

- Reduce criteria pollutants in South Coast Air Basin by reducing diesel emissions from transportation and movement of goods
- Accelerate introduction and penetration of zero and near-zero emission fuel cell and hybrid technologies in cargo transport sector
- Execute a joint project with the Port of Los Angeles and Long Beach consisting of demonstration, data collection and analysis of seven fuel cell and hybrid trucks on five different vehicle architectures.

Accomplishments

- The project has experienced some administrative delays in executing contracts with sub recipients. It was expected that the contracts with the five sub recipients would be executed by mid-June 2015 and the kickoff for the project would follow. However, the sub recipients' contracting process has continued into the third quarter of 2015 due to complexities in the partners' funding agreements which have caused a delay in securing those funds, the SCAQMD review process, and negotiations with sub recipients over SOW's and terms and conditions of the contracts. The status of the funding agreements with the partners has improved with the execution of the \$250K funding agreement with SoCalGas, the receipt of the \$1M in funding from LADWP, and the September execution of the \$2.4M CEC funding contract. The Ports TAP funding agreement for \$1.1M was approved by Port of Long Beach Board of Harbor Commissioners on September 28, 2015 and that agreement will be executed within a couple of weeks. In addition the SCAQMD Board has already committed \$2.4M for the project.

Future Achievements

- Going forward, we will now be able to execute contracts with the sub recipients. The contracts with TransPower and U.S. Hybrid have been signed by each respective company and will be executed first. The GTI, CTE and IR contracts are still in process and, depending on each entity and their agreement to the terms and conditions, negotiations could take an additional month.



II.16.B. Technical Discussion

Background

The I-710 and CA-60 highways are key transportation corridors in the Southern California region that are heavily used on a daily basis by heavy duty drayage trucks that transport the cargo from the ports to the inland transportation terminals. These terminals, which include store/warehouses, inland-railways, are anywhere from 5 to 50 miles in distance from the ports. The concentrated operation of these drayage vehicles in these corridors has had and will continue to have a significant impact on the air quality in this region whereby significantly impacting the quality of life in the communities surrounding these corridors. To reduce these negative impacts it is critical that zero and near-zero emission technologies be developed and deployed in the region. A potential local market size of up to 46,000 trucks exists in the South Coast Air Basin, based on near-dock drayage trucks and trucks operating on the I-710 freeway. In areas with historically poor air quality like the South Coast Air Basin, zero-emission transportation technologies are being considered and may become standard. The South Coast Air Quality Management District (SCAQMD), California Air Resources Board (CARB) and Southern California Association of Governments (SCAG) — the agencies responsible for preparing the State Implementation Plan required under the federal Clean Air Act — have stated that to attain federal air quality standards the region will need to transition to broad use of zero and near zero emission energy sources in cars, trucks and other equipment (Southern California Association of Governments et al, 2011). The SCAG 2012 Regional Transportation Plan also lays out a long-term vision of a phased adoption of zero and near-zero emission technologies to meet air quality goals. The current near-dock rail yard development project known as the Southern California International Gateway (SCIG) has been the subject of significant public concern regarding air quality impacts from the project and may ultimately result in the use zero emission trucks and other equipment. The planned expansion of the existing near-dock rail yard known as the Intermodal Container Transfer Facility (ICTF) is expected to face pressures similar to the SCIG to employ zero emission technologies.

Introduction

The proposed project area is known as the Los Angeles Goods Movement and Industrial Corridor. This area is adjacent to the Ports of Long Beach and Los Angeles, the busiest port complex in North America. The area is in an industrial setting with diesel truck activity mingled with a variety of uses including residences, schools, daycares and senior centers. The area is also a known Environmental Justice Community made up of predominantly low-income and minority populations.

The proposed technologies, fuel cell range extenders and hybrid electric trucks, face many challenges in the process of commercialization: proper sizing of the fuel cell stack, battery and fueling system; system integration and packaging of power train components and systems for safe, efficient and economical deployment of the technologies are just a few of the challenges. Many options exist in sizing the energy systems for these type of vehicle architectures – making the battery, engine or fuel cell dominate in size; plug in charging versus operation in charge sustaining mode and sizing of the energy storage system. Considerations for the power requirements of vehicle under load and providing enough onboard energy to attain the range requirements for the drayage operation and duty cycles all come into play in the design of the energy storage and power systems. Another challenge is to design the energy and power train systems described above and then integrate them into a vehicle for safe and efficient operation that can be made economical in volume and series production.

Approach

The technical objective of our proposed application is to address some of the challenges of developing the fuel cell range extended and hybrid truck platforms with the cost and time constraints of this FOA. By bringing together small to medium sized vehicle integrator contractors along with global manufactures and developers we offer the best in innovation and experience in this project. Transportation Power, International Rectifier and U.S. Hybrid, who are extremely cost effective in demonstrating proof of concept and exploring design variants in a timely fashion; BAE Systems and Ballard Power Systems a global defense and security company and an international fuel cell manufacturer who both have experience in developing fuel cell transit buses. Together

our project contractors offer the opportunity to explore design variations concurrently and address many of the challenges mentioned above in a timely and cost effective manner. Some of the metrics that will be used to evaluate the design variants of the five fuel cell range extended and hybrid architectures are: Operational capabilities, Energy usage and efficiency, Fueling/charging requirements and Costs compared to diesel powered trucks.

ZECT 2 Projects:

BAE Systems will develop a battery electric truck with a hydrogen fuel cell range extender. The vehicle will operate in electric mode at all times and all speeds until the battery energy system reaches a lower operating state of charge level, at which point the hydrogen range extender would be activated to supplement power.

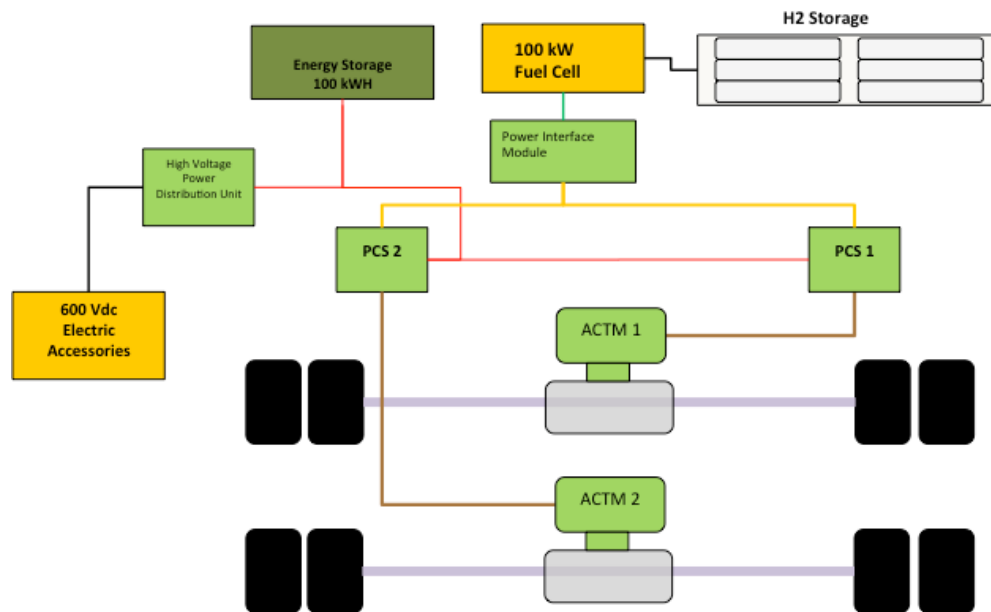


Figure II-65: Functional diagram of battery electric truck with H2 fuel cell range extender

TransPower will develop two battery electric trucks with hydrogen fuel cell range extenders. These trucks will employ a small fuel cell and stored hydrogen. One truck will be equipped with a 30 kW fuel cell and one with a 60 kW fuel cell, enabling a direct comparison of both variants.

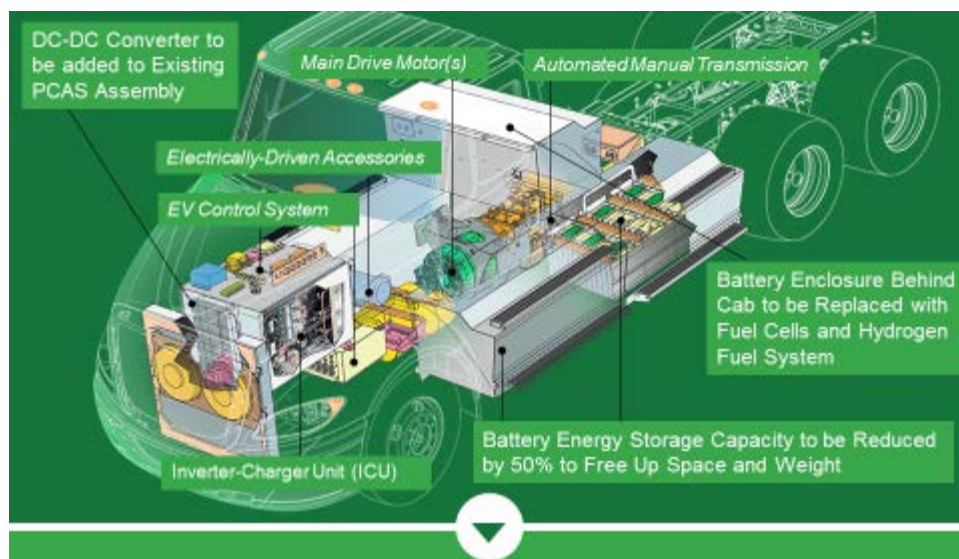


Figure II-66: Transpower truck subsystems

U.S. Hybrid will develop two equivalent battery electric trucks with an on-board hydrogen fuel cell generator. Each truck is estimated to have 20 kg of hydrogen storage at 350 BAR with an estimated fueling time under 10 minutes.

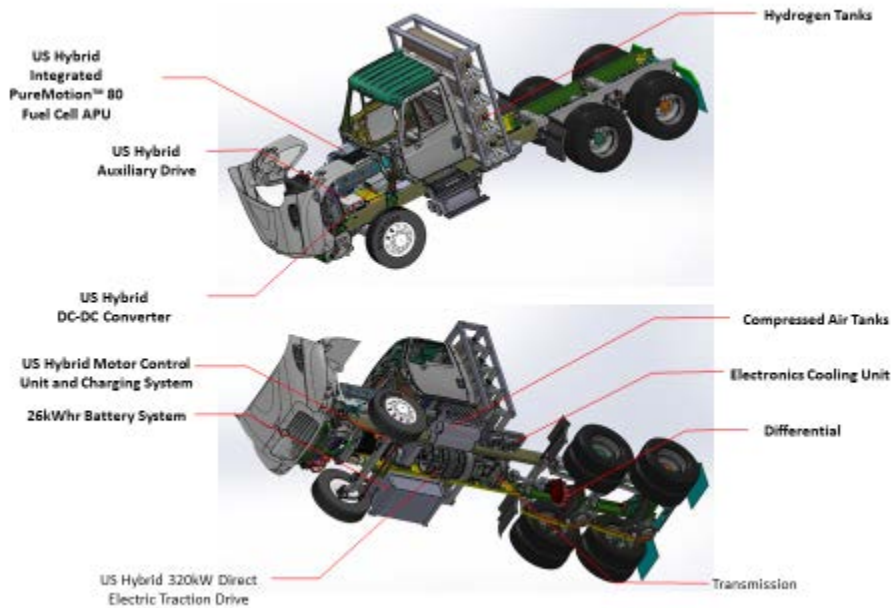


Figure II-67: U.S. Hybrid battery electric trucks with H2 fuel cell generator

BAE Systems and Kenworth will develop one hybrid battery electric truck with CNG range extender and catenary capability. The proposed technical concept provides an all-electric mode, a catenary electric mode to operate on a catenary system developed by Siemens and in a conventional hybrid mode using CNG.

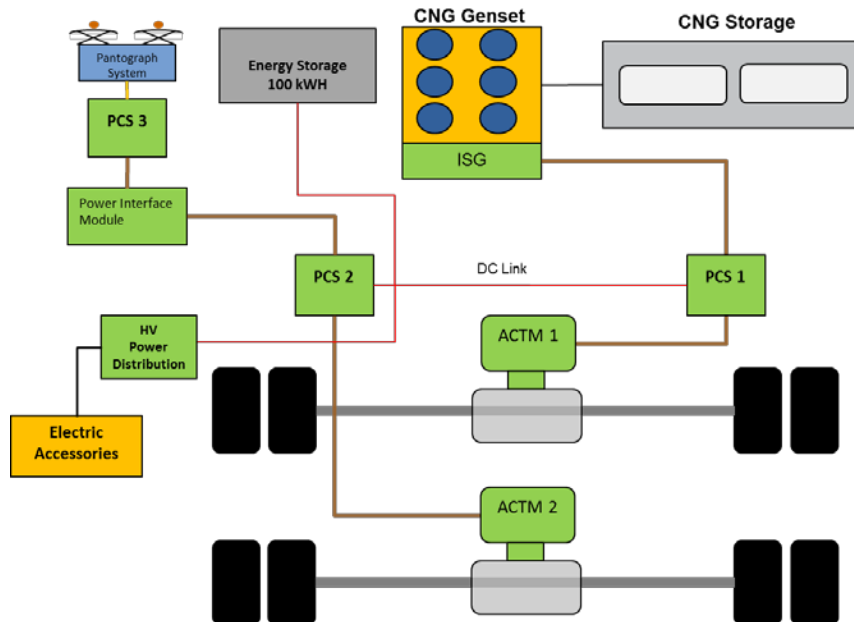


Figure II-68: Hybrid Electric Truck with CNG range extender

International Rectifier will develop a plug-in hybrid-electric truck, and ultra-fast chargers for use in or near the Ports. The vehicle concept will be capable of operating in a zero emissions (all-electric) mode in and around the Ports of Los Angeles and Long Beach. Outside that predetermined “Zero Emissions Zone”, the Class 8 hybrid electric vehicles will switch from all-electric to hybrid-electric mode where the vehicle will then operate at higher efficiencies to reduce diesel fuel consumption.

EV Architecture: Parallel PHEV

Modes of Operation:

1. All-electric drive mode
2. Hybrid mode
 - a) Motor-assisted start and acceleration
 - b) Brake regeneration
 - c) Engine start/stop
3. Zero-emissions Idle: IR EADS™ Electric Accessory Drive System

Recharging modes

1. Ultra-fast charging (15-20 minutes)
2. Diesel generation
3. Regenerative braking

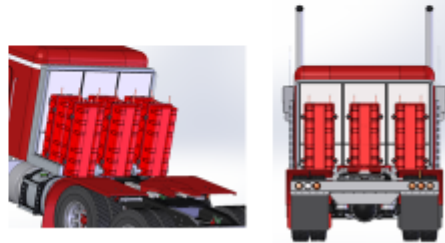


Figure II-69: Parallel PHEV truck

II.17. Hydrogen Fuel-Cell Electric Hybrid Truck Demonstration [DE-EE0005978] and Houston Zero Emission Delivery Vehicle Deployment [DE-E0005979]

Andrew J. DeCandis, Principal Investigator

Houston-Galveston Area Council
3555 Timmons Lane, Suite 120
Houston, TX 77027
Phone: (832) 681-2589; Fax: (713) 993-4508
E-mail: Andrew.DeCandis@h-gac.com

Lee Slezak, DOE Program Manager

Office of Energy Efficiency and Renewable Energy
E-mail: Lee.Slezak@ee.doe.gov

Charles Alsup, NETL Program Manager

Office of Energy Efficiency and Renewable Energy
Phone: (304) 285-5432
E-mail: Charles.Alsup@netl.doe.gov

Start Date: 10/01/2012

End Date: 09/30/2017

II.17.A. Abstract

Objectives

EE0005978

- Accelerate the introduction and penetration of electric transportation technologies (ETT) into the cargo transport sector.
- Demonstration of at least three (3) Class 8 zero-emission port drayage trucks
 - Vehicles will be selected through a Call for Projects process.
 - Vehicles will meet or exceed all applicable federal and state emission requirements and safety standards.
- Operate vehicles under real world conditions at or near the Port of Houston to measure and demonstrate operational cost-effectiveness and commercial viability.

EE005979

- Accelerate the introduction and penetration of electric transportation technologies (ETT) into the cargo transport sector.
- Deployment of thirty (30) all-electric delivery trucks.
- Project vehicles will be selected through a Call for Projects process.
 - Vehicles will be operated by selected fleet operators including large national fleets and progressive regional fleets with delivery operations.
- Testing and data collection for vehicles in real-world conditions to measure and demonstrate operational cost-effectiveness and commercial viability.

Accomplishments

EE0005978

- Developed and released a Call for Projects to solicit fleet partners for three (3) zero-emission Class 8 zero-emission trucks after originally proposed partners were unable to move forward with project as originally anticipated.
- Selected and contracted with Gas Technologies Institute for deployment and demonstration of three hydrogen-hybrid Class 8 drayage trucks.

EE0005979

- Developed and released a Call for Projects to solicit fleet partners for thirty (30) all-electric delivery vehicles after originally proposed partners were unable to move forward with project as originally anticipated.
- Selected and contracted with United Parcel Service (UPS) for the purchase of eighteen (18) all-electric delivery vehicles.
- Delivered the first contracted vehicle to UPS and began the UPS mandated 30-day testing period in preparation for deployment.

Future Achievements

EE0005978

- Full deployment and demonstration of at least three Class 8 zero-emission port drayage trucks.
- Release of technical report on cost-effectiveness of Class 8 zero-emission trucks in regional fleet(s).

EE0005979

- Complete deployment of the initial eighteen zero-emission all electric delivery vehicles.
- Contract with additional fleet(s) to deploy the final twelve (12) all-electric delivery vehicles.
- Reduce emission of 4,180 tons of criteria pollutants over the two year project deployment phase.
- Reduce emissions of greenhouse gases by 75 MMTCE over the two year project deployment phase.
- Reduce over 250,000 gallons of diesel fuel over the year project deployment phase.
- Release of technical report on cost-effectiveness and emission reductions related to vehicle deployment.



II.17.B. Technical Discussion

Background

EE0005978

The Houston-Galveston Area Council (H-GAC) is partnering with a project team (including a regional fleet and zero-emission Class 8 truck OEM) for a Zero-Emission Class 8 Drayage Truck Demonstration Project. The primary objective of the project is to accelerate the introduction and penetration of electric transportation technologies into the cargo transportation sector. The project will deploy vehicles, establish required fueling infrastructure, and demonstrate that vehicles will meet or exceed all emissions requirements.

To meet this objective, the grant will support development and demonstration of three Class 8 zero-emission trucks in the Houston-Galveston-Brazoria NAAQS 8-hour ozone nonattainment area. The project will

demonstrate vehicle operations, collect data, and report on project results for a period of two years after deployment.

Long-term benefits of the program may include improved air quality in highly traveled areas in the Houston region and particularly near the active port facilities. Additionally fleets may realize savings on fuel expenditures and can work towards meeting sustainability and corporate social responsibility goals.

EE0005979

The Houston-Galveston Area Council (H-GAC), Center for Transportation & the Environment (CTE), have partnered to establish the Houston Zero Emission Delivery Vehicle Demonstration Project. The primary objective of the project is to demonstrate the effectiveness of all-electric delivery vehicles to perform at the same level of operation as similarly sized diesel delivery vehicles, while reducing vehicle emissions and petroleum consumption.

To meet this objective, this project will support the deployment of 30 all-electric delivery trucks in the Houston-Galveston-Brazoria NAAQS 8-hour ozone nonattainment area.

Vehicles selected through a Call for Projects process will be demonstrated by selected national, regional, and/or local fleets. All vehicle deployment and operation of the vehicles will occur with the Houston-Galveston region. In addition to the deployment of delivery vehicles and charging infrastructure, the project will demonstrate vehicle operations, collect data, and report on project results for a period of two years after deployment.

Introduction

DE-EE0005978

This project supports ongoing efforts to reduce criteria pollutant emissions, greenhouse gas emissions, and fossil fuel use among drayage truck vehicles within the Houston region. As the project team works to create a demonstration of three zero-emission Class 8 drayage trucks, the vehicles will be monitored and fleet operators will be surveyed in order to measure and demonstrate operational cost-effectiveness and commercial viability of the trucks.

DE-EE0005979

The primary objective of this project is to deploy thirty zero-emission all electric trucks and demonstrate the effectiveness of the all-electric delivery vehicles to at the same level of operation as similarly sized diesel delivery vehicles while reducing vehicle emission and petroleum consumption.

The vehicles deployed will be selected through a Call for Projects process and will be deployed on delivery routes in the Houston-Galveston area. Large national fleets and progressive regional fleets that operate diesel and gasoline delivery vehicles in the region have been the initial targets for fleet deployment and testing. Integration of all-electric vehicles into their fleets will result in both emission and noise reductions over diesel and gasoline counterparts. The fleets will also reduce their reliance on petroleum-based fuels and realize significant cost savings.

Approach

EE0005978

Vehicles eligible to respond to the Call for Projects included zero-emission heavy-duty Class 8 drayage trucks. The vehicles were required to be cargo-carrying on-road trucks with an expected gross vehicle weight rating of at least 80,000 lbs. Project vehicles were required to be designed and used for the sole purpose of moving and/or delivering cargo, freight, goods. The vehicles were also required to be on-road legal and used under real-world drayage freight movement activities or through port or intermodal rail yard property for the purpose of loading, unloading or transporting cargo, such as containerized, bulk or break-bulk goods.

Project vehicles were required to be zero emission and use an electric motor for all of the motive power of the vehicles, including battery electric, fuel cell, and hydrogen hybrid electric fuel cell vehicles. The vehicles were also required to meet or exceed all applicable federal or state emission requirements and safety standards.

Testing

Qualitative evaluations and quantitative documentation for the tested parameters will be collected during the program using a combination of an on-board data collection system and input obtained by surveying drivers and maintenance personnel. These findings will be included in the monthly, quarterly and final reports.

Testing Variables

- Vehicle Operations
 - Daily Mileage
 - Operating Time
 - Payloads
 - Speed
 - State of Charge
 - Auxiliary Loading
 - Maintenance Costs
- Charging Operations
 - Daily Charge Times
 - State of Charge
 - Energy Consumption
 - Utility Costs
 - Maintenance Costs

Demonstration Period

The project will include a two-year demonstration of the zero-emission Class 8 vehicles under real world conditions.

Infrastructure Requirements

Recharging/refueling infrastructure needed for this project will be located to allow the proper charging of the trucks utilizing the facility.

Commercialization

The experience and data collected from this project will help validate hydrogen and/or electric as a feasible alternative fuel options. Confirming durability and driver acceptance are also key results expected from this demonstration that would advance commercialization of zero-emission Class 8 vehicles.

EE0005979

CTE will work with fleets and OEMs selected through the Call for Projects to plan, select, and model routes on which the vehicles will be deployed. The project team will also install and test the charging stations in preparation for vehicle deployment. Once the vehicles are delivered, the project team will conduct a series of tests to validate vehicle performance against the model. Once deployed in delivery service, the team will collect operational data and submit reports for two years.

As a result of the Call for Projects process, UPS and Workhorse were selected as the initial fleet/vehicle team for this project. UPS will be accepting 18 of the project's 30 vehicles. H-GAC and CTE continue to search for a fleet for the final 12 vehicles. The following information pertains to this project.

System Description

Workhorse is developing a new chassis for this project and for the commercial market. The W88 chassis is designed to meet the needs of a wide range of customers. At the same time, it is a universal chassis from an operations perspective.

The vehicle is 100% electric powered by a 120kWh battery pack giving it a useful range of 80 miles in a typical 120-150 stop per 8 hour package delivery shift. The range of the Workhorse truck will be more than adequate to cover the 50 to 65 mile per day routes in Houston. The vehicle has no transmission--it is a direct drive to the differential making it very efficient. The electric motive drive is a 2200NM regenerative drive capable of powering a 23,000 pound vehicle from a dead stop up a 23% incline.

Top speed of the vehicle is limited to 65 mph. Typical differential ratios are 4.78 to 1 and 5.1 to 1 for the direct drive. The vehicle has a supervisory controller that interfaces with the Battery Management System, the Body Control Module, and the Brake Module, and the charging system to control the vehicle. There is an onboard level two J1772 charger, either 7KW or 18Kw depending on the customer preference. The vehicle can also be fitted with inductive charging.

Testing

UPS as well as any additional recipient fleet, in partnership with CTE and Workhorse, will report vehicle and charger specifications and will collect operational and maintenance data for vehicles. Data collected may include powertrain and battery operational data. Additionally, data from non-electric fleet vehicles may be required for comparative analysis. All information collected shall be provided to CTE. CTE will analyze the data and summarize for submittal to DOE.

Testing Variables

- Vehicle Operations
 - Daily Mileage
 - Operating Time
 - Payloads
 - Speed
 - State of Charge
 - Auxiliary Loading
 - Maintenance Logs
- Charging Operations
 - Daily Charge Times
 - State of Charge
 - Energy Consumption
 - Utility Costs
 - Maintenance Logs
- Data Collected will be used to calculate a number of analytical factors, including, but not limited to:
 - Fuel Efficiency (i.e., \$/mile, kWh/mile, etc.)
 - Cargo Ton-Miles/Vehicle
 - Cargo Ton-Miles/Fleet
 - Reduction in Petroleum Consumption
 - Reduction of Green House Gas Emissions (Million Metric Tons of Carbon Equivalent (MMTCE)/year)
 - Reduction of Criteria Pollutant and Toxic Emissions
 - Expected Life Cycle Benefit Analysis

Demonstration Period

The project will include a two-year demonstration of each all-electric truck under real world conditions.

Data Collection Strategy

New vehicles are tested by Workhorse for durability and are equipped with data collection and monitoring systems to track variables from the battery management, drive system, cooling systems, etc. Coast-down testing is used to determine projected energy usage per mile; use case testing is accomplished to verify that vehicle energy usage is consistent with projected usage. Limits of charge and discharge are set as to ensure that the main battery will operate to its projected life without overstressing it.

Real time data is sent to a server for storage and analysis and parameters are modified as necessary to insure the vehicle performs to its design parameters.

Vehicles prototypes are tested on steep hills and anticipated normal driving conditions locally to get baseline data before TRC testing. Data is collected to determine energy usage per mile under various driving conditions and compared to predicted models to determine battery life, range, acceleration etc. Major vehicle maintenance for production vehicles can be performed at Workhorse dealers across the country.

Infrastructure Requirements

Each vehicle comes with a water-cooled J1772 level 2 charger on-board. The charger is typically 12kWh, 220 Vac. Vehicles may be optionally equipped with 25KW induction charging.

Commercialization

It is believed that the vehicles used in this project will result in a positive business case on a total cost of ownership basis for UPS and other selected fleets. This is due to the lower cost of electricity and lower maintenance costs as compared to fuel and maintenance of diesel medium- and heavy-duty vehicles.

Results

EE0005978

The new project team has been convened and is currently preparing to manufacture the vehicles. To date, no performance data has been collected.

Expected results:

H-GAC anticipates the following actions to occur as a result of this project:

- increased adoption of zero-emission Class 8 technology for drayage fleets
- increased adoption of technology for regional port operators as a result of outreach and exposure to the project
- increased adoption of technology through other outreach and education efforts to ports in other areas, through DOE meetings, participation in DOE Clean Cities/Clean Fleets partnership programs

EE0005979

The project team has contracted with United Parcel Service (UPS) to for the purchase of eighteen (18) all-electric delivery vehicles. These vehicles are currently in the manufacture process. One vehicle has been delivered to date, however performance data has not yet been collected.

Expected results:

H-GAC anticipates the following actions to occur as a result of this project:

- Reduction of petroleum use in the demonstration period during and after the project activities
- Reduction of greenhouse gases, criteria pollutants, and toxic emissions

- Demonstration and evaluation of market viability
- Opportunity to increase adoption of the demonstration technologies
- Expansion of U.S. manufacture and production of electric vehicles and U.S. suppliers of batteries and equipment for electric vehicles

Conclusions

EE0005978

This project will produce on-road experience and gather data which will serve to accelerate the introduction and penetration of electric transportation technologies. Specifically, at least three zero-emission Class 8 trucks will be deployed into the drayage cargo transportation sector. Current delays in project initiation will require an aggressive timeline for manufacture of advanced vehicle technologies and the establishment of adequate fueling and/or charging infrastructure in early 2016.

EE0005979

This project will produce on-road experience and gather data which will serve to accelerate the introduction and penetration of electric transportation technologies. Specifically, 30 zero emission all-electric trucks will be deployed across the Houston region. The project has experienced delays due to financial challenges faced by the originally intended OEM and in identifying appropriate routes in the Houston area as a result of typically longer travel routes. Continued outreach and education have identified routes and vehicles for deployment of vehicles in late 2015 early 2016.

II.17.C. Products

Presentations/Publications/Patents

EE0005978 & EE0005979

None to Date

II.17.D. References

None

II.18. Zero Emission Drayage Trucks Demonstration [DE-EE0005961]

Matt Miyasato, Principal Investigator, Deputy Executive Officer

South Coast Air Quality Management District
21865 Copley Drive
Diamond Bar, CA 91765
Phone: (909) 396-3249; Fax: (909) 396-3252
E-mail: mmiyasato@aqmd.gov

Brian Choe, Co-Principal Investigator, Program Supervisor

South Coast Air Quality Management District
Phone: (909) 396-2617; Fax: (909) 396-3252
E-mail: bchoe@aqmd.gov

Lee Slezak, DOE Technology Development Manager

U.S. Department of Energy
Phone: (202) 586-2335
E-mail: lee.slezak@ee.doe.gov

Start Date: 10/1/2012

End Date: 9/30/2017

II.18.A. Abstract

Objectives

- The objective of this project is to develop and demonstrate zero emission capable heavy-duty drayage trucks based on four different architectures, consisting of two battery electric drivetrains and two plug-in hybrid electric drives with all-electric range capability, to promote and accelerate deployment of zero emission cargo transport technologies.
- This project will also collect and analyze vehicle performance and O&M data to evaluate technical feasibility and market viability of zero emission truck technologies to support drayage operations.

Accomplishments

- Completed system and components design for all battery electric trucks (BETs)
- Incorporated design upgrades through validation and optimization processes
- Tested TransPower's BET on chassis dynamometer at University of California, Riverside
- Completed five BETs with three of them currently in demonstration with fleet partners at the Ports of Los Angeles and Long Beach, and the other two undergoing testing or upgrade
- Continue to collect and analyze vehicle performance and operational data.

Future Achievements

- Complete and deploy the remaining six vehicles in revenue drayage service for demonstration
- Complete validation testing including chassis dynamometer testing.



II.18.B. Technical Discussion

Introduction

On-road heavy-duty diesel trucks are one of the largest sources of diesel particulate matter and NOx emissions in the South Coast Air Basin. The impact on air quality and public health is more pronounced in the surrounding communities along the goods movement corridors near the Ports of Los Angeles and Long Beach, and next to major freeways in Southern California. As a measure to reduce the impact and to meet federal ambient air quality standards, South Coast Air Quality Management District (SCAQMD) has been working with regional stakeholders, including the Ports of Los Angeles and Long Beach, to promote and support the development and deployment of advanced zero emission cargo transport technologies. In 2012, SCAQMD received a \$4.17 million grant from the DOE Zero Emission Cargo Transport Demonstration Program to develop and demonstrate zero emission capable drayage trucks based on four different electric drive architectures in real world drayage environment. The objective is to promote zero emission truck technologies to fleet operators, the end users, by demonstrating that electric drayage trucks are capable of supporting demanding drayage operations reliably, thus helping to accelerate their market acceptance within the trucking industry. This project is also to collect and analyze vehicle performance and O&M cost data to evaluate the benefits over conventional diesel trucks and assess their market viability in drayage operations.

Approach

This project will develop eleven zero emission and near-zero emission heavy-duty drayage trucks for demonstration based on four different architectures, consisting of two types of battery electric vehicles (BEVs) and two types of plug-in hybrid electric vehicles (PHEVs) with all-electric range capability. Initial project scope had a total of thirteen trucks including Vision Motor's fuel cell hybrid electric trucks and Balqon's BETs but these two companies have since dropped out due to financial hardships and limited resources. With the departure of Vision Motors and Balqon, TransPower and US Hybrid, locally based EV system developers and integrators in Southern California, have been selected to develop plug-in hybrid electric trucks (PHETs) with all-electric range in addition to the BETs they are already building in this project as summarized in Table II-17.

Table II-17: 2012 Zero Emission Drayage Truck Demonstration Portfolio

Technology Demonstrator	Architecture	No. of Trucks
TransPower	BEV	4
US Hybrid	BEV	2
TransPower	PHEV	2
US Hybrid	PHEV	3
Total		11

Upon completion, these trucks will be deployed in revenue drayage service for two years of demonstration with fleet partners at the Ports of Los Angeles and Long Beach. During the demonstration, vehicle performance and O&M data will be collected and analyzed by National Renewable Energy Laboratory (NREL) to evaluate technical feasibility and market viability of the technologies for drayage operations. In addition, each technology will be tested on chassis dynamometer at the University of California, Riverside (UCR) for performance validation.

Battery Electric Trucks

a) TransPower

TransPower will develop four Class 8 BEV drayage trucks for demonstration. The motive power will be provided by a dual motor system with two 150 kW Fiskar motors leveraging mass produced components for cost savings and proven reliability. The motors will be coupled to an automated manual transmission (AMT) with proprietary software for high vehicle performance and improved efficiency. Also, TransPower will use an innovative Inverter-Charger Unit (ICU) that combines the functions of both vehicle inverter and battery charger to reduce the size and cost of power electronics.

Figure II-70 shows an illustration of the TransPower BEV system, which is comprised of:

- 300 kW dual motor assembly with two 150 kW motors coupled to an AMT
- Power control and conversion system with two ICUs, each rated at 150 kW for motor control and 70 kW for charging
- 215 kWh lithium iron phosphate battery pack, air cooled
- 70 to 100 miles of range in normal drayage operation
- Recharge time of 3-4 hours with one 70 kW ICU

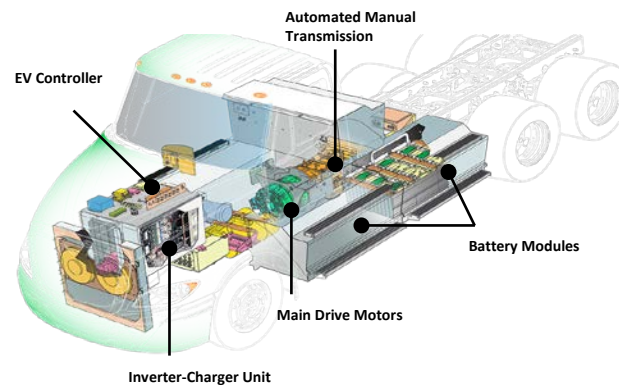


Figure II-70: TransPower BEV System

b) US Hybrid

US Hybrid will develop two Class 8 BEV drayage trucks. Each truck will be powered by a dual motor combination coupled with an AMT to provide higher continuous torque and power rating without compromising efficiency. A 240 kWh lithium-ion battery pack will provide an estimated operating range of 80-100 miles in normal drayage operations.

Figure II-71 shows an illustration of the US Hybrid BET, which is equipped with:

- 320 kW powertrain with a dual motor combination and automated manual transmission
- 320 kW Motor Control Unit
- Lithium-ion battery pack with 240 kWh in total capacity, air cooled
- 80 to 100 miles of range in normal drayage operations
- Recharge time of 4-5 hours with 60 kW on-board charger

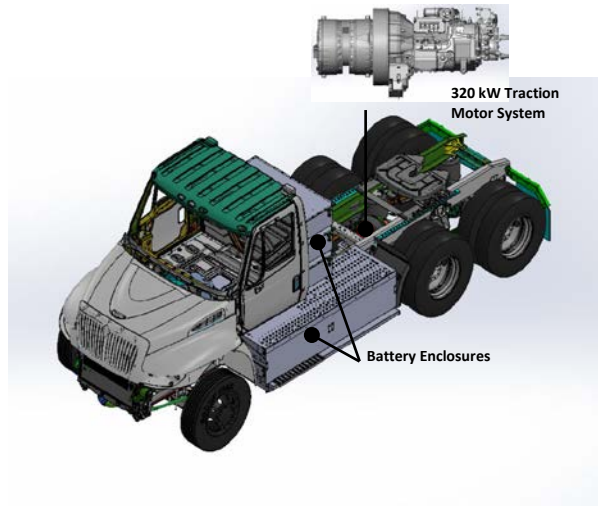


Figure II-71: US Hybrid BEV System

Plug-In Hybrid Electric Trucks

a) TransPower

Two Class 8 CNG plug-in hybrid electric drayage trucks will be developed by TransPower with a targeted operating range of 150-200 miles, including 30-40 all-electric miles. The hybrid technology is based on the electric drive system TransPower has developed for their BETs, which are currently in demonstration with fleets at the Ports of Los Angeles and Long Beach. In addition, TransPower will utilize commercially available and widely used CNG engines and components, which will help to make these trucks more cost-competitive and well-positioned for commercialization.

Figure II-72 shows an illustration of the TransPower’s CNG PHEV system, which is based on their BEV drive system with highlighted design changes including incorporating CNG engine-generator and fuel line behind the cab and reducing the battery capacity in half. The system will be comprised of:

- Series hybrid system with a smaller 3.7L CNG engine-generator
- 300 kW dual motor assembly coupled to 10-speed AMT
- Power control and conversion system with two ICUs, each rated at 150 kW for motor control and 70 kW for charging
- 107 kWh lithium iron phosphate battery pack, air cooled
- 30-40 all-electric miles
- 150-200 miles of total range in normal drayage operations

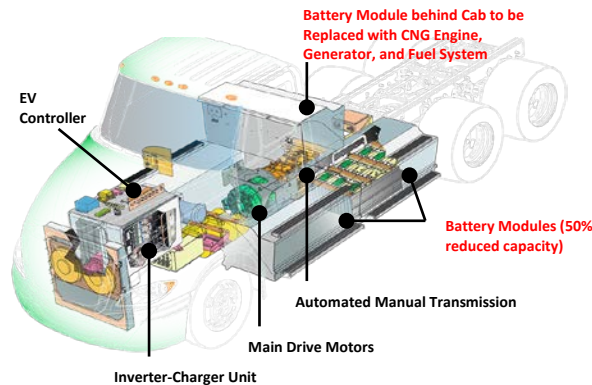


Figure II-72: TransPower CNG PHEV System

b) US Hybrid

US Hybrid will develop three Class 8 LNG plug-in hybrid electric drayage trucks for demonstration. US Hybrid is currently working to develop two LNG hybrid trucks by converting Autocar trucks with an 8.9L ISL-G engine for refuse hauler application. Leveraging this hybrid drive system, US Hybrid will convert three LNG drayage trucks into PHEVs with all-electric range capability.

Figure II-73 shows the proposed US Hybrid LNG PHEV topology, which will be comprised of:

- Parallel hybrid system with 8.9L LNG engine
- 240 kW powertrain with a dual motor combination and AMT
- 240 kW motor control unit and 20 kW on-board charger
- Lithium-ion battery pack with 80-100 kWh in total capacity, air cooled
- 30-40 all-electric miles
- 150-200 miles of total range in normal drayage operations

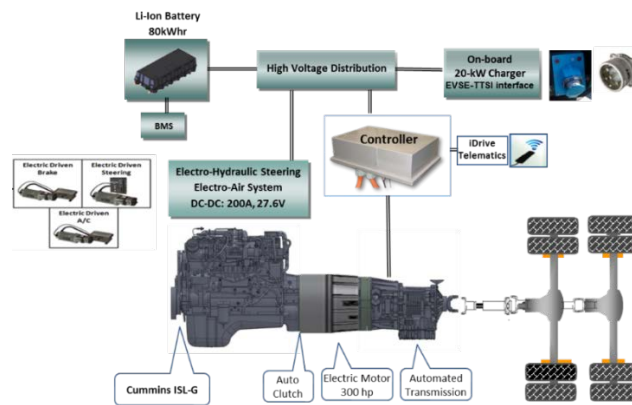


Figure II-73: US Hybrid LNG PHEV System

Results

Battery Electric Trucks

Despite setbacks due to the departure of Vision and Balqon, the project has made a good progress in FY2015. TransPower has completed all four trucks with three of them currently in demonstration in revenue drayage service at the Ports of Los Angeles and Long Beach. US Hybrid has also completed their first BET with chassis dynamometer testing scheduled in October 2015. US Hybrid expects to deliver the truck to TTSI for demonstration by this December and plans to deliver the second truck in March 2016. The achievements in FY2015 are further discussed below.

a) TransPower

TransPower completed and delivered all four BETs, EDD1 through EDD4, to fleet partners for demonstration as of August 2015. However, EDD1 had to be recalled to their facility in Poway California due to continuing issues with battery cells and BMS. This issue is limited to EDD1 because the problem was discovered early enough for TransPower to switch to more reliable cells and BMS for other EDD trucks. In order to effectively deal with this nagging issue, TransPower has decided to upgrade the energy storage system for EDD1 to the next generation cells and BMS with higher energy density and reliability. The upgrade is currently scheduled for December 2015.

The four BETs have collectively accumulated over 10,000 miles of on-road testing and revenue service demonstrations to date. Feedback from fleet operators described the trucks as quiet, clean and easy to drive especially in the stop and go traffic at the ports. The 80-mile range with average payloads works well for short haul applications, especially with the close port operators like SA Recycling, Cal Cartage and National Retail

Trucking (NRT). Those companies complete as many as 4 or 5 container “moves” or “turns” daily from the port terminals to their transfer stations. Averaging 10 miles an hour, the trucks can operate a full 8 hour shift in most cases. Some operators even run 10+ hours in a shift.



Figure II-74: TransPower EDD Trucks

EDD2 has seen the most service of the fleet, having been in demonstration service with TTSI since January 2015. The truck has accumulated over 2,800 drayage miles in 50 days of use over the past 9 months, averaging 52 miles per shift ranging from 19 miles to 135 miles per charge. Much of the downtime is related to administrative and logistical issues such as DMV registrations and driver training as well as EVSE installations to support electric trucks. EDD2 has not experienced any major technical issues to date. Some of the technical issues reported pertain to shift quality and sensing, advanced inverter controls, water clamps, water intrusion during heavy rain storms and two BMS circuit boards with shuffling issues. Most of these issues were promptly addressed with on-site fixes or software patches. With 9 months of operation in revenue drayage service, TransPower has been able to improve reliability and efficiency of the EDD trucks based on feedback from the operators.

UCR recently released a report on the chassis dynamometer testing they had conducted on EDD2 in October 2014. The testing was performed over several transient and steady state cycles representing simulated drayage operations for near dock and local operations around the ports as well as regional operations involving highway driving to warehouses and distribution centers located 30 to 40 miles inland from the ports. In all cases, EDD2 had favorable performance, improved fuel economy, and significant emission reductions compared to current model year conventional diesel HDVs as summarized below:

- EDD2 performed well on all test cycles from full to 20% SOC load. The truck also maintained sustained peak loads without loss of performance, deratings, or safety concerns in the range of 80 miles with 72,000 lbs. GCWR.
- The total energy usage was similar between the Near-Dock, Local, and the Regional cycles at 2.06 to 2.10 kWh/mi suggesting the energy rate per mile is not necessarily a function of average power for port driving operations.
- EDD2 recovered between 12 to 22% in regen energy with the highest recovery efficiency achieved for the Near-Dock cycle, suggesting these electric trucks are well suited for short haul applications near the ports with many stop and go operations.
- The fuel efficiency ranged from 17.9 to 18.3 MPGde for the transient port cycles and reached as high as 19.2 MPGde for the 55 mph cruise cycle. The efficiency far surpassed that of conventional diesel trucks as shown in Figure II-75.

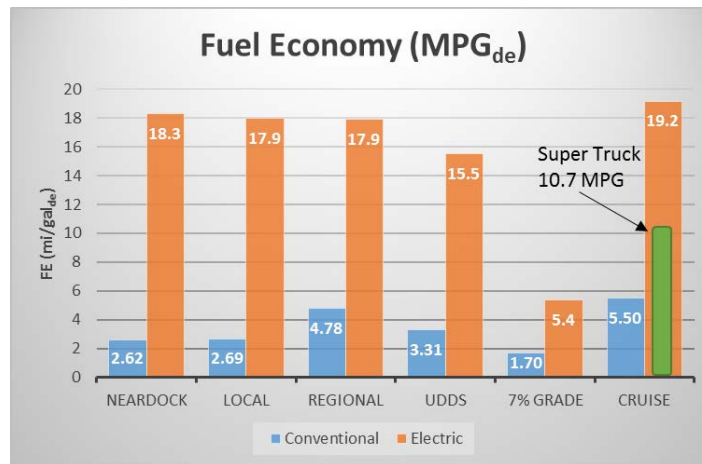


Figure II-75: Fuel Economy Comparison: EDD2 vs Conventional Diesel Trucks
Performance Evaluation of TransPower All-Electric Class 8 On-Road Truck Final Report/UCR CE-CERT

EDD trucks are continuing to generate interest within the local and national trucking industry. After starting out with only two fleets for demonstration, namely TTSI and SA Recycling in January 2015, many more fleet operators have since inquired about signing up for drayage fleet trials including Cal Cartage, NRT, Knight Transportation, PASHA, Osterkamp, APM, Seaside, and 3 Rivers Trucking. In August 2015, EDD3 and EDD4 were delivered to Cal Cartage and NRT respectively for demonstration and other fleets are waiting for completion of additional EDD trucks that are funded in a separate project by California Energy Commission, SCAQMD, and Ports of Los Angeles and Long Beach.

b) US Hybrid

US Hybrid has also made significant progress in FY 2015 having completed their first demonstration truck (Figure II-76) in September 2015. The truck is now undergoing commissioning process to check proper operation of each subsystem and is scheduled for a chassis dynamometer testing at UCR in October. US Hybrid expects to deliver the truck to TTSI for demonstration by this December with a plan to deliver the second BET in March 2016.



Figure II-76: US Hybrid Fully Integrated BET

The following summarizes some of their accomplishments in FY 2015:

- Performed power cycling test to validate the energy and power density of battery packs using the worst case scenario. With 11 packs in parallel, the available energy will be 210 kWh with 385 kW in total available power, sufficient to support the 320 kW drive system.

- Tested the command display and data collection system. The system was able to display captured vehicle performance data including battery SOC, fuel economy, speed and temperature readings as well as the remaining range.
- Tested a prototype with 240 kW motor to measure required power to maintain 55 mph during freeway driving and uphill conditions.
- US Hybrid is developing a 60 KW on-board charger for demonstration vehicles. The on-board charger will provide simplified charging logistics for fleets compared to bulky off-board chargers.

Plug-In Hybrid Electric Trucks

Since both technologies were recently added to the project, contracts have not been finalized. However, given that both TransPower and US Hybrid will be utilizing hybrid drive systems already developed from related projects, it is expected that the product developments will be fairly quick with the first demonstration vehicles to be completed within six to nine months from contract executions.

II.18.C. Products

Presentations/Publications/Patents

None

II.18.D. References

None

III. Vehicle Technology Evaluations

III.1. Advanced Technology Vehicle Lab Benchmarking (L1&L2)

Kevin Stutenberg (Level 1); Eric Rask (Level 2), Principal Investigators

Argonne National Laboratory
9700 South Cass Avenue
Lemont, IL 60439
Phone: (630) 252-6788; Fax: (630) 252-3443
E-mail: kstutenberg@anl.gov, erask@anl.gov

Lee Slezak, DOE Program Manager

U.S. Department of Energy
Phone: (202) 586-2335
E-mail: Lee.Slezak@ee.doe.gov

Start Date: October 1, 2014
End Date: September 30, 2015

III.1.A. Abstract

Objectives

- Provide independent evaluation of advanced automotive technology via benchmarking of advanced technology conventional vehicles (CVs), hybrid electric vehicles (HEVs), plug-in hybrid electric vehicles (PHEVs), battery electric vehicles (BEVs), and alternative fuel vehicles (AFVs) for the Vehicle Technologies Office of the U.S. Department of Energy (DOE).
- Establish the baseline for state-of-the-art automotive technology in powertrain systems and components through acquisition of independent and publicly available test data and analysis.
- Disseminate vehicle and component testing data to partners of the DOE, such as other national laboratories, the U.S. Council for Automotive Research (USCAR), OEMs, suppliers and universities.
- Provide data to support both codes and standards development and powertrain simulation model development and validation.

Accomplishments

- Level 1, Noninvasive technology assessments accomplishments
 - Completed technology assessment of nine advanced technology vehicles. Vehicles evaluated were of multiple classes and fuel types. These included:
 - 2014 Chevrolet Cruze Diesel (Conventional)
 - 2014 Mazda 3 iEloop (Conventional)
 - 2014 Smart Electric (BEV)
 - 2014 BMW i3 with optional Range Extending Engine (PHEV)
 - 2014 BMW i3 (BEV)
 - 2015 Honda Accord Hybrid (HEV)
 - 2015 Kia Soul EV (BEV)
 - 2015 Chevrolet Spark Electric (BEV)
 - 2012 VW Passat Bi-Fuel (Gasoline and CNG)

- Level 2: Invasive technology assessments
 - Completed technology evaluation of the 2014 Honda Accord PHEV
 - Completion of preliminary testing and instrumentation of the 2014 BMW i3 with range extending engine

Future Achievements

- Continued evaluation of advanced technology powertrain systems and components in order to provide independent and public data and analysis to the DOE's Vehicle Technologies Office and its partners.
- Support the EV Everywhere Solution Center with analysis and data



III.1.B. Technical Discussion

Background

Since its inception, the Advanced Powertrain Research Facility (APRF) has been testing advanced-technology vehicles to benchmark the latest automotive technologies and components for the U.S. Department of Energy (DOE). The staff has tested a large number of vehicles of different types, such as advanced technology conventional vehicles (CVs), hybrid electric vehicles (HEVs), plug-in hybrid electric vehicles (PHEVs), battery electric vehicles (BEVs), and alternative fuel vehicles (AFVs).

Introduction

Since the late nineties, the researchers at the APRF have developed a broad and fundamental expertise in the testing of the next generation of energy-efficient vehicles. Over this period of time, many methods of vehicle instrumentation and evaluation have continuously been refined. Two levels of instrumentation and testing exist today. The first level (Level-1) involves comprehensive, but non-invasive, instrumentation of a vehicle, leaving the vehicle unmarked after the testing. Typically these L1 vehicles enter Idaho National Laboratory's (INL) fleet testing as part of the DOE's Advanced Vehicle Testing Activity (AVTA). The second level (Level-2) involves comprehensive invasive instrumentation of a vehicle and its powertrain components, which leaves the vehicle with irreversible alterations, but provides an in-depth assessment of the technology.

This report summarizes the Level-1 and Level-2 benchmark activities of FY 2015. The first section describes the test approach for the benchmark work followed by a second section which highlights some select test results and analysis.

Approach

Vehicle Acquisition

The Level 1 benchmark program leverages the DOE's AVTA activities. Through this program, INL in collaboration with Intertek Testing Services, procures new advanced-technology vehicles to evaluate through accelerated fleet testing. As part of the evaluation, these vehicles are benchmarked at Argonne National Laboratory's APRF. Figure III-1 illustrates the AVTA process.

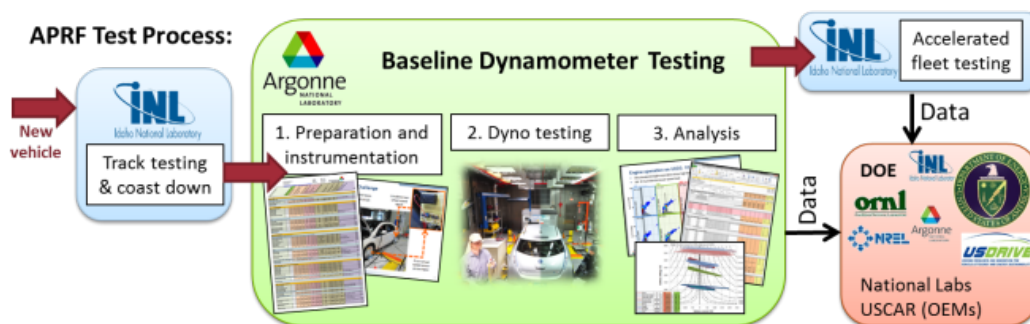


Figure III-1: Advanced Vehicle Testing Activity process.

Further information on the AVTA is available at avt.inel.gov/.

Additional test vehicles to those supplied within the AVTA program can be acquired for Level 1 evaluation in addition.

Level 2 vehicles are acquired by Argonne directly from dealerships. The typical Level 1 instrumentation is so invasive and complete that the vehicles are typically not road worthy at the completion of the program. The Level-2 test vehicles are maintained by Argonne to be used in future studies to support DOE investigations.

General Test Instrumentation and Approach

Typically, Argonne receives Level 1 test vehicles on loan; therefore, the vehicles need to leave the test facility in the “as-received” and road worthy condition. This requirement limits instrumentation to sensors that can be easily installed and removed without leaving any damage.

Despite this limitation, Argonne strives to achieve the maximum level of instrumentation to facilitate relevant data collection. If the vehicle has an internal combustion engine, instrumentation is applied to measure the engine speed, fuel flow and engine oil temperature (achieved through dipstick instrumentation). For electrified vehicles, a power analyzer is used to record the voltage and current from the high voltage energy storage system. If the vehicle requires charging, the electric power from the grid to the charger is measured. Furthermore, any sensors that can be fitted without permanent damage to the vehicle, such as temperature sensors, are typically included in locations of interest (a battery pack vent, for example). Additional APRF instrumentation focuses on the particular or unique technology, or technologies that enable the increased energy efficiency of the powertrain. A final aspect of Level 1 instrumentation is the recording of messages from the vehicle’s information buses, the content of which varies widely from vehicle to vehicle. This is completed by determining and recording both transmitted diagnostic and broadcast network messages.

The Level 2 benchmark, which included in-depth, testing, and analysis of new and emerging vehicle technologies, is specific to each vehicle. The particular Level 2 instrumentation is therefore described in the results and analysis section of the Level 2 vehicles of this report.

Advanced Powertrain Research Facility

In order to evaluate a vehicles in a variety of real-world conditions, the 4WD chassis dynamometer of the APRF is EPA 5-cycle capable. The test cell includes a thermal chamber and an air-handling unit with a large refrigeration system that enables vehicle testing at the EPA “Cold CO Test” ambient temperature of 20°F (-7°C), the standard test temperatures of 72°F (25°C) as well as the "SC03" test temperature of 95°F (35°C). Additionally, ambient test temperatures of 0°F (-17°C), and 40°F (4.5°C) maybe used. All temperatures can be evaluated with or without solar emulation lamps providing up to 850 W/m2 of radiant sun energy. The test cell is shown in Figure III-2.

Advanced Powertrain Research Facility
4WD Chassis Dynamometer Thermal Test Cell

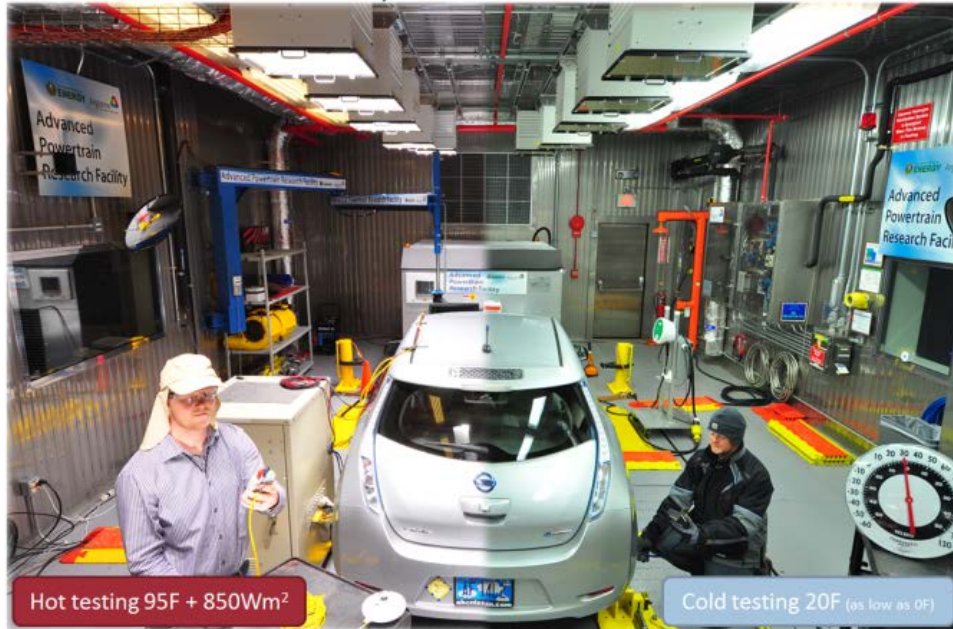


Figure III-2: Illustration of testing at 95°F with sun emulation (left) and at 20°F cold ambient temperature (right).

The APRF benchmark program goes well beyond the standard tests performed for EPA certification of fuel economy and emissions. To fully characterize the powertrain and the individual components the instrumented powertrains are tested on a wide range of ambient temperatures, drive cycles, performance tests and vehicle/component mapping tests.

Purpose of Benchmarking

A major goal of the benchmarking activity is to enable petroleum displacement through data dissemination and technology assessment. The data generated from the vehicle testing as well as the analyses are shared through several mechanisms, such as raw data, processed data, presentations and reports.

The independent and public data is a foundation enabling the development of rigorous and technology neutral codes and standards. The data also serves to develop and validate several modeling and simulation tools within the DOE system (i.e., Autonomie) as well as outside (i.e., EPA Alpha model, University modeling, and economic models). These activities in turn impact the modification of test plans and instrumentation for current and future test vehicles. Partners in the testing include U.S. manufacturers and suppliers, through the U.S. Council for Automotive Research. Many of the research activities of the DOE rely on the benchmark laboratory and fleet testing results to make progress towards their own goals. Figure III-3 details some of these DOE research activities and partners.

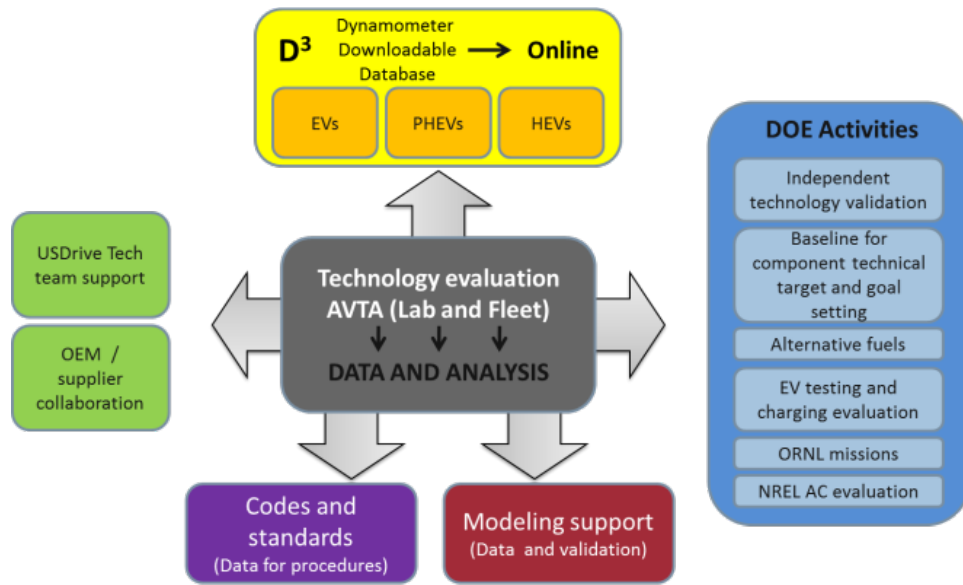


Figure III-3: Data dissemination and project partners

An additional avenue for data distribution is Argonne’s Downloadable Dynamometer Database (D3), which is a public website at anl.gov/D3. The D3 website provides access to a subset of data and reports.

Downloadable Dynamometer Database (D3)

D3 is a public web portal of highly detailed accurate public and independent vehicle test data, of critical utility in the research community. This web-based portal to Argonne vehicle test data is designed to provide access to dynamometer data that are typically too expensive for most research institutions to generate. Shared data is intended to enhance the understanding of system-level interactions of advanced vehicle technologies for researchers, students, and professionals engaged in energy-efficient vehicle research, development, or education. Figure III-4 shows the structure and content of the database.

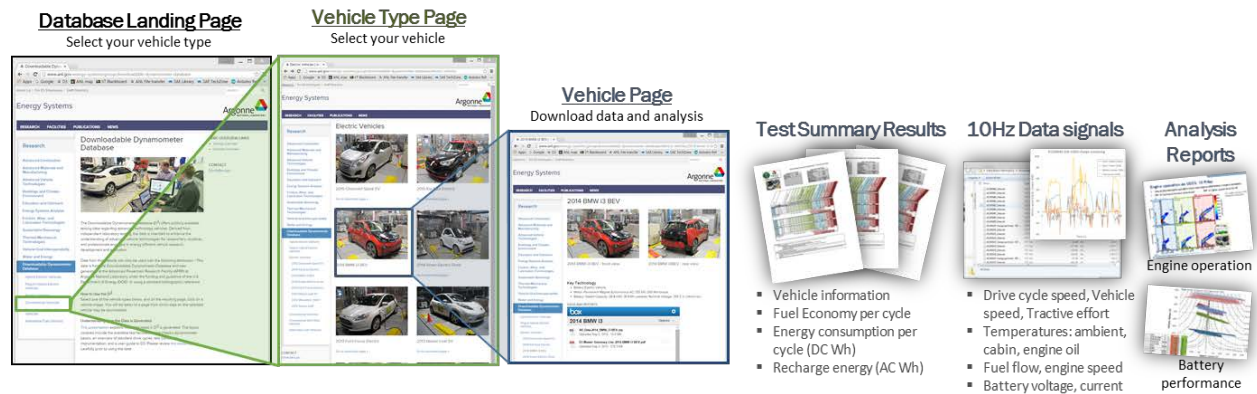


Figure III-4: Map of Downloadable Dynamometer Database content

The data and analysis from each vehicle tested through the non-invasive Level 1 benchmarking program is posted to D3.

Level 1 Evaluation Results

2014 Chevrolet Cruze Diesel

Vehicle Description

The 2014 Chevrolet Cruze Diesel is one of the first diesel compact vehicles from a domestic OEM sold within United States. A considerable amount of technological advancement in diesel engine and emissions after treatment technology enables high efficiency and low emissions. The Cruze has an advanced exhaust after-treatment system includes the injection system for diesel exhaust fluid, a diesel oxidation catalyst, diesel particulate filter, and selective catalyst reduction. The specifications of the vehicle are listed in Table III-1.

Table III-1: 2014 Chevrolet Cruze Diesel specifications

Architecture	Midsize Conventional, FWD
Engine*	2.0-Liter I4, Diesel Turbo DOHC FWD 148 HP, 349.8 Nm
Transmission*	6 Speed Automatic
EPA Label Fuel Economy (mpg)^	27 city / 46 hwy / 33 combined

* manufacturer's data

^ fuelconomy.gov

Vehicle Instrumentation

To capture the key technical aspects of the 2014 Chevrolet Cruze Diesel, testing and instrumentation focused on exhaust emissions and fuel consumption. The instrumentation focused on tailpipe emissions measured and analyzed with the emissions bench (bag and modal measurements) supplemented with a considerable amount of diagnostic powertrain messages. These vehicle reported parameters included: exhaust gas temperature, NO_x concentration, diesel particles filter accumulation, exhaust gas recirculation valve position, and many others relating to powertrain operation. Concurrently the APRF emissions bench was used to measure CO, CO₂, NO_x, THC and CH₄.

Points of interest

Vehicle Emissions Systems

Emissions reductions are enabled by an exhaust gas recirculation, an exhaust after treatment system and advanced fuel system components. The vehicle reported NO_x concentration in ppm pre and post after treatment on consecutive UDDS hot start cycles are shown in Figure III-5. The vehicle diagnostic data only began reporting following a system startup duration, resulting in after treatment values only beginning to report at ~175s into the cycle

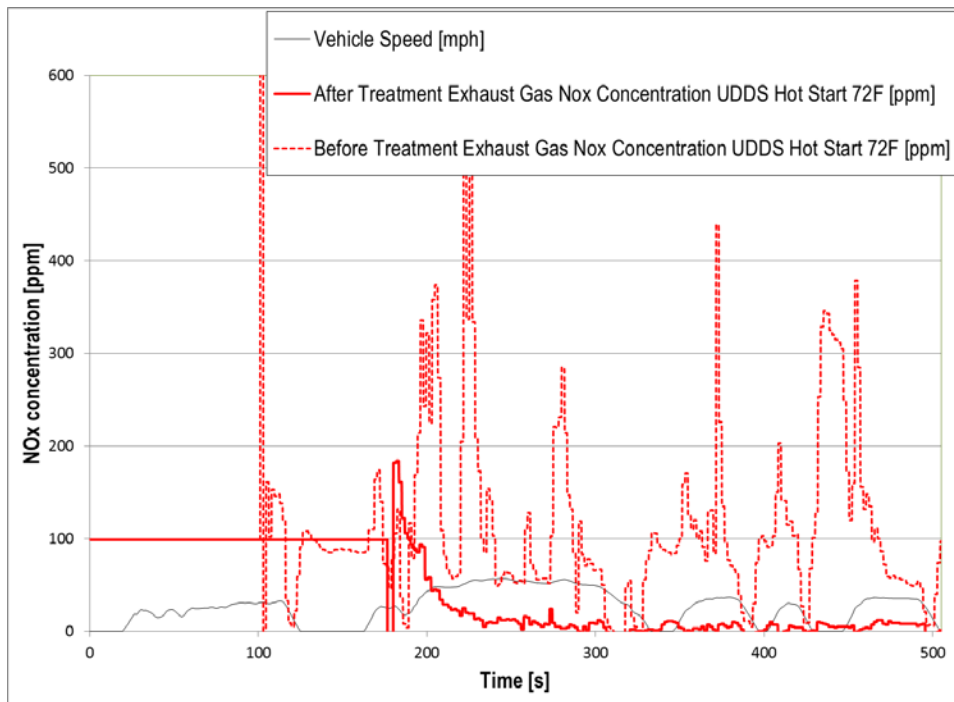


Figure III-5: NOx concentration before and after exhaust after treatment system, UDDS hot start and cold start 72F

Fuel Consumption throughout varying drive cycles

Fuel economy (in mpg of certification diesel fuel), for Chevrolet Cruze Diesel on the standard AVTA test cycles at varying temperatures can be found in Figure III-6.

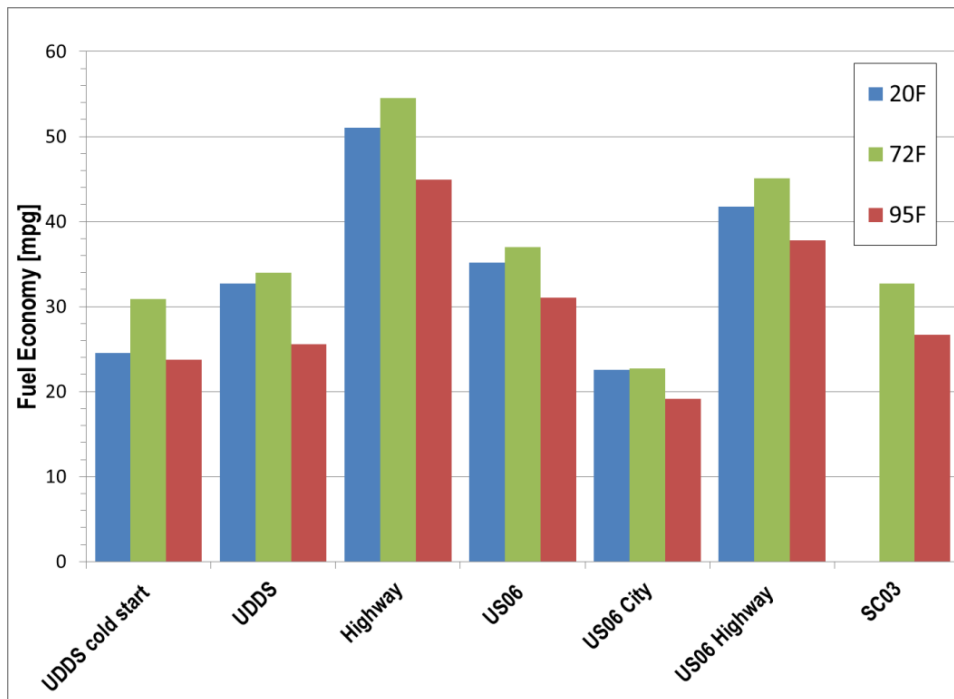


Figure III-6: 2014 Chevrolet Cruze diesel fuel economy (uncorrected)

The variation in the cold start penalty on the UDDS is more pronounced at colder ambient temperatures since the powertrain has to overcome high friction losses. The actual cold start penalty is shown in Table III-2.

Table III-2: 2014 Chevrolet Cruze diesel fuel consumption penalty at varying temperatures

Test Cycle	Penalty
20F	33%
72F	10%
95F with 850W/m2 solar emulation	8%

2014 Mazda 3 Skyactiv I-ELOOP

Vehicle Description

The Mazda 3 Skyactiv I-ELOOP is a variation of the popular conventional Mazda 3 incorporating Mazda's "i-ELOOP" technology. In this system, an advanced alternator is used to increase output voltage (up to 25V peak), and thus available 12V electrical power during vehicle decelerations. This electrical energy is then stored in a capacitor for later use in powering vehicle accessories. This system reduces the alternator load on the engine during vehicle cruise or accelerations, thus resulting in increased fuel economy. General specifications of the vehicle can be found in Table III-3.

Table III-3: 2014 Mazda 3 Skyactive i-ELOOP specifications

Architecture	Conventional vehicle (Gasoline fuel)
Engine*	2.3-L DOHC I4, VVT, 13.0:1 compression ratio 137 kW (184 HP), 250.8 Nm (185 ft-lb)
Transmission*	6-speed automatic*
Motor *	N/A
Battery *	Q85 Type
EPA Label Fuel Economy (mpg)	29 city / 40 hwy / 34 combined*

* Manufacturer’s data

Vehicle instrumentation

Instrumentation of the vehicle focused on capturing all possible parameters of the i-Eloop system. Electrical voltage and current measurements were recorded at multiple locations on the vehicle low voltage bus. This included voltage at the alternator and 12V battery, and current at the alternator, DCDC in, DCDC out, and the negative terminal of the 12V battery. Additionally, vehicle diagnostic messages were used to develop an understanding of the charging system operation and the powertrain operation. This included electrical measurements from vehicle stated current and voltage at different locations of the i-ELOOP, as well as powertrain parameters such as speeds, torques, temperatures, and transmission states. Additionally, standard facility instrumentation including emissions, fuel flow, and test cell information were captured as well.

Points of interest

Supercapacitor System Enables Improved 12V Auxiliary Load Generation

Unlike conventional battery-alternator system, the i-ELOOP enables the boosting of alternator voltage of levels up to 25V, in order to recapture the kinetic energy of the vehicle during vehicle braking, somewhat similar to regenerative on a hybrid powertrain but at a greatly reduced in capacity. Power from the alternator can be stored in the capacitor, allowing the alternator to become unloaded while power is delivered from that stored in the capacitor. Additionally alternator modes such as the alternator directly supplying to the low voltage bus (by passing the capacitor), and capacitor directly supplying to the low voltage bus (by passing the alternator), are enabled by switching within the DCDC converter. Additionally, Figure III-7 illustrates the varying operational modes of the i-ELOOP system during operation on a highway cycle.

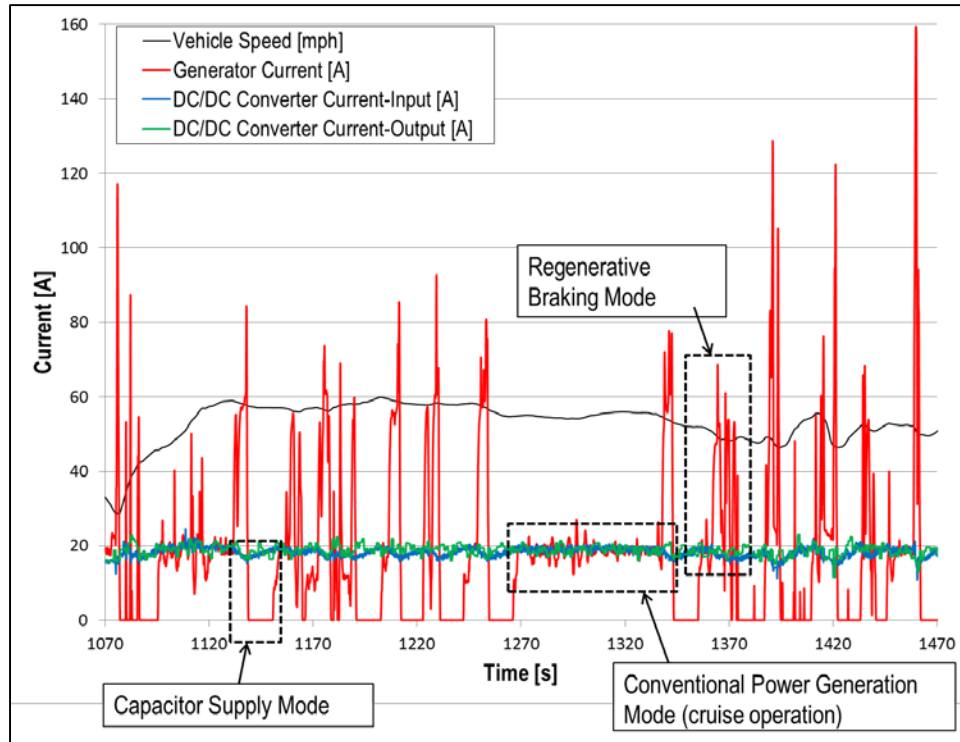


Figure III-7: Alternator and capacitor operation during a highway cycle at 72F

2014 Smart Fortwo Electric Drive

Vehicle Description

The 2014 Smart Fortwo Electric Drive is a lightweight, two seat, rear wheel drive battery electric vehicle within the subcompact segment. As is common with other recent BEV's the vehicle is an electric conversion of a conventional gasoline powered vehicle. Due to its subcompact size the Smart is relatively lightweight, at an EPA Equivalent test weight of 2375 lbs. General vehicle specifications can be found in Table III-4.

Table III-4: 2014 Smart Fortwo Electric drive specifications

Architecture	Battery Electric Vehicle
Motor*	AC Synchronous Permanent Magnet Electric Motor 55 kW (74hp) / 130 Nm (96 lb-ft) torque
Battery*	Li-ion 17.6 kWh net capacity
EPA Label Fuel Economy (mpg)+	122 City, 93 Highway, 107 Combined

Vehicle instrumentation

Instrumentation of the vehicle focused understanding of vehicle energy flow. The electrical measurements of current and voltage from the HV Battery, DCDC out, AC Charge Energy, and 12V battery were essential to the end. Additionally, a thorough amount of broadcast CAN was captured, with messages including vehicle reported high voltage battery, drive system, and climate control system parameters.

The vehicle was evaluated with a modified SAE J1634 testing procedure, with set soak times occurring between the standard test cycles. Test cycles completed include UDDS, Highway, and US06 cycles at the test temperatures of 20F, 72F, and 95F with 850 W/m² of solar emulation. Additional maximum performance and mapping testing was completed at 72F to determine vehicle capabilities.

Points of Interest

Vehicle operation at varying temperatures

Unlike other battery electric vehicles evaluated, the Smart Electric was not equipped with automatic climate control. Due to this, the climate control setting used were similar to that required with a conventional vehicle with manual climate control. At 95F the temperature selection was set to full cold, with recirculation and the blower fan at full speed. As is standard with manual climate control settings during 20F testing, the settings were HVAC to "full hot", on defrost, and high fan through the first 505 seconds of the UDDS cycle. Following this, the fan is then switched to "full hot", low fan, and floor ventilation.

The DC energy consumption results shown in Figure III-8 were obtained following the described test methodology.

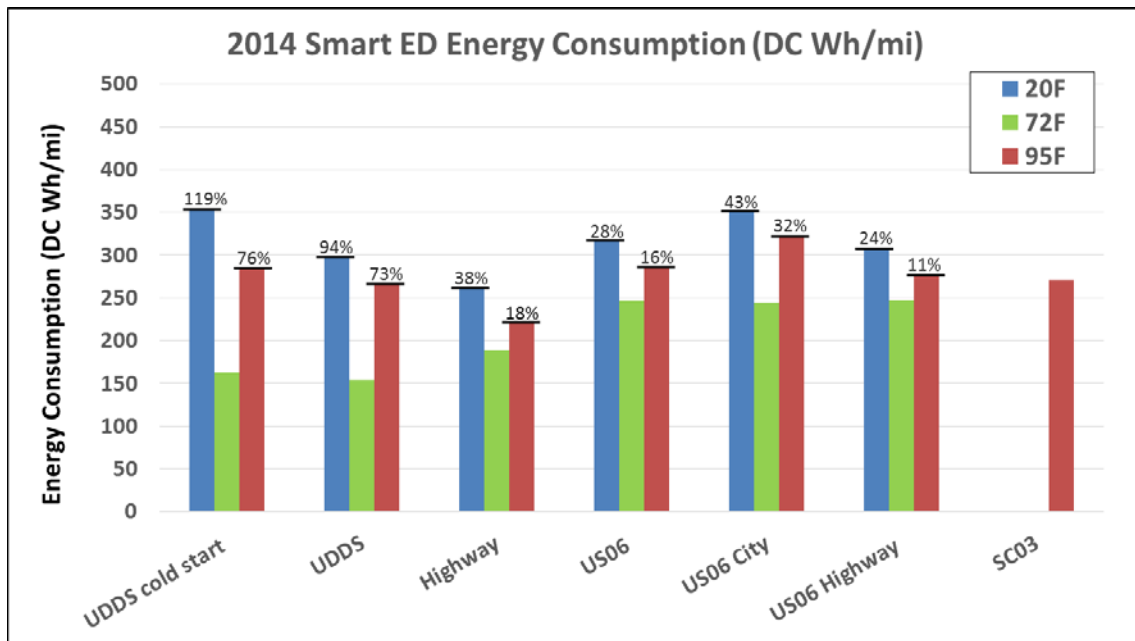


Figure III-8: 2014 Smart Electric energy consumption

As can be seen, the Smart Electric demonstrated a consistently higher energy consumption at the test temperature of 20F as compared to 72F. This increase and well as the amount of increased consumption is consistent with most other electric vehicles utilizing a resistance heater for cabin heating. Of note is the above average increase in energy consumption at the 95F test temperature. This is a result of excessive cabin cooling, based on the vehicle climate control setting selected for standardized test results. These values can be considered the highest load scenario for energy consumption at that temperature, as most individuals in a real world setting would reduce cooling load for comfort. This demonstrates the impact of climate control settings on energy consumption. It appears that an automated climate control system can save some energy and thus increase the range of the electric vehicle.

2014 BMW i3 REx

Vehicle Description

The BMW i3 was released during the second quarter of 2014 in the US. The BMW i3 is available both an electric vehicle (referred to later as BEV) and a plug-in hybrid vehicle that to an optional range extender (referred to as REx). During the FY2015, both versions of this model have been tested at the APRF through vehicles supplied by the AVTA program. Additionally, the level 2 test vehicle was a 2014 BMW i3 REx, allowing for leveraging of components and testing knowledge between the two testing regimes. Table III-5 gives the specifications of the BMW i3 with optional range extending engine (REx).

Table III-5: 2014 BMW i3 REx specifications

Architecture	BEV-X: Battery electric vehicle with range extending engine
Engine*	0.65L In-line 2, PFI, DOHC 28kW (37.5 hp) Generator Output- 26.6 kW at 5000rpm
Transmission*	1 Speed
Motor*	Synchronous PM Electric Motor 125 kW [170 hp] / 250Nm [184 lb-ft]
Battery*	Lithium Ion 18.8 kWh Net Capacity
EPA Label Fuel Economy (mpg)^	117 combined 72 miles EPA estimated EV Range

*Manufacturer's data

^ fueleconomy.com

Vehicle instrumentation

As vehicle energy use was of key interest on this vehicle, high voltage instrumentation was an area of particular focus. Instrumentation included a high voltage tap and current measurements at multiple locations. These current measurement locations included: at high voltage battery pack, A/C compressor, the PTC heater, the range extending generator, and the low voltage supply from the vehicles DCDC converter.

Additional electrical data and vehicle operation signals were captured and logged from diagnostic and broadcast CAN messages. These included state of charge of the HV battery pack, vehicle reported HV system voltage and current, traction and generator motor torque and speed, accelerator pedal positions, wheel speeds, and HVAC system parameters.

Tests were conducted at the standard AVTA temperatures of: 20F, 72F and 95F with 850 W/m² of solar emulation with standard cycles including the UDDS, HWY, US06, and SC03. A refined version of the J1634 multi-cycle tests were conducted to evaluate charge depleting operation on standard drive cycles. At each test temperature, the vehicle was evaluated in charge sustaining operation. To complete this, the vehicle was prepped as a hybrid, and evaluated using the standard APRF test series for evaluation of a hybrid vehicle in charge sustaining operation. This consisted of consecutive UDDS cycles until the engine reached thermal equilibrium, followed by sets of HWY and US06 cycles. Further exploratory testing also occurred in both charge sustaining and depleting operation in order to determine energy efficiency and operation.

Points of interest

Range Extender Operation

Of interest was the operational envelop of the vehicle when the range extending engine was in operation. The engine generator of the i3 REx is activated when the state of charge goes below a desired limit, at which time it activates in order to provide additional range. As the generator is limited to providing 26.3kW of power, any demand above this level must be delivered from that stored within the high voltage battery. If the power demand is above this limit for an extended duration of time, the vehicle will enter a state of reduced available power. This state then limits vehicle maximum speed, and acceleration. Test data looking into the operation limits of the range extending engine was captured through several custom drive cycles in which the vehicle was driven at a constant speed under varying loads. Figure III-9 shows the vehicle state of charge, battery power, and REx supplied power over a series of these speeds.

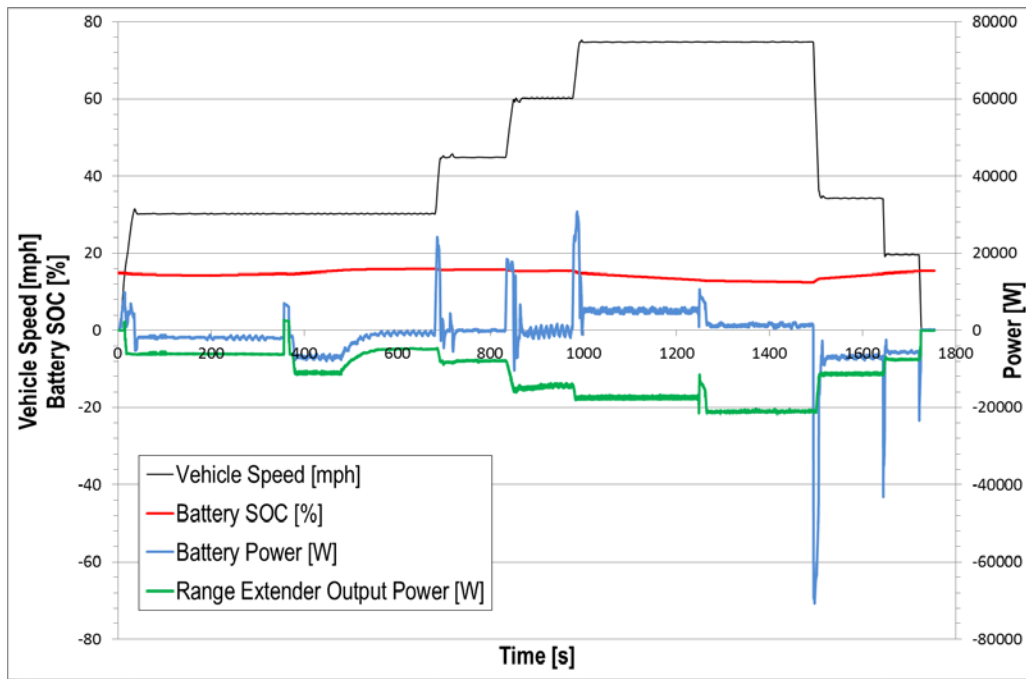


Figure III-9: Range extending engine power and battery power for a steady state speed test at 72F (in charge sustaining mode).

During the test in Figure III-9 at 0% grade, at 75mph a reduction in HV battery state of charge (SOC) is noticeable. At a lower SOC boundary the REX output reached 21.5 kW of electric power. Additional testing was performed with the dynamometer set to emulate a grade of 6%, as may be expected as an extreme scenario when traveling in a mountainous region. The results of the 6% grade test can be seen in Figure III-10.

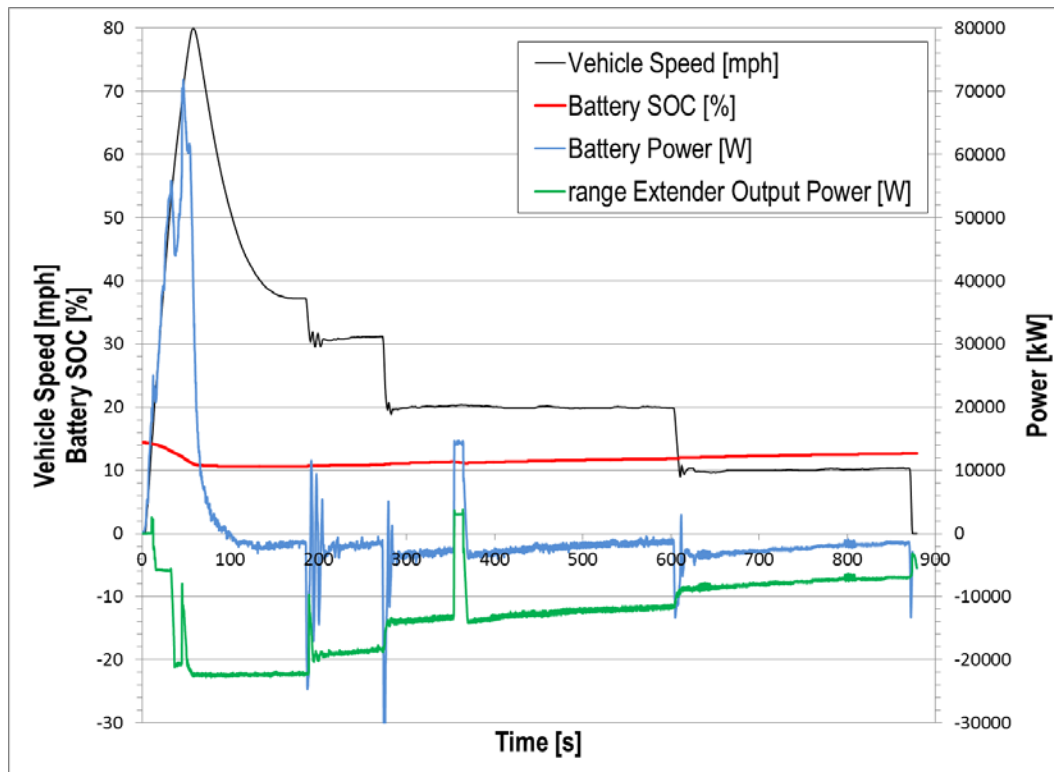


Figure III-10: Range extender power and battery power for a steady state speed 6% grade test at 72F (charge sustaining mode).

At 6% grade, the vehicle was accelerated. At a given point, the available electric drive power was de-rated as the SOC reached a lower limit. The derating of the battery power, as well as the quick increase in generator power can be seen as the vehicle approached a speed of 80pmh. After that point, power from the high voltage battery was gradually reduced, and the vehicle reached a steady state speed of approximately 37mph. At that speed the REx was found to supply the vehicle with a power level of 22.7kW to the high voltage DC bus.

In addition to an overview of the power limitations while in range extending mode, an overview can be given of the fuel economy on standard drive cycles, with which expected vehicle range while in charge sustaining operation could be determined. This resulting fuel economy for the standard set of AVTA drive cycles are shown in Figure III-11.

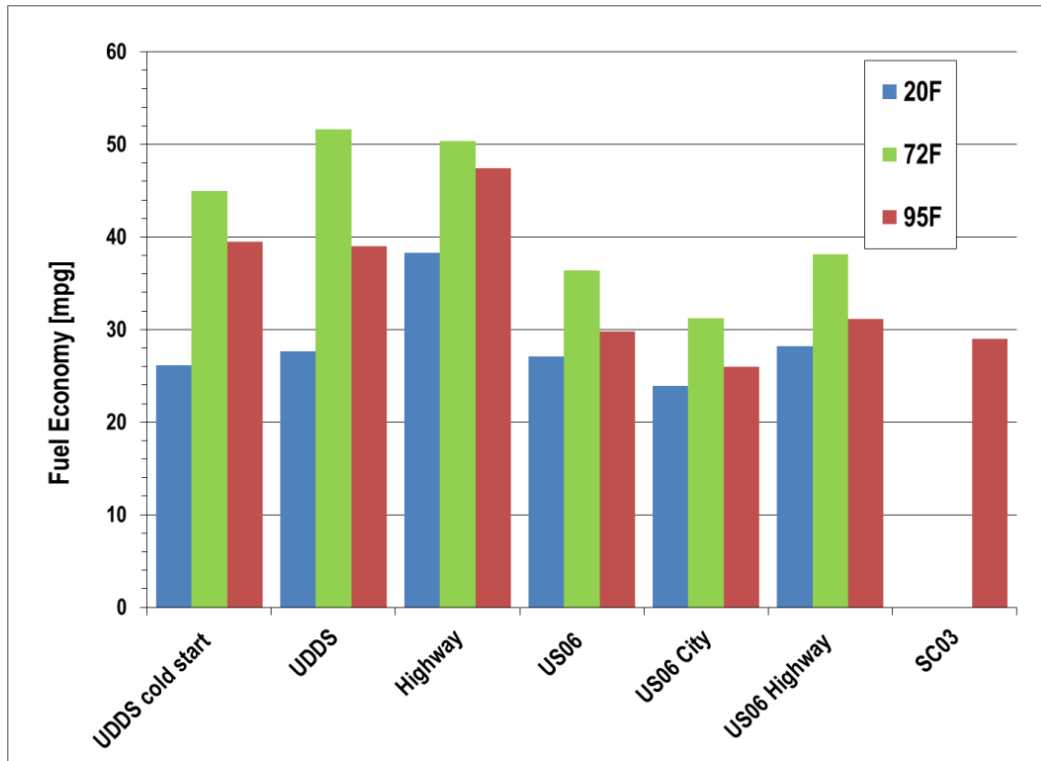


Figure III-11: BMW i3 Rex fuel economy during charge sustaining operation (uncorrected).

Of note is the reduction in the fuel economy at low temperatures. Though this vehicle generates waste heat from the engine, a PTC heater is used at low temperatures for cabin heating. This results in increased loading of the vehicles high voltage bus, as compared to the conventional and hybrids vehicles with an internal combustion engine which make use of waste heat within the vehicles thermal loop for cabin heating.

2014 BMW i3 BEV

Vehicle Description

The BMW i3 BEV refers to the battery electric only (without range extender) version of the BMW i3. The BEV had a heat pump system for cabin heating which was not present on the PHEV version. A summary of the specifications of the 2014 BMW i3 BEV can be found in Table III-6.

Table III-6: 2014 BMW i3 BEV Specifications

Architecture	All Electric Vehicle
Transmission*	1 Speed Automatic
Motor*	Synchronous PM Electric Motor 125 kW [170 hp], 250Nm [184 lb-ft]
Battery*	Lithium Ion 18.8 kWh Net Capacity
EPA Label Fuel Economy (mpg)^	137 City/111 Hwy/ 124 Combined

*manufacturer's data

^ fueleconomy.gov

Vehicle instrumentation

Due to the similarities with the BMW i3 Rex, instrumentation of this vehicle was identical to that listed previously, with the exclusion of all sensors related to the range extender and for the emissions bench measurement which are unnecessary for an all-electric model.

Testing was consistent with that performed on the i3 Rex, with the elimination of charge sustaining testing, and the inclusion of additional test temperatures for the BMW i3 BEV of 0F and 40F in order to more fully capture the operation of the heat pump within the vehicle. The vehicle was evaluated with a modified SAE J1634 testing procedure, with set soak times occurring between the standard test cycles. Test cycles completed include UDDS, Highway, and US06 cycles. Additional maximum performance and mapping testing was completed at 72F to determine vehicle capabilities.

Points of interest

Temperature effect on energy consumption

It has been well discussed that currently available electric vehicles have a high increase in energy use at cold temperatures due to cabin heating requirements. In order to reduce this sensitivity, the vehicle is equipped with a heat pump system which uses control of the vehicle refrigeration loop to reverse locations of heat capture and rejection, allowing for cabin heating from the already equipped refrigerant system. Heat pumps generally are only effective at moderate temperature- but below a transitional point icing can occur, greatly reducing system efficiency and heating capacity. Due to this restriction, and to provide greater heating power, the BMW i3 BEV is equipped with a high voltage PTC heater as is commonly seen on BEV's.

To quantify the overall energy use and understand the operation of the heat pump, this vehicle was evaluated at 5 separate cell temperatures, with the additional temperatures being 0F and 40F. The resulting energy consumption across standard cycles can be seen in Figure III-12.

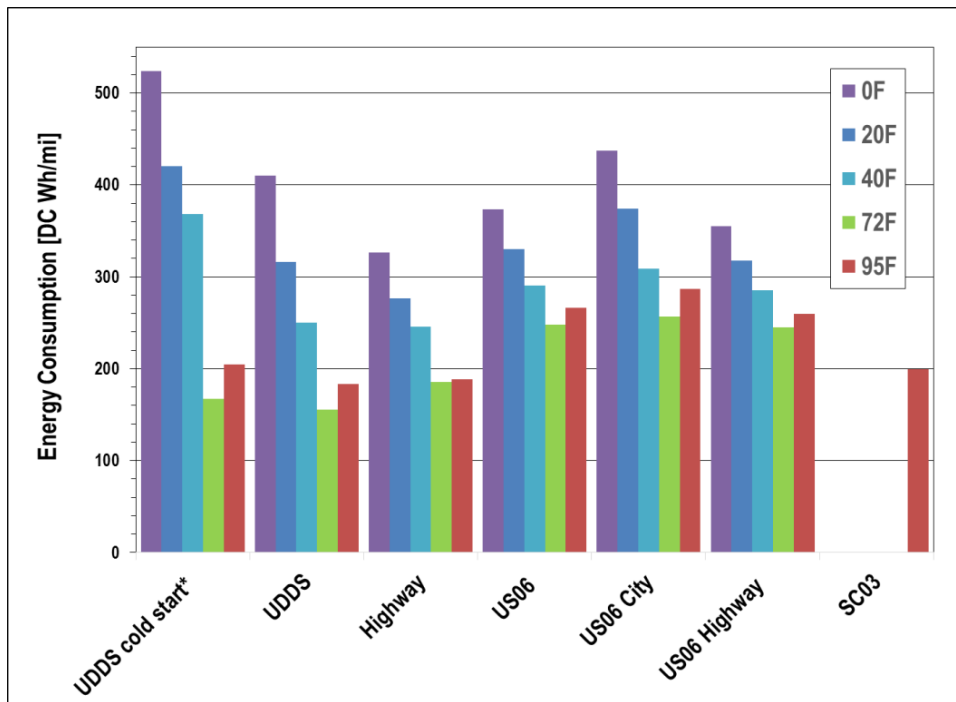


Figure III-12: 2014 BMW i3 BEV energy consumption at varying temperatures.

On the UDDS cold start cycle the vehicle interior must be heated to the desired cabin temperature from the test cell ambient temperature- requiring the highest energy consumption from the HVAC system through the test series. Following this cold start, heat remains within the vehicle cabin, reducing the startup heating load. On the UDDS cold start cycle at the ambient temperature of 40F, vehicle energy consumption was found to increase by 120% over the 72F baseline. As expected, this continued to increase as the test temperature dropped, with a 151% increase at 20F, and a 213% increase at 0F.

Due to the measurement of current at varying locations on the high voltage bus, energy consumption can be separated by high voltage component as seen in Figure III-13. Figure III-13 displays the energy consumption during the two first two UDDS (urban) cycles with the initial a cold start cycle, and the second "hot start" following a 10 minute soak preceding a highway cycle.

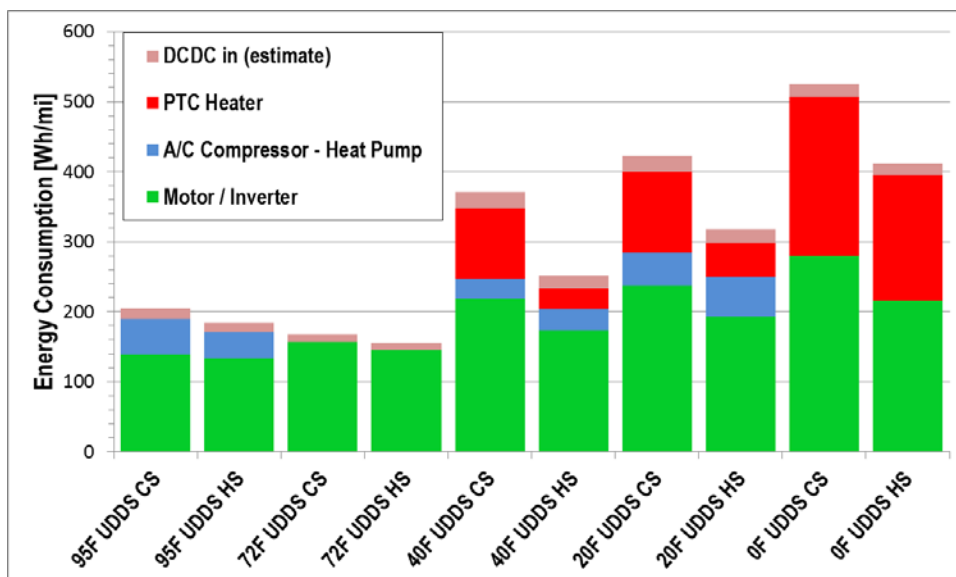


Figure III-13: Temperature effect on UDDS hot and cold start energy consumption.

The heat pump was found to be operational at the test temperatures of 20F and 40F, though was not utilized when the ambient temperature was at 0F. Furthermore the amount of percent of energy use provided by each component on the UDDS CS cycle is shown in Figure III-14.

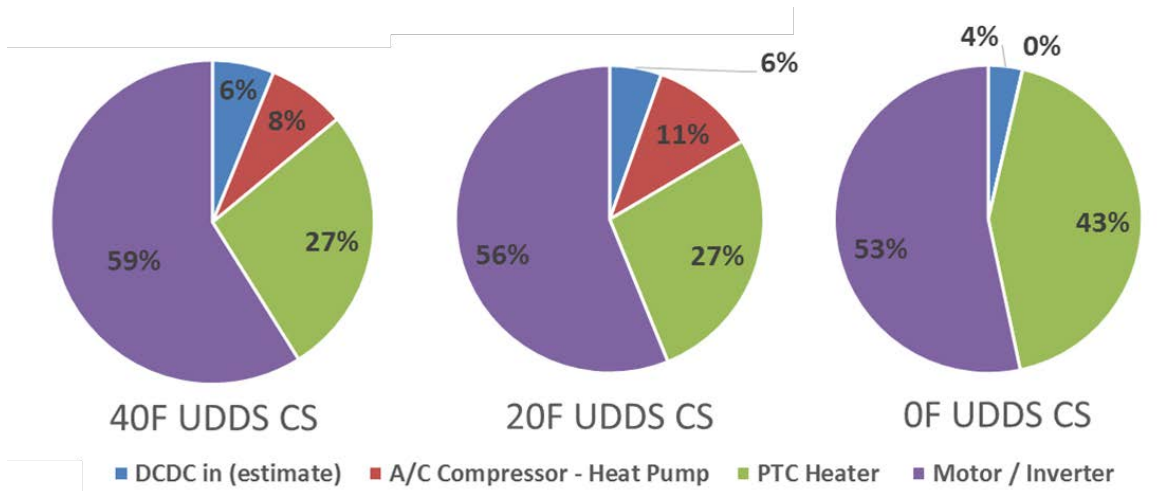


Figure III-14: BMW i3 BEV high voltage component energy use at cold temperatures

Further comparison of this vehicle with others utilizing a heat pump, along with tabulated data can be found in the following section pertaining to another battery electric vehicle evaluated with a heat pump system- the 2015 Kia Soul EV.

2015 Kia Soul EV

Vehicle description

The Kia Soul EV is an electrified version of the Kia Soul gasoline model, released in the 2015 model year. The Soul EV is referred as an “urban passenger vehicle” and differs from other electric vehicles by its relatively high capacity battery, and relatively heavy weight of 3625 lbs. (test weight). Of key interest was powertrain operation, the large capacity battery usage, and the operation of the heat pump. As was discussed within the section on the 2014 BMW i3 BEV, additional testing was included in order focus on the effects of a heat pump on BEV energy consumption while at cold ambient temperatures. General specifications for 2015 Kia Soul BEV can be found in Table III-7.

Table III-7: 2015 Kia Soul BEV Specifications

Architecture	All Electric Vehicle
Transmission*	1 speed gear reduction Ratio 8.206
Motor*	AC Synchronous Permanent Magnet Electric Motor 81.4 kW [109 hp] / 285 Nm [210 lb.-ft]
Battery*	Lithium Ion 27 kWh capacity
EPA Label Fuel Economy (mpg)^	120 City/ 92 hwy/ 105 Combined

*Manufacturer’s data

^ fueleconomy.com

Vehicle instrumentation

Instrumentation of the Kia Soul EV focused on component energy consumption and efficiency. This drove the instrumentation of the high voltage (HV) electrical bus at several locations. A HV tap was installed in the vehicles front junction box, while current was measured at the following locations: the HV battery, the electric powertrain control unit (EPCU), A/C compressor and the PTC heater. The low voltage system was measured via current out of the DCDC converter and at the ground of the 12V battery. Additionally, messages from broadcast and diagnostic CAN were decoded and recorded. These messages included: HV system parameters (voltage, current, SOC), charger system electrical data (current, voltage), HVAC system parameters, powertrain parameters.

Data were established for standard UDDS, HWY, US06 and SC03 cycles for 20F, 72F and 95F ambient temperatures. Additionally, several custom tests were conducted to evaluate vehicle operation and energy consumption.

Point of interest

Vehicle Energy consumption

As the vehicle represented a heavier than average BEV, vehicle energy consumption was of interest for a comparison point to other EV's. The standard set of certification cycles were performed, establishing a consistent baseline for comparison with other EV's. A summary of these test results can be seen in Figure III-15.

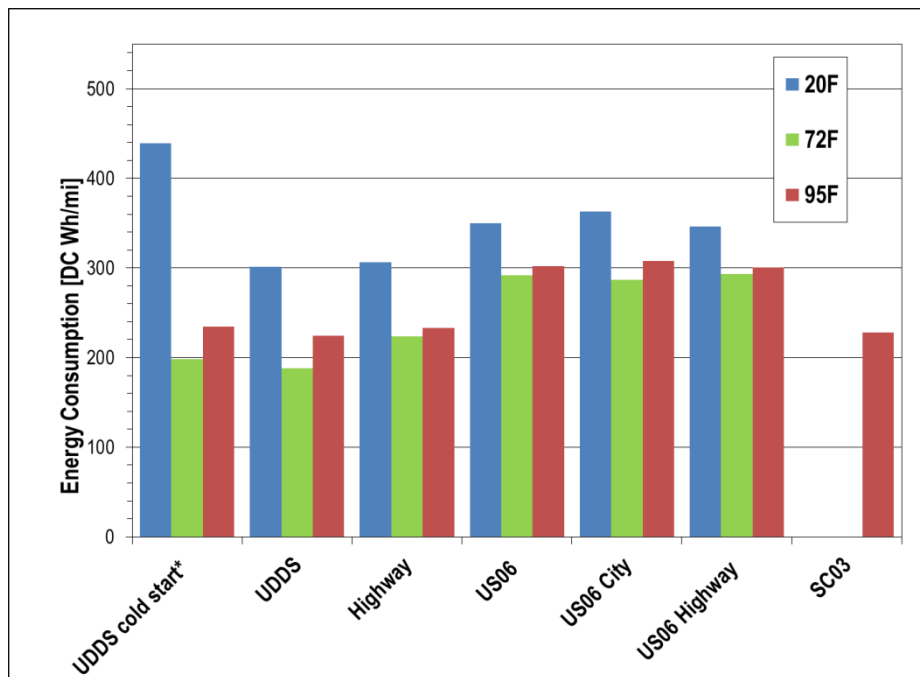


Figure III-15: Kia Soul EV Energy Consumption.

Of note is the large impact of the 20F test temperature on vehicle energy consumption, as compared to the second UDDS following a 10 minute soak following previous cabin heating. The cold start penalty on the UDDS resulted in an increase in energy consumption of 140 Wh/mi, or 50% over the UDDS hot start test at 20F.

Operation at varying temperature

The high voltage instrumentation enables a comparison to other heat pump equipped BEV's. The percent of energy used by each high voltage component for the 2014 Kia Soul EV, the 2014 BMW i3 BEV, and the 2013 Nissan leaf can be seen in Figure III-16.

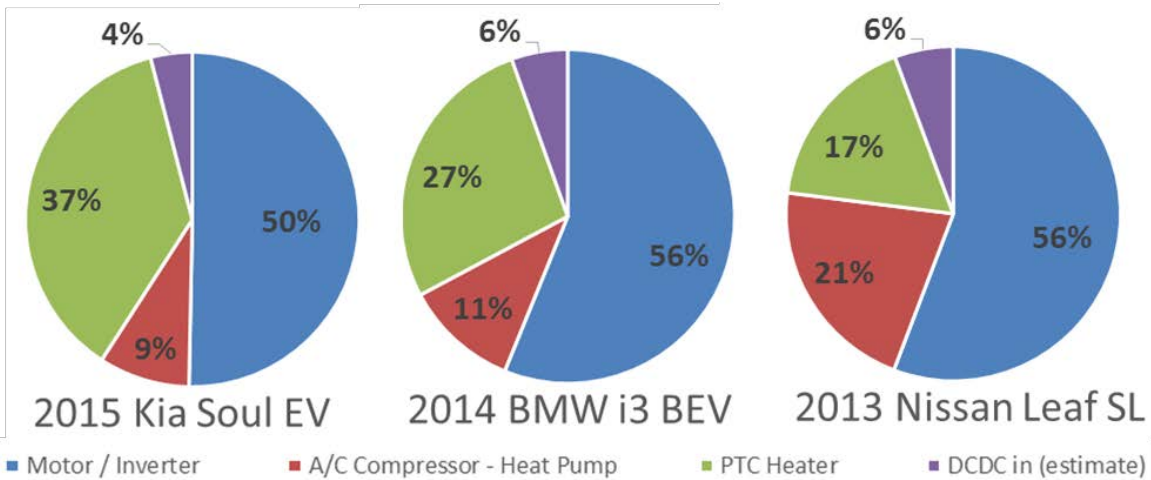


Figure III-16: Percent of energy consumption by component on the 20F UDDS CS cycle

Table III-8: 20F UDDS CS energy use by component for varying BEV's

[DC Wh/mi]	Motor / Inverter	A/C Compressor - Heat Pump	PTC Heater	DCDC in (estimate)	Total
2013 Nissan Leaf	217.9	82.9	67.6	22.2	390.5
2014 BMW I3 BEV	237.5	46.7	115.6	23.0	420.5
2015 Kia Soul EV	221.1	38.8	161.7	17.7	439.3

On the UDDS cold start cycle, the Nissan Leaf represented the highest energy use with the heat pump system as compared to the other vehicles. Though all 20F tests listed had the driver demanded temperature set to 72F, each vehicle will operate in its own manner to establish that temperature.

Additional tests were completed while holding the vehicle at constant speeds from 0 to 80 mph, at both a 0% and an increased grade of 6%. This results can be found in Figure III-17.

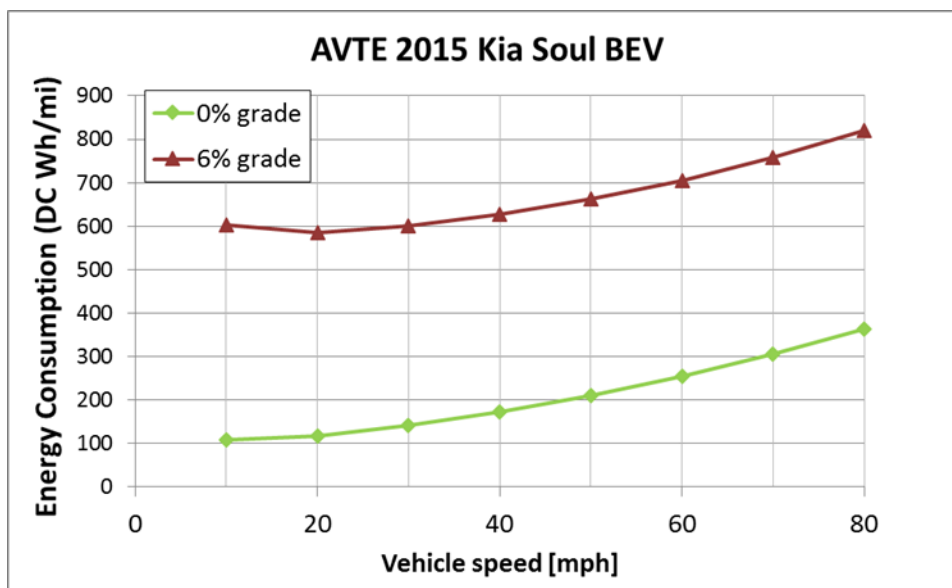


Figure III-17: Kia Soul BEV energy consumption at varying speeds and grade

2015 Honda Accord Hybrid

Vehicle Description

Similar to the L2 Honda Accord PHEV, the HEV's powertrain includes a 2.0L 4 cylinder engine, coupled to an e-CVT with two high voltage motors. Varying from other powersplits, the Accord HEV incorporates a clutch to enable engine only operation at higher vehicle speeds. The HV battery of the Accord PHEV is a Li-Ion pack consisting of a 6 modules of 12 cells, connected in series with a nominal voltage of 259.2V. General specifications of the Honda Accord Hybrid are given in Table III-9.

Table III-9: 2015 Honda Accord Hybrid Specifications

Architecture	Hybrid Electric Vehicle
Engine*	In-Line 4-cylinder 16-valve DOHC i-VTEC Displacement 1993 cm ³ 105kW (141 hp) Compression ratio 13.0:1
Transmission*	E- CVT with engine lock up clutch Final gear 3.421
Motor*	AC Synchronous Permanent Magnet Electric Motor 124 kW (166Hp), 306 Nm (226 lb-ft)
Battery*	Lithium-Ion 259.2V
EPA Label Fuel Economy (mpg)^	50 City/ 45 HWY/ 47 Combined

*Manufacturer's data

^ fueleconomy.com

Vehicle instrumentation

Electrical measures (current and voltage) were captured by installation of a set of current clamps at the HV battery, AC compressor, powertrain control unit (PCU), the DC/DC converter (high and low voltage), and at the ground of the 12V battery.

Decoded messages from both broadcast and diagnostic CAN data, were able to be transferred from the PHEV Accord, providing a considerable amount of vehicle insight. A highlighted list of these include: control pedal positions, powertrain components speed (engine, motor, generator) and torque (motor, generator), and HV battery data (current, voltage, SOC).

Tests were conducted at temperatures varying from 20F to 95F. As is standard through the AVTA program, drive cycles included both standard (UDDS, HWY, US06, SC03) and custom cycles at these three ambient temperatures.

Point of interest

Comparison of charge sustaining fuel economy of the hybrid with plug-in hybrid model

Both the PHEV and the HEV versions of the Honda Accord are supplied with similar powertrain components, the key variation remains in the high voltage battery and accompanying electronics. During evaluation of both the Accord PHEV and HEV, vehicle diagnostic messages were logged (powertrain parameters such as speeds

and torques, temperatures and operational state). An example of the difference, and the benefits to the capture and logging of vehicle diagnostic data can be seen in Figure III-18.

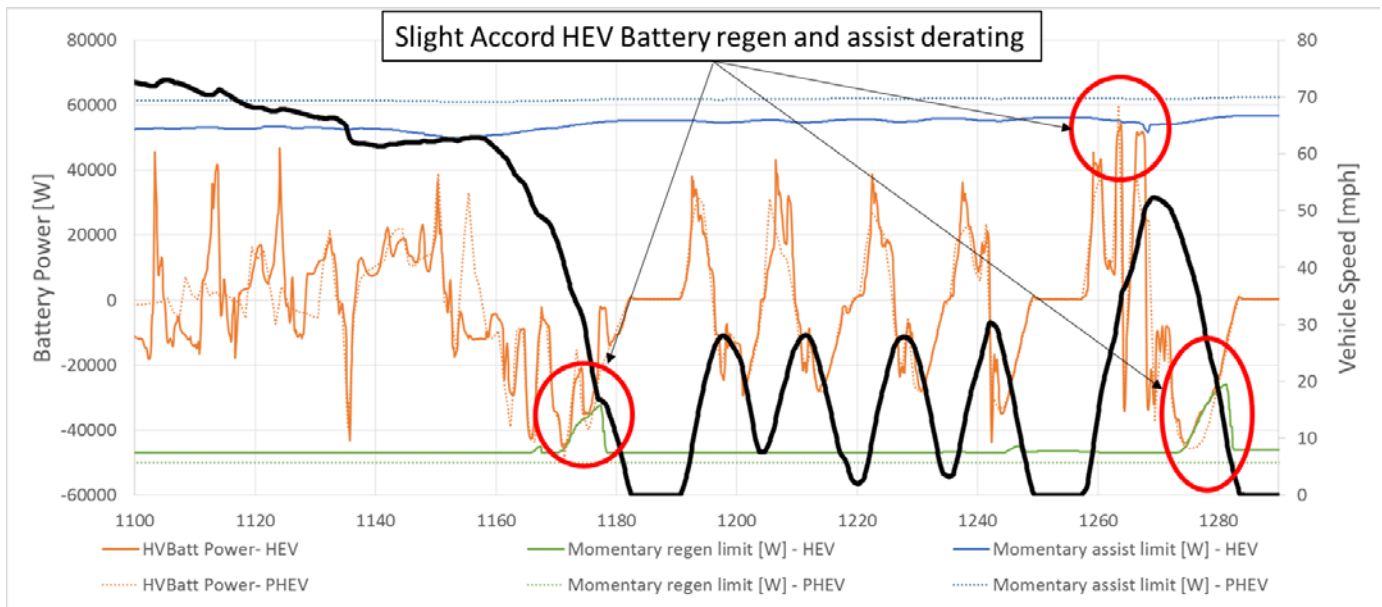


Figure III-18: Comparison of HEV and PHEV battery power during high power demand

Displayed above are the momentary assist and regen power limits plotted against actual vehicle battery power on the final city phase of the US06 cycle- a section of the standard cycles which displays the greatest power requirements. The steady state power limits for both the PHEV and HEV can be seen with the HEV shown as a solid line, and the PHEV as a dotted. Also of note is the offset between the signals- the steady state power limits for assist were approximately 62kW/56kW and regeneration were 50kW/46kW for the PHEV and HEV respectively.

Several times over this section of the US06 cycle, the momentary limits were seen to reduce on the HEV, thus limiting battery power. The most pronounced occurs at approximately 1275 seconds, where the regenerative limit is seen to reduce, thus limiting the power able to be captured during the regenerative braking event.

2015 Chevrolet Spark EV

Vehicle description

The Chevrolet Spark EV is a compact all-electric vehicle with a weight of 3157 lb. The vehicle offers insight into an all electric design from General Motors, equipping an existing vehicle platform with a powerful electric drive system. Vehicle specifications are detailed in Table III-10.

Table III-10: 2015 Chevrolet Spark EV Specifications

Architecture	Electric Vehicle
Transmission*	1-Speed Direct Drive
Motor*	AC Synchronous Permanent Magnet Electric Motor 140 hp; 327 lb-ft
Battery*	Lithium ion phosphate 19 kWh Capacity
EPA Label Fuel Economy (mpg)^	128 City/109 HWY/ 119 Combined

*manufacturer's data

^ fuelconomy.gov

Vehicle Instrumentation

Of interest from the Spark EV was the vehicles energy use and operation. Electrical measures (current and voltage) were captured by installation of a set of current clamps at the HV battery, AC compressor, PTC heater, the DC/DC converter, and at the ground of the 12V battery. Captured vehicle diagnostic and broadcast network data consisted of HV system parameters (temperature, voltage, current, state of charge, coolant system parameters), powertrain torques, motor parameters, and other data such as wheels speeds and accelerator pedal position.

The vehicle was evaluated with a modified SAE J1634 testing procedure, with set soak times occurring between the standard test cycles. Test cycles completed include UDDS, Highway, and US06 cycles at the test temperatures of 20F, 72F, and 95F with 850 W/m² of solar emulation. Additional maximum performance and mapping testing was completed at 72F to determine vehicle capabilities.

Point of interest

Effects of vehicle preconditioning on energy consumption

One option available on many electrified vehicles is the ability to precondition the vehicle prior to driving. During preconditioning, either the high voltage battery, or the cabin of the vehicle is increased to a desired temperature. Powertrain preconditioning generally only occurs when the vehicle is plugged in, unless an excessively low temperature is reached. Cabin preconditioning can be initiated with a driver command, either from a vehicle setting or by press of a button on the key fob. Cabin preconditioning can be completed either with the vehicle plugged in, or not. Of interest to the APRF was the impact to vehicle energy use and BEV range when either the vehicle's powertrain, cabin, or both were preconditioned.

As a starting reference, the energy consumption results for the 2015 Chevrolet Spark EV are shown in Figure III-19. An ambient temperature of 20F the energy consumption is 230% of the UDDS cold start at 72F.

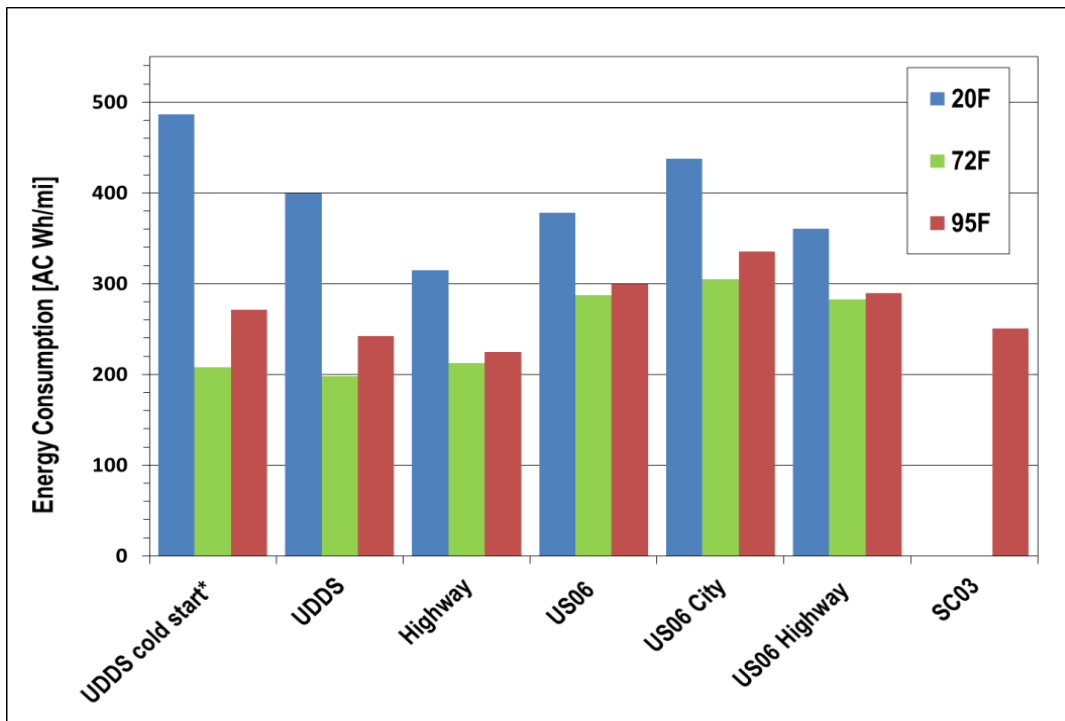


Figure III-19: 2015 Chevrolet Spark EV energy consumption.

Separate days of testing were completed in order to compare effects of 1) powertrain conditioning, and 2) both powertrain and cabin conditioning. The 2015 Spark EV was found to automatically precondition the powertrain if the vehicle were plugged in at an ambient temperature of 20F. Additionally, the vehicles key fob enables the cabin conditioning for up to 40 mins (two 2 x 20 mins sets). The cabin pre-conditioning is paired with the powertrain warm up. A third baseline test was conducted with the vehicle charged fully and then unplugged the night prior, which resulted in the vehicle and its powertrain to soak at the 20F the test cell temperature with no powertrain or cabin preconditioning.

For each preconditioning setting, the first four tests of a J1634 multi cycle test were completed in order to extract impact on vehicle range. The corresponding energy used from the high voltage battery can be seen in Figure III-20.

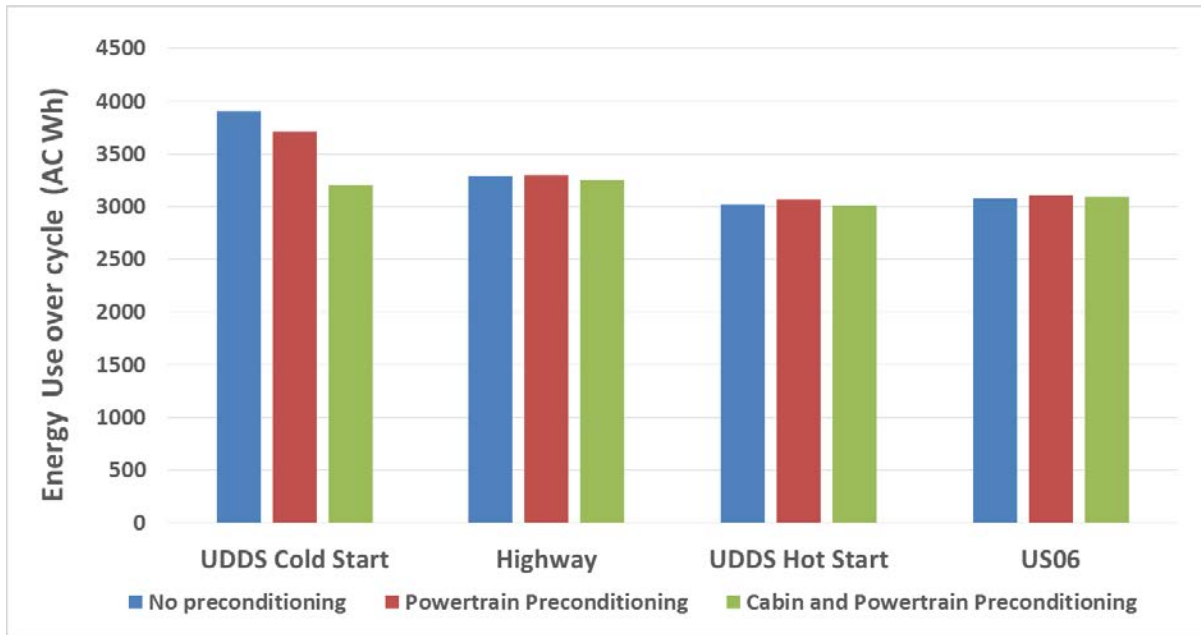


Figure III-20: Energy use over the comparing preconditioning over the MCT

As would be expected, the greatest impact is seen on the first cycle of the series. Following this initial cold start test, the remaining cycle show similar energy consumption result. Further investigating this first cycle, the energy consumption separated by component is shown in Figure III-21. This data set is also listed with the UDDS CS at 72F and 95F with solar emulation for an expanded frame of reference.

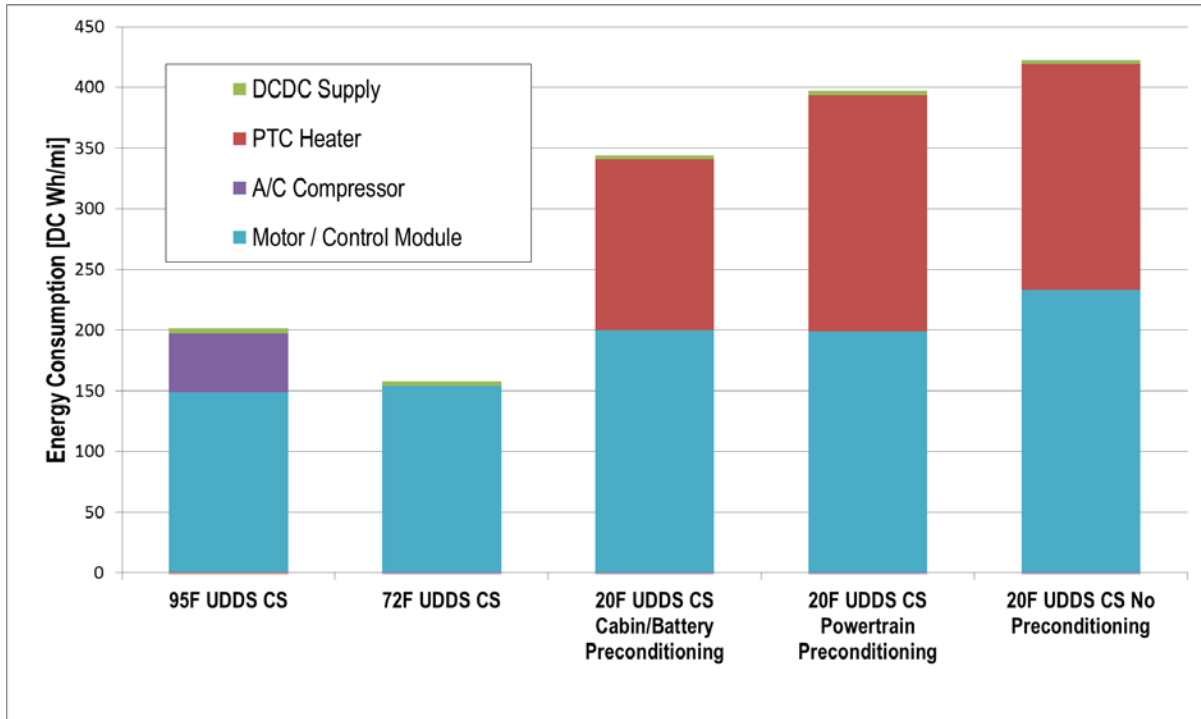


Figure III-21: Components Consumption for Hot and Cold Starts UDDS Cycles.

The energy consumption by component shows a similar powertrain energy used to drive the vehicle (1480 vs 1490h) between the cabin preconditioning and the cabin and powertrain preconditioning on the UDDS. That powertrain energy increases (400Wh) when the powertrain is not preconditioned as the friction losses in the powertrain are higher at the colder temperature.

2012 VW Passat EcoFuel TSI (Bifuel)

Vehicle description

The VW Passat Ecofuel TSI demonstrates an advanced bifuel gasoline/CNG powertrain. Similarly to a range extended electric vehicle this dual fuel vehicle uses the gasoline fuel as back up and the natural gas is the main fuel. On road, the vehicle is provided gaseous fuel from a set of steel CNG tanks with a max pressure of 3000 psi. A high-low pressure regulator is located with the vehicle engine bay, where the fuel is reduced to a rail pressure between 70 to 130 psi, which is varied dependent on engine loading. This gaseous fuel is then dispensed through port fuel injection, while gasoline operation is enable by direct injection in the cylinder.

An added unique aspect of this vehicle is that the engine is equipped with both a supercharger and a turbocharger, allowing for control of engine boost pressure at a wide range of engine speeds. This provides the ability to take advantage of the increased octane of CNG, by increasing boost pressure, while still allowing a reduced boost level while operating on gasoline. Due to this, manufacturer data claims that the vehicle torque and output power is unaffected by a change in operating fuels. This vehicle is European import, and it was leveraged from a separate APRF project for Level 1 testing.

Table III-11: 2012 VW Passat Ecofuel TSI Specifications

Architecture	Bifuel Vehicle (CNG/Gasoline)
Engine*	1.4L In-line 4, DI- gasoline, PFI- CNG, DOHC 110kW (148 hp), 220Nm (162 lbft)
Transmission*	6-Speed Manual
EPA Label Fuel Economy (mpg)^	N/A- Vehicle not available within US

Vehicle Instrumentation

Due to the leveraging of this vehicle from other APRF research work, the Passat Ecofuel was equipped with instrumentation beyond that of standard level 1 testing. This included a considerable amount of analog engine data including multiple engine signals such as intake pressures, component speeds, and operating states, and CNG system pressures and operational states. Additional data was collected during testing from the broadcast and diagnostic vehicle data, as well as APRF facility including gaseous and liquid fuel flow, and standard facility information.

The Passat Ecofuel was evaluated following the standard level 1 testing program, consisting of the standard UDDS, HWY, US06 at three different temperatures and SC03 drive cycle at 95F. Additional custom cycles to measure vehicle performance and operation were conducted as well.

Throughout this process, the APRF data acquisition system was modified in order to automatically calculate, and disseminate testing data related to bifuel operation.

Point of interest

Comparison of fuel economy and emissions varying fuels

Of interest on the VW Passat Ecofuel TSI is the effect of that the fuel of choice has on overall vehicle energy consumption and emissions. This can be reviewed with a comparison of test results of the standard test cycles,

with the vehicle operating in each mode. As the specific fuel properties of both the gaseous and liquid fuels are known, the energy content of each fuel can be calculated, and a mile per gallon equivalent (MPGe) of each fuel used for comparison. A summary of these results can be found in Figure III-22.

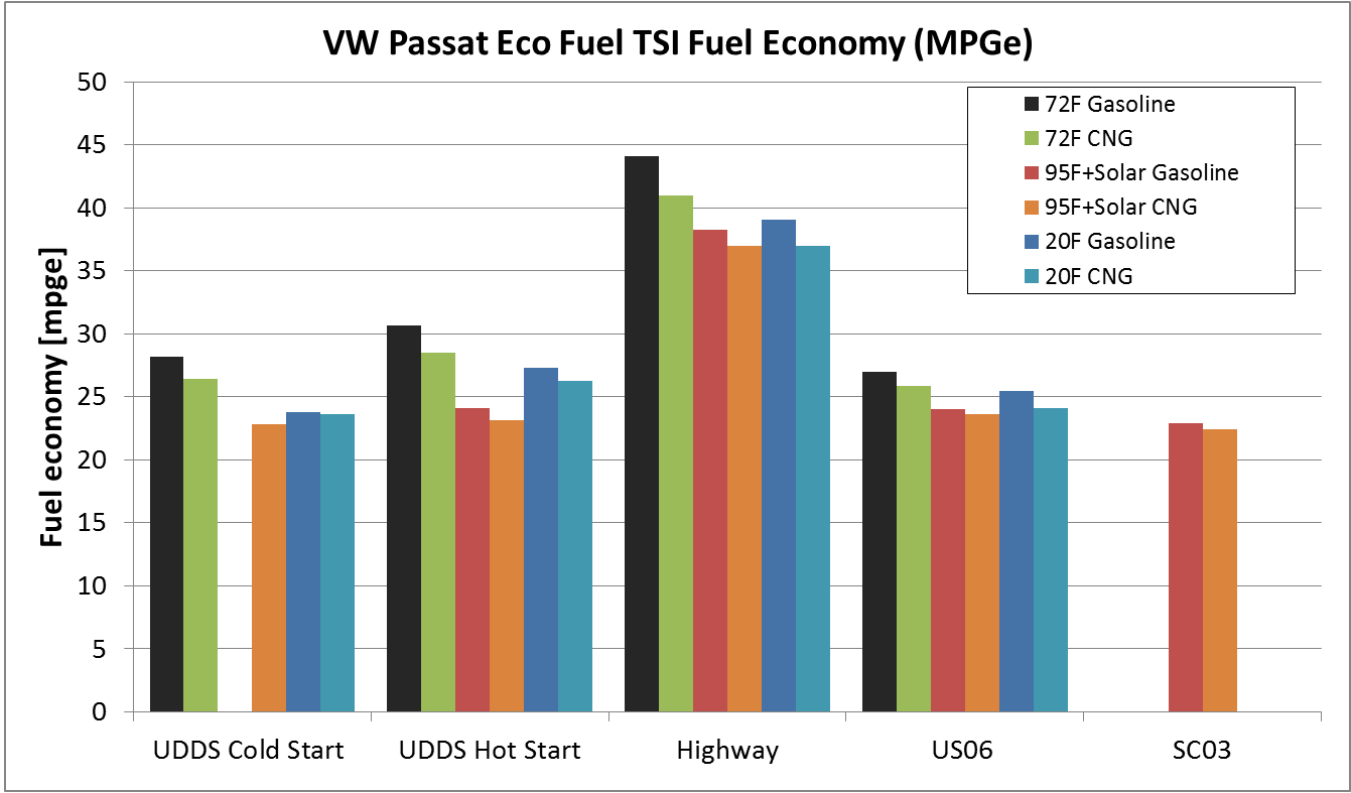


Figure III-22: Fuel Economy of the 2012 VW Passat EcoFuel TSI

5.

As can be seen, the vehicle fuel economy on CNG was found to consistently decrease each cycle, with a variation from 1%-7% by drive cycle and test cell temperature. Though the reduction in fuel economy can be seen from the calculated data, the impact of fuel to emissions of interest, which can be found in Table III-12.

Table III-12: VW Passat Ecofuel TSI emissions of the standard US drive cycles

VW Passat Ecofuel TSI Fuel Economy (MPGe) and Emissions (g/mi)													
Test	Temp [F]	Bag MPGe		CO ₂ x(.001)		CO		NO _x		THC		CH ₄	
		Petrol	CNG	Petrol	CNG	Petrol	CNG	Petrol	CNG	Petrol	CNG	Petrol	CNG
UDDS cold start	72	28.2	26.39	311.08	240.16	1.934	0.582	0.022	0.051	0.042	0.024	0.019	0.070
UDDS hot start	72	30.7	28.50	288.14	222.53	0.729	0.407	0.027	0.089	0.001	0.010	0.001	0.032
Highway	72	44.1	40.98	200.76	155.04	0.150	0.147	0.002	0.003	0.001	0.000	0.001	0.001
US06	72	27.0	25.85	325.24	245.71	1.940	0.227	0.065	0.079	0.010	0.009	0.007	0.026
Test	Temp [F]	Bag MPGe		CO ₂ x(.001)		CO		NO _x		THC		CH ₄	
		Petrol	CNG	Petrol	CNG	Petrol	CNG	Petrol	CNG	Petrol	CNG	Petrol	CNG
UDDS cold start	20	23.8	23.6	361.24	268.29	6.291	0.763	0.027	0.115	0.329	0.062	0.094	0.184
UDDS hot start	20	27.3	26.3	323.93	241.20	0.751	0.456	0.261	0.075	0.006	0.010	0.002	0.030
Highway	20	39.0	37.0	226.59	171.80	0.443	0.160	0.003	0.002	0.002	0.000	0.002	0.002
US06	20	25.5	24.1	346.34	263.64	1.067	0.229	0.037	0.078	0.008	0.010	0.005	0.029

A consistent reduction in CO₂ emissions, ranging from 30-35% dependent on drive cycle and test cell temperature was found. As can be seen the reduction in emissions for CO, NO_x, THC, and CH₄ was quite variable, as at the low level of emissions found small peaks in vehicle emissions created a large impact on overall cycle. This variability makes it challenge to draw any set conclusions, demonstrating the benefit of capturing modal emissions data, something which is a standard in level 1 though is outside of the scope of this summary.

Level 2 Evaluation Results

Level 2 evaluations differ from level 1 testing in two main areas: 1) extensive, invasive instrumentation, and 2) extended testing designed to full map the component. As an extensive amount of work goes into each vehicle, the vehicles are often utilized for multiple comparative projects over their lifetime.

Analysis within the FY2015 has included the thermal impacts on varying generations of HEV and PHEV powertrains, verifications of test methods for maximum power of hybridized powertrains, evaluation of test procedures for vehicle coast down standards, and added research projects for academic collaborations. As a specific area of discussion for FY2015, testing was leveraged with the FY2014 research vehicle, the 2014 Honda Accord PHEV. Test data was generated in order to compare the vehicle operation with other blended plug in electric vehicles.

2014 BMW i3 with Range Extending Engine

Vehicle Description

The vehicle selected for the FY2015 in depth testing and analysis was the MY2014 BMW i3 with optional range extender. This vehicle represents one of many battery electric vehicles to recently reach the market, though equipped with several unique features leading to a desire for in depth evaluation. Of key interest was a low power, 28kW range extending generator option for the standard BEV. This generator, directly mounted to the engine, provides electric power as a series hybrid only upon depletion of the high voltage battery. Figure III-23 shows the vehicle mounted on the 4WD chassis dynamometer at the Advanced Powertrain Research Facility undergoing testing.



Figure III-23: 2014 BMW i3 REx mounted in APRF for evaluation.

Vehicle Instrumentation

Preliminary instrumentation and testing

In contrast to the instrumentation performed on vehicles through the AVTA program, invasive instrumentation provided an in-depth signal list which allows the measure the full energy flow across different components

within the powertrain. The fitment of additional sensors, capture of additional vehicle parameters, and an extensive barrage of testing reveals the powertrain operation and component maps.

In contrast to Level 1 test vehicles, purchase and mileage accumulation of a set 4000 mile duration were completed under moderate instrumentation and data collection by APRF. Following break-in, a preliminary evaluation of the vehicle was completed in order to accomplish two goals. The first goal was to establish baseline test results to which the fully instrumented vehicle could be compared. Though all instrumentation is implemented in order to not impact vehicle operation, this preliminary testing provides data for verification. The second goal is to provide some preliminary data early for analysis and to help guide the plan development to areas of interest. This insight then results in specific instrumentation, and focused testing once the full Level 2 instrumentation is completed.

Preliminary instrumentation was similar to that of a Level 1, or non-invasive vehicle evaluation. As mentioned, the desire was to test the vehicle in an undisturbed state, thus rendering invasive instrumentation undesirable. This preliminary instrumentation included the mapping of the vehicles multiple CAN and FlexRay bus', followed by decoding of both the broadcast and diagnostic CAN messages. A short list of some messages captured includes: vehicle operational states, powertrain speeds and torques, varying system temperatures, and high voltage battery parameters such as voltage, current, state of charge.

Additional preliminary instrumentation included fuel flow measurements via a fuel scale located at the fuel supply connection within the powertrain bay, cabin temperature, engine oil temperature, emissions measurement, and standard APRF facility data.

Preliminary testing included evaluation on with J1634 shortcut multi cycle test, and additional testing with the vehicle in charge sustaining operation. Following evaluation for preliminary testing, the vehicle was removed from the dynamometer, and invasive instrumentation process began. This included additional instrumentation of the vehicles low voltage equipment, cooling systems, exhaust, and installation of axle torque sensors as detailed next.

In depth instrumentation- High and low voltage bus instrumentation

As energy flow and efficiency are of key interest, the vehicle was equipped with a high voltage tap, and multiple current measurements at specific areas of interest. Through the process of initial instrumentation, it was determined that the easiest location for a high voltage tap would be within a cable itself, resulting in splicing, and remolding of the main battery supply cable. Power flow was measured with a power analyzer, with the high voltage tap at the aforementioned location, and current measurement seen as clamps at the locations listed in Figure III-24.

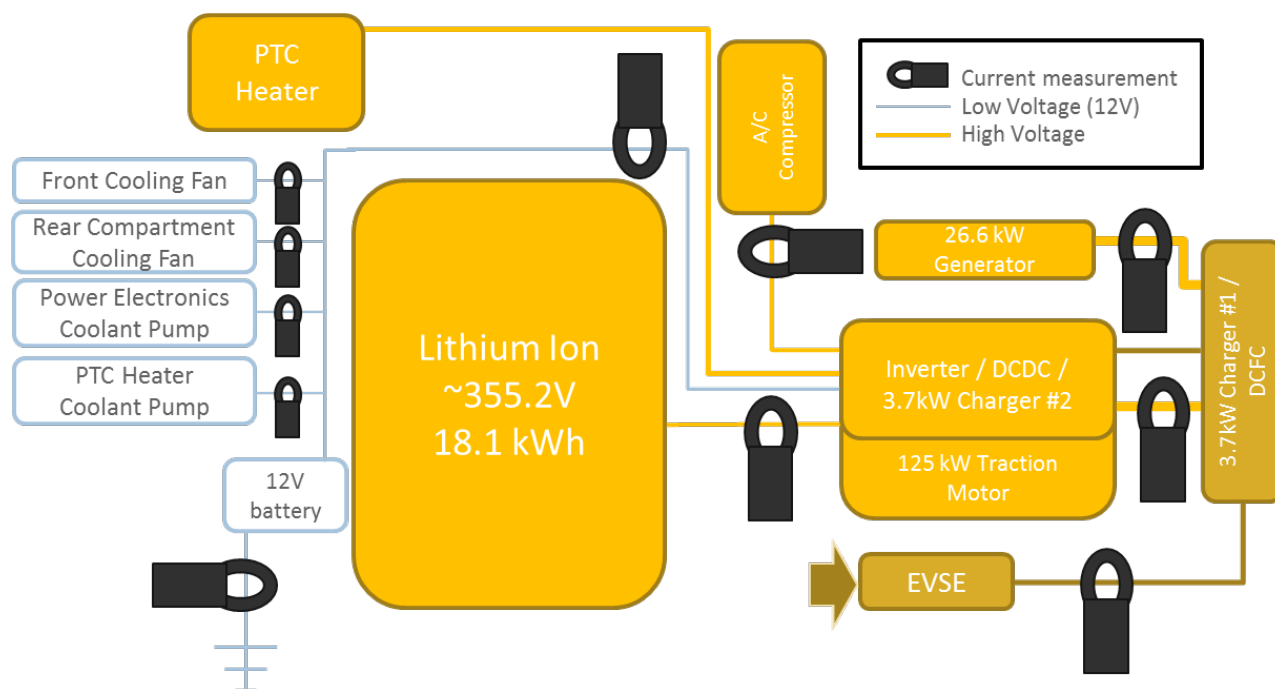


Figure III-24: Vehicle high voltage and low voltage bus description

The high voltage instrumentation includes: total high voltage battery power, range extending generator power, charger 1 (within the charging module), charger 2 (within the inverter packaging), HVAC compressor and heater, and AC power delivered into the vehicle charge port. Current measurements at these locations required modifications of the cabling to remove the shielding in order to provide an accurate measurement. This aspect will be discussed in greater detail later in the document.

Cooling system

The coolant system of the 2014 BMW i3 REx can be split into 3 systems, with a heat exchanger providing an exchange of thermal energy between two main systems via a liquid to liquid heat exchanger. The first of these three systems include a cooling loop similar to that of the i3 BEV, which provides separate cooling paths, in parallel for the drive motor and inverter, charging electronics, and range extender motor and inverter. Downstream of these components exists the heat exchanger, in which heat from the second loop of the range extending IC engine is rejected. A third coolant loop exists to provide cabin heat, consisting of only a PTC heater, pump, and interior heater coil.

In order to assess the operating temperatures of the coolant, and understand the losses associated with the various components, in-line coolant temperature sensors were installed across most important thermal nodes of the vehicle. In addition to the temperature sensors, coolant flow was also measured for various sections of the vehicle's overall thermal system. As with temperature, in-line sensors were installed to appropriately assess all coolant flows within the system.

A schematic of the first and second cooling loop, and associated instrumentation can be found with Figure III-25.

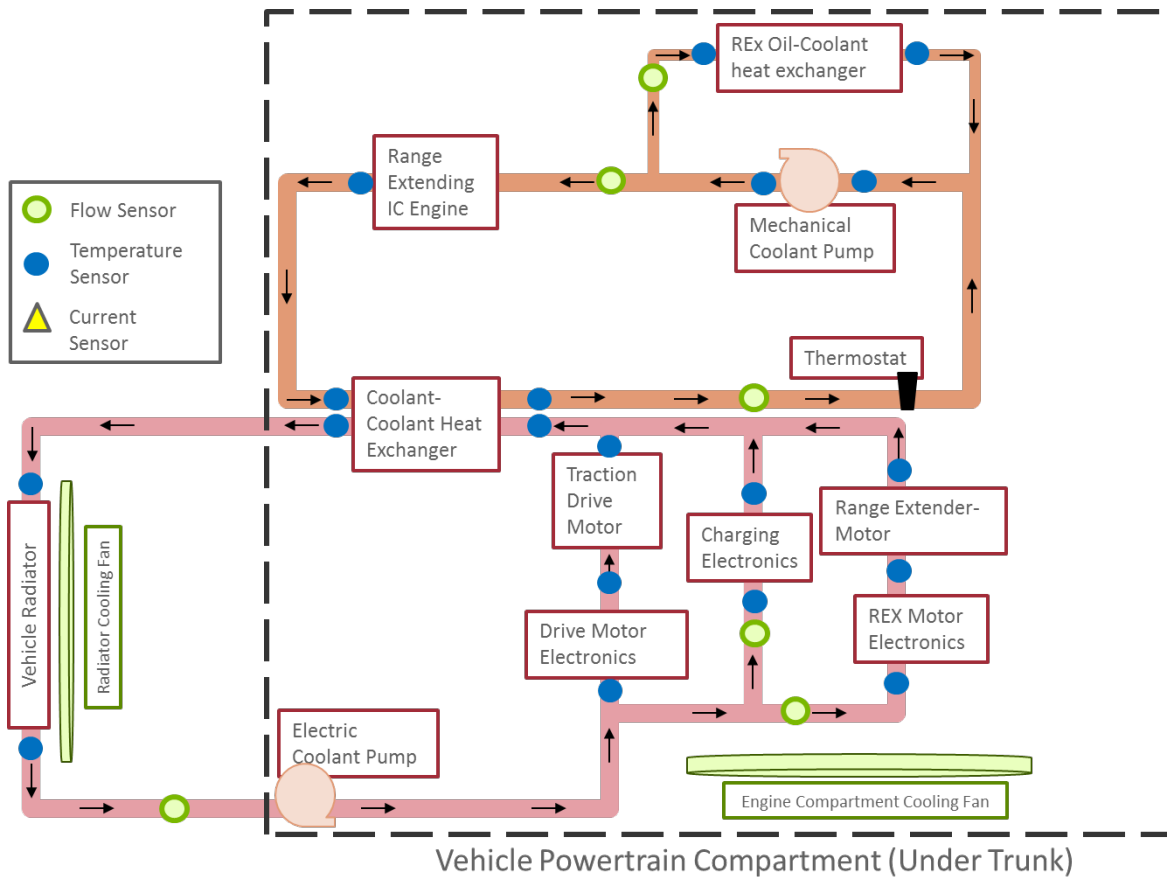


Figure III-25: BMW i3 REX Level 2 cooling system instrumentation

Exhaust system description

The range extending engine on the i3 Rex is equipped with a basic exhaust system, with no active external EGR system, resulting in simplification of exhaust system instrumentation. Both catalyst bricks are measured with thermocouples which coupled with the emissions data will provide some insight on the system effeteness. Additional temperature measurements were made at the manifold, between catalysts, and muffler entrance. Exhaust system instrumentation can be seen in Figure III-26.

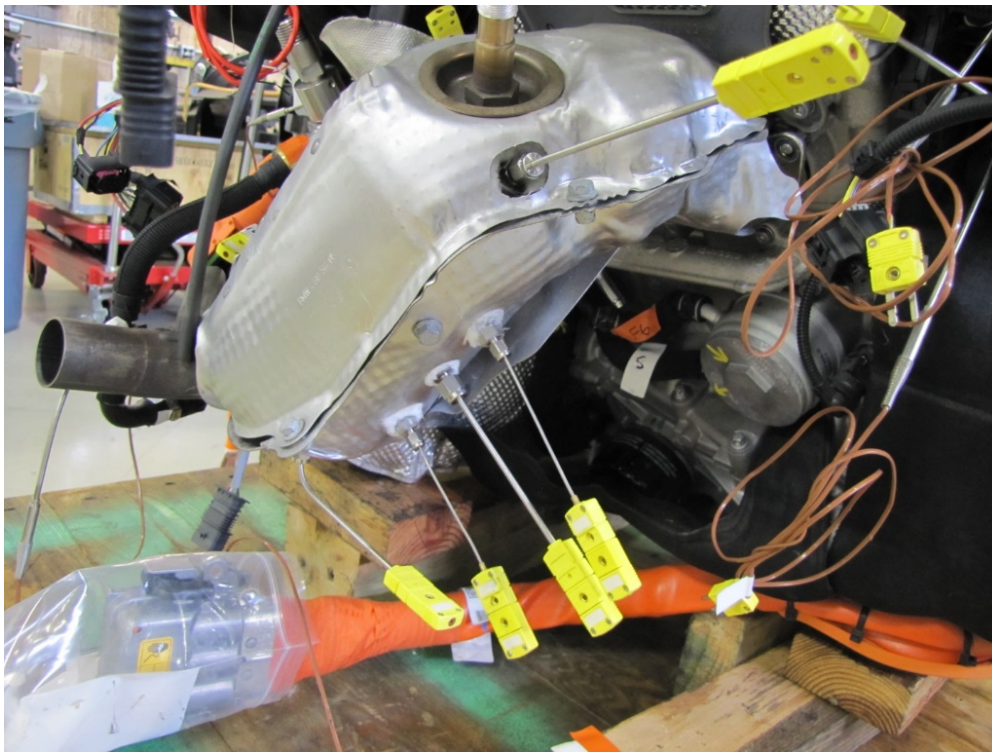
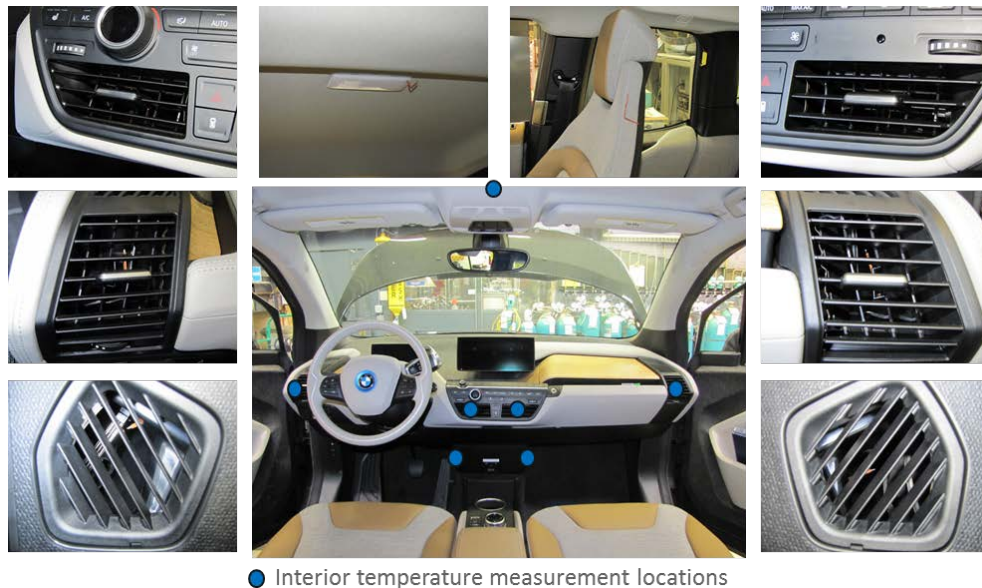


Figure III-26: Exhaust system instrumentation

Cabin and vent temperature instrumentation

To aid on-going DOE research related to vehicle HVAC usage and electrical loads, cabin and vent temperatures have been instrumented to capture an understand of heating, cooling, constraints across a range of ambient temperatures and conditions. Temperatures included all interior vents and various positions through the vehicle interior. Analog instrumentation was supported with diagnostic data relating to vehicle interior temperatures, HVAC system flap positions, and driver demanded settings. Interior instrumentation of in-cabin temperature signals can be seen in Figure III-27.



o

Figure III-27: Interior cabin and vent temperature instrumentation

3 phase voltage taps

In continuation of a successful collaboration with Oak Ridge National Laboratories (ORNL) power electronics benchmark group the 3 phase voltage of the vehicle traction motor was instrumented allowing for externally capture during testing. This instrumentation provides a greater understanding of the drive systems operation and aids in supporting other DOE efforts. The inverter voltage tap locations can be seen in Figure III-28 below.

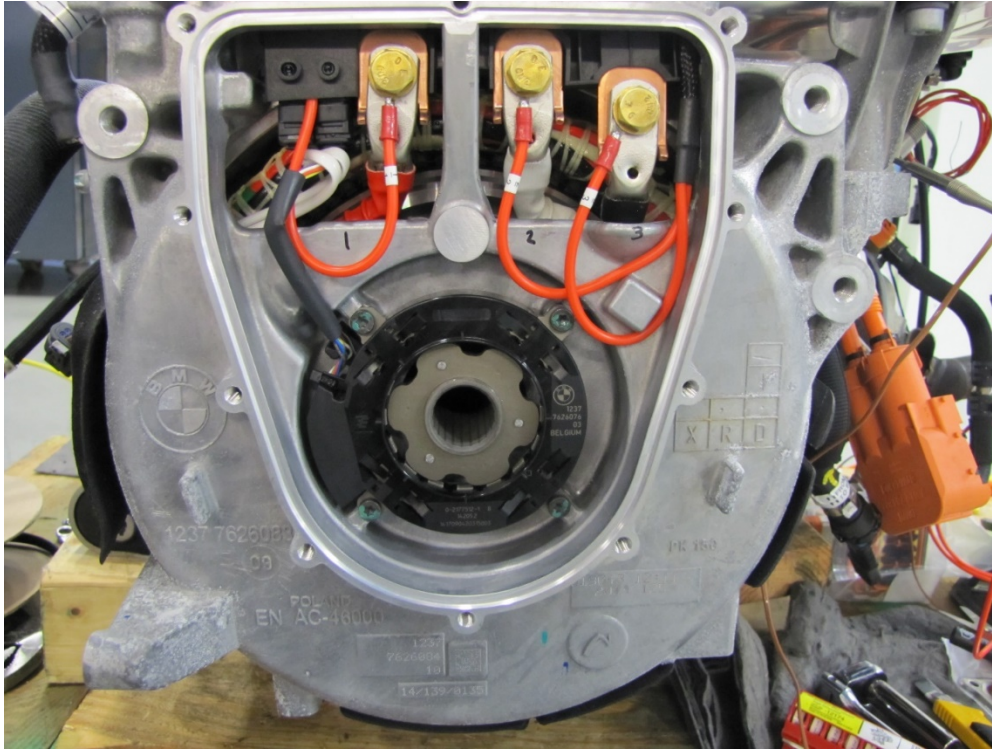


Figure III-28: Three phase voltage taps routed internal to the drive unit.

Instrumentation verification and challenges

Of key importance for these elaborate Level 2 benchmark vehicles is the validation of the instrumentation. As technology quickly advances, a proper understanding of how these advances change measurement requirements is critical to ensure proper testing allowing for accurate, repeatable results. Electrical energy use throughout electrified vehicles is typically a direct measurement of current and voltage on the components of interest. During Level 2 testing of the BMW i3 BEV, energy use was found to be variable with respect to low voltage system loads on multiple current clamp measurement locations. This current flow can be seen over the UDDS cycle in Figure III-29.

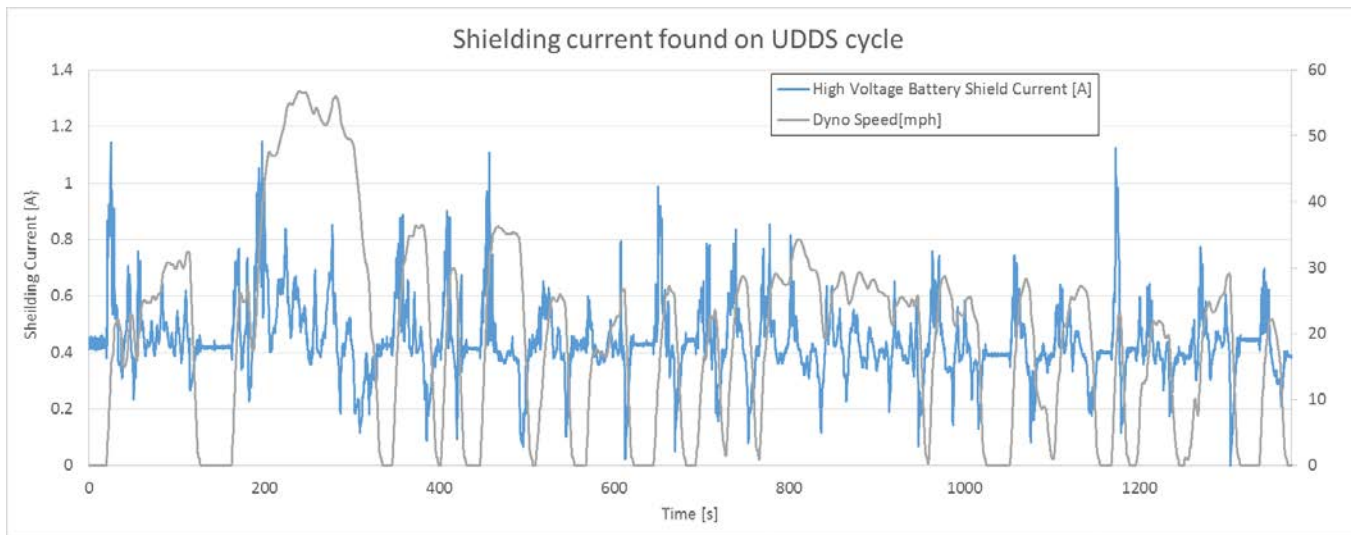


Figure III-29: Shielding current over UDDS CS on the 2014 BMW i3 Rex

Though this value is relatively small, it is not negligible. Over the duration of the UDDS drive cycle shown above it was found to account for a "phantom" energy use of 72Wh. If this energy were to be accounted for on the high voltage bus, cycle energy consumption would increase from 1228Wh to 1300Wh- an increase of 5.8%, in energy consumption from 164 Wh/mi to 174 Wh/mi. This increase in consumption would then integrate over the duration of a full charge test, resulting in inaccurate energy battery usable energy capacity results. These results demonstrate the need for a revision in instrumentation to ensure good test results.

Level 2 testing results and analysis

Due to the instrumentation challenge, the depth of instrumentation and amount of data available from this vehicle, and the current length of this report, results and analysis for the level 2 vehicle will be distributed through other platforms. Some of this information will be made available via the APRF's portal for publicly available data and analysis, the downloadable dynamometer database.

PHEV operation and range based on battery sizing and available power

A major benefit to the large number of test vehicles evaluated at the APRF is the ability to provide comparisons between varying vehicle platforms. This plethora of data was utilized in FY2015 to provide a comparison of three recently released plug in hybrid architectures including the Ford Fusion Energi, Toyota Prius PHEV, and the FY2014 test vehicle, the Honda Accord PHEV.

The plug in hybrid electric vehicles are similar in that they all provide a limited portion of the electric driving range available only within an limited electric power envelop. Driver demands outside of the electric power envelop will activate an internal combustion engine to meet torque demand. These vehicles also offer varying levels of EV-only capacities due to both drivetrain components and battery capacities (power and energy). Vehicle specifications such as weight, and available battery capacity as detailed in Figure III-30 below.



>Power-Split
 Test Weight: **3500 lbs**
 Nominal Batt Capacity:
4.4 kWh*
 Observed DC kWh:
 ~2.5 kWh (57% util)

>Series/Parallel (1 gear)
 Test Weight: **4000 lbs**
 Nominal Batt Capacity:
6.7 kWh**
 Observed DC kWh:
 ~3.0 kWh (45% util)

>Power-Split
 Test Weight: **4266 lbs**
 Nominal Batt Capacity:
 7.6 kWh***
 Observed DC kWh:
 ~5.9 kWh (78% util)

Figure III-30: General specifications of the 3 PHEV's under comparison

The battery energy capacity will define the electric driving range of a plug-in hybrid vehicles as long as the vehicle is operated within the available electric power of the battery and the drive system. Real world driving conditions may push the power demand beyond the available electric power and cause the engine to turn on. In normal operation varying levels of EV power result in large variability in percent of EV operation. To demonstrate this, the electric operation envelopes for all three vehicles was derived from test data as shown in Figure III-31.

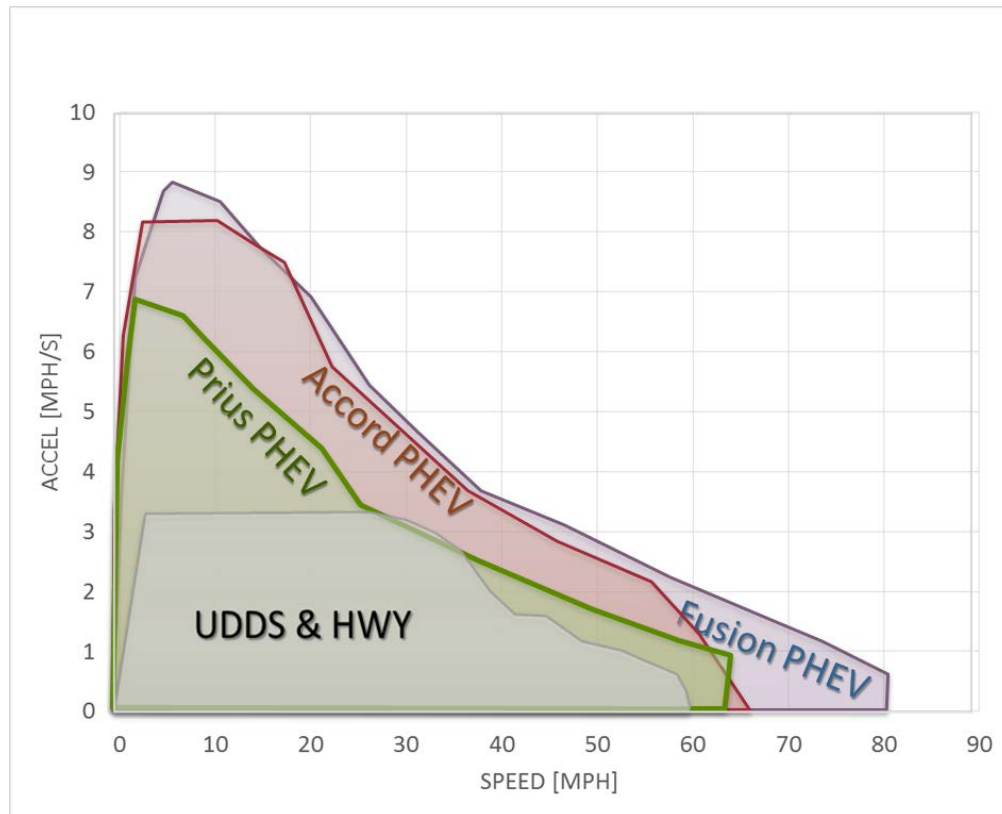


Figure III-31: Comparison of electric-only acceleration and maximum speed

Figure III-32 and Figure III-33 show the electric driving range for these vehicles on the UDDS and the US06 respectively. These vehicle operate in the electric driving mode for almost all of the UDDS cycle which has

rather mild accelerations and low speeds. The more aggressive cycle shows that the vehicle with a wider electric driving envelop can displace more fuel compared to the vehicle with a smaller electric driving envelope which has to use the engine frequently to meet the drive cycle power demands.

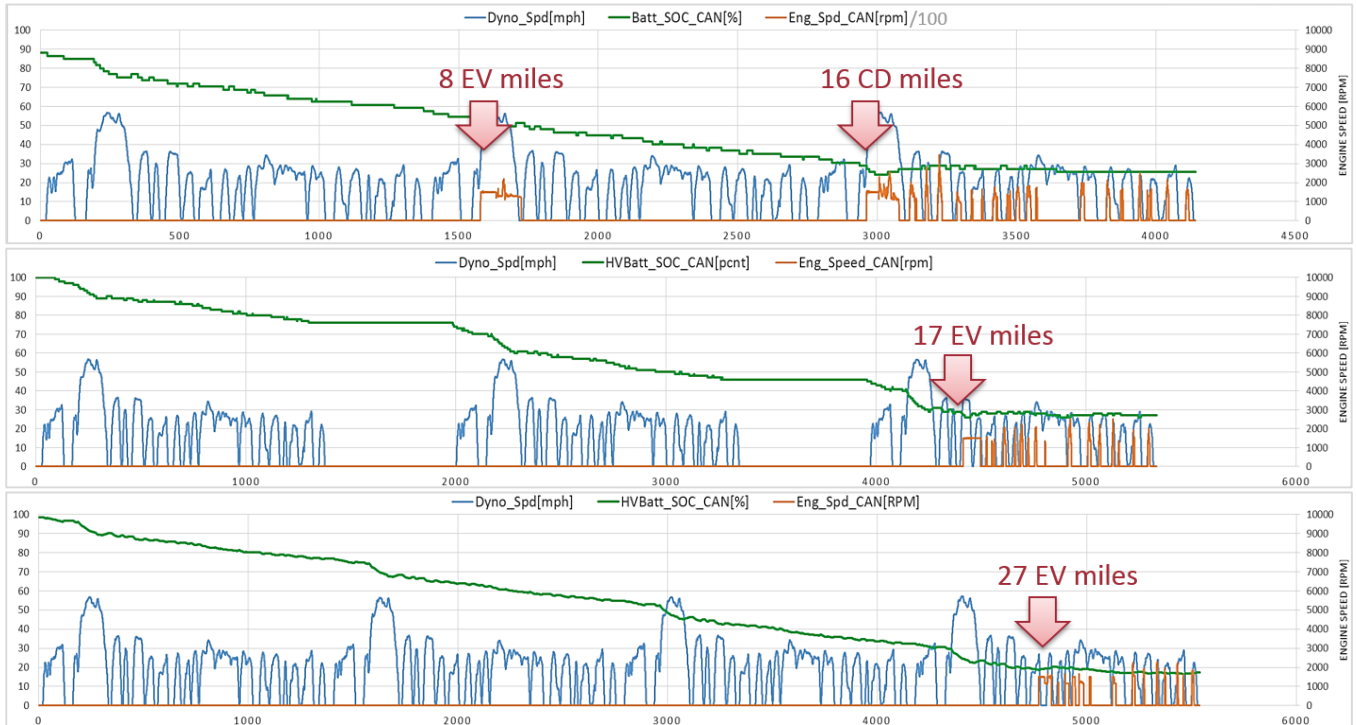


Figure III-32: UDDS operation of the Prius PHEV, Accord PHEV, and Fusion PHEV (in order)

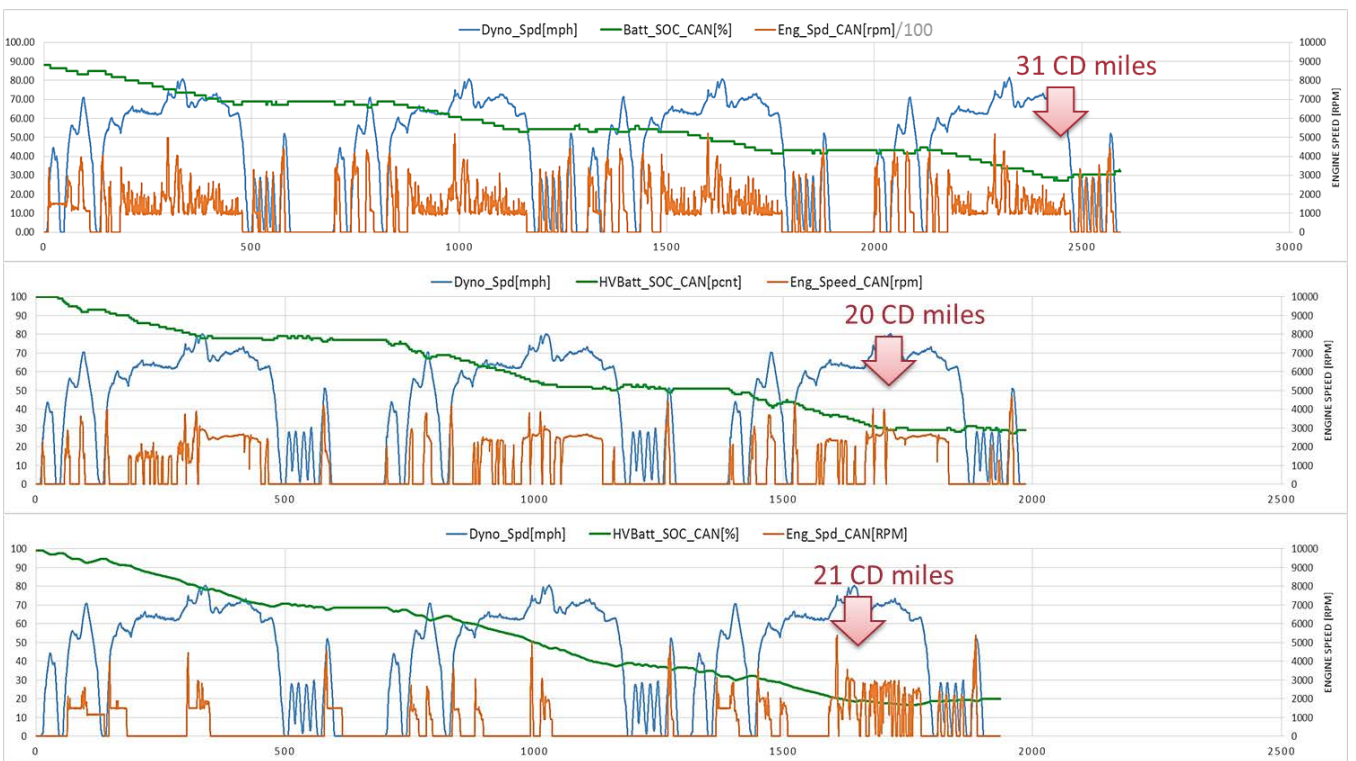


Figure III-33: US06 operation of the Prius PHEV, Accord PHEV, and Fusion PHEV (in order)

High power requirements from the second hill of the UDDS cycle result in an engine start at a range of 8 miles for the PHEV Prius, followed by the remainder of the cycle operating in EV mode. Both the Accord PHEV and Fusion PHEV completed at least two UDDS cycles in electric mode exclusively due to a wider electric drive operation envelopes. In comparison, the results of the US06 demonstrate vehicle operation under aggressive driving, resulting in higher power level demands. On all vehicles, engine starts occurred by the second acceleration of the US06 cycle, though amount of engine-on time between vehicles was quite varied.

This increased engine operation slows down the battery energy usage and thus the fuel displacement. While the engine is operating, it can be desirable to increase engine loading, thus providing power from the IC engine and in turn reducing the power demand and thus energy depletion of the HV battery. This effect of drive style on depletion rate to charge sustaining operation can be seen in Figure III-34 below.

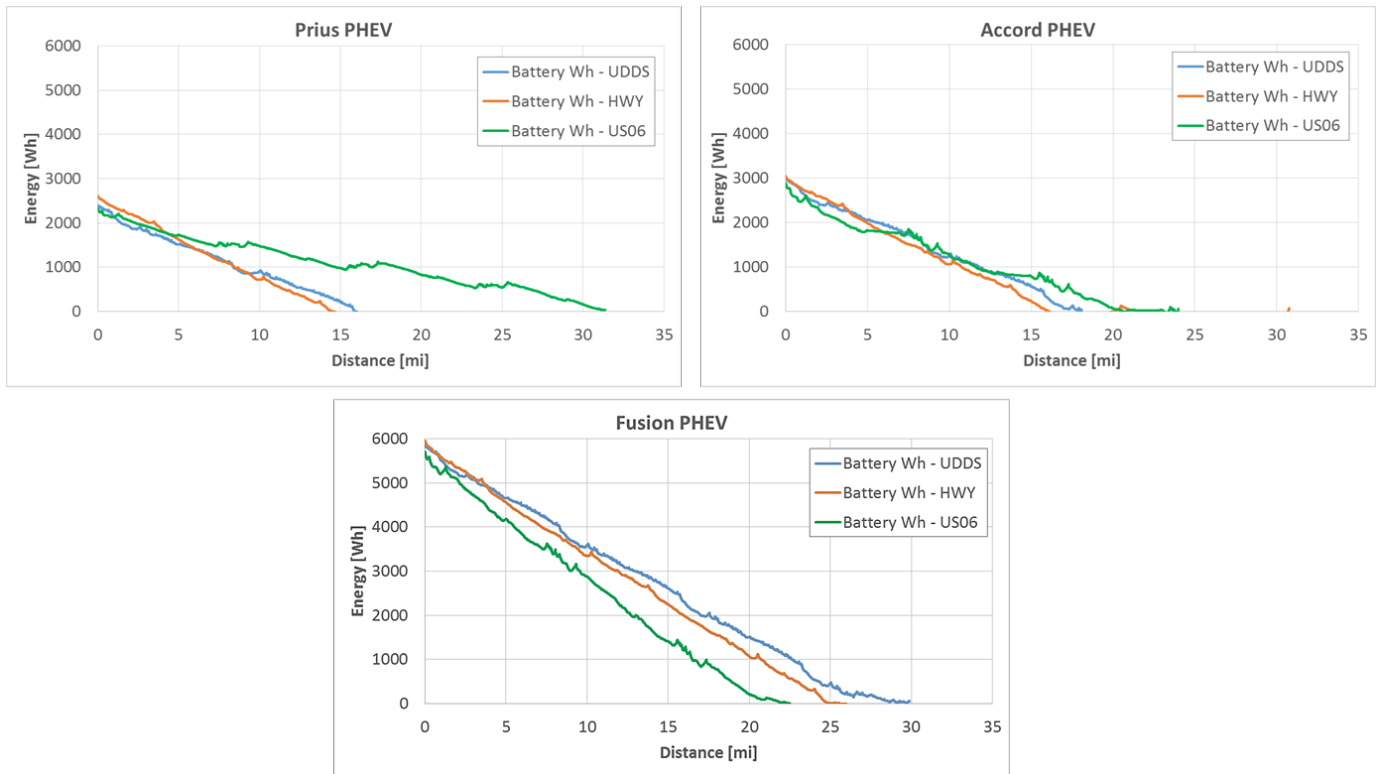


Figure III-34: Depletion summary of HV battery energy depletion

In summary, the example provide an overview of analysis that can be derived from APRF test data and the value in maintaining a fleet of Level 2 test vehicles. The available size of the electric driving envelop has impact in the real world driving which may not show on the certification city drive cycle.

Conclusions

The APRF benchmarked nine Level 1 vehicles which represented a rather wide range of powertrains and technologies. This report only highlights a small subset of data and analysis. The test results and analyses were distributed through several mechanisms such as reports, presentations, and sharing of raw data.

As is consistent with Level 2 in- depth vehicle evaluations of previous years, a significant amount of time and effort is spent on vehicle instrumentation, evaluation, and analysis. Instrumentation was directed toward specific systems of interest on a vehicle selected due to their capacity and depth of advanced technology.

The testing activity helped directly in the development of some codes and standards and supported the model development and validation. For more in-depth work regarding this and many additional advanced vehicles, the reader is pointed toward the Argonne Downloadable Dynamometer Database at anl.gov/D3.

The work conducted within this report is based on the hard work from a dedicated staff with a deep expertise. The principal investigators would like to acknowledge the hard work and prolonged efforts of the testing technicians: Mike Kern, Zach Stauber, and Geoff Amann, Facilities support including Dave Shimcoski and George Tsigolis, and the research aids Romain Macquart and Simeon Iliev.

III.1.C. Products

Presentations/Publications/Patents

1. Henning Lohse-Busch, "Off-Cycle Factors for Advanced Vehicle (xEV) Range and Energy Consumption", SAE 2015 Government/Industry Meeting, Washington DC, January 21-23, 2015
2. Henning Lohse-Busch, "Vehicle Electrification Increases Efficiency and Consumption Sensitivity", SAE ICE2015 12th International Conference on Engine and Vehicles, Keynote speech, Capri, Italy September 13-17, 2015
3. Namwook Kim, Jongryeol Jeong, Aymeric Rousseau, Henning Lohse-Busch, "Control Analysis and Thermal Model Development for Plug-In Hybrid Electric Vehicles", SAE Journal Article, 2015-01-1157
4. Jay Anderson, Scott Miers, Thomas Wallner, Kevin Stutenberg, Henning Lohse-Busch, Michael Duoba, "Performance and Efficiency Assessment of a Production CNG Vehicle Compared to Its Gasoline Counterpart", SAE Technical Paper 2014-01-2694
5. Namwook Kim, Aymeric Rousseau, Daeheung Lee, Henning Lohse-Busch, "Thermal Model Development and Validation for 2010 Toyota Prius", SAE Technical Paper 2014-01-1784
6. Namdo Kim, Aymeric Rousseau, Henning Lohse-Busch, "Advanced Automatic Transmission Model Validation Using Dynamometer Test Data", SAE Technical Paper 2014-01-1778
7. Jake Bucher, Thomas Bradley, Henning Lohse-Busch, Eric Rask, "Analyzing the Energy Consumption Variation during Chassis Dynamometer Testing of Conventional, Hybrid Electric, and Battery Electric Vehicles", SAE Journal Article 2014-01-1805

III.2. Advanced Vehicle Testing Activity

James Francfort, Principal Investigator

Idaho National Laboratory
 P.O. Box 1625
 Idaho Falls, ID 83415
 Phone: (208) 526-6787; Fax: (208) 526-0828
 E-mail: james.francfort@inl.gov

Lee Slezak, DOE Program Manager

U.S. Department of Energy
 Phone: (202) 586-2335
 E-mail: Lee.Slezak@ee.doe.gov

Start Date: October 2012
 End Date: September 2018

III.2.A. Abstract

Objectives

- Provide fuel efficiency, maintenance, and life-cycle cost data for advanced hybrid electric vehicles (HEVs), plug-in hybrid electric vehicles (PHEVs), battery electric vehicles (BEVs), and internal combustion engine vehicles.
- Benchmark battery performance and life in HEVs, PHEVs, and BEVs to support progress in battery development.
- Support federal fleets' petroleum reduction activities.
- Support New York State Energy Research Development Authority's (NYSERDA) electric vehicle charging station deployment project.

Accomplishments

- Advanced Vehicle Testing and Evaluation
 - Nine new models deployed in testing program
 - Baseline performance reports
 - Mileage and fuel reports
 - Maintenance and operations costs reports
 - Battery benchmarking reports
- Federal Fleet Support
 - Plug-in electric vehicle (PEV) fleet readiness reports published
 - Final federal fleet analysis report published
 - Twenty reports were published documenting the potential for federal fleets to replace internal combustion engine vehicles with plug-in electric vehicles (PEVs) and HEVs
- NYSERDA Electric Vehicle Supply Equipment (EVSE) Demonstration Project
 - Quarterly reports published

Future Achievements

- Continue rapid HEV, PHEV, and BEV mileage accumulation and benchmarking activities with a focus on new technologies.
- Partner with original equipment manufacturers to collect extensive field data through collaboration.

- Collect data and report on field demonstration for extended-range electric vehicle vans and pickup trucks
- Compilation and analysis of existing data from AVTA testing and PEV demonstrations to quantify variation in PEV overall cost of ownership
- Continuation of collection, analysis, and reporting of data from electric vehicle supply equipment (EVSE), including EVSE installed in New York State in partnership with Energetics and the New York State Energy Research & Development Agency. This may include the acquisition of new EVSE use data to fill knowledge gaps from previous data collection and analysis efforts, including new EVSE networks in and between metropolitan areas
- Continued analysis of data from PEVs to determine how electric vehicle miles traveled is affected by vehicle type, seasonal variations, region, and other factors.
- Continuation of PEV testing in cold weather to determine the impact of ambient temperature, battery conditioning, and cabin pre-conditioning on driving range and charging efficiency
- Evolve INL's data management and reporting process to produce new methods for sharing information and data to provide greater accessibility
- Continued support of the EV Everywhere Solutions Center.



III.2.B. Technical Discussion

Background

The Advanced Vehicle Testing Activity (AVTA) is the only activity tasked by the U. S. Department of Energy (DOE) to conduct field evaluations of vehicle technologies that use advanced technology systems and subsystems in light-duty vehicles to reduce petroleum consumption. A secondary benefit is a reduction in exhaust emissions.

Most of the advanced technology vehicles and components AVTA tests include use of electric drive propulsion systems and advanced energy storage systems. However, other vehicle technologies that employ advanced designs, control systems, or other technologies with production potential and significant petroleum reduction potential are also considered viable candidates for testing by AVTA.

The AVTA light-duty activities are conducted by Idaho National Laboratory (INL) for DOE. INL has responsibility for technical direction and management, along with data collection, analysis, and test reporting, for work performed under the Advanced Vehicle Testing and Evaluation project performed by Intertek Testing Services North America. INL is supported in this role by various subcontracts for specific tasks when greater value can be achieved for DOE. The AVTA sections of this task jointly cover the testing work performed by INL in addition to work over which INL maintains technical oversight. When appropriate, the AVTA partners with other governmental, public, and private sector organizations provide maximum testing and economic value to DOE and the United States' taxpayers via various cost-sharing agreements.

Introduction

AVTA is evaluating grid-connected PEV technologies in order to understand the capability of electric grid-recharged electric propulsion technology to significantly reduce petroleum consumption when vehicles are used for transportation. In addition, many companies and groups are proposing, planning, and have started introducing PEVs into their fleets.

It should be noted that grid-connected PEVs include several vehicle/energy storage powertrain types that include BEVs (or simply EVs), such as the Nissan Leaf and Volkswagen e-Golf; PHEVs, such as the Toyota Prius Plug-in; and extended-range electric vehicles (EREVs), such as the Chevrolet Volt.

Today's original equipment manufacturer-produced PEVs mostly have 4 to 16 kWh of onboard battery storage in PHEVs and EREVs, and more than 20 kWh of onboard storage for BEVs. AVTA makes extensive use of in-vehicle and in-charging infrastructure data loggers to collect a variety of vehicle and infrastructure-generated performance parameters. Experience has shown that automated data collection in fleet environments is the only way to ensure accurate and complete data are collected.

The concept of advanced onboard energy storage and grid-connected charging raises questions that include the life and performance of these larger batteries; the charging infrastructure required; how often the vehicles will actually be charged (i.e., driver and smart grid behavior and controls); and the actual amount of petroleum displaced over various missions, drive cycles, and drive distances; all of this is achieved with embedded data loggers.

AVTA also tests HEVs and advanced internal combustion engine technologies that can displace petroleum consumption through high-efficiency drivetrains. Low emissions capability is also a consideration for these advanced technologies.

Other activities conducted under the umbrella of AVTA include U.S. Department of Defense-related work that supports the DOE memorandum of understanding with the U.S. Department of Defense, supports DOE's Federal Energy Management Program (FEMP), and generally supports aiding federal fleet petroleum reduction efforts.

Approach

AVTA Fleet Testing

Under the Advanced Vehicle Testing and Evaluation project, three basic types of test methods are used to evaluate vehicles and their subsystems, each of which is discussed in detail as follows.

Baseline Performance Testing

To understand the capabilities of a vehicle when it is new and to independently verify performance ratings, vehicles are track and dynamometer tested. Track testing includes acceleration, constant-speed range, braking, and fuel consumption (both electricity and gasoline, or any other fuels that are being used) throughout the operating range of the vehicle. The vehicles are also coast-down tested to determine dynamometer coefficients, which are used during the various urban and highway dynamometer test cycles. Note that the AVTA dynamometer testing is conducted by Argonne or Oak Ridge National Laboratories in collaboration with AVTA. This sharing of vehicles and testing expertise reduces costs to DOE and leverages capability and knowledge base. Reports are published to document how the vehicles performed during each test, with a focus on fuel consumption.

Accelerated Testing

For experimental vehicles or cutting edge technologies, dedicated drivers are used to complete a series of drives and charges (for PEVs) on city and highway streets. This testing often is used to ensure PEVs can accomplish several charge and drive cycles in a day. For some vehicles, this can include more than 5,000 miles of operation per month. More commonly, and for most production advanced vehicles, AVTA partners with various fleets that utilize light-duty vehicles in high-mileage missions (e.g., document couriers or taxis).

Fleet Testing

This type of testing is normally conducted by placing vehicles into fleets with various missions to ensure a wide variation in drive cycles. AVTA partners with government, private, and public fleets for fleet testing because these fleets are often overwhelmingly the earliest adopters of advanced technology vehicles. Note that AVTA fleet testing normally does not include operation by the general public due to the level of management needed to ensure strict reporting for data quality assurance.

PHEVs and EREVs can operate on gasoline, even when the vehicles' battery packs are not charged. Therefore, with some exceptions, fuel-use reporting is normally broken down into the following three operating modes for these vehicle technologies:

- **Charge-Depleting Mode:** During each entire trip, electric energy in the traction battery pack provides either all-electric propulsion or electric assist propulsion throughout the entire trip.
- **Charge-Sustaining Mode:** During a trip, no electrical energy is available in the PHEV or EREV traction battery pack to provide any electric propulsion support beyond normal HEV battery operations.
- **Combined Charge-Depleting and Charge-Sustaining Mode:** For this mode, electrical energy is available in the traction battery pack at the beginning of a trip. However, during the trip, the PEV battery is fully depleted and the vehicle functions like a hybrid vehicle for the remainder of the trip.

Breaking down vehicle operations into these modes and characterizing the usage patterns is useful for understanding a technology's petroleum displacement potential and the results realized under the usage scenario the vehicle was placed in for rapid mileage accumulation. Data are recorded on a second-by-second basis during driving and charging, such that energy can be precisely tracked. The conditions under which the vehicle was operated are documented and presented with the fuel and energy consumption data.

Federal Fleet Support (Includes the Department of Defense)

This was a joint Energy Efficiency and Renewable Energy and FEMP-funded project during which data were collected from the diagnostic port of conventional fleet vehicles and electronically logged. Analysis was performed to determine vehicle usage patterns; those patterns were compared to the capabilities of several commercial PEVs and the results were compiled into reports. These reports support identification of vehicles and missions that are suitable for replacing current internal combustion engine vehicles with various electric drive vehicle technologies, with the main emphasis being on introducing PEVs.

NYSERDA EVSE Demonstration Project

Data were captured from 405 vehicle charging ports throughout the State of New York beginning in October 2013; data collection is presently ongoing. INL processes the charging data that is provided by several models of EVSE into a database that is used to generate reports and help answer questions about charging behavior. This system readily allows the data to be reduced by several different metrics that can be used to describe the charging station.

Results

AVTA Fleet Testing

The accelerated testing of HEVs, PHEVs, BEVs, and internal combustion engine vehicles is performed by Intertek Testing Services North America in Phoenix, Arizona. Intertek is working with INL on data collection, analysis, reporting, and procedure development. Ninety-five advanced technology vehicles were operated as part of the AVTA test fleet in 2015. Several models continued testing from previous years, while eight new models were introduced. The new models are listed as follows, along with their technology of interest:

- 2014 Chevrolet Cruze Diesel (advanced engine and emissions control system)
- 2014 BMW i3 Range Extender (battery, electric drive, and gasoline range extender system)
- 2014 BMW i3 EV (battery, electric drive, and Society of Automotive Engineers (SAE) Combined Charging System (CCS) fast charging)
- 2015 Kia Soul EV (battery, electric drive, and CHAdeMO fast charging)
- 2015 Chevrolet Spark EV (battery, electric drive, and SAE CCS fast charging)
- 2015 Honda Accord Hybrid (battery and hybrid drivetrain)

- 2015 Volkswagen e-Golf (battery, electric drive, and SAE CCS fast charging)
- 2015 Mercedes-Benz B-Class BEV (battery, electric drive, and extra battery range option).

All new HEVs, BEVs and PHEVs were tested for battery performance when they were new. This testing occurs five times throughout the test duration. Figure III-35 shows the charge and discharge power capability for a model year 2013 Chevrolet Volt that continued testing in 2015. The full results of battery testing are compiled into battery testing results reports.

Additionally, the new vehicles were tested on a closed test track for performance following a break-in period. A new test vehicle fitted with measurement instrumentation is shown in Figure III-36.

Dynamometer testing follows track testing to give consistent conditions for performance and energy consumption measurements, across which models can be fairly compared. Data from these tests were compiled into baseline performance testing reports that detail the performance and energy consumption both from the track and dynamometer testing. Following testing, the vehicles were instrumented with data logging equipment and released to fleets for mileage accumulation. Operation data summary reports were compiled for each test vehicle to show how each vehicle was used and the resulting fuel and electrical energy consumption. The distribution of electrical energy consumption is shown for a 2014 BMW i3 EV in Figure III-37.

Electronically logged data are continuously sent from the vehicles to INL servers and are processed daily. These data are used for specific subsystem studies at INL; they also have been provided to other national laboratories to support their modeling and simulation efforts. All reports referenced in the discussion of the project results were posted on the INL AVTA website (avt.inl.gov).

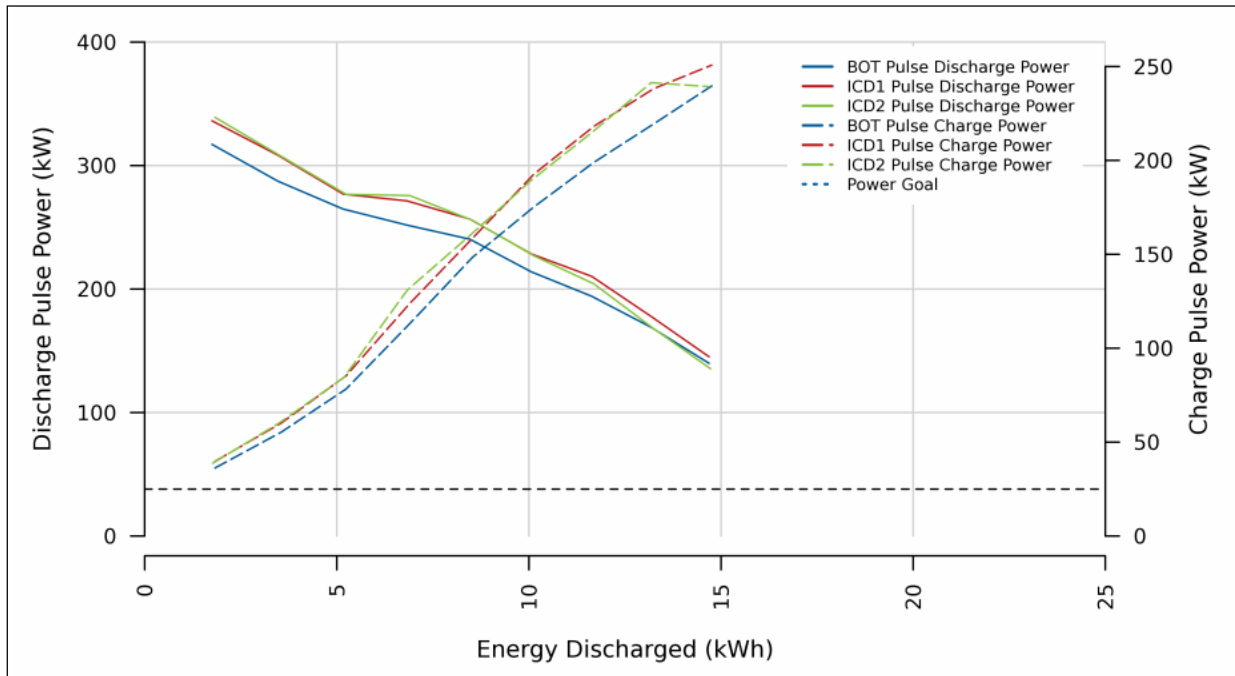


Figure III-35: Battery performance data are shown for a 2012 Chevrolet Volt. The data shown are from tests performed at 4,000; 14,000; and 60,000 miles. Two additional tests will be performed prior to completion of testing to characterize battery performance through the life of the battery. The Volt battery exceeded the United States Advanced Battery Consortium (USABC) power goal for a PHEV-40 for all tests.

INL



Figure III-36: A 2014 BMW i3 electric vehicle fitted with testing and measurement equipment for track testing.
Intertek Testing Services North America

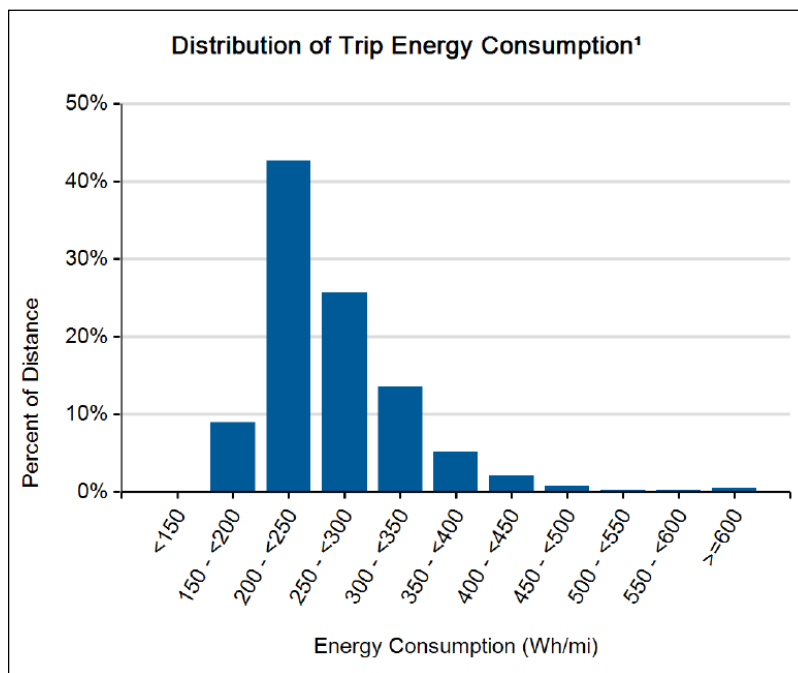


Figure III-37: Electrical energy consumption data are shown for a 2014 BMW i3 electric vehicle. The data shown are from on-road operations logged over several thousand miles.
Idaho National Laboratory

Federal Fleet Support (Includes the Department of Defense)

Following the previous year’s data collection efforts, analysis was performed and reports published for six federal fleets on PEV suitability. These reports support identification of vehicles and missions that are suitable for replacing current internal combustion engine vehicles with various electric drive vehicle technologies, with the main emphasis on introducing PEVs. This is a joint Energy Efficiency and Renewable

Energy and FEMP-funded project. Readiness reports have been completed for several federal agencies and fleet locations which are detailed in the publications list below. A graphic with supporting text from the final federal agency PEV suitability report is shown in Figure III-38.

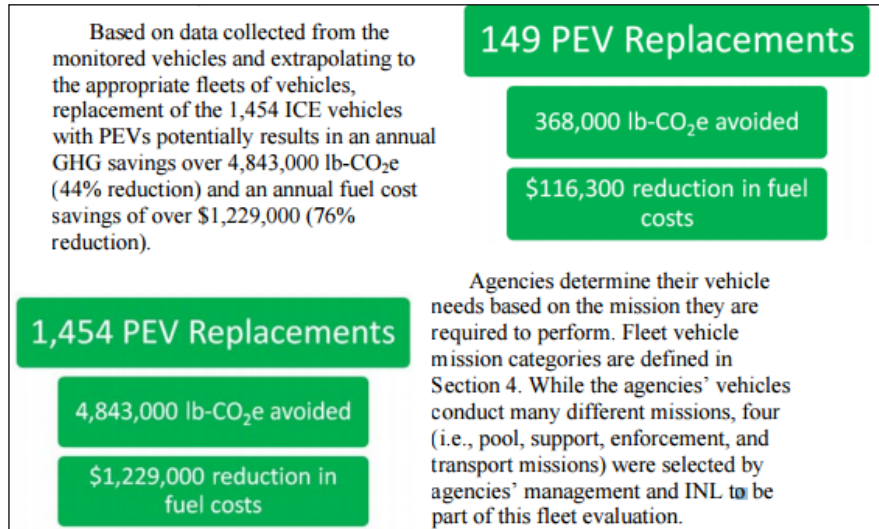


Figure III-38: Final report's executive summary about federal agency PEV suitability, which explains the economic, energy, and emissions reductions possible through replacement of conventional vehicles with PEV equivalents.

Idaho National Laboratory

Data loggers were placed on federal fleet vehicles in order to identify internal combustion engine vehicle missions that were suitable for the introduction of PEVs and HEVs. In addition, base studies were conducted at three Department of Defense bases that also included charging infrastructure location analysis. The federal departments and agencies supported by these activities included:

- United States Coast Guard Headquarters
- Marine Corps Base Camp Lejeune
- Joint Base Lewis McChord
- Marine Corps Logistics Base Barstow
- Marine Corps Base Camp Pendleton
- Marine Corps Air Station Miramar
- Marine Corps Air Ground Combat Center 29 Palms
- Naval Air Station Whidbey Island
- Idaho National Laboratory
- National Institute of Health
- Department of Health and Human Services – ASPR
- NASA Stennis Space Center
- NASA Glenn Research Center
- NASA White Sands Test Facility
- National Park Service: Sleeping Bear Dunes National Lakeshore
- Department of Veterans Affairs – James J. Peters VA Medical Center, Bronx, New York
- Department of Veterans Affairs – VA Manhattan Campus.

NYSDERDA EVSE Demonstration Reporting

As of June 2015, this project had deployed 405 electric vehicle charging ports in the state of New York. Data were collected from several distinct EVSE networks spread over five geographic districts. Aside from geographic location, the EVSE were also distributed among several fee structures, venues (e.g., retail, workplace, and hotel), access type locations (i.e., public and private), and land-use types (e.g., urban, suburban, and rural). INL’s reporting includes an overview for all EVSE; it also slices the data to examine variation in usage for each of the factors listed above. One year of data have been received and processed in Fiscal Year 2015, with reports produced for three quarters and the final quarter currently being processed. New York City boasts, by more than a factor of two, the highest average energy consumed per charging event, which is about 13 kWh in 2015. This indicates that more high-capacity electric vehicles charge at the New York City stations than other station locations. The vehicles in New York City also show a trend of longer charging times. The utilization of EVSE ports, by region, is shown in Figure III-39.

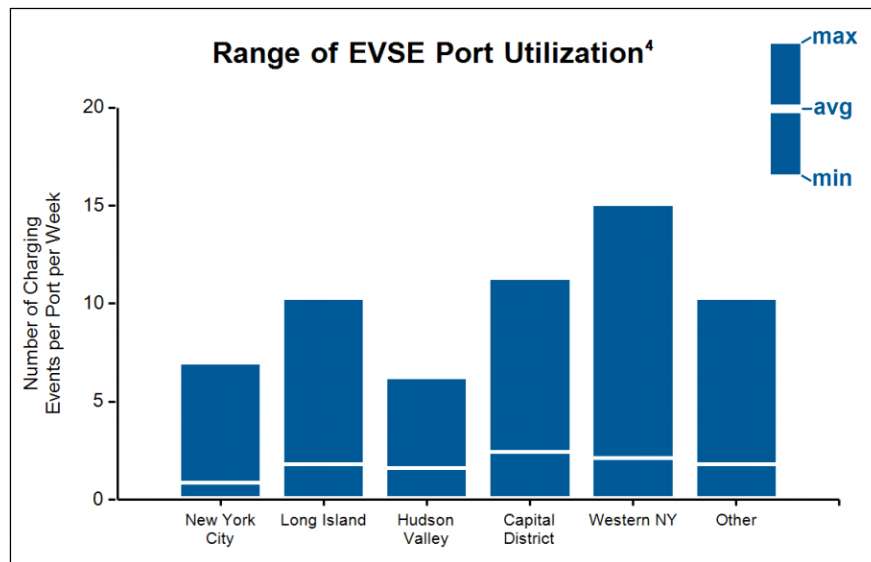


Figure III-39: The range and mean of EVSE port utilization is shown by region.

INL

Conclusions

AVTA will continue to provide the real-world testing needed to benchmark DOE technology investments, including the critical tasks of determining suitability for deployment, lifetime performance, and life-cycle costs of new technology components and vehicle systems. This testing provided information used to help understand the infrastructure requirements, operating costs, and petroleum displacement of PEVs, other alternative fuels, and HEVs, as well as proper placement of supporting infrastructure. The quality of the vehicles and the batteries (i.e., expected operational life) has improved significantly and fleets have been found that can significantly accumulate high per-vehicle mileage. Hybrid and internal combustion engine vehicle fleet testing mileage targets are set at 195,000 miles per vehicle. The PHEVs entering testing will accumulate 160,000 miles per vehicle and the BEVs will operate for 30,000 miles per vehicle. These targets are a combination of the practical limits of mileage accumulation and the period of interest (i.e. about 3 years) for the new technologies. Though the durability of these vehicles has improved significantly, the need for on-road testing is still very relevant to understand off-cycle performance and how on-road usage compares to standardized test procedures.

III.2.C. Products

Presentations/Publications/Patents

1. "Fleet Testing Fuel Economy, Series of Fact Sheets," INL/MIS-14-32657, Idaho National Laboratory, 2015.
2. "Baseline Performance Testing, Series of Reports," Idaho National Laboratory, Intertek Testing Services North America, 2015.
3. "Battery Testing Results, Series of Reports," INL/MIS-14-31587, Idaho National Laboratory, 2015.
4. "Maintenance History Reports, Series of Fact Sheets," Idaho National Laboratory, 2015.
5. "Vehicle Fact Sheet, Series of Fact Sheets," INL/MIS-14-32657, Idaho National Laboratory, 2015
6. "Plug-In Hybrid Electric Vehicle Operation Data Summary, Series of Fact Sheets," INL/MIS-11-22875, Idaho National Laboratory, 2015.
7. "Electric Vehicle Operation Data Summary, Series of Fact Sheets," INL/MIS-15-36519, Idaho National Laboratory, 2015.
8. "Hybrid Electric Vehicle Operation Data Summary, Series of Fact Sheets," INL/MIS-15-36685, Idaho National Laboratory, 2015.
9. "NYSERDA Electric Vehicle Charging Infrastructure Report, Quarterly Reports," INL/MIS-14-31250, Idaho National Laboratory, 2015.
10. Schey, S. and J. Francfort, "AVTA Federal Fleet PEV Readiness Data Logging and Characterization Study for United States Coast Guard Headquarters," INL/EXT-15-34869, Idaho National Laboratory, November, 2014.
11. Schey, S. and J. Francfort, "Electric Vehicle Preparedness: Task 1, Assessment of Fleet Inventory for Marine Corps Base Camp Lejeune," INL/EXT-15-34744, Idaho National Laboratory, January 2015.
12. Schey, S. and J. Francfort, "Electric Vehicle Preparedness: Task 2, Identification of Vehicles for Installation of Data Loggers for Marine Corps Base Camp Lejeune," INL/EXT-15-34744, Idaho National Laboratory, February 2015.
13. Schey, S. and J. Francfort, "AVTA Federal Fleet PEV Readiness Data Logging and Characterization Study: Final Report," INL/EXT-15-35799, Idaho National Laboratory, June 2015.
14. Schey, S. and J. Francfort, "Assessment of Fleet Inventory for Naval Air Station Whidbey Island: Task 1," INL/EXT-15-34754, Idaho National Laboratory, January 2015.
15. Schey, S. and J. Francfort, "Electric Vehicle Preparedness: Task 2, Identification of Vehicles for Installation of Data Loggers for Naval Air Station Whidbey Island," INL/EXT-15-34855, Idaho National Laboratory, March 2015.
16. Schey, S. and J. Francfort, "Utilization Assessment of Target Electrification Vehicles at Naval Air Station Whidbey Island: Task 3, Idaho National Laboratory," INL/EXT-15-35637, Idaho National Laboratory, May 2015.
17. Schey, S. and J. Francfort, "Assessment of Charging Infrastructure for Plug-in Electric Vehicles at Naval Air Station Whidbey Island: Task 3," INL/EXT-15-35636, Idaho National Laboratory, July 2015.
18. Schey, S. and J. Francfort, "AVTA Federal Fleet PEV Readiness Data Logging and Characterization Study for Idaho National Laboratory," INL/EXT-15-35443, Idaho National Laboratory, May 2015.
19. Schey, S. and J. Francfort, "AVTA Federal Fleet PEV Readiness Data Logging and Characterization Study for NASA Stennis Space Center," INL/EXT-15-34825, Idaho National Laboratory, November 2014.
20. Schey, S. and J. Francfort, "AVTA Federal Fleet PEV Readiness Data Logging and Characterization Study for NASA Glenn Research Center," INL/EXT-15-34769, Idaho National Laboratory, October 2014.

III.3. Electric Drive Vehicle Climate Control Load Reduction – FY 2014

John P. Rugh, Principal Investigator

National Renewable Energy Laboratory
15013 Denver West Parkway, MS 1633
Golden, CO 80401
Phone: (303) 275-4413; Fax: (303) 275-4415
E-mail: John.Rugh@nrel.gov

David Anderson and Lee Slezak, DOE Technology Managers

Vehicle Technologies Office
Phone: (202) 287-5688, (202) 586-2335
E-mail: David.Anderson@ee.doe.gov, Lee.Slezak@ee.doe.gov

Start Date: 10/01/2012

End Date: 9/30/2015

III.3.A. Abstract

Objectives

- Minimize the impact of climate control on electric-drive vehicle (EDV) range
- Reduce the battery size by minimizing:
 - Energy consumption of vehicle climate control system
 - Time the battery exceeds the desired temperature range
- Develop new strategies for thermal comfort evaluation
- Increase electric range by 10% during operation of the climate control system through improved thermal management while maintaining or improving occupant thermal comfort.

Accomplishments

- Completed warm weather outdoor thermal testing of Ford Focus Electric vehicles
- Demonstrated the potential for vehicle body insulation to reduce steady-state heating energy by up to 3.3%
- Used computational fluid dynamics (CFD)/RadTherm/human model to demonstrate 28% reduction in air conditioning (A/C) capacity and equivalent comfort with an overhead A/C vent
- Evaluated a combined A/C system configuration that included thermal load reduction and zonal cooling strategies, demonstrating:
 - Energy savings of up to 66.5% (0.92 kWh) after 20-minute cool-down
 - Improved cooling of driver air temperature (1.8°C lower than baseline after 20 min.)
 - Estimated range improvement of up to 11%–33% over baseline A/C.

Future Achievements

- Evaluate climate control load reduction strategies for cold weather
 - Zonal heating strategies
 - Improved defrost/defog performance
- Complete cold weather testing of Focus battery electric vehicles (BEVs)
- Demonstrate potential for 10% electric vehicle (EV) range improvement during cold weather climate control operation.



III.3.B. Technical Discussion

Background

As in conventional vehicles, passenger compartment climate control is required in EDVs for comfort and safety (e.g., demisting and defrosting). A challenge with EDVs is that electrical energy consumed for climate control can significantly reduce the vehicle range. A Ford Focus Electric tested at Argonne National Laboratory's Advanced Powertrain Research Facility showed a reduction in range of 53.7% due to A/C and 59.3% due to heating over the Urban Dynamometer Driving Schedule (UDDS) drive cycle [1]. Air conditioning and heating have also been shown to reduce the UDDS driving range of a Nissan Leaf by 18% and 48%, respectively [2]. Range anxiety will impact customer acceptance of EDVs and the penetration of these vehicles into the national fleet.

Introduction

Currently, conventional vehicles heat cabins with engine waste heat, but because EDVs do not have an engine, automobile manufacturers are presented with new climate control challenges. Using the battery for cabin electrical resistance heating takes valuable energy away from propulsion. Thus, larger batteries are often required to meet range targets that include climate control operation. Traction batteries can also be impacted by the interior cabin temperatures. Designing batteries to account for high-temperature degradation leads to larger and higher-cost batteries. Therefore, it is critical to minimize climate control loads in EDVs to maximize vehicle range.

The objective of this task is to increase in-use EDV range by minimizing climate control energy requirements. The goal is to increase range by 10% with improved thermal management during operation of the climate control system. The target range improvement is expected to increase customer acceptance of EDVs through the reduction of range anxiety. In addition, improving thermal comfort upon entry into a hot-soaked or cold-soaked vehicle may lead to additional motivation for drivers to adopt EDVs and improved safety through reduced driver distraction due to thermal stress.

Over the past two years, National Renewable Energy Laboratory (NREL) researchers have investigated climate control load reduction strategies using complementary experimental and analytical techniques. After installing numerous temperature and power sensors, thermal soak and transient conditioning tests were conducted to measure the power requirements of the Ford Focus Electric's on-board cooling and heating systems. Baseline tests characterized the inherent differences between the vehicles and enabled accurate measurement of the impact of load reduction technologies. Computational models have been developed and exercised to pre-screen technologies and to evaluate strategies that are difficult or costly to evaluate experimentally.

Approach

Our approach is to collaborate with the automotive industry to research and develop techniques that will reduce cooling and heating loads on EDVs to improve range. The following areas will be considered:

- Thermal load reduction technologies
- Occupant thermal comfort optimization
- Intelligent heating, ventilating, and air conditioning (HVAC) control to minimize energy use
- Thermal preconditioning.

Testing and analysis will be used in conjunction to develop and evaluate the effectiveness of strategies to reduce climate control loads in warm and cold weather.

Results

Thermal Analysis

Thermal analysis tools (including CFD, RadTherm, and human thermal comfort) were used to evaluate the effectiveness of potential strategies to reduce the climate control loads. Under a cooperative research and development agreement (CRADA), Ford provided the CAD geometry of a Focus Electric. Using this geometry, RadTherm and CFD meshes were developed. These meshes are fundamentally different as CFD uses a volume mesh, and RadTherm uses a surface mesh. Thermal soak simulations were performed to calibrate and validate the model. After calibration, the model was used for transient cool-down and human comfort simulations.

RadTherm Thermal Comfort Analysis Methodology

A virtual manikin based on NREL's ADAM thermal test manikin was added to both the RadTherm and Fluent models. The virtual manikin is a key element for enabling the human thermal comfort analysis.

Thermal comfort analysis is performed with RadTherm and the human comfort plugin developed by ThermoAnalytics, Inc. The plugin uses a human physiology model and calculates heat loss or gain to the environment to predict the thermal sensation and thermal comfort of a human. Inputs to the model include clothing ensemble and metabolic rate. Thermal boundary conditions include the local air velocity and temperatures from around the virtual manikin calculated in Fluent. Several thermal comfort and sensation metrics are output by the thermal comfort analysis, including Berkeley sensation and comfort, predicted mean vote (PMV), predicted percentage dissatisfied (PPD), and dynamic thermal sensation (DTS).

Fluent/RadTherm Transient Analysis Methodology

Fluent and RadTherm are run consecutively (not in parallel) and use bidirectional communication. For a steady-state analysis run, this can be done manually, but for a transient analysis run, the process must be automated to maintain time synchronization. A script was developed to execute the Fluent/RadTherm analysis on NREL's Linux supercomputer Peregrine. Using this script, a complete 20-minute cool-down transient analysis can be completed in three days using 128 processors. This was a significantly faster turn-around time compared to running locally.

Fluent/RadTherm Model Development – Overhead A/C Vent

Previous testing and simulation results indicated a potential for an overhead A/C vent to enable reduction in A/C energy use. An original equipment manufacturer-quality overhead vent was developed during the Ford-led thermoelectric HVAC project. This overhead vent geometry and ducting were incorporated into the Focus BEV model as shown in Figure III-40 and Figure III-41. The use of this vent enabled a more realistic evaluation of this technology. The modified geometry was remeshed, and both Fluent and RadTherm models were created.

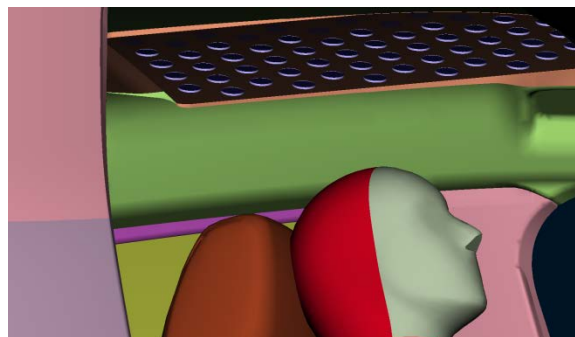


Figure III-40: Overhead Vent Incorporated into Focus BEV Model

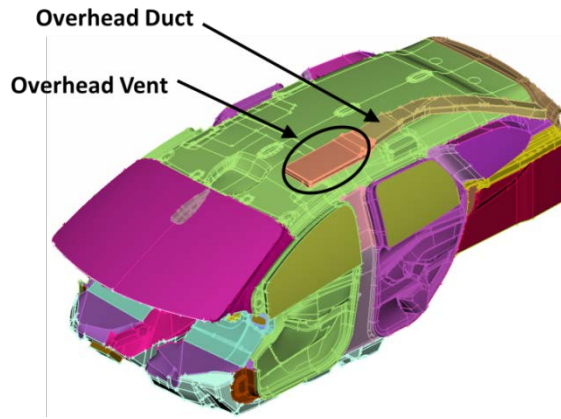


Figure III-41: Overhead Vent and Duct Geometry Incorporated into Focus BEV Model

Simulation Results – Overhead A/C Vent

In the overhead vent configuration, the air flow to the passenger side panel vents was eliminated, the air flow to the overhead vent was set to 60 cfm, and the flow to the driver side panel vents was reduced until thermal comfort matched the baseline case. The inlet air temperatures were taken from test data. Figure III-42 shows the comparison of thermal comfort and sensation for the baseline and overhead vent cases, which match very closely throughout the cool-down.

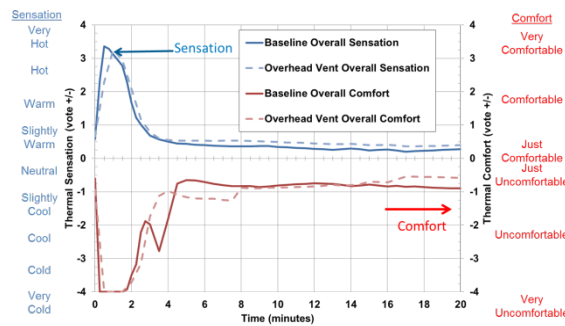


Figure III-42: Thermal Sensation and Comfort Results, Overhead A/C Case Compared to Baseline

The results show that the A/C air flow and thus the A/C capacity can be reduced by 28% while maintaining nearly identical thermal comfort and sensation.

Simulation Results – Insulated Headliner

The effect of adding insulation to the headliner was investigated. Adding insulation to the vehicle body may serve to reduce the interior temperature by preventing heat transmission from hot exterior surfaces into the vehicle interior during a hot soak. To test this theory, the headliner insulation was increased by a factor of ten. The remainder of the model and the boundary conditions were the same as those of the baseline case. Figure III-43 shows the soak temperatures of the baseline and insulated headliner cases. As expected, for a situation where the baseline roof temperature was hotter than the baseline headliner temperature, the roof temperature will increase and the headliner temperature will decrease due to the addition of insulation between the two surfaces. The breath level air temperatures in the case with the insulated headliner are approximately 2°C cooler than the baseline case. Figure III-44 shows the temperature difference (baseline minus insulated case) of several key interior surfaces during a cool-down simulation. The results show a moderate benefit for the headliner surface temperature but minimal impact to other interior surfaces during a cool-down. There was also a minimal impact to breath-level temperatures due to adding additional headliner insulation. There is little benefit to A/C energy use by adding headliner insulation for cool-down in high solar and moderate ambient temperature conditions. The effect of adding body insulation for a cold weather case will be investigated during additional heating mode simulations.

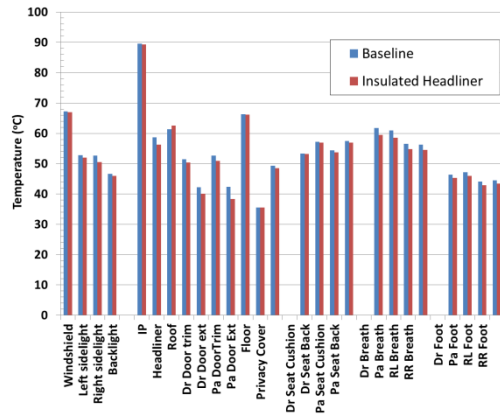


Figure III-43: Comparison of Baseline to Insulated Headliner Soak Temperatures

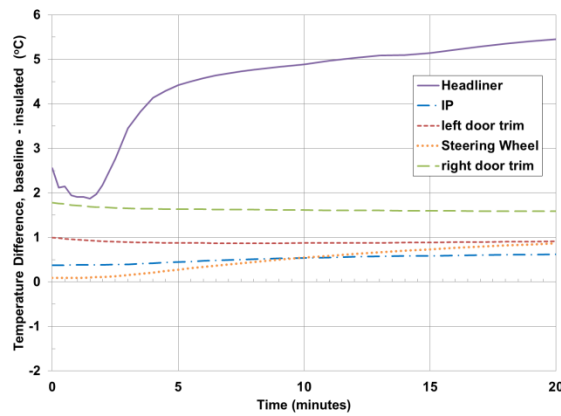


Figure III-44: Interior Surface Temperature Difference with Insulated Headliner during a Cool-down Simulation

Simulation Results – Stationary vs. Moving Vehicle

Vehicle testing at NREL is conducted with stationary vehicles. A simulation was performed to assess the impact of a moving vehicle vs. a stationary vehicle. The model simulated a constant 45-mph vehicle velocity during cool-down.

Figure III-45 shows a comparison of baseline and moving vehicle glass temperatures. As expected, the glass temperatures are lower in the moving vehicle. The ambient air is cooler than the vehicle interior air, and with movement, the heat transfer coefficients are higher, resulting in more heat transfer and cooler temperatures.

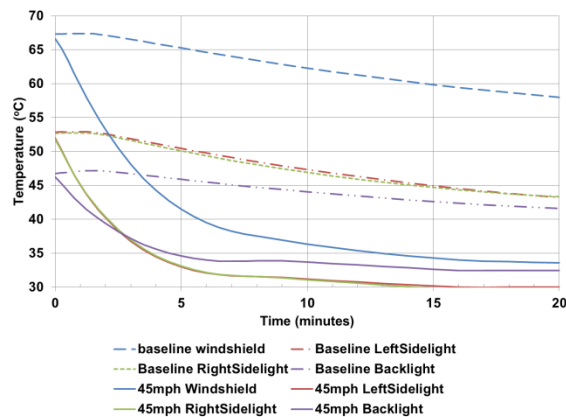


Figure III-45: Comparison of Glass Temperatures during Cool-down, Stationary vs. Moving Vehicle

Figure III-46 shows a comparison of baseline and moving vehicle average breath and foot air temperatures. The results show that the average breath temperatures are approximately 5°C lower during a moving vehicle cool-down as compared to a stationary vehicle. This indicates that the A/C power in a stationary vehicle would be higher than in a moving vehicle. An occupant would normally adjust the A/C setting to increase the temperature set point or reduce the blower speed. Because results are normally compared to a baseline case, percent improvements or reductions should be similar in stationary and moving vehicles.

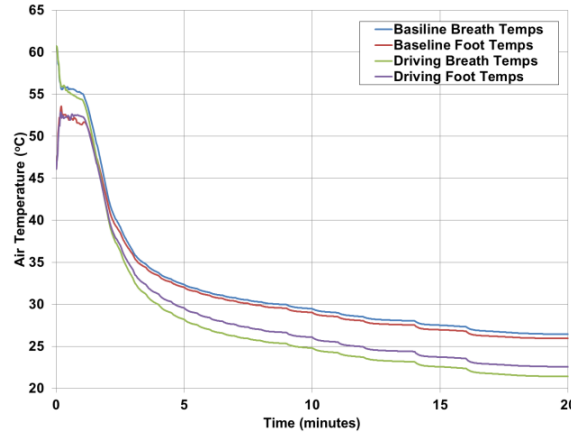


Figure III-46: Comparison of Breath Temperatures during Cool-down, Stationary vs. Moving Vehicle

Fluent/RadTherm Model Development – Heat/Defrost

The model that was used for the A/C studies was modified by adding defrost ducts, “frog leg” ducts, and footwell duct outlets for heating studies. The additional ducts are shown in Figure III-47, with the steering wheel included for orientation. The modified geometry was remeshed, and both Fluent and RadTherm models were created.

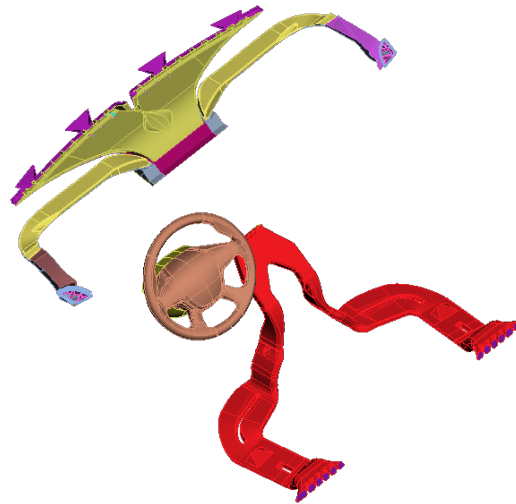


Figure III-47: Defrost and Frogleg Ducts

Simulation Results – Heating Baseline Comparison

A steady-state soak simulation was performed using weather data from the baseline test day of February 10, 2014. The analysis was performed both to check the accuracy of the model and to obtain an initial state for the warm-up simulation.

The simulation steady-state soak temperatures at 5:30 a.m. MST were compared to soak test data from February 10, 2014, averaged over 15 minutes from 5:15 a.m. to 5:30 a.m. MST. Minor adjustments were made to model parameters to improve the correlation. The baseline soak analysis temperatures shown in Figure

III-48 compared favorably to the test data. The most important locations (breath air, dash, windshield, and driver’s seat) matched within 1°C. The simulated foot-level temperatures had the greatest difference from the data, but even those differences were less than 3°C.

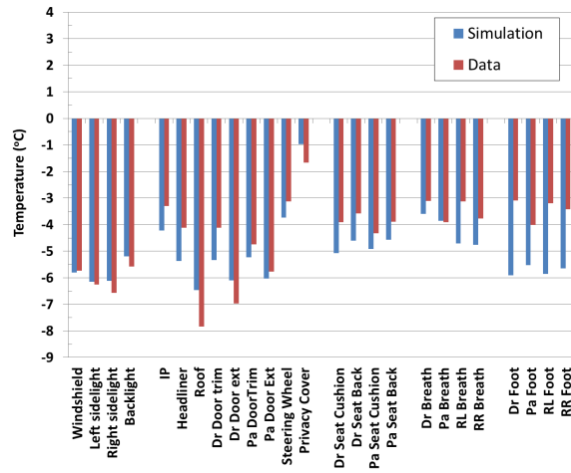


Figure III-48: Comparison of Cold-Soak Temperatures

The next step was to perform a transient warm-up analysis and compare the model results to the data. Experimental data from the same day were used, and the simulation was compared to data for the first 20 minutes of the warm-up beginning at 6:00 a.m. MST. The simulation used the same conditions as the warm-up test: Auto 72°F heating and 100% recirculation. The model used the vent flow splits obtained from Ford. The vent air velocities were validated by measurement. The transient temperatures at the vents were obtained from test data.

Figure III-49 and Figure III-50 show comparisons of temperatures predicted by the simulation to temperature measurements of a warm-up test performed February 10, 2014. The breath air temperatures were heated up faster than the data, but after 10 minutes were within 5°C and after 20 minutes were within 1°C for the driver and passenger. The predicted interior surfaces compared well to data. The results show that the model can be used to predict the thermal conditions during soak and warm-up trade studies. The model will be used in FY 2015 to predict the thermal results of additional tests and can be used to predict vehicle thermal behavior under conditions that are difficult to test.

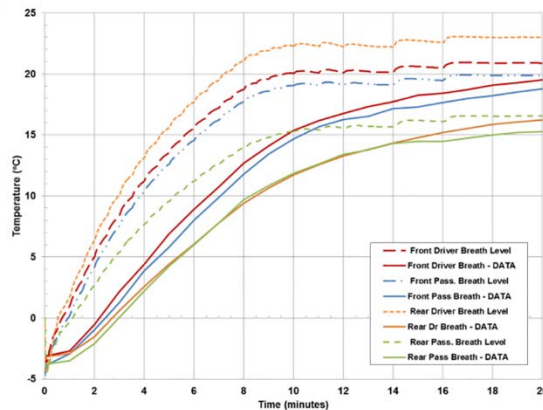


Figure III-49: Comparison of Simulation Data to Test Data for a Baseline Warm-up Test, Breath Air Temperatures

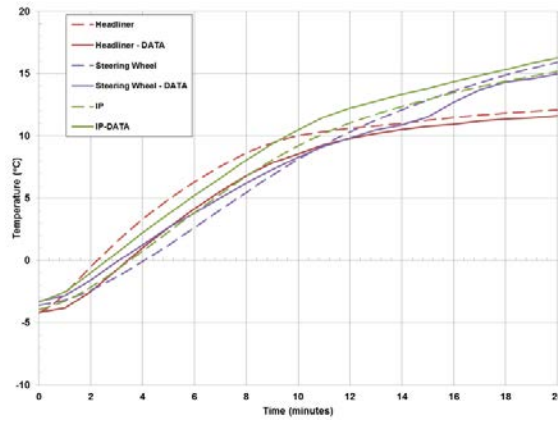


Figure III-50: Comparison of Simulation Data to Test Data for a Baseline Warm-up Test, Interior Surface Temperatures

Vehicle Thermal Testing

Under a CRADA, Ford has provided two Focus Electric vehicles to NREL for outdoor thermal testing. The battery electric vehicles (BEVs)—shown parked at NREL’s Vehicle Testing and Integration Facility (VTIF) in Figure III-51—have been instrumented with numerous thermocouples to measure interior and exterior air and surface temperatures. They each contain a power sensor on the high voltage battery circuit to calculate and record energy consumption of the HVAC system. Thermal soak and transient heating/cooling tests were conducted throughout FY 2014 to evaluate zonal climate control configurations and thermal load reduction strategies.



Figure III-51: Ford Focus Electric Vehicles at NREL's VTIF

Warm Weather Testing Approach

The procedure developed for warm weather climate control load reduction testing includes a thermal soak period followed immediately by a transient cool-down. The thermal soak begins overnight and lasts until noon standard time the next day, during which the test vehicles remain parked and undisturbed under full solar loading. This procedure allows technologies to be evaluated in terms of thermal soak temperature reduction at peak solar load as well as for cool-down performance improvements.

To assess zonal cooling strategies, NREL collaborated with Measurement Technologies Northwest to utilize their Automotive HVAC thermal test manikin. This manikin is instrumented with 60 sensors spread around the body form to provide high resolution measurements for the temperature and velocity of air surrounding a vehicle occupant.

NREL also used a vehicle test engineer to evaluate the occupant thermal sensation and comfort impacts of zonal cooling strategies—specifically, those configurations incorporating a thermoelectrically-cooled automotive seat.

Thermal Load Reduction Test Configurations

Thermal load reduction testing was continued in FY 2014. Three new test configurations were evaluated to compare to test results obtained in FY 2013. First, a shading canopy (shown in Figure III-52) was used to quantify the maximum possible solar load reduction to provide a benchmark for other solar load reduction strategies. Next, a prototype advanced infrared (IR)-reflective windshield was evaluated because glazing film tests from FY 2013 showed promising thermal load reduction potential. This production-quality windshield meets automotive safety standards and has improved solar properties compared to standard glazing. The third new configuration tested the IR-reflective windshield in combination with a just-in-time (JIT) pre-ventilation strategy. The IR-reflective windshield reduces solar energy entering the cabin and pre-ventilation removes stored energy from the cabin to further reduce the thermal load on the cooling system before an anticipated drive. For this pre-ventilation strategy, the onboard HVAC blower and existing air ducts were used to purge hot-soaked air from the cabin for 15 minutes before the start of cool-down. The blower was powered externally and was controlled to the maximum blower speed.

As with previous thermal load reduction tests, the A/C capacity of the modified vehicle was reduced during the 20-minute cool-down (by using a reduced blower speed) to achieve energy savings while maintaining an equivalent or lower interior air temperature throughout the cool-down.



Figure III-52: Shading Canopy Test Configuration

Thermal Load Reduction Test Results

Figure III-53 shows the results of the three new thermal load reduction tests along with three from FY 2013. These tests were evaluated based on the reduction in interior air temperature of the modified vehicle compared to the control vehicle at the end of the thermal soak period. The shading canopy represents the maximum soak temperature reduction that is possible by blocking direct solar radiation. Two configurations—the white film applied to all glazing (from FY 2013) and the IR-reflective windshield combined with pre-ventilation (from FY 2014)—achieved about half the temperature reduction of the shading canopy case. All other test cases led to 4°C–6°C reduction in soak temperature.

The soak temperature reductions that were achieved allowed the A/C capacity of the modified vehicle to be reduced for the 20-minute transient cool-down while still providing equivalent or better cooling. The lower A/C capacity led to significant savings in HVAC energy consumption, ranging from 21.2% for the IR-reflective windshield up to 74.4% for the shading canopy. The IR-reflective windshield and pre-ventilation are realistic thermal load reduction strategies that could be implemented in vehicles today.

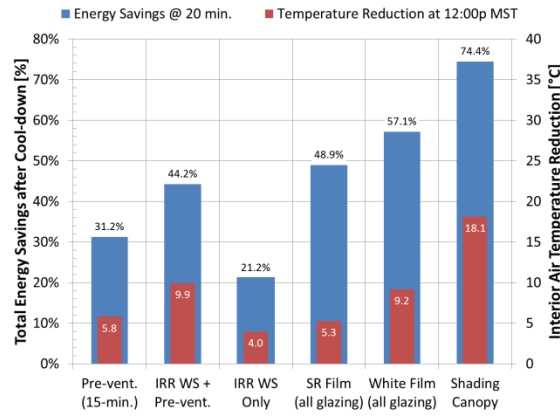


Figure III-53: Soak Temperature Reduction and Cool-down Energy Savings for Warm Weather Thermal Load Reduction Test Cases

Zonal Cooling Test Configurations

Zonal cooling tests were also continued in FY 2014 to expand upon the configurations evaluated in FY 2013 based on lessons learned and to evaluate the impact of combining strategies. The driver-only vent configuration tested previously used the vehicle’s default air flow distribution, which utilized only the panel vents for cooling. This configuration was modified to use the driver panel and footwell vents to improve the zonal cooling effect. The improved configuration is labeled “All Driver Vents” to distinguish it from the “Driver Panel Vents” configuration. Researchers also evaluated a combined cooling configuration that incorporated several thermal load reduction and zonal cooling strategies that were previously tested individually. The solar load reduction strategies implemented into the combined configuration include the prototype IR-reflective windshield and solar-reflective glazing film applied to the sidelites and backlite. These are passive technologies designed to decrease the amount of solar energy that enters the cabin through the glazing. Cabin pre-ventilation capability was included in the combined configuration to remove stored energy from the cabin, lowering the interior soak temperature prior to cool-down. Lastly, a zonal vent configuration was used for the combined configuration to focus all cold air near the driver. This zonal vent configuration used the existing driver panel and footwell vents as well as an overhead vent that was added above the driver seat. The combined configuration was intended to demonstrate the maximum potential improvement for this particular vehicle test setup and cooling procedure.

A prototype thermoelectrically cooled driver seat was also assessed as part of the zonal approach to cooling. This seat was developed with a novel approach to using thermoelectric devices for automotive seat cooling to improve response time and reduce energy consumption compared to other cooled seats. Because the HVAC manikin is not capable of sensing seat temperatures, engineering evaluation was used to assess the impact of the cooled seat. A test engineer sat in an office environment for 30 minutes prior to the start of the cool-down test to initialize to a thermally neutral state. Care was taken to ensure similarity between tests; clothing levels, food and drink consumption, activity levels, etc., were all kept consistent. After initialization, the test engineer sat in the driver seat of the modified BEV and evaluated driver thermal sensation at two-minute intervals during transient cool-down. The thermoelectric (TE) seat was tested individually and as part of the combined cooling configuration described above that included thermal load reduction and zonal cooling strategies. The supplemental cooling provided directly to the driver by the TE-cooled seat allowed the A/C system capacity to be reduced without compromising occupant thermal comfort.

Zonal Cooling Test Results

The zonal cooling test configurations shown in Figure III-54 were evaluated in terms of the average air temperature around the driver (as measured by the HVAC Manikin) and the savings in cumulative HVAC energy after a 20-minute cool-down. The driver air temperature was used as a proxy for occupant thermal sensation so it could be evaluated along with measured energy savings. Results of tests completed in FY 2013 are shown on the left in Figure III-54 (light blue/green columns), and new test configurations are shown on the right (dark blue/green columns). For the same blower speed (blower level 5), the modified driver vent case shows improved cooling over the driver panel vent case by almost 3°C and approximately matches the baseline

temperature after 20 minutes. This test configuration saved 0.58 kWh (45.5%) of cooling energy. The combined configuration shows the advantage of zonal cooling after utilizing several thermal load reduction techniques. The lower thermal load allowed the blower speed to be reduced to level 4 from the maximum level 7 for the cool-down. The combined case resulted in cool-down energy savings of 0.92 kWh (66.5%) and better cooling of the driver than the baseline (by 1.8°C).

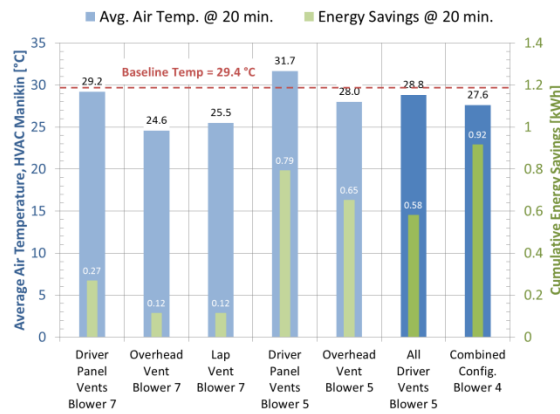


Figure III-54: Driver Air Temperatures and Cumulative Energy Savings after 20-minute Cool-down for Zonal Cooling Configurations

The prototype thermoelectric driver seat was evaluated by a test engineer rather than the HVAC thermal test manikin in order to capture the impact of cooling seat contact surfaces. A test was first conducted without seat cooling to establish a baseline for driver thermal sensation and HVAC energy consumption during the cool-down. The driver reached neutral thermal sensation after 22 minutes for the baseline test (Figure III-55). For the next test, the TE seat was set to maximum cooling and the A/C capacity was reduced by lowering the HVAC blower speed from level 7 to level 5. This led to energy savings of 43.5% (0.71 kWh) and improved time to neutral sensation compared to the baseline test. The TE-cooled seat was added to the combined cooling configuration discussed above and re-tested with the blower speed reduced to level 4. This test further reduced the time to neutral sensation (6 minutes faster than baseline) and resulted in almost 65% (1.05 kWh) energy savings after 20 minutes. This result shows the combined impact of reducing thermal loads prior to cool-down and using a cooled seat as part of a zonal cooling strategy, which can drastically reduce A/C energy consumption while maintaining or improving driver thermal comfort. These results are the maximum potential savings due to the test conditions that included a long thermal soak with higher solar load, maximum A/C settings, and the focus on the transient cool-down.

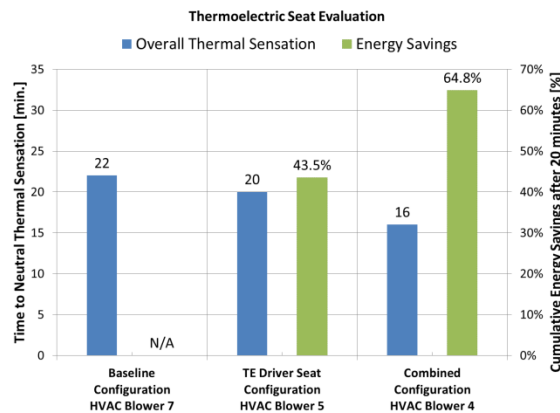


Figure III-55: Results of a Thermoelectrically-cooled Seat on Driver Thermal Sensation and HVAC Energy Consumption

Cold Weather Testing Approach

Climate control load reduction testing was continued into the winter of FY 2014 to evaluate strategies for improved heating performance for EVs. The procedure for cold weather testing consisted of an overnight thermal soak period followed by transient heating in the early morning. The heating portion of the test was completed before sunrise to avoid solar heating impacts.

Engineering evaluation was used to assess zonal climate control configurations in cold weather. Similar to the warm weather procedure, the test engineer initialized to a thermally neutral state in an office environment for 30 minutes prior to the warm-up test. The engineer sat in the modified vehicle and initiated the warm-up by starting the HVAC systems in both vehicles simultaneously, using a remote control and voice commands for the unmodified vehicle. The unmodified vehicle used Auto 72°F settings during warm-up. The climate control settings for the modified vehicle were adjusted from Auto 72°F to reduce energy consumption while maintaining driver comfort. Both vehicles used maximum air recirculation. Overall thermal sensation and comfort ratings were recorded by the engineer during initialization, just before the start of warm-up, and every two minutes during the transient warm-up test.

Zonal Heating Test Configurations and Results

Zonal heating tests conducted in cold weather include a baseline test and four zonal heating configurations. All configurations used the onboard HVAC system. The baseline test used the stock vent configuration and Auto 72°F climate control settings. Figure III-56 shows that neutral thermal sensation was reached after 10 minutes of heating.

The first two zonal heating strategies altered the air flow distribution and reduced the blower speed from the baseline case to conserve energy while providing approximately equivalent heating to the driver. For the “Driver Footwell Vents Only” case, all passenger vents were closed to restrict airflow to the driver using only the footwell vent. For the “Driver Footwell + Lap Vent” case, an air duct was added near the driver’s lap to supply additional warm air to the driver, and a recirculation air duct was added to return warm air from the driver’s footwell area to the vehicle HVAC package. These two cases resulted in energy savings of 39.8% and 20.7%, respectively, after 20 minutes of heating but required longer heating time to reach neutral thermal sensation, indicating that the air flow rate was not high enough to maintain equivalent driver thermal sensation as the baseline. Thus, the energy savings for these two cases are over-predicted.

The third zonal heating case used the same air flow configuration as the “Driver Footwell + Lap Vent” case—now called “Zonal HVAC” for simplicity—and included the heated driver seat to improve the zonal heating effect. The seat was set to maximum heating for the entire warm-up, and the HVAC air flow rate was further decreased. This configuration resulted in improved time to neutral sensation (two minutes faster than baseline) and saved 31.9% of heating energy from the 20-minute warm-up.

The last zonal heating configuration, called “Zonal HVAC + All Heated Surfaces,” added a heated steering wheel and a custom-built heated floor mat to the heated seat and zonal air flow of the third configuration. This test case provided direct heating to all points of contact between the driver and the vehicle. The energy savings were approximately the same but the time to neutral sensation was decreased by an additional four minutes over the third configuration.

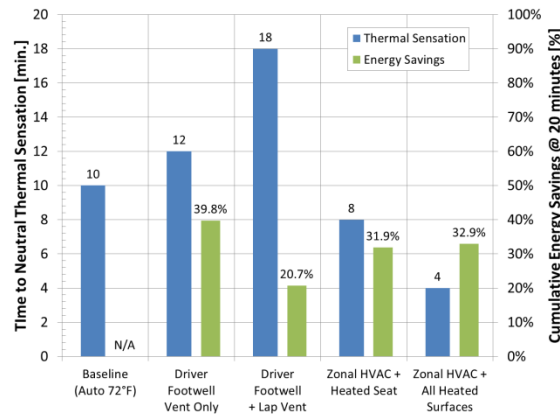


Figure III-56: Time to Neutral Thermal Sensation and Cumulative Energy Savings after 20 Minutes for Zonal Heating Tests

These zonal heating tests demonstrate the potential to reduce heating loads while maintaining occupant thermal comfort by focusing warm air near the occupant and providing supplemental heating directly to the occupant through heated contact surfaces.

Thermal Load Reduction Test Configurations and Results

In addition to zonal heating, thermal load reduction tests were also conducted in cold weather. A steady-state heating test was used to evaluate three configurations of vehicle insulation—glazing surfaces only, opaque (painted) surfaces only, and all cabin surfaces (glazing + opaque). The ¾-inch-thick foam insulation was applied to the exterior of the vehicle. It was intended to simulate the maximum potential improvement from increasing vehicle insulation.

Figure III-57 shows that adding insulation to the entire vehicle cabin (including glazing) resulted in 17.1% energy savings during steady-state heating. This represents the maximum savings against which other thermal resistance improvements can be measured. The 8.9% savings for the “Glazing Surfaces Only” case is not realistically achievable due to glazing visibility standards and other design constraints (such as thickness, weight, abrasion resistance, etc.), but the results indicate how much heat is lost through the vehicle glazing during steady-state heating and highlights the potential benefit of glazing with higher thermal resistance. Energy savings of 3.3% were measured for increased insulation on all opaque vehicle cabin surfaces. This configuration represents the most realistic results that manufacturers should strive to achieve with improved insulation.

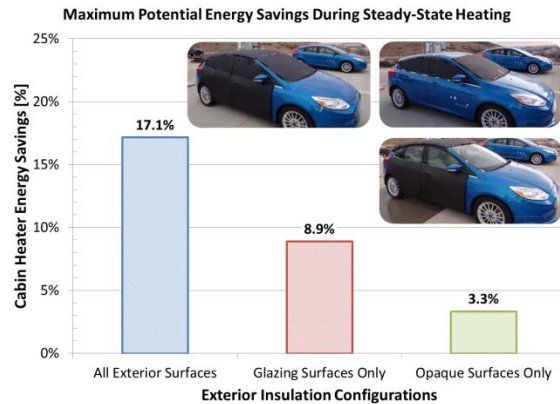


Figure III-57: Energy Savings from Exterior Insulation for Steady-state Heating

Vehicle Simulation Analysis

Range Impact Estimation Approach

The vehicle simulation tool Autonomie was used to assess the impact of climate control on range. Argonne National Laboratory provided NREL with a model of the Focus Electric. The model was modified to enable input of measured A/C compressor power from vehicle tests. Four conditions were compared: no A/C, baseline A/C, overhead A/C, and a combined overhead A/C with load reduction. The ambient temperature during the A/C tests was approximately 27°C with a solar load of 925 W/m². The Focus Electric uses a 23-kWh capacity lithium-ion battery pack. The battery utilization was assumed to be 85%; therefore, 19.55 kWh of usable energy was calculated for the battery pack [1].

Calculating the vehicle efficiency over a single 10-minute SC03 drive cycle and applying it to calculate the overall range would overestimate the impact of A/C because the A/C loads decrease when the passenger compartment temperatures attain steady state. Because the average vehicle trip duration in the United States is approximately 20 minutes, the average vehicle efficiency was calculated over several drive cycles that lasted approximately 20 minutes. The drive cycles used were: UDDS (22.8 minutes), back-to-back SC03 cycles (19.8 minutes), and back-to-back HWFET cycles (25.5 minutes). The compressor power applied to the vehicle was a composite profile (Figure III-58) that included measured compressor power at maximum A/C setting for the first 10 minutes (simulating a pull down), and then the measured compressor power for Auto 72°F setting for the remainder of the drive cycle (simulating steady state).

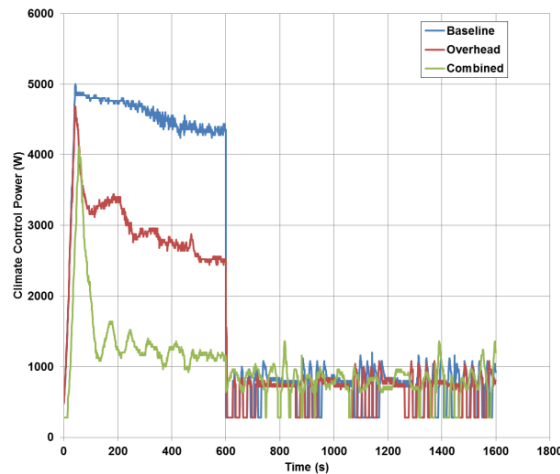


Figure III-58: Climate Control Power vs. Time

Range Impact Estimation Results

Table III-13 shows the predicted range of the Focus Electric. For the SC03 drive cycle, the baseline A/C reduces the range by 37%, from 109.6 to 69.4 miles. The reduction in range using baseline A/C varies from 16% to 37%.

Table III-13: Predicted Focus Electric Range (miles)

Drive Cycle	No A/C	Baseline A/C	Overhead A/C	Combined A/C
SC03	109.6	69.4	80.0	92.4
UDDS	111.9	70.6	81.4	93.3
HWFET	97.6	82.2	87.1	91.3

Table III-14 shows the improvement in range over baseline that is achieved by using the overhead vent or the combined configuration. The combined configuration increased the range 11% to 33% compared to operation with the baseline A/C system. The percent increase for the HWFET cycle is less than for the other two cycles

because the energy needed for propulsion for the high-speed HWFET cycle is much greater than for the low-speed urban cycles, resulting in the A/C energy usage being a smaller percentage.

Because the A/C power use is higher during the first 10 minutes of a cool-down, the impact of A/C will be higher than on a longer drive cycle. The assumption of maximum A/C also amplifies the impact of A/C because drivers typically turn down the A/C as they attain thermal comfort. In addition, the test conditions were under high solar and ambient temperature, so A/C usage may be lower under more moderate conditions.

Table III-14: Predicted Range Improvement over Baseline A/C

Drive Cycle	Baseline A/C (miles)	Overhead A/C (%) ^a	Combined A/C (%) ^a
SC03	69.4	15.2%	33.1%
UDDS	70.6	15.3%	32.2%
HWFET	82.2	5.9%	11.2%

^a % increase over Baseline A/C

Conclusions

As part of a four-year CRADA project with Ford, NREL researchers investigated strategies to reduce climate control loads for EDVs. Warm- and cold-weather outdoor thermal tests were conducted to assess a variety of thermal load reduction and zonal heating/cooling configurations.

A shading canopy showed a maximum possible temperature reduction of 18.1°C by blocking all direct solar energy from the parked vehicle. A prototype IR-reflective windshield was combined with cabin pre-ventilation to reduce the interior soak temperature by 9.9°C, saving up to 44.2% of A/C energy during a 20-minute cool-down. A thermoelectrically cooled driver seat was used to reduce A/C energy by up to 43.5% when tested alone, and up to 65% as part of a combined cooling configuration. These test results represent maximum savings due to test conditions that included a long thermal soak with high solar load and maximum A/C settings during the 20-minute transient. Energy savings in moderate environments would be less. However, these results demonstrate the potential benefit of solar load reduction and zonal air flow to reduce energy consumed for cooling, especially in environments where the range loss due to A/C is a major problem.

Zonal heating with a driver-focused vent configuration and heated seat resulted in approximately 32% energy savings and two-minute faster driver warm-up compared to the baseline. Adding a heated steering wheel and floor mat to the combined configuration further increased the speed of driver warm-up and saved approximately 33% of heating energy. Exterior insulation on the opaque vehicle cabin surfaces showed up to 3.3% energy savings during steady-state heating. For cold weather, increased vehicle body insulation and zonal heating including heated contact surfaces reduce transient and steady-state climate control loads, leading to increased EV driving range.

A combined CFD/RadTherm/human thermal comfort model was used to assess an overhead A/C vent for cooling. The overhead vent used the geometry of a production-ready vent. The results show the potential to reduce A/C capacity by up to 28% for a high solar and high ambient condition.

Vehicle simulations using an Autonomie model of the Focus Electric were used to estimate impact of climate control loads on vehicle range. For the UDDS cycle, an overhead A/C vent increased driving range by approximately 15%. Combined with thermal load reduction strategies, zonal cooling with an overhead A/C vent increased range approximately 32%.

HVAC Auxiliary Load Reduction Working Group/ Thermal Systems Analysis: Approach and Results

At the EV Everywhere Vehicle Design Workshop, the automotive industry participants recommended the formation of a working group to discuss vehicle thermal challenges that cross industries and branches of the government. NREL led the thermal working group effort by inviting potential participants, organizing

meetings and participating in the discussions. The overall working group goal was to guide crosscutting thermal research that could enhance national and energy security by reducing fuel use and improving military preparedness and survivability. Meetings were held that included the following stakeholders:

- Light Vehicle Manufacturers: Ford, GM, Chrysler
- Heavy Vehicle Manufacturers: Kenworth
- Suppliers: Delphi, Halla Visteon, Denso, Red Dot, Dana
- Universities: University of Maryland, University of Illinois
- Government Agencies: U.S. EPA
- National Laboratories: Argonne National Lab
- Military: TARDEC

During the meetings, key thermal challenges were identified. In cold environments, the lack of free waste heat to warm the passenger compartment in small internal combustion engine (ICE) vehicles and EDVs is a significant challenge. Using onboard stored electrical energy has a large negative impact on range and is a barrier to customer acceptance of EDVs. In vehicles that do have significant waste heat from ICEs, research on technologies to recover energy from waste heat was recommended. Additional research was suggested in seating and interiors, electric powertrains, and electronics. New thermal comfort tools for use in developing efficient climate control systems were also recommended.

One issue that was identified multiple times was that thermal issues usually become apparent late in the design cycle. Robust and validated analysis tools that identify thermal issues early in the design cycle would be valuable to the automobile industry. There was also interest in the potential for these analysis tools to be used to quantify off-cycle greenhouse gas credits. An extended discussion on the impact of designing a vehicle for use in all environments (hot/cold) and all missions (short drive, long drive, no cargo load, full cargo load) was held. The conclusion was that the automobile manufacturers are required to design the vehicle for all use cases, but there is an efficiency cost that is incurred by the owner during partial-use conditions.

From a military vehicle perspective, the highest priority is waste heat, fan, and heat exchanger research. Also, the heat generated from electronics equipment is a large thermal load on the interior and the size of their vehicles are a different scale than most cars.

Acknowledgements

- Co-authors: Lawrence Chaney, Matthew A. Jeffers: NREL
- Cory Kreutzer, Daniel Leighton, Jeff Tomerlin: NREL
- James Gebbie, Paul Hoke, Ken Jackson, Clay Maranville: Ford Motor Co.
- Rick Burke: Measurement Technologies Northwest
- Mark Hepokowski, Craig Makens, Tony Schwenn: ThermoAnalytics, Inc.
- Lat Franklin, Tarek Makansi: Tempronics
- Photo credit (Figures 12, 13, 18): Matthew A. Jeffers: NREL

III.3.C. Products

Presentations/Publications/Patents

1. Jeffers, M.; Chaney, L.; and Rugh, J. "Climate Control Load Reduction Strategies for Electric Drive Vehicles." Proceedings of 2014 SAE Thermal Management Systems Symposium, Presentation #14TMSS-0031, Society of Automotive Engineers, Denver, CO.

III.3.D. References

1. Argonne National Laboratory Advanced Powertrain Research Facility data, Vehicle Systems Analysis Technical Team (VSATT) meeting presentation, Eric Rask, April 2, 2014.
2. Argonne National Laboratory Advanced Powertrain Research Facility data, EV Everywhere Workshop presentation, Le
e Slezak, September 13, 2012.

III.4. Electric Drive Vehicle Climate Control Load Reduction – FY 2015

John P. Rugh, Principal Investigator

National Renewable Energy Laboratory
15013 Denver West Parkway, MS 1633
Golden, CO 80401
Phone: (303) 275-4413; Fax: (303) 275-4415
E-mail: John.Rugh@nrel.gov

David Anderson and Lee Slezak, DOE Technology Managers

Vehicle Technologies Office
Phone: (202) 287-5688, (202) 586-2335
E-mail: David.Anderson@ee.doe.gov, Lee.Slezak@ee.doe.gov

Start Date: 10/01/2012

End Date: 9/30/2015

III.4.A. Abstract

Objectives

- Minimize the impact of climate control on electric-drive vehicle (EDV) range
- Increase electric range by 10% during operation of the climate control system through improved thermal management while maintaining or improving occupant thermal comfort.

Accomplishments

- Completed outdoor cold weather thermal testing of Ford Focus Electric vehicles
 - Achieved 5.5% reduction in heating energy during warm-up with zonal air flow for the driver using existing air ducts and vents
 - Demonstrated up to 28.5% reduction in heating energy by combining driver zonal air flow with heated surfaces while maintaining or improving human thermal sensation
- Quantified the impact of a zonal HVAC strategy to reduce the range penalty due to heating
 - Calculated a potential 6.9% to 18.7% improvement in range compared to range with baseline heating if driver zonal air flow with heated surfaces is implemented
 - Calculated a national weighted improvement in range of 7.1% over the baseline heating range if driver zonal air flow with heated surfaces is implemented (33% reduction in range penalty)
- Using zonal heating strategies in conjunction with reduced thermal conductivity of the vehicle shell and other energy efficiency improvements such as implementation of a heat pump or thermal preconditioning can be part of a combined strategy to minimize the impact of heating on EDV range

Future Achievements

- Communicate research findings to industry, academia, and government representatives
 - Present results at the Society for Automotive Engineering's (SAE) 2015 Thermal Management Systems Symposium
 - Document research results in a technical paper and present at SAE's 2016 World Congress and Exhibition.



III.4.B. Technical Discussion

Background

As in conventional vehicles, EDVs require cabin climate control for passenger thermal comfort and safety. Heating and cooling can have a large negative impact on a vehicle's energy efficiency. For conventional vehicles, this results in lower fuel economy and higher per-mile travel costs, but for EDVs, this means a reduction in the vehicle's maximum driving range, presenting a major challenge for many drivers and a barrier to widespread adoption of electric vehicles.

Introduction

The negative impact of cabin heating is a relatively new challenge for automobile manufacturers because conventional vehicles traditionally used abundant waste heat from the engine. EDVs do not have sufficient waste heat to fulfill cabin heating requirements. Using electric resistance heaters for cabin conditioning takes valuable battery energy away from propulsion and reduces electric range. Oversizing traction batteries to overcome range limitations is too costly to be a viable solution. Therefore, it is critical to minimize climate control loads in EDVs to maximize vehicle range. Maximum heating at -7°C can reduce range by 20%–59%, according to the tests conducted at Argonne National Laboratory's Advanced Powertrain Research Facility [1].

The goal of this task is to increase in-use EDV driving range by 10% with improved thermal management during operation of the climate control system. The target range improvement is expected to increase customer acceptance of EDVs through the reduction of range anxiety. In addition, improving thermal comfort upon entry into a hot-soaked or cold-soaked vehicle may lead to additional motivation for drivers to adopt EDVs and improved safety through reduced driver distraction due to thermal stress.

Over the past three years, National Renewable Energy Laboratory (NREL) researchers have investigated climate control load reduction strategies using complementary experimental and analytical techniques. NREL has collaborated closely with Ford who, under a cooperative research and development agreement, provided two Focus Electric vehicles and engineering support. In the FY2014 annual report and in an SAE technical paper [2], techniques to reduce energy consumption for cooling the passenger compartment in hot environments were presented. In this report, the focus is reducing energy used for vehicle passenger compartment heating in cold weather.

Approach

Experimental and analytical techniques were used in conjunction to investigate thermal load reduction strategies. Outdoor vehicle testing was conducted at NREL to establish baseline climate control performance for the validation of thermal models and to evaluate vehicle technologies. Computer modeling and analysis were used to explore load reduction strategies that are difficult and/or costly to evaluate experimentally and to extrapolate test results to estimate impact on EDV range.

Vehicle Thermal Testing

Thermal soak and transient conditioning tests were conducted with instrumented test vehicles to measure the power requirements of the Ford Focus Electric's onboard cooling and heating systems. Baseline tests characterized the inherent differences between the vehicles and enabled accurate measurement of the impact of load reduction technologies. In FY2015, cold weather thermal soak and warm-up tests evaluated zonal climate control strategies to reduce heating loads. Thermal manikins and engineering evaluation have been used to quantify occupant thermal sensation impacts.

Thermal Analysis

A CFD/RadTherm/human thermal comfort modeling process was used to assess the thermal load reduction configuration with the largest potential to reduce heating energy consumption. A combined Fluent/RadTherm model simulated the air flow inside the vehicle and heat transfer across every surface during a soak and

warm-up. A thermal comfort analysis was performed using the human comfort plugin in RadTherm. The plugin uses a human physiology model and calculates heat loss or gain to the environment to predict the thermal sensation and thermal comfort of a human. Additional information on the modeling approach is located in [2].

Results

Vehicle Thermal Testing

Cold Weather Testing Approach

The test vehicles each contained over 40 calibrated thermocouples to measure interior and exterior air and surface temperatures. The cabin air temperature was calculated as the average of eight interior air temperature measurements: one breath-level thermocouple and one foot-level thermocouple at each of the four primary passenger seats. The instrumentation on the vehicles also included measurement of the climate control power and data acquisition from select channels on the vehicle CAN bus. Environmental conditions—including air temperature and relative humidity, wind speed and direction, and solar irradiance—were recorded by the Vehicle Testing and Integration Facility's onsite weather station.

Throughout the testing, one of the two vehicles remained unmodified to serve as a control vehicle, while the other vehicle was modified for each test configuration that was evaluated. Testing the vehicles side-by-side under the same weather conditions allowed a direct comparison of thermal performance of the load reduction strategy.

The cold weather test procedure included an overnight thermal soak period during which the vehicles remained closed and undisturbed, followed by a stationary transient warm-up beginning at 5:30 a.m. MST. Tests were conducted on days when the overnight ambient temperature was near 0°C. All tests had a warm-up duration of 20 minutes and were completed before sunrise to avoid any impact of solar heating. The timing, duration, and climate control settings for the warm-up procedure were selected to represent an early morning commute during the winter months. Auto 72°F settings were used for the onboard climate control systems during warm-up.

Zonal Heating Configurations

Four zonal heating configurations were evaluated during cold weather testing. They are shown in Figure III-59, listed in order of increasing zonal heating effect. For Zonal Configuration #1, all passenger air vents were closed and only the driver air vents were used to supply warm air to the cabin. This configuration required no major modifications to the vehicle's air ducts or HVAC blower. It provided a higher flow rate of warm air to the driver while lowering the total HVAC air flow rate. Zonal Configuration #2 also used the existing driver air vents as well as a lap vent that was added near the center console to deliver warm air to the driver's arms, lap, and lower torso. This improved the convective heating for the driver air space. Zonal Configuration #3 consisted of the zonal air vents from Zonal Configuration #2 and a heated driver seat. The heated seat was operated at the maximum heating setting for the duration of the warm-up test. Lastly, Zonal Configuration #4 included the zonal air vents and the heated seat from the previous configuration and also incorporated a heated steering wheel (42 W average) and a custom-built heated floor mat (129 W average).

These four configurations provided increasing levels of zonal heating to the driver by focusing air flow on the occupant and by providing direct heating through contact surfaces. With each incremental improvement, the overall heating load was reduced while maintaining or improving driver thermal sensation. This reduction in heating energy was accomplished by reducing the air flow rate of the HVAC system from the measured baseline value for each zonal configuration.



Figure III-59: Zonal heating test configurations

(Photo credit: NREL)

Zonal Heating Test Results

The results of the heating tests are shown in Figure III-60. The zonal heating strategies were evaluated in terms of the reduction in cumulative heating energy during the 20-minute warm-up for the modified vehicle compared to the unmodified control vehicle. Engineering evaluations were used to assess driver thermal sensation for the baseline and zonal heating tests to ensure the driver's thermal sensation was not compromised. During the baseline warm-up test, it took 12 minutes for the occupant to reach neutral overall thermal sensation. The energy savings for each zonal case were the result of the decreased total air flow rate of the HVAC system. The energy savings are shown as the percent decrease for the modified vehicle compared to the control vehicle and were adjusted to account for minor day-to-day weather variation.

Zonal Configuration #1 resulted in a 5.5% decrease in energy consumption with a warm-up time of 8 minutes. This configuration used the vehicle's existing air ducts and vents, and simply restricted air flow to the driver. Zonal Configuration #2 increased the convective heating for the driver's air space by adding a lap vent near the center console area. This led to a 9.4% reduction in heating energy and a slightly faster time to neutral thermal sensation than the baseline warm-up. Zonal Configuration #3 incorporated the Focus Electric's heated seat with the zonal air vents, achieving a 13.6% energy reduction and equivalent warm-up time. Finally, Zonal Configuration #4, which combined convective and conductive heating, demonstrated 28.5% energy savings and a slightly faster warm-up time. This highlights the importance of heating an occupant's extremities during a warm-up from cold soak. The hands and feet are major drivers of overall thermal sensation and comfort in cold weather and can have a large impact on potential energy savings of heating strategies.

It should be emphasized that these warm-up tests were conducted with stationary vehicles; moving vehicles would have greater heat loss to the cold outside environment during a warm-up, which would increase the amount of heating energy required for each case including the baseline. Also, the thermal sensation results were intended as a test-to-test reference point to produce equivalent warm-up times; they do not necessarily represent the average thermal response of the national driving population. Zonal heating is expected to have greater benefit during transient heating than during steady-state heating so the potential reduction in heating energy would be less for drive profiles longer than 20 minutes. However, short-duration drives are more common for electric vehicles than for conventional or hybrid vehicles.

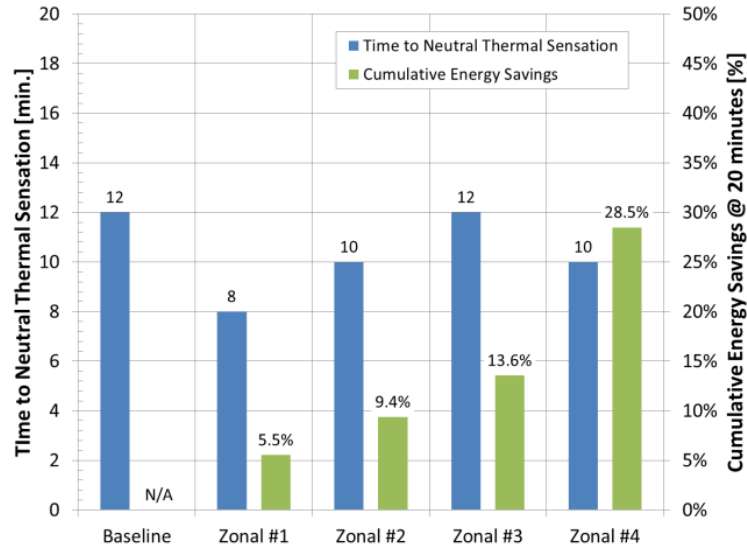


Figure III-60: Zonal heating test results

Thermal Analysis

Baseline Model Validation

A steady-state soak simulation was performed using weather data from the baseline test day of January 13, 2015. The analysis was performed both to check the accuracy of the model and to obtain an initial state for the warm-up simulation.

The steady-state soak temperatures from simulation at 5:30 a.m. MST were compared to soak test data averaged over 15 minutes, from 5:15 a.m. to 5:30 a.m. MST. The baseline simulation soak temperatures compared favorably to the test data. The most important locations (breath-level air, instrument panel, windshield, and driver’s seat) matched within 1°C. The simulated foot-level temperatures had the greatest difference from the data, but even those differences were less than 3°C.

The next step was to perform a transient warm-up analysis and compare the model results to the data. Experimental data from the same day were used, and the simulation was compared to data for the first 20 minutes of the warm-up beginning at 5:30 a.m. MST January 13, 2015. The simulation used the same conditions as the warm-up test: auto 72°F heating and 100% recirculation. The model used vent flow splits obtained from Ford, and the vent air velocities were validated by measurement. The transient vent temperatures were obtained from test data.

Figure III-61 shows the comparison of the average cabin air temperature predicted by the simulation to test data from the warm-up test. The simulated average air temperature initially increased slightly faster than the test data with a maximum deviation of 3.5°C, but after 10 minutes was within 1.6°C for the remainder of the simulation. Although not shown, the predicted interior surfaces compared well to test data. Because the transient simulation performance was reasonable and the steady-state temperatures matched well, the model can be used to predict the thermal conditions during soak and warm-up trade studies.

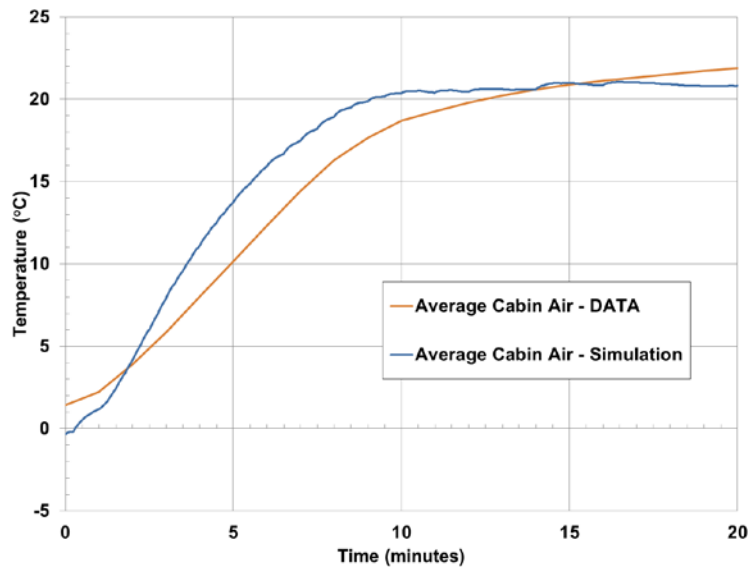


Figure III-61: Comparison of simulated cabin air temperature to experimental data for baseline warm-up

Zonal Heating Analysis

A zonal heating analysis was conducted to verify that a zonal testing approach would maintain or improve driver thermal comfort compared to the baseline. The baseline model boundary conditions were modified to reflect the test setup. This included no air flow to the passenger vents and adding flow to the driver lap vent. Due to the zonal strategy focused on the driver, the analysis was run with a 50% reduction in total air flow compared to the baseline to maintain thermal comfort. The zonal analysis was performed both with and without a heated steering wheel and heated seat to understand the effect of those heated surfaces on thermal comfort.

Figure III-62 shows the driver sensation for Zonal Configuration #4 is nearly identical to the baseline case. Without the heated surfaces, the driver is predicted to be colder than baseline. This means the heated surfaces are required or the heater air flow would need to be increased to maintain the same thermal comfort as the baseline. This analysis confirms the test approach of reducing blower airflow to lower energy consumption by using zonal air flow and heated surfaces while maintaining human thermal comfort.

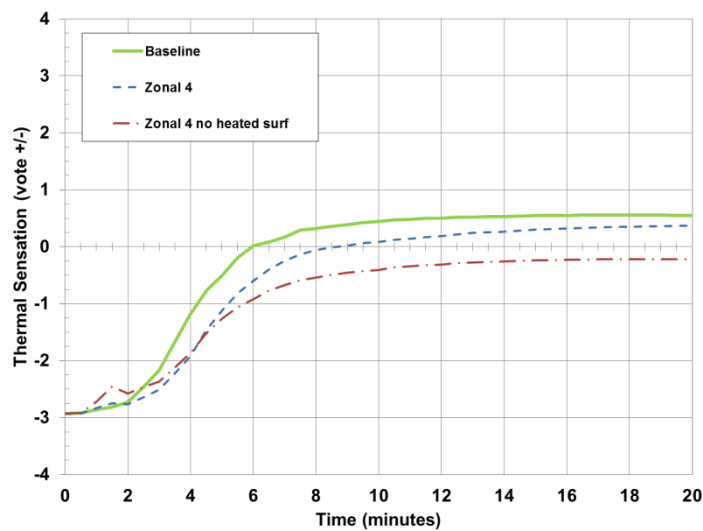


Figure III-62: Predicted thermal sensation for baseline and zonal heating

CoolCalc Thermal Modeling

Model Development

CoolCalc is a rapid HVAC load estimation tool built as a plugin to SketchUp drawing software. CoolCalc was developed at NREL from an early version of DOE's OpenStudio energy modeling tool and it uses EnergyPlus as the heat transfer solver. More detailed background information is available in [3].

A CoolCalc thermal model of the Ford Focus Electric was developed using CAD files of the vehicle geometry and other vehicle information provided by Ford, along with measurements made at NREL. This included information on surface and material properties, cabin thermal mass, air infiltration rate, and HVAC system specifications. Figure III-63 shows an image of the CoolCalc model geometry next to a photo of the Focus Electric test vehicle. A simplified HVAC system was added to the model to provide cabin climate control. The simplified system delivers the thermal load necessary to meet cabin temperature set points.

Model Validation

The CoolCalc model of the Focus Electric was validated against experimental data from warm and cold weather vehicle tests. The simulations were set up to match the conditions of the stationary outdoor vehicle tests, including vehicle configuration and HVAC system settings. Actual weather data recorded from the outdoor vehicle tests were supplied to the model as environmental boundary conditions. These conditions included ambient temperature and relative humidity, wind speed and direction, and solar irradiance. Warm and cold thermal soak simulations were performed to verify that the passive thermal behavior of the model matched the diurnal trends from the vehicle tests. The model results were in very close agreement with the test data for both warm and cold weather thermal soak conditions, as shown in Figure III-63. Transient warm-up simulations were also performed to verify the inputs to the simplified HVAC system. The average cabin temperature from the test was input as a boundary condition for the model, and the heater power was calculated. For equivalent cabin air temperature, transient heating energy of the simulation matched test data within 3.8%.

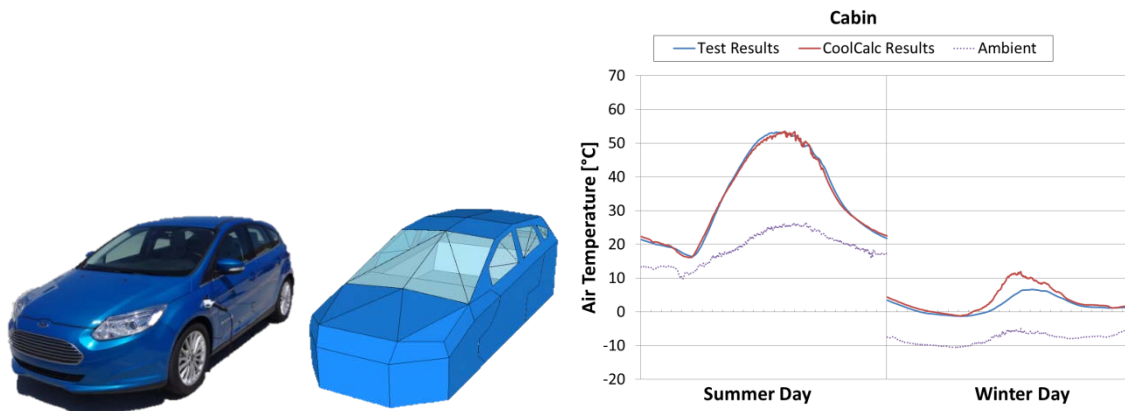


Figure III-63: Focus Electric test vehicle and CoolCalc model; results of model validation to test data for summer and winter days

(photo credit: NREL)

Modal Application & Results

The validated CoolCalc model was applied to evaluate the potential impact of polycarbonate (PC) glazing on steady-state heating loads. The conductivity of the window material was reduced to 0.2 W/mK to simulate a polycarbonate glazing. Simulations were performed with no solar loads during heating, so the solar spectral properties of the glazing would not have an impact. The ambient temperature was -5°C , and the cabin air temperature was maintained at 22°C .

The three configurations evaluated used polycarbonate in place of auto glass for: 1) the rear (fixed) glazing only; 2) the rear glazing and all sidelites (passenger door windows); and 3) all glazing, including the

windshield. The baseline configuration used standard automotive glass for all window locations. Figure III-64 shows the simulation results in terms of the average thermal power for steady-state heating for each configuration and the percent reduction from baseline for the three polycarbonate configurations. Heating power was reduced by 0.79%–3.27%. Automobile manufacturers face challenges implementing polycarbonate for movable glazing and windshields. Using polycarbonate for the fixed glazing is the most feasible configuration, but produced only a 0.79% reduction in heating energy.

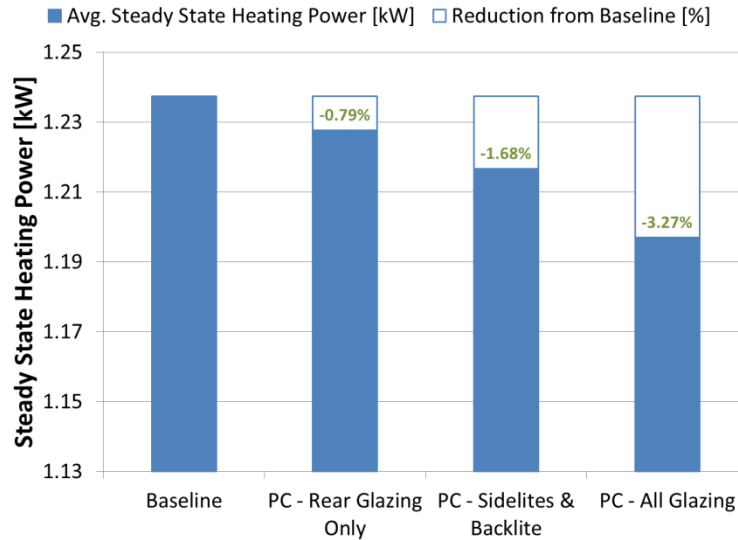


Figure III-64: Results of CoolCalc analysis of polycarbonate glazing

EDV Range Calculation

Range Impact Simulation Approach

The vehicle simulation tool Autonomie was used to calculate the impact of cabin heating on EDV driving range. A model of the Ford Focus Electric provided by Argonne National Laboratory was used for the simulations along with experimental measurements of the heating power for the baseline and Zonal Configuration #4 cases, including power for heated surfaces. It should be noted that the transient and steady-state warm-up tests were conducted at ~ 0°C ambient temperature with the HVAC control set to Auto 72.

The Focus Electric uses a 23-kWh capacity lithium-ion battery pack. The battery utilization was assumed to be 85%; therefore, 19.55 kWh of usable energy was calculated for the battery pack [1]. Calculating the vehicle efficiency over a single short-duration drive cycle and applying it to calculate the overall range would overestimate the impact of HVAC use because the heating loads decrease when the passenger compartment temperatures attain steady state. Because the average vehicle trip duration in the United States is approximately 20 minutes [4], the average vehicle efficiency was calculated over several drive cycles of approximately 20-minutes duration. The drive cycles simulated were Urban Dynamometer Driving Schedule (UDDS) (22.8 minutes), back-to-back Highway Fuel Economy Test (HWFET) cycles (25.5 minutes), and back-to-back US06 cycles (20 minutes). The model was simulated over these drive cycles for three climate control conditions: no cabin heating, baseline HVAC heating, and Zonal Configuration #4 heating. Using the average vehicle efficiency and the usable battery energy, the total range was calculated for each drive cycle.

Range Impact of Zonal Test Results

The results of the vehicle drive cycle simulations are shown in Figure III-65. The impact of baseline heating using the standard HVAC system is substantial, ranging from 20.1% loss of driving range for US06 up to 47.6% range loss for the UDDS cycle. These results are in general agreement with published EDV range reductions due to heating. While cabin heating is required, the good news is that some of this range penalty can

be recovered. For the same drive cycles and trip durations, the combined zonal heating strategy shows the potential to increase driving range by 6.9%–18.7% over the baseline heating case.

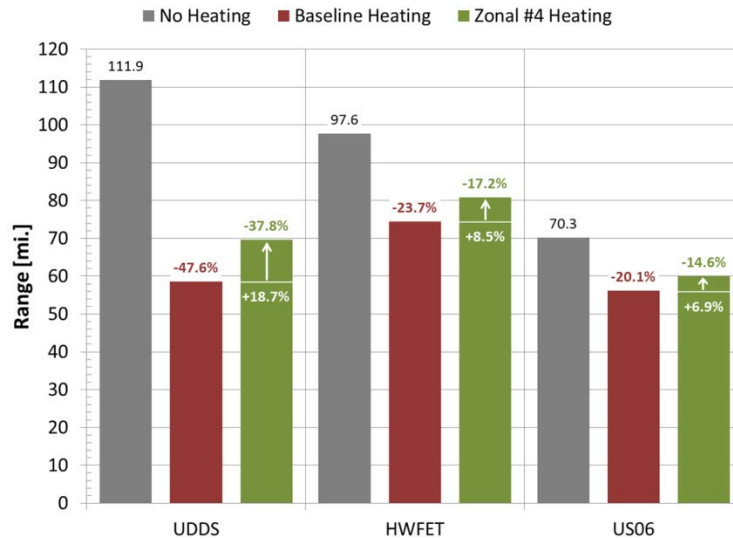


Figure III-65: Calculated driving range for no heating, baseline heating, and zonal heating

National Range Impact Estimate

A national-level analysis was conducted to identify where energy efficient heating systems will have the greatest benefit and to calculate the overall national impact. A process similar to the air conditioning fuel use analysis was used [5]. Using the UDDS drive cycle to represent current usage of EDVs primarily in urban locations and the environmental data for each state, the impact of baseline heating is shown in Figure III-66. As expected, there is a large reduction in range in colder climates.

To calculate the national-level impact, the current EDV distribution is used in the analysis. While conventional vehicles have a nearly uniform distribution with population, EDVs make up a small portion of the light-duty vehicle fleet and the distribution of these vehicles is influenced by local incentives and regulations. Figure III-66 shows the percent of EDVs per state, with California having over 40 percent of the EDVs in the United States. Based on this distribution, a baseline heating load reduces the EDV range by 17%. If all vehicles used Zonal Configuration #4, the range would be improved by 7.1% over the baseline heating range. This equates to a 33% reduction in range penalty.

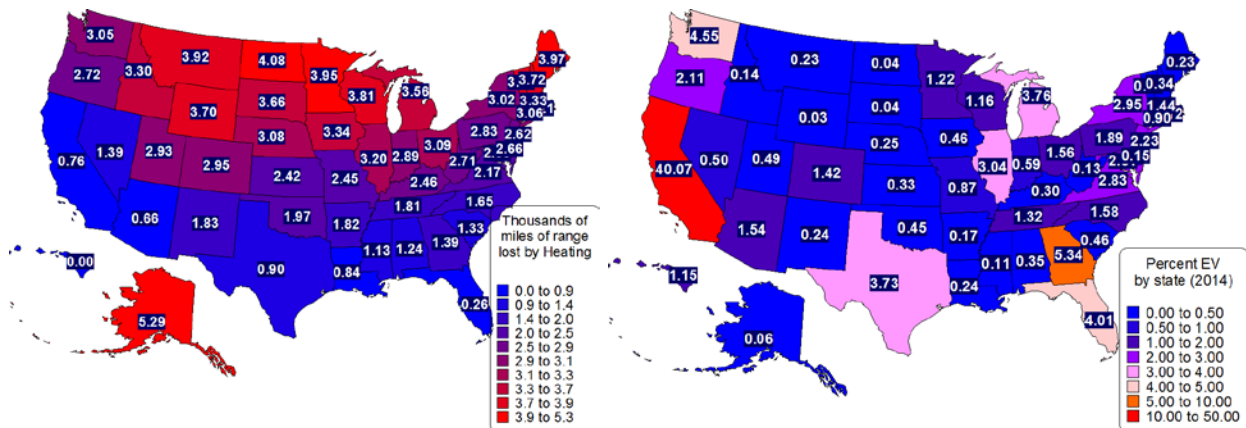


Figure III-66: Reduction in range due to cabin heating by state; fraction of the national EDV fleet per state

The range improvement estimates were based on drive cycle simulations using measured weather conditions and heating power from outdoor vehicle tests at ~ 0°C. As noted previously, the heater power profile was more heavily weighted to a transient heater load for a 20-minute simulation. The range improvements due to zonal strategies in moderate environments and for longer drive cycles will be lower. If the vehicle is thermally preconditioned during outdoor charging or parked indoors, the higher transient load would be eliminated. If vehicle use is not limited by the maximum EDV range, the heater power would be inconsequential.

Conclusions

Outdoor vehicle tests and thermal modeling were used to assess strategies for reducing vehicle cabin heating loads. Testing showed that using only existing HVAC vents and focusing the conditioned air on the driver, a 5.5% reduction in heating energy can be realized. A combined heating configuration that included zonal air flow as well as heated surfaces—seat, steering wheel, and floor mat—reduced the heating energy by 28.5% while maintaining nearly equal thermal sensation. Vehicle simulations showed a 7% to 19% improvement in range is achievable with zonal air and surface heating, thus reducing the range penalty for heating by 33%.

Analyses showed that a small reduction in heating energy can be attained by using polycarbonate glazings, which have a lower thermal conductivity than glass. Testing in FY2014 quantified the potential benefit of insulation on opaque surfaces in reducing the heating load.

Using zonal heating strategies in conjunction with reduced thermal conductivity of the vehicle shell is recommended to reduce the heating loads in EDVs. Other energy efficiency improvements such as implementation of a heat pump or thermal preconditioning can be part of a combined strategy to minimize the impact of heating on EDV range. Energy savings from HVAC load reduction solutions translate directly into increased energy for vehicle propulsion, which improves driving range and can lead to wider EDV adoption.

Acknowledgements

- Co-authors: Lawrence Chaney, Matthew A. Jeffers: NREL
- Cory Kreutzer, Jeff Tomerlin: NREL
- James Gebbie, Paul Hoke, Ken Jackson, Clay Maranville: Ford Motor Co.
- Mark Hepokowski: ThermoAnalytics, Inc.
- Todd Barnhart: Gentherm

III.4.C. Products

Presentations/Publications/Patents

1. Jeffers, M.; Chaney, L.; Rugh, J. 2015. "Climate Control Load Reduction Strategies for Electric Drive Vehicles in Warm Weather." Proceedings of 2015 World Congress and Exhibition, Paper #2015-01-0355, Society of Automotive Engineers, Detroit, MI.
2. Chaney, L.; Jeffers, M.; Rugh, J., 2015. "Climate Control Load Reduction Strategies for Electric Drive Vehicles in Cold Weather." Proceedings of 2015 SAE Thermal Management Systems Symposium, Presentation #15TMSS-0045, Society of Automotive Engineers, Troy, MI.

III.4.D. References

1. Argonne National Laboratory's Advanced Powertrain Research Facility data, Vehicle Systems Analysis Technical Team (VSATT) meeting presentation, Eric Rask, April 2, 2014.
2. Jeffers, M.; Chaney, L.; Rugh, J. 2015. "Climate Control Load Reduction Strategies for Electric Drive Vehicles in Warm Weather." Proceedings of 2015 World Congress and Exhibition, Paper #2015-01-0355, Society of Automotive Engineers, Detroit, MI.
3. Lustbader, J., Rugh, J., Rister, B., Venson, T. 2011. "CoolCalc: A Long-Haul Tuck Thermal Load Estimation Tool," Proceedings of 2011 SAE World Congress, Paper # 2011-01-0656, Detroit, MI.

4. Santos, A., McGuckin, N., Nakamoto, H.Y., Gray, D., et al. 2011. "Summary of Travel Trends: 2009 National Household Travel Survey." Federal Highway Administration, U.S. Department of Transportation, June 2011.
5. Johnson, V. 2002. "Fuel Used for Vehicle Air Conditioning: A State-by-State Thermal Comfort-Based Approach." Proceedings of Future Car Congress 2002, Paper #2002-01-1957, Society of Automotive Engineers, Arlington, VA, June 2002.

III.5. Increasing EDV Range through Intelligent Cabin Air Handling Strategies

Daniel Leighton, Principal Investigator

National Renewable Energy Laboratory
Transportation and Hydrogen Systems Center
15013 Denver West Parkway, MS 1633
Golden, CO 80401
Phone: (303) 275-4489; Fax: (303) 275-4415
E-mail: daniel.leighton@nrel.gov

John P. Rugh, Task Leader

Phone: (303) 275-4413
E-mail: john.rugh@nrel.gov

David Anderson and Lee Slezak, DOE Program Managers

Vehicle Technologies Office
Phone: (202) 287-5688, (202)586-2335
E-mail: david.anderson@ee.doe.gov, lee.slezak@ee.doe.gov

Start Date: October 1st, 2014
End Date: September 30th, 2015

III.5.A. Abstract

Objectives

- Identify cabin air recirculation strategies to increase the fraction of recirculation possible without causing windshield fogging to reduce electric vehicle (EV) cabin heating energy consumption in cold weather.

Accomplishments

- Computational fluid dynamics (CFD) simulations of a Ford Focus Electric demonstrated that a split flow heating, ventilating and air conditioning (HVAC) system with rear recirculation ducts can reduce cabin heating loads by up to 57.4% relative to full fresh air usage under some conditions (steady state, four passengers, ambient temperature of -5°C).
 - The primary challenge is the increased complexity and cost due to packaging constraints.
- Simulations also showed that implementing a continuous recirculation fraction control system into the original equipment manufacturer (OEM) HVAC system can reduce cabin heating loads by up to 50.0% relative to full fresh air usage under some conditions (steady state, four passengers, ambient temperature of -5°C).
 - This is a substantial energy savings benefit that is attainable at the relatively low cost of additional control logic and potentially a redesigned recirculation actuator door.
- Identified that continuous fractional recirculation control of the OEM system can provide significant energy savings for EVs at minimal additional cost, while a split flow HVAC system with rear recirculation ducts only provides minimal additional improvement at significant additional cost.
 - Recommend implementation of continuous recirculation fraction control for OEM system instead of split flow system.



III.5.B. Technical Discussion

Background

Plug-in hybrid electric vehicles, battery electric vehicles (BEVs), and internal combustion engine vehicles with fuel-efficient, down-sized engines increasingly lack sufficient “free” waste heat to condition the cabin in cold weather. The lack of sufficient waste heat to fully condition the cabin means that they must resort to alternative heating systems such as electrical resistance heaters and heat pumps. These heating technologies consume additional energy for thermal management, which reduces vehicle efficiency. In BEVs this effect is particularly acute due to the complete absence of engine waste heat and the limited battery energy available for vehicle propulsion. In fact, testing of a 2012 Nissan Leaf by Argonne National Laboratory demonstrated that operating the vehicle at an ambient temperature of 20°F approximately halved the vehicle range for the Urban Dynamometer Driving Schedule (UDDS) drive cycle when compared to 72°F [1], which is predominately due to energy used to heat the cabin via an air-side electrical resistance heater. Technologies that are able to reduce the amount of energy spent by the battery to condition the vehicle cabin will help to increase customer acceptance of electric drive vehicles (EDVs) by reducing range anxiety, which will in turn increase EDV penetration into the national vehicle fleet.

Introduction

Denso Corporation found that as much as 60% of the energy used to heat cabin air in a light-duty vehicle is due to the necessity of conditioning outside fresh air, which is also known as the ventilation losses [2]. This represents a significant potential EDV range increase in cold weather through a reduction in the amount of fresh air used during cabin heating. To reduce the energy consumption dedicated to conditioning fresh air, recirculated air from the cabin can be re-conditioned. Using current technologies, cabin air recirculation is limited due to issues of windshield fogging. One method to increase the fraction of air that can be recirculated is to focus fresh air on areas that need it the most, namely the windshields and occupant faces. To achieve higher recirculation fractions, the conditioned cabin air can be split into two separate airstreams, one fresh and one recirculated stream. These separate airstreams can then be directed through the cabin based on occupancy and fogging prediction.

The literature contains several examples of approaches for split flow systems that separate the fresh and recirculated air streams. Denso Corporation manufactures a split flow HVAC module that separates the flow streams within the HVAC module itself using a variable-diameter blower wheel and separation baffling for the heat exchangers [2]. Ford Motor Company holds a patent on suction surfaces that are distributed throughout the vehicle, as shown in Figure III-67 [3]. These suction surfaces are powered recirculation return ducts that can be embedded within the seats and structure of the vehicle both at the front and rear seating rows rather than the typical single recirculation “door” that opens on one side of the HVAC module itself. The HVAC module is typically located within the instrument panel on the passenger side of the vehicle, which theoretically sets up a cabin air flow pattern with a limited amount of recirculation air that reaches the rear of the vehicle.

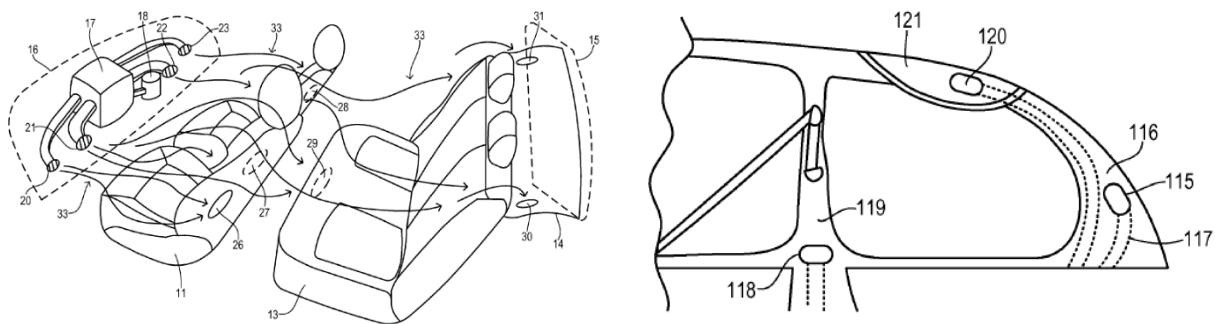


Figure III-67: Ford Motor Company patent drawings for proposed “suction surface” locations

Source: Ford Motor Company, US Patent 20120315835A1, “Automotive HVAC System with Suction Surfaces to Control Local Airflow”

CFD simulations were performed to efficiently explore the different split flow configuration options. The simulations allowed multiple configurations for recirculation return ducting and exhauster placement without needing to construct the physical ducting in an experiment vehicle. The CFD simulations also allowed direct quantification of the relative humidity (RH) of the air at all of the glass surfaces of the vehicle to detect fogging conditions, as well as quantification of the energy savings benefits of a variety of recirculation enhancement strategies.

Approach

A three-dimensional (3D) computer-aided design (CAD) model of the interior cabin of a Ford Focus BEV was provided to the National Renewable Energy Laboratory by Ford Motor Company. This 3D CAD model was used to create a mesh of the cabin interior airspace for 3D CFD modeling of the interior cabin airflow [4]. The model was then modified to add split flow ducting as shown in Figure III-68. The CAD model shown represents the final iteration of duct locations used in the final results.

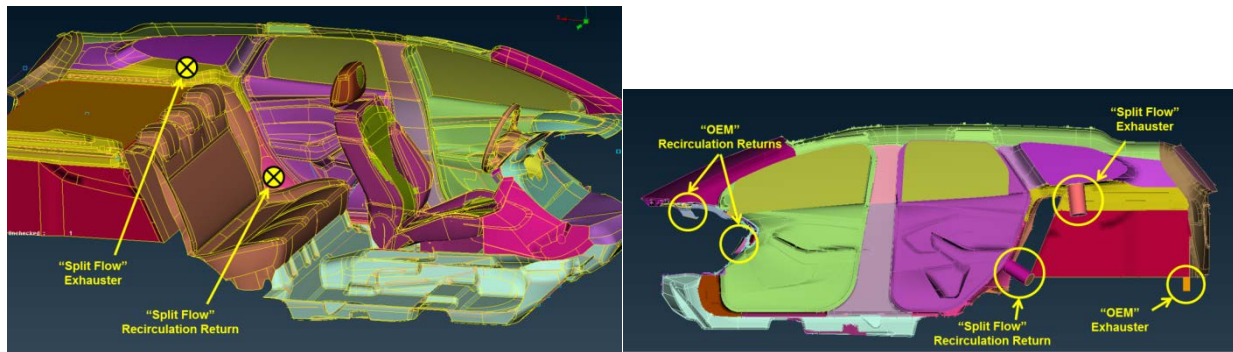


Figure III-68: Recirculation return and exhauster locations in Ford Focus CAD cabin model

The results from vehicle cabin simulations using steady-state CFD analysis were used to measure the impact of various enhanced cabin airflow techniques, including a split flow system with rear recirculation ducts. The effect of these technologies on windshield fogging during heating mode was assessed, the energy savings due to reduced fresh air usage was quantified, and best design practices were identified.

The CAD model includes the vent ducting of the HVAC system itself to capture the effect of vent design on the local airflow. This is important because the ducting can impart swirl and other turbulence into the air flow distribution, which affects the windshield fogging predictions. The defrost/demist vents are highlighted in green on the left of Figure III-69. In the case of split flow, this is where the fresh air enters the vehicle. The red floor outlets for the front and rear passengers are where the recirculated air flow re-enters the vehicle cabin.

The CAD model also includes four human passenger models, which provide wall boundary conditions for airflow as well as moisture inlet boundaries to the cabin. The human passenger models are shown on the right side of Figure III-69. Mouth and chest mass flow inlet boundaries are created on each of the four human models to simulate the respiration and perspiration water mass flow rates into the cabin air volume. The total water introduced to the cabin air from the human models is 280 grams per hour, which is a flow of 70 grams per hour per passenger as specified in SAE standard J902 [5]. This is executed as 15 grams per hour of respiration and 55 grams per hour of perspiration.

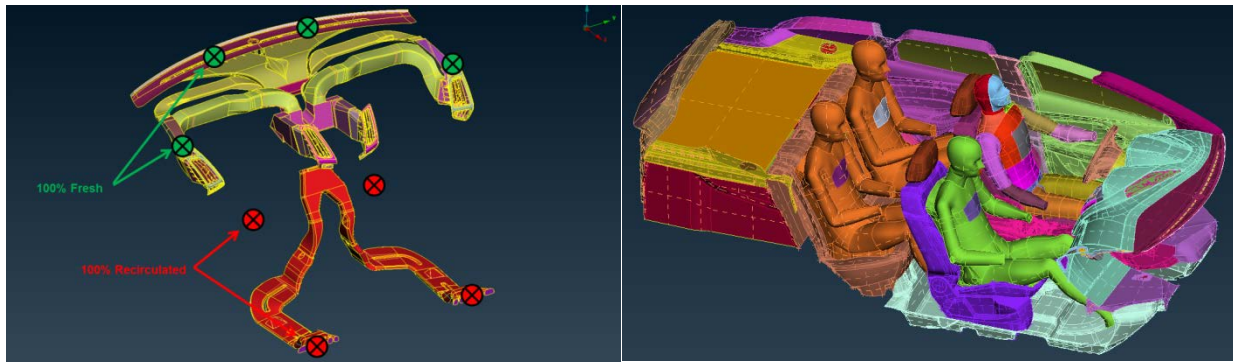


Figure III-69: Left - Cabin inlet vent CAD geometry; Right - Human passenger CAD models in four seating locations within cabin

To simplify the simulations and focus on exploring different configurations for the split flow system, a single representative test condition was chosen as a metric for comparison between the different technologies. The ambient outdoor air temperature was chosen as -5°C because it represents a substantial heating case in which the recirculation is limited by windshield fogging. It was assumed that the outdoor RH was worst case, at 100%. It is worthy to note that at such low ambient temperatures the absolute humidity is very low even at 100% RH. The air velocity over the outside of the vehicle was fixed at 30 miles per hour, head-on, which represents the moderate speeds seen in mixed city/highway driving during a commute. This moderate vehicle speed was used to calculate the convection coefficients on the exterior shell surfaces as part of the calculation of the heat lost through the vehicle walls. The conduction through the walls was calculated based on known material properties and dimensions, and the interior convection coefficients were calculated by the CFD model. The CFD simulations are steady-state, and therefore require representative cabin HVAC air flow rate and vent temperatures. A vent inlet temperature of 50°C was chosen based on experimental measurements, and an HVAC blower volumetric air flow rate of 105 cfm was chosen based on maintaining reasonable cabin air comfort temperatures for the steady-state simulation. This represents roughly half of the maximum possible blower air flow rate.

Based on experimental data, 37% of the volumetric air flow rate through the HVAC system was distributed to the defrost/demist vents, and 63% was distributed to the foot well vents in the OEM system. In the fractional recirculation control simulation case, the OEM system ducting is used. The recirculation air leaving the cabin mixes with fresh outside air within the HVAC module and is then distributed to all of the cabin inlet vents. When continuous fractional recirculation control is used, it only affects the proportion of mixed recirculation and fresh air; the air flow rates to the vents remain constant. In the split flow configuration simulations, 100% of the recirculation outlet air is reconditioned separately and sent to the floor vents, while 100% fresh outside air is conditioned and sent to the defrost/demist vents. When the split flow recirculation fraction is changed, the air flow rates to the defrost/demist vents and floor vents are proportionally altered. For example, if the recirculation fraction is 75%, then 75% of the 105 cfm total air flow rate is sent to the foot vents, and the remainder is sent to the defrost/demist vents. Table III-15 summarizes the different configurations presented in the results.

Table III-15: Test configuration descriptions

Configuration	Exhauster Location	Recirculation Location
OEM Fresh	Trunk floor	None
Fractional Recirculation Control	Trunk floor	HVAC module (within dashboard)
Split Flow	Behind C-pillar	Rear passenger waist level
Split Flow w/ OEM Exhausters	Trunk floor	Rear passenger waist level
Split Flow w/ OEM Exhausters and Recirculation	Trunk floor	HVAC module (within dashboard)

Results

An example of the air flow patterns in the split flow configuration is shown in Figure III-70 for a 63% recirculation fraction. It is notable that the highest air flow velocities occur at the inlet vents and outlet recirculation return ducts and exhausters. The area of these duct openings must be sized to prevent excessive air velocities that may cause discomfort and noise. In the center of the cabin, the airflow velocity is generally very low. The original theory was that in a split flow system, the foot well vents that supply re-conditioned recirculation air will flow through the bottom level of the cabin and exit through the recirculation ducts near the rear passengers' waists, while the fresh air supplied at the defrost/demist vents will flow through the upper level of the cabin past the passengers' heads and out of the exhausters near the rear windshield behind the C-pillar. Although this two-layer flow pattern undoubtedly occurs to a small degree, simulations showed that the expected distinctly separate regions of flow are not apparent.

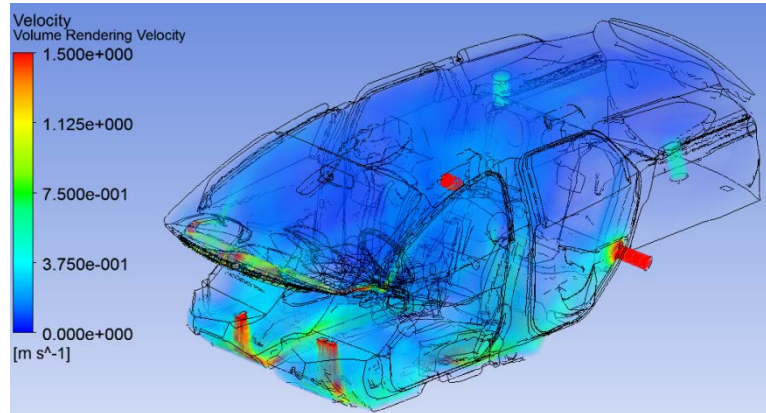


Figure III-70: Cabin air velocity field of split flow case with rear split flow recirculation return ducts and exhausters at 63% recirculation

The fogging prediction of the windshield is a key parameter used to determine the maximum allowable fraction of recirculated cabin air. To this end, the RH at the inner glass surfaces will be the metric used to compare different cases. RH is a function of the water content of the air flowing over the windshield, but is also a function of the glass surface temperature itself. Figure III-71 shows the inner surface temperature of the front windshield in the fractional recirculation control case to demonstrate the effect of the defrost vents heating the inside of the glass while the exterior airflow is cooling the glass. It is apparent that the average windshield inner surface temperature is dominated by the heat transfer from the defrost vent air, but that there are strong non-uniformities caused by differences in local defrost flow velocity.

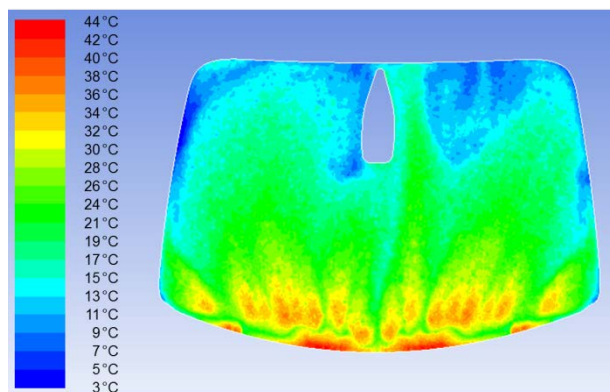


Figure III-71: Front windshield interior surface temperatures of the fractional recirculation control case

A comparison between the fractional recirculation control case and the split flow system using the rear recirculation return ducts and split flow exhauster locations is shown in Figure III-72. This figure shows the inner front windshield surface RH levels when a recirculation fraction of 63% is used in both cases. In both

cases, the entire windshield surfaces are below 100% RH, which indicates that no fogging occurs under these conditions. The notable difference between the two cases is that the split flow system has a qualitatively lower average RH, which is expected since it is receiving 100% fresh outside air, whereas the fractional recirculation control system windshield is receiving the mixed fresh/recirculation air at a 37%/63% fraction. In this comparison the air flow rate and temperature of the defrost vents is the same in both configurations.

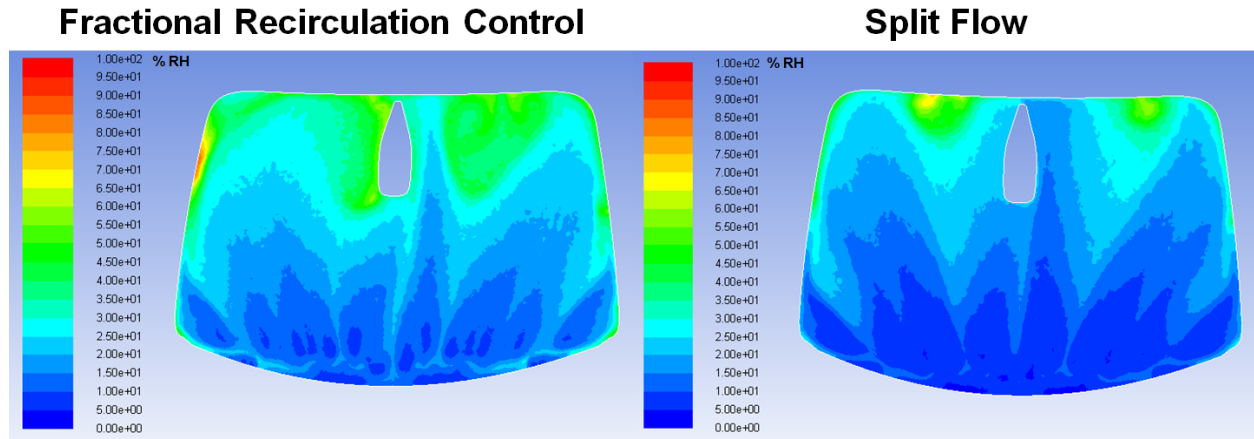


Figure III-72: Windshield RH of fractional recirculation control (left) and split flow (right) at 63% recirculation fraction

Of more interest is how high the recirculation fraction can be increased before windshield fogging begins, which is determined to occur when the RH reaches 100% in any section of the windshield. Again, a comparison between the windshield RH for the fractional recirculation control system and the split flow system using the rear recirculation return ducts and split flow exhauster locations is shown in Figure III-73. In this case, the recirculation fraction of the split flow system has been increased to 84.5%, which means that the flow rate of the 100% fresh air being delivered by the defrost vents must be reduced as a fraction of the total 105 cfm HVAC air flow rate. This equates to a 58.1% reduction in air flow rate from the defrost vents when compared with the fractional recirculation control case. In the fractional recirculation control case, the recirculation fraction has been increased to 75%, which means that the absolute humidity of the vent air is increased compared with the previous case, which elevates the RH at the interior windshield surface. The most notable effect occurs in the split flow case, where it is apparent that the windshield surface RH near the defrost vent outlet is still very low, but that the lower flow rate does not "project" very far up the height of the windshield, which allows the higher humidity cabin air to flow back as a plume onto the upper windshield, which becomes the limiting factor for fogging.

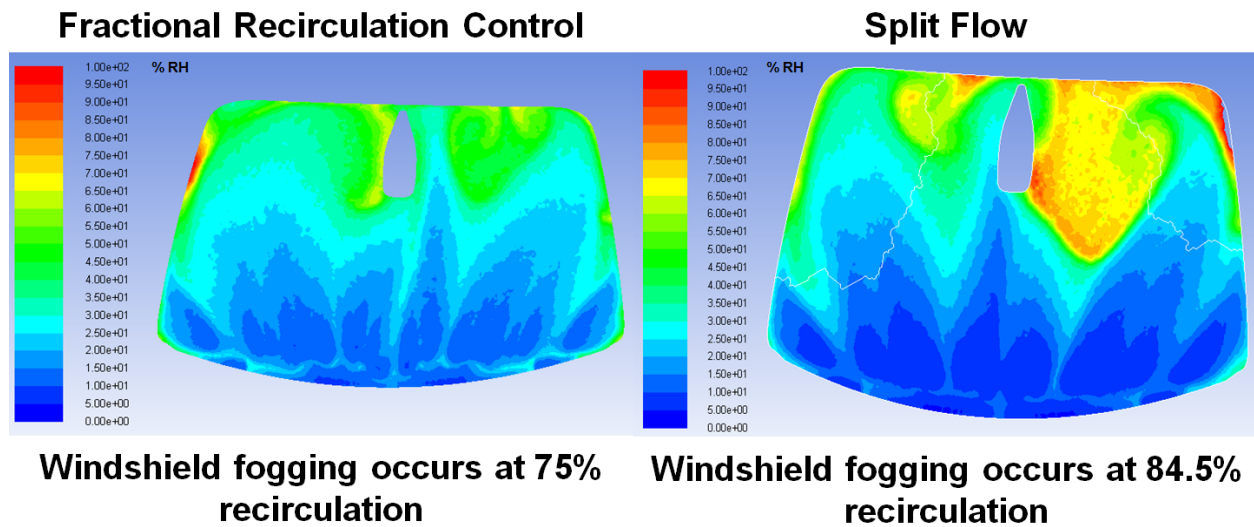


Figure III-73: Windshield RH of fractional recirculation control (left) and split flow (right) at highest recirculation fractions before fogging point

When examining what the maximum allowable recirculation fractions are for the various system configurations, it is important to examine not only the RH at the inner surface of the front windshield, but also the RH at the inner surfaces of the other glass panes within the vehicle. Figure III-74 shows three different simulation cases for the RH at the inner glass surface for the front windshield (left side), side windshields (three panes each side), and rear windshield (right side). The two cases discussed previously for the maximum allowable recirculation fractions before front windshield fogging occurs show that there are small areas of predicted fogging on other portions of the glass surfaces (top and middle plots). In fact, the split flow system produced moderate amounts of fogging at the rear glass. Based on this result, the simulation was re-run for the split flow case using the OEM exhausters that are below the rear glass at the floor of the trunk instead of the "split flow" exhausters that are behind the C-pillar. The result is shown in the third (bottom) plot, and it is apparent that the OEM exhausters are superior to the "split flow" exhausters due to more flow over the rear glass. Because these OEM exhauster locations are typical for vehicle packaging, it is recommended that they be used for the split flow system to reduce complexity and cost. The OEM exhausters were used in the remaining analysis of the split flow system. It is also important to note that simple 2D wall conduction models are used, not detailed 3D wall simulations. The consequence of this is that at the junction of different wall surface materials, the accuracy of the wall temperature prediction is reduced, such as at the edges of the glass surfaces where they connect with sheet metal walls.

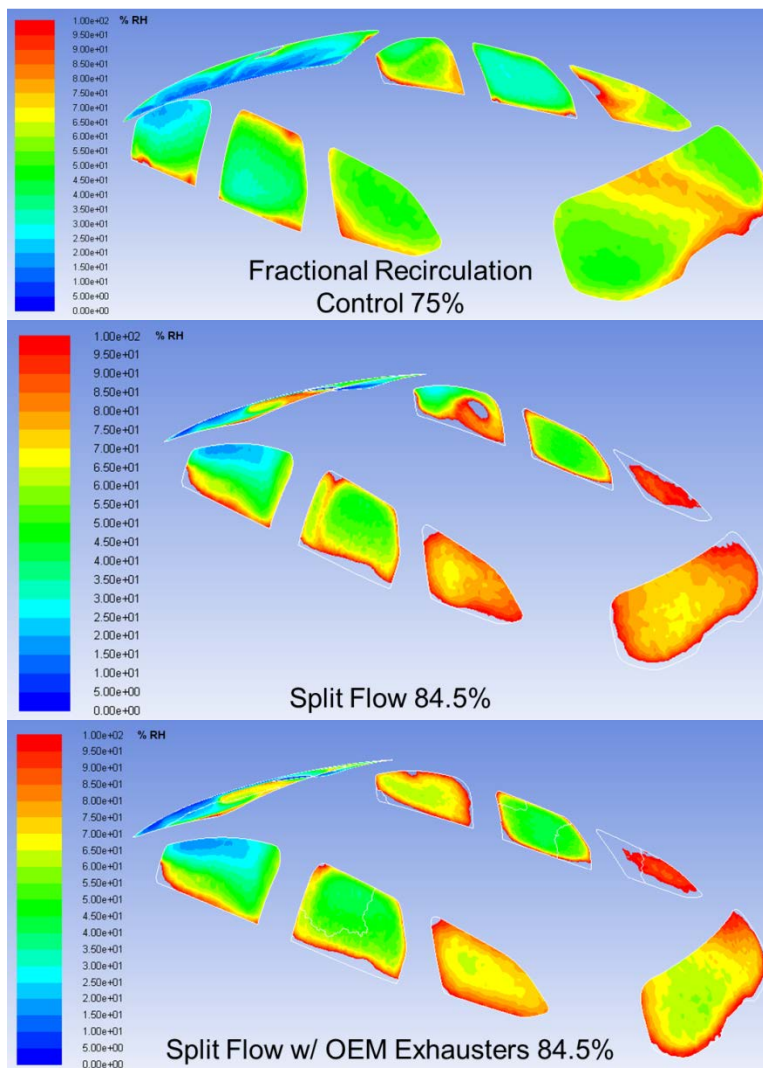


Figure III-74: Vehicle glass surface RH of fractional recirculation control at 75% recirculation (top); split flow at 84.5% recirculation (middle); and split flow with OEM exhausters at 84.5% recirculation (bottom)

Another question of interest is how well a split flow HVAC module works when using unmodified OEM exhausters and recirculation return, i.e., a drop-in of a split flow HVAC module. A recirculation fraction of 63% was used to make a performance comparison between the three different system configurations in Figure III-75. The comparison shows that the drop-in split flow HVAC module (middle) performs similarly to the fractional recirculation control case (top) with the exception of superior performance at the front windshield. A comparison of the split flow drop-in (middle) with the split flow system using rear recirculation return ducts (bottom) shows that the performance difference is generally positive, but small.

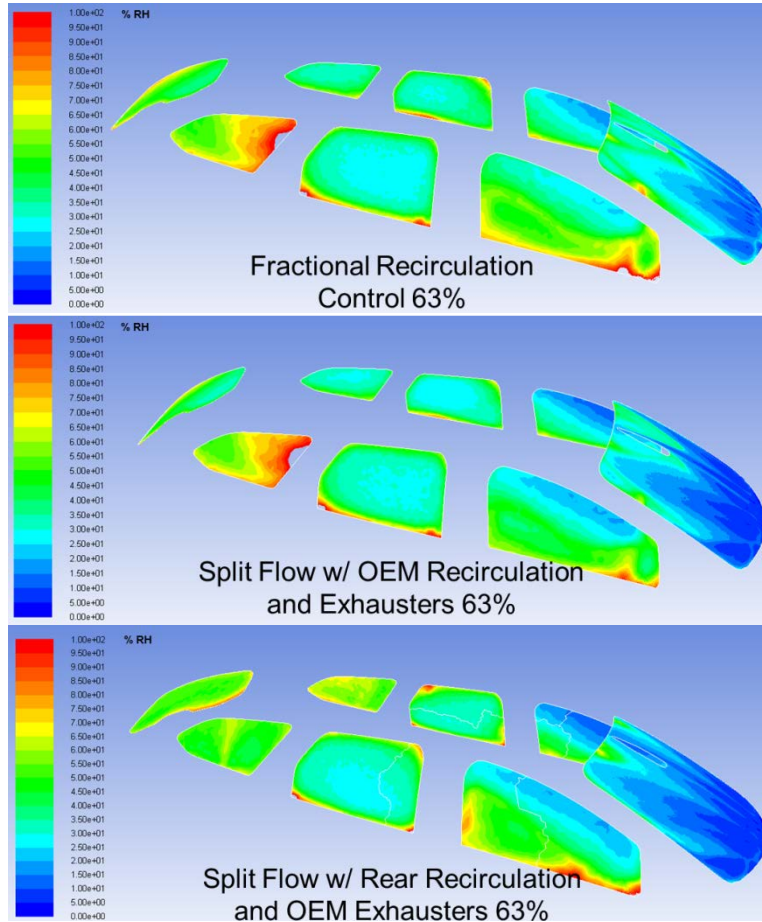


Figure III-75: Vehicle glass surface RH at 63% recirculation for fractional recirculation control (top); split flow with OEM recirculation ducts and exhausters (middle); and split flow with rear recirculation ducts and OEM exhausters (bottom)

The RH of the bulk cabin air is another metric that is informative for discerning what is occurring within the vehicle air space. Figure III-76 compares the air RH for the fractional recirculation control case at 63% recirculation (top) to the split flow system with rear recirculation ducts (bottom) over a virtual plane down the center of the vehicle from front to back. The most notable finding in this comparison is that the split flow system with rear recirculation return ducts can significantly lower the average air RH in the rear seating area of the vehicle, which can be disadvantageous to rear occupant comfort under some conditions. The other notable outcome is that two-layer flow does not significantly develop as discussed previously for the air velocity plot; the RH gradient in the vertical direction is slight, if any.

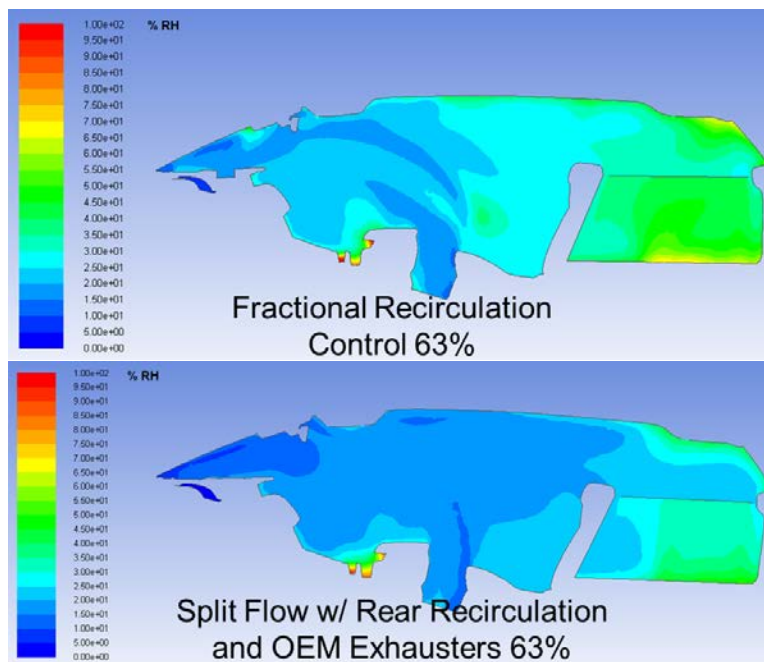


Figure III-76: Air RH at center plane along length of vehicle of fractional recirculation control at 63% recirculation (top) and split flow with OEM exhausters at 63% recirculation (bottom)

The maximum energy savings associated with the different configurations is calculated at the point where any further increase in the recirculation fraction will induce windshield fogging. It is assumed that the reduced thermal load of the cabin is directly proportional to the amount of energy required to provide it. This is approximately true for electrical resistance heating or a heat pump, although results could differ slightly depending on the exact system design. The required heating capacity for the cabin is calculated based on the simulation results for inlet and outlet conditions at the tested recirculation fraction. Table III-16 summarizes the energy savings. It is important to note that these energy savings results are only for the specific case tested, which is a steady-state case with four passengers where the vehicle is travelling at a constant 30 mph at an ambient temperature of -5°C . In other common cases, such as a transient cabin warm-up period, the energy savings benefits would likely be reduced.

Table III-16: Steady-state energy savings summary

Configuration	Recirculation Fraction	Required Heating Capacity	Energy Savings
OEM Fresh	0%	2.98 kW	0%
Fractional Recirculation Control	75%	1.49 kW	50.0%
Split Flow w/ OEM Exhausters	84.5%	1.27 kW	57.4%

Conclusions

CFD simulations demonstrated that continuous fractional recirculation control using standard OEM ducts and recirculation doors allows a recirculated air fraction of up to 75% before windshield fogging occurs when there are four passengers and the ambient temperature is -5°C . A 75% recirculation fraction results in a cabin heating load reduction of 50.0% relative to using full fresh air, which equates to a 50.0% energy savings for a generic heating system such as an electrical resistance heater or heat pump. This is a substantial energy savings for EDVs in cold weather at the relatively low cost of additional control logic, sensor, and potentially a

redesigned recirculation actuator door. The actual EDV range increase that this energy savings would equate to would be heavily dependent on vehicle usage.

The primary investigation of this CFD simulation study was to measure the effect of a split flow recirculation system. CFD results showed that having split fresh and recirculation air streams with a return duct at the rear of the vehicle allowed up to a 84.5% recirculation fraction before windshield fogging, which equates to an energy consumption reduction of 57.4% relative to full fresh air use. Although the split flow system provides significant benefit, the slight difference in energy savings of the split flow system over the fractional recirculation control system is unlikely to be justifiable due to the increased system complexity. The increased complexity is particularly apparent in the packaging challenge of running recirculation return ducts from the rear of the vehicle to the instrument panel. Also, the energy savings estimate is based on thermal load reduction and does not take into account any potential increase in HVAC blower electrical power due to the additional pressure drop of the return ducts. With that in mind a fractional recirculation control system is recommended as an effective option to reduce heating loads. In fact, Corporate Average Fuel Economy (CAFE) regulations provide off-cycle greenhouse gas credits to OEMs for implementing improved recirculation strategies, and OEMs are beginning to implement fractional recirculation controls.

Although the additional energy savings benefit of the split flow system over the fractional recirculation control system is small, an auxiliary benefit of the split flow system is potentially improved passenger thermal comfort. The split flow system provides drier air to the front windshield, which would allow a reduction of airflow through the defroster/demister vents. This is advantageous because defrost/demist flow can cause discomfort for the front passengers due to "dry eyes."

III.5.C. Products

Presentations/Publications/Patents

1. Leighton, Daniel. "CFD Modeling of Cabin Airflow Using Split HVAC and Dynamic Extractors." SAE 2015 Thermal Management System Symposium, Troy, MI, September 29 - October 1, 2015.

III.5.D. References

1. Losche-Busch, Henning. "Advanced Powertrain Research Facility AVTA Nissan Leaf Testing and Analysis." Argonne National Laboratory, October 12, 2012.
2. Shikata, Kazushi; Uemura, Yukio; Ichitani, Yutaka; Uchida, Goro; Kato, Yasushi. "Development of Two Layer Flow HVAC Unit," SAE Congress 1999, Paper # 1999-01-1199, March 1-4, 1999.
3. Maranville, Clay, et al. Automotive HVAC System with Suction Surfaces to Control Local Airflow. U.S. Patent 20120315835A1, filed June 9, 2011, and issued December 13, 2012.
4. Jeffers, Matthew A.; Chaney, Larry; Rugh, John P. "Climate Control Load Reduction Strategies for Electric Drive Vehicles in Warm Weather," SAE Congress 2015, Paper # 2015-01-0355, April 21-23, 2015.
5. SAE Standard J902. "(R) Passenger Car Windshield Demisting and Defrosting Systems." SAE International, August 2011.

III.6. Integrated Vehicle Thermal Management – Combining Fluid Loops on Electric Drive Vehicles

Daniel Leighton, Principal Investigator

National Renewable Energy Laboratory (NREL)
15013 Denver West Parkway
Golden, CO 80401
Phone: (303) 275-4489; Fax: (303) 275-3765
E-mail: daniel.leighton@nrel.gov

John P. Rugh, Task Leader

Phone: (303) 275-4413
E-mail: john.rugh@nrel.gov

David Anderson and Lee Slezak, DOE Program Managers

Phone: (202) 287-5688, (202) 586-2335
E-mail: David.Anderson@ee.doe.gov, Lee.Slezak@ee.doe.gov

Start Date: 1/1/2011
End Date: 12/31/2014

III.6.A. Abstract

Objectives

- Improve vehicle range and reduce weight and volume of electric drive vehicle (EDV) thermal systems by combining fluid loops
- Collaborate with industry partners to plan future vehicle-level demonstration of combined fluid loop technology.

Accomplishments

- Transient drive cycle hot-weather bench testing was completed
- Power electronics and electric motor (PEEM) and energy storage system (ESS) thermal conditioning was sufficient at all temperatures
- Transient drive cycle cold-weather bench testing was completed
- PEEM waste heat recovery increased vehicle range by 2% at tested ambient temperatures
- Heat pump operated down to -12°C
- Estimated impact of combined fluid loop technology on EDV range
 - National vehicle usage versus ambient temperature weighting predicts a 9.0% increase in vehicle range using a non-optimized prototype combined fluid loop system.

Future Achievements

Work with industry suppliers and a vehicle manufacturer to conduct future vehicle-level development and demonstration of combined fluid loop technology.



III.6.B. Technical Discussion

Background

Relative to traditional internal combustion engine vehicles, EDVs have increased vehicle thermal management complexity through the addition of a battery pack, or ESS, as well as PEEM components. These drivetrain subsystems have specific thermal requirements that have necessitated a separate thermal loop for each subsystem. The ESS must be cooled during hot ambient conditions to prevent degradation of battery cell life and must be heated during cold ambient conditions to enable adequate discharge power. The typical range of temperature control for the ESS battery cells is 15°C to 35°C [1]. The PEEM systems must be cooled so that they remain below their maximum operating temperature limits to prevent thermal damage or failure. The typical thermal limits for the PE and EM components are around 150°C [2,3].

Separate cooling loops typically entail additional heat exchangers at the front end of the vehicle, water/ethylene glycol (WEG) coolant, piping, and WEG pumps. The disadvantage of multiple cooling loops is that they increase vehicle weight, volume, aerodynamic drag, and fan/pump power, thus reducing EDV range. Due to the lack of abundant engine waste heat that is typically available in traditional vehicles, EDVs also suffer from significant range loss when heating the cabin in cold weather conditions. Cold-weather range loss can be as high as 50% [4], which reduces customer acceptance of EDVs by increasing range anxiety, and presents a barrier for the penetration of EDVs into the national vehicle fleet. The goal of the combined fluid loop (CFL) technology is to improve EDV range and reduce weight and volume by capturing the synergistic benefits of unifying the thermal management systems.

The CFL technology being investigated unifies the cabin, ESS, and PEEM thermal management into a single coolant-based system that has separate hot and cold fluid streams that are directed to the thermal components as required. The unified system has a single heat exchanger at the front end of the vehicle that either rejects or absorbs heat based on the CFL system's operating mode. The design of the system piping allows the coolant to be directed based on operating requirements, including actively heating or cooling the ESS, using the high-temperature coolant stream to cool the PEEM, and recovering the waste heat from the PEEM to Cold-weather range loss can be as high as 50% [4], which reduces customer acceptance of EDVs by increasing range anxiety, and presents a barrier for the penetration of EDVs into the national vehicle fleet. The goal of the combined fluid loop (CFL) technology is to improve EDV range and reduce weight and volume by capturing the synergistic benefits of unifying the thermal management systems.

The CFL technology being investigated unifies the cabin, ESS, and PEEM thermal management into a single coolant-based system that has separate hot and cold fluid streams that are directed to the thermal components as required. The unified system has a single heat exchanger at the front end of the vehicle that either rejects or absorbs heat based on the CFL system's operating mode. The design of the system piping allows the coolant to be directed based on operating requirements, including actively heating or cooling the ESS, using the high-temperature coolant stream to cool the PEEM, and recovering the waste heat from the PEEM to supplement cabin heating. The CFL system also enables hot or cold coolant to be directed to the passenger cabin, which means that the system can act as either an air-conditioner or heat pump without reversing the refrigerant cycle. This is advantageous because refrigerant cycle reversal induces refrigerant charge and oil migration issues, as well as requiring the heat exchangers to act as both condensers and evaporators depending on the operating mode. This dual usage of the heat exchanger makes heat exchanger design more difficult because performance trade-offs must be made so that the heat exchangers perform adequately in both operating configurations rather than optimizing each for a single application.

It is expected that the CFL system will increase cold-weather EDV range by minimizing electrical resistance heating of the cabin through recovery of PEEM waste heat and heat pump operation. Minimizing the area and number of heat exchangers at the front end of the vehicle has the potential to reduce the aerodynamic drag. An additional benefit of combining cooling loops is that the ESS, passenger compartment, and thermal management fluid loops can be preconditioned when the vehicle is connected to grid power.

Approach

Feasibility Study

Using component bench data, National Renewable Energy Laboratory (NREL) researchers conducted an initial feasibility study to predict CFL thermal performance through software simulation. The key results of this study were that the ESS and PEEM thermal demands could be met using a combined approach without significant impact on cabin conditioning [5]. This is an important finding because CFL technology must be capable of maintaining the PEEM component temperatures below the required limits using the hot coolant circuit instead of the cold coolant circuit, which would have a large negative impact on cabin cooling capacity. After determining feasibility through simulation, an experimental bench test system was constructed using available prototype components to validate the simulation findings and measure thermal system performance for cooling and heating conditions. Although sufficient for bench testing, it is expected that the prototype components could be further optimized for improved system capacity and efficiency.

Bench Test Apparatus

To perform the experimental study, a bench test apparatus capable of evaluating the steady-state and transient performance of EDV thermal systems was constructed. The purpose of the test apparatus is to measure the impact of the CFL technology on EDV range. The test apparatus is a hardware-in-the-loop system that imposes actual thermal loads on the experimental system and measures the resulting energy consumption and thermal performance. To impose realistic EDV loads on the thermal system, the test bench incorporates a vehicle powertrain model, thermal and efficiency PEEM and ESS models, and a thermal cabin model. The model-based portions of the bench test apparatus are adapted into a control and data acquisition LabVIEW program for continuous feedback based on thermal system performance. The vehicle powertrain model is a LabVIEW adaptation of NREL's power-based FASTSim model [6], the PEEM and ESS models are based on the previous NREL CFL simulation work [5], and the cabin model is from prior work by Gado [7]. The PEEM, ESS, and cabin models are all lumped capacitance physics-based models. Some of the basic parameters of the models are given in Table III-17.

Table III-17: Selection of basic model inputs

Vehicle type	Mid-sized battery electric vehicle
Battery capacity	24 kWh
Usable state of charge range	90%
Maximum powertrain power	80 kW
ESS mass (including housing)	348 kg

The physical bench test apparatus consists of two separate air ducts, a cabin air simulator, and an outdoor air simulator, as shown schematically in Figure III-77. The cabin air simulator recreates the conditions seen inside of the heating, ventilation, and air-conditioning (HVAC) module in the instrument panel of a vehicle, and therefore houses the experimental system's heater core and cooler core heat exchangers. It can achieve air flow rates up to 250 CFM and can simulate temperatures from -30°C to 63°C. The outdoor air simulator recreates the conditions seen by the heat exchangers at the front end of the vehicle, and therefore houses the low-temperature radiator of the experimental system. It is capable of air flow rates up to 2,000 CFM, and can simulate temperatures from -30°C to 43°C. The airflow rate is continuously scaled based on the simulated vehicle speed to capture the effect of vehicle ram air on heat exchanger performance. In order to simulate a given ambient temperature condition, the test apparatus draws in fresh air from the laboratory and heats it to the control temperature. The bench test apparatus is not capable of actively cooling the intake airstream, and therefore must always be operated in an environment which is at a lower temperature than the simulated ambient temperature.

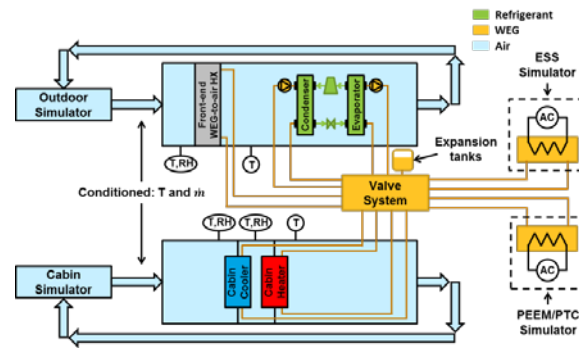


Figure III-77: Basic schematic of CFL bench test apparatus

The bench test apparatus has two electrical resistance coolant heaters; one to simulate the heat from the vehicle PEEM and supplemental heat from the Positive Temperature Coefficient (PTC) electrical resistance heater; and the other to simulate the heat from the hot-soaked ESS. The ESS simulator also has a coolant-to-air heat exchanger that can reject heat to the ambient laboratory air when simulating the thermal load of a cold-soaked ESS. The coolant outlet conditions from the PEEM and ESS components were predicted with the software models for a virtual vehicle and imposed on the actual experimental system with the coolant heaters. In the model, the full coolant mass flow rate passes through the PE before subsequently passing through the EM; however, this is imposed on the experimental system as a single coolant load. A picture of the assembled bench test apparatus is shown in Figure III-78.



Figure III-78: CFL bench test apparatus

Experimental CFL System

The experimental CFL system was constructed with six heat exchangers and a thermostatic expansion valve (TEV) provided by Delphi. The heat exchangers included a production radiator as the front-end low-temperature radiator, a production heater core, a prototype cooler core that was a coolant-to-air heat exchanger used to cool the cabin, a prototype plate-type evaporator, a prototype plate-type condenser, and a prototype plate-type sub-cooler. To complete the system a prototype electric automotive compressor was provided by Halla Visteon Climate Control. The electric automotive compressor was powered with a high-voltage direct current (DC) power supply that simulated the power provided by an EDV traction battery pack. The compressor was a variable speed scroll-type, and the refrigerant used was R-134a. The refrigerant system components are shown in Figure III-79.

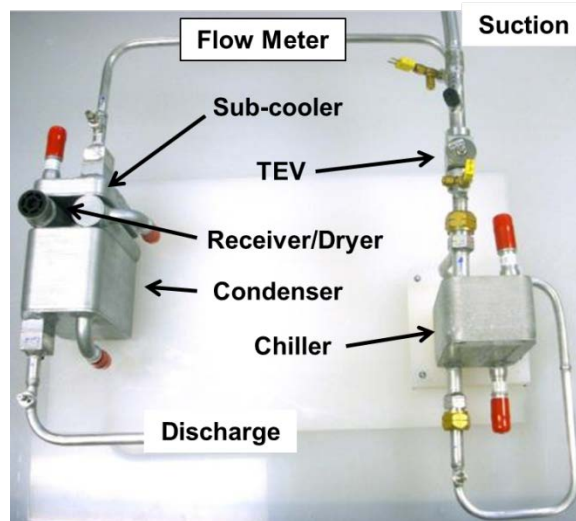


Figure III-79: Delphi prototype refrigerant system components

The flow path of the refrigerant system was configured so that low-temperature, low-pressure vapor is compressed by the compressor to a high-temperature, high-pressure vapor. The refrigerant vapor then passes through the condenser where it rejects heat and condenses to a high pressure liquid, before passing through the sub-cooler where further heat is rejected to achieve a sub-cooled liquid. The liquid is then expanded through a TEV to a low-pressure, low-temperature two-phase refrigerant that is passed through the evaporator to absorb heat and vaporize the remaining liquid. The low-temperature, low-pressure vapor then completes the circuit back to the compressor.

The experimental system used a 50%/50% mixture of water and ethylene glycol by weight as the coolant working fluid. The coolant circuit was formed with $\frac{3}{4}$ in. inner diameter automotive radiator hose, with two automotive 12 V DC electric coolant pumps that separately pumped the hot and cold fluids. The coolant pumps were operated at full speed for all test conditions and consumed approximately 60 watts each. Laboratory-grade ball valves were used to control the circuit flow paths and to provide variable bypass capability of the heat exchangers. The experimental system piping and valving arrangement was designed to allow maximum flexibility for experimental bench testing, and is not representative of the configuration expected for in-vehicle applications. A schematic of the fully assembled experimental system is shown in Figure III-80.

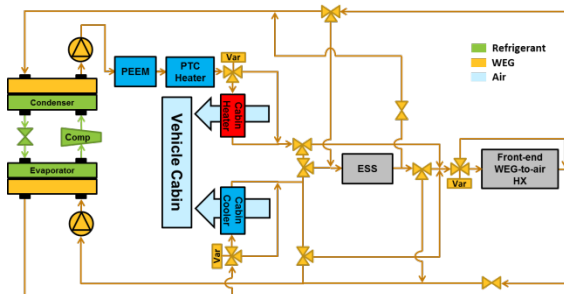


Figure III-80: Schematic of full experimental CFL system

The experimental CFL system piping and valving design allows for a number of test configurations, including cooling of the PEEM and ESS systems when the compressor is deactivated by using the ambient air as a heat sink via the front-end heat exchanger. For the purposes of this study, there are two main configurations of interest that can be used to judge the energy efficiency of the system—cooling mode and heating mode. In the cooling mode configuration, the hot-side coolant sequentially absorbs heat from the condenser, absorbs heat from the PEEM systems, rejects heat through the front-end heat exchanger, and finally completes the hot circuit back to the condenser. On the cold-circuit side, the coolant sequentially rejects heat to the evaporator, absorbs heat from the cabin, absorbs heat from the ESS, and completes the cold circuit back to the evaporator. This configuration enables cabin air-conditioning (A/C), cooling of the PEEM system using the hot coolant

instead of the actively cooled cold coolant, and active cooling of the ESS. A schematic demonstrating the coolant flow paths for cooling mode is shown in Figure III-81.

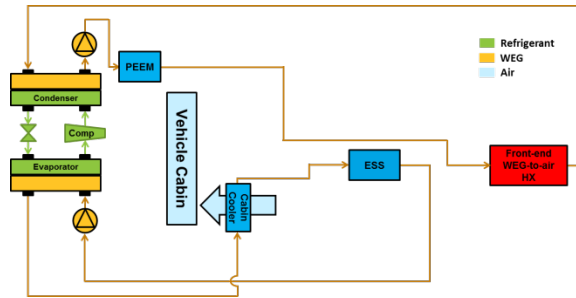


Figure III-81: Schematic of experimental CFL system cooling mode

For heating mode, the hot-side coolant sequentially absorbs heat from the condenser, absorbs heat from the PEEM systems, absorbs heat from the supplemental PTC heater (when operating), rejects heat to the cabin, rejects heat to the ESS, and finally completes the hot-circuit back to the condenser. On the cold-circuit side, the coolant rejects heat to the evaporator, absorbs heat from the front-end heat exchanger, and finally completes the cold-circuit back to the

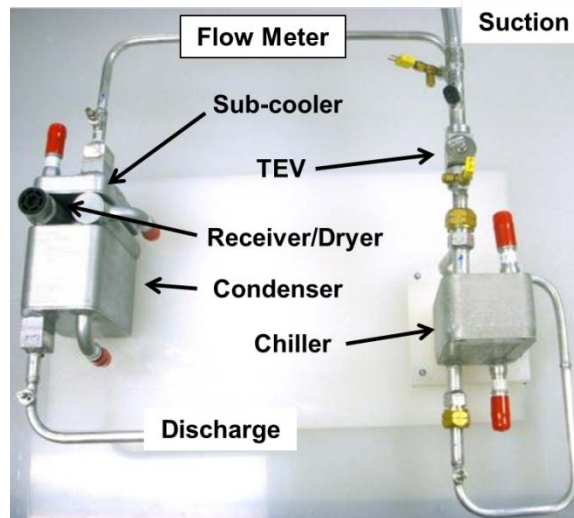


Figure III-82: Delphi prototype refrigerant system components

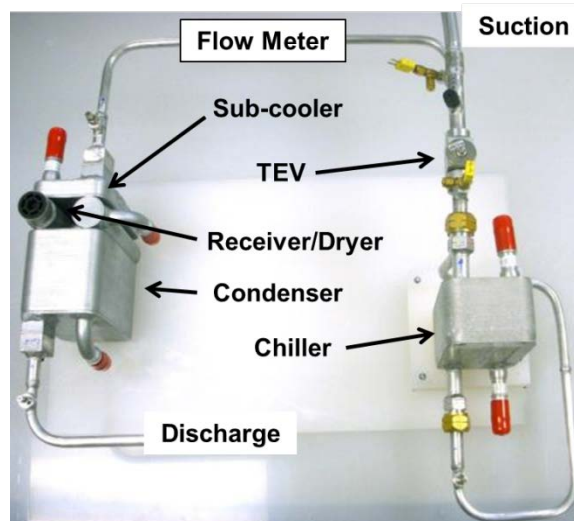


Figure III-83: Delphi prototype refrigerant system components

The flow path of the refrigerant system was configured so that low-temperature, low-pressure vapor is compressed by the compressor to a high-temperature, high-pressure vapor. The refrigerant vapor then passes through the condenser where it rejects heat and condenses to a high pressure liquid, before passing through the sub-cooler where further heat is rejected to achieve a sub-cooled liquid. The liquid is then expanded through a TEV to a low-pressure, low-temperature two-phase refrigerant that is passed through the evaporator to absorb heat and vaporize the remaining liquid. The low-temperature, low-pressure vapor then completes the circuit back to the compressor.

The experimental system used a 50%/50% mixture of water and ethylene glycol by weight as the coolant working fluid. The coolant circuit was formed with 3/4 in. inner diameter automotive radiator hose, with two automotive 12 V DC electric coolant pumps that separately pumped the hot and cold fluids. The coolant pumps were operated at full speed for all test conditions and consumed approximately 60 watts each. Laboratory-grade ball valves were used to control the circuit flow paths and to provide variable bypass capability of the heat exchangers. The experimental system piping and valving arrangement was designed to allow maximum flexibility for experimental bench testing, and is not representative of the configuration expected for in-vehicle applications. A schematic of the fully assembled experimental system is shown in Figure III-84.

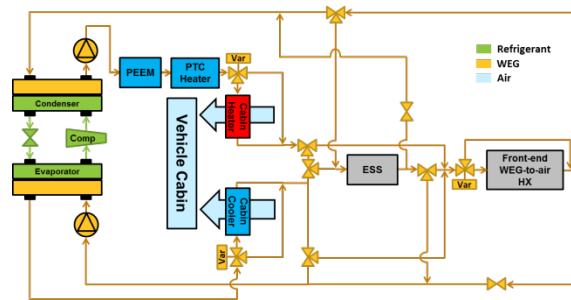


Figure III-84: Schematic of full experimental CFL system

The experimental CFL system piping and valving design allows for a number of test configurations, including cooling of the PEEM and ESS systems when the compressor is deactivated by using the ambient air as a heat sink via the front-end heat exchanger. For the purposes of this study, there are two main configurations of interest that can be used to judge the energy efficiency of the system—cooling mode and heating mode. In the cooling mode configuration, the hot-side coolant sequentially absorbs heat from the condenser, absorbs heat from the PEEM systems, rejects heat through the front-end heat exchanger, and finally completes the hot circuit back to the condenser. On the cold-circuit side, the coolant sequentially rejects heat to the evaporator, absorbs heat from the cabin, absorbs heat from the ESS, and completes the cold circuit back to the evaporator. This configuration enables cabin air-conditioning (A/C), cooling of the PEEM system using the hot coolant instead of the actively cooled cold coolant, and active cooling of the ESS. A schematic demonstrating the coolant flow paths for cooling mode is shown in Figure III-85.

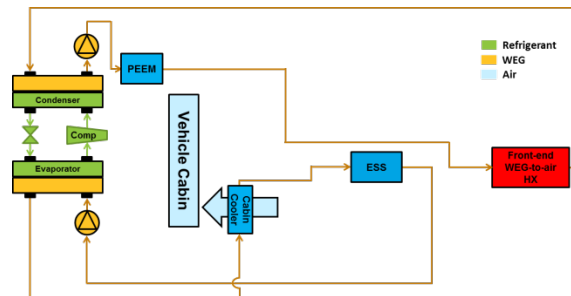


Figure III-85: Schematic of experimental CFL system cooling mode

For heating mode, the hot-side coolant sequentially absorbs heat from the condenser, absorbs heat from the PEEM systems, absorbs heat from the supplemental PTC heater (when operating), rejects heat to the cabin, rejects heat to the ESS, and finally completes the hot-circuit back to the condenser. On the cold-circuit side, the coolant rejects heat to the evaporator, absorbs heat from the front-end heat exchanger, and finally completes the cold-circuit back to the evaporator. This configuration enables PEEM waste heat recovery, cabin

heating, and active ESS heating. A schematic demonstrating the coolant flow paths for heating mode is shown in Figure III-86.

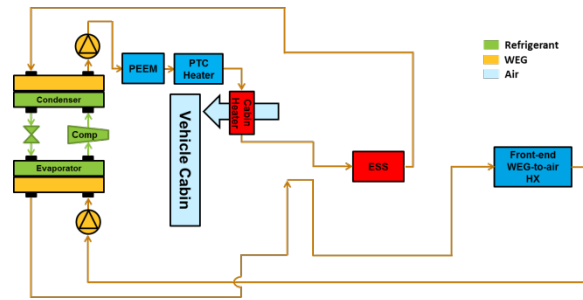


Figure III-86: Schematic of experimental CFL system heating mode

System Controls and Testing Metrics

The experimental CFL system and test apparatus were controlled using software PID control loops as well as simple thermostats programmed into the LabVIEW data acquisition and control program. There are two sets of controls: the test apparatus controls used to stabilize the thermal inputs into the system such as inlet air temperatures, and the CFL system controls that mimic automatic vehicle climate control. Depending on the ambient temperature, the system controls entered into either heating or cooling mode, with separate control algorithms for each. The CFL system controls that mimic automatic vehicle climate control were designed to be as simple and repeatable as possible. The degrees of freedom for these controls included compressor speed, cabin blower speed, supplemental PTC heating power, and on/off coolant flow to the ESS, as shown in Table III-18. Controlled variables included cabin air temperature, cabin vent temperature, and ESS temperature.

Table III-18: Control parameters

Variable	Lower Limit	Upper Limit
Compressor	10%	100%
Cabin blower	50 CFM	250 CFM
PTC heater	0 kW	6 kW
ESS coolant flow	0%	10%

The cabin air “comfort” control point was set to 25°C for both the heating and cooling cases. In cooling mode, frosting of the cooler core air-side is a key constraint. To prevent frost accumulation, the cabin vent air temperature is set to 3°C, which is maintained by varying the compressor speed. This is analogous to conventional belt-driven automotive HVAC systems that use compressor on/off clutch cycling or variable displacement to prevent frosting. Cabin blower speed is used to control the cabin air temperature to the set point, which means that the blower operates at maximum speed during the transient pull-down of the hot cabin and then reduces speed as the set point is reached. When the vehicle cabin air set point is reached, the cabin blower speed drops, which reduces the air-side capacity of the cooling system and therefore causes a compressor speed reduction to maintain the cabin vent set point. The cabin recirculation damper control is configured so that the inlet air temperature to the cabin cooler core is set to the equivalent of 100%/0% outside/recirculated air when the cabin air temperature is above the ambient temperature and 15%/85% outside/recirculated air when the cabin air temperature is below ambient temperature. In summary, these controls result in a system that maximizes cooling for the hot-soaked vehicle until it is pulled-down to the comfort temperature, and then minimizes energy consumption of the system to maintain cabin comfort.

Frost prevention control of the cooler core is no longer applicable in heating mode. Instead, compressor speed is used to control the cabin vent temperature to 50°C to simulate realistic vehicle HVAC performance. Cabin blower speed is still used to control the cabin air temperature at the 25°C comfort set point. Testing demonstrated that based on the compressor capacity of the experimental system, the warm-up performance of

the heat pump alone is insufficient for ambient temperature test conditions at or below 8°C, and that supplemental electrical resistance PTC heating is needed. The simulated PTC heater is set to control the cabin vent temperature to 49.5°C when the ambient temperature is below 8°C, and has a maximum design capacity of 6 kW. In practical terms, this control strategy means that in very cold ambient temperatures, the heat pump and PTC heater will simultaneously operate at maximum capacity until the vent outlet set point is approached, at which point the PTC capacity will be reduced to zero before the compressor speed begins reducing to maintain the 50°C set point. As the cabin temperature set point is approached the blower speed will reduce, which will lower the heating capacity required to maintain the 50°C vent outlet set point. In extremely cold conditions, the heat pump capacity is low and the heating load of the cabin is high, necessitating the continuous operation of the supplemental PTC heater at partial capacity in addition to the compressor at full speed to maintain cabin comfort. The cabin heater core inlet air temperature recirculation damper control is set to 15%/85% outside/recirculated air for the entire duration of all of the heating mode tests. clutch cycling or variable displacement to prevent frosting. Cabin blower speed is used to control the cabin air temperature to the set point, which means that the blower operates at maximum speed during the transient pull-down of the hot cabin and then reduces speed as the set point is reached. When the vehicle cabin air set point is reached, the cabin blower speed drops, which reduces the air-side capacity of the cooling system and therefore causes a compressor speed reduction to maintain the cabin vent set point. The cabin recirculation damper control is configured so that the inlet air temperature to the cabin cooler core is set to the equivalent of 100%/0% outside/recirculated air when the cabin air temperature is above the ambient temperature and 15%/85% outside/recirculated air when the cabin air temperature is below ambient temperature. In summary, these controls result in a system that maximizes cooling for the hot-soaked vehicle until it is pulled-down to the comfort temperature, and then minimizes energy consumption of the system to maintain cabin comfort.

Frost prevention control of the cooler core is no longer applicable in heating mode. Instead, compressor speed is used to control the cabin vent temperature to 50°C to simulate realistic vehicle HVAC performance. Cabin blower speed is still used to control the cabin air temperature at the 25°C comfort set point. Testing demonstrated that based on the compressor capacity of the experimental system, the warm-up performance of the heat pump alone is insufficient for ambient temperature test conditions at or below 8°C, and that supplemental electrical resistance PTC heating is needed. The simulated PTC heater is set to control the cabin vent temperature to 49.5°C when the ambient temperature is below 8°C, and has a maximum design capacity of 6 kW. In practical terms, this control strategy means that in very cold ambient temperatures, the heat pump and PTC heater will simultaneously operate at maximum capacity until the vent outlet set point is approached, at which point the PTC capacity will be reduced to zero before the compressor speed begins reducing to maintain the 50°C set point. As the cabin temperature set point is approached the blower speed will reduce, which will lower the heating capacity required to maintain the 50°C vent outlet set point. In extremely cold conditions, the heat pump capacity is low and the heating load of the cabin is high, necessitating the continuous operation of the supplemental PTC heater at partial capacity in addition to the compressor at full speed to maintain cabin comfort. The cabin heater core inlet air temperature recirculation damper control is set to 15%/85% outside/recirculated air for the entire duration of all of the heating mode tests.

When active cooling of the ESS was needed for hot ambient conditions, a simple on/off coolant flow control thermostat was used. This controller allowed 10% of the total WEG coolant mass flow to pass through the ESS when in the “on” configuration. It was desirable to maintain the ESS temperature between 15°C and 35°C; therefore the cooling mode thermostat was set to 32.5°C with a 2.5°C band. This thermostat control allowed the ESS to be conditioned to the desired upper temperature limit for longevity, but minimized the load on the compressor to maximize vehicle range. The thermal mass of the ESS was large enough so that the cycle time of the thermostat due to self-heating of the battery under load was long. In fact, after initial cool-down of the battery the thermostat did not cycle back on within the durations of the drive cycles tested. When active heating of the ESS was required to maintain adequate power output performance, the thermostat was set to heat with 10% coolant flow until the ESS temperature was above 15°C. After being warmed to 15°C, self-heating of the ESS under load maintained the temperature for the remainder of the drive cycles tested. Because the battery model was a lumped-capacitance model instead of a cell-level model, issues of non-uniformity among cell temperatures were not considered. The control scheme was designed to be simple and repeatable, and is therefore only representative of the potential impact of ESS thermal management. The actual impact of ESS thermal management will vary significantly depending on the vehicle implementation and control design.

To predict the impact of the CFL technology on EDV range, realistic transient test conditions need to be imposed. Transient operation is vital for accurately capturing the effects on the thermal sub-systems such as the cabin, PEEM, and ESS. This is particularly true for determining whether or not the CFL system can adequately condition the PEEM components using the hot coolant stream. In terms of energy consumption, a key aspect of transient testing is the duration of the test as this will dictate the weighted effect of the transient cabin cool-down/warm-up loads versus the steady-state cabin comfort maintaining loads.

In the United States the average commute travel time is 22.85 minutes [8]. This is a relatively short duration, which heavily weights transient cabin conditioning for hot or cold soaked vehicles. To most accurately predict the impact of the CFL system on vehicle range, it was desirable to select drive cycles that closely matched this duration. There are also significant differences in vehicle power output, and therefore PEEM and ESS thermal demands, between continuous highway driving and stop-and-go city driving. The method used to measure vehicle efficiency was a 45%/55% weighting of the Urban Dynamometer Driving Schedule

(UDDS) city cycle and the Highway Fuel Economy Test (HWFET) highway cycle. With a duration of 22.9 minutes, the UDDS cycle almost exactly matches the average commute travel time. When the HWFET cycle is doubled by running two full cycles back-to-back, the total duration is 25.5 minutes, which is sufficiently close to the average commute. A plot of vehicle speed versus time for the two drive cycles used is shown in Figure III-87.

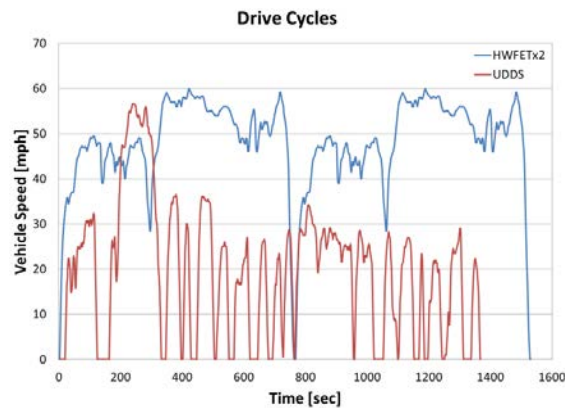


Figure III-87: Drive cycle profiles for UDDS and double HWFET

Results

Cooling

Cooling mode in the experimental investigation is considered to be the simulated ambient temperature test conditions from 23°C to 43°C in increments of 5°C. In addition to the heat transfer between the ambient air and cabin air calculated by the cabin model, all of the cooling mode tests also included a 1 kW solar load imposed on the cabin air to simulate high, but realistic solar loading of a south-facing mid-sized vehicle. All of the test conditions also included a single passenger, which is simulated as a 100 W internal cabin load. “Soak” test cases simulated a cabin that was hot soaked in the sun while facing south on a clear solar day. The simple input parameter is that the average cabin air and average interior mass temperatures were uniformly 20°C above the ambient temperature at the start of all soak test cases, a realistic value based on experimental vehicle testing results. The coolant and refrigerant system temperatures started at the ambient temperatures for the soak cases rather than the elevated soaked cabin temperature. The soak test cases were used to measure the impact of hot soaking the vehicle on the CFL system performance and subsequently the vehicle range. The humidity of the air in the test apparatus was low enough so that the cooler core did not accumulate water vapor condensation under any of the test conditions.

One of the major findings of the cooling mode testing was that the PEEM component temperatures were kept well within the 150°C limitation for all of the ambient temperatures tested when using the hot coolant stream

to remove PEEM waste heat. The maximum instantaneous temperature observed during any of the cooling mode conditions tested was less than 100°C for the PE and 90°C for the EM. An example of this is shown in Figure III-88 for a double HWFET drive cycle at an ambient temperature of 38°C.

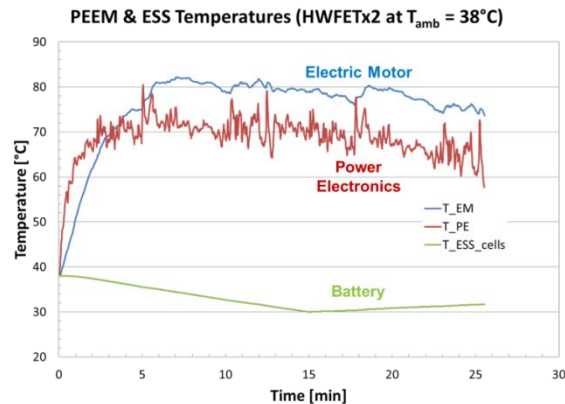


Figure III-88: Component temperatures for cooling mode, double HWFET cycle, $T_{amb} = 38^{\circ}\text{C}$, no soak, PEEM and ESS cooling case

The data demonstrate the rapidly fluctuating PE temperature due to its relatively low thermal mass, which necessitates continuous cooling to avoid rapidly exceeding its thermal limits. The EM temperature fluctuates more slowly than the PE because of the larger thermal mass, but the transient nature of the drive cycle powertrain system load can still be observed. The ESS has a very large thermal mass; because of this, it is apparent that the average ESS temperature is independent of the changing power load and is more closely related to the cooling capacity and starting temperature. This indicates that the ESS is the component that would benefit most from thermal pre-conditioning. Approximately 15 minutes into the drive cycle, the ESS thermostat control cycles off the coolant flow to the ESS. The effect of removing the ESS thermal load from the cooling system can be observed in the cabin cooling rate as demonstrated in Figure III-89 for the same test.

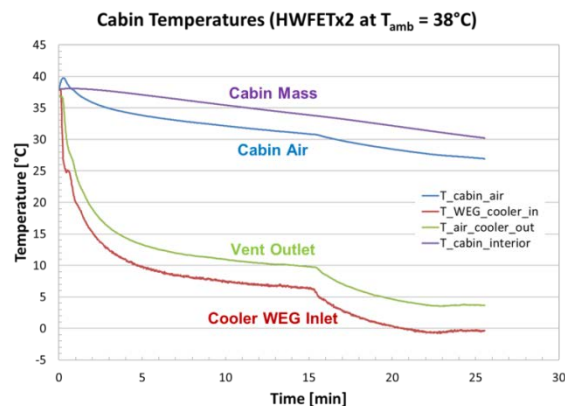


Figure III-89: Cabin temperatures for cooling mode, double HWFET cycle, $T_{amb} = 38^{\circ}\text{C}$, no soak, PEEM and ESS cooling case

At the beginning of the test, it can be observed that the cabin and cooling system started at an initial temperature equal to the ambient temperature, and then began to cool down when the compressor started. The slight increase in cabin air temperature at the start was due to the sudden solar load on the non-solar soaked vehicle. Essentially this is representing the cabin behavior if the vehicle was parked in the shade and then driven into the direct sun at time zero of the drive cycle. The air temperature increases because the solar load exceeds the A/C cooling capacity for the first 30 seconds of the test. When the ESS thermostat control turns the coolant flow off after 15 minutes, the compressor cooling capacity is able to control the vent outlet temperature to 3°C, which maximizes the rate of cabin cooling.

An observation of the experimental testing is that the experimental system thermal mass was larger than a realistic implementation of an in-vehicle system. This is due to the larger number of laboratory-grade valves,

additional piping and WEG coolant, sensors, and other thermally massive components necessary for experimental testing. The consequence of the larger thermal mass is that the cooling system capacity to the cabin is lower than it would be in an actual vehicle system, resulting in a longer cool-down period, which requires additional compressor energy consumption. This was deemed acceptable for the purposes of concept bench testing, but it is expected that an actual vehicle system would have superior performance and energy efficiency.

Eight drive cycle tests were conducted for each cooling mode ambient temperature, with four unique test configurations that were each tested with the UDDS and double HWFET drive cycles. The first test quantified the energy consumption of operating just the A/C system without conditioning the PEEM or ESS systems, shown as the “A/C Penalty” in Figure III-90. This represented the performance of a secondary loop A/C system that does not utilize the CFL integration technology. The second test included PEEM cooling to measure the impact on A/C performance. The third test added ESS cooling to the PEEM cooling, to measure the energy consumption of using active ESS cooling. The final test included all of the above conditions in addition to a hot-soaked cabin to measure the sensitivity of the system performance to initial cabin temperature. The total possible range of the vehicle if the A/C, ESS cooling, and PEEM cooling were not operated is represented by the summation of the data bars for a given ambient temperature in Figure III-90.

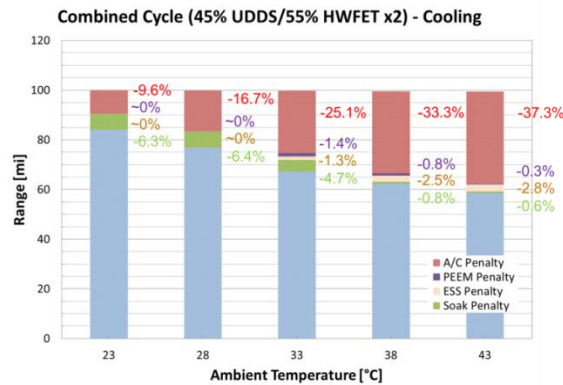


Figure III-90: Summary of combined drive cycle cooling results for vehicle range

As expected, the cabin A/C energy consumption, or “A/C Penalty” increased with increasing ambient temperature. This reflects the additional compressor power required for higher condenser pressures at higher ambient temperatures as well as the longer runtimes of the compressor at maximum speed during higher temperature cabin cool-downs. The vehicle range loss due to cabin A/C varies from 9.6% for mild cooling to 37.3% at the highest ambient temperatures. The additional load of PEEM cooling on the CFL system was negligible for ambient temperatures of 28°C or less. For higher temperatures, the maximum range loss due to PEEM cooling is only 1.4%, and is less than 1% at the highest ambient temperatures. This loss is due to the slightly increased condenser pressure due to the elevated temperature of the hot coolant loop. ESS cooling was only activated by the thermostat control systems at the tested ambient temperatures of 33°C and above and therefore had no impact on range at lower temperatures. The range loss due to ESS conditioning increased with increasing ambient temperature up to 2.8% at the highest ambient temperatures. This is a moderate impact on range, but necessary in order to condition the ESS for longevity.

The impact of a hot-soaked cabin on the A/C energy consumption is significant due to the longer period of full speed compressor operation required for cool-down to cabin comfort. The reduction in vehicle range is as high as 6.4% for ambient temperatures below 38°C. For the 38°C and 43°C cases, the effect is less than 1% due to the control strategy and system sizing. For cases below 38°C, the cabin temperature reaches the 25°C set point within the duration of the drive cycle, but in the hotter ambient temperature cases without soak the cabin never reaches cabin comfort within the drive cycle duration, as demonstrated in Figure III-89. The consequence of this is that there is not a significant difference in energy consumption when compared with the soaked case because the compressor operates at maximum speed for the entire duration of both cases. The small increase in energy consumption of the soaked case is because of the slightly higher average cabin cooler inlet air temperature. The higher average inlet temperature is due to the recirculation mode control engaging later in the drive cycle because it takes longer for the cabin air temperature to drop below the ambient temperature.

Heating

Heating mode for the experimental investigation is considered to be the simulated ambient temperature test conditions below 23°C in increments of 5°C. All of the test conditions still included a single passenger, which is simulated with a 100 W internal cabin load. The heating mode tests assume zero solar loading on the cabin to simulate a severe heating case. “Soak” test cases were not conducted, and the cabin air, cabin mass, coolant, and refrigerant system temperatures were set to the ambient temperature at the start of the tests. The cabin air remained in recirculation mode (85% recirculation/15% fresh) for the entire drive cycles. Supplemental PTC heating was used for ambient temperatures of 8°C or lower. The humidity of the air in the test apparatus was low enough so that the front-end low-temperature radiator did not accumulate frost under any of the test conditions.

One of the major findings of the heating mode testing was that the PEEM component temperatures were kept well within the 150°C limitation for all of the ambient temperatures tested when using the hot coolant stream to recover PEEM waste heat. The maximum instantaneous temperature observed during any of the heating mode conditions tested was less than 80°C for the PEEM components. Examples of the component and cabin temperatures for a UDDS drive cycle at an ambient temperature of -2°C are shown in Figure III-91 and Figure III-92, respectively.

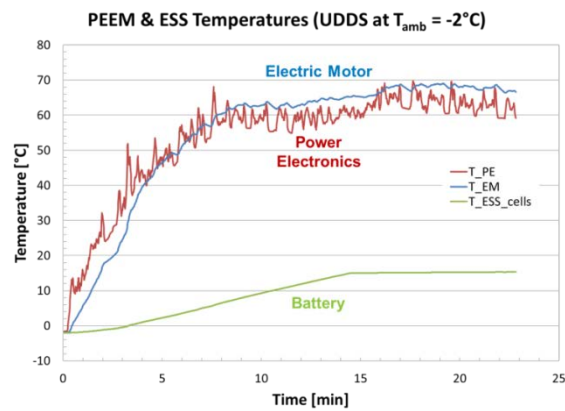


Figure III-91: Component temperatures for heating mode, UDDS cycle, $T_{amb} = -2^{\circ}\text{C}$, PEEM and ESS conditioning case

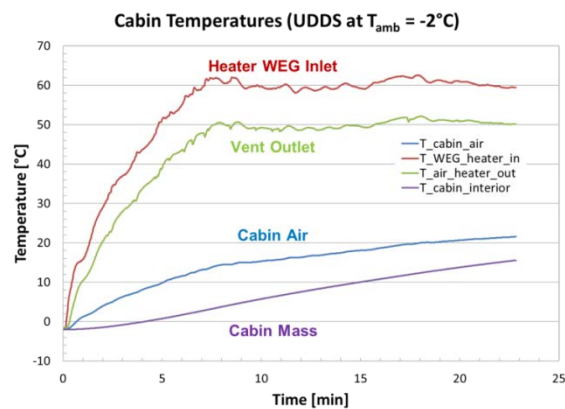


Figure III-92: Cabin temperatures for heating mode, UDDS cycle, $T_{amb} = -2^{\circ}\text{C}$, PEEM and ESS conditioning case

It is apparent that the warm-up rate of the hot-side coolant at the heater core inlet and the PEEM components is similar. This is an expected result, as they are thermally linked by the hot coolant loop. For the first 3.5 minutes of the drive cycle, the EM does not contribute waste heat for cabin heating as the initial waste heat is used to self-heat the thermal mass of the motor. The thermal mass of the PE is small enough so that it contributes waste heat at the start of the cycle. After the target vent outlet air temperature control point is reached after 7.5 minutes the supplemental PTC heating is reduced. Another notable result is that the ESS is actively heated until 14 minutes into the drive cycle when it reaches its 15°C control point. Once the

thermostat control system deactivates active ESS heating, the ESS self-heats slightly during the remainder of the drive cycle. A consequence of the ESS thermostat cycling off is that the total required heating load decreases, which reduces the supplemental PTC heating to zero and allows a reduction in the compressor speed control. This effect is shown in Figure III-93.

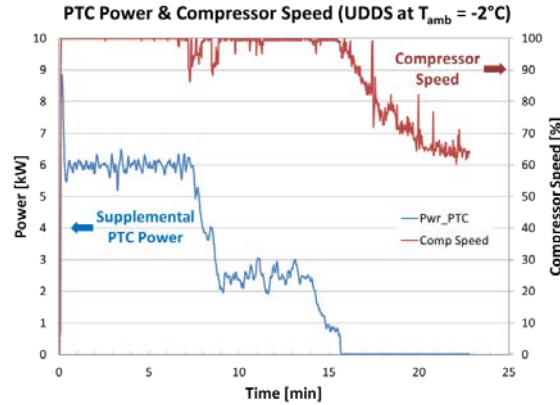


Figure III-93: Supplemental PTC heating power and compressor speed for heating mode, UDDS cycle, Tamb = -2°C, PEEM and ESS conditioning case

Four drive cycle tests were conducted for each heating mode ambient temperature, with two unique test configurations that were each tested with the UDDS and double HWFET drive cycles. The first test consisted of heating the cabin and ESS using the heat pump system without PEEM waste heat recovery, shown as the “HP” case in Figure III-94. From this test, the equivalent thermal performance of a PTC-based heating system was derived by assuming a 100% efficient PTC heater that output the same heating capacity as the heat pump system. This was done to ensure that the warm-up performance of the baseline PTC heating case matched the heat pump case, and so that the energy consumption of the PTC heating case could be calculated without requiring an additional experimental test. This is shown as the “PTC Only” case in Figure III-94, and it represents the performance of a PTC coolant heater system that does not utilize the CFL integration technology, but does provide active ESS heating. The second test added PEEM waste heat recovery to the heat pump to measure the performance of the fully integrated CFL system. The total possible range of the vehicle if the cabin heating, ESS heating, and PEEM waste heat recovery were not operated is represented by the summation of the data bars for a given ambient temperature in Figure III-94.

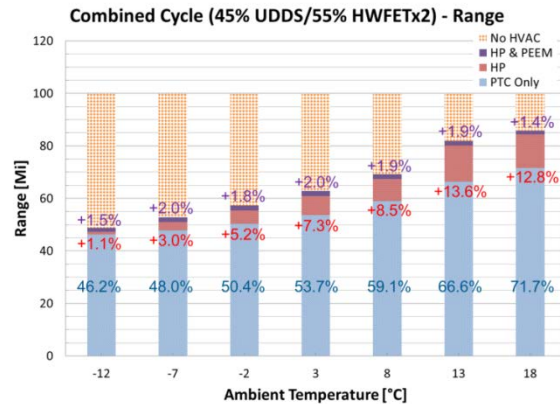


Figure III-94: Summary of combined drive cycle heating results for vehicle range

As expected, the vehicle range decreased with decreasing temperature because the heating system energy consumption increases as the temperature decreases. This is predominantly due to the increasing transient and steady-state vehicle heating loads. For PTC-only heating, the vehicle range loss varies from 28.3% at an ambient temperature of 18°C, to 53.8% at an ambient temperature of -12°C. When operating the heat pump system, the recovered vehicle range varies from 12.8% at 18°C down to only 1.1% at -12°C. This shows that the heat pump system provides a very large energy efficiency benefit for mild heating conditions, but becomes

ineffective at extremely low temperatures. This is due to the decreasing performance of the heat pump as the suction pressure decreases with decreasing ambient temperature. One possible way to improve the low temperature performance would be to use a larger capacity compressor to offset more of the supplemental PTC heating. Under all of the tested conditions, the PEEM waste heat recovery benefit to vehicle range was around 1.5% to 2%. This is a moderate benefit when compared with the heat pump at mild temperatures, but it remains relatively consistent even at the lowest temperatures, making it a valuable contribution. An in-vehicle application of the CFL technology would have a significantly lower thermal mass on the coolant side compared with the experimental system. This would be achieved through a reduction in pipe length, number of valves and sensors, and coolant volume, which would improve cold weather performance by decreasing the supplemental PTC heating needed during warm-up.

One of the important findings of the cold weather testing is that the heat pump system only operated down to a minimum temperature of -12°C. For ambient temperatures colder than -12°C, the suction pressure was below atmospheric pressure, creating possible issues of air entrainment in the refrigerant cycle. At this low ambient temperature the heating capacity of the heat pump system is reduced to a point at which the benefit is approaching zero. For an in-vehicle application, vehicle usage at extreme low temperatures (below -12°C) would necessitate using only the supplemental PTC heater as a source for cabin and ESS heating. PEEM waste heat recovery could still be applied at these extremely low temperature conditions, although the benefit will be reduced due to the cold-soaked EM mass at the start of the drive cycle. One way to improve the extreme cold weather performance would be to switch from a TEV to an electronic expansion valve (EEV). Due to the physics of a TEV, it is difficult to design a valve that is capable of maintaining the desired 5°C of superheating at a wide range of suction pressures that include A/C and heat pump mode. The experimental bench testing showed that the TEV superheat can approach 10°C during operation at an ambient temperature of -12°C. This causes the suction pressure to be lower than desired, which decreases the performance of the compressor. An EEV can be software-tuned so that it does not have this limitation.

Annual Weighting

To accurately predict the impact of the CFL system technology on EDV range at a national level, the measured performance needed to be compared to real world usage data. A study conducted by Duthie took into account the national geographical population distribution, temporal usage data, and weather conditions for light-duty vehicles in the United States [9]. These data were used to weight vehicle usage versus ambient temperature to determine the weighted average effects of CFL system efficiency at various temperatures. Percentage-based vehicle usage versus ambient temperature data are shown in Figure III-95.

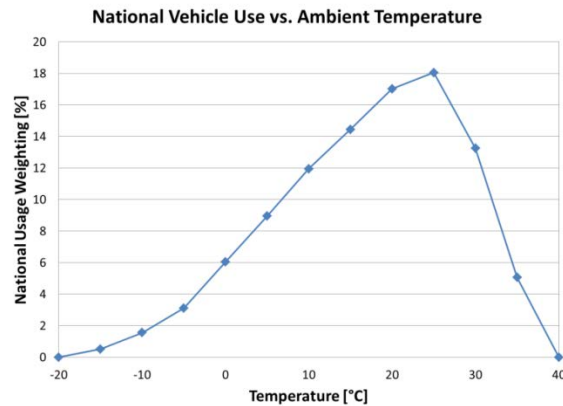


Figure III-95: National vehicle use weighting for ambient temperature

It is apparent from the usage data that the majority (>80%) of driving is done in moderate climate conditions, from 5°C to 30°C. The usage data also show that the extreme hot case tested at 43°C represents a very small fraction of the population. Testing revealed that the CFL heat pump operation could not extend below -12°C, but the weighted data extends to -20°C. To account for this extreme cold weather usage it was assumed that the heat pump would be deactivated for conditions colder than -12°C and instead the supplemental PTC heating would provide 100% of the heating capacity. These assumptions were used to extrapolate system performance

down to -20°C. The error introduced on the final result by the extrapolation is negligible because the usage weighting at these temperatures is on the order of 1%.

To compare the CFL system to the standard secondary loop system used as a baseline, the data from Figure III-90 and Figure III-94 were combined to represent the performance for the entire tested temperature range. The baseline system represents A/C only in cooling mode, meaning that PEEM and ESS cooling are not included. In heating mode, the baseline system does include ESS heating in addition to cabin heating, but does not include PEEM waste heat recovery and uses only supplemental PTC heating, not heat pumping. The CFL system includes ESS and PEEM cooling in cooling mode and PEEM waste heat recovery, ESS heating, and heat pumping in heating mode. In both the baseline and CFL system cases, vehicle cabin soak is not included. Details of the configurations are listed in Table III-19. The CFL system versus baseline system data are shown in Figure III-96.

Table III-19: CFL versus baseline configurations

Configuration	Cooling Mode	Heating Mode
Baseline System	Secondary loop A/C	PTC cabin heating PTC ESS heating
CFL System	Secondary loop A/C PEEM cooling ESS cooling	HP cabin heating HP ESS heating PEEM heat recovery

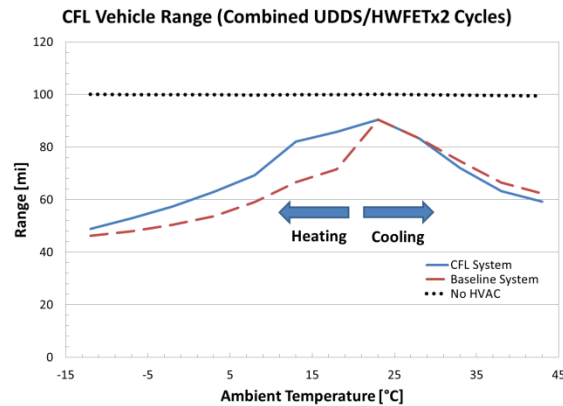


Figure III-96: CFL versus baseline system for combined drive cycle vehicle range

It is apparent that the majority of the energy efficiency benefit of the CFL technology occurs in mild to moderate heating mode conditions. This is where the maximum benefit of the heat pump and PEEM waste heat recovery occurs. Another significant finding is that the CFL technology has little negative impact for mild cooling conditions up to 33°C. This is important to note because on a national level this is where the majority of cooling mode driving occurs and the moderate range loss at the extreme hot conditions have only a minor impact. It is also important to note that this is a comparison of the CFL technology with active ESS cooling to a baseline system without active ESS cooling, which is a conservative assumption because many EDVs already include active ESS cooling. This is critical because the energy consumption for active ESS cooling is the main source of range loss at the highest ambient temperatures, but that is where it is the most critical to ensuring battery cell longevity. If the CFL technology was compared to a baseline system that also included active battery cooling, the performance difference would be minor.

When the national vehicle usage weighting was applied to the entire data set, it was found that the predicted vehicle range for the baseline case was 71.4 miles, and the predicted range for the CFL system was 77.8 miles. This is a 9.0% increase in predicted vehicle range at a national level. As a note of comparison the predicted vehicle range without using any thermal management system is 99.9 miles (not accounting for powertrain frictional loss or battery energy storage dependence on temperature). This means that the CFL system is

recovering 22.5% of the range that is lost due to operating the baseline system, i.e., it is 22.5% more efficient than the baseline system.

Conclusions

Experimental bench testing of the CFL technology has demonstrated both the feasibility of the approach and energy savings at a national level. The PEEM and ESS thermal demands were met by the CFL system under all of the drive cycles and ambient temperatures tested without the need for separate cooling loops. It was shown that incorporating the PEEM cooling system into the hot-side loop had only a minor negative impact on range during cooling conditions, typically below 1% and only under very hot weather conditions. During both mild-cold and extreme cold weather, the PEEM waste heat recovery increased range by around 2%. Overall, the experimental, non-optimized CFL system showed an EDV range increase of 9% when weighted for U.S. national population and annual vehicle use, a 22.5% improvement over the experimental baseline. It is expected that an in-vehicle system will be capable of exceeding this 9% range increase when the components and control strategies are optimized for the application. There are no major remaining breakthroughs needed for the technology, and the next development stage will be vehicle-level demonstration by suppliers and vehicle manufacturers. In summary, bench testing of the CFL technology verified that EDV cooling loops can be combined to reduce the weight and volume of the system while providing the necessary thermal management of EDV subsystems and increasing vehicle range at a national level.

III.6.C. Products

Presentations/Publications/Patents

1. Leighton, D., and Rugh, J. P., (2013) "Bench Testing Cooling Performance of a Combined Fluid Loop Thermal Management System for EDVs," Proceedings of the SAE Thermal Management Systems Symposium, October 22–24, 2013, Troy, MI.
2. Leighton, D., and Rugh, J. P., (2014) "EDV Range Improvement using a Combined Fluid Loop Thermal Management Strategy," Proceedings of the SAE Thermal Management Systems Symposium, September 22–24, 2014, Denver, CO.

Acknowledgements

The author would like to thank Delphi and Halla Visteon Climate Control for material and engineering support for the project. The author would also like to thank David Anderson and Lee Slezak in the Vehicle Technologies Office at the U.S. Department of Energy for sponsoring this work. Additional thanks to those at NREL who assisted with the project including: Kevin Bennion, Cory Kreutzer, and Jeff Tomerlin.

Photo credits: Figure III-78 – Daniel Leighton; Figure III-82 – Daniel Leighton

III.6.D. References

1. Rugh, John P., Pesaran, Ahmad, and Smith, Kandler, Electric Vehicle Battery Thermal Issues and Thermal Management Techniques. SAE 2011 Alternative Refrigerant and System Efficiency Symposium, Scottsdale, AZ, September 2011.
2. Bayerer, Reinhold, (2010), Advanced Packaging Yields Higher Performance and Reliability in Power Electronics. *Microelectronics Reliability*, Vol. 50, pp. 1715-1719.
3. Kamiya, Munehiro, Kawase, Yoshihiro, Kosaka, Takashi, and Matsui, Nobuyuki, Temperature Distribution Analysis of Permanent Magnet in Interior Permanent Magnet Synchronous Motor Considering PWM Carrier Harmonics, International Conference on Electrical Machines and Systems, Seoul, Korea, October 2007.
4. Lohse-Busch, Henning, Duoba, Mike, Rask, Eric, and Meyer, Mark, Advanced Powertrain Research Facility AVTA Nissan Leaf Testing and Analysis. Argonne National Laboratory Report, October 2012.

5. Rugh, John P., and Bennion, Kevin, Electric Vehicle Thermal Modeling to Assess Combined Cooling Loop Concepts. SAE 2012 Thermal Management Systems Symposium, Scottsdale, AZ, October 2012.
6. “NREL: Vehicle Systems Analysis – Future Automotive Systems Technology Simulator.” Available at nrel.gov/vehiclesandfuels/vsa/fastsim.html. Accessed: 18-Sep-2013.
7. Gado, Amr, Development of a Dynamic Test Facility for Environmental Control Systems. University of Maryland Ph.D. Dissertation, 2006.
8. Santos, Adella T., McGuckin, Nancy, Nakamoto, Hikari Y., Gray, Danielle, and Liss, Susan, Summary of Travel Trends: 2009 National Household Travel Survey. Report # FHWA-PL-11-022, U.S. Department of Transportation, June 2011.
9. Duthie, Graham S., Average Mobile A/C Customer Usage Model: Development and Recommendations. SAE Automotive Alternate Refrigerant Systems Symposium, Scottsdale, AZ, July 2002.

III.7. In-Vehicle Test Platform Evaluation of Lower-Energy Energy Storage System (LEESS) Devices

Jeffrey Gonder, Principal Investigator

National Renewable Energy Laboratory (NREL)
15013 Denver West Parkway
Golden, CO 80401
Phone: (303) 275-4462; Fax: (303) 275-3765
E-mail: Jeff.Gonder@nrel.gov

David Anderson and Lee Slezak, DOE Program Managers

Phone: (202) 287-5688, (202) 586-2335
E-mail: David.Anderson@ee.doe.gov, Lee.Slezak@ee.doe.gov

Start Date: 1/1/2012
End Date: 12/31/2015

III.7.A. Abstract

Objectives

- Evaluate performance of lower-energy energy storage system (LEESS) devices to support power-assist or “full” hybrid electric vehicles (HEVs).
 - HEVs with lower cost or better performing energy storage systems could improve their cost-versus-benefit ratio, market penetration, and aggregate fuel savings.
- Continue automobile manufacturer and supplier collaboration for conducting the project.
 - Complete installation and testing of multiple LEESS devices in the reusable HEV test bed (converted 2012 Ford Fusion Hybrid).
- Conduct LEESS performance evaluation, to include bench, on-road, and dynamometer testing at a variety of temperatures.
 - Maintain stock operating capability, enabling back to back performance comparisons of the production battery and alternative LEESS configurations.

Accomplishments

- Completed bench testing, vehicle installation, and performance evaluation of multiple LEESS devices and configurations.
 - Fiscal Year 2015 (FY15) efforts focused on testing ultracapacitor modules provided by Maxwell Technologies in multiple restricted and unrestricted energy configurations.
 - Previous testing assessed in-vehicle operation with lithium-ion capacitor (LIC) modules provided by JSR Micro in a similar range of restricted and unrestricted energy configurations.
- On-road vehicle testing demonstrated similar performance while operating on the LEESS devices when compared to the production nickel-metal-hydride (NiMH) battery pack.
 - Starting accelerations (0–60 mph) and passing accelerations (40–60 mph) showed particularly close performance.
- Dynamometer testing further revealed comparable fuel economy performance, with the LEESS configurations achieving all or most of the hybrid benefit realized by the production battery over standard test cycles.

Future Achievements

- Complete preparation, submission and publication of a final paper on the project with the Journal of Power Sources.



III.7.B. Technical Discussion

Background

Automakers have been mass producing hybrid electric vehicles (HEVs) for over 15 years, and the technology has proven to be very effective at reducing per-vehicle fuel use. However, the cost of an HEV such as the Toyota Prius or Ford Fusion Hybrid remains several thousand dollars higher than the cost of a comparable conventional vehicle, which has limited HEV market penetration. In recent years, HEV sales have accounted for less than three percent of all new car sales [1]. The battery energy storage system [2] (ESS) is one of the greatest contributors to this cost increment, so any ESS cost reductions and/or performance improvements could help improve the overall vehicle cost vs. benefit relationship, potentially leading to greater HEV market penetration and larger aggregate fuel savings.

Introduction

In recognition of this potential, the United States Advanced Battery Consortium (USABC) asked the National Renewable Energy Laboratory (NREL) several years ago to collaborate with a designated Workgroup and analyze the trade-offs between vehicle fuel economy and reductions to the historic minimum energy requirements for power-assist HEVs [3] (which were initially established in the late 1990s). NREL's analysis, together with the Workgroup's, indicated that significant fuel savings could still be delivered from an ESS with much lower energy storage than the previous targets, which prompted USABC to issue a new set of lower-energy ESS (LEESS) targets as well as issue a request for proposals to support device developers working on new technologies that could satisfy the new targets [4, 5].

Around the same time, General Motors funded NREL to evaluate an ultracapacitor (also known as an electric double layer capacitor, or EDLC) as an alternate ESS in a 42-V Saturn Vue mild hybrid. For the project, NREL worked with General Motors to modify the vehicle so that it could switch between using the production nickel-metal hydride (NiMH) battery and using the ultracapacitor [6]. The track and chassis dynamometer testing results from this mild hybrid conversion showed that the low-energy ultracapacitor configuration could perform at least as well as the stock configuration with respect to acceleration and with respect to fuel efficiency over several standard test cycles.

These results were encouraging and supported the premise that LEESS devices can be effective in automotive applications. In full or power-assist HEVs, the fuel saving potential may be even greater, but a LEESS device would be challenged to satisfy a greater number of HEV functions, with greater potential limitations caused by its lower energy content. To validate the fuel savings and performance of a full HEV platform using such a LEESS device, the U.S. Department of Energy Vehicle Technologies Office initiated a jointly funded research project through its Energy Storage and Vehicle Systems research programs. Under this project, NREL was tasked to establish a full-hybrid test platform in which alternate LEESS devices could be installed and evaluated.

Approach

To accomplish the evaluation of LEESS devices in a full HEV platform, NREL established a cooperative research and development agreement with Ford Motor Company to support the conversion of a Ford Fusion Hybrid into a test platform for evaluating different LEESS devices (in comparison with operation using the vehicle's production NiMH battery). NREL purchased the vehicle, a front wheel drive 2012 Ford Fusion Hybrid equipped with a 2.5L 156-hp gasoline engine mated to a two-speed continuously variable transmission and including 79kW AC electric motor.

The conversion involved configuring the vehicle to allow the production NiMH high voltage traction battery (HVTB) to remain in place while allowing this system to be disconnected from the vehicle. When disconnected, a replacement system made up of LEESS devices can connect to the powertrain and serve as the HVTB, supplying the vehicle with power assist during acceleration and capturing regenerative braking energy

in the same way as the production battery. Figure III-97 shows a picture of the production HVTB unit, which mounts between the rear seat and the trunk area in the Fusion Hybrid, and includes several key submodules, including the high-voltage bussed electrical center (BEC), the battery pack sensor module (BPSM), and the battery energy control module (BECM). The BEC acts as an interface between the high-voltage output of the HVTB and the vehicle's electric motor, air conditioning compressor, and direct current converter for stepping down to the 12V accessories. The BPSM measures the voltage and temperature of the HVTB's cells and communicates with the BECM, which manages the charging/discharging of the ESS and also communicates with the other vehicle control modules over the high-speed controller area network (CAN) bus.



Figure III-97. Fusion Hybrid's HVTB and associated components.
 (Photo credit: John Ireland, NREL)

NREL purchased a duplicate HVTB and reconfigured the accompanying BEC, BPSM, and BECM submodules to work with the replacement LEESS devices under test. All of these were then connected to a dSpace MicroAutoBox (MABx) that is used to intercept certain CAN signals pertaining to the BECM's calculations for the production NiMH battery (state of charge, power capability, etc.) and to replace them with corresponding calculations for the alternate LEESS under test. The MABx also served as the data logger and provided safety controls during the testing. Figure III-98 illustrates these connections and their interface points with the vehicle.

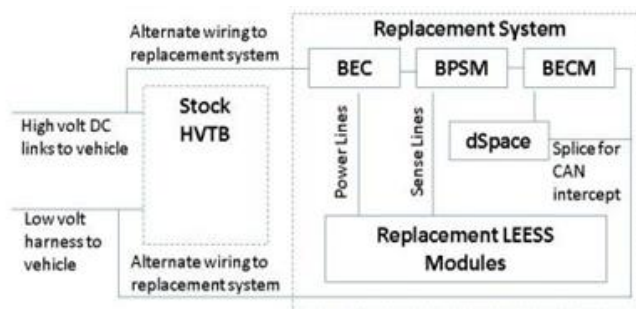


Figure III-98: Schematic of connections between replacement components and the vehicle.

These modifications enabled installation and testing of different LEESS devices in the vehicle, and easy switching between the production battery and the LEESS under test. This report includes results from evaluating two distinct lower-energy energy storage technologies in the Fusion Hybrid test platform.

JSR Micro, Inc., provided a lithium-ion capacitor (LIC) system as the first LEESS technology to be evaluated. The LICs are asymmetric electrochemical energy storage devices possessing one electrode with battery-type characteristics (lithiated graphite) and one with ultracapacitor-type characteristics (carbon). In 2014, NREL completed bench testing on the LIC replacement pack and integrated the modules into the Fusion Hybrid test platform for on-road and chassis dynamometer testing.

Maxwell Technologies, Inc., provided an EDLC system as the second LEESS technology to be evaluated in the full-hybrid test platform. The bench and on-road testing of the EDLC system began in 2014 and were completed in 2015.

Results

Bench Testing

Initially, both the LIC and EDLC systems are tested in a benchtop laboratory setting to establish their capability to operate over a power demand profile from a vehicle drive cycle, as well as to gather data to use as inputs for the state estimator in the MABx prototype controller. Hybrid pulse power characterization and capacity tests are performed for both systems at three test temperatures (-20°C, 25°C, and 45°C) in order to include capacity- and temperature-dependence in the state estimator model. Operation over a sample US06 charge/discharge drive trace obtained from previous production Fusion Hybrid chassis dynamometer testing conducted at Argonne National Laboratory (ANL) confirms the ability of both devices to operate as expected, satisfying the power and energy demands of a representative duty cycle. In addition, these tests highlight the lower impedance inherent to the LEESS devices relative to the production NiMH pack.

Testing over the power profile provided by ANL (Figure III-99) produces slightly charge-gaining results when run using a LEESS device as opposed to charge-sustaining performance from the dynamometer-tested production battery configuration. This is because the lower impedance of the LEESS device leads to higher round-trip discharge/charge efficiency, which may help counteract potential adverse performance impacts due to the reduced energy availability during testing in the conversion configuration.

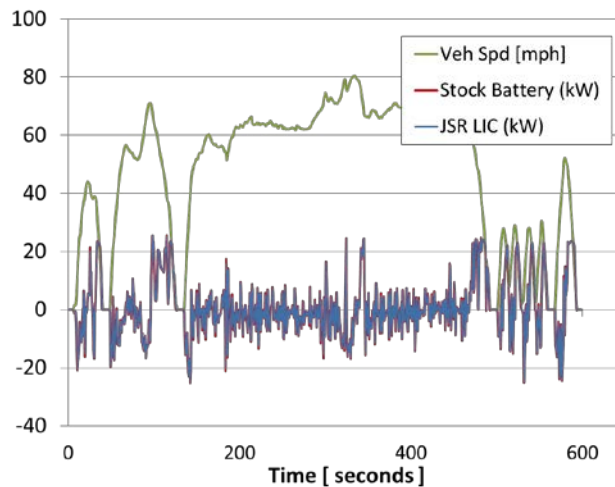


Figure III-99: ANL-provided ESS power trace over the US06 test cycle.

Table III-20 summarizes the differences between the production battery system and the two baseline LEESS configurations under test in the vehicle. In addition to these baseline configurations, a select number of in-vehicle tests are performed using even tighter energy restrictions (such as by artificially lowering the LEESS upper voltage limit) in order to emulate the performance of smaller LEESS configurations.

Table III-20: Baseline ESS Device Comparisons

Device Configuration	# of Cells	Nominal Voltage	Total Energy (Wh)
Production Sanyo NiMH ^a	204	275	1,370
8 JSR Micro 192 F LIC modules	96	300	260 ^b
7 Maxwell 83 F modules	126	300	130 ^b

^a Based on an Idaho National Laboratory fact sheet: <http://avt.inl.gov/pdf/hev/batteryfusion4699.pdf>.

^b Assuming 175 V – 350 V maximum in-vehicle operating window.

Vehicle Testing

The LEESS test platform is evaluated in two environments for both the LIC and EDLC systems: a closed road to measure on-road acceleration performance, and a chassis dynamometer test facility to measure fuel economy. Note that because the vehicle is modified from its production configuration (in addition to the fact that these tests are performed at high elevation), they are not intended to be verification of or comparable to factory claims. Rather they are performed to provide “A to B” comparisons of the different energy storage systems.

As shown in Figure III-100, the on-road testing demonstrates very similar 0–60 mph and passing acceleration performance between the production battery configuration and the baseline LEESS configurations. The baseline LIC and EDLC configurations are closely aligned to the production system voltage levels and show essentially equivalent acceleration distances for each of the tests performed despite lower available energy. The bottom portion of Figure III-100 shows passing acceleration results for the baseline (“high energy”) EDLC configuration along with two different levels of further energy restriction (“mid energy” and “low energy”). These results indicate that 40–60 mph passing acceleration performance is maintained across the evaluated energy cases, but that the mid- and low-energy EDLC cases require progressively longer distances to complete the 60–80 mph acceleration maneuver (due to the lower energy configurations more quickly reaching SOC levels at which the vehicle controllers impose ESS discharge power limitations). The test results indicate that about 70 watt-hours (Wh) of ESS assist was provided by the high energy EDLC configuration in the 60–80 mph passing maneuver whereas the low-energy configuration only had about 70 Wh total available if it were to start the maneuver at its maximum SOC level (which it did not). This same trend was observed in the restricted-energy LIC testing, and was further illustrated by observing the ESS discharge power limit signal from the BECM over the 60-80 mph acceleration maneuvers. For instance, in the production NiMH configuration the discharge power limit signal held steady through almost the entire 60-80 mph maneuver before dropping slightly to around 90% of the unrestricted level by the end of the maneuver. In the most energy restricted LIC configuration tested, the discharge power limit drops steadily throughout the 60-80 mph maneuver and finishes the maneuver with a discharge power capability less than half of the unrestricted level.

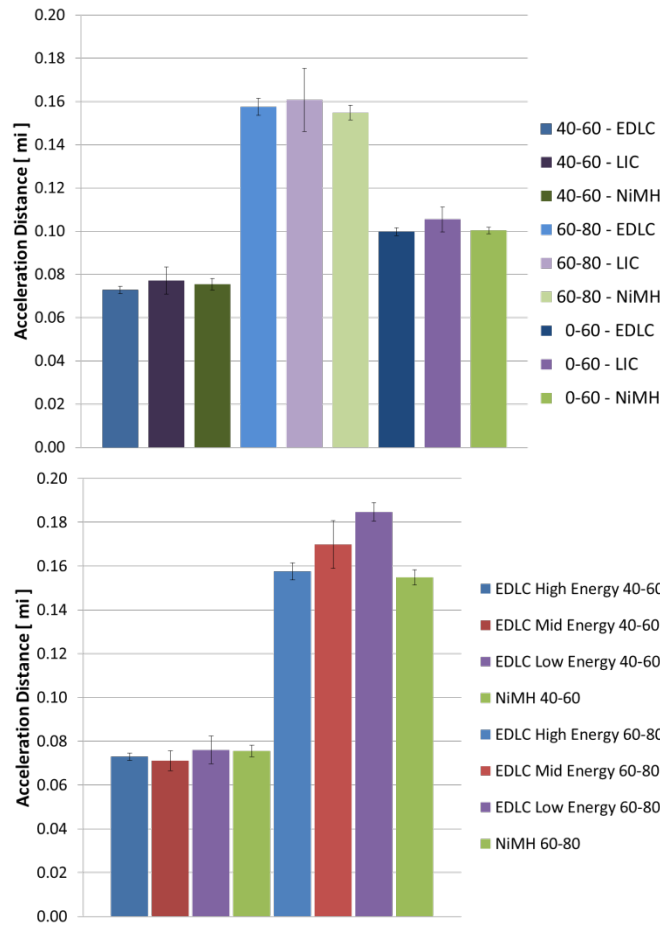


Figure III-100: Passing and 0-60 mph acceleration distances for NiMH compared with unrestricted LIC and EDLC configurations (top) and compared with restricted-energy EDLC configurations (bottom).

It should also be noted from the track testing that the vehicle begins to experience some drive quality issues when the emulated ESS is restricted to available energy levels much below 70 Wh. At these levels, routine acceleration and braking events cause rapid changes in the ESS SOC, which in turn cause the vehicle to switch quickly between charging and assist modes, degrading driving smoothness. These issues related to potential drive quality and acceleration performance degradation are legitimate concerns with very low energy ESS devices; however, it is also true that inherent limitations in the conversion vehicle configuration may exaggerate their magnitude in the test vehicle. A more rigorous and production-intent controls calibration for a very low energy full hybrid configuration would have the potential to significantly mitigate if not eliminate such concerns.

With respect to the chassis dynamometer testing, the evaluation results indicate that the converted LEES configuration retains much if not all of the hybridization fuel savings as the baseline production battery HEV configuration. While the ESS usage profile does vary based on its available energy content, the net fuel consumption differences remain small relative to the hybrid’s fuel savings over a comparable non-hybrid Fusion for the same drive cycles. Figure III-101 highlights a LEES configuration comparison test that shows one of the largest differences relative to the production battery HEV configuration. Over the aggressive US06 driving cycle, the production battery energy profile spans a usage window of over 150 Wh, including a significant period of charge depletion during the extended high-speed driving section in the middle of the cycle. This is contrasted with the energy profile for the lowest restricted-energy LIC scenario, which spans a usage window a little less than 70 Wh.

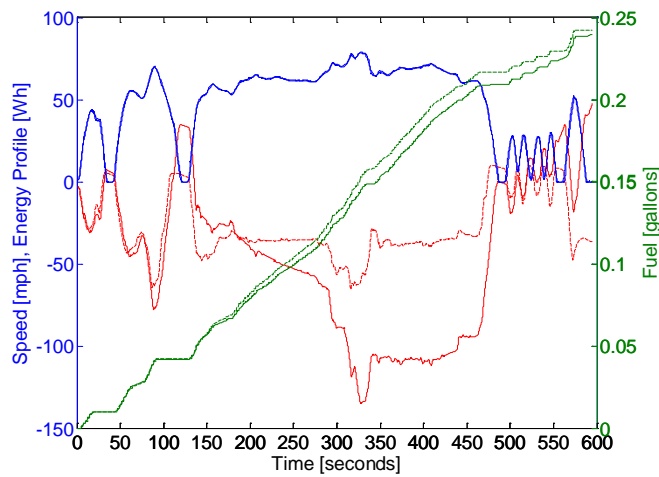


Figure III-101: Performance comparison of the production battery and the lowest restricted-energy LIC configuration over the US06 cycle.

Figure III-101 also shows a gradual separation of the cumulative fuel use curves between the two ESS configuration cases during the extended high-speed portion of the drive cycle. During this period, the bulk depletion by the NiMH battery enables the vehicle to use slightly less fuel, and the steep decelerations at the end of the cycle enable the battery to recapture regenerative braking energy and remain charge neutral over the course of the entire drive cycle.

Figure III-102 shows individual fuel consumption vs. energy window data points for multiple configurations tested on the US06 cycle, including the two from Figure III-101 (roughly 3.0 gallons [gal]/100 miles [mi] and 150 Wh for the NiMH and roughly 3.1 gal/100 mi and 70 Wh for the lowest restricted-energy LIC scenario). In general, comparisons across consistent test conditions show comparable fuel consumption over a range of energy usage windows. While the very lowest restricted-energy configurations indicate slightly higher fuel consumption on this test cycle, note that the differences are minimal compared with the 3.8 gal/100 mi fuel consumption performance of a comparable conventional Fusion over the US06 cycle. This conventional data represents testing at three test temperatures (similar to what is shown for the HEV) with the spread in fuel consumption results across the different test temperatures falling within 0.05 gal/100 mi of the average shown in the figure.

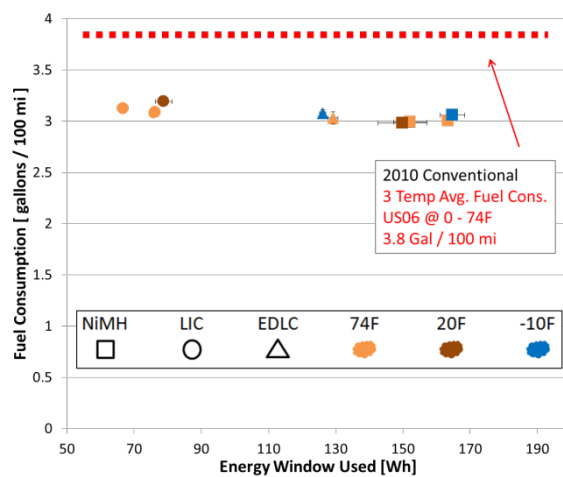


Figure III-102: US06 fuel consumption vs. energy window for multiple vehicle configurations.

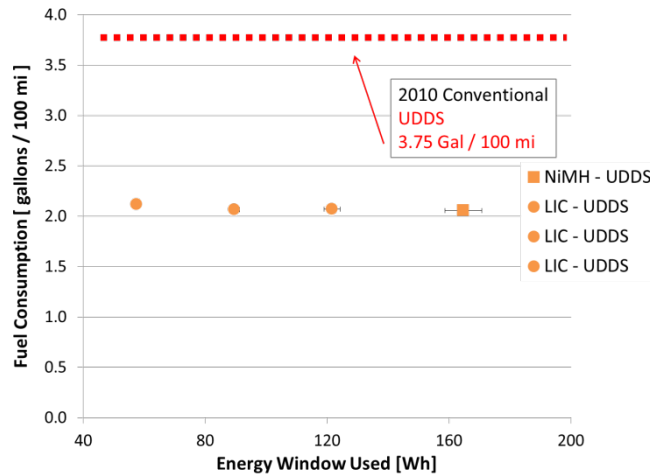


Figure III-103: UDDS fuel consumption vs. energy window for LIC and NiMH configurations.

All other drive cycle tests show fuel consumption at least as low as the production battery configuration for all LEESS configurations tested. For instance, Figure III-103 provides a fuel consumption comparison over the Urban Dynamometer Driving Schedule (UDDS), a drive cycle used for city fuel economy testing that is less aggressive than the US06 cycle. For these tests, the energy window spread between the production configuration and the lowest energy-restricted LIC configuration is even greater than for the US06 test, but this did not translate into any discernable fuel consumption differences. All of the tested HEV configurations show a roughly 40% fuel consumption advantage relative to the comparable conventional Fusion on this test cycle.

This finding of consistent fuel efficiency at low energy also holds for evaluations over the standard cold temperature (20°F or -6.7°C) Federal Test Procedure (FTP), which includes cold and hot start evaluation using the UDDS speed profile. To further explore potential performance differences at very cold temperatures, FTP tests are also run at -10°F (-23°C), with each test preceded by a 12-hour soak of the vehicle at that test temperature. Specifically comparing the performance of the production NiMH configuration to the baseline EDLC conversion, this test shows a lower energy window, but also better than 10% lower fuel consumption for the EDLC configuration. This is primarily attributed to charge and discharge power limitations imposed on the production battery at these very cold temperatures, which limited availability of hybrid functions for improving fuel efficiency. In contrast, the EDLC configuration is able to operate in these conditions without encountering temperature-induced power limitations.

The top portion of Figure III-104 illustrates the relative NiMH configuration power and ESS usage limitations during the first part of a cold-start test at -10°F. The bottom portion of Figure III-104 indicates that the EDLC configuration also experiences power limits; however, these limits are very short in duration and are not caused by temperature restrictions. The limits shown in the bottom portion of Figure III-104, which are representative of those encountered by EDLC configuration city cycle testing across all considered temperatures, instead arise when the EDLC system approaches its maximum SOC. The overall results, however, show that these situations are short enough and infrequent enough so as to have a negligible impact on the EDLC configuration’s ability to apply fuel-saving hybrid functions over the city test cycles.

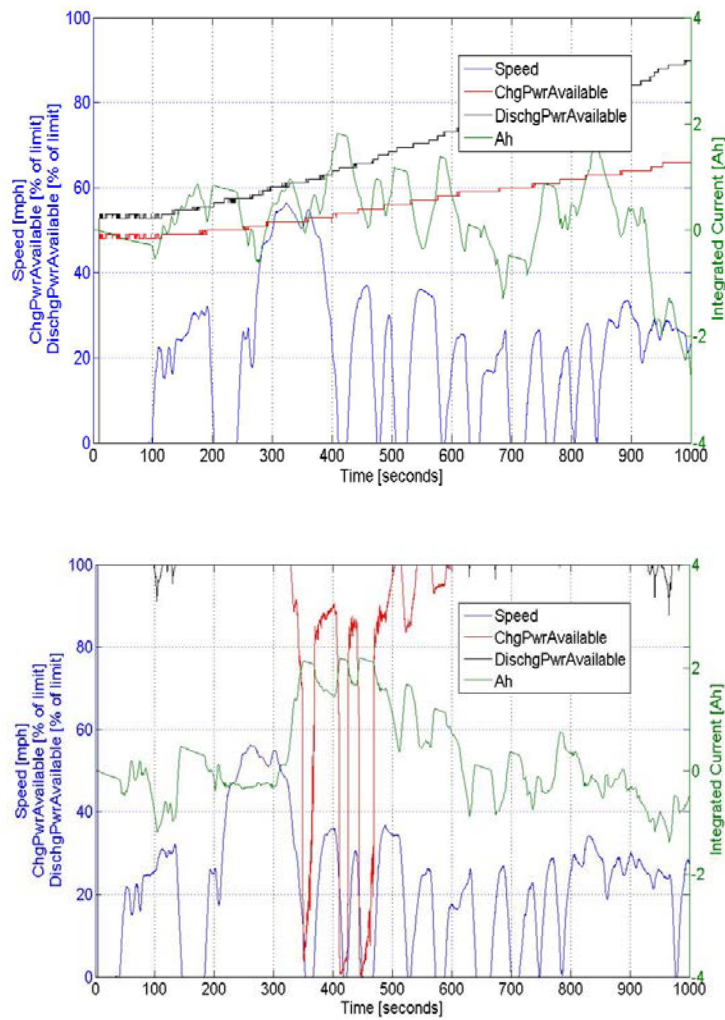


Figure III-104: NiMH and EDLC configuration power limits during cold start city cycle testing at -10°F.

Evaluations over the standard Highway Fuel Economy Test show similar results to the city cycle findings. Figure III-105 compares test results from the production battery configuration with those from the most restricted low-energy LIC configuration. The most striking difference is the larger amount of assist at the beginning of the cycle and the larger amount of regenerative braking energy recaptured at the end of the cycle for the production NiMH configuration. However, this does not correspond to any significant difference in the cumulative fuel consumption over the two tests. The small incremental performance differences at the very beginning and very end of the cycle represent a small fraction of the overall test, and any marginal benefit from the larger charge/discharge cycling of the NiMH configuration may also be offset by the slightly higher round trip charge/discharge efficiency of the LEES configuration.

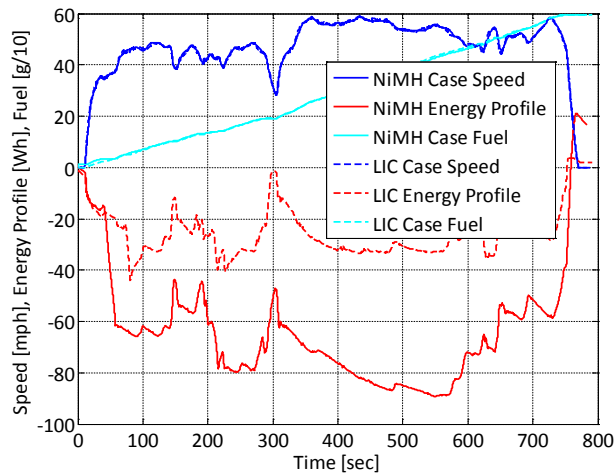


Figure III-105: Highway Fuel Economy Test showing similar fuel consumption for widely varying energy windows between the production NiMH and the lowest-energy LIC configurations.

The final set of chassis dynamometer testing is conducted at hot ambient conditions (95°F or 35°C), where the LEESS devices may see larger auxiliary loads due to vehicle air conditioning. When operating over the 95°F SC03 cycle¹ with the vehicle’s air conditioning system set to 72°F (22°C), both of the LEESS configurations demonstrate fuel consumption and engine on/off cycling similar to that of the NiMH configuration. Figure III-106 shows this for one of the restricted-energy LIC configurations as compared to the production NiMH configuration. The small differences between the system operation in the two configurations resulted in one fewer engine stop/start events for the LIC (14 events) compared with the NiMH (15 events), with both systems possessing between 42%–43% “engine on” time over the cycle.

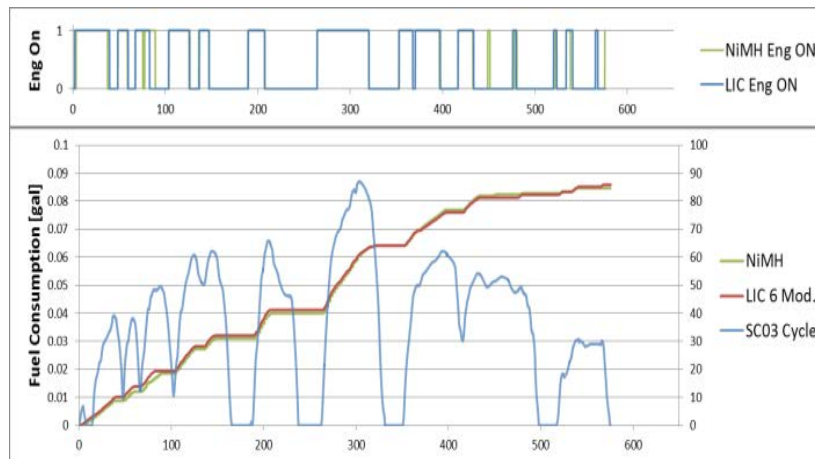


Figure III-106: Engine stop/start cycling and fuel consumption comparison between the production NiMH and a restricted-energy LIC configuration over the 95°F SC03 cycle.

An additional potential concern about HEV LEESS systems is that they might require excessive engine on/off cycling when running the air conditioning while parked and idling. To address this issue, the research team considered a scenario where a steady-state 1-kW accessory load is required to run the air conditioning for maintaining occupant comfort while parked and idling on a hot day. Under such a scenario, an ESS with as little as 50 Wh of available energy could permit three minutes of engine-off time between engine-on events to recharge the ESS, which seems reasonable.

¹ Note: SC03 cycle standard test procedures were followed with the exception of the use of heat lamps to simulate solar loading. No heat lamps were available at test time.

Conclusions

This report presents an evaluation of two LEESS technologies under several energy-restriction configurations in a full HEV application. The activities included bench testing of the LEESS devices to collect the necessary data for completing the conversion, which confirmed the lower impedance level of the LEESS devices relative to traditional battery systems. The developed vehicle conversion permitted back-to-back comparison tests of the LEESS configurations relative to vehicle performance using the production NiMH battery pack found in the 2012 Ford Fusion Hybrid.

On-road evaluation, including standing and passing acceleration tests as well as general drive quality observation, demonstrated that most of the vehicle's original performance can be maintained while operating on the lower energy devices. Under the most energy-restricted configurations tested (in-use energy limited to less than 70 Wh), the results indicated that high-speed passing acceleration performance and overall drive quality may begin to degrade. However, it is possible that a more rigorous and production-intent controls calibration than what could be implemented for this conversion testing would be able to mitigate some, if not all, of this performance degradation.

Chassis dynamometer testing results similarly indicated that LEESS configurations could match the hybridization fuel savings achieved by the production NiMH configuration. For scenarios where artificial limitations were again imposed to evaluate further restricted-energy LEESS configurations, some specific hybrid functions can also become restricted (such as providing extended assist via bulk ESS depletion over certain sections of driving or recapturing large amounts of regenerative braking energy through successive deceleration events). Even so, for all of the cycles tested, even the most energy-restricted LEESS configurations experienced minimal fuel consumption impact when compared to the fuel savings offered by the HEV relative to a comparable conventional vehicle.

Edge cases evaluated on the chassis dynamometer included very cold testing at -10°F, where the LEESS devices actually offered a performance advantage relative to the production NiMH battery due to their superior cold temperature tolerance. Further evaluation included 95°F testing with air conditioning, for which the results suggested that LEESS devices could perform in an acceptable manner for consumers.

Overall, the bench, track, and chassis dynamometer testing demonstrated the technical feasibility for non-traditional ESS devices to perform well in a power-assist HEV platform. Increased competition from LEESS technologies in the HEV energy storage space could be beneficial, but the onus will be on the manufacturers of these technologies to translate lower energy requirements into lower system costs before they are likely to beat out incumbent technologies in very large numbers. If they are able to do so and ultimately translate these savings into an improved benefit vs. cost relationship at the vehicle level, then broad fuel savings benefits could be achieved from aggregate increases in HEV sales.

III.7.C. Products

Presentations/Publications/Patents

1. Cosgrove, J.; Gonder, J.; Pesaran, A. "Performance Evaluation of Lower-Energy Energy Storage Alternatives for Full-Hybrid Vehicles." Presentation at the Supercapacitors USA International Conference and Tradeshow, November 2013.
2. Gonder, J.; Cosgrove, J.; Pesaran, A. "Performance Evaluation of Lower-Energy Energy Storage Alternatives for Full-Hybrid Vehicles." Proceedings of the SAE 2014 Hybrid and Electric Vehicle Technology Symposium, February 2014.
3. Gonder, J.; Cosgrove, J.; Pesaran, A.; Keyser, M. "In-Vehicle Evaluation of Lower-Energy Energy Storage System (LEESS) Devices." DOE Vehicle Technologies Annual Merit Review – Project ID#: VSS129, June 2014.
4. Gonder, J.; Cosgrove, J.; Shi, Y.; Saxon, A.; Pesaran, A. "Lower-Energy Energy Storage System (LEESS) Component Evaluation." NREL Milestone Report MP-5400-62853, September 2014.

5. Cosgrove, J.; Gonder, J.; Pesaran, A. "Lower-Energy Energy Storage System (LEESS) Component Evaluation: Draft Report on Devices Tested in the Ford Fusion HEV Test Platform." NREL Milestone Report, July 2015.

III.7.D. References

1. Cobb, J. Jan. 6, 2015. "2014 December 2014 Dashboard." HybridCars. Accessed on 09/01/2015. hybridcars.com/december-2014-dashboard/
2. Lukic, S. Cao, J. Bansal, R. Rodriguez, F. Emadi, Ali. "Energy Storage Systems for Automotive Applications." IEEE Transactions on Industrial Electronics, VOL. 55, NO. 6, June (2008) 2 pp. <http://ieeexplore.ieee.org/stamp/stamp.jsp?arnumber=4450599&tag=1>
3. "FreedomCAR Power Assist HEV Battery Goals." USCAR. Accessed on 09/01/2015. uscar.org/commands/files_download.php?files_id=83
4. J. Gonder, A. Pesaran, D. Howell, H. Tataria. "Lower-energy requirements for power-assist HEV energy storage systems—Analysis and rationale." Proc. 27th International Battery Seminar and Exhibit, March 15–18, 2010, Fort Lauderdale, FL (2010) 26 pp. nrel.gov/docs/fy10osti/47682.pdf
5. United States Advanced Battery Consortium (USABC). "Request for Proposal Information (RFPI), Development of advanced energy storage systems for high power, lower-energy energy storage system (LEESS) for power-assist hybrid electric vehicle (PAHEV) applications." Accessed on 09/01/2015. uscar.org/commands/files_download.php?files_id=219
6. J. Gonder, A. Pesaran, J. Lustbader, H. Tataria. "Hybrid vehicle comparison testing using ultracapacitor vs. battery energy storage." Proc. SAE 2010 Hybrid Vehicle Technologies Symposium, February 10–11, 2010, San Diego, CA (2010) 30 pp. nrel.gov/docs/fy10osti/47355.pdf

III.8. Medium-Duty Electric Vehicle Data Collection and Performance Assessment

Kenneth Kelly, Principal Investigator

National Renewable Energy Laboratory
15013 Denver West Parkway, MS 1633
Golden, CO 80401

Phone: (303) 275-4465

E-mail: Kenneth.Kelly@nrel.gov

Lee Slezak, DOE Program Managers

U.S. Department of Energy

Phone: (202) 586-2335

Email: Lee.Slezak@ee.doe.gov

Start Date: 10/01/2010

End Date: 12/30/2015

III.8.A. Abstract

Objectives

The objective of this project is to securely collect, store, and analyze vehicle data transmitted from medium-duty plug-in electric vehicles (EVs) and equipment being deployed as a part of U.S. Department of Energy (DOE)-funded activities under the American Recovery and Reinvestment Act (ARRA) Transportation Electrification Awards. The project includes extensive data collection from Smith Newton and Navistar eStar EVs, Cascade Sierra Solutions (CSS) truck stop electrification, and Odyne plug-in hybrid electric vehicle (PHEV) utility trucks. Objectives for FY15 included:

- Obtain second-by-second vehicle and component performance data from each EV participating in the ARRA data collection, to be logged and stored at the National Renewable Energy Laboratory (NREL)
- Obtain truck stop electrification usage records that provide a timestamp and energy consumption information each time a plug-in site is used
- Report data and progress of the data collection efforts and analyzed vehicle/equipment performance data to the DOE and the general public
- Provide for the secure storage of data with routine backups
- Refine and optimize processing routines to handle an increasing volume of data as more vehicles come online
- Process results to protect proprietary and private information and post on an NREL website quarterly for public review.

Accomplishments

Data collection and reporting activities for medium-duty EVs in FY15 included the addition of Odyne PHEV utility vehicles along with continued data collection from the truck stop electrification data through February 2015 and second generation Smith Electric vehicles through June 2015. Accomplishments from individual ARRA deployment projects are highlighted below:

- Smith Electric Vehicles: Data transmission, analysis, and reporting of performance from the Smith Newton EVs to NREL
 - First Generation Vehicles: Two international conference papers characterizing operation use and drive cycle behavior were published in FY15. These publications were presented at the 2014 IEEE International Electric Vehicle Conference and the 2015 Electric Vehicle Symposium.

- Second Generation Vehicles: NREL began receiving data from second-generation Smith vehicles in FY14. Data from a total of 200 second-generation vehicles were recorded through June 2015. This represented over 48,000 vehicle-days of operation covering nearly 1.5 million miles over 30 months.
- ShorePower Truck Stop Electrification: A cumulative report covering data collected from January 2013 through February 2015 has been created and includes monthly usage statistics over this period. As of February 2015, all 50 DOE-funded sites were active and had recorded 5,611 plug-in events using 56,073 kWh of electricity.
- Odyne PHEV Utility Trucks: NREL began receiving Odyne PHEV data from EPRI in December 2014 through June 2015. Usage gradually increased as data collection progressed. NREL is currently refining the processing routines and reporting templates for this project. Results will be made publically available on the NREL website.
- Reports: Detailed cumulative and quarterly reports for all of the projects listed above can be found on the NREL website: nrel.gov/vehiclesandfuels/fleettest/

Future Achievements

- Analysis of the data received in mid FY15 from the Odyne plug-in hybrid electric bucket trucks will continue. Similar data collection, screening, and analysis efforts will be completed in FY16 for this data set, and reports will be posted for public consumption.
- Efforts for FY16 will focus on improved integration with data sets from other projects and expanding the number of metrics that are being considered.
- A final technical report will be published in FY16.



III.8.B. Technical Discussion

Background

ARRA deployment and demonstration projects are helping to commercialize technologies for medium-duty HEVs, PHEVs, all-electric vehicles, and electric charging infrastructure for commercial fleets.

This effort, which is funded by the DOE’s Vehicle Technologies Office within the Vehicle & Systems Simulation and Testing Activities, will utilize data collected from the medium- and heavy-duty ARRA EV demonstration projects. Data from EVs from Smith Electric Vehicles (Smith), Navistar, and Odyne will be collected, compiled, and analyzed. Data from ARRA-funded ShorePower truck stop electrification sites have also been included. A project framework schematic is shown in Figure III-107.

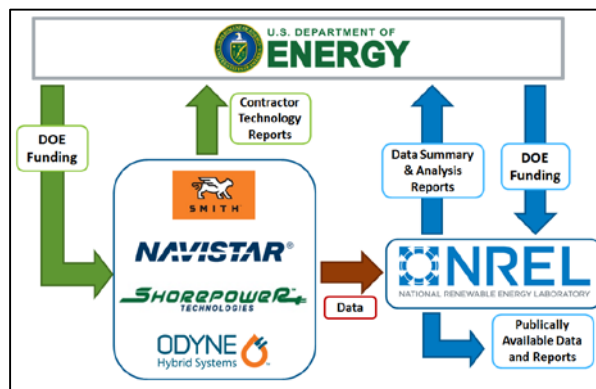


Figure III-107: Project framework schematic

Introduction

NREL will compile the data received from each original equipment manufacturer (OEM) through the NREL Commercial Fleet Data Center (CFDC). This includes more than 25 parameters, which are recorded each second from each vehicle and transmitted to NREL on a regular basis. Compiled data products will be used to better understand the behavior and operating characteristics of electric-drive vehicles being operated in the field. This is in direct support of the Vehicle Technology Office’s goals of developing and deploying plug-in EVs.

Information gathered on vehicle drive cycle characteristics along with data collected on specific components, such as electric motors, power electronics, auxiliary loads, and battery performance, can be used to support other DOE-sponsored research and development activities.

NREL will prepare and deliver detailed non-proprietary summary reports of vehicle performance to the DOE. This information, which will be processed to protect any proprietary or private information, will also be made available on the NREL website for public review.

Approach

Overall Approach

On-board diagnostic data are collected, typically from the controller area network bus, along with global positioning system and any additional sensors. The data are transmitted wirelessly back over the cellular network and eventually on to the OEM. The data are then uploaded by the OEM to the NREL secure FTP site, usually as a text file. Once the data have arrived at NREL, a number of automated processes handle downloading, filtering, sorting, and processing the data. The raw and processed data are stored in the CFDC PostgreSQL central database, and summary reports are generated for the DOE and general public. This process is outlined in the schematic shown in Figure III-108.

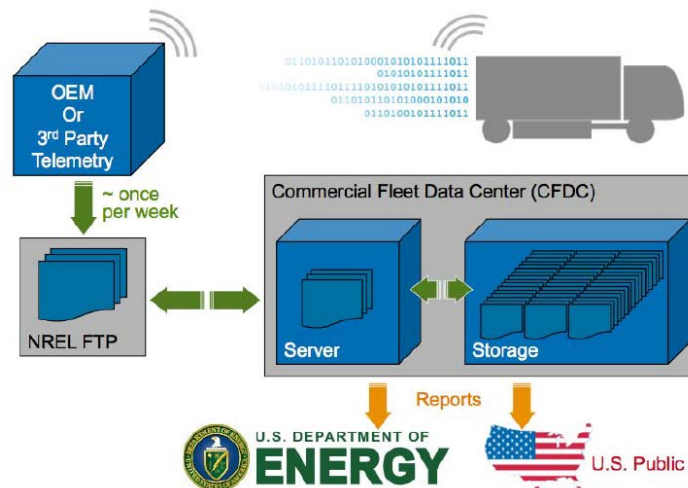


Figure III-108: Data flow from vehicle to final reporting

The procedure for data processing within the CFDC can be broken down into a number of steps, including data transfer, quality assurance, storage, analysis and reporting. The two primary software packages used for calculations and analysis are MATLAB and Python. Raw data can be loaded directly from individual files or read from the CFDC PostgreSQL central database. All data received by the secure FTP site are stored; however, if data are found to be erroneous or corrupt during the filtering process, they are flagged and are not included in the subsequent processing steps. Time and date are adjusted for geographic location, and then binned into “driving days” that capture one full day of driving and any subsequent charging, even if the charge cycle goes past midnight. Specific analysis is then carried out on individual aspects, including drive cycle, powertrain, power electronics, batteries, and any individual components of interest. These routines include

code and calculations specifically designed for these projects, as well as incorporating more universal calculations from NREL's Fleet Analysis Toolkit, which allows the performance of these vehicles and vehicle components to be compared across a large number of current and past projects within the secure data center. This information can be combined with demographic data to better understand localized trends and markets. Final data products are then posted to the NREL website for public access. This process is outlined in the schematic shown in Figure III-109.

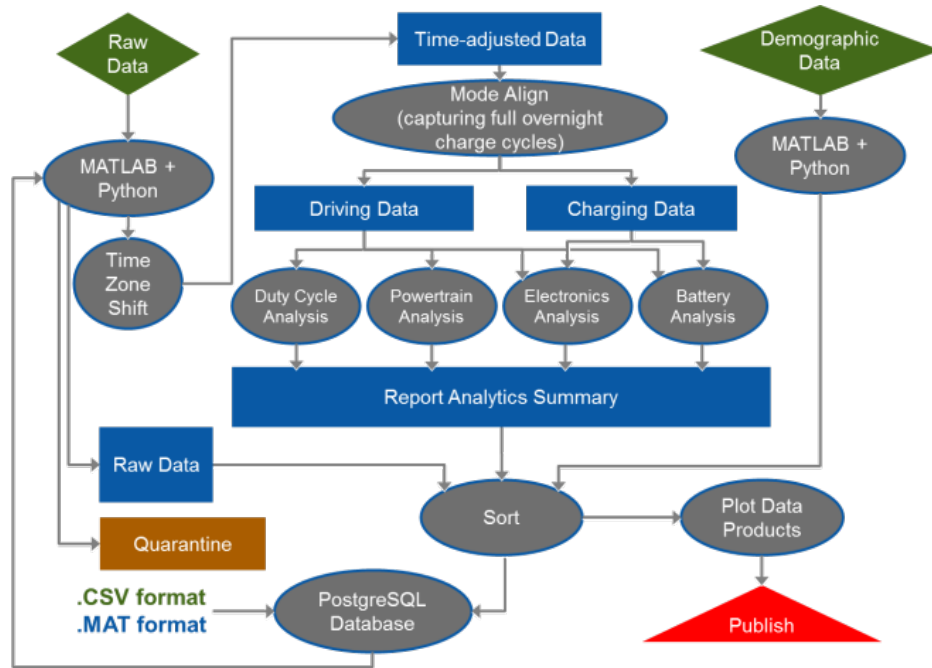


Figure III-109: Data processing and analysis

The main focus for the Smith Newton deployment project in FY15 was to continue to acquire and incorporate data from second-generation vehicles (Smith Gen 2) into the normal processing routine as well as reformat the database for security and efficiency. This required refining the processing scripts to handle new file formats and adjustments for increasing the speed of calculations as vehicle usage and raw data volume increased.

The main data storage structure for the Smith EV data is a PostgreSQL database. This is not only neater and cleaner from an organizational standpoint when compared with the raw files, but also adds functionality in which the database allows multiple users to interact with the data while simultaneously processing results. The database also integrates with the new Python scripting and calculations, allowing raw data to be extracted from the database, calculations made, and results saved back to the database all in one step. Mirrored copies of the raw data for all ARRA projects are stored on the NREL High Performance Computing Data Center's mass storage system, which is linked to NREL's high-performance supercomputer, Peregrine. Peregrine is used to apply the Smith EV in-use performance data to tune large-scale EV and battery simulation models for vehicles and components in similar applications.

A Smith Newton delivery vehicle is shown in Figure III-110.



Figure III-110: Smith Newton delivery vehicle
NREL 22848

Currently, all the Smith Newton full electric-drive vehicles participating in this demonstration project have 80-kWh battery packs, with the exception of a handful of utility trucks that have 120-kWh packs, but which are not in regular service at this time. Battery packs for these vehicles were supplied by Valence and A123. The vehicle is advertised as having a number of battery pack size options ranging from 40 kWh to 120 kWh and comes in a number of chassis configurations feeding a number of vocations, including box truck, step van, refrigerated, aerial lift, utility, flat bed, shuttle bus, and military transport. The vehicles participating in this demonstration project are primarily delivery, distribution, and utility maintenance vehicles. Participating fleets include Frito-Lay, Staples, FedEx, Duane Reade, PG&E, and Coca-Cola. The second-generation vehicles benefit from improved battery chemistry, an updated battery management system, and a redesigned driveline. Some vehicle specifications are listed in Table III-21.

Table III-21: Smith Newton Vehicle Specifications

Gross vehicle weight rating	16.5k–27k lbs.
Drag coefficient	~0.5
Charging standards	J1772 or 3-phase
Onboard charger power	5–6 kW
Battery capacity	80–120 kWh
Inverter efficiency	94%
Peak motor power	134 kW
Motor efficiency	90%

NREL has been receiving data from Smith as part of this demonstration project since November 2011 for first-generation vehicles and since September 2013 for second-generation vehicles. The latest cumulative report posted to the web captures all data that have passed through the filtering and analysis steps described above.

Figure III-111 shows the home locations of Smith vehicles reporting data under this project. Figure III-112 and Figure III-113 give a breakdown of the total data received by state for Gen1 and Gen 2 vehicles, respectively.

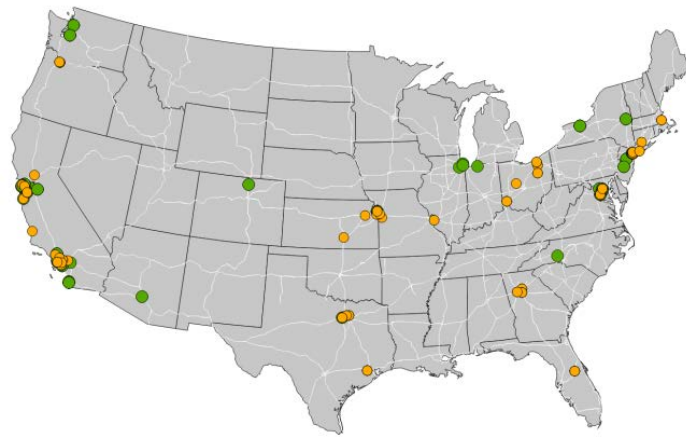
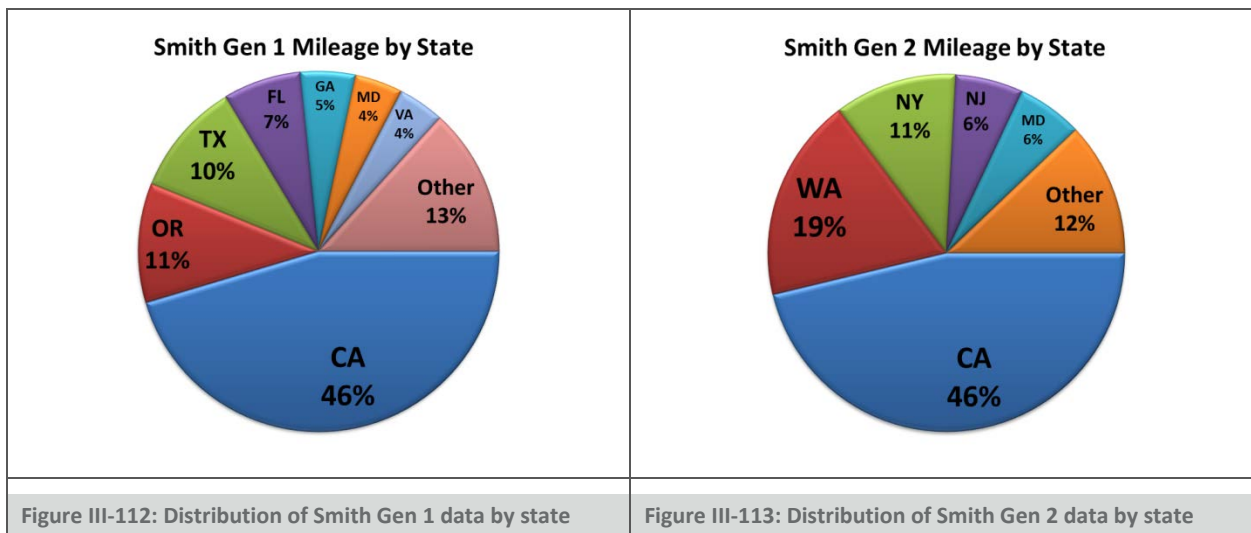


Figure III-111: Home locations of Smith Vehicles: Gen1 (orange), Gen2 (green)



NREL has completed additional univariate analysis on the Smith Gen 1 EVs and has reported daily driving duration and distance distributions. The results of this analysis are shown in Figure III-114 and Figure III-115, respectively. It is interesting to note that the Gen 1 delivery vehicles spend only a small portion of their working day driving.

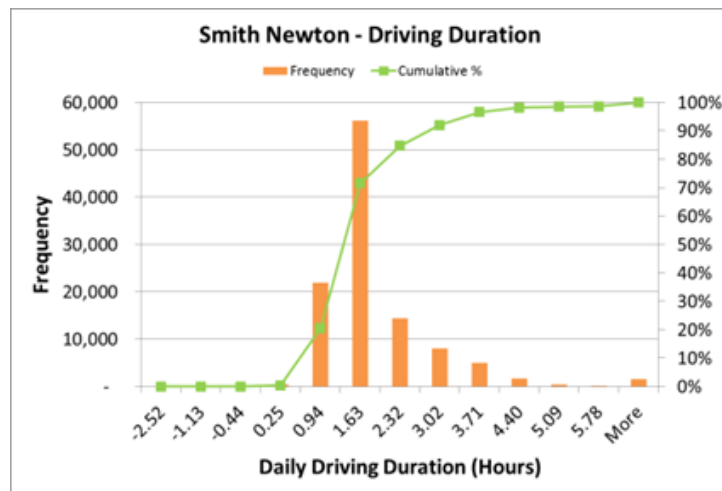


Figure III-114: Average daily driving duration for Gen 1 Smith EVs

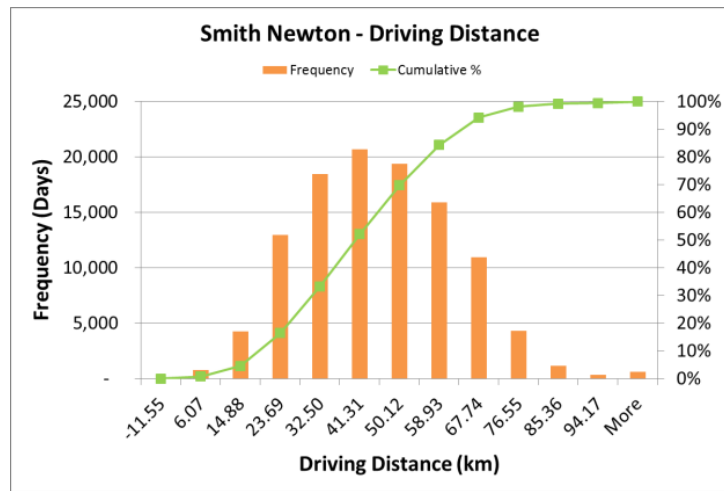


Figure III-115: Average daily driving distance for Gen 1 Smith EVs

Figure III-116 shows a representative drive cycle developed from the in-use data using NREL’s Drive-Cycle Rapid Investigation, Visualization, and Evaluation Analysis Tool (DRIVE). NREL’s DRIVE tool employs a deterministic multivariate hierarchical clustering method to generate representative drive cycles from source data. Using the in-use data collected under ARRA project funds, the DRIVE tool processes all data points to build a singular, time-based, weighted, virtual drive cycle that contains the driving profile for each day of in-use data. This composite cycle made up of all data points is then characterized by more than 175 drive cycle metrics. Using these metrics, the tool then deconstructs the composite cycle into numerous micro trips, which are then used to reconstruct an appropriate representative drive cycle with a user-specified duration. The custom drive cycle generated as a result of this process is approximately 1 hour in length. This drive cycle was recently used in partnership with NREL’s Energy Storage program as input to a life cycle model to predict battery life under real-world commercial driving conditions. Shorter length representative cycles, such as a 20-minute cycle for chassis dynamometer testing, can also be developed from the field data using DRIVE.

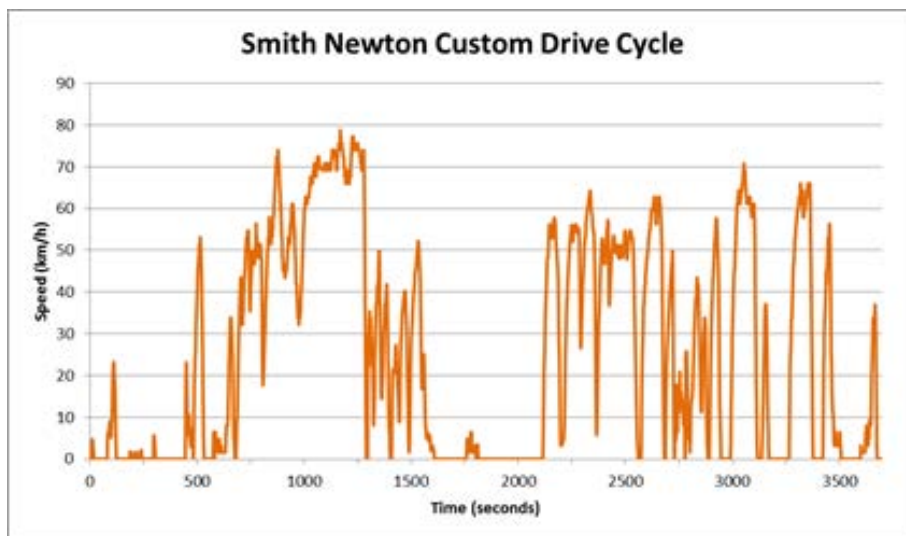


Figure III-116: Gen 1 Smith EV representative custom drive cycle

The latest reports and more detailed results, including data through June 2014, can be found at: nrel.gov/vehiclesandfuels/fleettest/research_electric.html

Results: Navistar Data Collection, Analysis, and Reporting

All of the Navistar eStar vehicles that reported data to NREL through June 2014 are first-generation vehicles with 80-kWh battery packs. The Navistar eStar is shown in Figure III-117, and some vehicle specifications are presented in Table III-22.



Figure III-117: Navistar eStar, Battery Electric Delivery Vehicle
PIX# 18624

Table III-22: Navistar eStar Vehicle Specifications

Gross vehicle weight rating	12,122 lbs.
Payload (max)	5,100 lbs.
Curb weight	7,022 lbs.
Charging standard	J1772
Battery capacity	80 kWh
Motor power	70 kW
Top speed	50 mph
Advertised range	Up to 100 miles

The ARRA-funded Navistar eStar cumulative statistics were reported in the FY14 milestone report. The following additional analysis was completed in FY15. As with the Smith Gen 1 vehicles, additional analysis was performed on the Navistar EV data set to better understand in-use driving behavior. Figure III-118 and Figure III-119 show the 3-sigma distribution for daily driving duration and daily driving distance respectively. Compared to the Smith Gen 1 vehicles, the Navistar vehicles spend considerably more time driving.

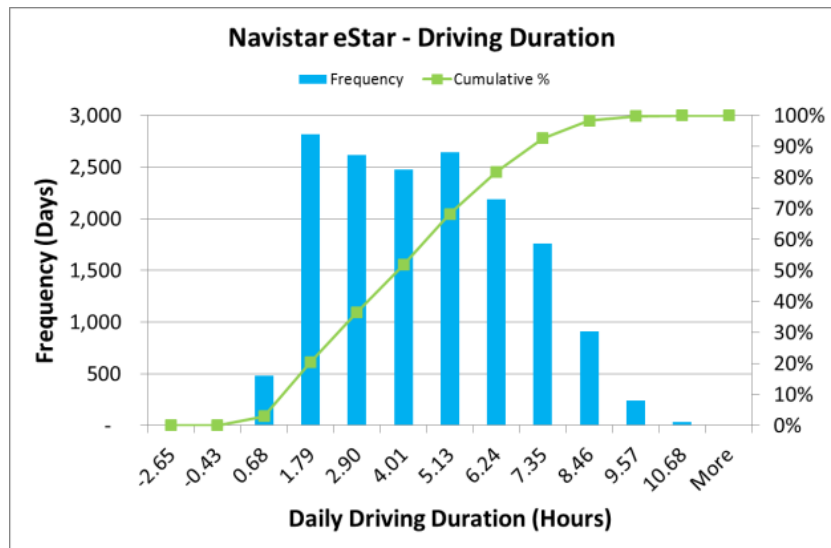


Figure III-118: Navistar driving duration – 3 sigma distribution

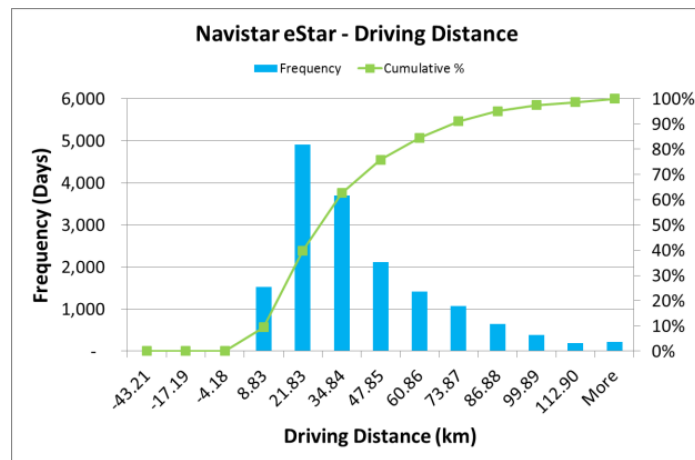


Figure III-119: Navistar driving distance – 3 sigma distribution

Figure III-120 shows the average acceleration as a function of the number of stops per kilometer, for both the Smith Gen 1 and Navistar EVs. It is evident that the lighter and smaller Navistar vehicles on average have both acceleration and deceleration rates of greater magnitude than the Smith vehicles.

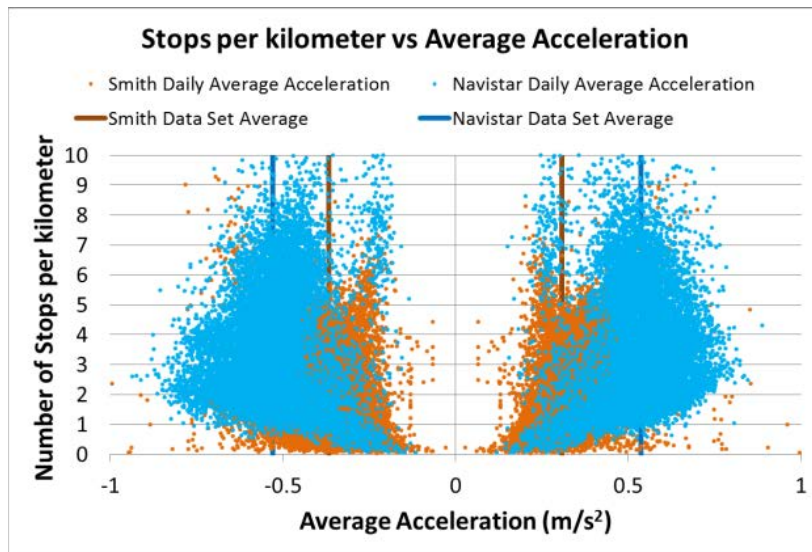


Figure III-120: Stops per kilometer vs. average acceleration

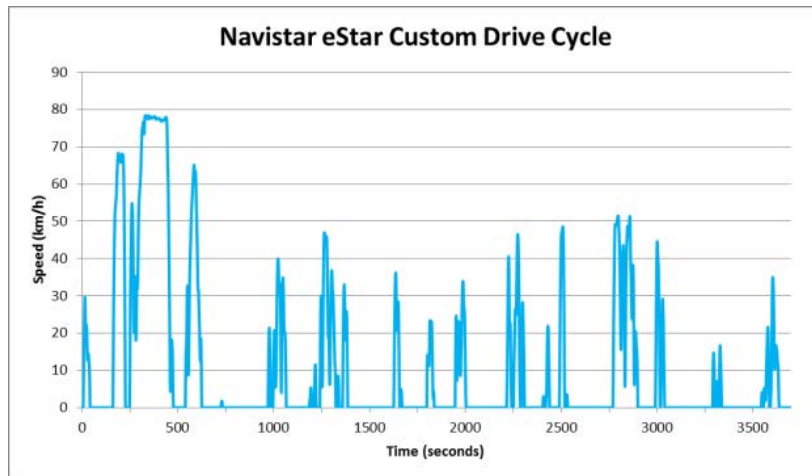


Figure III-121: Navistar eStar custom representative drive cycle

The latest reports and more detailed results can be found at: nrel.gov/vehiclesandfuels/fleettest/research_electric.html

Results: Shorepower Technologies / Cascade Sierra Solutions Data Collection, Analysis, and Reporting

In mid- FY13, CSS began sending truck stop electrification usage statistics to NREL. In early FY14, CSS entered receivership, but utilization data continue to be supplied by Shorepower Technologies. Each funded site has several pedestals, and each pedestal has four connection points where vehicles equipped with electrified equipment can be plugged in. The data set includes a summary of each transaction, which contains location, date, person/business contact information, hours booked, total energy used, and a reference ID that can be linked to truck equipment, if available. This reference ID is the only link between energy consumption and the equipment on the truck. The latest cumulative report shows usage statistics through the end of February 2015. Some summary statistics from this report are shown in Table III-23:

Table III-23: Utilization summary

Idle-reduction rebate approvals	4,686
Completed equipment installations	4,353
Number of TSE sites with >90% uptime	50
Number of plug-in events	5,611
Total hours booked	77,273
Total kWh used	56,073
Average kWh/event	10.0
Estimated gallons of diesel fuel saved ¹	61,818
Metric tons of CO ₂ avoided ²	629

¹ Diesel fuel saved calculated using booking time x 0.8 gal/hr (EPA-420-F09-038) to estimate offset engine idle fuel use.

² Metric tons of carbon dioxide calculated using U.S. EPA greenhouse gas guidelines of 10,180 g CO₂ / gallon of diesel.

The map in Figure III-122 shows the total energy consumption by location and by Petroleum Administration for Defense District (PADD) over the current reporting period.

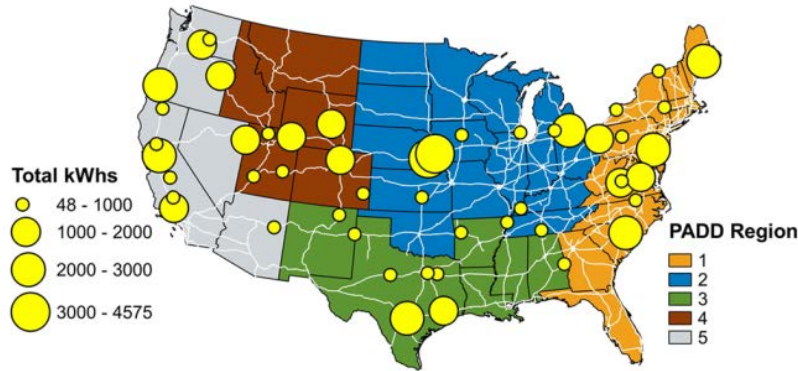


Figure III-122: Map showing energy consumption by ARRA site and PADD regions through February 2015

Figure III-123 and Figure III-124 show weekly and seasonal trends of site utilization. From an energy standpoint, Tuesday shows the lowest use, whereas Friday and Saturday see the highest use. This is typical for truck stop use where drivers may spend a considerable period of time at one stop over the weekends, waiting for a business to open the following Monday. On a seasonal scale, usage appears to be highest during the winter months; however, these trends are complicated by the fact that some individuals received free credits in 2013, and some of the utilization drop-off in mid-2014 could also be due to issues revolving around the CSS receivership. More data are needed to establish a sound trend in usage patterns.

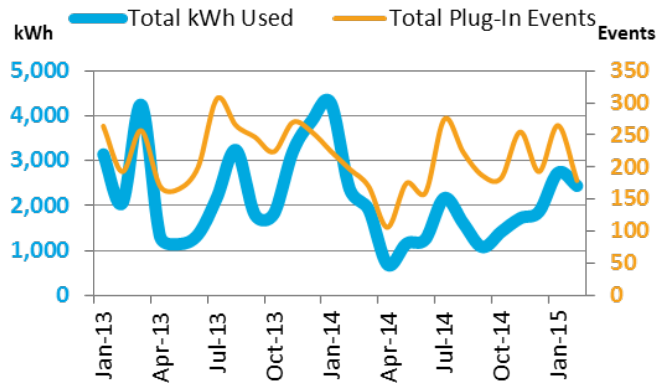


Figure III-123: Shorepower seasonal utilization

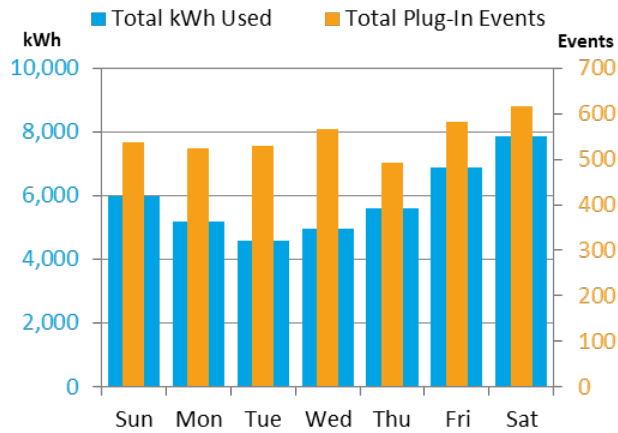


Figure III-124: Shorepower weekly utilization

Figure III-125 shows the average duration of each usage as the number of hours booked per event. The most typical usage was between 9 and 12 hours in length, which correlates well with drivers being required to take a mandatory 10-hour break after each day of driving.

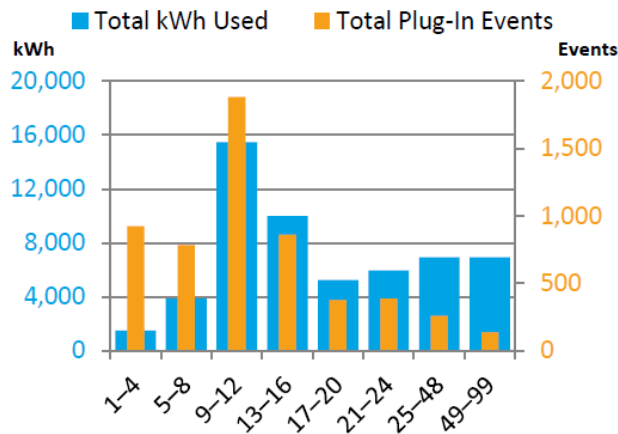


Figure III-125: Hours booked per plug-in event

The latest reports and more detailed results can be found at nrel.gov/vehiclesandfuels/fleetttest/

Odyne Plug-In Hybrid Electric Utility Trucks Background

Introduction

Odyne Systems has developed a plug-in hybrid electric power take-off (PTO)-based system for use with medium- and heavy-duty vehicles. Its system interfaces with Allison 2000, 3000, and 4000 series transmissions and targets vocational vehicles in the utility and maintenance sector. As part of the medium- and heavy-duty demonstration projects under ARRA, Odyne has deployed 119 vehicles into real-world service that will be reporting data back to NREL for further analysis. A schematic of the hybrid system is shown in Figure III-126, and a CAD model is shown in Figure III-127.

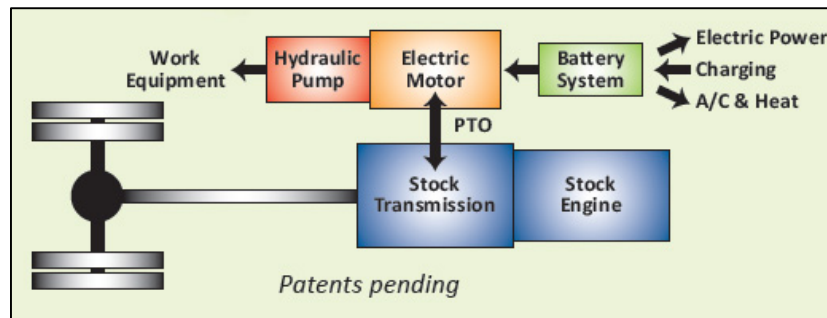


Figure III-126: Odyne Parallel Hybrid Architecture schematic
NREL 34049

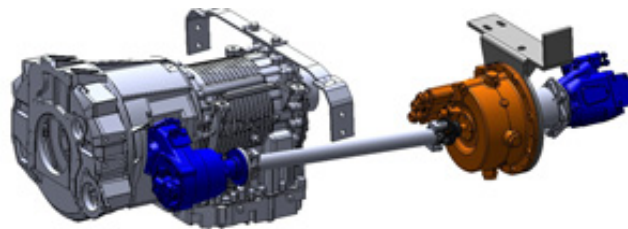


Figure III-127: Odyne Parallel Hybrid Architecture graphic model with system components shown in color
Compliments of odyne.com/

The system interfaces through the stock transmission's PTO port, which feeds power to a double-ended electric motor shaft attached to the PTO clutch on one side and the hydraulic pump on the other. The Remy HVH250 electric motor is rated at 56 horsepower for continuous use and 95 horsepower for peak power and is also used to capture up to 40 kW of energy during regenerative braking that is transferred back into the system for improved fuel economy when traveling to a jobsite. The vehicles are configured with 28.4-kWh battery packs from Johnson Controls. Once on site, the PTO clutch can be disengaged and the electric motor can drive the hydraulic work equipment; heating, ventilating and air conditioning; and electric accessories without the need to idle the engine. Figure III-128 and Figure III-129 show two configurations for utility vehicles with the Odyne system installed.



Figure III-128: Vocational vehicle configured with aerial bucket and the Odyne PHEV system
NREL 34050



Figure III-129: Digger vocational vehicle the Odyne PHEV system
NREL 34048

Approach

In FY15, Odyne completed a number of vehicles and has started delivering them to final customers. Data uploads from Odyne to EPRI and from EPRI to NREL’s FTP site began in December 2014 with the last data transfer containing data from June 2015. Figure III-130 shows the number of vehicle files received month by month from EPRI compared to the original target of 119 vehicles.

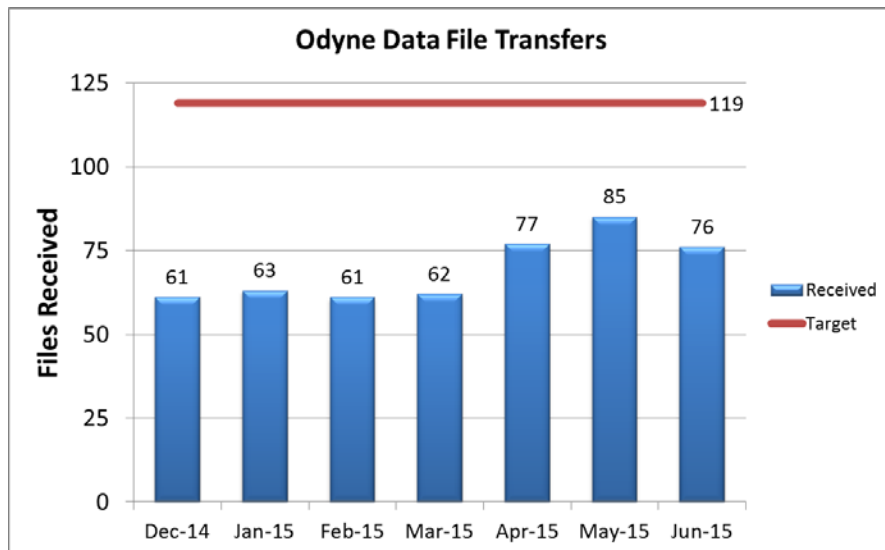


Figure III-130: Completed Odyne vehicle file transfers

Results

Processing routines and reporting templates are still being developed for this new data set. Initial analysis included a breakdown of vehicles by type, as seen in Figure III-131; the majority of the 119 vehicles are configured as bucket trucks with the next most common configured as walk-in vans.

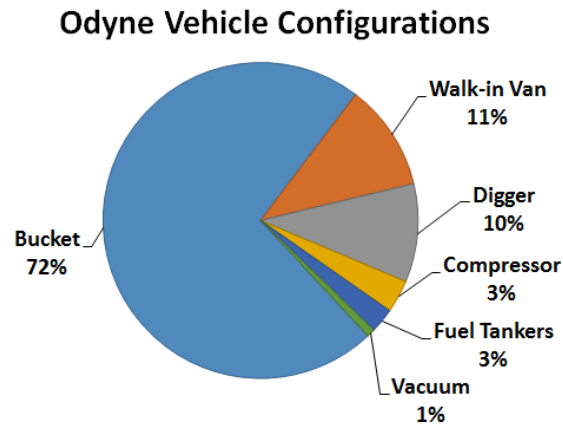


Figure III-131: Distribution of ARRA funded vehicle types

Figure III-132 shows a typical daily vehicle usage profile for a bucket truck, indicating the battery pack state of charge throughout the day as the vehicle drives (shown in red) and is operated on the jobsite in electric PTO (ePTO) mode (shown in blue).

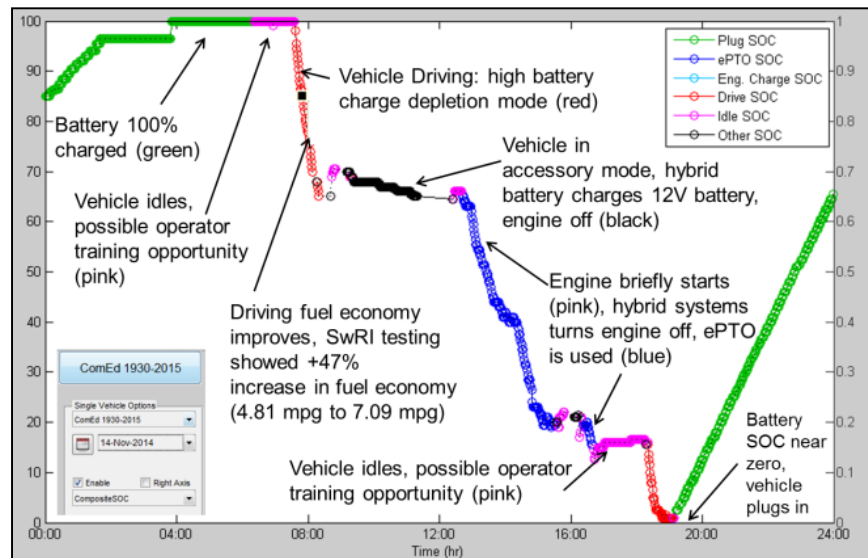


Figure III-132: Typical daily vehicle usage profile for a bucket truck

Graph Courtesy of Odyne Systems LLC

Conclusions

As these vehicles were put into service, there was a consistent increase in usage over the first few months. EPRI's last data transfer included operational data on 76 vehicles through June 2015. The processing routines and report templates are currently in progress.

Conclusions

Using ARRA Data in Support of Other DOE Efforts

The primary focus for the projects presented above has been on data collection, filtration, secure storage, and primary analysis for summary reporting. However, this data set has been used in support of other DOE efforts at NREL and will continue to be a valuable resource in the future. The vast amount of real-world operation in vocational duty cycles will continue to help aid the development of the next generation of hybrid and all-electric drive systems for medium- and heavy-duty vehicles.

Summary of Vehicle Data

- NREL continues to receive data from 259 first-generation and 200 second-generation Smith EVs (vehicles with data that can pass through the data filters to meet minimum usage requirements). NREL has also received data from 101 Navistar eStar vehicles through the end of June 2014. All of these Smith and Navistar vehicles are battery electric delivery vehicles. The data received include over 25 parameters of 1-Hz data.
- The Smith Newton EVs have been driven more than of 145,000 days, covering over 3.8 million miles.
- The Navistar eStar vehicles have been driven a total of 17,447 days, covering a combined 353,733 miles, for an average of 20.3 miles per day.
- The Shorepower Truck Electrification Project has all 50 funded sites active with >90% uptime through February 2015. A total of 77,273 hours booked and 56,073 kWh used were reported, offsetting an estimated 61,818 gallons of diesel fuel.
- As the Odyne hybrid utility analysis continues, it will be incorporated into the automated processing and analysis routines for the ARRA project.

Reporting

- Recent quarterly and cumulative reports have been posted to the web for the Smith and Navistar projects. Example reports are shown below in Figure III-133; these (and all reports) can be found at: nrel.gov/vehiclesandfuels/fleettest/
- Additional quarterly reports will continue to be added to the website beginning in October 2014 once all the September data are in, continuing the quarterly and cumulative report series.

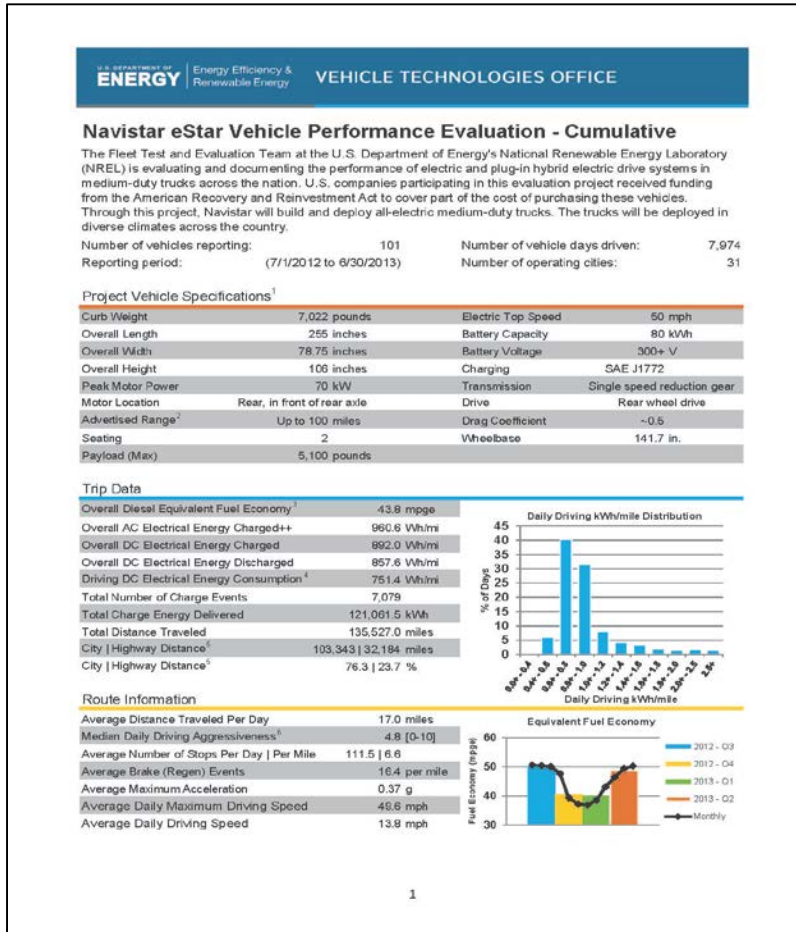


Figure III-133: Example summary report
 Available at nrel.gov/vehiclesandfuels/fleettest/

III.8.C. Products

Presentations/Publications/Patents

- Adam Duran, Adam Ragatz, Robert Prohaska, Kenneth Kelly, and Kevin Walkowicz. "Characterization of In-Use Medium Duty Electric Vehicle Driving and Charging Behavior," December 2014.
- Robert Prohaska, Adam Duran, Adam Ragatz, Kenneth Kelly. "Statistical Characterization of Medium-Duty Electric Vehicle Drive Cycles," May 2015.

III.9. Electric Bus Facility and Grid Integration

Kenneth Kelly, Principal Investigator

National Renewable Energy Laboratory
15013 Denver West Parkway, MS 1633
Golden, CO 80401
Phone: (303) 275-4465
E-mail: Kenneth.Kelly@nrel.gov

Lee Slezak and David Anderson, DOE Program Managers

Phone: (202) 586-2335; (202) 287-5688
Email: Lee.Slezak@ee.doe.gov, David.Anderson@ee.doe.gov

Start Date: 2015

End Date: 2016

III.9.A. Abstract

Objectives

This project will collect data from transit agencies operating electric buses and evaluate innovative approaches to electric vehicle (EV) charge management to assist in offsetting facility electric demand charges and grid infrastructure issues. U.S. transit authorities are beginning to incorporate all-electric transit buses into their fleets at significant numbers. Transit duty cycles may be well suited or exceedingly tough on lithium-ion batteries—the unique requirements of heavy-duty (HD) charging infrastructure further blur the picture. HD EV charging adds significant electricity demand to transit facilities.

The lack of validated field data on battery next-generation electric transit buses (BEBs) is a significant barrier to adoption of commercial BEBs. The National Renewable Energy Laboratory (NREL) will conduct an independent evaluation of BEBs and the accompanying 500-kW fast-charger, including vehicle and component performance data, duty cycle, driving range, fuel efficiency, and emissions offsets.

FY15 objectives included:

- Conduct field testing evaluation on 35-foot Proterra BEBs at Foothill Transit in West Covina, California
- Analyze in-use vehicle data and evaluate usage compared to other compressed natural gas (CNG) transit buses in the same fleet
- Investigate facility implications of fast charger integration
- Analyze controlled charging data to evaluate battery health as a factor of use and drive cycles and share data with DOE VTO Energy Storage team to simulate battery degradation in a vehicle.

Accomplishments

- Executed non-disclosure agreement with Proterra, Inc., for transfer of in-use vehicle controller area network (CAN) data.
- Received four separate one-month segments of high frequency (2 Hz) in-use vehicle CAN data from 12 buses operating at Foothill Transit
- Added transit bus data to Fleet DNA database for use on other DOE projects
- Performed initial analysis on data and presented results to Foothill Transit, Proterra, and the California Air Resources Board (CARB).

Future Achievements

- Proterra is currently refining its battery health tests, after which the data will be made available to NREL for analysis
- Perform a detailed drive cycle and performance analysis of Foothill Transit’s BEBs and fast chargers
- Collect in-use data from CNG baseline vehicles on various routes to use as a comparison for performance and emissions
- Develop FASTSim vehicle model to investigate feasibility of the electrification of other routes
- Conduct laboratory chassis dynamometer testing of both the BEB and the conventional CNG baseline bus to accurately quantify fuel and emissions savings
- Collect and evaluate charging profile data from the Eaton 500-kW fast chargers.



III.9.B. Technical Discussion

Background

NREL’s Fleet Test and Evaluation team has found medium-duty and HD vehicle fleets to be good candidates for deploying low-emitting advanced technologies due to their large numbers, high vehicle miles traveled—and consequently high petroleum fuel consumption and emissions—and frequent operation in large population centers, as well as common return-to-base fueling regimes and consistent driving routes.

Previous testing and analysis conducted by NREL have illustrated the influence of drive cycle and vehicle usage on both energy consumption (from liquid fuels and high-voltage hybrid battery packs) and exhaust (or well-to-wheels) emissions. Drive cycle has also been shown to influence the all-electric range of battery EVs, the charge-depleting range of plug-in hybrid EVs, and the potential fuel economy benefit of hybrid EVs. Accordingly, fleet customers can benefit from a further understanding of advanced vehicle technology deployment to minimize fuel consumption and emissions. It has also been shown that large-scale deployments of EVs in a localized area can lead to power quality and power cost issues due to increased peak demand.

Introduction

Working in conjunction with a previously funded CARB project, NREL’s Fleet Test and Evaluation group partnered with the electric bus manufacturer Proterra to perform a detailed performance evaluation of its BEBs in-use at Foothill Transit. Proterra provided the in-use raw vehicle data for this analysis as Proterra collects and maintains detailed (2 Hz) data for monitoring and development work.

These data will be used to understand the overall usage and effectiveness of the BEBs in transit fleet operations and will also be compared to operations of conventional counterparts in the same location. Through this collaboration with Proterra, NREL hopes to provide a more focused investigation to understand the implementation and performance of BEBs.

Approach

Data were received electronically from Proterra via a secure FTP site starting in the summer of 2015. A total of 774 days of operational data were provided for 12 buses during the following four periods throughout the year (to account for any seasonal variation).

- July – August 2014
- October – November 2014
- January – February 2015
- April – May 2015.

Data channels include details on vehicle speed; GPS location; battery pack state of charge (SOC); battery pack current; battery pack voltage; inverter current; inverter voltage; motor heating, ventilating, and air conditioning (HVAC) status; and more. These data will be used to assess vehicle and component performance and conduct detailed drive cycle analysis, as well as to build and refine vehicle models for further analysis.

Battery lifetime uncertainty is a major barrier to fleet manager decisions regarding the adoption of EVs of all types. To reduce life uncertainty, NREL and Proterra are working to develop a study to perform benchmarking tests of Proterra's BE35 battery packs at regular stages throughout their life.

Proterra is currently finalizing its in-field battery pack health test procedure, which will be used on every vehicle at least every 12 months and at every individual customer facility at least once per quarter. NREL will perform an independent test to validate this procedure, and then Proterra will provide the results of the in-field testing from the Foothill Transit buses.

The battery health benchmarking test results will provide valuable in-use data. These data will allow NREL to better quantify battery pack health and track battery performance changes over life as well as validate battery life assumptions to help develop a fleet business case.

Results

Initial analysis was performed on the location-based data to ensure data integrity and to better understand the operation of the BEBs on an electrified route. Figure III-134 and Figure III-135 show Foothill Transit line 291 with the fast charger located approximately in the middle at the Pomona Transit Center. This route consists of two loops, a 9.3 mile northern loop and a 6.8 mile southern loop, for a total distance of 16.1 miles.

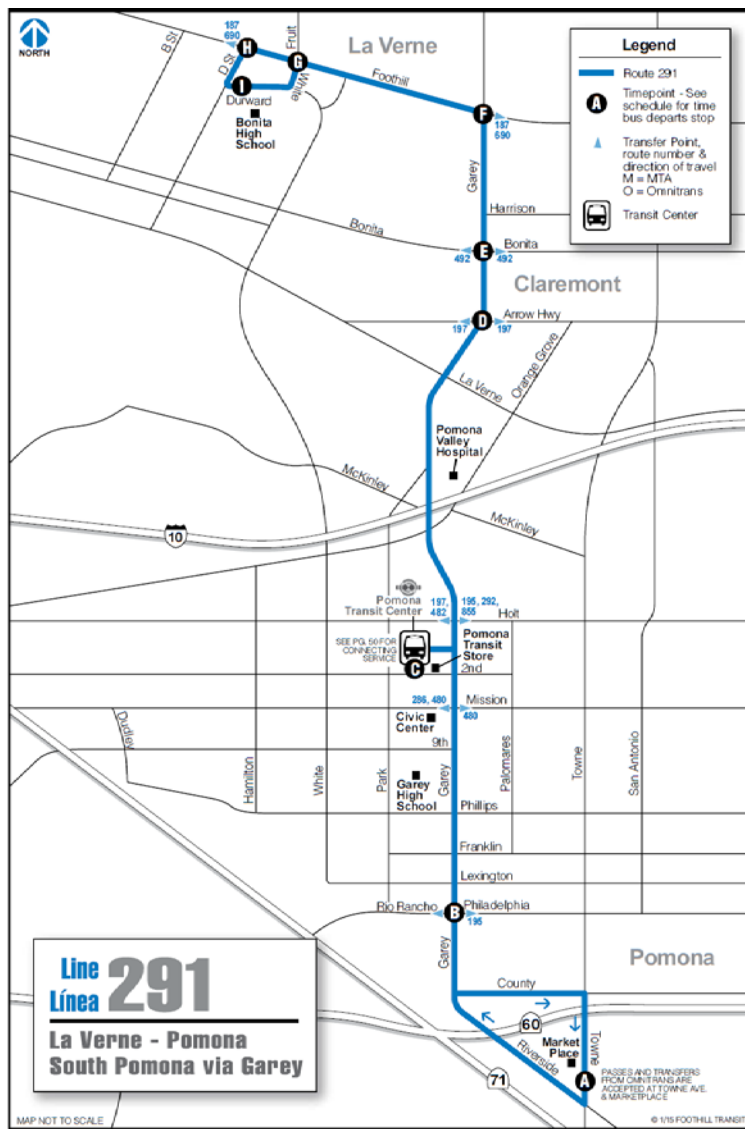


Figure III-134: Foothill Transit Line 291 route map

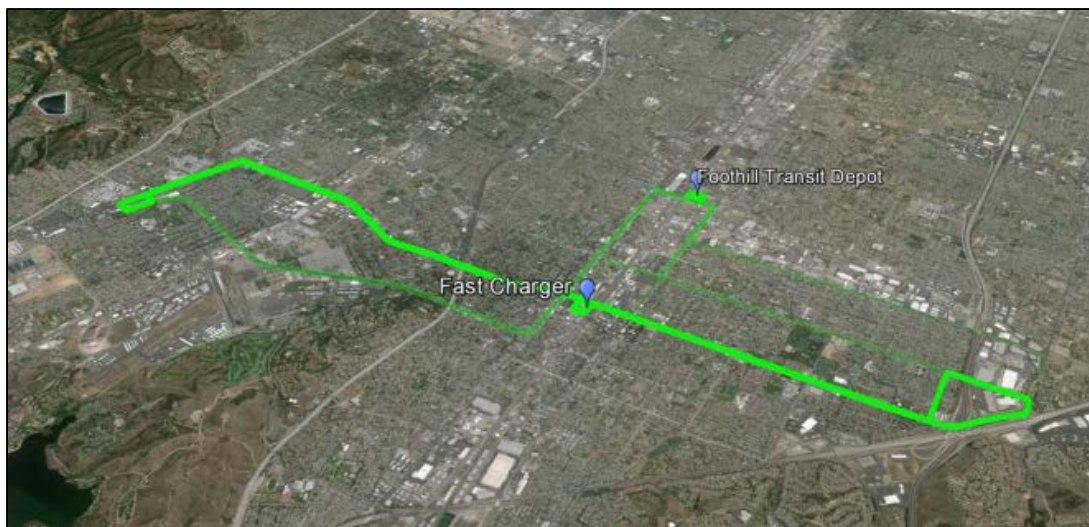


Figure III-135: Foothill Transit route 291 shown with GPS data

Looking more closely at the GPS data, the location of the fast charger stations at the Pomona Transit Center can be seen in Figure III-136 as green traces of bus activity pulling into the charging station.

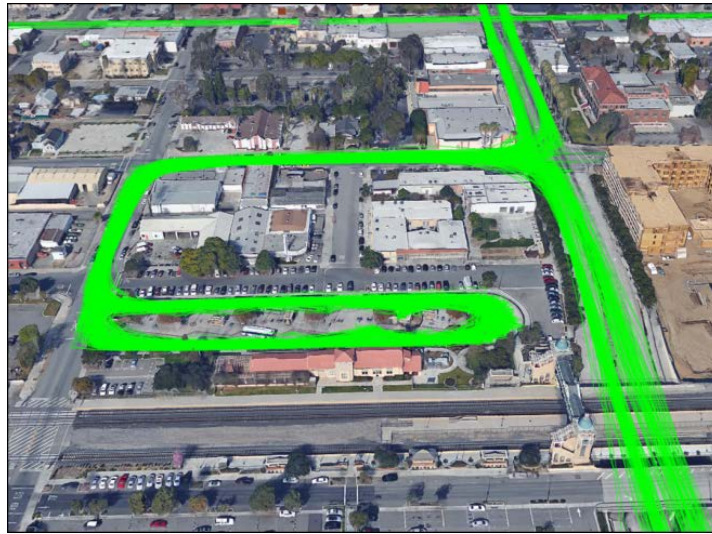


Figure III-136: Fast charger location on Foothill Transit’s line 291

Using NREL’s Drive-Cycle Rapid Investigation, Visualization, and Evaluation Analysis (DRIVE) tool, preliminary drive cycle statistics were calculated using for all 774 driving days and are shown in Table III-24.

Table III-24: Foothill Transit daily drive cycle statistics

Daily Average	Foothill Transit
Average speed (including idle time) (mph)	8.42 mph
Average driving speed (mph)	17.66
Kinetic intensity (1/mi)	1.71
Stops per mile	3.70
Number of stops per day	444
Distance traveled (miles)	119.30
Daily hours of operation (hours)	13.9 total / 6.72 driving
Acceleration (ft/s ²)	1.44
Deceleration (ft/s ²)	-1.81
Percent of total time charging	5.56%

Additional drive cycle metrics were also calculated for the Foothill Transit data set as well as for the existing NREL Fleet DNA mass transit data set. Figure III-137 shows the kinetic intensity vs. average driving speed for these two data sets as well as for four standard chassis dynamometer test cycles.

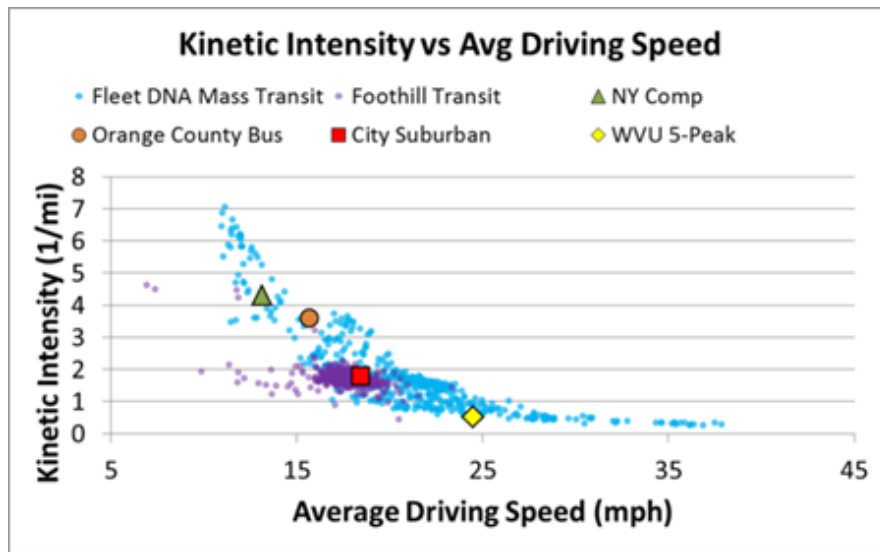


Figure III-137: Kinetic intensity shown as a function of average driving speed for all Foothill Transit data (purple) and all Fleet DNA mass transit data (blue) compared to select standard chassis dynamometer test cycles

When comparing the Foothill Transit data set to the existing Fleet DNA mass transit database, one can see that on average the Foothill Transit buses stop more frequently and, as shown in Figure III-138, have a more consistent (tightly clustered) pattern on a per-mile basis than the other vehicles.

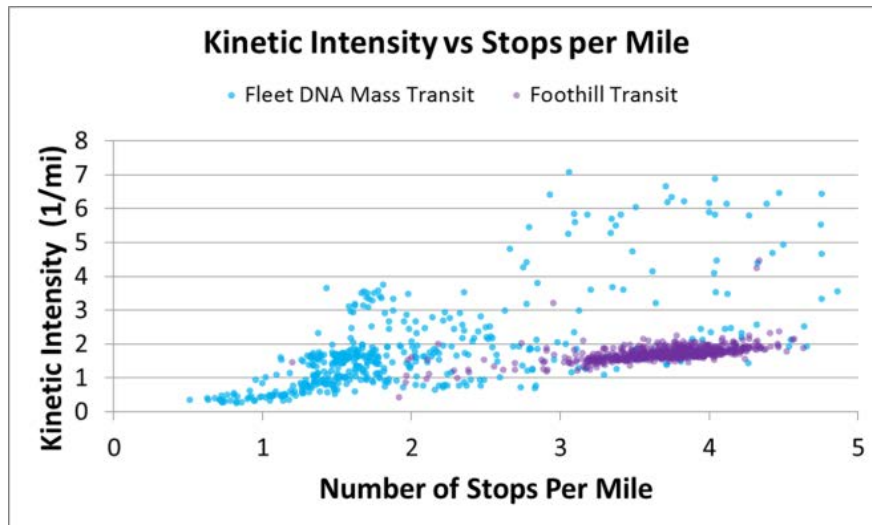


Figure III-138: Kinetic intensity as a function of daily average stops per mile for both the Fleet DNA mass transit database and the Foothill Transit BEBs

Further investigation into the operation of these BEBs confirms that not only do these buses stop quite often when on route, they spend very little time at the fast charging stations while their battery packs are recharged. Figure III-139 shows a single 16.1-mile loop on line 291 with three separate charging events. The green line shows the cumulative distance for the day. It can also be seen that in between charges, the battery pack SOC fluctuates between approximately 30% and 80%.

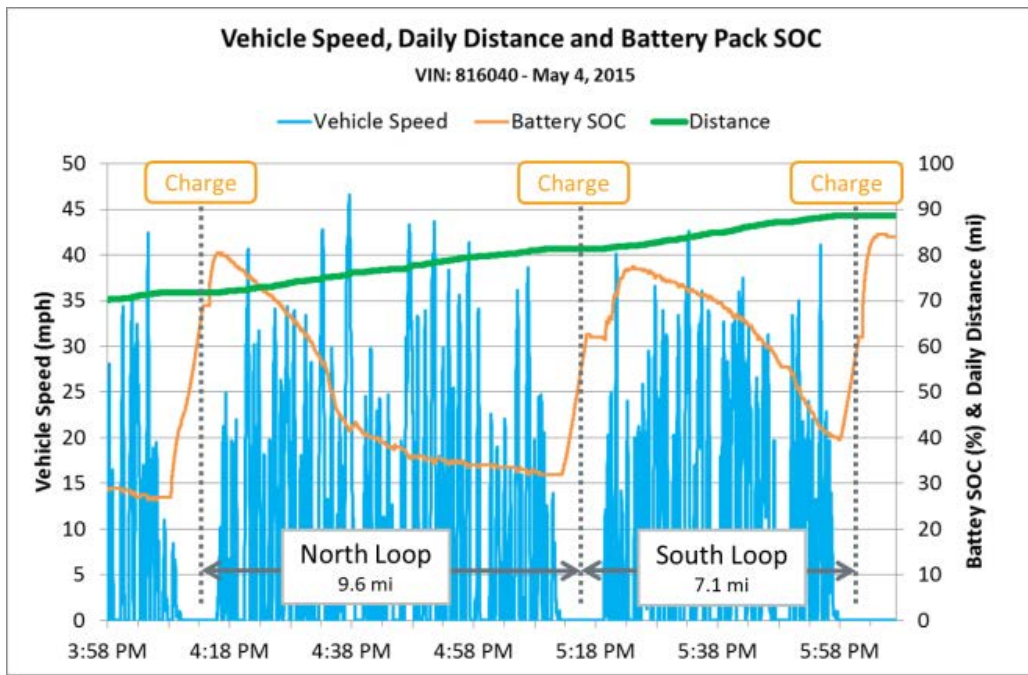


Figure III-139: Vehicle speed, distance, and battery pack SOC shown for one full "loop" on line 291

When looking at the average battery pack histogram shown in Figure III-140, it can be seen that the majority of the time the battery pack is between 60% and 90% SOC with a mean of 75.4% and a standard deviation of 11.3%. This indicates there may be an opportunity to shift the usage window to a lower SOC on average to help prolong battery pack life.

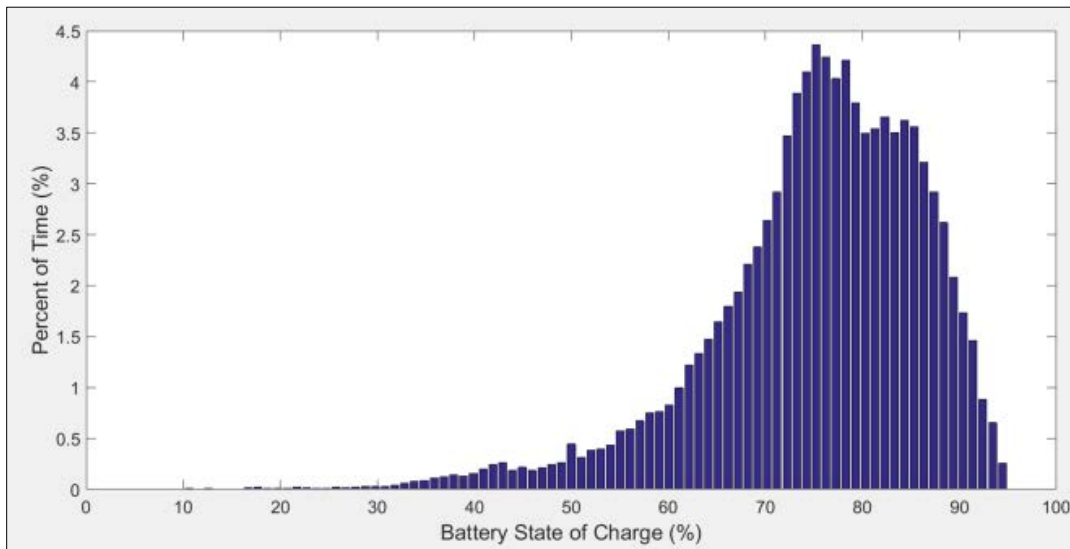


Figure III-140: Average battery pack SOC for all vehicles sampled at 2 Hz while vehicle was logging data

More detailed analysis will be performed on power electronics and accessory loads in the future. Figure III-141 shows an example of the buses' heater cycling on and off while stationary, allowing for isolation of this 8.3-kW load.

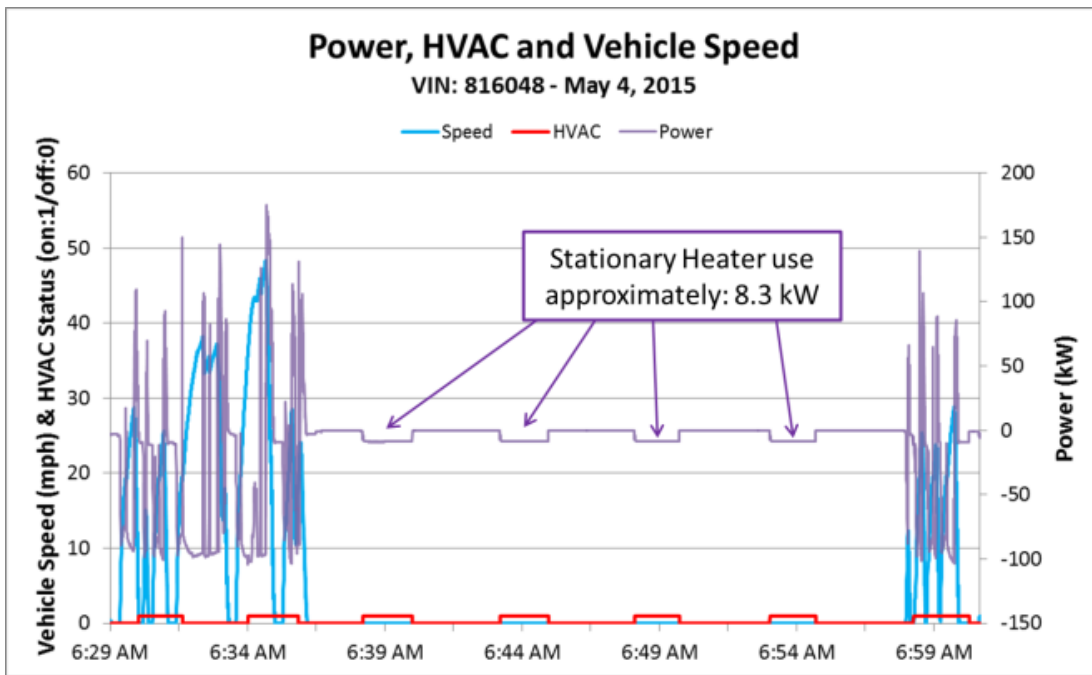


Figure III-141: Auxiliary load analysis example showing the power impact of the resistive element heater during stationary use

Figure III-142 shows a “heat map” illustrating the relationship between calculated battery power and vehicle speed. In this figure, positive power represents charging or regenerative braking, and negative power is power being drawn from the pack. There are two areas of interest in this figure: the first is at zero speed where there is a concentration of power going into the pack; and the second is at 20 mph, which shows a higher concentration of regeneration braking energy into the pack during at what appears to be the downshifting sequence where the transmission holds speed for a brief amount of time while the shift occurs.

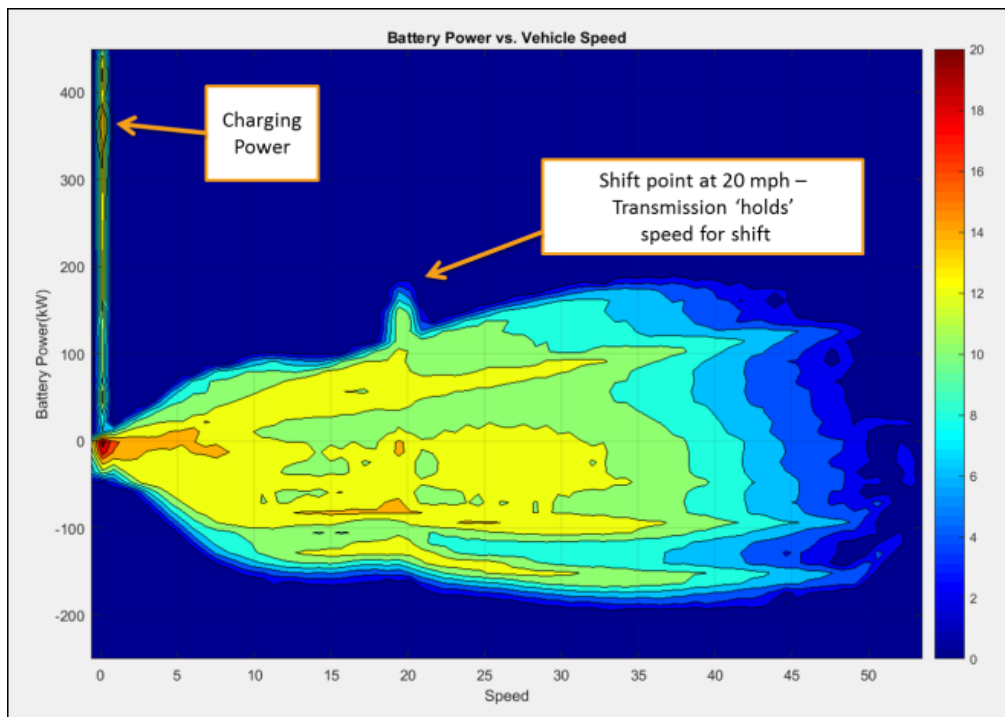


Figure III-142: Heat map showing the distribution of battery power as a function of vehicle speed (positive power indicates energy into the pack)

Conclusions

Additional analysis is still required to draw significant conclusions on the technology, but the findings to date include the following:

- Average energy efficiency was found to be 3.25 kWh/mi over 399,663 miles of use.
- The average battery pack SOC is equal to 75.4%, indicating a possibility for a usage window shift.
- Average runtime per day is 13.2 hours with an average of 12.5 charges per day. Each charge averages 20 kWh energy delivered.
- Accessory loads contribute to the overall range capability as over 50% of "system on" time is spent at a speed of 0 mph where lighting and HVAC loads are still required.

III.9.C. Products

Publications

Only initial data have been collected and analyzed to date. No publications have been produced at this time. A final technical report is planned during FY16.

III.10. Fleet DNA

Kenneth Kelly, Principal Investigator

National Renewable Energy Laboratory (NREL)
15013 Denver West Parkway, MS 1633
Golden, CO 80401
Phone: (303) 275-4465
E-mail: Kenneth.Kelly@nrel.gov

Lee Slezak, DOE Program Manager

U.S. Department of Energy (DOE)
Phone: (202) 586-2335
Email: Lee.Slezak@ee.doe.gov

III.10.A. Abstract

Objectives

The objective of Fleet DNA is to accelerate the evolution of advanced vehicle development and support the strategic deployment of market-ready technologies that reduce costs, fuel consumption, and emissions. The Fleet DNA clearinghouse of commercial fleet transportation data helps vehicle manufacturers and developers optimize vehicle designs; helps fleet managers match appropriate advanced vehicle technologies to their fleets; and provides in-use data for standard drive-cycle development, research and development, tech targets, and rule making. Specific objectives of the Fleet DNA project in FY15 include:

- Continue to grow the Fleet DNA database through the inclusion of additional data
- Improve project visibility through ongoing refinement of the Fleet DNA website and publication of associated research
- Enhance integration of Fleet DNA with existing DOE tools and computational capabilities
- Improve existing data processing routines and database structure to optimize speed when processing data.

Accomplishments

- Significantly increased volume of data stored in Fleet DNA database; Fleet DNA now houses data on more than 1,600 unique vehicles
- Performed analysis and published results examining impact of road grade on simulated commercial vehicle fuel economy
- Examined methods to estimate vehicle fuel economy based on drive cycle metrics. Results of the research were released as an SAE publication.
- Performed a sweep study exploring the effects of vehicle parameters such as aerodynamic drag, rolling resistance, and mass on heavy-duty vehicle fuel consumption. Results were published and presented at SAE Commercial Vehicles Congress.
- Fleet DNA's unique capabilities and data were leveraged to support multiple project partners including the California Air Resources Board, the South Coast Air Quality Management District, and the U.S. Environmental Protection Agency (EPA).

Future Achievements

- Additional efforts will be made to continue to grow the volume and variety of data stored in the Fleet DNA database. In the first two quarters of FY16, NREL expects to receive data on an additional 8,000 vehicles are expected to be received, continuing Fleet DNA’s exponential growth trajectory.
- Continued leveraging of Fleet DNA data and capabilities to support projects within DOE’s portfolio
- Updated reporting and enhanced data availability through ongoing improvements to the Fleet DNA project website
- Development and refinement of additional novel data analysis capabilities.



III.10.B. Technical Discussion

Background

The Fleet DNA clearinghouse of commercial fleet transportation data helps vehicle manufacturers and developers optimize vehicle designs while assisting fleet managers with the selection of advanced technologies for their fleets, all with the goal of reducing petroleum consumption and improving energy efficiency. This online database and tool—available at nrel.gov/fleetdna—provides both static and interactive data summaries and visualizations representative of the real-world “genetics” for medium- and heavy-duty commercial fleet vehicles.

The data for each visualization/report have been drawn from multiple fleets operating in a variety of vocations for each vehicle type, across multiple locations within the United States. This extensive breadth of data is necessary to capture the wide range of vehicle operation resulting from different geographies and fleet applications demonstrated by medium- and heavy-duty vehicles. In addition to providing public access to commercial fleet data summaries and visualizations, Fleet DNA serves as a portal for users to explore related DOE programs and projects such as NREL’s fleet testing activities and reports, the DOE Office of Energy Efficiency and Renewable Energy’s Alternative Fuels Data Center, and the Clean Cities’ National Clean Fleet Partnership program.

Designed by NREL in partnership with Oak Ridge National Laboratory, this online database and the accompanying reports help vehicle manufacturers and fleets understand the broad operational range of many of today’s commercial vehicle vocations.

Introduction

FY15 saw significant growth in the Fleet DNA project, both in terms of data stored in the database and applications of data to support ongoing research efforts. Ongoing partnerships with fleets, industry leaders, and other government and research organizations resulted in the addition of over 1,000 new vehicles to the database, and ongoing research efforts led to the publication of 3 new Society of Automotive Engineers technical research papers. Contained in this report will be a review of the current NOSQL database data fusion approach adopted by the Fleet DNA project in FY14, as well as a discussion of the major areas of accomplishment in FY15. Details regarding the ongoing growth of data stored in the Fleet DNA database will be examined, Fleet DNA’s enhanced capabilities will be presented, and the results of applying Fleet DNA to exploratory simulation and model activities will be explored. Finally, the report will close with an overview of ongoing project support activities, reporting enhancements and a summary of major conclusions.

Approach

The Fleet DNA database serves as an excellent example of the power of “big data” fusion techniques when applied to transportation research. Through the controlled analysis and fusion of multiple datasets, studies that

were once limited due to data ability can now be performed. Additionally, more complex research questions can be explored due to the ability to link multiple large data sets, as shown in the example in Figure III-143.

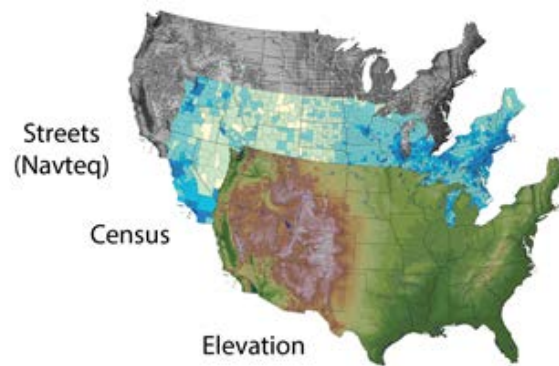


Figure III-143: Illustration of data fusion in Fleet DNA with multiple data layers

Credit: NREL

In Figure III-143 the U.S. elevation dataset is being merged with the U.S. Census dataset and the Navteq streets layer providing information that allows researchers to explore the correlations between population, road grade, and infrastructure. Each individual data layer provides very detailed and informative information; when combined, the layers provide opportunities for deeper analysis and observation of more complex phenomenon.

To address the need for better handling of the ever increasing volume and complexity of data stored in the Fleet DNA database, NREL researchers adopted a NoSQL database structure in FY14. The NoSQL database structure was chosen as a means of overcoming the limitations of traditional SQL-based databases when handling data with nonuniform columns and data labels. Traditional databases store data as tables with a fixed structure. To find data within a table, the whole table is read off a disk and then divided into a subset of smaller pieces for analysis. When dealing with billions of records, the approach will scale well as long as the number of columns within a table is minimized. When the number of columns in a table increases, the speed at which data can be accessed decreases exponentially. The loss of efficiency is the result of the increased amount of data needed to be sorted within a table. Further, all tables in a database require the data being archived to have a fixed structure so that every time records are inserted, the same columns are always available.

To ensure that the normalized Fleet DNA data archive can handle variability in the number of columns archived while not sacrificing efficiency, a NoSQL data storage approach was implemented. NoSQL is a combination of tools and methods for web-scale data storage. The approach is more robust, because it does not rely on a rigid data table structure and focuses on organizing data in a way in which only what is needed is ever read off a disc. This allows for greater flexibility in the types and volume of data stored in the database. For example, data channels specific for electric vehicles (EVs), such as state of charge and battery voltage/current, can be stored in the NoSQL database for each vehicle that has this type of data without wasting database space by devoting empty storage arrays for vehicles, such as a conventional diesels, that may not generate this type of information. This is also helpful when working with historical data and data sourced via project partners. As data collection continues to decrease in cost, more and more information is being captured for future use in research and development activities. The NoSQL configuration provides researchers with the agility needed to adapt the Fleet DNA database to handle ever more complex and detailed data without running into scalability issues.

Results

Additional datasets

One of the greatest areas of growth for the Fleet DNA project in FY15 came as a result of continued growth and expansion of the data stored within the database. With the addition of NREL's existing Smith and Navistar EV datasets, as well the contributions from a number of commercial vehicle manufacturers, the Fleet DNA database saw the number of vehicles stored in the database grow from 550 vehicles in FY14 to nearly 1,700

vehicles in FY15. This represents a nearly three-fold increase in the volume of individual vehicle data stored in the database. Looking at the number of individual days of operation, the Fleet DNA database grew from approximately 8,000 days in FY14 to just under 177,000 days in FY15. Much of this growth can be attributed to the inclusion of the Smith and Navistar data collected by NREL for the past three years as part of a separate American Reinvestment and Recovery Act (ARRA) project. Finally, looking at the total mileage growth from FY14 to FY15, the number of miles available for analysis grew from 480,000 miles to just under 7,670,000 miles. Again, much of this growth can be attributed to the inclusion of the ARRA datasets; however, the Fleet DNA project continues to demonstrate exponential growth in data stored and available for analysis, as shown in Figure III-144.

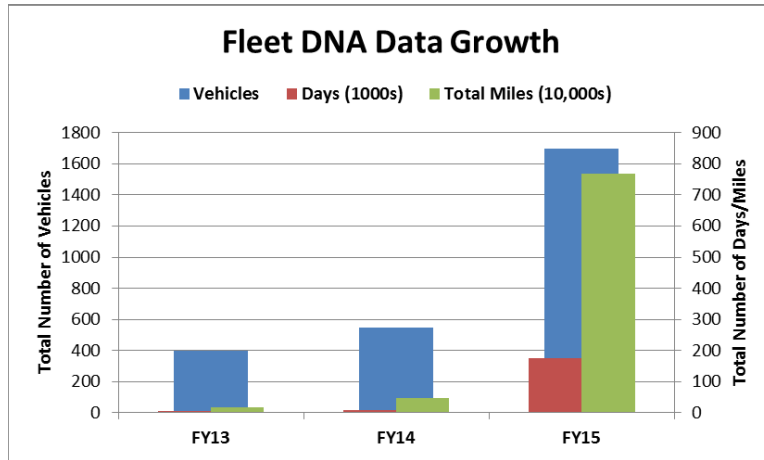


Figure III-144: Historical growth of Fleet DNA project

Credit: NREL

In addition to expansion in the volume of data stored in Fleet DNA, another way to look at the growth in the database can be to examine the increase in geographic diversity of the data. At the conclusion of FY15, Fleet DNA contained data coverage for roughly one-third of the United States, as shown in Figure III-145, with coverage expected to increase dramatically in FY16 with the inclusion of additional long-haul and regional delivery datasets which are expected to traverse more of the interior United States via highway shipping corridors.

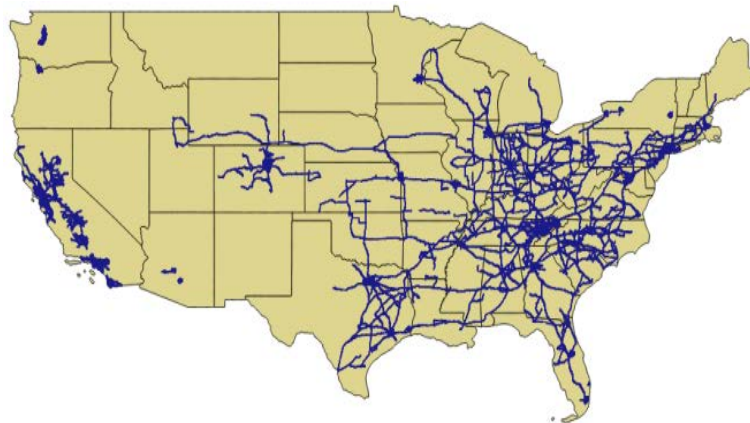


Figure III-145: Current geographic coverage of Fleet DNA data

Credit: NREL

Expanded capabilities

FY15 saw the improvement of existing road grade estimation capabilities through the development of a novel road grade estimation method utilizing two new Fleet DNA national data layers. While supporting EPA's

phase 2 greenhouse gas (GHG) regulation development efforts, NREL researchers were able to integrate TomTom's national road network layer and national road grade layer into the Fleet DNA database. These new data layers allow researchers to accurately determine road grade for a vehicle traveling on any major roadway in the United States based on its geographic location information (latitude and longitude) and direction of travel. An analysis of this new method compared to the existing U.S. Geological Survey's Digital Elevation Model-based approach was performed to quantify the differences between the methods. Results of this analysis can be found in the report titled "EPA GHG Certification of Medium- and Heavy-Duty Vehicles: Development of Road Grade Profiles Representative of U.S. Controlled Access Highways" located in NREL's publication database at nrel.gov/docs/fy15osti/63853.pdf.

In addition, NREL also incorporated EPA's Motor Vehicle Emission Simulator (MOVES) model containing estimated vehicle emissions and daily vehicle miles traveled on a county by county basis throughout the United States. This allows NREL researchers to combine Fleet DNA's drive cycle data with the national-scale models to perform novel predictive traffic analyses, as shown in Figure III-146.

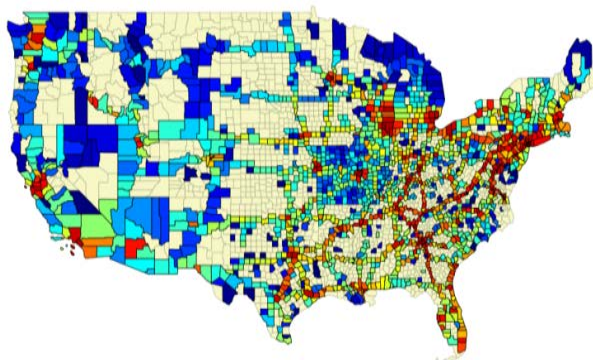


Figure III-146: U.S. major highway corridors, color coded by vehicle miles traveled

Credit: NREL

Modeling and simulation

In addition to expanding the data stored in the Fleet DNA database and further improving project analysis capabilities, significant effort was made in FY15 to apply the data stored in the Fleet DNA database to address the complex problems facing the commercial vehicle industry and DOE. One of the key areas of need is a better understanding and quantification of the effects of drive cycle on fuel consumption in medium- and heavy-duty vehicles. To address this need, NREL researchers attempted to first determine the drive cycle metrics strongly correlated to fuel consumption while developing a method to predict vehicle fuel economy solely by examining drive cycle characteristics. An additional area of interest to commercial vehicle fleets is a better understanding of the effects of vehicle parameters such as aerodynamic drag and tire rolling resistance on fuel economy. Some limited information is available documenting the effects of individual vehicle improvements on fuel economy, however little is known about the correlation and potential compounding effects of multiple vehicle parameter changes. To address this need, NREL researchers performed simulation-based sweep studies to quantify the effects of key parameters—such as aerodynamic drag, rolling resistance, and vehicle mass—on a simulated Class 8 beverage delivery truck operating on three standard chassis test cycles. Finally, limited data is available documenting the effects of road grade on commercial vehicle fuel economy, and there is a significant need by industry to understand road grade effects when attempting to implement future fuel saving strategies. Past chassis dynamometer testing has suggested that road grade could have as much as a 25% impact on the fuel economy of a fully loaded transit bus. To address this need, NREL researcher combined FASTSim modeling with the vocational data stored in the Fleet DNA database and examined the effects both mass and road grade have on simulated fuel economy for a variety of medium- and heavy-duty vehicle vocations. The results of this research will be presented in the following subsections.

Effects of Drive Cycle Properties of Fuel Consumption

A polynomial model, a black box artificial neural net model, a polynomial neural network model, and a multivariate adaptive regression splines (MARS) model were developed and verified using data collected from

chassis testing performed on a parcel delivery diesel truck operating over the Heavy Heavy-Duty Diesel Truck (HHDDT), City Suburban Heavy Vehicle Cycle (CSHVC), New York Composite Cycle (NYCC), and hydraulic hybrid vehicle (HHV) drive cycles. Each model was trained using one of four drive cycles as a training cycle and the other three as testing cycles. By comparing the training and testing results, a representative training cycle was chosen and used to further tune each method. HHDDT as the training cycle gave the best predictive results, because HHDDT contains a variety of drive characteristics, such as high speed, acceleration, idling, and deceleration. Among the four model approaches, MARS gave the best predictive performance, with an average percent error of -1.84% over the four chassis dynamometer drive cycles. To further evaluate the accuracy of the predictive models, the approaches were applied to real-world data. MARS outperformed the other three approaches, providing an average percent error of -2.2% over four real-world road segments. The MARS model performance was then compared to powertrain modeling results over HHDDT, CSHVC, NYCC, and HHV drive cycles using NREL’s Future Automotive Systems Technology Simulator (FASTSim). The results indicated that the MARS method achieved comparable predictive performance with FASTSim.

Among the four chassis dynamometer test cycles, each cycle was considered as a training cycle and the other three as testing cycles. By comparing the training and testing results, a representative training cycle can be chosen. Table III-25 shows the summary of training and testing performance for fuel consumption (FC). “Measured Ave. FR” is defined as measured average fuel rate and “Predicted Ave. FR” is defined as predicted average fuel rate. The results indicate that HHDDT as a training cycle gives the best performance. This is likely because HHDDT contains a variety of driving characteristics, such as idling, accelerating, cruise, and decelerating. In the following nonlinear study examining 3 common methods (Artificial Neural Network (ANN), Polynomial Neural Network (PNN), and Multivariate Adaptive Regression Splines (MARS)), the HHDDT was chosen as the training cycle and the other three were used as the testing cycles.

Once the appropriate test and training cycles had been identified, a FASTSim conventional diesel truck model (Table III-25) was developed and run over the HHDDT, CSHVC, NYCC, and HHV cycles, and then the results were compared with that of the MARS model, as summarized in Table III-26.

Table III-25: Information on the Conventional Diesel Truck Model

Vehicle Type	Diesel Conventional Truck
Vehicle Tested Weight (lb)	15,410
Coefficient of Rolling Resistance	0.0071
Coefficient of Aerodynamic Drag	0.71
Frontal Area (m2)	6
Rated Engine Power (HP)	200

Table III-26: Predictive Results of FASTSim and MARS Approaches

Approach\Cycle		HHDDT	CSHVC	NYCC	HHV
FASTSim	Measured. Ave. FR (L/h)	8.53	5.67	4.51	8.47
	Predicted. Ave. FR (L/h)	8.72	5.60	4.17	8.92
	Relative Error (%)	2.24	-1.27	-7.53	5.34
MARS	Measured. Ave. FR (L/h)	8.53	5.67	4.51	8.47
	Predicted. Ave. FR (L/h)	8.53	5.94	4.24	8.09
	Relative Error (%)	0.00	4.79	-5.79	-4.53

Examining Table III-26, it can be seen that MARS gave the best predictive performance with an average percent error of 1.84% for the four chassis dynamometer test cycles. The models were also applied to real-world data for further evaluation of accuracy. MARS gave the best predictive results with an average percent error of -2.2%. Ultimately, the performance of the MARS approach was compared with that of FASTSim; the results showed that the MARS approach achieved an accuracy comparable to that of FASTSim.

Quantitative Effects of Vehicle Parameters on Fuel Consumption

A quantitative study was performed analyzing the impacts of various factors on FC and fuel economy (FE) by modeling and simulating a Class 8 beverage delivery truck. The data used for this study was captured via onboard data logging of a vehicle similar to the one shown in Figure III-147.



Figure III-147: Example beverage delivery truck

Credit: NREL

To perform the parametric sweep study, researchers input the vehicle specifications shown in Table III-27 into FASTSim to develop digital vehicle model for use in the analysis.

Table III-27: Vehicle Specifications

Vehicle Type	Class 8 Truck
Vehicle Tested Weight (lb.)	33,237
Tire Size	305/70R22.5
Coefficient of Rolling Resistance	0.0085
Coefficient of Aerodynamic Drag	0.7963
Frontal Area (m ²)	9.5
Engine Power (HP)	284
Test Cycle	HHDDT, WVU City, and CILCC

Once the model was developed, a series of parametric sweep studies were performed using real-world drive cycle data stored in the Fleet DNA database. The simulation studies were done to examine the effects of changing a number of vehicle factors on simulated fuel economy. Factors included vehicle weight and the coefficients of rolling resistance and aerodynamic drag. Simulation results from a single parametric study revealed that FC was approximately a linear function of the weight, coefficient of aerodynamic drag, and rolling resistance over various drive cycles. The study of the impact of two technologies on FE suggested that,

depending on the circumstances, it may be more cost effective to reduce one parameter (such as coefficient of aerodynamic drag) to increase FE, or it may be more beneficial to reduce another parameter (such as the coefficient of rolling resistance). It also provided a convenient way to estimate FE by interpolating within the parameter values and extrapolating outside of them. The simulation results indicated that FC could be reduced from 38.70 L/100 km, 50.72 L/100 km, and 38.42 L/100 km in the baseline truck to 26.78 L/100 km, 43.14 L/100 km, and 29.84 L/100 km over the California Air Resources Board (CARB) Heavy Heavy-Duty Diesel Truck (HHDDT), West Virginia University (WVU) City, and Composite International Truck Local and Commuter (CILCC) drive cycles, respectively, when DOE's three targeted new technologies were applied simultaneously. A visualization of the multivariate sweep performed on the HHDDT cycle can be seen in Figure III-148.

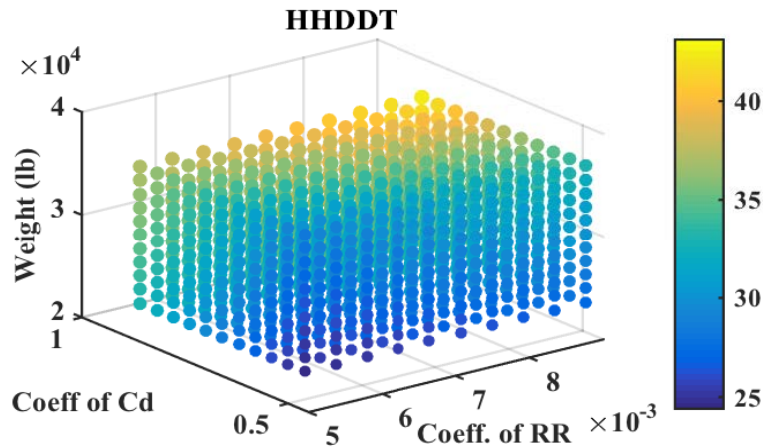


Figure III-148: Effects of aerodynamic drag and rolling resistance on fuel consumption

Credit: NREL

Impact of Road Grade on Simulated Fuel Economy

Understanding the drivers of fuel use in commercial applications is a necessary step in designing more efficient engines, powertrains, and vehicles. Existing studies have demonstrated incremental fuel use resulting from commercial vehicle operation on grades ranging from 10%–30%. While insightful, these studies generally focused on specific vocations (most commonly Class 8 line haul) and were often limited to a small number of routes and drive cycles. The literature lacked an aggregate quantification of the impact of road grade on fuel use in commercial applications over a wide range of operating conditions. The study performed by NREL set out to characterize the increase in fuel use incurred due to road grade through large-scale simulation of commercial vehicle operation using real-world drive cycles and road grade data. The study used real-world commercial vehicle drive cycles drawn from NREL's Fleet DNA database to simulate the effects of road grade on fuel economy across a range of vocations, operating conditions, and locations. Drive cycles were matched with vocation-specific vehicle models and simulated with and without road grade. The results of the study suggested that road grade accounts for 1%–9% of fuel use in commercial vehicles on average and up to 40% on select routes. Examining the results of the study in greater detail provides insight on a number of informative trends while also reinforcing many past intuitive observations. For example, Figure III-149 demonstrates an increasing trend in fuel consumption as average grade increases.

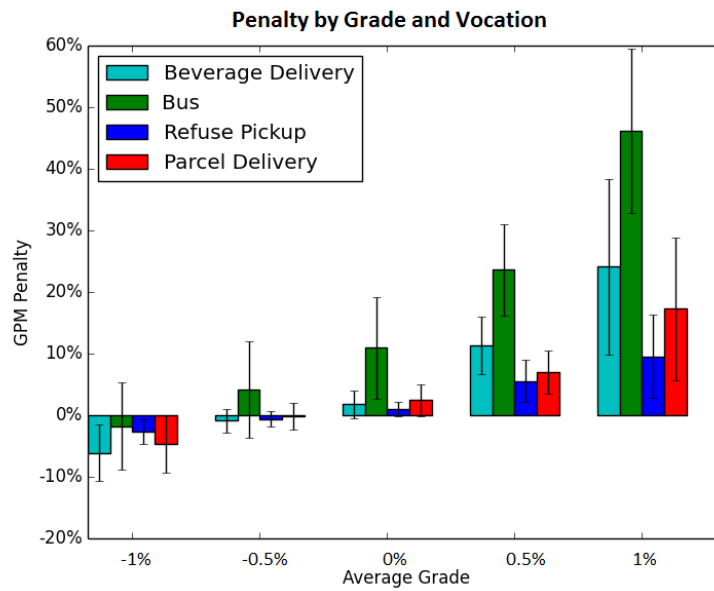


Figure III-149: Overall simulated road grade fuel economy penalty

Credit: NREL

Looking closer at Figure III-149, one can also see that trips with small average grade can still have significant fuel penalties. These penalties can be explained by root mean squared (RMS) grade. Figures III-7 and III-8 compare fuel use between vocations by isolating trips with roughly net-zero elevation change, or equivalently distance-averaged absolute grade between 0.0% and 1.0%. RMS grade is used as an indication of the average magnitude in grade across a trip. RMS grade distinguishes between a trip with no climbs or descents and a trip with equal amounts of climbs and descents. Figure III-150 suggests that for RMS grade close to 3%, average fuel penalties range from 4% to 15% by vocation. However, for the few trips with very large RMS grade (above 6%), penalties can exceed 30% of fuel use.

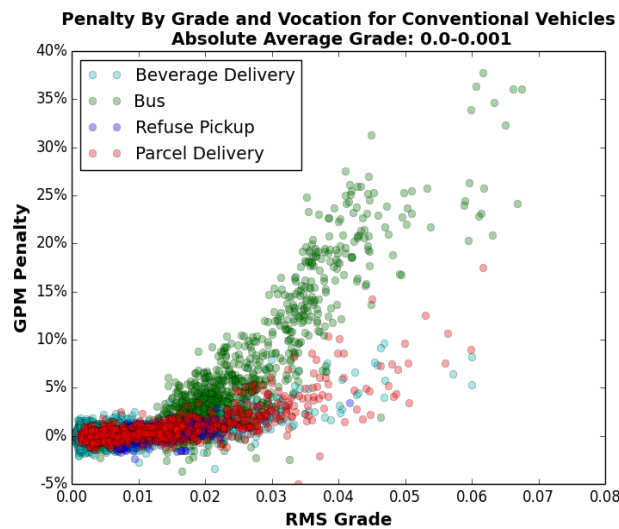


Figure III-150: Effect of grade on fuel economy penalty

Credit: NREL

The relationship between RMS grade and fuel use also appears to vary by vocation. In Figure III-150, for example, even while attempting to account for both average grade and RMS grade, the bus vehicle model had a higher fuel penalty curve. This increase is partially explained by average grade.

In addition to exploring the effects of road grade on fuel consumption in isolation, additional work was performed exploring the effects of vehicle payload over the same range of drive cycles and vehicle vocations. For all vocations examined, the average penalty increased with the increase in mass. Figure III-151 shows the effect of increasing mass on fuel penalty considering different levels of RMS grade for the parcel delivery vocation. The other vocations were similar, with the higher mass corresponding to an additional increase in penalty. The variation in penalty also increases with both RMS grade and mass.

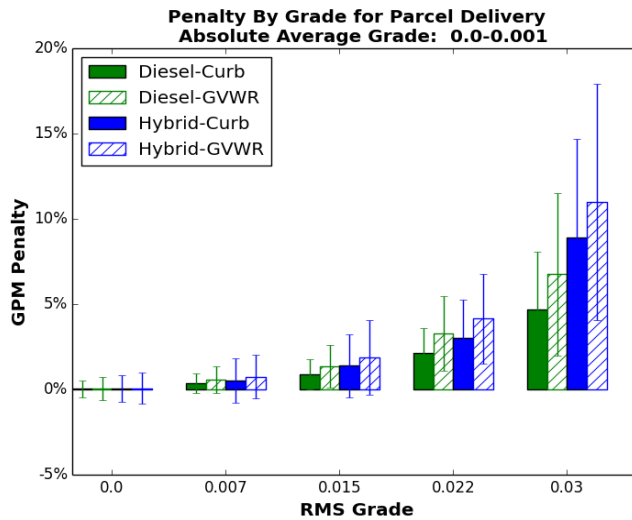


Figure III-151: Effect of vehicle payload on fuel economy over range of road grade conditions
Credit: NREL

Reporting

In FY15, updates to existing reports hosted on the Fleet DNA website were made to reflect the increase in available Fleet DNA data along with expanded analysis capabilities. As shown in Figure III-152, additional composite data charts were developed and the Fleet DNA website was redesigned to improve user accessibility.

Fleet DNA: Commercial Fleet Vehicle Operating Data

The Fleet DNA clearinghouse of commercial fleet vehicle operating data helps vehicle manufacturers and developers optimize vehicle designs and helps fleet managers choose advanced technologies for their fleets. This online tool provides data summaries and visualizations similar to real-world "genetics" for medium- and heavy-duty commercial fleet vehicles operating in a variety of vocations.

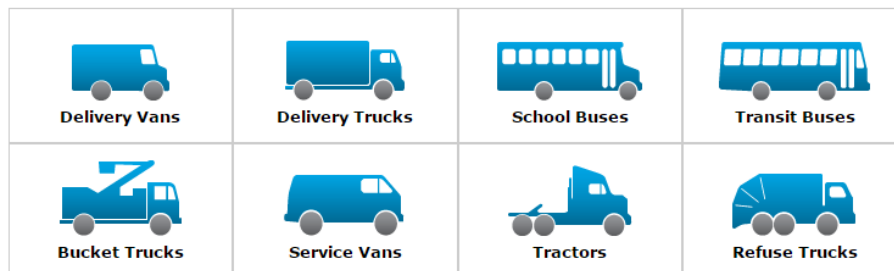
Contribute Data

Learn how to [contribute to Fleet DNA](#) anonymously to help other fleets analyze and improve their drive cycle metrics.

For more information, refer to the [Fleet DNA fact sheet](#).

Data by Vehicle Category

View and download data, charts, and reports by vehicle category.

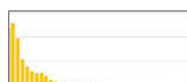


Composite Data for All Categories

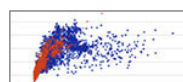
View charts with data for all the vehicle categories above or download the [composite data for all vehicles](#). Fleet DNA has 4,705 days of driving data from 486 vehicles operating in the United States.



Daily Average Driving Speed and Kinetic Intensity for All Vehicle Categories



Daily Stops per Mile Distribution for All Vehicle Categories



Average Acceleration and Number of Stops for All Vehicle Categories

Show More Charts

Figure III-152: Fleet DNA website interface

Credit: NREL

Additional enhancements and updates are planned for early FY16, including the addition of fuel economy and road grade data products to both the static and interactive data reports. Additionally, there are plans to improve access to the drive cycle data stored in Fleet DNA by providing speed-time traces for download.

Supporting additional efforts

One of the major accomplishments in FY15 was the continued deployment of Fleet DNA data and analyses in support of both internal and external DOE projects. Fleet DNA continued to support numerous project partners including the EPA; DOE’s Clean Cities, 21st Century Truck, and Fuel Cell Technology programs; and California’s Air Resource Board and the South Coast Air Management District. Additionally, NREL supported modeling efforts at both Oak Ridge National Laboratory (ORNL) and ANL for their annual operating plan activities by providing real-world drive cycles for simulation and design activities. NREL also leveraged unique data capabilities to partner with Eaton, Smith Electric Vehicles, and ORNL to win a competitively bid DOE funding opportunity for the design of a multispeed transmission for electric vehicles.

Conclusions

The Fleet DNA project has demonstrated the value of “big data” when applied to the transportation research sector. The ongoing growth of the database, publication of novel research and reports, and continued collaboration with industry partners, other national labs and government entities has demonstrated the value of a concentrated and focused transportation data center.

It is the ongoing goal of the Fleet DNA project to provide continually growing support for DOE programs under the Vehicle Technologies Office umbrella and to continue to work closely with other national labs, industry partners, and project collaborators to maximize the benefits and reach of the research and data. Through maintained collaborative efforts and a focus on data dissemination and publication, Fleet DNA will continue to provide value and act as a multiplier for DOE for years to come.

III.10.C. Products

Presentations/Publications/Patents

Three SAE publications were developed in FY15:

1. Lopp, S., Wood, E., and Duran, A., "Evaluating the Impact of Road Grade on Simulated Commercial Vehicle Fuel Economy Using Real-World Drive Cycles," SAE Technical Paper 2015-01-2739, 2015, doi:10.4271/2015-01-2739.
2. Wang, L., Kelly, K., Walkowicz, K., and Duran, A., "Quantitative Effects of Vehicle Parameters on Fuel Consumption for Heavy-Duty Vehicle," SAE Technical Paper 2015-01-2773, 2015, doi:10.4271/2015-01-2773.
3. Wang, L., Duran, A., Gonder, J., and Kelly, K., "Modeling Heavy/Medium-Duty Fuel Consumption Based on Drive Cycle Properties," SAE Technical Paper 2015-01-2812, 2015, doi:10.4271/2015-01-2812.

III.11. Fleet DNA Database Development and Support

Oscar Franzese, Ph.D.

Oak Ridge National Laboratory
2360 Cherahala Boulevard
Knoxville, TN 37932
Phone: (865) 946-1304
E-mail: franzeseo@ornl.gov

David Anderson, DOE Program Manager

Vehicle Technologies Office
Phone: (202) 287-5688
E-mail: david.anderson@ee.doe.gov

Start Date: October 1, 2012
End Date: September 30, 2015

III.11.A. Abstract

Objectives

- To merge the existing ORNL Heavy Truck Duty Cycle (HTDC) and Medium Truck Duty Cycle (MTDC) databases into the Fleet DNA data repository at National Renewable Energy Laboratory (NREL) by
 - Identifying and standardizing in conjunction with NREL, high priority 1Hz drive cycle data channels (such as speed, elevation, and other necessary data) recognizing DOE and other partner preferences;
 - Filtering and correcting, where feasible and without degradation of the information, the data collected by Oak Ridge National Laboratory (ORNL) for inclusion into the database;
 - Porting the extracted information into the format required by the Fleet DNA project. (Accomplished in Year 1)
- To provide summary statistics of each the five vocations included in the HTDC and MTDC databases (Accomplished in Year 2).
- To provide additional indexing and cataloguing of the information contained in the HTDC and MTDC databases for quick searching and retrieval of specific duty cycles (Accomplished in Year 2).

Accomplishments

- Development of a methodology and procedures to correct short segments of the data collected in the HTDC and MTDC projects that contain errors due to short losses of global positioning system (GPS) signals, sensor issues, databus issues, and data-collection equipment issues. (Year 1)
- Development of visualization software to quickly display direct current (DC) characteristics of the files that ORNL include in the Fleet DNA database. This tool was used to visually inspect the files and allowed identifying any errors that were not corrected by the ORNL data-correction methodology. (Year 1)
- Submission to NREL of the ORNL Fleet DNA files. A total of 3,241 files (1,562 HTDC files, 930 MTDC 1 files, and 749 MTDC 2 files) were uploaded and distributed to NREL. (Year 1)
- Submission to NREL of revised Fleet DNA files with four additional channels where requested by NREL –i.e.; 1) actual engine percent torque, 2) actual gear ratio, 3) percent load, and 4) current gear. (Year 2)
- Development and deployment of a methodology to organize and catalogue the duty cycles contained in the Fleet DNA database. These files were processed and indexed so they could be searched using user defined criteria. (Year 2)

Future Achievements

- N/A. Project Ended



III.11.B. Technical Discussion

Background

Fleets DNA was funded in FY12 through National Renewable Energy Laboratory (NREL) by the Vehicle Systems Simulation and Testing (VSST) project within DOE's Vehicle Technologies program. The project was designed to provide a common location for storage and basic analysis of medium and heavy-duty drive cycles. Work performed within NREL, Oak Ridge National Laboratory (ORNL), other labs and DOE as well as other state and federal agencies has generated data but a common portal and processing routine does not currently exist to store, access, and apply all of this data. As VSST's primary medium and heavy duty data collection laboratories, NREL and ORNL have agreed to collaborate and bring together data analysis techniques and previously collected data, while coordinating future data collection activities. This and future efforts will provide industry (original equipment manufacturers (OEMs) and fleets), other DOE programs and other federal agencies with valuable drive cycle information to be used to intelligently deploy and design advanced technology vehicles.

Introduction

Previous projects sponsored by DOE and performed by ORNL have generated a highly detailed dataset of real-world information for five vocations including long-haul operations, regional delivery, public transit (buses), electrical utility vehicles, and tow and recovery vehicles. These databases include 60 or more channels of information collected at 5Hz or five readings every second.

During the first year of this project, ORNL worked with NREL to derive from the data collected in the heavy truck duty cycle (HTDC) and medium truck duty cycle (MTDC) efforts, a database of duty cycle information that was in accordance to the guidelines of the NREL Fleet DNA project. The data was parsed and selected channels extracted and filtered using different techniques and methodologies developed exclusively for this project, and included in the Fleet DNA database.

In the second year of the project, ORNL developed methodologies and algorithms to build searching tools that would allow to extract from the ORNL Fleet DNA database duty cycles with user's selected criteria such as percentage of stop time compared to total DC time; DCs with total distance traveled that falls within a user-defined range; DCs with average speed that is within a user-defined range; and other

Approach

The work accomplished in the first year of this project generated the Fleet DNA database. The database, which covers five vocations (i.e.; long-haul operations, regional delivery, public transit (buses), electrical utility vehicles, and tow and recovery vehicles), includes a time channel; three vehicle information channels: vehicle speed, vehicle engine speed, and fuel rate; three spatial location channels: latitude, longitude, and altitude; and where available, three channels with the vehicle mass information: steer-axle weight, driver-axle weight, and trailer axle weight. The Fleet DNA database includes information derived from 3,241 files (each file corresponding to a 24-hr period) that were extracted from the ORNL HTDC and MTDC databases (1,562 HTDC files, 930 MTDC 1 files, and 749 MTDC 2 files) and were resampled (from 5Hz to 1Hz) and formatted according to NREL specifications.

The extensive information included in the Fleet DNA database makes it difficult to manually search for specific duty cycles that have certain characteristics of interest for researchers and/or industry. To alleviate this problem, during the second phase of this project ORNL first developed a methodology to catalogue and characterize the information contained in the Fleet DNA database. Software was written to identify duty cycles

(i.e., segments of data between engine power-on/power-off events) and then to characterize those duty cycles according to given parameters. For example, the data collected in each duty-cycle was used to generate probability distributions of vehicle speed (other parameters, such as vehicle weight or vocation type –i.e., only long-haul operations were included– were not processed since the project was put on hold four month after start).

These probability distributions were used later on to quickly characterize each DC in terms of average speeds, percentage of stops, distance traveled, etc. A second application was developed by ORNL to combine and integrate information from different duty cycles so a given user’s selected criterion (or criteria) could be used to identify and extract from the Fleet DNA duty cycles that comply with these criteria.

The duty cycle selection and extraction processes works as follows. The user is presented with a dialog box shown in Figure III-153 below and he/she selects the vehicle number (there are 18 vehicles included in the Fleet DNA database), the type of criteria (only speed in this version of the software), and enters any resampling frequency if needed.

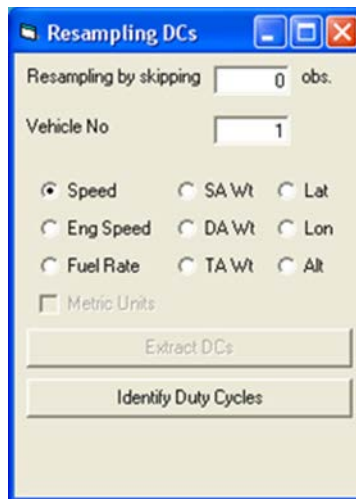


Figure III-153: Fleet DNA DC Extraction Tool - Parameters

After pressing the “Identify Duty Cycles” button (see Figure III-153), the utility presents the user with the dialog box shown in Figure III-154. The user then specifies ranges for criteria of interests such as lower and upper bounds of the percentage of stops that a duty cycle in the database has to have to be selected; the lower and upper bounds of distance covered in the DC; upper and lower bounds of the minimum, maximum, and average speeds registered in the duty cycle; the number of DCs needed, and many other parameters.

DC Selection

BASIC INFORMATION

Vehicle No: Number of DCs: Start with a Stop Interval:

LB % of Stops: UB % of Stops: LB Distance [m]: UB Distance [m]:

TOPOGRAPHY (Min and Max Slopes over 1/4 mile)

LB Min Slope [%]: UB Min Slope [%]:
 LB Max Slope [%]: UB Max Slope [%]:
 LB Avge Slope [%]: UB Avge Slope [%]:

VEHICLE DYNAMICS

LB Min Spd [mph]: UB Min Spd [mph]: LB Min Acc [ft/sec2]: UB Min Acc [ft/sec2]:
 LB Max Spd [mph]: UB Max Spd [mph]: LB Max Acc [ft/sec2]: UB Max Acc [ft/sec2]:
 LB Avge Spd [mph]: UB Avge Spd [mph]: LB Avge Acc [ft/sec2]: UB Avge Acc [ft/sec2]:

ROAD TYPE AND REGION TYPE

LB % Freeways: UB % Freeways: LB % Urban: UB % Urban:

Search:

RESULTS

Final % of Stops: Start At Index:
 Start File: Start Record:
 End File: End Record:

Stop Time [sec]	Moving Time [sec]	Total Time [sec]	Total Distance [m]
<input type="text"/>	<input type="text"/>	<input type="text"/>	<input type="text"/>

Min Speed [mph]	Max Speed [mph]	Avge Speed [mph]	Avge Sp Total [mph]
<input type="text"/>	<input type="text"/>	<input type="text"/>	<input type="text"/>

Duty Cycle 1

Avge Steer Axle Wt [lbs]	Avge Drive Axle Wt [lbs]	Avge Trailer Axle Wt [lbs]
<input type="text"/>	<input type="text"/>	<input type="text"/>
Min Slope [%]	Max Slope [%]	Avge Slope [%]
<input type="text"/>	<input type="text"/>	<input type="text"/>
Min Sp [mph]	Max Sp [mph]	Avge Sp [mph]
<input type="text"/>	<input type="text"/>	<input type="text"/>
Min Acc [ft/sec2]	Max Acc [ft/sec2]	Avge Acc [ft/sec2]
<input type="text"/>	<input type="text"/>	<input type="text"/>
Freeways [%]	Surface Streets [%]	Urban [%]
<input type="text"/>	<input type="text"/>	<input type="text"/>
		Rural [%]
		<input type="text"/>

Figure III-154: Fleet DNA DC Selection Criteria

Results

The implementation of the cataloging and search methodologies developed during the second phase of the project resulted in the development of an application that allows users to identify and extract from the extensive Fleet DNA database DCs that comply with user’s-defined criteria in a quick and efficient manner.

As an illustration of the methodology developed in this project, Figure III-155 below shows that the user is interested in extracting 1 DC which should have a percentage of stop time compared to total time that is between 0% and 1% and the DC should cover a distance that is between 140 and 150 miles, the terrain should present maximum slopes between 5% and 8%, the maximum speed should be between 60 mph and 75 mph, and the average speed between 50 mph and 60 mph, and the maximum acceleration should be below 0.5 ftss, the percentage of the DC traveled on freeways should be between 70% and 80%, and the DC should be between 60% and 70% urban. When the user presses the “Search” button, the utility uses the catalogue (over 7,000 Class-8 DCs) and other functions developed by ORNL to identify 1 DC from the Fleet DNA/HTDC database for vehicle 1 that have the characteristics specified by the user. Once the results are obtained, the application presents on the screen information about the first DC found (bottom half of Figure III-155). In this particular example, the DC corresponds to the Fleet DNA file SD1_20070205_HTDC_1. This DC starts at record 76, 974 and ends at record 86,400, has 0.88% of stops, a duration of 9,427 seconds, covering a total distance of 142 miles, with an average speed of 54.2 mph and a maximum speed of 72.4 mph.

DC Selection

BASIC INFORMATION

Vehicle No

Number of DCs Start with a Stop Interval

LB % of Stops UB % of Stops

LB Distance (m) UB Distance (m)

TOPOGRAPHY (Min and Max Slopes over 1/4 mile)

LB Min Slope [%] UB Min Slope [%]

LB Max Slope [%] UB Max Slope [%]

LB Avge Slope [%] UB Avge Slope [%]

VEHICLE DYNAMICS

LB Min Spd [mph] UB Min Spd [mph] LB Min Acc [ft/sec2] UB Min Acc [ft/sec2]

LB Max Spd [mph] UB Max Spd [mph] LB Max Acc [ft/sec2] UB Max Acc [ft/sec2]

LB Avge Spd [mph] UB Avge Spd [mph] LB Avge Acc [ft/sec2] UB Avge Acc [ft/sec2]

ROAD TYPE AND REGION TYPE

LB % Freeways UB % Freeways LB % Urban UB % Urban

RESULTS

Final % of Stops <input type="text" value="0.88"/>	Start At Index <input type="text" value="8,068"/>	Duty Cycle 1	Avge Steer Axle Wt [lbs] <input type="text" value="10,525"/>	Avge Drive Axle Wt [lbs] <input type="text" value="18,237"/>	Avge Trailer Axle Wt [lbs] <input type="text" value="20,325"/>
Start File <input type="text" value="SD1_20070205_HTDC_1.csv"/>	Start Record <input type="text" value="76,974"/>		Min Slope [%] <input type="text" value="0.00"/>	Max Slope [%] <input type="text" value="7.09"/>	Avge Slope [%] <input type="text" value="0.00"/>
End File <input type="text" value="SD1_20070205_HTDC_1.csv"/>	End Record <input type="text" value="86,400"/>		Min Sp [mph] <input type="text" value="0.0"/>	Max Sp [mph] <input type="text" value="72.4"/>	Avge Sp [mph] <input type="text" value="54.2"/>
Stop Time [sec] <input type="text" value="83"/>	Moving Time [sec] <input type="text" value="9,344"/>		Min Acc [ft/sec2] <input type="text" value="-0.1"/>	Max Acc [ft/sec2] <input type="text" value="0.3"/>	Avge Acc [ft/sec2] <input type="text" value="0.0"/>
Min Speed [mph] <input type="text" value="1.6"/>	Max Speed [mph] <input type="text" value="72.4"/>		Freeways [%] <input type="text" value="78.16"/>	Surface Streets [%] <input type="text" value="21.84"/>	Urban [%] <input type="text" value="64.47"/>
					Rural [%] <input type="text" value="35.53"/>
Total Time [sec] <input type="text" value="9,427"/>	Total Distance [m] <input type="text" value="142"/>				
Avge Speed [mph] <input type="text" value="54.7"/>	Avge Sp Total [mph] <input type="text" value="54.2"/>				

Figure III-155: Fleet DNA DC Selection Criteria and Search Results

Figure III-156 presents a mapping of the identified DC, showing that about 62% of the DC is in urban areas and 78% on freeways, as specified by the user.

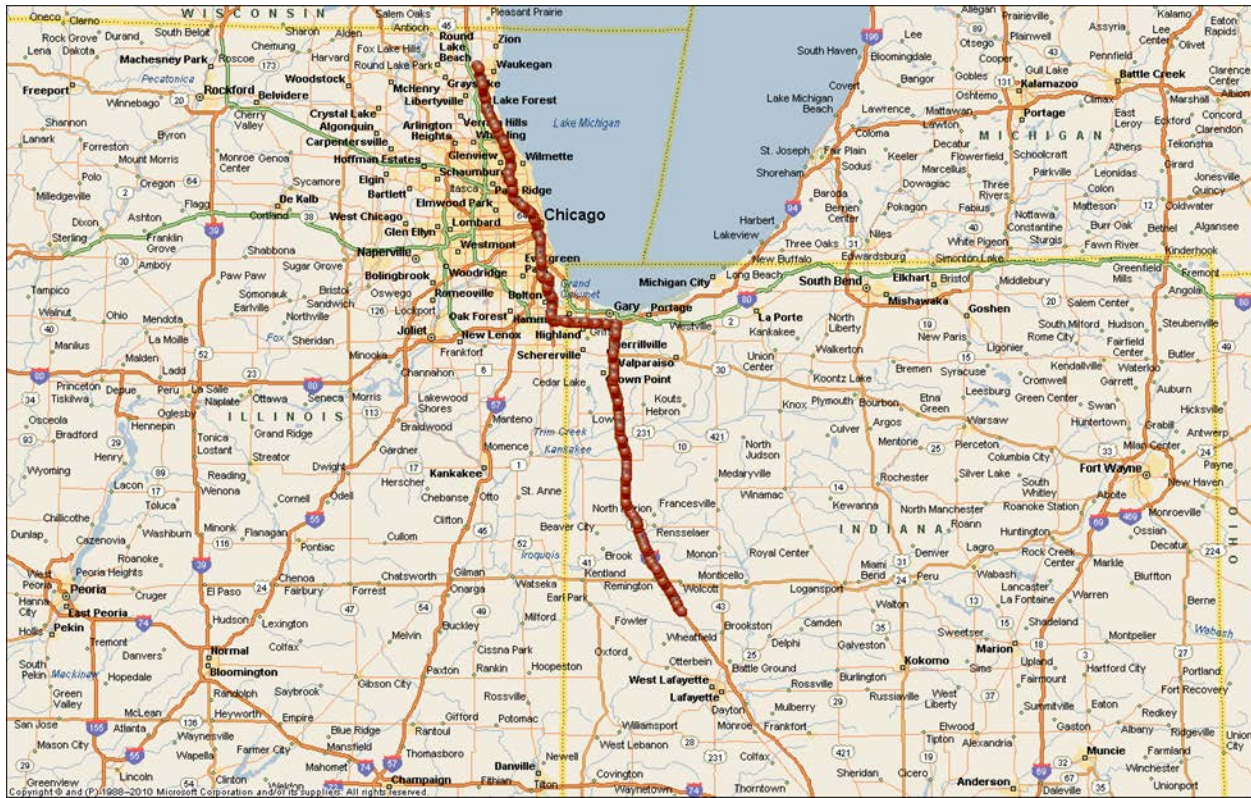


Figure III-156: User Selected DC

Only the summary for the first identified/extracted DC is shown on the screen (see Figure III-155). If nothing is shown, it is an indication that the Fleet DNA database does not contain any DCs with the user’s specified criteria for the selected vehicle. In that case, the user can relax some of the constraints to identify more DCs with the most relevant parameters specified. Once these DCs are identified, the information corresponding to each one of the DCs is added to a comma-separated values (csv) DCID summary file for further analysis. For example, Table III-28 below shows the result of a search requesting 5 DCs with the following characteristics: 1) percentage of stop time compared to total time that is between 9% and 11%, 2) each DC should cover a distance that is between 50 and 70 miles, and 3) all other parameters are relaxed (e.g., the percentage of the DC that is on freeways is between 0% and 100%). The table presents just some of the parameters included in the DCID summary file. It shows that all of the 5 identified DCs comply with the criteria selected by the user (i.e., all of them have percentage of stops between 9% and 11% and traveled distance between 50 and 70 miles). The table presents the user with additional information that could be used to refine the DC selection. Perhaps the user is interested only on DCs that have an average speed that is larger than 45 mph, in which case only the first DC in the table would qualify. Or perhaps the use is interested only on DCs that have maximum speeds below 70 mph in which case only DCs 2 and 4 would qualify.

The tools developed in this research were also used to characterize the DCs in the Fleet DNA database. To do so, all the HTDC DCs in the database were extracted (a DC was defined as a segment of data going from engine off to engine on to engine off) and distributions of their main parameters built. Figure III-157 to Figure III-165 present those distributions (obtained from 5,904 DCs with a distance traveled >=25 miles).

Table III-28: Identified DCs - Selected Parameter Information

Final% Stops	Start File Name	Start Rec. #	End File Name	End Rec. #	Total Distance [m]	Avg. Speed [mph]
10.5	SD1_20061114_HTDC_1	47,395	SD1_20061114_HTDC_1	52,679	67.7	46.15
9.1	SD1_20061116_HTDC_1	78,994	SD1_20061117_HTDC_1	4,714	66.1	36.81
10.1	SD1_20061127_HTDC_1	39,088	SD1_20061127_HTDC_1	44,053	50.3	36.43
9.1	SD1_20061201_HTDC_1	24,855	SD1_20061201_HTDC_1	30,284	58.0	38.48
10.7	SD1_20061215_HTDC_1	18,049	SD1_20061215_HTDC_1	24,918	61.2	32.08

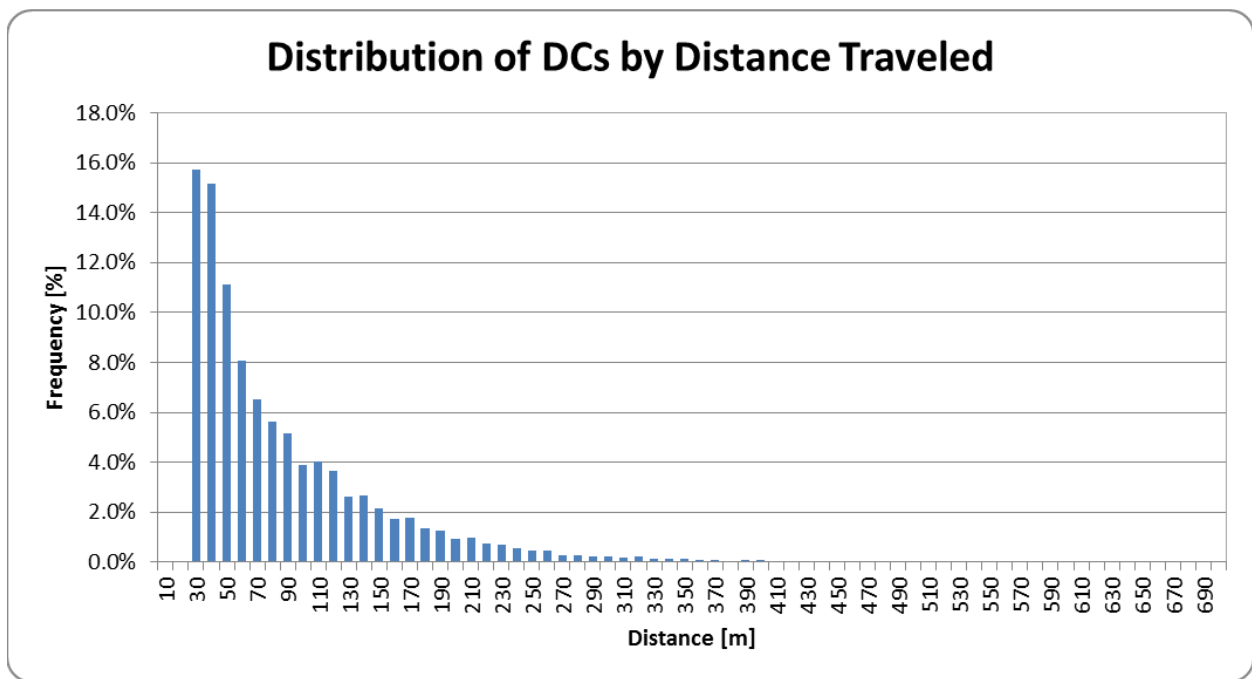


Figure III-157: Distribution of DCs by Distance Traveled

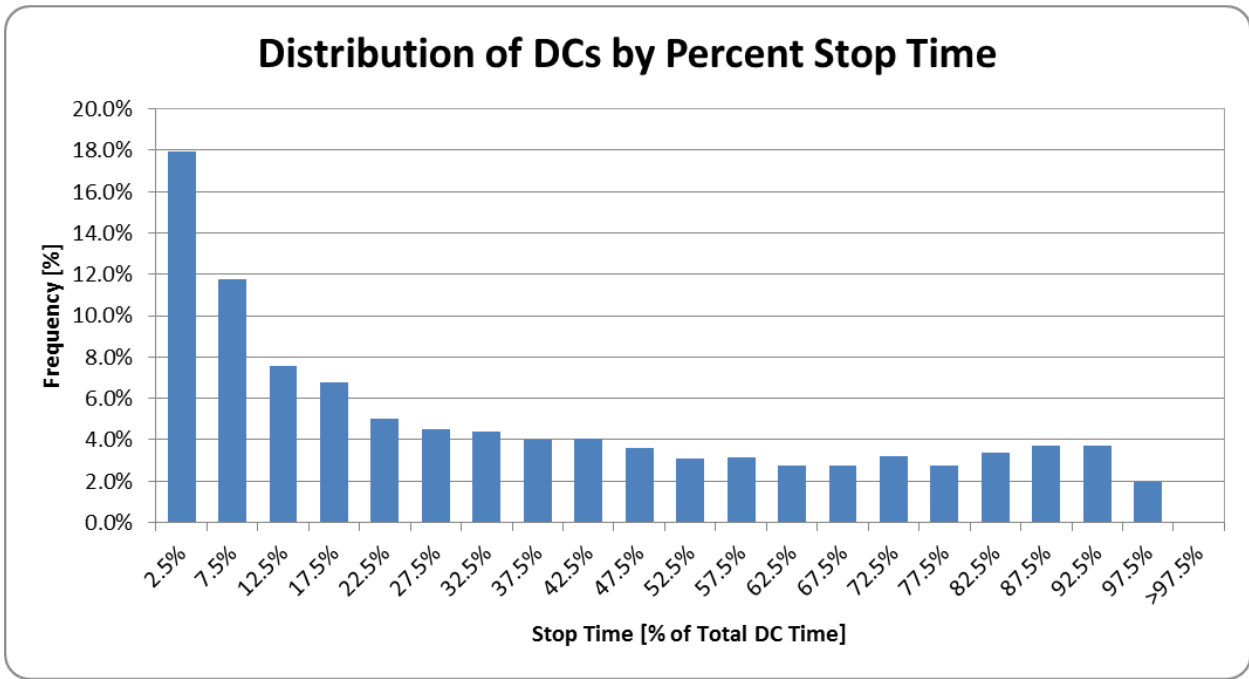


Figure III-158: Distribution of DCs by Percent Stop Time

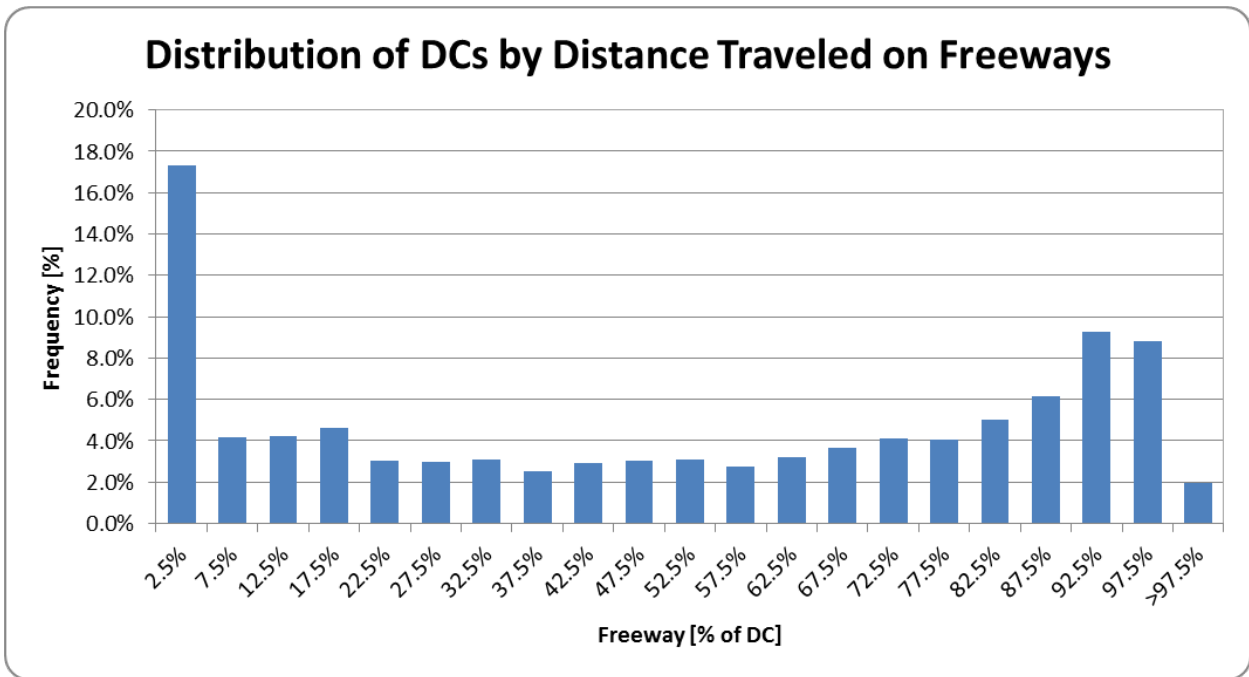


Figure III-159: Distribution of DCs by Distance Traveled on Freeways

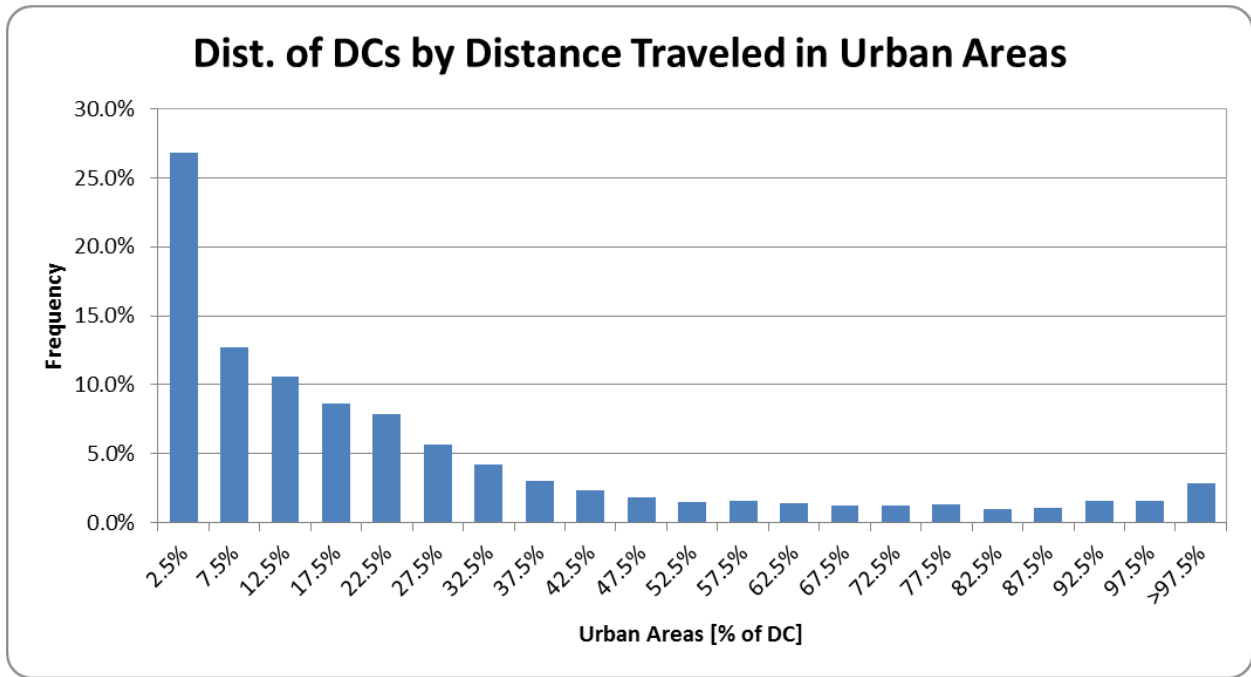


Figure III-160: Distribution of DCs by Distance Traveled in Urban Areas

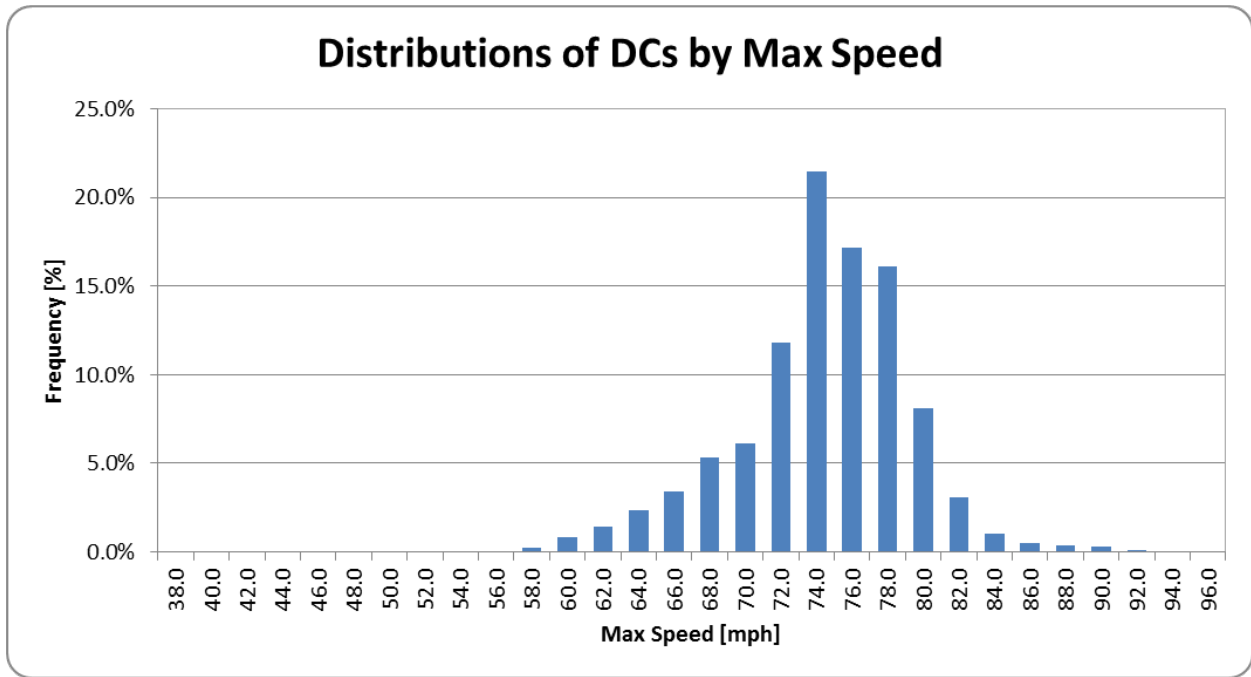


Figure III-161: Distribution of DCs by Maximum Speed

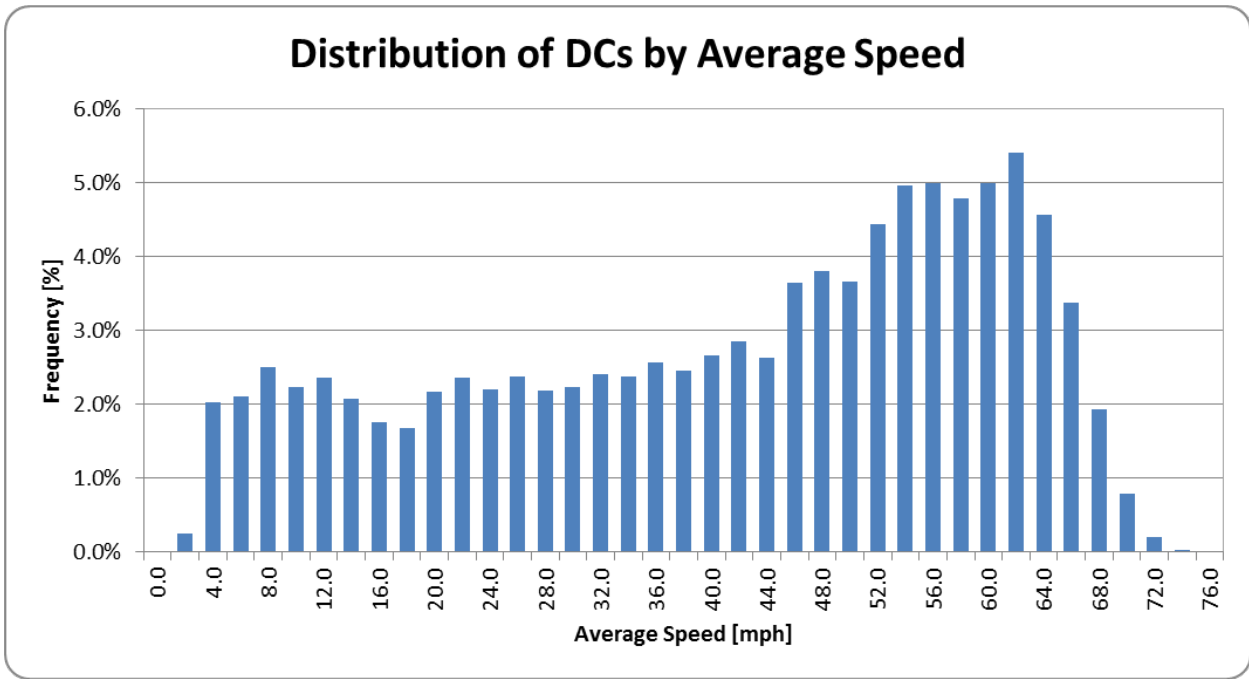


Figure III-162: Distribution of DCs by Average Speed

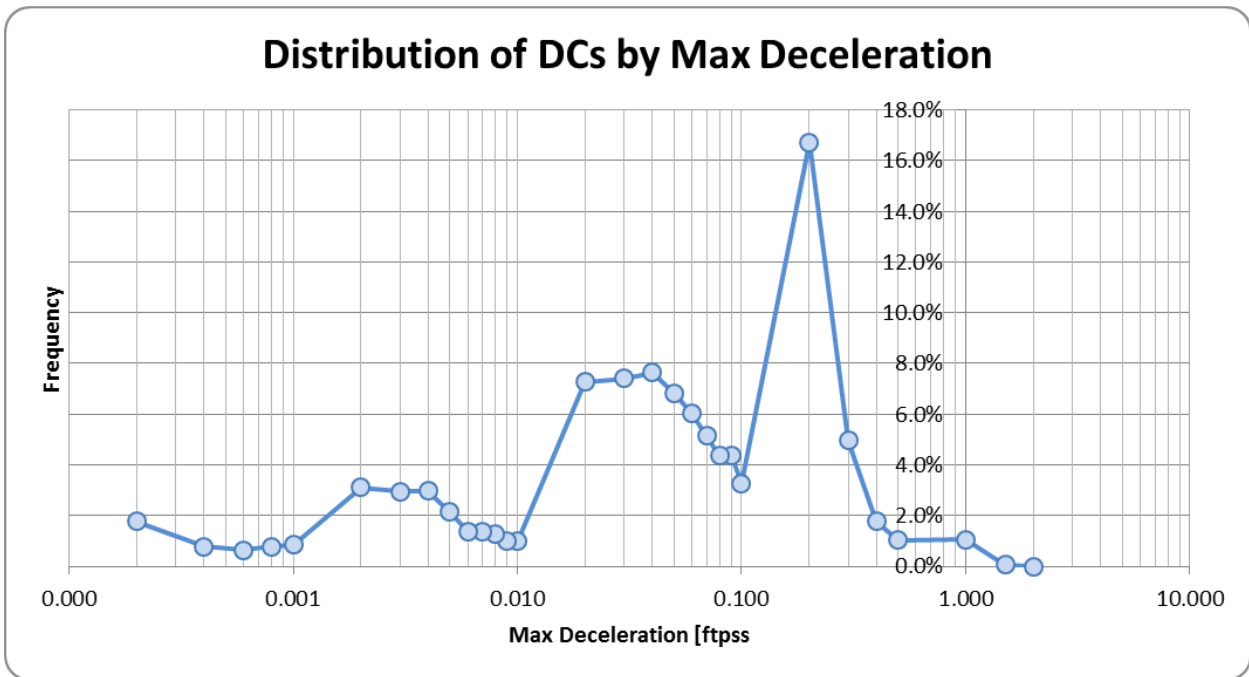


Figure III-163: Distribution of DCs by Maximum Deceleration (Logarithmic Scale)

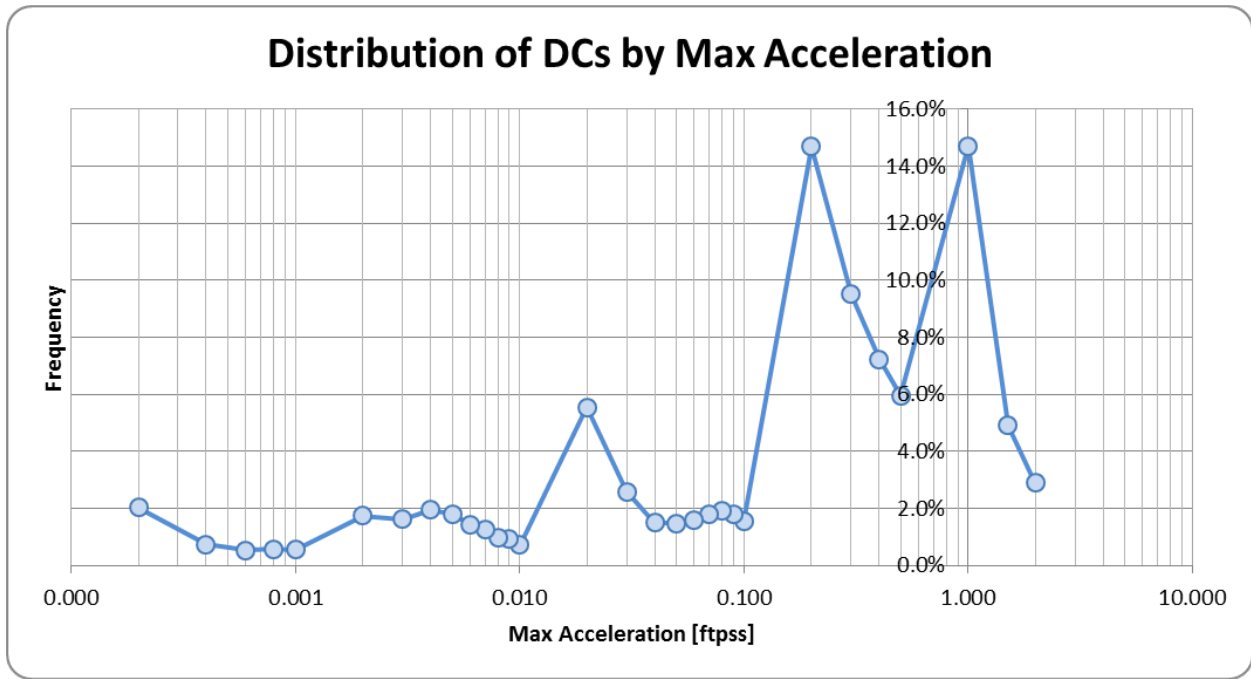


Figure III-164: Distribution of DCs by Maximum Acceleration (Logarithmic Scale)

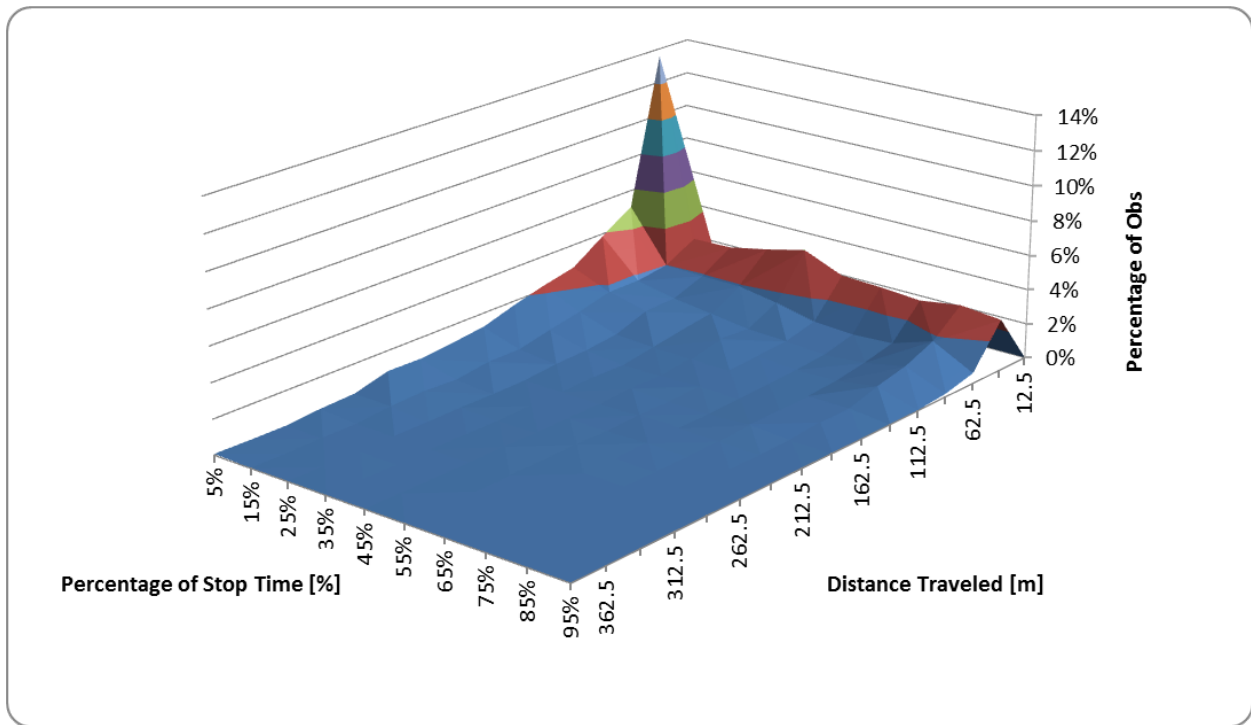


Figure III-165: Distribution of DCs by Distance Traveled and Percentage of Stop Time

Conclusions

During the first phase of the project, data collected as part of the HTDC and MTDC 1 and 2 projects was organized, resampled at one-second resolution (from the original 5 Hz), and cleansed. The Fleet DNA files (version 1) contain ten main channels: time (elapsed time since midnight, each file corresponds to a date), latitude, longitude, altitude, vehicle speed, engine speed, fuel consumption, and steer, drive, and trailer axle weight information (where available). In the first phase of this project, errors that were due to equipment problem (mostly loss of GPS signal) were corrected without changing the information of the main channels. For cases in which these corrections were not possible because they would have changed the raw data for key channels (e.g., files for which vehicle speed information was missing at the start of a trip when the data collection equipment was turned on as the vehicle engine was turned on), the file was not included in the Fleet DNA database.

In the second phase of the project the focus was on the addition of other channels that were originally collected but were not included in the phase-one files (e.g., engine torque, cruise control engagement, etc.). The information contained in the files included in the Fleet DNA database was catalogued and characterized by certain parameters of interests (only speed since the project was put on hold at month 4 after start). For example, even within a given vocation (there are 5 vocations included in the Fleet DNA database) there may be many different types of duty cycles (different lengths, different shapes, etc.). Those duty cycles were catalogued according to a given set of parameters and using predefined ranges for these parameters, the corresponding duty cycles were indexed to allow users to quickly find duty cycles with specific characteristics of interest.

The indexing and cataloging of the extensive Fleet DNA database will allow industry users and researchers to better identify real world duty cycles with certain characteristics of interest that could serve as the basis for testing new engine and vehicle technologies. Also with this objective in mind, the DCs contained in the Fleet DNA database were characterized and distributions of their main parameters presented.

III.11.C. Products

Presentations/Publications/Patents

N/A

III.11.D. References

1. G.J. Capps, O. Franzese, H.E. Knee, M.B. Lascurain and P. Otaduy, [Class-8 Heavy Truck Duty Cycle Project Final Report](#), ORNL/TM-2008/122, Oak Ridge National Laboratory, Oak Ridge, TN (2008).
2. M.B. Lascurain, O. Franzese, G. Capps, A. Siekmann, N. Thomas, T. LaClair, A. Barker, H. Knee, ["Medium Truck Duty Cycle Data from Real-World Driving Environments: Project Final Report,"](#) ORNL/TM-2012/240, Oak Ridge TN, November 2012.

III.12. Medium- and Heavy-Duty Field Testing

Kenneth Kelly

National Renewable Energy Laboratory
15013 Denver West Parkway, MS 1633
Golden, CO 80401
Phone: (303) 275-4465
E-mail: Kenneth.kelly@nrel.gov

Lee Slezak

Phone: (202) 586-2335
E-mail: Lee.Slezak@ee.doe.gov

III.12.A. Abstract

Objectives

The main goal of this project is to test and/or validate advanced propulsion technologies in medium- and heavy-duty applications and to provide data and results from independent evaluation to help facilitate transitioning these vehicles from the research and development /prototype stage into the marketplace. This will be accomplished by means of the following:

- Testing and analyzing near-term advanced technologies in vehicles and comparing them to conventional technologies in vehicles in similar service
- Providing data and feedback to the research and development community (including other offices and programs within the U.S. Department of Energy [DOE]) to guide technology development that will lead to fuel-saving commercial products.

Accomplishments

FLNA Plug-In Electric Delivery Truck Case Study

- Completed data collection and analysis of Smith electric vehicles (EVs) in service with Frito-Lay North America (FLNA) in Federal Way, Washington
- Instrumented the Federal Way depot building to properly align charge-management schemes with local minima in their daily power consumption
- Refined facility power simulation model to evaluate managed charge opportunity at Federal Way facility
- Applied facility power model to evaluate benefits of onsite integrated solar arrays.

Miami-Dade County Hydraulic Hybrid Refuse Truck Case Study

- Executed non-disclosure agreement with hydraulic hybrid system supplier, Parker Hannifin
- Completed initial field data collection of first-generation hybrid vehicles and analysis of preliminary data
- Performed preliminary analysis on vehicle operation and performance of conventional diesels and first-generation hydraulic hybrids.

CGI / EV2G School Bus Case Study

- Kicked-off project in the second quarter of FY15
- Reached agreement with Zonar Systems to provide telematics data on entire Torrance, California, school bus fleet

- Worked with Napa Valley Unified School District to identify 10 buses as targets for data logger installation based on TransPower EV bus potential route operation
- Completed initial round of vehicle instrumentation in Napa Valley Unified School District
- Reported on Napa and Torrance bus use statistics to working group
- Modeled vehicle-grid integration opportunities from charge management to vehicle-to-grid energy storage.

Economy and Emissions Impacts from Solazyme Fuel in UPS Delivery Vehicles

- Completed vehicle instrumentation and in-field data collection of 12 UPS tractors and delivery vans
- Completed drive cycle analysis
- Completed fuel properties testing of Solazyme synthetic diesel
- Conducted heavy-duty chassis dynamometer testing on UPS tractor and delivery van using representative drive cycles.

Future Achievements

FLNA Plug-In Electric Delivery Truck Case Study

- Explore additional opportunities for onsite integration of renewables (i.e., solar, wind)
- Compile findings and publish final technical report in FY16.

Miami-Dade County Hydraulic Hybrid Refuse Truck Case Study

- Perform laboratory chassis dynamometer testing of second-generation hydraulic hybrid refuse truck and comparable baseline conventional diesel
- Travel to Miami-Dade County to collect in-use data on second-generation vehicles and conventional diesel vehicles
- Collect and analyze maintenance data as provided by Miami-Dade County Public Works and Waste Management Department
- Compile findings and publish final technical report in 2016.

CGI / EV2G School Bus Case Study

- In FY16, the National Renewable Energy Laboratory (NREL) plans to use data analysis to develop School Bus drive cycle using NREL's Drive-Cycle Rapid Investigation, Visualization, and Evaluation (DRIVE) drive cycle evaluation tool
- Construct vehicle model using Future Automotive Systems Technology Simulator (FASTSim) to investigate performance potential
- Collaborate with TransPower to collect and analyze EV bus data when EV buses are deployed
- Collaboration with DOE/NREL Grid Integration team to test vehicle-to-grid hardware and controls
- Contribute data to Fleet DNA project
- Produce technical report of project status and outcomes.

Economy and Emissions Impacts from Solazyme Fuel in UPS Delivery Vehicles

- Complete analysis of results and present to National Clean Fleet Partnership and UPS stakeholders



III.12.B. Technical Discussion

Background—General

DOE funds an array of research and development projects to develop technologies and subsystems for advanced vehicles. Testing, validating, and providing data and analysis of real-world service requirements and performance of vehicles and systems can help with the transition of DOE's and other energy-saving technologies into widespread marketplace adoption. To accomplish this, DOE's Vehicle Systems Office provides a process to document testing, validating, and benchmarking the advanced technologies and provide data and technology evaluations from an unbiased party. The information provided by this project is vital to original equipment manufacturers to identify areas of improvement and to fleets to aid them in making purchase decisions that will be appropriate for the unique operational characteristics of a given vocation. DOE can also utilize this information to help identify future research and development opportunities.

Approach—General

This project will cooperate with fleet and/or original equipment manufacturer partners to select, test, and validate advanced technologies in commercial vehicle applications. Specific technologies will be selected based on (1) their potential for reducing fuel consumption, (2) their potential for widespread commercialization, and (3) interest at DOE (including the 21st Century Truck Partnership and other DOE programs). After a technology area has been identified, NREL will collect vehicle data on system performance, maintenance (if applicable), and/or operational costs relative to the new technology. The data will be analyzed, and results will be presented to DOE and the project teams. The potential for improvement in real-world service, including operational costs, maintenance, and emissions, will be compared to data collected from conventional technology vehicles.

The approach for the FY15 medium- and heavy-duty field evaluation projects included:

- Working cooperatively with commercial fleets to collect operational, performance, and cost data for advanced technologies
- Characterizing vehicle drive/duty cycles
- Analyzing performance and cost data during a period of 6 months to 1 year or more
- Testing and analyzing in-use performance of advanced technologies in a laboratory setting to duplicate observed real-world conditions
- Producing fact sheets and reports on advanced heavy-duty vehicles in service
- Providing updates on new advanced technologies to DOE and other interested organizations as needed.

FLNA Plug-In Electric Delivery Truck Case Study

Background and Introduction

NREL's Fleet Test and Evaluation Team has found medium- and heavy-duty vehicle fleets to be good candidates for deploying low-emitting advanced technologies because of their large numbers, high vehicle miles traveled—and consequently high petroleum fuel consumption and emissions—and frequent operation in large population centers, as well as common return-to-base fueling regimes and consistent driving routes.

Previous testing and analysis conducted by NREL have illustrated the influence of drive cycle and vehicle usage on both energy consumption (from liquid fuels and high-voltage hybrid battery packs) and exhaust (or well-to-wheels) emissions. Drive cycle has also been shown to influence the all-electric range of battery EVs, the charge-depleting range of plug-in hybrid EVs, and the potential fuel economy benefit of hybrid EVs. Accordingly, fleet customers can benefit from a further understanding of advanced vehicle technology deployment to minimize fuel consumption and emissions. It has also been shown that large-scale deployments of EVs in a localized area can lead to power quality and power cost issues.

Introduction

In a separate project, NREL is funded by DOE to collect operational data on Smith EVs being deployed as part of the American Reinvestment and Recovery Act (ARRA). Data collected from the ARRA-funded EVs (up to 500, some of which are located at FLNA facilities) will be used to understand the overall usage and performance of EVs in medium-duty commercial fleet facilities and operations. The FLNA Plug-In Electric Delivery Truck Case Study, covered here, will provide a more detailed investigation to understand the implementation and performance of medium-duty EVs compared to conventional vehicles in a large-scale commercial facility.

Approach

The technical approach for this project follows the general approach for conducting fleet evaluations described above. The specific technical approach for the Frito-Lay project includes the following:

- Initial fleet identification and selection
- Initial route and in-vehicle data collection
- Twelve-month fleet data collection
- Battery life degradation study.

Detailed discussion of the approach and results from the fleet identification and the route and vehicle data collection steps were covered in the FY14 Annual Report. The following section provides a high-level summary of key results from that previous work along with a description of progress in FY15.

Results

Progress to Date

Initial Fleet Identification and Selection

During FY13, NREL engaged with FLNA and Smith to establish a program to evaluate the performance of plug-in electric delivery vans in direct comparison to conventional diesel vehicles. Based on the availability of comparable vehicles, NREL and FLNA decided that the FLNA Federal Way, Washington, fleet depot would be the ideal target site for research. Table III-29 lists the vehicles that were instrumented.

Table III-29: Federal Way vehicles monitored in second logger deployment

Manufacturer	Model	Year
International	4200 SBA 4X2	2005
International	4200 SBA 4x2	2003
International	4700 4x2	2001
International	4200 SBA 4X2	2005
International	4200 SBA 4x2	2006
Hino	HINO 238	2012
International	4200 SBA 4x2	2007
International	4200 SBA 4X2	2005
International	4700 4x2	2001

Initial Route and In-Vehicle Data Collection

Data collected from the nine diesel vehicles provide the baseline to which Smith EV performance was compared. NREL gathered data from the 10 Smith EVs stationed at Federal Way during the 17 days of logging in 2014 (April 16 to May 1) and found several correlations among FLNA diesel and EV operations. The routes for both sets of vehicles span similar ranges across the territory served by the Federal Way depot.

Traveling on similar routes as the diesel trucks, FLNA’s Federal Way EVs operated at much higher fuel economies. As shown in Figure III-166, the EVs drove nearly three times as far on the same energy as the diesels, at times exceeding 25 miles per gallon of gasoline equivalent (mpge).²

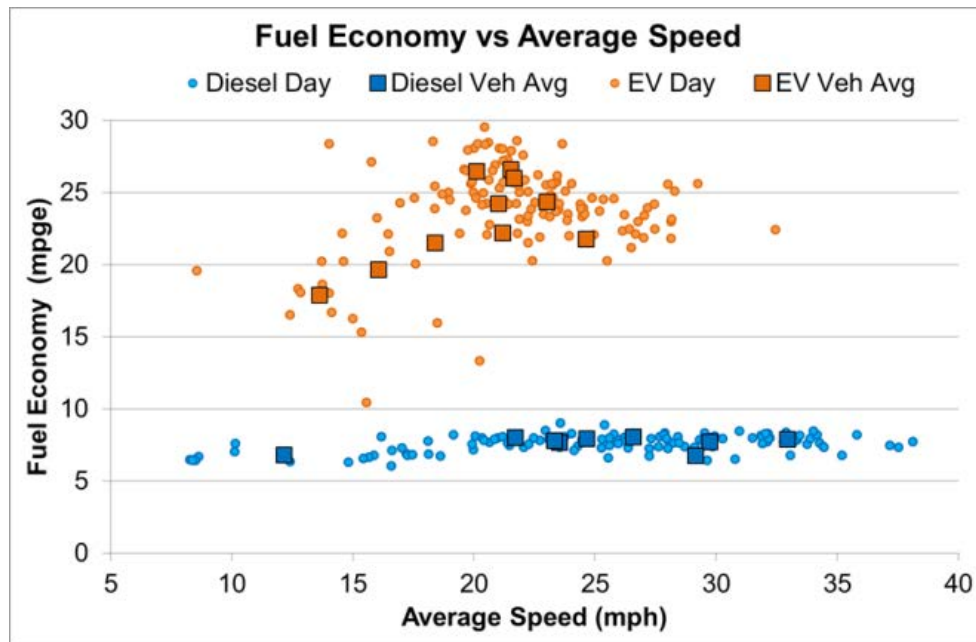


Figure III-166: Fuel economy comparison of diesels and EVs

The diesel trucks averaged 7.7 mpg at \$3.85/gal—roughly the average in Seattle at the time these data were collected—and the EVs averaged 23.3 mpge at \$0.102/kWh³; thus, the same ratio in fuel economy applies to fuel savings for EVs. Frito Lay spent \$0.50 for every mile driven with diesel trucks compared to \$0.15 for every mile driven by an EV. Figure III-167 shows the average energy consumed as a function of daily distance traveled. It can be seen that, as expected, there is a relatively strong linear correlation between the two variables.

² Fuel economy assessments for Smith EVs are represented as AC energy and thus assume a 90% charger efficiency as found in earlier ARRA data analyses for Smith’s onboard chargers. A gallon of diesel fuel was assumed to contain 37.6 kWh of energy.

³ Utility bills collected from the site energy manager at the Federal Way depot during 2013 were averaged to price each kWh at \$0.102, including access and demand charges.

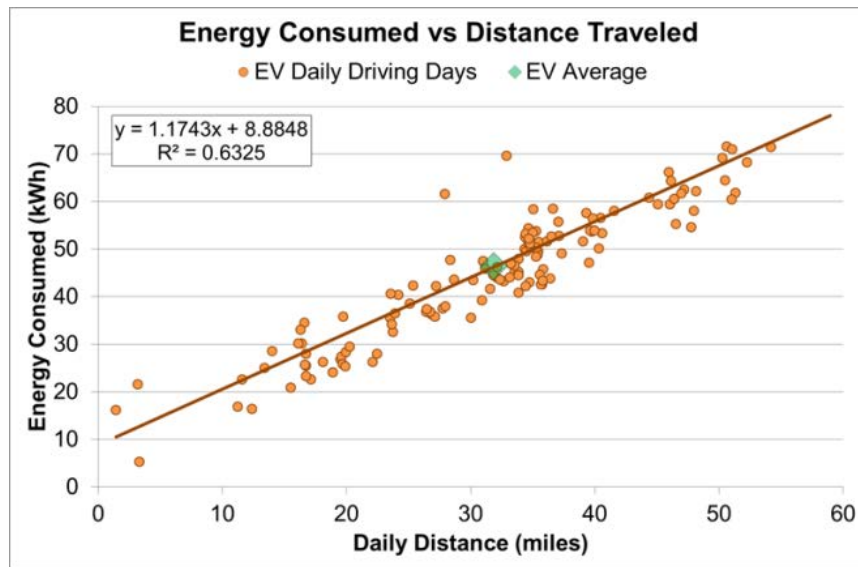


Figure III-167: Energy consumption as a function of distance traveled for the Smith EVs

To provide more detailed information regarding grid impact from the EVs, NREL worked with one of FLNA’s partners to collect the charging station power meter data. During the two consecutive months of continuous data collection, the charging demand from the bank of 10 vehicles peaked at slightly more than 77 kW, with 23,085 kWh (AC) delivered. This load adds \$462.77 in demand charges to the Federal Way utility bill during the months of April through September. The demand charge averaged \$693.77 for each month from October through March⁴ in addition to the \$1,479.10 monthly energy charges. Electricity costs roughly \$2,470 per vehicle each year on average, whereas Frito-Lay spent nearly \$6,000 per diesel truck in fuel costs.

Figure III-168 shows an example of the data recorded by the Federal Way charging station energy management system. Each stacked color represents the power recorded over time (energy) delivered by a single charging station. NREL found that each of the Federal Way EVs charged an average of 47.1 kWh AC per day. With an average charger efficiency of 90%, FLNA’s routes consumed approximately 53% of an EV’s full 80-kWh battery pack capacity each day. Each individual electric vehicle supply equipment (EVSE) station was then analyzed to evaluate both the average and peak power delivered while charging, as seen in Figure III-169.

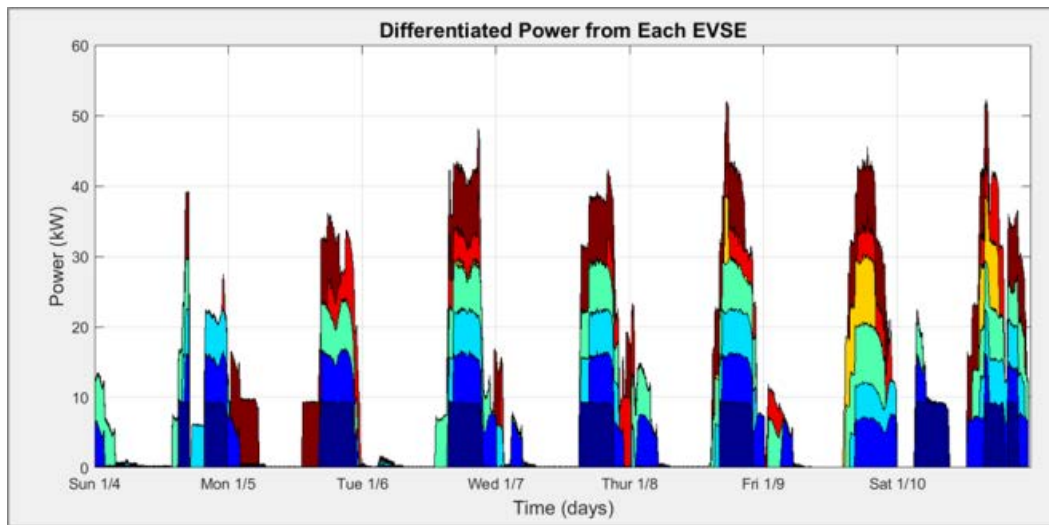


Figure III-168: Subset of data from Chateau Energy management system January 4–10, 2015 shown

⁴ The FLNA Federal Way depot is on Puget Sound Energy’s Tariff G rate schedule: a \$9.01/kWh demand charge from October through March and \$6.01/kWh demand charge from April through September. Energy costs \$0.064072/kWh above 20,000 kWh consumed.

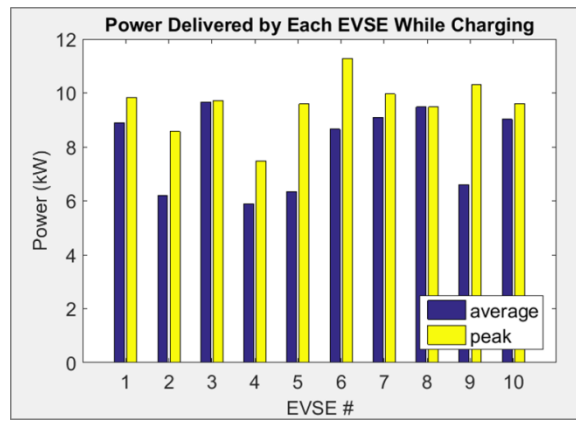


Figure III-169: Average and peak power delivered by each EVSE while charging

As shown in Figure III-170, the EVs charge overnight until early morning, when the delivery shifts begin. Adding load throughout the afternoon and into the early evening coincides with many facility loads and has nearly doubled the Federal Way FLNA depot’s demand (see Figure III-171). Working with the local energy management engineer at Federal Way, NREL acquired the depot’s utility bills, which indicated that peak demand nearly doubled after the 10 plug-in EVs were put into service in early 2013.

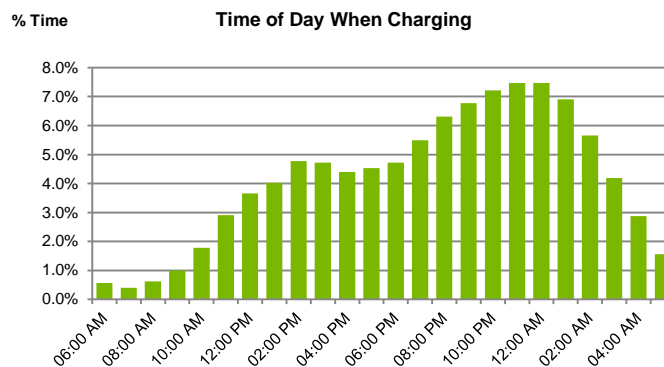


Figure III-170: Time of day when vehicles are charging during the diesel comparison period (April–May 2014)

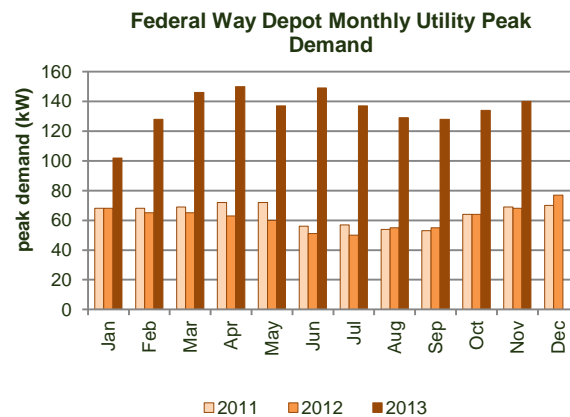


Figure III-171: Fleet depot utility bill monthly peak demand

In November of 2014, NREL installed a high-speed, transient power quality monitor on the main utility feed at the Federal Way depot to better understand the overall facility power consumption behaviors. The detailed facility data allowed for much deeper analysis of the dynamics between facilities and EV power requirements.

When examining the power requirements of the Federal Way facility at a daily level, one can see a direct correlation between EVSE usage and an increase in facility power requirements, as shown in Figure III-172.

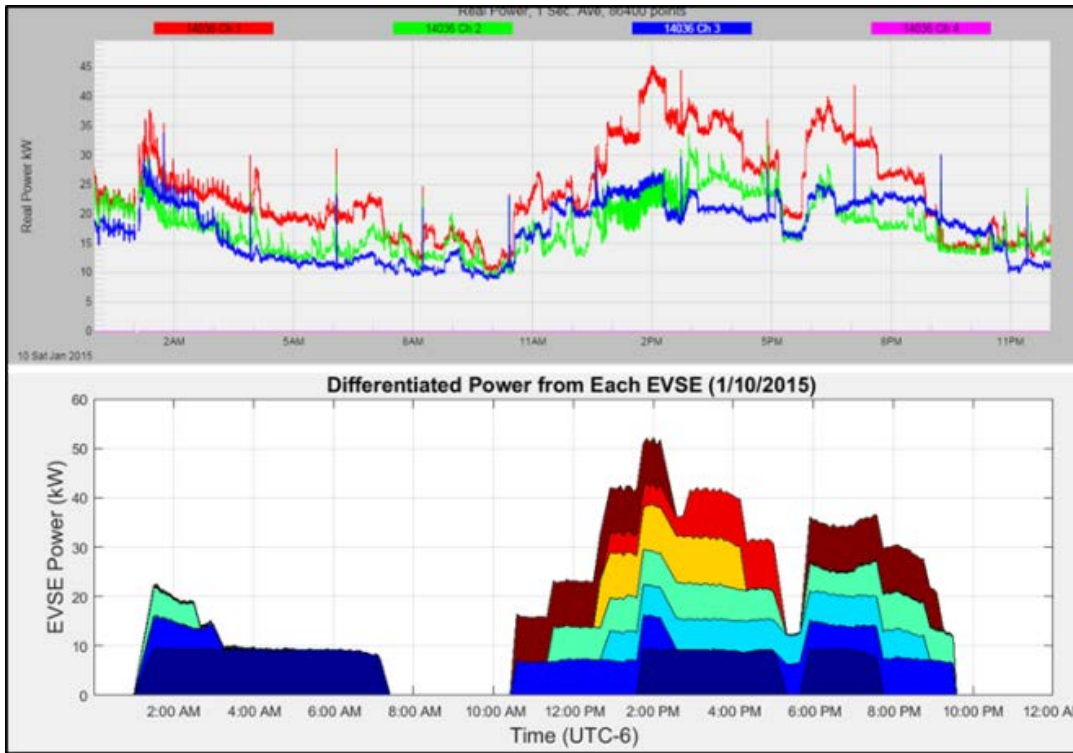


Figure III-172: Comparison of Federal Way facility power consumption and EVSE usage (data from 01/10/2015)

Figure III-173 shows the additive effect of the EVs as their charging times often coincide with the facility’s peak base loads.

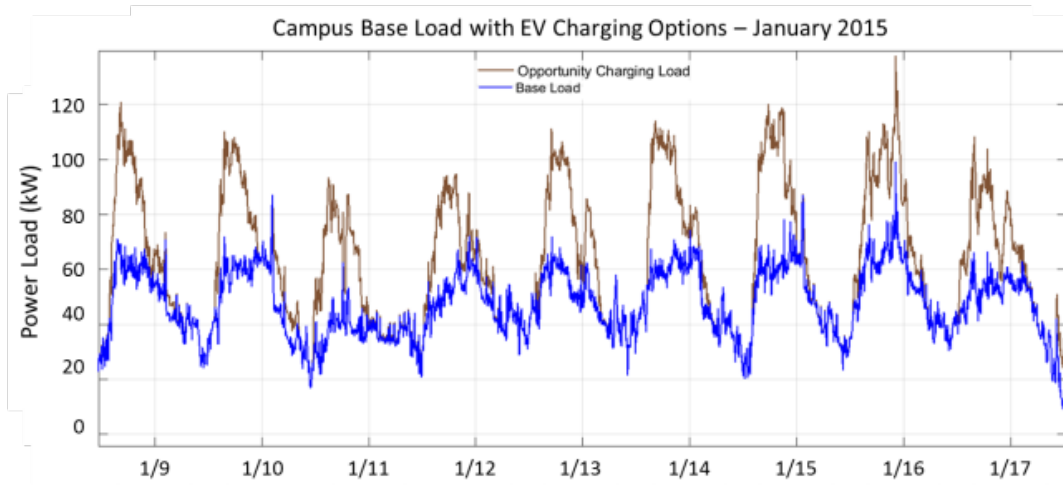


Figure III-173: Campus base load and EV charging contribution

Using this detailed facility load data, a facility energy model was created to demonstrate the opportunity for managed plug-in EV charging. Some of the key assumptions driving this energy model include the state of charge when the vehicle is plugged in, the time the vehicle will be used next, and the base facility load as a function of time. With the addition of a tuning parameter based on the historical peak loads, a peak demand reduction of up to 23% was demonstrated for the Federal Way facility. The modeled power load for nine days can be seen in Figure III-174.

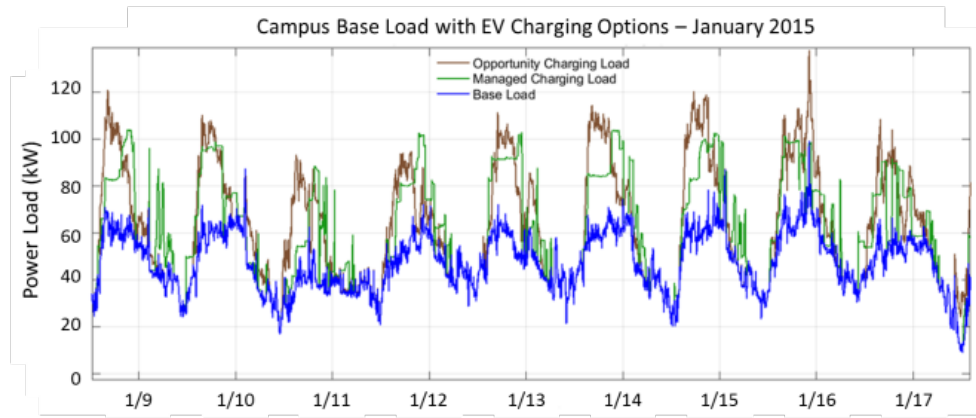


Figure III-174: Charge management schemes developed by NREL could save FLNA in peak demand charges

When considering managed EV charging at a facility, it is important to understand the timing of different loads. For example, at the Federal Way facility there is a significant overlap in peak facility loads and peak charging loads. This fact greatly diminishes the potential to reduce peak demand charges. Additionally, there are limitations with this model as it relies on communication of the vehicles’ state of charge, which is not currently available from these vehicles.

Taking the EV integration analysis one step farther, one can consider the potential benefits of the integration of onsite renewables. Using the same base facility model as previously discussed, a 100-kW solar array was modeled using NREL’s PVWatts® Calculator, which is a web application that estimates the electricity production of a grid-connected roof- or ground-mounted photovoltaic system. The calculator estimates the monthly and annual electricity production of a photovoltaic system using an hour-by-hour simulation over a period of one year.

Evaluating the hour-by-hour electricity production on an annual basis as a function of solar array orientation, the PVWatts model shows a total annual output at 111,396 kWh for a southern-facing array and an annual output of 97,203 kWh for a western-facing array. While the southern-facing array has a greater total annual output, using the facility power and charging data with the facility power model, it was found that the generation from a western-facing solar array would actually align better with late afternoon/evening charging of this fleet. Figure III-175 shows the annual hourly power distribution as a function of solar array orientation and can be compared to the charging times show previously.

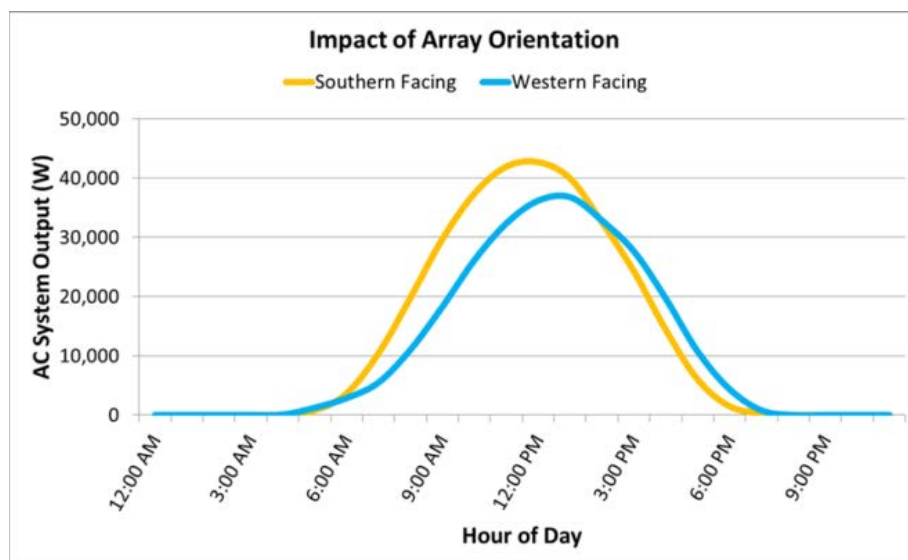


Figure III-175: Modeled 100-kW AC system located at FLNA Federal Way facility average hourly output based on array orientation

Additional analysis is being performed to integrate the time series facility data, EVSE data, and solar load data with local power company rate structures to further enhance the facility model.

Conclusions

Traveling on similar routes as the diesel trucks, FLNA's Federal Way EVs operated at much higher fuel economies. The EVs drove nearly three times as far on the same energy as the diesels, at times exceeding 25 mpg. The diesel trucks averaged 7.7 mpg at \$3.85/gal—roughly the average in Seattle at the time of this report—and the EVs averaged 23.3 mpg at \$0.102/kWh; thus, the same ratio in fuel economy applies to fuel savings for EVs. FLNA spent \$0.50 for every mile driven with diesel trucks compared to \$0.15 for every mile driven by an EV.

Electricity costs roughly \$2,470 per EV each year on average, whereas FLNA spent nearly \$6,000 per diesel truck in fuel costs (assuming an average of slightly more than 4 gal/day/truck at \$3.85/gal).

Due to the significant overlap in facility and charger peak demand times and relatively lower peak demand charges in the area, managed charging would save FLNA on average only \$270–\$370 per month across Federal Way's 10 vehicles based on current power prices, thereby reducing the overall utility bill 6%–12%.

NREL will complete all data collection and analysis and publish a final report on the results of this study in FY16.

Miami-Dade County Hydraulic Hybrid Refuse Truck Case Study

Background

Working with the Southeast Florida Clean Cities Coalition, NREL has partnered with Miami-Dade County's Public Works and Waste Management Department (PWWMD) to evaluate the on road-performance of Parker Hannifin's hydraulic hybrid system on refuse trucks.

With a fleet of 190 refuse vehicles, Miami-Dade County's PWWMD provides waste collection and recycling services to more than 320,000 households in unincorporated Miami-Dade County and eight municipalities in southern Florida—Aventura, Cutler Bay, Doral, Miami Gardens, Miami Lakes, Palmetto Bay, Pinecrest, and Sunny Isles Beach. It processes more than 1.2 million tons of waste a year, with 240,000 tons of material being processed into a biomass fuel. The county owns an advanced waste-to-energy facility operated by Covanta. The 77-megawatt facility produces enough energy to run the plant and meet the electrical needs of approximately 45,000 homes.

Miami-Dade County is a long-recognized leader in its commitment to reducing greenhouse gas (GHG) emissions. It has an impressive track record of implementing numerous programs and policies that contribute to the regional GHG reduction target of 80 percent below 2008 levels by 2050.

Miami-Dade County placed their its hydraulic hybrid vehicle order in April 2010, and by November 2012 it had a total of 35 hydraulic hybrid vehicles (HHVs) in service, shown in Figure III-176. These 35 first-generation MY2012 HHVs were all configured as automated side-loading refuse trucks on an Autocar E3 chassis with Heil DuraPack 7000 bodies and 2010 EPA-compliant Cummins ISL diesel engines, as shown in Figure III-177.



Figure III-176: Miami-Dade County's first generation (MY2013) hydraulic hybrid refuse trucks at the PWWMD facility
 NREL 32729



Figure III-177: Miami-Dade County, first generation (MY2013) Hydraulic Hybrid Refuse Truck on route
 NREL 32783

Late in 2014 Miami-Dade County placed an order for an additional 29 MY2015 HHVs with Parker Hannifin's latest HHV technology on the Autocar E3 chassis with Cummins 2010 EPA compliant ISL diesel engines. These vehicles were configured as automated side-loaders with New Way Sidewinder XTR bodies. The changes between the MY2013 and MY2015 hybrid systems are primarily focused on increased reliability and cost reduction, but Parker Hannifin has stated that there is a slightly different energy recovery profile to further improved efficiency.

Table III-30 presents additional details on Parker Hannifin's Powersplit infinitely variable transmission hydraulic hybrid system. Figure III-178 shows a schematic of its hydraulic hybrid RunWise system. This system is not strictly parallel or series in architecture, but a combination of both architectures. It is a dual path system capable of transmitting power hydraulically or mechanically or a combination of both. The system uses a gearbox to mix power input from both the diesel engine and the hydraulic motor to the wheels, to the hydraulic motor from the wheels for regeneration, or from the hydraulic motor to the engine flywheel to start the engine. The system also shuts off the diesel engine when it is not needed.

Table III-30: Hybrid Propulsion-Related Systems

Category	Hybrid System Description
Manufacturer/integrator	Parker Hannifin Corporation
Transmission	Parker Power Drive Unit (3-mode)
Drive mode max power	335-hp C24 variable displacement bent-axis hydraulic pump/motor
Regen mode max power	335-hp C24 variable displacement bent-axis hydraulic pump/motor
Energy storage	Composite bladder accumulator (MY13) Steel vessel accumulator (MY15) 3,500–4,000 psi nominal pressure range 5,400 psi max pressure

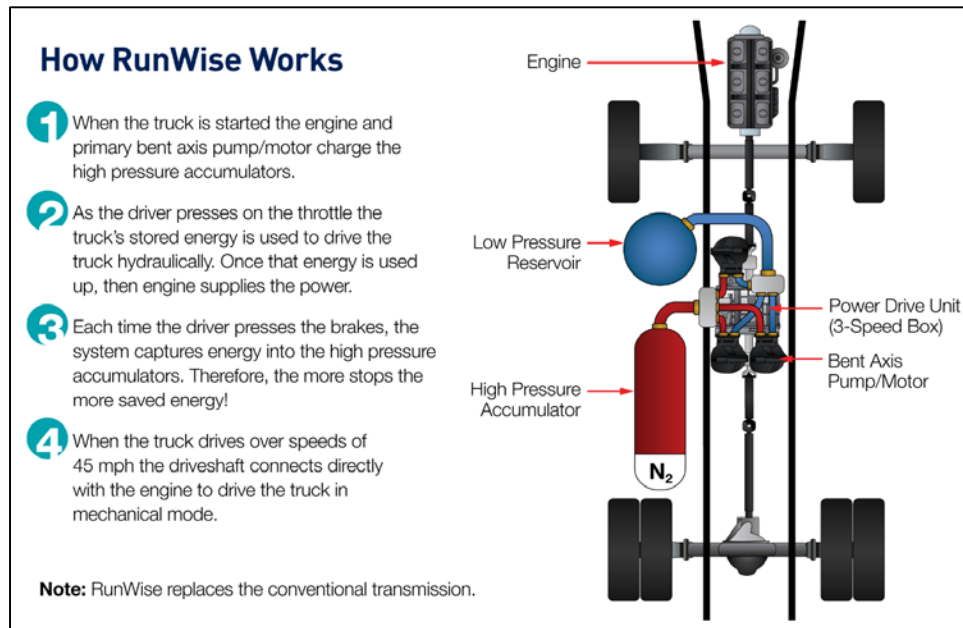


Figure III-178: Parker Hydraulic Hybrid schematic
NREL 34464

Introduction

This field evaluation project discusses an in-use evaluation of MY13 and MY15 HHV refuse vehicles in service in Miami-Dade County. Laboratory chassis dynamometer testing is planned for FY16 to validate the in-field findings and quantify both fuel and emissions savings over standard chassis dynamometer cycles.

The HHV refuse trucks with hydraulic drive systems manufactured by Parker Hannifin feature an infinitely variable hydraulic transmission for low-speed operation and a mechanical mode for speeds over 45 mph.

Host Site Profile—Miami-Dade County PWWMD

The host site in Doral, Florida, is a large service facility serving all Miami-Dade county PWWMD vehicles. This home terminal offers not only service and repair facilities but also onsite refueling of both diesel fuel and

diesel exhaust fluid. The residential waste collection schedule in Miami-Dade County is based on two pick-ups per week either Monday and Thursday or Tuesday and Friday depending on location. All collected waste is taken to either a transfer station or directly to the local Covanta waste-to-energy plant.

Approach

The technical approach for this project follows the general approach for conducting fleet evaluations described above. The specific technical approach for the Miami-Dade County Hydraulic Hybrid Refuse Truck Case Study includes the following:

- Initial fleet identification and selection
- Technology partnership
- Initial route and in-vehicle data collection
- Follow-up route and in-vehicle data collection
- Twelve-month fleet data (maintenance/operations) collection.

Detailed results from discussion and results from each of these steps are covered in the following section.

Results

Progress to Date

Initial Fleet Identification and Selection

Through coordination with both the Southeast Florida Clean Cities Coalition and the fleet managers at Miami-Dade County PWWMD, NREL was able to establish the project framework for this research project. Miami-Dade is interested in this research to better quantify the fuel savings it has seen with the first-generation HHVs and to more objectively evaluate the performance of its newest vehicles.

Technology Partnership

NREL and Parker Hannifin executed a non-disclosure agreement in May 2015 and Parker has agreed to support this research project by providing technical information into the operation of their hydraulic hybrid system as well as access to test vehicles for chassis dynamometer testing.

Initial Route and In-Vehicle Data Collection

Starting in March 2015, NREL deployed ten data logging devices (Isaac Instruments DRU900/908) with global positioning system (GPS) antennas and J1939 controller area network (CAN) bus connections to the Miami-Dade fleet. This initial deployment was primarily focused on collecting data on the first-generation hybrid vehicles already in service. At the same time, two 2007 Freightliner Condors with Caterpillar C11 diesel engines and LaBrie automated side-loader bodies were also instrumented. While these conventional vehicles are slightly older than the hybrids, they are the newest conventional diesel vehicles configured as automated side loaders operating in the Miami-Dade refuse fleet. These data along with future data from conventional diesel vehicles in the fleet will serve as the baseline for performance comparisons.

Initial GPS route analysis was performed to help validate data integrity and provide a general sense of how and where the vehicles are operated on a daily basis. Examples of the routes are shown in Figure III-179 and Figure III-180.

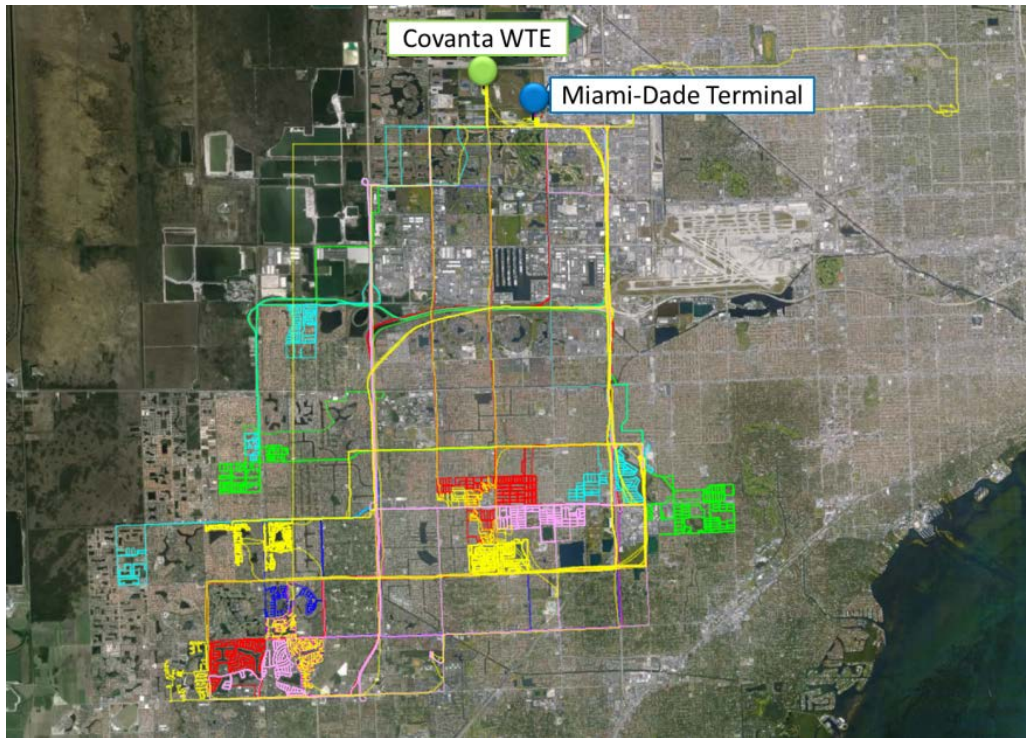


Figure III-179: Several vehicle routes shown in Miami-Dade County with the locations of the Covanta Waste to Energy (WTE) facility and main terminal indicated



Figure III-180: Neighborhood detail showing GPS vehicle routes

Initial drive cycle analysis of the in-use data was performed to gain a better sense of how the vehicles are driven on a daily basis. The first component of this evaluation was to confirm that the hybrid vehicles and the conventional vehicles were being operated on comparable routes. Two strong indicators for this comparison are kinetic intensity and average driving speed. Figure III-181 shows these two variables for both the HHVs and the conventional vehicles. It can be seen visually in the figure and statistically with P-values much greater

than 0.05, that there is no statistical difference between the two data sets in terms of average driving speed on route and kinetic intensity of with P-values of 0.21 and 0.44 respectively.

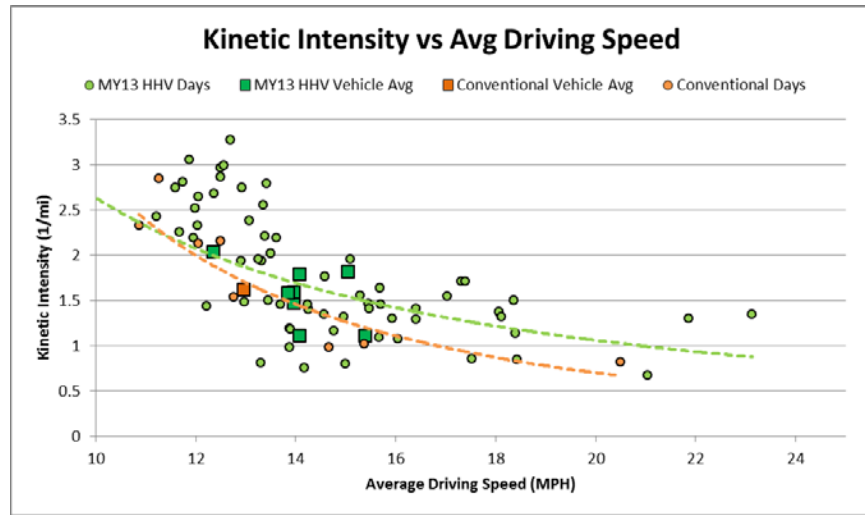


Figure III-181: Kinetic intensity vs. average driving speed for first-generation HHVs and conventional vehicles

Additionally, the number of stops per mile is of importance when evaluating refuse vehicle drive cycles. Figure III-182 shows the average daily kinetic intensity as a function of the number of stops. It can be seen that both vehicle groups share statistically similar characteristics in terms of stops per mile with a P-value of 0.15 and average kinetic intensity with a P-value of 0.44, which reaffirms that the conventional diesel vehicles are being operated in a comparable way to the hybrids.

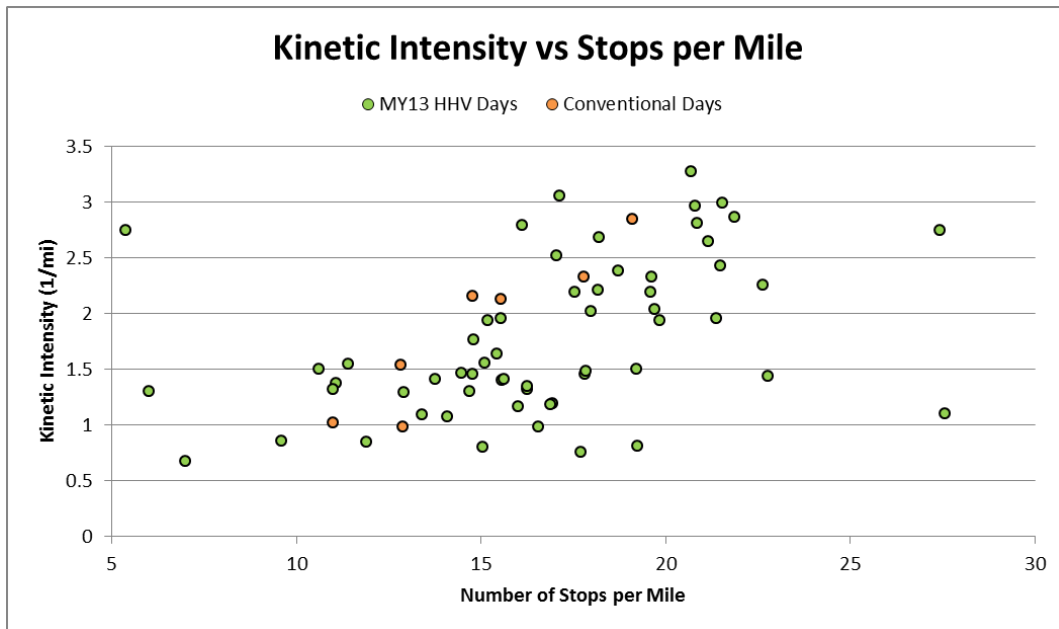


Figure III-182: Kinetic Intensity vs. average stops per mile for first-generation HHVs and conventional vehicles

While additional conventional diesel vehicle data is will be collected to before final conclusions or recommendations are made, the initial data set offers some interesting findings. Figure III-183 shows the J1939 reported fuel economy of both the first generation HHVs and the conventional diesel vehicles. It can be seen that for a given level of kinetic intensity, the HHVs consistently have a higher average fuel economy.

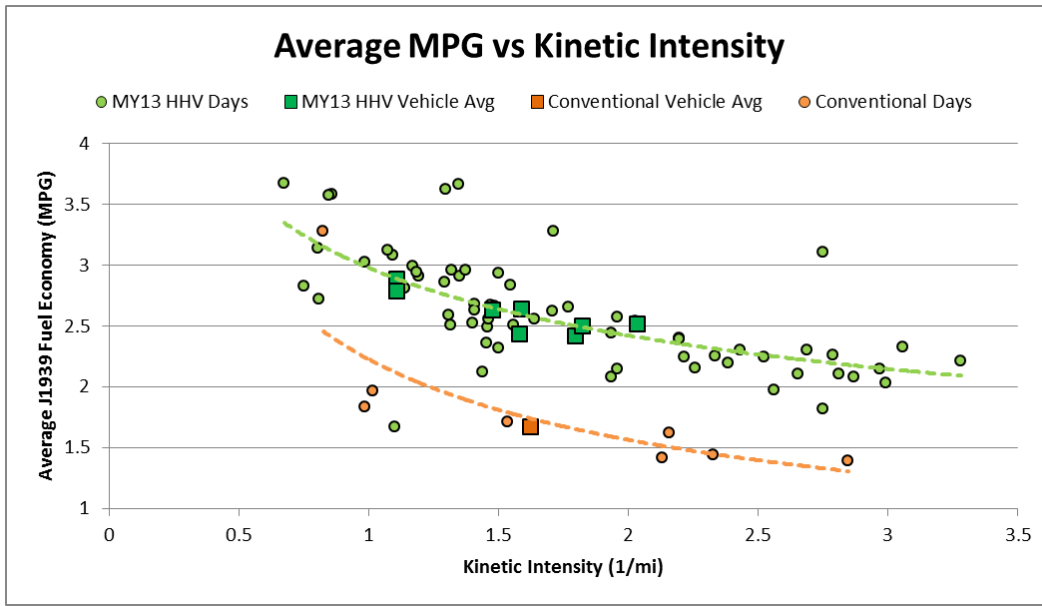


Figure III-183: Average fuel economy vs. kinetic intensity

Another way to look at this relationship is to compare average daily acceleration rate and average J1939 reported daily fuel economy, as shown in Figure III-184. For a given daily average fuel economy, the hybrid vehicles are able to accelerate more quickly than the conventional diesel vehicles. The hybrid vehicle fuel economy is also less sensitive to increasing acceleration rates as shown by a shallower trend line.

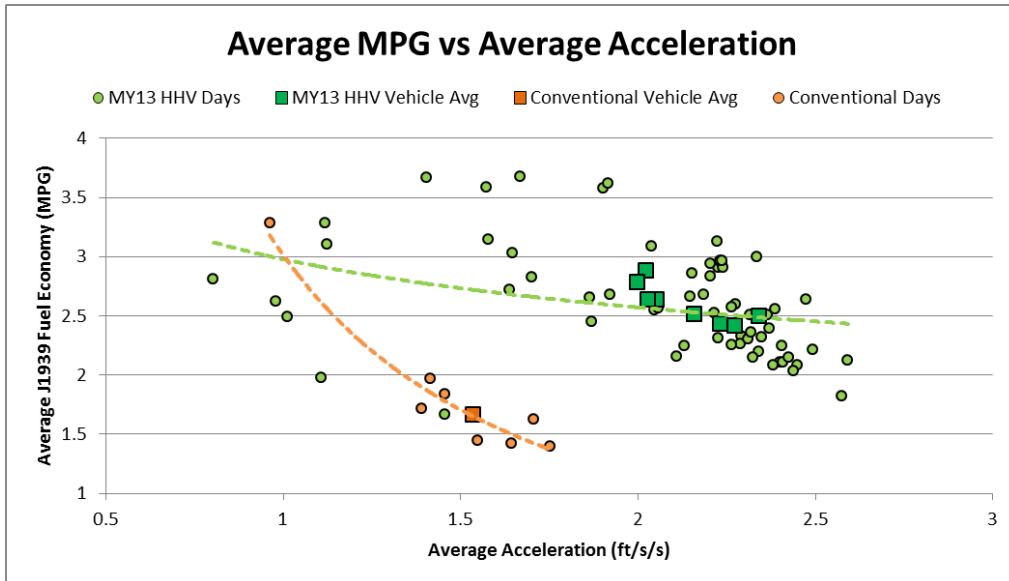


Figure III-184: Average fuel economy vs. average acceleration

Follow-up route and in-vehicle data collection

The first eight of 29 second-generation MY15 HHVs were put into service in June 2015 with the remainder going into service over the following three months. After the vehicles have undergone their break-in process by accumulating a few thousand miles, additional data will be collected on the HHVs and their conventional diesel counterparts. Another data logger deployment this will likely be in early FY16.

Twelve-month fleet data (maintenance/operations) collection

The 12-month fleet data collection process on the second generation HHVs will start in FY16.

Conclusions and Summary

Limited data have been collected and analyzed to date. Preliminary analysis indicates an average fuel economy improvement of over 40% with the first-generation HHVs over the 2007 conventional diesels when operated on similar routes. Early analysis also shows evidence of Parker Hannifin's stated improved efficiency due to quicker acceleration rates for a given level of fuel consumption, but more data will need to be collected and analyzed to draw a full conclusion.

CGI / EV2G School Bus Case Study

Background

NREL's Fleet Test and Evaluation Team is leveraging investment of the Clinton Global Initiative (CGI) technical and project team with funding from the CEC and the SCAQMD and many cost share elements. Collaboration between the Fleet Test team and the Vehicle Grid Integration team on field data will support grid integration efforts and vice versa. The project will contribute data to the Fleet DNA database and knowledge base on school bus duty cycles and their electrification potential.

Introduction

NREL is currently funded by DOE to collect operational data on conventional school buses in the districts receiving electric vehicle-to-grid (EV2G) buses and on the EV2G buses once they are deployed in the second or third quarter of 2016. The project will document the total cost of ownership of all CGI electric school buses with vehicle-to-grid (V2G) capability and contribute to TransPower's bus conversion efforts through the duty cycle characterization of current conventional and hybrid vehicles in service.

Approach

The technical approach for this project follows the general approach for conducting fleet evaluations described above. The specific technical approach for the EV2G school bus project includes the following:

- Initial route and in-vehicle data collection
- One school year of EV2G fleet data collection
- Battery life degradation study
- Energy Systems Integration Facility (ESIF) V2G evaluation.

Results

Progress to Date

Initial Fleet Identification and Selection

During FY15, NREL engaged with CGI to offer assistance in the area of duty cycle analysis and alternative vehicle application understanding. NREL then coordinated with Napa Valley Unified School District (NVUSD) and Torrance Unified School District (TUSD) to gather needed baseline data for the planned EV2G retrofit demonstration project in those districts. Zonar, the telematics provider for TUSD, agreed to provide in-kind 1-Hz data for 2 weeks on the TUSD 32 bus fleet to NREL for the purpose of this evaluation. NREL worked with NVUSD to identify 8 buses as targets for data logger installation based on TransPower EV bus potential route operation and completed the instrumentation plan in April. NREL reported on the NVUSD and TUSD baseline bus utilization data gathering to the Statistics Working Group on June 24, 2015.

Initial Route and In-Vehicle Data Collection

Data collected from the school districts was used to produce data products to help TransPower understand the usage environment its product will be placed into. Figure III-185 shows a histogram of daily distances traveled by buses in NVUSD and TUSD fleets. Note that 80% of observed days had fewer than 50 miles driven, and less than 10% of days had greater than 70 miles driven.

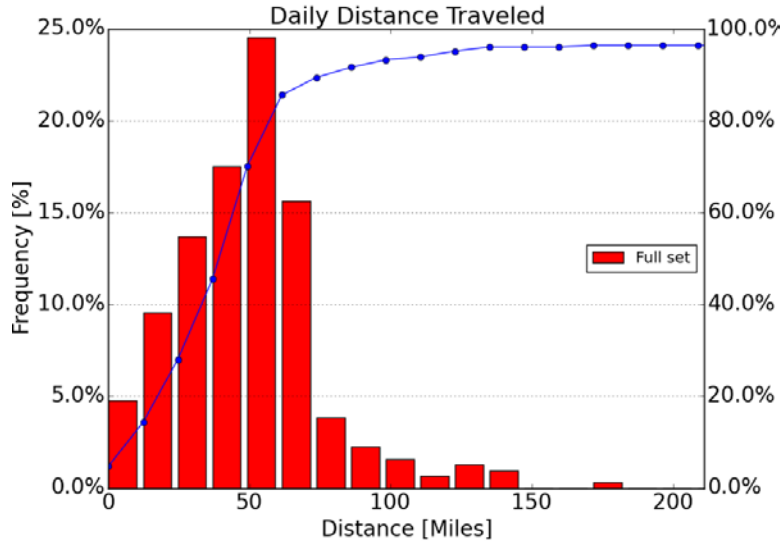


Figure III-185: School bus distance driven daily

Figure III-186 shows a histogram of the average speed driven by buses in the NVUSD and TUSD fleets. NVUSD had lower average trip speeds than TUSD, but also had more trips at higher average speeds, likely due to longer distance drives in rural areas of the district.

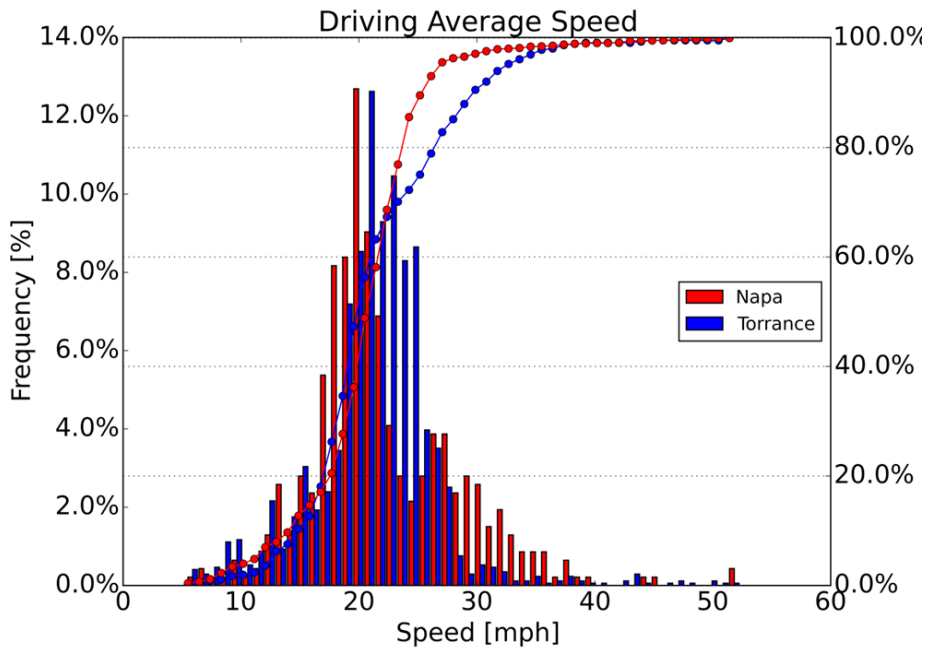


Figure III-186: School bus average speed driven

Figure III-187 shows a histogram of percent of miles traveled by time of day, an important point if an EV needs to charge between morning and afternoon runs or if the school district wants to participate in grid activities. NVUSD drives about 6% of its miles between 9 a.m. and noon, while TUSD drives almost 20% of its miles during that period. TUSD also had more buses in operation supporting student after school activities.

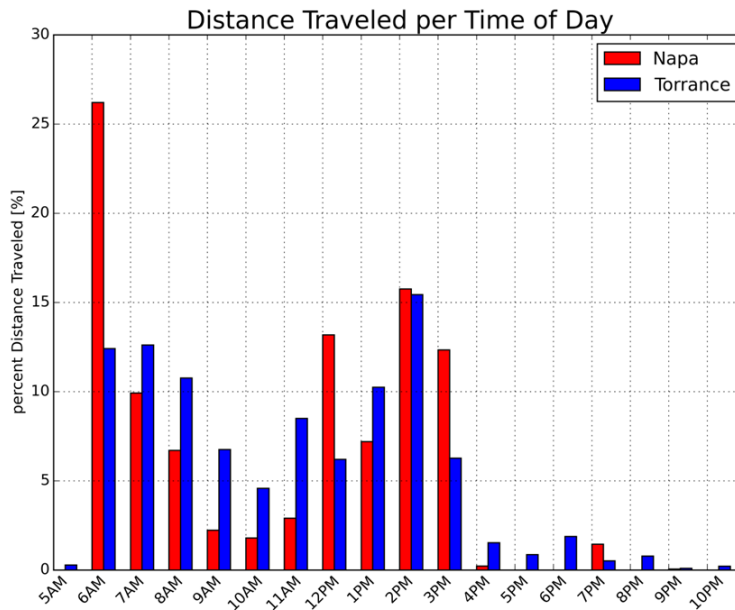


Figure III-187: School bus distance travelled by time of day

Figure III-188 shows stops per mile vs. kinetic intensity of all the observed days at both NVUSD and TUSD. The majority of driving in both districts has relatively low stops per mile and kinetic intensity, much lower than standard transit bus cycles. This indicates the EV buses may not have significant opportunities to regenerate energy in-route.

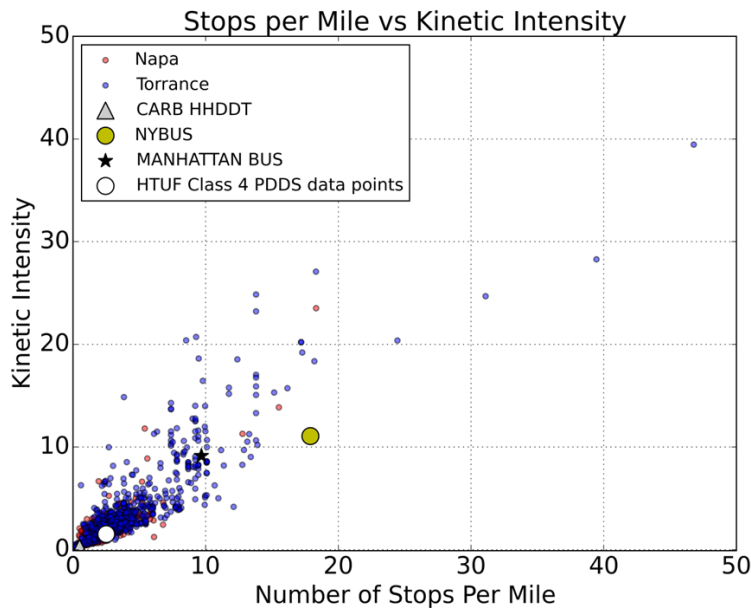


Figure III-188: School bus stops per mile vs. kinetic intensity

Economy and Emissions Impacts from Solazyme Fuel in UPS Delivery Vehicles

Background

UPS is one of the largest users of renewable diesel in the world. It recently announced an agreement for the purchase of up to 46 million gallons of renewable fuels over the next three years [1]. Part of that commitment to renewable fuels includes renewable diesel supplied by Solazyme. Renewable diesel is considered a "dropped in" replacement for petroleum diesel and does not require any modifications to existing trucks or equipment. The renewable diesel is held to the same standard as conventional fuel and must comply with the ASTM D975 standard for diesel fuel oil.

Two categories of vehicle were investigated during this fleet evaluation. The first was the package car, shown on the left in Figure III-189. All package cars for this in-field evaluation were model P100D and were equipped with Cummins ISB diesel engines on a Freightliner chassis. The second vehicle category was the day cab tractor, shown on the right in Figure III-189. The day cab tractors had various engine and chassis makes, but all were class 7–8 and used for regional haul operations.



Figure III-189: UPS package car (left) and day cab tractor (right)

NREL Image Gallery: #34441

In total, 12 vehicles were instrumented for real-world data collection, six package cars and six day cab tractors, all in the Houston area. Data were collected from April 20, 2015, to May 8, 2015. Drive cycle analysis was then used to select appropriate standard test cycles for further evaluation on NREL's heavy-duty chassis dynamometer at the Renewable Fuels and Lubricants (ReFUEL) Laboratory.

Introduction

NREL's Fleet Test and Evaluation Team aims to analyze near-term advanced technologies and provide unbiased performance data back to potential vehicle customers, equipment manufacturers and the R&D community at large. Clean Cities brings together stakeholders in the public and private sectors to deploy alternative and renewable fuels that help advance the nation's economic, environmental, and energy security by reducing petroleum consumption in transportation. Together, as part of a joint effort, a team was gathered to instrument and collect real-world drive cycle data from six package delivery cars and six day cab tractors operating in the Houston area, followed by further fuel economy and emissions analysis at NREL's ReFUEL facility. The goal of this work was to better understand what fuel economy and emissions impacts may arise from switching a fleet of vehicles from conventional petroleum to synthetic renewable diesel.

Approach

The technical approach for this project follows the general approach for conducting fleet evaluations described above. The UPS Solazyme fuel evaluation included:

- Vehicle instrumentation and in-field data collection
- Drive cycle analysis to determine the most representative standard cycles
- Fuel properties testing
- Heavy-duty chassis dynamometer testing on conventional diesel and Solazyme renewable diesel fuel to determine fuel economy and emissions impacts.

Results

Vehicle instrumentation and in-field data collection

Six package cars and six day cab tractors were selected for instrumentation at a Houston-area UPS depot. Selected vehicles were equipped with Isaac DRU900/908 data recorders on April 17, 2015. The devices were configured to watch for over 100 public on-board diagnostic parameters on the vehicle controller area network (CAN) bus. Not all parameters reported, but typically over 50 parameters are recorded each second, including vehicle speed, transmission gear, engine fuel rate and air flow, driver demanded and estimated output torque, and various temperatures and pressures throughout the engine and aftertreatment. In addition to CAN data, the devices also collected 1-Hz GPS location and speed information. The loggers remained on the vehicles until May 8, 2015, capturing three full weeks of vehicle operation. Figure III-190 shows the collected GPS information from both sets of vehicles with a close-up of the Houston metro area on the right.

Blue – Regional Tractor Trailers

Red – Package Cars

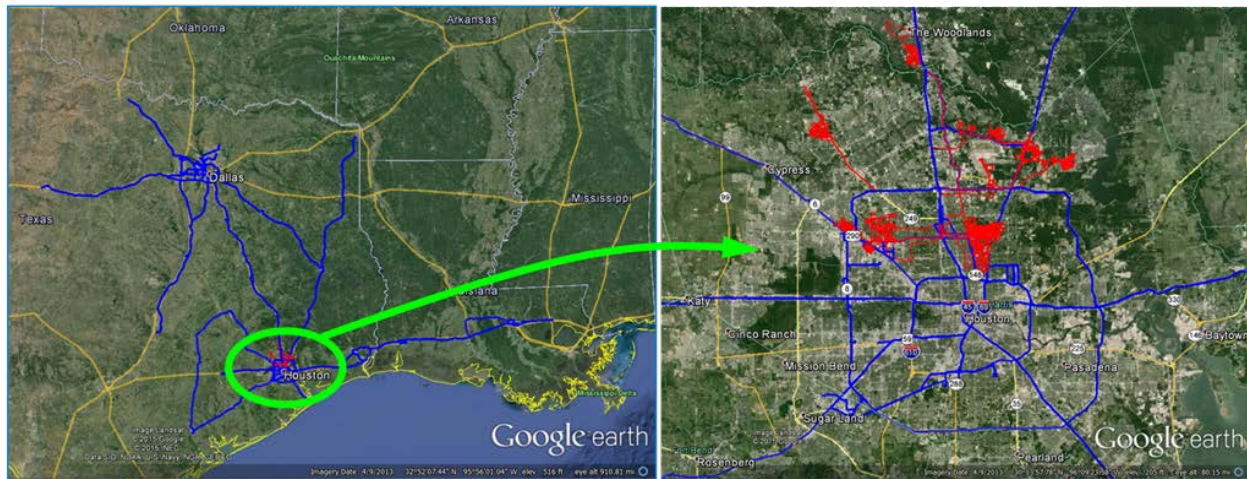


Figure III-190: UPS vehicle activity map

Images were generated using Google Earth

The regional haul day cab tractors travel between major UPS hubs and cover a large area connecting Houston to Dallas, Baton Rouge, Texarkana, Abilene, Austin, and many areas in between. The package cars travel from stop to stop making individual deliveries in dense urban areas. Therefore, this results in two distinctly and vastly different operating behaviors. Summary statistics for the vehicles are shown in Table III-31. As expected, the package cars and tractors differ significantly in average speed and kinetic intensity, a measure of drive cycle aggressiveness.

Table III-31: Vehicle summary statistics

ISAAC Logger #	3	5	12	13	15	17	29	30	32	33	34	35
Truck Number	147513	143085	148105	147509	147431	147544	274845	273701	271971	274850	274835	271919
Vehicle Type	Package	Package	Package	Package	Package	Package	Tractor	Tractor	Tractor	Tractor	Tractor	Tractor
Total Time [hr]	58.3	75.2	55.0	62.7	65.6	69.5	199.3	11.5	182.0	104.9	205.9	106.7
Idle Time [hr]	9.4	15.7	11.3	9.4	10.5	12.0	10.9	0.9	28.9	6.5	12.3	12.8
Idle Time [%]	16%	21%	20%	15%	16%	17%	5%	8%	16%	6%	6%	12%
Total Dist [mi]	1,162	1,158	766	1,143	1,355	1,354	10,703	654	6,513	5,505	11,649	4,686
Total Work [kWh]	1,119	1,762	1,116	1,470	1,774	1,691	29,374	1,734	11,373	12,433	31,041	10,998
Avg Speed [mph]	19.9	15.4	13.9	18.2	20.7	19.5	53.7	57.0	35.8	52.5	56.6	43.9
BSFC [g/kWh]	287	259	282	265	258	271	198	209	242	203	195	219
Fuel [Gallons]	98.5	140.2	96.7	119.5	140.5	140.5	1783.5	111.2	844.9	775.2	1862.7	739.7
Fuel Econ. [mpg]	11.8	8.3	7.9	9.6	9.6	9.6	6.0	5.9	7.7	7.1	6.3	6.3
KI [1/mi]	0.71	2.81	2.85	1.53	1.04	1.21	0.08	0.13	0.19	0.10	0.09	0.13

Figure III-191 shows a graph of kinetic intensity vs. driving average speed (while the vehicle is in motion, excluding stops). The small dots show individual driving days for both types of vehicle, and the larger symbols of the same color show vehicle averages, as well as several standard cycles that were selected for testing. The Heavy Heavy-Duty Diesel Truck (HHDDT), U.S. EPA Highway Fuel Economy Test (HWFET), and SAE J1376 - Commuter cycles were selected for the day cab tractor testing. The HHDDT, NY Composite, and HTUF 4 were selected for the package car. However, to date only the NY Composite cycle has been tested due to a chassis dynamometer component failure, and it is unclear if the other cycles can still be completed under current budget and timeline constraints.

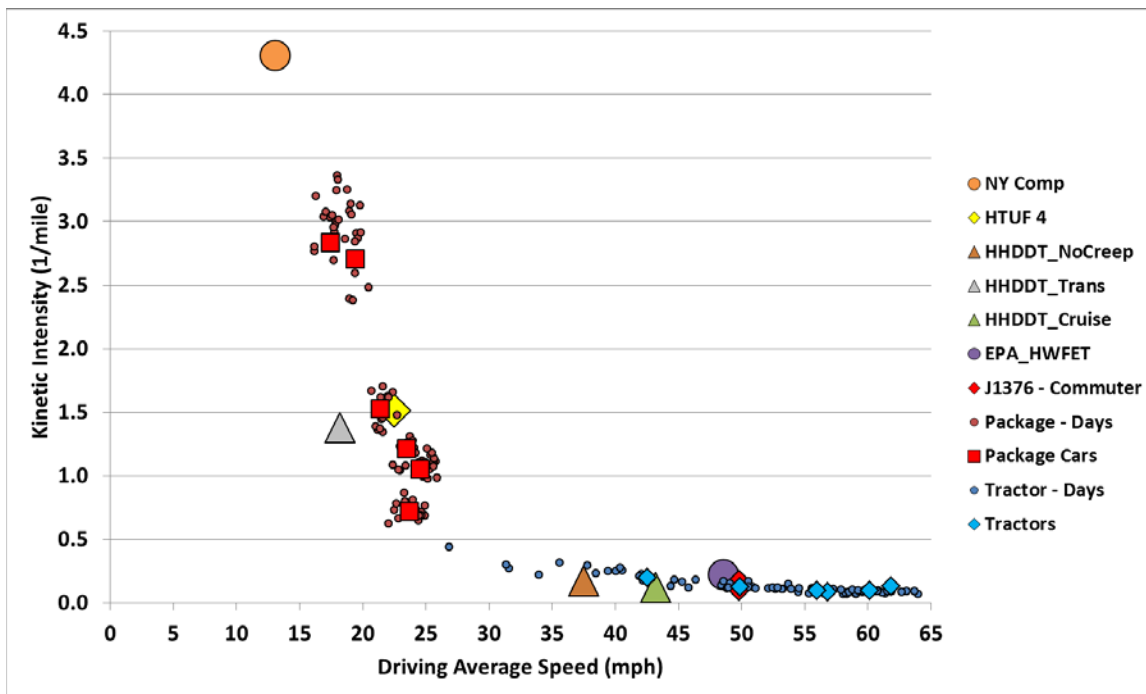


Figure III-191: Kinetic intensity vs. speed

The selected drive cycle time traces are shown in Figure III-192, followed by summary statistics in Table III-32.

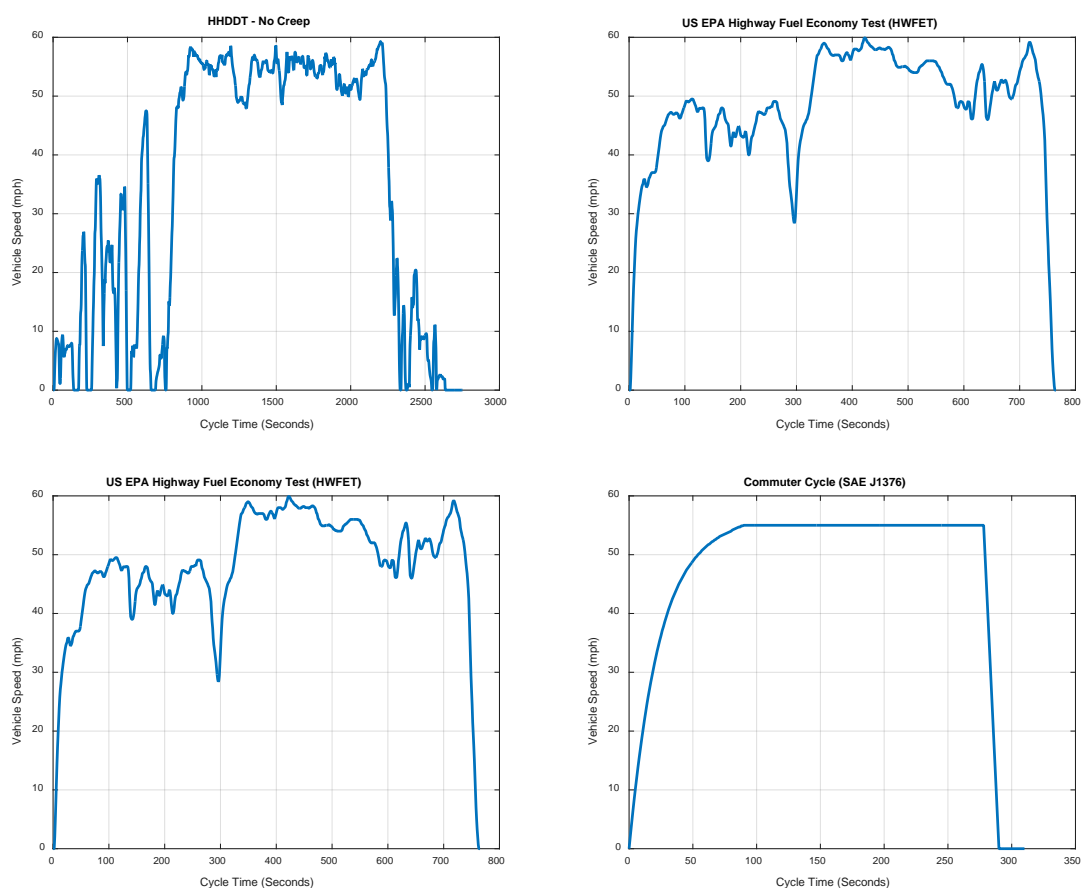


Figure III-192: Standard drive cycles

Table III-32: Standard Test Cycle Summary Statistics

Standard Test Cycle	Cycle Time	Distance	Avg Speed	Avg D Speed	KI	Stops	Stops
	Seconds	mi	mph	mph	1/mi	#	#/mi
New York Composite Cycle	1,029	2.51	8.8	13.1	4.30	20	7.98
HTUF Class 4	3,336	11.17	12.1	22.5	1.51	28	2.51
HHDDT Cycle Speed Data - Transient Mode	668	2.85	15.3	18.2	1.38	4	1.40
HHDDT - No Creep	2,751	25.92	33.9	37.5	0.17	10	0.39
HHDDT - Cruise Mode	2,083	23.07	39.9	43.2	0.12	6	0.26
US EPA Highway Fuel Economy Test (HWFET)	765	10.26	48.2	48.6	0.22	1	0.10
Commuter Cycle (SAE J1376)	310	4.00	46.3	49.8	0.14	1	0.25

Fuel properties testing

Regular summer blend pump fuel was used as the baseline petroleum diesel for the chassis dynamometer tests, and renewable diesel test fuel was supplied directly by Solazyme. Before testing began, fuel samples were extracted from each batch of fuel and sent out for analysis. Some tests, such as density, cloud point, percent biodiesel, and derived cetane, were conducted in-house by NREL's Fuels Performance Group. The remaining tests were conducted at Southwest Research Institute. The resulting fuel properties are shown in Table III-33. Distillation curves are shown in Figure III-193. It is worth noting that the Solazyme fuel has slightly higher hydrogen content and mass-based lower heating values, which will later be shown to reduce tailpipe carbon dioxide emissions and reduce mass-based fuel consumption. However, Solazyme's lower density is significant enough to result in a lower volume-based heating value, increasing volume-based fuel consumption and reducing fuel economy.

Table III-33: Fuel Properties

SwRI + NREL Fuel Analysis				
Test Method / Test		Units	ULSD Pump Fuel	Solazyme Fuel
D5291 CH	Carbon	wt%	85.36	83.69
	Hydrogen	wt%	13.48	14.95
D93	Flash Point	°F	144	139
	Flash Point	°C	62	60
Density		g/cm ³	0.834	0.779
Cloud Point		°C	-16.3	-7.3
% Biodiesel		%	4.61	2.59
Lower Heating Value		J/g	45,509	46,942
Lower Heating Value		J/cm ³	37,941	36,549
Derived Cetane		DCN	50.5	75.4

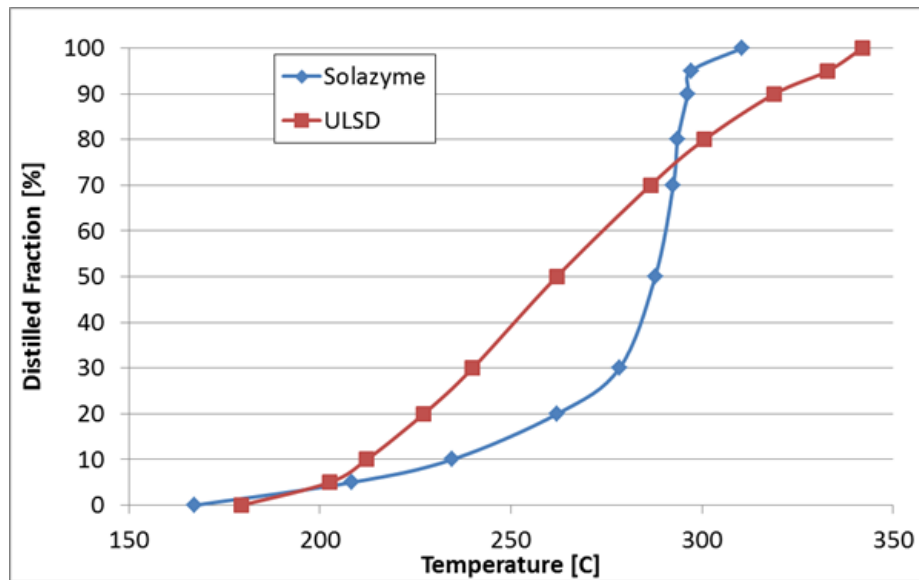


Figure III-193: Fuel distillation profile

Heavy-duty chassis dynamometer testing

Vehicle testing was performed using the heavy-duty chassis dynamometer at NREL's ReFUEL Laboratory. The chassis dynamometer is capable of simulating transient loads on heavy-duty vehicles from 8,000 up to 80,000 pounds at speeds up to 60 mph. To assure the accuracy and consistency of road load simulation, an automated dynamometer warm-up procedure is performed prior to testing until the dynamometer temperatures stabilize and measured parasitic losses in the dynamometer are stabilized. After each test run, a loaded coast-down procedure is performed to further ensure stability of vehicle and dynamometer parasitic losses and accurate road load simulation during testing. Vehicle fuel consumption was measured with a gravimetric scale. The fuel returning from the vehicle was cooled with an ambient air-to-liquid heat exchanger to maintain consistent temperatures. The scale mass measurements were recorded in real time along with all of the test data. Engine intake air was conditioned for pressure, humidity, and temperature as well as HEPA filtered to eliminate background particulate matter. Engine intake air was maintained at 20°C with a dew point of 12°C, which is a relative humidity of approximately 50%. The intake air pressure was maintained at a slight positive gage pressure of about 4~5 mbar above ambient pressure, which is typically around 840 mbar for Denver. Vehicle exhaust was diluted through the use of a constant volume sample (CVS) full dilution system. The CVS

system relies on sonic flow across orifices to measure exhaust flow rates and dilution ratios. The dilution air for the exhaust is supplied by the same system that supplies air to the intake of the engine. Gaseous emissions were measured with a Horiba MEXA 7100DEGR Bench.

Cold start and warm-up tests have been omitted for the results shown below. Each data point is an average of a minimum of three consecutive hot-start tests with a 20-minute soak period in-between. Error bars on all figures indicate 95% confidence intervals. Figure III-194 shows the measured gravimetric fuel consumption for all tests. The solid bars indicate tests conducted on the day cab tractor, and the patterned bars indicate tests conducted on the package car. Although three cycles were selected for the package car, only one was completed due to a dynamometer component failure. Cycle-to-cycle, the HWFET and HHDDT exhibited similar results. The Commuter cycle showed an increase in fuel consumption, likely due to the short duration of the test and therefore higher weighting of acceleration up to speed relative to cruising. The NY Composite is a more aggressive low-speed test, which would typically increase fuel consumption; however, the change in the vehicle's weight and aerodynamic drag properties more than makes up the difference, resulting in lower overall fuel consumption.

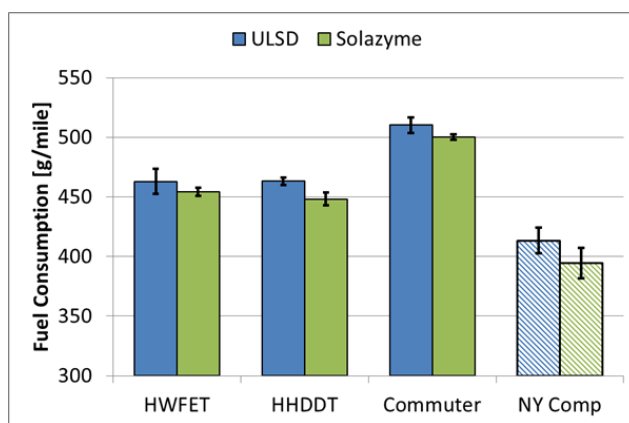


Figure III-194: Fuel consumption

As noted in the fuel properties results section, typically a decrease in fuel consumption would result in an increased fuel economy as the two are inversely proportional. However, in this case the density of the Solazyme fuel is lower than ultra-low sulfur diesel (ULSD) by a greater ratio than the gains in fuel consumption, resulting in an increased volumetric fuel consumption and lower fuel economy. The fuel economy results are shown in Figure III-195.

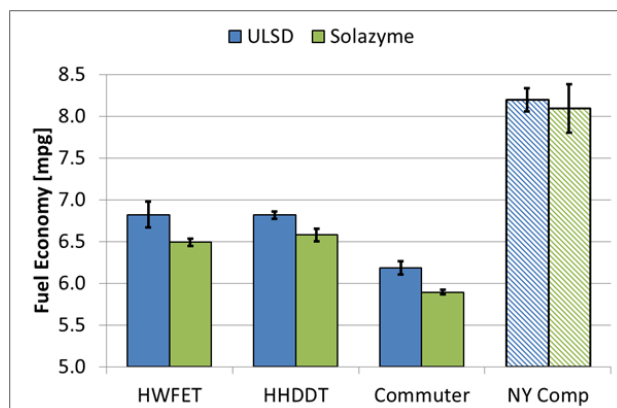


Figure III-195: Fuel economy

Figure III-196 shows the relative change in tailpipe carbon dioxide emissions, fuel consumption, and fuel economy when switching from ULSD to Renewable Solazyme fuel for the three day cab tractor tests. Variability in the NY Composite test cycles did not result in a statistically significant difference and has therefore been omitted. All three cycles show a consistent 4.2% decrease in tailpipe carbon dioxide emissions.

Fuel consumption and economy showed more variability from cycle to cycle, but both trended as expected with Solazyme's higher mass-based and lower volume-based heating values due to its lower density.

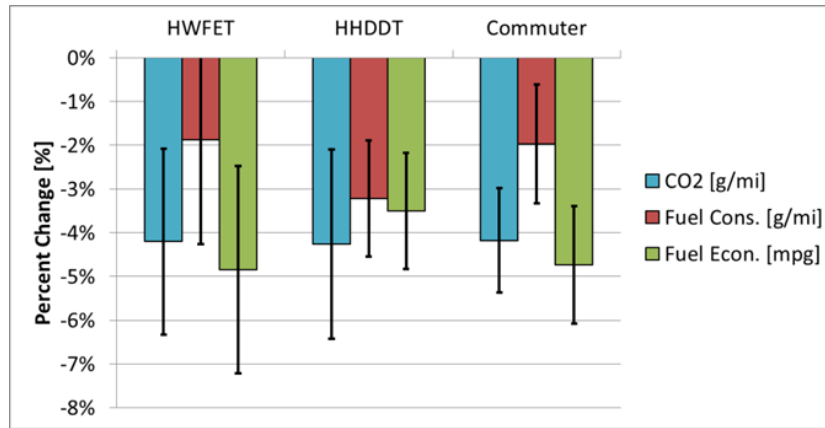


Figure III-196: Relative difference

Conclusions

A three week in-field data collection period on six day cab tractors and six package cars yielded 170 usable days of real-world vehicle operation that were used to select representative standard cycles for further testing. Fuel economy and emissions tests at NREL's ReFUEL Laboratory showed that in general when switching from conventional petroleum diesel to renewable diesel, the thermal efficiency of a cycle remains relatively constant and observed changes in tailpipe carbon dioxide, fuel consumption, and fuel economy are primarily driven by changes in fuel properties such as hydrogen-to-carbon ratio, density, and lower heating value.

III.12.C. Products

Publications

Only initial data have been collected to date; therefore, no technical publications have been produced at this time. However, the following project kickoff documents have been published or are in progress.

- NREL Highlights Fact Sheet: "NREL Evaluates Performance of Hydraulic Hybrid Refuse Vehicles"
- NREL Project Startup: "Evaluating the Performance of Hydraulic Hybrid Refuse Vehicles"
- Southeast Florida Clean Cities: "Local and Federal Government Partnership Progresses"

III.12.D. References

1. pressroom.ups.com/pressroom/ContentDetailsViewer.page?ConceptType=PressReleases&id=143811177421-236

III.13. Commercial EV Battery Degradation Field Evaluation

Kenneth Kelly, Principal Investigator

National Renewable Energy Laboratory
 15013 Denver West Parkway, MS 1633
 Golden, CO 80401
 Phone: (303) 275-4465
 E-mail: Kenneth.Kelly@nrel.gov

Lee Slezak and David Anderson, DOE Program Managers

Phone: (202) 586-2335, (202) 287-5688
 E-mail: Lee.Slezak@ee.doe.gov, David.Anderson@ee.doe.gov

Start Date: 2013

End Date: 2015

III.13.A. Abstract

Objectives

The lack of validated field data needed to predict battery life is a barrier to adoption of commercial electric vehicles (EVs). The National Renewable Energy Laboratory (NREL) has developed and will implement a field testing approach for conducting in-situ battery capacity tests. NREL will leverage an ongoing EV field data collection effort with Frito-Lay North America (FLNA), and work with the DOE VTO Energy Storage team to build life-cycle prediction capabilities for advanced transportation batteries. FY15 objectives included:

- Conduct field testing on Smith EVs at Frito-Lay locations with varying climates
- Begin analyzing data to evaluate battery health as a factor of usage and drive cycles and share data with DOE VTO Energy Storage team to simulate battery degradation in a vehicle.

Accomplishments

- Battery degradation testing and preliminary analysis were conducted on eight Smith EVs at four Frito-Lay fleet locations across the country, as well as one control vehicle at Smith Electric’s manufacturing facility.
- In FY15, a second round of tests was conducted at Clifton Park, New York, and a third round of tests was conducted at Casa Grande, Arizona, and Federal Way, Washington.
- Data from the tests have undergone preliminary analysis and have been presented to engineers at Smith Electric and fleet managers at Frito-Lay.

Future Achievements

- Battery degradation testing is currently planned to continue every six months to ten months on seven in-use Smith EVs at four Frito-Lay locations throughout FY16 and into FY17.
- To date, the degradation analysis procedure has been applied to a small number of vehicle histories for which NREL’s controlled degradation tests are available to validate the technique.
- Going forward, battery state of health will be estimated for the vehicles in the Smith data set collected under the American Recovery and Reinvestment Act (ARRA) to construct a life model of the pack based on in-use field data. Such a model would be of great value to fleet managers interested in pairing EVs with appropriate vocations in their fleet.



III.13.B. Technical Discussion

Background

NREL's Fleet Test and Evaluation Team has found medium- and heavy-duty vehicle fleets to be good candidates for deploying low-emitting advanced technologies due to their large numbers, high vehicle miles traveled—and consequently high petroleum fuel consumption and emissions—and frequent operation in large population centers, as well as common return-to-base fueling regimes and consistent driving routes.

Previous testing and analysis conducted by NREL have illustrated the influence of drive cycle and vehicle usage on both energy consumption (from liquid fuels and high-voltage hybrid battery packs) and exhaust (or well-to-wheels) emissions. Drive cycle has also been shown to influence the all-electric range of battery EVs, the charge depleting range of plug-in hybrid EVs, and the potential fuel economy benefit of hybrid EVs. Accordingly, fleet customers can benefit from a further understanding of advanced vehicle technology deployment to minimize fuel consumption and emissions. It has also been shown that large-scale deployments of EVs in a localized area can lead to power quality and power cost issues.

Introduction

NREL is currently funded by the DOE to collect operational data on Smith EVs being deployed as part of ARRA. Data collected from these vehicles (up to 500, some of which are located at FLNA facilities) will be used to understand the overall usage and effectiveness of EVs in medium-duty commercial fleet facilities and operations and also compare to operations of conventional counterparts in the same location. Through this collaboration with FLNA, NREL hopes to provide a more focused investigation to understand the implementation and performance of medium-duty EVs in a large-scale commercial facility.

Battery lifetime uncertainty is a major barrier to fleet manager decisions regarding the adoption of plug-in EVs. To reduce life uncertainty, NREL, Smith, and FLNA have developed a study to perform benchmarking tests of EV batteries at regular stages throughout their life.

Approach

Battery degradation testing is currently planned to continue every six to ten months on seven Smith EVs throughout FY16 and into FY17. The original scope included testing eight separate vehicles; however, unit FLNAR42175 (see Table III-34) was relocated to another terminal within Frito-Lay. To validate the technique, the degradation analysis procedure has been applied to a small number of vehicles for which NREL's controlled degradation tests are available. Going forward, battery state of health will be estimated for the entire Smith ARRA data set through time and potentially be used to construct a life model of the pack based on in-use field data. Such a model would be of great value to fleet managers interested in pairing EVs with appropriate vocations in their fleet.

The benchmarking test results provide ground truth data that support a larger battery health trending analysis of the ARRA telemetry data set. These methods will allow NREL to quantify battery pack health and track battery performance changes over life as well as validate battery life assumptions (as envisioned in Figure III-197) to help develop a fleet business case.

Table III-34: Smith EV subjects of battery degradation testing

Location	Vehicle ID	In-Service Date	Test Date
Kansas City, MO	SMITHFE110	N/A	6/13/13
Casa Grande, AZ	FLNAR42175	2/4/13	9/11/13
			5/6/14
			Moved
	FLNAR42176	2/4/13	9/10/13
			5/7/14
			7/7/15
Federal Way, WA	FLNAE27123	1/9/13	9/24/13
			4/16/14
			7/21/15
	FLNAE27124	4/10/13	9/25/13
			4/15/14
			7/22/15
Clifton Park, NY	FLNAE27144	9/24/13	6/3/14
			11/5/14
	FLNAE27148	9/24/13	6/4/14
			11/4/14
Manteca, CA	FLNAE27157	5/28/13	6/18/14
	FLNAE27159	5/28/13	6/17/14

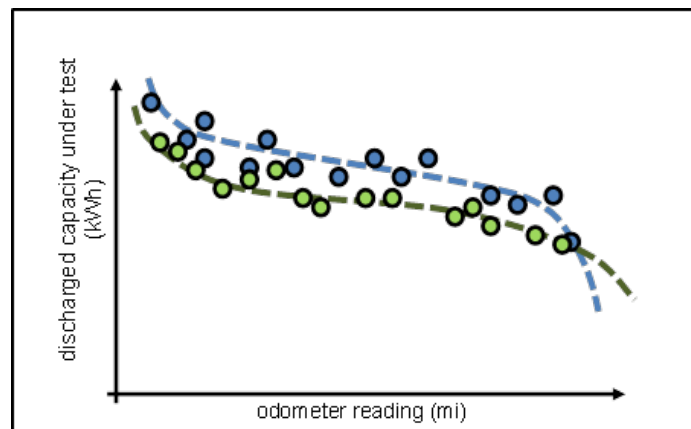


Figure III-197: Intended data collection—collecting several points over a period of years will help to validate life models

Results

The benchmarking tests are being performed onsite at four FLNA fleet depot locations with a total of eight Smith Gen 2 trucks. Smith's Gen 2 vehicles are box trucks with two 40-kWh A123 battery pods (80 kWh total). Table III-34 lists the vehicles tested along with their locations and battery test dates.

In 2013, NREL and Smith developed a test to perform a controlled discharge of Smith EV batteries in-situ, without removing them from the truck. NREL ships test equipment to each fleet location prior to an NREL visit, including a 14.5-kW programmable DC load bank and data recording and electrical interface boxes. Prior to the test, the truck is fully charged overnight using the normal charge protocol. NREL test engineers electrically disconnect the battery from the truck and route the electrical leads to the test equipment. The test equipment discharges the battery at a C/6 rate, with periodic rests to measure open circuit voltage and resistance. The data are recorded both from the vehicle controller area network (CAN) and using an independent data logger. A representative schematic is shown in Figure III-198. Following the six-hour discharge, the truck is returned to its original condition and placed on charge to resume normal service the following day. This one-day test is minimally invasive to fleet operations.

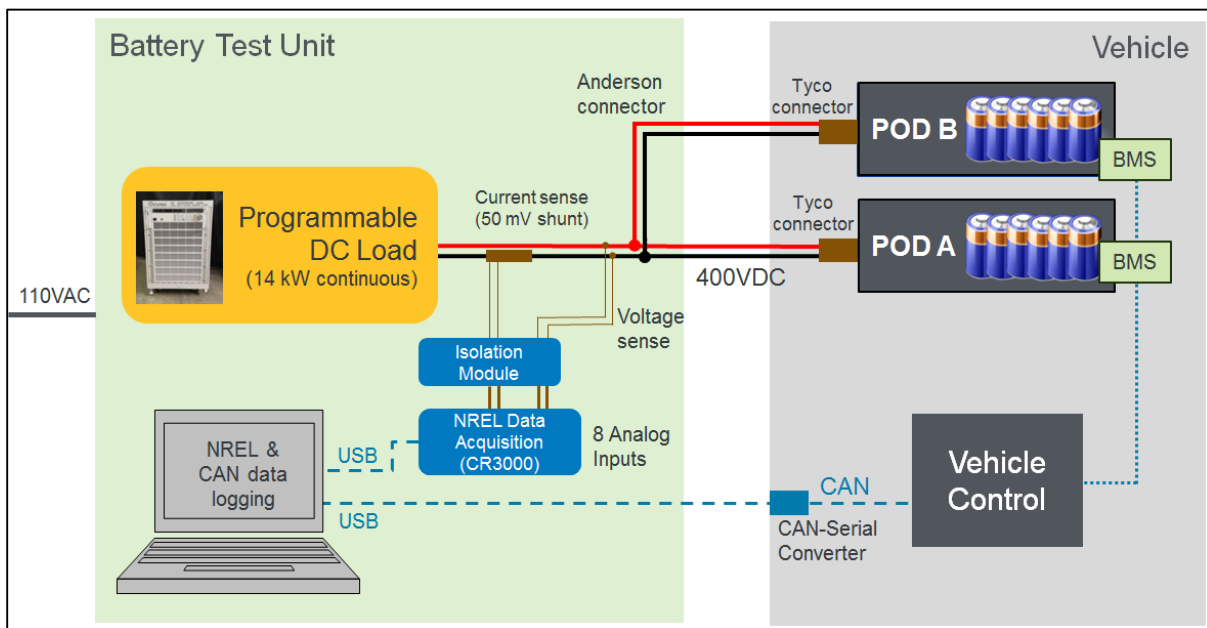


Figure III-198: Schematic of load bank and data acquisition set-up

NREL validated proper operation of the test and test equipment at Smith's U.S. headquarters in Kansas City, Missouri, in 2013 (see Figure III-199) on a new vehicle. Data were collected at Smith headquarters on this new truck to act as a benchmark for beginning-of-life performance of Smith EV packs. During September 2013, the load bank was shipped to FLNA's Arizona and Washington facilities, documenting battery performance for two trucks at each location that entered service the same year. In the summer of 2014, testing was started at two additional locations on two vehicles in each location; these distribution centers are located in Manteca, California, and Clifton Park, New York. In the fall of 2014, NREL returned to the Clifton Park site for follow-up testing of the same two trucks. In the summer of 2015, NREL performed testing on the two vehicles in Federal Way as well as one vehicle in Casa Grande, Arizona. The total number of vehicles under test is presently seven as vehicle FLNAR42175 originally under test at Casa Grande was relocated to another facility.



Figure III-199: Load test conducted at Casa Grande, AZ
NREL 29613

Given that these vehicles are operating in their native FLNA environment, it is expected that a minimum of three years of testing may be required to discern any actionable trends in degradation from the seven vehicles under test. NREL has strong support from Smith EV and FLNA to continue the testing for several years. Each test takes less than one day per truck and is conducted without removing the battery pack from the truck. A successful outcome of the project is dissemination of credible, multi-year battery performance data to support increased adoption of EVs in commercial fleets.

Conclusions

At this point, results are still preliminary because all vehicles tested have relatively low mileage (6,000 to 22,000 miles) and any variations measured in capacity are still within the error margins of NREL's test equipment. Data will be presented as more data points are collected in the coming years, which will average out any errors.

Battery duty cycles harvested from large data sets of in-use operation provide an excellent opportunity to monitor and better understand the real-world aging process in EV battery packs. For this effort, the ARRA Smith EV data set is being used to identify combinations of drive cycles and climates that result in accelerated degradation.

Time series histories of pack current and voltage are applied to an electrical model of the pack that considers zero-order current-resistance dynamics and a single-particle model of electrode concentration gradients (used to describe transient voltage relaxation). Modeled pack voltage is compared to the historical data, and a constrained non-linear optimization algorithm is used to minimize the root mean square of model error (usually achieving root mean square of model error values of tens of millivolts per cell). Figure III-200 shows an example of the analysis. Note that the vertical scale on the upper graph has been omitted and the voltages have been skewed on the lower graph to protect intellectual property.

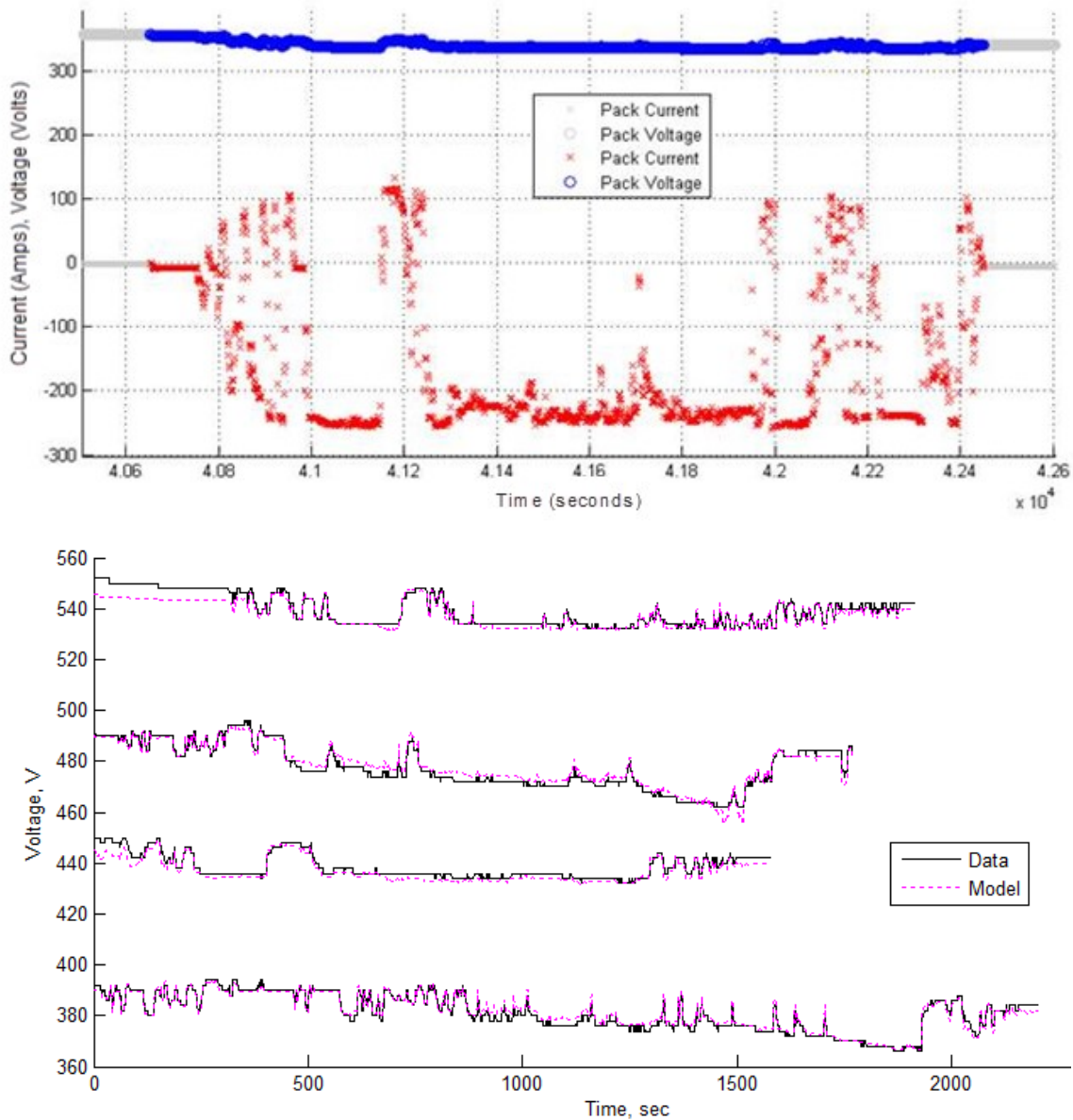


Figure III-200: Example of sample drive cycle data from the ARRA Smith data collection project (top) used to generate models fit to a root-mean-square error of less than 6% open circuit voltage (bottom).

Error is minimized by updating model parameters such as pack capacity, bulk resistance, initial thermodynamic state of charge, and multiple diffusion coefficients. Following optimization of the model over each individual drive cycle, estimated parameters used to describe pack available energy and power are reported through time and compared to controlled performance tests conducted by NREL engineers in the field.

III.13.C. Products

Publications

Only initial data has been collected to date. No publications have been produced at this time.

III.14. Truck Platooning Follow-on Study

Kenneth Kelly, Principal Investigator

National Renewable Energy Laboratory
15013 Denver West Parkway, MS 1633
Golden, CO 80401
Phone: (303) 275-4465
E-mail: Kenneth.Kelly@nrel.gov

David Anderson and Lee Slezak, DOE Program Managers

Phone: (202) 287-5688, (202) 586-2335
E-mail: David.Anderson@ee.doe.gov, Lee.Slezak@ee.doe.gov

Start Date: 2015

End Date: 2016

III.14.A. Abstract

Objectives

This project is planning follow-on analysis and testing paths to further understand the factors affecting potential fuel savings from highway truck platooning beyond what the National Renewable Energy Laboratory (NREL) demonstrated in FY14 testing. Platooning technology is an early application and supports development of autonomous vehicle technology. Truck platooning is gaining significant attention from industry with public investments in the technology by Volvo, UPS, Nokia, Intel, and Lockheed Martin. However, all the variables impacting possible fuel savings from following distances and the number of vehicles in platoon to the impact of fleet logistics on the percent of miles that can be platooned still remain a significant unknown. In FY14, NREL showed the technology has the potential to reduce fuel use by 3%–6% (tandem average). Analysis of the results indicated a potential opportunity to further optimize the system performance.

FY15 objectives included the following:

- Collaborate with Lawrence Livermore National Laboratory (LLNL) to investigate specific aerodynamic features to address trailing truck ram air cooling needs
- Investigate potential benefits of other configurations such as three or four trucks in platoon
- Plan follow-on track testing of platooning systems to better understand key performance parameters and opportunities to improve overall fuel and emissions performance
- Conduct high-level analysis of platooning applicability for national energy displacement benefits.

Accomplishments

- Built relationship and collaboration path with LLNL to investigate questions raised by track testing with a wind tunnel test plan to be implemented in early October 2015
- Championed and completed three-way Non-Disclosure Agreement (NDA) between NREL, LLNL, and PACCAR to enable sharing of computational fluid dynamics (CFD) shape files to support LLNL/NREL CFD investigation into questions raised during track testing and follow-on wind tunnel testing
- Searched for and identified a large fleet willing to supply telematics data in support of “big picture” platooning fuel savings analysis
- Secured an NDA with Con-way Freight to disclose high-resolution telematics data from over 8,000 vehicles

- Completed contract with Con-way Freight to reimburse them for cellular costs incurred due to NREL's data collection activities
- Completed contract with Vnomics to collect and transmit the high-resolution telematics data from Con-way Freight
- Presented results of the testing and discussed future plans at the Transportation Research Board Automated Vehicle Symposium in July 2015
- Provided technical assistance and equipment to enrich platooning track testing conducted by Auburn University at the Transportation Research Center track and funded by the Federal Highway Administration.

Future Achievements

The truck platooning study conducted so far has received positive feedback from a number of industry partners. Several opportunities exist for improving the understanding and potentially optimizing the benefits of this technology. These include:

- Additional testing to confirm the trends shown in FY14, including greater following distances to clarify the optimum configuration
 - Wind tunnel testing in partnership with LLNL
 - Modeling CFD in partnership with LLNL
 - Incorporating direct aerodynamic study into track testing (truck-mounted anemometer, smoke trails, etc.) to confirm wind tunnel and CFD findings
- Designing aerodynamic aids specific to platooning to address the loss of cooling airflow over the radiator of the trailing tractor
- Assessing current highway truck travel
 - What percent of large fleet and national highway truck miles would be conducive to platooning?
 - How often do trucks typically travel together and at what following distance?
- Assessing any impact of platooning on criteria emissions (e.g., NO_x).



III.14.B. Technical Discussion

Background

Vehicle automation is a promising petroleum reduction technology. Platooning systems for heavy-duty vehicles are likely to be an early commercial application of vehicle automation technology. These systems may employ existing technologies such as radar or laser range finders, global positioning system, dedicated vehicle-to-vehicle communications, and braking and engine torque authority to enable vehicles to follow safely in close proximity, with the goal of reducing fuel consumption through improved aerodynamics as well as reducing traffic congestion and possibly collisions. Figure III-201 illustrates how platooning is intended to make two trucks appear more like one object to the airflow, resulting in reduced turbulence behind the lead truck and reduced forebody drag on the trailing truck.

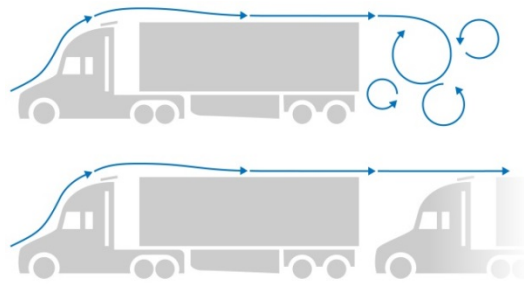


Figure III-201: Truck Platooning Air Flow

In FY14, NREL teamed with Intertek and Peloton to evaluate the fuel efficiency of line-haul trucks operated in platooned pairs under controlled track testing. The first round of track testing of the Peloton system was completed in March 2014. The technology showed potential to improve fuel use by 3%–6% (tandem average). Figure III-202 shows the actual FY14 test vehicles in platoon formation.



Figure III-202: Trucks in Platoon Formation during Testing

NREL #31237

Introduction

Under this project, NREL is planning studies to increase understanding around the dynamic interactions between platooning vehicles that impact fuel savings as well as the logistics of what percent of truck miles can be platooned. This project is intended to answer questions raised by results from a FY14 series of 10 modified SAE Type II J1321 fuel consumption track tests that were performed to document the fuel consumption of two platooned vehicles and a control vehicle at varying steady-state speeds, following distances, and gross vehicle weights.

FY15 planning activities included the following:

- Additional testing to confirm the trends shown in FY14, including greater following distances to clarify the optimum configuration
 - Wind tunnel testing in partnership with LLNL
 - Modeling CFD in partnership with LLNL
 - Incorporating direct aerodynamic study into track testing (truck-mounted anemometer, smoke trails, etc.) to confirm wind tunnel and CFD findings
- Designing aerodynamic aids specific to platooning to address the loss of cooling airflow over the radiator of the trailing tractor
- Assessing current highway truck travel
 - What percent of large fleet and national highway truck miles would be conducive to platooning?
 - How often do trucks typically travel together and at what following distance?
- Assessing any impact of platooning on criteria emissions (e.g., NO_x).

Approach

This research project, which was funded by DOE, intends to increase understanding around the dynamic interactions between platooning vehicles that impact fuel savings and determine the best application scenarios. This will be accomplished with a two-pronged effort. The first is to better understand the specific impacts of platooning at varying distances through collaborative wind tunnel and CFD testing with LLNL, which will inform more track testing by NREL. The second is to estimate the impact of large-scale platooning adoption at fleet and national levels using "big data" to understand what percent of highway truck miles could potentially be platooned under several scenarios.

Results

Partnerships and Collaborations

Partnership with LLNL to increase understanding of aerodynamic envelope governing truck platooning

A partnership was created with LLNL to investigate some of the questions raised in the FY14 track tests about close following conditions, long following distances, alignment sensitivity, and three-truck platoons. These questions will be addressed with a series of scale wind tunnel scenarios and CFD work. Wind tunnel testing will commence at the end of September 2015 and will include ideas for boat tail designs to aid following vehicle radiator cooling at close following distances. CFD work to follow. A three-way NDA among NREL, LLNL, and PACCAR was secured to enable PACCAR to share shape files of the Peterbilt 386 trucks used during the FY14 track testing to help the CFD modeling to be more accurate. NREL will plan a second track study to confirm at full scale what was indicated by wind tunnel and CFD testing.

Big picture fuel savings at fleet and national scales

NREL solicited a dozen highway truck fleets looking for a partner to supply large-scale high-resolution fleet vehicle level telematics data for platooning analysis. Con-way Freight agreed to participate, and an NDA protecting sensitive data was signed. Vnomics, Con-way's telematics provider, was also contacted, and a technical way forward was established. Contracts to pay Vnomics for engineering work to supply 1-Hz data and reimburse Con-way for incurred costs due to increased cellular data usage on 8,000+ class 8 tractors are in final stages of completion. Once in hand, this data set will enable a large-scale geospatial analysis of what percent of highway miles driven could potentially be available for platooning savings given scheduling of vehicles together, road type, speeds, etc.

Conclusions

Wind tunnel testing is to begin at the beginning of October 2015. Telematics data from the Con-way Freight fleet are planned to be flowing through Vnomics to NREL by the end of November 2015.

III.14.C. Products

Presentations/Publications/Patents

As this activity took significant effort to establish relationships and data is just beginning to be produced, no public data products were produced this fiscal year.

IV. Modeling and Simulation

IV.1. Autonomie Maintenance and Model Based System Engineering (MBSE) Enhancements

Phillip Sharer, Principal Investigator

Argonne National Laboratory
9700 S. Cass Avenue, Building 362
Argonne, IL 60439
Phone: (630) 252-9739; Fax: (630) 252-3443
E-mail: psharer@anl.gov

David Anderson, U.S. Department of Energy (DOE) Program Manager

Office of Vehicle Technologies, Department of Energy
Phone: (202) 287-5688
E-mail: David.Anderson@ee.doe.gov

Start Date: 10/1/2015
End Date: 9/30/2016

IV.1.A. Abstract

Objectives

- Enhance and maintain Autonomie as needed to support the U.S. Department of Energy (DOE) and the user community
- Enhance Autonomie to expand its model-based system engineering scope

Accomplishments

- User Interface Enhancements
 - Improved robustness of the import functionality
 - Implemented a more user-friendly vehicle selection control
 - Designed a process to define and run combinations of vehicle parameters, files, and systems in parallel
- Model Based System Engineering (MBSE) Enhancements
 - Invented a way to select different workflows in Autonomie
 - Enhanced tool that manages large-scale datasets produced for Baseline and Scenario Analysis (BaSce)
 - Adopted the SAE J3049 Standard for Model Architecture
 - Added Support for Functional Mockup Interface (FMI) 2.0
 - Migrated the automated testing used as part of the internal MBSE process to the Jenkins framework
- Incorporating Industry Feedback
- Supporting Government Activities

Future Achievements

- Continue to enhance Autonomie to support DOE and technology transfer



IV.1.B. Technical Discussion

Background

Autonomie is a plug-and-play powertrain and vehicle model architecture and development environment that supports the rapid evaluation of new powertrain/propulsion technologies to improve fuel economy through virtual design and analysis in a math-based simulation environment. Autonomie has an open architecture to support the rapid integration and analysis of powertrain/propulsion systems and technologies. This architecture allows rapid technology sorting and evaluation of fuel economy under dynamic/transient testing conditions.

Introduction

To better support the U.S. Department of Energy (DOE) and its user community, several new features have been implemented in Autonomie. Some of the most significant accomplishments are described in this report.

Approach

There are always more ideas for new Autonomie features and enhancements than time to actually implement them. Feedback on which items to prioritize and include is collected in several ways.

First, users of Autonomie register suggestions for improving the software or models by email, in person, or through our online issue-tracking system at Autonomie.net. Second, direct interaction with partners and sponsors while working on shared projects contributes to collecting new requirements. Finally, DOE studies often drive the improvement of existing capabilities and/or the development of new ones.

Model Based System Engineering (MBSE) enhancements focused on longer-term strategies for the future of vehicle modeling and simulation, such as an emphasis on parallelization for running larger number of simulations. Another emphasis was the integration of tools that, themselves, integrate tools, thereby increasing the breadth of the Autonomie ecosystem.

Results

User Interface Enhancements

Improved Robustness of the Import Functionality

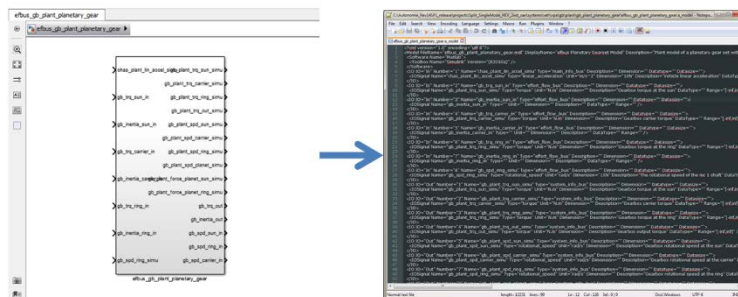


Figure IV-1: Import Functionality—Converting Models to Improved Autonomie Metadata

Autonomie provides both search and compatibility features to users, attributes that enable them to manage their own library of system models and calibrations. As a user defines their specific vehicles, they are guided by Autonomie in selecting the appropriate model for each system. Just as important as search and compatibility, a user can declaratively state what calibrations are within the vehicle without having to worry about interdependencies between calibrations. That is, Autonomie determines the proper order in which to apply calibrations. These features, searching, compatibility, and interdependency analysis, provide considerable benefit to the Autonomie user, and are reasons why original equipment manufacturers (OEMs)

and suppliers choose Autonomie to be their MBSE software. All three of these features rely on good static analysis of models and calibrations. Such static analysis involves reading the model diagram; parsing the diagram structure; and tracing internal connections to determine the number, names, and types of inputs and outputs to the model. Static analysis on the calibrations involves parsing the calibration file any equations in the file, and any pure data files referenced by the calibration file. The input and output names are then recorded along with their types. This syntactic analysis of the models and calibrations is quite involved, but it is necessary for Autonomie to deliver its search, compatibility, and dependency analysis features. The speed and accuracy of the model and calibration parsing was improved in this version. All users of Autonomie, from those who run only the default Autonomie library to users with their own vast internal libraries, derive benefit from Autonomie's improved import functionality.

Implemented a More User-Friendly Vehicle Selection Control

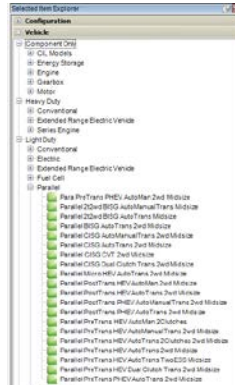


Figure IV-2: Vehicle Tree View—Browsing the New Vehicle Tree View

Apparently, simple changes to the user interface can result in significant productivity gains for users. For each individual the time saved may be small, but when repeated over and over again throughout the day, across all users, the time saved can be considerable. One example of such a productivity-boosting gain is the new design for the Vehicle Selection Control. This control started as a flattened list of vehicles, which was fine when the list of vehicles was small. However, as the number of vehicles in Autonomie grew, so too did the cognitive load on the engineers using this control. A redesign was in order. After careful consideration of several replacement options, a tree was chosen as the best replacement for the Vehicle Selection Control to yield productivity gains. This action of choosing a vehicle is so fundamental to the current version of Autonomie that the change from flattened list to tree benefits all users. On the surface this change appears to be simple, but changes needed to be made throughout the software in numerous controls and metadata files to support the new system classification tree.

Designed a Process to Define and Run Combinations of Vehicle Parameters, Files, and Systems in Parallel

The Autonomie backend and application programming interface is used to run large studies. These studies involve hundreds of thousands of vehicles, each vehicle represented by a forward, fully transient, fully controllable model running at 100 hertz. Setting up the assumptions for each vehicle can take a considerable amount of time. Assumptions are not defined for each vehicle, but for each class and type of vehicle. Being able to run such large-scale studies directly from the Autonomie graphical user interface is the ultimate goal. However, to manage these large scale studies, the needs of small- to medium-scale studies need to be addressed first. These large-scale studies have been the domain of various government departments and agencies; the small- to medium-scale studies, which have hundreds of vehicles, are of great interest to OEMs and suppliers. Several OEMs and suppliers have requested that this ability to set up small- to medium-scale studies be added to Autonomie. The new process addresses these requests. A root vehicle is chosen as the starting point. Systems can then be applied to the root vehicle to yield different types of vehicles. Both architectural modifications and model fidelity changes to the vehicle can be made by changing systems. For example, a system change can take a conventional vehicle and transform it into a hybrid vehicle or take a map-based engine and transform it into a physical engine. Next, calibrations can be selected on for each system. These calibrations represent different technologies, such as engine fuel types or battery chemistries. Finally,

such parameters as engine power, frontal area, and coefficient of drag, among hundreds of others, can be changed through the interface. These modifications can be layered onto one another, allowing for studies that run the gamut of advanced vehicle technologies.

The user interface that was developed flows naturally, allowing the user to specify vehicle definitions in columns with modifications to the vehicle in rows. This tabular form can be exported to Microsoft Excel, then modified in Excel and imported back into the user interface. This enables the study definition to be scripted outside of the user interface for medium-scale studies, but still allows the user to bring the study back into Autonomie for modification. Besides providing a tabular view up front for defining vehicles, behind the scenes compatibility checking is constantly running to ensure that the user can only choose compatible systems and calibrations. As a user makes selections in any given column, the set of compatible systems and calibrations changes; it is different for each column. There is substantial behind-the-scenes work involved in giving the user an accurate, current list of compatible systems and calibrations for each column in the table. All of this is feels fast, fluid, and seamless for the user, ultimately magnifying the user’s productivity.

If the interface makes setting up a vehicle study fast, running the simulations then becomes the bottleneck. Unless using Autonomie, a user has no choice but to either run simulations in sequence or spend hundreds of hours developing their own multithreaded solution. However, this process executes simulations in parallel for the user, eliminating the hundreds of hours an OEM would spend developing and maintaining their own solution. The user only needs to specify the number of current sessions to run, and Autonomie manages the rest. Scheduling and synchronizing the child processes is handled for the user with no additional effort on their part.

The great power of Autonomie is realized when one realizes that this is a modifier that can be applied to any cycle or procedure in Autonomie, or even to other modifiers, such as optimization or design of experiment routines. Modifiers can be stacked on top of each other like Legos, allowing the user to create their own vehicle simulation workflows.

System Path	Change	Unit	Run 1	Run 2	Run 3	Run 4	Run 5
	Output Folder Name		Folder_0	Folder_1	Folder_2	Folder_3	Folder_4
	Run Description		Diesel	Gasoline	Run Description 2	Run Description 3	Run Description 4
vehlvpa	veh.plant.init.mass.total	kg	1550	1550	1550	1550	1600
vehlvpa/chas/plant	chas.plant.init.coeff_drag		0.27	0.27	0.29	0.30	0.30
vehlvpa/chas/plant	chas.plant.init.frontal_area	m^2	2.0	2.0	2.0	2.0	2.0
vehlvpa/whl/plant	whl.plant.init.coeff_roll1		0.0075	0.0075	0.0075	0.0075	0.0075
vehlvpa/fd/plant	Initialization		fd_plant_274.a_init	fd_plant_274.a_ini	fd_plant_274.a_ini	fd_plant_274.a_ini	fd_plant_274.a_ini
vehlvpa/eng	System		eng_ci.a_system				
vehlvpa/eng/plant	Scaling		eng_plant_s_pwr_lin.a	eng_plant_s_pwr_	eng_plant_s_pwr_	eng_plant_s_pwr_	eng_plant_s_pwr_

Figure IV-3: Multi-Option Vehicle Study—Embarking on a New Way to Define and Launch Large-Scale Studies

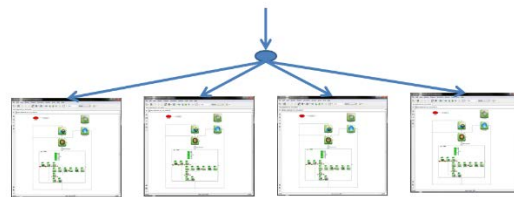


Figure IV-4: Multiple Instances of Simulink—Benefiting from Running Simulations in Parallel

Model Based System Engineering (MBSE) Enhancements

Invented a Way to Select Different Workflows in Autonomie

The concept of workflows is part of the design philosophy of Autonomie, and Autonomie has had great success in supporting user-defined workflows for vehicle simulation because of modifier and process composition. However, under MBSE, many other workflows exist, such as model verification and validation, Design of Failure Modes Analysis (DFMEA), vehicle validation and correlation, test data quality assurance,

system based hardware-in-the-loop, system based software-in-the-loop, system based model-in-the-loop, large-scale study, and large-scale data analysis. Numerous OEMs and even other government entities have used these workflows and would benefit if they were supported in Autonomie. This project addresses these additional workflows by modifying the framework of Autonomie to support customized workflows that do not directly involve loading a single vehicle and running a simulation. Before addressing these other workflows, compatibility with the current workflow must be maintained and demonstrated

The user begins by choosing the MBSE workflow that matches their requirements. For this example, a vehicle simulation on a cycle may be chosen. The workflow is loaded and Autonomie presents to the user a flow chart showing the steps in the current workflow. The workflow starts with Setup Matlab and then progresses to Select a Vehicle, then Initialize the Cycle, Run the Simulation, and finally Data Analysis. The workflow is clear, easy to grasp, and informs the user on what steps are involved to accomplish the work. Much of the visual noise has been removed while the core functionality of the tool has been retained. This is still just a basic example to demonstrate the ability of the Autonomie to handle different workflows, starting with its own current workflow. Notice that the last control is the Data Analysis control, which is the same one that appears in Autonomie now. This shows significant flexibility in that the workflow reuses the data analysis control. The control is now pluggable into any workflow, not just the default Autonomie workflow. The idea is to extend the plug-and-play philosophy of Autonomie beyond the models it simulates to the tool itself, thereby broadening the scope of Autonomie as an MBSE framework.

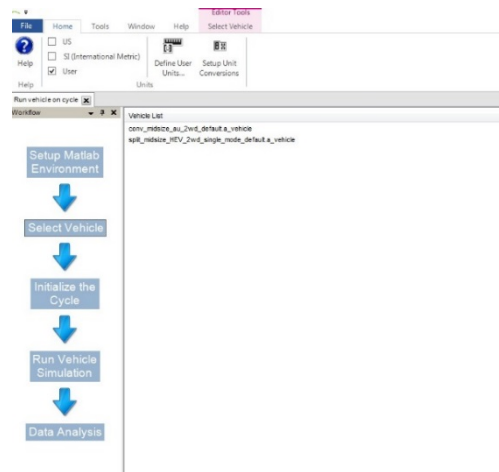


Figure IV-5: A Vehicle Simulation Workflow—Getting to the Point, Increasing a User's Productivity

Project for Developing Autonomie Plug-and-Play Steps

Continuing with the theme of supporting user workflows, a method to allow users to define their own process steps was developed and documented. Users can now implement an interface and have their own personalized control appear in the user interface of Autonomie. In future work, these steps can be migrated to the new Autonomie workflow framework.

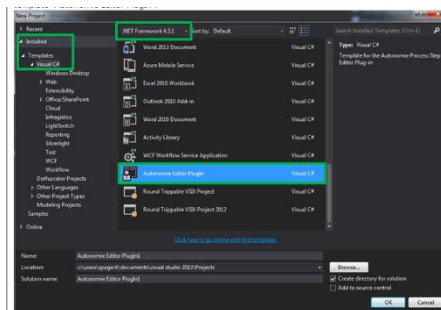


Figure IV-6: A Visual Studio Project is Provided—Simplifying the Integration

Enhanced Tool that Manages Large-Scale Datasets Produced for BaSce

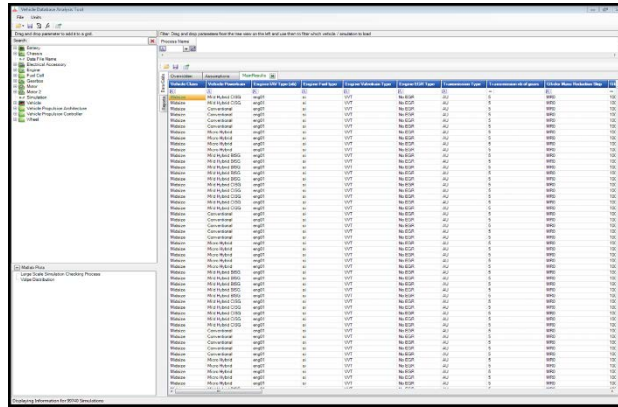


Figure IV-7: Database Tool—Managing Datasets Produced by Large-Scale Simulations

The workflow of analyzing large datasets is provided by the large-scale data analysis tool; this tool had numerous improvements to support DOE studies, such as BaSce. These improvements include adding additional named tabs that allow results to be grouped and filtered as the user desires. For example, a separate tab can be created for each powertrain component: engine, battery, motor, and others. These tabs can be exported as spreadsheets that can then be delivered to DOE. In addition to Excel files, the tool can now generate HTML reports.

This HTML reporting feature is integrated in the tool’s scripting interface, allowing a user to load data from various datasets, filter the results, and then plot them. The HTML report is generated from a standard template report generated by Autonomie.

Besides having a general HTML reporting feature that the user can customize, specialized HTML reports have also been developed for specific studies. They can either be called from the scripting interface or stand alone as analysis files. The reports have some sophisticated features, such as calling predefined distribution plots that would be of interest to a user.

This tool operates as a standalone now, but it will be integrated into Autonomie once the MBSE workflow framework has been completed.

Vehicle Class	Technology Tree	Technology	Absolute / Incremental	Average value (%)	Minimum value (%)	Maximum Value (%)	Baseline vehicle (ANL) (%)	VOLPE result (%)	Distribution plots
Midsize	Engine	02-Discrete VVL (DVLD)	Absolute	4.0	2.3	5.2	4.2	3.6	Click for distribution
Midsize	Engine	03-Direct Injection (GDI)	Absolute	6.1	4.2	7.4	6.3	5.2	Click for distribution
Midsize	Engine	04-Cylinder Deactivation (DEACD)	Absolute	12.4	7.2	17.1	13.8		Click for distribution
Midsize	Engine	05b-Reduced Friction VVT	Absolute	0.8	-1.1	2.6	1.0		Click for distribution
Midsize	Engine	05a-Discrete VVL (DVLS)	Absolute	6.6	4.1	8.1	7.1		Click for distribution
Midsize	Engine	07a-Direct Injection (GDIS)	Absolute	8.8	0.5	10.2	9.2		Click for distribution
Midsize	Engine	08a-Cylinder Deactivation/DEACS	Absolute	15.4	9.9	20.4	16.5		Click for distribution
Midsize	Engine	12-Turbocharging and Downsizing-1 (TRBD1)	Absolute	16.7	13.0	20.3	16.5		Click for distribution
Midsize	Engine	13-Turbocharging and Downsizing-2 (TRBD2)	Absolute	19.6	13.7	24.5	20.3	5.2	Click for distribution
Midsize	Engine	14-Cooled EGR-1 (CEGR1)	Absolute	19.8	14.3	24.3	20.1	5.2	Click for distribution
Midsize	Engine	15-Cooled EGR-2 (CEGR2)	Absolute	19.9	15.1	25.2	19.7		Click for distribution
Midsize	Engine	17-Advanced Diesel(ADLS)	Absolute	22.9	18.5	26.5	22.1		Click for distribution
Midsize	Engine	02-Discrete VVL (DVLD)-DOHC	Incremental	4.0	2.3	5.2	4.2	3.6	Click for distribution
Midsize	Engine	03-Direct Injection (GDI)-DOHC	Incremental	2.1	0.6	3.2	2.2	2.2	Click for distribution
Midsize	Engine	04-Cylinder Deactivation (DEACD)-DOHC	Incremental	6.8	2.4	11.0	8.0		Click for distribution
Midsize	Engine	12-Turbocharging and Downsizing-1 (TRBD1)-DOHC	Incremental	4.8	2.2	10.2	3.2	7.5	Click for distribution
Midsize	Engine	13-Turbocharging and Downsizing-2 (TRBD2)-DOHC	Incremental	3.6	-0.5	5.9	4.5	3.5	Click for distribution
Midsize	Engine	14-Cooled EGR-1 (CEGR1)-DOHC	Incremental	0.1	-1.0	2.4	-0.2	3.5	Click for distribution
Midsize	Engine	15-Cooled EGR-2 (CEGR2)-DOHC	Incremental	0.1	-2.2	2.1	-0.5	1.4	Click for distribution
Midsize	Engine	17-Advanced Diesel(ADLS) DOHC	Incremental	3.8	-5.8	9.1	3.0		Click for distribution
Midsize	Engine	05b-Reduced Friction VVT-SOHC-RedFrict1	Incremental	0.8	-1.1	2.6	1.0		Click for distribution

Figure IV-8: New Dataset Report—Reviewing and Understanding the Results from a Large-Scale Simulation

Adopted the SAE J3049 Standard for Model Architecture

Increasingly, global vehicle engineering teams span domains of engineering and physics within organizations and include external collaborations among commercial businesses (OEMs and suppliers), government agencies, and research institutions. For increased efficiency, reduced costs, faster design iterations, and fewer hardware prototypes, these teams use math-based engineering methods to build and test virtual ground vehicles in simulation environments. These types of inter-organizational engineering collaborations require a common shared simulation model for an entire ground vehicle system and/or the related subsystems of which it is composed. Use of dynamical modeling and simulation for virtual engineering development and testing of the functional performance of ground vehicles by inter-organizational teams have increased; this has resulted in a need for standardizing the architecture and interfaces of a ground vehicle system model by partitioning it into subsystem models to enable plug-and-play of subsystem simulation models. A standardized ground vehicle system model with an architectural structure partitioned into subsystem models, and with defined subsystem model interfaces, enables (1) model reuse; (2) division of modeling tasks across multifunctional teams; (3) parallel model development, verification and validation; and (4) rapid and efficient integration of subsystem models for reduced development time and costs.

The configuration based on this standard was implemented in Autonomie. A new configuration had to be created, along with models that matched the new interface defined by this standard.

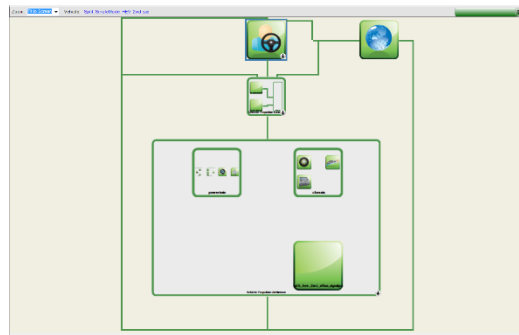


Figure IV-9: SAE Configuration—Applying the SAE J3049 Standard

Added Support for Functional Mockup Interface FMI 2.0

Autonomie support was added for FMI 2.0, which is an important enhancement in support of MBSE. Support was added for FMI 1.0 last fiscal year, but because FMI is an evolving standard, new options related to FMI 2.0 had to be added to the user interface to allow Autonomie to leverage the new features in FMI 2.0. Autonomie interfaces with Modelon toolbox, which generates an s-function from an FMU that can be used in Matlab.

Migrated the Automated Testing Used as Part of the Internal MBSE Process to the Jenkins Framework

Testing is an integral part of MBSE to verify that a model met the requirements. The same is true for software. Not only do the models of Autonomie need to be tested, but the entire Autonomie code base requires testing to satisfy Software Quality Assurance requirements. A Jenkins server was set up to manage and launch both Autonomie unit tests and integration tests. After each check in of source code to Team Foundation Server (TFS), a quick set of unit tests are run to verify the code. At the end of each day, a set of integration tests is run to verify the basic functionality of Autonomie. At the end of the week, a full set of tests is run to exercise all of Autonomie's features. The tests produce two types of reports: an HTML report for a quick high-level overview of each test with indicators of a pass or fail, and an Excel report with detailed results from each simulation run, which can help diagnosis the cause of the failure.

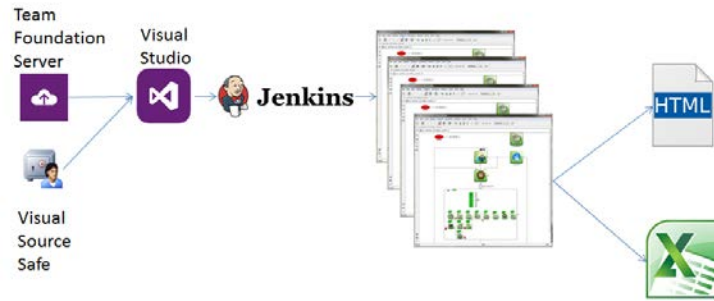


Figure IV-10: Automated Testing Setup—Illustrating the Testing Workflow and Manage Unit and Integration Tests

Jenkins has its own web interface, shown in Figure IV-10. From this interface, any Autonomie developer can launch tests on demand. It also allows the developer to customize their tests. For instance, they can pull either the latest source code or use the latest release to run their tests.

Incorporating Industry Feedback

Since Autonomie's inception, industry feedback has been a driving force behind its design. The REV14SP1 release is no different. On the basis of feedback from several OEMs, improvements to Autonomie were made.

Improved Building Speed and Model Simulation Speed

The first improvement involves speeding up one of the premier features of Autonomie, the automated building of vehicle models. Several options were added to the user interface to balance the speed of the build with the aesthetics of the build. Capturing system pictures, adding terminators, and propagating port names can now all be turned off; this leads to a less-attractive diagram, but the build can be up to 10% faster. In addition to these aesthetics changes, there is also an option to prune unused signals from the buses. Many signals are sent out as diagnostic information from models that are not used by any other models. These diagnostic-only signals can now be removed from the bus. This option does not yield a faster build, but it does produce a faster running model. Especially for some OEMs that have diagnostic signals as a significant portion of their model's output signals, the improvement in speed was significant. This feature required a great deal of backend work to properly trace the path of signals through a vehicle, find all systems where a signal is used, discover if no signals are used, and remove them from the bus. This feature also needed to look for signal collisions where the same signal was received at one input from two different locations; changes were made to allow the user to select the appropriate source for their signal.



Figure IV-11: Building Options Control—Reducing the Simulation Time

Support Lightweight Projects

Another OEM needed to combine several variations of a vehicle in the same project. Although a more formal implementation of projects is coming in the next version of Autonomie, some of the OEM's requirements could be satisfied now by using a lighter weight version of projects. The implementation is shown below. With some modifications to the Multi-Option Vehicle Study, multiple instances of the same vehicle each with different processes, could be stored, within one run file. Even though this is a variation on the Multi-Option Vehicle Study, several changes had to be made to support the nesting of the modifier, which was necessary to

deliver this feature. The overall modifier was more stable, and because of the nesting feature it allows users more flexibility in defining vehicles in their run files.

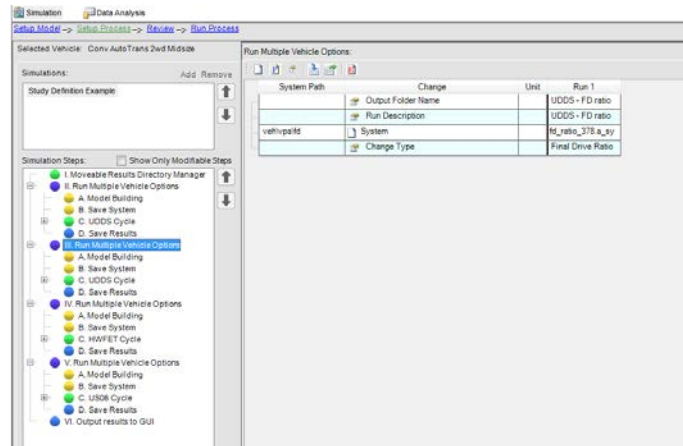


Figure IV-12: Simple Projects—Reusing Features to Provide a Rudimentary Notion of Projects

Document Application Programming Interface

Autonomie has an Application Programming Interface (API), which is used extensively internally to run studies; OEMs have expressed interest in using this API to run their own large-scale studies. Although each file is thoroughly commented, the documentation for the API cannot be found in a single location. In addition, the API is constantly being extended, so a tool had to be developed that dynamically builds the API documentation from the current API comments. The results of this API document generator are shown below.

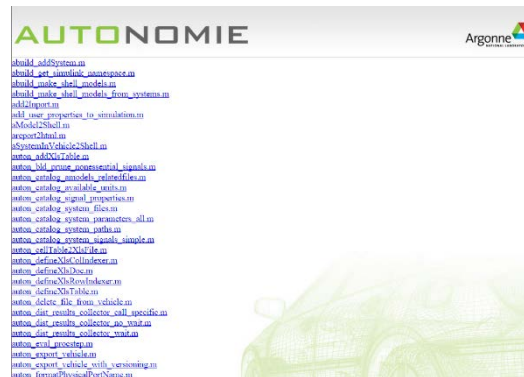


Figure IV-13: Documentation Index—Finding Help on Functions in the Auto-Generated API Documentation

Run Autonomie Backend on Large Linux Clusters

Many high-performance clusters are running some version of Linux, and some OEMs have their own high-performance cluster on which they wanted to run Autonomie simulations. To support these OEMs and a broad range of high-performance computing hardware, Autonomie's backend was ported to run on a Linux cluster. In addition, Autonomie's distributed computing API was updated so that a user could easily launch vehicles on a cluster, even when using a non Mathworks job scheduler. These improvements will benefit studies, such as BaSce, that, as time progresses, increasingly require more computing resources.

Looking toward the Future

Finally, as further evidence of the desire to respond to industry needs, a tech-to-market survey was performed that gathers feedback from across the industry. The results of this survey will help guide the Autonomie development roadmap. The tech-to-market survey's goals include assessing the state of ground vehicle system and subsystem modeling and simulation, identifying the current and desired primary applications and uses for

virtual engineering of ground vehicle systems and subsystems, identifying the deficiencies in the roadmap and processes, and proposing projects to address deficiencies and prioritize projects. Understanding where the industry is going is paramount in tailoring Autonomie to meet the changing and emerging needs of industry.

Supporting Government Activities

DOE develops a platform that many other governments departments and agencies derive benefit from by having a strong foundation off of which they can build their own capabilities.

DOE—BaSce

The Autonomie framework and models are leveraged by DOE to assist them in evaluating their research portfolio, by predicting the effect advanced technologies have on fuel economy and cost. Improvements in the large scale database tool have improved this process and reduced the cost of providing results.

Volpe

Autonomie is used by the U.S. Department of Transportation (DOT) to run an immense number of vehicle simulations, which include millions of simulations with hundreds of thousands of vehicle combinations. Improvements in the distributed computing interface and the large-scale database tool have benefited Volpe. The amount of data generated for this study is so large that Volpe was provided with only a tiny fraction of the data from the Autonomie simulation runs, and even that fraction was a database several gigabytes in size.

DOT NATC

Because of the prior development of a link with CarSim, Autonomie has the capability to run vehicles with CarSim to which new vehicle architectures can be integrated. A hybrid vehicle was developed and added to Autonomie, which leverages this link with CarSim to support NATC's work on a DOT Funding Opportunity Announcement. This new feature enhances the overall value of Autonomie for all current and future users. This new hybrid electric vehicle link to CarSim was released this year.

TARDEC OneSAF Integration

Because Autonomie is trusted by several government agencies and OEMs, the Tank Automotive Research Development and Engineering Center (TARDEC) supported development to link their tool the One Semi-Automated Forces (OneSAF) to Autonomie.

Conclusions

Several versions of Autonomie were released this year; these include numerous new features developed on the basis of the feedback from DOE and the user community.

IV.1.C. Products

Presentations/Publications/Patents

1. L. Michaels, "Increasing the Robustness of Hybrid Electric Vehicle Controls via System Simulation," presented at the SAE 2013 Hybrid Powertrain Complexity and Maintainability Symposium, Dearborn, MI, Oct. 22, 2013.
2. A. Rousseau, Y. Ding, "Impact of Worldwide Test Procedures on Advanced Technology Fuel Efficiency Benefits," presented at EVS27, Barcelona, Spain, Nov. 17–20, 2013.
3. A. Rousseau, "Fuel Efficiency Benefits of Electrified CNG Vehicles," presented at EVS27, Barcelona, Spain, Nov. 17–20, 2013.
1. N. Kim, E. Rask, A. Rousseau, "Control Analysis under Different Driving Conditions for Peugeot 3008 Hybrid 4," 2014-01-1818, SAE World Congress, Detroit, Apr. 8–10, 2014.
2. D. Lee, A. Rousseau, E. Rask, "Development and Validation of the Ford Focus Battery Electric Vehicle Model," 2014-01-1809, SAE World Congress, Detroit, Apr. 8–10, 2014.

3. N. Kim, A. Rousseau, H. Lohse–Busch, “Advanced Automatic Transmission Model Validation Using Dynamometer Test Data,” 2014–01–1778, SAE World Congress, Detroit, Apr. 8–10, 2014.
4. S. Pagerit, P. Sharer, A. Rousseau, “Complex System Engineering Simulation through Co-Simulation,” 2014–01–1106, SAE World Congress, Detroit, Apr. 8–10, 2014.
5. L. Michaels, “Model–Based Systems Engineering at Argonne National Laboratory,” presented at the 2014 NAFEMS Americas Conference, Colorado Springs, CO, May 28–30, 2014.
6. L. Michaels, “Future of Automotive Simulation Software: What Capabilities Should One Expect?” Panel Discussion, IEEE Transportation Electrification Conference, Dearborn, MI, June 16–18, 2014.
7. A. Rousseau, S. Halbach, L. Michaels, N. Shidore, Na. Kim, N. Kim, D. Karbowski, M. Kropinski, “Electric Drive Vehicle Development and Evaluation using System Simulation,” Journal of the Society of Instrument and Control Engineers, Vol. 53, 2014 (sice.jp).
8. N. Shidore, N. Kim, R. Vijayagopal, D. Lee, A. Rousseau, J. Kwon, B. Honel, E. Haggard, “Battery in the Loop: Battery Evaluation in a Systems Context,” presented at the IEEE Transportation Electrification Conference (ITEC), Beijing, China, Aug. 31–Sept. 3, 2014.
9. A. Rousseau, P.B. Sharer, S. Pagerit, "Flexible Evaluator for Vehicle Propulsion Systems." UChicago Argonne LLC, assignee. Patent 8510088B2. Aug. 13, 2013.

IV.2. VTO Baseline and Scenario (BaSce)

Neeraj Shidore, Principal Investigator

Argonne National Laboratory
9700 South Cass Avenue, Building 362
Argonne, IL 60439
Phone: (630) 252-7416; Fax: (630) 252-3443
E-mail: nshidore@anl.gov

David Anderson, Jacob Ward, DOE Program Manager

Office of Vehicle Technologies, Department of Energy
Phone: (202) 287-5688, (202) 586-7606
E-mail: David.Anderson@ee.doe.gov, Jacob.Ward@ee.doe.gov

Start Date: 10/1/2014

End Date: 9/31/2015

IV.2.A. Abstract

Objectives

- Simulate multiple vehicle platforms, configurations, and timeframes to analyze the impact of U.S. Department of Energy (DOE) Vehicle Technologies Office (VTO) technologies on component operating conditions, component size, vehicle energy consumption, and cost.
- Evaluate the fuel consumption displacement and cost of fuel cell vehicles based on an updated set of assumptions. The results will be used to update the levelized cost of driving results and provide inputs to multiple market penetration models.

Accomplishments

- Simulated and sized more than 4,000 vehicles for light duty applications.
- Simulated new vehicles when assumptions or platforms were revised or when additional configurations or timeframes were requested.
- Updated deliverables to DOE – results spread sheet, spread sheet with market penetration results, and presentation with main assumptions on technology, cost and main results, based on fuel cell reruns and bug fixes
- Generated spread sheet with additional information (component cost, size) needed for life cycle analysis (GREET) inputs.

Future Achievements

- Further enhance the large-scale simulation process to improve post processing on sets of simulations and conduct additional quality assurance.
- Continue to provide analytical data to support BaSce in 2016.



IV.2.B. Technical Discussion

Background

Through the Office of Planning, Budget, and Analysis, the DOE Office of Energy Efficiency and Renewable Energy (EERE) provides estimates of program benefits in its annual Congressional Budget Request. The Government Performance and Results Act (GPRA) of 1993 provided the basis for assessing the performance of federally funded programs. Often referred to as “GPRA Benefits Estimates,” these estimates represent one piece of EERE’s GPRA implementation efforts — documenting some of the economic, environmental, and security benefits (or outcomes) that result from achieving program goals.

Introduction

The simulation tool Autonomie was used to evaluate the fuel economy of numerous vehicle configurations (including conventional, hybrid electric vehicles [HEVs], plug-in HEVs [PHEVs], and all-electric vehicles), component technologies (gasoline, diesel, and compressed natural gas [CNG], as well as fuel cells), and timeframes (2015, 2020, 2025, 2030, and 2045). The uncertainty of each technology is taken into account by assigning probability values for each assumption. Argonne’s database tool also allows the detailed simulation results provided by Autonomie to either be distilled into a format that can be easily distributed and analyzed horizontally across many simulations, or examined via a deep, vertical dive into one simulation. Both aspects are critical for the full-scale vehicle analysis that VTO benefit analysis requires.

The process is composed of two distinct phases. The objective of the first phase is to set up the simulations to be performed, and launch all the runs through a distributed computing toolbox and be able to perform analysis of individual results to ensure the simulations are performed properly as shown in Figure IV-14.

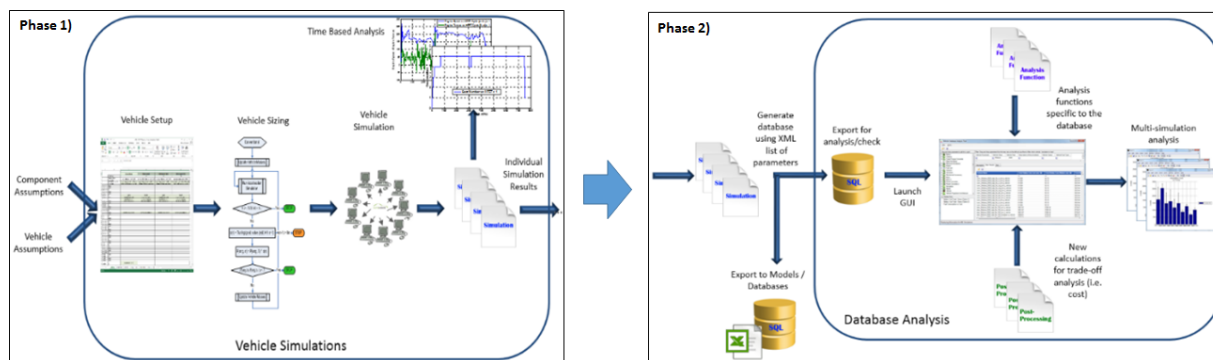


Figure IV-14: Study process for running and analyzing large-scale simulation

The second phase of the process allows users to analyze a limited number of parameters from the individual simulations to perform large-scale analysis. As shown in Figure IV-14, this process starts with the development of a standardized query language (SQL) database based on a list of parameters defined by the users. The objective of the database analysis tool is then to, for example, select the most cost-beneficial technologies and understand uncertainties.

Approach

To evaluate the fuel efficiency benefits of advanced vehicles, the vehicles are designed on the basis of component assumptions. The fuel efficiency is then simulated on the Urban Dynamometer Driving Schedule (UDDS) and Highway Fuel Economy Test (HWFET). The vehicle costs are calculated from the component sizing. Both cost and fuel efficiency are then used to define the market penetration of each technology to finally estimate the amount of fuel saved. This report focuses on the first phase of the project: fuel efficiency and cost.

To properly assess the benefits of future technologies, the following options were considered:

- Different vehicle classes: compact car, midsize car, small sport utility vehicle (SUV), medium SUV, and pickup truck.
- Five timeframes: 2015, 2020, 2025, 2030, and 2045.
- Five powertrain configurations: conventional, HEV, PHEV, fuel cell HEV, and electric vehicle.

Also, to address uncertainties, a triangular distribution approach (low, medium, and high) was employed. For each component, assumptions regarding efficiency, power density, and so forth were made, and three separate values were defined to represent the (1) 90th percentile, (2) 50th percentile, and (3) 10th percentile. A 90% probability means that the technology has a 90% chance of being available at the time considered. For each vehicle considered, the cost assumptions also follow the triangular uncertainty. Each set of assumptions is, however, used for each vehicle, and the most efficient components are not automatically the least expensive ones. As a result, for each vehicle considered, we simulated three options for fuel efficiency. Each of these three options also has three values representing the cost uncertainties.

In order to address all of these combinations, the VTO benefit analysis requires the definition and simulation of more than 4,000 vehicles (Figure IV-15).

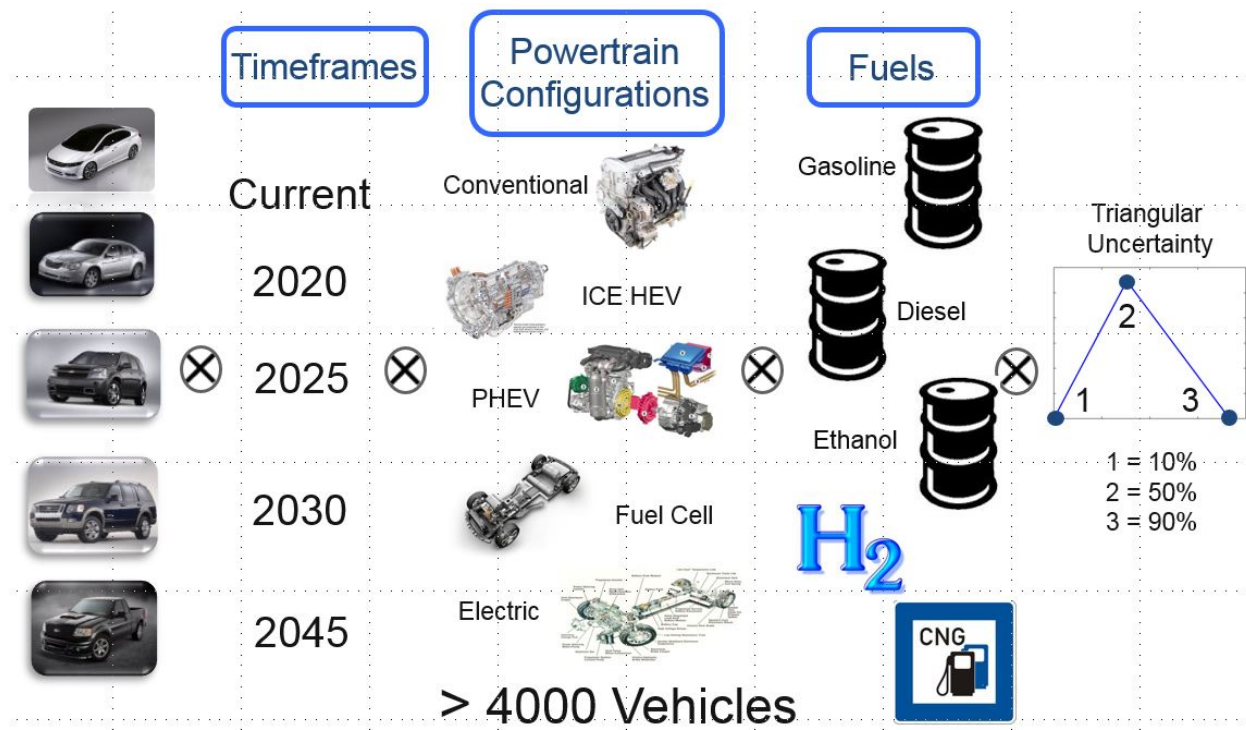


Figure IV-15: Vehicle classes, timeframes, configurations, and fuels considered

The assumptions described below have been defined on the basis of inputs from experts and the U.S. Drive Team targets (when available).

Engine

Several state-of-the-art internal combustion engines (ICEs) were selected as the baseline for the fuels considered: gasoline (spark ignition or SI), diesel (compression ignition or CI), ethanol (E85), and compressed natural gas (CNG). The engines used for reference conventional vehicles were provided by automotive car manufacturers. The proprietary engine data used for HEVs and PHEVs are based on Atkinson cycles. Figure IV-16 shows the engines peak efficiency for conventional vehicle in the study.

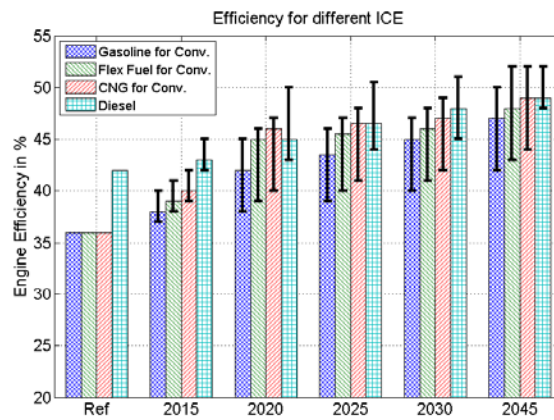


Figure IV-16: Engine peak efficiency for conventional vehicle

Fuel Cell Systems

Figure IV-17 shows the evolution of the fuel-cell system peak efficiencies. The peak fuel-cell efficiency is assumed to be at 59% currently, and will increase to 69% by 2045.

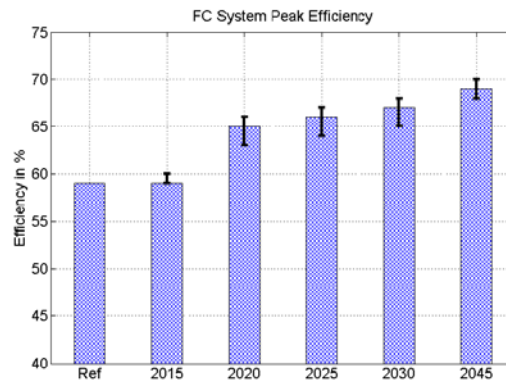


Figure IV-17: Fuel-cell system efficiency

Integrated Traction Drive System

Two types of electric machine will be used as references in the study:

- The power-split vehicles are powered by a permanent magnet electric machine (similar to Toyota Camry), which has a peak power of 105 kW and a peak efficiency of 95%.
- The series configuration (fuel cell) and electric vehicles use an induction electric machine with a peak power of 72 kW and a peak efficiency of 95%.

Energy Storage System

The HEV reference case includes a Ni/metal hydride battery. It is assumed that this technology is the most likely to be used until 2015 for the low uncertainty case. This technology is similar to that found in the Toyota Prius. Both the medium and high uncertainty cases use a lithium-ion battery. For PHEV applications, all the vehicles are run with a Li-ion battery from Argonne.

After a long period of operation, batteries lose some of their power and energy capacity. To be able to maintain the same performance at the end of life (EOL) compared to the beginning of life (BOL), an oversize factor is applied while sizing the batteries for both power and energy. These factors are supposed to represent the percentage of power and energy that will not be provided by the battery at the EOL compared to the initial power and energy given by the manufacturer. The oversize factor decreases over time to reflect an

improvement in the ability of batteries to uniformly deliver the same performance throughout their life cycles. Figure IV-18 shows the battery energy density for high energy application in the study.

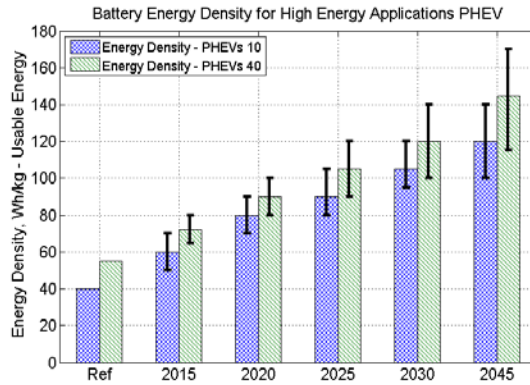


Figure IV-18: Battery energy density for high energy application PHEV

Vehicle

One of the main factors affecting fuel consumption is vehicle weight. Lowering the weight (light-weighting) reduces the forces required to follow the vehicle speed trace. As a result, the components can be downsized, resulting in smaller components and decreased fuel consumption. However, the impact of light-weighting is not the same for all the powertrain configurations. Figure IV-19 shows the glider mass reduction factor applied to each vehicle classes.

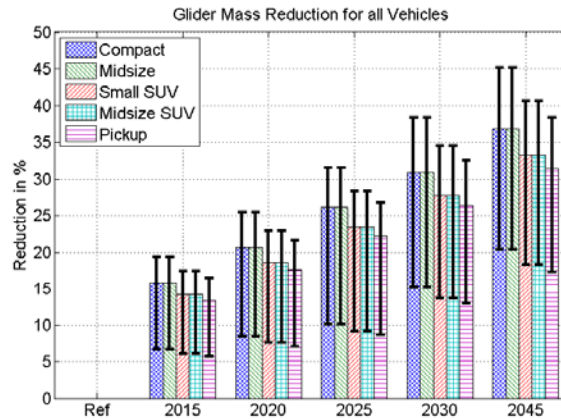


Figure IV-19: Glider mass reduction for all vehicle classes

Vehicle Powertrain Assumptions

All the vehicles have been sized to meet the same requirements:

- 0–60 mph in 9 s ± 0.1 seconds
- Maximum grade of 6% at 65 mph at gross vehicle weight
- Maximum vehicle speed of >160 km/h

For all cases, the engine or fuel cell powers are sized to complete the grade requirement without any assistance from the battery. For HEVs, the battery was sized to recuperate the entire braking energy during the UDSS. For the PHEV case, the battery power is defined as its ability to follow the UDSS in the electric mode for the 10- and 20-mile cases and the US06 drive cycle for the 30- and 40-mile cases, while its energy is calculated to follow the UDSS for a specific distance regardless of distance.

Input modes for the power-split configurations, similar to those used in the Toyota Camry, were selected for all HEV applications and PHEVs with low battery energies. Extended Range Electric Vehicle (EREV) configurations were used for PHEVs with high battery energies (e.g., range of 30 miles and up in EVs on the UDDS). The series fuel cell configurations use a two-gear transmission to allow them to achieve the maximum vehicle speed requirement.

Results

The vehicles were simulated on both the UDDS and HWFET drive cycles. The fuel consumption values and ratios presented below are based on unadjusted values.

Evolution of HEV vs. Conventional

The comparisons between power-split HEVs and midsize conventional gasoline vehicles (same year) in Figure IV-20 show that the fuel consumption ratios decrease slightly for all fuel cases with time. The advances in component technology will significantly benefit HEVs.

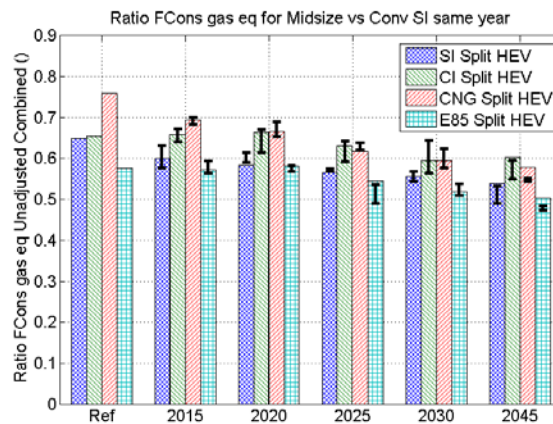


Figure IV-20: Ratio of fuel consumption gasoline equivalent (unadjusted) for HEV to that of conventional Gasoline vehicle of same year and case

Figure IV-21 shows the vehicle cost ratio between HEV and conventional vehicles. As expected, HEVs remain more expensive than conventional vehicles, but the difference significantly decreases because costs associated with the battery and electric machine fall faster than those for conventional engines.

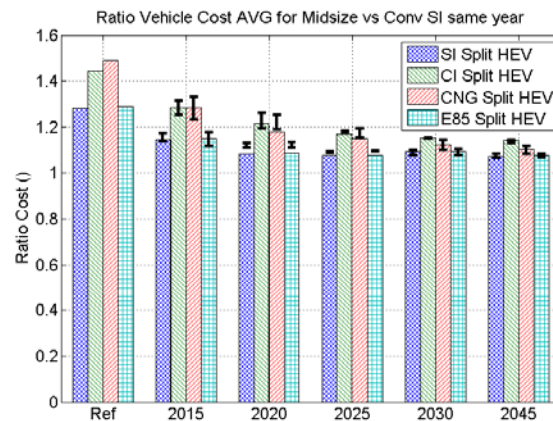


Figure IV-21: Vehicle cost ratio for HEVs compared to gasoline conventional vehicle of the same year and case

Evolution of HEV vs. Fuel Cell

The fuel-consumption ratios for all types of power-split HEVs versus fuel-cell HEVs (Figure IV-22) are higher than 1, showing that fuel-cell technology offers consistently lower fuel consumption than power-split HEV technology. However, the ratios vary over time, and it is pertinent to study the evolution for each fuel. In the reference case, the gasoline engine vehicle consumes nearly 50% more fuel than a fuel-cell HEV; in 2045, however, this difference is reduced to the 25% to 30% range.

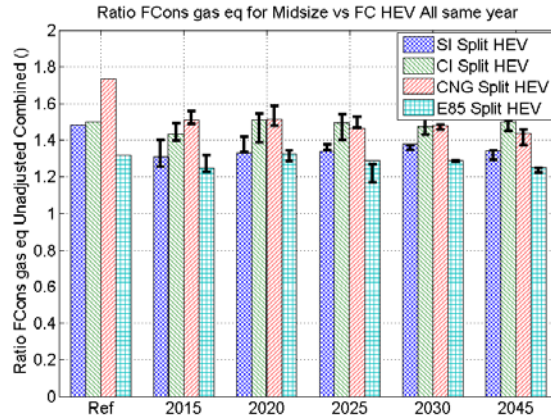


Figure IV-22: Ratio of fuel consumption gasoline equivalent (unadjusted) for HEV to that of fuel cell HEV of same year and case

Evolution of PHEVs

Figure IV-23 indicates that the fuel-consumption evolution for power-split PHEVs is similar to that for power-split HEVs with a gasoline engine.

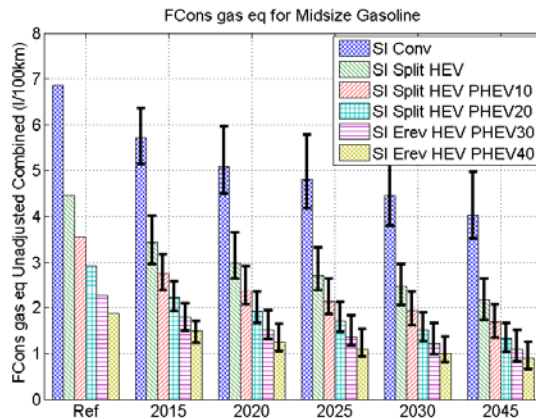


Figure IV-23: Fuel consumption evolution for HEV, PHEVs, gasoline engine vehicle for midsize class

Figure IV-24 shows the manufacturing cost evolution of PHEVs for gasoline engine. The overall trend is the same for all electric ranges; only the actual costs vary. PHEV40 costs show a sharp decrease over time, whereas PHEV10s show a very slight decrease over time. This observation can be explained by improvements in batteries over time.

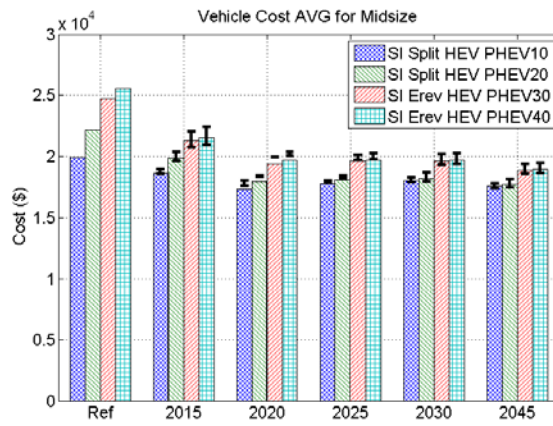


Figure IV-24: Manufacturing cost of PHEVs for gasoline engine

Trade-off between Fuel Efficiency and Cost

Figure IV-25 shows similar trends for HEVs, independently of ICE technology. The overall trend is decreasing, which means lower fuel consumption and lower cost. Gasoline and ethanol HEVs offer the best trade-offs over time, with the diesel HEV becoming competitive in the 2045 timeframe.

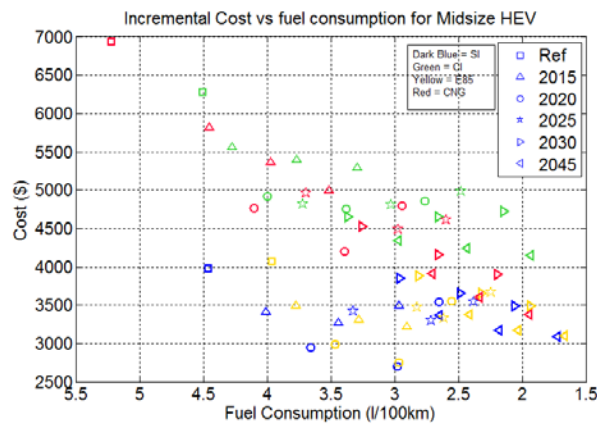


Figure IV-25: Incremental manufacturing cost (in comparison with the reference conventional gasoline vehicle manufacturing cost) as a function of fuel consumption for midsize HEVs

Figure IV-26 shows the trade-offs of incremental manufacturing cost versus fuel consumption for fuel-cell HEVs and PHEVs compared with the reference conventional gasoline vehicles. For the PHEVs, we found a diminishing return on investment, since little fuel-efficiency gain is achieved for the higher AER despite a higher manufacturing cost. Overall, all configurations trend toward good fuel efficiency at a low manufacturing cost.

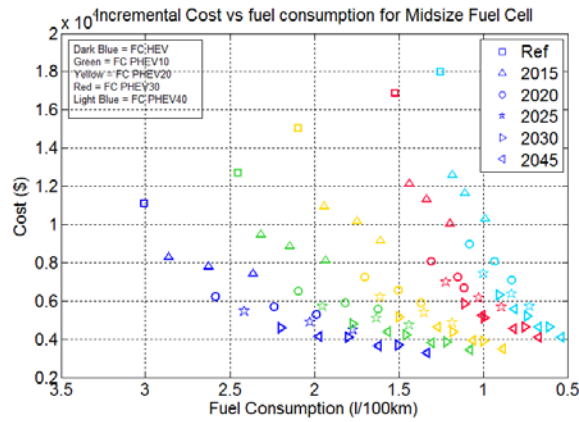


Figure IV-26: Incremental manufacturing cost (in comparison with the reference conventional gasoline vehicle manufacturing cost) as a function of fuel consumption for fuel-cell vehicles

Conclusions

- More than 4000 vehicles were simulated for different time frames (up to 2045), powertrain configuration, and component technologies. Both their fuel economy and cost were assessed to estimate the potential of each technology. Each vehicle was associated with a triangular uncertainty.
- The database tool and the plotter were used to generate the bar plots and scatter plots for analysis.
- The combination of the technology improvements leads to significant fuel consumption and cost reduction across light duty vehicle applications. Due to the uncertainty of the evolution of the technologies considered, research should continue to be conducted in the different area showing high fuel displacement potential. Due to expected improvements, advanced technologies are expected to have significant market penetration over the next decades. In the short term, both engine HEVs and PHEVs allow for significant fuel displacement with acceptable additional cost. While electric vehicles do provide a promising solution, they are likely to remain expensive and range limited in the near future.
- The simulation and analysis process will be further enhanced through the development of dedicated post processing for a large database (large-scale database analysis) and development of quality assurance/quality control (QA/QC) methods.

IV.2.C. Products

Presentations/Publications/Patents

None.

IV.2.D. References

1. Autonomie web site, accessed at autonomie.net
2. N. Kim, J. Jeong, A. Rousseau, and H. Lohse-Busch, “Control Analysis and Thermal Model Development of PHEV”, SAE 2015-01-1157, SAE World Congress, Detroit, April15
3. N. Kim, A. Rousseau, and H. Lohse-Busch, “Advanced Automatic Transmission Model Validation Using Dynamometer Test Data”, SAE 2014-01-1778, SAE World Congress, Detroit, Apr14
4. N. Kim, E. Rask and A. Rousseau, “Control Analysis under Different Driving Conditions for Peugeot 3008 Hybrid 4”, SAE 2014-01-1818, SAE World Congress, Detroit, Apr14
5. D. Lee, A. Rousseau, E. Rask, “Development and Validation of the Ford Focus BEV Vehicle Model”, 2014-01-1809, SAE World Congress, Detroit, Apr14

6. N. Kim, A. Rousseau, D. Lee, and H. Lohse-Busch, "Thermal Model Development & Validation for the 2010 Toyota Prius", 2014-01-1784, SAE World Congress, Detroit, Apr14
7. N. Kim, N. Kim, A. Rousseau, M. Duoba, "Validating Volt PHEV Model with Dynamometer Test Data using Autonomie", SAE 2013-01-1458, SAE World Congress, Detroit, Apr13
8. N. Kim, A. Rousseau, E. Rask, "Autonomie Model Validation with Test Data for 2010 Toyota Prius", SAE 2012-01-1040, SAE World Congress, Detroit, Apr12
9. N. Kim, R. Carlson, F. Jehlik, A. Rousseau, "Tahoe HEV Model Development in PSAT", SAE paper 2009-01-1307, SAE World Congress, Detroit (April 2009).
10. Cao, Q., Pagerit, S., Carlson, R., Rousseau, A., "PHEV hymotion Prius model validation and control improvements," 23rd International Electric Vehicle Symposium (EVS23), Anaheim, CA, (Dec. 2007).
11. Rousseau, A., Sharer, P., Pagerit, S., Duoba, M., "Integrating Data, Performing Quality Assurance, and Validating the Vehicle Model for the 2004 Prius Using PSAT," SAE paper 2006-01-0667, SAE World Congress, Detroit (April 2006).
12. Pasquier, M., Rousseau, A., Duoba, M, "Validating Simulation Tools for Vehicle System Studies Using Advanced Control and Testing Procedures," 18th International Electric Vehicle Symposium (EVS18), Berlin, Germany, 12 pgs. (October 2001).
13. Rousseau, A., Deville, B., Zini, G., Kern, J., Anderson, J., and Duoba, M., "Honda Insight Validation Using PSAT," Future Transportation Technology Conference, Costa-Mesa, 01-FTT49 (August 2001).
14. Rousseau, A., and Pasquier, M., "Validation of a Hybrid Modeling Software (PSAT) Using Its Extension for Prototyping (PSAT-PRO)," Global Powertrain Congress, Detroit (June 2001).

IV.3. VSATT, TSDC and Miscellaneous Support

Jeffrey Gonder, Principal Investigator

National Renewable Energy Laboratory (NREL)
15013 Denver West Parkway
Golden, CO 80401
Phone: (303) 275-4462; Fax: (303) 275-3765
E-mail: Jeff.Gonder@nrel.gov

David Anderson and Lee Slezak, DOE Program Managers

Phone: (202) 287-5688, (202) 586-2335
E-mail: David.Anderson@ee.doe.gov, Lee.Slezak@ee.doe.gov

Start Date: 10/1/2014

End Date: 9/30/2017

IV.3.A. Abstract

Objectives

- Support the U.S. Driving Research and Innovation for Vehicle efficiency and Energy sustainability (U.S. DRIVE) Vehicle Systems Analysis Technical Team (VSATT)
- Operate and enhance the Transportation Secure Data Center (TSDC)
- Perform other miscellaneous modeling and simulation activities, such as maintaining and applying the Future Automotive Systems Technology Simulator (FASTSim).

Accomplishments

- Hosted the annual VSATT Deep Dive Project Kickoff Meeting
- Delivered presentations to VSATT automaker and national lab partners on studies of pre-competitive interest to advance commercialization of vehicle efficiency technologies
 - Included active engagement with the derivative workgroup on "Quantifying Vehicle Usage Parameters Based on Existing Data"
 - Received and incorporated partner feedback to improve NREL's research projects and provided input to help similarly improve partners' studies
- Supported analyses for hundreds of TSDC users that would not otherwise be possible without access to the real-world travel data
 - Users include U.S. Department of Energy (DOE) national laboratories, universities, automakers and regulators, with cost-share support provided by the U.S. Department of Transportation (DOT) Federal Highway Administration
 - Thanks to DOE's and NREL's involvement, the enabled analyses often focus on real-world implications for electrified and other advanced vehicle technologies, multiplying DOE's impact to advance research in this space
- Maintained and applied FASTSim
 - Published a detailed paper on the tool to accompany the freely-available version that is posted on-line
 - Applied the tool to analyze the impact of road grade on medium- and heavy-duty commercial vehicle fuel economy and published a paper on the investigation.

Future Achievements

- Continue supporting VSATT, including participation in the FY16 Deep Dive Project Kickoff Meeting in October

- Add further TSDC datasets and enhancements to continue improving geographic representation and to even better support advanced vehicle studies by users both inside and outside the national lab system
 - Respond to questions and improvement suggestions by TSDC users and research partners
- Maintain and update the publicly downloadable version of FASTSim.



IV.3.B. Technical Discussion

Background

This report summarizes NREL's fiscal year 2015 (FY15) activities supporting the VSATT, operating the TSDC, and performing other miscellaneous modeling and simulation activities.

Introduction

VSATT is one of several technical teams participating in the U.S. DRIVE program. NREL provides ongoing support for VSATT, to include responding to DOE-approved requests from the automaker participants. NREL's roles include application of modeling and simulation tools, conducting vehicle systems testing, and performing real-world analysis.

For the TSDC project, the U.S. DOT Federal Highway Administration (FHWA) provides cost share funding to maintain the data center and perform data processing that supports travel activity and other transportation-focused analyses. The DOE, via this task, contributes the remainder of the operational support needed, which also enables further data processing focused on facilitating vehicle fuel use and energy analyses.

Approach

The approach for VSATT includes regular participation in team meetings along with any pertinent derivative workgroups, presentation of research plans and results, responding to any analysis requests, and hosting the FY15 VSATT Deep Dive Project Kickoff Meeting.

The overall approach for the TSDC project includes operating the data center in a manner that first and foremost protects survey participant privacy, but secondarily maximizes usability within the privacy protection constraints. To help accomplish these balanced priorities, NREL maintains three distinct areas for the TSDC: (1) an enclave for raw data processing and archiving with no external access, (2) a public website where cleansed data are available for download (with detailed location and other potentially identifying information removed), and (3) a secure portal for detailed spatial data that permits controlled access to users who complete an application and approval process.

The approach for the miscellaneous modeling and simulation support activities includes maintaining NREL's FASTSim tool, and applying the tool in combination with data enhancements from the TSDC and from NREL's medium- and heavy-duty commercial vehicle real-world driving database (Fleet DNA) to conduct analysis.

Results

FY15 accomplishments in support of VSATT included hosting the annual Deep Dive Project Kickoff Meeting at NREL during the first quarter of the fiscal year. As host, NREL supported presentation coordination, tour organization, and general logistics management. Throughout the year, NREL participated in VSATT's regular bimonthly meetings and supported preparation of VSATT deliverables, such as NREL's input on behalf of the team into the U.S. DRIVE Accomplishments Report.

As a spinoff activity from VSATT, NREL has actively engaged with a U.S. Council for Automotive Research (USCAR)/national lab workgroup on "Quantifying Vehicle Usage Parameters Based on Existing Data." The formation of this group was largely motivated by industry interests in defensible quantification of Corporate Average Fuel Economy (CAFE) off-cycle credits, combined with corresponding DOE/national lab interest in seeing technologies that achieve real-world fuel savings move forward for commercialization. NREL's presentations to the workgroup have included descriptions of data layers that could be applied toward such real-world fuel economy calculations, such as those illustrated in Figure IV-27.

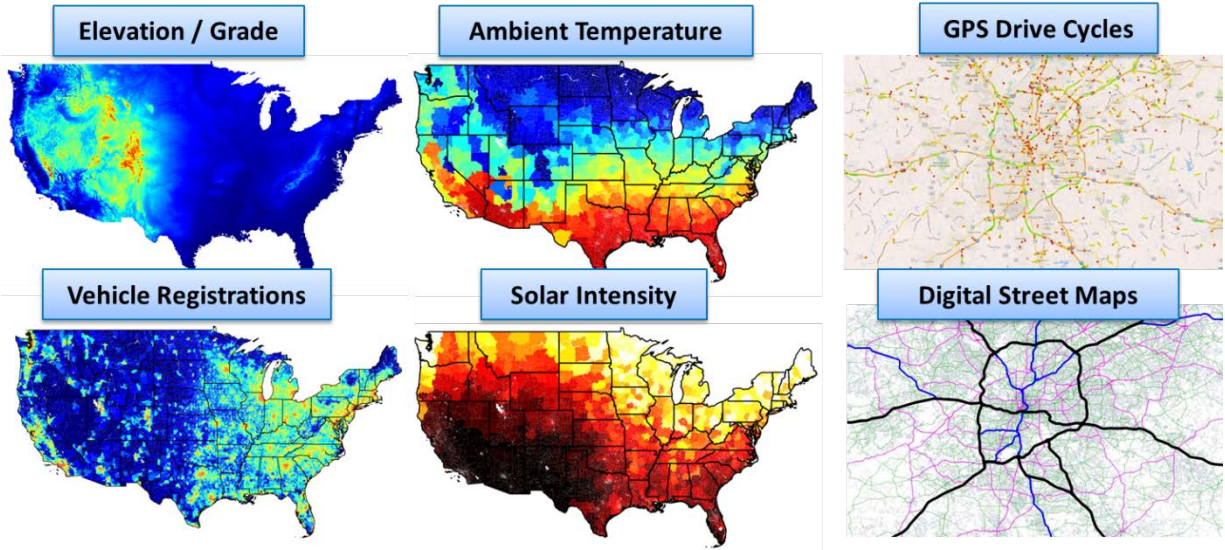


Figure IV-27: Examples of the Types of Datasets Discussed in Data Inventory Presentations to the Derivative Workgroup from VSATT on "Quantifying Vehicle Usage Parameters Based on Existing Data"

TSDC-related activities have had some overlap with those for VSATT, such as NREL's several presentations for VSATT and for the derivative vehicle usage parameters workgroup that leveraged TSDC data. When engaging with the travel survey community, NREL also continues to articulate the interests of VSATT stakeholders for specific survey feature enhancements, such as inclusion of signals from vehicle on-board diagnostic systems in the data collection and further emphasis of longitudinal data collection (i.e., over months or years of time).

Other TSDC-specific accomplishments have included providing support for over 900 registered users of the TSDC cleansed public download data and over 50 users who have applied to interface with TSDC datasets through its secure portal operating environment. Figure IV-28 illustrates the trends in continued user growth.

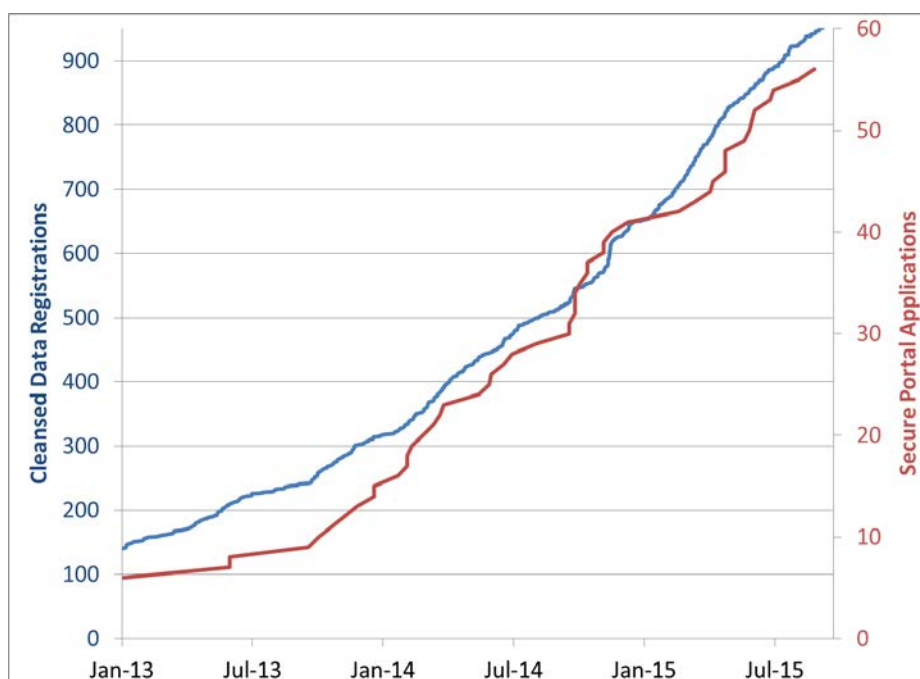


Figure IV-28: Trends in TSDC User Growth for the Two Data Access Environments

Functional enhancements that have helped manage the user growth included establishing a dedicated tsdc@nrel.gov e-mail address that can be monitored by several TSDC support team members to address user inquiries. Individuals using the data include researchers from NREL, other national labs, universities, automakers, regulators, and a variety of other organization types. TSDC users apply the data to support a wide variety of research projects, many of which focus on electrified vehicle and/or transportation energy analysis. Another interesting topic being pursued by a recent TSDC secure portal applicant from the EPA is to explore using GPS data from the TSDC to improve calibration of EPA’s Motor Vehicle Emission Simulator (MOVES) model.

To begin making it easier to track publications that have made use of the TSDC-hosted data, NREL established a copy/paste-ready citation that is now posted on the website for users to include in derivative publications [1]. NREL also maintains an Application Examples subpage on the TSDC website, which currently lists over 40 example publications that have benefitted from having access to the data made available through the TSDC.

New datasets added to the TSDC include household travel panel surveys conducted from 2010 to 2012 in Seattle and Atlanta by the DOT’s Volpe National Transportation Systems Center, add-on GPS travel data collected on behalf of the Southern California Association of Governments as part of the 2010–2012 California Household Travel Survey, GPS data from the Regional Transportation Commission of Southern Nevada collected as part of its 2014 Household Travel Survey in the Las Vegas area, and GPS data from the Delaware Valley Regional Planning Commission’s 2012–2013 Household Travel Survey in the Philadelphia area.

Bolstered by work with partner agencies such as FHWA and EPA, NREL has also added new reference datasets that can be linked to light-duty vehicle GPS data from the TSDC and medium-/heavy-duty data from the complementary Fleet DNA project to further enhance aggregated energy analyses. These datasets include road network, travel mileage, traffic speed and volume information from public sources, as well as private providers such as INRIX, HERE, and TomTom. Figure IV-29 provides an illustrative example of some of the added reference data, specifically showing a heat plot of link-by-link annual average daily travel estimates from FHWA’s Highway Performance Monitoring System.

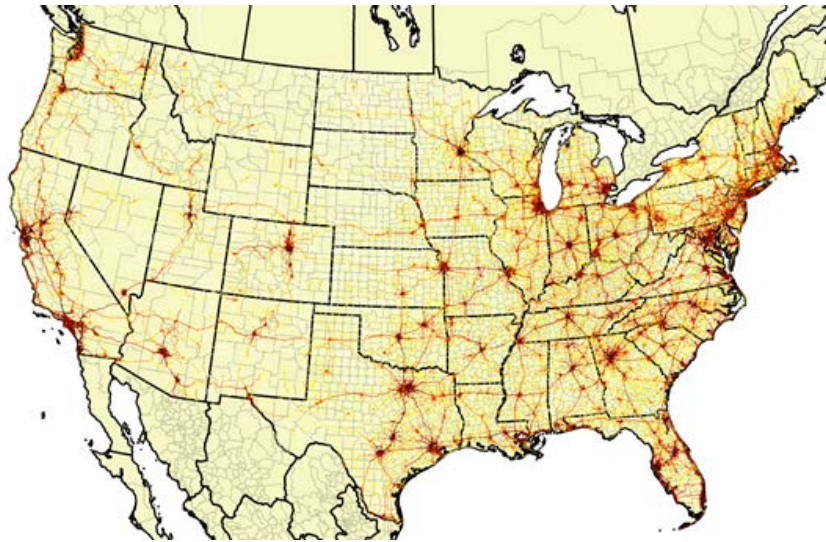


Figure IV-29: Heat Plot of Travel Estimates for Individual Roads, Available for Use in Combination with TSDC Data

Some of FHWA's cost share contributions have been specifically directed to support travel to data-related events, which has continued to build overall awareness for the TSDC. In FY15, NREL gave TSDC presentations at the ISCTSC International Conference on Travel Survey Methods [2], the Transportation Research Board Annual Meeting, and the UC Davis spring Sustainable Transportation Energy Pathways Symposium. At the Transportation Research Board Annual Meeting, NREL also convened a meeting of the TSDC Advisory Committee, which includes a variety of data provider and user stakeholders who provide objective inputs on the TSDC's ongoing goals to maximize research utility from real-world travel data in a way that preserves survey participant privacy.

With respect to FASTSim, specific FY15 accomplishments included preparation of a pair of papers for publication and presentation at SAE International events. The first paper provides a detailed overview of the tool [3] to accompany the freely available on-line posted version [4]. The second paper presents a follow-on analysis to an investigation published in FY14 about the impact of road grade on light-duty vehicle fuel economy [5], with the FY15 effort leveraging medium- and heavy-duty vehicle FASTSim powertrain models and corresponding grade-appended driving profiles from the Fleet DNA project to perform an analogous analysis [6].

The FY15 study found that the impact of road grade on average fuel use for medium- and heavy-duty vehicles ranges from a 1% to a 9% increase in fuel use, depending on the vehicle's vocation and its payload/mass. The study also found that, on average, the increased fuel use needed to ascend an incline exceeds the decreased fuel use benefit of descending it, so that individual trips with net-zero elevation but significant grade can see fuel use increases of up to 40%. As shown in Figure IV-30, this fuel use "penalty" from road grade tends to increase with higher vehicle mass.

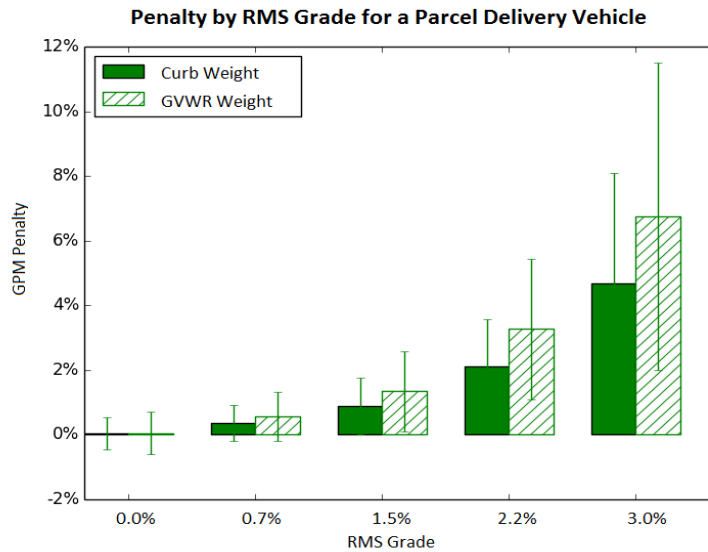


Figure IV-30: NREL-Simulated Fuel Penalty due to Grade over a Subset of Trips with Net Elevation Gain Close to Zero

Conclusions

This report summarizes NREL's FY15 accomplishments from engaging with VSATT, operating the TSDC, and completing additional ad hoc modeling and simulation activities (such as maintaining and applying FASTSim). The interactions with VSATT have served to inform USCAR and lab partners about findings from NREL research, provide opportunities for NREL to better understand specific auto industry challenges, and ensure that NREL efforts are appropriately addressing the barriers to widespread penetration of fuel-saving technologies. Through the TSDC project, NREL has continued to build the database of real-world driving profiles and useful reference data layers, which support increasingly sophisticated vehicle efficiency analyses both at NREL and at other organizations. NREL's FASTSim model is one key tool for supporting these analyses. In FY15, NREL published supporting information on the tool to accompany the freely available version that is posted on-line.

IV.3.C. Products

Presentations/Publications/Patents

1. "Transportation Secure Data Center." (2015). National Renewable Energy Laboratory. Accessed September 2015: nrel.gov/tsdc.
2. Gonder, J., Burton, E., Murakami, E. "Archiving Data from New Survey Technologies: Enabling Research with High-Precision Data while Preserving Participant Privacy." To be published in the Transportation Research Procedia from the 10th International Conference on Transport Survey Methods.
3. Brooker, A., Gonder, J., Wang, L., Wood, E., Lopp, S., Ramroth, L. "FASTSim: A Model to Estimate Vehicle Efficiency, Cost and Performance." SAE Technical Paper 2015-01-0973, Proceedings of the SAE World Congress, Apr. 2015, Detroit, MI.
4. "Future Automotive Systems Technology Simulator." (2015). National Renewable Energy Laboratory. Accessed September 2015: nrel.gov/fastsim.
5. Lopp, S., Wood, E., Duran, A. "Evaluating the Impact of Road Grade on Simulated Commercial Vehicle Fuel Economy Using Real-World Drive Cycles." SAE Technical Paper 2015-01-2739, to be published in the Proceedings of the SAE Commercial Vehicle Engineering Congress, October 2015.

IV.3.D. References

1. "Transportation Secure Data Center." (2015). National Renewable Energy Laboratory. Accessed September 2015: nrel.gov/tsdc.
2. Gonder, J., Burton, E., Murakami, E. "Archiving Data from New Survey Technologies: Enabling Research with High-Precision Data while Preserving Participant Privacy." To be published in the Transportation Research Procedia from the 10th International Conference on Transport Survey Methods.
3. Brooker, A., Gonder, J., Wang, L., Wood, E., Lopp, S., Ramroth, L. "FASTSim: A Model to Estimate Vehicle Efficiency, Cost and Performance." SAE Technical Paper 2015-01-0973, Proceedings of the SAE World Congress, Apr. 2015, Detroit, MI.
4. "Future Automotive Systems Technology Simulator." (2015). National Renewable Energy Laboratory. Accessed September 2015: nrel.gov/fastsim.
5. Wood, E., Burton, E., Duran, A., Gonder, J. "Contribution of Road Grade to the Energy Use of Modern Automobiles across Large Datasets of Real-World Drive Cycles." SAE Technical Paper 2014-01-1789, Proceedings of the SAE World Congress, Apr. 2014, Detroit, MI.
6. Lopp, S., Wood, E., Duran, A. "Evaluating the Impact of Road Grade on Simulated Commercial Vehicle Fuel Economy Using Real-World Drive Cycles." SAE Technical Paper 2015-01-2739, to be published in the Proceedings of the SAE Commercial Vehicle Engineering Congress, October 2015.

IV.4. Long-Haul Truck Idle Climate Control Load Reduction

Jason Lustbader, Principal Investigator

Co-Authors: Bidzina Kekelia, Jeff Tomerlin, Cory Kreutzer

National Renewable Energy Laboratory

15013 Denver West Parkway

Golden, CO 80401

Phone: (303) 275-4443

E-mail: Jason.Lustbader@nrel.gov

DOE Program Manager: David Anderson

U.S. Department of Energy

Phone: (202) 287-5688

E-mail: David.Anderson@ee.doe.gov

DOE Program Manager: Lee Slezak

U.S. Department of Energy

Phone: (202) 586-2335

E-mail: Lee.Slezak@ee.doe.gov

Start Date: 2011

End Date: 2015

IV.4.A. Abstract

Objectives

- Demonstrate a more than 30% reduction in long-haul truck rest period climate control loads
- Reduce long-haul truck rest period idling by working with industry partners to research and develop commercially viable climate control solutions
- Develop technologies that could help reduce the estimated 667 million gallons of fuel used annually for rest-period idling to increase national energy security and sustainability.

Accomplishments

- Overall heat transfer coefficient (UA) testing of a long-haul truck thermal load reduction package demonstrated a 43% reduction in rest period heating loads, complementing the 35.7% reduction in cooling loads shown previously and exceeding the 30% reduction goal
- Adding an additional layer of advanced insulation with a reflective barrier to the thermal load reduction package improved it further, resulting in a heating UA reduction of 53.3%
- Filed a provisional patent application for NREL's Thermal Barrier Curtains for Long-Haul Trucks design
- Initial fuel use analysis shows 774 gallons saved per year per truck for cooling using a battery electric air conditioning (A/C) system with advanced thermal load reduction technologies. Thermal load reduction technologies reduced the battery size by half, decreased the thermal power demand, saved additional fuel, and have the potential to reduce heating demands.

Future Achievements

- Improve and complete national-level fuel use analysis and use the results to inform future research and technology trade-offs for long-haul truck rest period climate control fuel use reduction.



IV.4.B. Technical Discussion

Background

In the United States, long-haul trucks (trucks that travel more than 500 miles per day) use approximately 667 million gallons of fuel annually for rest period idling [1]. Sleeper cab climate control is one of the primary reasons for idling the main engine during these driver rest periods. This rest period idling is approximately 6.8% of the total long-haul truck fuel use and represents a zero freight efficiency operating condition for the truck. With the recent high prices of diesel, fuel is one of the largest trucking costs per mile, averaging 35% of the total from 2008 to 2013 [2]; therefore, the increasing cost and cost volatility of fuel provides a significant financial incentive to reduce fuel use. Recent federal, state, and city anti-idling regulations [3] are providing further incentives to reduce truck idling. One example is the idle reduction technology credit in the Heavy-Duty Greenhouse Gas Emissions Standards, effective starting in 2014 [4].

By reducing thermal loads and enabling more effective idle-off climate control systems, there is an opportunity to reduce fuel use and associated emissions. Enhancing the thermal performance of long-haul truck sleepers will enable smaller, lighter, and more cost-effective idle reduction solutions. In addition, if fuel savings from new technologies provide a one- to three-year payback period [5], fleet owners will be economically motivated to incorporate the new technologies. Therefore, financial incentive provides a pathway to rapid adoption of effective thermal load and idle reduction solutions.

Introduction

The U.S. Department of Energy's National Renewable Energy Laboratory's (NREL's) CoolCab project is researching efficient thermal management systems to maintain cab occupant comfort without the need for engine idling. The CoolCab project uses a system-level approach that addresses three aspects: reducing the thermal loads, efficient delivery of climate control for occupant thermal comfort, and maximizing equipment efficiency. By reducing thermal loads, the occupant's climate control needs are reduced, and reduced-capacity equipment can then provide the conditioning. To advance the goals of the CoolCab project and the broader goals of increased national energy security and sustainability, the CoolCab team works closely with industry partners to develop and apply commercially-viable solutions to reduce national fuel use and industry costs. To reduce thermal and resulting idle loads in long-haul trucks, NREL has identified four thermal load reduction technology focus areas: (1) conductive pathways, (2) the solar envelope, (3) the occupant environment, and (4) efficient equipment. Working closely with industry partners, NREL applied modeling tools and experimental methods to identify and evaluate promising complete-cab heating, ventilating, and air conditioning (HVAC) load reduction solutions comprised of technologies in each of these focus areas.

To achieve an effective solution, NREL first conducted baseline testing of vehicles to quantify their thermal behavior. This information was then used to build and validate a CoolCalc model. CoolCalc is NREL's rapid HVAC load estimation tool [6]. In FY14, CoolCalc thermal models were then used in conjunction with experimental screening tests to identify promising thermal load reduction technologies. The most promising technologies were combined into a Complete-Cab Thermal Load Reduction Package. Previous tests showed that this reduced A/C electrical loads by more than 35.7%, exceeding the 30% goal [7]. In FY15 NREL tested the impact of this Complete Cab Thermal Load Reduction Package on heat loads using an overall heat transfer coefficient, UA, test procedure. This showed a 43% reduction in heating loads. The Complete-Cab thermal load reduction package was then updated with improved insulation (an additional thin layer of advanced insulation with reflective barrier was added to the previously tested thermal insulation package), resulting in a UA heating load reduction of 53.3%. A model of the base Complete-Cab thermal load reduction package was then used to understand the national impact of the climate control load reduction technologies on thermal performance, climate control loads, and fuel consumption, spanning the wide range of use and environmental conditions that occur in the United States.

Approach

Complete-Cab Thermal Load Reduction Package

NREL has identified four key climate control load technology focus areas: conductive pathways, the solar envelope, occupant environment, and efficient equipment. The first three of these technologies impact the cab's heat transfer and resulting thermal loads and are the focus of this report. The efficient equipment focus area translates the thermal loads into mechanical or electrical loads. The four technical focus areas are described below.

1. The conductive pathways focus area addresses heat transfer through walls and other surfaces of the cab/sleeper. Technologies in this area include insulation, advanced materials, and glass.
2. The solar envelope describes the interaction of surfaces with radiant energy from the sun and the surrounding environment. It is predominantly driven by radiant heat transfer and is most relevant during daytime operation; however, nighttime radiation to the sky is also included. This focus area includes the study of opaque and transparent surface properties of paints and glass, respectively. It also includes devices to modify these properties, such as window shades.
3. The occupant environment includes the volume of conditioned air, occupant heat exchange with the surroundings, and human factors such as thermal sensation/comfort. Designing the thermal environment to make every occupant comfortable rather than to meet the traditional temperature-based metric has a significant impact on design. Technologies in this area include sleeper curtains and control of the microenvironment.
4. The use of efficient equipment impacts conversion of thermal loads to mechanical, electrical, or chemical loads. A range of technology options and design considerations falls into this category. These options include battery electric A/C, fuel-fired heaters, and auxiliary power units. For the purposes of this study, battery electric idle-off systems were used; however, the idle-off thermal load reduction technologies applied to the cab/sleeper are largely independent of the equipment used.

Prior work used testing and modeling to down-select technologies from each of these focus areas to develop a Complete-Cab thermal load reduction package. The baseline experimental configuration for the test cab contained sections of insulation as part of the vehicles stock insulation configuration. The stock insulation was affixed to portions of select upholstery panels that composed the sleeper compartment, Figure IV-31A. For the advanced insulation package, prefabricated insulation panels were installed throughout the sleeper compartment to occupy the void space between the upholstery panels and exterior frame wherever possible (Figure IV-31: B). The advanced insulation package consisted of Thinsulate automotive acoustic insulation provided by Aearo Technologies. The areas of the sleeper cab insulation included the rear sleeper wall, sleeper ceiling, sleeper side walls, and portions of the cab ceiling. The installed insulation package contained a combination of one- and two-inch-thick blanket insulation with a nominal thermal conductivity of between 0.03 and 0.05 W/m-K. Prior testing of this load reduction package showed it to be effective for electrical load reduction for an electric-powered A/C unit. To improve on this load reduction package, an additional layer of Thinsulate insulation with a reflective radiation barrier was added between the interior trim and cab structure to reduce thermal shorts between the wall structure and the interior (Figure IV-31: C).



Figure IV-31: A (left), Stock Insulation; B (center), Advanced Insulation; C (right), Additional Layer with Reflective Barrier

Experimental Test Setup

An overall heat transfer coefficient, UA, test program was conducted at NREL's Vehicle Testing and Integration Facility, shown in Figure IV-32A, during the months of May through August. The facility is located in Golden, Colorado, at an elevation of 5,997 feet at latitude 39.7 N and longitude 105.1 W. The experimental setup included two current model Volvo cab test "bucks." Both bucks were the cab section from a representative truck in current production provided by Volvo Trucks North America. One buck was utilized as the control buck, and the other was modified as the test buck.

For the experimental setup, test and control bucks were oriented facing solar south and separated by a distance of 25 feet to maximize solar loading and minimize shadowing effects. To keep the firewalls from receiving direct solar loads, a firewall shade cloth was implemented on both the control and test bucks. In each vehicle, the sleeper curtain and four shades were available for use, depending on the test being conducted. The shades available were the front privacy, cab skylight, and two bunk window curtains.

The UA test procedure used to measure the heating performance of the Complete Cab Thermal Load Reduction Package was conducted at night to eliminate solar loading effects. The sleeper air temperature of both bucks was controlled to 32°C using a forced air heater, Figure IV-32B. This temperature was selected to provide a sufficient temperature difference of at least 10°C with the environment over the extended test season. This heater design and vent exit orientation provided sleeper air temperature uniformity within ±2°C. Unless noted otherwise, the sleeper curtain and all four shades were utilized on the vehicles. All curtains and shades were employed to match the expected standard configuration during a rest period operation.

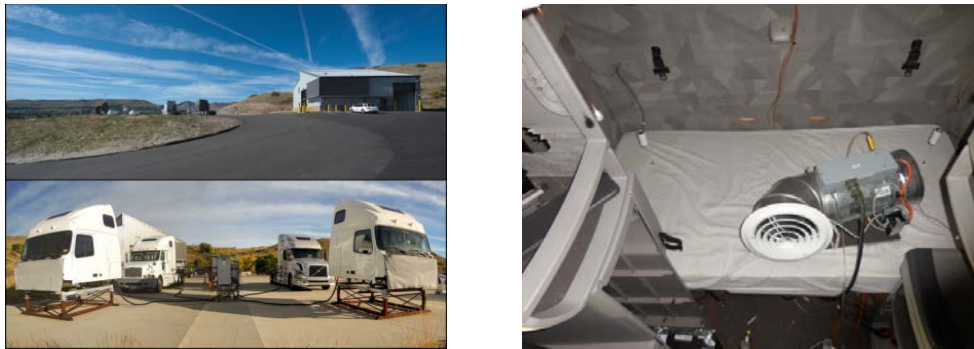


Figure IV-32: A (left), NREL's Vehicle Testing and Integration Facility; B (right), UA Test Heater in Sleeper

The UA value of the sleeper was calculated by measuring the heater power and the temperature difference between the interior air temperature and ambient temperature as described in Equation 1:

$$UA = \frac{Q}{\bar{T}_{Sleeper} - \bar{T}_{Ambient}} \quad (1)$$

where UA is the overall heat transfer coefficient [W/K], Q is the heater power, $\bar{T}_{Sleeper}$ [°C] is the average sleeper cab air temperature measurements, and $\bar{T}_{Ambient}$ [°C] is the local air temperature taken inside a naturally aspirated radiation shield at the weather station collocated at the test site.

If the total area of heat transfer in the sleeper is known this test can be used to determine a truck's thermal resistance, R-value, as described in Equation 2:

$$R = \frac{A}{UA} \quad (2)$$

where R [$m^2 \cdot K/W$] is the total sleeper cab resistance, and A is the total area of the sleeper boundaries [m^2]. Due to the uncertainty in defining the total area of heat transfer in the sleeper, results are reported in terms of UA. It is worth noting that UA is inversely proportional to the overall resistance.

To account for normal day-to-day variations in weather conditions, the control buck was used as a reference. All vehicles will have some thermal performance variation due to differences in A/C systems, manufacturing,

leakage, and other factors. To account for this, the control cab was calibrated to the test cab while both bucks were in a baseline configuration. The control cab can then be used as an accurate reference for the behavior of the test cab in a baseline configuration.

To further minimize the impact of weather variation on the test results, environmental screening criteria were established for a valid heating test day. Net downwelling infrared radiation (IR) was measured using Kipp & Zonen CG4 pyrgeometer located at NREL's Solar Radiation Research Laboratory's weather station to characterize the cloud cover at night. Net downwelling IR is the difference between upward radiation from a surface to the sky and the downwelling, incoming, radiation from the atmosphere. Cloud cover will increase the downwelling IR from the atmosphere to the surface and thus decrease the net loss of heat from the surface. A net downwelling IR of more than 85 W/m^2 lost from the surface was determined to indicate a clear night sky condition. Hourly average wind speeds were filtered to below 3.58 m/s to limit the impact of wind variability. Wind speed below this limit was found to have little influence on UA.

To minimize the impact of transient effects, one-hour segments were selected that met stability criteria for ambient temperature and heater power. The maximum allowable ambient temperature change in the hour interval was 3°C , and the maximum allowable power change was 15%. The one-hour segments also had to be after midnight and before daybreak to avoid any influence of sunset or sunrise.

The average interior sleeper air temperature was calculated by averaging eight thermocouples, with six located in accordance with the American Trucking Association Technology Maintenance Council's recommended practice RP422A [8], as shown in Figure IV-33B. Similarly, the average cab air temperature was calculated by averaging six thermocouples with four located in accordance with RP422A, illustrated in Figure IV-33A. The addition of two thermocouples located in both the cab and sleeper air spaces improved the average air temperature measurement by more accurately capturing the air temperature distribution.

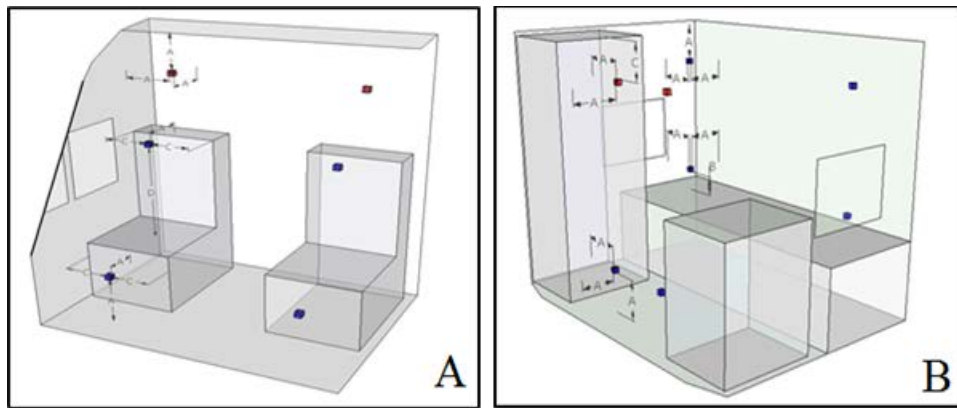


Figure IV-33: (A) Cab and (B) Sleeper Thermocouple Locations. Dimensions: A = 12", B = 6", C = 18". Blue: TMC standard [8]; red: NREL added

A National Instruments SCXI data acquisition system was used to record measurements at a sampling frequency of 1.0 Hz, which was averaged over 1-minute intervals. Among the four vehicles, more than 200 calibrated type K thermocouples were used for a variety of surface and air temperatures. An isothermal bath and reference probe were used for thermocouple calibration, achieving a U95 uncertainty of $\pm 0.32^\circ\text{C}$ in accordance with American Society of Mechanical Engineers standards [9]. Air temperature sensors were equipped with a double concentric cylindrical radiation shield to prevent errors due to direct solar radiation. The heater electrical power consumption was measured using Yokogawa watt meters with the accuracy of $\pm 0.2\%$ reading. Weather data were collected from both NREL's Solar Radiation Research Laboratory and NREL's Vehicle Testing and Integration Facility [10] weather station, which together feature more than 160 instruments dedicated to high-quality measurements of solar radiation and other meteorological parameters.

Results

Baseline Testing

For the Complete-Cab thermal load reduction package experimental evaluation, a heater system calibration was completed for the test and control bucks using the baseline configuration in both bucks. Two configurations were calibrated: a standard original equipment manufacturer insulation package with standard sleeper curtain and privacy shades, and a privacy-shade-only case with no sleeper curtain. The bucks were painted different colors, but because the testing was conducted at night and the paint emissivity was very similar, any effects due to this were negligible. The calibration data for the Complete-Cab thermal load reduction package UA baseline is shown in Figure IV-34. The figures contain only data that meet the weather and stability screening criteria described in the approach section. Both data sets show a strong linear correlation with a coefficient of determination (R²) of 0.934 and 0.962 for the standard and no-curtain configurations respectively.

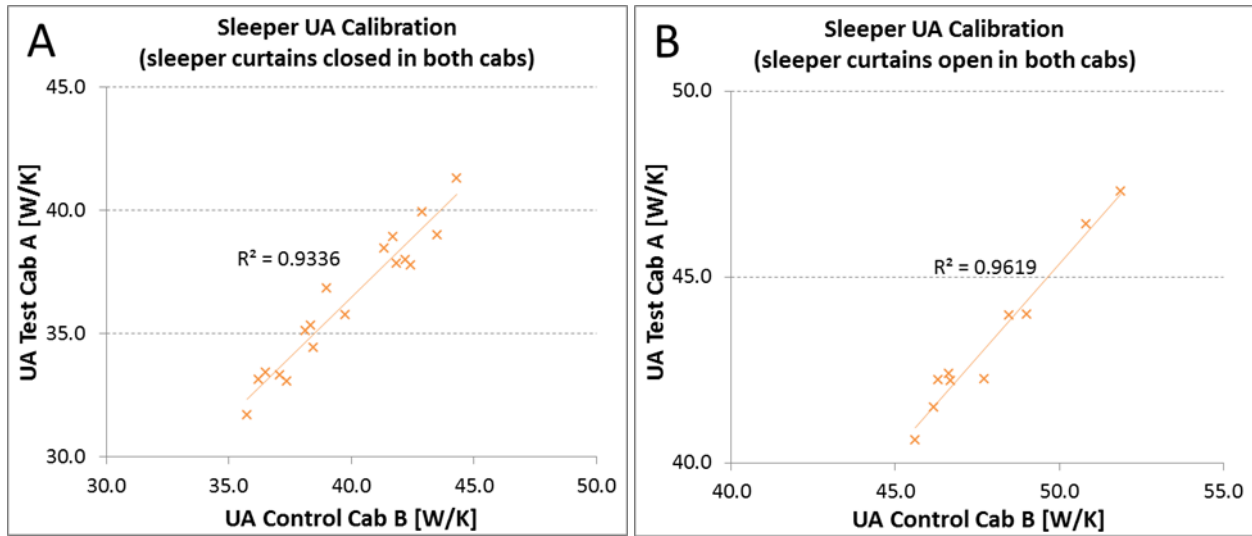


Figure IV-34: UA Calibration Results for: A. Sleeper with Standard Sleeper Curtain and Shades, B. Sleeper with Window Shades Only and No Curtain

Thermal Load Reduction Package Testing

The test buck thermal load reduction package was tested for multiple configurations as summarized in Table I-35. Applying only the advanced curtains and shades to the standard insulation resulted in a 20.6% reduction in UA. The advanced insulation alone was also effective at reducing the heating load, yielding 20.7% reduction in UA. Applying the full thermal load reduction package with both advanced curtains and shades resulted in a 43% reduction in UA.

Table I-35: Thermal Load Reduction with Advanced Insulation

Configuration	Insulation	Privacy shades on windshield	Sleeper curtains	Reduction in UA
Baseline with sleeper curtains closed	Standard	Standard	Standard	-
Advanced curtains	Standard	Advanced	Advanced	20.6%
Advanced insulation	Advanced	Standard	Standard	20.7%
Complete cab solution	Advanced	Advanced	Advanced	43.0%

To build on these results, the insulation was improved further by adding an additional insulation layer with a reflective barrier to the walls and ceiling as previously described. This is the "advanced plus thermal load reduction" configuration. This layer fit between the structural members and the inner panels. The "advanced plus configuration" results are shown in Table I-36. This insulation improvement resulted in an increase in the UA reduction for the insulation-only case with a 33.6% reduction in UA. Adding this insulation improved the full thermal load reduction package, reducing UA by 53.3%. The third case in Table I-36 compares the advanced insulation and privacy shades without a curtain to the baseline with a standard curtain. This would provide more space to the occupant, but does reduce the overall improvement substantially. By opening the curtain a larger volume of air will be conditioned and walls without improved insulation will be exposed to higher interior temperatures as compared to the baseline case with the standard curtains closed, resulting in higher thermal losses to the colder surroundings.

Table I-36: Thermal Load Reduction with Advanced Insulation

Configuration	Insulation	Privacy shades on windshield	Sleeper curtains	Reduction in UA
Baseline with sleeper curtains closed	Standard	Standard	Standard	-
Advanced+ insulation	Advanced+	Standard	Standard	33.6%
Complete cab solution+	Advanced+	Advanced	Advanced	53.3%
Adv+ insulation & adv shades	Advanced+	Advanced	- Open -	21.6%

In some cases drivers may want a more spacious feeling and not use a sleeper curtain during rest periods. In order to investigate the impact of the insulation and privacy shades on a vehicle not using a sleeper curtain, the second calibration process was used, as shown in Figure IV-34B. The impact of the insulation technologies was then compared against the baseline with no sleeper curtain as shown in **Error! Reference source not found.** These results also show strong improvements over the no sleeper curtain baseline.

Table I-37: Thermal Load Reduction with Sleeper Curtains Open

Configuration	Insulation	Privacy shades on windshield	Sleeper curtains	Reduction in UA
Baseline with sleeper curtains open	Standard	Standard	- Open -	-
Adv insulation & adv shades	Advanced	Advanced	- Open -	27.4%*
Adv+ insulation & adv shades	Advanced+	Advanced	- Open -	34.1%*

*Calibrated with open sleeper curtains in both test and control cabs

In order to understand the impact of these thermal load reduction technologies on long-haul trucks nationally, NREL's CoolCalc rapid HVAC load analysis tool was used. First, the 200 weather stations that best represent the national long-haul truck vehicle miles traveled and their relative weightings were determined. The cab thermal model was then simulated for a typical meteorological year for each location. These national-thermal results were then converted into electrical discharge loads using performance maps created with NREL's A/C modeling framework, CoolSim, which is built in Simulink. A battery model was then used in conjunction with the vehicle simulation tool Autonomie to calculate the fuel cost of recharging the batteries over various drive cycles. These fuel costs were then used to calculate a drive cycle weighted average fuel cost per battery energy used. Using rest period time assumptions, this allowed calculation of fuel consumption for each scenario. Analysis showed an average of 990 hours of A/C operation per year. This resulted in 792 gallons of fuel used per year for cooling by the baseline idling truck. Adding an A/C idle-off system with the Complete-Cab solution reduced fuel use to 17 gallons per year, resulting in \$6,968 saved per year for \$3/gal price of diesel fuel. Analysis also showed that the Complete-Cab thermal load reduction package required half as many

batteries and required a smaller system to meet power demands resulting in a lower-cost system. Additional fuel savings for the battery electric A/C system due to the advanced insulation were also seen. Heating analysis has not yet been completed, but initial results indicate possible additional savings between the baseline and advanced insulation configurations. These savings provide a suitable budget for implementing thermal reducing technologies while improving the performance of the system. This process and its results are described in detail in the rapid HVAC modeling section of this annual report [11].

Conclusions

NREL's CoolCab project aims to reduce HVAC loads and resulting idling fuel consumption while maintaining driver comfort when long-haul trucks are parked during a rest period. To achieve this, NREL researchers have collaborated with partners Volvo Group North America, Aearo Technologies, and PPG Industries to develop and test a thermal load reduction package that uses ultra-white paint, advanced insulation, and advanced curtains and window shades. Overall heat transfer coefficient (UA) testing of this package demonstrated a 43% reduction in heating loads, complementing the 35.7% reduction in cooling loads shown previously and exceeding the 30% reduction goal. Adding an additional layer of advanced insulation improved this to a 53.3% reduction in heating loads. NREL's rapid HVAC load analysis tool, CoolCalc, was used to model the baseline insulation and advanced insulation packages. Simulations over a typical meteorological year were performed for 200 weather stations identified as most representative of long-haul truck vehicle miles traveled. Initial simulations and assumptions resulted in \$6,968 savings for \$3/gal price of diesel fuel, showing the potential for cost-effective idle reduction systems improved by use of advanced climate control load reduction technologies.

IV.4.C. Products

Presentations/Publications/Patents

1. Lustbader, J.; Kreutzer, C.; Tomerlin, J.; Adelman, S.; Yeakel, S. "Advanced Technologies for Long-haul Truck idle load reduction." SAE Commercial Vehicle Engineering Congress, Oct. 7, 2014.
2. Lustbader, J.; Kreutzer, C.; Adelman, S.; Yeakel, S.; Zehme, J. "Sleeper Cab Climate Control Load Reduction for Long-Haul Truck Rest Period Idling." SAE World Congress, April 14, 2015.
3. Lustbader, J.; Kreutzer, C.; Jeffers, M.; Adelman, S.; Yeakel, S.; Zehme, J.; Brontz, P.; Kopetz, C.; Ohlinger, J. "Complete Cab Thermal Load Reduction Package for Long-Haul Truck Rest Period Idling." SAE Thermal Management Systems Symposium, Sept. 30, 2015.
4. Lustbader, J.; Kreutzer, C.; Jeffers, M.; Tomerlin, J.; Langewisch, R.; Kincade, K. "CoolCab Test and Evaluation & CoolCalc HVAC Tool Development." DOE Annual Merit Review, June 10, 2015; VSS075.
5. U.S. Provisional patent application entitled NREL PROV/15-54 "Thermal Barrier Curtains for Long-Haul Trucks," submitted to USPTO, filed September 30, 2015.

IV.4.D. References

1. Gaines, L.; Vyas, A.; Anderson, J. "Estimation of Fuel Use by Idling Commercial Trucks." Presented at 85th Annual Meeting of the Transportation Research Board, Washington, D.C., Jan. 22–26, 2006; Paper No. 06-2567.
2. Torrey, F.; Murray, D. "An Analysis of the Operational Costs of Trucking: A 2014 Update." American Transportation Research Institute. Atlanta, GA. 2014.
3. "Idling Regulations Compendium." American Transportation Research Institute, accessed September 16, 2013: <http://atri-online.org/2013/02/20/idling-regulations-compendium/>.
4. "Greenhouse Gas Emissions Standards and Fuel Efficiency Standards for Medium- and Heavy-Duty Engines and Vehicles, Final Rule." Federal Register 76 (15 September, 2011): 57106-57513.
5. Roeth, M.; Kircher, D.; Smith, J.; Swim, R. "Barriers to the Increased Adoption of Fuel Efficiency Technologies in the North American On-Road Freight Sector." Report for the International Council for Clean Transportation. NACFE. July 2013.

6. Lustbader, J.; Kreutzer, C.; Adelman, S.; Yeakel, S.; Brontz, P.; Olson, K.; Ohlinger, J. "Impact of Paint Color on Rest Period Climate Control Loads in Long-Haul Trucks." Presented at SAE World Congress, April 8, 2014. nrel.gov/docs/fy14osti/61084.pdf
7. Lustbader, J.; Kreutzer, C.; Adelman, S.; Yeakel, S.; Zehme, J. "Sleeper Cab Climate Control Load Reduction for Long-Haul Truck Rest Period Idling." SAE World Congress, April 14, 2015.
8. "Cab Insulation Testing Methodology." RP422A-1-9. Technology and Maintenance Council's Recommended Maintenance Practices Manual, 2010–2011 edition. Arlington, VA: American Trucking Association, p. RP422A 1.
9. Dieck, R.H.; Steele, W.G.; Osolsobe, G. Test Uncertainty. ASME PTC 19.1-2005. New York, NY: American Society of Mechanical Engineers. 2005.
10. "Vehicle Testing and Integration Facility." National Renewable Energy Laboratory, nrel.gov/midc/vtif_rsr/
11. Lustbader, J.A.; Kreutzer C.; Kekelia B.; Jeffers, M.; Schilling, S. "CoolCalc Rapid HVAC Load Estimation Tool." Vehicle and Systems Simulation and Testing 2015 Annual Progress Report.

Acknowledgements

1. Special thanks to our industry partners Volvo Group North America, Aearo Technologies LLC, and PPG Industries.
2. Additional thanks to John Rugh and Lisa Fedorka (NREL).

IV.5. VTCab, Rapid Vehicle HVAC Load Estimation Tool

Jason Lustbader, Principal Investigator

Co-Authors: Cory Kreutzer, Bidzina Kekelia, Matt Jeffers, and Sam Schilling

National Renewable Energy Laboratory

15013 Denver West Parkway

Golden, CO 80401

Phone: (303) 275-4443

E-mail: Jason.Lustbader@nrel.gov

David Anderson, DOE Program Manager

U.S. Department of Energy

Phone: (202) 287-5688

E-mail: David.Anderson@ee.doe.gov

Lee Slezak, DOE Program Manager

U.S. Department of Energy

Phone: (202) 586-2335

E-mail: Lee.Slezak@ee.doe.gov

Start Date: FY15

End Date: FY17

IV.5.A. Abstract

Objectives

- Develop modeling tools to help quantify the impact of advanced load-reduction technologies and show progress toward at least a 30% reduction in long-haul truck idle climate control loads with a three-year or better payback period
- Reduce the risk of advanced technology adoption by improving the quantification of thermal load reduction technology impacts for both design points and in-use estimation
- Investigate opportunities to reduce truck cab thermal loads through modeling and simulation to decrease the estimated 667 million gallons of fuel used for truck rest period idling.

Accomplishments

- Developed beta release of VTCab, a standalone version of CoolCalc, which has a complete set of basic tools to build and simulate a vehicle model. This improved stability, greatly reduced maintenance requirements, and allows for future integration with CoolSim.
- Determined method of weighting weather stations by long-haul truck traffic density and used this to down select to the most representative 200 weather stations.
- Developed fuel use estimation process that combines a VTCab thermal model, CoolSim air conditioning (A/C) model, and a vehicle model at the national level. This process was used to simulate an idle-off electric A/C system combined with a thermal load reduction package that showed 774 gallons of annual fuel savings per truck for A/C. At diesel fuel prices of \$3/gal, these fuel savings translate into \$6,968 savings over the first three years of operation. In addition to fuel savings, the thermal load reduction package lowers auxiliary heating, ventilating, and air conditioning (HVAC) system battery energy requirements to meet the 99% cooling day by about half, thus requiring fewer batteries. This combined with the reduced peak power demands could allow for reduced size and improved performance of a "no-idle" A/C system.

Future Achievements

- Complete evaluation of thermal load reduction technologies on heating fuel use
- Use combined A/C and heating model to simulate the payback period of various technology configurations, enabling fuel use and payback period-driven design
- Apply tools to the broader commercial vehicle applications and identify opportunities for climate control and idle load reduction



IV.5.B. Technical Discussion

Background

A/C and heating are two of the primary reasons for long-haul truck main engine operation when a vehicle is parked. In the United States, trucks that travel more than 500 miles per day use 667 million gallons of fuel annually for rest period idling [1]. Including workday idling, more than 2 billion gallons of fuel are used annually for truck idling [1]. By reducing thermal loads and improving efficiency, there is an opportunity to reduce the fuel used and emissions created by idling. Enhancing the thermal performance of cabs/sleepers will enable cost-effective idle-reduction solutions. If the fuel savings from new technologies can provide a one- to three-year payback period [2], fleet owners will be economically motivated to incorporate them. This provides a pathway to the rapid adoption of effective thermal and idle load-reduction solutions.

The U.S. Department of Energy's (DOE's) National Renewable Energy Laboratory (NREL) CoolCab project is researching efficient thermal management strategies that keep the vehicle occupants comfortable without the need for engine idling. To achieve this goal, NREL is developing tools and test methods to assess idle-reduction technologies. The heavy-duty truck industry needs a fast, high-level analysis tool to predict thermal loads, evaluate load reduction technologies, and calculate their impact on climate control fuel use over a wide range of temperatures and use conditions.

To meet the needs of industry, NREL developed the Vehicle Thermal Cab Simulator (VTCab), a software tool, to assist the industry in reducing climate control loads for vehicles. VTCab is a simplified HVAC load estimation tool that enables rapid exploration of idle reduction and climate control design options for a range of climates. VTCab is also general enough to perform HVAC analysis for light-duty vehicles.

Introduction

VTCab is an easy-to-use, simplified, physics-based HVAC load estimation tool that requires no meshing, has flexible geometry, excludes unnecessary detail, and is less time intensive than more detailed computer-aided engineering (CAE) modeling approaches. For these reasons, it is ideally suited for performing rapid tradeoff studies, estimating technology impacts, and sizing preliminary HVAC designs. VTCab complements more detailed and expensive CAE tools by providing the ability to explore the design space to identify promising technologies and specific parameters that require deeper investigation.

CoolCalc, described in more detail in [3], was originally built as a plug-in extension for Trimble's SketchUp three-dimensional design software. VTCab, a new standalone version of CoolCalc, is being developed to gain independence from SketchUp, improve long-term stability, and greatly reduce maintenance needs. DOE's EnergyPlus software (developed for building energy modeling) is used as the heat transfer solver for VTCab.

VTCab fills an important role in the CoolCab project's suite of experimental and analytical tools. It enables rapid evaluation of technologies over a range of weather types and locations to help understand their impacts as the technologies will be used on long-haul trucks. VTCab also provides industry partners with a valuable and cost-effective research and design tool.

Approach

The goals of the CoolCab research project are to reduce thermal loads, improve occupant thermal comfort, and maximize equipment efficiency to eliminate the need for rest period engine idling. To accomplish these goals, NREL is closely collaborating with original equipment manufacturers and suppliers to develop and implement commercially viable thermal management solutions.

VTCab is a critical tool for achieving the CoolCab project goals. It enables rapid evaluation of thermal load reduction technologies, not only at extreme design points, but also over the wide range of weather and use conditions that the vehicles will experience. Each phase of the CoolCab project approach leverages VTCab. After baseline testing is completed, VTCab models of the test vehicles are built, starting from computer-aided design models and other information provided by original equipment manufacturer and suppliers. Best engineering estimations are used when data are not available. Next, models are validated against test data collected at NREL's Vehicle Testing and Integration Facility. Local weather data collected at the Vehicle Testing and Integration Facility are input into the VTCab simulation to ensure that the model behaves similarly to the test vehicle under the same weather conditions. VTCab is then used to identify opportunities to reduce thermal loads via rapid simulation of technologies and thermal management strategies. Top candidates from parametric simulations are selected for further investigation through outdoor testing.

After testing promising thermal load reduction technologies, the information is used to improve VTCab models as needed and verify the accuracy of the model results. VTCab simulations are then used to analyze cab thermal performance at a national level under typical weather conditions. Results can be coupled with HVAC and vehicle models to understand the impact on system performance. VTCab supplies thermal loads to NREL's CoolSim A/C model, which calculates the required electrical A/C system power. The model is then coupled with Autonomie, Argonne National Laboratory's simulation environment for rapid evaluation of vehicle powertrain and propulsion technologies, to predict fuel use for weather and use conditions. This analysis will provide industry with the necessary information to adopt solutions that reduce or prevent engine idling and save fuel.

Results

VTCab Improvements and New Features

The beta version of VTCab, a SketchUp-independent version of CoolCalc was completed and released for feedback from industry partners. CoolCalc was initially developed as a plug-in to the SketchUp program environment. For rapid preliminary tool development and the demonstration of CoolCalc, use of the SketchUp environment was very beneficial; however, this dependency is also a disadvantage because of updates that are required for CoolCalc to remain compatible with SketchUp as the SketchUp product changes over time. For this reason, development of VTCab was initiated.

The primary purpose of VTCab is to retain and improve upon existing CoolCalc functionality with stand-alone execution of the software. VTCab is currently being developed to use EnergyPlus as the thermal solver; however, future development could include the addition of a thermal solver developed in the MATLAB/Simulink environment. VTCab provides additional programming flexibility and control while eliminating unnecessary SketchUp tools and features that were not used in CoolCalc projects. VTCab also simplifies the installation process with a single installer, providing a faster and simpler procedure for new users. A picture of the VTCab interface is shown in Figure IV-35A.

The VTCab beta version has all the basic tools needed to build a model from imported geometry, set up parametric variables, and run the model using the graphic user interface (GUI).

Various enhancements have been made to VTCab. These include the following:

1. The COLLADA, COLLABorative Design Activity, file importer has been upgraded to be more robust. It can import complex three-dimensional geometries without any of the stability limitations found in the previous version. Figure IV-35B shows an example of imported geometry from a SketchUp

COLLADA file of a light-duty vehicle developed as part of another NREL thermal load reduction project [4].

2. Parametric simulation capability has been implemented in VTCab. This allows a user to define multiple values for a model input parameter (e.g., insulation thickness or conductivity) and evaluate the impact parametrically. Interdependent variables can be grouped together to ensure associated values are simulated together in the desired sequence. Weather files can also be set up as parametric variables (and grouped by state, geographic region, population density, etc.). This feature provides full control over the parameter combinations in the Run Simulation GUI, up to full factorial parametric simulations.
3. Figure IV-35C shows a new exploded view that has been added to allow users to more easily view and select surfaces in a model. A surface transparency option was also implemented to help reveal surfaces of zone interfaces or internal geometry that are otherwise hidden from view.
4. A zone rendering view has been added as a user-friendly way to assign surfaces to zones in the model after importing geometry from a COLLADA file. Each zone is distinguished by a unique color that the user may customize freely (Figure IV-35C). This speeds up the zone assignment process considerably as the user no longer has to manually click on each surface object in the Object Browser and select the appropriate zone from the list. This also serves as a visual aid for the user to ensure that all surfaces are assigned correctly.
5. VTCab now contains the option to create a zone interface from imported geometry. This option duplicates a surface and applies the appropriate boundary conditions to each surface to properly simulate two adjacent thermal zones. Fully enclosing all thermal zones at their interfaces is an important step that previously was not always obvious to a user. This feature makes zone-to-zone interfaces easier for the user to define.

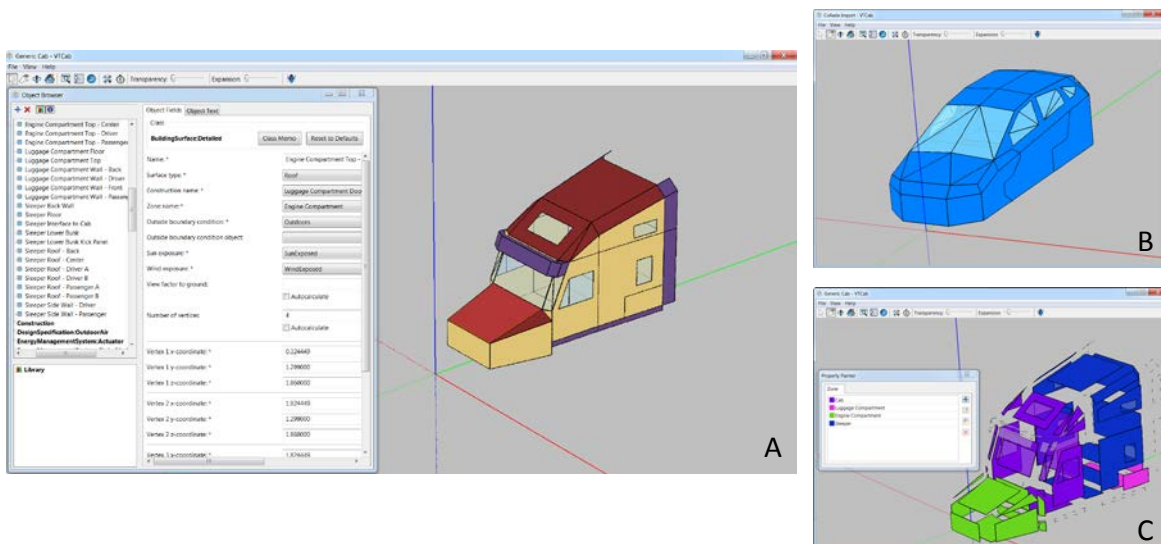


Figure IV-35: VTCab interface: A. Standard rendering, B. Imported light-duty model, C. Zone assignment tool with exploded view

Rest-Period Climate Control Fuel Use Estimation

To estimate the fuel use of thermal load reduction technologies during rest-period climate control operation, a fuel use estimation process was developed in VTCab. A high-level overview of the developed process is shown in Figure IV-36 and includes the relationship between each step in the process and the associated type of energy evaluated or converted in the step. For national-level analysis, additional components are added to this fuel use estimation process and include national weather station selections, vehicle-miles-traveled (VMT)

weighting, as well as high-performance computing task distribution and results post-processing steps. Each subtask is described in the following sections.

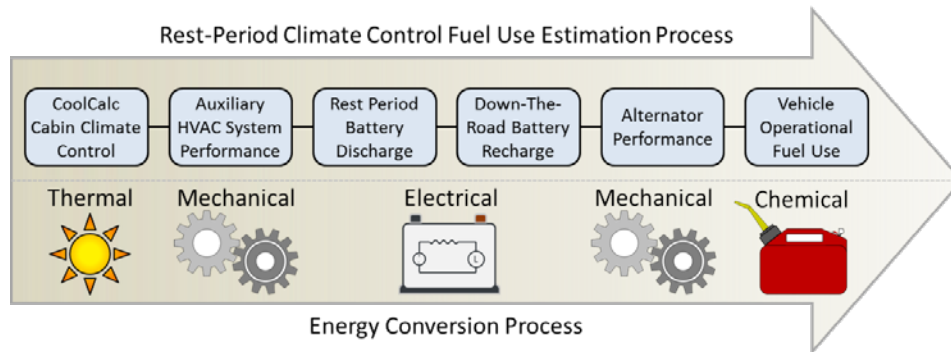


Figure IV-36: Relationship between the rest-period climate control fuel use estimation process and energy conversion

Weather Station Weighting by Truck VMT

The impact of thermal load-reduction technologies on long-haul trucks is dependent on weather conditions. The location and time of year, therefore, are important inputs for a VTCab thermal analysis. VTCab simulations use Typical Meteorological Year weather data to simulate vehicle thermal behavior at many different locations throughout the United States. The distribution of weather stations, however, is not correlated with the distribution of long-haul truck traffic throughout the United States. Thus, the simulation results from each weather station cannot be weighted equally when distilling results into a single, representative national-average value for a technology's impact on rest-period idling. For a national-level VTCab analysis, the results of simulations in different cities are weighted by the fraction of long-haul trucks operating in and around each of those cities. It is assumed that the geographic distribution of trucks during rest periods is proportional to the distribution of on-road truck traffic. Therefore, an analysis was performed to determine the relative importance of each weather station in the contiguous United States in terms of its proximity to long-haul truck traffic.

Truck traffic density data for long-haul trucks were available from the Freight Analysis Framework (FAF3) dataset [5]. The traffic data were uploaded into GIS software [6], which divided truck routes into small traffic segments with average number of trucks traveling the segment per day. The truck traffic data were imported into MATLAB for analysis. First, the data were filtered to remove unwanted segments: those pertaining to truck routes outside the contiguous United States and those containing zero truck traffic. The daily average VMT for each segment were calculated from the segment length and the average number of trucks traveling on that route per day. For each route segment, the distance to every weather station was calculated, the closest weather station was identified, and the VMT for the segment were allocated to the closest weather station. The total VMT for each weather station were calculated, and a VMT-weighting was determined for each weather station.

Weather Station Down-Selection

Not every weather station contributes significantly to the results of a national-level analysis because many of the stations represent a very small percentage of the national total VMT. To reduce the time required to run the national-level simulations and to process and analyze the results, it was necessary to reduce the number of weather stations used for the analysis. The goal was to identify a small subset of weather stations that were representative of the weather conditions experienced by the vast majority of the long-haul truck fleet.

Figure IV-37B shows the cumulative total of VMT per weather station, summed in order of decreasing station VMT. Over 50% of the national total VMT was accounted for by fewer than 20% of the weather stations, according to the initial VMT-weighting analysis. The top 200 weather stations comprised approximately 55% of the national total VMT. Two hundred stations were found to be a good balance between the need to retain good geographic distribution of stations with the need to reduce computation time.

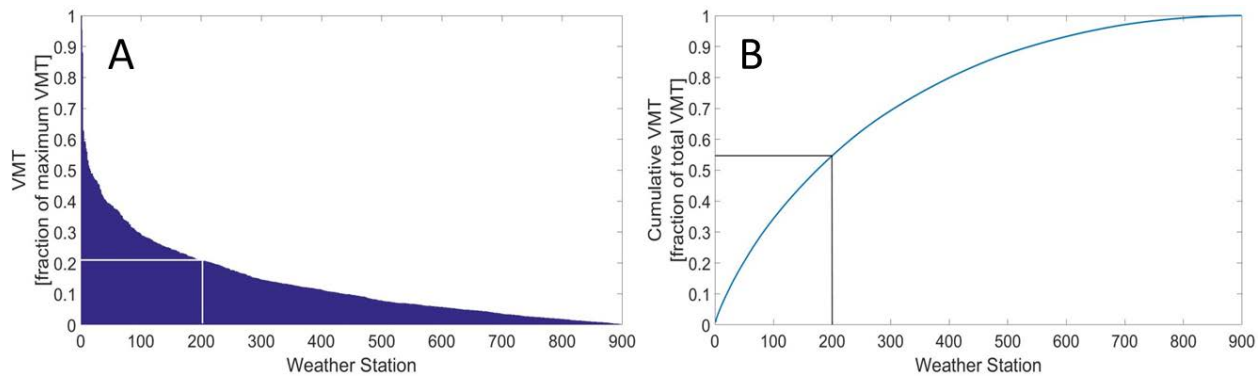


Figure IV-37: A (left), VMT per weather station; B (right), Cumulative total of VMT by weather station

An iterative process was developed to down select the list of weather stations. Beginning with the full set of approximately 900 stations (Figure IV-38A), the closest weather station was identified for every route segment. The VMT for each route segment were allocated to the closest weather station, the total VMT per weather station was calculated, and the stations were sorted by total VMT per station. The weather station that represented the fewest VMT was eliminated from the list and was not considered for the remainder of the analysis. For the next iteration, the closest weather station for every segment was again identified, now with one fewer station to choose from. The segment VMT were applied to the closest weather station and the total VMT per station was recalculated. In this way, the VMT that were originally applied to the eliminated station were reallocated to the next nearest weather station(s), conserving the number of total truck VMT across the United States. The iterative process was continued until only the desired number of weather stations remained. The 200 weather stations remaining in the list are shown in Figure IV-38B. VTCab simulations were performed using weather conditions for each of these stations, and the results were weighted by the final VMT weightings for each station.

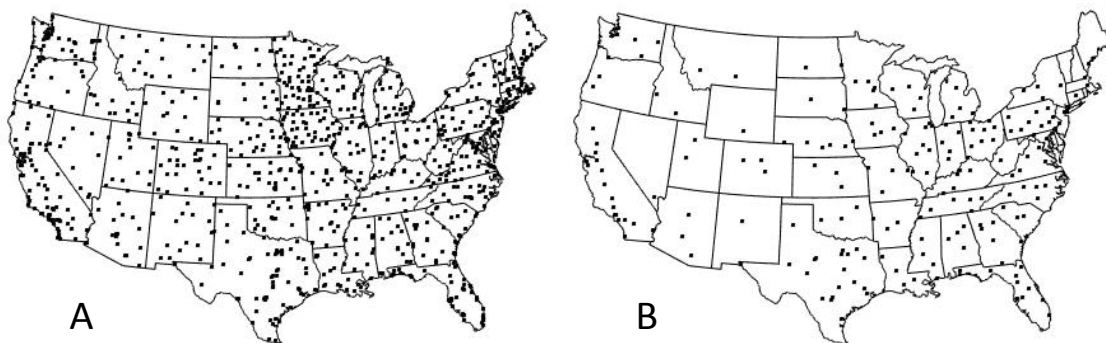


Figure IV-38: Map of weather station locations for A) all stations, and B) remaining top 200 stations

VTCab Cabin Climate Control

After the weather station weighting by VMT, a VTCab model of the vehicle cabin was created and validated with local experimental data. The vehicle cabin model contained the thermal load reduction package and the baseline package. An HVAC system was created for the sleeper compartment with heating and cooling target temperatures at 72°F and 65°F, respectively. A high-performance computer was used to perform an annual simulation at each of the 200 down-selected weather locations for both the complete cab and baseline model configurations. The primary outputs of the VTCab analysis were the time-dependent cooling and heating thermal power required to maintain the sleeper compartment target temperature throughout the entire year for each location. Once thermal load results were populated, the information was used to convert the thermal loads into HVAC system electric loads as described in the subsequent step.

Auxiliary Electric HVAC System Performance

To convert time-dependent thermal load results for both the complete cab package and the baseline configuration, a model of a generic example auxiliary electric A/C system was created using the CoolSim modeling tool previously developed [7]. Due to the large quantity of results obtained and the difference in run-time between VTCab and the HVAC system model, the A/C system performance was evaluated as a function of ambient temperature and flow rate of the evaporator blower. The A/C system was operated at each combination of ambient temperature and flow rate until steady-state operation was achieved. Once steady state was achieved, the corresponding thermal power demand of the evaporator and the system electrical power consumption were calculated. These were used to generate look-up tables of thermal load and system electrical power consumption as functions of ambient temperature and blower flow rate. The look-up tables were then used together to convert the thermal load and ambient temperature VTCab cabin model results into HVAC system electrical energy consumption at each time step. Maximum system coefficient of performance (COP) is at moderate blower speeds and lower ambient temperatures.

Rest-Period Battery Discharge

Once the auxiliary A/C system electrical energy consumption was calculated for each time interval, the fuel use estimation process used an internal resistance-based battery model in conjunction with a battery discharge algorithm to quantify the impact of the A/C system electrical energy consumption on the on-board battery pack for the vehicle. For the analysis, eight 104-Ah, 12-V group 31 absorbed-glass-mat (AGM) deep-cycle batteries were modeled as the battery pack for the vehicle based on capacity recommendations from the A/C system manufacturer. The battery model was written in the MATLAB programming environment, and the model type chosen was an internal resistance battery model adapted from ADVISOR [8] selected for its ability to accurately and simply model lead-acid type batteries. A process diagram describing the battery model function is provided in Figure IV-39A. For the battery discharge process, data over a 24-hour period of time for each configuration and location was selected. At the beginning of the 24-hour period, the battery pack was initialized to be fully charged. As the A/C system electrical energy was discharged over the 24-hour period, losses in the HVAC system inverter were included. The battery discharge process then proceeded by calculating the battery state of charge (SOC) throughout the day based on the A/C system energy consumption at each time interval. At the end of the 24-hour period, the final SOC of the batteries was saved for subsequent evaluation. If the loads for the 24-hour period fully depleted the batteries, a full depletion event was saved and the battery pack reinitialized to a full SOC for subsequent depletion. In this case, both a fully depleted and a partially depleted SOC for the 24-hour period were collected.

Down-The-Road Battery Recharge

After the discharge process was completed, each discharge event was then cycled through a recharge event. The battery recharge process utilized the same internal resistance battery model described for the discharge process. In addition to the battery model, a battery-charging algorithm was needed to accurately model the battery management system function for the battery pack. A three-phase charging algorithm was selected and included a bulk phase, absorb phase, and float phase. However, because the float phase maintains an existing charged battery, it was omitted in the analysis. Assuming adequate supply from the alternator, the bulk phase of the charging algorithm supplied 0.2 times the C-rate for the battery until the actual current consumption by the battery was reduced to below 90% of the supply current. Thereafter, for the absorb phase, the battery management system held the supply voltage at 14.9 V for a duration of 1.5 times the duration of the bulk phase. The charging algorithm was subjected to reduced supply capacity at any time interval if the alternator was unable to provide the necessary power. Due to the coupling of the battery recharge event to alternator and vehicle performance, recharging, vehicle accessory load calculation, and down-the-road fuel use estimations were performed simultaneously and are described in subsequent sections.

Alternator Performance

To supply the auxiliary A/C system battery pack with adequate power for recharging during down-the-road operation, a high-capacity engine alternator was modeled. For the model, the performance of a claw-pole brushed alternator was used, and the maximum current output of the alternator as a function of alternator speed in addition to the alternator efficiency as a function of current and speed were used for the analysis. The alternator was sized to have a 275-A rating to adequately charge the eight group 31 AGM deep-cycle batteries

over a typical long-haul driving period. The alternator efficiency as a function of alternator speed and supply current is provided in Figure IV-39B. To determine the alternator speed at a given engine speed, a pulley ratio of 2.5:1 was used. Finally, in addition to the energy needed for recharging the battery pack, additional electrical accessory loads on the alternator were included. The model included 0.35 kW of electrical accessory load on the alternator at all times to represent operation of additional electric components for the vehicle such as headlights and radio. The 0.35 kW was selected based on the U.S. Environmental Protection Agency (EPA) Greenhouse Gas Emissions Model (GEM) Model Class 8 combination tractor modeling parameters used for heavy-duty greenhouse gas emissions credits [9].

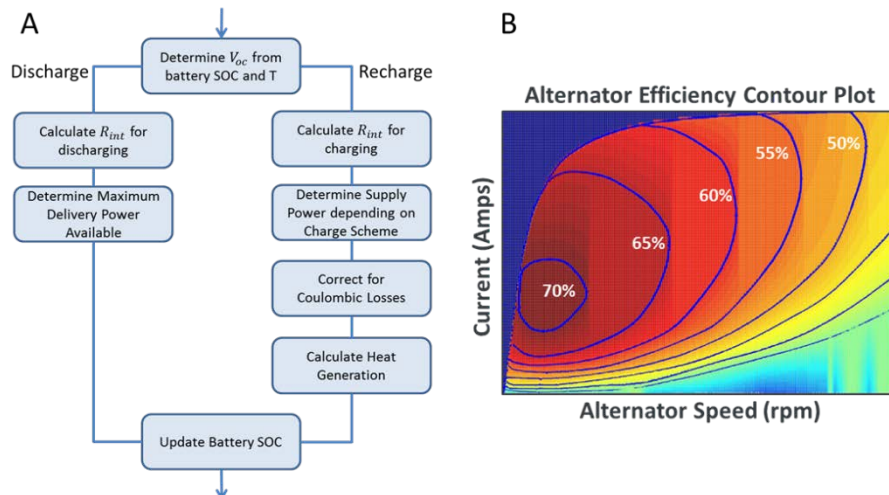


Figure IV-39: A. Process diagram for the internal resistance battery model used for the fuel use estimation process, B. Alternator efficiency as a function of speed and current for the fuel use estimation process

Vehicle Operational Fuel Use Estimation

In order to calculate the vehicle fuel use used during the down-the-road auxiliary A/C system battery recharge process, a vehicle model was needed. The vehicle model provided the link between mechanical accessory power demand of the alternator to the fuel used by the engine. For the fuel use estimation process, Autonomie was used for the vehicle model platform and a non-proprietary open-use Class 8 long-haul truck vehicle model developed by Oak Ridge National Laboratory was used. The vehicle model was modified to match the EPA GEM Model Class 8 combination tractor modeling parameters [9], and electrical accessory loads were disabled for the model. In addition, three Heavy Heavy-Duty Diesel Truck (HHDDT) schedule components were used: HHDDT 65 Cruise cycle, HHDDT Cruise cycle, and the HHDDT Transient cycle. The vehicle model was operated over a range of mechanical accessory loads, vehicle weights, and the three drive cycles. The average fuel consumption at each combination was quantified and was used to generate a fuel performance curve as a function of the input variables. It was determined that the impact of vehicle weight variation due to thermal load reduction technologies on cycle average fuel consumption was insignificant and therefore gross vehicle weight was held constant at 29,000 kg for the analysis.

A visual description of the beginning and end of a single recharge event is provided in Figure IV-40. The recharge process began by selecting a drive cycle and ending SOC from the rest-period discharge sequence. For each time interval in the recharge event, the charge current from the battery-charging algorithm was determined and added to the additional accessory electrical loads (i_{other}). The combined current demand was then used in conjunction with the cycle averaged engine speed to calculate the alternator efficiency. If the current demand exceeded the maximum current at the specified speed, only the maximum alternator current would be supplied. Next, the vehicle mechanical accessory power was calculated based on the current and bus voltage, in addition to the power regulator efficiency, alternator efficiency, and alternator-to-engine belt efficiency. The accessory power and drive cycle were then used as inputs to the vehicle performance map to determine the fuel use rate. In parallel, the process was repeated at each step without the battery charging electrical load and only accessory electrical loads. The difference between the fuel use with and without the battery charging at each time interval was calculated. The process was repeated for each time interval

throughout the recharge process, and the cumulative fuel use difference with and without battery charging was calculated. The entire recharge process was then repeated for each of the three drive cycles. Every ending SOC was saved from the rest-period discharge process. Once the drive cycle specific fuel use for each recharge event was calculated, cycle weighting fractions from the EPA GEM analysis transient cycles of 86% for the HHDDT 65 Cruise, 9% for the HHDDT Cruise, and 5% for the HHDDT [9] were applied to the result to determine a composite fuel use for each recharge event. Finally, the daily electrical HVAC load profile obtained early in the analysis was integrated, and the corresponding fuel use was used to generate a fuel use rate per electrical HVAC energy. This fuel use rate per electrical energy was then applied to the HVAC load profile for the day to generate an approximate fuel use at each time interval for use with additional post-processing tools.

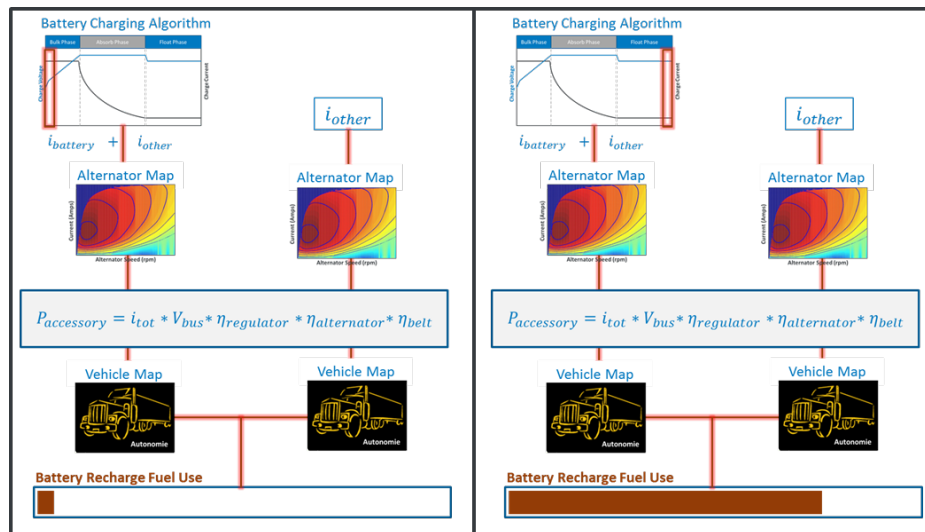


Figure IV-40: Auxiliary A/C system battery pack recharge process sequence for fuel use estimation. A (left), beginning of a recharge event; B (right), end of a recharge event (right).

Results—Comparison of Cases

Using VTCab, annual simulations were carried out for the 200 selected locations for unmodified (Standard) sleeper cab and a sleeper cab modified with a Complete-Cab Thermal Load Reduction Package (TLRP) and with a "no-idle" electric A/C unit. Initial assumptions were made for the fuel use analysis process, and several A/C cases were simulated.

VTCab simulation results showed that on a national scale, application of the TLRP reduced cooling thermal loads by up to 57%. With average annual COP of approximately 1.83, corresponding electrical loads were reduced by 46%, exceeding an initial goal of a 30% reduction in cooling loads. The benefits from reducing idle time and cooling loads due to application of these technologies are summarized in Table IV-38. The analysis was based on the following assumptions. The number of operational days for a long-haul truck with a rest period was assumed to be 260 annually. This assumption is on the conservative side of prior estimations of 250–300 days [10]. To be consistent with current rest period regulations, a 10-hour rest period within each 24 hours of operation was assumed. These 10 hours were assumed to be equally probable throughout each 24-hour period. This assumption could be replaced with a time-of-day probability when this information is available. Idling fuel consumption of a truck engine was assumed to be 0.8 gal/h [10]. It should be noted that this analysis assumes trucks idle only when there is an HVAC load. This is a conservative assumption since actual trucks will usually continue to idle before or after HVAC loads are zero, resulting in additional fuel consumption. The difference between this assumption and the maximum number of cooling hours (idling the full duration of rest periods on days whenever air conditioning is needed) is approximately 14%, which would result in additional 164 hour and 131.2 gallons of fuel saved for cooling. Table IV-38 summarizes different A/C scenarios for three different price points of diesel fuel.

Table IV-38: A/C national-level fuel use simulation result summary

Truck Configuration	Annual A/C On Time During Rest Periods [hour]	Fuel Use for Cooling During Rest Periods [Gal/year]	Diesel Fuel Price [\$/Gal]	Fuel Cost for Cooling During Rest Periods [\$/year]	Annual Savings in Fuel Costs	3 Year Savings in Fuel Costs
Standard Cab - idling *	989.6	791.7	\$ 2.50	\$ 1,979	\$ -	\$ -
Complete-Cab TLRP - idling	806.9	645.6		\$ 1,614	\$ 365	\$ 1,096
Standard Cab with electric A/C system		34.8		\$ 87	\$ 1,892	\$ 5,677
Complete-Cab TLRP with electric A/C system		17.4		\$ 44	\$ 1,936	\$ 5,807
* Rest period idling hours assume that idling only occurs when an HVAC load is present. If trucks are idled the full duration of rest periods (even after HVAC load goes to zero), then an additional 164 hours per year should be added to the "Annual A/C On Time". This would increase standard cab annual fuel use for cooling by 131.2 gal/year. At nominal diesel fuel price of \$3/gal this would provide an additional savings of \$393.60/year or \$1,180.80 in 3 years.			\$ 3.00	\$ 2,375	\$ -	\$ -
				\$ 1,937	\$ 438	\$ 1,315
				\$ 104	\$ 2,271	\$ 6,812
				\$ 52	\$ 2,323	\$ 6,968
			\$ 4.00	\$ 3,167	\$ -	\$ -
	\$ 2,582	\$ 584	\$ 1,753			
	\$ 139	\$ 3,028	\$ 9,083			
	\$ 70	\$ 3,097	\$ 9,291			

For the last five years (2010-2015) US national weekly average diesel fuel prices have fluctuated from \$2.48 to \$4.16 per gallon with an average price of \$3.58/gal [11]. As of October 15, 2015 the US national weekly average price for diesel fuel was \$2.56/gal. With the projected increase in diesel fuel price over the next year [11], \$3.00/gal nominal price was used in the following discussions.

1. Equipping a standard sleeper cab with TLRP

Based on the simulated results, installation of TLRP alone could significantly reduce truck idle time for cooling. The TRLP-reduced thermal load on the cab would translate into less time needed for running an engine to operate a mechanically driven, standard A/C unit of the truck. Preliminary analysis showed that with the price of diesel fuel at \$3.00/gal, annual savings of \$438 were possible, accumulating to \$1,315 in three years. At \$4.00/gal, the savings increase to \$584/year and \$1,753 for three years. Part of the TLRP is ultra-white paint with higher reflective properties than national average paint for reducing solar load. At certain locations with colder climates, this could negatively affect (increase) morning and evening heating loads of the cab, reducing the beneficial effect of the solar load for heating. This loss of solar heat should be offset by the total amount of heating load reduction due to increased insulation and reduced heat losses of the cab. Detailed studies of these effects will be carried out in the coming year, but due to significantly reduced overall heating loads, additional fuel savings benefits are expected when using fuel-fired heaters.

2. Equipping a standard sleeper cab with "no-idle" electric A/C system

Installation of an auxiliary electric battery-operated A/C unit in the standard cab resulted in elimination of cooling-related idling of the engine and associated fuel consumption during rest periods. Energy is needed, however, to recharge batteries for the A/C unit, which still requires some fuel. This was estimated using the methodology described above and modeling tools at 34.8 gal/year (\$104 to \$139/year at \$3 to \$4/gal diesel fuel prices, respectively). This resulted in significant savings ranging from \$6,812 at \$3/gal to \$9,083 at \$4/gal. Over a three-year period of operation, the initial aftermarket installed investment cost of a "no-idle" auxiliary A/C system, estimated at \$6,000, should be recovered.

3. Equipping a standard sleeper cab with TLRP and "no-idle" electric A/C system

Adding a TLRP to a standard cab equipped with a "no-idle" auxiliary A/C system reduces cooling loads, reducing the peak power and electric energy required for the auxiliary A/C system. This reduced fuel used for battery recharge down to 17.4 gal/year. This results in only \$52 to \$70 of annual fuel costs for recharging the A/C unit batteries. In addition to lowering operating costs, the electric A/C energy requirement to meet the 99% national daily maximum 10-hour window cooling loads drops from 9.2kWh for a Standard Cab to 4.7 kWh for Complete Cab TRLP solution (see Figure IV-41A).

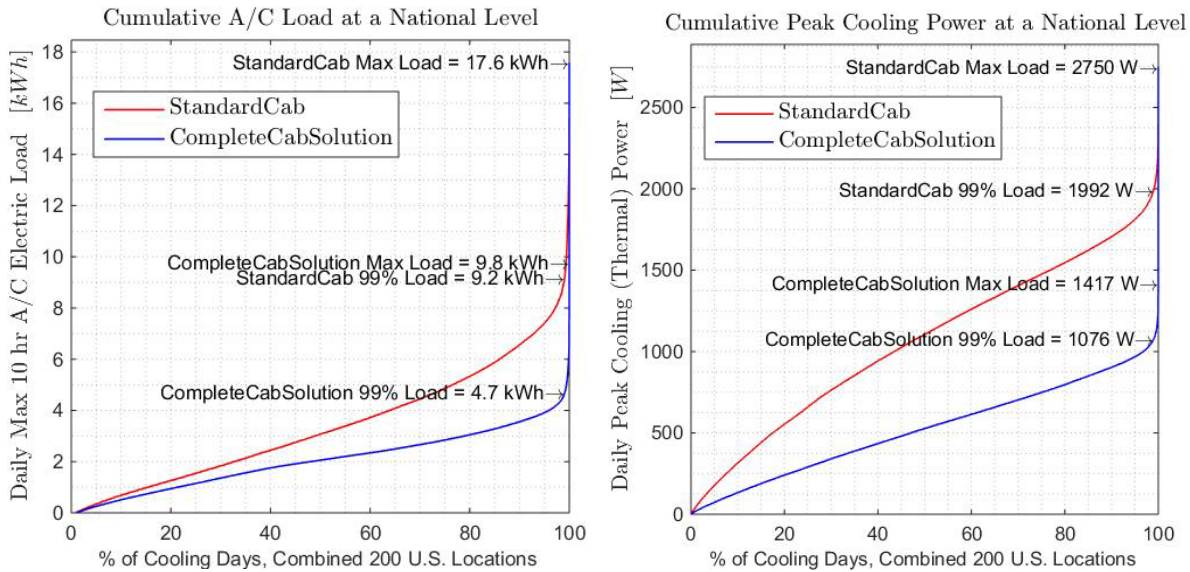


Figure IV-41: A (left), daily maximum 10-hr window A/C electric loads (left) B (right), daily peak cooling power for combined cooling loads of 200 US locations

Lowering the A/C energy requirement reduces the battery size requirement which provides significant additional cost savings and incentive for the auxiliary A/C system installation. Assuming an inverter efficiency of 90%, a 9.2-kWh A/C electrical load for a Standard Cab would need at least eight 104-Ah (≈ 1.25 kWh) batteries. A cab with TLRP would require approximately four units to meet 4.7 kWh of A/C electrical load. Assuming that during a three-year period of use, the pack of batteries has to be replaced once, the cost savings could add up to \$1,400 (see Table IV-39).

Table IV-39: Battery sizing impacts of TLRP

"No-Idle" Electric A/C System Configuration	Number of 104 Ah (1248 Whr @ 12V) Batteries	Cost per Battery	Initial Cost Reduction of Electric A/C System	Number of Replacements During 3-year Period	Battery Replacement Cost During 3-year Period	Savings During 3-year Period
Standard electric A/C system	8	\$ 175	\$ -	1	\$ 1,400	\$ -
Electric A/C system with reduced battery pack	4	\$ 700	\$ 700	1	\$ 700	\$ 1,400

Reduction in peak cooling power demand from 1,992 W, meeting 99% of peak cooling days for a Standard Cab (see Figure IV-41B), to 1,076 W for a TLRP-equipped cab would also allow a smaller and potentially cheaper auxiliary A/C unit. This, again, would provide potential cost savings.

Alternatively, if the A/C unit or the standard battery pack size for the auxiliary A/C system is kept unchanged, it would provide essentially 100% coverage of cooling days for a cab with TLRP, improving the unit's high-load handling capability and reducing operator anxiety regarding its performance for prolonged operation.

Conclusions

NREL's HVAC load estimation software, VTCab, was used to model long-haul truck rest-period thermal load reduction technologies at a national level. A fuel use estimation process was developed to combine these thermal loads with an A/C system performance model to calculate required electrical loads. These electrical loads were then coupled with a vehicle model to determine fuel use impacts from the battery charging. A methodology was developed to calculate long-haul truck VMT weightings for each weather station. This information was then used to perform an elimination process to identify the 200 most representative weather stations and their weightings based on long-haul truck traffic. Preliminary analysis performed using these tools showed that adding a thermal load reduction technology package and auxiliary electric A/C system to a standard cab could save up to 774 gallons of fuel annually per truck. At a diesel fuel price of \$3/gal, this fuel

savings translates into \$6,968 over the first three years of operation. In addition to fuel savings, the thermal load reduction package lowers HVAC battery energy requirements to meet the 99% cooling day by about half, thus requiring fewer batteries. This combined with the reduced peak power demands could allow for reduced size and improved performance of a "no-idle" A/C system. Additional benefits are also expected for fuel-fired heater performance, which is currently being investigated. Consequently, thermal load reduction technologies could reduce the initial investment cost and cost of ownership, enabling broader adoption of such systems.

IV.5.C. Products

Presentations/Publications/Patents

1. Lustbader, J.; Kreutzer, C.; Adelman, S.; Yeakel, S.; Zehme, J. "Sleeper Cab Climate Control Load Reduction for Long-Haul Truck Rest Period Idling." SAE World Congress, April 14, 2015.
2. Lustbader, J.; Kreutzer, C.; Jeffers, M.; Adelman, S.; Yeakel, S.; Zehme, J.; Brontz, P.; Kopetz, C.; Ohlinger, J. "Complete Cab Thermal Load Reduction Package for Long-Haul Truck Rest Period Idling." SAE Thermal Management Systems Symposium, Sept. 30, 2015.
3. Lustbader, J.; Kreutzer, C.; Jeffers, M.; Tomerlin, J.; Langewisch, R.; Kincade, K. "CoolCab Test and Evaluation & CoolCalc HVAC Tool Development." DOE Annual Merit Review, June 10, 2015; VSS075.
4. VTCab rapid HVAC load estimation tool beta version. Only available to industry and laboratory partners at this time.

IV.5.D. References

1. Gaines, L.; Vyas, A.; Anderson, J. "Estimation of Fuel Use by Idling Commercial Trucks." 85th Annual Meeting of the Transportation Research Board, Washington, D.C., Jan. 22–26, 2006; Paper No. 06-2567.
2. Roeth, M.; Kircher, D.; Smith, J.; Swim, R. "Barriers to the Increased Adoption of Fuel Efficiency Technologies in the North American On-Road Freight Sector." Report for the International Council for Clean Transportation. NACFE. July 2013.
3. Lustbader, J.; Kreutzer, C.; Adelman, S.; Yeakel, S.; Brontz, P.; Olson, K.; Ohlinger, J. "Impact of Paint Color on Rest Period Climate Control Loads in Long-Haul Trucks." SAE World Congress, April 8, 2014.
4. Rugh, J.; Jeffers, M; Chaney, L. "Electric Drive Vehicle Climate Control Load Reduction." DOE Annual Report. 2015.
5. http://ops.fhwa.dot.gov/freight/freight_analysis/faf/index.htm accessed on 9/15/2015
6. <http://grass.osgeo.org/> or QGIS Brighton 2.6
7. Kiss, T.; Lustbader, J. "Comparison of the Accuracy and Speed of Transient Mobile A/C System Simulation Models." SAE International Journal of Passenger Cars—Mechanical Systems (7), August 2014; pp. 739–754; doi:10.4271/2014-01-0669.
8. Johnson, V. "Battery Performance Models in ADVISOR." Journal of Power Sources, 2002, v. 110, pp. 321–329.
9. U.S. Environmental Protection Agency. "Greenhouse Gas Emissions Model (GEM) User Guide." EPA-420-B-11-019. August 2011. epa.gov/otaq/climate/documents/420b11019.pdf
10. Lim, H. "Study of Exhaust Emissions from Idling Heavy-Duty Diesel Trucks and Commercially Available Idle-Reducing Devices." U.S. Environmental Protection Agency. EPA420-R-02-025, October 2002.
11. U.S. Energy Information Administration. "U.S. Gasoline and Diesel Retail Prices." Release Date: 10/13/2015. eia.gov/petroleum/data.cfm#prices

IV.6. ACEC Technology Analysis and Evaluation

Zhiming Gao (PI), Scott Curran, David Smith, Stuart Daw, Principal Investigators

Oak Ridge National Laboratory (ORNL)
2360 Cherahala Boulevard
Knoxville, TN 37932-6472
Phone: (865) 946-1339; Fax: (865) 946-1354
E-mail: gaoz@ornl.gov

David Anderson and Lee Slezak, DOE Program Managers

Vehicle Technologies Office, EERE, DOE
Phone: (202) 287-5688, (202) 586-2335
E-mail: david.anderson@ee.doe.gov, lee.slezak@ee.doe.gov

Start Date: October 1, 2014
End Date: September 30, 2015

IV.6.A. Abstract

Objectives

- Evaluate the merits and barriers of advanced light-duty (LD) vehicles equipped with high efficiency clean combustion engine powertrains, leading-edge catalysts, and renewable fuels over realistic driving conditions.
- Support DOE advanced combustion engine (ACE) fuel and lubricant technologies (FLT), and vehicle systems(VS) R&D programs in leveraging activities that will assist U.S. automakers to meet 2025 fuel economy standards and EPA Tier III emissions regulations.

Accomplishments

- Supported completion of the DOE advanced combustion and emission control (ACEC) R&D program's FY15 JOULE milestone, demonstrating 30% gasoline equivalent fuel economy improvement.
- Evaluated the impacts of RCCI fueling strategies, including diverse combinations of conventional and renewable fuels, on LD drive-cycle engine efficiency and emissions in conventional and hybrid vehicles.
- Updated, refined and validated our 1D diesel oxidation catalyst (DOC) model capable of accurately simulating carbon monoxide (CO), unburned hydrocarbons (HC), and nitrogen oxides (NO_x) oxidation for conventional diesel combustion (CDC) and RCCI exhausts.
- Explored LD vehicle engine efficiency and RCCI HC and CO emissions control that can be realized by using a combination of a conventional DOC catalyst and a proactive RCCI control strategy that manages CDC/RCCI switching and regulates exhaust temperature.
- Published the results of drive cycle simulations for various high efficiency combustion technologies on fuel economy and exhaust properties in LD vehicles (Applied Energy, 2015).

Future Achievements

- Continue refining and updating RCCI performance maps for evaluations of fuel efficiency and emissions control of RCCI-enabled engines used in conventional and hybrid vehicles.
- Assess emission control technologies that operate at low temperatures (<150°C) as a means to enable fuel-efficient engines with low exhaust temperatures to meet current and future emission regulations.

- Develop high-fidelity predictive vehicle engine models by describing the behavior of detailed engine subsystems that yield precise evaluations of engine transient behavior
- Coordinate closely with the USDRIVE ACEC tech team, DOE ACE/FLT/VS R&D programs, and CLEERS to ensure access to the latest engine combustion, emissions control, and alternative fuels technology information in order to best address industry needs.



IV.6.B. Technical Discussion

Background

To meet 2025 Corporate Average Fuel Economy (CAFE) standards, EPA Tier III emissions regulations and the Renewable Fuel Standard (RFS), the integrated technologies of high-efficiency clean combustion engines, leading-edge catalysts and renewable fuels will become particularly important. High efficiency clean combustion engine technologies, such as RCCI, provide a high engine thermal efficiency while dramatically lowering engine-out NO_x and particulate matter (PM) emissions. Renewable fuels, including high-octane ethanol blends, can help to increase thermal efficiency and enable engine downsizing while extending the high efficiency clean combustion operating range. However, these combustion approaches inherently lead to a significantly lower exhaust temperature (typically <150°C), while the engine-out CO and HC emissions are increased considerably. Innovative aftertreatment devices become a necessity since the performance of conventional aftertreatment systems becomes inadequate in such a cool exhaust stream. In this project, we developed and applied models for the engine, aftertreatment system, and other components to evaluate high efficiency engines, leading-edge catalysts, and renewable fuels in diverse vehicle configurations and evaluated their performance in realistic driving conditions. Our overall goal is to provide comprehensive vehicle system simulations that support DOE R&D efforts in evaluating and identifying innovative technologies and leverage activities that will assist U.S. automakers in meeting future fuel economy standards and emissions regulations. The models and simulations rely on measurements from multiple facilities at ORNL, and can be implemented directly in simulation platforms such as Autonomie. These models also provide guidance to experimental teams in targeting future measurements. This close interaction between simulation and experiments provides DOE with the best possible basis for identifying promising vehicle technologies that maximize energy efficiency and minimizing any negative environmental impacts from transportation.

Introduction

In FY15, we continued to collaborate with partners at ORNL and DOE ACE R&D programs to evaluate and identify the impacts of multiple RCCIs on fuel economy and emissions from conventional and hybrid vehicles using vehicle system simulations. We concentrated our efforts this year on the following research topics:

- Development of new engine maps for a 1.9-L GM engine with updated piston component that are intended to enable steady-state and transient mixed-mode operation between CDC and dual-fuel RCCI with a fueling strategy for UTG96 gasoline and ultra-low sulfur diesel (ULSD).
- Developed stoichiometric E10 engine maps for a Ford EcoBoost 1.6L GTDI 4-cylinder engine with a turbocharger, direct injection, dual variable cam timing and with a 10.1:1 compression ratio.
- Achieved the DOE ACEC R&D program's FY15 JOULE milestone by demonstrating a 30% gasoline equivalent fuel economy improvement in the latest RCCI-enabled GM engine, as compared to a 2009 PFI gasoline baseline engine in a mid-size sedan.
- Evaluated the impact of several RCCI fueling strategies, including (i) biodiesel and gasoline; (ii) E30 and diesel; and (iii) gasoline and diesel, on light-duty engine efficiency and emissions in conventional and hybrid vehicles for multiple types of drive cycles.
- Updated, refined and validated a 1D DOC model that employs a new global kinetic reaction mechanism to accurately account for steady-state and transient CO, HC, and NO_x oxidation. The

model was used for analysis of CDC and RCCI exhausts during cold starts and the transition to mixed-mode operation.

- Exploration of more sophisticated RCCI utilization strategies that manage CDC/RCCI switches and regulate exhaust temperature to significantly improve the performance of conventional diesel oxidation catalysts in removing CO and HC from RCCI exhaust during transient drive cycles.

Approach

Evaluating the fuel economy and emissions benefits of high efficiency clean combustion engine technologies requires computationally efficient and physically accurate models for different types of engines and aftertreatment devices. Our transient engine models adopt a coarse representation of the internal engine heat transfer and use simplifying assumptions about how engine-out emissions species change as the engine heats up. The transient exhaust properties in the model are predicted from steady-state or pseudo-steady-state engine data by applying dynamic first-order correction terms and empirical parameters to account for the inherent thermal and combustion lags in the engine as it shifts from one operating state to another. We also adopt physics- and chemistry-based computational models for lean and stoichiometric exhaust emissions control devices including DOC, LNT, DPF, selective catalytic reduction (SCR), and passive hydrocarbon traps. These models incorporate 1-D differential transient mass and energy balances with global reaction kinetics and heat and mass transport information to simulate the performance of each aftertreatment component. The integration of the engine and separate aftertreatment models enables calculation of the instantaneous properties of the exhaust stream as it flows from the engine and through each aftertreatment component during a complete drive cycle. The ORNL engine and aftertreatment models, together with other critical component models, are integrated into Autonomie, developed by Argonne National Laboratory (ANL). These comprehensive vehicle powertrain, emissions and fuel economy models are used to explore the impact of low-temperature combustion strategies, innovative aftertreatment devices, and renewable fuels technologies in different vehicle powertrain configurations, including hybrids.

Results

Engine mapping

We continued collaborations with the DOE ACE R&D program to construct new RCCI-enabled engine maps using ORNL dynamometer measurements completed in FY15 for a GM 1.9-L engine updated with a new piston design. The low- and high-reactivity fuels used in the RCCI fuel strategy were conventional gasoline and diesel. Figure IV-42(a) shows a detailed engine map showing the steady-state engine efficiency. Compared to our previous RCCI maps generated in FY12-FY14, the range of RCCI operation for the FY15 engine is significantly reduced, particularly at high loads. However, compared to CDC, this RCCI strategy still increases net engine efficiency by 4-7% in the RCCI-enabled regime and reduces exhaust temperatures by 55-130°C. We also utilized ORNL engine dynamometer measurements to construct engine maps for a Ford EcoBoost 1.6L stoichiometric GTDI engine which is a turbocharged gasoline direct injection engine with dual variable cam timing and a compression ratio of 10.1:1. The engine is designed for the Ford Fusion and Escape. Figure IV-42(b) shows the steady-state engine efficiency while operating with E10 fuel

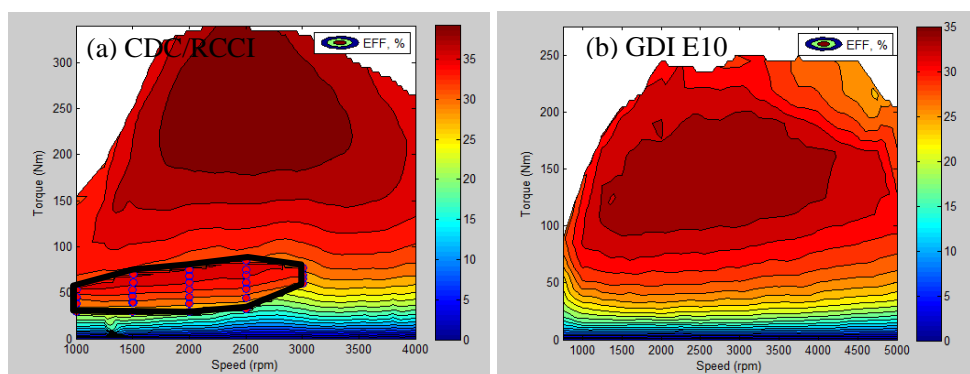


Figure IV-42: Example of steady-state engine maps for the GM 1.9L engine with the RCCI-enabled zone highlighted (a) and for the 1.6L GTDI stoichiometric engine, (b) the pink marks in Figure IV-42(a) indicate measured RCCI operating conditions.

The new RCCI-enabled engine maps were utilized to simulate and compare the fuel economy of a mid-size sedan equipped with the RCCI engine to designs with conventional PFI gasoline, stoichiometric GDI, and diesel engines for city and highway driving. The vehicle configuration was based on the 2014 Chevrolet Cruze conventional powertrain. This activity supported the DOE ACE R&D program's FY15 JOULE milestone to demonstrate the benefits of RCCI-enabled engines over several 2009 engine designs: a conventional 2.7L PFI gasoline engine, 1.6L stoichiometric GTDI E10, and a 2.0L DI diesel engine. Our results indicate that implementation of RCCI can improve gasoline equivalent fuel economy by around 15% relative to the GDI engine. Compared to the 2.7L PFI gasoline operation, utilization of RCCI can boost fuel economy by nearly 30%, consistent with the DOE FY 2015 JOULE milestone.

Aftertreatment modeling

We developed and refined our DOC model using CDC and RCCI CO/HC oxidation data measured on the GM 1.9-L turbocharged diesel engine equipped with a 1.2-L high-Pt DOC catalyst provided by EmeraChem. The DOC model accounts for CO/HC/NO oxidations with a single-step global kinetic mechanism, where HC emissions are assumed to consist of C₃H₆ and C₃H₈. The model was initially established from test data measured in the DOC with the GM engine operating in CDC mode. The kinetic reaction rates were optimized using Matlab optimization functions for each DOC performance at 1500rpm and 3000rpm operations. The model was then refined and updated with RCCI operation data to account for the RCCI exhaust emissions control. The measured RCCI data set includes only six points but covers an exhaust temperature range of 185–300 °C and engine speed from 1500 to 2300 rpm. Figure IV-43 shows a comparison of predicted CO emissions with experimental measurements associated with CDC and RCCI exhausts. In general, the DOC model is capable of predicting CO and HC oxidation reduction for both CDC and RCCI regimes with reasonably accuracy. For the updated DOC model, we found that the limited RCCI operation data set does not adequately cover the entire RCCI operation regime, thus we need to work closely with the ORNL-FEERC experimental teams to obtain additional data to improve the DOC model in the future. The DOC model has also been used to explore sophisticated RCCI utilization strategies that manage CDC/RCCI switches via regulating exhaust temperature. These strategies improve the performance of conventional diesel oxidation catalysts in removing CO and HC from the RCCI exhaust.

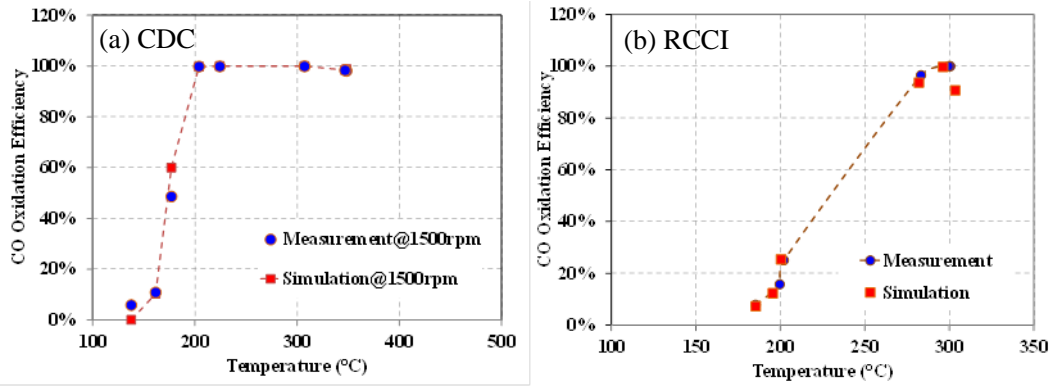


Figure IV-43: Example comparison of the simulated and measured DOC oxidation efficiencies of CO emissions in the CDC and RCCI exhaust stream as a function of exhaust temperature.

Fuel economy simulations

The most common fuel combination for RCCI is a blend consisting of conventional gasoline and diesel. Alternative fueling strategies that use a blend of ethanol and gasoline and/or replace conventional diesel with biodiesel blends have been used to increase the span of the RCCI reactivity gradient through reducing port fuel reactivity. To compare the benefits and challenges of these strategies on energy efficiency and emissions control, we simulated the light-duty drive cycle performance, based on the GM 1.9L engine at ORNL, of three types of RCCI implementation with blends of B20/gasoline, Diesel/E30 and Diesel/gasoline. B20 consists of 20% biodiesel and 80% 2007 certification ultra-low sulfur diesel; and E30 was splash blended with 30% anhydrous ethanol and 70% 87 AKI gasoline. The simulated conventional and hybrid powertrains were based on a conventional 2012 Ford Fusion and a 2010 Ford Fusion hybrid with a power-split planetary gear, respectively. The example result shown in Figure IV-44 indicates that the engine efficiencies of the simulated RCCIs are higher than or close to those of the CDC. Renewable fuels enable extending the RCCI operation regime and enhancing the engine efficiency over the driving cycles, which makes RCCIs containing E30 and B20 better than the non-renewable implementations. However, although the fuel economy results for RCCIs are substantially higher than PFI, they show little or no benefit in fuel economy over CDC. Significant consumption of the low-reactivity fuel in RCCIs offsets the actual fuel economies because of its lower energy density compared to diesel. Consequently, fuel energy density differences related to different RCCI fuel combinations need to be wisely considered in reporting fuel economy for RCCIs.

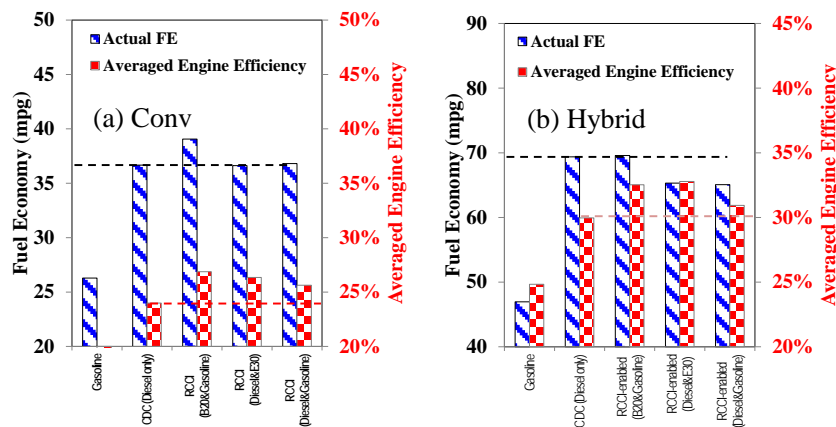


Figure IV-44: Comparison of fuel economies and engine efficiencies between CDC and different RCCI fueling strategies in the simulated vehicles over a UDDS drive cycle.

In addition, we utilized the 2015 RCCI engine maps for 1.9-L GM engines with updated piston components to carry out fuel economy simulations of the new RCCI operations and compare to other engine combustion modes, in support of the DOE ACEC R&D program’s FY15 JOULE milestone. The brief results have been summarized in the section of engine mapping.

Emissions simulations

RCCI exhaust temperatures are typically below 200°C during a considerable portion of city driving. Moreover, RCCI produces significant higher CO and HC emissions. The combination of higher CO and HC engine-out emissions poses difficulty in the oxidation of CO and HC in the aftertreatment system and typically shifts HC “light-off” temperatures from ~200°C up to ~250°C. Our simulations indicate that the majority of these CO/HC emissions are produced between 160-240 °C. Besides developing low-temperature aftertreatment catalysts, it is important to develop RCCI operation strategies for managing CO and HC emissions as well as engine exhaust and catalyst temperature. We explored a proactive RCCI control strategy. Briefly, the conventional DOC temperature is monitored in the strategy; the engine has to switch from RCCI to CDC during the normal RCCI operating regime once the DOC temperature is below 250 °C; the engine keeps running in CDC mode until exhaust temperature returns above 250 °C, then the engine reverts to RCCI if the engine operation is within the appropriate RCCI regime. Figure IV-45 shows that the strategy significantly shifts low-temperature engine-out CO and HC emissions to a more reasonable (higher) exhaust temperature environment, closely matching conventional DOC performance.

Moreover, this proactive RCCI control strategy allows a significant improvement of conventional DOC on RCCI CO and HC emissions reduction. Figure IV-46(a) and Figure IV-46(b) show that the proposed strategy reduces the DOC-out CO and HC emissions from RCCI significantly, although it still results in a slightly higher CO and HC emissions compared to CDC. On the other hand, the strategy generates slightly higher NOx emissions than RCCI without the proactive control strategy (see Figure IV-46(c)), but NOx emissions of the former are still considerably less than CDC. In the simulations, the DOC-out NOx emission, in units of g/mile, is slightly higher than the engine-out NOx, due to the mechanism of NO oxidization to NO2 which increases NOx mass flow rate. However, the simulation results also demonstrate that the strategy reduces CO and HC emissions with a mild penalty on engine efficiency. Figure IV-46(d) shows the impact of the proactive RCCI control strategy on engine efficiency. Although there is a slightly penalty of engine efficiency relative to the control strategy, the controlled RCCI still achieves better energy efficiency than CDC alone. Thus the tradeoff between the benefits of RCCI CO/HC emissions reduction and the penalty on energy efficiency deserves further study in the future.

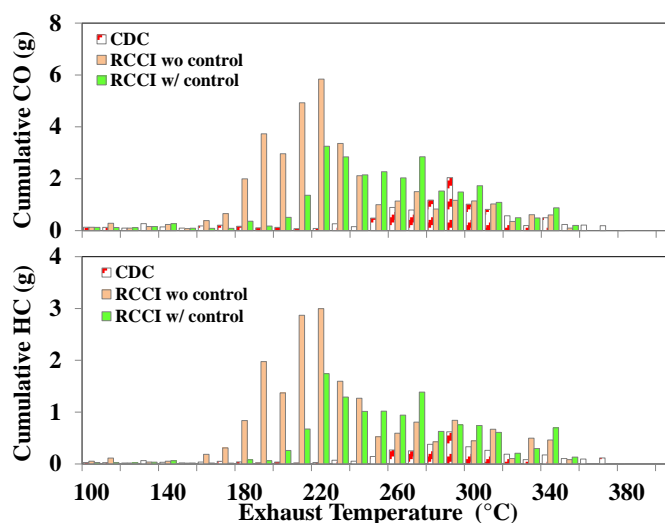


Figure IV-45: Effect of the proactively RCCI control strategy on cumulative engine-out CO/HC emissions as a function of exhaust temperature in the hybrid vehicles over the cold-start FTP cycle. The RCCI fueling strategy is a combination of conventional diesel and gasoline.

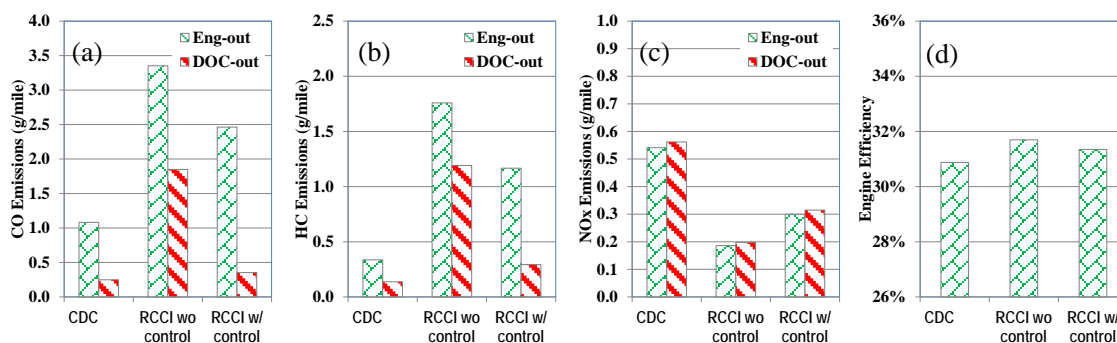


Figure IV-46: Effect of the proactive RCCI control strategy on engine efficiency and cumulative CO/HC emissions in hybrid vehicles with DOC, over the cold-start FTP cycle. The RCCI fueling strategy is a combination of conventional diesel and gasoline.

Conclusions

Two sets of new engine maps were constructed for 1.9-L GM engines enabled with mixed-mode operation between CDC and RCCI and for a Ford EcoBoost 1.6L gasoline turbocharged direct injection engine. Simulation results indicate that this RCCI implementation can improve gasoline equivalent fuel economy by around 15% relative to the GDI engine. Compared to our previous 2.7L PFI gasoline operation, utilization of RCCI can boost fuel economy by nearly 30%, which is consistent with the DOE FY15 JOULE milestone.

Comparison of various RCCI fueling strategies was also carried out in conventional and hybrid vehicles. The simulated RCCI fueling strategies include the combination of biodiesel and gasoline, E30 and diesel, and gasoline and diesel. Renewable fuels, such as E30 and B20, are capable of extending the RCCI operating regime and enhancing engine efficiency over city and highway driving cycles. The results also indicate that actual fuel economies of RCCIs are substantially higher than PFI gasoline, but differ little from CDC fuel economy levels. Significant consumption of low-reactivity fuels in RCCIs offsets actual fuel economies because of their lower energy density compared to diesel.

A 1D DOC model that uses a new global kinetic reaction mechanism was developed, refined and validated. The model accounts for CO, HC, and NO_x oxidation for CDC and RCCI exhausts during cold start and the transition to mixed-mode operation and has been used in exploring sophisticated RCCI utilization strategies. The simulated results show that RCCI utilization strategies that manage CDC/RCCI switches via regulating exhaust temperature could significantly improve the performance of conventional diesel oxidation catalysts in removing CO and HC from RCCI exhaust during transient drive cycles.

IV.6.C. Products

Presentations/Publications/Patents

1. Z. Gao, et al., Comparison of three RCCI fueling strategies on light-duty drive-cycle engine efficiency and emissions, *Fuel* (Journal), in preparation.
2. Z. Gao, S. Curran, J.E. Parks, D.E. Smith, R.M. Wagner, C.S. Daw, K.D. Edwards, J.F. Thomas, Drive cycle simulation of high efficiency combustions on fuel economy and exhaust properties in light-duty vehicles. *Applied Energy* (Journal), in press (invited).
3. S. Curran, Z. Gao, R.M. Wagner, Reactivity-controlled compression ignition drive cycle emissions and fuel economy estimations using vehicle system simulations, *International Journal of Engine Research* (Journal), in press.
4. Z. Gao, S. Curran, C.S. Daw, D.E. Smith, J.E. Parks, Comparison of the simulated light-duty drive-cycle fuel economy and engine exhaust properties for three different RCCI fuel combinations, 9th US Combustion Meeting, May 2015.

5. S. Curran, Z. Gao (PI), D.E. Smith, C.S. Daw, Impacts of Advanced Combustion Engines, 2015 U.S. DOE Hydrogen Program and Vehicle Technologies Program Annual Merit Review and Peer Evaluation Meeting, June 9, 2015.
6. Z. Gao, S. Curran, C.S. Daw, ACEC Technology Analysis and Evaluation, 2014 Annual Report, DOE Vehicle Technologies office, October, 2014.

IV.6.D. References

1. NA

IV.7. Technology Requirements and Evaluations for High Power Applications of Wireless Power Transfer

Omer C. Onar, Principal Investigator and Perry T. Jones, Project Manager

Oak Ridge National Laboratory
 Power Electronics and Electric Machinery Group
 National Transportation Research Center
 2360 Cherahala Boulevard
 Knoxville, TN 37932
 Phone: (865) 946-1351 and (865) 946-1772
 Fax: (865) 946-1262 and (865) 946-1568
 E-mail: onaroc@ornl.gov and jonespt@ornl.gov

Lee Slezak and David Anderson, DOE Program Managers

Vehicle Systems Program, Vehicle Technologies Office
 Phone: (202) 586-2335; (202) 287-5688
 E-mail: Lee.Slezak@ee.doe.gov and David.Anderson@ee.doe.gov

Start Date: October 2014

End Date: October 2015

IV.7.A. Abstract

Near-field electromagnetic resonant induction based wireless power transfer systems have achieved great developments in recent years for charging portable electronics, medical devices, home and industrial devices, and electric vehicles. Currently, for electric vehicles, most of developments are designed for 3.3kW power levels and only very few applications can demonstrate >10kW power transfer rate. For heavy duty vehicles including fleet and cargo trucks and shuttles, a minimum 30-80kW would be required for reasonable charging times. For larger busses and semi-trucks, >100kW power transfer rate is typically desired.

For high power applications important challenges remain for areas in electromagnetic coupler architecture and design, high power – power electronic converter (inverter and rectifier) design, and the thermal management for both the coupler and the power electronics. The other significant challenge is the greater airgaps that is likely to occur for a wireless power transfer (WPT) deployment in heavy duty vehicles that results in lower coupling factor, lower mutual inductance, reduced efficiency, higher field emissions, and higher reactive power burden on the high frequency power inverter required for magnetizing the mutual inductance branch.

Although high power WPT systems have been investigated recently, there is limited literature work that has focused on the design methodology of the high power WPT system with high efficiency, low fringe field emissions, and low flux density. This project reviews the existing literature, addresses the limitations, and provides preliminary simulation results.

Objectives

- Advance technology maturity; identify commercialization, standardization and safety of high power wireless charging technology.
- Address barriers, technical challenges, issues, and risks with the detailed technology analysis, evaluation, and design.
- Support J2954/2 Bus and Heavy Duty Wireless Charging Standards Development Taskforce with development, test data, experimental lessons learned, and design experience.
- Identify limitations and design a high power wireless power transfer components meeting heavy duty vehicle expectations of overall WPT technical targets.
- Design, model, and simulate system architecture after initial analysis and evaluations.

- Build test bench-top system for future integration to a medium-duty (MD) application in collaboration with partner(s).

Accomplishments

- Existing power electronics architectures and magnetic coupling technologies have been reviewed and their advantages, drawbacks, and limitations have been identified,
- High power wireless power transfer system methods identified and example systems modeled - ongoing and future focused standards support,
- Design and operation challenges addressed through modeling and simulations,
- Safety and protection systems in hardware and software have been developed to protect the equipment and people operating the system in the case of a fault or if an over-voltage, over-current, short-circuit, or over-temperature event occurs,
- The integration requirements of different vehicles in terms of voltage range, current range, power level, ramp rates, ripple restrictions, and other on-board charging (OBC) and energy storage systems (ESS) requirements have been identified and provided solutions for.

Future Achievements

- Design and build high power wireless power transfer components meeting heavy-duty (HD) vehicle expectations of overall WPT technical targets.
- Build test bench-top system for future integration to an MD application in collaboration with partner(s).
- Integrate the technology into a heavy duty vehicle with high power charge capability.



IV.7.B. Technical Discussion

Background

Currently, big rigs, delivery vans, and other medium and heavy-duty trucks account for 7% of all the vehicles in the United States. However, they consume more than 25% of the oil. At the same time, there is a lot of room for improvement in the fuel economy of a standard bus or truck. For instance, most commuter busses operate at 4-6 miles per gallon (MGP) fuel economy rate. In addition, they have considerable higher fuel consumption which would result in more petroleum displacement if electrified. These vehicles also have much higher average fleet emissions and they idle more than passenger vehicles. The large volume of fuel used by these vehicles represents a great opportunity for tremendous reductions in fuel consumption. Moreover, these vehicles need very heavy and expensive battery packs with high power rating and high energy storage capacity. On the other hand, these vehicles often operate on a known route; therefore, installation locations, power ratings, and infrastructure use is predictable. With quasi dynamic or opportunistic charge of these vehicles, the size and the cost of the battery packs can be significantly reduced.

Furthermore, for heavy duty vehicles, particularly for rapid transit and metro systems, the infrastructure is usually un-inspiring and aesthetically acceptable in modern cities. Examples of these systems powered by wires are given in Figure IV-47.



Figure IV-47: Examples of infrastructure powering transit systems by wires.

Introduction

This project identifies the technology requirements and evaluates the technologies for high power applications of wireless power transfer systems for medium and heavy duty vehicles. This project supports the Vehicle Systems Simulation and Testing (VSST) power train electrification goals: demonstrates market readiness of wirelessly grid-connected vehicles, develops methods to reduce impact on infrastructure due to electric vehicle charging, and addresses the codes and standards needed to enable the wide-spread adoption of electric-drive transportation technologies. This project reviews the existing literature, addresses the limitations, and provides preliminary simulation results based on a feasibly design for realizing the high power wireless power transfer. The overall expectations for a high power wireless power transfer system can be summarized as follows:

- Compact, light-weight coupler design,
- Highly efficient (>80%),
- >100kW power rating,
- Misalignment tolerant up to 10-15%,
- Low flux density / smaller fringe fields, meeting international guidelines, and
- Electrically safe, having built-in protection features for the equipment, vehicle, and people.

Approach

Through the literature review, modeling, design, and simulations, the issues and barriers of the high power wireless charging systems with design validation are addressed. The challenges and needs for high power wireless charging systems can be summarized as follows:

- **Reduced coupling factor:** Typically, HD vehicles have larger ground clearances requiring higher airgaps for power transfer. Larger airgap reduces the coupling factor. As coupling factor, k , goes down, the mutual inductance also drops: $= k\sqrt{L_1L_2}$. Lower mutual inductance requires highly reactive and relatively larger primary coil current that the inverter has to deliver. Inverter device rating and coil wire current rating are stressed. Both the inverter reactive power rating and the coil current rating (wire gauge) should be increased. In addition to the reactive power supplied from the inverter, more reactive power rating from the tuning capacitors is needed which also results in higher voltage rating requirement. The other reason for higher voltage rating for tuning capacitors is that higher primary current is needed for high power applications and the capacitor voltage increases with the higher current.
- **Power electronic device restrictions:** Typically, device voltage and current ratings go down as the switching frequency increases. Metal-Oxide Semiconductor Field-Effect Transistors (MOSFETs) can switch at frequencies around 100 kHz but their power rating cannot exceed a few kilo-Watts. Silicon controlled rectifier (thyristors, SCR) and gate turn-off thyristors (GTO) can handle MW level powers, but their switching frequency is restricted to less than a kHz or a few kHz at most. On the other hand, for effective field generation, high frequency, ideally >20 kHz is needed. Insulated gate bipolar transistors (IGBTs) with smaller voltage-current ratings ($<300V$, $<100A$) can switch up to 20-30 kHz but high power 4500-6500V devices can only handle a few kilo-Hertz. Therefore, advanced power electronics architectures are needed to overcome these issues. The power rating and frequency relationship is depicted in Figure IV-48.

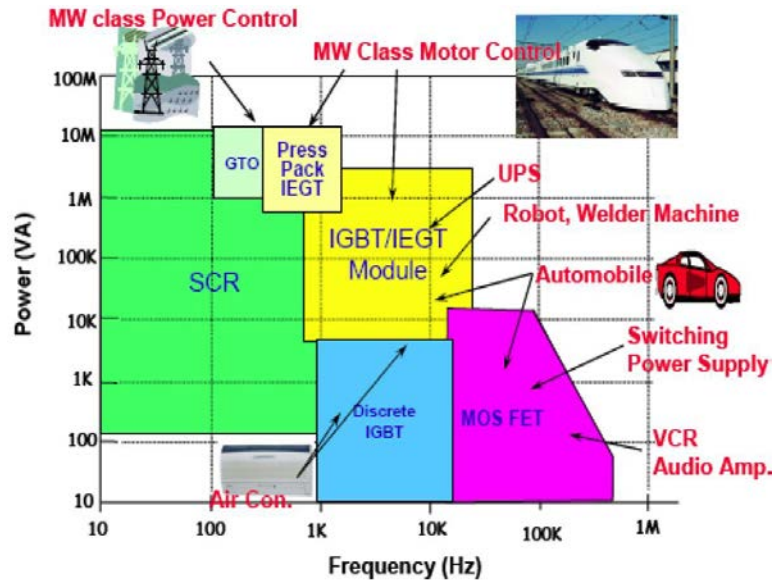


Figure IV-48: Power semiconductor devices power and frequency relationship.

Hongfang Wang, "Investigation of power semiconductor devices for high frequency high density power converters," Virginia Tech.

- **Power transfer efficiency:** The overall end-to-end system efficiency is typically expected to exceed 80%. For high power, most critical power conversion efficiency is the coil-to-coil efficiency that is defined by (ideally):

$$\eta = \frac{1}{1 + \frac{R_2}{R_L} + \left(\frac{R_L + R_2}{\alpha \cdot \omega \cdot L_2}\right)^2 \cdot \frac{R_1}{R_L}}$$

where R_1 and R_2 are the primary and secondary winding resistances, α is the coupler turns ratio, which is defined as $k\sqrt{L_1L_2}$; k is the coupling factor which is defined as $M/\sqrt{L_1L_2}$; M is the mutual inductance, ω is the angular frequency, and L_1 and L_2 are the primary and secondary self-inductances.

Inverter efficiency depends on the switching (turn-on and turn-off) losses and the conduction losses of the semiconductor device and also the reverse-recovery losses of the internal body diodes.

- **Magnetic flux density:** Relatively higher airgap in heavy duty vehicles results in very low flux linkage between the primary and secondary hence large leakage flux is emitted to the air from the primary. Field emissions should be less than $6.25 \mu\text{T}$ at all locations where the human may be exposed to magnetic field at frequencies 0.8 to 150 kHz. According to IEC (International Electrotechnical Commission) 62110, the field radiation is evaluated at three locations; 20cm away from the surface of the source and 50, 100, and 150cm vertically above from the ground. Field emission normally depends on frequency, number of turns on primary, primary current, and the primary inductance. Ferrite layout or magnetic core design of the couplers is of significant importance to reduce field emissions and increase efficiency.
- **Power electronics kVA rating and thermal management:** Ideally, tuning capacitors should eliminate the reactive power (VAr: Volt-Amp-reactive). However, the pickup circuitry feeding a voltage-source-based load (i.e., battery) through a rectifier requires reactive power that is reflected back to the primary side inverter. This means that the inverter should be oversized / overrated to compensate for all the additional VAr loads that can be presented from secondary or multiple pickups. Current ratings of the devices are usually defined for 25°C temperature. However, even at 97% efficiency, while transferring 100kW, the total power converted to heat is 3kW which increases the device temperatures well above 100°C and current rating is reduced. Either very advanced controlled chillers or the overrated systems should be utilized.
- **State-of-the-art coupling device configurations:** This classification has two major subgroups called “Flat Spiral Coils” and “Long Track / Rail / Wire Loop based Couplers.” The subgroups are detailed below:
 - Flat spiral coils (can be with or without flux guiding ferrites):
 - Solenoid (polarized coils)
 - DD and DDQ coils (polarized)
 - Circular (non-polarized) (shown in Figure IV-49)
 - Rectangular (non-polarized)
 - Long track / rail / wire loop based couplers:
 - Flat pickup (shown in Figure IV-50)
 - Flat E-pickup
 - E-pickup (shown in Figure IV-51)
 - S or S-pickup
 - U-pickup (shown in Figure IV-52)
 - I-core transmit
 - T-core transmit
 - U-core transmit
 - Double-sided
- **High power systems also classified based on their compensation network or tuning configurations.** A comparison table created for the conventional compensation configurations and presented in Table II-2.
 - Conventional tuning configurations:
 - Series-series
 - Series-parallel
 - Parallel-series
 - Parallel-parallel
 - Unconventional tuning configurations
 - LCL
 - LCCL
 - LCC



Figure IV-49: Circular coil.

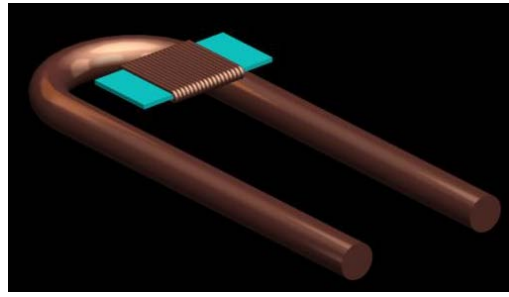


Figure IV-50: Flat pickup coil.

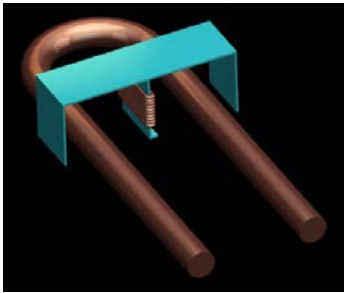


Figure IV-51: E-pickup coil.

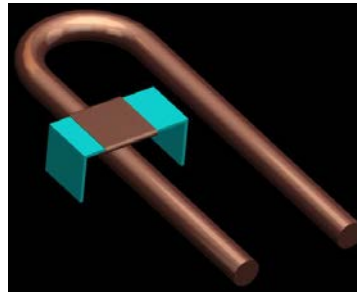


Figure IV-52: U-pickup coil.

Table IV-40: Tuning configuration comparisons.

	Series-parallel	Series-series	Parallel-series	Parallel-parallel
Dependence on load and coupling factor	Secondary side tuning capacitor depends on load and coupling factor	Primary and secondary tuning capacitors are not a function of load and coupling factor	Primary side compensation capacitor depends on load and coupling factor.	Both primary and secondary side compensation capacitor depends on load and coupling factor.
Inverter device voltage rating	Lower DC link voltage is required. – lower inverter efficiency if a transformer is not used	Lower DC link voltage is required. –lower inverter efficiency if a transformer is not used	Higher voltage is needed than SS and SP	Higher voltage is needed than SS and SP
Inverter device current rating	Equals to the primary coil current	Equals to the primary coil current	Equals to the active component of the primary coil current (ideally)	Equals to the active component of the primary coil current (ideally)
Restriction on flux linkage	Magnetic field independent of the load current since secondary is parallel compensated	Secondary coil is equal to the load current, field is limited by load current	Secondary coil is equal to the load current, field is limited by load current	Magnetic field independent of the load current since secondary is parallel compensated

- Regarding the coupling technology and Eddy current model is developed that captures the frequency domain analysis as well as the ohmic and core loss calculations. Furthermore, the magneto-static model has been built to represent the inductance and coupling factor dynamics. The visuals of this model are given in Figure IV-53. The magnetic field, B-vector in the cross-sectional plane in between and around the coils is given in Figure IV-54. Finally, the B-field magnitude of the flux guiding ferrite plates and on the coil structural elements is shown in Figure IV-55.

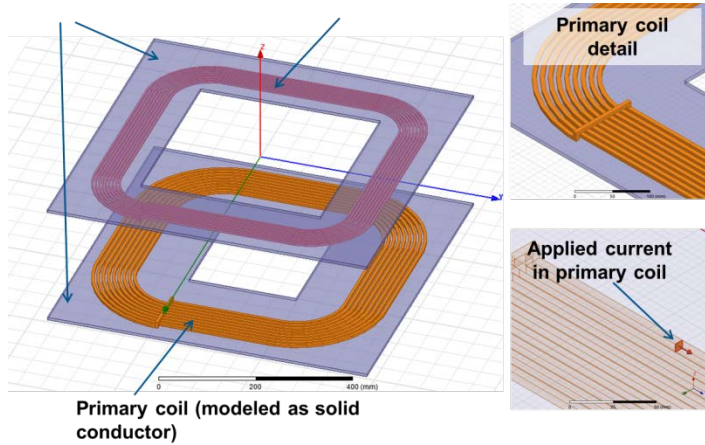


Figure IV-53: Eddy current model of coupling coils for frequency domain analysis.

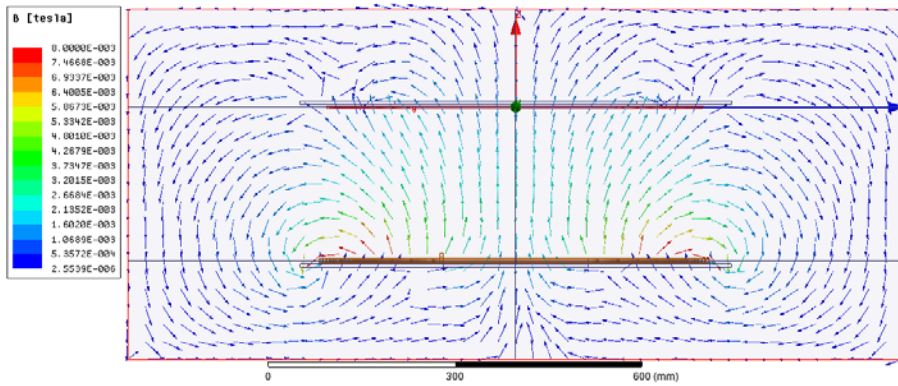


Figure IV-54: B-vector in the cross-sectional plane.

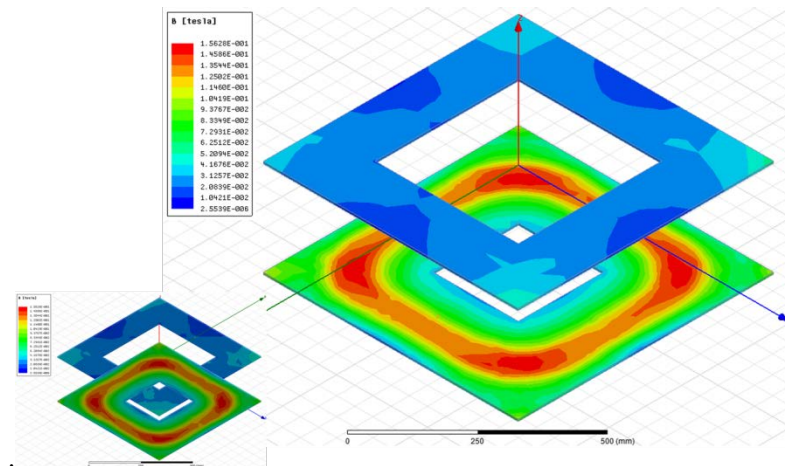


Figure IV-55: B-field magnitude of the flux guiding ferrite plates.

- Currently, there are many methods introduced in the literature for high power wireless power transfer systems. However, most of these systems are not practically realized or they have either design or operational drawbacks. Oak Ridge National Laboratory (ORNL) power electronics approach utilizes

three 50kW inverters, sharing the same input that can be supplied from a direct current (DC) power supply or by the rectified three-phase 480V alternating current (AC) voltage. Here, inverter output voltages are added up and more current at higher voltage is obtained at "ORNL designed integrated magnetics structure." High current drives the primary coil that generates magnetic field that is linked to secondary. High voltage on induced on secondary is rectified, filtered, and used to recharge heavy-duty vehicle battery. The ORNL proposed high power WPT architecture is presented in Figure IV-56 whereas Table IV-41 shows the preliminary system parameters.

$$R_{L1} = R_{L2} = 9.06m\Omega$$

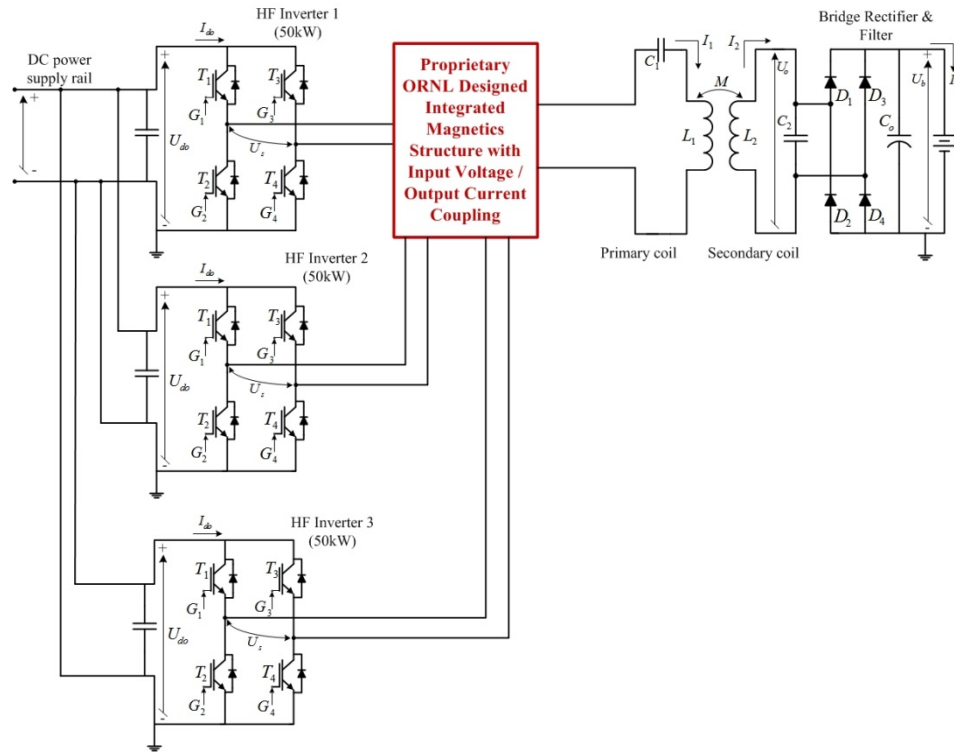


Figure IV-56: ORNL power electronics approach utilizing three inverters and an integrated magnetic structure.

Table IV-41: Preliminary system design parameters.

Parameter	Value
Source supply	480V, 3-phase rectified (675 Vdc)
Primary and secondary inductance	$L_1 = L_2 = 447.08\mu H$
Primary and secondary tuning capacitor	$C_1 = C_2 = 117.06n$
Capacitor internal resistance	$C_{R1} = C_{R2} = 3m\Omega$
Coil winding internal resistance	$R_{L1} = R_{L2} = 9.06m\Omega$
Coupling factor	$k = 0.19$
Mutual inductance	$M = 84.94\mu H$
Vehicle battery	Li-ion, 600Vdc nominal
Switching frequency	22 kHz

Results

This section summarizes the simulation results of the proposed high power system. Results obtained while transferring 121.8 kW to the vehicle battery and include the stage by stage efficiencies obtained at each input-output pair of the power conversion stages. Accordingly, following efficiency figures have been obtained:

- Inverter efficiency: 97.88%
- Transformer efficiency: 96.32%
- Coil-to-coil efficiency (@ $k=0.19$ coupling factor due to relatively higher airgap): 91.83%
- Vehicle side rectifier efficiency (using ultra-fast recovery Schottky barrier diodes): 99.34%
- Overall end-to-end efficiency: 86.02%

The efficiency diagram is provided in Figure IV-57.

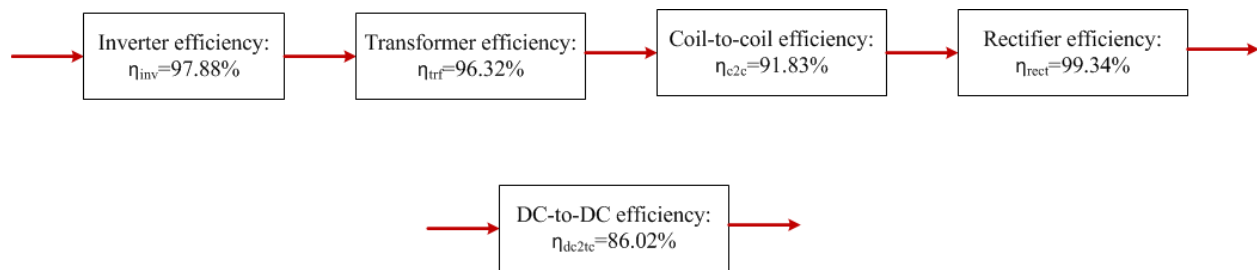


Figure IV-57: Preliminary simulation results based on ~122kW power transfer.

Conclusions

This report summarizes the ORNL activities on high power wireless power transfer systems. In this study; a literature review is completed based on coupling technologies and resonant tuning configurations. The ORNL coupling coil design is validated with the Eddy current model and the magneto-static model developed in this project. An integrated magnetic structure is proposed for combining three 50kW inverters for high power. Although this structure needs a considerable design work before implementation, the results are promising. The proposed system modeled and simulated and state by stage efficiencies recorded. The results evaluated and the areas needing improvement are identified. Hardware design and fabrication will be completed in next phases for a high power design validation. In order to improve the coil-to-coil efficiency, following recommendations can be concluded:

- Improve coupling factor to reduce iron losses,
- Improve coupler wiring with a thicker AWG wire to reduce copper losses,
- Improve integrated magnetic structure (transformer) efficiency with different core material,
- Improve inverter devices by evaluating wide bandgap device materials; i.e., SiC or other devices with reduced thermal stress.

IV.7.C. Products

Presentations/Publications/Patents

1. Conference papers/presentations:
 - a. O. C. Onar and P. T. Jones, “System parameters, modeling, design, and simulations of high power wireless charging for heavy duty vehicles,” in Proc., SAE Hybrid & Electric Vehicle Technologies Symposium, February 2015, Los Angeles, CA.
2. Invited talks and panels:
 - a. O. C. Onar, “Recent Advances in Wireless Power Transfer Systems,” IEEE Applied Power Electronics Conference and Exposition, Industry Special Session on Recent Development in Wireless Power Transfer, March 2015, Charlotte, NC.
 - b. J. M. Miller (Moderator), Ted Bohn, O. C. Onar, J. Taiber, and M. de Rooji, “Wireless Power Transfer: Facts and Fictions,” RAP Session at the IEEE Applied Power Electronics Conference and Exposition, March 2015, Charlotte, NC.

IV.8. Vehicle Thermal System Model Development in Simulink

Jason A. Lustbader, Principal Investigator

Gene Titov, Eric Miller, and Daniel Leighton, Co-Authors

National Renewable Energy Laboratory

15013 Denver West Parkway

Golden, CO 80401

Phone: (303) 275-4443

E-mail: Jason.Lustbader@nrel.gov

David Anderson, Lee Slezak, DOE Program Managers

Vehicle Technologies Office

Phone: (202) 287-5688, (202) 586-2335

E-mail: David.Anderson@ee.doe.gov, Lee.Slezak@ee.doe.gov

Start Date: 2014

End Date: 2017

IV.8.A. Abstract

Objectives

- Develop a flexible, publicly available framework for analysis of advanced thermal management systems for electric, hybrid, and conventional vehicles
 - Use the popular MATLAB/Simulink environment as an implementation platform
 - Model the vapor compression cycle and the coolant distribution network in a manner applicable to combined and separate loop architectures
 - Account for transients and ensure real time or faster simulations on commodity hardware
 - Co-simulate with Autonomie.
- Develop tools aimed at analysis of design-stage-evolving thermal management system architectures. Rapidly assess the impact of emerging concepts and technologies
- Apply the analysis tools with industry partners to assess the impact of technologies that reduce thermal load, improve climate control efficiency, reduce vehicle fuel consumption, and extend range.

Accomplishments

- The National Renewable Energy Laboratory's (NREL's) CoolSim MATLAB/Simulink modeling framework was improved by including a newly developed coolant loop solution method aimed at reducing the simulation effort for arbitrarily complex thermal management systems. The new approach does not require the user to identify specific coolant loops and flow directions in these loops. The user is only expected to connect the fluid network elements in a manner consistent with the desired schematic, and the solution method will account for flow in the loops.
- Using the new solution method, a model of NREL's advanced combined coolant loop system for electric vehicles (EVs) was created that reflected the test system architecture. This system was built using component data provided by Delphi Automotive (now part of the MAHLE Group) and included both air conditioning (A/C) and heat pump modes. Validation with test bench data and verification with the previous solution method were performed for 10 operating points spanning a range of ambient temperatures from -2°C to 43°C. The largest root mean square (RMS) difference between the data and the simulation results was less than 7%. Simulated capacities of heat exchangers lay inside error bars of the measurements for nine out of 10 simulations.
- An improved cabin model was developed and validated using a new dataset provided by MAHLE. Cooldown, heating, and steady-state simulation results were compared with the data. Updates to the model resulting from the validation included addition of an instrument panel module sub-model that

accounted for notable heat exchange between the ducted air, cabin air, and the module surface. As part of the validation, a two-zone variant of the model was considered that accounted for differences between breath and floor level air temperatures.

- Using the Simulink framework, NREL built a model of a long-haul truck air conditioning (A/C) system in collaboration with Cummins and Oak Ridge National Laboratory (ORNL). The model is currently being calibrated and will be used to study accessory electrification trade-offs and to inform future testing.
- CoolSim was used for a number of Funding Opportunity Announcement projects with industry partners, including MAHLE, Halla Visteon (now part of the Hanon Systems), and Hyundai. It was also used with Daimler Trucks on the SuperTruck project.

Future Achievements

- Develop full cab model in CoolSim, including environmental loads, to allow integration with the VTCab rapid heating ventilation and air conditioning (HVAC) analysis tool
- Use the framework to build specific models to identify design improvement opportunities and estimate the impact of advanced thermal management systems on light- and heavy-duty vehicle performance, fuel use, and range
- Develop generic component libraries for components such as electric and mechanical compressors, refrigerant-to-air, refrigerant-to-coolant, refrigerant-to-refrigerant heat exchangers, expansion valves, etc. Make the components modifiable and provide calibration harnesses for the users to specialize the components for their needs
- Extend the range of supported refrigerant types to include HFO-1234yf refrigerant. Streamline the procedure of incorporating new types of refrigerants with the CoolSim framework
- Use CoolSim in collaboration with Oak Ridge National Laboratory and Cummins to provide high-fidelity simulations of proposed A/C architectures, understand the impacts on the vehicle load, and provide support for future hardware-in-the-loop testing.
- Update and improve integration with Autonomie.

IV.8.B. Technical Discussion

Background

Thermal management systems are increasingly important for effective and efficient advanced heavy- and light-duty vehicle design. Developing flexible and cost-effective tools to understand vehicle thermal trade-offs at the system level is critical to designing advanced electrified traction drive systems and their associated thermal controls. When operating, the A/C system is the largest auxiliary energy consumer in a conventional vehicle. A/C loads account for more than 5% of the fuel used annually by light-duty vehicles in the United States [1]. Climate control loads can have an even larger impact on hybrid EV, plug-in hybrid EV, and all-electric vehicle performance. Hybrid EVs show a 22% lower fuel economy with the A/C on [2]. For all-electric vehicles, the effect of the climate control system usage is even more severe. Due to a shortage of waste heat, heating of the passenger cabin in EVs has to rely on battery energy and complicated heat pump operations. Cooling the cabin can also take a high portion of the energy available in the battery, significantly reducing vehicle efficiency and range. Mitsubishi reports that the range of the i-MiEV can be reduced by as much as 68% with heating and 46% with cooling of the cabin on Japan's 10–15 cycle [3]. The Advanced Powertrain Research Facility at Argonne National Laboratory has reported 59.3% and 53.7% reductions in range due to maximum heating and maximum cooling, respectively, for the Ford Focus EV operating on the Urban Dynamometer Driving Schedule cycle [4]. In addition to these climate control impacts, electric-drive vehicles may have additional cooling requirements for the electric traction drive system components, including batteries, power electronics, and electric machines.

To address these challenges, alternative heating methods and more efficient cooling systems are needed for EVs. These methods and systems often involve running the A/C system in heat pump mode to reduce the

heating power requirements of the cabin. In some advanced concepts, the traditional liquid coolant-based thermal management is supplemented with refrigerant-based cooling systems, which can make the thermal management system as a whole significantly more complex. When developing a thermal management system for an internal combustion engine vehicle, it has traditionally been sufficient to simulate the A/C systems and the liquid coolant-based cooling systems separately. For advanced vehicles, especially for hybrid and all-electric vehicles, the benefits of interconnectedness of the thermal management and A/C systems outweigh the associated complexity. This requirement motivates the development of a more integrated simulation approaches.

The more complex thermal management systems of advanced vehicles typically allow for various alternative modes of operation that can be selected based on driving and ambient conditions. Investigating a number of system alternatives and determining the best ranges for various operating modes with experimental methods can be very time consuming. A good system simulation tool can greatly reduce the time spent and expense of the development of these complex systems. Such tools should also be able to efficiently co-simulate with vehicle simulation programs and should be applicable for evaluating various control algorithms. MATLAB/Simulink simulation environment is popular in the automotive industry and is well suited for development of such models while meeting the requirements of dynamic modeling of complex systems.

Introduction

To meet the needs of advanced vehicle thermal system simulations, NREL is building an integrated single- and two-phase thermal system modeling framework in Simulink called CoolSim. This integrated approach allows for rapid system analysis and design in a flexible and open modeling environment. Simulink is a common engineering platform that allows for co-simulation with Autonomie [5]. NREL previously developed an A/C system simulation modeling framework in MATLAB/Simulink and validated its results against test bench data. To match the wide range of A/C modeling needs, NREL developed models with three different levels of detail: Fully-Detailed, Quasi-Transient, and Mapped-Component.

The three models involve different levels of trade-offs between speed and accuracy to meet a wide range of modeling needs. The Fully-Detailed model captures the system transient behavior accurately but runs at 1/10 times real-time speed [6]. The Quasi-Transient and Mapped-Component models are progressively more simplified while trying to maintain accuracy. These models run at real time and 10 times real-time speed, respectively [7]. The goal of these newer model versions was to provide faster simulation tools for less detailed, vehicle-focused, drive-cycle-based evaluations of A/C systems. For steady-state conditions, the Quasi-Transient model provides essentially the same accuracy as the Fully-Detailed model. The Mapped-Component model does lose some accuracy in steady-state conditions. For the SC03 cycle, the averaged results of power and heat exchange rates obtained with the Quasi-Transient model are within 3% of the Fully-Detailed model results. The Mapped-Component model results are within 15% of the Fully-Detailed model results. Short transients, such as those occurring during compressor cycling, produce the most deviation from the Fully-Detailed model for both simplified models. Conversion from the Quasi-Transient A/C system model approach to the other two models is relatively simple within the CoolSim framework. This allows a new system model to be developed with the Quasi-Transient version before the results are refined using the slower Fully-Detailed version or accelerated using the faster Mapped-Component model version.

As outlined in the background section, there is a need for coupled thermal system simulations due to the interconnectedness of the refrigerant and liquid coolant circuits used in advanced thermal management systems, especially the ones developed for EVs. To address this need, NREL's refrigerant circuit simulation model was extended with a liquid-coolant circuit simulation capability. The original coolant fluid network solution method was selected for its speed and algorithmic simplicity. This approach works well for relatively simple systems that do not involve features such as changes in fluid flow direction, a large number of operating modes, etc. The complexity and flexibility of next-generation integrated systems, however, put a higher burden on the user for setting up the models using the originally developed fluid network approach. Certain system configurations with changing flow directions based on mode and operating conditions were also found to be challenging to simulate. To improve modeling of these more complex thermal systems, a more general method that considers the coolant as a compressible medium with an artificially large bulk modulus was developed. This approach is similar to that used for two-phase flow of refrigerant. While this

approach comes at a higher computational cost, the flexibility and ease of model development make it a preferable alternative for complex fluid networks. Furthermore, it was determined that the bulk of computational effort is typically spent on the refrigerant circuit, making the additional computational expenses for the coolant relatively small. An additional benefit for developers comes from the fact that the solution methods for both single- and two-phase flows become similar.

A model built with this updated version of CoolSim was developed for NREL's combined fluid loop (CFL) thermal management test bench in both active cooling and heating modes. Comparisons of simulated results with measured data validate the new coolant loop solution approach. Additional verification was obtained by comparisons with results produced by the original solution method.

Approach

A New Approach to Coolant Loop Modeling

The Advanced Combined Fluid Loop modeling method (ACFL) integrates the "Quasi-Transient" modeling method for the refrigerant circuit with a similar approach for coolant loops. The details of the two-phase refrigerant loop solution method are discussed in [7]. This report focuses on details of the single-phase coolant loop modeling. The original approach to coolant loops in CoolSim relies on a theory similar to the Kirchhoff's law for electric circuits. This approach is efficient and will continue to be of use for simpler systems; however, it proved too complicated for quick development of more sophisticated models with many modes of operation. The advantage of the new approach is more obvious when used for complicated models such as MAHLE-led UTEMPRA.

Similar to the Quasi-Transient refrigerant circuit approach, coolant loops in the new method are represented by 0-D volumes connected with 1-D pipes, valves, or orifices. In general, any system component that can provide a flow rate due to a pressure differential can be attached to these 0-D volume blocks. For the coolant loop network topology, these 0-D volume blocks are referred to as junctions, as opposed to actual fluid reservoirs used in refrigerant circuits such as accumulators, headers, compressor suction/exit volumes, etc. However, these coolant junction simulation blocks can still be used to model large volumes of coolant if needed.

The 1-D pipe block assumes a constant coolant mass flow rate along its length. The flow rate then becomes a simulation state variable. At each time step, the coolant pressure differential across lines is compared to pressure differences between the junctions attached to them. A numerical method is applied to continuously adjust the coolant mass flow rate in each of the lines. The goal of this method is to match the pressure drop in the line to the pressure drop between the junctions that the line connects. This causes the coolant mass flow rate to respond with a delay, but it approaches the solution that would develop under steady-state conditions.

The implications include lost accuracy for fast transients (on the order of seconds) such as pump cycling. For steady-state conditions, however, the conservation of mass and energy for each junction and each of the 1-D pipes in the model is ensured. A typical thermal management network is a slowly drifting "quasi-steady" system, especially in cases with constant RPM electric pumps. In such cases, a true conservation of mass and energy will be closely approximated by this method.

Junction Modeling

In the case of junctions, a mathematical concept of "artificial mass" of coolant is introduced and the conservation equations are written for this artificial mass. This allows for adjustment of system "stiffness." Mass and enthalpy flows into and out of a junction are obtained from adjacent blocks. The heat transfer rate across the solid boundary of a junction is obtained separately. The time derivative for the artificial mass in a junction volume is the difference between the sum of incoming and the sum of outgoing mass flow rates as formulated by equation (1):

$$\frac{dm_a}{dt} = \sum_i \dot{m}_{in,i} - \sum_j \dot{m}_{out,j} \quad (1)$$

where m_a [kg] is the artificial mass, t [s] is time, and $\dot{m}_{in,i}$ and $\dot{m}_{out,j}$ [kg/s] are incoming and outgoing mass flow rates, respectively. Conservation of energy is treated in a similar manner, in the form of a control volume equation. The volume is constant, which implies that there is no work done by solid boundaries. The resulting time derivative of the total energy in a junction volume is the sum of incoming enthalpy flow rates minus the sum of outgoing enthalpy flow rates plus heat addition:

$$\frac{dU}{dt} = \sum_i \dot{H}_{in,i} - \sum_j \dot{H}_{out,j} + \dot{Q} \quad (2)$$

where U [J] is the internal energy, \dot{H}_{in} and \dot{H}_{out} [W] are the enthalpy flow rates in and out of the volume, respectively, and \dot{Q} [W] is the heat transfer rate into the volume through its boundaries.

Naturally, m_a and U are simulation state variables. By integration, Eqs. (1) and (2) produce the artificial mass and total energy in a junction, making these values available before values of all the other variables are computed as time is advanced by a step.

The artificial coolant mass is introduced to allow changing how pressure and density are related through the coolant material property equations. This approach assumes a uniform coolant bulk modulus valid for all conditions, making pressure a function of the artificial density only. The bulk modulus is also proportional to the volume. This ensures that all junction volumes in the model have adjustable and identical "stiffness." This approach allows a larger simulation time step and therefore much faster model execution. Accordingly, the pressure in a junction is:

$$p = B \cdot \left(\frac{m_a}{V} - \rho_{ref} \right) \quad (3)$$

where B [Pa] is the bulk modulus, V [m³] is the volume, and ρ_{ref} [kg/m³] is a reference density. Note that while volume V is varying from junction to junction in the system, B/V for each junction remains the same. B/V and the volume are input parameters from which B is calculated. The lower the value of B/V , the "softer" the system will be. By dividing the total enthalpy by the artificial mass, the specific enthalpy in the volume can be obtained as:

$$h = \frac{U + pV}{m_a} \quad (4)$$

where h [J/kg] is the specific enthalpy. Temperature is calculated from the specific enthalpy, using the generic enthalpy-temperature relationship for a specific coolant.

Equations (1) and (2) become accurate for conservation of mass and energy when applied to steady-state conditions. If the sum of incoming mass flow rates is greater than the sum of outgoing mass flow rates, the artificial mass will increase, and therefore the pressure in the volume will increase. Such a pressure rise will tend to reduce the incoming mass flow rates and will increase the outgoing mass flow rates. As a result, the system will be driven to a steady-state solution. A similar statement can be made for enthalpy, provided the mass flow rates in and out have already reached a steady state; therefore, Eqs. (1) and (2) approach the rigorous mass and energy conservation equations in steady-state conditions, and they will tend to drive the system towards a correct steady-state solution from any transient state.

1-D Pipe Modeling

For the 1-D pipe model, the governing equations are also developed with the goal of approximating quasi-steady solutions. The approach assumes a constant coolant mass flow rate along the length of a pipe at any time. However, the flow rate is allowed to vary in time. A finite volume formulation is used to determine the lengthwise distribution of flow parameters. With the coolant mass flow rate fixed along the length of the pipe, the finite volume equations can be applied with a marching scheme in the direction of the flow. For each finite volume (or segment), and at each time step, the flow variables at the outlet boundary of the segment can be calculated from the flow variables at the inlet to that segment and the wall temperature of the segment. Assuming that the magnitude and direction of the coolant flow are known, it can be considered that the inlet

boundary conditions of the first segment are those prevailing in the junction attached at the upstream side of the pipe block. Starting with this condition, the pressure at the exit boundary of the first segment, p_{out} , is calculated using the Darcy-Weisbach equation (Eq. 5.8.7 in [8]).

$$p_{out} = p_{in} - 1/2 f \frac{L}{D_H} \rho_{in} v_{in}^2 \quad (5)$$

where p_{in} [Pa], ρ_{in} [kg/m³], and v_{in} [m/s] are the pressure, density, and velocity at the inlet boundary of the segment; L [m] is the length of the segment; and D_H [m] is the hydraulic diameter. v_{in} is the constant mass flow rate, \dot{m} , divided by the inlet boundary density, ρ_{in} . The dimensionless wall friction coefficient, f , is obtained from the Hagen-Poiseuille equation (Eq. 5.10.12 in [8]) for laminar flows and from a modified version of the Colebrook equation (Eq. 5.10.13 in [8]) for turbulent flows. Next, the local heat transfer coefficient is calculated with the Dittus-Boelter correlation [9] and the effectiveness-number-of-transfer-units (E-NTU) method [9] to obtain the coolant exit temperature assuming that the pipe wall temperature is uniform. This approach ensures that the coolant exit temperature from the segment does not overshoot the wall temperature:

$$T_{out} = T_{in} - (T_{in} - T_w) \cdot \left(1 - \exp \frac{\alpha A}{\dot{m} C_p} \right) \quad (6)$$

where T_{in} [K] is temperature at the inlet boundary, T_w [K] is the segment wall temperature, A [m²] is the heat transfer area (segment length times inner channel perimeter), α [W/(m² · K)] is the heat transfer coefficient, and C_p [J/(kg · K)] is the constant pressure specific heat. The heat transfer rate from the coolant to the wall can be calculated as follows:

$$\dot{Q} = C_p \cdot \dot{m} \cdot (T_{in} - T_{out}) \quad (7)$$

Once the heat transfer rate is computed with Eq. (7), the specific enthalpy on the outlet boundary can also be calculated with:

$$h_{out} = \frac{\dot{H}_{in} - \dot{Q}}{\dot{m}} \quad (8)$$

where \dot{H}_{in} [J/s] is the enthalpy flow rate through the inlet boundary of the segment. With h_{out} and p_{out} obtained, all other coolant properties can be calculated at the outlet boundary of the first segment. The procedure is repeated for each subsequent segment of the line with outlet conditions at a previous segment serving as the inlet conditions for the subsequent one. This constitutes a “marching” scheme that starts at the upstream boundary of a pipe and proceeds until the downstream boundary is reached. The pressure obtained at the outlet of the pipe can now be compared to the pressure inside the junction connected to the pipe at its downstream boundary. Ideally these two pressures would match, which would mean that the coolant mass flow rate used in the calculations was accurate; however, these pressures typically differ significantly. One approach to resolve the difference is to iterate the coolant mass flow rate until the pressures match, which was found to be computationally expensive. A faster alternative approach was adopted in which only one iteration of the marching is completed per pipe for each time step. Instead of fully converging the system to an intermediate steady state, the pipe flow solution is advanced one time step toward the steady state. After a step is completed, the outlet pressure is compared to that of the junction downstream to calculate a rate of change for the coolant mass flow in the pipe. This rate of change is used at the next global iteration to increase convergence speed. Because the coolant mass flow rate is calculated by integrating this rate of pressure change, the coolant mass flow rate becomes a simulation state variable and therefore available at the beginning of each time step. The equation applied to calculate the derivative of the mass flow rate is as follows:

$$\frac{d\dot{m}}{dt} = C \cdot \frac{p_{d,calc} - p_d}{p_u - p_d} \cdot \dot{m}, \quad (9)$$

where \dot{m} [kg/s] is the coolant mass flow rate, p_u and p_d [Pa] are the pressures in the upstream and downstream junction blocks respectively, $p_{d,calc}$ [Pa] is the 1-D pipe downstream boundary pressure calculated at the current time step, and C is a dimensionless input parameter that adjusts the rate of the numerical “pull” towards the steady-state solution at the given intermediate boundary conditions.

Cabin Model Improvements

Data obtained from collaborators and onsite experimentation suggest that the behavior of the vapor compression cycle in HVAC systems is affected by ducts that deliver air from the outside and distribute it inside the cabin. These ducts may be heated by solar radiation or affected by contact with the outside air as well as exchanging heat with the cabin air. The cabin model was updated to account for such interactions. Figure IV-58 shows the cabin air temperatures predicted by a model built with an updated CoolSim framework in comparison with data provided by MAHLE for a cabin heating case at an ambient temperature of -10°C . Fresh air is drawn through the module into a positive temperature coefficient (PTC) heater, warmed, and then delivered through a duct into the cabin. After the ducts were accounted for in the model, good agreement with the data was obtained. Figure IV-59 illustrates a similar comparison with data for a cooling case. Note that no additional tuning was needed. This allows for use of a single cabin model for a full range of simulations.

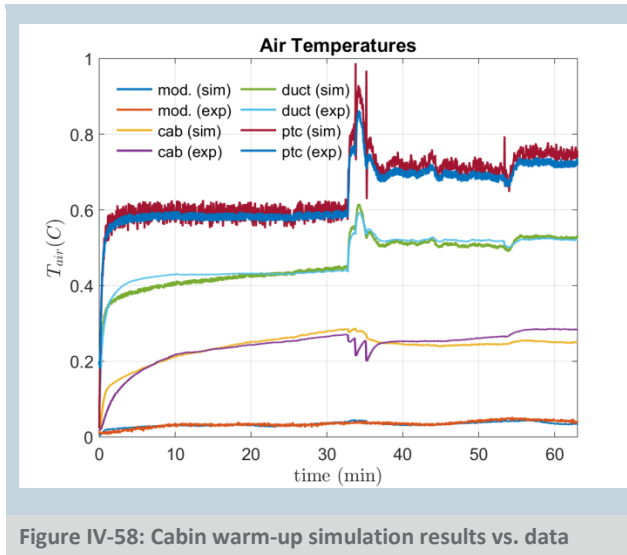


Figure IV-58: Cabin warm-up simulation results vs. data

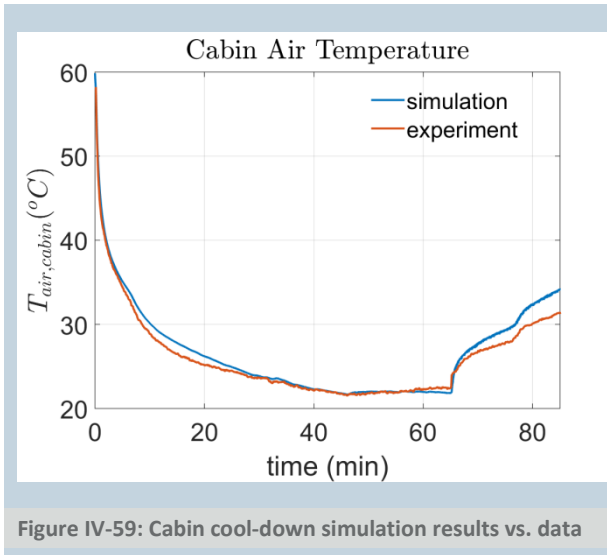


Figure IV-59: Cabin cool-down simulation results vs. data

Results

Validation of the New Coolant Modeling Approach

NREL's CFL electric-drive vehicle thermal management system test bench [10], illustrated in Figure IV-60 and Figure IV-61, was selected for validation and demonstration of the new coolant loop solution method. Two modes of operation were selected for validation which were of primary interest in connection with emerging thermal management systems of EVs: active A/C cooling, and heating that utilizes heat pumping from the outside using a vapor compression cycle. NREL's test bench allows for testing of a wide range of advanced A/C, heat pump, and cooling loop configurations [10]. In this system, a refrigerant circuit operating in the vapor compression cycle is used as both an A/C unit (providing cooling) and as a heat pump (providing heating). The refrigerant loop exchanges heat with the liquid coolant in the chiller and in the condenser. The liquid coolant is used to provide cooling and heating to the cabin.

With the new coolant loop solution method presented in this report, no identification of coolant loops by the user is needed. The selection of operating modes is done in a more natural way by opening and closing the valves. This is different from the previous approach presented in the FY 2014 Annual Progress Report [11], where Figures V-174 through V-176 illustrated user-specified coolant loops and is a significant improvement in usability of the CoolSim framework for complex systems.

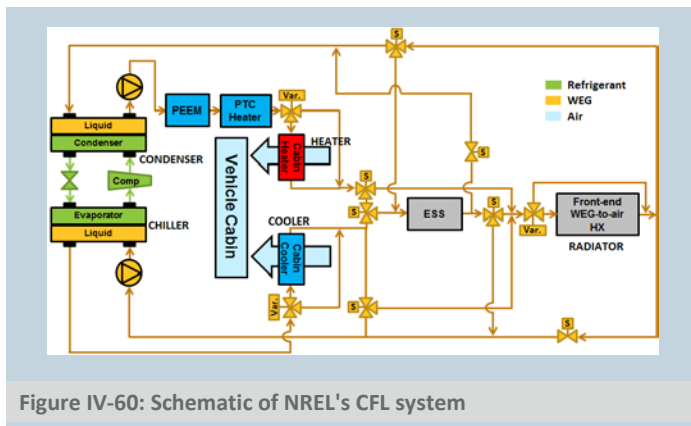


Figure IV-60: Schematic of NREL's CFL system



Figure IV-61: NREL's CFL test bench

Figure IV-62 and Figure IV-63 show steady-state results obtained with the updated coolant loop solution method for the active heating and active cooling modes of the CFL system illustrated in Figure IV-60 and Figure IV-61. Simulation results are compared to the measured data as plots of major parameters versus ambient temperature. The RMS difference between the simulation results and data characterizing the simulation error for capacities of coolant-to-air heat exchangers was 4.18%, and the RMS difference for the coolant temperatures was found to be 1.56%. Similarly, the RMS difference between simulated and measured refrigerant pressures was found to be 6.71%, and for chiller and evaporator capacities within 5%, not presented here. Except for extreme cooling conditions, simulated results lay within error bars of the measurements as illustrated in Figure IV-62.

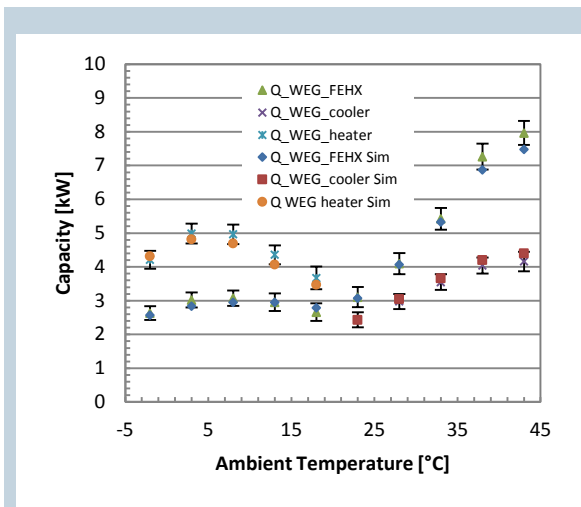


Figure IV-62: Simulated and measured capacities of coolant-to-air heat exchangers

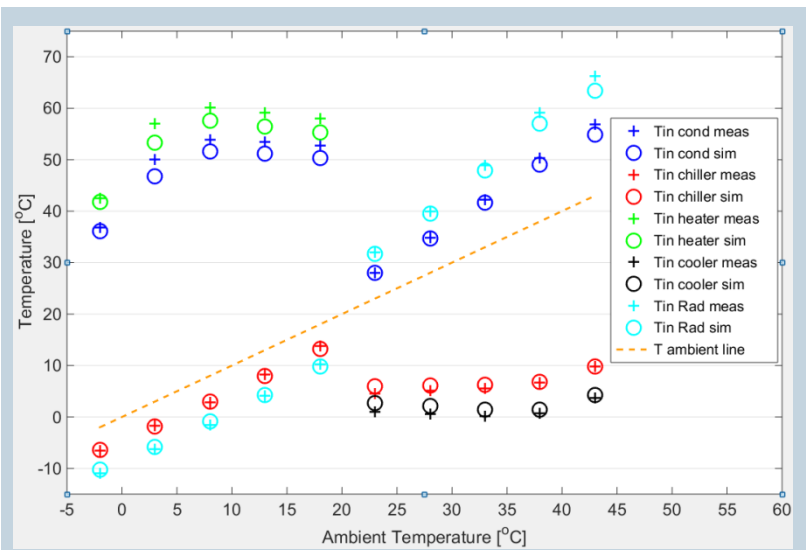


Figure IV-63: Simulated and measured system temperatures

A Heavy-Duty A/C System Model Using CoolSim

Utilizing the CoolSim framework, NREL is collaborating with ORNL and Cummins, providing simulation expertise on heavy-duty truck cab air conditioning in support of vehicle accessory electrification studies. The system schematic and a top-level representation expressed in MATLAB/Simulink are shown in Figure IV-64 and Figure IV-65, respectively.

The overall goal of the project is to reduce line-haul truck idling fuel use through the use of a hybridized/electrified accessory load system. The A/C system is a critical component when evaluating optimized accessory systems. NREL's CoolSim model is being used to provide an accurate high fidelity air conditioning model that can be used to evaluate system architectures, help understand the impacts on the vehicle load, and provide support for future hardware-in-the-loop testing. NREL has built a baseline A/C model and successfully compared it to test data from ORNL.

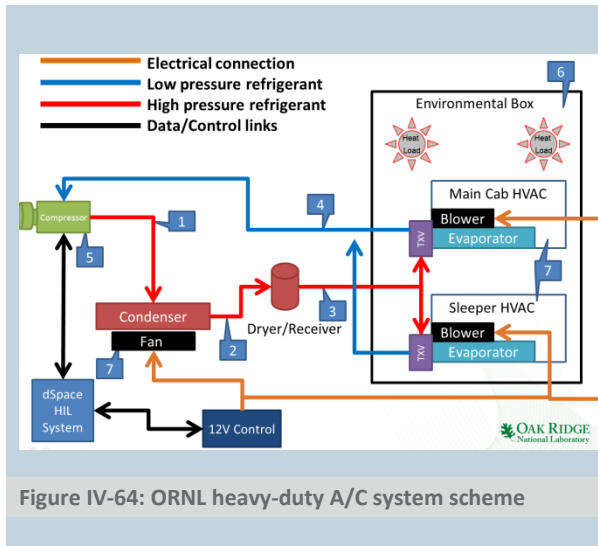


Figure IV-64: ORNL heavy-duty A/C system scheme

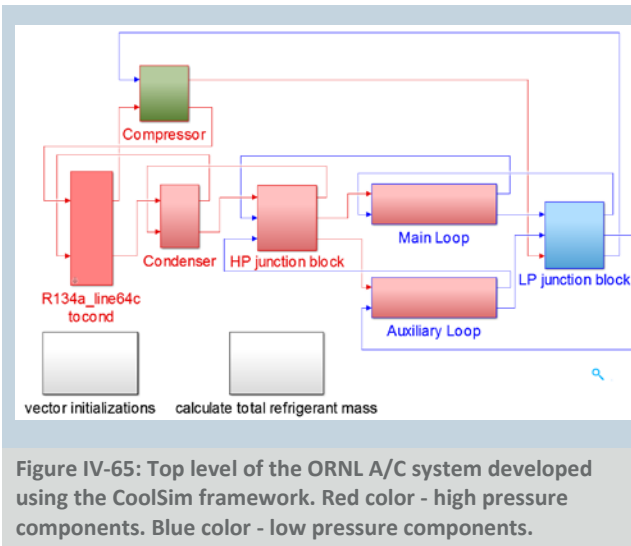


Figure IV-65: Top level of the ORNL A/C system developed using the CoolSim framework. Red color - high pressure components. Blue color - low pressure components.

Conclusions

NREL's MATLAB/Simulink thermal modeling framework, CoolSim, was improved with an alternative simulation method for liquid coolant networks. The new method makes it possible to apply CoolSim to networks with changing flow patterns and flow directions regardless of complexity. This allows the use of a single model whose top-level representation in MATLAB/Simulink closely follows the system schematics for all modes of operation. Such a capability is of special interest to emerging combined refrigerant/coolant loop networks of advanced electric and hybrid vehicles, which may include tens of operating modes. Developing control algorithms for such networks can be greatly simplified by application of CoolSim. Several separate projects that utilize this capability are now underway with industry partners.

The new simulation method also reduces user effort needed to create more complex system models by eliminating the time-consuming definition of coolant loops required by the original approach. The new method determines loop configurations on its own, relying on valve configurations specified by the user. The original solution method, however, has a computational speed advantage and will continue to be used for simpler systems or for established systems that no longer require fast prototyping and design modification. The new approach was validated with data obtained by NREL's combined loop experimental test bench and showed the same level of agreement with data as the original, previously validated approach. The RMS differences between the data and the simulation for coolant loop parameters were 4.18% for liquid-to-air heat exchange capacities and 1.56% for coolant temperatures. Except for extreme cooling conditions, the results are within uncertainties of the measurements and constitute an acceptable level of agreement with the data.

CoolSim's cabin model was also improved and compared against data provided by MAHLE. It was found that the module that included the ambient air inlet ducting and ducts distributing air inside the cabin experienced significant heat exchange with ambient and cabin air, as well as receiving heat from solar radiation. These heat exchanges affected the air temperature inside the ducts and needed to be accounted for. CoolSim's cabin model was extended to include a module sub-model that accounts for the effects of this heat exchange. The resulting model experienced up to several degrees of difference in the evaporator inlet air temperature in both full ambient and cabin air recirculation modes. The updated model results compare favorably with the test data provided by MAHLE.

Collaboration between NREL, ORNL, and Cummins leverages the CoolSim capabilities to help evaluate hybrid/electric accessory system architectures for heavy-duty truck applications. An initial model compares well to test data and is providing insight into A/C component sizing. Future modeling will in part be focused on the conditions beyond the available test facility.

CoolSim's improving capabilities and NREL's expertise in thermal system modeling are currently utilized by the following projects:

- MAHLE's UTEMPRA system, which will use CoolSim to assist with control algorithm development of a combined coolant loops architecture with 22 modes of operation
- Halla Visteon's EV thermal management system, which includes options for thermal energy storage
- Daimler Truck HVAC system modeling
- Hyundai hybrid vehicle energy-efficiency improvement by application of advanced technologies
- ORNL-Cummins Accessory Electrification CRADA

IV.8.C. Products

Presentations/Publications/Patents

1. T. Kiss; J. Lustbader; D. Leighton. 2015. "Modeling of an Electric Vehicle Thermal Management System in MATLAB/Simulink." SAE International World Congress. April. Paper #2015-01-1708
2. J. Lustbader; E. Titov; E. Miller; T. Kiss. 2015. "Vehicle Thermal System Modeling Framework in Simulink." Poster. DOE Annual Merit Review, June 9, 2015; VSS134.
3. E. Titov; E. Miller; D. Leighton; J. Lustbader. 2015. "MATLAB/Simulink Modeling of Parallel Coolant Loop Architecture for Modern Electric Vehicle Thermal Management Systems." SAE Thermal Management Systems Symposium. Sept. 29 – Oct 1, 2015, Troy, MI. Paper 15TMSS-0072.

IV.8.D. References

1. J. Rugh et al. 2004. Earth Technologies Forum and Mobile Air Conditioning Summit.
2. J. Francfort; T. Murphy. "Operational and Fleet Testing, A. Hybrid Electric Vehicle Testing." Chapter V. Advanced Vehicle Technology Analysis and Evaluation Activities: FY 2007 Annual Report. Washington, D.C.: Vehicle Technologies Program, U.S. Department of Energy, 2007; p. 145.
3. K. Umezu et al. 2010. SAE Automotive Refrigerant and System Efficiency Symposium.
4. K. Umezu et al. "Air-Conditioning system For Electric Vehicles (i-MiEV)" 2010. SAE Automotive Refrigerant and System Efficiency Symposium.
5. E. Rask et al. 2014. "Ford Focus BEV In-depth (Level 2) Testing and Analysis." Presentation. DOE Annual Merit Review.
6. "Autonomie." autonomie.org.
7. T. Kiss; L. Chaney; J. Meyer. 2013. "A New Automotive Air Conditioning System Simulation Tool Developed in MATLAB/Simulink." SAE International Journal of Passenger Cars—Mechanical Systems 6(2); doi:10.4271/2013-01-0850.
8. T. Kiss; J. Lustbader. 2014. "Comparison of the Accuracy and Speed of Transient Mobile A/C System Simulation Models." SAE International Journal of Passenger Cars—Mechanical Systems (7), August; pp. 739–754; doi:10.4271/2014-01-0669.
9. V.L. Streeter; E.B. Wylie. 1979. "Fluid Mechanics." 7th edition, McGraw-Hill, New York, ISBN 0-07-062232-9.
10. F.P. Incropera; D.P. DeWitt. 1996. "Fundamentals of Heat and Mass Transfer." 4th edition, John Wiley and Sons: New York, NY.
11. D. Leighton; J. Rugh. 2014. "Electric Drive Vehicle Range Improvement Using a Combined Fluid Loop Thermal Management Strategy." Presentation at the SAE Thermal Management Systems Symposium, Sept. 22–24, 2014, Denver, CO.
12. "Vehicle and Systems Simulation and Testing 2014 Annual Progress Report." Section V.O. Vehicle Thermal System Model Development in MATLAB/Simulink; pp. 240–247.

Acknowledgements

1. Special thanks to ORNL and our industry partners MAHLE and Cummins
2. Additional thanks to John Rugh and Lisa Fedorka (NREL).

IV.9. Advanced Transmission Selection to Provide Accurate VTO Benefits

Namdoo Kim, Principal Investigator

Argonne National Laboratory
 9700 South Cass Avenue, Building 362
 Argonne, IL 60439
 Phone: (630) 252-2843; Fax: (630) 252-3443
 E-mail: nkim@anl.gov

David Anderson, DOE Program Manager

Office of Vehicle Technologies, Department of Energy
 Phone: (202) 287-5688
 E-mail: David.Anderson@ee.doe.gov

Start Date: 10/01/2014

End Date: 09/30/2015

IV.9.A. Abstract

Objectives

- The objective is to develop algorithms for proper transmission selection (i.e., gear ratios, gear spread, final drive ratio) and shift parameter optimization based on engine and powertrain technology, to rigorously evaluate the impact of the Vehicle Technologies Office (VTO) technologies on fuel displacement and the costs of advanced vehicles.
 - In previous years, Argonne developed and validated new model and control algorithms for advanced transmissions—i.e., dual-clutch transmission (DCT) and continuously variable transmissions (CVT). The objective in Fiscal Year 2015 is to develop transmission selection (gear selection, gear spread, final drive ratio, etc.) for specific component technologies and powertrain configurations.
 - Performing an unbiased evaluation of VTO technology benefits requires the proper selection of the transmission technology.
 - The project will provide a solid foundation to assess the impact of advanced transmissions and the accurate evaluation of VTO benefits. Targets achieved will guide future research and development (R&D).
 - The algorithms can be leveraged to optimize gear ratios for the electrified powertrains.

Accomplishments

- Argonne continues to develop and validate advanced transmission models. Some achievements include:
 - Developed and validated plants and controllers for DCT and continuously variable transmissions.
 - Used validated models to assess the impacts of advanced transmissions on other components (including cost considerations), evaluate the VTO benefits guide, and plan future R&D.
- Developed a process to optimize shift parameters, based on engine technology.
- Combined the algorithm for transmission gear ratio and final drive selection with the shift parameter optimization to co-optimize the gear ratio selection with the shift parameter optimization for powertrain technology.
 - The process can be further enhanced by considering other factors like emissions.
 - Gear ratios can be optimized for electrified powertrains to minimize fuel consumption, while meeting vehicle technical specifications (VTS).

Future Achievements

- Co-optimization of gear ratio selection and shift parameter optimization with energy management parameters for maximizing petroleum displacement for the other electrified powertrains.
- Combine optimization with vehicle sizing algorithms to simultaneously meet VTS and minimize energy consumption.



IV.9.B. Technical Discussion

Background

As a result of more stringent regulations and customer expectations, auto manufacturers have considered numerous technology options to improve vehicle fuel economy. One example is transmission technology, since transmission improvements are some of the most cost-effective options. In previous years, specific transmission models (i.e., CVT, DCT) and shifting algorithms have been developed and validated. Recent studies and production vehicles have demonstrated that matching the transmission to the proper engine powertrain is critical to properly evaluate technology benefits. To properly evaluate the VTO benefits and targets to guide future R&D, we developed an algorithm to select the main transmission parameters (i.e., gear selection, gear spread, final drive ratio, etc.) as functions of the component and powertrain configurations as well as the shifting calibrations. A specific set of rules was developed to ensure proper drivability based on vehicle test data and inputs from experts. Partners: Chrysler, Argonne's Advanced Powertrain Research Facility (APRF)

Introduction

The selection of transmission parameters (span, gear ratios, number of gears, etc.) as a function of powertrain and configuration types ensures an unbiased review of powertrain and/or engine technology. Based on the review of test data from APRF, inputs from original equipment manufacturers (OEMs), and literature review transmission ratio selection and shift parameter optimization routines are developed. The control parameters of the shifting algorithm is also part of the multi-objective optimization process. The developed routines will be available in releases of Autonomie, for use by VTO and the national labs.

Approach

The project workflow is shown in Figure IV-66. This study leverages numerous vehicle test data collected at the APRF. With the numerous vehicle test data collected at the APRF (i.e., fuel economy or time from 0 to 60 mph, based on several signals) for several types of transmissions, we analyzed the advanced powertrain system. We also developed and validated the advanced transmission model and shifting algorithm in Autonomie.

In Fiscal Year 2015, using Argonne's optimization algorithm "Pounder," which is available for use through the Autonomie User Interface [1], the process was developed to optimize the shift parameters and gear ratio selections for automobile transmissions for engine technology. This study leverages Autonomie's optimization methods to optimize gear ratios for alternate powertrains, and it also enhances the transmission selection process to merge with the control optimization and vehicle sizing processes.

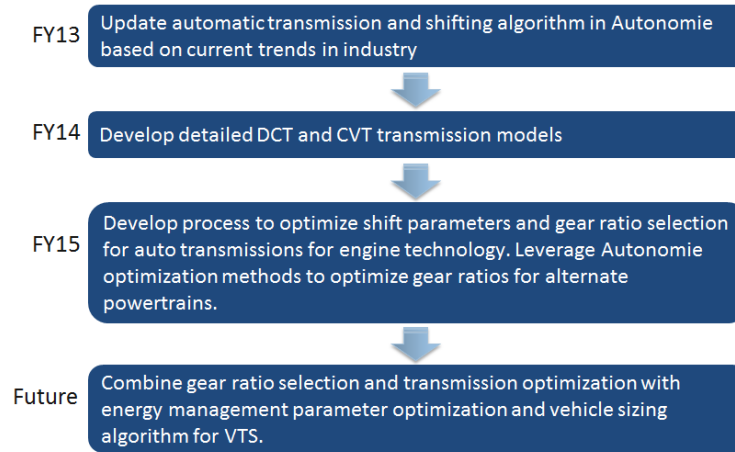


Figure IV-66: Study process for developing advanced transmission models and optimization processes

The main objective of the algorithm is to optimize the parameters of the transmission shift map and gear ratio, to evaluate the potential for shift parameter optimization or gear ratio selection, to further reduce the energy consumption of each powertrain over a combined (Urban Dynamometer Driving Schedule [UDDS] + Highway Fuel Economy Driving Schedule [HWFET]) cycle. In this study, midsize vehicle models used for DOE Analysis (BaSce) Model Year 2025 were chosen for their alternate powertrains, because the model year 2025 vehicles assume an optimistic technology scenario.

Results

Conventional Transmission Vehicle

To properly evaluate the engine operation for powertrain configurations, a rigorous selection of transmission gear ratios, final drive ratios, and gear shift parameters is important. As stated previously, using Argonne’s optimization algorithm Pounder, shift parameters are optimized for a conventional vehicle, to evaluate the potential for shift parameter optimization. The following shift parameters and gear ratio selection parameter are chosen for optimization algorithm.

1. Pedal command for downshift in eco mode
2. Pedal command for upshift in eco mode
3. Vehicle speed for downshift to below gear
4. Vehicle speed for upshift to next gear
5. Progression factor for gear ratio selection

Figure IV-67 shows the shifting curves and shifting parameters selected for optimization using Pounder.

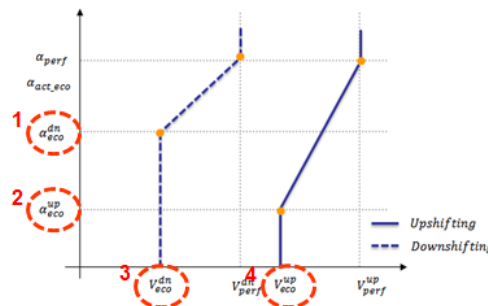


Figure IV-67: Shifting curves and parameters selected for optimization

On the basis of industry trends in gear spans, top gear and final drive progressive gear ratios [2] are designed for six over automatic transmissions using the following formula.

$$i_n = i_z \left[\frac{\text{Span}}{5 \phi_2^{0.5(z-1)(n-1)}} \right]^{\frac{z-n}{z-1}} \quad z \neq 1$$

Where,

z = total number of gears,

n = gear number in consideration for design (varies from 1 to z),

ϕ_2 = progression factor (independent variable—normally between 1 and 1.2),

i_z = top gear ratio, and

i_n = nth gear ratio.

The independent variable ϕ_2 is also chosen for optimization to meet the VTS and simultaneously maximize the fuel economy over a combined cycle.

On the basis of a literature review [3] and chassis dyno test data [4], the following criteria are selected for the transmission (gear ratio), final drive, and shift parameters.

- The vehicle acceleration performance should be 0–60 mph in 9.0 seconds.
- The number of gear shifts for an 8-speed transmission, UDDS cycle, should be around 160 to 165.
- The gear span and final drive ratios should be based on industry trends for the midsize vehicle class.
- Engine operation will be restricted in the low-speed high-torque region, to prevent noise, vibration, and harshness (NVH) issues and ensure drive quality.

Figure IV-68 shows the trajectory taken by the Pounder optimization algorithm, with the 8-speed transmission, for the UDDS cycle. The data points in red represent fuel consumption results which are unacceptable, based on the criteria laid out in the previous section. The green data points are a set of acceptable results.

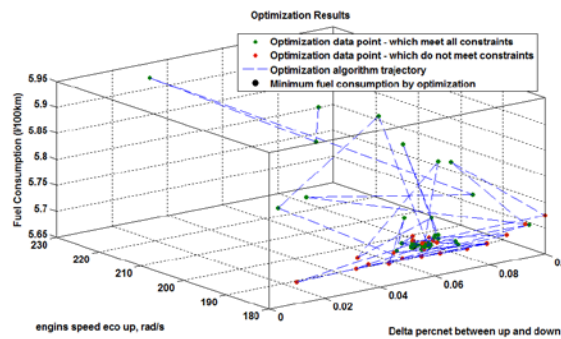


Figure IV-68: Fuel consumption as a function of the trajectory of the optimization algorithm

Figure IV-69 shows the comparison of fuel economy for the conventional midsize 8-speed transmission vehicle with and without optimization. As can be seen from the plot, the co-optimization of gear ratio selection and shift parameter optimization can result in significant fuel economy improvement for conventional powertrains.

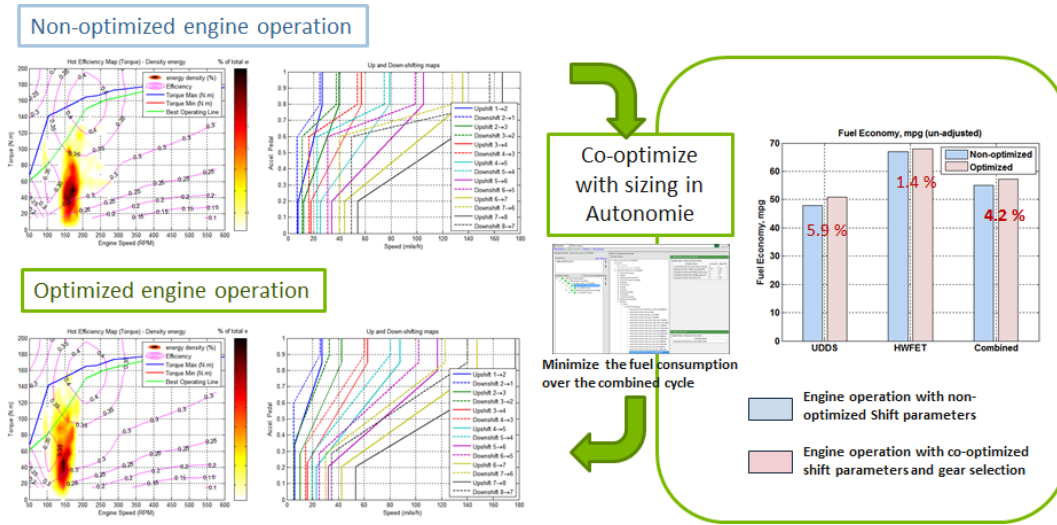


Figure IV-69: Comparison of fuel economy benefits with and without the use of optimization

Power Split Hybrid Electric Vehicle

The same principal we used for the conventional transmission is applied to the power-split powertrain for the hybrid electric vehicle (HEV). For the power-split powertrain, the ratio of ring gear teeth to sun gear teeth could be optimized to reduce energy consumption with same VTS simultaneously. Figure IV-70 is a schematic diagram of the single-mode power-split transmission with a reduction gear. Since the input power from the engine is split at the planetary gear (PG) which is located at the input side, and the power transmission characteristic is represented by a single relationship for the whole speed range, this power-split configuration is called the “input-split type”[5].

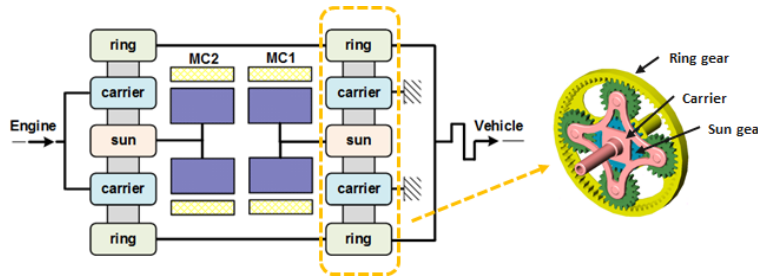


Figure IV-70: Schematic of the input-split type

The ratio of ring gear teeth to sun gear teeth and the electric machine (MC1) peak power are chosen for optimization to meet VTS and simultaneously maximize the fuel economy over a combined cycle. On the basis of a literature review and developed auto-sizing algorithm [6], the following criteria are selected to merge with the vehicle sizing process.

- The vehicle acceleration performance should be 0–60 mph in 9.0 seconds.
- Maximum vehicle speed \geq 100 mph.
- Engine sized to meet 70% of peak power required to meet VTS (acceleration performance or grade 6% at 65 mph at gross vehicle weight rating [GVW]). So, the engine peak power is a function of the vehicle weight.

- Battery power sized to recuperate 100% energy on UDDS.
- Electric machine (MC2) sized as following: 1) MC2 should crank up the engine at peak speed on UDDS, 2) MC2 should control the engine to provide the maximum power of the engine when the vehicle starts for acceleration performance, and 3) MC2 should control the engine at max grade condition.
- The constraint for the total system cost per fuel economy improvement (< \$70/%).
- Vehicle weight is a function of the engine peak power, electric machine peak power, and battery cell number.

Figure IV-71 shows the comparison of fuel economy for the power split midsize HEV with and without optimization. In Figure IV-71, the electro-mechanical power ratio is plotted with respect to the speed ratio (SR). In this analysis, it is assumed that there is no power loss through the all-mechanical path and the only electric machine loss is considered by using the efficiency maps of the electric machines. The power ratio is defined as the ratio of the electro-mechanical power to the engine input power and the SR is defined as the ratio of the engine input speed to the output speed. When the SR is around 0.6–0.7, the electro-mechanical power ratio becomes 0, and all the power is transmitted through the mechanical part. This mechanical part is called the mechanical point. The system efficiency shows the highest value at the mechanical point.

As can be seen from the plot, the co-optimization of the sizing algorithm and the gear ratio selection optimization can result in an improvement in fuel economy, particularly in the highway cycle. In optimized results, the mechanical point moves to the low SR range and the negative value (power circulation) of the electric-mechanical power ratio is also reduced. Once the power circulation occurs, the electro-mechanical infinitely variable transmission (EVT) efficiency decreases due to the relatively low efficiency of the electro-mechanical power path. However, the electric-mechanical power ratio at a high SR range shows a relatively high value in the optimized results. The high electric-mechanical power ratio requires large electric machines and the cost increases, which is a reason why we use the constraint for total system cost per fuel economy improvement.

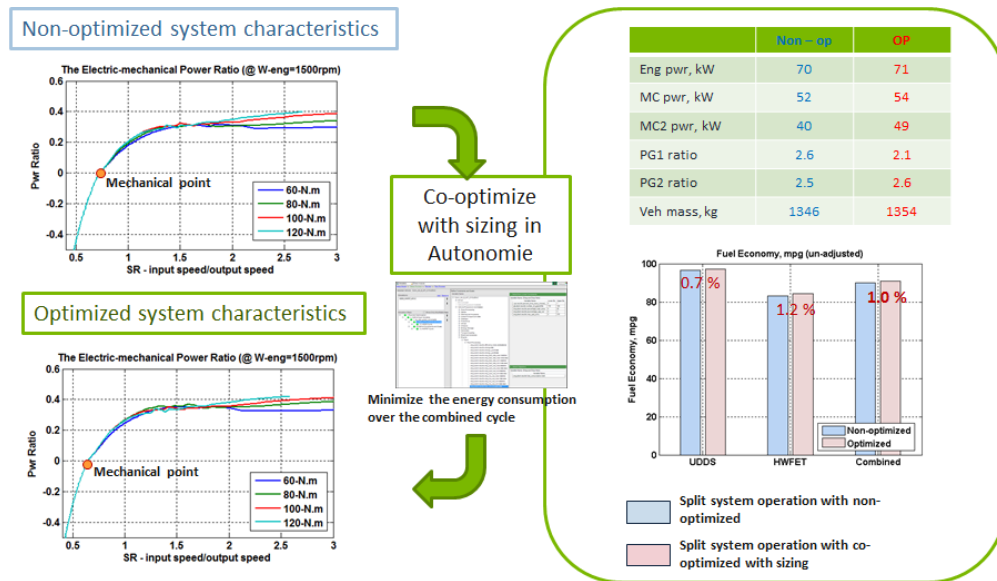


Figure IV-71: Comparison of fuel economy benefits with and without the use of optimization

Conclusions

Argonne continues to develop and validate advanced transmission models.

- Developed and validated plants and controllers for DCT and CVT.

- Validated models will be used to assess the impacts of advanced transmissions on other components (including cost considerations), evaluate VTO benefits guide, and plan future R&D.
- The optimization process can result in a significant improvement in fuel economy for conventional powertrains and power-split powertrains.
- The design of progressive gear ratios coupled with shift-parameter optimizations provides maximum fuel consumption benefits.
- Optimized gear ratios for electrified powertrains to minimize fuel consumption, while meeting VTS.
- The process can be further enhanced by considering other factors like emissions.

IV.9.C. Products

Presentations/Publications/Patents

1. Son, H., N. Kim, S. Ko, A. Rousseau, and H. Kim, “Development of Performance Simulator for a HEV with CVT and Validation with Dynamometer Test Data,” EVS28 conference, 2015.

IV.9.D. References

1. Autonomie; available at autonomie.net.
2. GETRAG Products, accessed at getrag.com/en/products/products.html.
3. Shidore, N., “Impact of Advanced Vehicle Technologies on Engine Operation and Vehicle Energy Consumption Benefits,” presentation at the U.S. Department of Energy Annual Merit Review, June, 2014.
4. Naunheimer, H., B. Bertsche, and J.R.W. Novak, Automotive Transmissions: Fundamentals, Selection, Design and Application, 2nd edition, Springer, ISBN 978-3-642-16213-8, 2010.
5. Kim, N., J. Kwon, and A. Rousseau, “Trade-off between Multi-mode Powertrain Complexity and Fuel Consumption,” The 25th World Battery, Hybrid, and Fuel Cell Electric Vehicle Symposium and Exhibition, 2010.
6. Sharer, P., A. Rousseau, S. Pagerit, and P. Nelson, “Midsize and SUV Vehicle Simulation Results for Plug-in HEV Component Requirements,” SAE 2007-01-0295, 2007.

IV.10. Benefits of Connected Route-Based Energy Management for Light-Duty Electrified Vehicles

Dominik Karbowski, Principal Investigator

Argonne National Laboratory
9700 S Cass Avenue, Building 362
Argonne, IL 60439
Phone: (630) 252-5362; Fax: (630) 252-3443
E-mail: dkarbowski@anl.gov

David Anderson, DOE Program Manager

Office of Vehicle Technologies, Department of Energy
Phone: (202) 287-5688
E-mail: David.Anderson@ee.doe.gov

Start Date: 10/1/2014

End Date: 9/30/2015

IV.10.A. Abstract

Objectives

- Provide a practical way of generating a speed profile for a future trip.
- Demonstrate savings of route-based energy management for a PHEV.

Accomplishments

- Modelled different intersection types in a traffic micro-simulator.
- Built predictive models of main intersection features, such as queue length and wait times.
- Designed models to generate 1 Hz speed profiles for stop signs.
- Improved robustness of the optimal controller for a PHEV.
- Performed a large sensitivity study showing achievable fuel saving potential for a PHEV with route-based control.

Future Achievements

- Finish integration with existing speed prediction algorithm.
- Improve the optimal control prediction algorithm.
- Perform larger study for evaluating fuel saving benefits.



IV.10.B. Technical Discussion

Background

Increased powertrain complexity, connectivity and high-accuracy digital maps provide an opportunity to make vehicles more energy efficient by adjusting the energy management of the vehicle to the particular route travelled. This is especially important for electrified vehicles (HEVs), where appropriate management of the fuel and battery energy is critical for fuel efficiency. Conventional vehicles can also benefit from route-based energy management, as for example in gear management in cruise-control.

Optimal control theory provides a range of methods to find the control strategy that will lead to minimum fuel consumption. Dynamic programming is one of them which finds the global optimum [1]. However, it is computer intensive and is impractical for online real-time control. The Pontryagin Minimum Principle (PMP) [2], and associated methods such as the Equivalent Consumption Minimization Strategy (ECMS) [3], provide a more realistic way of achieving an optimum, because they can easily be implemented online. One critical input to all these methods is the full knowledge of the trip ahead, meaning second-by-second speed and grade.

Several concepts or even products have leveraged digital maps and positioning for energy efficiency. The first application has been topography-dependent cruise-control for conventional engine powered vehicles: the cruise-control would adjust the target speed and the shifting before hills, especially during uphill grades [4, 5]. This concept was extended to hybrids, where proper conditioning of the battery SOC before grades can lead to significant savings, as demonstrated by an early experiment by Nissan [6], and has been made available to Mercedes-Benz S-Class and C-Class. One major enabler was the development of horizon providing capabilities, either directly by map providers (e.g. Navteq/HERE) or suppliers (e.g. Continental, Bosch).

Route-based energy management for PHEVs is more challenging, as it requires a much longer prediction. Optimization, only necessary at distances longer than the electric range, often involves spreading the engine operations throughout the trip while targeting a depleted battery at the end. The Ford C-Max Plug-in HEV (PHEV) [7], now in production, comes with the “EV+” feature that adjusts the control to “increase the amount of electric vehicle (EV) mode driving, particularly near a destination in which an ignition-off event may occur.” There is limited published data on the details and performance of this system.

Introduction

The energy efficiency of vehicles, electrified ones in particular, can be greatly improved using optimal control theory and prediction of future speed, i.e. route-based energy management. In previous years, Argonne has created a novel speed prediction algorithm combining the stochastic aspect of driving (from real-world vehicle trip profiles) and the deterministic nature of it (knowledge of the future route and its attributes thanks to digital maps). This speed prediction can then be used by an optimal energy management strategy that relies on the Pontryagin minimum principle. Our vision for route-based control can be summarized in Figure IV-1. Our contribution is to on the route prediction, route-based optimization and vehicle control.

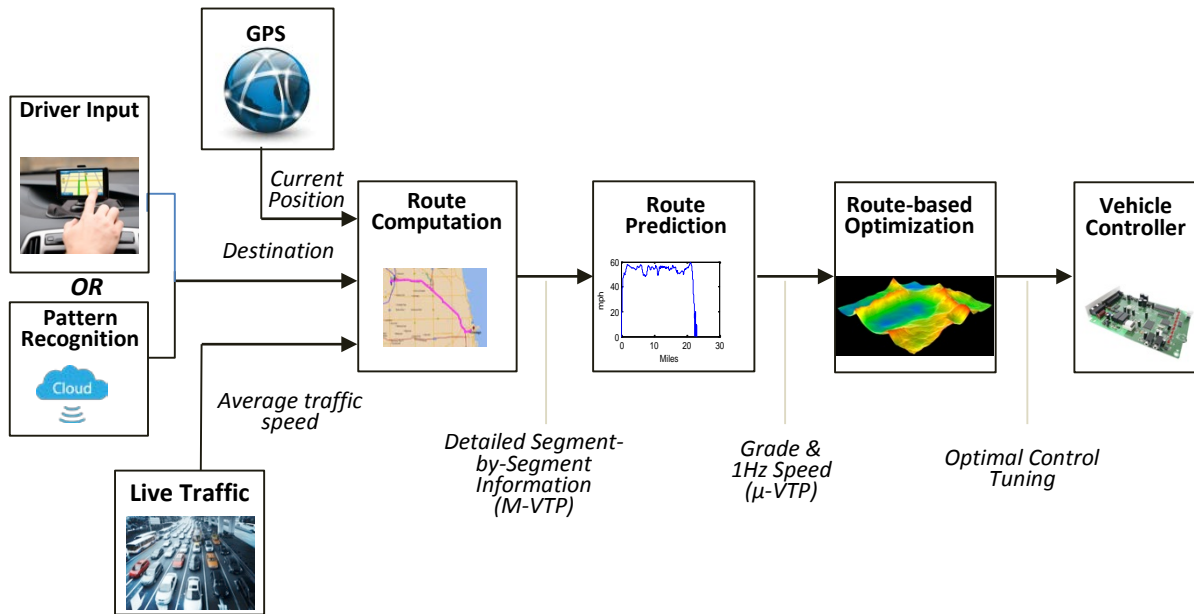


Figure IV-72: Route-based energy management concept

Our route-prediction algorithm augments a macroscopic vehicle trip profile or VTP (M-VTP) into a microscopic VTP (μ -VTP). A VTP is a set of attributes describing a journey made on the road; a M-VTP contains macroscopic attributes for each subsection of the trip, including road category, speed limit, traffic signs, etc. A μ -VTP contains a time-series for the entire trip with a frequency of 1 Hz or less, including vehicle speed and grade. In our case, the M-VTPs are provided by a HERE digital map, accessed through their ADAS-RP tool. In such M-VTP, the trip is divided in segments of a few hundred meters up to a few kilometers, and for each segment, the average speed and the speed limit can be known, as well as whether the segment ends with a stop. We designed a constrained stochastic model that creates second-by-second speed profiles matching the M-VTP. It consists in running a Markov chain [8,9] in a loop until the main characteristics (distance, average speed, speed limit, final speed) of the outcome match the ones of the M-VTP subsection used as an input. When this algorithm is run for each subsection of the M-VTP, it results in an entire μ -VTP. In FY15, the goal was to improve the way the intersection approach is modeled, so that μ -VTPs are closer to real-world driving.

The vehicle we consider in this study is the Toyota Prius PHEV, the model of which has been implemented in Autonomie, a vehicle simulation tool developed at Argonne [10]. The model of Toyota Prius PHEV has a 200-V, 21-Ah Li-ion battery with 168 cells. The top speed in all-electric mode is 100 km/h, and its all-electric range (AER) is 23 km on the Japanese test cycle JC08. The vehicle controller executes the energy management, and has two main operating modes: charge-depleting (CD) mode, during which the battery gets discharged of its grid electricity until a low SOC threshold (set to 30%), after which the battery SOC hovers in a narrow range, in a charge-sustaining (CS) mode. The reference CD strategy consists in using electric-only operations as long as component constraints permit it, and using the engine if they don't; this results in the fastest battery discharge. The optimized CD (for trips longer than the AER) mode is an implementation of the PMP.

Approach

Intersection Approach Modeling

In our original algorithm, the modeling of intersections was relatively simple: for intersections with stop signs, there would be a constant wait time, and for traffic light, there would be a random probability of stopping and another probability for wait time. In actuality, there may be queues, several traffic light cycles and wait time may vary.

The general approach consists in:

- Modeling intersections in PTV VISSIM, a microscopic traffic flow simulator, with various intersection types, and a wide sweep of parameters (speed limits, traffic volumes, entry speed, etc.);
- Identifying a simple set of macroscopic variables (e.g. queue length) that suffice to predict the speed profile at the intersection;
- Building a predictive model linking these variables with the data (intersection type, average speeds, speed limits, etc.) available for prediction from the digital map;
- Creating a speed profile generator (given knowledge of variables);
- Integrating with existing algorithm.

Intersection with stop signs

Two-way and four-way stops were modelled in VISSIM. After multiple simulations, a relationship was found between queue length N_q , average speed V_{avg} and speed limit, as illustrated in Figure IV-73. There is also a relationship for the delay time T_d , i.e. the time stopped at the intersection. The queue length is the number of vehicles stopped and waiting to clear the intersection.

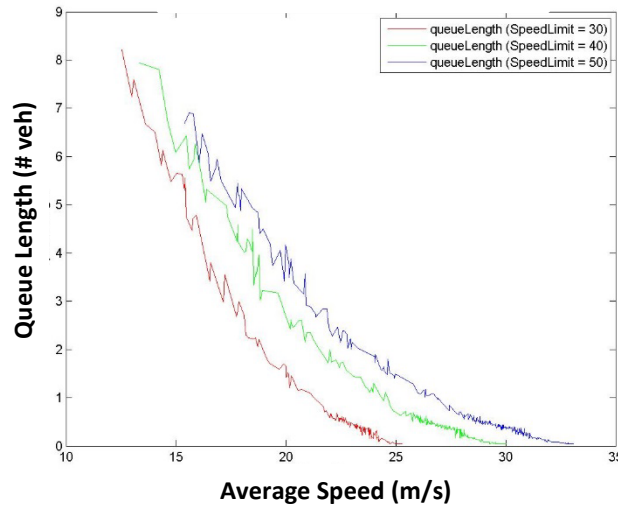


Figure IV-73: Evolution of queue length as a function of average speed for various speed limits (30, 40 and 50 km/h) for a 4-way stop intersection

These relationships translate into the following equations:

$$N_q = N_0 + a \cdot V_{avg} + b \cdot V_{avg}^2 \quad , \quad T_d = T_0 + c \cdot V_{avg}$$

The parameters N_0 , a , b , c , T_0 are different for the 3 speed limits considered, and are specific to the intersection type (2- or 4-way stop).

Intersections with Traffic lights

An intersection with a traffic light is modeled in VISSIM. Various volumes are applied, and the individual speed traces are analyzed, eventually leading to the identification of 4 canonical patterns:

- One stop: the vehicle encounters a red light, stops before the intersection; the queue is short enough that vehicle can clear the intersection once the light turns green.
- Two-stop: this situation is similar to the one-stop, but in this case, the queue is too long, and the vehicle must wait through another red phase before being able to clear the intersection. As a result, it has to stop twice.
- Deceleration: the light is green when the vehicle arrives at the intersection, but the queue from the red light is still clearing; as a result, it has to slow down, then reaccelerates and clears the intersection.
- No effect/free flow: the vehicle arrives at a green light, and does not alter its course

The probability of each scenario depends on the volume of cars entering the link, as shown in Figure IV-74. As the volume increase, all vehicles must stop at the light, and half of them need to stop twice.

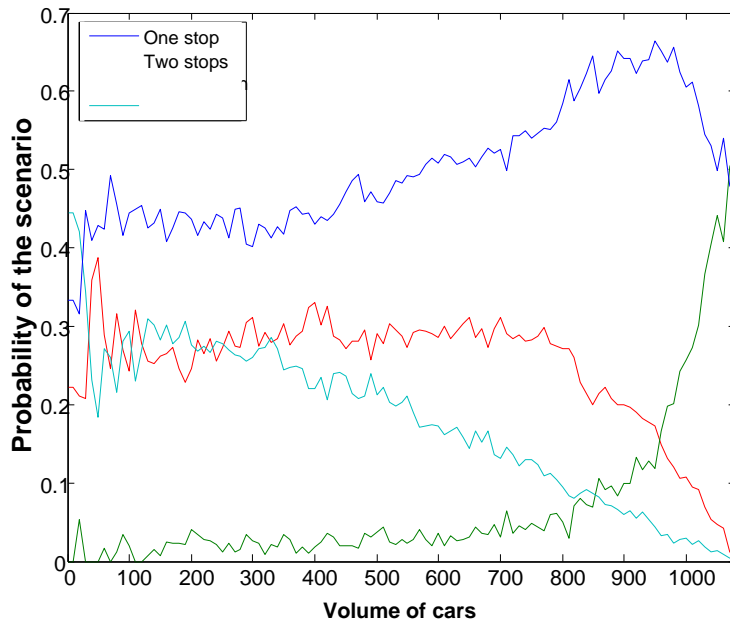


Figure IV-74: Probability of approach scenario as a function of the volume for an intersection with traffic lights

Similarly to stop sign intersections, there is a relationship between traffic volume and average speed, which can be provided by the digital map. Each scenario has a different set of features that uniquely describe it. For example, the one-stop scenario can be defined by the distance of the stop from the intersection and the stop time. We then build a probabilistic model for these two parameters, using joint distributions, and using traffic volume is an input. A similar approach can be applied to the other scenarios. As a result there is a clear path from average speed to scenario features. Once the scenario features are defined, the constrained Markov model can be used to generate a second-by-second speed profiles that matches the scenario feature.

Optimal Controller for a PHEV

The optimization aims at minimizing the fuel used on the entire trip, with the final SOC being the CS mode SOC target. According to the PMP [11], an optimal solution to that problem is to minimize at each time step the Hamiltonian H of the system:

$$H = P_f + r_0 \theta(P_b, S_b) P_b$$

Where P_f and P_b are respectively fuel and battery power, S_b is the battery SOC, r_0 is the equivalence factor (EQF), and θ is a dimensionless function whose value is close to 1.

The challenge in the PMP is to find the EQF that leads to the desired final condition (SOC=30%). If the EQF is too high, electricity is more costly and used less, leading to a partially discharged battery and, very likely, higher fuel consumption. If the EQF is too low, electricity is less costly and used more, the optimized CD mode ends prematurely, and there is a missed opportunity to optimize on the entire trip.

To evaluate the impact of route-based control on fuel consumption, we ran a large simulation experiment involving:

- 30 trips defined in 3 metro areas (Chicago, San Francisco, Pittsburgh), leading to 30 M-VTPs.
- 8 generations for each trip, resulting in 240 μ -VTPs; generating multiple μ -VTPs per M-VTP allows to model the stochastic nature of driving.
- 3 different initial SOC (90%, 70% and 50%).
- 9 EQFs: the optimal EQF for each μ -VTP, as well as 8 suboptimal values around the optimal one.

For each micro-VTP, the optimal EQF is the one that results in the operations as close as possible to the ideal situation, which is the SOC reaching the target SOC (30%) at the end of the trip and not before. The optimal EQF is computed using an ad hoc Newton method.

Results

Synthesized speed profiles at intersection approach

Figure IV-75 and Figure IV-76 respectively show examples of speed profiles in the case of intersection approach, with stop signs and with traffic lights.

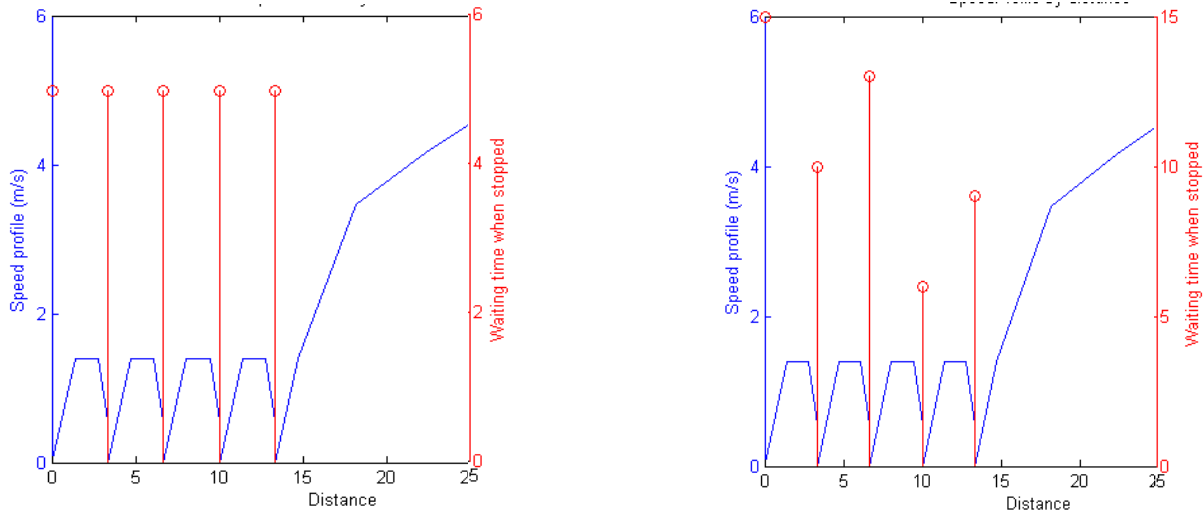


Figure IV-75: Example of Speed profile at intersection with stop signs: four-way stop (left), two-way stop (left)

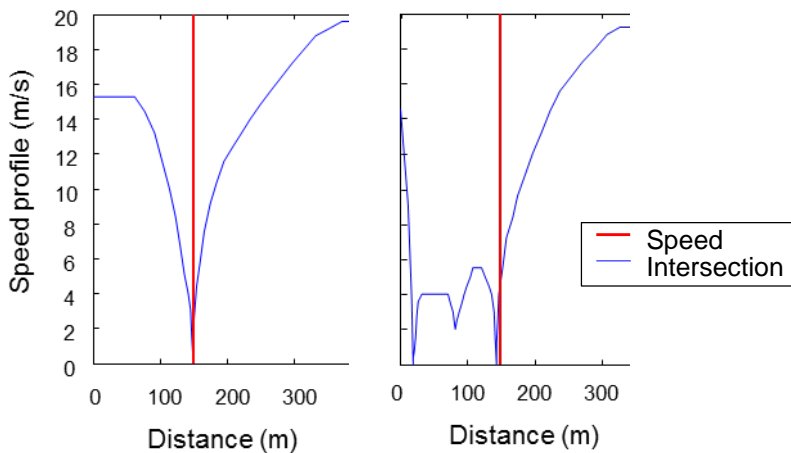


Figure IV-76: Example of Speed profile at intersection with traffic light; one stop scenario (left), two stop scenario (right)

Fuel savings with route-based control

Figure IV-77 shows energy use and fuel savings for one example trip. To compare the fuel savings, we adjust the fuel consumption based on the difference with the target SOC for both the reference and the optimal controllers. The left figure shows how adjusted and unadjusted fuel savings compare. The adjusted fuel savings for optimal EQF are then 7.5%; higher EQFs produce even higher adjusted fuel savings, but they are not desirable because they do not lead to a depleted battery, and in practice use more fuel.

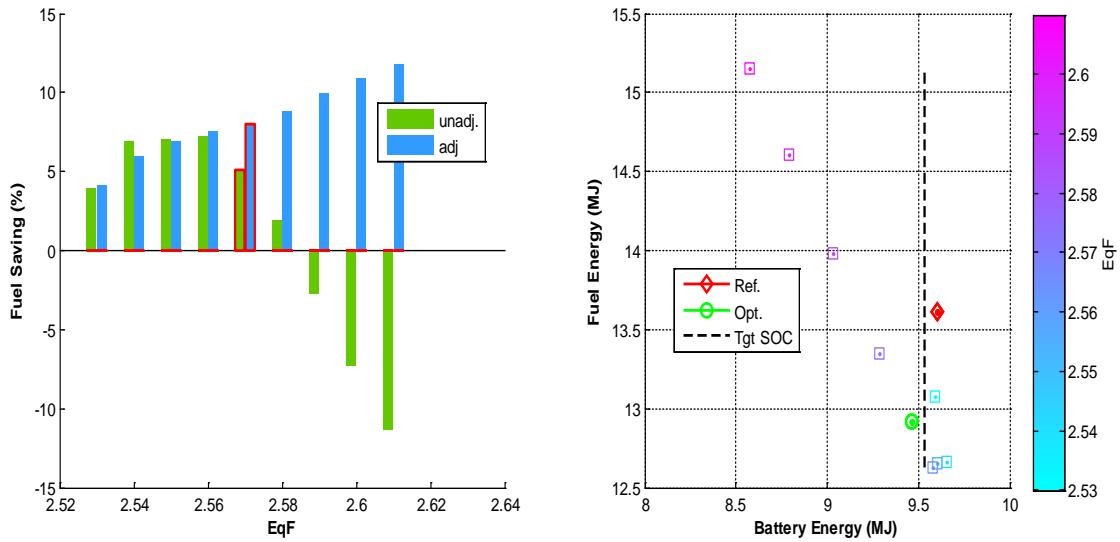


Figure IV-77: Unadjusted and SOC-adjusted fuel savings of PMP as a function of EQF (left); Total fuel energy and total battery energy for various EQF values (right)

The adjusted fuel savings for all μ -VTPs are shown in Figure IV-78, as a function of trip distance. Different colors represent different initial SOC. μ -VTPs where optimization was not necessary are not represented, i.e. when the trip can be done on electricity alone. Fuel savings are generally significant, with a very sizeable portion above 5%.

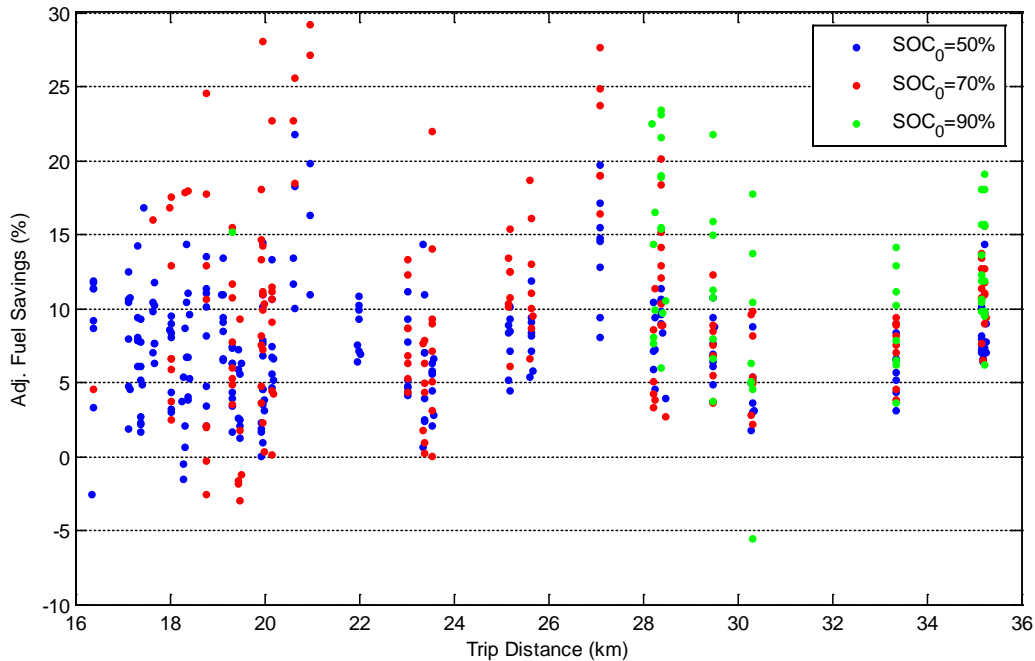


Figure IV-78: SOC-adjusted fuel savings of the PMP controller with optimal EQF for all μ -VTPs

Conclusions

The route prediction algorithm was improved:

- We analyzed intersection approach using a traffic flow microsimulation tool (VISSIM)
- For the stop sign intersection, it was found that the key features are queue length and time delay, and they are function of average speed and speed limit.
- For intersections with traffic lights, 4 canonical situations were identified, each with different features (stop time, position from intersection, etc.); probabilistic models were adopted in order to predict these features given an input (average speed) from the digital map.
- Once the macroscopic features are known, existing code can be re-used to generate speed profiles

Improvements on the route-based control were also achieved, and a study was performed:

- We improved the robustness of the PMP controller.
- We designed a process for large-scale evaluation the controller.
- We demonstrated that in a PHEV context, savings are significant.

IV.10.C. Products

Presentations/Publications/Patents

1. D. Karbowski, Namwook Kim, A. Rousseau. Route-based online energy management of a PHEV and sensitivity to trip prediction. IEEE Vehicle Power and Propulsion Conference 2014.
2. Dominik Karbowski, Namwook Kim, Aymeric Rousseau, Route-Based Energy Management for PHEVs: A Simulation Framework for Large-Scale Evaluation, 28th International Electric Vehicle Symposium (EVS28), Goyang, Korea, May 2015
3. Dominik Karbowski, Vadim Sokolov, Aymeric Rousseau, Vehicle Energy Management Optimization through Digital Maps and Connectivity, 22nd ITS World Congress, Bordeaux, France, October 2015

IV.10.D. References

1. D. Karbowski, A. Rousseau, et al. (2006). Plug-in Vehicle Control Strategy: From Global Optimization to Real Time Application. 22th International Electric Vehicle Symposium (EVS22), Yokohama.
2. Namwook Kim, S. Cha, H. Peng (2011). Optimal Control of Hybrid Electric Vehicles Based on Pontryagin's Minimum Principle. IEEE Transactions on Control Systems Technology, Vol. 19, Issue 5, pp. 1279–1287
3. G. Paganelli, S. Delprat, et al. (2002). Equivalent Consumption Minimization Strategy for Parallel Hybrid Powertrains. 55th IEEE Vehicular Technology Conference, 2076–2081.
4. P. Sahlholm, K. Henrik Johansson (2010) Road Grade Estimation for Look-Ahead Vehicle Control Using Multiple Measurement Runs. Control Engineering Practice, 1328–1341.
5. D. Rotz, A. Bracht, K. Moran, et al. (2010). Quality Assurance and Robustness for Predictive Cruise Control Using Digital Map Data. SAE Technical Paper 2010-01-0467, 2010.
6. Y. Deguchi, K. Kuroda, et al. (2004). HEV Charge/Discharge Control System Based on Navigation Information. SAE Technical Paper 2004-21-0028.
7. A. Schamel, P. Schmitz, J. d'Annunzio and R. Iorio (2013). Ford C-Max Plug-in Hybrid. MTZ worldwide, issue no. 2013-03.
8. A. Ivanco, A. Charlet, Y. Chamaillard, P. Higelin, (2009). Energy Management Strategies for Hybrid-Pneumatic Engine Studied on a Markov Chain Type Generated Driving Cycle. SAE Technical Paper 2009-01-0145.

9. Tae-Kyung Lee, Zoran S. Filipi (2011). Representative Real-World Driving Cycles in Midwestern US. Proceedings of Int. Scient. Conf. on Hybrid and Electric Vehicles (RHEVE 2011), IFPEN.
10. Autonomie, autonomie.net, accessed July 2015.
11. D. Karbowski, Namwook Kim, A. Rousseau (2014). Route-based online energy management of a PHEV and sensitivity to trip prediction. IEEE Vehicle Power and Propulsion Conference 2014.

IV.11. Honda PHEV Thermal Model Validation

Jongryeol Jeong, Principal Investigator

Argonne National Laboratory
9700 S Cass Avenue, Building 362
Argonne, IL 60439
Phone: (630) 252-5362; Fax: (630) 252-3443
E-mail: dkarbowski@anl.gov

David Anderson, DOE Program Manager

Office of Vehicle Technologies, Department of Energy
Phone: (202) 287-5688
E-mail: David.Anderson@ee.doe.gov

Start Date: 10/1/2014

End Date: 9/30/2015

IV.11.A. Abstract

Objectives

- Develop a model of a novel configuration of plug-in hybrid electric vehicle (PHEV), the 2014 Honda Accord Plug-in (Accord PHEV) with sensitivity to thermal conditions.
- Create the vehicle in Autonomie to support future studies.
- Further improve vehicle validation expertise.

Accomplishments

- Analyzed the operations of the 2014 Honda Accord Plug-in (Accord PHEV) based on test data.
- Analyzed sensitivity to thermal conditions: cold start, cold ambient, hot ambient, cabin heating and cooling.
- Developed and calibrated a vehicle model representative of the Accord PHEV in Autonomie.
- Developed supervisory control logic, including sensitivity to temperature.
- Validated the Accord PHEV vehicle model under different ambient temperatures.

Future Achievements

- Write paper on the validation of the PHEV Accord



IV.11.B. Technical Discussion

Background

Argonne has analyzed the control behaviors of advanced vehicles, such as hybrid electric vehicles (HEVs), PHEVs, and battery electric vehicles (BEVs), to develop simulation models and reproduce vehicle performances with simulation techniques [1–3]. Since many studies related to transportation technologies conducted at Argonne rely on simulation techniques [4], validated models are critical.

This project leverages the test data produced at Argonne's Advanced Powertrain Research Facility (APRF), which houses a 4-wheel drive chassis dynamometer set in an environmental chamber. The APRF replicates a

broad range of conditions, from -7°C or 35°C , with or without solar load. Once analyzed, the results are used to calibrate individual component models, including the thermal aspects. One of the main reasons to develop thermal models is that the impact of temperature on vehicle performance is significant, especially for electrified vehicles. Not only are the component losses affected by temperature, but so too is the vehicle-behavior because the supervisory control adjusts for the effects of ambient temperature.

This project investigates in detail the operations of the Accord PHEV, which was tested at the APRF with advanced instrumentation ("Level 2"), including half-shafts torque sensors.

Introduction

The Accord PHEV is a mid-size sedan with an EPA-rated all-electric range of 13 miles [5-7]. It features a powertrain design that has not seen significant commercial development before: a series-parallel without multi-gear transmission. In electric vehicle (EV) mode ("EV drive"), a 124 kW motor moves the car, linked to the 6.7 kWh Li-ion battery. In series mode ("Hybrid drive"), that motors remains the prime mover, but draws its energy from the generator set. In that configuration, the 102 kW Atkinson engine provides mechanical power to a generator that converts it to electricity. In parallel mode ("Engine drive"), the engine is connected to the wheels via a single ratio of 2.73:1, thus avoiding the losses incurred by the double energy conversion occurring in series mode. The switch between series and parallel mode is governed by a clutch: when the clutch is locked, the vehicle is in parallel mode, and is in EV or series mode otherwise.

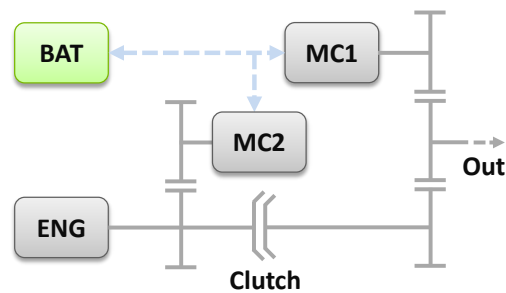


Figure IV-79: Series-parallel configuration of the Accord PHEV

Approach

The approach starts with test data import and enhancement. After this initial phase, data analysis, model development and vehicle validation occur in a closed-loop until convergence towards a validated vehicle model.

- Test data import and enhancement.** The raw test data is imported using Autonomie, which has tools facilitating the data analysis. During this phase, the signals are formatted (SI units, phase correction, standardized renaming), and additional signals are calculated from measured data. For example, the additional signal "clutch state" is computed from vehicle speed and engine speed, and the additional signal "engine torque" is calculated from half-shaft torque and motor torque. Thus, either through direct measurement or through calculation all of the relevant efforts and flow signals can be obtained from the test data. These test signals can then be directly compared to their equivalents from Autonomie simulation.
- Data analysis.** The enhanced test data is then thoroughly analyzed to understand component operations, control logic and sensitivity to thermal state and battery state-of-charge (SOC). The analysis is often used to calibrate component models, e.g. engine fuel rate maps.
- Model development.** A specific model for the Accord PHEV is implemented in Autonomie, based on published specifications and measured data (e.g. coupling ratios). If the observed operations are different from existing models, new ones are developed. The models are then calibrated using the test data.

- Vehicle validation.** Finally, all signals are compared between testing and simulation. A vehicle is validated not only if the fuel consumption is within the test-to-test variability, but also if the operations and efficiencies of the main components are properly replicated in simulation.

Results

Component operations

The operations of the main components of the vehicle (engine, battery, electric machines, tires) are analyzed, and efficiency and thermal parameters or maps are computed from the test data: engine fuel rate map (as a function of speed, torque and coolant temperature), battery internal resistance, engine thermal capacity, etc. Examples of such maps are shown in Figure IV-80.

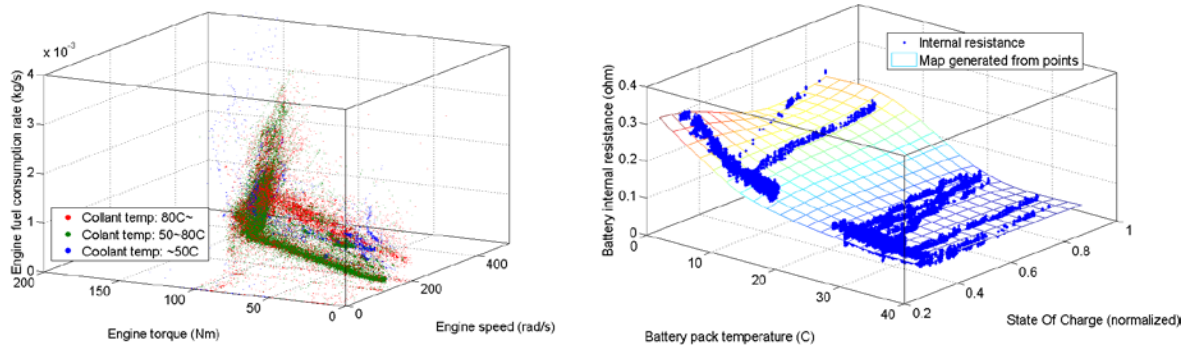


Figure IV-80: Engine fuel rate map (left) and Battery internal resistance (right), with temperature as a variable

Control analysis

When charged, the Accord PHEV is first operated in charge-depleting (CD) mode until a SOC of 35% is reached, at which point it switches to charge-sustaining (CS) mode. In CD mode, the priority is given to using electricity for propelling as much as possible. However, due to the limitations of the main electric machine, the engine is turned on at high power demand (~45kW) or when vehicle speed exceeds 100 km/h.

In CS mode, the goal is to use the engine as the main source of power and use the battery as a buffer, to perform typical HEV operations: electric-only (EV) mode, regenerative braking. Driver power demand was identified as the main trigger for engine ON events. At higher SOC (>30%), the threshold is approximately 14 kW, and decreasing as SOC falls below 30% SOC.

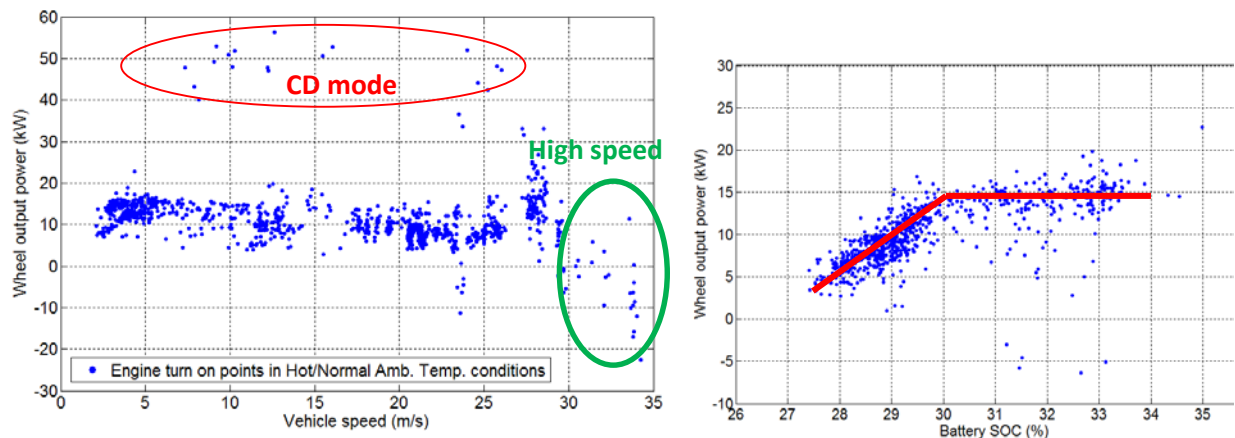


Figure IV-81: Wheel output power at engine starts as a function of vehicle speed (left) and battery SOC (right)

The other discrete control variable is the clutch state: when locked, the vehicle is in parallel mode, and when unlocked it is in series mode. The results clearly show that the parallel mode occurs at high vehicle speed (>70km/h), and when the driver power demand is positive but moderate (<40kW) - see Figure IV-82. In any other case, the vehicle operates in series mode. This behavior can be explained by the fact that the engine can only operate at low engine speed and low power when connected to the wheels, due to the low single multiplication ratio: At 40 mph, the engine cannot deliver more than 25 kW. The series operations always allow higher available power at the wheels, which explains why it is used at low speed or high power demand. On the other hand, the efficiency of the parallel mode is arguably higher, due to high torque, low speed operations and lack of electric conversion losses.

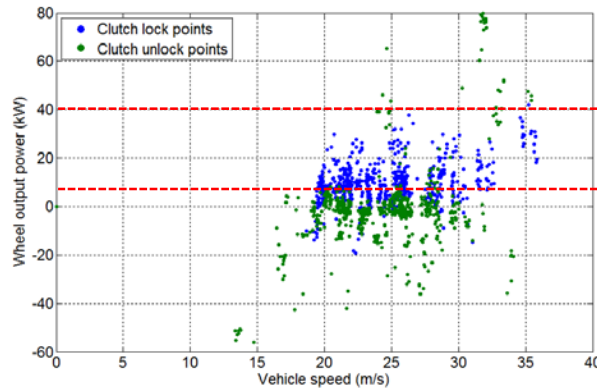


Figure IV-82: Clutch locking patterns - wheel output power at clutch lock and unlock

When the engine is ON, it is generally operated along what appears to be an "optimal efficiency" line, at least during relatively steady operations. In series, this is a natural choice: since the engine speed is decoupled from the vehicle speed, the generator-set can deliver any desired output power while following a narrow operating line. It is a less conventional approach in parallel mode, because the speed is constrained, therefore forcing the engine to operate at a power dictated by vehicle speed, not driver power demand. As a result, the difference must be provided or absorbed by the battery, which can be seen in Figure IV-83. However the battery is not charged beyond 10 kW, which means that the engine must then operate off target, at lower torque and therefore lower efficiency.

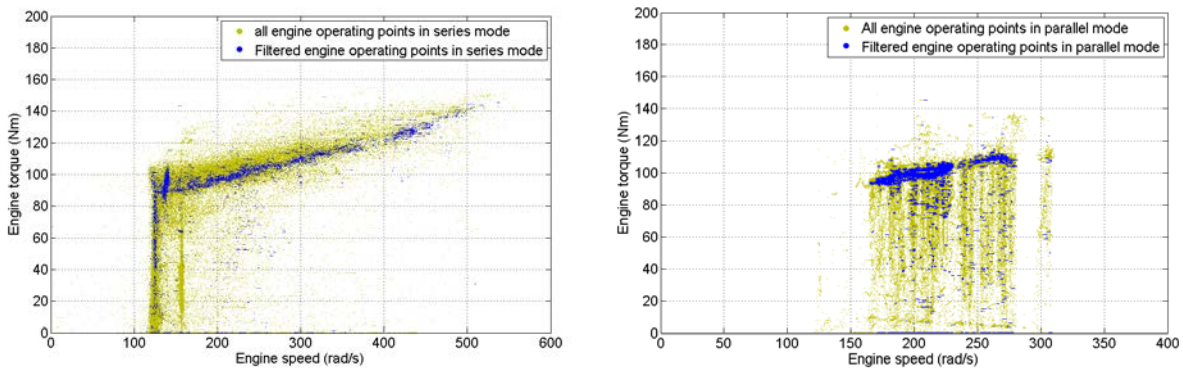


Figure IV-83: Steady-state (blue points) engine operating points in series (left) and parallel (right) mode

Impact of Thermal conditions

The control of the Accord PHEV is impacted by the temperature to some extent. In CD mode, there is no particular change in control in cold ambient temperatures. That is because the Accord PHEV has an electric heater, and does not require the engine to provide waste heat for cabin heating purposes. Even when the engine is turned ON, it is behaving similarly to normal ambient conditions.

In CS mode however, the engine coolant temperature is maintained above 65C, certainly for efficiency and emission reasons, but also because waste engine heat is used for cabin heating and not the electric heater. Cold starts involve idling the engine until it warms up, letting it spin at higher angular speed (+300RPM) without load. In cold ambient conditions, we also observe that some of the engine starts are triggered by the engine coolant temperature dropping below the 65C threshold.

Validation

A model of the vehicle, including calibrated plants and controllers was implemented in Autonomie. The validation process is iterative, and combines data analysis, model development and model calibration.

The main goal is to closely match all effort and flow signals, as well as state signals (engine ON, battery SOC, engine coolant temperature). Figure IV-84 shows an example of a cold start in cold ambient temperature. Once a good match is obtained, total fuel consumption results is within the test-to-test uncertainty, as shown in Table IV-42 and Table IV-43.

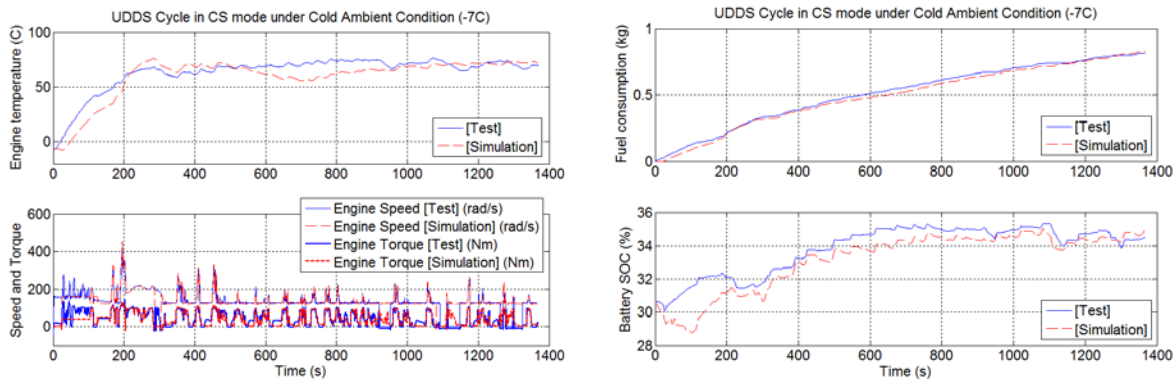


Figure IV-84: Comparison of tested and simulated signals for UDDS cycle in cold ambient conditions

Table IV-42: Validation results (Urban/UDDS)

Ambient Temperature (C)	Driving mode	Fuel Consumption (g)		Final SOC (%)	
		Test	Simulation	Test	Simulation
22C	CD	0	0 (-)	61.1	61.4 (0.64%)
	CS	360.3	360.7 (0.11%)	29.7	28.9 (-2.71%)
35C	CD	0.6	0 (-)	54.5	54.5 (0.01%)
	CS	424.1	444.7 (4.85%)	28.6	26.8 (-5.98%)
-7C	CD	338.6	345.0 (1.89%)	33.8	34.2 (1.01%)
	CS	815.0	826.1 (1.36%)	34.5	34.9 (1.28%)

Table IV-43: Validation results (Highway)

Ambient Temperature (C)	Driving mode	Fuel Consumption (g)		Final SOC (%)	
		Test	Simulation	Test	Simulation
22C	CD	-	-	-	-
	CS	429.9	430.8 (0.20%)	31.4	31.4 (0.23%)
35C	CD	0.3	0 (-)	48.2	50.6 (4.99%)
	CS	589.2	590.7 (0.26%)	31.1	30.3 (-2.79%)
-7C	CD	262.7	250.3 (-4.75%)	31.4	33.1 (5.49%)
	CS	828.4	814.6 (-1.67%)	33.5	32.9 (-2.02%)

Conclusions

- 2014 Honda Accord PHEV test data was imported in Autonomie from Argonne's APRF. It is the first series-parallel configuration validated at Argonne.
- Configuration and control strategy were developed in Autonomie.
- Vehicle energy management strategy analysis completed using APRF test data, including:
 - Engine ON/OFF, clutch lock (i.e. series/parallel modes)
 - Engine operation target, battery SOC balancing
 - Operations in hot and cold ambient temperatures with cold starts
- The model was validated within the test-to-test uncertainty

IV.11.C. Products

Presentations/Publications/Patents

1. Jeong, Jongryeol, Namwook Kim, Eric Rask and Dominik Karbowski, "Model Validation of the Honda Accord Plug-In", submitted for SAE World Congress 2016

IV.11.D. References

1. Rousseau, A., Kwon, J., Sharer, P., Pagerit, S., et al., "Integrating Data, Performing Quality Assurance, and Validating the Vehicle Model for the 2004 Prius Using PSAT," SAE Technical Paper 2006-01-0667, 2006.
2. Kim, N., Rousseau, A., and Rask, E., "Vehicle-level Control Analysis of 2010 Toyota Prius Based on Test Data," IMechE Part D: J. Automobile Engineering, 226(11):1483-1494, Nov. 2012.
3. Kim, N., Rousseau, A., Lee, D., and Lohse-Busch, H., "Thermal Model Development and Validation for 2010 Toyota Prius," SAE Technical Paper 2014-01-1784, 2014.
4. Government Performance and Results Act; available at whitehouse.gov/omb/mgmt-gpra/index-gpra
5. Higuchi, Naritomo, Yoshihiro Sunaga, Masashi Tanaka, and Hiroo Shimada. "Development of a New Two-Motor Plug-In Hybrid System." SAE Technical Paper 2013-01-1476 (April 8, 2013). doi:10.4271/2013-01-1476.

6. Ohkubo, Naoto, Satoshi Matsushita, Masayuki Ueno, Kohei Akamine, and Kunimichi Hatano. "Application of Electric Servo Brake System to Plug-In Hybrid Vehicle." SAE Technical Paper 2013-01-0697 (April 8, 2013). doi:10.4271/2013-01-0697.
7. Yonekawa, Akiyuki, Masaki Ueno, Osamu Watanabe, and Naohiro Ishikawa. "Development of New Gasoline Engine for ACCORD Plug-in Hybrid." SAE Technical Paper 2013-01-1738 (April 8, 2013). doi:10.4271/2013-01-1738.

IV.12. EcoCAR3 Support

Ram Vijayagopal, Larry Michaels, and Aymeric Rousseau, Principal Investigators

Argonne National Laboratory
9700 S. Cass Avenue, Building 362
Argonne, IL 60439
Phone: (630) 252-9739; Fax: (630) 252-3443
E-mail: ram@anl.gov

David Anderson, DOE Program Manager

Office of Vehicle Technologies, Department of Energy
Phone: (202) 287-5688
E-mail: David.Anderson@ee.doe.gov

Start Date: 10/1/2015

End Date: 9/30/2016

IV.12.A. Abstract

Objectives

- Integrate component performance data from the different sponsors
- Integrate higher fidelity plant models from MathWorks
- Integrate new/enhance existing processes in Autonomie working with MathWorks (i.e., Verification and Validation [V&V])
- Develop training material
- Provide support to the universities participating in EcoCAR3

Accomplishments

- All of the component data provided by event sponsors were imported to Autonomie, and baseline vehicle models were provided to the teams. These models were used for vehicle sizing.
- MathWorks provided physical models for certain components and a procedure to import them to Autonomie was developed. The teams were free to use Autonomie models or MathWorks models within or outside of Autonomie.
- Verification and validation procedures were developed and were included in the training sessions for the EcoCAR teams.
- Webinars were conducted to introduce the students to the methodology of progressing from Model in Loop (MIL) to Software in Loop (SIL) to Hardware in Loop (HIL).
- All questions from EcoCAR teams have been answered. All issues faced by the teams in their simulation effort, even if not directly related to Autonomie, have been looked into and explained to the teams.

Future Achievements

- General Motors (GM) withheld some actual vehicle specifications in the initial stage because the new Camaro had not yet been released. GM released the data to Argonne National Laboratory (Argonne) and teams in August 2015. These data need to be examined, and the vehicle models will be updated if necessary.

IV.12.B. Technical Discussion

Background

Argonne has extensive experience in modelling and simulating advanced vehicles. Autonomie is a plug-and-play powertrain and vehicle model architecture that is ideal for the powertrain selection and technology evaluation required in a project like EcoCAR.

Introduction

GM provides the specifications for the vehicle it donates to the universities, and Argonne is responsible for building a baseline vehicle model in Autonomie. This year, Autonomie was not the sole modelling environment available for the students. MathWorks too took the initiative to build a vehicle using Simulink and their physical modelling toolboxes.

Teams had the options to use

- Models developed by their respective universities,
- Models provided by Autonomie, or
- Models provided by MathWorks.

Approach

EcoCAR teams were trained to use Autonomie as they started the project in late 2014. The release of a new version of Autonomie and introduction of many new features made it necessary to conduct follow-up training in early 2015. For any kind of support, the teams could send emails to the Autonomie support team; Argonne responded to their questions within a few days. Several personnel, based on their areas of expertise, were involved in answering the questions from the EcoCAR teams.

Training materials were also developed by the Autonomie team. Three webinars were organized to demonstrate how Autonomie could be used for the verification and validation process during the various stages of the competition.

Results

Many teams used Autonomie as their primary simulation tool during the first year for the hybrid architecture selection and the component sizing. We believe that a majority of the teams are planning to use Autonomie in future stages of the competition as well.

Conclusions

Use of Autonomie is helping EcoCAR teams in their technology selection stage. We wish to expand the use of Autonomie-based modelling and simulation in the EcoCAR program, there by introducing the students to model based systems engineering. Demonstrating an actual hybrid controller development, as required for the EcoCAR competition will be a good step in this direction. Such a demonstration would also provide more insights into new features that have to be developed to make the process easier.

Tools and Data

Autonomie (autonomie.net)

IV.13. Evaluation of Benefits of DOE Vehicle Technology Research on Real-World Driving

Neeraj Shidore, Investigator

Argonne National Laboratory
 9700 South Cass Avenue, Building 362
 Argonne, Illinois 60439
 Phone: (630) 252-7416; Fax: (630) 252-3443
 E-mail: nshidore@anl.gov

David Anderson, DOE Program Manager

Office of Vehicle Technologies, Department of Energy
 Phone: (202) 586-2333
 E-mail: david.anderson@ee.doe.gov

Start Date: 10/1/2015

End Date: 9/30/2016

IV.13.A. Abstract

Traditionally, vehicle technology evaluation is performed on standard drive cycles and procedures. For the past several years, the benefits of vehicle technology research performed by the Office of Vehicle Technologies (VTO) at the U.S. Department of Energy (DOE), have been evaluated on these standard drive cycles. Argonne National Laboratory's (Argonne's) Vehicle System Simulation Software, Autonomie, has been used to predict vehicle fuel consumption and component utilization information for the advanced powertrain technologies researched by VTO. In this study, leveraging large-scale simulation processes, the benefits of VTO research on vehicle technologies has been performed on real-world drive cycles.

IV.13.B. Objectives

Leverage the large-scale simulation process in Autonomie to answer key questions:

- What is the evaluation of the real-world impact of VTO technology research on petroleum displacement?
- How do VTO technology benefits compare between the standard drive cycles and the Real-World Design Challenge (RWDC)?
- What is the sensitivity of the results to the choice of real-world cycles?

Accomplishments

- Developed a large-scale simulation approach to evaluate the impact of VTO technology benefits on real-world driving.
- Developed in Autonomie, Daily Driving Trips (multiple drive cycles with key-off) which meet the National Household Travel Survey (NHTS) average daily miles travelled. These daily driving trips are a close statistical representation of daily driving.
- The results show that apart from plug-in hybrid electric vehicles (PHEVs), benefits of VTO technology are 'overrepresented' by standard drive cycles.
- Based on preliminary results, real-world profiles that match the NHTS average daily miles travelled would show similar VTO technology benefits.

Future Achievements

- The evaluation of the impact of VTO technologies will be expanded to consider other real-world scenarios, like fleet distribution, thermal, and intelligent transportation systems (ITS).
- For the current study, additional sets of real-world daily trip profiles will be used to evaluate the impact of VTO technology benefits.



IV.13.C. Technical Discussion

Background

Evaluation of the VTO technology research portfolio is a key function of vehicle systems research. Traditionally, vehicle technology evaluation is performed on standard drive cycles and procedures. It is important to evaluate technology on non-standard drive cycles, so as to ascertain the benefits of technology research in real-world situations.

Introduction

Argonne National Laboratory (Argonne) has developed a process to run large-scale simulation studies using Argonne's vehicle system simulation tool—Autonomie. Autonomie is being used to evaluate VTO technology benefits over standard cycles, in the DOE analysis or baseline and scenario analysis (BaSce) process. Leveraging this large-scale simulation process, the analysis is now being expanded to real-world (non-standard) drive cycle scenarios, like real-world drive cycles (RWDC), fleet distribution, thermal analysis and ITS. This study provides an evaluation of technology benefits over real-world drive cycles.

Approach

The travel survey [1] conducted by the National Highway Transportation Safety Administration (NHTSA) in 2009 was used to generate a distribution of average daily miles travelled. In addition, several daily driving trips were generated from the real-world drive cycles from the National Transportation Secure Data Center [2] at National Renewable Energy Laboratory (NREL). Figure IV-85 shows a conceptual flow chart of the process.

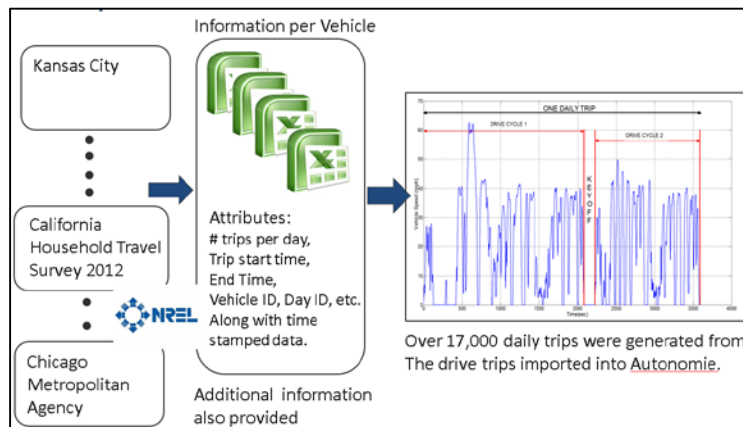


Figure IV-85: Generation of daily driving events from real-world drive cycles from NREL

Sets of such daily drive events or were then combined into sets of daily driving events, such that each set matched the distribution of average daily miles travelled generated from the NHTSA survey (Figure IV-86).

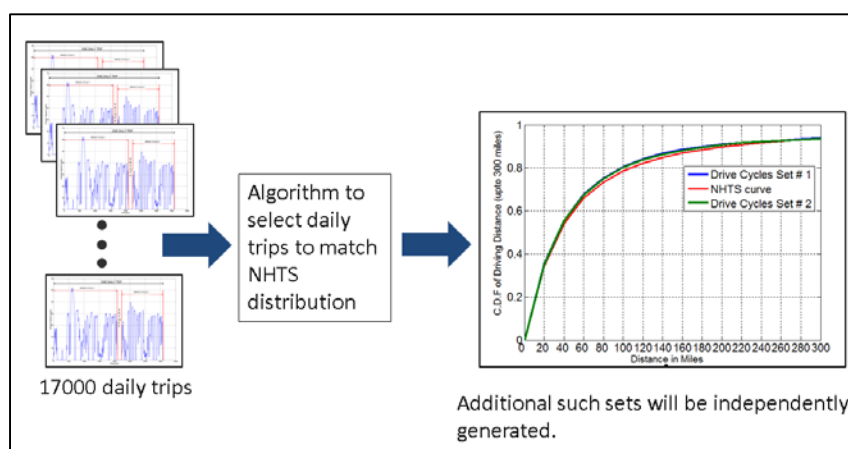


Figure IV-86: Generation of sets of daily driving trips to meet the NHTS distribution

Vehicles, representing VTO facilitated technology improvements in vehicle model years 2015 (current technology vehicles) and model year 2025 were chosen to compare the real-world versus standard drive cycle impact. For the vehicle model year 2025, simulation models developed with optimistic DOE targets were used. For each of the future years, DOE technology targets are set at three levels—no DOE involvement (pessimistic targets), optimistic targets, and an average case in between. Conventional vehicles with gasoline and diesel technology, a charge sustaining hybrid with a gasoline Atkinson Cycle engine, battery electric vehicles (EV) with 100-mile and 300-mile EV ranges, and PHEVs with a 10-mile and a 40-mile electric range were chosen, to represent a spectrum of powertrain technologies of the future. Vehicles on the road in 2015 and 2025 represent vehicles which are in the 'lab' in 2010 and 2020 respectively, and hence, in the further references in the document, these vehicles will be referenced as 2010 simulation year and 2020 simulation year, respectively. In addition to real-world daily driving trips, the vehicles were also simulated on standard drive cycles and standard procedures for the hybrid, electric, and plug-in hybrid procedures.

The NHTS distribution represents a one-day distribution of multiple vehicles making multiple trips. Therefore, aggregate fuel consumption from all the real-world driving trips, for a particular vehicle powertrain, for a given simulation and/or lab year, is calculated using the following formula:

$$RW \text{ fuel consumption} = \frac{\sum fc_i \times d_i}{\sum d_i}$$

where

fc_i = fuel consumption of the i th daily trip

d_i = driving distance of the i th daily trip

As such, the aggregate fuel consumption represents a fleet average value.

Results

As stated above, several sets of daily driving events or trips were generated, each set representing the distribution of daily driving per the NHTS curve. The following results are for the first such set of daily driving trips, which have over 1,000 daily driving events, and 22 different powertrains (2010 and 2020), and represent over 22,000 simulation runs.

Table IV-44 shows the comparison in VTO technology impact for conventional (gasoline and diesel) and charge sustaining hybrid technologies, between the real-world and the combined (Urban Dynamometer Driving Schedule [UDDS] and Highway Fuel Economy Test [HWFET]) 2-cycle procedure.

Table IV-45 shows the comparison for a charge sustaining hybrid powertrain with a gasoline spark-ignition (SI) engine. It shows that in both cases—conventional (gasoline [SI] and diesel compression-ignition [CI]) and hybrid—the impact of VTO technology benefits is lower with real-world daily driving.

Table IV-44: Impact of VTO Technology Benefits for Conventional Powertrain (Real-World and Standard Procedure)

	Powertrain	2010 (L/100 km) gasoline eq	2020 (L/100 km) Gasoline eq	% Improvement
Real-World (distance weighted)	Conv SI	7	4.8	31.4%
Combined (UDDS and HWFET)	Conv SI	6.6	4.4	33.3%
Real-World	Conv CI	5.8	4.3	25.2%
Combined	Conv CI	5.3	3.7	30.1%

Table IV-45: Impact of VTO Technology Benefits for Hybrid Powertrain (Real-World and Standard Procedure)

	Powertrain	2010 (L/100 km)	2020 (L/100 km)	% Improvement
Real-World	Hybrid - SI	4.9	3.9	20.4
2-cycle Procedure	Hybrid - SI	4.1	3	27.7

Figure IV-87 shows the ratio of electric to total miles travelled for a PHEV-40, i.e., a plug-in hybrid capable of 40 miles of electric driving on the UDDS drive cycle, on the set of real-world daily driving trips, for both 2010 and 2020 cases. It can be seen that there is hardly any difference in the ratio due to VTO technology improvements.

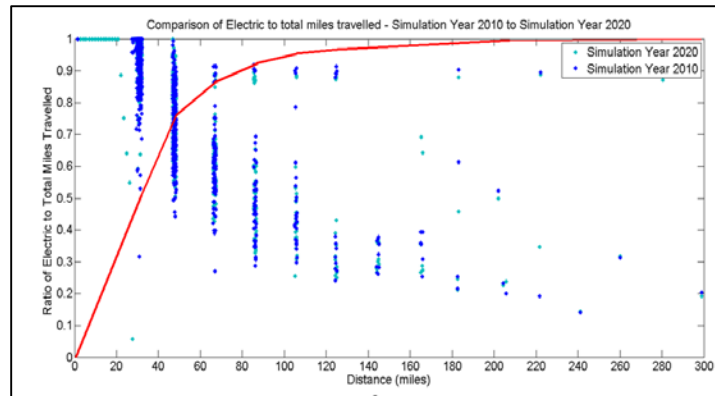


Figure IV-87: Ratio of electric to total miles across different daily driving distances

Table IV-46 compares the gains between real-world and standard procedures, in electrical energy consumption (Wh/mi) for a battery electric vehicle (BEV)-100, i.e., an electric vehicle capable of a range of 100 miles on the UDDS cycle, due to VTO technology enhancements. It can be seen that the impact of VTO technology benefits is lower in the case of real-world driving, when compared to the U.S. Standard Procedure for electric vehicles (EVs) (SAE J1634). A similar impact also is seen in the case of the BEV-300.

Table IV-46: Impact of VTO Technology Benefits for an Electric Powertrain (Real-World and Standard Procedure)

	Powertrain	2010 (Wh/mi)	2020 (Wh/mi)	% Improvement
Real-World	BEV-100	326	225	31
Standard Procedure	BEV-100	283	213	25

As stated earlier, multiple sets of daily trips have been developed to match the NHTS distribution. Table IV-47 compares the benefits of real-world to standard procedure for two such sets of daily trips, for a BEV-100. It shows that for both sets of real-world data, the technology benefits are similar.

Table IV-47: Impact of VTO Technology Benefits for an Electric Powertrain (Real-World and Standard Procedure) for two sets of Daily Driving Schedules

	Powertrain	2010 (Wh/mi)	2020 (Wh/mi)	% Improvement
Real-World Set 1	BEV-100	326	225	31
Real-World Set 2	BEV-100	286	215	24
Standard Procedure	BEV-100	283	213	25

Conclusions

- A large-scale simulation approach has been developed to evaluate the impact of VTO technologies' benefits on Real-World Driving.
- Daily Driving Trips (multiple drive cycles with key-off) which meet the NHTS average daily miles travelled are a close statistical representation of daily driving.
- Several such sets of Daily Driving Trips have been developed from the NREL database and are available to Autonomie users.
- Apart from PHEVs, the benefits of VTO technologies are 'overrepresented' by standard drive cycles.
- Based on preliminary results, Real-World Profiles that match NHTS average daily miles travelled would show similar VTO technology benefits.

IV.13.D. Products

Presentations/Publications/Patents

1. E. Islam, N. Shidore, and A. Rousseau, 'Evaluation of VTO Technology Benefits over Real-World Drive Cycles—Research Update,' presented to the U.S. Department of Energy, September 28th, 2015.

IV.13.E. References

1. U.S. Department of Transportation, Federal Highway Administration, 2009 National Household Travel Survey. URL: nhts.ornl.gov.
2. National Renewable Energy Laboratory (NREL), Transportation Research, nrel.gov/transportation/secure_transportation_data.html

IV.14. Analyzing Real-World Light-Duty Vehicle Efficiency Benefits

Jeffrey Gonder, Principal Investigator

National Renewable Energy Laboratory (NREL)
15013 Denver West Parkway, MS 1634
Golden, CO 80401
Phone: (303) 275-4662; Fax: (303) 275-3765
E-mail: Jeff.Gonder@nrel.gov

David Anderson, DOE Program Manager

U.S. Department of Energy (DOE)
Office of Energy Efficiency and Renewable Energy (EERE)
Phone: (202) 287-5688 (David Anderson)
E-mail: David.Anderson@ee.doe.gov
Phone: (202) 586-2335 (Lee Slezak)
E-mail: Lee.Slezak@ee.doe.gov

Start Date: 10/1/2013
End Date: 9/30/2016

IV.14.A. Abstract

Objectives

- Evaluate the real-world fuel savings opportunities for technologies that are difficult to assess using standard certification cycles
 - DOE and regulatory bodies want to maximize real-world fuel savings
 - Original equipment manufacturers (OEMs) want to get credit for actual fuel savings achieved
- Develop and evaluate a novel analytical methodology for accurately and objectively evaluating real-world efficiency impacts from off-cycle technologies
 - Leverage detailed vehicle testing efforts at Argonne National Laboratory (ANL)
 - Technologies considered could include thermal retention/engine encapsulation, start/stop hybridization, high-efficiency alternators, high-efficiency lighting, glazing technology, and/or automated and connected vehicle features.

Accomplishments

- Successfully developed and implemented analytical framework for real-world evaluation
 - Leveraged existing DOE lab capabilities for objective evaluation of energy efficiency technologies, including past and ongoing NREL activities using large data sets to determine real-world distributions of on-road operating conditions (such as vehicle loads from driving speed and acceleration, road grade, ambient temperature, and solar loads)
- Applied analytical framework to assess real-world benefits from three hypothetical off-cycle technologies: solar reflective window glazing, accessory load reduction, and powertrain thermal retention (such as via engine encapsulation)
 - Results indicated that the real-world analytical methodology is important to capture the benefit of some but not all such technologies
- Thermal retention is one technology where such an analytical framework is needed; the hypothetical benefit calculation estimated over 5 g CO₂/mi potential greenhouse gas emissions reduction and savings over 1% higher than that estimated by the traditional two-cycle approach for Corporate Average Fuel Economy (CAFE) evaluation

- This is significant, as broad implementation of even a seemingly modest 1% fuel saving technology for conventionally powered vehicles would have the equivalent aggregate benefit of taking 2.5 million vehicles off the road.

Future Achievements

- Further model validation and refinement via on-road data collection
- Additional statistical analysis and enhancements to the analytical driving profile binning by road type
- Other proposed efforts include applying the methodology to evaluate actual off-cycle technologies for which the National Renewable Energy Laboratory (NREL) can obtain test data (as opposed to just hypothetical examples), and extending consideration to other types of off-cycle technologies (such as actual real-world impacts of start/stop hybridization or of connected and automated vehicle features).



IV.14.B. Technical Discussion

Background

NREL has significant experience managing large GPS databases and interfacing data with vehicle simulation. Some recent studies focused on 1) real-world fuel economy distributions and sensitivities, 2) comparisons between real-world driving profiles and standard certification test cycles, 3) enabling road grade simulation and quantifying impact, and 4) synthesis with national climate data for evaluation of thermal technologies [1–5].

Additionally, through the Internal Combustion Engine Energy Retention Project, NREL developed and implemented a novel approach of simplifying experimental data into a predictive model to improve understanding of the real-world thermal and driving effects on vehicle efficiency [6].

This project—Analyzing Real-World Light-Duty Vehicle Efficiency Benefits—builds on these previous bodies of work.

Introduction

Off-cycle technologies represent an important pathway to achieving real-world fuel savings and provide an opportunity for OEMs to earn compliance credits for CAFE regulations. DOE's national labs are well positioned to provide objective input on such technologies using large national data sets in conjunction with OEM-specific testing.

This project demonstrates an approach that combines vehicle testing (in-lab and on-road) with powertrain modeling and simulation over large, representative data sets to quantify real-world fuel economy. Such an approach can be applied to off-cycle technologies (including engine encapsulation, start/stop, connected vehicles, etc.) in A/B comparisons to support calculations of realistic real-world impacts.

Approach

The testing and model-based evaluation process included in-laboratory and on-road activities, leveraging work performed at ANL with a highly-instrumented test vehicle.

Dynamometer testing

First, ANL conducted hundreds of miles of in-laboratory dynamometer testing at its Advanced Powertrain Research Facility to generate data over a range of conditions in a controlled environment. While the vehicle

under test was a 2011 Ford Fusion representative of a modern mid-sized sedan, this project's testing and analysis activities were designed to be extended to other chassis and powertrain designs.

ANL performed a matrix of 16 dynamometer tests over various drive cycles, start conditions, and ambient temperatures. In addition to the 16-cycle sweep, ANL tested the vehicle under the U.S. Environmental Protection Agency's (EPA's) standard 5-cycle test procedure (FTP, HWFET, US06, SC03, Cold FTP).

Simulation

Then, NREL calibrated a vehicle model against the laboratory test data using the Future Automotive Systems Technology Simulator (FASTSim). Developed by NREL, the FASTSim vehicle simulation tool evaluates the impact of various technologies on vehicle performance, cost, and utility in conventional and advanced powertrains. FASTSim calculates the power necessary to meet a given speed trace and overcome road loads (rolling, aerodynamic, kinetic, and potential) while considering component limitations, system losses, and auxiliary loads [7].

FASTSim is particularly well suited to rapid simulation of very large numbers of drive cycles over multiple conditions, which is what was done for this study utilizing the data in the Transportation Secure Data Center (TSDC). Maintained by NREL for DOE and the U.S. Department of Transportation, the TSDC is an online repository for the secure archival of personal travel data. It features more than a million miles of 1-Hz GPS travel histories from personally owned light-duty vehicles. Its geographical coverage includes highways and city streets in multiple urban and rural areas across the United States. NREL processing routines join data points to the road network, link U.S. Census and other spatial data layers, and add information such as road grade [8].

The simulations were run over combinations of the real-world driving profiles with typical climate conditions across the United States and were weighted based on total driving occurring under the different conditions to generate national averages. NREL designed the evaluation process to be model-agnostic so that other organizations could reproduce results using various modeling platforms.

Validation

Finally, ANL made the Ford Fusion test vehicle available to NREL for on-road evaluation as a sanity check that the model calibrated against data from laboratory testing under controlled conditions can accurately represent real-world fuel use in an uncontrolled environment. The vehicle's instrumentation was reconfigured for mobile data logging, which included adding a GPS and in-line flow meter for on-road measurements. The on-road data collection is ongoing and will include collection of thousands of miles of data to complete this validation sanity check and any model recalibration if needed.

National datasets supporting results extrapolation

NREL employed a variety of national datasets, including 1) TomTom Multinet, a digital street map of U.S. highways and city streets consisting of more than 3 million links; 2) the Federal Highway Administration (FHWA) Highway Performance Monitoring System (HPMS), which features national vehicle miles traveled (VMT) estimates by vehicle type, geography, and functional class; 3) the U.S. Geological Survey's Digital Elevation Model, a national elevation data used to derive road grade; and 4) NREL's National Solar Radiation Database (NSRDB), which contains typical meteorological year data for more than 1,000 U.S. weather stations with hourly resolution.

Results

Good model/data agreement

Figure IV-88 shows example time series data of measured and modeled engine fueling rate, with the measured test data from chassis dynamometer (solid black) overlaid with the model estimate (dashed magenta). As the figure demonstrates, good model/dynamometer data agreement was achieved for fuel use. The model calculates fuel consumption to within 5.2% on all 16 test conditions and within 2.2% on average.

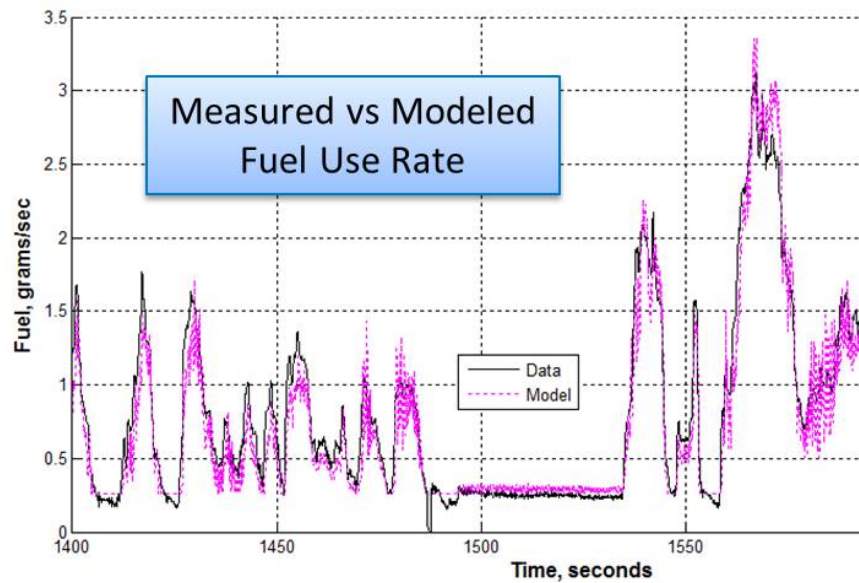


Figure IV-88: Good agreement was achieved between the simplified powertrain model's fuel consumption estimates and fuel consumption measurements from laboratory chassis dynamometer testing

Source: NREL

Good model/dynamometer data agreement was achieved for thermal states as well—specifically for exhaust catalyst, engine oil, and engine coolant temperatures. Figure IV-89 illustrates this with the model's predictions compared with measured test data on engine oil temperature during warm-up (i.e., after initial vehicle start) and cool-down (i.e., after the vehicle stops and is turned off).

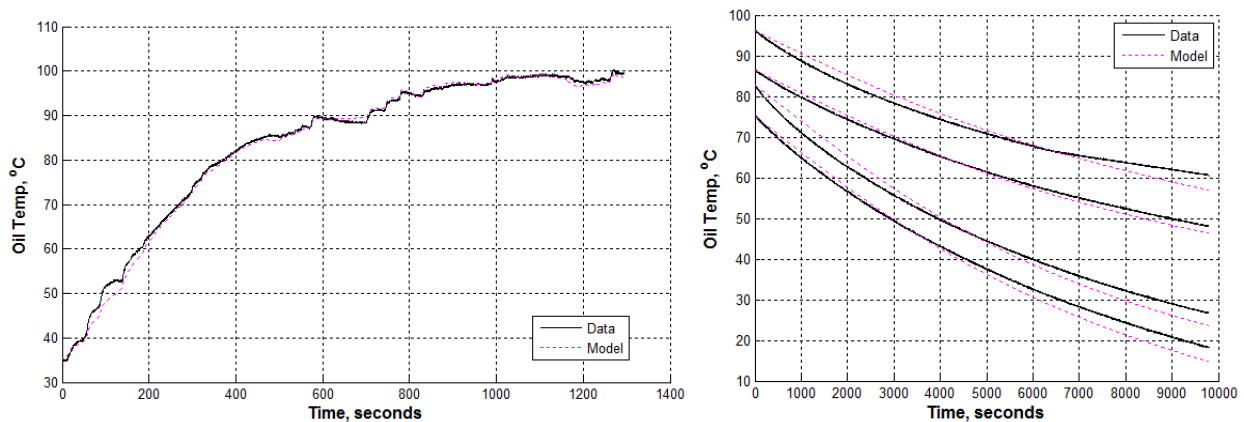


Figure IV-89: Good agreement was achieved between the simplified powertrain model's thermal predictions and measured temperatures from the laboratory chassis dynamometer testing (shown here for engine oil as an example)

Source: NREL

Additionally, initial on-road testing has confirmed that the model performs well on rural, controlled-access highways, and on-going testing will evaluate the model's accuracy in a variety of driving conditions—including significant road grades typical of travel through the Rocky Mountains.

Model snapshots

Figure IV-90 shows a snapshot of modelling results encompassing a 50-minute window (two trips) and drawing on real-world drive cycle data from the TSDC and climate data from the NSRDB. Figure IV-91 and Figure IV-92 feature the same simulation results, but zoomed out to a 13-hour window and a 7-day window, respectively. These figures illustrate how the model captures vehicle thermal conditions over time (as a function of driving style, local temperature and solar conditions, and real-world parking durations between

driving trips). The model then estimates vehicle fuel consumption based on power demands to satisfy the speed and acceleration profile as well as the specific thermal conditions present, which influence fuel demands for enrichment (accelerating catalyst heating), overcoming engine friction (oil viscosity), and cabin climate control (i.e., air conditioning).

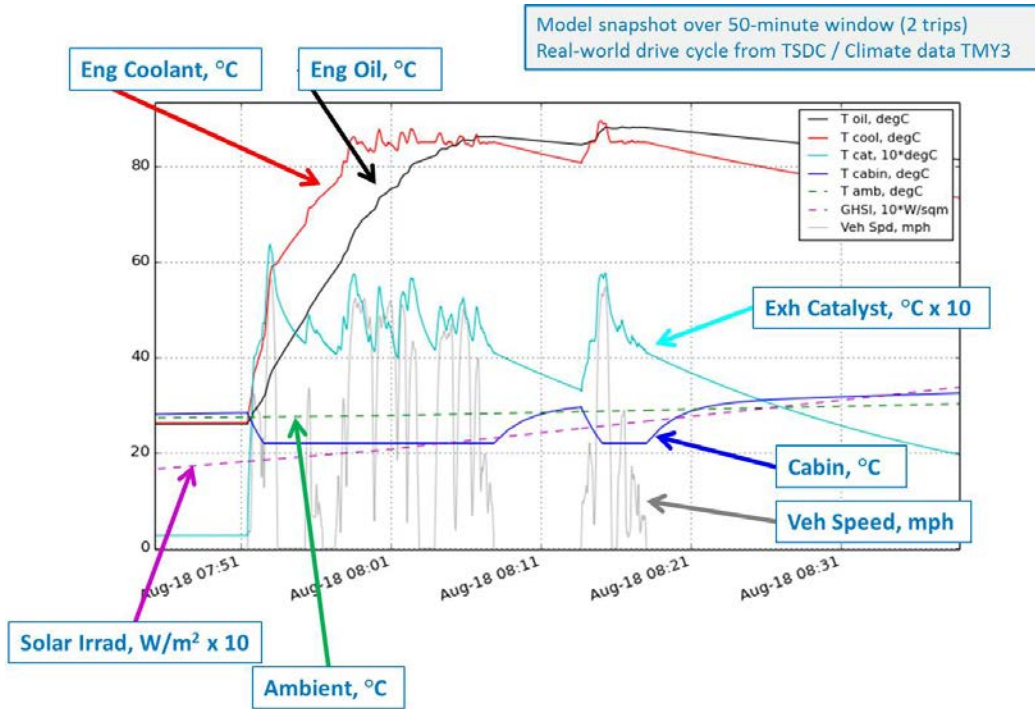


Figure IV-90: Model snapshot: 50 minutes

Source: NREL

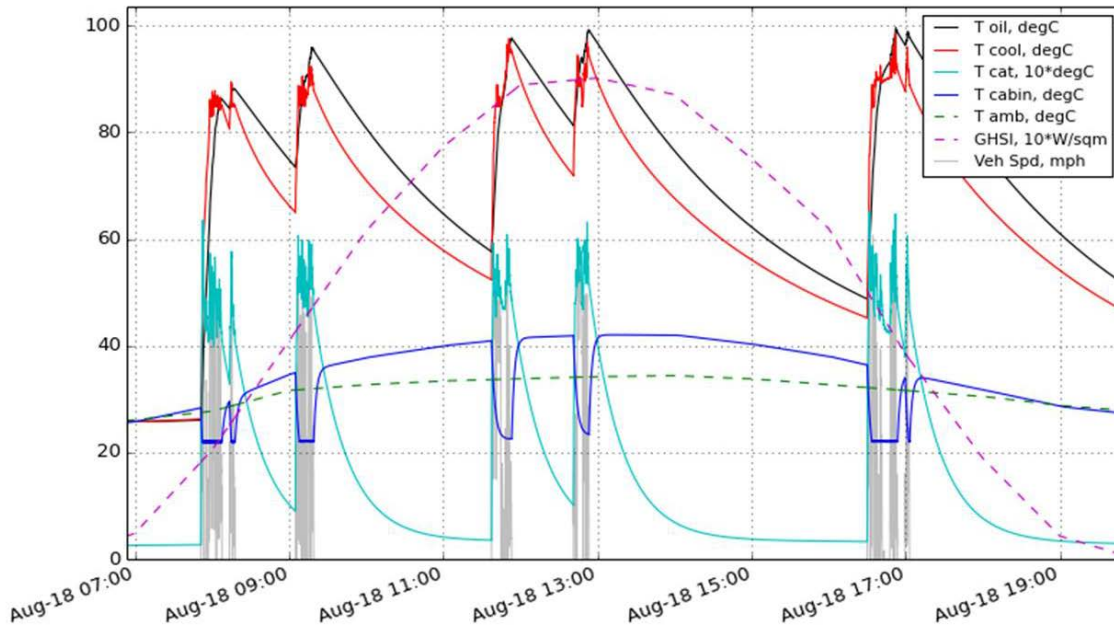


Figure IV-91: Model snapshot: 13 hours

Source: NREL

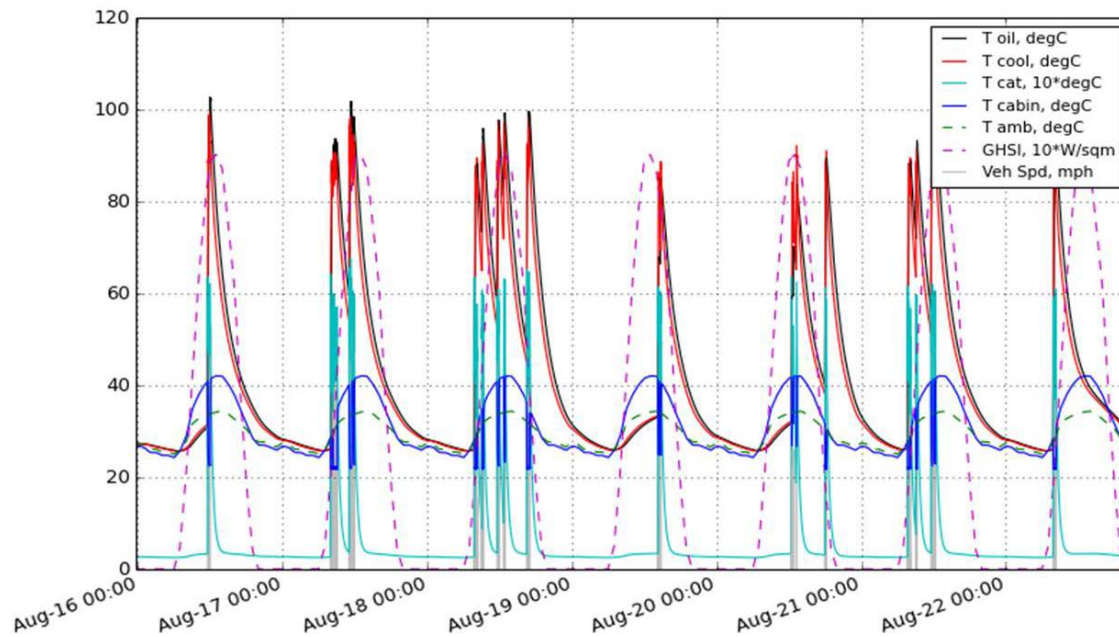


Figure IV-92: Model snapshot: 7 days
Source: NREL

Mapping vehicle operational space and climate differences

NREL established an approach to "map" the operational space of light-duty vehicles by running the model over a large spectrum of real-world operation. For this initial evaluation, NREL selected a subset of TSDC data from the 2012 California Household Travel Survey (CHTS), which includes a GPS sample with 2,900 seven-day vehicle histories, 500,000 miles of driving, and a mix of urban/rural and city/highway operation. NREL aggregated simulation results by road type using FHWA definitions. The figure below shows FHWA road classifications for the state of California, with urban vs. rural delineations on the left and road functional classifications on the right.

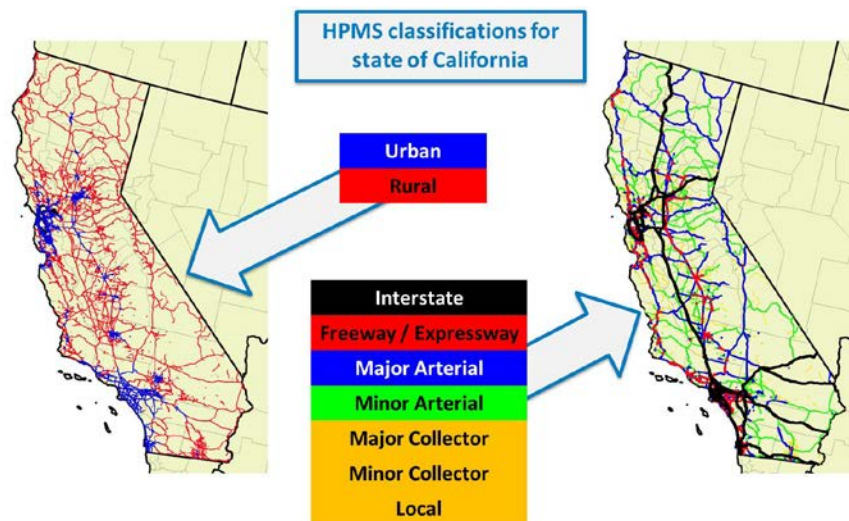


Figure IV-93: FHWA HPMS road classifications in California
Source: NREL

When looking at average driving speed distributions by urban/rural and HPMS functional class binning, results showed 1) large distributions across functional classes, 2) reduced speed on roads with lower capacities, and 3) higher speeds on rural roads, which generally have lower congestion and fewer intersections. The average

speed trends between the road type bins generally translate to discernable fuel economy trends between the bins (e.g., when average driving speed is higher on a given rural functional class relative to its urban counterpart, then average fuel economy tends to also be higher on the rural road). The magnitudes of the fuel economy distributions tend to be lower than those of the speed distributions due to tradeoffs in the road-load equation. These initial results show some convergence of the average fuel economy calculations in each road type bin when over 20,000 miles of real-world driving are available over that road type. Additional analysis in the next fiscal year will include examining driving differences in other parts of the country relative to comparable road types in California, adding to the real-world driving data for road types with relatively lower representation in the CHTS dataset, and considering additional metrics (such as ways to capture relative road congestion) for modifying the road type binning.

In the absence of these future improvements, NREL made the simplifying assumption in this analysis iteration that the binned drive profile characteristics from the CHTS dataset are representative of driving in the same road type bins nationally. NREL then quantified climate impacts by superimposing this binned real-world driving data over the range of ambient conditions found nationally across seasons and geographies. Exemplar climate data were selected by canvassing the complete set of location and day-of-year combinations in the NSRDB Typical Meteorological Year 3 (TMY3) dataset, including 1,020 locations, 365 days, and 372,300 location-days.

The plots in Figure IV-94 show the results of some 40 million miles of simulated driving, representing fuel economy relative to urban/rural designation, HPMS functional class, and average ambient temperatures. Simulated fuel economy increases from -40°C to +20°C (due to reduced viscous losses and enrichment), then drops due to cabin air conditioning load at high temperatures (where the trend becomes more noisy due to variable solar load in the exemplar location-days). The figure suggests that rural interstate fuel economy is less sensitive to ambient temperature than other functional classes, which is likely the result of unique drive cycle characteristics (high speed, long distances).

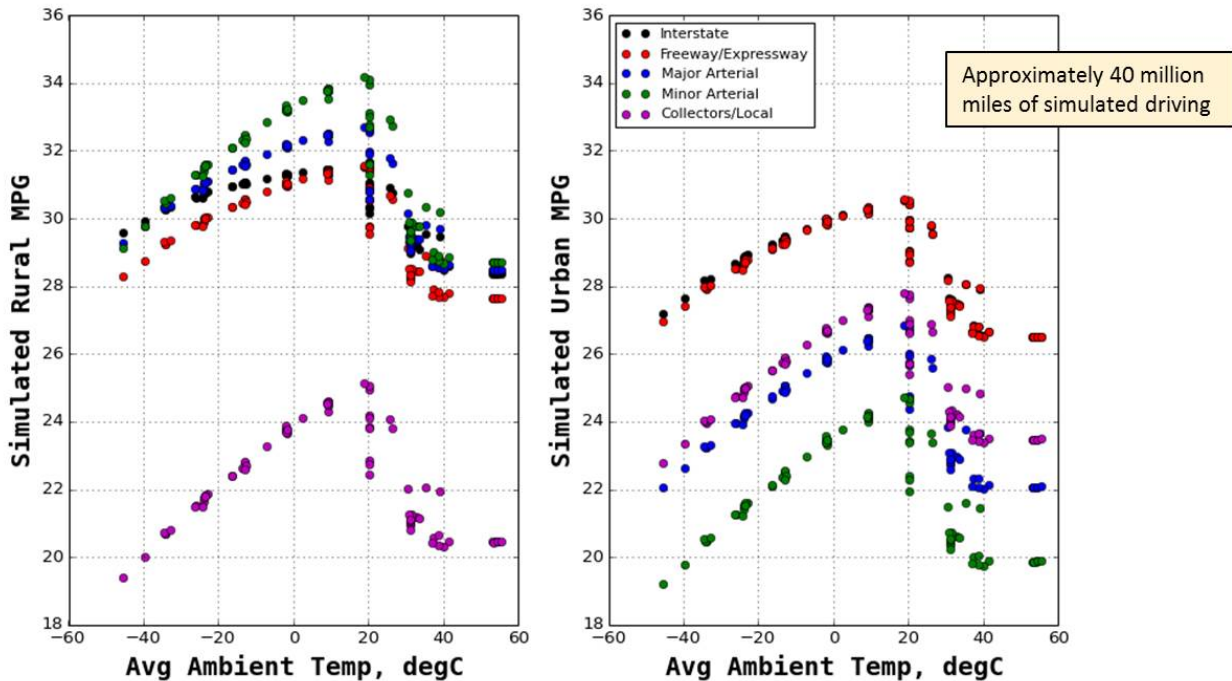


Figure IV-94: Operational mapping results: Simulated real-world fuel economy relative to urban/rural designation, HPMS functional class, and average ambient temperature (solar load impacts also captured but not illustrated on the plot)

Source: NREL

Extrapolating to national statistics

NREL next took the "rates" generated from the operational mapping with the real-world simulations and applied them to national VMT data, disaggregated to cities and overlaid with typical climate data (as is visualized in Figure IV-95). The calculations involved included 1) calculating the mean fuel economy for each day of the year in each city by distance-weighting road types, 2) calculating the mean for each city by distance-weighting across days of the year, and 3) calculating the national mean by distance-weighting all U.S. cities.

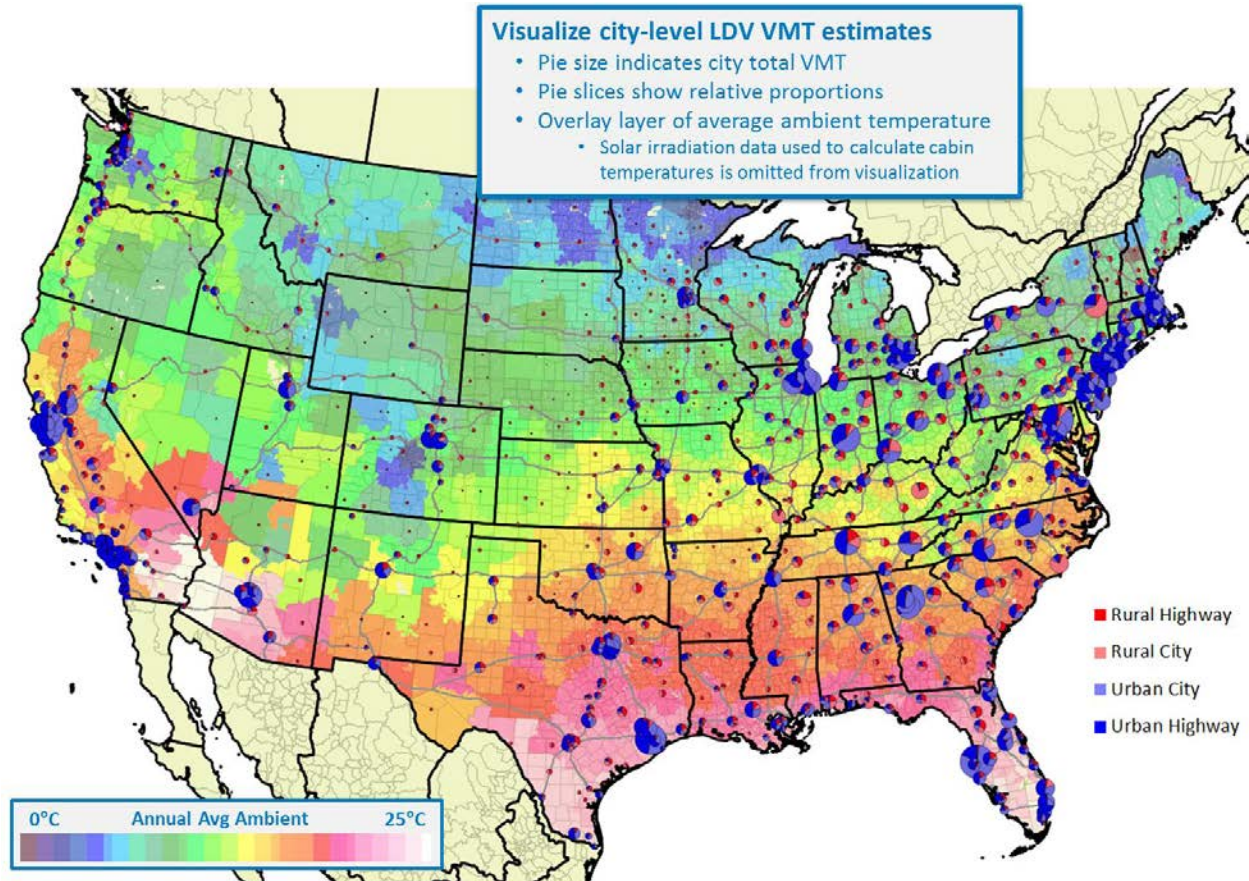


Figure IV-95: National FHWA VMT data disaggregated to cities and overlaid with typical climate data

Source: NREL

As an illustrative example of the calculations, consider the process to estimate the contribution of a single area, such as Chicago, Illinois, to the national total. On January 1, the typical average temperature in Chicago is 5.2°C, and the average solar irradiation is 31 W/m². Taking the operational mapping described above over five HPMS functional class categories and urban/rural designations at these ambient conditions gives ten representative fuel economy values for each road type bin. The HPMS VMT data for the same ten bins can then provide the distance-weighted fuel economy over all roads in the Chicago area on January 1. Repeating this process for each day of the year yields interim results as illustrated in the following figure. The figure shows estimated fuel economy and corresponding average temperature over the course of a year, plotted in 15-day increments. Note that fuel economy is highest in the spring and fall when moderate temperatures prevail, whereas cold-temperature operation in the winter months and air conditioning loads in the summer months cause reduced fuel economy at those times.

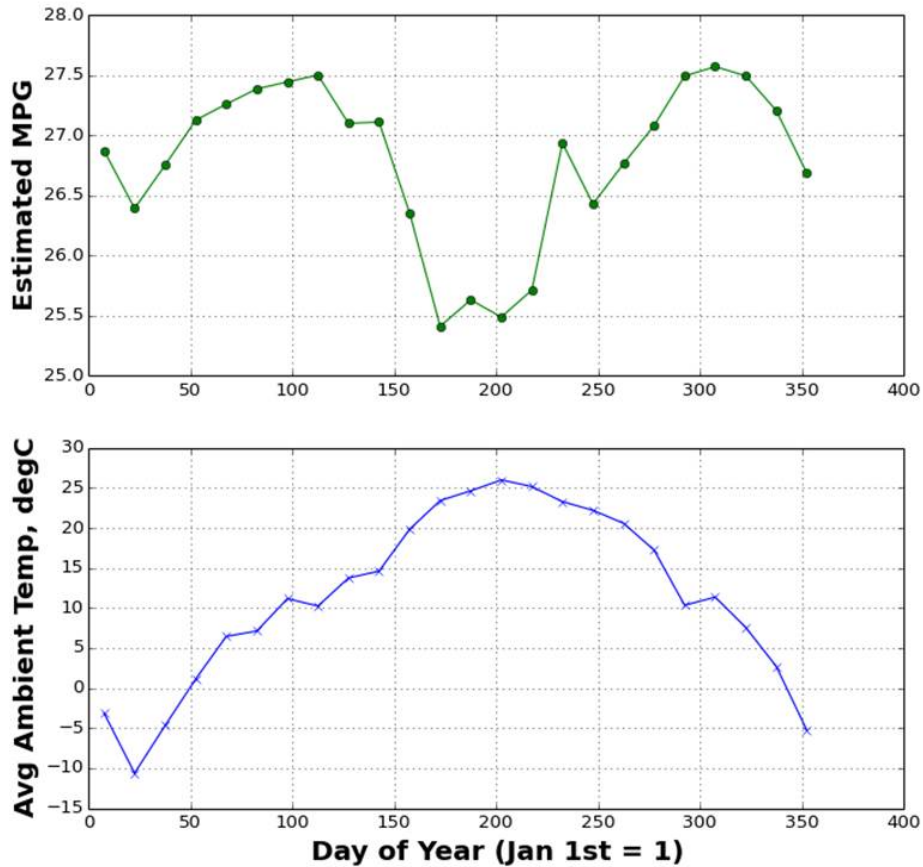


Figure IV-96: Example calculation results over the course of a year in Chicago
 Source: NREL

Repeating this typical climate and road type weighting for all of the disaggregated cities produces a set of city-level fuel economy estimates which can then be distance weighted together by each area's relative contribution to national light-duty vehicle VMT to produce a national-level fuel economy estimate. The scatter plot in Figure IV-97 shows the city-level fuel economy estimates organized relative to the percentage of highway driving in that particular city (i.e., VMT on interstates, freeways, or major arterials, as opposed to minor arterials, collectors, and local roads) and the annual average ambient temperature in that area. The sizes of the circles in the figure are proportional to the relative VMT contribution to the national total from the area represented by each fuel economy calculation. Note that the cities with the highest average fuel economy feature large highway VMT percentages in moderate climates, whereas the cities with the lowest fuel economy estimates have low percentages of highway VMT and/or are in extreme climates, with greater VMT weighting typically being found in areas with very high as opposed to very low temperature extremes. Distance-weighting all of the city-level fuel economy estimates for this baseline evaluation results in a national estimate of 27.0 mpg.

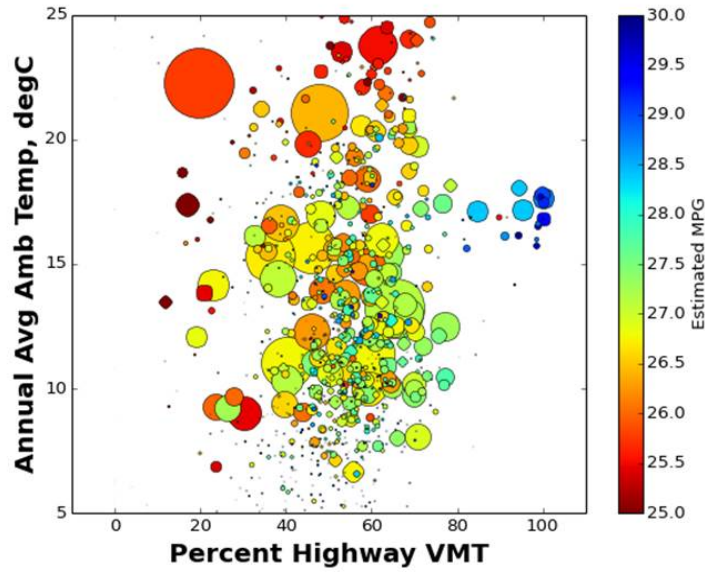


Figure IV-97: City-level fuel economy estimates plotted relative to the percentage of highway driving and the annual average temperature in each city. The size of each circle is proportional to that city's relative VMT contribution to the national total. Source: NREL

A/B technology evaluations

Having now developed and tested the above analytical framework, NREL next applied it to estimate the real-world impact from several hypothetical off-cycle technologies. These included 1) a hypothetical window glazing technology that reduced effective solar load by 5% (slightly reducing steady-state air conditioning load over long trips in hot and sunny weather conditions); 2) an accessory load reduction technology, such as increased alternator efficiency, that reduces accessory power demand by 10% over all driving conditions; and 3) a hypothetical thermal retention technology that doubles the time constant for engine cool-down after turning off the vehicle (resulting in more warm starts in subsequent trips and reduced cold-start fuel penalty). Table IV-48 through Table IV-50 summarize the estimated fuel economy and grams of CO₂/mile impacts from these three hypothetical technology cases using EPA's standard 2-cycle and 5-cycle calculation procedures and using the real-world estimation approach described in the previous sections of this report.

Table IV-48: Estimates for hypothetical window glazing technology

Calculation Approach	Baseline MPG	Technology-enabled MPG	g CO ₂ /mi Benefit	Percent benefit
EPA 2-cycle	30.9	30.9	0.0	0.0%
EPA 5-cycle	24.0	24.0	0.0	0.0%
Real-world estimate	27.0	27.0	-0.1	0.0%

Table IV-49: Estimates for hypothetical accessory load reduction technology

Calculation Approach	Baseline MPG	Technology-enabled MPG	g CO ₂ /mi benefit	Percent benefit
EPA 2-cycle	30.9	31.1	-1.8	-0.6%
EPA 5-cycle	24.0	24.2	-1.7	-0.5%
Real-world estimate	27.0	27.1	-1.6	-0.5%

Table IV-50: Estimates for hypothetical thermal retention technology

Calculation Approach	Baseline MPG	Technology-enabled MPG	g CO ₂ /mi benefit	Percent benefit
EPA 2-cycle	30.9	31.0	-1.3	-0.4%
EPA 5-cycle	24.0	24.2	-2.3	-0.6%
Real-world estimate	27.0	27.4	-5.3	-1.6%

Under the selected assumptions, the hypothetical glazing technology shows no benefit using the 2-cycle or 5-cycle approach, and insignificantly greater benefit using the real-world estimation approach. The assumptions included that the air conditioning would still run at its maximum load to initially cool the cabin, so that the technology would only provide a slight load reduction benefit on longer driving trips in hot and sunny conditions by marginally reducing the steady-state air conditioning load. The limited magnitude combined with the fractional VMT weighting for these conditions resulted in a negligible overall benefit estimate from the calculations. That said, activities in the next fiscal year will ideally include implementation of a higher-fidelity cabin model into the vehicle simulation along with a basic thermal comfort model, which will allow us to revisit the benefit calculation for this type of technology and determine the conditions that would make it significant.

For the hypothetical accessory load reduction technology, the real-world estimation approach predicts a measurable g CO₂/mi and fuel economy benefit; however, the benefit is not substantially different from that calculated by the standard 2-cycle and 5-cycle approaches. This is perhaps unsurprising in the absence of assumptions about specific or limited driving conditions over which the accessory load reduction would occur.

For the hypothetical thermal retention technology, the 2-cycle and 5-cycle approaches again estimate some level of benefit; however, the real-world estimation approach predicts significantly larger gains. The modest benefit estimated by the standard cycles largely results from more rapid engine warm-up during cold-start cycles whereas the benefit calculation in the real-world estimation approach derives from improved engine warm-up AND better heat retention between trips. Note also that broad implementation of a seemingly modest 1% fuel saving technology for conventionally powered vehicles could have an equivalent aggregate impact of taking 2.5 million vehicles off the road. This underscores the importance of accurately and objectively estimating the real-world impact from such technologies, for which this on-going research effort shows great promise.

Conclusions

Off-cycle technologies represent an important pathway to achieving real-world fuel savings through which OEMs can receive credit toward CAFE compliance. As a DOE national lab, NREL is well positioned to objectively assess these technologies using large, national, publically available datasets in conjunction with vehicle-specific testing. This project demonstrates an approach that combines vehicle testing (chassis dynamometer and on-road) with powertrain modeling and simulation over large, representative data sets to quantify real-world fuel economy. The approach can be applied to specific off-cycle technologies in A/B comparisons to support calculation of realistic real-world impacts.

The example A/B comparison calculations performed thus far underscore that the standard 2-cycle and 5-cycle approach can be sufficient for some technologies, but that an alternative real-world analytical methodology, such as described in this report, may be quite important for other off-cycle technologies. Specifically for a hypothetical thermal retention technology (such as engine encapsulation) that doubles the time constant for cool-down following engine off, the real-world analytical methodology estimated three times greater fuel savings benefit than the standard cycle approaches. The aggregate national benefit of such a technology deployment could be significant.

Future work on this project will include further model validation and refinement via on-road data collection, and additional statistical analysis and enhancements where possible to the driving profile binning by road type. Other proposed efforts include applying the methodology to evaluate actual off-cycle technologies for which NREL can obtain test data (as opposed to just hypothetical examples), and extending consideration to other types of off-cycle technologies (such as actual real-world impacts of start/stop hybridization or of connected and automated vehicle features).

IV.14.C. Products

Presentations/Publications/Patents

1. Gonder, J., Wood, E., Lopp, S. "Analyzing Real-World Light Duty Vehicle Efficiency Benefits." DOE Vehicle Technologies Annual Merit Review – Project ID#: VSS155, June 2015.
2. Jehlik, F., Wood, E., Gonder, J., Lopp, S. "Simulated Real-World Energy Impacts of a Thermally Sensitive Powertrain Considering Viscous Losses and Enrichment." SAE International Journal of Materials and Manufacturing Vol. 8 (2) 14 April 2015 pp. 239-250. (Conference version pre-print: nrel.gov/docs/fy15osti/63255.pdf).

IV.14.D. References

1. Earleywine, M., Gonder, J., Markel, T., Thornton, M. "Simulated Fuel Economy and Performance of Advanced Hybrid Electric and Plug-in Hybrid Electric Vehicles Using In-Use Travel Profiles." Proceedings of the 6th IEEE Vehicle Power and Propulsion Conference (VPPC); Sept.1-3, 2010, Lille, France.
2. Neubauer, J., Wood, E., "Accounting for the Variation of Driver Aggression in the Simulation of Conventional and Advanced Vehicles." SAE Technical Paper 2013-01-1453, 2013, doi:10.4271/2013-01-1453.
3. Neubauer, J., Wood, E. "Thru-Life Impacts of Driver Aggression, Climate, Cabin Thermal Management, and Battery Thermal Management on Battery Electric Vehicle Utility." Journal of Power Sources, Volume 259, 1 August 2014, Pages 262-275, doi:10.1016/j.jpowsour.2014.02.083.
4. Wood, E., Burton, E., Duran, A., Gonder, J. "Contribution of Road Grade to the Energy Use of Modern Automobiles across Large Datasets of Real-World Drive Cycles." SAE Technical Paper 2014-01-1789, Proceedings of the SAE World Congress, Apr. 2014, Detroit, MI.
5. Wood, E., Burton, E., Duran, A., Gonder, J. "Appending High-Resolution Elevation Data to GPS Speed Traces for Vehicle Energy Modeling and Simulation." Technical Report NREL/TP-5400-61109, 2014.

6. Wood, E., Gonder, J., Lopp, S., Jehlik, F. "Simulated Real-World Energy Impacts of a Thermally Sensitive Powertrain Considering Viscous Losses and Enrichment." Proceedings of the SAE Thermal Management Systems Symposium, Sept. 2014, Denver, CO.
7. Brooker, A., Gonder, J., Wang, L., Wood, E., Lopp, S., Ramroth, L. "FASTSim: A Model to Estimate Vehicle Efficiency, Cost and Performance." SAE Technical Paper 2015-01-0973, Proceedings of the SAE World Congress, Apr. 2015, Detroit, MI.
8. "Transportation Secure Data Center." (2015). National Renewable Energy Laboratory. Accessed September 21, 2015. nrel.gov/tsdc.

IV.15. Thermal Impact of Energy Consumption on Real-World Drive Cycles

Neeraj Shidore, Principal Investigator

Argonne National Laboratory
9700 S. Cass Avenue, Building 362
Argonne, IL 60439
Phone: (630) 252-7416; Fax: (630) 252-3443
E-mail: nshidore@anl.gov

David Anderson, DOE Program Manager

U.S. Department of Energy (DOE)
Office of Vehicle Technologies (VTO)
Phone: (202) 287-5688
E-mail: David.Anderson@ee.doe.gov

Start Date: 10/1/2014
End Date: 9/30/2015

IV.15.A. Abstract

Objectives

- Assess the impacts from thermal conditions on vehicle energy consumption for multiple powertrain configurations.
- Compare the impacts from thermal conditions on vehicle energy consumption for standard and real-world drive-cycle (RWDC) scenarios.

Accomplishments

- A thermal model of a tire was developed and added to the suite of models of thermal powertrain plants in Autonomie.
- The thermal behavior of a conventional vehicle system simulation model was validated through a comparison with chassis dynamometer test data.
- The impacts from thermal conditions on vehicle energy consumption for multiple powertrain configurations were assessed.
- The impacts from thermal conditions on vehicle energy consumption for standard and RWDC scenarios were evaluated.

Future Achievements

- The impacts from thermal conditions will be combined with the impacts from additional real-world scenarios (fleet distribution, grade, ITS) to provide a realistic evaluation of technology benefits.



IV.15.B. Technical Discussion

Background

Argonne has analyzed the control behaviors of advanced vehicles, such as hybrid electric vehicles (HEVs), plug-in HEVs (PHEVs), and battery electric vehicles (BEVs), to develop simulation models and reproduce the

performance of vehicles with simulation techniques [1, 2]. Since many studies related to transportation technologies conducted at Argonne rely on simulation techniques [3], validated models are critical.

This project leverages the test data produced at Argonne's Advanced Powertrain Research Facility (APRF), which houses a four-wheel-drive chassis dynamometer set in an environmental chamber. The APRF allows a broad range of conditions to be replicated, from -7 to 35°C , with or without solar load. Once analyzed, the results are used to calibrate individual component models, including their thermal aspects. One of the main reasons for developing thermal models is that the impact of temperature on vehicle performance is significant, especially for electrified vehicles. Not only are component losses affected by temperature, but the vehicle-level control is different.

Introduction

An evaluation of system technologies developed with the support of DOE VTO is a critical part of the vehicle systems research portfolio. This evaluation covers vehicle energy consumption benefits and includes a technology utilization analysis. Because of the increased focus on the real-world benefits that result from powertrain technology, it is critical that current and future technology trends be evaluated under real-world scenarios. These include RWDCs, realistic thermal conditions and grades, and intelligent transportation systems.

Approach

Due to the significant impact that thermal conditions can have on real-world vehicle performance and fuel economy, realistic predictions of the benefits from technological advances using system simulations need validated vehicle-level control and plant/powertrain models. In previous years, MATLAB-Simulink-based, one-dimensional thermal models for several powertrain components (e.g., engines, batteries, electric motors) were developed through standard energy flow equations for use in Argonne's vehicle system simulation tool, Autonomie. On a powertrain (system) level, the behavior of the powertrain system and vehicle energy management under extreme thermal conditions were calibrated by leveraging the chassis dynamometer test data from Argonne's APRF. In previous years, thermal models were developed and validated for an electric vehicle (EV), an HEV (a power-split vehicle), an extended-range EV (EREV) plug-in hybrid, and a charge-depleting power-split PHEV.

In fiscal year 2015 (FY15), a validated conventional vehicle thermal model was added, with additional improvements made in the representation of tire thermal behavior.

The validated system simulation models developed have been used to evaluate the impacts on vehicle energy consumption from thermal conditions for standard and RWDC scenarios, by leveraging a large-scale simulation process with Autonomie.

The travel survey [4] conducted by the National Highway Transportation Safety Administration (NHTSA), along with several daily driving trips generated from the RWDCs from the National Transportation Secure Data Center [5] at the National Renewable Energy Laboratory (NREL), were used to generate a set of daily driving trips that matched the average national daily driving distribution obtained from the NHTSA survey. This set of daily driving trips formed the RWDC scenario used for the thermal impact evaluation. Each daily driving trip involved multiple drive cycles with key-off events in-between.

Results

Thermal Model of Tire

Vehicles tested at Argonne's APRF with advanced ("Level 2") instrumentation have torque sensors that measure the input torque to the wheel, while the torque applied by the wheels to the dynamometer rolls is measured by the dynamometer controller. This allows measurements of the torque losses due to friction and estimates of their sensitivity to temperature, as shown in Figure IV-80.

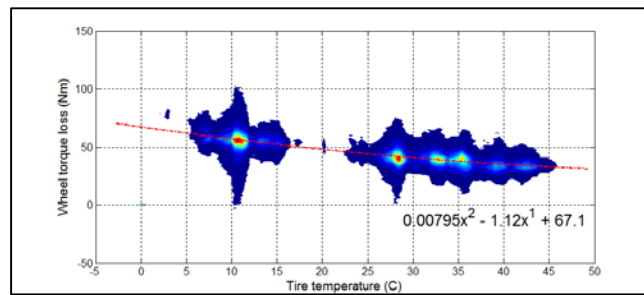


Figure IV-98: Wheel torque losses as a function of temperature for the Ford Fusion

Thermal Model of Conventional Car

Test data on the 2012 Ford Fusion were imported in Autonomie and analyzed. The engine consumes more fuel when it is cold, primarily due to increased friction and higher viscosity of the oil. By analyzing the temperature of engine oil during cold engine operation and engine cool-down, it is possible to find the sensitivity of engine efficiency to temperature and to adjust the engine efficiency map in Autonomie. Figure IV-99 shows how the main signals in the test and in the simulation compare with each other and demonstrates the successful validation of the vehicle.

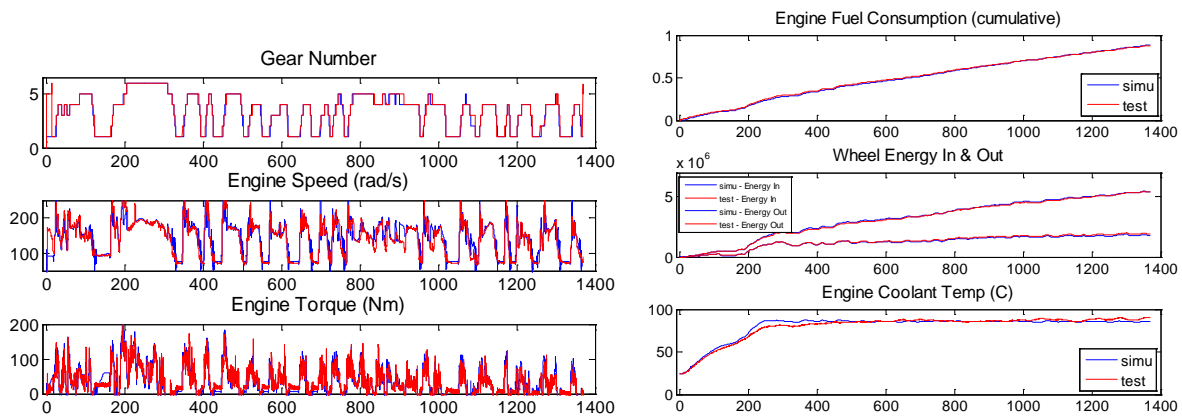


Figure IV-99: Comparison of test and simulation signals (Urban Dynamometer Driving Schedule [UDDS], cold start, normal ambient temperature)

The conventional thermal model thus developed, along with thermal models for other powertrain types, were evaluated under standard and real-world scenarios. It can be seen that the thermal impacts (cold and hot ambient temperatures) were lower for the RWDC.

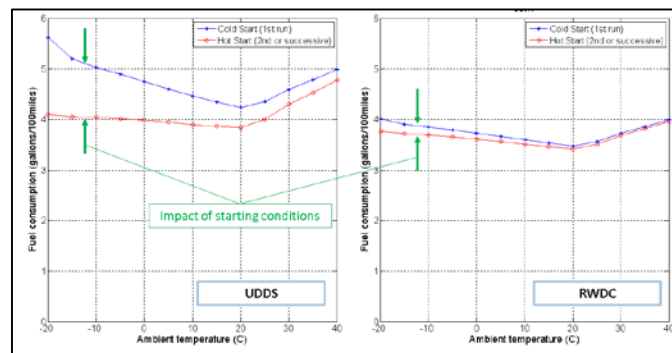


Figure IV-100: Impact of thermal conditions on UDDS and RWDCs for a conventional vehicle

At each ambient temperature (x axis), the fuel consumption for the RWDC is the mean fuel consumption for the set of real-world daily driving trips chosen to meet the NHTS daily driving distribution. These trips are, on average, longer than the UDDS drive cycle. In addition, for this first version of real-world evaluation, the key-off event between the drive cycles that constitute the trip has been modelled as being only 10 seconds, and it does not reflect the real key-off time, which allows the engine to cool down and increases the real-world thermal impact. In the next generation of daily trips, the actual key-off time has been incorporated. Figure IV-101 shows the comparison for a hybrid vehicle, and a similar impact can be seen.

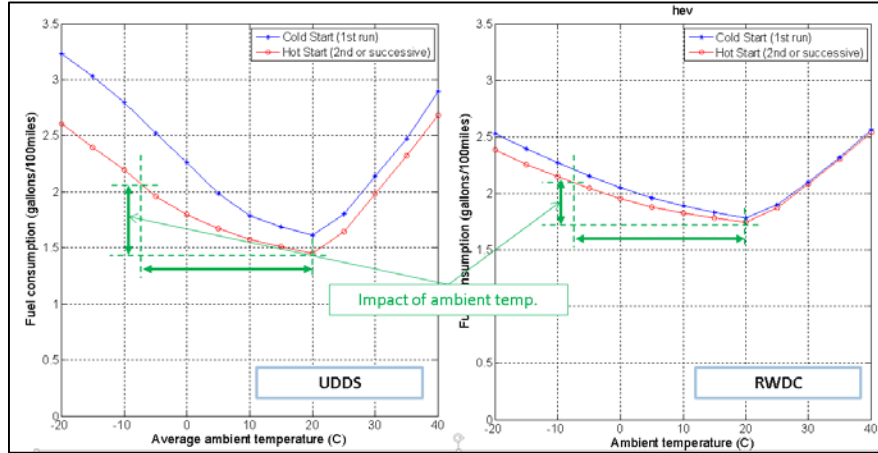


Figure IV-101: Impact of thermal conditions on UDDS and RWDCs for a hybrid vehicle

Figure IV-102 shows the impact of temperature on the energy consumption for a BEV. Unlike a conventional vehicle or a hybrid vehicle, in which waste engine energy in the heater core loop is used to heat up the cabin, traction energy has to be "diverted," which results in range reduction. Also, for the RWDC case, the change in energy requirements with temperature is more significant than the change experienced by vehicles with internal combustion engines.

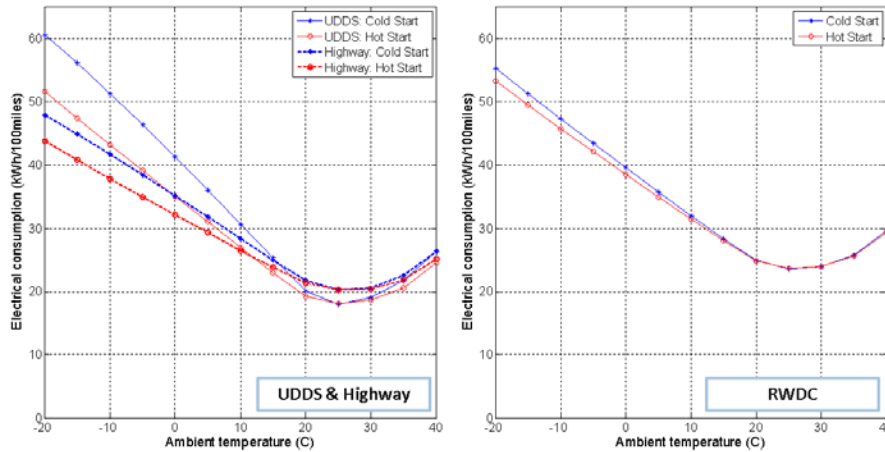


Figure IV-102: Impact of thermal conditions on the UDDS, Highway Fuel Economy Test (HWFET), and RWDCs for a BEV

Conclusions

- Thermal models were improved as follows:
 - New tire thermal model and
 - Validated thermal model of a conventional car (Ford Fusion).
- Several vehicles now have validated models in Autonomie and are used for studies: conventional vehicles, HEVs, PHEVs, EREVs, and BEVs.

- Daily driving trips (multiple drive cycles with key-off) that meet the NHTSA average daily miles travelled are a close statistical representation of daily driving and have been used for RWDC evaluation.
- The impact of ambient thermal conditions is lower for real-world driving than for standard drive cycles due to longer distances.
- A rigorous evaluation of thermal impacts on statistically representative real-world driving would require a consideration of powertrain cool-down times during key-off parts of daily driving.

IV.15.C. Products

Presentations/Publications/Patents

1. Kim, Namwook, Namdoo Kim, and Aymeric Rousseau, "Thermal Model Developments for Electrified Vehicles," presented at 28th Electric Vehicle Symposium (EVS28), Goyang, South Korea, May 2015
2. Jeong, Jongryeol, Namwook Kim, Dominik Karbowski, and Aymeric Rousseau, "Impact of Thermal Conditions on Vehicle Control," presented at IFAC Workshop on Engine and Powertrain Control, Simulation and Modeling (ECOSM '15), Columbus, Ohio, August 2015.

IV.15.D. References

1. Rousseau, A., et al., "Integrating Data, Performing Quality Assurance, and Validating the Vehicle Model for the 2004 Prius Using PSAT," SAE Technical Paper 2006-01-0667, 2006.
2. Kim, N., et al., "Vehicle-Level Control Analysis of 2010 Toyota Prius Based on Test Data," IMechE Part D: J. Automobile Engineering 226(11):1483-1494, Nov. 2012.
3. Kim, N., et al., "Thermal Model Development and Validation for 2010 Toyota Prius," SAE Technical Paper 2014-01-1784, 2014.
4. U.S. Department of Transportation/Federal Highway Administration, 2009, "National Household Travel Survey," <http://nhts.ornl.gov>.
5. National Renewable Energy Laboratory, "Transportation Research," nrel.gov/transportation/secure_transportation_data.html.

V. Codes and Standards

V.1. Green Racing Technical Support

P.T. Jones, Principal Investigator

Bob Larsen (OboTech), Senior Technical Lead

Oak Ridge National Laboratory

2360 Cherahala Boulevard

Knoxville, TN 37932

Phone: (865) 946-1472

Email: Jonespt@ornl.gov

Lee Slezak, DOE Program Manager

Phone: (202) 586-2335

E-mail: Lee.Slezak@ee.doe.gov

Start Date: 10/01/2013

End Date: 9/30/2016

V.1.A. Abstract

Objectives

- Incentivize vehicle manufacturers to develop, validate, and promote advanced technologies relevant to production vehicles through motorsport participation. Increase the use of renewable fuels and petroleum alternatives in racing, and provide an avenue to introduce new fuels or bio-fuel blends.
- Strengthen the link between BioEnergies Technologies Office (BETO) and Green Racing Initiative (GRI).
- Increase the use of electric drive technologies in racing.
- Use racing as a platform to educate the public:
 - On the benefits of using renewable fuels and the concept of well-to-wheels fuel life cycles;
 - On the performance and efficiency benefits and capabilities of advanced vehicle technologies.
- Diversify the success of the Green Racing Initiative beyond the TUDOR United Sportscar Championship (TUSC) to include other racing series with the final goal of establishing advanced transportation technologies as a foundation for all motorsports.
- Gain the support of the automotive industry in the validation of “green racing” in the United States and internationally.
- Maintain collaborative partnership with the U.S. Environmental Protection Agency (EPA) and Society of Automotive Engineers (SAE) International.

Accomplishments

- All of the full-season GT Le Mans (GTLM)-class cars racing with the TUSC used E85R fuel with cellulosic ethanol sourced from INEOS, a DOE grant recipient. This fuel reduced oil consumption by over 62% and provided more than 65% reduction in greenhouse gas (GHG) emissions compared to conventional racing fuels with no renewable content. (For the International Motor Sport Association (IMSA) this would be a 2005 baseline.)
- Building on the Green Racing partnership with IMSA (valid through 2019), IMSA leadership applied and were approved for Green Racing status under SAE J2880 for each of the four classes of sports cars competing in TUSC.

- The Green Racing scoring system was upgraded to simplify the terms that everyone can understand and relate to. For example, the Fast term is now expressed in kilometers per hour (kph) relative to the leader. Shifting the terms to more easily understood measures improved the acceptance of the Green Racing scores.
- Widespread changes in the future rules of international sports car racing presented the opportunity to align future IMSA fuels with those used in Europe, Asia, and most importantly, the 24 Hours of Le Mans. Lower classes in the United States will double the use of renewable fuels and more fuel options will be available in the professional classes raced around the world. A casualty of this decision is to prohibit diesel-powered LMP2 (Le Mans Prototype) cars from 2017 on. Since the P2 class is the top Prototype class competing in IMSA races, this decision had the unfortunate effect of eliminating a highly efficient engine technology from competing in North America in IMSA races. Diesel-powered cars are still eligible in LMP1 - the highest technology race cars in the world - aimed at original equipment manufacturer (OEM) participation.
- IMSA further demonstrated its commitment to the GRI by agreeing in principle to adopt the fuel emerging from the DOE Optima R&D initiative, projected to have even a higher proportion of renewable content than their current base fuel. It is hoped that making this fuel available to every TUSC class will incentivize the rest of global sports car racing to also move towards fuels with both road relevance and higher renewable fuel content.
- IMSA also reinforced their commitment to renewable fuels by switching the fuel for the Prototype spec class Prototype Challenge cars to E85R fuel for the 2016 season.
- A new sponsor for the Green Racing activities in TUSC was very active in supporting and promoting Green Racing during the 2015 season - DEKRA (dekra.com/en/home). DEKRA awarded Green Racing trophies to the teams in the GTLM class at each of the ten races this past season. The trophies proudly showed the logos of the three participating agencies in the GRI as well as the DEKRA branding. The winners were selected through the Green Racing scoring system also used to compile the winner of the season-long Green Racing OEM award presented by the GRI.
- The winner of the season-long Green Racing OEM award in the GTLM class in TUSC was BMW Motorsports. Presented at the Night of Champions award ceremony by DOE Deputy Assistant Secretary Rueben Sarkar, this year's winners showed the best combination of Clean, Fast, and Efficient performance over the ten-race season. This year's competition was the closest ever, with Chevrolet and Porsche finishing the season with scores only two points behind the winner, BMW. This was only the second time BMW has won this prestigious award since 2008.
- Mazda fielded two cars with their street-based diesel engine in the TUSC Prototype category in 2015. Development continued on this mighty 2.2 liter diesel that uses the production block and head along with more than 50% of stock components. A 100% renewable synthetic diesel fuel with a cetane of 75 made available to Mazda through the DOE's Green Racing program technical support remains key in the power production and improved reliability of the stock-based engine. The engine was able to nearly quadruple its output, when compared to a stock engine, to over 550 hp.
- The light weight, downsized-engine Elan DeltaWing coupe raced in six rounds of the TUSC, leading several races finishing as high as fourth place in the Prototype class. The DeltaWing competes with a 350hp engine compared with 550+hp engines in a typical Prototype race car.
- Transported and displayed the Green Racing Simulator (a model-based E85 Corvette hybrid electric vehicle (HEV) race car simulator) at three TUSC races and several additional events around the country with EPA and BETO support including a major event in Washington, DC at DOE headquarters.
- Multiple discussions were held with INDYCAR about becoming a Green Challenge race series in 2016 and how to incorporate energy recovery technologies features in their new engine formula expected to be introduced in 2017. The advantages of using 2nd Generation (cellulosic) ethanol in support of the series and an offer to assist in obtaining a supplier of cellulosic ethanol were made.
- Developed an SAE J2880 Application Announcement and process for applying for Green Racing recognition through the SAE Green Racing website.

- HEV LMP1 cars from Porsche dominated the 24 Hours of Le Mans and the World Endurance Championship (WEC) in 2015 with an advanced HEV powered by a downsized, boosted V-4 SI engine with waste heat recovery and multiple electric drives. HEVs took the first 9 places at Le Mans in addition to winning every WEC race to date in the 2015 season.
- Four different HEV architectures competed in the WEC in 2015 breaking lap records at almost every track - all while using 30% less fuel. Each of the four factory HEV entries in the WEC LMP1 uses different forms of energy storage illustrating the diversity of technical solutions relevant to road cars: Audi with an electro-mechanical flywheel, Toyota with ultracapacitors, Porsche with Li-Ion batteries, and Nissan with multiple mechanical flywheels.
- In Formula 1 (F1), 2015 was the second season using HEV powertrains based on small turbocharged V6 engines with waste heat and kinetic recovery and greatly expanded electric drive capabilities. The premier racing series in the world employs energy allocations (100kg of fuel) and maximum fuel flow rates with real-time fuel flow metering to incentivize maximum efficiency in the races. These efficiency-encouraging steps have long been a part of the GRI philosophy and resulted in a greater than 30% reduction of energy consumption in F1 that was nevertheless able to set lap records at several circuits (Figure V-1). With these changes and the addition of a third race in North America (Mexico City), F1 has become eligible for a Green Cup Award starting in the 2015 season.

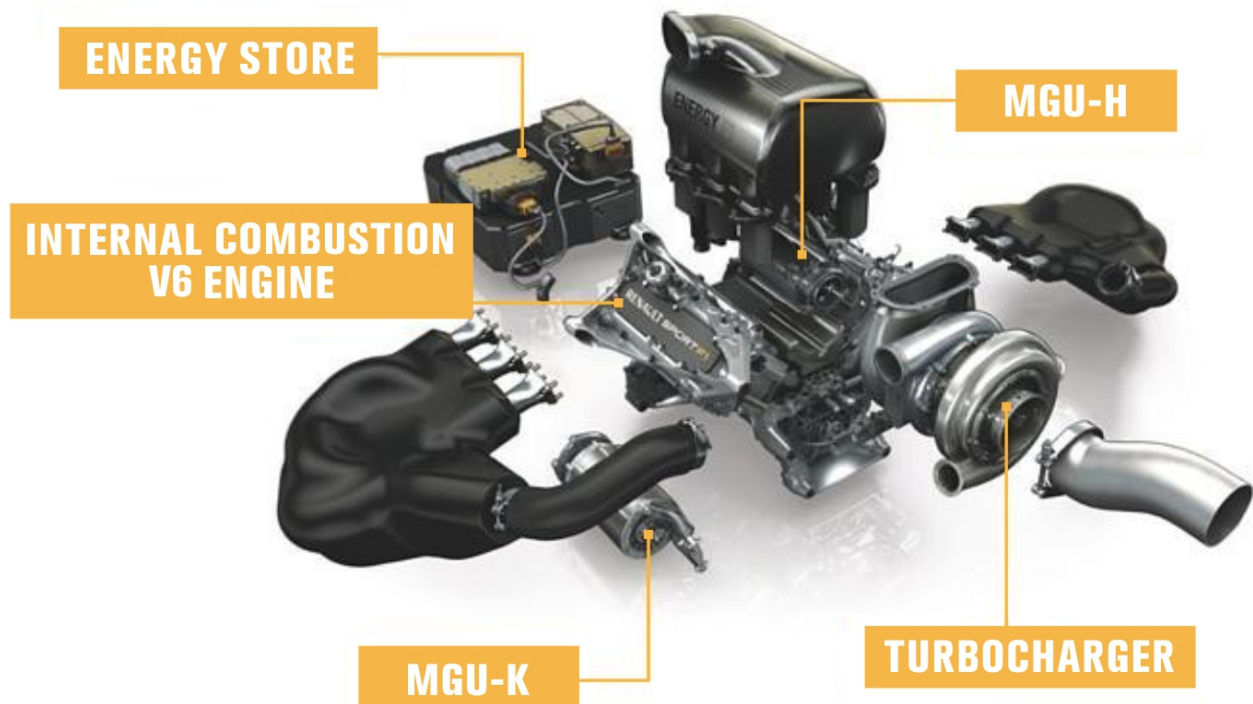


Figure V-1: Typical Formula 1 Hybrid Power Unit: two motor generator units (MGU) are used: 1 by the kinetic energy of the car (MGU-K) connected to the engine flywheel, and 2, driven by waste heat from a common shaft on the turbocharger (MGU-H; produces electricity fed to the energy storage and/or the MGU-K). The energy storage is limited to 4 MJ that is available for propulsion each lap. The 1.5 L V-6 engine's revs are capped at 15,000 rpm; the entire power unit weighs 145 kg (340 lbs.) and produces over 600 hp.

(photo: news.com.au)

- The HySpy fuel flow meter was approved by the Federation Internationale de l'Automobile (FIA) to be the exclusive real-time fuel consumption measurement device to implement fuel allocations for the 2016 Formula 1 and LMP1 category in the WEC to incentivize powertrain and vehicle efficiency. The availability of a highly accurate fuel flow measuring device further increases the potential for fuel allocations - a key efficiency-enhancing feature of SAE J2880 - to be used in other series around the world.

- 2015 marked the end of the first season of Formula E (FE), the FIA-sponsored electric vehicle race series. Based on spec cars with identical electric powertrains and energy storage and using innovative spec tires from Michelin, the series had a smooth, if somewhat underwhelming, first season (Figure V-2). However, the ability to hold a race series for electric vehicles (EVs) was demonstrated in some of the most iconic city centers in nine countries around the world. Most importantly for Green Racing, the FIA announced a schedule for moving away from a spec series towards a technology-driven series that is in keeping with the spirit and letter of Green Racing. In 2016, teams will be free to use different electric machines and power electronics; in 2017 a choice of energy storage systems will be available, and in 2018 full bespoke cars will be allowed. By 2018 it is expected that a single car will be used for the 45 minute sprint race instead of needing to switch cars in the middle of the race as is done now. At that time, FE will have evolved into the technology-leading development and demonstration platform that fully supports Green Racing philosophy and technical content.



Figure V-2: 2014-15 Formula E car; note the batteries behind the driver with power electronics above and electric motor behind attached to five-speed transaxle.
(photo: mmdi.co.uk)

Future Achievements

- Work with TUSC to incorporate E85R into the PC class in 2016 and adopt Optima-based fuels with a higher percentage of renewable content into all classes as soon as the 2018 season.
- Continue to make advanced renewable fuel sources available to IMSA and INDYCAR for spark-ignition (SI) engines.
- Develop Green Racing integration plan with INDYCAR as they qualify as a Green Racing series under SAE J2880, and help them move towards achieving Green Challenge status with additional efficiency-enhancing technology.
- Work with the FIA to establish a Green Cup Award in F1 in 2017 or 2018. Under the revised J2880, F1 qualifies for recognition and award status starting in 2015.
- Work with the ACO to recognize the LMP1 category in WEC as a Green Racing series in 2016.
- Support and incentivize the use of energy recovery technology in race cars, and identifying methods available to properly limit and/or record use of technologies to allow for performance balancing.
- Expand working relationship with BETO including additional biofuels suppliers and inclusion of BETO information on the Green Racing website update.

- Move towards a scoring system based on energy allocation, working with industry partners to develop fuel flow measurement technologies applicable in a racing vehicle.



V.1.B. Technical Discussion

Background

Green Racing History

The Green Racing Initiative (GRI) started in 2006 with a working group of industry, government and national lab representatives. The team sought to take advantage of the efforts and opportunities in motorsports to further develop advanced transportation technologies that could be applied to street vehicles. This effort focused on providing a proving ground for technology advancements and petroleum displacement in a competitive setting. Once the working group had built the foundation for GRI, a set of protocols was approved through SAE and in 2008 the J2880 ‘Recommended Green Racing Protocols’ were established.

The American Le Mans Series (ALMS) acknowledged these protocols and awarded the first Green Challenge Award in October 2008. When the ALMS merged with GRAND-AM to become the United Sports Car Championship in 2014, the Green Racing element of the competition was adopted as a signature element of the new racing series.

The Green Challenge Award and the Michelin Green X Challenge soon became an integral part of sports car racing in North America, where Michelin recognized the teams and the Department of Energy (DOE), Environmental Protection Agency (EPA), and the Society of Automotive Engineers (SAE) recognized the manufacturers who perform best when evaluated using the Green Racing formula for competition. The scoring formula takes into account measured performance and fuel consumption to determine a total score: Clean, Fast and Efficient terms are calculated in real time for each lap for each vehicle in the appropriate racing categories. In 2015, DEKRA became the official Green Racing partner with International Motor Sports Association (IMSA), replacing Michelin but carrying on the same award structure. In addition, DEKRA became a partner in the technical and safety inspections of TUDOR United Sports car Championship (TUSC) cars.

Introduction

The 2015 racing season in the United States came to an end right after the end of FY2015 generating a record that showed sustainable motorsports activities advanced both technology and performance in the multiple racing series they were adopted in. Once again, the 2015 season has been extremely competitive in the renewable fuel-powered GT Le Mans (GTLM) class of the TUSC, often being acknowledged as the world's premier sports car racing class. Teams have applied new technologies and sanctioning bodies have confirmed future rules which incorporate sustainable practices and require advanced technologies for future racing vehicles. Cellulosic ethanol from multiple producers, many of whom have received DOE funds to develop their process, have been provided fuel to IMSA through a relationship with VP Racing fuels which was established through the GRI. In a similar fashion, the GRI was instrumental in providing a fully synthetic renewable diesel fuel for the Prototype class in TUSC. The GRI seeks to coordinate the strategies and guide motorsports requirements to optimize efforts within motorsports to highlight advances in transportation technologies.

Approach

Motorsports are the only professional sport that can directly help attain national energy and environmental objectives. The rapid developmental cycles in racing, the focused development of advanced technologies and alternative fuels, and the search for more efficient and capable vehicles inherent in racing, all tie directly with our national transportation goals. These efforts reduce our dependence on petroleum and lower the carbon footprint of vehicles – and still provide the entertainment and drama that has made racing one of the most

followed forms of sports around the world. Racing is one of the best platforms for reaching a large audience with the message that through advanced vehicle technologies and renewable fuels we can maintain the personal mobility and performance customers want while moving toward the energy security and sustainable transportation the country needs.

Racing brings out the best in automotive technology and places it in a demanding competitive environment allowing a technology showcase that resonates with the public. Racing also inherently values efficiency as successful teams operate in alignment with sanctioning body rules to optimize fuel use with other racing parameters, like distance between required tire changes. Efficiency and petroleum displacement are attributes that underpin our national energy and environmental objectives. Building on core values in racing and adding renewable fuels and advanced transportation technologies as ways to improve sustainability, we have developed the GRI with our partners.

Results

The 2015 racing season had a number of highlights in advancing transportation technologies through motorsports. Of particular interest was the domination of hybridized racing vehicles in the world's most important sporting event, the 24 Hours of Le Mans. Audi, Nissan, Porsche and Toyota each brought hybridized Le Mans Prototype (LMP1) vehicles to the event, with the Porsche hybrid electric vehicles (HEVs) taking the first three positions on the grid and finishing in first and second place overall (Figure V-3). LMP1 race cars are considered the most technologically advanced cars ever produced, bristling with energy-efficiency technologies that enable them to post faster lap times than ever before while using more than 30% less energy.



Figure V-3: Porsche 919 HEVs took first and second place in the 2015 24 Hours of Le Mans (left) and in cutaway to show electric front drive, energy storage in the center of the car, and 2 liter V4 engine with energy recovery and electric transaxle in rear (right).

(photos: Porsche AG)

In 2014, the Automobile Club de l'Ouest (ACO) refined their rule package for the LMP1 premiere category vehicles in the World Endurance Championship (WEC) expanding the size and type of energy recovery and hybrid technologies by a factor of 4 as well as allowing a limited amount of energy (fuel) per lap depending on the level of hybrid technologies applied to each car. These ACO rules were developed to enhance efficiency and not performance in consultation with the GRI. The rules are remarkably open with regards to technologies allowing the factory teams to be innovative in creating and applying advanced technologies. This shift of motorsports to using energy allocations, rather than purely speed, as a way to structure future competition represents a substantial change in the perspective of sanctioning bodies, and places a renewed relevance in the sport, as energy efficiency is something the manufacturers deal with in every vehicle they produce. WEC continues to use E20 cellulosic as the base fuel for all its categories, lowering its well-to-wheels (WTW) GHG emissions by 18.5% and boosting its oil displacement to 19.5%.

The GRI retains its integral part of the TUSC in its second year of operation. Green Racing content will spread to other classes in TUSC in an official ceremony at the 2016 Rolex 24 at Daytona in January. Working in close collaboration with TUSC and the ACO from which a significant amount of the sporting regulations are drawn, the GRI continues to explore ways where advanced technologies can be showcased and renewable fuels

utilized for racing in the future. The experimental DeltaWing from the innovative Garage 56 at the 2012 Le Mans race returned in more competitive form in the TUSC in 2015, being able to lead several races this season (Figure V-4). A completely new chassis and ongoing developments spawned a transformation into a road car design in 2015. It remains a fan favorite due to its innovative, light weight design and tiny front wheels.



Figure V-4: The DeltaWing showed more pace in 2015, leading several races. Note the absence of traditional wings and highly aerodynamic design; most of the downforce is developed under the side pods. It has a remarkable drag/lift ratio, together with its light weight allowing it to be competitive with about 60% of the engine power of its rivals.

(photos: DeltaWingracing.com)

The 2015 TUSC season continued to offer advanced renewable fuels for use by its competing teams. In the GTLM class, E85R dominated as the fuel of choice in this ultra-competitive category. All the top three finishers in all the races used E85R fuel. The GT class is based on cars that are on the road today and puts rival teams in door-to-door competition that may be the most competitive class in racing anywhere in the world. All the BMW, Corvette, Dodge, Ferrari, and Porsche factory cars and most of the privately entered cars used this renewable fuel with great success. The wholesale movement to E85R was primarily motivated by the performance potential of this excellent fuel, but the message with respects to its upstream impact and its energy security and environmental advantages have provided an excellent outreach opportunity for DOE goals. The Green Challenge scoring system accurately reflects each fuel's characteristics in terms of its greenhouse gas (GHG) and oil replacement attributes without rewarding a team's selection of bio-fuels over conventional fuels (Figure V-5). That makes this switch to renewable fuels at this level of motorsports all the more impressive and significant. This noteworthy accomplishment demonstrates that these fuels are capable of outstanding performance, reliability, and capable of widespread use in street vehicles.



Figure V-5: DEKRA Green Challenge Awards were given in all ten TUSC races in 2015
 (photo: speedvile.com)

In the LMP class in TUSC, Mazda's ongoing commitment to their diesel-powered prototype race car was a major story (Figure V-6). The remarkable performance from a production-based diesel engine was highlighted by its use of 100% synthetic renewable diesel fuel made from waste vegetable oil thanks to the Green Racing program. Its high cetane, zero sulfur content allowed impressive power density – achieving nearly four times the production engine's power - and virtually no particulate matter (PM) emissions. This engine's performance became better and better as the season unfolded, now producing in excess of 550 hp. Mazda also made a major contribution to Science, Technology, Engineering, and Mathematics (STEM) education by bringing a race car and drivers to local high schools near the race tracks to show how important STEM education was to open exciting futures for high school students. Using their commitment to racing as their model, they explained how practical and specific applications of science and technology will shape the future and offered real-life examples of how that knowledge can be put to work.



Figure V-6: Mazda Skyactiv-Diesel production-based race engine competed in all ten TUDOR United SportsCar Championship races using 100% renewable synthetic diesel fuel.

(photo by mazdamotorsports.com)

Due to the success of last year's Green Racing Simulator (GRS), the mobile outreach simulator was deployed again this season for the Green Racing program (Figure V-7). The GRS, developed by Argonne National Laboratory, incorporates a program that is based on real engine, battery, and electric motor maps and calculates the amount of regenerative braking energy captured and fuel used during two laps of simulated racing. This simulator was set up at three IMSA races in 2015 as well as events at DOE Headquarters and auto shows. It served as a notable means of disseminating the DOE's Green Racing key message that the use of renewable fuels and hybrids can displace a substantial amount of imported petroleum to thousands of racing fans.



Figure V-7: Fans and professional racing drivers alike try their hand at the GRS. Tommy Milner of Corvette Racing puts the simulated E85/Hybrid Corvette to the test.

Conclusions

Motorsports in FY2015 was a year that showed significant world-wide acceptance of Green Racing content in the premier racing series around the world: WEC LMP1, F1, TUSC, and INDYCAR. Significant petroleum reduction was recorded in the GTLM class in TUSC of 62.5% with a 65.5% reduction in GHG emissions when compared to a baseline of the 2005 series. All vehicles season-long participants in the GTLM class are running on E85 racing fuel, while the Mazda has successfully employed an advanced synthetic renewable diesel fuel to power their two-car team Prototype team in the TUSC. Green Racing continues to expand in the elite levels of

racing, illustrating how advanced transportation technologies and renewable fuels are leading the way to sustainable transportation through motorsports.

Important accomplishments regarding the incorporation of energy recovery systems into world class racing were showcased multiple times during the year. The adoption in F1 of both exhaust and kinetic energy recovery was an important part of reducing energy consumption in that series by 30%. The domination of HEVs in the WEC LMP1 class with hybrid vehicles fielded by four major OEMs shows that recovering energy is an essential element in the future of racing at the highest levels. Making advanced renewable fuels available to TUSC and INDYCAR shows that using these fuels is the easiest and most cost-effective way to reduce the carbon emissions and oil consumption of race series.

The adoption and publications of the updates to SAE J2880, the Green Racing Protocols, in 2014 provides a flexible set of guidelines for racing series around the world to adopt elements of Green Racing that fit their situation. In addition, the updated J2880 contains a set of recognitions and rewards that incentivize series' progressing to greater levels of Green Racing content and sustainability. The Protocols form a solid foundation for advancing the development of technologies and fuels used in future road vehicles.

The relationship between DOE, IMSA and partners at EPA and SAE International is strong and there are many opportunities for building acceptance of Green Racing principles contained in the Green Racing Protocols. The GRI continues to impact the future of motorsports in alignment with DOE's transportation goals.

V.1.C. Products

Presentations/Publications/Patents

- Presentation of Annual Green Racing Challenge Award by DAS-T Sarkar (New York, New York, October 2014)
- Motorsports Engineering Science Conference (Indianapolis, Indiana, December 2014)
- 2015 Florida 12 hours of Sebring TUSC Technical conference (Sebring, Florida, March 2015)

V.1.D. References

7. SAE J2880, Green Racing Protocols (http://standards.sae.org/j2880_201406/)

V.2. Test Standards Development for EV, PHEV and HEVs

Michael Duoba, Principal Investigator

Argonne National Laboratory
9700 South Cass Avenue
Argonne, IL 60439
Phone: (630) 252-6398
E-mail: mduoba@anl.gov

Lee Slezak, DOE Program Manager

Phone: (202) 586-2335
E-mail: Lee.Slezak@ee.doe.gov

Start Date: October 1, 2014
End Date: September 31, 2015

V.2.A. Abstract

Objectives

- Power Rating: Organize and chair an SAE standards task force to define methods for testing and validating the powertrain power rating for hybrid electric vehicles.
 - Collaborate and communicate with several international committees also involved with hybrid vehicle system power definition.
 - Leveraging existing vehicles, instrumentation, hardware and test equipment, invent new approaches to testing for system power rating.
 - Ensure that final standard is fair for hybrid vehicles and comparable to other vehicle powertrain types.
- Road Load Investigation: Test the accuracy and robustness of current coastdown test methods compared to alternative road load determination methods for electrified vehicles that have the powertrain always connected to the wheel (no mechanical neutral gear).
 - Leveraging existing vehicles, instrumentation, hardware and test equipment to run the various test approaches.
 - Analyze results, make recommendations for accurate road load testing for electrified vehicles.

Accomplishments

- Power Rating
 - Validated that both chassis and hub dynamometer provide equivalent power rating measurements.
 - Invented several test method approaches for finding the maximum powertrain power using a wide variety of vehicle configurations
 - Discovered that a fair amount of flexibility is required to accommodate the profound differences in powertrain architecture and operation among electrified vehicles.
 - Narrowed down reporting possibilities to three distinct options (consensus building in progress).
- Road Load Investigations
 - Measuring torque directly from axle sensors was found to be a robust method of road load determination for all speed ranges.
 - Differences were found between an electric drive vehicles with a mechanically disconnected neutral compared to another vehicle that did not.
 - Data analysis methods and techniques were developed to use the axle torque readings for best accuracy.

Future Achievements

- Power Rating
 - Harmonization of J2908 with J2907, ISO 20762, and the UN ECE workgroup in the methods of defining HEV system power. These other methods are being developed now and will finish in the future.
 - Finish draft of J2908 and ballot the document successfully thus providing the framework for fair comparisons between all electrified vehicles and conventional vehicles.
- Road Load Investigations
 - Test a few more vehicles to investigate the now-understood problem of irregular motor drag profiles interfering with traditional coastdown polynomial force fitting.
 - Investigate designs for quick-install and/or reusable wheel or axle torque measuring hardware making it less expensive and costly to perform the new steady-speed testing methods.



V.2.B. Technical Discussion

Background

Vehicle technology is undergoing many radical changes and the US Department of Energy (DOE) is investing in advanced technologies to provide pathways to achieve reductions in transportation petroleum usage. A new technology's capability to increase efficiency and lower environmental impact can only be quantified by using appropriate laboratory tests. To ensure that these new technologies are properly and accurately evaluated, Argonne National Laboratory has been developing new, robust analytical testing techniques for close to two decades that match the unique characteristics of advanced vehicles (such as HEVs, BEVs, PHEVs, and others). This expertise has provided leadership and guidance for SAE committees that are involved in many vehicle testing standards/procedures.

Introduction

In addition to participation in many active standards committees, two research efforts were conducted in the area of understanding and improving specific methods for testing electrified vehicles. They are:

J2908 Hybrid Net System Power Rating

The first effort involves developing methods and guidelines for defining the system power for hybrid electric vehicles. Currently there isn't a uniform approach to reporting a hybrid's power rating. Providing objective research into this standard is another way to ensure the best chance for further adoption of advanced vehicle technology. Argonne staff holds the chair of the SAE task force for document J2908 Hybrid Net System Power Rating. A fair amount of testing with different vehicles and test equipment are needed to provide informed recommendations to the task force (standards development is based on consensus building).

Road Load Investigations

The second effort was a general investigation into road load determinations for electrified vehicles. Standard practices call for a "Coast Down" test that allows the road load to be determined by using the vehicles deceleration rate to define the losses as a function of speed. However, in electrified vehicles, the rotating motor(s) cannot be disengaged and this adds inertia and extra losses leading to some concern about its accuracy and applicability.

Approach

J2908 Hybrid Net System Power Rating

The approach was to investigate all the options and methods which would be most appropriate (in the judgement of the task force). Argonne's 2WD chassis dynamometer was used with instrumented vehicles. All the relevant test vehicles had axle torque sensors installed to provide direct power measurements at the axle. In addition, a hub dynamometer was rented for 4 months exclusively for this project to experiment and validate that both it and the chassis dynamometer provided equivalent results.

The testing objectives were to investigate different testing approaches and analysis techniques. There are many stakeholders concerned that this new test method would require additional costs for new equipment. An important objective was to ensure that any valid method could be run on either a hub dyno (dynos measure power directly at the hub) or a chassis dyno (requires added sensors to measure axle or wheel torque). The equipment used is shown in Figure V-8.

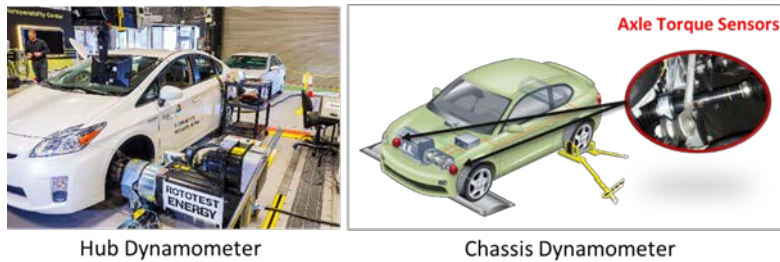


Figure V-8: Dynamometer Equipment Used in Experiments

Photos and Artwork: Argonne National Lab

Because of its large scope, it was apparent that this program should look at a diverse set of vehicles each with a unique powertrain configuration and operation. Leveraging test vehicles from Argonne's advanced vehicle benchmarking program, the following vehicles (Argonne owned Level 2 benchmark vehicles) were selected for testing: Sonata HEV, Accord PHEV, Focus BEV, Prius HEV, Gen 2 Insight HEV, Volt PHEV (EREV), and one conventional vehicle, the Fusion v6 as shown in Figure V-9.



Figure V-9: Experimental Vehicles Used for Developing System Power Rating Test

Photos: Argonne National Lab

Road Load Investigations

The current approach to making a vehicle's road load determination is described in SAE J2263 [1] and J1263 [2]. All vehicles driven solely by an engine possess a launch device in the powertrain, i.e., a clutch or torque

converter. When a vehicle is placed in neutral gear, the engine is disengaged from the wheels using the launch device with only a small amount of gear and bearing drag added to the total vehicle drag.

Many electric-driven vehicles (HEVs, PHEVs and BEVs) do not have the need for a launch device and thus depending upon their configuration do not have the capability to mechanically disengage their power-producing components. This brings up a host of questions. Are new electric and hybrid electric vehicles getting a fair and balanced result during traditional coast-down testing? Are there inherent biases? Are the baseline assumptions for axle inertia sound? These are all questions that need to be addressed by this project and frames the approach taken in the testing.

The conventional coast down test is the basis for all chassis dynamometer testing of fuel economy and emissions. Using Newton's Second Law (the sum of the forces equals the mass times acceleration) coast down testing calculates the total road load as a function of vehicle speed. Refer to Figure V-10 and for the simple solution to solving for road load case (i). The fact that in neutral gear there are no other forces acting to slow the vehicle down, ensures accurate vehicle road load results can be determined. However, for the electric vehicle (and some hybrids) the motor introduces other forces that complicate the coast down test, Figure V-10 case (ii).

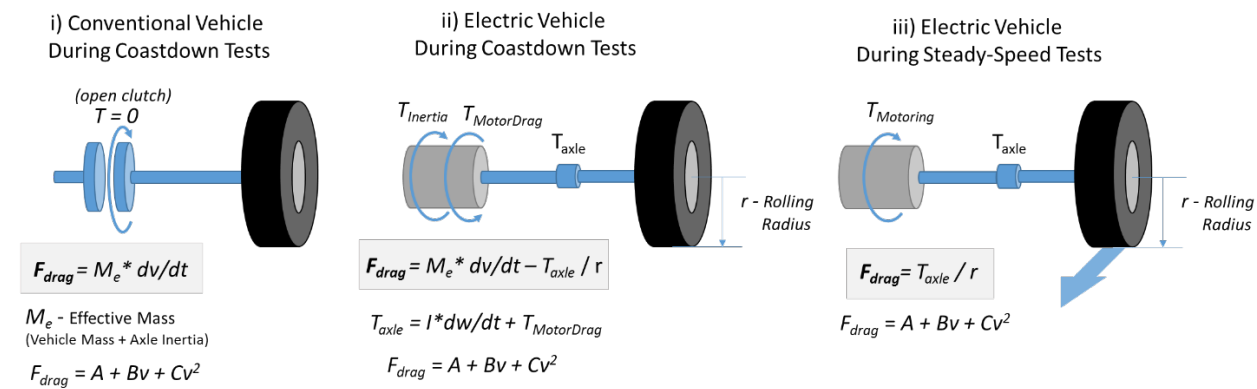


Figure V-10: Description of Forces during Tests to Determine Road Load (Force of drag)

Graphic: Argonne National Lab

The approach is to test for errors or uncertainties in the conventional coast down procedure by providing a 2nd determination method for road load that is not effected by the extra forces in the motor itself. In Figure V-10 case (iii), road load is found by directly measuring the torque required to maintain a specific speed. If a set of stable steady-state speeds can be driven, the road load curve found by curve fitting the point throughout the speed range. Both tests approaches require a long, flat road surface such as that at a proving ground or on public roads in a rural, flat location. The protocol for both tests are that runs are repeated in both directions on the same patch of road, thus any influences due to wind or grade are averaged out.

Several existing Argonne test vehicles have instrument-grade torque sensors installed on both axle shafts. They will be used for this study. Note that these include some of the same vehicles used in the Hybrid System Power study. The Chevy Volt PHEV and the Ford Focus BEV are the two vehicles highlighted in this report because they are the most interesting. Whereas both vehicles are driven by a large electric motor, the Volt PHEV has the ability to open all its clutches in neutral gear (motor is at rest) but the Focus BEV motor is permanently geared to the output (wheels). The comparison of results from both vehicles will reveal the strengths and limitations of various road load determination techniques.

Results

J2908 Hybrid Net System Power Rating

Literally hundreds of tests were run using both the Argonne 2WD chassis dynamometer and the rented hub dynamometer. After experimenting all the vehicles running many different test approaches it became clear that rigid and specific prep procedures will not work for all types of powertrain designs. Whereas procedures for

emissions and fuel economy dynamometer testing detail very specific prep conditions leading up to the beginning of a test, the results in this study show that as long as the vehicle is not limiting power because of low SOC or out of range component temperatures, results are valid and repeatable. The exact method used to prep the vehicle shall be left to the test engineer. For example, some hybrids turn their engine on and off up to speeds as high as 70 mi/hr with the SOC always rising or falling. Controlling for initial SOC requires ending the warmup based upon SOC instead of ending at an exact time limit.

It also became apparent that the specific dynamometer mode and procedures must allow for the engineer to choose among several test approaches to achieve the best final results. For example, if the procedure mimics a road load acceleration run, through a range of speeds, vehicles like the Sonata hybrid would only experience maximum power for a very short moment right before a gear change. However, running the vehicle with a fixed vehicle speed (like how engines are rated on a test stand) the proper gear can be held to achieve the correct maximum total vehicle power. Several tests types were invented and developed to accommodate the various operational behaviors encountered in months of testing (Figure V-11).

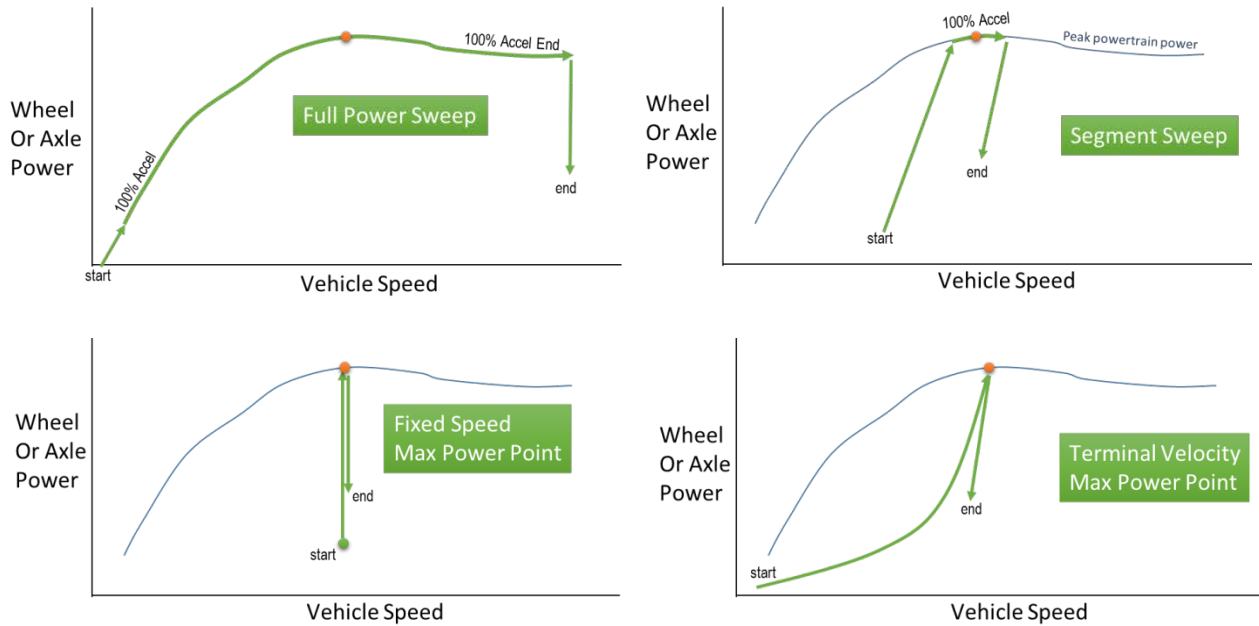


Figure V-11: Power Test Options Invented/Explored During Testing Program

Graphics: Argonne National Lab

After completing development of the test options, the next challenging task was taking all the data from the tests and finding the right way to report the results. The fundamental math used to account for "Net Hybrid Power" is currently not consistent among manufacturers. Vehicles with different hybrid powertrain types use different ways to sum up the system power. While some methods apply easily to some hybrid configurations, others do not. After many months of analyzing data, having frequent discussions with the task force, and setting up one-on-one meetings with industry and other standards entities, three (3) different fundamental approaches emerged for providing the basis for "Net Hybrid Power" (see Figure V-12).

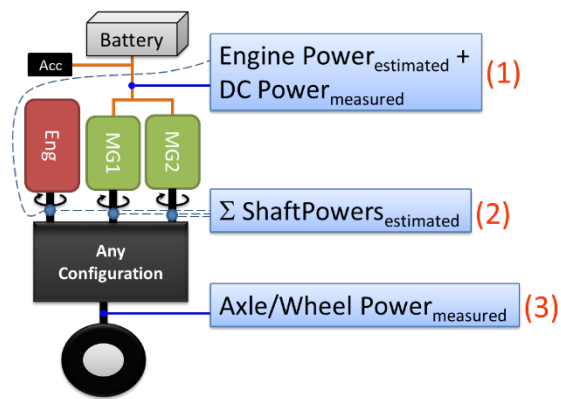


Figure V-12: Three Fundamental Ways to Determine "Net Power" from a Test

Graphics: Argonne National Lab

Method (3) represents the most direct approach to finding a single measurement encompassing the entire powertrain. Power is measured at the both axles or both wheel hubs. Analysis of data on the Hub Dynamometer showed that if care is taken to prevent excessive brake drag, the power measured at the axles and at the wheel hubs are within 1-2% of each other. One strength of this method is that it can be tested by a third party without requiring any estimates of component operation or additional knowledge about the vehicle. However, if the primary focus of this standard is to report the information to the consumer, consumers will be confused or misled because conventional vehicles are defined by their engine power, not the power at the wheel (which can be much lower). Look to Figure V-13 to see an example. The measured axle power is 125 kW, however the other approaches provide power levels 26 - 33 kW higher.

Method (1) is currently being used by manufacturers of power-split hybrids. This method adds the measured battery power to the expected engine power. A typical assumption for an HEV (not a plug-in) is that the engine power is at its maximum power (rated power) at the moment of maximum powertrain power. Full engine power can be validated by monitoring a host of engine parameters during a test (engine RPM, MAP, throttle angle, etc.). However for plug-in hybrids, we found that the engine is not always at its rated power at maximum powertrain power and in this case, the engine power level needs to be estimated. Estimating engine power during a test may require additional data about the engine (look-up tables or maps) that can be matched up to the parameters monitored, or that real-time torque and speed data reported by the vehicle network be accurate and trustworthy. The strengths of Method (1) are that it is more in line with current conventional vehicle power reporting (power reported upstream of the transmission and gearing) and it can at times be easy to reproduce and verify (in the case that the engine achieves rated power during maximum powertrain power, like in Figure V-13). However, there will be times when the engine power must be estimated to report the system power.

Method (2) defines "Net System Power" as the sum of all the mechanical power-producing powertrain components. Like the other methods, it is designed to be valid for any type of hybrid configuration. For example, in Figure V-13 the results for Method (2) are shown as the engine rated power plus the reported motor power off the vehicle CAN bus. The test results in Figure V-14 are from series hybrid operations, in this case the positive engine power is assumed to be equal to the negative generator power and thus the "Net Power" is only the motor power output. For hybrids with only a modestly-sized battery, the difference between Method (1) and Method (2) may not be significant to cause concern. However, looking at the results in Figure V-14, it is apparent that as we evaluate vehicle with bigger and bigger batteries, these two methods significantly depart. Taken to the logical conclusion, if Method (1) were applied to an EREV type PHEV the vehicle power output would be defined by the battery power, not the motor power. Imagine if an OEM produced both a BEV and a series hybrid PHEV using the exact same motor as the prime mover. The PHEV would be rated noticeably higher than the BEV even though these two vehicles have the very same electric motor. Discussions like these have led the committee to consider expanding the scope of J2908 to include BEVs to avoid discontinuities in "Net Power" ratings among vehicle types.

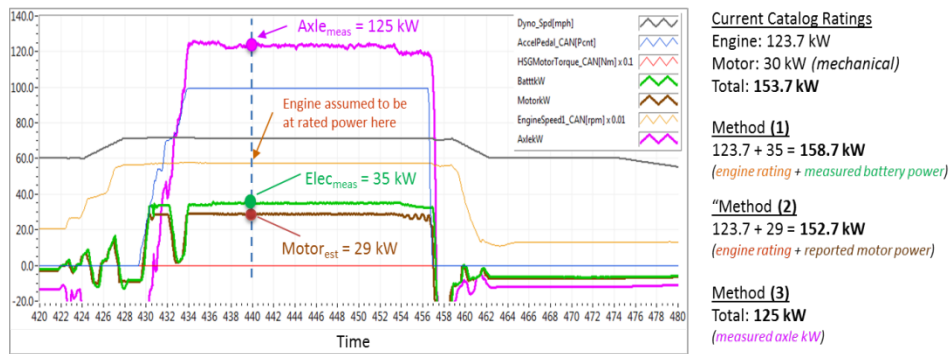


Figure V-13: All Three Methods Applied to a Parallel HEV during Max Power
 Graphics: Argonne National Lab

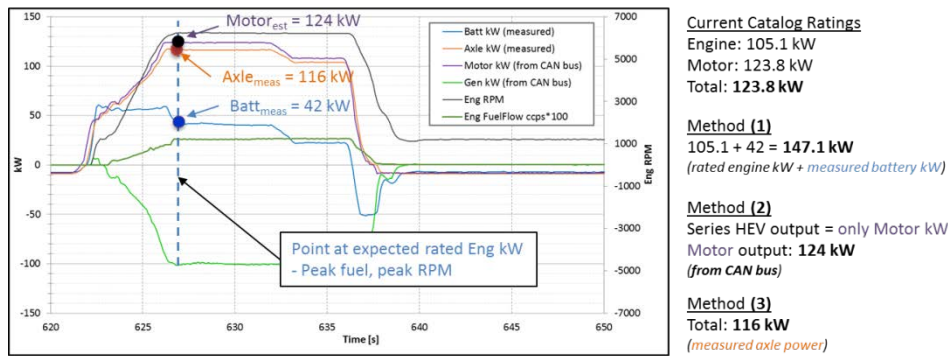


Figure V-14: All Three Methods Applied to a PHEV in Series Mode during Max Power
 Graphics: Argonne National Lab

Road Load Investigations

Both traditional coast down tests and experimental steady-speed load tests were conducted on the same road surface on the same day (best for comparisons) for both test vehicles, the Chevy Volt and the Ford Focus BEV. The results from testing the Chevy Volt are provided in Figure V-15. Keep in mind that the Volt has a mechanically disengaged neutral gear like most cars and the results show nothing out of the ordinary. The plot on the left of Figure V-15 is the individual steady-state road load measurement in pounds force calculated from the axle torque sensors. On the right is that data curve-fitted and placed over the fitted road load curves derived from a number of coastdown tests. Both test types provided road load results that are fairly close in magnitude.

It was found that running steady-state speeds is much easier to conduct if the vehicle's own cruise control system is utilized. One weakness however is that the cruise control normally does not work below 25 mi/hr. This is a shame because the most uncertainty in road load force found in coastdown testing is at low speeds.

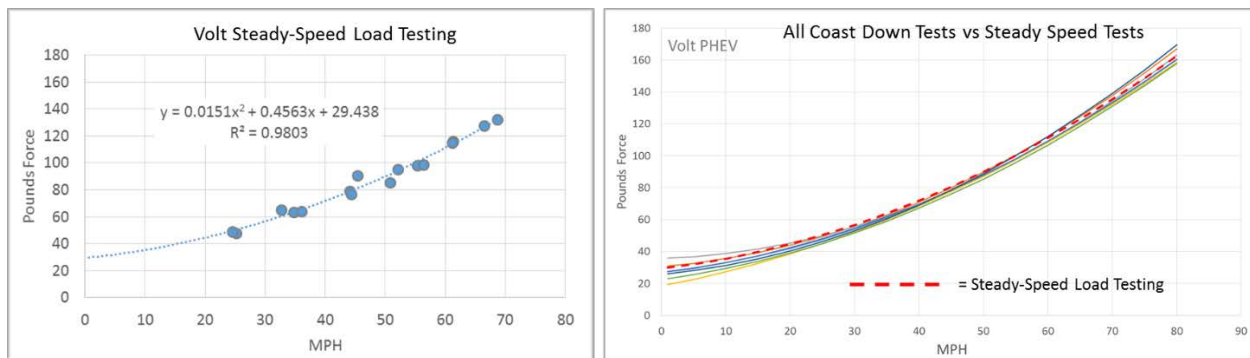


Figure V-15: Chevy Volt Road Load Testing (vehicle has mechanically disengaged neutral gear)

The results of the electric vehicle with the motor permanently geared to the wheels (Focus BEV) showed some important differences to the Volt that requires some further investigation. The left side of Figure V-16 is a plot of the steady-speed road load results. Note that this time we achieved steady-state data at ~5 mi/hr, this helps the overall curve fit. This is data taken in drive but with 0% accelerator pedal input, this vehicle operates a "creep" mode that was used for the lowest speed data (thus no data is available between 5 mi/hr and the lowest cruise control speed of 23 mi/hr). The curve fit of that data is plotted on the right graph alongside the coastdown road loads calculated normally with one exception: using a higher "added mass" multiplier to account for the added inertia of the spinning electric motor. The added mass assumption used in calculating road load force is typically assumed to be 3% of the vehicle mass. The actual total axle was found to be 4.57% of vehicle mass from a special accel/decel test conducted on the dynamometer.

Refer back to Figure V-10 (ii) to help explain why the coastdown road load curves do not match the steady-speed results for the Focus BEV as they did for the Volt. The drag of the motor is adding to the coastdown road load, but is not part of the steady-speed road load measured at the axle. Our initial thought was that one could look at the axle torque reading during the coastdown tests to make a correction to the vehicle road load, but again looking at Figure V-10 (ii) one can see that the motor inertia is providing decelerating torque in the opposite direction of the its drag. It became apparent that another test was needed. A test that will quantify the steady-state motor drag as a function of speed. This was best accomplished on the dynamometer.

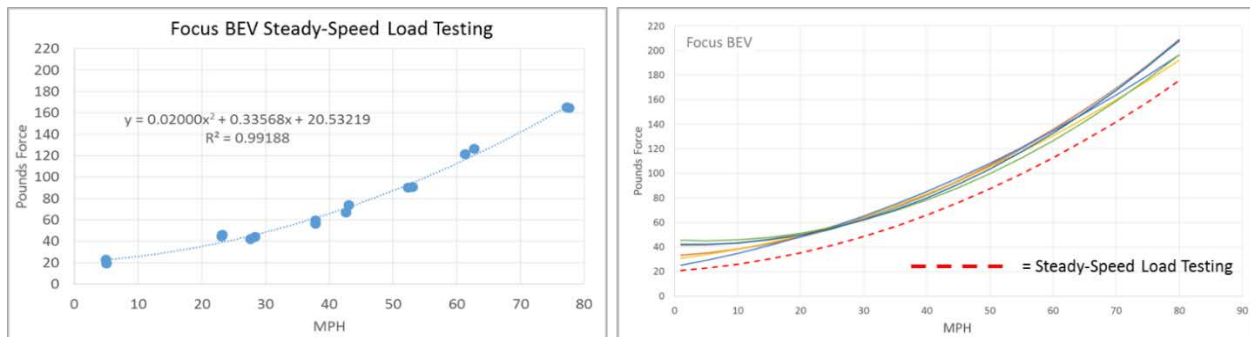


Figure V-16: Ford Focus BEV Road Load Testing (motor is always mechanically engaged)

The vehicle was mounted to the chassis dynamometer and the wheels motored in neutral (dynamometer providing the power to remain at a steady speed). On the left plot in Figure V-17 the measured motor drag is shown as a function of at speed. Notice that the motor drag data points are not easily fit to a 2nd order polynomial curve like road load is traditionally defined. This irregular motor drag could be due any number of electric motor control design features (field weakening, etc.) that changes at various motor rotational speeds. This would explain why there are times that the road load determination (the dynamometer procedure to match on-road load coefficients) will match in one part of the speed range but poorly match in others for electrified vehicles. The motor is forcing the vehicle losses to a shape not easily described with a 2nd order curve fit.

Continuing with the analysis, if the on-dyno force required to maintain steady-speeds matches the on-road steady-speed load curve, then we can feel more assured that running the traditional process for road load determination could be valid for BEVs without a mechanically disengaged neutral, even though the road load result includes the motor drag during the coastdown testing process.

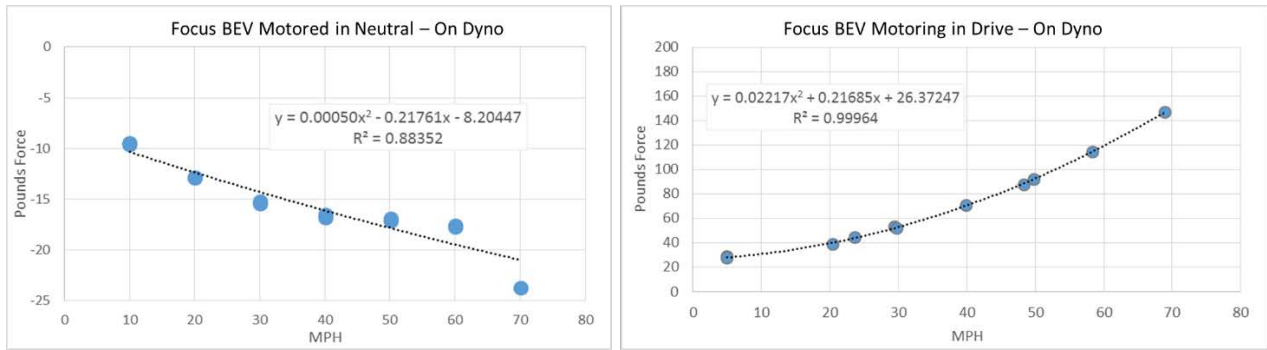


Figure V-17: Ford Focus BEV On-Dyno Motor Load Testing
 Graphics: Argonne National Lab

Figure V-18 shows several road load curves for analysis. The upper curve, higher than the others is the average of the coastdown load curves. Also shown are the steady-speed force curves from on-road testing and from the dyno with the dyno setting based upon a road load determination of the coastdown average, and finally, the coastdowns load curve corrected by subtracting the motor drag curve (from the left plot in Figure V-17).

Whereas the average coastdown load curve is significantly higher than the steady-speeds curve, after corrected for motor drag, all three curve sources match. There is a little uncertainty and deviations at higher and lower speeds, they will be addressed in future testing. A curve fit is only as good at the range of data provided, perhaps starting the coastdown testing at much higher speeds (90 mi/hr) may reduce the uncertainties in the desired speed range (< 80 mi/hr). Low-speed accuracy is always a problem for coastdown testing. Here the steady-speed on-road test at the creep speed may provide a robust point for the load curve fit. But are there other ways that the low speed road load can be found directly. This was also investigated with the Focus BEV.

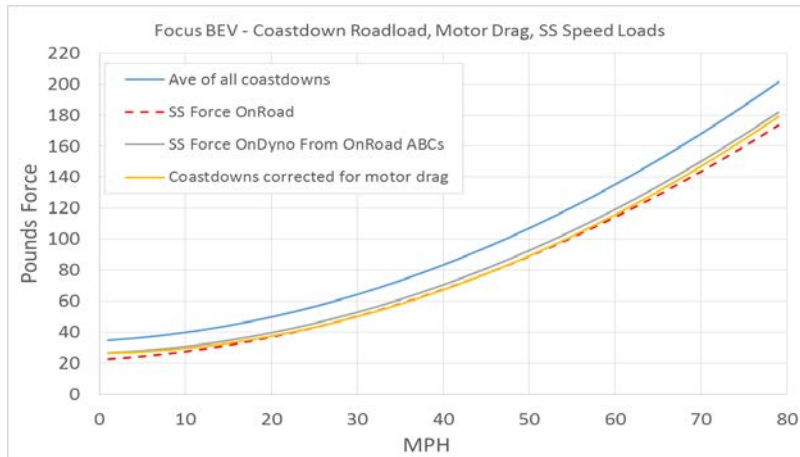


Figure V-18: A comparison of Ford Focus BEV Road Load Curves
 Graphics: Argonne National Lab

A simple experiment was conducted where the vehicle was pulled at a low speed with a winch (after a warmup driving period). The winch cable was fitted with a load cell measuring cable tension. Different stiffness of elastic cable was used to dampen out the spikes and valleys (it turns out that pavement and surprisingly, indoor concrete floors that by all appearances seem flat, does induce variations in cable tension while pulled). Figure V-19 shows several pull tests of the Focus BEV. Although the tension measurements include short peaks at 50 lbs and fall to 10 lbs for moments, it is assumed that as long as the tension is greater than zero and the test covers a significant distance, then the average tension must be the true force required to maintain a very slow speed. Refer to

Table V-1 to compare the A-Terms of the various methods to the pull test results. The 23.09 lbf result from pull testing seems slightly low compared the other tests (the creep test at ~ 5 mi/hr was 27.4 lbf). The vehicle weights during test were different (1 person in the pull test, 2 plus extra equipment in the road tests) this could

account for roughly ~2 lbf. Additional attempts to use a perfectly flat surface and a better tension system could provide better direct determination of the A-Term in order to make road load determinations robust and accurate for future road load testing when axle torque sensors are not installed in a vehicle.

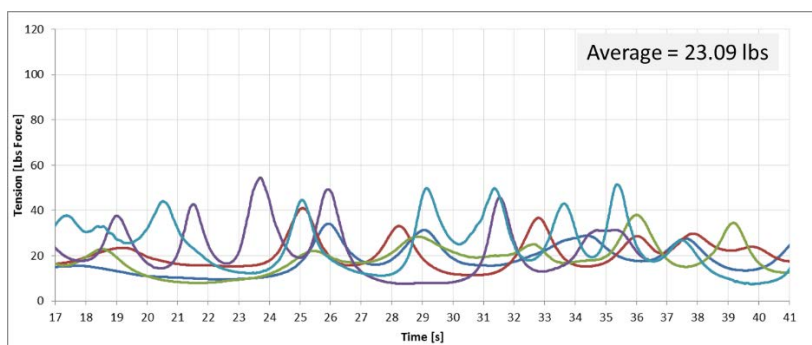


Figure V-19: Several Runs of a Simple Pull Test to Determine Low-Speed Road Force

Graphics: Argonne National Lab

Table V-1: Focus BEV Load Curve Summary

c	A	B	C
SS Force On-Road	21.90	0.33568	0.0200
Ave of all On-Road Coastdowns	34.37	0.31334	0.02278
From SS Force and OnRoad ABCs	26.37	0.21685	0.02217
Motor Drag	-8.20	-0.21761	0.0005
Coastdowns - Motor Drag	26.17	0.09573	0.02328

Conclusions

A common thread among all the DOE-sponsored work in the area of vehicle test standards is the notion that as new technology enters the market it must be properly and accurately evaluated so that it does not over-predict or under-predict performance. As experts in testing and in advanced vehicle technology, Argonne provides an important risk management function to all the DOE Vehicle Technology programs to ensure that advanced technology vehicles are integrated into the fleet with testing methods that properly and accurately quantify their merit.

J2908 Hybrid Net System Power Rating

Currently the "net power" of hybrid vehicles are being reported by manufactures in different ways. The challenge is to find a fair and appropriate method agnostic to any specific powertrain configuration or design. It should also make comparisons to other vehicles without unfair bias or confounding discontinuities. There are a number of key conclusions from the work in FY15 on the development of a standard way to test and describe the "Net System Power" for a hybrid vehicle:

- A significant testing program was conducted with both chassis and hub dynamometer systems that yielded a framework to conduct "Net System Power" testing for an array of vehicle technologies.
- A dyno-forced fixed-speed test is the most direct way to find the peak powertrain power, however because of gear shifting and other transients (e.g., engine speed-up) several alternative tests

approaches were created and developed that were used with success in many of the vehicles. The Argonne-developed "terminal velocity" test method provided some of the best data in relation to all the test options.

- After much analysis and discussion among task force members, three fundamental ways to collect and report "Net System Power" were defined. The committee is currently coming to a consensus on the most appropriate approach for SAE J2908.
- Depending upon which way the committee decides, the scope of J2908 could include defining "Net System power" for BEVs thus creating compatibility in the approach and reporting for all HEVs, PHEVs, and BEVs.
- There are currently three other international efforts actively working on the definition of system power (ISO, UN ECE, and Korean regulations). It is a significant effort to maintain coordination with the many committees and members.
- Some of the OEM-reported hybrid system power ratings are currently higher or lower than others only because the methods used vary from one OEM to another. There is no doubt that if OEMs adopted SAE J2908, then some of today's advertised power ratings would change. These changes would be a victory for the continued introduction of new HEVs, PHEVs and BEVs. By using a single, comparable, standard method, consumer understanding and acceptance will improve and reduce chances of consumer frustrations with new technology vehicles.

Road Load Investigations

Anecdotal anomalies and uncertainties in conventional road load determinations for HEVs with large electric motors have been circulating through the testing community ever since Argonne and OEM sponsors performed coastdown and dynamometer testing to evaluate the efficiency and emissions of university prototypes in the DOE/USCAR 1996-1999 FutureCar Challenge. It is not until recently that a specific effort was taken to address it (EPA engineering staff also looked into the issue this year but with only one vehicle and without axle torque sensors). Leveraging existing test vehicles from the DOE vehicle benchmarking program, some important insights was gained, they are summarized below:

- The viability of an alternative approach to defining road load, the steady-speed load test, was proven for a couple test vehicles. Further improvements can be made to the results with more tests and better controlled road and wind conditions.
- Comparisons of coastdowns and steady-speed loads yielded very comparable results for the vehicle with a disengaged neutral gear (Volt PHEV). A significant difference in testing outcomes were found between it and the other test vehicle with no mechanical neutral (Focus BEV). The additional load was verified to be the motor drag by conducting more experimental tests on the chassis dynamometer.
- The true test to determine if the traditional coastdown procedures provide the correct dynamometer settings for the Focus BEV, is to compare the axle loads as a function of speed on the road to the axle loads on the dynamometer. The two curves match up well for the Focus BEV. Because this fact, it can be concluded in the case of the Focus BEV that using traditional coastdown techniques does provide accurate settings to mimic true road load on the dynamometer. It would be prudent to investigate more vehicles using the same comparison technique.
- Sometimes road load coefficients are used to determine the required driving energy for a vehicle on specific cycles or for quantifying vehicle powertrain efficiency. Without accurately taking into account the additional drag cause by the motor, these calculations would be in error. This is a point only particularly relevant to those doing very specific energy consumption analysis work.
- It was found that the motor drag points form an irregular shape and do not conform to a 2nd order load curve like that used for road load definition. These irregularities could prevent a robust load curve fit when doing road load matching on the dynamometer. There were several occasions over the last few years during benchmark testing when the road load curve of an electric vehicle was not fitting well over all speed ranges satisfactorily. This should be a topic for further exploration.

- There are assumptions in current standards that each axle adds 1.5% of mass to the Newton's Law calculations for coastdown road load (refer to Figure V-10: Description of Forces during Tests to Determine Road Load (Force of drag). The Focus front axle inertia alone was tested to be 3.1%. However, the calculations were made with and without the correct axle inertia and found to cause only small changes, perhaps within the range of uncertainty expectations, thus any bias to this effect may not be as significant as once thought.
- A general trend was that low speed loads were less certain in coastdown testing. A direct pull method was developed to address this issue. Based upon our initial testing, this test method may be helpful by using it in conjunction with traditional coastdown data. The A-term value can be constrained by the direct pull results and a least squares fit could be made by solving for the other two coefficients with the coastdown load curves. This test method will be explored further and presented to important OEM and regulatory stakeholders for their feedback.
- A general conclusion based upon this study was that the steady-speed testing provided more robust data than traditional coastdown methods. A curve is better fitted with highly stable values of less speed points (steady-speed testing), than many speed points of less certain load results (coastdown testing). Coastdown loads are calculated by taking derivatives of speeds signals, there are always noise issues to consider when taking derivatives of collected digital signals.
- Cruise control was very helpful in collecting steady-state speed data. Driving for long distances on a road/track is recommended (at least 1.5 - 2 miles) if wind and road features are present. Shorter distances may be possible in better-controlled weather and road conditions

V.2.C. Products

Presentations/Publications/Patents

1. Numerous SAE Committee Meeting Presentations (roughly 20 in number during FY15)
2. "Observed Variations in Blended PHEV Operation - Advantaged and Limitations," Michael Duoba, 2015 Hybrid Symposium, San Diego, CA, Feb 2015.
3. SAE J2908 Update, presented to VSATT, Aug 5, 2015.

V.2.D. References

1. SAE J2263_200812: Road Load Measurement Using Onboard Anemometry and Coastdown Techniques, SAE International Standard, 2008.
2. SAE J1263_201003: Road Load Measurement and Dynamometer Simulation Using Coastdown Techniques, SAE International Standard, 2010.

V.3. SAE Standards Development Support

Rick Pratt, Principal Investigator

Pacific Northwest National Laboratory (PNNL)
 P.O. Box 999, M/S: K5-17
 Richland, WA 99354
 Phone: (509) 375-3820
 E-mail: rmpratt@pnl.gov

David Anderson, DOE Program Manager

Vehicle Systems
 Phone: (202) 287-5688
 E-mail: David.Anderson@ee.doe.gov

Start Date: October 1, 2014
 End Date: September 30, 2015

V.3.A. Abstract

Objectives

- PNNL will contribute to accelerating the development and harmonization of vehicle to grid communication standards by supporting the SAE technical working groups to develop use cases and technical requirements in the development of the following standards:
 - J2836/3 - Communication for Plug-in Vehicles as a Distributed Energy Resource
 - J2836/5 - Customer to vehicle communication.
- PNNL will evaluate the effects of V1G PEV / grid integration using simulation tools and develop an estimate of PEV owner value from PEV charging providing multiple grid services.

Accomplishments

- PNNL performed technical reviews and helped SAE committees in the development of the following standards:
 - J2836/3 - Communication for Plug-in Vehicles as a Distributed Energy Resource
 - J2836/5 - Customer to vehicle communication
- The J3072 - Interconnection Requirements for Onboard, Utility-Interactive Inverter Systems was published.
- PNNL evaluated the economics of using PEV & V1G charging as a grid resource, developed recommendations for additional investigation, and tested foundational capabilities needed to develop the PEV / Grid Integration Value proposition.
- Completed the Multi-Lab PEV Smart Grid Integration Requirements and Opportunities Study.

Future Achievements

- The PEV Smart Grid Integration Requirements and Opportunity Study that will identify high value use cases for V1G PEV / Grid Integration. The study results are scheduled for submission in October 2015.
- The V1G PEV / Grid Integration Communications Requirements document that includes support of participation in regulation services market, mitigation of TOU peak power and reduced duration of TOU peak power are scheduled for submission in November 2015.



V.3.B. Technical Discussion

Background

EV Standards Development provides the requirements and testing processes needed to enable interoperability between vehicles, charging stations and electric utilities. These standards are critical to the success of electric vehicle deployment. SAE, ISO and IEC are leading the US standards development to define the communication architectures, protocols and messages.

To expedite the standards development process DOE / EERE / VS has been funding national laboratories (PNNL, ANL, ORNL and INL) to provide technical support for the SAE, ANSI, and NIST standards development process.

FY 2015 SAE communications standards development began with a recognition that standards needed to be updated (e.g., J2847/2, J2836/3), several needed to be completed (e.g., J2836/5), and a gap analysis recognized that a new standard; J3072 - Interconnection Requirements for Onboard, Utility-Interactive Inverter Systems; was needed to enable OEMs to deliver vehicles with on-board inverters that meet utility requirements.

Introduction

In order to promote the widespread adoption of electric vehicles, interoperable charging infrastructure must be made available. While the majority of electric vehicle charging events currently take place at home using residential AC Level 1 or Level 2 charging equipment, the availability of public and commercial (such as workplace and retail) charging infrastructure may alleviate “range anxiety,” increasing driver confidence and the overall value of electric vehicles. Workplace charging can enable broader PEV adoption and contribute to meeting renewable energy consumption and greenhouse gas (GHG) emission reduction goals by extending the PEV travel range by providing a one-way travel charging alternative rather than waiting until returning home to recharge, providing alternative charging locations for customers with limited residential PEV charging capability, and enabling variable resource integration during work hours.

Approach

PNNL participates in the monthly SAE Hybrid standards committee meetings and actively contributed to the development and technical review of SAE EV/EVSE communication standards J2847/3, J3072 and J2836/5.

PNNL evaluated national and international research to identify the potential economic benefits of intelligent vehicle charging for the consumer and the utility. The research suggested that optimal PEV charging control must be capable of adapting to temporal and regional markets. The regional market differences include the value of regulation services (higher on the East Coast), demand charges, and the cost of electricity (which also depends on participation in TOU programs). The foundational capabilities needed to develop a realistic PEV / Grid Integration Value proposition were tested.

Results

PNNL participated in the SAE Hybrid committees to develop the J2836/5 standard, provide technical support to update the J2836/3 standard, and perform technical reviews of the J3072 standard. Several new use cases including sub-metering and vehicle telematics have been developed for inclusion in the SAE J2836/5.

In addition to the standard support, PNNL performed analyses to identify the potential grid impact and value of Intelligent Charging and performed distribution feeder analyses to evaluate the effect of growing PEV adoption including:

- The effects of increased PEV adoption on the prototypical distribution system analyzed are directly related to individual PEV charging rate as well as the number of vehicles charging. In 2013, the Level 2 Nissan Leaf charging rate was increased from 3.3kW to 6.6kW. The 6.6kW chargers have twice the peak power of the 3.3kW chargers as simulated by the 3.3kW charger (black line) and the 6.6kW charger (red line).
- Increased battery capacity has the positive effects of extending vehicle travel range and reducing range anxiety. But, larger batteries take longer to charge and typically have higher charging rates. This increases the distribution feeder loading effects as shown by the 6.6kW/160-mile range line.

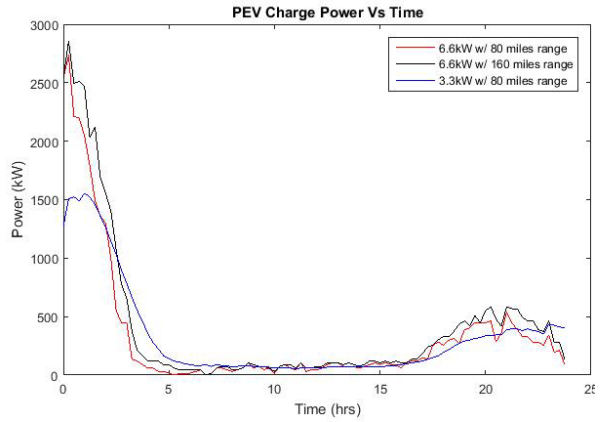


Figure V-20: PEV Charging Power vs. Time

- Plotting the temporal San Francisco EV Project PEV charging power data with the hourly time of use rates revealed that only 68% of the PEV charging energy was delivered during the lowest Time-Of-Use (TOU) periods. The inflections in the charging data at 9PM and 11PM show that some customers were intentionally starting charging at exact times of rate changes. This raises the question of why is over 30% of the charging energy being dispersed at the higher TOU rates.

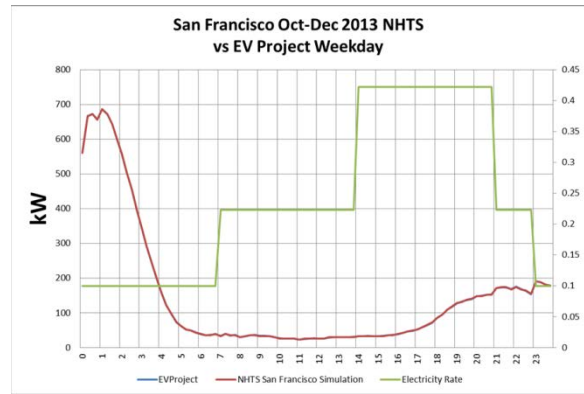


Figure V-21: San Francisco NHTS versus EV Project - Weekday

- GridLAB-D (distribution system simulator) simulations were run using 4th quarter 2013 San Francisco EV Project data scaled from the measured population of 1132 vehicles down to a population of 500 vehicles to evaluate the effects of a growing population of PEVs on a prototypical distribution feeder with 1000 residences (typical feeder has between 800-1200 residences). Sequential simulations increased the PEV population by 500 until the substation transformer limit (5.3MVA) was exceeded. It took a population of ~1750 3.3kW PEVs charging at 1000 residences to exceed the substation transformer limit. This equates to ~1.75PEVs per residence. Subsequent simulations showed that ~0.85 PEVs/home is needed to exceed the substation limits with 6.6kW chargers. Increasing battery range from 80-miles to 160-miles further reduces the PEVs/home to ~0.7 before the substation limit is exceeded.

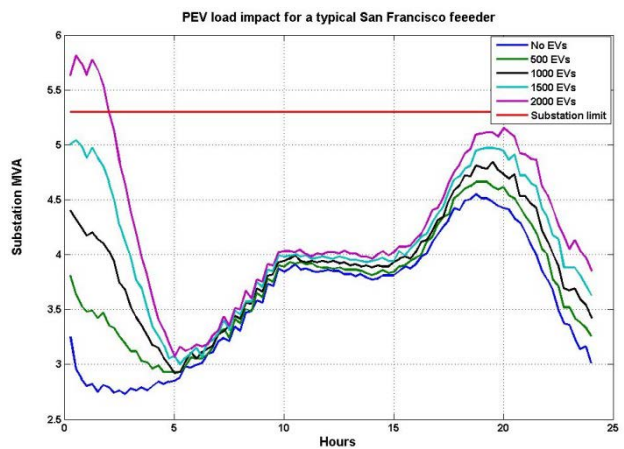


Figure V-22: 3.3kW PEV impact on typical San Francisco distribution feeder

The analysis concluded:

- Increasing PEV charging power reduces the time needed to fulfill existing PEV energy requirements and opens the opportunity to use multiple low-rate TOU periods to spread the large peak demand at about 1AM. This requires no additional PEV communication requirements and will help to delay exceeding the substation transformer limits.
- Increasing the PEV battery range or offering workplace charging offers a greater population to potentially adopt PEVs. Longer PEV ranges are expected to be accompanied by higher PEV charging rates which are just as effective in causing substation power limits to be exceeded as a larger PEV population. Workplace charging is typically during times of highest PV generation which better enables renewables to be used for transportation.

Conclusions

The PEV charging impact on distribution feeders was analyzed at the substation transformer level and found to not only be a function of the total number of vehicles charging, but also directly to the PEV charging rate. The effect on the substation transformer is identical if the charging rate is increased from 3.3kW to 6.6kW or the number of electric vehicles charging is doubled.

An analysis of EV Project temporal charging data showed that TOU rates help shift PEV charging loads to times of lower total power consumption, but there remains a significant amount of charging that occurs during periods of higher TOU rates. Possible contributors to this charging behavior include: range anxiety, PEV owner travel requirements, net metering with residential rooftop solar or customer preference.

V.3.C. Products

Presentations/Publications/Patents

1. Markel, T, A. Meintz, K. Hardy, B. Chen, T. Bohn, J. Smart, D. Scoffield, R. Hovsopian, S. Saxena, J. MacDonald, S. Kiliccote, K. Kahl, and R. Pratt. "Multi-Lab EV Smart Grid Integration Requirements Study, Providing Guidance on Technology Development and Demonstration", Technical Report. May 2015. NREL/TP-5400-63963.
2. Pratt RM, YP Agalgaonkar, D Wu, and NE Stanton. 2015. "PEV / Grid Integration Study." Presented by Rick Pratt at Vehicle Technologies Annual Merit Review, Washington, DC, DC on June 9, 2015. PNNL-SA-109462.
3. Pratt RM. 2015. "PEV / VOLTTRON Integration." Presented by Rick Pratt (Invited Speaker) at Technical Meeting on the Software Framework for Transactive Energy, Arlington, VA on July 24, 2015. PNNL-SA-111792.

V.4. Codes and Standards and Technical Team Activities

James Francfort, Principal Investigator

Idaho National Laboratory
 P.O. Box 1625
 Idaho Falls, ID 83415-2209
 Phone: (208) 526-6787
 Email: James.francfort@inl.gov

Lee Slezak, DOE Program Manager

Phone: (208) 586-2335
 Email: Lee.slezak@ee.doe.gov

Start Date: October 2013

End Date: Ongoing

V.4.A. Abstract

Objectives

- To contribute vehicle, component, fueling, and charging infrastructure testing knowledge gained by Idaho National Laboratory (INL) staff from onroad and laboratory evaluations to industry and government groups developing and modifying standards, codes, best practices, and regulations.

Accomplishments

- Recognition as an industry expert and a voting member of these industry and government committees is a major accomplishment in itself
- The current committees/organizations that INL staff contribute to include the following:
 - Society of Automotive Engineers (SAE) J2954 Wireless Charging Task Force
 - SAE J2894 Power Quality Requirements for Plug-in Electric Vehicle Chargers
 - National Institute of Standards and Technology's U.S. National Work Group on Measuring Systems for Electric Vehicle Fueling and Sub-Metering
 - U.S. Drive: Vehicle Systems Analysis Tech Team
 - U.S. Drive: Grid Integration Tech Team
 - Electric Power Research Institute – National Electric Transportation Infrastructure Working Council.

Future Achievements

- Continue future participation on various committees and panels, representing U.S. Department of Energy (DOE) interests and providing expertise and testing results from testing of cutting-edge advanced vehicle technologies.
- Continue providing high-fidelity performance testing, analyses, procedure development, methodology validation, reporting and other support related to the various codes and standards committees INL is part of, as well as the DOE US DRIVE Grid Interaction Technical Team, the EPRI-sponsored Infrastructure Working Group, and other C&S committees, as directed by DOE.



V.4.B. Technical Discussion

Background

DOE's Advanced Vehicle Testing Activity (AVTA) is part of DOE's Vehicle Technologies Office, which is within DOE's Office of Energy Efficiency and Renewable Energy. AVTA is the only DOE activity tasked by DOE to conduct field evaluations of fueling infrastructure and light-duty vehicle technologies that use advanced technology systems and subsystems in light-duty vehicles to reduce petroleum consumption. A secondary benefit is reduction of exhaust emissions.

Most of the advanced technology vehicles, subsystems, and fueling infrastructure that AVTA tests include the use of electric drive propulsion systems and advanced energy storage systems. However, other vehicle technologies that employ advanced designs, control systems, or other technologies with production potential and significant petroleum reduction potential are also considered viable candidates for testing by AVTA. AVTA and INL's first priority is providing DOE feedback on the performance of advanced technologies that DOE has made funding investments in.

AVTA's light-duty activities are conducted by INL for DOE. INL has responsibility for AVTA's execution, direction, management, and reporting. INL is supported in this role by various subcontracts for specific tasks when greater value can be achieved for DOE if INL conducts research in partnerships with other organizations.

The AVTA sections of the Fiscal Year 2015 Annual Program Report jointly cover testing work performed by INL and any subcontractor conducting work that INL manages. When appropriate, AVTA partnered with other governmental, public, and private sector organizations to provide maximum testing and economic value to DOE and the United States' taxpayers via various cost-sharing agreements.

Introduction

DOE's AVTA evaluates grid-connected plug-in electric vehicle (PEV) technology in order to understand the capability of electric grid-recharged electric propulsion technology to significantly reduce petroleum consumption when vehicles are used for transportation. In addition, many companies and groups are proposing, planning, and starting to introduce PEVs into their fleets.

Knowledge gained from 20 years of testing electric drive, other vehicle technologies, and fueling infrastructure for more than 232 million miles, is used by INL staff to contribute to various industry and government groups that are primarily interested in developing policies, standards, codes, and regulations that ensure safety and interoperability within technology sectors.

Approach

As a member of a technical committee or industry group, participation is intended to contribute to the common body of knowledge being applied to develop standards and other industry practices. Participation is also intended to represent DOE interests.

Results

SAE International

SAE J2954 Wireless Charging Task Force:

INL supports the SAE J2954 committee as a full voting member by providing detailed test results from wireless charging systems and providing detailed test setup information and text that are incorporated into the standard document. Testing involves both bench testing and vehicle testing. Results from both forms of testing detail the system efficiency and electromagnetic field strength across a wide range of coil misalignment, coil gap, and charge power. More information on these test results can be found in the Vehicle Systems Efficiency Improvements section of this report.

Information from both the bench and vehicle testing directly fed into the test setup development for the document. Test setup specifications (such as coil alignment apparatus specifications, means of varying the coil gap for testing, and common test setup components for both the bench and vehicle testing) have been incorporated into the document. Figure V-23 and Figure V-24 show representative graphics of the bench test setup and vehicle test setup.

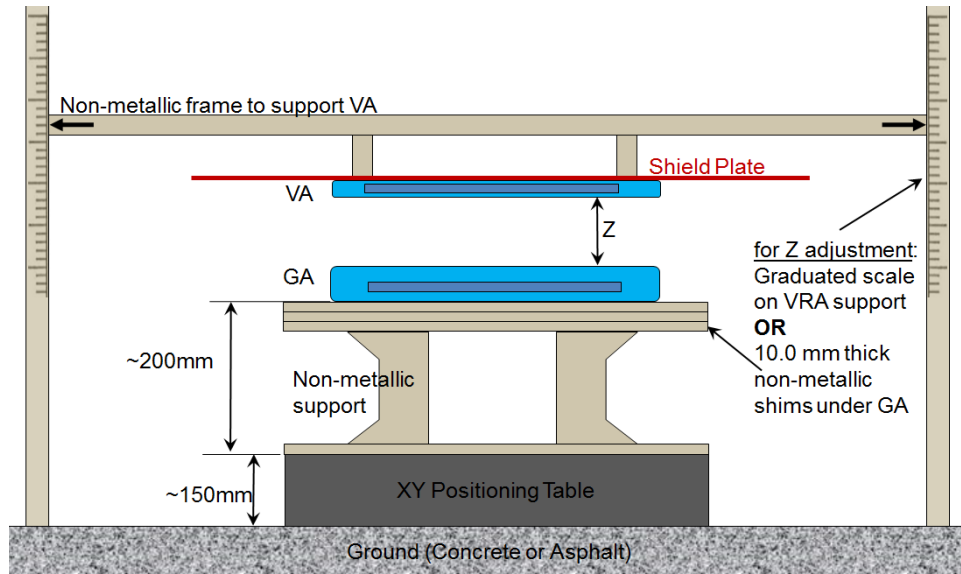


Figure V-23: Bench test setup for wireless charging for SAE J2954.

INL/SAE J2954

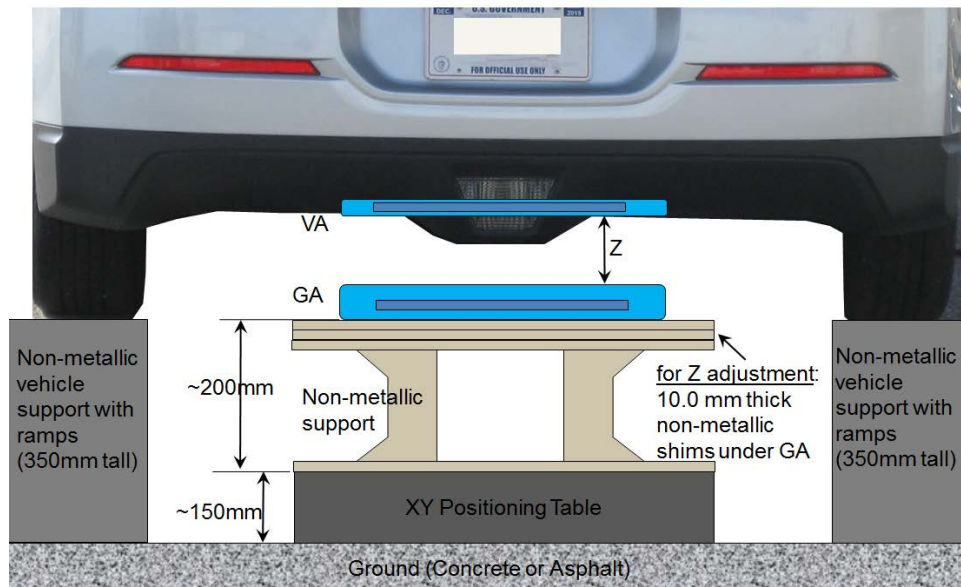


Figure V-24: Vehicle test setup for wireless charging for SAE J2954.

INL/SAE J2954

The bench test setup is used to evaluate wireless charging systems without vehicle specific interaction. This is useful when comparing charger technologies because no vehicle interaction occurs with the electromagnetic field. The bench setup is likely to be used during the early stages of system development. In contrast, vehicle testing includes wireless charging system interaction with the vehicle, which is the most representative of real-world operation. Vehicle testing will likely be the final measure of system performance when installed in a specific vehicle model. Both test setups minimize the use of metallic and conductive devices in order to minimize electromagnetic field impact and interaction.

These two setups contain a significant amount of shared components, specifically the XY positioning table and non-metallic support for the ground assembly (GA). The XY positioning table accurately and repeatably locates the GA under the vehicle assembly, which enables evaluation of the X and Y misalignment impact on system performance without the need to reposition the vehicle during testing. The non-metallic support for the GA, positions the GA for accurate and repeatable coil gap. The non-metallic support is comprised of a fixed height base and several 10-mm spacers that enable accurate and repeatable change in Z height. This enables evaluation of the impact of coil gap on system performance. The benefit of having common components between the two setups is reduced time to change from one setup to the other and reduced cost due to reuse of components for both setups.

The vehicle test setup elevates the vehicle through use of vehicle supports and ramps over the GA, support, and positioning device. The vehicle support is the same height as the GA support and positioning device, such that the nominal test condition coil gap is equivalent to the GA sitting on top of the floor (i.e., vehicle and GA sitting on same surface height).

The bench test setup uses a non-metallic frame to suspend the vehicle assembly and vehicle mimic shield plate over the GA, support, and positioning device. This frame is adjustable in height and tilt to allow for more test flexibility. Ultimately, the frame is merely intended to mimic the vehicle; therefore, generating the need for a vehicle mimic shield plate.

INL evaluated the impact of the height of the GA support with respect to electromagnetic field interaction with the XY positioning table, because it is composed of aluminum and steel, which will interact with and alter the electromagnetic field. The evaluated support height ranged from 50 to 500 mm. The lowest support height (i.e., 50 mm) showed significant electromagnetic field interaction with the XY positioning table, whereas minimal interaction was measured with support heights greater than 150 mm. Because the GA support and the vehicle support/ramps need to be of equal height, a GA support height of 200 mm is chosen. A GA support height of 200 mm is commercially available; non-metallic vehicle supports and ramps are also available at this height requirement.

SAE J2894 Power Quality Requirements for Plug-In Electric Vehicle Chargers:

The SAE J2894 committee is developing requirements and test procedures to ensure PEV chargers do not cause power quality issues and PEVs can continue to function properly in the presence of power quality issues caused by adjacent loads.

Testing done at INL has informed many decisions made by the SAE J2894 subcommittee. For the past year, the J2894 subcommittee has been working on updating the recommended practices found in J2894/1. In this process, efficiency testing done at INL has helped the subcommittee determine if the limits for minimum full power conversion efficiency in the recommended practice are still applicable for modern PEVs. Likewise, power quality testing done at INL has helped the subcommittee determine if the limits for maximum allowed total harmonic distortion in the recommended practice were still applicable for modern PEVs. For the J2894 committee, INL input and testing results are considered a valuable resource of expertise and hands-on experience for the committee.

Figure V-25, Figure V-26, and Figure V-27 show key insights from testing the following PEVs: 2012 Chevy Volt, 2012 Nissan Leaf, 2015 Nissan Leaf, and 2014 BMW i3. Figure V-25 shows charging efficiency of the onboard charger vs. alternating current drawn by the PEV. Figure V-26 shows the power factor of the onboard charger vs. alternating current drawn by the PEV. Figure V-27 provides the total harmonic distortion of the onboard charger vs. alternating current drawn by the PEV. Some general trends seen across all PEVs are that PEV charging is most efficient and has the best power quality when charged at the maximum charge rate. Also, for some PEVs, the efficiency and power quality rapidly deteriorate as the charge rate is reduced, while for other vehicles, this is not the case. There is a lot of variation in the efficiency and power quality characteristics between the various brands and model years of PEVs that were tested. This underscores the importance of continued testing of PEVs to understand evolution through time.

U.S. Environmental Protection Agency Energy Star

Electric Vehicle Supply Equipment Test Method Development in Collaboration with Energy Star:

The U.S. Environmental Protection Agency will be introducing Energy Star ratings for Level 1 and Level 2 electric vehicle supply equipment (EVSE) standby power consumption and power loss during charging. INL is collaborating with the U.S. Environmental Protection Agency and other national laboratories (i.e., Argonne National Laboratory, and Lawrence Berkeley National Laboratory) to develop a test method document that details the requirements of the test method, including measurement equipment and detailed test procedures. INL drafted the measurement equipment requirements, including input and output measurement connection modules that are necessary to safely and effectively measure the input and output current and voltage, and the control pilot signal. The specified connection modules alleviate the need to modify the EVSE input and output cord sets. Additionally, a controllable load bank is required to draw power through the EVSE at specified current rates. INL also developed and drafted test procedures for evaluation of EVSE for standby power consumption and power loss during charging. Standby power consumption is consumption by the EVSE while not providing current to the vehicle. This is measured during each operation state per SAE J1772 definition (State A, B, C, and D), which is important because EVSE may operate in one or more of the modes for a significant amount of time. Standby power consumption is often a result of various EVSE functions drawing power such as status lights, touch screen display, a control module, or a smart grid communication module. The measurement of power loss during charging is also detailed in the document. Current is drawn through the EVSE in the same manner as a vehicle charging and at prescribed current levels that are representative of the typical charge levels of production PEVs (i.e., 1.1 kW, 3.3 kW, 6.6 kW, and 10 kW). Input and output power are accurately measured during the steady-state current draw; differences between the two measurements are EVSE power losses during charging. These losses are often due to resistive losses of wire, contacts, and other connections, as well as standby loads that are still present during charging.

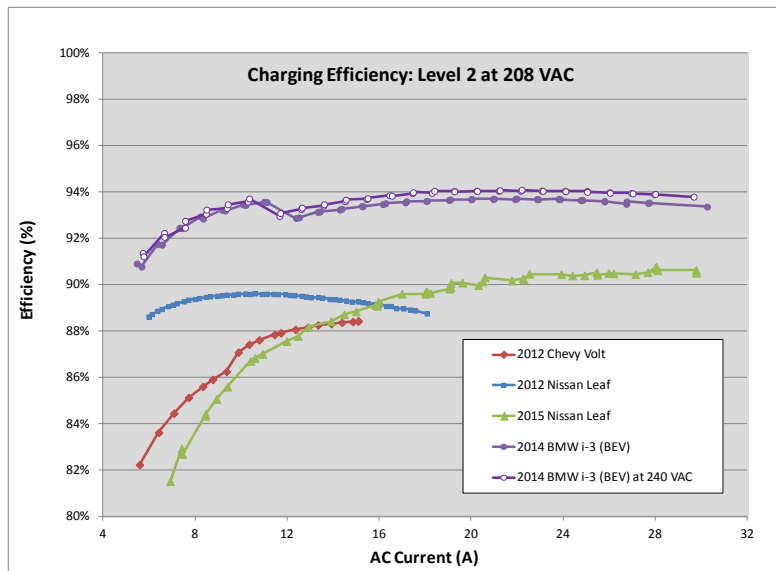


Figure V-25: Charging efficiency of onboard charger vs. alternating current (A) for several production PEVs.

INL/SAE J2894

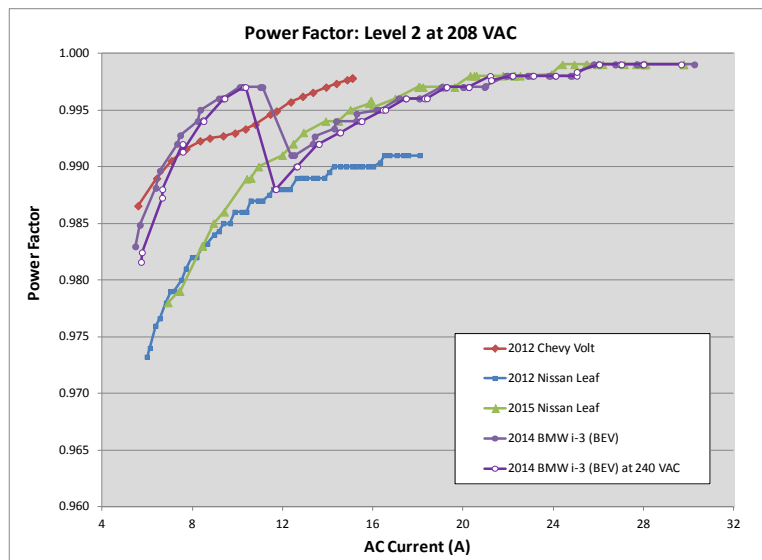


Figure V-26: Power factor of onboard charger vs. alternating current (A) for several production PEVs. INL/SAE J2894

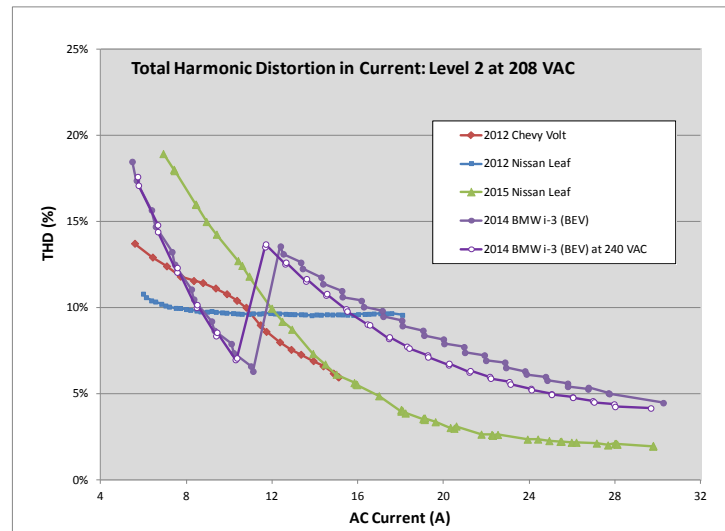


Figure V-27: Total harmonic distortion in current of onboard charger vs. alternating current (A) for several production PEVs. INL/SAE J2894

In support of developing the test method draft document, INL tested numerous EVSE to validate the test procedures and evaluate alternative measurement methods. Numerous production EVSE were tested using the draft test procedure and the required equipment. The results were analyzed to identify any outlying results or anomalies due to test procedure inconsistencies. No issues were found. Additionally, INL presented at the Energy Star webinar to discuss and receive public comments on the draft test method document. The webinar included a proposed alternative method for measuring EVSE loss by a differential measurement technique. After the webinar, INL conducted testing on the same EVSE, but used the proposed differential measurement technique. The results were analyzed and compared with the Energy Star test procedure results. A comparison of the two techniques was conducted for review by the Energy Star engineering and management staff.

National Institute of Standards and Technology

U.S. National Work Group on Measuring Systems for Electric Vehicle Fueling and Sub-Metering:

The National Institute of Standards and Technology committee is developing a draft standard of rules and regulations that EVSE must adhere to if the EVSE sells power or is the point of metering. INL staff

participation in this meeting is important because, in the future, EVSE will need to be tested to ensure they meet the National Institute of Standards and Technology requirements. By participating in this standard development, INL staff engineers are helping to direct future requirements development for EVSE testing needs, methods, and procedures that will be required to support a code at a national level of acceptance. Future INL activities will be focused on aiding in development of the necessary supporting operational and testing procedures for the device code.

U.S. Drive (United States Driving Research and Innovation for Vehicle Efficiency and Energy Sustainability)

Vehicle Systems Analysis Tech Team:

INL is a long-time member of the Vehicle Systems Analysis Tech Team due to INL's history of testing performed for DOE. INL staff contributes, via presentations and papers, the results of benchmarking the advanced automotive powertrain components and subsystems from INL's whole vehicle system and component testing. This testing includes fuel use, efficiencies, auxiliary loads, and energy storage results that are subsequently used by other team members as modeling inputs.

Grid Integration Tech Team:

Because of the nature of the infrastructure testing INL performs for DOE, INL is a founding member of the Grid Integration Tech Team. This includes wireless power transfer and conductive charging, which includes direct current fast charging, and INL's data collection, analysis, and reporting on how 8,000 PEV drivers utilize 17,000 Level 2 EVSE and direct current fast chargers.

Electric Power Research Institute – National Electric Transportation Infrastructure Working Council

Infrastructure Working Council:

INL is a 20-year member of the Infrastructure Working Council, which is sponsored by the Electric Power Research Institute and is a group of individuals whose organizations have a vested interest in the emergence and growth of the electric vehicle, plug-in, and hybrid electric vehicle industries, as well as electrification of truck stops, ports, and other transportation and logistics systems. Infrastructure Working Council members include representatives from electric utilities, vehicle manufacturing industries, component manufacturers, government agencies, related industry associations, and standards organizations. The various committees meet several times a year to address electric vehicles, plug-in hybrid electric vehicles, truck stop and port electrification, and infrastructure research and development. INL supports the Plug-in Hybrid and Electric Vehicle Working Group, the Transportation Electrification Committee, and serving on the Infrastructure Steering Committee. Results from INL's testing of vehicles and infrastructure and from data collection with data loggers from 24,000 vehicles and charging infrastructure units is of great interest and support to the Infrastructure Working Council's decision processes.

Conclusions

The intent of this work was to leverage benchmark testing results and staff knowledge gained as a resource for various industry groups that are putting into place industry-lead or government-lead codes, standards, requirements, or best practices.

V.4.C. Products

Presentations/Publications/Patents

1. The intent of this work is not to publish results as products of INL, because the outcomes are usually the sole intellectual rights of other organizations such as SAE.
2. The work described in this section will not result in INL patents. The intent of this work is to provide technical support to DOE and industry in the development of standards.

V.5. PEV-Grid Connectivity

Keith Hardy, Director, EV-Smart Grid Interoperability Center, Principal Investigator

Argonne National Laboratory

6900 S. Cass Avenue

Argonne, IL 60439

Phone: (630) 816-7383 (mobile); (630) 252-3088 (ANL); (202) 488-2431 (DC); Fax: (202) 488-2413

E-mail: khardy@anl.gov

Lee Slezak, DOE Program Manager

DOE Vehicle Technologies Office

Phone: (202) 586-2335

E-mail: Lee.Slezak@ee.doe.gov

Start Date: 10/01/2015

End Date: 9/30/2018

V.5.A. Abstract

Objectives

The primary objectives of this project are development of technology and standards for vehicle-grid connectivity, communication and interoperability (i.e., grid integration) and facilitation of global harmonization of interoperability requirements/standards. The project includes direct support of codes & standards development committees, development of enabling technologies for vehicle-grid integration and facilitation of global cooperation on vehicle interoperability with the charging infrastructure.

Developing technology and standards for interoperability is essential to widespread adoption of plug-in electric vehicles (PEVs) and achieving the goals of sustainable transportation and smart grid integration. Key elements of the codes & standards activities and specific topics are listed below:

- Codes & Standards
 - SAE committees related to charging, communication and grid integration; NIST Handbook 44 sub-committee on metering electric fuel delivery; related ISO/IEC/DIN and IEEE committees.
- Technology Development and Standards Verification
 - Workplace charging (devices for integrated metering, communication and control)
 - Wireless charging (automated magnetic interoperability testing)
- Metering Technology Development and Implementation
 - End-Use Measurement Device (EUMD) and current sensor application engineering
 - NIST HB44 electric fuel metering (AC Level 2 EVSE)
- Harmonization, International Cooperation and Grid Modernization
 - Multi-Lab EV-Smart Grid Integration Requirements Study
 - Cooperative activities in Europe; European Commission's Joint Research Centre - Institute for Energy & Transport (JRC-IET), Global InterOP and German Ministry
 - Cooperative activities in China and APEC
 - Grid Modernization Lab Consortium (GMLC) FY 2016 planning/proposal process

Accomplishments

- Codes and Standards
 - Chaired SAE J2953 (interoperability) committee
 - Led NIST Handbook 44 sub-committee on methodology to measure electric fuel delivery
 - Actively contributed to SAE committees; SAE J1772 (PEV charging coupler), SAE J2984 (PEV charging power quality), SAE J3068 (heavy duty 480vac coupler), SAE J2847/2 (PEV off-board

- DC communication), SAE J2847/6 (J2931/6) (wireless charging communication), SAE J2931/7 (cybersecurity of PEV-EVSE-network), SAE J3072-J2836/3-J2847/3 (utility interactive PEV requirements), SAE J2954; UL2750;
- Actively contributed to ANSI C63.30 (wireless charging safety-interoperability) and EPA EnergySTAR framework requirements for EVSE
 - Coordinated with ISO/IEC/DIN standards committees on AC, DC and wireless charging communication
 - Liaised with IEEE committees (representing J2953 interoperability committee); P2030.7/P2030.8 (micro-grid controller definition/tests), IEEE P2030.5 (Smart Energy Profile, SEP, communication), IEEE 1547.4 (utility interactive inverter requirements) and IEEE P2413 (framework for Internet of Things)
- Technology Development and Standards Verification
 - Coordinated and hosted Interoperability 'Festival'; a round robin DC charging event supported by automotive OEMs, EVSE manufacturers and test equipment suppliers from eight countries
 - Installed and networked EVSE, building systems and solar array in the Smart Energy Plaza
 - Developed and demonstrated a Common Integration Platform (CIP), a universal electronic module with embedded open source software to connect EVSE and other devices to the grid
 - Demonstrated integrated metering, communication and charge control of EVSE using 'Internet of Things' (IoT) approach in the Smart Energy Plaza
 - Developed prototype design and demonstrated proof-of-concept Sub-metering/Load Control Adaptor (SLCA) to enable communication with and control of legacy EVSE
 - Designed and fabricated EVSE modules using off-the-shelf technology to establish a low-cost reference for multiple EVSE with individual sub-metering, communication and control
 - Metering Technology Development and Implementation
 - Continued development and evaluation of EUMDs based on a low-cost, single Programmable System-on-Chip (PSoC) and current sensor options
 - Continued sensor application engineering; compared performance of PC Board micro shunt to Rogowski/integrator coreless sensor and proof-of-concept stand-alone DFGM current sensor
 - Developed, tested and commissioned a NIST Handbook 44 capable electric fuel compliance/benchmark comparison metering system
 - Harmonization, International Cooperation and Grid Modernization
 - Contributed to the Multi-Lab EV Smart Grid Integration Requirements Study
 - Authored "Enabling PEV-to-Grid Integration" chapter; focused on standards and enabling technologies
 - Identified the key factors to enable PEV to grid integration
 - Performed a comprehensive literature research to identify the issues/barriers of VGI in the areas of interface technology, communication, controls, and standardization
 - Provided recommendations for future R&D to enable PEV to grid integration
 - Published a conference paper presented at 2015 IEEE Transportation Electrification Conference & Expo (ITEC'15)
 - Supported cooperative activities in Europe
 - Contributed to reports and briefed USG representatives in Brussels, Berlin and Washington regarding collaboration with JRC-IET, Global InterOP and Germany
 - Participated in/presented at several US-EU and US-Germany technical coordination events
 - Published joint conference paper with JRC-IET, BMW and Ford Europe at the 2014 European Electric Vehicle Congress
 - Worked with JRC-IET to develop technical annexes to the DOE-JRC Scientific and Technology Agreement between JRC and ANL; to authorize joint activities at JRC-IET and ANL on E-vehicle testing/interoperability and smart grid interoperability
 - Completed the instrumentation of the BMW i3 reference vehicle for comparative testing at Argonne and JRC-IET in FY 2016
 - Cooperative activities in China and APEC economies

- Developed proposal to MIIT to establish cooperative interoperability center in China; participated in meetings in Beijing and Washington
- Contributed to the US proposal for an APEC EV Roadmap; presented the proposal and overview of the interoperability centers at the 2015 APEC meeting in Manila
- Supported DOE Grid Modernization Initiative/Lab Consortium
 - Participated in the multi-lab, multi-year plan for Devices and Integrated Systems Testing (DIST); contributed to scope and objectives from vehicle-grid integration perspective.
 - Contributed to four GMLC Foundational Proposals (Interoperability, GMLC Testing Network, Standards and Test Procedures for Interconnection and Interoperability, Definitions, Standards and Test Procedures for Grid Services from Devices) and two Program-Specific proposals to the Vehicle Technologies Office (Vehicle-to-Building Integration Pathway, Research Supporting Standards and Interoperability) and one specific to the Building Technologies Office

Future Achievements

- Codes and Standards
 - Continue leadership of SAE J2953 (interoperability) committee; shift focus to DC and wireless charging; continue active participation in SAE committees related to charging and communication; continue liaison to related IEC/ISO, DIN, IEEE, ANSI committee activities
 - Continue support of NIST Weights & Measures HB44 effort to define methodology to measure electric fuel delivery by DC EVSE; collaborate with the California Department of Food and Agriculture regarding type approval of HB44 compliant EVSE/charging network transaction recording and displaying equipment
- Technology Development and Standards Verification
 - Integrate and demonstrate the Common Integration Platform (and IoT software) with the controllable devices in the Smart Energy Plaza, i.e., EVSE, building systems and solar inverter
 - Demonstrate prototype Sub-metering/Load Control Adaptor (SLCA) with multiple legacy EVSE in the Smart Energy Plaza
- Metering Technology Development and Implementation
 - Integrate and demonstrate low-cost EUMDs (i.e., PSoC, DFGM current sensor and commercial packaging) in the ANL IOC test facilities and with an industry partner
 - Develop a NIST Handbook 44 capable electric fuel compliance/benchmark comparison metering system for DC charging.
- Harmonization, International Cooperation and Grid Modernization
 - Address recommendations from Multi-Lab EV Smart Grid Integration Requirements Study in the testing infrastructure, including communication and control/power HIL connected to the workplace charging testing environment.
 - Complete Level 2 testing at Argonne and joint testing of the BMW i3 reference vehicle in the JRC-IET test facility; compare and document differences in test procedures and methods to analyze/report data.
 - Develop a joint work plan with JRC-IET for FY 2016-18 activities
 - Continue support of USG cooperative/diplomatic efforts in Europe and Asia
 - Develop FY 2016-18 work plan for the ANL-IOC that integrates/incorporates the tasks proposed in response to DOE VTO and GMLC lab calls



V.5.B. Technical Discussion

Background

US and European interoperability centers were established in an agreement between the US Department of Energy (DOE) and the European Commission's Joint Research Centre (JRC), signed in November 2011, with the intent of harmonizing EV and battery test procedures as well as EV interoperability. The agreement stipulated the activities listed below; much progress has been made since then and the accomplishments/status of the ANL IOC prior to FY 2015 with respect to each activity is shown in parentheses:

- Establish state-of-the-art facilities for development and testing of EV-grid interface technologies (Embedded controls lab and PEV-EVSE integration/test lab were fully operational; plans to add control HIL, building systems and solar power to support grid integration are complete)
- Play an active role in standardization (ANL IOC staff actively contributed to SAE committees related to charging/communication for several years and had recently assumed responsibility for the NIST Handbook 44 sub-committee on measuring electric fuel delivery)
- Undertake projects to enhance interoperability (ANL IOC staff had developed compact sub-meters, communication control modules and test tools to verify compliance with SAE PEV charge connector and AC charging interoperability standards ... all requisite technologies to development/implement PEV-EVSE interoperability)
- Participate in inter-laboratory 'round-robin' testing (Plans were in place to acquire and instrument a reference vehicle for testing in the ANL and JRC-IET test facilities; planning was underway for the international DC charging 'Festival')

The details of these and other technical accomplishments of the ANL IOC have been reported in the DOE VTO Annual Merit Reviews, annual reports, several conference publications and numerous presentations.

Programmatically, the launch of cooperative projects between the ANL and JRC IOCs awaited the completion of JRC-IET vehicle test facilities in Ispra, Italy (aka JRC Ispra). Efforts to establish cooperative activities with China had not yielded results and the possibility of cooperation with the APEC economies had been proposed.

At the diplomatic level, a more streamlined process for establishing collaborative agreements between US and EU labs was being developed; based on an umbrella Science and Technology Agreement that would define the areas of cooperation, as well as common terms and conditions, projects would be authorized with technical annexes that were mutually agreed upon by the labs.

Introduction

'EV-smart grid interoperability' is the ability of any PEV and EVSE to connect and communicate with the infrastructure in a standard manner to enable 'smart' charging (or discharging as the case may be) as an integral element of a managed network of grid-connected devices.

Realizing widespread interoperability necessitates harmonized connectivity and communication standards across industries and international borders as well as enabling technologies. The ANL IOC addresses these issues from a communication/control perspective; supporting the development and verification of codes & standards, developing communication control modules/platforms, facilitating harmonization with Europe and Asia, and providing the vehicle perspective in DOE's grid integration/modernization initiative.

This report summarizes ANL IOC activities and accomplishments in FY 2015, as well as proposed future activities, related to codes & standards; technology development and standards verification; metrology; harmonization/international cooperation; and grid modernization.

Approach

Codes and Standards Development

The DOE/ANL interoperability center was established to facilitate harmonization of technology and standards for connectivity and communication between plug-in vehicles, the charging infrastructure and the future grid with ‘smart’ control capabilities. The integration required to achieve smart energy management throughout the grid necessitates involvement with several standards definition organizations (SDOs) that span the vehicle, building and the electric power supply infrastructure domains. Figure V-28 summarizes the SDOs and standards that must be addressed to harmonize physical connectivity, communication and information exchange (Ref. 1).

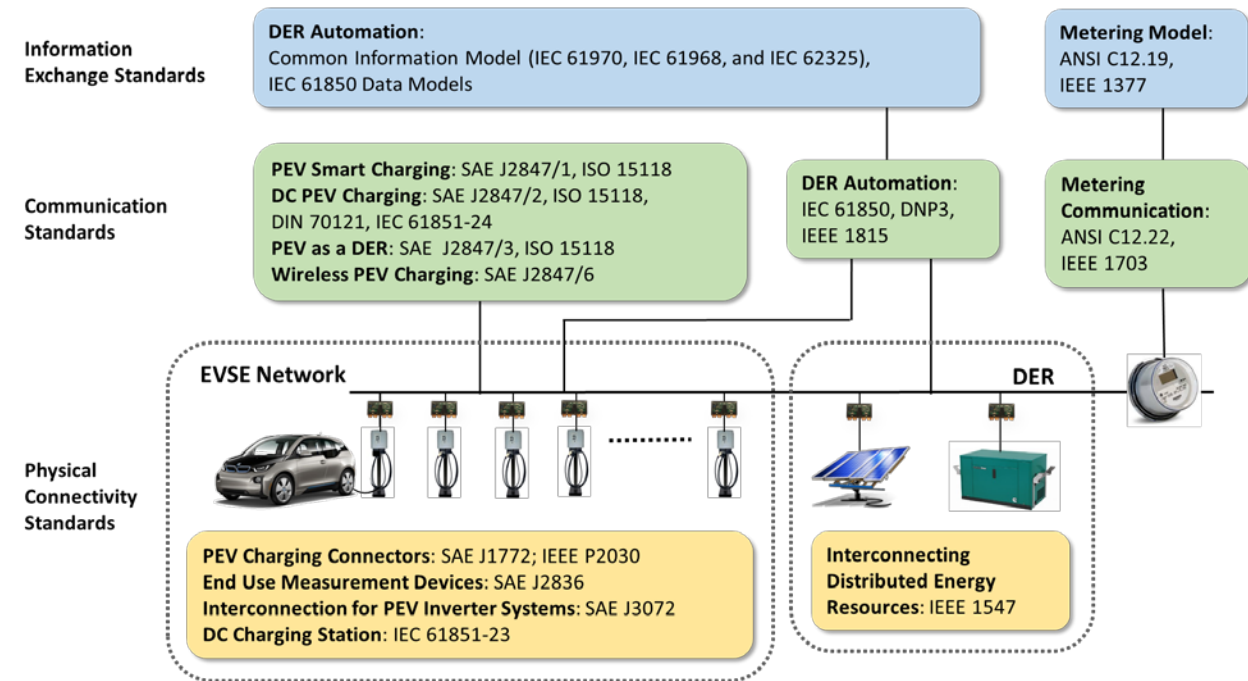


Figure V-28: Standards Definition Organizations and Standards Related to PEV-Grid Integration

Source: ANL

Generally SAE and ISO focus on vehicles/charging standards while IEEE, IEC and ANSI address electric infrastructure and building systems - anything that connects to the grid. Others are involved regarding the infrastructure (e.g., NFPA and NEC), but the SDOs in the figure are directly involved with communication.

Argonne subject matter experts either lead, provide direct support or monitor committee activities of the SAE, NIST, IEEE and ISO/IEC/DIN - those that define standards for interfaces between PEVs and EVSE; connectivity to charging networks, building systems and electricity distribution; metering and electric fuel delivery. Roles vary depending on the maturity of the standard and the need for specific ANL expertise or development/testing capabilities. The committees, status and contributions are summarized in Table V-2.

In addition to supporting coordination between SAE and international SDOs (e.g., IEC/ISO/DIN), the ANL and JRC interoperability centers directly contribute to international harmonization through collaboration on interoperability testing procedures and equipment as part of the Global InterOP team. The multi-national team, made up of German and US automotive OEMs plus the IOCs, facilitates cooperation with EVSE and test equipment suppliers to address immediate PEV-EVSE incompatibilities and attempt to ensure global interoperability in the future. The team is defining use cases (i.e., PEV-EVSE interactions), translating the use cases to requirements (hardware states and measurable parameters), defining test procedures and developing a universal specification for test equipment to verify compliance with interoperability standards (AC by 2016, DC and wireless schedule TBD).

Table V-2: Status of Key Standards and Committee Participation

Standard	Status	Role	Contribution
SAE J2953 PEV-EVSE Interop.	v1 published v2 in draft	Committee chair	Chaired; facilitated ID of gaps to be addressed in v2 based on lessons from AC interoperability testing
NIST Handbook 130/44; EPO30; EV fueling method of sale/measure	HB44 EV Fueling section ratified	Sub-committee chair	EVSE section adopted at 7/2015 Natl Conf. on Weights & Measures (NCWM). WM; hosted sub-committee on Exam Procedure 30 (EPO30) HB44 compliance and methods for national type certification; developed tools and methods
SAE J1772 PEV Coupler	v6 sent to publisher	Active Contributor	Contributed DC charging timing diagrams in FY14 that were refined in J1772-v6
SAE 2894 PEV Charge Power Qual.	v1 published	Active Contributor	Contributed to definitions, supporting data - impact of line impedance on peak inrush currents during turn on
SAE J3068 Heavy Duty 480vac Coupler	Launched in 2015	Active Contributor	3 phase/480vac (not J1772 compatible) harmonized with EU-China HD PEV charging coupler standards
SAE J2847/2 PEV Off-board DC Comm	v3 to be publ. in 2015	Active Contributor	Assisted the chair with changes to harmonize J2847/2 to DIN70121; utilizing ANL J1772 DC diagrams
SAE J2847/6 (J2931/6) Wireless Charging Comm.	Both published in 2015	Active Contributor	Paralleled and harmonized DC charging standards; assisted standards editors in clarifying intent of these charging functions
SAE J2931/7 Cybersecurity	Stalled, new chair	Active Contributor	Relinquished chair; assist incoming leaders with comments/requested changes to standard
SAE J3072-J2836/3-J2847/3 Utility Interactive PEV Req.	v1 to be published in 2015	Active Contributor	Contributed to figures/reference vehicle-grid configurations of V2G/V2B demonstrated to date; in the context of vehicles as power sources/loads
SAE J2954; UL2750; ANSI C63.30 Wireless Charging Safety/Interoperability	On track for TIR in 2016	Active Contributor	Content/support data via committee task groups; testing (safety, performance, robustness), WPT EMC-EMF, Magnetic Field Interop., Alignment and Comm., Verification testing (UL2750-J2954).
EPA EnergySTAR Reqmts. for EVSE	Draft released 2015	Active Contributor	Supported test procedures/cases, rationale of criteria to achieve EnergyStar rating.
ISO/IEC/DIN Standards	Ongoing	Support	Coordinate SAE standards with ISO15118 (AC/DC), DIN70121 (DC), IEC61980 (wireless)
IEEE P2030.7/P2030.8 Micro-grid	Launched in 2014/2015	Support	Provide PEV interoperability perspective (SAE J2953)
IEEE P2030.5 SEP Communication	Publ. 2013; rev. in 2016	Support	Provide PEV interoperability perspective (SAE J2953)
IEEE 1547.4 Utility Interactive Inverter	Publ. 2011; rev. in 2016	Support	Provide PEV interoperability perspective (SAE J2953)
IEEE P2413 Framework for IoT	Launched in 2014	Support	Provide PEV interoperability perspective (SAE J2953)

Argonne contributed their experience with AC interoperability requirements, procedures and test equipment to verify compliance with the SAE J2953 standard (documented in the FY 2014 annual report). JRC worked with test equipment manufacturers in Europe to evaluate the gaps in existing equipment to address the needs of the Global InterOP team. The team worked together on roughly 100 use cases for AC charging, i.e., the expected communication between, and reactions of, PEV and EVSE in typical and unpredictable situations (e.g., identification, communicating vehicle status, initiating and terminating charge, power failure/recovery, etc.). The benefit of this team approach is development of a common, detailed understanding of technical issues to address in both the SAE and IEC/ISO standards committees.

In addition to PEV interoperability, the DOE-JRC cooperative agreement includes harmonization of vehicle and battery test procedures. Preparations for joint vehicle testing activities began in FY 2015 with the acquisition and instrumentation of a reference vehicle that will be tested at both Argonne and JRC-IET; testing at ANL will be completed by Q2 FY 2016 and the vehicle will be shipped to JRC Ispra for comparative testing. Battery-related testing will be coordinated with the Argonne battery group (outside the IOC), but will not begin until JRC's new battery facility is completed in FY 2016.

Technology Development and Standards Verification

This group of tasks focused on communication technology R&D for AC/DC charging, including workplace charging with integrated control of EVE, building systems and/or distributed energy resources (e.g., solar).

Workplace charging

This group of tasks addressed technical issues associated with integrating PEVs in the workplace, including assessment of interoperability issues, building up a real communication and control test environment to support grid integration studies (i.e., the Smart Energy Plaza) and developing enabling technologies:

- Coordination and hosting of an international interoperability 'Festival'; a 2-day ad hoc testing event that included PEVs and EVSE (equipped with the Combo Coupler System, CCS) as well as stand-alone communication control electronics
- Installation of building systems, solar and communication networks in the Smart Energy Plaza
- Design and development of a Common Integration Platform (CIP), a universal electronic module with embedded open source software; to connect EVSE and 'controllable' devices to the grid
- Demonstration of integrated metering and control of EVSE using an 'Internet of Things' approach
- Design and development of a Sub-metering/Load Control Adaptor (SLCA) to enable communication with SAE J1772 compliant EVSE (to integrate legacy EVSE)
- Design of EVSE modules using off-the-shelf technology to establish a low-cost reference for multiple EVSE with individual sub-metering, communication and control

DC Charging (CCS) Interoperability Test Event

BMW, TU Dortmund, and ANL coordinated a round-robin DC charging test festival (aka 'Festival') in conjunction with the ISO/IEC interoperability working group meeting held in Q1, FY 2015 at Argonne. Two days of working group meetings were followed by two days of testing in the EV-Smart Grid Interoperability Center; attendees included vehicle OEMs, EVSE manufacturers, laboratories and universities from eight countries. The event paired various PEVs and DC EVSE equipped with the Combo Coupler System for ad-hoc testing. Outcomes from the event were promising; results showed that most systems were able to properly charge after some adjustments, suggesting that refinement of the DIN 70121 specification can lead to DC fast charge (DCFC) interoperability. The success led to additional interest/participation in events hosted by the Japan Automobile Research Institute (JARI) in Tokyo in April 2015 and an event scheduled for November 2015 at TU Dortmund in Germany.



Figure V-29: DC charging interoperability testing with PEVs, EVSE and communication modules at the ANL IOC-hosted testing festival ('Festival') in November 2014

Source: ANL

Common Integration Platform (CIP)

As 'smart' networked devices are increasingly integrated into buildings, homes and public infrastructure, the need to monitor and communicate with these devices to enable system control, data analytics and visualization becomes paramount. Argonne is pursuing an open source approach to control networked devices to minimize barriers to commercial implementation of smart energy management. Two applications were considered for potential use in a common integration platform; VOLTTRON, developed by PNNL with DOE support, and Node-RED, developed privately by IBM. It should be noted that these are not mutually exclusive options; preliminary development activities demonstrated that VOLTTRON and Node-RED can work together. These applications are briefly described and initial impressions are summarized in the following paragraphs.

VOLTTRON is a PYTHON-based virtual environment that deploys software agents to perform specific tasks (Ref. 2). These agents communicate via a publish/subscribe information exchange bus (IEB) based on the ZeroMQ protocol. Documentation is straightforward and allows a novice to get a VOLTTRON environment up and running. However, the application lacks a graphical user interface (GUI) and there is not an extensive library of agents developed by third parties. The initial impression is that there is a substantial learning curve to develop 3rd party agents for the VOLTTRON environment.

Node-RED is described as the "visual tool for wiring the Internet of Things" (Ref. 3). Within the Node-RED environment, nodes are wired together to create flows, these flows perform a specific task similar to the concept of agents in VOLTTRON. Node-RED allows browser-based flow editing with real-time debugging and deployment options. Node-Red is built on Node.js, taking full advantage of its event-driven, non-blocking model. Node.js' package repository, npm, is the largest ecosystem of open source libraries in the world.

Node-RED does not have a core capability to visualize data or an information exchange bus, though it is compatible with a suite of open source tools that appear to provide the necessary functionality based on the IOC's experience to date. For example, Freeboard is a real-time customizable dashboard, enabling monitoring of devices and visualization of data. MQTT is a machine-to-machine (M2M)/"Internet of Things" connectivity protocol. It was designed as an extremely lightweight publish/subscribe messaging transport. Mosquitto is an open source MQTT Broker that can be utilized with the built-in MQTT nodes of Node-RED to enable a common integration platform information exchange bus that can be deployed locally and/or in the cloud. The initial impression of Node-RED is that when combined with other open source projects, such as Freeboard and MQTT, it provides a common integration platform that is scalable and capable of rapid development and deployment.

Integration of Devices and Infrastructure in the Smart Energy Plaza

The scope of PEV-grid integration goes beyond EVSE, extending to buildings, homes and other grid-connected devices. An integrated communication and control testing environment has been developed by combining the bank of EVSE located outside the Building 362 High Bay and a 'mobile grid unit' with representative building systems (e.g., HVAC, lighting, etc.) and a 9 kW solar array, shown in Figure V-30.

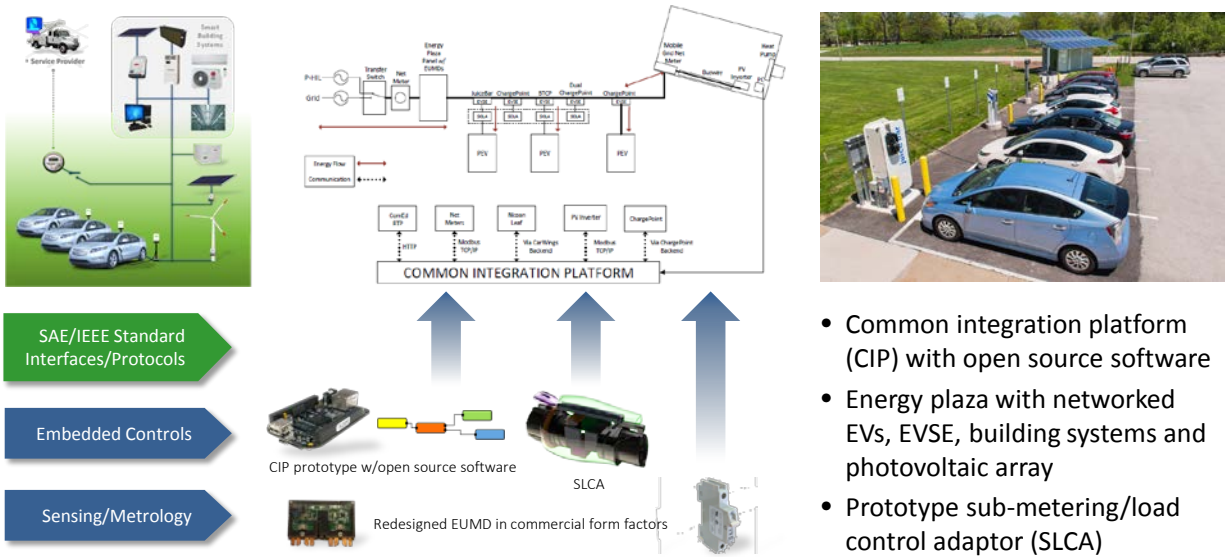


Figure V-30: Mechanization of the Smart Energy Plaza

Source: ANL

Integration of devices in the Smart Energy Plaza using the IoT approach began in Q4 FY 2015. The Fronius solar inverter, ChargePoint EVSE, and Measurlogic smart meters have been 'integrated' into the platform, i.e., Node-RED flows have been developed to communicate with and/or control these devices. Node-RED and the associated suite of tools enabled data logging and visualization on the monitor in the mobile grid unit; this approach will be used for integrated communication/control development in FY 2016.

An example of data integration and visualization is shown in Figure V-31, i.e., a graph of power consumed by loads (blue) and solar generation (yellow) on a recent summer day in the Smart Energy Plaza. The labels on the axes are faint in this screenshot from the monitor in the mobile grid unit; the max power on the y-axis is 8000 watts and the time on the x-axis is from 0500 to 1800 hours. The load power data implies that 3 charge sessions occurred during the day: a ~6.6 kW peak charge session in the early morning, followed by ~3.3 kW peak charge session around 11 am and another ~6.6 kW peak charge session around 12:30 pm. The periodic repetitive small loads are the heat pump turning on to cool the mobile grid unit mid-morning through the afternoon. There was little cloud cover this day, as evidenced by the bell curve of solar power generation.

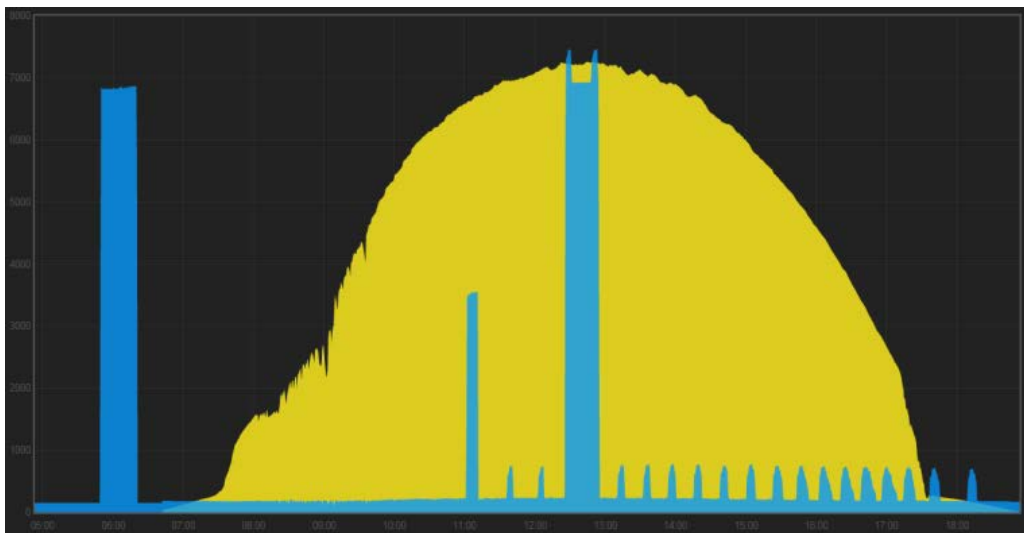


Figure V-31: Example of Solar Power Generation and Loads in the ANL IOC Smart Energy Plaza

Source: ANL

Sub-metering/Load Control Adapter (SLCA)

Most deployed PEVs and EVSE lack the communication, monitoring and control capability necessary for grid integration; the SLCA has all these capabilities and allows any PEV or EVSE compliant with SAE J1772 to be integrated into a building energy management system (BEMS) or vehicle-grid integration (VGI) platform. The SLCA is PEV/EVSE agnostic and will not limit which PEV/EVSE can be integrated into a VGI platform. From a technical standpoint the SLCA is an IoT device with the potential to minimize proliferation of proprietary protocols and communications for EVSE and PEVs as well as the aggregation and grid integration challenges of today's PEV charging infrastructure.



Figure V-32: Proof-of-concept Sub-metering/Load Control Adapter (SLCA)

Sources: ANL, C.A.D.

The SLCA is portable and can be connected between an SAE J1772-compliant AC Level I or II EVSE and PEV. It has two modes of operation: pass-through and emulation. In pass-through mode the SLCA monitors the charge session and the embedded smart sub-meter measures energy and instantaneous power of the charge session. This information is communicated to a common integration platform for data analysis in real time. In emulation mode, the SLCA seamlessly enables full control of the charging session by the common integration platform, i.e., start, stop, increase or reduction of charging power. Figure V-32 is a rendering of the proof-of-concept SLCA prototype. The SLCA will be a valuable research tool for developing smart charging algorithms, aggregation and workplace charging use cases, as well as charging diagnostics given its ability to provide communication, monitoring, and control of a PEV's charge session.

Modular, Low-Cost EVSE

Hardware studies were conducted to develop a baseline for implementing multiple EVSE in the workplace, i.e., a 'reality check' to serve as a basis for benchmarking progress/cost reduction in the EVSE market. The first study (below left, Figure V-33) focused on integrating contactors from Phoenix Contact with metering and communication by Argonne; the objective was to minimize the overhead/control cost. Though the packaging was promising, the proprietary firmware was still under development and integrated control could not be implemented.

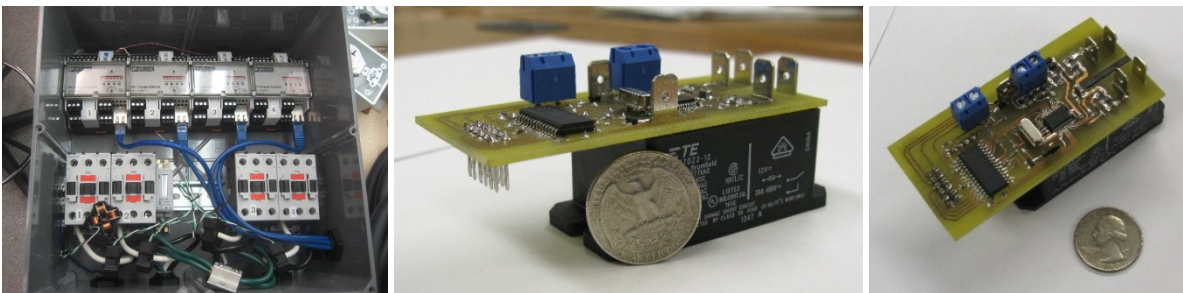


Figure V-33: Multiple EVSE hardware studies; Quad EVSE and EVSE building block

Source: ANL

The second study (above right, Figure V-33) combined off-the-shelf and custom components in an EVSE building block; comprised of a 30 Amp contactor, an EUMD measuring current and voltage to calculate power

and energy, the PWM driver circuitry, and a microcontroller. When plugged into a system bus that provides power (+5V, +12V, -12V) and a master microcontroller each EVSE module will be able to handle one vehicle up to 30 Amps. Any number of EVSE modules can be plugged into a system bus and a master microcontroller can individually dictate, via the EVSE module, how much current the PEV is allowed to draw.

This design results in a cost for each EVSE module of ~\$40 (~\$20 for the EUMD). Two small EUMD capacitors (~\$10 total) have been included that may or may not be necessary. If not, the overall module price drops to ~\$30. The cost for the system bus as currently configured works out to \$40 (the power transformer is about half that at ~\$20). This includes the transformer, +5V, +12V, -12V, a GFCI protection circuit, a master microcontroller, USB communications, and a real time clock circuit. With a 30 Amp, 20 ft. cable set costing ~\$165 (today), a 4 channel system would cost less than \$900 (or \$225/EVSE).

Wireless charging

The wireless charging test system was detailed in the FY 2014 annual report, hence this is an update of continued developments in FY 2015 in support of semi-automated magnetic interoperability testing.

- The previous computer-automated coil positioning system (ground and vehicle side) was extended to include a computer-automated electromagnetic field probe positioning system (large swept volume) and central host (PC-based) DAQ system to coordinate/record data from each to the test instruments and actuators.
- In preparation for potential use outside Argonne, three international grade custom packing crates were fabricated and the ability to transport the entire test system via commercial carrier was verified. Setup and commissioning was accomplished in less than 1 day.
- The wireless charging test system was commissioned with the Toyota (first generation) wireless charging system in three test environments; RF chamber, indoors on concrete with rebar and outdoors in the Smart Energy Plaza.

As described previously, support for SAE J2954 (Wireless PEV Charging) includes assessing performance, safety, interoperability and other aspects of wireless vehicle charging systems. One of the most important aspects of wireless charging is that the equipment on the vehicle and stationary wireless charging equipment on the ground will not likely have come from the same manufacturer. Interoperability of the ground assembly (GA; stationary side) and the vehicle assembly (VA; mobile side) needed to be assured.

To clarify the challenge, not only will there be different manufacturers' approaches to making an SAE J2954 compliant wireless charging product, but there are three different height classes for different sized vehicles (Z1-Z3) and three different power classes (WPT1-WPT3). Interoperability for J2954 will be based on the use of a master reference coil, for which the specifications are still under discussion. Figure V-34 shows several coils that are similar to the reference coils for SAE J2954 (Ref. 4). The proposed reference coils were still under discussion in the J2954 committee at the end of FY 2015. FY 2016 effort includes characterizing the performance of a matched pair of GA-VA reference coils and electronics. This will be the baseline for measuring the interoperability of mismatched GA-VA coils with the reference coil.

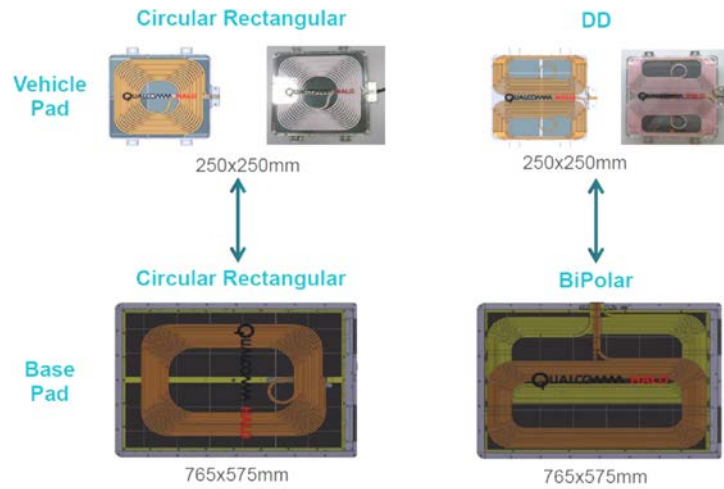


Figure V-34: Example coil topologies similar to proposed reference coils

Source: wiseharbor.com

The ANL wireless test fixture was expanded in FY15 to include the computer automated (ground and vehicle side) coil positioning system, computer automated electromagnetic field (3 meter swept volume) probe positioning system and central host DAQ system (PC based, Figure V-35) to coordinate/record data from each of the test instruments and actuators.

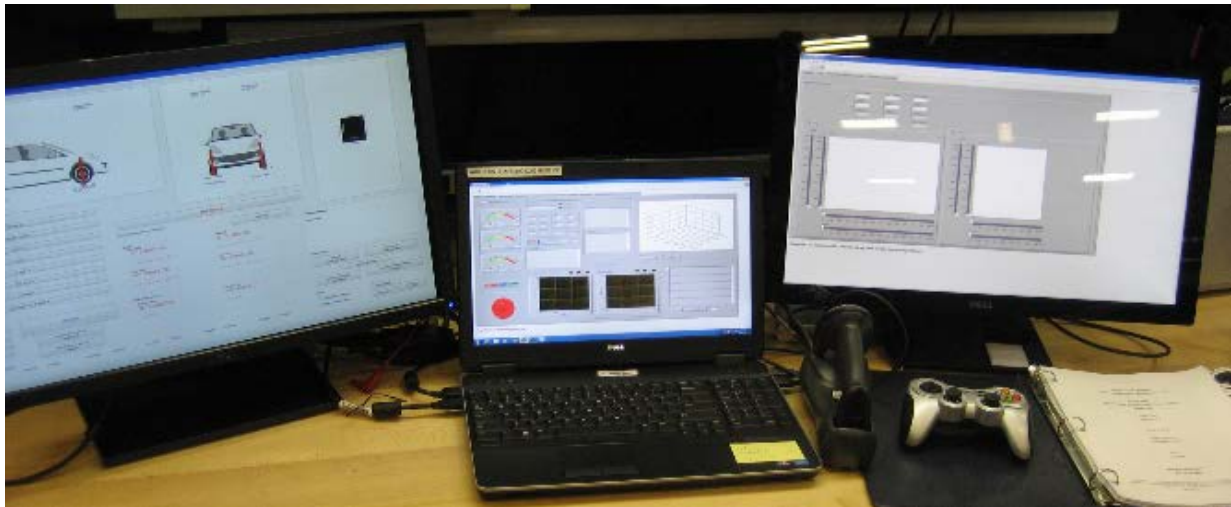


Figure V-35: Wireless Charging test system DAQ Graphic User Input screens from left to right; vehicle/coil positioning, data and probe positioning

Source: ANL

The field probe positioning system is shown the lower left of the Figure V-36. The coil positioning system, probe positioning system, Z-axis lifts, safety equipment and DAQ system pack in the three international shipping crates shown. A single operator can uncrate and set up the test system within a day.



Figure V-36: ANL Wireless test system with field probe/coil positioners-DAQ; custom international shipping crates
 Source: ANL

As part of the safety plan and subject matter expert reviews, the wireless charging testing system at ANL was commissioned on a Toyota wireless charging system in three test environments; RF chamber, indoors on a concrete floor with rebar and outdoors in the Smart Energy Plaza (Figure V-37).

The wireless charging test system was also commissioned for alignment assessment at the component and vehicle level using the 3.3kW Evatran (20 kHz) wireless charging system. The figure also shows the system installed on a Chevy Volt and in the RF chamber.

The intent is to collaborate with OEMs/vendors on testing pre-production wireless charging systems, with and without vehicles, to support the soon-to-be-published SAE J2954 (TIR) standard; focusing on validation and refinement of test procedures and the implications for test results.



Figure V-37: Commissioning wireless test fixture in the RF chamber and outdoors (above) and for component/vehicle level alignment assessment using Evatran system (below)
 Source: ANL

Reverse power flow (off-board inverter)

This project was proposed as an extension of the FY 2014 V2G activity with the ARRA-funded Chrysler RAM pickup; Argonne modified the SpEC module for this project and added CCS to the vehicle. However, the project was cancelled because FCA decided not to allow the vehicle to remain at Argonne beyond FY 2014.

Metering Technology Development and Implementation

Design and development of fourth generation, compact End-Use Measurement Devices continued; focused on utilization of the low-cost PSoC by Maxim, the Max71315 IC.

Application engineering of the proof-of-concept digital flux gate magnetometer (DFGM) current sensor continued; the performance was compared to PC board micro shunt and Rogowski/integrator coreless sensors.

In support of NIST Weights and Measures, a NIST Handbook 44 capable electric fuel compliance/benchmark comparison metering system was developed and commissioned; it utilized the Maxim MAX71315 IC and an EUMD developed by ANL.

Fourth Generation End-Use Measurement Device (EUMD)

As an extension of previous versions of the ANL modular metering EUMDs, a version based on the low-cost Maxim Max71315 IC (now < \$3) was designed and tested on the evaluation board platform. Packaging for the previous versions (1-3), as shown on the left in Figure V-38, was limited to open frame (EVSE daughter card/direct current measurement) in the 60A disconnect format, combining metering and disconnect in a standard low-cost base socket. These versions were capable of using current transformer (CT), hall-effect, PC board resistive micro shunt, and digital flux gate magnetometer (DFGM) current sensors. Communication included isolated serial port, Zigbee/SEP1.x, and powerline carrier over the main circuit as well as auxiliary serial inputs to monitor EVSE data and/or the state of the EVSE charging process. The processor and supporting parts were based on the software-intensive Freescale Coldfire processor used by most of the 'smart' meters at the time. Software development and support costs were perceived by industry as obstacles to adoption of this compact meter.

To address the shortcomings of previous versions and further reduce cost, Argonne's efforts this year focused on the Maxim Max71315 chip and several current sensor options. The figure also shows a mockup of the draft 2" x 2" PC board layout next to several of the proposed packages with different mounting and sensor options.

A CAD rendering of the design to replace a standard circuit breaker is shown at right; the LCD panel is shown on the top, where the circuit breaker trip lever is normally. Connectors on the side for power, current sensors and data output are where the output lead (load) of the circuit breaker terminal is normally located.

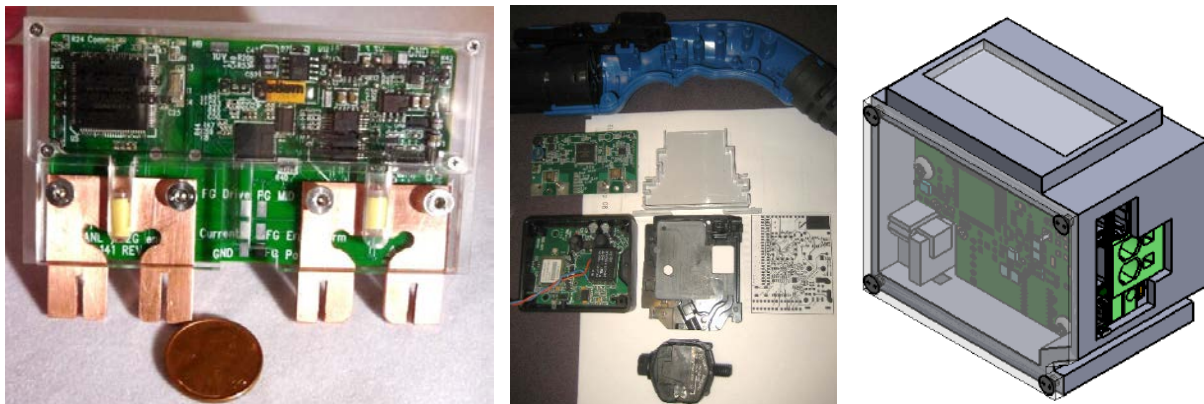


Figure V-38: ANL EUMD design (versions 1-3) on left; Preliminary 2" x 2" board layout and potential commercial packaging formats; CAD rendering of the EUMD design to replace a standard circuit breaker

Sources: ANL, 2G Engineering

Future work includes hardware and software development/integration for selected commercial applications and form factors in cooperation with supplier/utility partners.

Current Sensor Development

Argonne has supported the development of DFGM-based current sensors for several years (described in previous annual reports). To summarize the method of current sensing in a DFGM, a high frequency ramp current is driven into the sensor coils to the point of nulling the flux created by current in the wire being measured. Using signal conditioning algorithms, the ramp signal is turned into sensed current. Due to their small size and low cost, they are a good candidate for the latest generation EUMD using a small, low cost PSoC. The small size is evident in Figure V-39, which shows the 3mm x 8mm sensors in loose form and as a sensor pair molded on the EUMD bus bar. The figure also shows the latest design of the analog signal conditioning circuit using a single PSoC.



Figure V-39: DFGM sensors and sensor pair on EUMD bus bar; analog signal conditioning circuit with PSoC; comparison of previous and PSoC-based designs

Source: ANL

Two forms of drive circuit/signal conditioning were implemented by ANL and Magnetic Sensor Systems, the support contractor, for comparison of performance, and cost/volume/performance tradeoffs. Figure V-40 shows linearity and accuracy data of the DFGM sensor with analog signal conditioning, PSoC drive/EMF symmetry (metric of closed loop high accuracy measurement) and modeling of the magnetic field from the current carrying wire interacting with the DFGM sense coil.

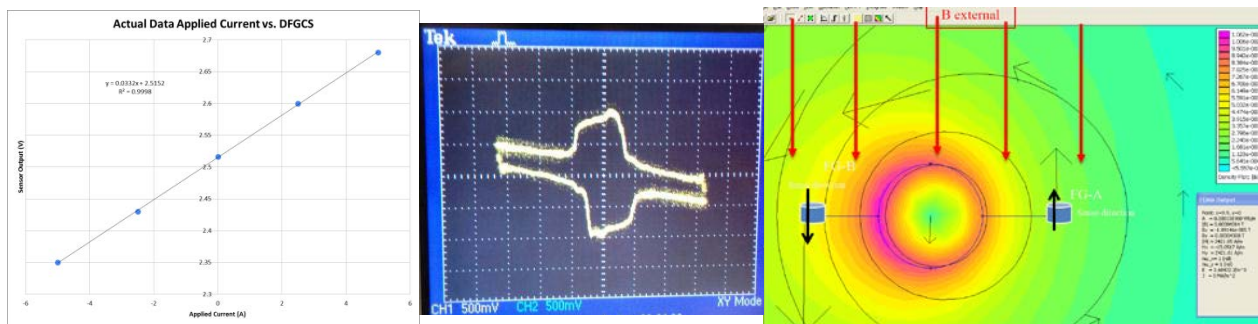


Figure V-40: Output current signal from DFGM; drive versus EMF signal symmetry; magnetic sense field modeling

Sources: ANL, Magnetic Sensor Systems

In addition to molding the DFGM sensor coils along the sides of a very uniform bus bar (as shown previously in Figure V-39), a board holding the sensor coils has been designed for a molded part that can snap onto a DIN rail (shown in the mockup of Figure V-41). This DIN rail-mounted sensor array could be part of a circuit breaker load center. The molded part holds the circuit board in place with a notch/clip in the back for the conductor being measured. The two square 'boxes' next to the clip (rightmost drawing) hold the 3mm sense coils below the PSoC board. Since there is no ferrite core or other magnetic concentrating component to

encircle the flux of the conductor, the DFGM current sensor can be attached to live circuits without the need to power down/disconnect leads.

The target cost and accuracy for the production DFGM current sensor is less than \$3 with signal conditioning and better than .2% from 10% to full scale. DFGM drive circuit current can be managed by magnetic field modeling. The sensor can measure 5 amps or 5000 amps full scale if properly spaced near the conductor being measured, i.e., component cost per ampere is a function of packaging/mounting, not sensors.

In FY15 ANL and collaborators studied the challenges in tuning the single chip PSoC approach (digital registers) vs analog circuit with manual tuning bulk resistance as a function of net performance. Future work includes completing the performance benchmarking of both signal conditioning approaches, on several mounting packages for the sensor heads, and completing a report on the tradeoffs of cost, complexity, ease of tuning, and net sensor system performance. One possibility is a compromise (hybrid circuit) between an analog and mixed signal PSoC approach, using digital tuning elements instead of a full-on PSoC device with a large number of unused circuits inside.

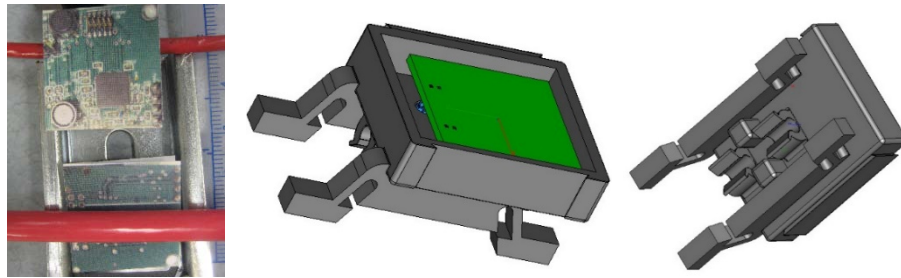


Figure V-41: Design of DFGM-based current sensor in DIN rail mounted case/wire guide

Sources: ANL, Magnetic Sensor Systems

NIST HB44 AC EVSE Electric Fuel Meter

DOE VTO decided in FY 2014 to support the efforts of NIST Weights and Measures to measure electric fuel delivery (analogous to measuring liquid fuel pumped at a gas station). Since that time an ANL IOC staff member has served as the chair of the NIST Handbook 44 (HB44) sub-committee on requirements for measurement systems related to commercial dispensing of electricity as a fuel and designed a test tool for evaluating EVSE compliance with HB44.

The "Smart Load DAQ©" (copyright asserted) is shown in Figure V-42. Based on the EUMD metrology module, and packaged by 2G Engineering, the 12" x 12" x 12", 20lb device travels in a zippered carrying case with wireless printer and tablet PC. The system is powered by the tablet and AC source during testing. A photo during a field trial of the menu-driven system (tablet, printer and Smart Load DAQ©) is shown as well.



Figure V-42: Smart Load DAQ© internal construction, system components and in a field trial

Source: ANL, 2G Engineering

The name describes the three main functions of the device:

'Smart' – Runs a test script to emulate a PEV that is 'fueling' from the EVSE that is being assessed for HB44 compliance. Emulation includes a real electronic load and J1772 capable pilot signal interlock.

'Load' – Within the compact UL listed 5.6kW resistance load is a 200 kHz active electronic AC/DC regulator with similar input characteristics to a PEV onboard charger. The regulator is based on next generation silicon carbide (wide bandgap) field effect transistors with very low switching losses that allow faster switching speeds which, in turn, allow smaller passive magnetic components. (upper left corner).

'DAQ' – The data acquisition system is based on an Argonne EUMD metrology module, and industry standard Linux single-board PC with MODBUS over USB communication. It is connected to the tablet PC running a Labview-based display terminal application. (i.e. all data acquisition functions for measuring charging state, power, energy, time on charge, etc., are located in the Smart Load DAQ©).

This Smart Load DAQ© test system was demonstrated at the 2015 National Conference on Weights and Measures where the proposed 2016 code cycle version of HB44 was put up for ballot, and subsequently adopted. Many Weights and Measures code officials commented that demonstration of the ability to meet the HB44 test requirements using the Smart Load DAQ© before the code was ratified had a significant effect on the outcome of the ballot for this yet-to-be deployed standard for measurement of electricity as a fuel.

Future work on metering technology for HB44 includes collaboration with California's Department of Food and Agriculture who is taking the lead in running the California Type Evaluation Program (CTEP). CTEP can issue a type certification to HB44 compliant EVSEs with energy/time/money transaction recording and displaying equipment. California is the first state to adopt HB44-2015 as enforceable for commercial EV fueling transactions.

Harmonization, International Cooperation and Grid Modernization

The ANL IOC was established in 2011 to support harmonization of technology and standards for PEV connectivity and communication with the charging infrastructure and future smart grid. The IOC has focused on PEV-EVSE compatibility and interoperability; as evidenced by the IOC's involvement in standards, test procedures and equipment for both domestic and international initiatives (described previously in this report).

In FY 2014, the scope expanded to include PEV-grid integration, with implications for technology and standards beyond the EVSE, including buildings, distributed energy resources and grid storage. The broader scope was reflected in the Multi-Lab EV Smart Grid Integration Requirements Study that was initiated in Q4 FY 2014. Six national labs cooperated to provide guidance on technology development and demonstration for DOE VTO; the study was completed in Q2 FY 2015 and the final report was published in May 2015 (Ref.1).

IOC tasks were aligned with the recommendations from study, i.e., developing enabling technologies (such as a common integration platform), an integrated testing infrastructure and tools to verify compliance with standards. In addition, the working relationships developed in the multi-lab study group directly influenced the decision to jointly propose grid integration tasks in response to the DOE Grid Modernization Lab Call of Q4 FY 2015; these tasks are expected to be initiated in Q2 FY 2016.

Since many of the FY 2015 tasks supporting harmonization have been covered adequately in sections of this report related to standards, development or implementation, this section addresses the following activities:

- Multi-Lab EV Smart Grid Integration Requirements Study
- Cooperative activities in Europe
- Cooperative activities in China and APEC
- Grid modernization

Multi-Lab EV Smart Grid Integration Requirements Study

Initiated in Q4 FY 2014, ANL participated in the grid integration requirements study with NREL, INL, LBNL, ORNL and PNNL. The objectives of the study were to define PEV-grid integration scenarios, understand

system implementation requirements, and suggest research opportunities to develop technologies that are needed to enable vehicle-grid integration (VGI).

ANL's responsibilities included identifying key factors/enablers for using PEVs as a grid resource, understanding the current status of these key areas, and providing recommendations for future research and development to enable PEV grid integration. The outcomes of ANL study were presented in the Chapter 3, "Enabling PEV to Grid Integration," of the final project report. Six factors were recognized as key to enabling seamless VGI, including uniform reference architecture; harmonized interface standards or protocol translators for interoperability; standard use cases and demonstrations to quantify the costs and benefits; control paradigms that enable coordinated control and active grid management; advanced metering infrastructure (AMI) and sensing technology for grid quality, reliability and real-time energy management; and cyber security.

Although the availability of private and public EVSE has increased to accommodate the increasing numbers of PEVs in the market, most existing EVSE lack the sophistication (i.e., communication and control capability) to be integrated in a managed grid in a manner that is required to implement the higher level PEV-grid service functions. Various challenges remain to integrate PEVs in a future smart grid, including system architecture, communication and information exchange standards, regulation and business models. Recommendations for future research and development to overcome these issues/barriers and enable VGI include following:

- Adopt or define a uniform reference architecture and the scope of analytical and hardware studies
- Implement control paradigms for active management of distributed generation, storage, and mobile PEVs
- Establish connectivity and communications standards
- Develop VGI enabling technologies, such as a standardized integration platform, low-cost and standards-compliant smart meters and sensors
- Build a testing infrastructure/tools to verify compliance with connectivity/communications standards
- Demonstrate and quantify the cost and benefit of VGI

Cooperative activities in Europe

The focus is on fulfillment of the DOE-JRC agreement while supporting industry in their efforts to globalize interoperability requirements and facilitate timely development, refinement and adoption of universal interoperability standards. The primary activity is with the European Commission (EC) and their research arm, the JRC; maintenance of this relationship requires briefings to the State and Commerce, representatives of the EC/Transatlantic Economic Council and DOE International Affairs in Washington and Brussels (Ref. 5, 6). In addition, IOC involvement in Global InterOP necessitates coordination with the German ministry that directly supports an EV infrastructure and interoperability tool development for the initiative.

Cooperation with JRC-IET

The working relationship with JRC-IET has developed well in the past three years; the technical staffs have worked together, and with industry, to develop global interoperability requirements and tools to verify compliance with the requirements (Figure V-43). JRC's new vehicle test facilities in Ispra, IT and battery test facilities in Petten, NL will be inaugurated in Q1 and Q3 FY 2016, respectively, allowing comparative reference testing to harmonize PEV test procedures.



Figure V-43: Interoperability Center Activities Supporting Global Harmonization
 Sources: ANL, JRC

Preparation for reference vehicle testing began in FY 2015 with the Argonne’s acquisition and instrumentation of a PEV common to both markets, the BMW i3 EREV. Instrumentation adequate for Level 2 testing is now complete; measuring axle torques, voltage and current of low- and high-voltage circuits, temperatures in the low- and high-temperature coolant loops, interior temperatures, CAN diagnostics, etc. The vehicle will complete the Level 2 test program in Argonne's Advanced Powertrain Research Facility (APRF) in Q1 FY 2016; including vehicle and component performance on a variety of test cycles, vehicle loss determination (i.e., coast down), component mapping, charging (in charge depleting and sustaining modes) ... all with the added dimension of ambient temperatures of 0 F, 20 F, 72 F and 95 F.

The vehicle will be shipped to JRC Ispra in Q2 FY 2016 where it will be tested in a similar manner in the VELA-8 dynamometer facility to allow direct comparison and identification of differences in test procedures and/or results. Use of the same vehicle avoids potential differences in vehicle characteristics or instrumentation, allowing the focus to be on comparison of procedures, data acquisition, analysis and results.

Comparative vehicle testing is one of several projects that will be conducted under the new Science and Technology Agreement between DOE and the JRC. Expected to be adopted before reference vehicle testing at Ispra begins, the ‘umbrella agreement’ includes a streamlined technical annex process for collaboration between JRC and the DOE national labs. Three technical annexes were jointly developed with JRC-IET to be initiated in FY 2016 in anticipation of the new S&T agreement:

- "E-vehicle testing and interoperability, Technical Annex to the Scientific Collaboration Arrangement between JRC and ANL", June 2015
- "Smart grid interoperability, Technical Annex to the Scientific Collaboration Arrangement between JRC and ANL", July 2015
- "Battery testing and testing methodologies, Technical Annex to the Scientific Collaboration Arrangement between JRC and ANL", July 2015

Cooperation with Germany

German automotive manufacturers are among the most successful in the world due to the popularity of their products. Cooperation between German and US OEMs – and their respective governments – can greatly influence the expansion of vehicle electrification globally. In addition, Germany and the US are key players in

the transatlantic trade discussions; sharing multi-national corporations that benefit from removal of barriers such as discriminating and/or differentiating standards. Hence, both countries' automotive industries support the US and EU interoperability centers as well as the Global InterOP activity. The USG fosters a mutually beneficial relationship with Germany, as reflected in the establishment of the Joint Committee on Science & Technology Cooperation. The IOC directly supports joint technical meetings and coordination with the German Ministry that supports interoperability standards and verification (Ref. 7, 8, 9)

Cooperative activities in China and APEC

Efforts to establish a PEV interoperability center with China continued and similar cooperation with the Asia Pacific Economic Council (APEC) economies was initiated by DOE International Affairs at the end of FY 2014, resulting in a US proposal to APEC in FY 2015.

Cooperation with China

The IOC continued supporting meetings of the US-China EV Initiative (Ref. 10); this forum has been a useful means of updating each other on technical developments of mutual interest as well as discussing potential areas of cooperation on pre-competitive/non-sensitive technical issues. In fact, discussions of establishing a cooperative interoperability center began in this forum over two years ago. The idea appears to be making some progress since the Ministry of Industry and Information Technology (MIIT) got involved. Several meetings with MIIT this year and a specific proposal by the ANL IOC resulted in the topic being included in the agenda of President Xi's visit to the US in September 2015. At the end of FY 2015, the intent and scope of such an agreement were still being discussed.

Cooperation with APEC

Establishment of cooperative EV interoperability and research centers was one element of an EV Roadmap proposed by the US to the APEC Automotive Dialog (AD). ANL was asked to present the Roadmap and provide an overview of the EU and US EV-Smart Grid Interoperability Centers at the APEC AD meeting in Manila in April 2015 (Ref. 10, 11). The response was positive, resulting in direct queries by many AD delegates and subsequent substantive comments on the proposal. The roadmap is undergoing final review at the AD level and will be presented to the APEC Committee on Trade and Investment in Q1 FY 2016. The method of cooperation has not been determined; both joint technical activities and a 'virtual center' (based on sharing information) have been discussed. Realistically, the level of cooperation will be determined by the terms of the agreement, DOE priorities and resources available to the ANL IOC for international cooperation.

Grid Modernization

Though the ANL IOC has focused on PEV interoperability since its inception, the DOE-JRC agreement also included addressing EVs and the charging infrastructure as an integral part of a future smart grid, or in today's terminology, PEV-grid integration as part of the DOE grid modernization initiative.

The objective of grid modernization, from the interoperability perspective, is to enhance the grid with the ability to monitor, communicate with and control grid-connected devices, using a standardized approach, for the mutual benefit of energy producers, distributors and consumers. All IOC activities have supported this objective, e.g., development/verification of standards, enabling technologies (such as sensors, sub-meters, communication modules, and the common integration platform), numerous test tools and an integrated testing environment.

Grid-related activities of the IOC are now considered part of DOE's Grid Modernization initiative; described as 'an integrated and coordinated approach for national labs to support development of a future smart and robust grid' at the launch of the Grid Modernization Lab Consortium in November, 2014 (Ref. 12). The technical objectives/needs of grid modernization were detailed in the DOE Grid Modernization Laboratory Call issued by NETL in June 2015 (Ref. 13); the labs jointly responded to the Call, resulting in 40+ proposals. The ANL IOC participated in four 'Foundational' (cross-cutting) proposals supporting Devices and Integrated Systems Testing (DIST), two proposals specific to the Vehicle Technologies Office and one specific to the Building Technologies Office. The common element of the Argonne's roles in the proposals (listed below) is vehicle connectivity and communication with the grid; with contributions ranging from grid integration strategies to development, testing and implementation of enabling technologies. The proposals are included here because

they required substantial time and effort of IOC staff to support (in addition to the effort required to respond to the Vehicle Technologies Office AOP Lab Call), the tasks proposed in responses to the Calls are synergistic and it reflects a significant level of cooperation between the labs in FY 2016-18.

Foundational proposals

- Interoperability (with PNNL, NREL and LBNL)
- Establishment of Grid Modernization Laboratory Consortium – Testing Network (with SNL, NREL, PNNL, ORNL, INL, LBNL, SRNL, BNL and LLNL)
- Standards and Test Procedures for Interconnection and Interoperability (with NREL, PNNL, LBNL, SNL, ORNL and INL)
- Definitions, Standards and Test Procedures for Grid Services from Devices (with PNNL, NREL, ORNL, SNL, LBNL, INL and LLNL)

Program-Specific, Vehicle Technologies Office

- Vehicle to Building Integration Pathway (with INL, LBNL, NREL and PNNL)
- Systems Research Supporting Standards and Interoperability (with INL, LBNL, NREL, ORNL and PNNL)

Program-Specific, Buildings Technologies Office

- VOLTTRON to Vehicles (with INL, LBNL, NREL, ORNL and PNNL)

Results

The Approach section included descriptions of IOC tasks and associated results; this section summarizes the results by technical area.

Codes and Standards

- Led the SAE J2953 (PEV-EVSE interoperability) committee and NIST Handbook 44 sub-committee on metering methodology for EVSE electric fuel delivery
- Contributed substantially to the Global InterOP team; transfer of use cases, requirements and test procedures developed in support of the SAE J2953 and SAE J1772 committees

Technology Development and Standards Verification

- Hosted an international DC charging test festival at the ANL IOC; attended by OEMs and EVSE manufacturers from 8 countries; ad hoc testing of PEVs, EVSE and communication control modules implied that further refinement of the DIN 70121 specification could lead to DC fast charge (DCFC) interoperability.
- Developed and demonstrated the preliminary design of a Common Integration Platform (CIP) for communication between and control of grid-connected devices - based on an open source, Internet of Things (IoT) approach; demonstrated integrated communication, control and data visualization of EVSE, solar inverter, smart meters and external grid information in the Smart Energy Plaza.
- Evaluated VOLTTRON (PNNL) and Node-RED (IBM) platforms for integrating PEVs and other grid-connected devices; demonstrated that they can work together
- Completed first phase of Smart Energy Plaza mechanization with addition of mobile grid unit and networked solar array, controllable building systems and smart metering.
- Developed prototype design and demonstrated proof-of-concept Sub-metering/Load Control Adaptor (SLCA); portable device for use between PEV and EVSE to enable grid connectivity of any SAE J1772-enabled PEV/EVSE and smart energy management (e.g., smart charging, demand response, etc.).

Metering Technology Development and Implementation

- Designed fourth generation EUMD based on small, low-cost Maxim programmable system on chip (PSoC) and DFGM current sensors; packaging layouts completed for standard DIN formats.
- Designed DFGM-based current sensor for integration in commercial form factors; performance characterized.
- Developed and demonstrated NIST Handbook 44 AC electric fuel delivery measurement device; collaboration with NIST Weights and Measures will continue with development of a similar device for DC EVSE.

Harmonization, International Cooperation and Grid Modernization

- Identified key enablers for vehicle-grid integration and recommended R&D to address key issues/barriers in the Multi-Lab EV Smart Grid Requirements Study; initiated/refined several activities in response to the recommendations (e.g., open source common integration platform and communication/control testing infrastructure)
- Maintained cooperative relationships and supported joint events with the European Commission, Joint Research Centre, German Ministries and representatives of the US Departments of State and Commerce at embassies in Brussels and Berlin; specific cooperation planned through FY 2017.
- Developed Technical Annexes to the DOE-JRC Science and Technology Agreement that authorize collaborative EV interoperability and grid integration activities that begin in FY 2016.
- Contributed to and presented the US-proposed EV Roadmap to the APEC Automotive Dialog at the Manila meeting in Q3 FY 2016; included establishment of a cooperative EV interoperability and research center; acceptance by the APEC Committee on Trade and Investment is expected in the Q1 FY 2016 meeting.
- Developed working relationships with national labs resulting in six joint proposals in response to the DOE Grid Modernization Laboratory Call; the GMLC and VTO AOP projects are synergistic and could lead to substantive cooperation through FY 2018.

Conclusions

Argonne has significantly contributed to the development of technology and standards for vehicle-grid integration and universal interoperability with the charging infrastructure. The ANL IOC has leveraged its expertise in embedded controls, electrical/electronic design and system integration to produce enabling technologies, tools and testing environments to support development and validation of sensing, communication and control for vehicle-grid integration. Patents, copyrights and licenses of the unique enabling technologies and tools are expected continue; increasing industry participation and bringing further recognition to the DOE-sponsored activities at the ANL IOC.

Meaningful working relationships have been developed and maintained with governments, industry and the scientific community internationally - initiated by government commitment and sustained by mutual recognition of the benefits of combining subject matter experts from industry and the national laboratories. Additional joint projects are planned to utilize the new facilities at JRC-IET in FY 2016; further strengthening the relationships between government programs, the national labs and industry that are the basis of cooperation and harmonization between the US and EU. Efforts to establish similar working relationships in Asia will continue; but at a pace determined by the progress at the diplomatic level between the US, China and APEC.

In summary, the technical and programmatic achievements of DOE/Argonne EV-Smart Grid Interoperability Center to date provide a solid basis for the 'Future Accomplishments' presented in this report, the grid integration projects in support of the DOE Grid Modernization Initiative and productive international cooperation.

V.5.C. Products**Presentations/Publications/Patents**

1. "EV-Smart Grid Interoperability Center in Europe and the US", Presentation to the US-EU Energy Policy Working Group, K. Hardy, Washington and Brussels, 20 Nov. 2014
2. "Progress toward Harmonization of EV Interoperability Requirements in Europe and the US", Publication by K. Hardy, H. Scholz (JRC-IET), D. Dobrzynski, A. Lajtkep (BMW) and W. Selle (Ford), European Electric Vehicle Congress, Brussels, 5 Dec. 2014
3. "Harmonization of Standards, Technology and Testing, EV-Smart Grid Interoperability Centers in Europe and the U.S.", K. Hardy, J. Harper and D. Dobrzynski, Presentation to the Global InterOP/Golden Test Device Workshop, Wolfsburg, 9 Dec. 2014.
4. "E-mobility ... Perspectives, Challenges and Globalization", K. Hardy, Presentation at the US Embassy-sponsored US-Germany Symposium, Die Stadt der Zukunft – Die Zukunft der Stadt, Konrad Adenauer Stiftung, Amerikazentrum Hamburg, GE, 18 February 2015
5. "EV-Smart Grid Interoperability Centers ... Progress and Potential", K. Hardy, Presentation at the US-China EV and Battery Technology Workshop, Beijing, 30 March 2015
6. "Enabling Technologies and Standards for V2X and EV Interoperability", Presentation to the IEA-HEV Task 28, Expert Workshop 'V2X Technologies and the Power System', K. Hardy, Bern University of Applied Sciences, Burgdorf, Switzerland, 15-16 April, 2015
7. "US/EU EV-Smart Grid Interoperability Centers ... Harmonization of PEV standards, technology and test procedures, K. Hardy, Presentation at the 22nd APEC Automotive Dialog, Manila, 22 April 2015
8. "APEC Actions to Promote Widespread Usage of Electric Vehicles: US Proposal for EV Roadmap Template", Presentation at the 22nd APEC Automotive Dialog, Manila, 22 April 2015
9. "US/EU EV-Smart Grid interoperability Centers, Update", K. Hardy, Presentation at the 2nd Meeting of the US-Germany Joint Committee on Science & Technology Cooperation, Washington, DC, 6 May 2015
10. "US/EU EV-Smart Grid Interoperability Centers, Harmonization of PEV standards, technology and test procedures", Presentation to the COTEVOS Industry Summit, K. Hardy, Rome, 25 May 2015
11. "US/EU EV-Smart Grid Interoperability Centers, Progress and Next Steps", K. Hardy, Presentation to the US Mission to the EU, Brussels, 28 May 2015
12. "Multi-Lab EV Smart Grid Integration Requirements Study - Providing Guidance on Technology Development and Demonstration", T. Markel and A. Meintz (NREL), K. Hardy, B. Chen and T. Bohn (ANL), J. Smart, D. Scofield and R. Hovsopian (INL), S. Saxena, J. MacDonald and S. Kilicotte (LBNL), K. Kahl (ORNL), R. Pratt (PNNL), NREL/TP-5400-63963, May 2015.
13. "Towards Standardized Vehicle Grid Integration: Current Status, Challenges, and Next Steps," B. Chen, K.S. Hardy, J.D. Harper, T.P. Bohn, and D.S. Dobrzynski, 2015 IEEE Transportation Electrification Conference & Expo (ITEC'15), Dearborn, MI, June 14-17, 2015.
14. "DC Charging Infrastructure Overview", J. D. Harper, IEEE Transportation Electrification Conference & Expo (ITEC'15), Panel 11: Charging Technology, Logistics, and Infrastructure, Dearborn, MI, June 14-17, 2015
15. "PEV SMART CHARGE MODULE", J.D. Harper, D. Dobrzynski, Submitted Patent, Argonne National Laboratory, IN-14-066.
16. "SAE Charger Emulator Graphical User Interface", J. D. Harper, Copyright 2015, Argonne National Laboratory, SF-14-134.

V.5.D. References

1. "Multi-Lab EV Smart Grid Integration Requirements Study - Providing Guidance on Technology Development and Demonstration", T. Markel and A. Meintz (NREL), K. Hardy, B. Chen and T. Bohn (ANL), J. Smart, D. Scofield and R. Hovsopian (INL), S. Saxena, J. MacDonald and S. Kilicotte (LBNL), K. Kahl (ORNL), R. Pratt (PNNL), NREL/TP-5400-63963, May 2015

2. energy.gov/eere/buildings/volttron
3. nodered.org/
4. wiseharbor.com/pdfs/WiseHarbor%20Spotlight%20Report%201%20Efficacy%202015Aug18.pdf
5. "EV-Smart Grid Interoperability Center in Europe and the US", Presentation to the US-EU Energy Policy Working Group, K. Hardy, Washington and Brussels, 20 Nov. 2014.
6. "US/EU EV-Smart Grid Interoperability Centers, Progress and Next Steps", K. Hardy, Presentation to the US Mission to the EU, Brussels, 28 May 2015
7. Coordination meetings with the German Ministry of Economics and Energy Affairs; the Environmental Innovation and E-mobility Division sponsors the SLAM Project that significantly contributes to Global InterOP; Jan. 2015 (Washington) and Feb. 2015 (Berlin)
8. "E-mobility ... Perspectives, Challenges and Globalization", K. Hardy, Invited presentation at the US Embassy-sponsored US-Germany Symposium, Die Stadt der Zukunft – Die Zukunft der Stadt, Konrad Adenauer Stiftung, Amerikazentrum Hamburg, GE, 18 February 2015
9. "US/EU EV-Smart Grid interoperability Centers, Update", K. Hardy, Invited presentation at the 2nd Meeting of the US-Germany Joint Committee on Science & Technology Cooperation, Washington, DC, 6 May 2015
10. "US/EU EV-Smart Grid Interoperability Centers ... Harmonization of PEV standards, technology and test procedures, 22nd APEC Automotive Dialog, Manila, 22 April 2015
11. "APEC Actions to Promote Widespread Usage of Electric Vehicles: US Proposal for EV Roadmap Template", K. Hardy, 22nd APEC Automotive Dialog, Manila, 22 April 2015
12. energy.gov/articles/launch-grid-modernization-laboratory-consortium
13. netl.doe.gov/File%20Library/Business/solicitations/2016GMLabCall_1.pdf

VI. Vehicle Systems Efficiency Improvements

VI.1. DOE's Effort to Improve Heavy Vehicle Fuel Efficiency through Improved Aerodynamics

Kambiz Salari, Principal Investigator

Lawrence Livermore National Laboratory
7000 East Avenue L-090
Livermore, CA 94551
Phone: (925) 424-4635
Email: salari1@llnl.gov

Lee Slezak, DOE Program Manager

Phone: (202) 586-2335
E-mail: Lee.Slezak@ee.doe.gov

Start Date: 9/01/2014
End Date: 10/30/2018

VI.1.A. Abstract

There are roughly 2.2 million combination trucks on the road today, each traveling an average of 65,000 miles/year and consuming 12,800 gallons of fuel/year for a total of 36 billion gallons of fuel/year. These trucks consume roughly 11-12% of the total United States petroleum usage. At highway speeds, a class 8 tractor-trailer uses over 50% of the usable energy produced by the vehicle engine to overcome aerodynamic drag. To improve the fuel economy of these vehicles Lawrence Livermore National Laboratory (LLNL) has been conducting research on enhanced aerodynamics through the use of add-on devices and new tractor-trailer shape design. LLNL has demonstrated new drag reduction techniques and concepts for tractor-trailers and tanker-trailers. A new body shape design is proposed for the next generation of highly aerodynamic heavy vehicles with geometry, flow, and thermal integration that radically reduces aerodynamic drag and improves fuel efficiency. This project relies extensively on computational simulations and wind tunnel testing for the development of the new integrated aerodynamic body design. For the selected aero devices and concepts additional track and on-the-road tests are performed. An important part of this effort is to join with industry in getting aerodynamic add-on devices on the road and to provide guidance to industry in design of the next generation of highly integrated heavy vehicles.

In collaboration with National Renewable Energy Laboratory (NREL) the fuel saving benefits of heavy vehicles platooning will be investigated. NREL is responsible for track testing part of this activity. NREL has established a process for conducting accurate and objective track evaluations of heavy vehicles platooning.

Objectives

- Provide guidance to industry to improve the fuel economy of class 8 tractor-trailer through the use of aerodynamics
- Develop innovative aerodynamic concepts for heavy vehicles that are operationally and economically sound
- Demonstrate the potential of new drag-reduction concepts
- Design the next generation of an integrated highly aerodynamic tractor-trailers and tanker-trailers
- Establish a database of experimental, computational, and conceptual design information
- In collaboration with NREL investigate the potential fuel savings of heavy trucks platooning

Accomplishments

- Designed a new heavy vehicle body shape for the Next Generation of highly aerodynamic and integrated Class 8 tractor-trailers – Generic Speed Form 1 (GSF1)
- Tested various configurations of aerodynamic add-on devices such as skirts and trailer tails
- Developed aerodynamics fairings to improve fuel economy for tanker-trailers
- Compiled wind tunnel test results for the new tractor-trailer design GSF1 and modified tanker-trailer conducted at NASA Ames Research Facility operated by Army Research Development and Engineering Command



VI.1.B. Technical Discussion

Analysis of GSF1 aerodynamic performance - “Sailing Effect”

We conducted a 1/8th scale wind tunnel study of GSF1 at NASA Ames 7x10 wind tunnel in collaboration with Navistar and the U.S. Army Research, Development and Engineering Command. One of the key observations of this study was the drag behavior of a highly streamlined heavy vehicle model at larger yaw angles (Figure VI-1). With increasing vehicle yaw angles, the drag coefficient of the model rose to a local maximum and then decreased with further increases in the yaw angle (Figure VI-2a). When vehicle underbody skirts were installed, the drag coefficient decreased even further and became negative for yaw angles greater than 22 degrees (Figure VI-2b). This observation is similar to that which Cooper highlighted for a simplified, streamlined heavy vehicle model investigated by the University of Maryland [1]. For that configuration, the streamlined model was fully skirted with no ground clearance and had an extended boattail that was tapered on the sides. At a yaw angle of 20 degrees, the vehicle also had a drag coefficient of zero, which indicated that the model was beginning to sail.

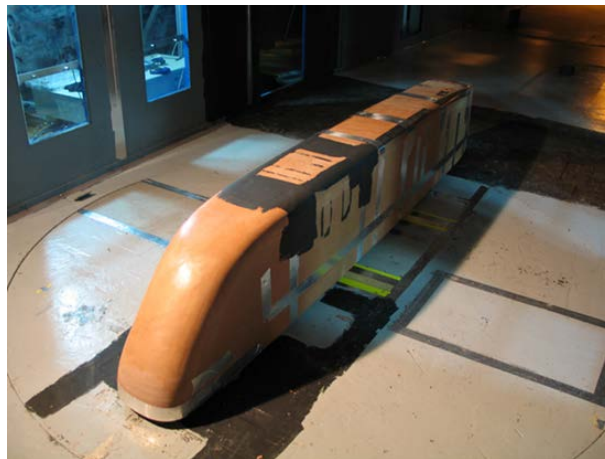


Figure VI-1: GSF1 1/8 scale wind tunnel model in the NASA Ames 7×10 wind tunnel.

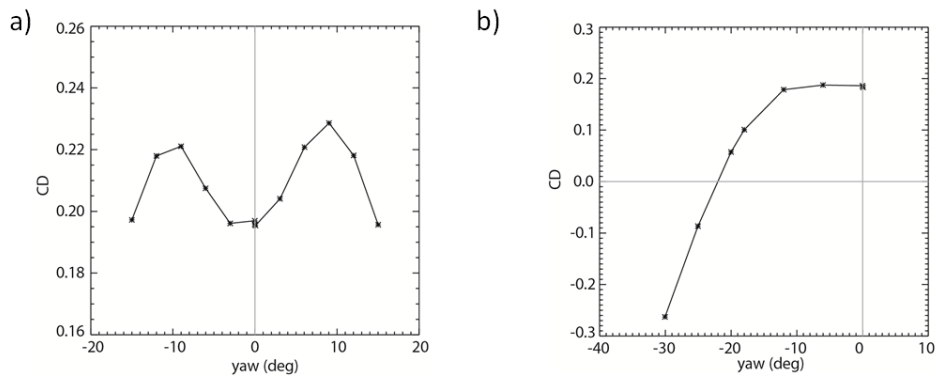


Figure VI-2: Drag coefficient as a function of yaw angle for the streamlined heavy vehicle in Figure VI-1 a) without and b) with skirts.

We further investigated this “sailing effect” phenomena using computational fluid dynamics (CFD) at highway speed in a 15 degree crosswind. There were two important findings from this study. The first was that a streamlined heavy vehicle benefits from having a boattail that is longer than that typically placed on conventional heavy vehicles today. For example, the drag coefficient decreased from 0.052 to 0.003 when the boattail length was increased from 42” (Figure VI-3a) to 138” (Figure VI-3b). Furthermore, the longer boattail almost entirely eliminated the presence of the vehicle wake (Figure VI-3c-Figure VI-3d). This behavior is unlike that of a conventional heavy vehicle, in which boattails longer than approximately 20” have minimal impact on reducing the aerodynamic drag [2]. The second important finding was that the drag coefficient continues to decrease for boattail deflection angles greater than the optimum deflection angle (~ 11 to 15 deg) for conventional heavy vehicles (Figure VI-4). Both of these findings indicate that the industry rules of thumb that have been established for heavy vehicles do not necessarily apply to streamlined heavy vehicles. As a result, further study is required to better understand the “sailing effect” and its implications upon the design of next-generation heavy vehicles.

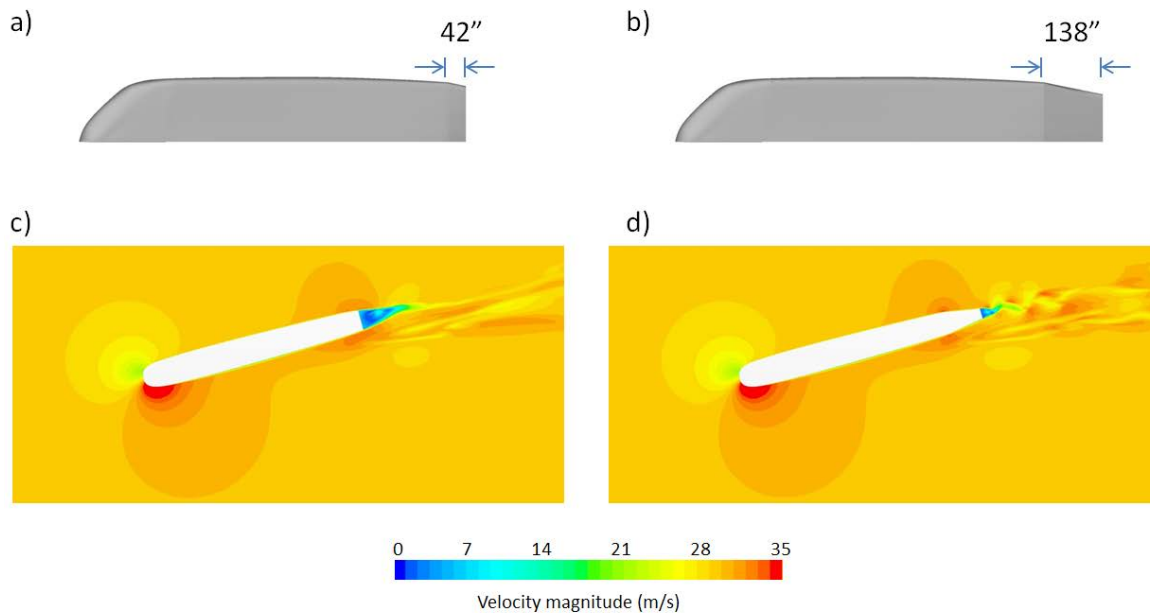


Figure VI-3: Streamlined heavy vehicle geometry at 15 degrees yaw with a) 42" and b) 138" boattail. c-d) Corresponding velocity magnitude contours.

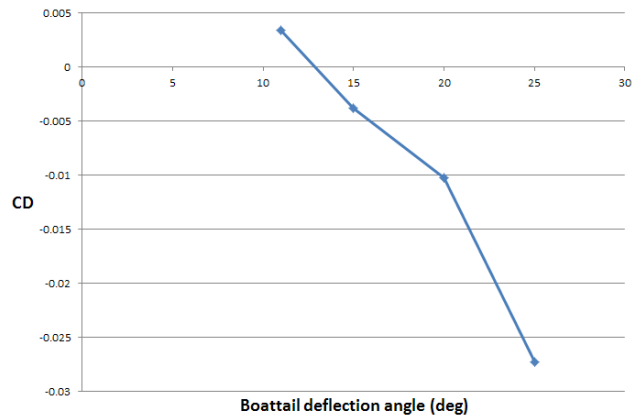


Figure VI-4: Drag coefficient as a function of boattail angle for a streamlined heavy vehicle at 15 degrees yaw.

Particle Image Velocimetry Data Analysis

An extensive, high-resolution 3D particle image velocimetry (PIV) dataset was analyzed in the wake of a 1/8th scale heavy vehicle with and without a trailer boattail (Figure VI-5). The experimental setup (Figure VI-6) is comprised of a horizontal laser sheet formed by two lasers located on each side of the wind tunnel. Two cameras are positioned above the lasers to image the region in the vehicle wake. A theatrical smoke system is used to seed the flow within the wind tunnel, thereby making the laser sheet visible to the cameras. Since the two cameras provide a stereoscopic view of the sheet, all three flow velocity components are acquired. To measure the velocity field at various horizontal planes (Figure VI-7), the laser optics are attached to a vertical traverse system. From the PIV data, velocity field data is acquired, highlighting the changes in the wake structure when a trailer boattail is installed (Figure VI-8-Figure VI-9). This data will subsequently be used to computational fluid dynamics (CFD) code validation.



Figure VI-5: Heavy vehicle model (1/8th scale) in the NASA Ames 7x10 wind tunnel.

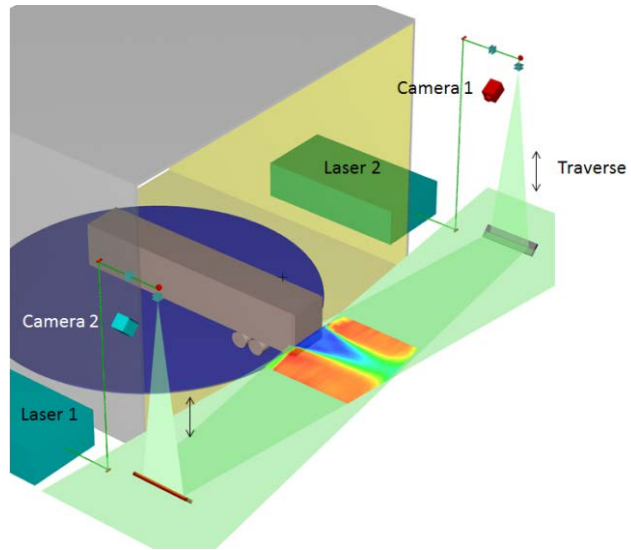


Figure VI-6: Experimental setup for the PIV system in the NASA Ames 7x10 wind tunnel.

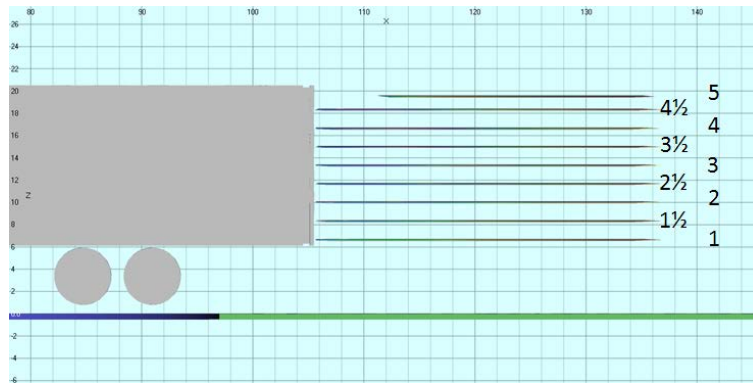


Figure VI-7: Locations of the horizontal PIV imaging planes in the heavy vehicle wake.

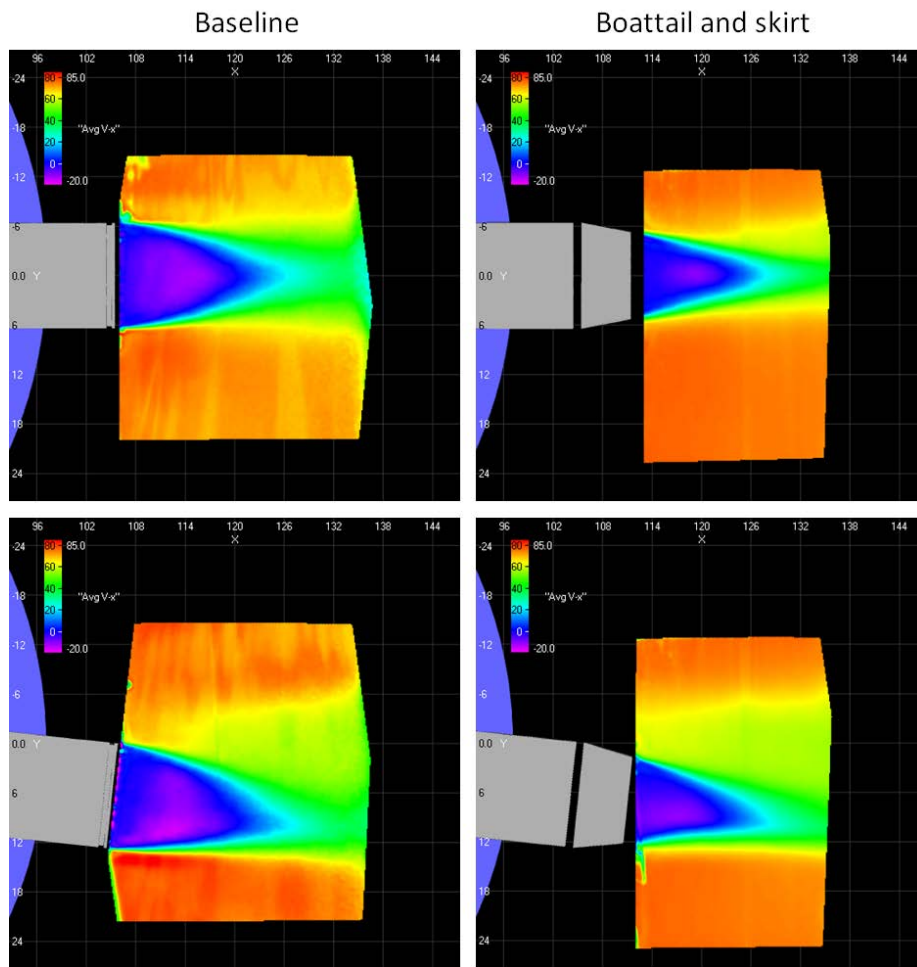


Figure VI-8 Time-averaged velocity magnitude at the mid-height of the trailer at 0 deg (top) and 6 deg (bottom) yaw.

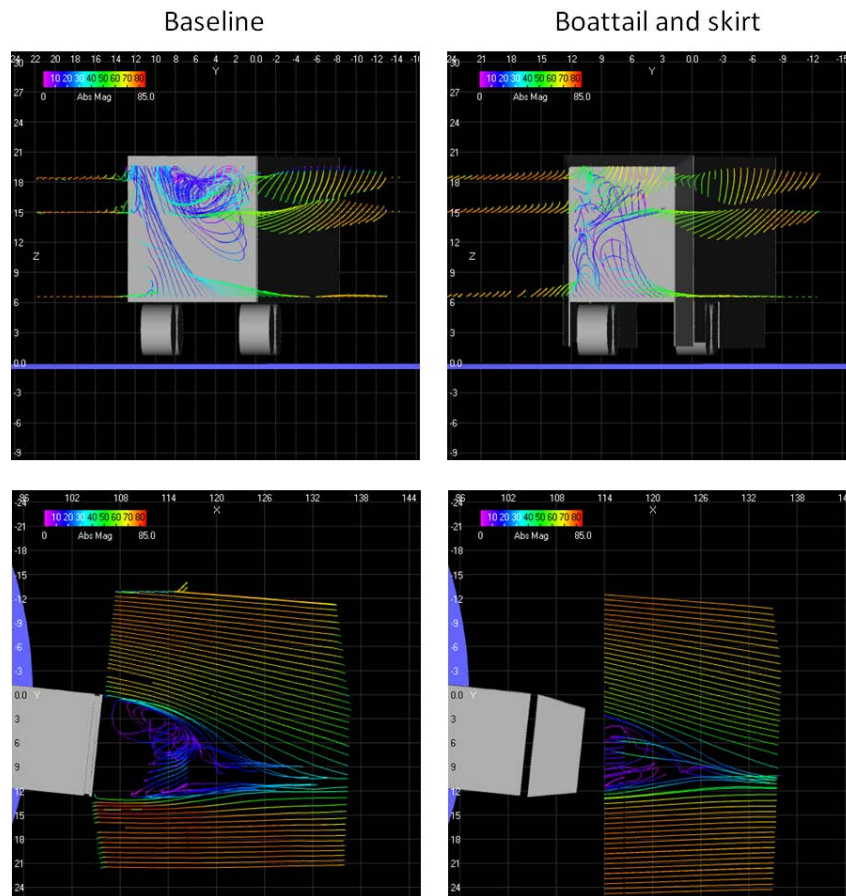


Figure VI-9: Time-averaged velocity streamlines in the trailer wake at 6 deg yaw.

Platooning Heavy Vehicles

Previous studies have shown that a platoon of heavy vehicles results in a decrease in the average drag coefficient across the individual vehicles in the platoon [3-6]. However, the close spacing between the vehicles reduces the amount of cooling flow provided to the radiator, thus requiring the engine fan to operate. This, in turn, reduces the engine fuel efficiency. To better understand the impact of the vehicle spacing upon both the average drag coefficient and the engine cooling flow, we will be conducting a wind tunnel study at NASA Ames in September 2015 on a 1/50th scale heavy vehicle platoon. In preparation for this study, we have designed the splitter plate and load-cell systems for a three-vehicle platoon outfitted with trailer skirts (Figure VI-10). The splitter plate positions the platoon above the tunnel floor, thereby reducing the boundary layer thickness in the vicinity of the model platoon. Each vehicle is mounted on a linear bearing that is attached to a load-cell for making drag force measurements at various vehicle spacings (Figure VI-11). The amount of cooling flow provided to engine is estimated by means of a pressure port mounted on the grill of each model. Through these force and pressure measurements, we will obtain an optimal vehicle spacing for both aerodynamic drag reduction and engine cooling efficiency.

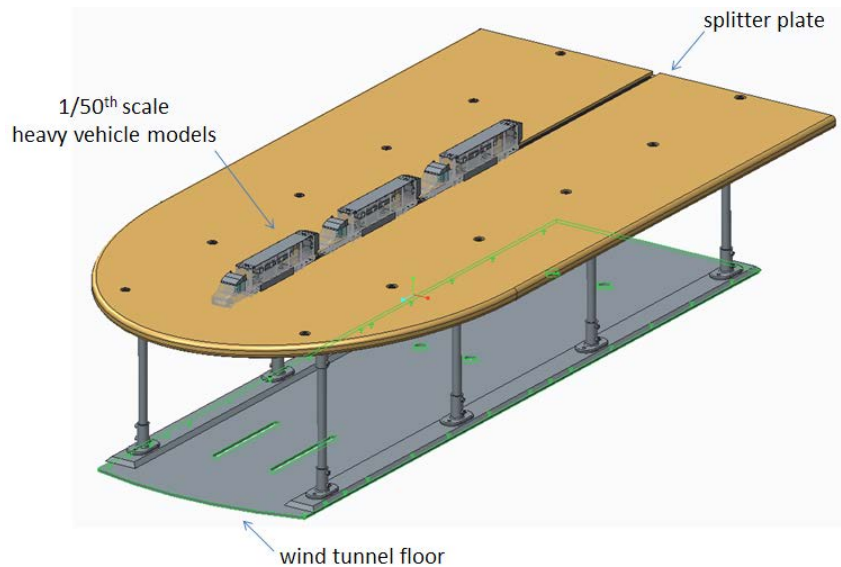


Figure VI-10: Model heavy vehicle platoon (1/50th scale) and splitter plate design.

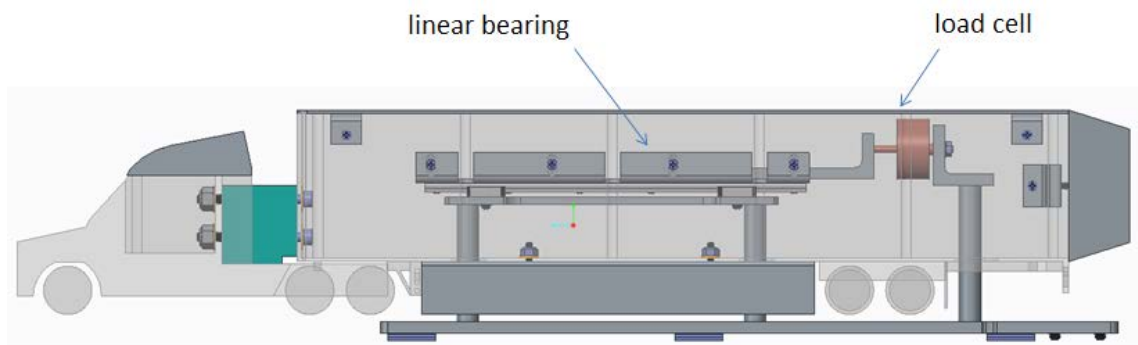


Figure VI-11: Internal details of the 1/50th scale platoon model.

VI.1.C. References

1. Sherwood, A.W. Wind Tunnel Test of Trailmobile Trailers. University of Maryland Wind Tunnel Report No. 85. College Park, MD, April 1974.
2. Cooper, K.R. Truck Aerodynamics Reborn--Lessons from the Past. SAE Technical Paper Series 2003-01-3376, 2003.
3. Lammert, M., Duran, A., Diez, J., Burton, K. et al., Effect of Platooning on Fuel Consumption of Class 8 Vehicles Over a Range of Speeds, Following Distances, and Mass, SAE Int. J. Commer. Veh. 7(2):2014, doi:10.4271/2014-01-2438.
4. Browand, F., Zabat, M. Tokumaru, P. Aerodynamic Benefits from Close-Following. In Ioannou, P.A. (Ed.) Automated Highway Systems, Plenum Press, NY, 1997.
5. Shladover, S.E., et al. Demonstration of Automated Heavy-Duty Vehicles, California PATH Research Report UCB-ITS-PRR-2005-23, June 2005.
6. Browand, F., Radovich, C., Boivin, M. Fuel Savings by Means of Flaps Attached to the Base of a Trailer: Field Test Results. SAE Paper 2005-01-1016, 2005.

VI.2. DOE/DOD Parasitic Energy Loss Collaboration

George Fenske, Principal Investigator

Aaron Matthews (Aerotek), Nicholaos Demas, Robert Erck, Co-Investigators

Argonne National Laboratory

9700 S. Cass Avenue

Argonne, IL 60439

Phone: (630) 252-5190

E-mail: gfenske@anl.gov

Ricardo, Inc., CRADA Contact

Lee Slezak, DOE Program Manager

Phone: (202) 586-2335

E-mail: lee.slezak@ee.doe.gov

Start Date: August 2012

End Date: March 2016

VI.2.A. Abstract

Objectives

- Develop a web-based tool kit based on friction mean effective pressure (FMEP) maps to predict the impact of key tribological engine parameters on vehicle fuel economy.
- Develop a high-fidelity database on key tribological parameters (boundary friction) for use in a tool kit for identifying low-friction solutions.

Accomplishments

- Completed a parametric study of a combustion chamber FMEP as a function of engine load (indicated mean effective pressure) and speed for a small spark-ignited engine.
- Developed engine three-dimensional (3-D) finite element models of power cylinder components for a medium-sized diesel engine.
- Analyzed FMEP simulation data using a linear-regression approach to develop an analytical tool that will predict FMEP and fuel consumption scaling factors as functions of load, speed, and lubrication properties.
- Completed a preliminary parametric study of asperity friction for commercial and advanced friction modifiers.

Future Achievements

- Complete development of a web-based tool kit to predict the impact of lubricant properties on fuel consumption in a heavy duty diesel engine (HDDE).



VI.2.B. Technical Discussion

Background

Multiple approaches are being pursued to improve the fuel economy of vehicles, including the development of advanced tribological systems involving lubricants, materials, coatings, and engineered surfaces to reduce

parasitic friction losses in engines (and drivelines). This project focuses on the development of a user friendly, web-based calculator to predict the impact of tribological parameters such as the boundary friction coefficient, lubricant viscosity, temperature, surface finish, speed, load, and visco-piezo properties on the fuel economy of engines typically used for ground transportation vehicles.

Introduction

Friction, wear, and lubrication affect fuel economy, durability, and emissions of engines used in ground transportation vehicles. Total frictional losses alone, in typical engines, may account for more than 10% of the total fuel energy (depending on the engine size, driving conditions, etc.). The amount of emissions produced by these engines is related to the fuel economy of each specific engine. In general, the higher the fuel economy, the lower the emissions. Higher fuel economy and lower emissions in future diesel engines may be achieved by the development and widespread use of novel materials, lubricants, and coatings. For example, with increased use of lower viscosity oils (that also contain lower amounts of sulfur- and phosphorus-bearing additives), the fuel economy and environmental performance of future engine systems can be dramatically improved. Furthermore, with the development and increased use of smart surface engineering and coating technologies, even higher fuel economy and better environmental soundness are feasible.

The main goal of this project is to use advanced models of engine-component friction and contact loading to predict the impacts of advanced surface engineering technologies (e.g., near frictionless carbon and superhard coatings) and energy-conserving lubricant additives on parasitic energy losses from diesel engine components. The project also aims to develop more realistic databases on the boundary or asperity friction that are used in advanced codes to predict total (asperity and hydrodynamic) friction losses and, in the future, to validate the predictions in tests using fired engines. Such information will help to identify critical engine components that can benefit the most from the use of novel surface technologies, especially when low-viscosity engine oils are used to maximize the fuel economy of these engines by reducing churning and/or hydrodynamic losses. The long-term objective of the project is to develop a database that provides a “look-up” capability to predict the impact of lubricant viscosity, asperity friction, surface finish on FMEP, and contact severity at different engine operating modes.

Approach

Under the Argonne/Ricardo cooperative research and development agreement (CRADA), multiple codes (PISDYN, RINGPAK, VALVDYN, and ENGDYN) were used to calculate from first principles the parasitic friction losses (FMEP) under prescribed engine conditions (load and speed) for a range of tribological parameters (asperity friction, lubricant viscosity). The results for a large diesel engine were analyzed to determine the dependence of asperity and hydrodynamic FMEP as a function of load, speed, viscosity, and asperity friction. Linear regression trends of FMEP were developed to predict FMEP difference maps and fuel consumption scaling factors. A regression was developed to calculate changes in FMEP and fuel consumption scaling factors (FCSFs) to predict changes in fuel consumption for different driving cycles.

Our primary task for this project was to perform FMEP calculations for a broad range of parameters including engine type [spark ignition (SI) or compression ignition (CI)], engine size, engine mode (speed and load), lubricant viscosity, asperity friction, surface finish, oil type (mineral or synthetic), and additive (friction modifier), as discussed previously [1–3]. The actual analysis was limited to a large diesel engine and it included both load and speed dependencies as well as lubricant viscosity and speed.

The approach used in this project to predict the impact in fuel consumption for arbitrary drive cycles (engine load and speed) for different lubrication conditions (viscosity and asperity friction) is based on the use of FMEP difference maps to calculate FCSFs, which together with fuel consumption maps and weighted drive factors, can be used to predict fuel consumption. The FMEP simulations were used to calculate FMEP for arbitrary conditions of load, speed, viscosity, and asperity friction. The fuel consumption rate for a given load, speed, viscosity, and asperity friction can be predicted using the FCSFs and known fuel consumption rates (as a function of load and speed) for a baseline case (e.g., 40WT oil, 0% reduction in asperity friction). Changes in the drive cycle are also used to weight the contributions for an arbitrary drive cycle.

Results

A suite of software codes developed by Ricardo, Inc. were used to model engine friction losses. The codes and components that were modeled include:

- PISDYN—a 3-D simulation code that predicts the dynamic motion of the piston and connecting rod assembly. Code used to predict friction losses between the piston skirt and liner as well as friction losses in the wrist pin.
- RINGPAK—a two-dimensional (2-D) simulation code that predicts ring pack dynamics, lubrication, and gas flow. Code used to predict friction losses between individual rings (top, second, and oil control) and liner, and also between rings and pistons (ring grooves).
- ENGDYN—a 3-D simulation code used to model the dynamic behavior of the crank train, engine structure, bearings, connecting rod, and engine mounts. Code was used to predict friction losses in the main bearings and in connecting rod large-end bearings.
- VALDYN—a simulation code that models the dynamic and kinematic responses of valvetrain components (drive chain, gears, valves, springs, etc.). Code was used to predict friction losses in the valve train system.

Approximately 200 case studies [4–6] were performed and analyzed for components typical of a large compression engine (9–12 L displacement). To model the impact of lubricant viscosity and boundary friction on overall engine friction, case runs were performed for 6 different viscosities (ranging from 3.9 cSt to 18.5 cSt @ 100°C) and 4 asperity friction levels (ranging from baseline to 30, 60, and 90% reduction from baseline). Table VI-1 summarizes the component interfaces modeled in these studies, the codes used for the simulations, the types of friction models (detailed hydro + boundary, or, a simple, i.e. a constant friction coefficient), and the baseline friction coefficient used for each component.

Table VI-1: Components modeled, code, friction model, and baseline friction coefficients used in calculations [4]

Component Interface	Code	Baseline Asperity Friction	Model
Rings/Liner	RINGPAK	0.12	Hydro/Boundary
Piston Skirt	PISDYN	0.08	Hydro/Boundary
Piston Pin — Piston	PISDYN	0.08	Hydro/Boundary
ConRod Small End	ENGDYN	0.12	Hydro/Boundary
ConRod Large End	ENGDYN	0.12	Hydro/Boundary
Main Bearing	ENGDYN	0.12	Hydro/Boundary
Cam-Follower	VALDYN	0.005	Simple/Constant
Cam-Cam Bearing	VALDYN	0.02	Simple/Constant
Rocker Arm — Rocker Support	VALDYN	0.02	Simple/Constant
Pushrod Socket — Pushrod	VALDYN	0.05	Simple/Constant
Rocker Tip — Valve Bridge	VALDYN	0.05	Simple/Constant

Table VI-2 summarizes the viscosity and asperity friction combinations used in the case studies.

Table VI-2: Lubricant viscosity and asperity friction coefficients used in calculations [5]

Lubricant Viscosity (cSt @ 100oC)	Asperity Friction Coefficient Reduction (Relative to Baseline)
--------------------------------------	---

3.9 (5WT)	0%, 30%, 60%, 90%
4.8 (10WT)	0%, 30%, 60%, 90%
8.5 (20WT)	0%, 30%, 60%, 90%
10.5 (30WT)	0%, 30%, 60%, 90%
14.5 (40WT)	0%, 30%, 60%, 90%
18.5 (50WT)	0%, 30%, 60%, 90%

For each of the 24 (viscosity and asperity friction combinations) cases studies, calculations were performed at 8 separate engine speed and/or load conditions. Figure VI-12 shows the speed and/or load points for the different modes used for the large bore diesel engine.

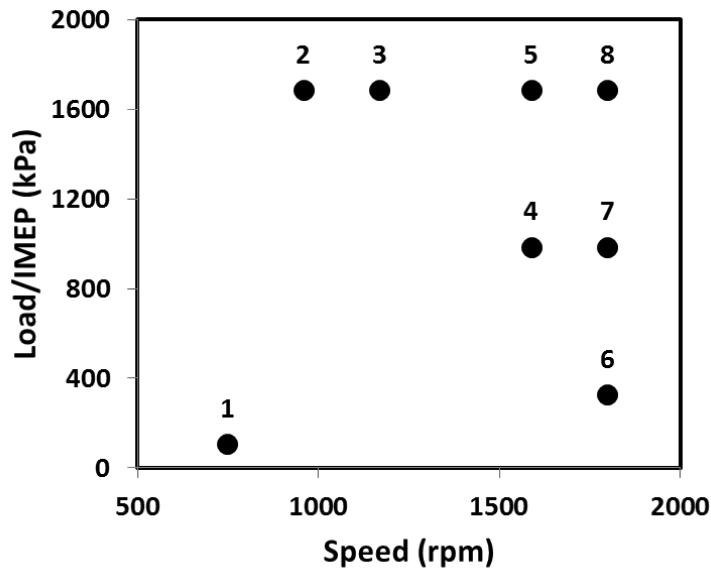


Figure VI-12: Location of eight load and/or speed locations used in the simulations

For each case, friction forces (N) and friction power (W) were calculated as a function of crank-angle (720°). Crank-angle-averaged values of the friction power losses were normalized to the speed and displacement using the concept of mean effective pressure (mep) where:

$$\text{mep (Pa)} \equiv (P \times n_c) / (V_d \times N) \quad \text{eq. 1}$$

Where:

P = Power (W)

n_c = number of revolutions per stroke (= 2 for a 4-stroke)

V_d = displacement volume (in cubic meters), and

N = speed (in revolutions per second)

The end result of the simulations of the friction losses was a series of tabulated values of FMEP data arising from hydrodynamic losses (i.e., viscous shear losses in the oil) and FMEP arising from asperity interactions ('metal-metal' contact between asperities).

Analysis of FMEP Trends: Results of the 200 case studies were analyzed to develop linear regressions to calculate the FMEP as a function of key critical parameters: engine load (IMEP – kPa), engine speed (rpm),

lubricant viscosity (kinematic viscosity at 100oC, and asperity friction reduction). Graphical analysis of the hydrodynamic and asperity FMEP data suggests the FMEP can be modeled using one of the following models:

$$\text{Linear Trend} \quad FMEP = y_0 + a \cdot \eta \quad \text{eq. 2}$$

where ‘y0’ and ‘a’ are linear regression coefficients and η is the kinematic viscosity

$$\text{Exponential Decay} \quad FMEP = y_0 + a \cdot [\exp]^{(-b \cdot \eta)} \quad \text{eq. 3}$$

where ‘y0’, ‘a’, and ‘b’ are linear regression coefficients and η is the kinematic viscosity

Figure VI-13 shows an example of the trends that were observed for the skirt and/or linear simulations for the baseline friction coefficients given in Table VI-1.

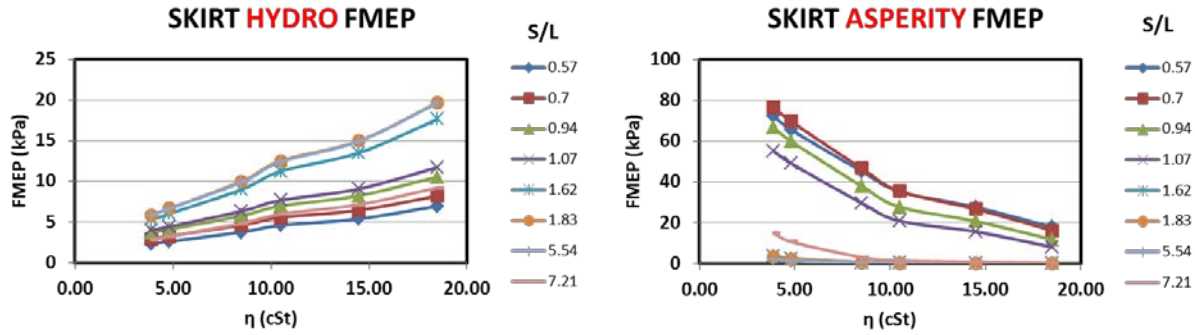


Figure VI-13: Calculated FMEP for the skirt and/or liner interface of a large diesel engine as a function of viscosity for different operating modes (Speed/Load)

For a given engine mode (e.g., speed and load), the hydrodynamic FMEP follows a linear trend with viscosity, while the asperity FMEP follows an exponential decay trend. The values of the regression coefficients (y_0 , a , and b) are dependent on the engine speed and load, which were in turn fitted to one of two regression trends:

$$\text{Cubic Trend:} \quad y_0 = y_0^i + y_0^{ii} \left(\frac{S}{L}\right) + y_0^{iii} \left(\frac{S}{L}\right)^2 + y_0^{iv} \left(\frac{S}{L}\right)^3 \quad \text{eq. 4}$$

where y_0^i , y_0^{ii} , y_0^{iii} , and y_0^{iv} are linear regression coefficients to the different y_0 values for different (S/L) values, and (S/L) is speed (rpm) and load (kPa). Similar regression coefficients for a and b , i.e.,:

$$a = a^i + a^{ii} \left(\frac{S}{L}\right) + a^{iii} \left(\frac{S}{L}\right)^2 + a^{iv} \left(\frac{S}{L}\right)^3 \quad \text{eq. 5}$$

$$b = b^i + b^{ii} \left(\frac{S}{L}\right) + b^{iii} \left(\frac{S}{L}\right)^2 + b^{iv} \left(\frac{S}{L}\right)^3 \quad \text{eq. 6}$$

$$\text{Polynomial Trend:} \quad y_0 = y_0^i + y_0^{ii} S + y_0^{iii} L + y_0^{iv} S^2 + y_0^v L^2 \quad \text{eq. 7}$$

where y_0^i , y_0^{ii} , y_0^{iii} , y_0^{iv} , and y_0^v are linear regression coefficients to the different y_0 values for different engine modes (S, L). Similar regression coefficients for a and b were determined, i.e.,:

$$a = a^i + a^{ii} S + a^{iii} L + a^{iv} S^2 + a^v L^2 \quad \text{eq. 8}$$

$$b = b^i + b^{ii} S + b^{iii} L + b^{iv} S^2 + b^v L^2 \quad \text{eq. 9}$$

Using regression coefficients derived from the 200 case runs, individual contributions to the asperity and hydrodynamic FMEP for the 6 different engine components can be predicted as functions of load, speed, and viscosity for the baseline friction coefficient using eqs. 2 through 9. The total FMEP, FMEP_t is the sum of the hydrodynamic FMEP, FMEP_h and asperity FMEP, FMEP_a:

$$FMEP_t = FMEP_h + BFR * FMEP_{a,1} \quad \text{eq. 10}$$

where BFR (boundary friction reduction) is the reduction (or increase) in the asperity friction (i.e., a 90% reduction in asperity friction corresponds to a BFR of 0.1, while a 60% increase in asperity friction corresponds to a BFR of 1.6), and $FMEP_{a,1}$ refers to the $FMEP_a$ for the baseline friction coefficients.

The difference in FMEP, $\Delta FMEP$, relative to a baseline case was used to predict the change in fuel consumed to produce the same required BMEP.

Fuel consumption scaling factors, FCSFs, were calculated using the following relationship:

$$FCSF \equiv (IMEP + \Delta FMEP)/IMEP \quad \text{eq. 11}$$

where

$$\Delta FMEP = FMEP_{\text{case}} - FMEP_{\text{reference}} \quad \text{eq. 12}$$

where $FMEP_{\text{reference}}$, and $FMEP_{\text{case}}$ refer to the FMEP values for the reference (e.g., 40WT, 0% BFR) and case conditions (e.g., 20 WT, 90% BFR), respectively. Figure VI-14 shows an example of the calculations for two cases relative to an SAE 40WT, 0% BFR reference map: a) yellow mesh — SAE 20WT relative to an SAE 40WT oil and b) Black mesh — SAE 20WT, 90% reduction in asperity friction relative to an SAE 40WT oil with baseline friction.

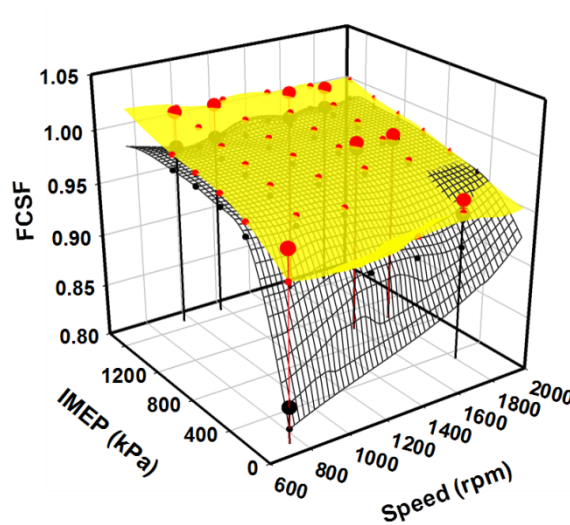


Figure VI-14: FCSF maps for a 20 WT, 0% BFR (yellow) and 20 WT, 90% BFR (black mesh) oil relative to a baseline oil (40 WT, 0% BFR)

CSF maps, such as those shown in Figure VI-14, together with fuel consumption data and/or maps (kgs fuel burned per hr. as functions of load and speed), and appropriate drive cycle weighting factors were used to calculate changes in fuel consumption relative to a specified reference case. Figure VI-15 illustrates the application of this approach for a reference case of an SAE 40WT oil with the baseline asperity friction data in Table VI-1.

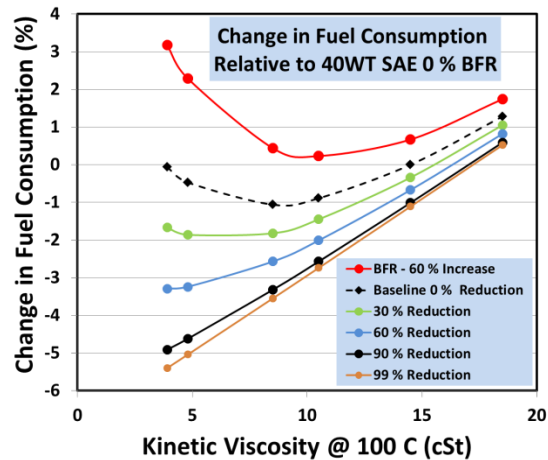


Figure VI-15: Predicted change in fuel consumption for a large diesel engine as functions of oil viscosity and asperity friction reduction

The results in Figure VI-15 show several trends:

- For the baseline viscosity, 40WT, reducing or eliminating all asperity friction will reduce fuel consumption by approximately 1%
- Reducing viscosity alone (e.g., no reduction in asperity friction) will reduce fuel consumption no more than 1%
- Reducing both viscosity and asperity friction together can achieve significantly greater savings in fuel consumption.
- It should be noted that these trends only address the impact of viscosity and asperity friction on fuel consumption for a large bore HDDE and do not consider the impact of low viscosity fluids on component reliability and durability.

Conclusions

Linear regression analysis of 200 cases of predicted FMEP contributions from different engine components for different lubricant viscosities and asperity friction coefficients was performed to develop an analytical approach to predict the impact of lubricant viscosity and boundary friction on fuel consumption. Results of the analysis will be incorporated into a web-based spreadsheet and/or tool kit and a final report will be issued during the 1st quarter of 2016.

VI.2.C. Products

Presentations/Publications/Patents

1. Engine Friction Reduction Technologies, G. Fenske, N. Demas, R. Erck, C. Lorenzo-Martin, A. Erdemir, and O. Eryilmaz, U.S. Department of Energy Vehicle Technologies Office Annual Merit Review and Peer Evaluation Meeting, June 11, 2015, Washington, D.C.
2. Modeling the Effect of Parasitic Friction Losses on Fuel Economy, G. Fenske, A. Matthews, and D. Dascalescu, Global Automotive Management Council Emissions 2015, June 23, 2015, Troy, MI.
3. Overview of Automotive Lubrication Research at Argonne National Laboratory, G. Fenske, Global Automotive Management Council Emissions 2015, June 23, 2015, Troy, MI.
4. DOE/DOD Parasitic Energy Loss Collaboration, G. Fenske, A. Matthews, N. Demas, and R. Erck, U.S. Department of Energy Vehicle Technologies Office Annual Merit Review and Peer Evaluation Meeting, June 16–20, 2014, Washington, D.C.

5. Engine Friction Reduction Technologies, G. Fenske, N. Demas, R. Erck, C. Lorenzo-Martin, A. Erdemir, and O. Eryilmaz, U.S. Department of Energy Vehicle Technologies Office Annual Merit Review and Peer Evaluation Meeting, June 16–20, 2014, Washington, D.C.
6. Application of FMPEP maps to model the impact of friction technologies on fuel economy, G. Fenske, A. Matthews, and D. Dascalescu, presentation at 2014 STLE Tribology Frontiers Conference, October 26–28, 2014.

VI.2.D. References

1. G. Fenske, A. Matthews, N. Demas, and R. Erck, “DOE/DOD Parasitic Energy Loss Collaboration,” FY 2014 Annual Progress Report, March 2015.
2. G. Fenske, A. Matthews, N. Demas, and R. Erck, “DOE/DOD Parasitic Energy Loss Collaboration,” FY 2013 Annual Progress Report, DOE/EE-1023.
3. G. Fenske, N. Demas, and R. Erck, “DOE/DOD Parasitic Energy Loss Collaboration,” FY 2012 Annual Progress Report, DOE/EE-0834.
4. I. Fox, T. Torbeck, and W. Brogden, Argonne Engine Friction Study Phase 1 Final Report, ANL-15/12, Sept 2015.
5. I. Fox, T. Torbeck, W. Brogden, Argonne Engine Friction Study Phase 2 Final Report, ANL-15/13, Sept 2015.
6. G. Weller, Final Report on Phase 3 of a Program to Evaluate the Fuel Consumption Effects of Low Friction Coatings in Diesel Engines, ANL-15/14, Sept 2015.

VI.3. Thermal Control through Airside Evaporative Heat Removal

Dileep Singh/Wenhua Yu, Principal Investigator

Argonne National Laboratory
9700 South Cass Avenue
Lemont, IL 60439
Phone: (630) 252-5009; Fax: (630) 252-5568
E-mail: dsingh@anl.gov

Lee Slezak/David Anderson, DOE Program Managers

U.S. Department of Energy
Phone: (202) 586-2335
E-mail: Lee.Slezak@ee.doe.gov

Start Date: October 2012
End Date: September 2016

VI.3.A. Abstract

Objectives

- Explore possibilities of using evaporative cooling in radiator airside heat removal applications.
- Determine potential radiator airside heat removal rate increases using evaporative cooling.
- Determine potential radiator size reductions using evaporative cooling.
- Optimize radiator evaporative fin designs.

Accomplishments

- Developed theoretical models for analyses of radiator airside evaporative cooling.
- Completed detailed calculations to establish the benefits of the concept.
- Conducted numerical simulations for investigations of the air flow effect on water droplets.
- Designed and fabricated an experimental test system simulating the air flow of moving vehicles.
- Conducted experimental tests for investigations of water droplet movement and evaporation on a fluxed and braze-treated surface.

Future Achievements

- Investigate coating or surface treatment methods and materials to generate proper surface tension.
- Conduct experiments for investigating water droplet movement and evaporation on coated or modified surfaces using warm water to account for water temperature effects.
- Design and test a water droplet supply and distribution system.



VI.3.B. Technical Discussion

Background

This project is aimed to explore the possibilities of reducing cooling system size and therefore aerodynamic drag on heavy-duty trucks by using evaporative cooling under extreme temperature, load, and road grade conditions that would be encountered in the United States.

Introduction

Aerodynamic drag is a major contributor to fuel consumption in heavy-duty trucks, especially at highway speeds. Aerodynamic drag, i.e. the resistance to truck's movement through the air, consists of two main components, pressure drag and shear drag. The shear drag for trucks usually is small compared to the pressure drag, and the basic shape of a truck imposes the pressure drag on the vehicle. Typically, a high-pressure zone is created in the front of the tractor due to the stagnation effect, and a low-pressure zone is created in the rear of the truck, both resulting in pressure drag. The frontal shape of the tractor is dictated in a large part by the radiator resulting in a large stagnation area. The method for reducing aerodynamic drag on trucks proposed in this study is to modify the frontal shape of the tractor by using a hybrid radiator-cooling system, a combination of conventional airside finned surface cooling and active evaporative water cooling.

Approach

Figure VI-16b shows the hybrid radiator compared to a conventional radiator of Figure VI-16a. The example hybrid radiator-cooling system shown in Figure VI-16b is similar to the conventional radiator with vertical coolant channels and fins between them on the air side. However, the channels have been extended beyond the fins on the downstream air side of the radiator. Liquid water flows downwards by gravity along the extended surfaces providing evaporative cooling to the engine coolant. In the case of the hybrid radiator, there is a liquid supply and distribution system not shown in Figure VI-16b.

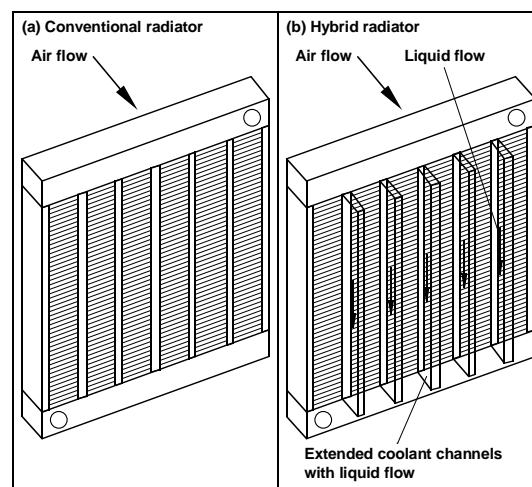


Figure VI-16: Hybrid Radiator System

Figure VI-17 shows a top view of a section of the hybrid radiator. In this schematic, the extended channel surfaces are cooled by evaporating water flowing downwards by gravity into the plane of the figure. The combination of the conventional cooling from the finned surfaces and the evaporative cooling from the extended channel surfaces is the total heat transfer from the radiator to the atmosphere. Under the thermal design condition, both cooling mechanisms would be functioning. However, at most thermal loads below the design condition, only the conventional air-side finned surface cooling would be required. Thus, the active cooling of the water evaporation would be used only at or very near the thermal design condition.

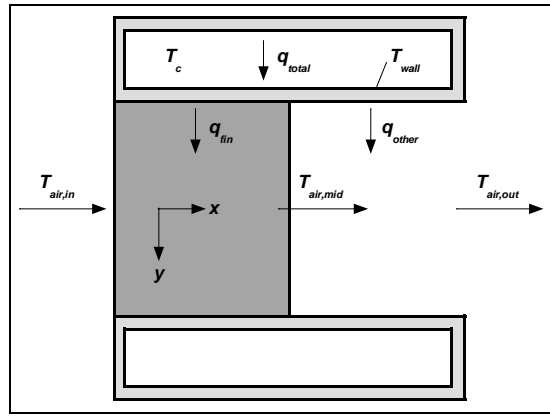


Figure VI-17: Top View of a Section of the Hybrid Radiator

This limited use of the active evaporative cooling component of the hybrid radiator cooling system is important because evaporative cooling requires a supply of water. Using evaporative cooling only at or very near the thermal design condition serves to optimize the parameters of reduced radiator size (or increased maximum radiator heat transfer) and minimized water use/transport.

Results

Heat Transfer Increase

Heat removal rates were calculated from the radiator of Figure VI-16 and Figure VI-17 with a 221.8-kW heat rejection rate and the outside air temperature was fixed at 47°C. The heat removal rate as a function of water consumption rate generated using falling liquid film evaporation is shown in Figure VI-18. It is noted that, at water consumption rates of 76 liter/hour (20 gallon/hour) and 189 liter/hour (50 gallon/hour), the total heat removal rate is increased by 42 kW and 102 kW, respectively, which is equivalent to the heat removal rate increase of 19% and 46%, respectively. A small part of this increase (~3 kW) is due to the increased surface area associated with the coolant channel extensions of the hybrid radiator design. The rest of the sizable increase in the heat removal rate is due to evaporative cooling. At both of these flow rates, the cooling water completely evaporated before reaching the bottom of the radiator.

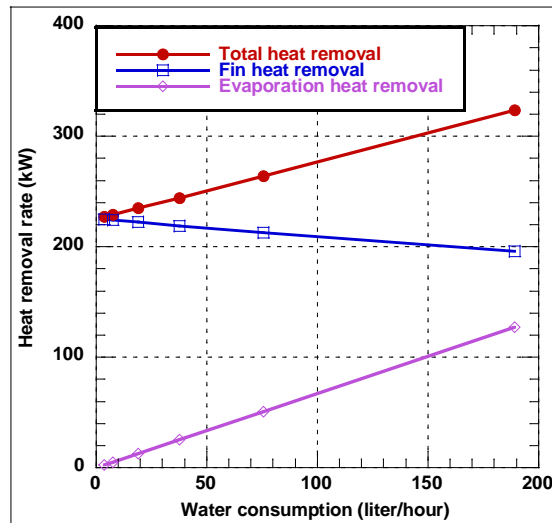


Figure VI-18: Increased Radiator Heat Transfer

Radiator Size Reduction

The results for the radiator width as a function of the water consumption rate, calculated from a thin falling film under the conditions of the engine speed of 1700 rpm with a 221.8-kW heat rejection rate and the outside air temperature of 47°C, are shown in Figure VI-19. The original width of the radiator in this study was 988 mm. It is noted that, at water consumption rates of 76 liter/hour (20 gallon/hour) and 189 liter/hour (50 gallon/hour), the width could be reduced to 778 mm and 478 mm, respectively, which corresponds to radiator frontal area decreases of 21% and 52%, respectively. In each case studied, the film was assumed to completely evaporate before reaching the bottom of the radiator. Using droplets instead of a film will give the same potential for area reduction as long as the droplets completely evaporate. It is also noteworthy to mention that if the frontal area of the tractor were modified, to account for the reduced radiator size that can be achieved by the hybrid cooling system, aerodynamic drag would also be reduced, thereby increasing fuel efficiency.

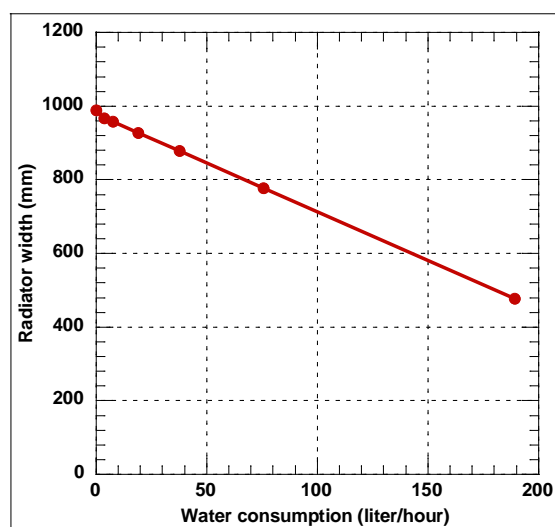


Figure VI-19: Reduced Radiator Size

Radiator Design Optimization

The design condition for truck and automobile radiators usually is the most severe condition possible: the highest air temperature and the steepest road grade. Many vehicles may never encounter such conditions found at places such as Baker Grade in California or Union Pass in Arizona in a hot summer afternoon. A good potential utilization of evaporative cooling is to size the finned portion of the radiator for an alternative design condition corresponding to a steep road grade away from the desert hills. Thus, water for evaporative cooling would be needed only when a vehicle travels through the desert hills under extremely hot conditions. An 11-kilometer (7-mile) stretch of land along Interstate Highway 24 near Monteagle, Tennessee is an example of a steep road grade that could be used for the alternative design condition for the finned portion of the radiator. According to the typical meteorological year for Chattanooga, Tennessee near Monteagle, the highest temperature can reach 37°C. If the radiator were sized at this location with the same coolant temperatures and heat transfer rates, then the radiator could be 22% smaller in width compared to the Baker grade design condition. Thus, on the majority of roads in the United States, the smaller radiator would be sufficient. Under conditions of 47°C and constant full engine power for a long period of time, the water flow rate of approximately 76 liter/hour (20 gallon/hour) would be needed to remove the remainder of the heat. Since it takes less than one hour to traverse 40-kilometer (25-mile) Baker Grade and 48-kilometer (30-mile) Union Pass, the amount of water consumed would be less than 76 liters (20 gallons) for either of them with this example design modification.

Surface Contact Angle Effect

At a 76-liter/hour (20-gallon/hour) flow rate, the actual flow rate on each extended surface of the hybrid radiator is only 0.107 milliliter/s. At this low flow rate, the liquid film across the 20-mm radiator extension surface is only 0.11 mm thick and has a tendency to break up into rivulets or droplets such as streaks. It is

because of this tendency that an analysis was performed with the evaporating liquid film replaced by evaporating discrete droplets falling downwards along the extended radiator channel surfaces. Such droplets have good potential to be maintained at the required thickness. For 100% evaporation of the droplets as they reach the bottom of the radiator, the amount of additional heat transfer using the droplets is similar to that using the falling film.

The droplet evaporation results showed that the thickness of the droplets from the radiator extension surfaces is the most important parameter governing both the evaporation rate of the droplets and the speed at which the droplets travel along the surfaces. As shown in Figure VI-20, the droplet moves downwards under the influence of gravity. By using this model, the droplet evaporation percentage is shown in Figure VI-21 as a function of the initial contact angle (a key factor for the thickness of the droplet). It can be seen that a small droplet contact angle or equivalent a small droplet thickness is necessary for complete evaporation.

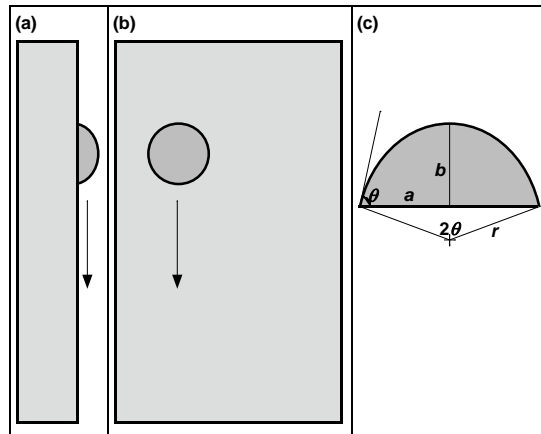


Figure VI-20: Droplet Movement

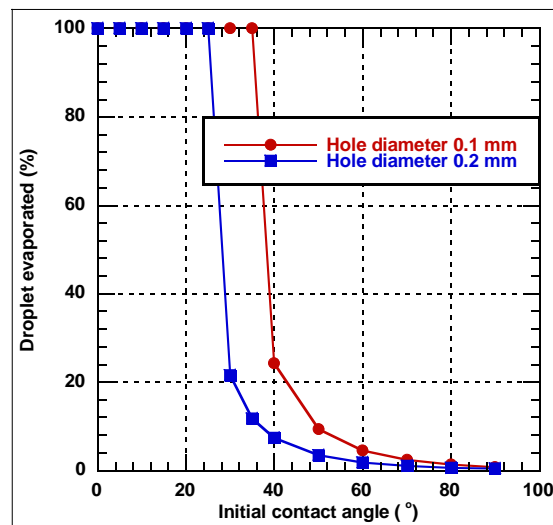


Figure VI-21: Droplet Evaporation

Air Flow Effect on Droplet Movement

For a moving vehicle, the droplet is under the influence of the drag force in addition to gravity. As shown in Figure VI-22, the droplet moves downwards and to the air flow direction during the evaporation process. The droplet movement is depended on the force balance among gravity (F_g), air drag force (F_d), and wall shear force (F_s). These forces and the velocity (u) are related by the following equations for a droplet volume of V

$$\begin{cases} F_d - F_s \frac{\bar{u}_x}{\sqrt{\bar{u}_x^2 + \bar{u}_z^2}} = \rho_w V \frac{d\bar{u}_x}{dt} \\ F_g - F_s \frac{\bar{u}_z}{\sqrt{\bar{u}_x^2 + \bar{u}_z^2}} = \rho_w V \frac{d\bar{u}_z}{dt} \end{cases}$$

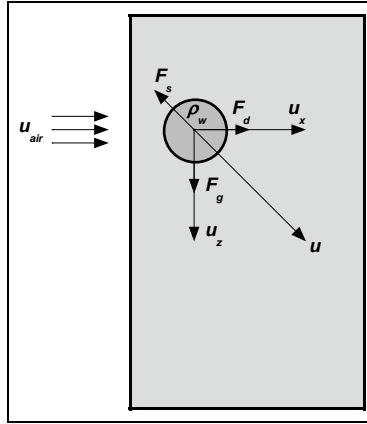


Figure VI-22: Air Flow Effect

To analyze the air flow effect on droplet movement, numerical simulations were conducted using the commercial software COMSOL Multiphysics for various air flow speed and droplet hole size combinations. Figure VI-23, where the evaporation percentage of the droplet is plotted as a function of its initial contact angle, shows an example for an air flow speed of $u_{air}=35$ mph at an extended surface width of 20 mm with the droplet hole sizes of 0.1 mm and 0.2 mm, respectively. As it can be seen from Figure VI-23 that droplets with a small initial contact angle were able to stay on the surface until they completely evaporated. Thus, the droplet generation and surface characteristics of the radiator extension surface must produce a small initial drop thickness for the most efficient operation of the hybrid radiator-cooling system. This condition requires a small droplet size and a small surface contact angle.

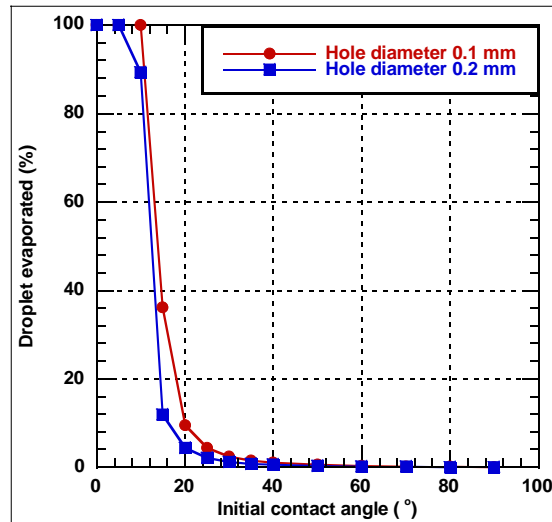


Figure VI-23: Droplet Evaporation with Air Flow Effect

There are several ways to increase the droplet evaporation percentage: (a) larger width of the extended surface, which is usually limited by the available space, (b) frontal extended surface arrangement instead of rear extended surface arrangement, which increases the effective surface width for droplet movement, and (c) smaller surface contact angle, which reduces the air drag force and enhances evaporation. Because the surface

contact angle for the common radiator material 3003 aluminum alloy is about 90°, surface treatment or coating will be necessary to reduce the surface contact angle to acceptable levels. Current technologies are able to attain such levels. Therefore, the third option provides a good potential for generating droplets with small thicknesses and achieving effective evaporative cooling of vehicle engines.

Experimental Test System

The experimental test system, shown graphically in Figure VI-24, was designed and fabricated to investigate the evaporation and movement of droplets under the air flow of moving vehicles. Experiments conducted using this experimental test system can study the effects of the surface contact angle, the initial droplet size, and the air flow velocity on the evaporation and movement of droplets. As shown in Figure VI-23, the experimental test system consists of mainly an enclosed experimental test system housing, a radiator, a fan, an experimental test strip, a droplet dispersing subsystem, a camera, a computer for controlling the droplet dispersing subsystem and for collecting experimental data, and a direct-current power supply (Electronic Measurements, Inc., Model EMHP 40-450-D-11111-0933, not shown in the photograph) for heating the test strip.

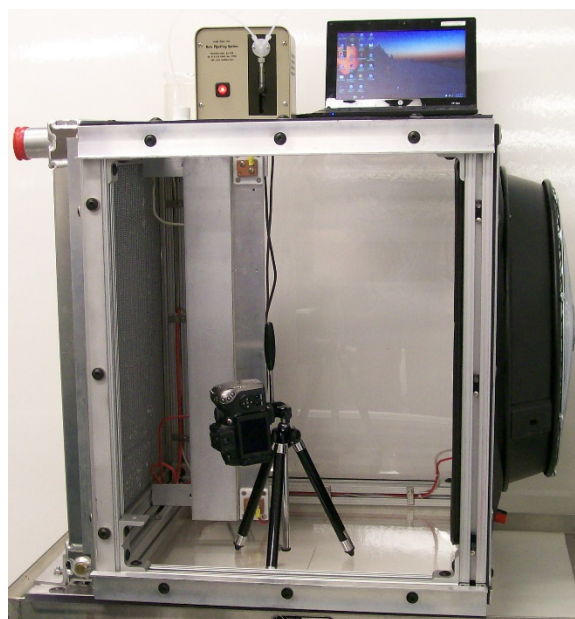


Figure VI-24: Experimental Test System Overview

Experimental Test System Housing

The purpose of the enclosed experimental test housing is to eliminate any air flow effects other than those from the fan. The experimental test system housing consists of two main parts: the frame and the walls. The frame is made from aluminum stock with extended slots on all four sides, which make it easy to mount the radiator, the fan, the walls, and any other necessary components. The walls are made of machinable Lexan sheets for the purpose of easily monitoring experimental tests. The Lexan sheet thickness is 1/2 inch for the base and 1/8 inch for the top and the sides.

Radiator and Fan Assembly

The radiator and fan assembly (Flex-A-Lite, 62180L) was chosen to represent the air flow of heavy-duty vehicles. The radiator and fan assembly was separated and then the radiator and the fan were integrated individually into the experimental test system as two side walls of the experimental test system housing. A fan cover was installed for safety purposes.

Experimental Test Strip

The purpose of the experimental test strip is to simulate the extended surfaces of the hybrid radiator coolant channels. The experimental test strip, shown schematically in Figure VI-25 of its assembly, is made from 24

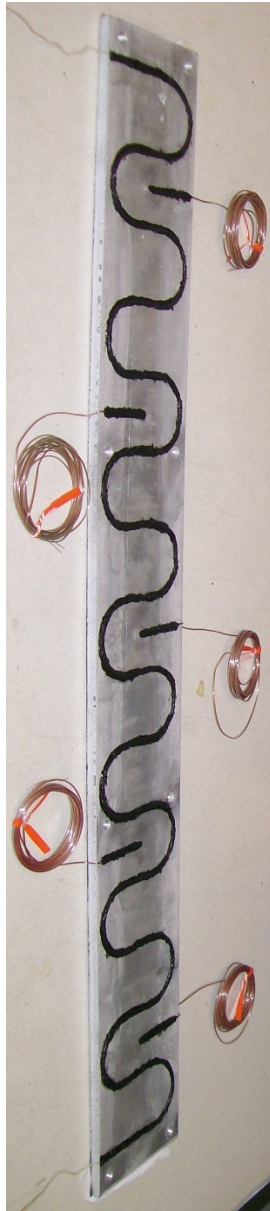


Figure VI-26: Heating Wire and Thermocouples

Droplet Dispersing Subsystem

A goniometer droplet dispensing system from Ramé-Hart is used for delivering droplets for experimental tests. This droplet dispersing system allows for the control of the total dispensed volume and the time interval during which the volume is displaced. While there is no direct control over the droplet size, manipulating the size of the opening tip changes the droplet size. The droplet dispersing process is controlled by Ramé-Hart's Dropimage software. The droplet dispersing head assembly, shown schematically in Figure VI-27, is attached to the top wall of the experimental test system housing and its opening tip height can be adjusted by adding or removing spacing washers.

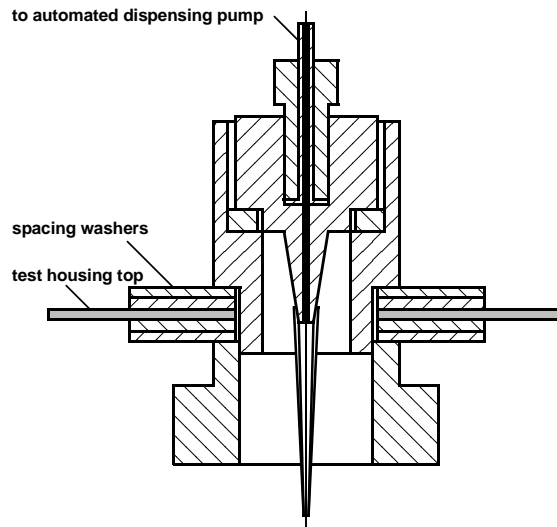


Figure VI-27: Droplet Dispersing Head Assembly

Experimental Tests of Droplet Movement and Evaporation

A series of experimental tests of the droplet movement and evaporation has been conducted on the unheated and heated strip surface to investigate the effects of the radiator fan speed, the droplet size, the strip surface temperature, and the droplet interval. All experimental tests were conducted on the Modine permanently fluxed and braze-treated Al 3003 strip surface.

Radiator Fan Speed Effect on Droplet Movement

Experimental tests were conducted under the following conditions: (a) the droplet tip size of $\sim 380 \mu\text{m}$, (b) the unheated strip surface, and (c) the droplet dispersing system outlet step volume of $20 \mu\text{L}$. The experimental test results are summarized in Table VI-3.

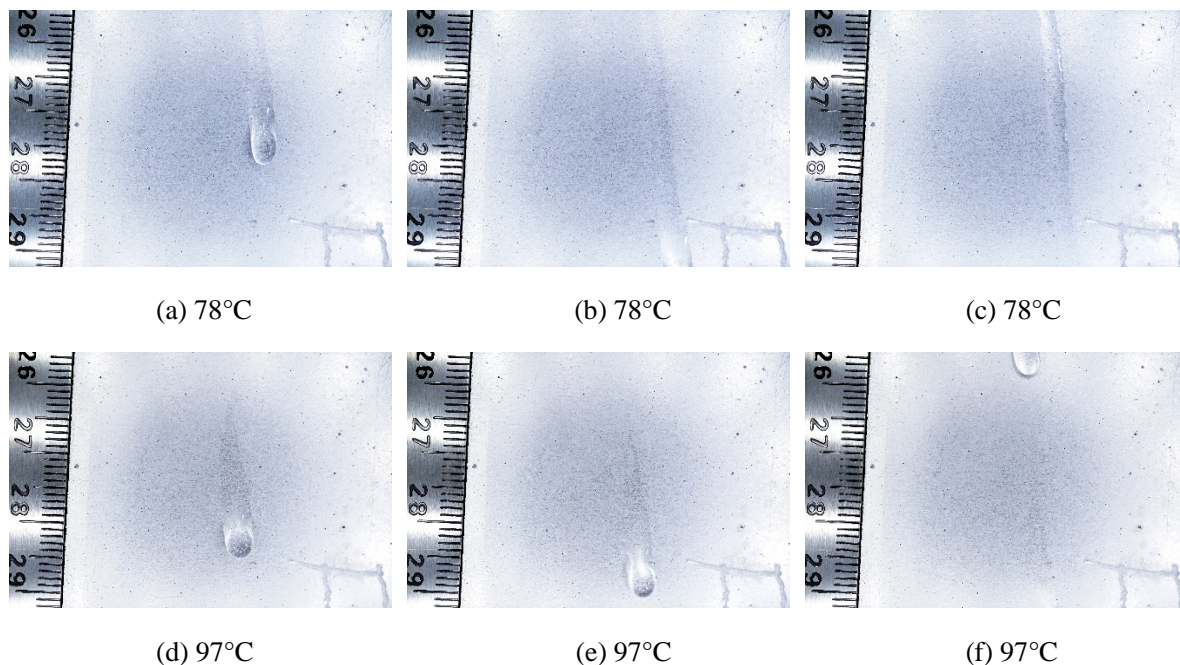
Table VI-3: Radiator Fan Speed Effect on Droplet

Fan Speed (m/s)	Surface Condition	Droplet Movement
0	Dry (without previous drop)	For one or two outlet steps, the droplet stays on the strip top, not moving down. For three outlet steps, the droplet moves fast to about 1/3 distance from the strip top, then slowly moves further, and finally stays on the surface. For more than three outlet steps, the droplet is able to move to the strip bottom.
0	Wet (with previous drops)	For any outlet steps, the droplet moves down along the previous droplet trace and increases the trace thickness.
1.7, 2.6, and 3.4 m/s	Dry and Wet (without/with previous drops)	The droplet moves in a similar way as that without the fan running. There is no significant horizontal drop movement compared to the fan not running. The droplet trace dries faster than that the fan not running.

One of the most important findings of these experimental tests is the insignificant horizontal movement of the droplet under various radiator fan speeds, including the full radiator fan speed. Due to this insignificant horizontal movement, the droplet will not be sheared off the downstream edge of the extended cooling channel surface and will be able to evaporate on the hot surface to remove heat from the radiator. Therefore, this phenomenon is a promising sign for the proposed technology to be used in practical heavy-duty vehicles. The possible reasons for the droplet not moving towards the edge include mainly: (a) the Modine permanently fluxed and braze-treated Al 3003 surface roughness increases the surface tension between the droplet and the surface (which increases resistance to droplet movement) and (b) the elongated droplet shape (drop with film wake/trace on surface), instead of the theorized spherical droplet shape, increases the contact surface area between the droplet and the surface (which also increases resistance to droplet movement) and decreases the thickness of the droplet (which decreases the force of the air flow on the droplet).

Surface Temperature Effect on Droplet Movement and Evaporation

Experimental tests were conducted to investigate the surface temperature effect on the droplet movement and evaporation. Pictures shown in Figure VI-28 were taken at the center location of the surface with a droplet volume of $\sim 73 \mu\text{L}$ at various surface temperatures. Figure VI-28 (a), (b), and (c) are for a surface temperature of 78°C . Figure VI-28 (a) shows the first droplet on the surface, Figure VI-28 (b) shows the same droplet moving downwards leaving a long trace (liquid film) behind, and Figure VI-28 (c) shows a second droplet following the trace left by the first droplet, which increased the trace thickness without forming a separate droplet on the surface. Figure VI-28 (d), (e), (f), and (g) are a continuous sequence of photos (approximately 0.1s apart) taken of two droplets (one following another) for a surface temperature of 97°C . It can be seen from the pictures that the trace left behind by the first droplet, (d) and (e), was short and thin. Therefore, the trace evaporated fast and the second droplet, (f) and (g), following the trace was able to form a separate droplet on the surface. Figure VI-28 (h) shows a droplet on the surface at a temperature of 104°C , which is similar to Figure VI-28 (d) through (g) at 97°C . However, when the surface temperature increased to 106°C in Figure VI-28 (i), in addition to evaporation, the droplet also boiled, which would accelerate the heat removal from the radiator.



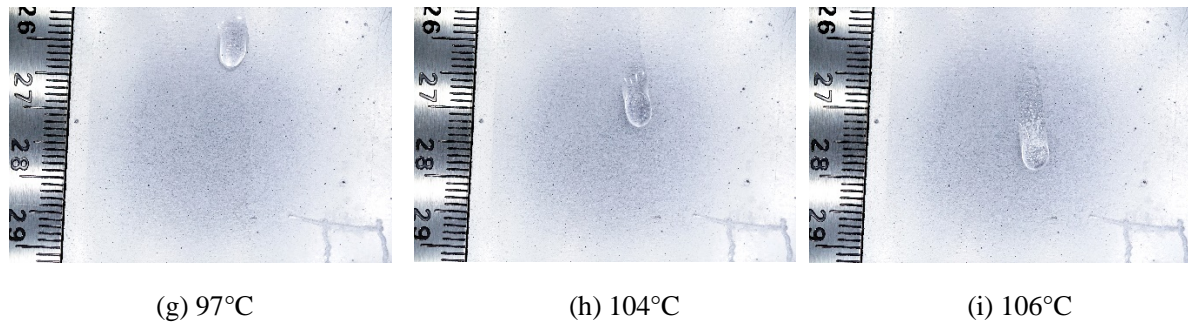


Figure VI-28: Surface Temperature Effect on Droplet Movement and Evaporation

The temperature effect on droplet boiling is shown clearer in Figure VI-29 with close-up views. Figure VI-29 (a) shows a droplet on the surface at a surface temperature of 102°C, and Figure VI-29 (b) shows a close-up view of that droplet. Figure VI-29 (c) shows a close-up view of a droplet on the surface at a surface temperature of 104°C. No boiling was observed when temperatures at and below 104°C. The droplets in figures I-14 (a), (b) and (c) are clear with the surface visible through them. The white dots in a ring on the drops, and downstream in their traces, are reflections from the lighting system used. When the surface temperature increased to 105°C or above, boiling occurred as shown in close-up views in Figure VI-29 (d), (e), and (f). Figure VI-29 (f) is a closer view of (e), and it is seen that bubbles are present in both the drop and trace regions. These tests show that only 5°C wall superheat is required at the onset of nucleate boiling compared to 10°C wall superheat generally required for internal water flows. Although this result must be taken into consideration in the hybrid-radiator optimization process, it does not present a barrier to implementation. In fact, heat transfer and evaporation rates are higher with boiling. Therefore, the occurrence of boiling can be viewed as a positive condition and a conservative situation for cooling the radiator.

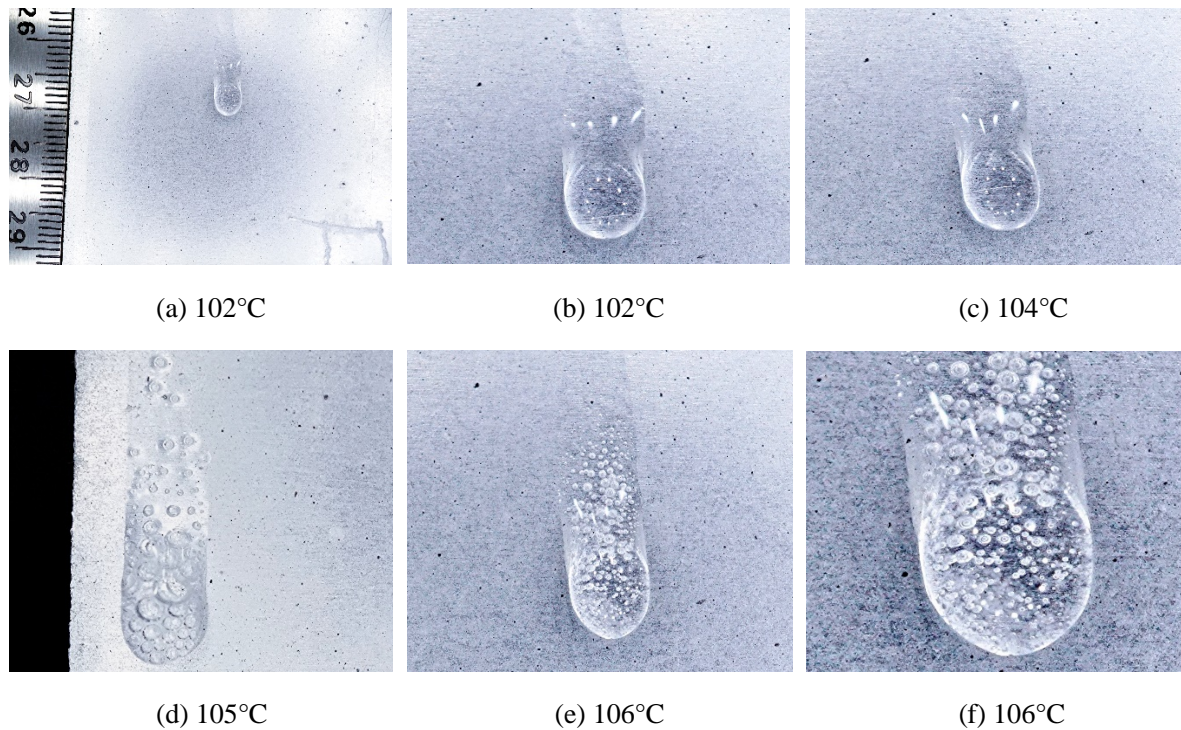


Figure VI-29: Surface Temperature Effect on Droplet Movement and Evaporation (Close-Up View)

Droplet Size Effect on Droplet Movement and Evaporation

Experimental tests were conducted to investigate the droplet size effect on the droplet movement and evaporation. Pictures shown in Figure VI-30 were taken at the bottom location of the surface with a surface temperature of 75°C at various droplet volumes. Figure VI-30, (a), (b), and (c) are for a droplet volume of 73

μL . The droplet on the heated surface became smaller and thinner with time as the droplet moved down the surface and almost completely evaporated upon reaching the bottom as shown sequentially in Figure VI-30 (a), (b), and (c). Figure VI-30 (d) shows two droplets (each with an initial $80\text{-}\mu\text{L}$ volume) on the surface with the volume of the first (lower) droplet less than that of the second droplet, indicating droplet evaporation with time. The droplets also nearly evaporated when they reached the bottom of the surface. Figure VI-30 (e), (f), (g), and (h) taken at a continuous sequence are for a droplet volume of $146\ \mu\text{L}$. It can be seen from the pictures that, as the droplet moved down along the surface, it left a long thin film trace behind; reduced its size on the way down due to evaporation of the droplet and the thin film behind; but was not completely evaporated as it reached the bottom of the surface. These results, along with others at higher surface temperatures, indicate that the optimized initial droplet volume is in the $73\text{-}80\ \mu\text{L}$ range for this test surface. Future testing, as defined below, will refine this optimum considering more vehicle operating conditions as well as extended radiator surface conditions.

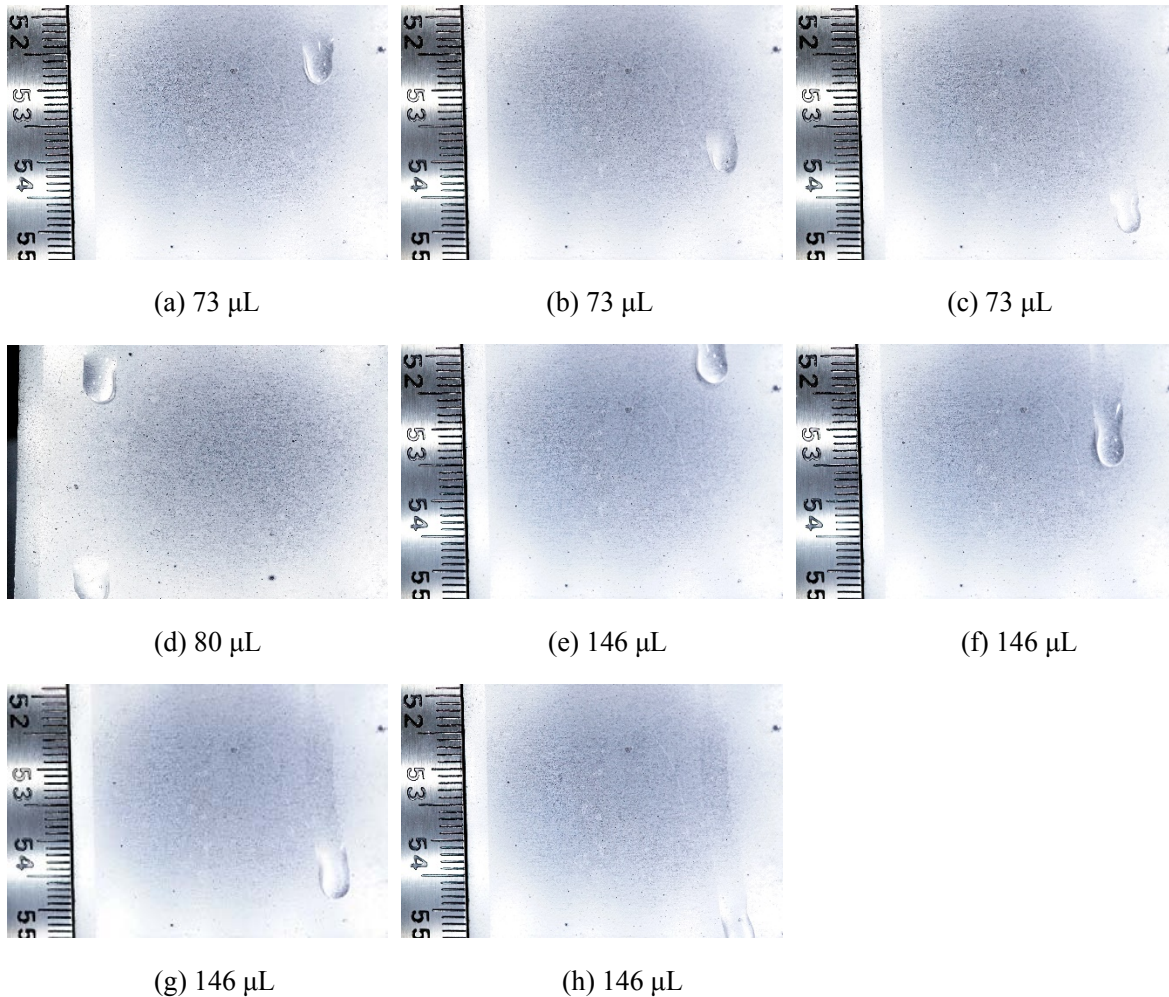


Figure VI-30: Droplet Size Effect on Droplet Movement and Evaporation

Conclusions

Coolant radiators in trucks and automobiles were shown to be amenable to evaporative cooling. Using a hybrid radiator, 19% and 46% heat transfer increases were obtained with 76-liter/hour (20-gallon/hour) and 189-liter/hour (50-gallon/hour) water flow rates, respectively. These results were dependent on the establishment of water flow with a small thickness along the radiator extended surfaces. It was found that such thickness could readily be obtained by using droplet flow with contact angle management.

An alternative to the heat transfer increase from an existing radiator with the addition of evaporative cooling is radiator size reduction. It was shown that, at the design heat load, the 76-liter/hour (20-gallon/hour) and 189-liter/hour (50-gallon/hour) water flow rates yield radiator area reductions of 21% and 52%, respectively.

A good potential utilization of evaporative cooling would be to design the finned portion of the radiator to accommodate all driving conditions except for desert hills. In this case, water for evaporative cooling would only be needed when a vehicle travels through desert hills under extremely hot conditions. It was found that the radiator area could be reduced by 21% when only 76 liters (20 gallons) of water were used to traverse an extreme desert hill such as Baker grade.

A series of numerical simulations was conducted using the commercial software COMSOL Multiphysics. It was shown that the key factor for effective usage of evaporative cooling is the initial droplet thickness, which depends largely on the droplet size and the surface contact angle. Small droplets and contact angles generate small droplet thicknesses with effective evaporative cooling.

An experimental test system simulating the air flow of moving vehicles was designed and fabricated for investigating the droplet evaporation and movement under realistic application conditions of heavy-duty vehicles.

A series of experimental tests of the droplet movement and evaporation has been conducted on the unheated and heated Modine permanently fluxed and braze-treated Al 3003 surface to investigate the effects of the radiator fan speed, the droplet size, the surface temperature, and the droplet interval. The very promising results from the experimental tests include: (a) the radiator fan speed has a minimum effect on the droplet horizontal movement, which means that the droplet will not be sheared off the edge of the extended cooling channel surface and will be able to evaporate on the hot surface to remove heat from the radiator, (b) droplets with a reasonable initial volume are able to completely evaporate on the heated surface before they reach the bottom, and (c) boiling in the drops and trace occurs at low wall superheat of 5°C enhancing heat transfer and drop evaporation rates, which aids in complete drop evaporation and adequate radiator cooling. These experimental results represent improved conditions compared to earlier computer simulations. Those simulations did not include the actual Modine fluxed surface nor the thin liquid trace found to follow the droplets increasing the area of water/surface contact for each drop. These effects produced the thin drops that the simulations showed to be a requirement for effective heat transfer and reduced the shear force tending to move them off the surface. Both results indicate the potential for the proposed technology to be used in practical heavy-duty vehicles. The boiling phenomenon was not expected at this low wall superheat and benefits the heat transfer when it occurs.

Future research will continue on experimental investigations of the effects of various surface coating and treatment methods and materials on the droplet movement and evaporation under the realistic air flow conditions of moving vehicles. The focusing areas include (a) conducting experimental tests of the droplet movement and evaporation on coated or modified surfaces using warm water to account for water temperature effects, (b) optimizing the droplet size and interval for the maximum evaporative cooling benefit, and (c) designing and testing a water droplet supply and distribution system usable for heavy-duty vehicles.

VI.3.C. Products

Presentations/Publications/Patents

1. D. M. France, D. S. Smith, W. Yu, Efficient, Active Radiator-Cooling System, SAE International Journal of Commercial Vehicles 6 (1) (May 2013) 249–256.
2. D. M. France, D. S. Smith, W. Yu, J. L. Routbort, Hybrid Radiator Cooling System, pending US patent, US 2013/0233517 A1, September 2013.

VI.4. Aerodynamics and Underhood Thermal Analysis of Truck Platooning

T. Sofu, Principal Investigator

Argonne National Laboratory
9700 S. Cass Avenue
Argonne, IL 60439
Phone: (630) 252-4500
E-mail: tsofu@anl.gov

Prasad Vegendla, Other Collaborators

E-mail: svegendla@anl.gov

Lee Slezak, DOE Program Manager

Phone: (202) 586-2335
E-mail: Lee.Slezak@ee.doe.gov

Start Date: 10-01-2014
End Date: 10-01-2015

VI.4.A. Abstract

In truck platooning, an external aerodynamics and underhood thermal analyses of medium-duty delivery trucks were studied to assess their fuel economy and thermal performance. In platooning configuration, the leading and trailing vehicles had similar geometrical dimensions, i.e., widths, heights, and lengths.

In this work, a total of five different truck platooning configurations were modeled and simulated in single- and multi-lane traffic. In single-lane traffic, the leading and trailing vehicles separated in longitudinal direction by 30ft, 60ft, 90ft and 150ft. Similarly, the vehicles were separated in two-lane traffic but with a latitude direction of 1.2 m. In single-lane traffic, a significant drop in fuel consumption was observed in trailing vehicle while decreasing the vehicle separation distance when compared to no-traffic vehicle. In contrast, the significant drop in fuel consumption was observed in trailing vehicle while increasing the longitudinal vehicle separation distance in two-lane traffic. In all side-by-side vehicle position configurations, the rise of fuel consumption was observed in all leading vehicles.

Apart from the aerodynamics simulations, the underhood thermal analyses were performed to analyze the cold mass air flow rates and cooling package temperatures. A significant temperature rise was observed in trailing vehicle cooling package (Charge Air Cooler (CAC), radiator and fuel-condenser) due to lower cold mass air flow rates through the cooling package in both single-lane and two-lane traffic.

Objectives

- Vehicle aerodynamic drag analysis
 - The aim of this project is to develop a methodology to simulate external aerodynamics of trucks. The main focus of the project is to optimize the fuel consumption.
- Vehicle thermal analysis
 - The aim of this project is to develop a methodology to simulate underhood thermal performance of trucks. The main focus of the project is to optimize the underhood compartment by modifying heat exchanger designs, i.e., the CAC and the radiator.

Accomplishments

- In single-lane vehicle platooning, a significant fuel savings were observed in both leading and trailing vehicles. The higher fuel saving potential was observed at lower vehicle separation distance. The fuel benefits were diminished with increasing vehicle separation distances.

- In two-lane vehicle platooning, trailing vehicle fuel savings benefit rose with increasing vehicle separation distance in longitudinal direction (latitude direction was kept at 1.2 m).
- In multi-lane side-by-side vehicle traffic, the rise of fuel consumption was observed in all leading vehicles.
- The higher fuel saving benefits were observed in trailing vehicle with two leading vehicle and side-by-side vehicle positions.
- In single- and two-lane leading and trailing vehicle platooning, the significant drop in cold mass flow rates (temperature rise) were observed in cooling package of trailing vehicle due to a big vortex (low velocity region) between both leading and trailing vehicles.

Future Achievements

- Underhood thermal analyses of platooning vehicles by adjusting an engine heat rejection rates based on the vehicle fuel consumption rates
- Investigation of road-tunnel influence on vehicle thermal and aerodynamics of different vehicle configurations in a confined wind obstruction roads
- Identifying the improvements in vehicles for efficient thermal and aerodynamics designs



VI.4.B. Technical Discussion

Background

In the automotive and transport industry, aerodynamic thermal improvements are highly desirable in the design of fuel-efficient vehicles. Over the last two decades, continuous efforts to build aerodynamic designs by modifying external vehicle surfaces and through add-on aerodynamic drag reduction devices are growing rapidly. In transport vehicles, external air-flows are heterogeneous and it can have a positive or even negative impact on both aerodynamics and thermal management, depending on the influence of vehicle traffic and vehicle position. Computational Fluid Dynamics (CFD) modeling offers an excellent alternative to experiments in modeling and designing of aerodynamics vehicles. Today's available High Performance Computing (HPC) allows the building of very robust aerodynamic and thermal fuel-efficient vehicles with minimal amounts of time and cost. This ongoing study is aimed at replacing costly experiments by designing feasible modeling prototypes of the heavy vehicle. CFD is the main tool as mentioned above in designing and optimizing the underhood configuration and the external aerodynamics of the heavy-duty vehicle.

Optimization of medium- and heavy-duty vehicle aerodynamic drag and thermal loads is an important design consideration with significant implications for fuel efficiency. A medium/heavy-duty vehicle's drag-producing components include the mirrors, side extenders, wheels, cabin, and trailer, and also including cooling devices and engine. A component-based analysis helps to identify improvements in aerodynamic drag and cooling performance. Aerodynamic drag optimization lies mostly in redesigning the external surfaces of the above-mentioned vehicle components. On the other hand, vehicle thermal design was focused on the underhood compartment, which comprises the engine, radiator, Charge Air Cooler (CAC) and fan. An efficient cooling system reduces thermal loads and maximizes the use of power because conventional underhood configurations allow conversion of only a fraction of the total fuel energy into mechanical power and the rest is lost through the exhaust system and heat rejection. An ideal temperature distribution in and around the engine allows redesign of a heavy vehicle's underhood configuration and helps to achieve fuel efficiencies through cooling system optimization.

Technical Barriers

- Developing methodology to analyze each phenomena/component separately and its effect on overall full-vehicle performance.
- Model validation with prototypes.

- Scarcity of acceptable-quality heat exchanger performance data and pressure drop.

Technical Targets

- Development of physics-based models and numerical techniques.
- Identification of potential fuel savings in vehicle platooning configurations and improvement of external vehicle surfaces to reduce aerodynamic drag.
- Identification of potential improvements in cooling package in platooning configurations.

Introduction

In the automotive industry, optimized efficiency in vehicle aerodynamics and thermal management of an engine cooling system and underhood components is highly desirable for achieving durable and fuel-efficient designs that meet today’s energy demand [1-2]. CFD analysis offers an inexpensive and fast alternative to experiments. Commercially available CFD simulation software such as StarCCM+® can be used to investigate and assess the various factors that affect aerodynamic drag and underhood thermal vehicle performance [1]. Aerodynamic and thermal optimization of vehicles can reduce fuel consumption and vehicle emissions while improving vehicle durability.

The objective of this work is to evaluate the fuel savings potential of on-highway platooning vehicles. Trucks operate in a heterogeneous aerodynamic environment that includes influences of multiple surrounding vehicles. Platooning involves the reduction of aerodynamic drag by grouping vehicles together and decreasing the distance between them in single and/or multiple lanes. Recent research studies have demonstrated that platooning can be effective at reducing the aerodynamic drag on all of the vehicles in the platoon, even in the lead vehicles [3-4]; however, the highest aerodynamic drag reduction occurs for the vehicles between the first and last truck. Moreover, fuel consumption depends on vehicle spacing, vehicle speed, vehicle position, and vehicle mass [5].

In this work, 3D CFD modeling and simulations were performed in STAR-CCM+® commercial tool [1,2,4]. Aerodynamic drag and thermal numerical results were analyzed for multiple vehicle interactions occurring while the vehicles were under the influence of the on-road traffic that may be impacted by the overall aerodynamic drag of the leading and the trailing vehicles in both single and multiple lanes.

Approach

Aerodynamic drag simulations: 3D isothermal steady-state simulations were conducted using the segregated flow solver in StarCCM+. Gas-phase turbulence was modeled using k-ε with standard parameters [6]. Operating and inlet conditions were listed in Table VI-4.

Table VI-4: Operating conditions for aerodynamic drag simulations

Operating Conditions	Values
Velocity Inlet [mph]	55
Temperature Inlet [K]	300
Yaw Angle [deg]	-6, 0 and 6
Outlet Pressure [bar]	1
Computational Domain [m3] [Length x Width x Height]	200x 500 x 100
Number of Hexahedral Cells [millions]	30 to 200
Side Walls	Periodic

Underhood thermal simulations: 3D non-isothermal steady-state simulations were carried out using the segregated flow solver in StarCCM+. Gas-phase turbulence was modeled using k- ε with standard parameters. For Fan, the Moving Reference Frame (MRF) is implemented. Operating and inlet conditions were shown in Table VI-4.

Results

Single-lane traffic

CONFIGURATION-1

As shown in Figure VI-31, leading and trailing vehicle separated only in longitudinal direction. The aerodynamic drag and underhood thermal simulations were performed to analyze the fuel consumption and cooling package temperatures.



Figure VI-31: Leading Vehicle (LV) and Trailing Vehicle (TV) configuration in single-lane traffic

As shown in Figure VI-32, the higher fuel saving benefits was observed at lower vehicle separation distance in both leading and trailing vehicles. The fuel consumption benefit drops with increasing vehicle separation distance. The higher fuel savings were observed in trailing vehicle than in leading vehicle. This was mainly due to reduced oncoming air flow velocity from the leading to the trailing vehicles, which leads to a lower drag in the trailing vehicle. It should be noted that the calculated fuel savings comparisons were based on the no-traffic vehicle. The fuel savings/penalty was roughly an half of the aerodynamic drag drop/rise compared to no-traffic vehicle.

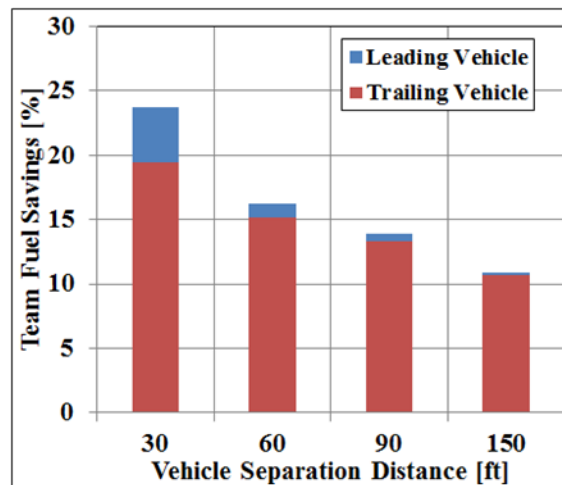


Figure VI-32: Comparison of fuel savings in single-lane traffic vehicles at different vehicle separation distances [averaged values of three different yaw angles 0°, -6°, and 6°].

In leading vehicle, the fuel benefit was diminishing with vehicle separation distance. This was due to influence of the trailing vehicle's pressure wave on the leading vehicle's wake region as shown in Figure VI-33. Similarly, lower pressures were observed in the trailing vehicle at front portion of the cabin, which leads to higher fuel savings than in no-traffic and leading vehicle.

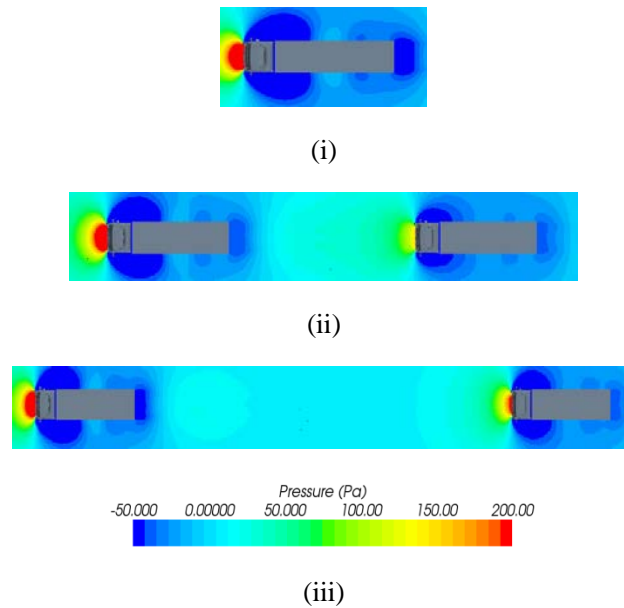


Figure VI-33: Static pressure distribution in 0° yaw angle (i) no-traffic, (ii) 60 ft, and (iii) 150 ft

Multi-lane traffic

CONFIGURATION-2

As shown in Figure VI-34, leading and trailing vehicle separated in longitudinal and latitude directions. The latitude direction was kept at 1.2 m. The aerodynamic drag and underhood thermal simulations were performed to analyze the fuel consumption and cooling package temperatures.

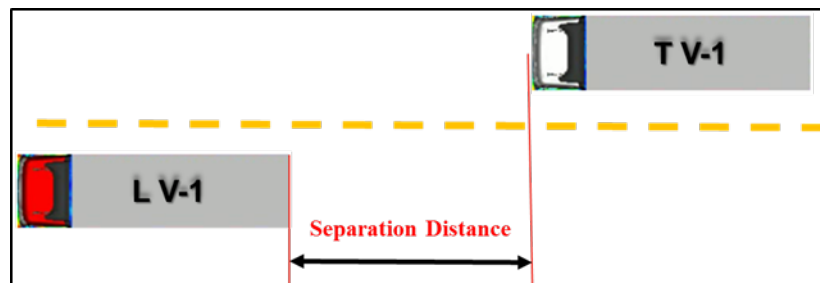


Figure VI-34: Leading Vehicle (LV) and Trailing Vehicle (TV) configuration in two-lane traffic

As shown in Figure VI-35, the fuel savings rise was observed in trailing vehicle when increasing the vehicle separation distance in longitudinal direction. The fuel savings in a leading vehicle follows the same trend as explained above in Figure VI-32 and Figure VI-33.

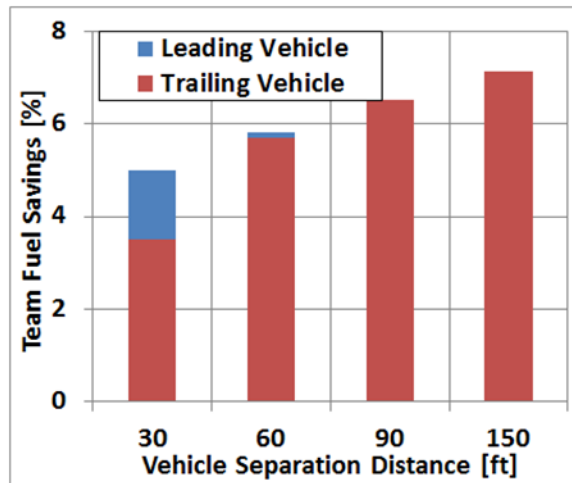


Figure VI-35: Comparison of fuel savings in one-way two-lane traffic vehicles at different vehicle separation distances [averaged values of three different yaw angles 0°, -6°, and 6°].

As shown in Figure VI-36, the spread of low velocity region increases with increasing vehicle separation distance. The influence of trailing vehicle on leading vehicle was observed at lower vehicle separation distance (less than 90ft).

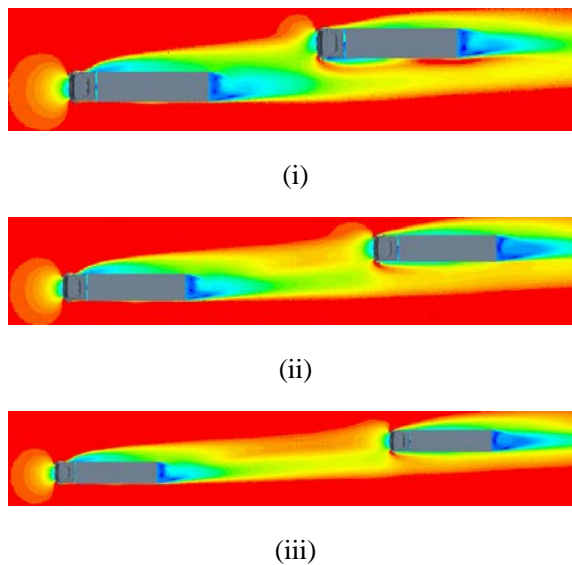
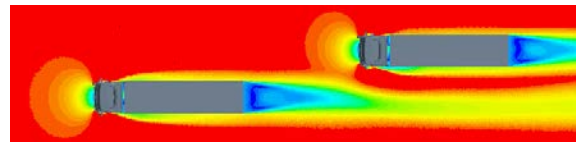
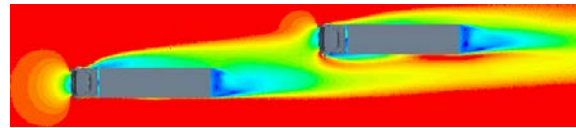


Figure VI-36: Velocity fields in 6° yaw angle (i) 30 ft, (ii) 60 ft, and (iii) 90 ft

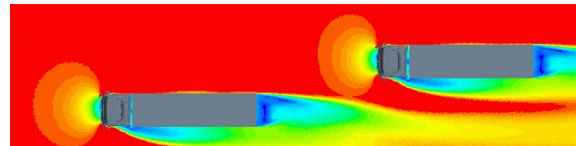
As shown in Figure VI-37, a significant low velocity region was observed at front portion of the trailing vehicle in 6° yaw angle when compared to 0 and -6° yaw angles. This was due to the wind flow direction towards trailing vehicle in two-lane traffic. In -6° yaw angle, the leading vehicle influence was negligible on the trailing vehicle.



(i)



(ii)



(iii)

Figure VI-37: Velocity fields in 30ft vehicle separation distance at different yaw angles (i) 0°, (ii) 6°, and (iii) -6°

CONFIGURATION-3

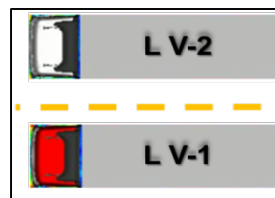


Figure VI-38: Two vehicles in side-by-side positions in multi-lane traffic

As shown in Figure VI-38 and Figure VI-39, two vehicles in side-by-side configuration had shown the highest fuel consumption and penalty was up to 5.5% in both vehicles. The fuel consumption rise was mainly due to the limited clearance to escape airflow from front cabins. This condition leads to higher static pressure at front portion of the cabin when compared to no-traffic condition as illustrated in Figure VI-40.

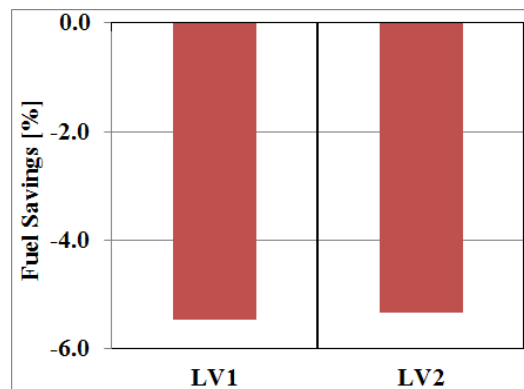
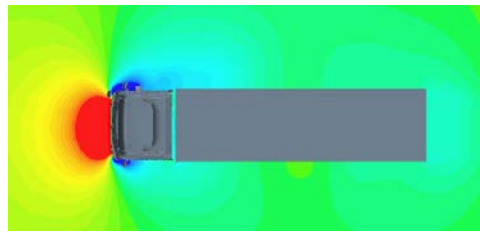
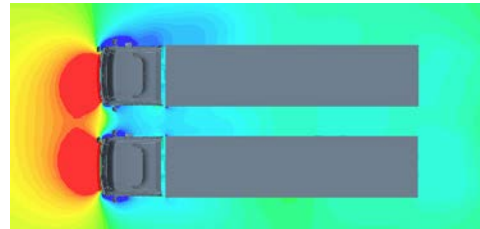


Figure VI-39: Comparison of fuel consumption for each of vehicle in one-way two-lane traffic [averaged values of three different yaw angles 0°, -6°, and 6°].



(i)



(ii)

Figure VI-40: Static pressure distribution in 6° Yaw angle (i) no-traffic and (ii) two-vehicles

CONFIGURATION-4

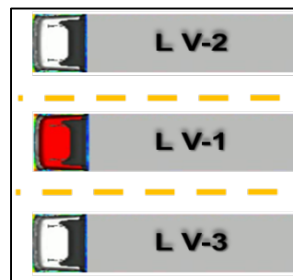


Figure VI-41: Three vehicles in side-by-side positions in multi-lane traffic

As shown in Figure VI-41 and Figure VI-42, three vehicles in side-by-side configuration had shown the highest fuel penalty, up to 12% in a center vehicle and 8% in an extreme left and right vehicles. The fuel penalty was mainly due to the limited clearance to escape airflow from front cabins as discussed above in configuration-3. The center vehicle had experienced most of the fuel consumption.

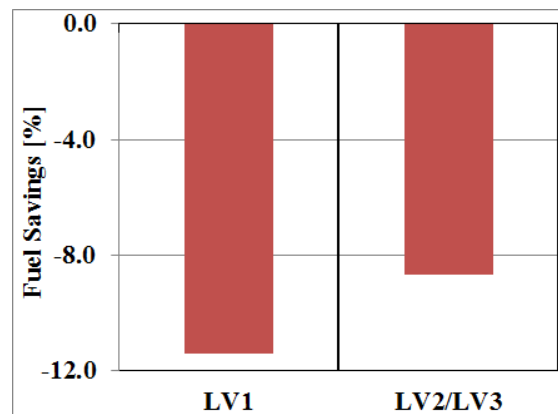


Figure VI-42: Comparison of fuel consumption for each of vehicle in one-way three side-by-side vehicles [averaged values of three different yaw angles 0°, -6°, and 6°].

CONFIGURATION-5



Figure VI-43: Three vehicle configuration; two leading vehicles are in side-by-side position and one trailing vehicle behind one of the leading vehicles.

As shown in Figure VI-44, the highest fuel benefit was observed in the trailing vehicle compared to all other configurations. This was mainly due to lower oncoming air flow from the leading vehicles were much stronger than in one-leading vehicle configurations as shown in Figure VI-45. On the other hand, both leading vehicles were also benefited when compared to two vehicles in side-by-side vehicle positions (Figure VI-39). This was mainly due to the stagnation pressure from the trailing vehicle communicated with the wake pressure of the leading vehicles causing an increased base pressure on the leading vehicle and an overall aerodynamic drag reduction (not shown). In this configuration, the leading and trailing vehicle was separated by a 30 ft distance in longitudinal direction.

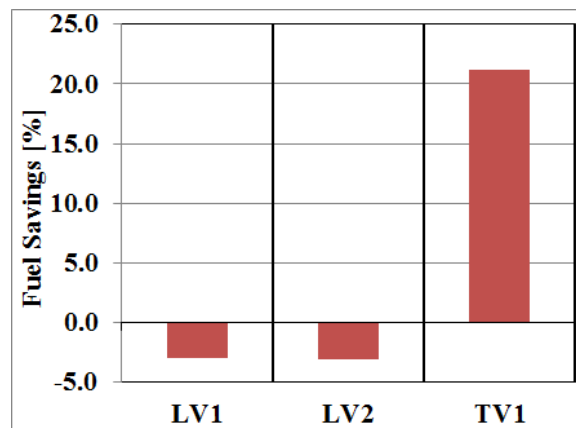
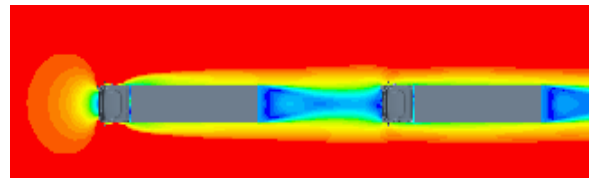
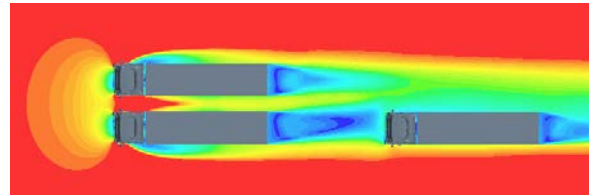


Figure VI-44: Comparison of fuel consumption for each of vehicle in one-way two-lane traffic at 30 ft vehicle separation distance [averaged values of three different yaw angles 0°, -6°, and 6°].



(i)



(ii)

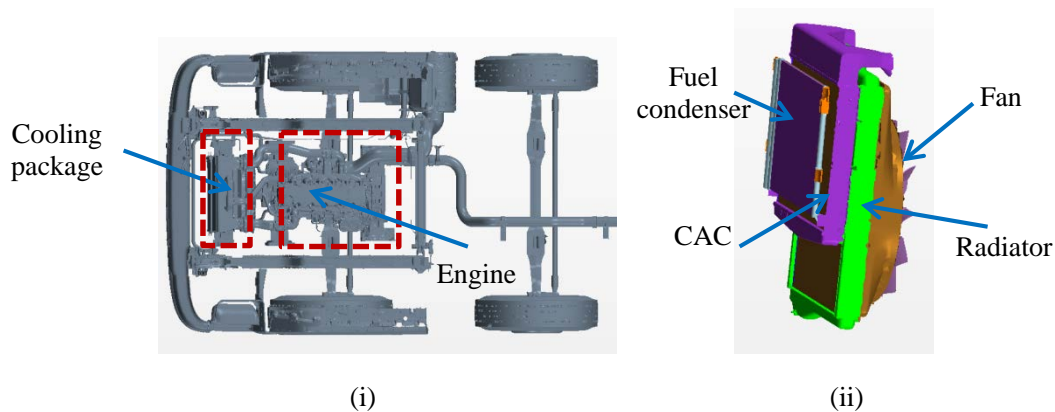
Figure VI-45: Velocity fields in 0° Yaw angle (i) one-leading vehicle and (ii) two-leading vehicles

Underhood Thermal Simulations

In both leading and trailing vehicle, heat exchangers, i.e. fuel condenser, CAC and radiator, were modeled using porous body with inertial and viscous resistances as shown in Table VI-5. The heat exchangers and fan locations were described in Figure VI-46. In both vehicles, the fan was operated at constant speed of 1400 rpm. The total heat rejection rates of fuel condenser, CAC and radiator were considered to be 11, 24.25 and 55 kW, respectively.

Table VI-5: Heat exchanger porous body modeling

	Fuel Condenser	CAC	Radiator
Inertial forces [kg.m ⁴]	66	67	330
Viscous forces [kg.m ⁴ .s ⁻¹]	66	415	335



(i)

(ii)

Figure VI-46: Vehicle underhood components; (i) top view and (ii) cooling package

Single-lane traffic

CONFIGURATION-1

In single-lane traffic, one vehicle behind another in the same lane (Figure VI-31). As shown in Figure VI-47, the trailing vehicle cooling package temperature rise was dropping with an increase of vehicle separation distance when compared to no-traffic vehicle (see Figure VI-31 for platooning configuration). This was mainly due to the amount of cold mass air flow rates increase with increasing the vehicle separation distances. At lower vehicle separation distance of 30 ft, around 20% (equivalent to 25% temperature rise) drop in mass flow rates was observed. This was mainly due to the low velocity vortex region occupied between both leading and trailing vehicles. On the other hand, there was no significant temperature rise in the leading vehicle when compared to no-traffic vehicle. It should be noted that the average temperatures were extracted from the three heat exchangers cold mass air flow rates ($Q=m.C_p.\Delta T$) and at three different yaw angles 0° , -6° , and 6° . As shown in Figure VI-48, the significant hot regions were observed in trailing vehicle when compared to leading vehicle.

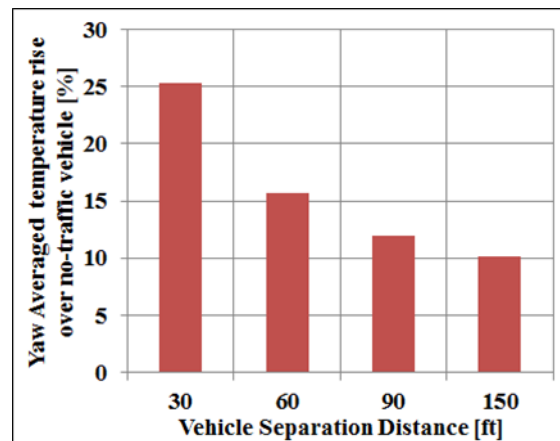


Figure VI-47: Comparison of fuel savings in one-way two-lane traffic vehicles at different vehicle separation distances [averaged values of three different yaw angles 0° , -6° , and 6°].

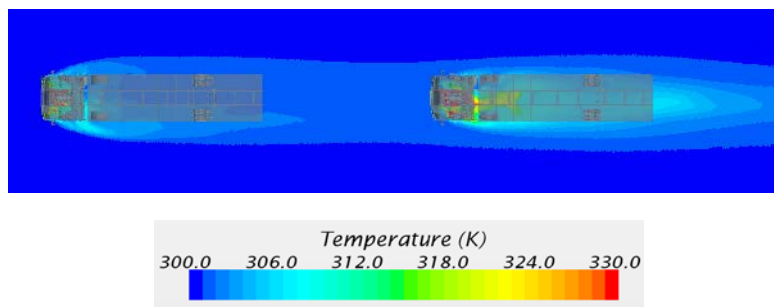


Figure VI-48: Temperature distribution in 0° Yaw angle at 30ft vehicle separation distance [horizontal plane at fan center position].

Multi-lane traffic

CONFIGURATION-2

In multi-lane traffic, one vehicle in one lane and the trailing vehicle behind and in the next lane (Figure VI-34). As shown in Figure VI-49, the rise in temperature was almost independent of the vehicle separation distance in two-lane traffic condition. This was mainly due to the average air flow velocities were almost same around the trailing vehicle cooling package. In the leading vehicle, no changes were observed in temperatures when

compared to no-traffic vehicle (similar to the single-lane traffic condition). As shown in Figure VI-50, the temperature rise was not significant in the trailing vehicle when compared to single-lane traffic (Figure VI-47).

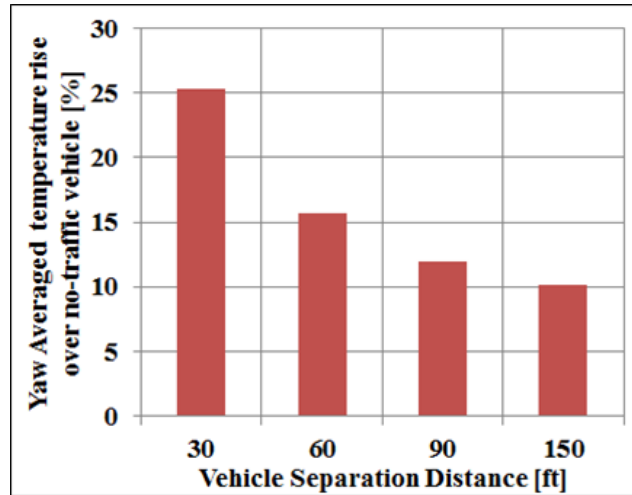


Figure VI-49: Comparison of fuel savings in one-way two-lane traffic vehicles at different vehicle separation distances [averaged values of three different yaw angles 0°, -6°, and 6°]

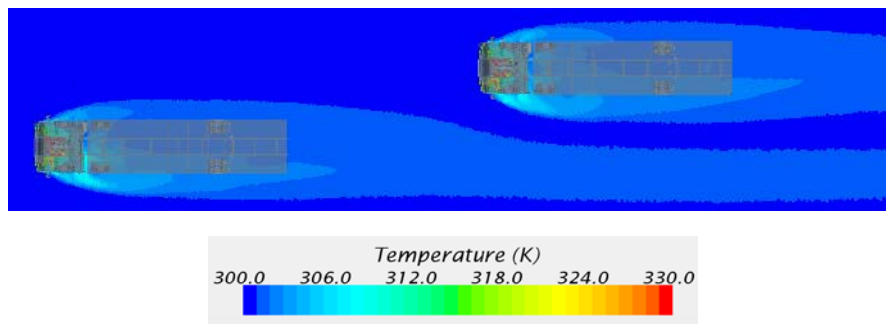


Figure VI-50: Temperature distribution in 0° Yaw angle at 30ft vehicle separation distance [horizontal plane at fan center position].

Conclusions

In single-lane traffic, one vehicle behind another in the same lane is the most common for platooning and had the highest fuel benefits, up to 23%. The fuel benefits were reduced with increasing vehicle separation distance between both leading and trailing vehicles.

In multi-lane traffic, one vehicle in one lane and the trailing vehicle behind and in the next lane. The fuel savings potential was minimum at a separation distance of 30 ft. Higher benefits were observed in the trailing vehicle with higher longitudinal separation distance due to a vortex shedding by the leading vehicle.

In multi-lane traffic and side-by-side vehicle position, the fuel consumption rise was observed due to high static pressure at the front portion of the cabin. The overall fuel consumption was increased by 5.5% in two vehicle and 14.5% in three vehicle configurations. In multi-lane traffic, three vehicles side-by-side configuration, the center vehicle had experienced most of the fuel consumption. In multi-lane traffic, two vehicles side-by-side and another vehicle following behind. The negative fuel consumption impact was on the leading vehicle with fuel economy penalty up to 2.25%. The trailing vehicle had experienced most of the fuel benefits compared to all other configurations.

Apart from the aerodynamic drag considerations, the trailing vehicle cooling performance drop was observed in both single-lane and multi-lane traffic due to lower mass air flow rates at front portion of the trailing vehicle cabin.

VI.4.C. Products

Presentations/Publications/Patents

1. Vegendla, S.N.P., Sofu, T., Saha, R., Kumar, M.M., and Hwang, L.K. (2015) 'Investigation of Aerodynamic Influence on Truck Platooning', 2015 SAE technical paper, 2015-01-2895.
2. Vegendla, S.N.P., Sofu, T., Saha, R., Kumar, M.M., and Hwang, L.K. (2015) 'Investigation of Aerodynamic Influence on Truck Platooning', 2015 SAE COMVEC conference, Rosemont, Illinois, USA.

VI.4.D. References

1. Vegendla, S.N.P., Sofu, T. and Lee, S. 'Aerodynamics and underhood thermal analysis of heavy/medium vehicles' US DOE Annual Report -Vehicle and System Simulation and Testing R&D, DOE-EE-1165. 2014, pp: 345-349.
2. Sofu, T. Aerodynamics and underhood thermal analysis of heavy/medium vehicles. US DOE Annual Report for Vehicle Technology Program, DOE/EE-1023.
3. Smith, J., Mihelic, R., Gifford, B., Ellis, M., "Aerodynamic Impact of Tractor-Trailer in Drafting Configuration," SAE technical paper, 2014, DOI:10.4271/2014-01-2436.
4. Vegendla, S.N.P., Sofu, T., Saha, R., Kumar, M.M., and Hwang, L.K. (2015) 'Investigation of Aerodynamic Influence on Truck Platooning', 2015 SAE technical paper, doi:10.4271/2015-01-2895.
5. Lammert, MP., Duran, A., Diez, J., Burton, K., et al., Effect of Platooning on Fuel Consumption of Class 8 Vehicles Over a Range of Speeds, Following Distances, and Mass," SAE technical paper, 2014, DOI:10.4271/2014-01-2438.
6. STAR-CCM+-v9.06.011, User Guide, 2014.

VI.5. Experimental Investigation of Coolant Boiling in a Half-Heated Circular Tube – CRADA with PACCAR

Dileep Singh/Wenhua Yu, Principal Investigators

Argonne National Laboratory
9700 South Cass Avenue
Lemont, IL 60439
Phone: (630) 252-5009; Fax: (630) 252-5568
E-mail: dsingh@anl.gov

Lee Slezak/David Anderson, DOE Program Managers

U.S. Department of Energy
Phone: (202) 586-2335
E-mail: Lee.Slezak@ee.doe.gov

Start Date: October 2011
End Date: September 2015

VI.5.A. Abstract

Objectives

- Understand and quantify engine coolant subcooled boiling heat transfer in heavy-duty vehicles.
- Experimentally determine subcooled flow boiling heat transfer rates and limits in the cylinder head region of heavy-duty vehicle engines.
- Develop predictive mathematical models for subcooled flow boiling heat transfer results.
- Provide measurements and models for development/validation of heavy-duty vehicle engine computer codes.

Accomplishments

- Completed the concept design, the technical design, and the fabrication of the experimental test facility and support systems.
- Completed the LabVIEW-based data acquisition system and test control hardware and software.
- Completed the heat loss calibrations of the experimental test facility.
- Completed single-phase convective heat transfer experiments and data reduction with three test fluids.
- Completed subcooled flow boiling heat transfer experiments and data reduction with three test fluids for all flowrates.
- Developed three experimental data-based predictive correlations for the subcooled flow boiling heat transfer coefficient.
- Modified the experimental test facility by adding a pressurizing system for higher-pressure subcooled flow boiling tests.
- Conducted experimental tests for investigating surface corrosion effects on subcooled flow boiling heat transfer.
- Conducted subcooled flow boiling heat transfer experiments and data reduction with a 50/50 ethylene glycol/water mixture at higher pressures.

Future Achievements

- Complete the final report of the project.



VI.5.B. Technical Discussion

Background

Started in FY 10 as a CRADA between Argonne National Laboratory and PACCAR Inc./DAF Trucks N.V. (PACCAR/DAF), this project aims to provide heat transfer and critical heat flux measurements and models of coolant subcooled boiling in the cylinder head region of heavy-duty vehicle engines for development and validation of heavy-duty vehicle engine computer codes.

Introduction

Currently, the engine cooling systems in heavy-duty vehicles are designed to use approximately 50/50 ethylene glycol/water (EG/W) mixture in the liquid state. Boiling is usually a phenomenon that has been avoided in conventional engine cooling systems in heavy-duty vehicles. However, while the conventional engine cooling systems in heavy-duty vehicles are designed to eliminate coolant saturation boiling, coolant subcooled boiling in the cylinder head regions is unavoidable at high thermal loads due to high metal temperatures. Because of its order-of-magnitude higher heat transfer rates, there is interest currently in using controllable nucleate-boiling precision cooling instead of conventional single-phase forced convection cooling in vehicle cooling systems under certain conditions or in certain areas to remove ever increasing heat loads, to eliminate potential hot spots in engines, or to further optimize the parasitic losses of the coolant pump. Theoretical, numerical, and experimental investigations have been conducted on the potentials and the practical applications of nucleate boiling cooling systems in heavy-duty vehicles. Consequently, there is great interest in the knowledge of flow boiling heat transfer rates and limitations under these application conditions.

One of the unique characteristics of coolant subcooled boiling in the cylinder head regions of heavy-duty vehicle engines is that boiling generally occurs only on the cooling channel side facing the flame plate because of the one-sided heating condition. Although there have been many investigations into subcooled flow boiling with one-sided heating, most of the effort was focused on fusion reactor system cooling with water as the coolant. Despite its importance in practical applications, theoretical and experimental studies of EG/W mixture boiling under engine cooling application conditions are generally lacking.

PACCAR/DAF is designing engines to take advantage of coolant subcooled boiling heat transfer below the critical heat flux, but the critical heat flux and the heat transfer rate have not been determined under realistic conditions. The experiments of this program address this situation using a design specified by DAF. The data will be used in computational fluid dynamics models and designs by PACCAR/DAF, which could result in more efficient engines for heavy-duty vehicles. The objective of this project is to measure heat transfer rates during subcooled flow boiling of engine coolants in a geometry typical of valve bridge areas in heavy-duty vehicle engines under various operating conditions.

Approach

The general approach for this project is to experimentally investigate subcooled flow boiling of water and EG/W mixtures for heavy-duty vehicle engine applications.

The experimental apparatus used in this study is shown in Figure VI-51. It consists of a closed-loop system with main components of a pump, two preheaters, an experimental test section, a heat exchanger (cooler), and a flowmeter. The system was designed and fabricated to study the heat transfer of subcooled flow boiling of water and EG/W mixtures with heat supplied only to the bottom half surface of the experimental test section. As shown in the schematic diagram of the experimental apparatus in Figure VI-51, the test fluid was pumped through the test loop by a turbine pump (MTH Pumps, Model T31FAB) and the system was open to the atmosphere through the fill port at the flowmeter. The turbine pump was driven by an alternating-current adjustable-frequency driver (Dayton Electric Manufacturing Company, Model 1XC95), which made it possible to fine adjust flowrates through the experimental test section. Exiting the pump, the test fluid flowed through two preheaters arranged in series, in which, for a given test, the fluid temperature was raised to the desired subcooled level and monitored through two in-stream thermocouples. Each preheater, being made of an AISI type 304 stainless steel tubing with a 9.779-mm inside diameter, a 15.875-mm outside diameter, and a 3.9624-

m resistance-heated length, was heated by passing current through its wall. A direct-current power supply (Sorensen Company, Model DCR 16-625T) was used for each preheater, the output power of which could be regulated from 0 to 10 kW with the maximum voltage drop and the maximum current of 16 volts and 625 amperes, respectively. As a safety precaution for protecting the preheaters from overheating, each preheater was provided with a temperature interlock. At the end of each preheater, the wall temperature was measured and then fed to a high-temperature limit switch (Omega Engineering, Inc., Model CN8500) that would terminate power to the preheater when a preset upper-temperature limit was reached. After passing through the preheaters, the fluid entered the horizontal experimental test section. The experimental test section was heated with a direct-current power supply (Electronic Measurements, Inc., Model EMHP 40-450-D-11111-0933) by passing current through a 1.6256-mm diameter AISI type 304 stainless steel heating wire attached to the bottom half of the experimental test section surface shown schematically in Figure VI-52. The output power could be regulated from 0 to 18 kW with the maximum voltage drop and the maximum current of 40 volts and 450 amperes, respectively. The voltage drop across the heating wire was measured directly, and the current through the heating wire was determined from a measurement of the voltage drop across a shunt resistor with known resistance of 0.00001 Ω . The heat input to the experimental test section was calculated using the product of the voltage drop and the current. Electrical isolation for eliminating ground loops was provided for the preheaters and the experimental test section by short high-pressure hoses, designated ISO in Figure VI-51. The test fluid out from the experimental test section was cooled in the compact plate-and-frame heat exchanger (Affiliated Steam Equipment Company, Model WP1-14) that used laboratory water as a heat rejection fluid. The volumetric flowrate of the test fluid was measured by an electromagnetic flowmeter (Endress+Hauser, Inc., Model 10H08-A00A1RA0B4AA). A thermocouple probe (Omega Engineering, Inc.) just upstream from the flowmeter provided a means to determine the density of the fluid and subsequently the mass flowrate of the fluid. Flowing out of the flowmeter, the test fluid returned to the pumps to close the test loop.

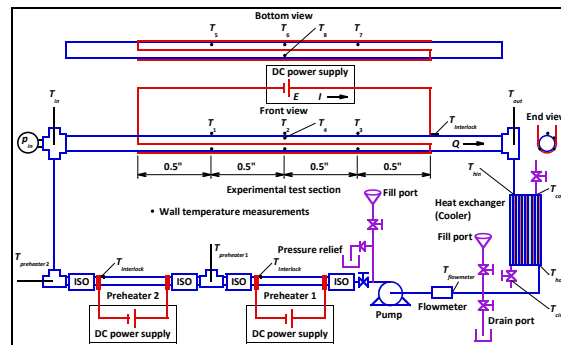


Figure VI-51: Schematic of Heat Transfer Facility

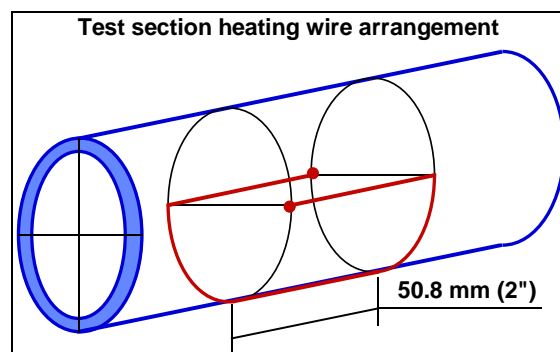


Figure VI-52: Test Section Heating Wire Arrangement

The experimental test section, shown schematically in Figure VI-51, was fabricated from a 10.9-mm-inside-diameter and 12.7-mm-outside-diameter AISI type 1010 carbon steel tube with a 50.8-mm heated length. The in-stream bulk fluid temperatures were measured at the inlet and the outlet of the experimental test section with type K thermocouple probes (Omega Engineering, Inc.). As shown schematically in Figure VI-51, the wall

temperatures were measured at 8 locations along the experimental test section and around the test section circumference over the heated length with type K thermocouple junctions (Omega Engineering, Inc.) spot welded to the test section surface. The inlet fluid pressure was measured in all tests with a diaphragm pressure transducer (Omega Engineering, Inc., Model PX309–100A5V). These measurements were incorporated in the data reduction to calculate the average in-stream temperatures and the average wall temperatures. As a safety precaution for protecting the experimental test section from overheating, the experimental test section was provided with a temperature interlock. At the end of the experimental test section, the wall temperature was measured and then fed to a high-temperature limit switch (Omega Engineering, Inc., Model CN8500) that would terminate power to the experimental test section when a preset upper-temperature limit was reached.

A data acquisition system consisting of a personal computer and a multiplexor (Hewlett-Packard Company, Model HP 75000 Series B) was assembled to record outputs from all sensors. A data acquisition program, including all calibration equations and engineering-unit conversions, was written with the LabVIEW graphical programming software. The data acquisition system functioned in two modes. During experimental test setup, the data acquisition system provided an on-screen display of analog signals from all sensors and graphs of representative temperature measurements as a function of time to facilitate determination of steady-state conditions. When the system reached a steady-state condition at desired parameters, the data acquisition system read all sensor-output voltages of in-stream temperatures, wall temperatures, ambient temperature, inlet pressure, volumetric flowrate, voltage drop across the heating wire, and current through the heating wire. These sensor-output voltages were read 30 times, averaged, and stored as a data set for future data reduction.

An overview of the completely-fabricated heat transfer test facility is shown graphically in Figure VI-53 before it was insulated.



Figure VI-53: Heat Transfer Facility Overview

Results

Heat Loss Calibration

Although the experimental test section is well insulated thermally from the atmosphere to minimize heat loss to the environment, the heat loss was not negligible during flow boiling heat transfer experiments because of the relatively high driving temperatures. Therefore, heat loss experiments were performed for the experimental test section wall temperatures up to the boiling heat transfer conditions, and the heat loss was subsequently incorporated into the data reduction procedures for single-phase convective and subcooled flow boiling heat transfer data. The heat loss was characterized through a special series of experiments with no fluid in the experimental test section. Power was applied to the experimental test section to bring its wall temperature to a selected level. The heat loss rate q_{loss} , the input power required for maintaining the wall temperature at the selected value and calculated by the product of the voltage drop across the heating wire and the current through the heating wire ($q_{\text{loss}}=EI$), is related to the difference between the experimental test section wall temperature T_w and the ambient temperature T_{ambient} . Experimental results confirmed a linear dependence of the heat

loss on this driving temperature difference. Then the heat loss rate was expressed approximately as $q_{loss}=c(T_w-T_{ambient})$ where the proportional constant c , which depends on the heat transfer coefficient and the heat transfer surface area between the experimental test section and ambient for this particular experimental apparatus, was determined from the heat loss experiments. Figure VI-54 shows the heat loss rate as a function of the driving temperature difference for the experimental test section. The test section heat loss was <3% of the applied input power to the experimental test section in all subsequent heat transfer tests.

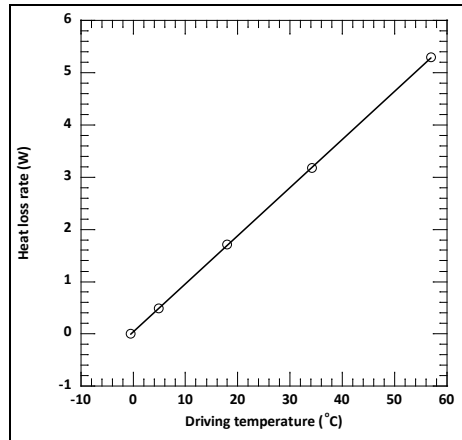


Figure VI-54: Heat Loss Calibration

Single-Phase Heat Transfer Experiments

Investigations of heat transfer under the condition of heat supplied only to one half surface of an experimental test section are limited in the engineering literature, and no standard data reduction process exists. Therefore, to validate the test apparatus in this study and to establish a base line, a series of single-phase heat transfer experiments was carried out prior to subcooled flow boiling experiments. For the single-phase heat transfer experiments, the system pressure was kept near atmosphere pressure similar to the subcooled flow boiling experiments. The single-phase heat transfer experiments were performed under the turbulent flow condition mirroring the flow region of the subcooled flow boiling experiments, and the liquid heat transfer coefficients were correlated as functions of the Reynolds number Re and the Prandtl number Pr by modifying the Dittus-Boelter equation. As shown in Figure VI-55, where the heat transfer coefficients are plotted, the experimental data are in good agreement with the predicted values from the above equation with a mean deviation of <4%. Almost all experimental data are within $\pm 5\%$ of the predictions. The fact that modification was required to the Dittus-Boelter equation is not surprising because the Dittus-Boelter equation is not based on one-sided heating conditions. The fact that different equations were needed for each fluid is also not surprising because the Dittus-Boelter equation was not developed for fluid mixtures. These equations were only used in the data reduction of this study to account for the single-phase heat transfer at the top of the experimental test section under subcooled boiling conditions at the bottom.

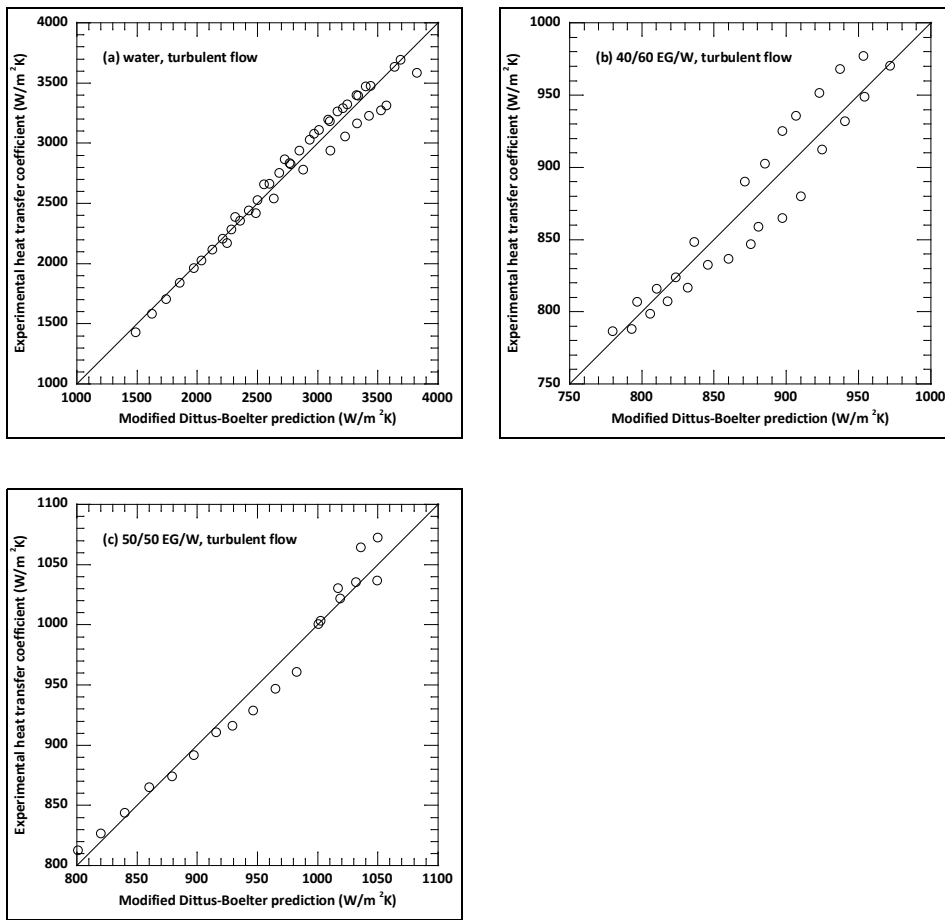


Figure VI-55: Turbulent Heat Transfer Coefficient Comparison

In addition to the turbulent flow, single-phase heat transfer experiments were also performed under the laminar flow condition with EG/W mixtures to establish a base line for the subcooled laminar flow boiling that occurred at the lowest flow velocity of EG/W mixtures. The liquid heat transfer coefficients were correlated as a function of the Reynolds number Re and the Prandtl number Pr by modifying the Shah equation. As shown in Figure VI-56, where the heat transfer coefficients are plotted, the experimental data are in good agreement with the predicted values from the above equation with a mean deviation of $<2\%$. All experimental data are within $\pm 5\%$ of the predictions.

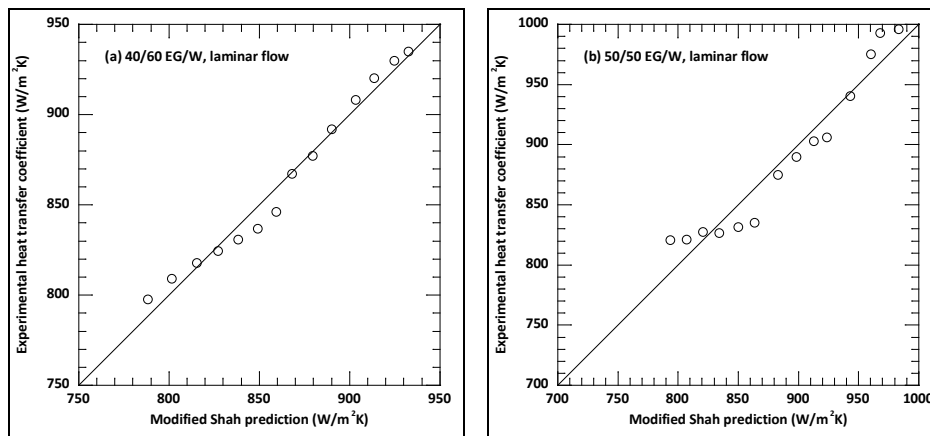


Figure VI-56: Laminar Heat Transfer Coefficient Comparison

Subcooled Flow Boiling Heat Transfer

A series of subcooled flow boiling heat transfer experiments was conducted for water under the turbulent flow condition with the Reynolds number in the range of 3500–51000 and for 40/60 and 50/50 EG/W mixtures under both the turbulent flow condition with the Reynolds number in the range of 2900–26000 and the laminar flow condition with the Reynolds number in the range of 1400–2200. The inclusion of the 40/60 EG/W mixture was to account for deviations from the 50/50 EG/W mixture specification occurred in practical cooling systems of heavy-duty vehicle engines. For each test fluid, the subcooled flow boiling heat transfer experiments were performed for parameters of five flow velocities and four fluid inlet temperatures. For each set of the subcooled flow boiling heat transfer experiments, the system pressure was kept close to atmospheric pressure through the open fill port at the flowmeter, the heating power of the preheaters was adjusted to maintain the test fluid inlet subcooling temperature at a desired level, and the heating power of the experimental test section was increased progressively until the top wall temperature of the experimental test section reached the upper-temperature limit that was preset to avoid subcooled flow boiling on the top wall of the experimental test section. Because of this limitation, the subcooled flow boiling in this study is generally in the weak boiling range, especially for the higher flow velocities. For each test section heating power increment, the test fluid changed gradually from single-phase convection-dominated heat transfer toward subcooled flow boiling heat transfer and, after enough time for the experimental system to reach a steady-state condition, all the test-related sensor outputs were averaged and recorded in a data set with appropriate engineering units for future data reduction such as generating boiling curves and computing heat transfer coefficients.

According to the above subcooled flow boiling experimental procedure, the top wall superheat was always below a certain threshold and consequently the top section heat transfer was single-phase convection for all time even when subcooled flow boiling occurred at the bottom section. Based on this assumption, the approach used for analyzing subcooled flow boiling heat transfer was to separate the overall heat transfer into two parts: top heat transfer and bottom heat transfer. The detailed results for boiling curves and boiling heat transfer coefficients are shown and discussed below.

Water Turbulent Flow Boiling Curves

A series of subcooled flow boiling heat transfer experiments was conducted for water under the turbulent flow condition at five flow velocities of 0.125, 0.25, 0.5, 1, and 1.5 m/s and four fluid inlet temperatures of 75, 80, 85, and 90°C. The fluid inlet temperatures were chosen to obtain the inlet liquid subcooling in the range of approximately 10–25°C. The corresponding boiling covers are shown in Figure VI-57. The essential feature shown in Figure VI-57 is that, for the unique experimental setup of this study with heating only from the bottom of the experimental test channel, the heat transfer can generally be divided into the single-phase convection dominated region and the subcooled flow boiling region, which is similar to heat transfer of fluids in channels with the all-around heating condition. Related to the two heat transfer regions, there are several important characteristics that can be seen from Figure VI-57. First, the wall superheats at which heat transfer changes from single-phase convection to subcooled flow boiling are at approximately 10°C. This transform temperature is most obvious for the lowest flow velocity and the lowest inlet liquid subcooling. Second, the boiling curves display different increase gradients for the single-phase convection dominated region and the subcooled flow boiling region. Because of these different increase gradients, for the same heat flux increment, the wall superheat increment in the subcooled flow boiling region is smaller than that in the single-phase convection dominant region. Third, for various inlet liquid subcooling levels, the boiling curves follow an approximately parallel pattern in the single-phase convection dominant region but a gradually merging pattern in the subcooled flow boiling region. It should be pointed out that, due to the limitation of the wall superheat and therefore the experimental data in the subcooled flow boiling region in this study, the merging pattern is most evident at the lowest flow velocity, then gradually becomes less noticeable with the increase of the flow velocity, and is almost unnoticeable at the highest flow velocity. Fourth, the boiling curves with the highest inlet temperature or the lowest inlet liquid subcooling show the sharpest trend change at the transform temperature from single-phase convection to subcooled flow boiling due to the above-mentioned gradually merging pattern. Finally, based on the gradually merging pattern in the subcooled flow boiling region, it is expected that the influence of the inlet liquid subcooling on overall heat transfer gradually becomes less significant with the increase of subcooled flow boiling.

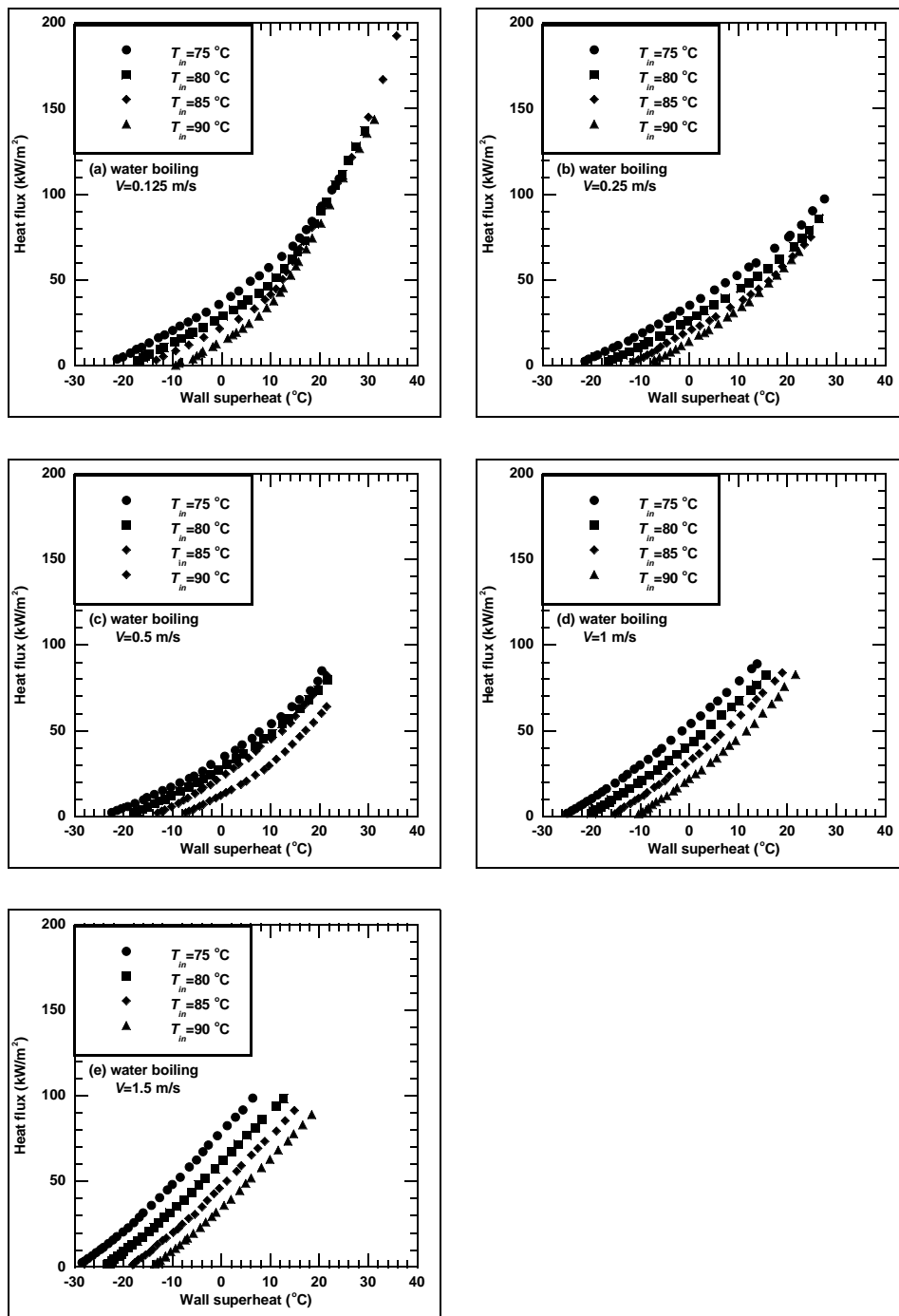


Figure VI-57: Water Turbulent Flow Boiling Curves

EG/W Mixture Turbulent Flow Boiling Curves

A series of subcooled flow boiling heat transfer experiments was conducted for 40/60 and 50/50 EG/W mixtures under the turbulent flow condition at four flow velocities of 0.25, 0.5, 1, and 1.5 m/s and four fluid inlet temperatures of 80, 85, 90, and 95°C for the 40/60 EG/W mixture and 82, 87, 92, and 97°C for the 50/50 EG/W mixture, respectively. The fluid inlet temperatures were chosen to obtain the same inlet liquid subcooling as that of water subcooled flow boiling in the range of approximately 10–25°C. The corresponding boiling covers are shown in Figure VI-58 for the 40/60 EG/W mixture and Figure VI-59 for the 50/50 EG/W mixture, respectively. Several characteristics can be seen from Figure VI-58 and Figure VI-59. First, the differences of the boiling curves between the 40/60 EG/W mixture and the 50/50 EG/W mixture are generally

small, based on which it is expected that a volume concentration deviation of ethylene glycol in practical vehicle cooling systems will not change coolant subcooled flow boiling too much. Second, the general trends identified above for water subcooled flow boiling are also applicable and are also more observable at lower flow velocities for EG/W mixture subcooled flow boiling. Finally, for the same wall superheat, the heat flux for water is higher than that for EG/W mixtures, which is consistent with the fact that water has a higher heat capacity than EG/W mixtures.

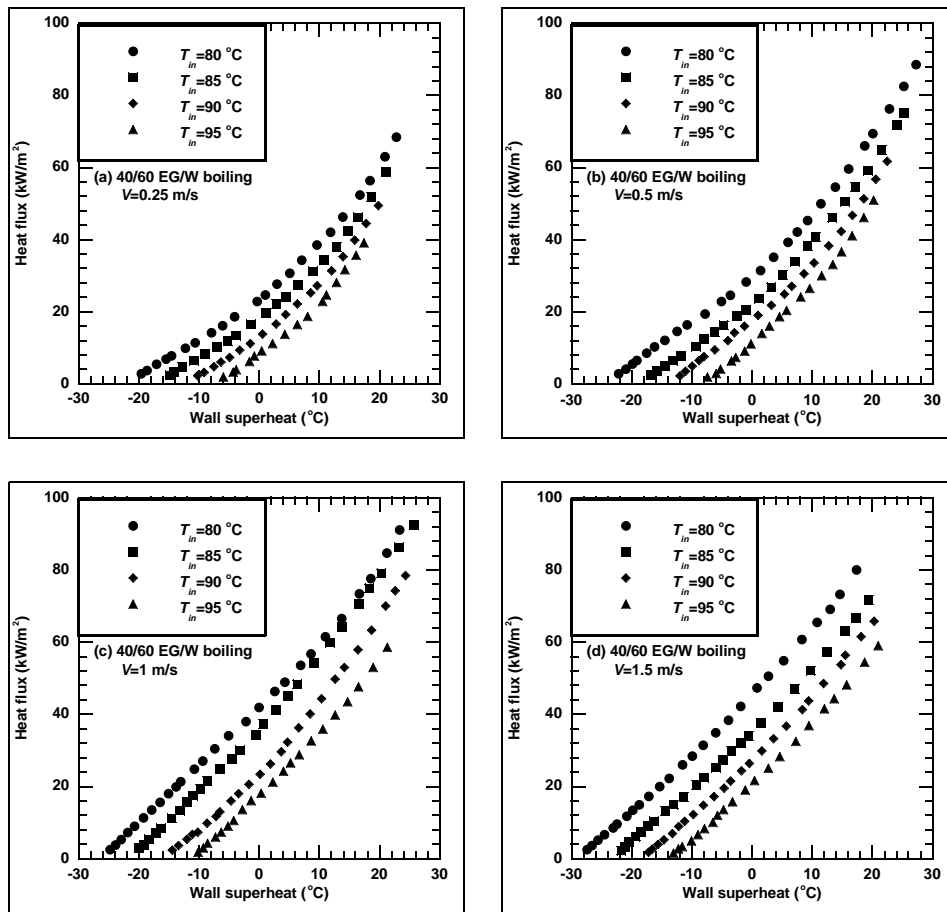


Figure VI-58: 40/60 EG/W Mixture Turbulent Flow Boiling Curves

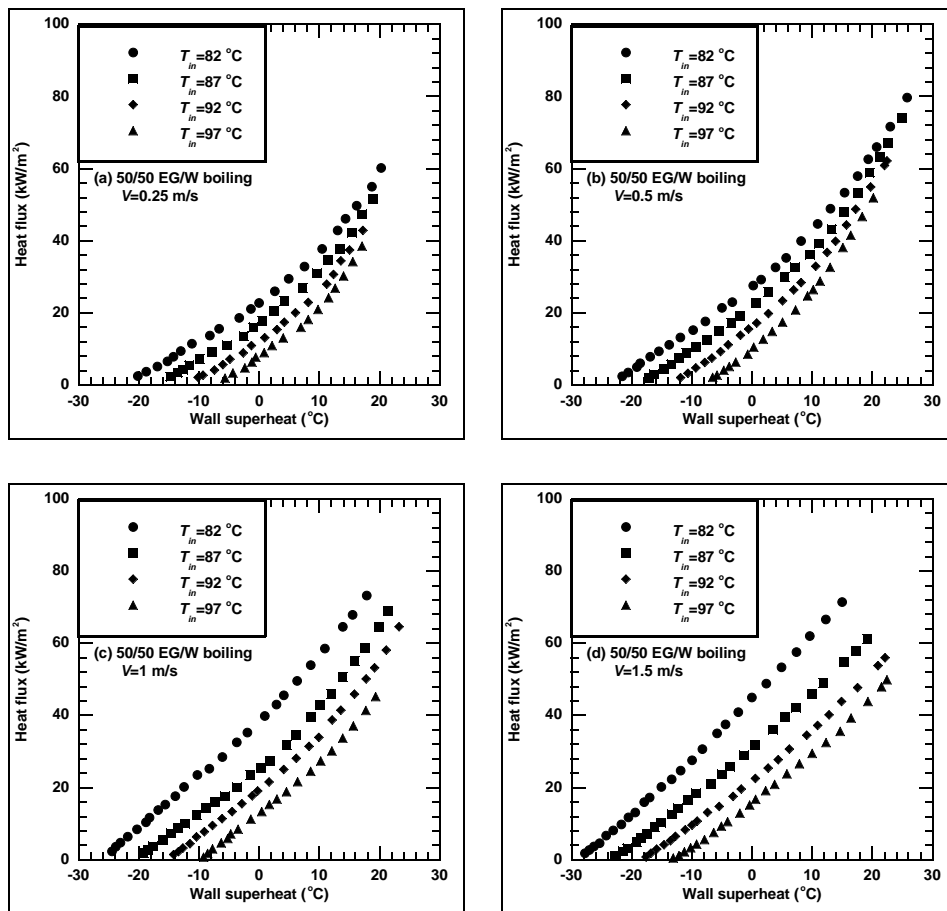


Figure VI-59: 50/50 EG/W Mixture Turbulent Flow Boiling Curves

EG/W Mixture Laminar Flow Boiling Curves

A series of subcooled flow boiling heat transfer experiments was conducted for 40/60 and 50/50 EG/W mixtures under the laminar flow condition at a flow velocity of 0.125 m/s and four fluid inlet temperatures of 80, 85, 90, and 95°C for the 40/60 EG/W mixture and 82, 87, 92, and 97°C for the 50/50 EG/W mixture, respectively. The fluid inlet temperatures were chosen to obtain the same inlet liquid subcooling as that of water subcooled flow boiling in the range of approximately 10–25°C. The corresponding boiling covers are shown in Figure VI-60a for the 40/60 EG/W mixture and Figure VI-60b for the 50/50 EG/W mixture, respectively. It can be seen from Figure VI-60 that the boiling curves for EG/W mixture subcooled flow boiling in laminar flow are very similar to those for EG/W mixture subcooled flow boiling in turbulent flow, except that the boiling curve trends mentioned above are more observable for EG/W mixture subcooled flow boiling in laminar flow due obviously to its lower flow velocity.

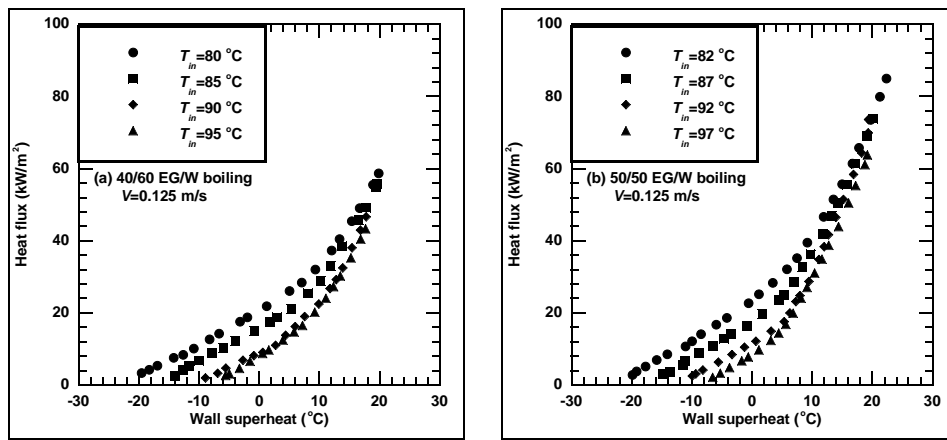


Figure VI-60: EG/W Mixture Laminar Flow Boiling Curves

Boiling Heat Transfer Coefficients

The subcooled flow boiling heat transfer coefficients with the wall superheat higher than the transform temperature are shown in Figure VI-61a for water and Figure VI-61b for EG/W mixtures as a function of the wall superheat. There are several features that can be seen from Figure VI-61. First, the subcooled flow boiling heat transfer coefficients increase with the wall superheat indicating the further development of subcooled flow boiling with the increase of the experimental test channel wall temperature. Second, the differences of the subcooled flow boiling heat transfer coefficients between the 40/60 EG/W mixture and the 50/50 EG/W mixture are insignificant, which is due to the relatively small difference of their ethylene glycol concentrations and is consistent with their boiling curve characteristics. Finally, for the same wall superheat, the subcooled flow boiling heat transfer coefficients for water are larger than for EG/W mixtures, which is caused by the higher heat flux for water boiling than for EG/W mixture boiling under the same wall superheat.

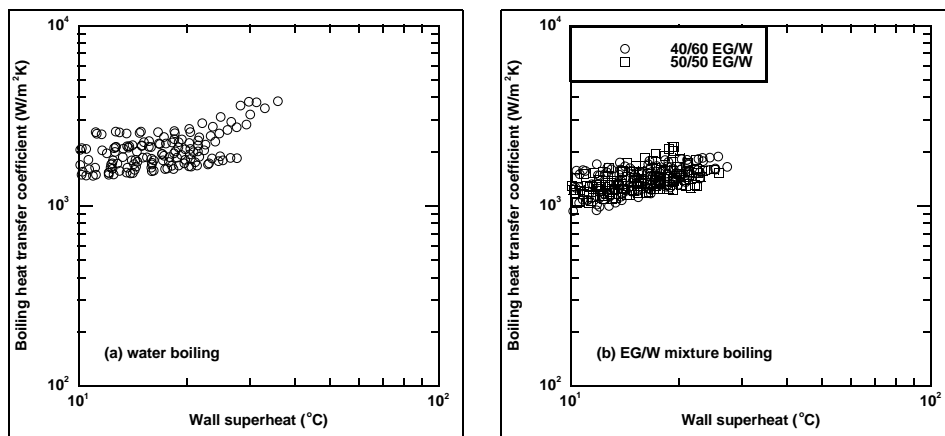


Figure VI-61: Boiling Heat Transfer Coefficients

Many predictive correlations have been developed for the subcooled flow boiling heat transfer coefficient. However, they were generally developed for the all-around heating condition but not for the one-side heating condition, especially not for the application condition of mixture boiling with one-side heating as in this study. While the correlations in the engineering literature may give reasonable predictions of the experimental data in this study, the prediction errors are expected to be high as shown in our previous report. Therefore, efforts were made in developing better predictive correlations based on the experimental data in this study. The details of the proposed correlations are discussed below.

Boiling Heat Transfer Coefficient Correlations

For the correlation of the experimental data in the present investigation of subcooled water and EG/W mixture flow boiling under the condition of heating supplied only from the bottom of the experimental test section, the wall superheat was correlated as functions of the boiling heat flux, the convective heat transfer coefficient predicted by the Dittus-Boelter correlation, the EG volume concentration, and a boiling number term based on the experimental data of water, EG/W mixtures, and all three tested fluids, respectively. Figure VI-62 shows the boiling number term $f_w(Bo)$ computed from the experimental wall superheats for water and EG/W mixtures, respectively. The predicted subcooled flow boiling heat transfer coefficients based on $f_w(Bo)$ for water and $f_M(Bo)$ for EG/W mixtures are compared with the experimental data in Figure VI-63a and Figure VI-63b, respectively. It can be seen from Figure VI-63a and Figure VI-63b that almost all of the experimental data are within $\pm 20\%$ of the predictions and the mean deviations for both water subcooled flow boiling and EG/W mixture subcooled flow boiling are $< 10\%$.

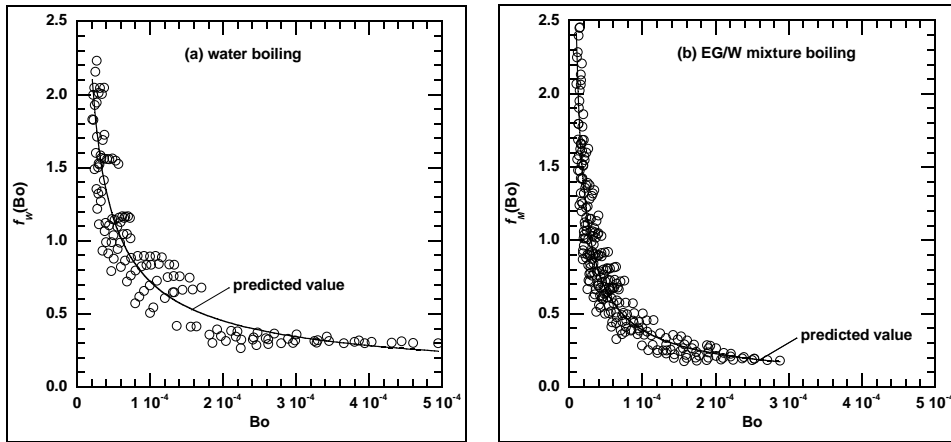


Figure VI-62: Correlation of Boiling Number Term

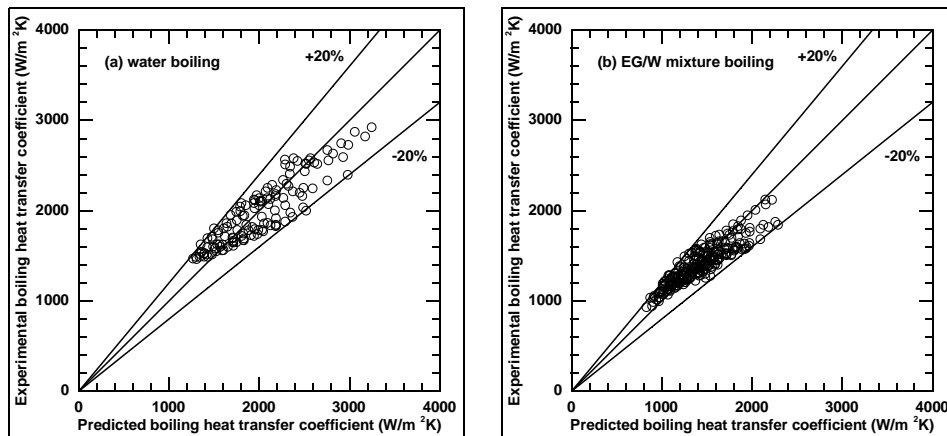


Figure VI-63: Heat Transfer Coefficient Comparison

Figure VI-64 shows the boiling number term $g(Bo)$ computed from the experimental wall superheats for all three tested fluids. The predicted subcooled flow boiling heat transfer coefficients based on $g(Bo)$ for all three tested fluids are compared with the experimental data in Figure VI-65. It can be seen from Figure VI-65 that almost all of the experimental data are within $\pm 20\%$ of the predictions and the mean deviations are $< 10\%$.

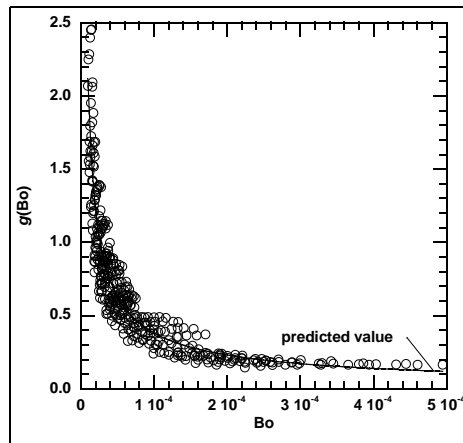


Figure VI-64: Correlation of Boiling Number Term for All Data

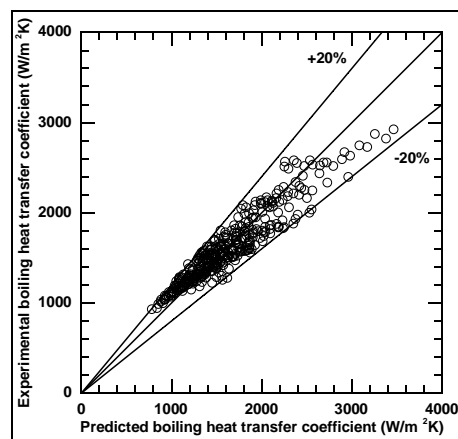


Figure VI-65: Heat Transfer Coefficient Comparison for All Data

Wall Temperature Simulations

To further validate the proposed predictive correlations for the subcooled flow boiling heat transfer coefficient, numerical simulations were conducted for computing wall temperatures and comparing them with the experimental measurements. The numerical simulations were carried out using the COMSOL Multiphysics commercial software with the model boundary condition of the heat transfer coefficient computed by the above proposed correlations. Figure VI-66 shows the comparison of the wall temperatures at the location of thermocouple 6 between the experimental measurements and the predicted results with 50/50 EG/W mixture boiling at various flow velocities and two fluid inlet temperatures. In obtaining the simulation results of Figure VI-66, the test section heat fluxes were same as the experimental values and the heat transfer coefficients as the model boundary condition were computed by the predictive correlation based on $g(Bo)$ for all tested fluids. It can be seen from Figure VI-66 that the simulation results agree with the experimental measurements very well with the differences $<6\%$.

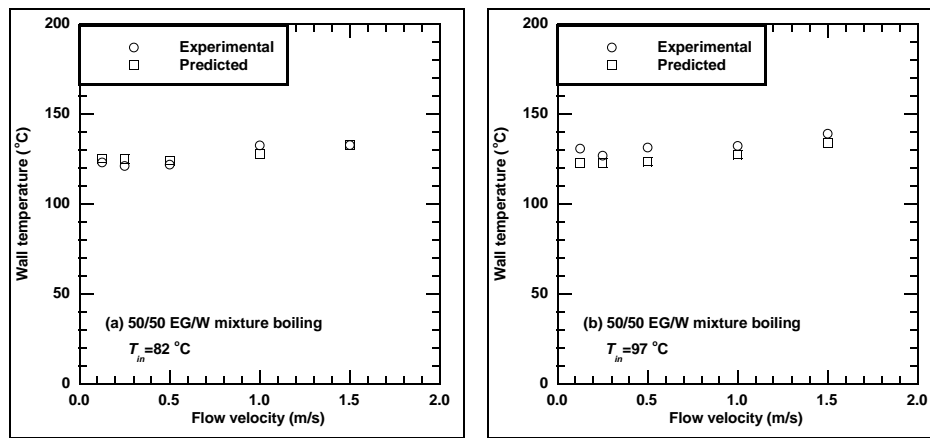


Figure VI-66: Wall Temperature Comparison

Experimental Test Facility Modifications

To prepare for experimental tests of higher-pressure subcooled flow boiling of water and EG/W mixtures, the experimental test facility was modified and a pressurizing system was added. As shown in Figure VI-67, a bladder-type hydraulic accumulator (Greer Hydraulics, Inc.), connected to a high-pressure nitrogen cylinder, will be used to pressurize and control the fluid pressure in the experimental test section within the experimental specifications by adjusting the pressure in the accumulator. As a safety precaution for protecting the experimental test section from overpressure, a pressure relief valve is attached to the accumulator with a preset relief pressure of 100 psi, high enough for the experimental test pressure requirements of <50 psi.

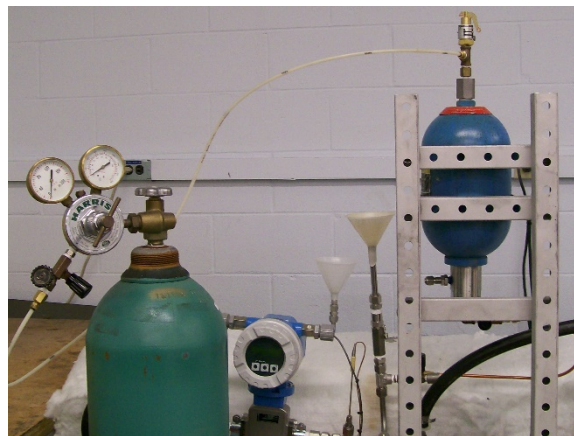


Figure VI-67: Pressurizing System

Surface Corrosion Effects

To simulate real cooling channels in heavy-duty vehicles, the experimental test section used in this study was made from AISI type 1010 carbon steel. Due to the material of the experimental test section and water content in the tested cooling fluids, iron oxide was generated on the internal surface of the experimental test section over the time of testing. In order to quantify the effects of this corrosion, experimental investigations were conducted to study the effects of the accumulated iron oxide on subcooled flow boiling heat transfer of a 50/50 EG/W mixture. Figure VI-68 shows experimental boiling curves of subcooled flow boiling of a 50/50 EG/W mixture at a flow velocity of 0.125 m/s and a fluid inlet temperature of 92°C at three conditions of the experimental test section: original test section, corroded test section, and cleaned test section. It can be seen from Figure VI-68 that (a) two different heat transfer regions (the single-phase convection dominated region and the subcooled flow boiling region) exist for all three test conditions, (b) the wall superheats at which heat transfer changes from single-phase convection to subcooled flow boiling are at approximately 6 - 10°C for all three test conditions, (c) the boiling curves display different gradients for the single-phase convection

dominated region and the subcooled flow boiling region, (d) because of these different gradients, for the same heat flux increment, the wall superheat increment in the subcooled flow boiling region is smaller than that in the single-phase convection dominant region, and (e) for the same heat flux, the wall superheat is highest for the corroded surface condition and lowest for the original surface condition, especially for the subcooled flow boiling region. The last feature indicates that the heat transfer performance of the corroded surface is worse than that of the original surface. Cleaning the corroded surface improved heat transfer performance. However, the heat transfer rate of the cleaned surface is still lower than that of the original surface in the subcooled boiling region. While the surface corrosion (rust) causes heat transfer deterioration between the wall surface and the heat transfer fluid, it should be pointed out that it generally is less of an issue for practical applications because engine coolants usually contain additives for preventing surface corrosion in the cooling system.

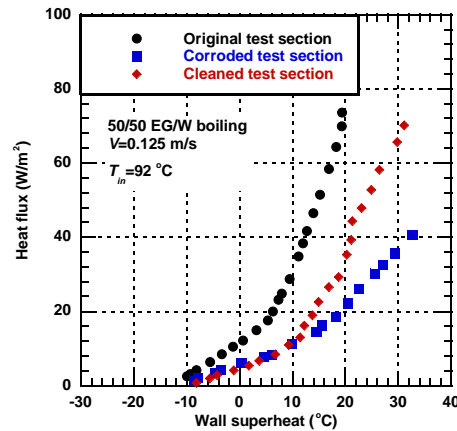


Figure VI-68: Surface Rust Effects

System Pressure Effects

Cooling systems of heavy-duty vehicles generally are operated at a system pressure higher than one atmosphere. Experimental tests were conducted with a 50/50 EG/W mixture to investigate subcooled flow boiling heat transfer performance at higher system pressures. Figure VI-69 shows the boiling curves of subcooled flow boiling of a 50/50 EG/W mixture at a flow velocity of 0.125 m/s, a fluid inlet subcooling level of 15°C and pressures of 1 atm. and 2 atm. absolute. It can be seen from Figure VI-69 that (a) the two boiling curves are very similar to each other with similar patterns, (b) two different heat transfer regions (the single-phase convection dominated region and the subcooled flow boiling region) exist for both system pressures with the transition occurring at lower wall superheat for the 2 atm. pressure test, (c) the wall superheats at which heat transfer changes from single-phase convection to subcooled flow boiling are at approximately 6 - 10°C for both system pressures, (d) the boiling curves display different gradients for the single-phase convection dominated region and the subcooled flow boiling region but do not differ with the pressure, (e) because of these different gradients, for the same heat flux increment, the wall superheat increment in the subcooled flow boiling region is smaller than that in the single-phase convection dominant region, and (f) for the same heat flux, the wall superheat is slightly higher for the system pressure of 1 atm. The last feature indicates that, in practical applications, the cooling fluid could remove more heat from metal components at higher system pressures than at lower system pressures.

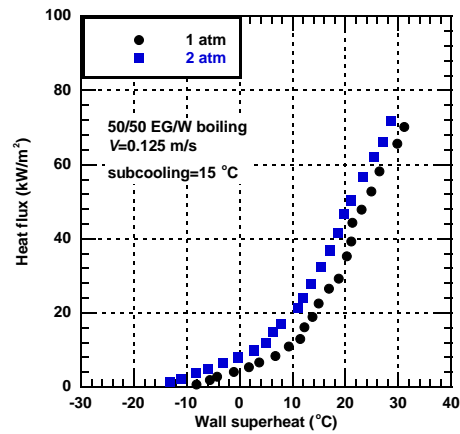


Figure VI-69: System Pressure Effects

Conclusions

In summary, the design and fabrication of the PACCAR heat transfer test facility have been finished; the LabVIEW-based data acquisition system and test control hardware and software have been established; the experiments and data reduction for single-phase convective heat transfer with three test fluids have been completed; the experiments and data reduction for subcooled flow boiling with three test fluids have been completed; three predictive correlations have been developed for the subcooled flow boiling heat transfer coefficient of water and EG/W mixtures; modifications to the experimental test facility have been made for higher-pressure subcooled flow boiling experiments of water and EG/W mixtures; and experimental tests have been conducted to investigate the surface corrosion effect and the system pressure effect on subcooled flow boiling of a 50/50 EG/W mixture. Future work will be focused on completing the final report of the project.

VI.5.C. Products

Presentations/Publications/Patents

1. Wenhua Yu, David M. France, Dileep Singh, Roger K. Smith, Jason Ritter, Thomas Vijlbrief, and Yves Menger, Subcooled Flow Boiling of Ethylene Glycol/Water Mixtures in a Bottom-Heated Tube, *International Journal of Heat and Mass Transfer* 72 (May 2014) 637–645.
2. W. Yu, D. M. France, W. Zhao, D. Singh, and R. K. Smith, Investigation of Subcooled Flow Boiling Heat Transfer to Water and Ethylene Glycol/Water mixtures in a Bottom-Heated Tube, accepted for publication in the *Experimental Heat Transfer*.

VI.6. Cummins MD&HD Accessory Hybridization CRADA

Dean D. Deter, Principal Investigator, R&D Staff Researcher

Oak Ridge National Laboratory (ORNL)

Oak Ridge National Laboratory

1 Bethel Valley Road

Oak Ridge, TN 37810

Phone: 865-576-8620

E-mail: deterdd@ornl.gov

David Anderson, DOE Program Manager

Vehicle and Systems Simulation and Testing

Phone: 202-287-5688

E-mail: david.anderson@ee.doe.gov

Start Date: July 1, 2013

End Date: January 16, 2016

VI.6.A. Abstract

Objectives

- Analytically verify novel heavy truck accessory hybridization and electrification approaches, and experimentally validate prototype hardware utilizing the ORNL Vehicle Systems Integration (VSI) Laboratory's component test cell and Cummins' test vehicle.
- Develop and validate medium/heavy duty accessory models by means of data collection on a test vehicle and extraction from Cummins' preexisting models.
- Using the project's generated models and market research, choose and develop an electric or hybrid architecture and controls for one or more accessories depending on fuel consumption reduction and perceived market acceptability.
- Integrate the conventional system and chosen prototype architecture in the component lab for system testing and controls development. This culmination, allows for good comparison of the two systems utilizing the repeatability of the lab environment.
- Add finished system to one of Cummins test vehicles for a proof of concept test.

Accomplishments

- Typical vehicle level models use a "lumped" mechanical and electrical accessory structure that is not detailed enough to represent dynamic accessory behavior. ORNL has integrated Cummins' accessory models into Autonomie's vehicle architecture to capture these behaviors at a vehicle level.
- Using test vehicle data the power steering model has been validated within the acceptable system assumptions.
- Exercised three different vehicles to determine which vehicle application would have the most impact of fuel consumption: a MD pickup/delivery truck, an HD class 8 bus, and an HD class 8 line haul sleeper cab.
- Validated the class 8 line haul sleeper cab to be accurate within 5% of a chassis tested vehicle.
- Using results from the simulation study as well as data from literature reviews, the CRADA team was able to determine that while line haul sleeper cabs made the smallest impact with hybrid accessories for driving when compared to MD, P&D, or HD bus, they made the biggest impact when looking into idle mitigation and overnight hotel loads.

- Based on the findings from the literature review and simulation study ORNL proposed and designed a hybrid Auxiliary Power Unit (h-APU) architecture that would allow for hybridization for the air conditioning, electrification of the condenser fans, and energy storage for other electrical hotel loads. This allows for the truck to eliminate or greatly reduce all over night idling by providing hotel loads from a battery pack that utilizes regenerative braking for charging.
- The baseline controls and system architecture have been designed and implemented in Autonomie for further testing and controls development.
- Two possible architectures were chosen and designed for driving the A/C compressor. One is a hybrid system which continues to utilize the existing compressor and the other being a fully electric compressor system.
- Two out of the three lab testing setups have been completed; the conventional and hybrid systems.
- Providing NREL with the proper resources, they have developed a baseline CoolSim Quasi-Transient air conditioning model that can be used with both the simulation portion of the project as well as the Hardware-In-the-Loop (HIL) portion of the project. This will provide a much needed high fidelity model for use in future simulation studies as well as controls development.

Future Achievements

- Using the data generated in ORNL's VSI Laboratory NREL will improve and validate their baseline model to provide even better accuracy for future use.
- ORNL will test the second compressor architecture that will allow Cummins to make a more educated test if the prototype system were to be chosen for commercialization.
- Cummins is currently testing the proposed h-APU system, providing a proof of concept for all of the work done by simulation and in the component test cell.



VI.6.B. Technical Discussion

Background

Medium and heavy duty trucks are a growing market and integral part of our society. From the home delivery of goods by medium duty trucks to the freight hauling of heavy duty line haul trucks, they are the main source of material and goods transport. Due to these trends, there is an overwhelming need to quickly address key problems with excess fuel usage and emissions production of these diesel vehicles.

Modern trucks have become much more advanced in terms of engine, aftertreatment, and transmission technologies which greatly reduced both fuel consumption and emissions. Due to these improvements, focus of truck OEMs has shifted to start looking at what other aspects of MD and HD trucks can be impacted by advanced technologies.

Introduction

There are many areas of MD and HD vehicles that can be improved by new technologies and optimized control strategies. Component optimization and idle reduction need to be addressed, this is best done by a two part approach that includes selecting the best component technology, and/or architecture, and optimized controls that are vehicle focused. While this is a common focus in the light duty industry it has been gaining momentum in the MD and HD market as the market gets more competitive and the regulations become more stringent.

When looking into systems optimization and idle reduction technologies, affected vehicle systems must first be considered, and if possible included in the new architecture to get the most benefit out of these new capabilities. Typically, when looking into idle reduction or component optimization for MD/HD, the vehicle's

accessories become a prime candidate for electrification or hybridization. While this has already been studied on light duty vehicles (especially on hybrids and electric vehicles) it has not made any head way or market penetration in most MD and HD applications. If hybrids and electric MD and HD vehicles begin to break into the market this would be a necessary step into the ability to make those vehicles successful by allowing for independent, optimized operation separate from the engine.

Approach

ORNL and Cummins began this project by discussing which approach would be most successful in reducing fuel consumption, but also which approach would gain acceptance by the market to enable this technology to penetrate the market more quickly. A two phased approach was selected due to ORNL’s test cell capabilities and Cummins market resources and access to a test vehicle for data and proof of concept test.

The first phase is a modeling/simulation/data collection and market study phase that is focused on determining, which accessories would be feasible to hybridized/electrify, what accessories have fuel consumption benefits if hybridized/electrify, the ideal vehicle application which would benefit most from these new technologies, and what architecture on the selected vehicle type would have the most impact on fuel consumption.

Phase one of the project started by collecting all of the data and resources ORNL and Cummins had to begin the modeling and simulation. Cummins was able to supply base models for the four major accessories that the project would be addressing: the engine’s cooling fan, the vehicle air conditioning system, the power steering system, and the vehicle’s air compressor and air brake system. ORNL opted to use Argonne National Laboratory’s Autonomie as the platform for simulation work on a vehicle level.

The first change to model was to switch the Autonomie accessory model structure from a “lumped” accessory structure (Figure VI-70) to a separated accessory structure (Figure VI-71) in order to capture all of the dynamic behaviors of each accessory and how those behaviors change based on vehicle type and drive cycle variability.

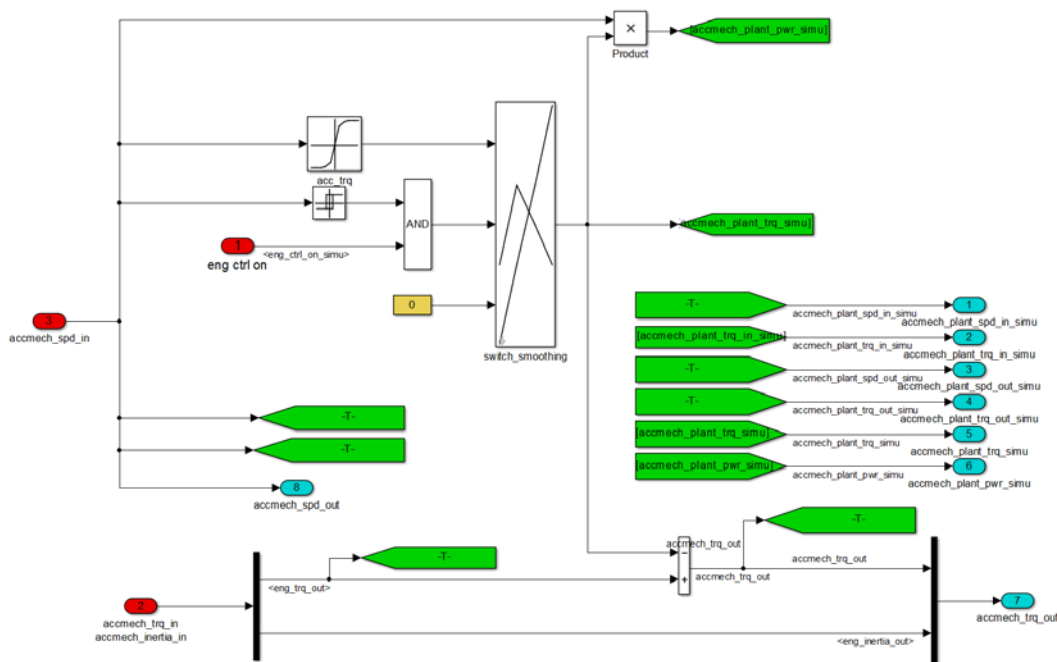


Figure VI-70: Original Autonomie “lumped” mechanical accessory model.

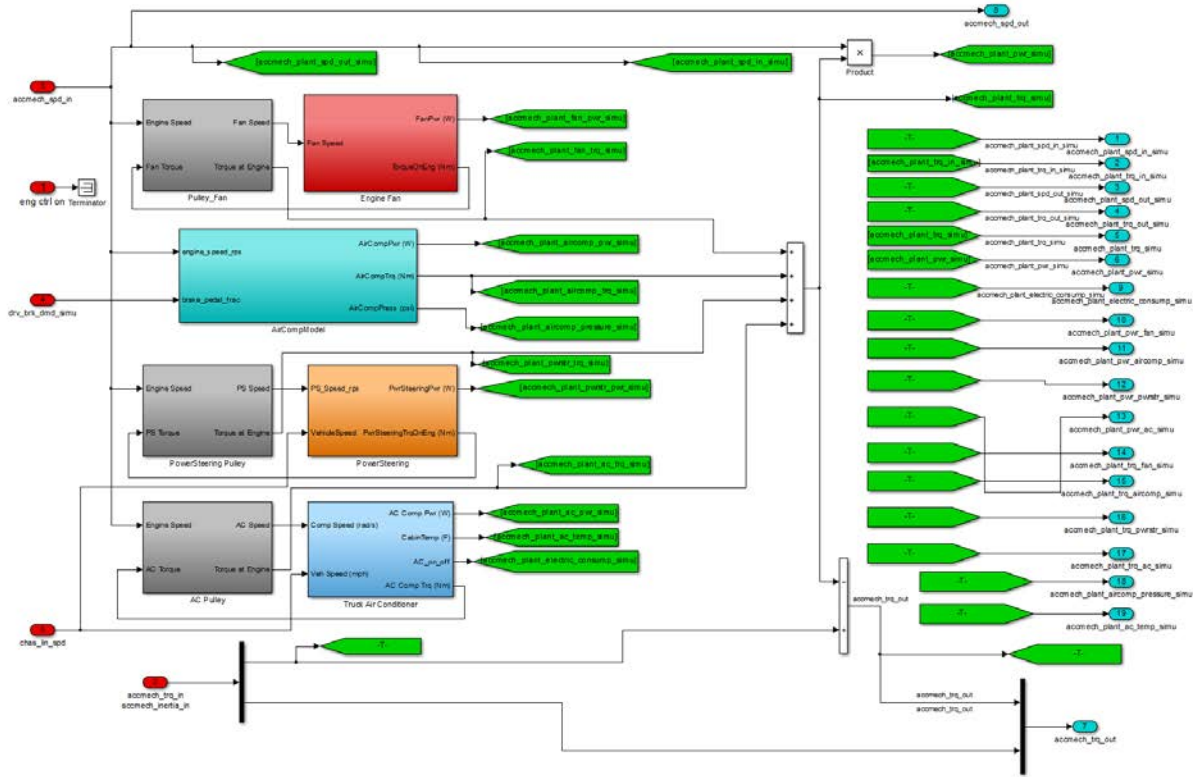


Figure VI-71: Separated accessory models. (cooling fan, air compressor, power steering, air conditioning, and electrical accessories)

Several vehicle types were considered but ultimately class 8 line haul (LH) sleeper cabin trucks were chosen as the project's focus. This vehicle was assessed due to its overwhelming market size and total amount of fuel consumed per year compared to the other two vehicles. Additionally, sleeper cabs spend a large amount of time idling, especially during the driver's overnight hoteling in the warm months of the year. ORNL had access to parameters and data on this vehicle type. The engine and transmission for this vehicle has been tested in ORNL's VSI lab as well as had access to vehicle parameters for a Kenworth T700 to further increase the fidelity of this vehicle model (Figure VI-72).

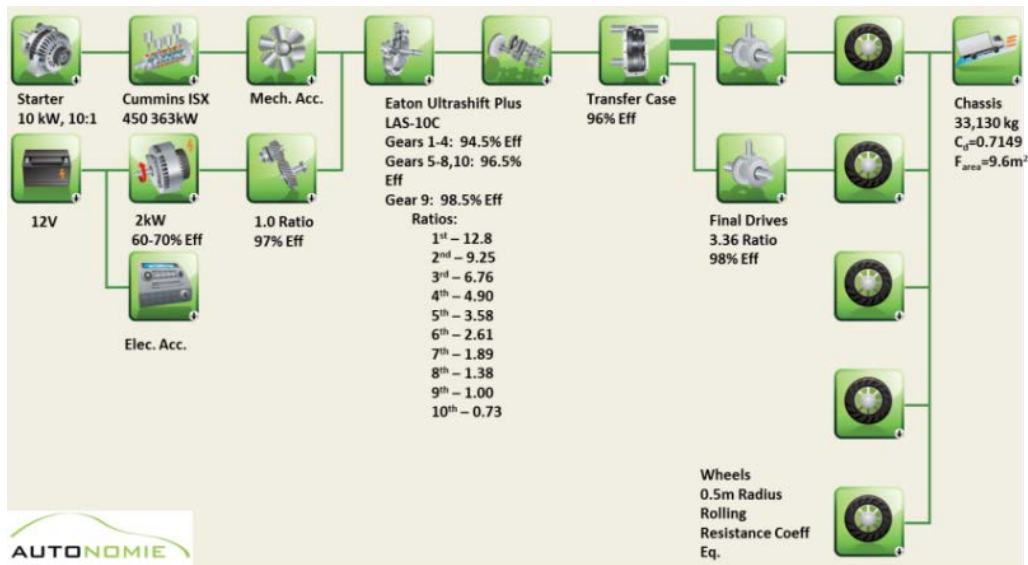


Figure VI-72: HD class 8 line haul sleeper cab based on a chassis tested Kenworth T700.

The second phase of the project is prototype development and component/vehicle testing phase which will be used to: validate the developed component and vehicle models, develop and build a prototype system based on simulation findings, create and test prototype controls in ORNL's VSI component test cell using HIL practices, and test the finished system in Cummins test vehicle for a final system proof of concept.

In order further develop and validate the accessory and vehicle models, Cummins was able to leverage a test vehicle from another project in order to instrument the accessories and get real world data from most of the accessories. After analyzing the data and making the HVAC system, the main focus of this project the team decided that testing the components of that system in a test cell would both help NREL further develop their CoolSim model, but also allows to more accurately compare the two different compressors chosen for the h-APU architecture. The first setup (Figure VI-73) tested is the conventional setup in the truck with the condenser changed to a remote setup allowing the fan to be electrified.

• **Instrumentation**

- 1-4: Pressure and Temperature
- 5: Mass Flow of Refrigerant
- 6: Delta Pressure and Temperature
- 7-8: Speed and Airflow from HVAC Boxes

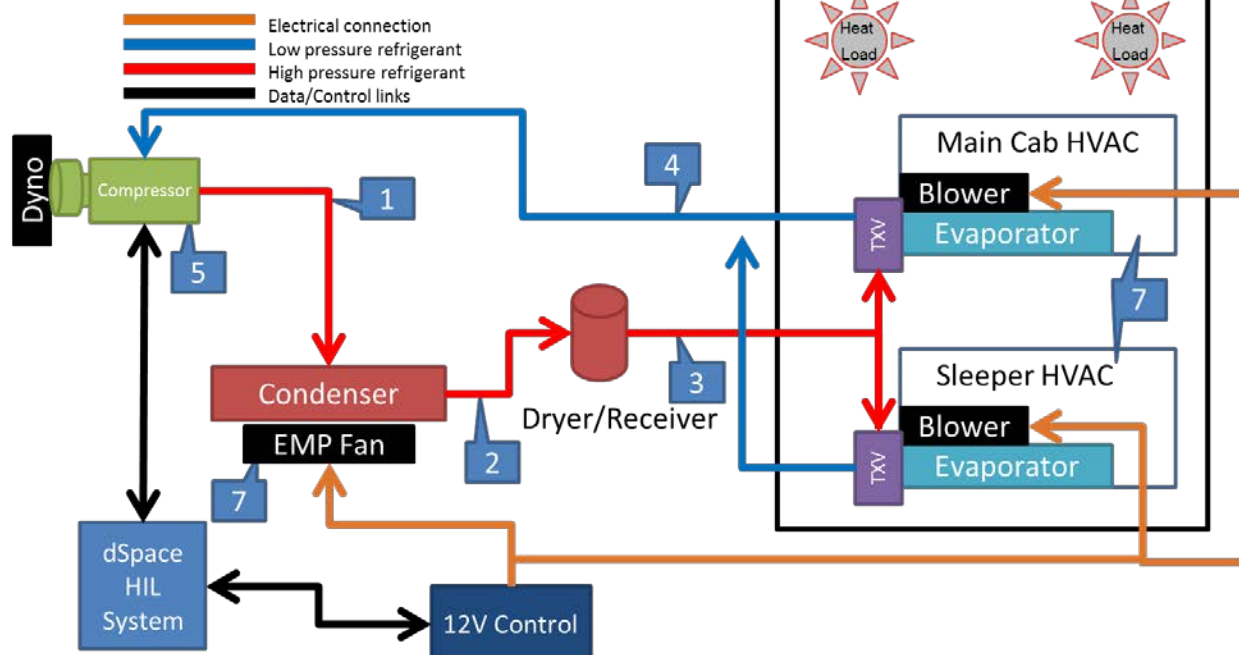


Figure VI-73: First component test cell setup. Conventional sleeper cab setup with electrified condenser fan.

The second setup (Figure VI-74) looks at replacing the conventional A/C compressor with an electrified unit that was supplied by Masterflux. It was essential to achieve the same cooling capacity as the conventional system at certain operating points, so the electric compressor is sized to achieve those selected points. Using two Hioki power analyzers we can characterize both the mechanical and electrical power/efficiency differences between the two systems. This will allow the team to make a choice of which setup best serves the finalized h-APU prototype.

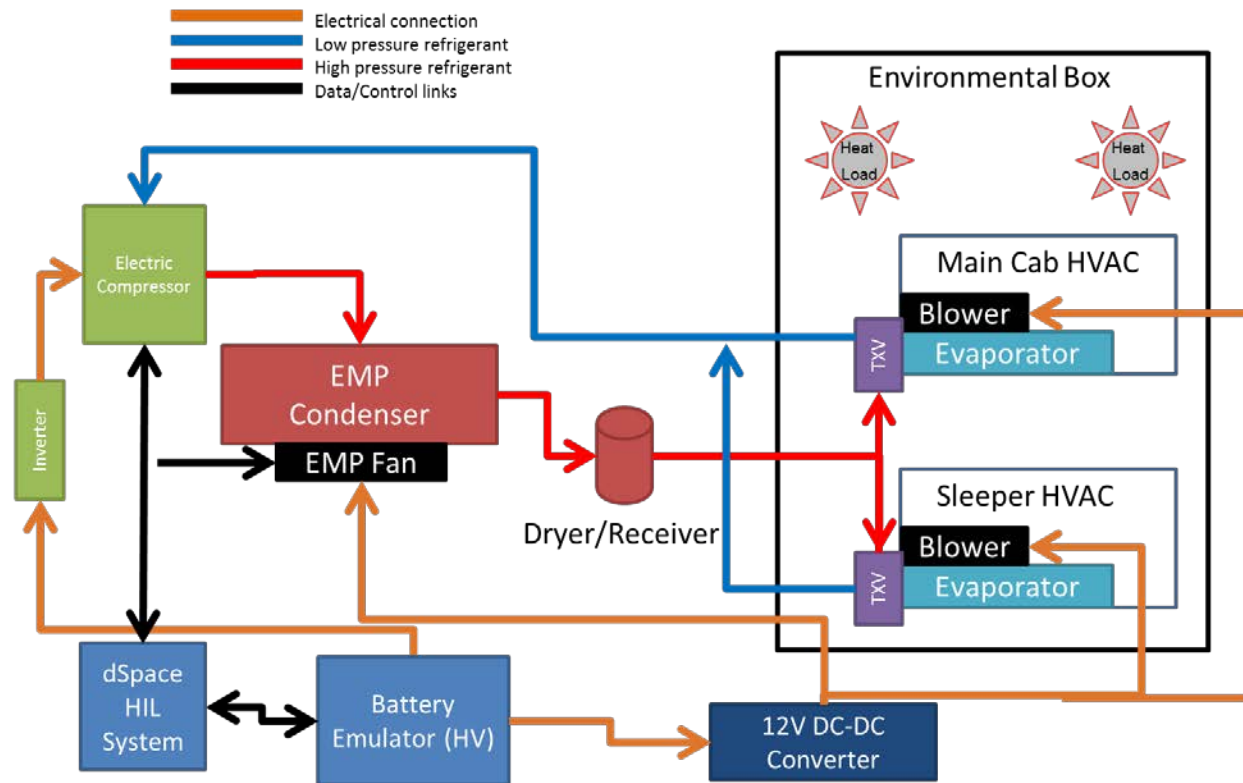


Figure VI-74: Second component test cell setup. Electrified compressor with electrified condenser fan.

While phase two is mostly complete, the specifics of the prototype h-APU architecture, its other components, and results are protected under the CRADA agreement.

Results

The on road portion of the vehicle utilization is only one factor that has to be taken into account when looking at accessory hybridization or electrification. When examining the amount of fuel burned during overnight hoteling in a sleeper cab, researchers found that the amount of fuel consumed was larger than any other application for saving during the on road entitlement studies (Table VI.6).

An idling line haul truck consumes between 0.4-0.88 gallons an hour. Required driver rest period is at least 10 hours which translates into 4-9 gallons consumed during idling not including idling that might incur during freight drop-off and pick up, an extended period of time at distribution hubs could also be a factor. Cummins and ORNL have chosen and developed an architecture which allows for idle reduction or elimination during these distribution hub times as well as overnight idling.

Table VI.6: Accessory Entitlements for the Cummins Proprietary Cycle (HD Class 8 Line Haul Sleeper Cabin)

Fuel Consumption Entitlements	
Data	Fuel Consumption % Decrease
A/C	0.123
Power Steering	0.438
Brake Air Compressor	0.282
Cooling Fan	0.344

With the A/C and hotel loads being the focus for idle reduction, a full mockup of a typical class 8 sleeper cabs HVAC system was installed into ORNL's VSI Component Laboratory (Figure VI-75). This lab is equipped to be able to control temperature up to 105°F and has an E-Storage emulator that can both supply power to electric test components, but also emulate the types of energy storages that the system may use.



Figure VI-75: ORNL's VSI Component test cell. Open configuration.

Two setups were used to test the different components. One setup with all of the A/C components was open to the ambient air of the test cell and the other used an insulated box to isolate the evaporator boxes from the ambient temperature of the test cell (Figure VI-76). During the first setup we are able to simulate pull down conditions within the truck; this was performed at the temperature set points of 105°F, 90°F, and 75°F. Regarding the second set of tests (using the insulated box) the focus was on finding the maximum cooling capacity of each system setup, and to test temperature regulation controls to find which strategy was the most efficient. In order to test the cooling capacity of the system at different operating points the ambient temperature was set to either 105°F or 90°F and the system is set to maintain 70°F inside the insulated box. A set of fans with known volumetric flows introduces hot ambient air into the box until the system is just able to maintain the desired 70°F, this allows for the calculation of how much heat load is being introduced into the system providing the cooling capacity at that operating point.

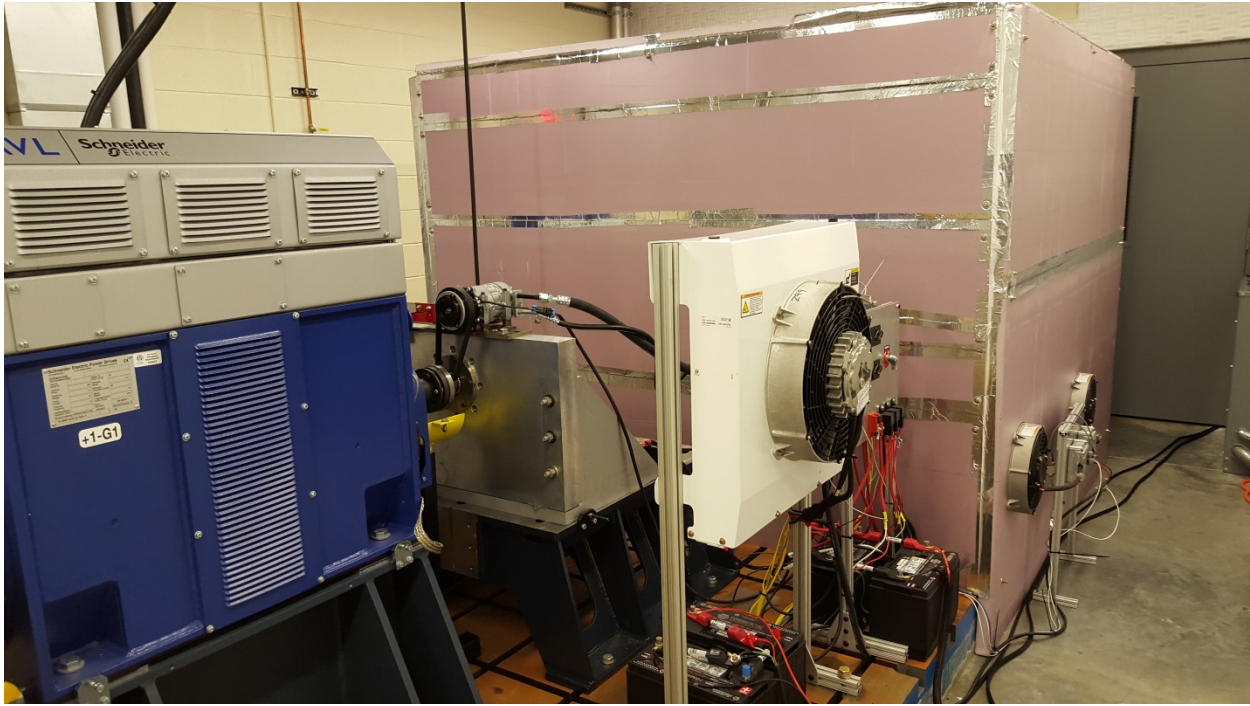


Figure VI-76: ORNL's VSI Component test cell with insulated environmental box.

With the conventional system and remote condenser systems tested ORNL was able to provide NREL with all of the HVAC components geometries, volumes, and other specs to build a baseline system in their CoolSim model. As more data is provided to NREL they will continue to validate and adapt the model to be used in both future simulations as well as providing us an Autonomie compatible model that is to be used in our HIL testing (Figure VI-77). This baseline model being developed with this project will be available for public use once a few proprietary parameters are removed and generic ones take their place. Ultimately the CoolSim model will be an invaluable tool once validated to perform offline simulations of the h-APU system controls on our selected and validated system.

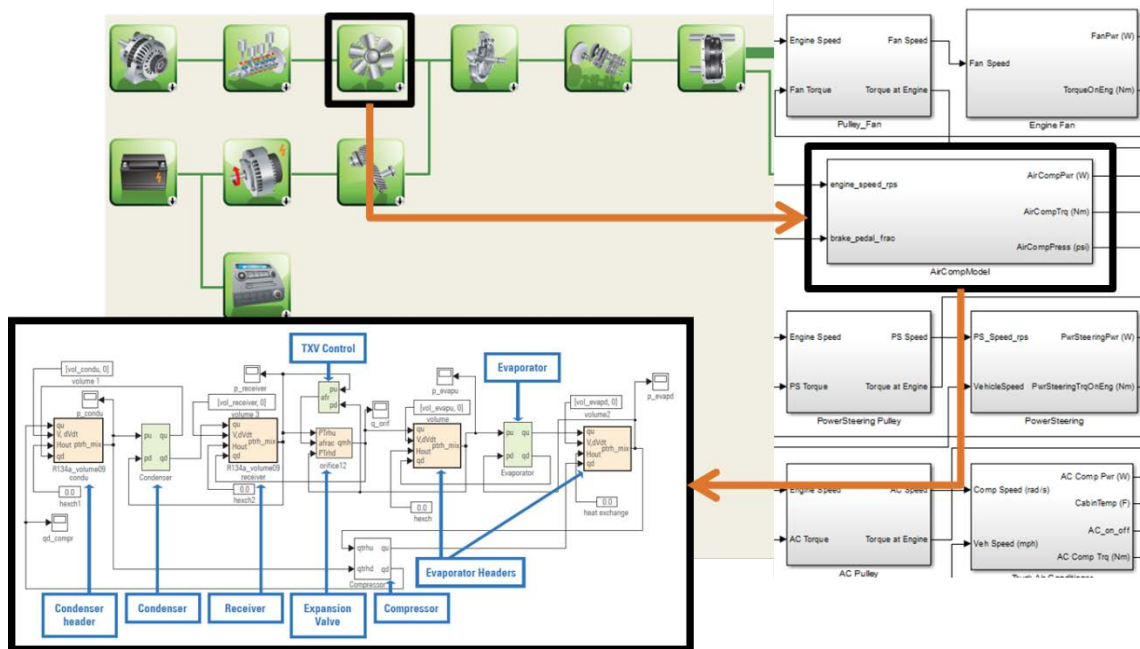


Figure VI-77: NREL's CoolSim model and the structure it will take inside our Autonomie model when validated.

Conclusions

Phase one of the project is largely completed. As more data from Cummins test vehicle, ORNL's test cell, and NREL's CoolSim model becomes available the models will continually be updated to provide more realistic results as well as continue to improve ORNL, NREL and Cummins' model libraries for future projects. Phase one has allowed Cummins and ORNL to create tools to evaluate future accessory technologies as well as discover the current landscape in accessory technologies and idle reduction devices.

Phase two is nearing completion. ORNL is concluding testing on the electric compressor system along with the temperate control strategies, and Cummins is finishing integration of the finished h-APU system into the test truck for the proof of concept demonstration. Phase two has also allowed NREL to build a baseline class 8 heavy duty sleeper cab CoolSim model that will be validated and available for public consumption minus a few propriety parameters from this project.

After reviewing the results of the study, Cummins and ORNL determined that an accessory architecture is the best solution for maximized potential in reducing emissions and fuel consumption; this method will either reduce or eliminate the need for idling in HD class 8 trucks. Choosing the accessory architecture best allows the project to address issues of idling for extended periods while accessory loads are still essential, as in overnight hoteling and idling while in queue at distribution hubs. The architecture for this has been chosen and developed based on the findings and testing done on this project, but is protected under the CRADA agreement.

VI.6.C. Products

Presentations/Publications/Patents

1. Invention Disclosure: 201503581
 - a. DOE S-Number: S-138,217
2. Invention Disclosure: 201503582
 - a. DOE S-Number: S-138,218
3. Invention Disclosure: 201503589
 - a. DOE S-Number: S-138,226

VI.7. Powertrain Controls Optimization for HD Hybrid Line Haul Trucks

David E. Smith, Principal Investigator

Oak Ridge National Laboratory
2360 Cherahala Boulevard
Knoxville, TN 37932
Phone: (865) 946-1324; Fax: (865) 946-1541
E-mail: smithde@ornl.gov

David Anderson, DOE Program Manager

Vehicle Technologies Office
Phone: (202) 287-5688
E-mail: david.anderson@ee.doe.gov

Start Date: 10/01/2013

End Date: 9/30/2016

VI.7.A. Abstract

Objectives

- Develop and validate accurate component models for simulating integrated engine, hybrid energy storage, emissions control, and supervisory control systems in Class 8 trucks.
- Evaluate the merits of specific alternative technologies and control strategies under realistic MD and HD drive cycle conditions.
- Investigate Reactivity Controlled Compression Ignition (RCCI) advanced combustion coupled with series hybrid electric operation.
- Introduce emissions controls to minimize criteria pollutants, with emphasis on challenges of low temperature combustion.
- Integrate actively controlled hybrid energy storage systems (battery plus ultracapacitor) for enhanced regenerative braking energy capture.
- Experimentally verify advanced combustion, hybrid energy storage, and aftertreatment systems utilizing actual hardware and virtual vehicle systems.

Accomplishments

- Updated engine and aftertreatment models based upon experimental powertrain results from ORNL VSI Laboratory.
- Completed detailed hybrid energy storage systems models and associated sizing.

Future Achievements

- This project is being refocused in FY2016 to explore powertrain optimization of conventional line haul vehicles.
- The research aligns more closely with 21st Century Truck Partnership needs and will focus on treating the engine and transmission as a system with a goal of fuel consumption and emissions reduction.



VI.7.B. Technical Discussion

Background

Hybrid medium and heavy-duty (MD and HD) powertrains offer large potential reductions in fuel consumption, criteria pollutants, and greenhouse gases. In addition to powertrain electrification, advanced combustion regimes could further reduce the fuel consumption for these vehicles. The most fuel-efficient MD and HD combustion engines are advanced diesels, which require aftertreatment for compliant emissions control. Diesel hybridization is challenging because the integrated aftertreatment, engine, and battery systems must be optimized to meet efficiency targets and simultaneously satisfy drive cycle and emissions constraints.

Introduction

This is a vehicle system level project, encompassing analytical modeling and supervisory controls development as well as experimental verification/validation testing at the component, powertrain, and full vehicle system level. This project supports the goal of petroleum consumption reduction for medium and heavy trucks through the development of advanced hybrid technologies and control systems. VSST has invested previously in R&D to support hybrid energy storage systems (Li-ion plus ultra-caps) for light duty, passenger car applications. This research will be extended to the MD and HD sector where current battery technology is not mature enough to handle the substantial regenerative braking power levels these trucks are capable of producing. With this hybrid energy storage system, substantial gains in overall vehicle efficiency are possible. In addition, advanced combustion technologies, such as RCCI, will be implemented into an advanced hybrid powertrain for a Class 8 line haul application. This powertrain, leveraged from other VSST work (Meritor, a current ORNL/VSST partner), is ideal for taking advantage of the benefits of RCCI operation due to its series hybrid mode of operation. Emissions control is also a focus of this project, especially due to the fact that RCCI creates a low temperature exhaust stream that must be addressed.

Approach

The project seeks to leverage multiple research areas into a single vehicle platform. The chosen hybrid powertrain is a fully capable Class 8 powertrain designed for line haul applications, and has the ability to be operated as an all-electric vehicle, series hybrid electric vehicle (at low to moderate speeds), and a parallel hybrid electric vehicle at moderate to highway speeds. This powertrain offers itself to improvement by the technologies investigated in this project.

There are four focus areas for this project, ranging from advanced combustion regimes and engine control strategies, emissions control technologies, pulsed energy storage systems (dual energy storage systems), and advanced energy management and supervisory controls. These four areas are shown graphically in Figure VI-78, and are summarized below.

Advanced engine control strategies

Research in this area is being leveraged with on-going projects at ORNL and being co-sponsored by the DOE VTO Advanced Combustion and Emissions Control program. ORNL has been engaged in the area of Reactivity Controlled Compression Ignition (RCCI) on multi-cylinder engines for improved fuel efficiency and reduced emissions. This mode of combustion offers increased fuel efficiency at the sacrifice of a narrow operating window and reduced exhaust gas temperatures. For this reason, a series HEV would be a good operating environment for this type of engine control, due to the ability to maintain complete control over the operating envelope of the engine.

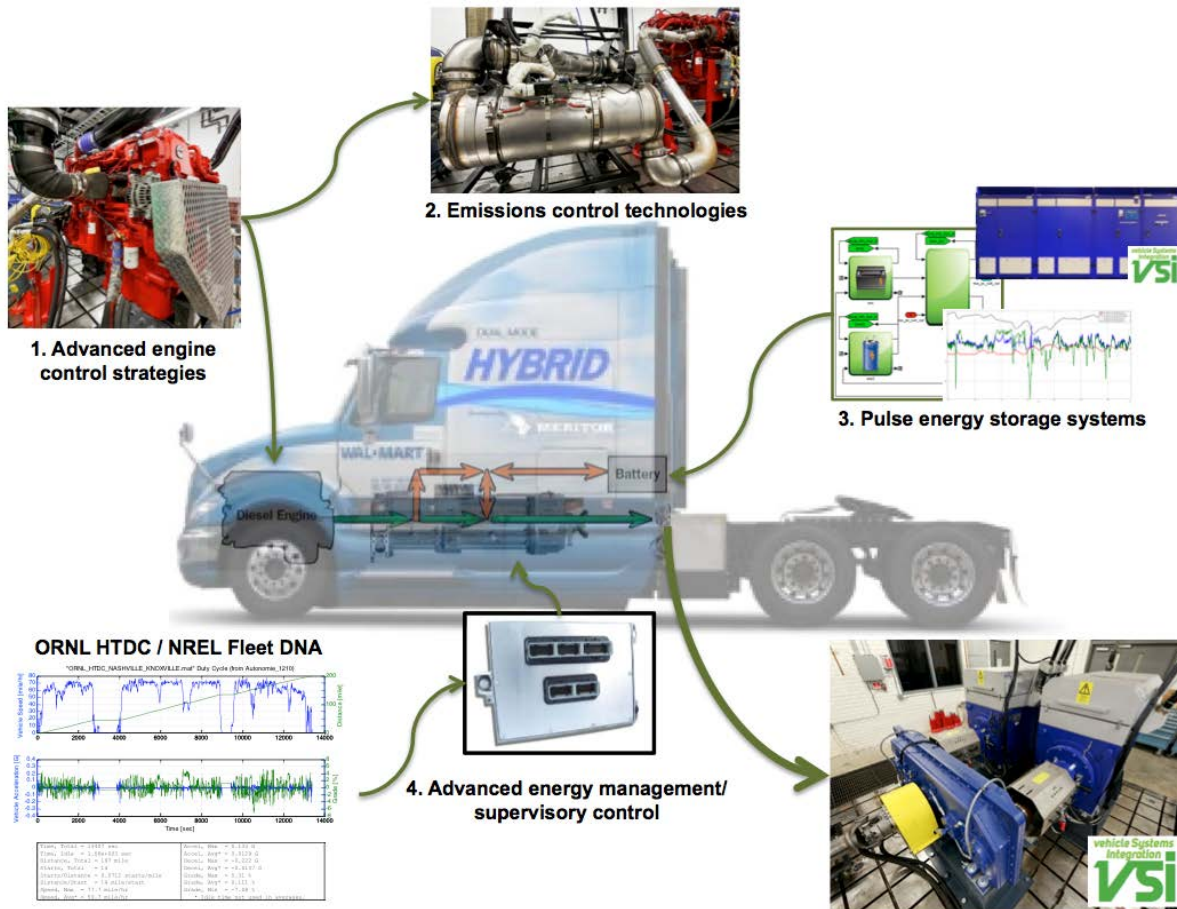


Figure VI-78: Project focus areas.

Emissions control technologies

Emissions control is essential for the success of RCCI due to lower exhaust temperatures. To further exacerbate the problem, the hybrid powertrain has the ability to operate solely on electric power, as well as intermittent engine start/stop operation. This leads to increased importance of coordinating engine operation and emissions control in order to maximize the benefits of powertrain electrification and advanced combustion.

Pulse energy storage systems

Perhaps the greatest opportunity for powertrain efficiency improvement is new approaches for increased regenerative braking energy collection for Class 8 line haul hybrid trucks. Current battery technology, while reasonably mature for light duty applications, is not capable of absorbing the large amounts of energy that is necessary to slow these trucks down. One approach that has been researched in the past for light duty applications is dual energy storage systems, or the combination of batteries with ultra-capacitors. This section of the research builds upon past research from Argonne National Laboratory that was done for light-duty vehicles. The approaches developed as part of that work will be adapted/extended to this heavy-duty line haul vehicle application.

Advanced energy management/ supervisory control

In order for each of the previous technologies to function seamlessly at the vehicle level, appropriate energy management strategies must be developed that will fully realize the compound benefits of all the candidate technologies being investigated in this project. Past HD HEV supervisory control experience will be leveraged and expanded to incorporate these new technologies in a meaningful and cohesive manner.

Results

Engine and emissions data enhanced

Engine fuel consumption and emissions data was enhanced due to leveraging against other on-going projects in the VSI laboratory. A complete test matrix was executed (and repeated for accuracy) for developing more reliable engine and emissions data. The laboratory setup of the test engine is shown in Figure VI-79 below.

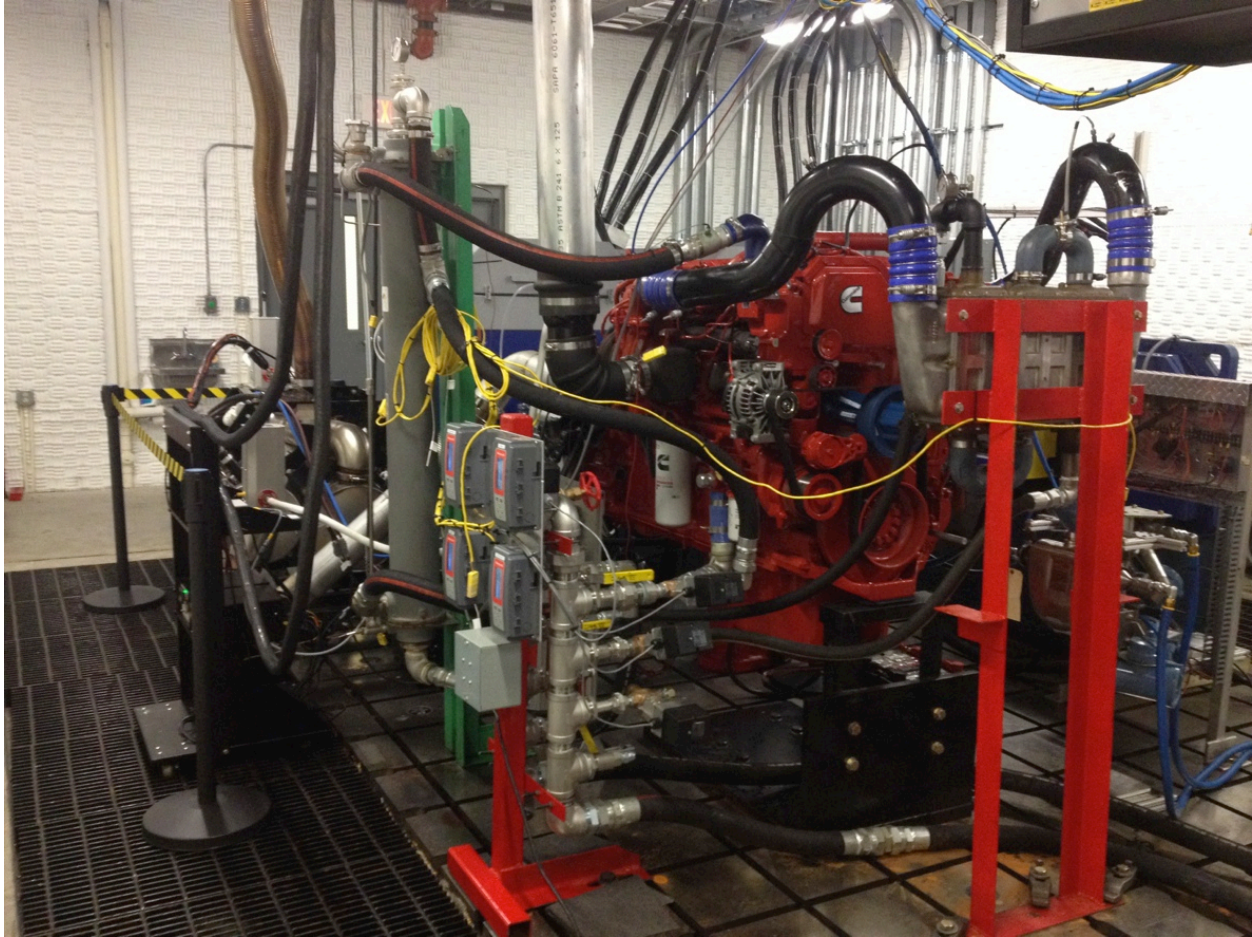


Figure VI-79: Engine dynamometer configuration.

The fuel consumption data was verified through comparison of actual fuel measurement, J1939 engine network data, and emission/air fuel calculations. In addition, essential parameters were logged and mapped that were necessary for developing the exhaust aftertreatment models, such as temperatures and mass flow rate of emissions species. Example maps of the data generated for use in the simulation models are represented in Figure VI-80.

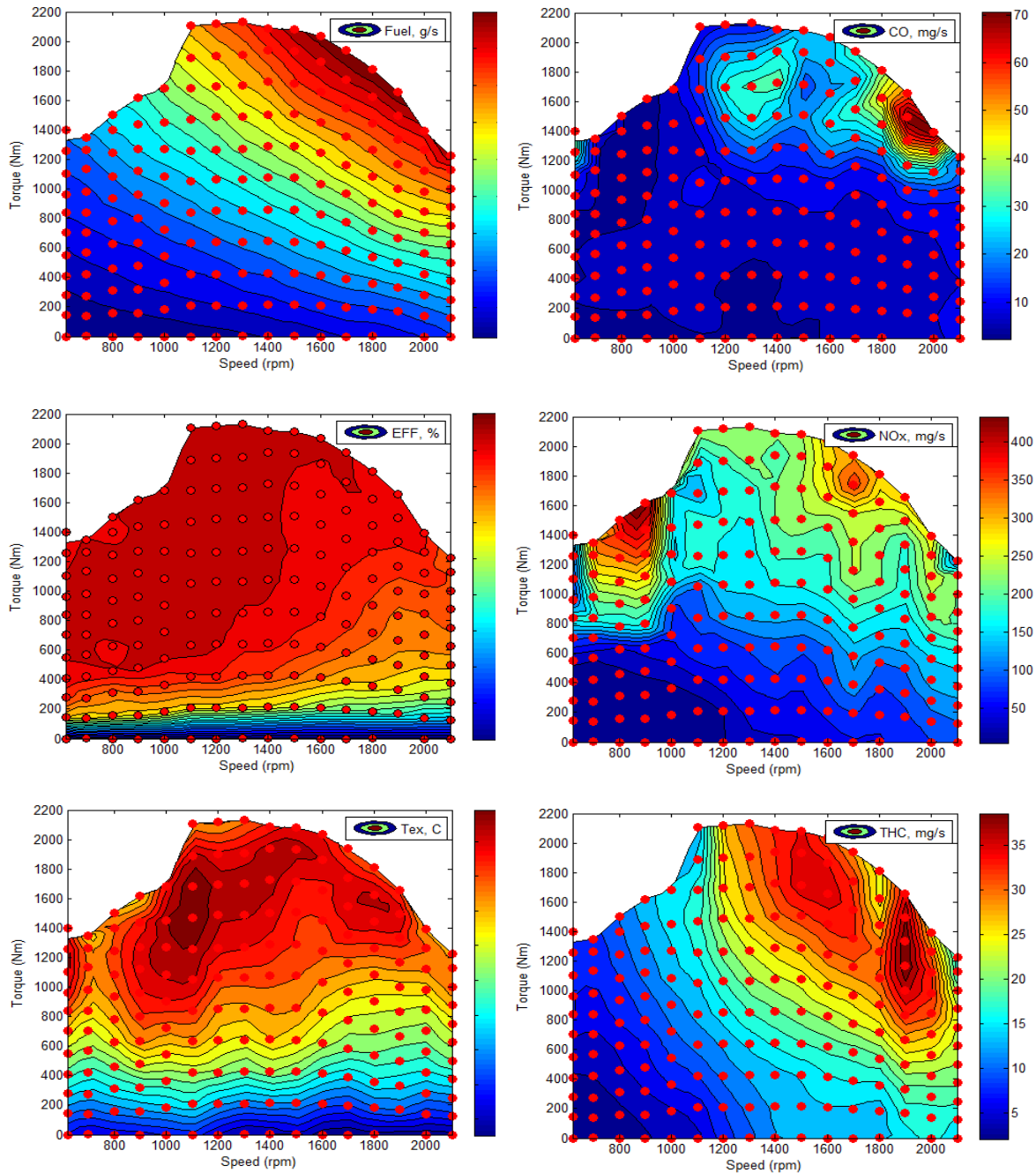
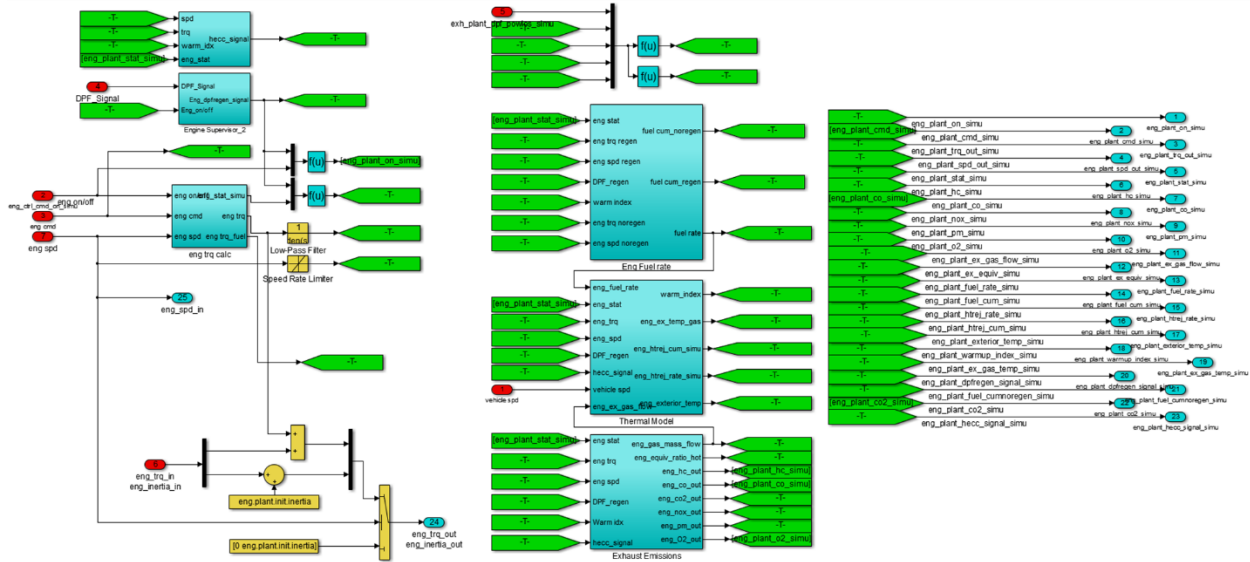


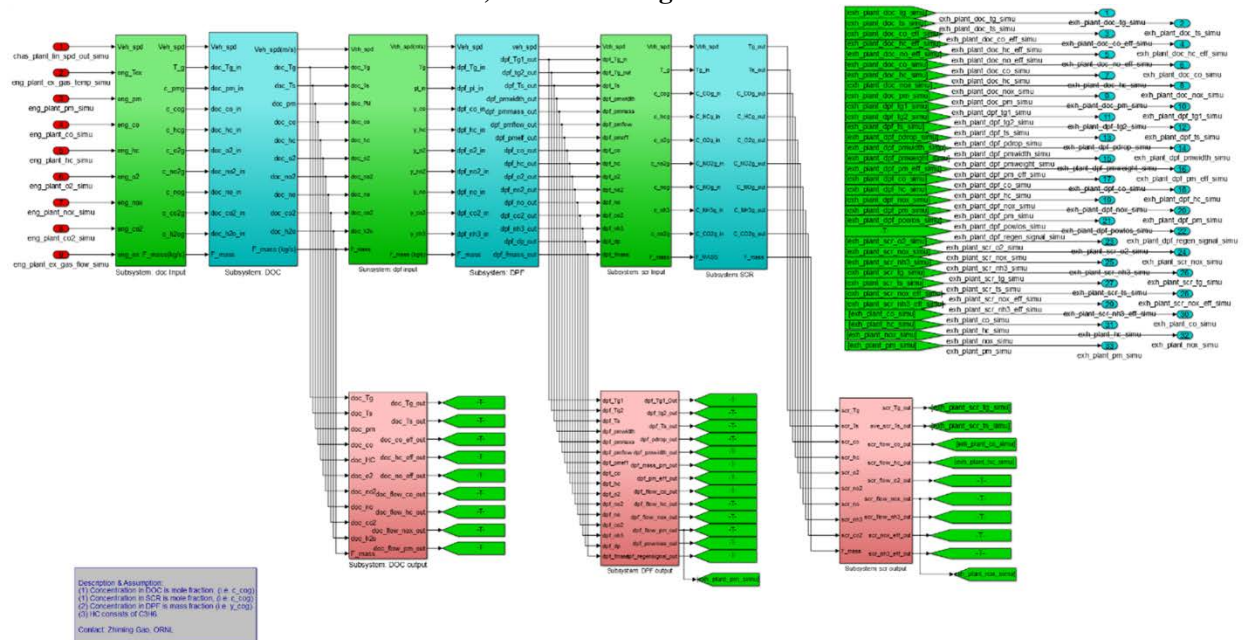
Figure VI-80: Updated fuel consumption and emissions maps.

Engine system models updated and validated

ORNL has implemented past transient engine modeling experience to develop a transient model of a Cummins ISX-450 15 liter engine and associated emissions aftertreatment system. The suite of engine and aftertreatment models developed for this engine is capable of simulating cold starts based upon a method developed by ORNL researchers utilizing quasi-statis data. The model was built in the SIMULINK environment and formatted for use in Autonomie. Figure VI-81 outlines the high level Autonomie implementation of the transient engine model, including a snapshot of the aftertreatment models.



a) Transient Engine Model



b) Exhaust Aftertreatment Models

Figure VI-81: ORNL transient engine model and associated aftertreatment models.

Emphasis was placed on completing the development and validation of the aftertreatment models for this powertrain in FY2015. Data was logged from the actual components in the ORNL VSI Laboratory and used to validate the resulting empirical models over a host of drive cycles. Figure VI-82 gives examples of the validation for predicted (simulated) versus actual measurements for the diesel particulate filter (DPF) exit flow temperature, differential pressure measurements across the DPF, and the diesel oxidation catalyst (DOC) exit flow temperature. Excellent correlation between the actual and predicted values was observed in all cases. Temperature predictions trended appropriately, and exhibited reasonable agreement.

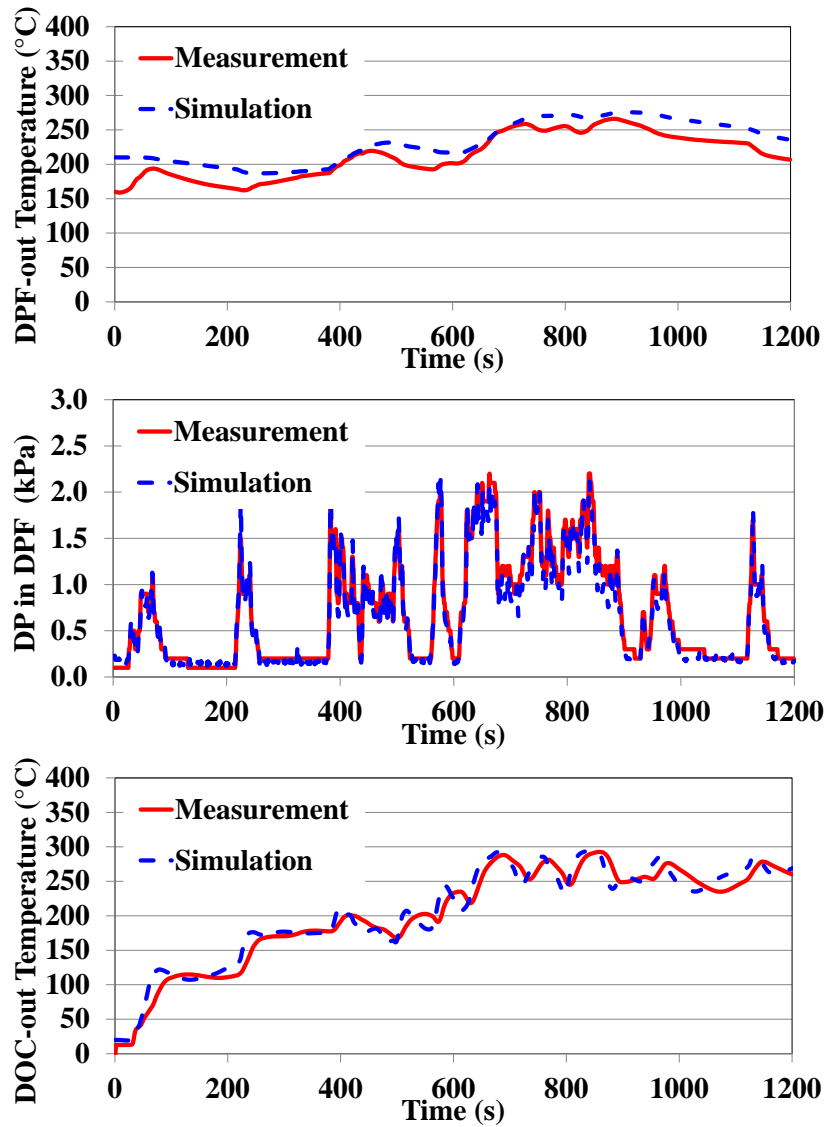


Figure VI-82: Aftertreatment model validation data.

Hybrid energy storage system (HESS)

The full-up simulation model for the dual energy storage system, modeled in PSIM V.10.0.2, is shown as Fig. 5.1 noting that the issue with external file importing has been corrected in this version along with the addition of an ultracapacitor parameter extraction tool that facilitates the voltage dependent modeling of any manufacturers ultracapacitor provided an appropriate single pulse discharge data set is available.

The parameter file shown in Figure VI-83 at left contains all the parameter values along with initial state of charge (SOC), lithium ion battery (LIB) capacity, C_b , and the setting on the buck/boost regulated voltage, U_{d0} . What happens with this architecture having a free-running buck/boost converter is that for a specified link voltage, U_{d0} , relative to the LIB nominal voltage at the specified SOC_0 the two energy storage units will try to charge/discharge until the voltages equilibrate. This can be seen in the short simulation run where the load file consists of a bipolar pulse of 100A discharge followed by 100A charge. In this case the HESS meets the load current profile but overall the LIB discharges into the ultra-capacitor (UC) attempting to restore its voltage. For this reason the DC-DC converter requires voltage mode control.

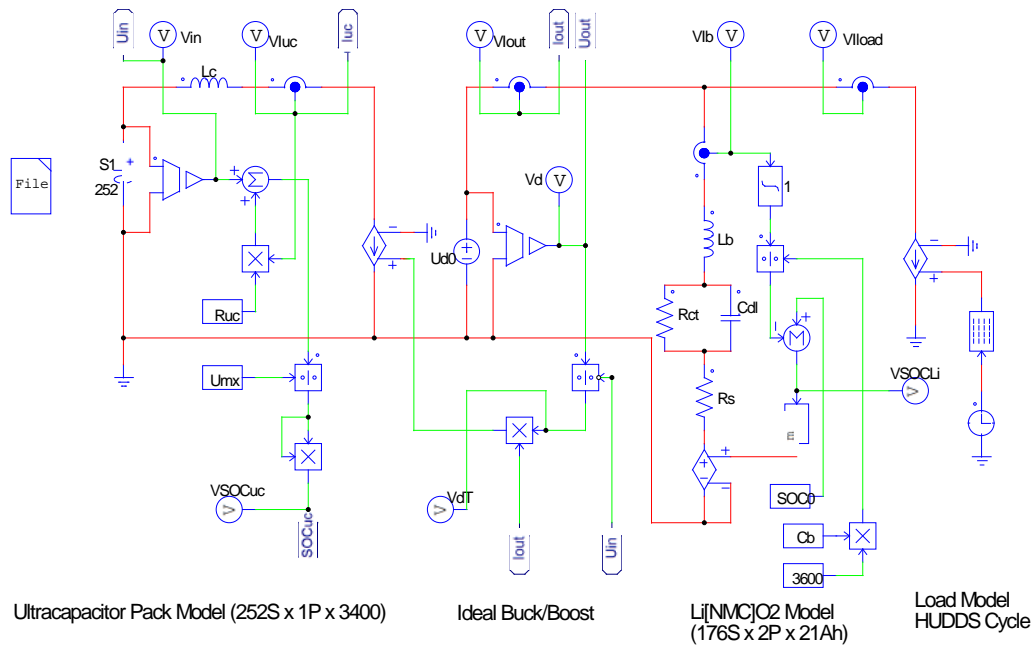


Figure VI-83: HD truck HESS simulation model.

The full HESS model of Figure VI-83 is modified to include voltage mode control of boosting and buck modes according to the loading conditions. This is needed so that the UC does not exceed its SOC_{uc} bounds of $0.25 < SOC_{uc} < 0.95$ thereby extracting nearly 75% of its energy but not imposing a high boost gain on the DC-DC converter. Figure VI-84 illustrates the contrived load current pulse train applied for model validation.

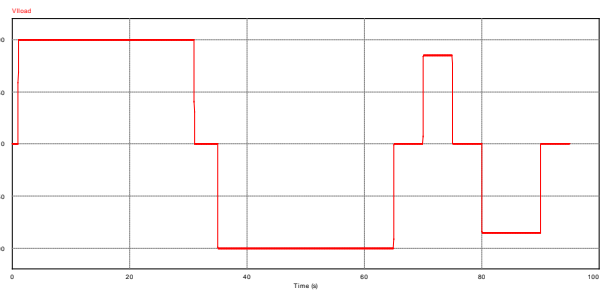


Figure VI-84: HD HESS load current profile: +/-100A; +/-80A.

Figure VI-85 shows how the full dual storage system has been modified. In this modification the switch (SS1) represents an inhibit signal that would be applied to the buck/boost converter thereby transitioning it to a high impedance state, Z. Figure VI-86 shows the buck/boost converter control logic (preliminary stage).

On the left hand side of Figure VI-86 the UC SOC_{uc} is windowed by the comparators against lower and upper limits. The LPF stages are needed to eliminate chattering since hysteresis has not been used in the comparator stages. At the right hand side of Figure VI-86 the load current is windowed against upper (motoring) and lower (regeneration) limits that help maintain C-rate loading of the battery to less than its maximum capability. The load current window values here are set relatively low to facilitate validation using the load current profile of Figure VI-84.

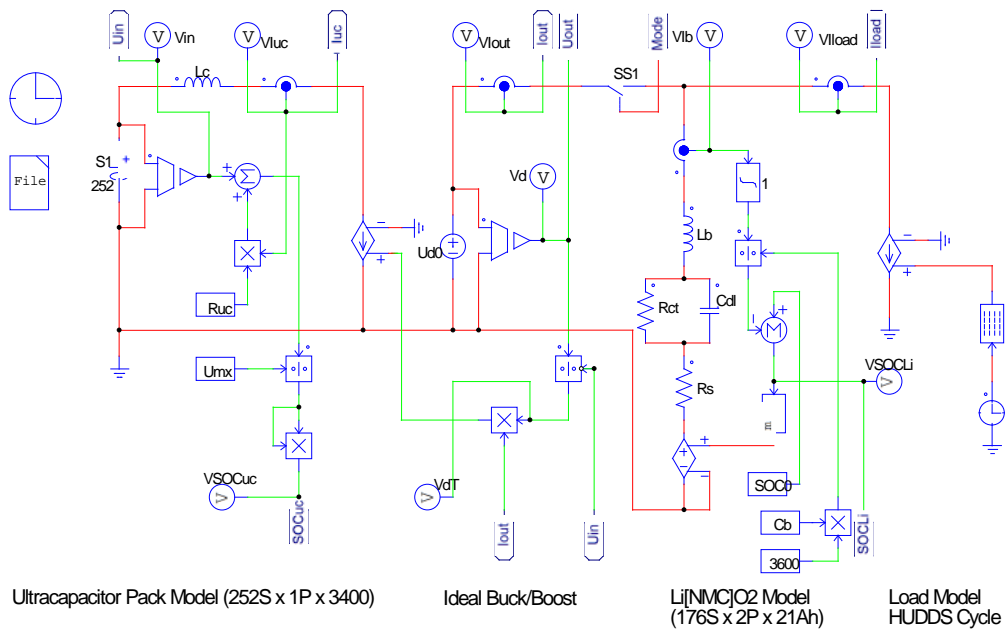


Figure VI-85: HD HESS modified for high-Z state of buck/boost cConverter.

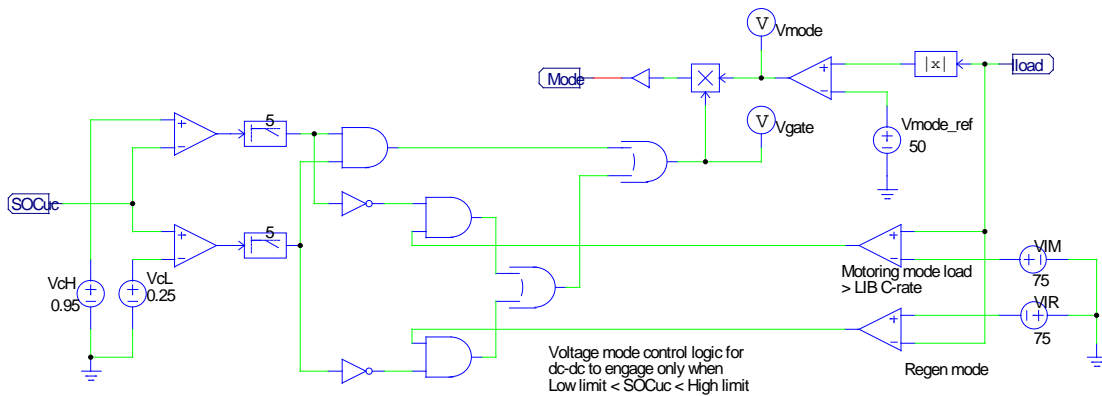


Figure VI-86: HD HESS buck/boost voltage mode control logic (initial power management strategy architecture).

Without going into dc-dc converter control mode changes it is worth exercising the model of Figure VI-85 and Figure VI-86 with the load current obtained for the HD Truck over the HUDDS cycle. In order to do this, four steps must be undertaken:

- i. Total propulsion power, $P(V)$, shown in Figure VI-87 must be decomposed into P_{mtr} and P_{gen} in order to segregate motoring power, which for a hybrid consists of ICE and M-G power, from regeneration and braking power. For this project, the H-UDDS drive cycle data is used.
- ii. Next, using the motoring power data, an exponential smoothening function having damping coefficient of 0.8 is used to smoothen (average) the propulsion power as P_{ICE} . This step is also performed in Excel using its Data Analysis features. Once the average is separated from the total motoring power, P_{mtr} , a difference is taken with this from the total P_{mtr} . For the fully loaded HD Truck on the HUDDS cycle this difference power may easily exceed the capability of the ISG unit (rated 400 kW). It will be seen whether the UC can source these peaks (only on the order of 6 or 7 occurrences in this case).
- iii. Third, and due to the M-G peak power capability, the regeneration power is limited to 400 kW. It is understood that any regeneration power exceeding the capability of the M-G is to be dissipated in the

HD Truck service brakes. This means of course that parallel regenerative brake system technology is being used.

- iv. Lastly, the now decomposed propulsion power, P_{diff} , and delimited regeneration power, P_{regen} , are summed into total hybrid energy storage system power, P_{HESS} . For a given dc-link voltage on the M-G subsystem, U_{d0} , this dynamic power, P_{HESS} , is converted to a load current, I_{load} (A_{dc}). This final set of data is what will be imported into the dual storage system model as its loading.

The following set of figures summarize the above four steps and show how the overall HD Truck propulsion power, $P(V)$, is decomposed into the dynamic power to be handled by the HESS. At this point it is necessary to understand the method used to separate out P_{diff} from P_{mtr} and P_{ICE} in order to constitute the motoring load on the HESS. Note in Figure VI-88 that exponential smoothening (red trace) persists even when total motoring power, P_{mtr} , is zero. Logical expressions are used in the Excel file that simply zero out these zones since they will later be filled with the delimited regeneration power.

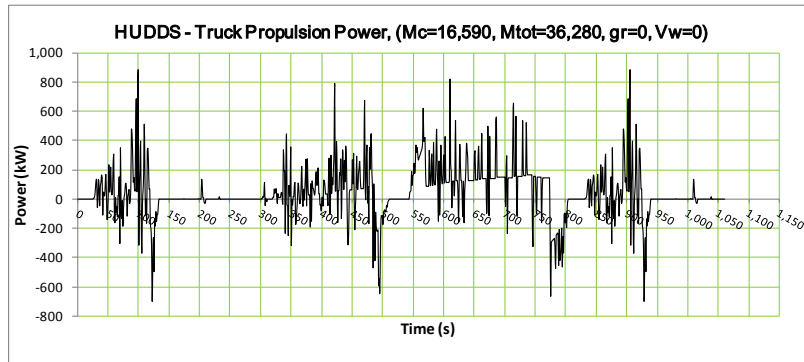


Figure VI-87: HD truck propulsion power, $P(V)$, (fully loaded trailer case).

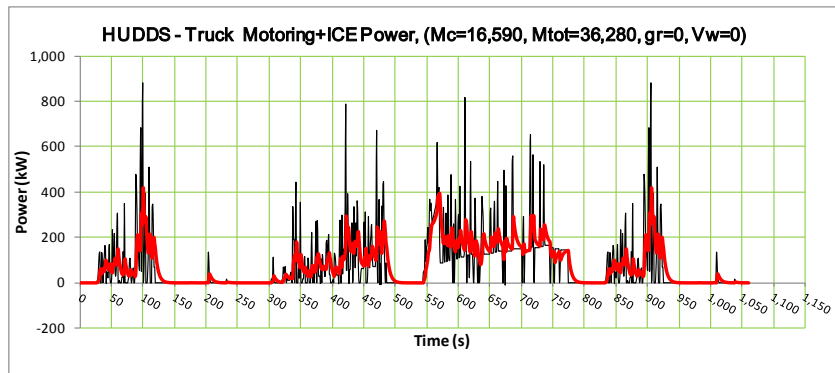


Figure VI-88: HD truck motoring power with filtered PICE.

It is clear in Figure VI-89 that the HD Truck easily exceeds the M-G regeneration capability in the four clustered zones of heavy deceleration. To accommodate the M-G limitations the regeneration power, P_{regen} , is clamped to 400 kW, with the remainder understood as being dissipated in the foundation brakes.

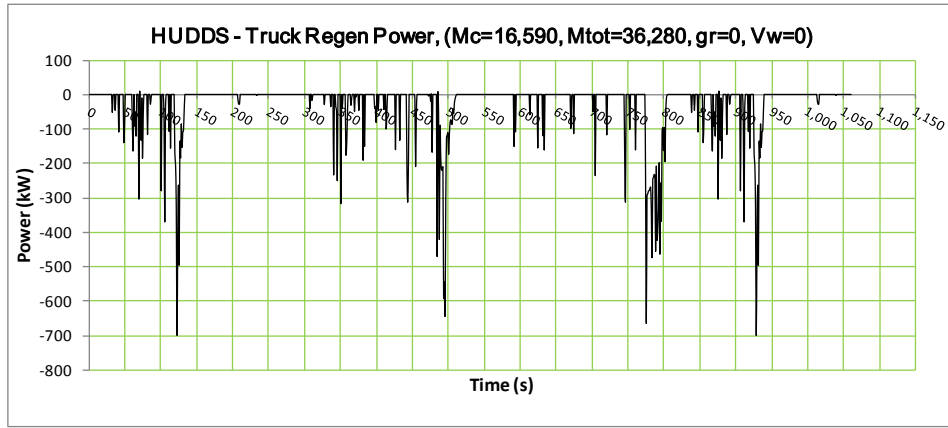


Figure VI-89: HD truck regeneration power (fully loaded trailer case).

With the above cited data limiting for regeneration power the next step is to reconstitute the total dynamic power that will be applied to the dual storage system. Figure VI-90 shows the reassembled power now as total dynamic power loading for the HESS. There is no sustained average power demand as before.

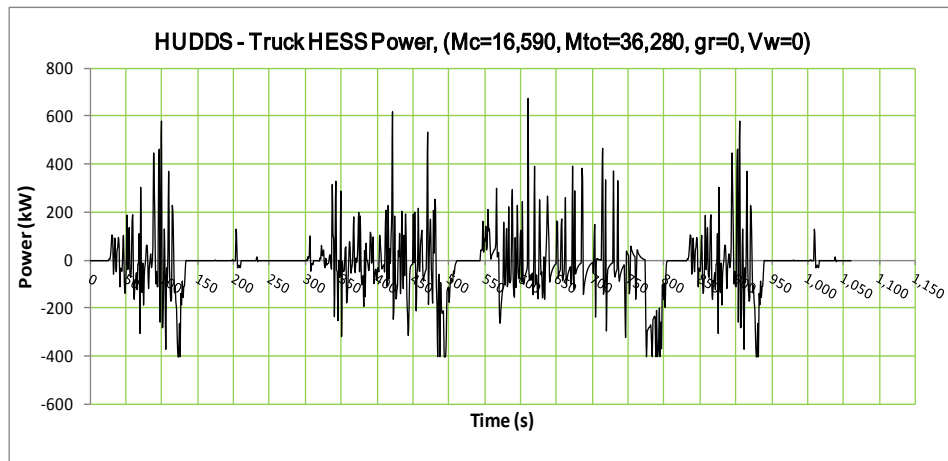


Figure VI-90: HD truck dynamic power (fully loaded trailer case).

Using the nominal dc-link voltage as specified by the dual storage system architecture ($U_{d0}=700V_{dc}$) the dynamic power shown as Figure VI-90 is converted to a dynamic load current, I_{load} as shown in Figure VI-91 below. Note that there will be instances of high discharge demand for those motoring power pulses that exceed 400 kW. The implication is that for a fully loaded trailer a 400 kW M-G will be over taxed meeting the dynamic loading. For this reason, a simulation to follow this work will evaluate the empty trailer case to determine how much the M-G should be up-rated to accommodate the load and drive cycle. In addition, the same should be done for the more demanding drive cycles. Figure VI-91 shows that regenerative current peaks will reach 571 A_{dc} but motoring peaks can be 800 A_{dc} to 900 A_{dc} in a handful of cases.

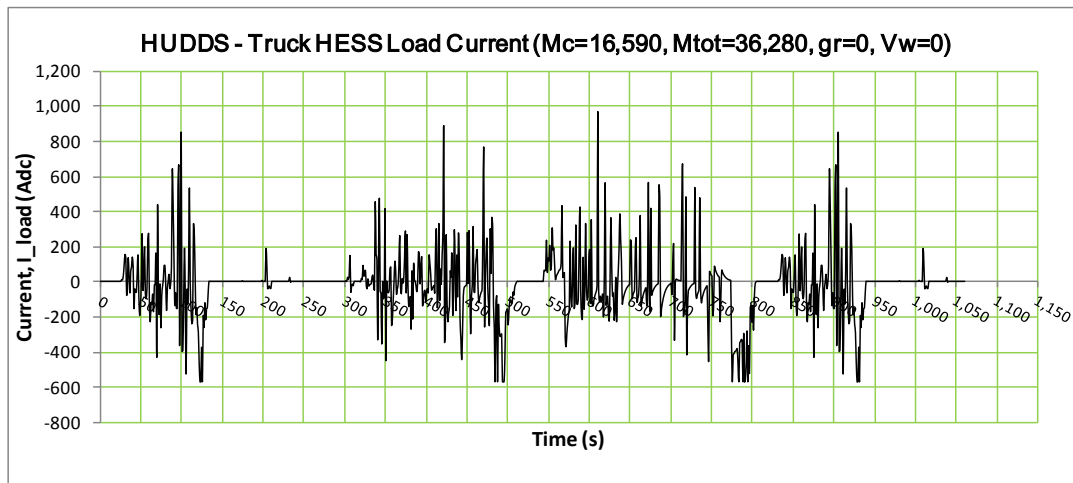


Figure VI-91: HD truck dynamic load current (fully loaded trailer case).

For the dynamic load current of Figure VI-91 and the dual storage design at hand, the LIB has the capability to discharge and charge up to $210A_{dc}$ (5C rate) at $U_{d0}=700V_{dc}$. For regeneration this leaves a dc-dc converter load side current $I_{out}=361 A_{dc}$. Assuming the buck gain, $D=0.5$, then $I_{uc}=I_{in}=(1/D)I_{out} = 722A_{dc}$, feasible for the UC pack, but putting a high current burden on the buck/boost converter semiconductors. For those isolated cases of extreme motoring current, $900A_{dc}$, the converter output side and input side currents will be $I_{out}=690 A_{dc}$ and $I_{in}=1380 A_{dc}$ respectively. For a modern power converter those are high, but still manageable current levels. It was found that when Excel regenerative braking data for the fully loaded trailer is limited to 400 kW that this is still a net charge situation for the HESS.

The high average regeneration current means the HESS will tend to fill both the UC and the LIB. To remedy this, the regeneration power limit in (5) is reduced to 310 kW for which $\langle I_{load} \rangle = -16.46 A_{dc}$, but with $\langle P_{mtr} \rangle = 15.2 kW$ and $\langle P_{gen} \rangle = -26.8 kW$ which should be manageable by the dual storage system.

The Excel file for HUDDS $I_{load}(t)$ vs. time is saved as a notepad *.txt file for import into the PSIM HESS model of Figure VI-85 for simulation of UC and LIB SOC variations. It will be a matter for the power management strategy to manipulate the buck/boost converter so that load current is appropriately shared between the UC and LIB. In Figure VI-92 it is clear that even this amount of P_{gen} causes the UC to fill-up.

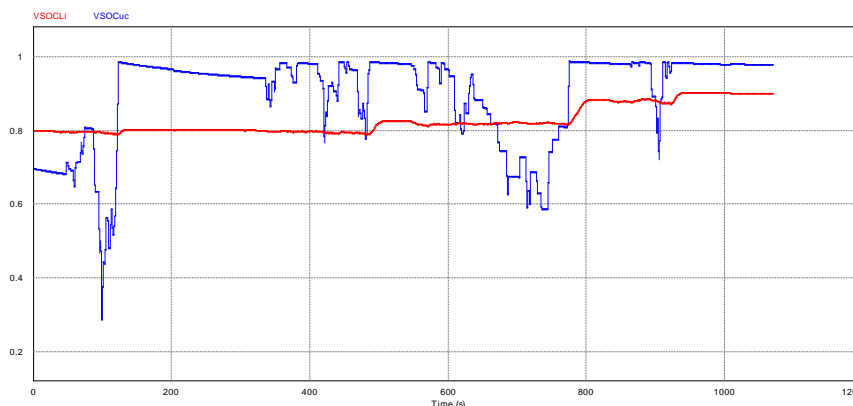


Figure VI-92: PSIM simulation of the HD truck HESS: Initial $SOC_b=0.8$, $SOC_{uc}=0.697$, $U_{d0}=680V_{dc}$

The UC model initial voltage, U_{c0} , is reduced from 2.38V/cell to 2.1V/cell which brings the pack initial $SOC_{uc0}=0.54$ from the earlier $SOC_{uc0}=0.697$. This will provide more energy storage capacity to the UC pack. The LIB pack remains at $SOC_b=0.8$ since the LIB is not absorbing as much energy due to its C-rate limit of 5C. The burden is clearly on the UC and its power converter. Figure VI-93 shows that with a lower initial SOC_{uc0} that it still fills quick during some initial heavy regeneration during the HUDDS cycle.

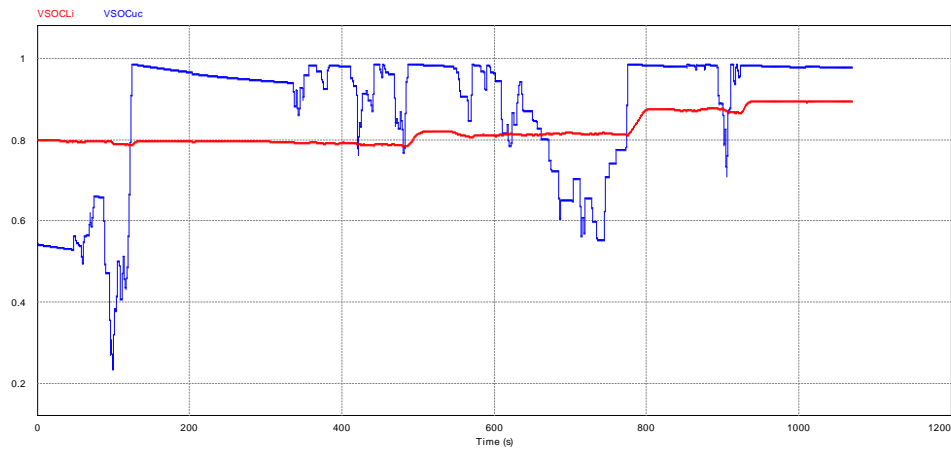


Figure VI-93: PSIM simulation of the HD truck HESS: Initial SOC_b=0.8, SOC_{uc}=0.54, U_{d0}=680V_{dc}

To put more realism into the HESS model a constant power load of 5kW is added to model accessory and ancillary loads that may be drawn from the LIB. In addition, and in order to shift more of the load current to the LIB, the buck/boost converter regulation limit is returned to 700 V_{dc} from 680V_{dc}. The reason for this change is to compensate for the battery current terminal voltage rise under high charging. Figure VI-94 shows the results and the fact that SOC_b is steadily increasing, an indication that the battery is playing more of a role in energy storage. Moreover, the UC exhibits full SOC_{uc} swings over the cycle.

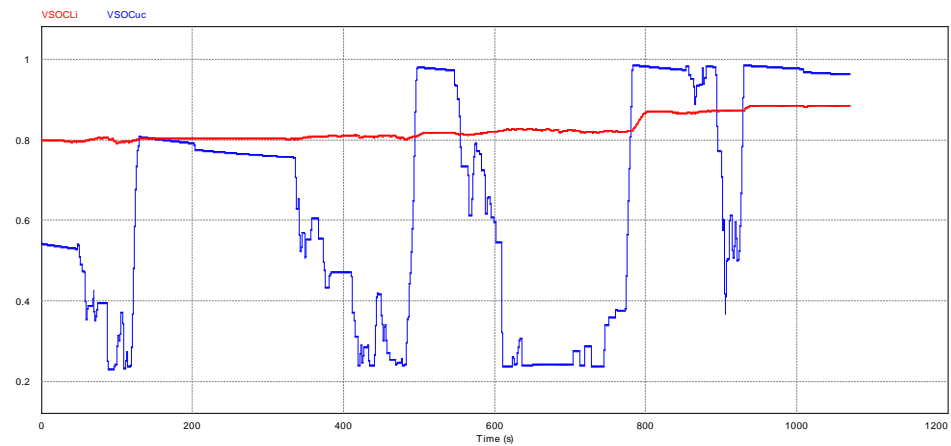


Figure VI-94: PSIM simulation of the HD truck HESS: Initial SOC_b=0.8, SOC_{uc}=0.54, U_{d0}=700V_{dc}

The final PSIM model of the dual storage plus interface buck/boost converter and with external file import is shown in Figure VI-95. Note that the UC, LIB, and dc-link voltage retain the values shown in the caption of Figure VI-94.

It can be seen in the full simulation model that the accessory/ancillary load has been included. This addition effectively absorbs a portion of the net regeneration current. This will manifest as a lower increase in SOC_b as well as SOC_{uc} as seen in Figure VI-96.

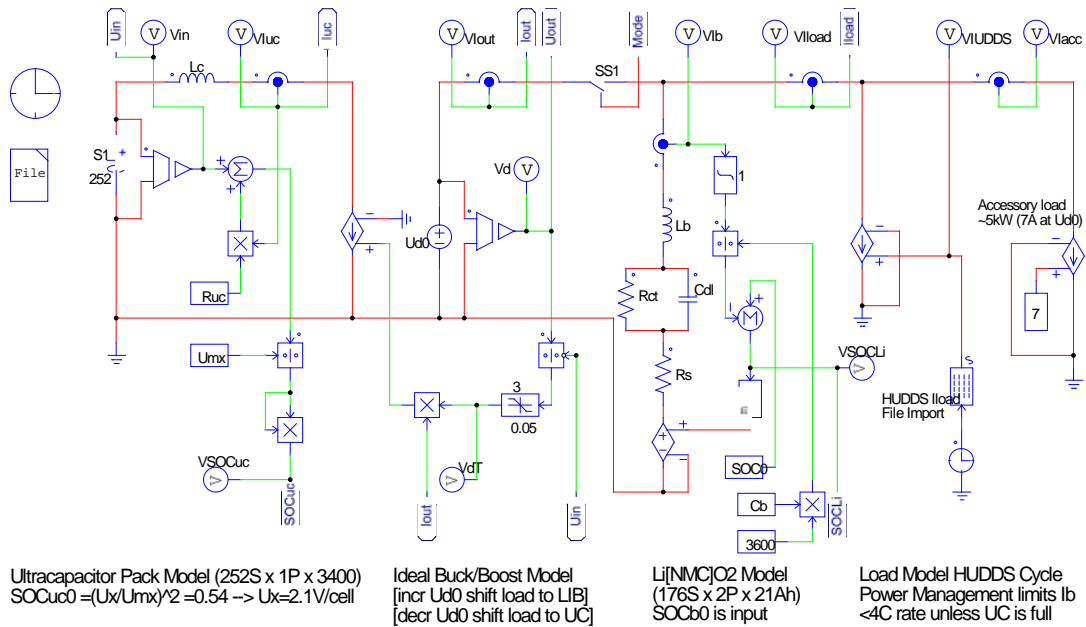


Figure VI-95: PSIM model of the HD truck HESS: Initial SOC_b=0.8, SOC_{uc}=0.54, U_{d0}=700V_{dc}

Note: Ideal Buck/boost Converter is Voltage Mode Controlled

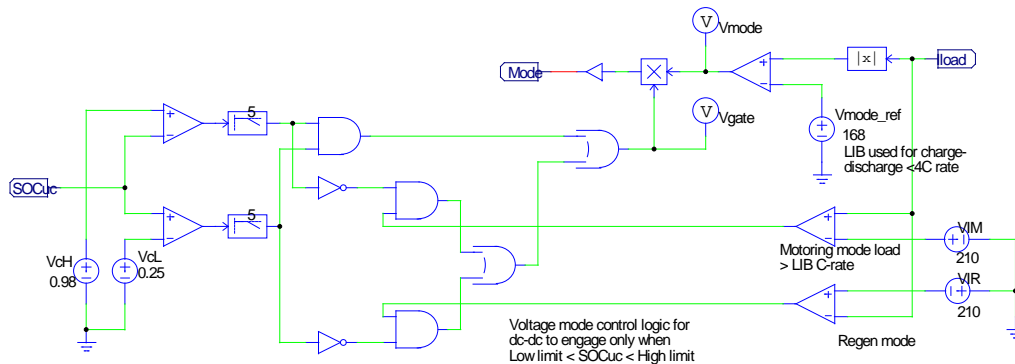


Figure VI-96: PSIM model mode control logic

The following sequence of graphics document the performance of the dual storage system under dynamic loading having a net positive regeneration power flow. The incorporation of representative ancillary and accessory loading of 5 kW effectively shunts a portion of this excess regeneration on the HUDDS cycle.

Figure VI-97 is the same as Figure VI-94 but with the addition of the ancillary and hotel loading. Note that with this additional loading it would be advisable to increase the initial SOC_{uc0} to minimize time near 0.25.

Figure VI-98 shows the buck/boost output current, I_{out}, and the Li[NMC]O₂ battery current, I_b. It is very clear in these plots that the battery is being exercised more, along with the UC. This illustrates the design freedom of dual storage: battery cycling is now under power management strategy control rather than simply reacting to drive cycle loading. Note that for the most part the power management strategy is limiting LIB C-rate except for those instances where the UC goes outside its SOC_{uc} bounds.

Figure VI-99 compares the UC voltage at input to the dc-dc, U_{in}, with the dc-link voltage, U_d. Under voltage mode control the dc-link voltage is regulated.

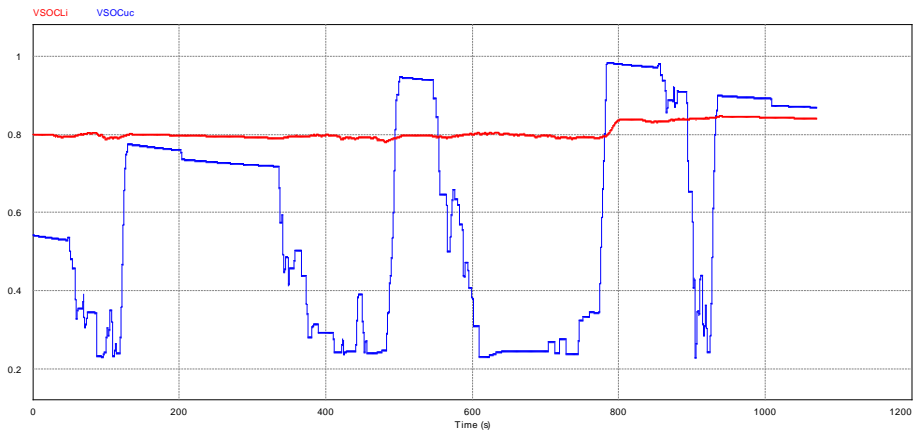


Figure VI-97: PSIM simulation of the HD truck HESS: Initial $SOC_b=0.8$, $SOC_{uc}=0.54$, $U_{d0}=700V_{dc}$

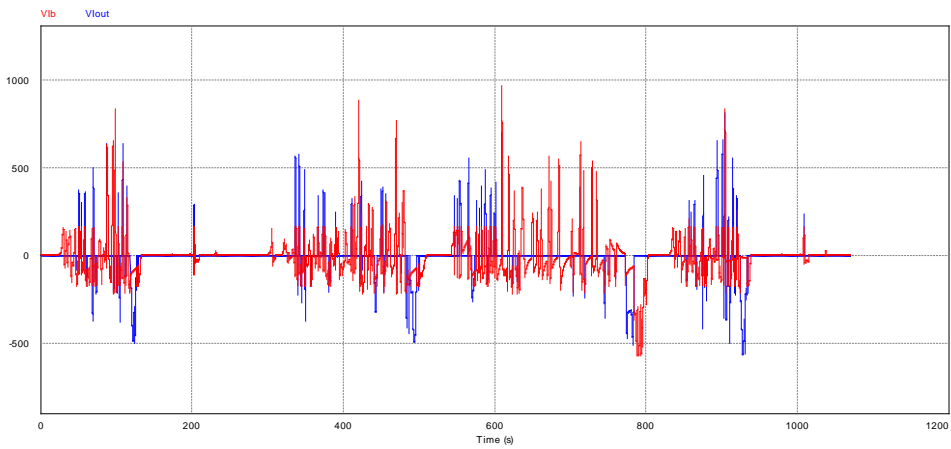


Figure VI-98: PSIM simulation of the HD truck HESS: dc-dc converter output and LIB currents.

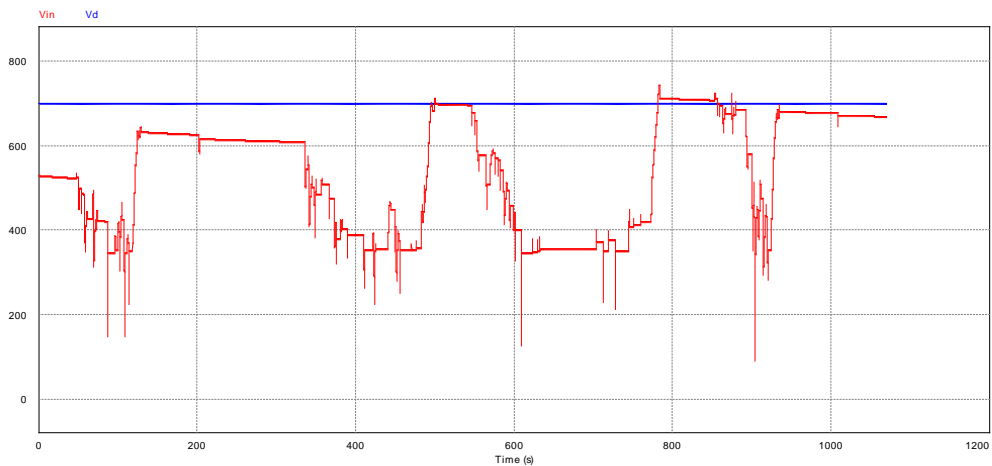


Figure VI-99: PSIM simulation of the HD truck HESS: dc-link voltage, U_d , and UC voltage, U_{in}

There is some insight to be gained by examination of the dc-dc duty ratio signal, $D = dT$, shown as Figure VI-100 and comparing it to the UC voltage shown in Figure VI-99. Notice that the four zones in Figure VI-99 where the UC voltage is high correspond to those times in the signal $dT(t)$ where it remains close to unity (low level boosting). The transients exceeding about 2.2 are due to mode control logic switching events.

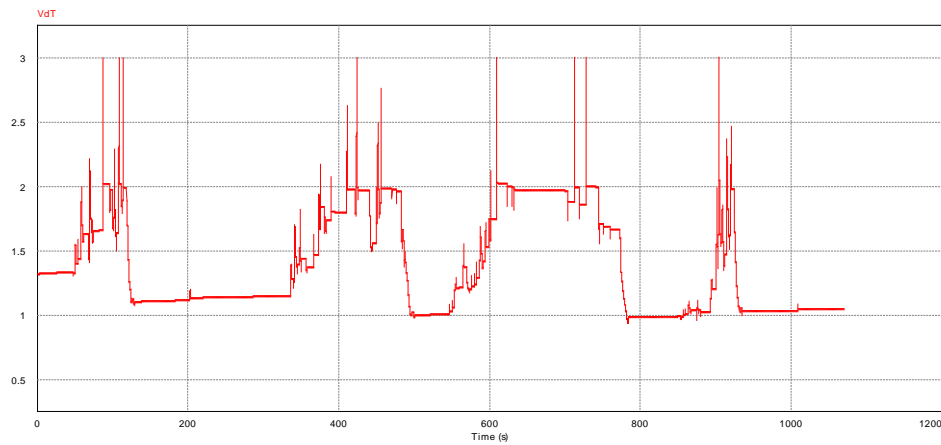


Figure VI-100: PSIM simulation of the HD truck HESS: dc-dc Converter Duty Ratio, $dT(t)$

Conclusions

The project is focused on advanced heavy-duty powertrain systems that will reduce energy consumption and criteria emissions for Class 8 line haul vehicles. A multi-faceted approach is being taken to minimize the fuel consumption and emissions of a Class 8 line haul powertrain utilizing advanced combustion, hybridization, and dual energy storage systems. Progress on the project includes completion of enhanced engine and aftertreatment models based upon experimental powertrain results from ORNL VSI Laboratory and completed detailed hybrid energy storage systems models and associated sizing. The project is being refocused in FY2016 to explore powertrain optimization of conventional line haul vehicles through controls integration and optimization of both the engine and transmission as a system.

VI.8. Thermal Control of Power Electronics of Electric Vehicles with Small Channel Coolant Boiling

Dileep Singh and Wenhua Yu, Principal Investigators

Argonne National Laboratory
9700 South Cass Avenue
Lemont, IL 60439
Phone: (630) 252-5009; Fax: (630) 252-5568
E-mail: dsingh@anl.gov

Lee Slezak and David Anderson, DOE Program Managers

Organization: U.S. Department of Energy
Phone: (202) 586-2335
E-mail: Lee.Slezak@ee.doe.gov

Start Date: October 2013
End Date: September 2016

VI.8.A. Abstract

Objectives

- Explore possibilities of using coolant boiling in cooling of vehicle power electronics.
- Eliminate the hybrid electric vehicle low-temperature cooling system and simplify the cooling system configuration.
- Increase the heat removal capacity and enhance cooling of vehicle power electronics.
- Control the junction temperature of vehicle power electronics and improve the efficiency and lifetime of electronic components.
- Cool high power-density electronics such as wideband-gap semiconductor-based power modules.

Accomplishments

- Developed thermal analysis models of coolant boiling in cooling of vehicle power electronics.
- Developed numerical simulation models of coolant boiling in cooling of vehicle power electronics using the commercial COMSOL Multiphysics software.
- Conducted numerical simulations investigating the effects of various parameters on the boiling cooling system.
 - Thermal conductivity of thermal interface materials.
 - Coolant flow velocity.
 - Fluid inlet temperature.
 - Heat flux of vehicle power electronics.
- Designed, fabricated, and characterized an experimental test system for investigating coolant boiling in cooling of vehicle power electronics.

Future Achievements

- Conduct VS_n models and results of coolant boiling in cooling of vehicle power electronics.



VI.8.B. Technical Discussion

Background

The current cooling technology for the power electronics in commercial hybrid electric vehicles (HEVs) uses a liquid-cooled heat sink with fins. In order for the fin-structure heat sink to remove heat from the power electronics, a separate low-temperature radiator and pumping system, in addition to the main engine radiator and pumping system, is required to provide a low coolant inlet temperature. This second radiator and pumping system increases the weight and the cost of the vehicle and decreases the fuel efficiency. This project is aimed to use subcooled or low-vapor quality saturation flow boiling for cooling of vehicle power electronics. It is expected that this cooling technology will enhance cooling of vehicle power electronics, control junction temperatures of vehicle power electronics, and eliminate the second cooling system currently used in hybrid electric vehicles.

Introduction

Various technologies have been proposed to enhance the cooling of the power electronics in HEVs and therefore reduce the system weight and volume of the power electronics and increase the efficiency and the life time of vehicles. These cooling technologies include the single-phase or two-phase jet impingement, the two-phase spray, the immersion pool boiling, and the two-phase saturation boiling. However, all of these previously studied technologies require installation of significant additional hardware to cool the power electronics.

In the present study, with subcooled flow boiling in the cooling channels of power electronics in HEVs, no major additional components are required. The low-temperature radiator and pumping system is replaced with the existing main engine radiator and pumping system, and boiling occurs only in the cooling channels of power electronics and nowhere else in the HEV cooling system. The uniqueness of this technology lies in the use of subcooled flow boiling in addition to liquid convection under controlled conditions in current power electronic cooling channels to improve the cooling capacity without exit vapor from the channels or major additional components in HEVs. These desirable conditions are in contrast to these other cooling technologies.

Approach

As illustrated in Figure VI-101, the subcooled flow boiling system proposed in the present study can be integrated into the main engine cooling system without major additional hardware installation. The conventional engine coolant, a 50/50 ethylene glycol/water (EG/W) mixture, is used for cooling of vehicle power electronics. The coolant flowing out from the radiator is pumped by the main engine coolant pump and divided into two flow paths. One follows the normal engine cooling route, and the other goes into the cooling channels of power electronics. The coolant in the cooling channels absorbs heat from the power electronics through subcooled flow boiling. Then the two coolant flows combine in the flow mixer to form a uniform-temperature fluid. The coolant then enters the radiator to reject the absorbed heat to air. The flow divider and mixer components are considered to be minor additions to an HEV as they may be little more than types of piping tees.

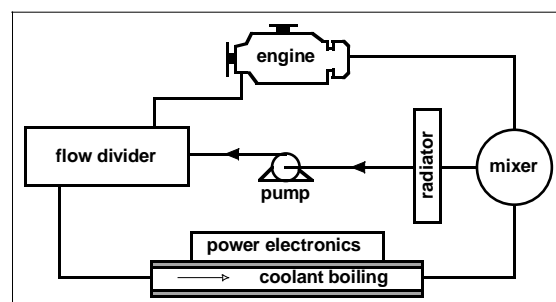


Figure VI-101: Concept of Subcooled Flow Boiling System

Results

The subcooled flow boiling technology for vehicle power electronics cooling has been studied in this project through numerical simulations conducted using the commercial COMSOL Multiphysics software. The effects on coolant subcooled flow boiling of various parameters, including the thermal conductivity of thermal interface materials (TIMs), the coolant flow velocity, the fluid inlet temperature, and the heat flux of vehicle power electronics, were studied. Furthermore, the subcooled flow boiling system was compared to the current single-phase liquid-cooled technology. Results presented subsequently show that coolant subcooled flow boiling in the cooling channels can enhance the cooling for vehicle power electronics and remove the low-temperature radiator and pumping system to simplify the cooling system in HEVs.

Simulation Models and Key Considerations

The vehicle power electronic package studied in the simulations is shown in Figure VI-102. There are two semiconductors on the top, an insulated gate bipolar transistor (IGBT) and a diode. The cooling channels on the bottom are divided by costly fins. A typical power electronics package in a HEV has about a dozen of these semiconductor pairs. This power electronics module was chosen for the simulations of this study because it is used in commercial HEVs. Furthermore, this package allows the cooling on both sides of the semiconductors. Figure VI-103 shows the side view of the configuration of Figure VI-102 identifying each layer of the power electronics and cooling channels, and Table VI-7 gives the materials and dimensions of each layer. The fin structure of the cooling channels for the vehicle power electronic package of Figure VI-102 is enlarged in Figure VI-104. There are 20 channels under each pair of semiconductors.

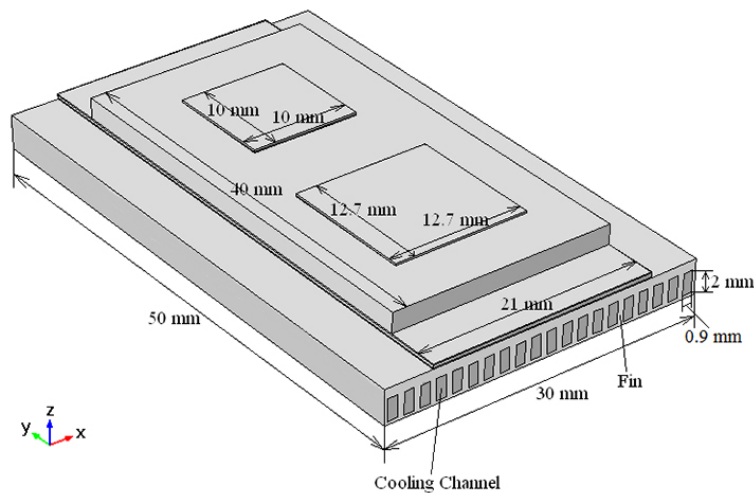


Figure VI-102: Vehicle Power Electronic Package

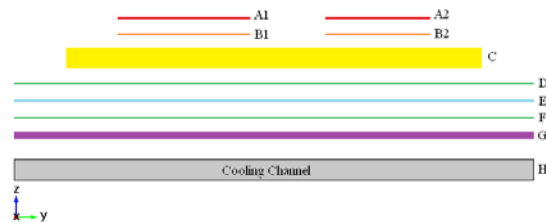


Figure VI-103: Side View of Vehicle Power Electronic Package

Table VI-7: Materials and Dimensions of Each Layer

Index	Material	X (mm)	Y (mm)	Z (mm)
A1	IGBT: Si	12.7	12.7	0.145
A2	Diode: Si	10.0	10.0	0.145
B1	Solder	12.7	12.7	0.076
B2	Solder	10.0	10.0	0.076
C	Heat spreader: Cu	21.0	40.0	1.85
D	TIM: Thermal grease	21.0	50.0	0.1
E	Substrate: SiN	21.0	50.0	0.3
F	TIM: Thermal grease	21.0	50.0	0.1
G	Heat sink: Al	30.0	50.0	0.6
H	Cooling channel	30.0	50.0	2.0

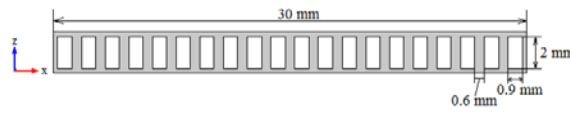


Figure VI-104: Fin Structure

The mesh structure in the numerical model of the configuration of Figure VI-102 is displayed in Figure VI-105. The simulation model consists of 2,007,316 domain elements, 443,403 boundary elements, and 15,374 edge elements. Based on a mesh independence study, these mesh elements are sufficient for the 3-D numerical simulations.

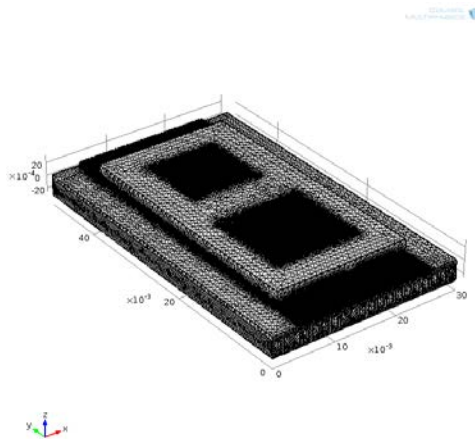


Figure VI-105: Mesh Structure (All Units in Meter)

For the simulation boundary condition of the subcooled flow boiling heat transfer coefficients in the cooling channels, the widely used Shah correlation in the engineering literature was chosen. While the Shah correlation was not developed for subcooled flow boiling of a 50/50 EG/W mixture, the differences between the experimental data from our current PACCAR CRADA project of 50/50 EG/W subcooled flow boiling and the

simulation results based on the Shah correlation are within 10% at various coolant flow velocities, which validates the applicability of the Shah correlation for the simulations.

Other key considerations include: (a) because the subcooled flow boiling system is integrated into the main engine cooling system, the conventional engine coolant, a 50/50 EG/W mixture, is used for cooling of power electronics; (b) the pressure in the cooling channels for power electronics in HEVs is 2 atm where the saturation point of a 50/50 EG/W mixture is 129°C; (c) in order to eliminate the low-temperature radiator and the associated pumping system, the coolant inlet temperature is assumed to be 105°C; (d) the coolant flow velocity is 0.16 m/s in order to keep the coolant outlet temperature below the saturation point and to generate desired subcooled flow boiling; (e) the coolant outlet temperature is below the saturation point with no net vapor in the rest of the system (outside the power electronics cooling channels); and (f) to have desired subcooled flow boiling, the cooling channel wall temperature is 10-30°C above the saturation point, i.e. a wall superheat of 10-30°C.

TIM Thermal Conductivity Effects

Figure VI-106 shows the junction temperature (the IGBT surface temperature) versus the TIM thermal conductivity for a double-sided cooling system with or without fins for a 100-W/cm² heat flux on the IGBT and diode surfaces, the current commercial heat flux level. The coolant inlet temperature is 105°C. Various TIM thermal conductivities of 1.5 W/mK, 7.5 W/mK, and 15 W/mK were considered. It can be seen from Figure VI-106 that use of subcooled flow boiling in the cooling channels reduces the junction temperature compared to single-phase convective heat transfer. Single-phase cooling at this 105°C coolant inlet temperature cannot keep the junction temperature below 175°C at any TIM thermal conductivities. With a 7.5-W/mK TIM thermal conductivity, the junction temperature is reduced to 175°C without fins in the cooling channel and to 137°C with fins by using subcooled flow boiling as shown in Figure VI-106 and Figure VI-107. At a TIM thermal conductivity of 1.5 W/mK, the junction temperature is still maintained far below the 175°C limit using the subcooled flow boiling system with fins. TIM thermal conductivities higher than 7.5 W/mK do not significantly reduce the junction temperature of the power electronics, as displayed in Figure VI-106, which means that there is little benefit to TIM thermal conductivities above 7.5 W/mK. By using a TIM thermal conductivity of 7.5 W/m K, fins can be eliminated in the double-sided subcooled flow boiling system while maintaining a 175°C junction temperature, which reduces the capital cost and pumping power. Using subcooled flow boiling with fins, the junction temperature can be reduced below 155°C with all TIM thermal conductivities studied, as displayed in Figure VI-106.

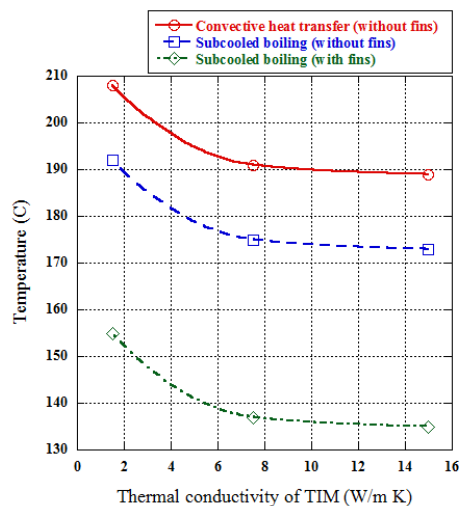


Figure VI-106: TIM Thermal Conductivity Effects

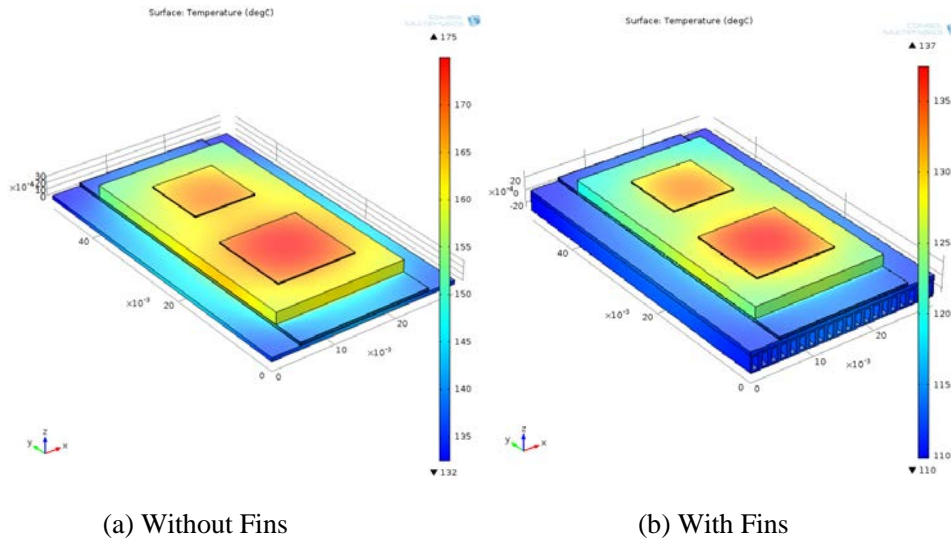


Figure VI-107: Junction Temperatures

Coolant Flow Velocity Effects

Figure VI-108 is a plot of the junction temperature versus the coolant flow velocity. It is for a double-sided cooling system with a 7.5-W/mK TIM thermal conductivity for a 100-W/cm² heat flux on the IGBT and diode surfaces. The coolant flow inlet temperature is 105°C. It is seen that the finned channels combined with subcooled flow boiling can reduce the junction temperature below 140°C for all coolant velocities. Without fins, the junction temperature can be controlled below 175°C when the coolant flow velocity is 0.16 m/s or higher. It is seen in Figure VI-108 that the coolant flow velocity does not have significant effect on the junction temperature for the subcooled flow boiling system.

Efficient cooling using subcooled flow boiling occurs at low coolant flow velocities, which reduces pressure drops and pumping power requirements. Using fins in the cooling channels, the coolant flow velocity range for subcooled flow boiling is between 0.06 m/s to 0.4 m/s, as shown in Figure VI-108. When the velocity is lower than the lower limit of this range, the coolant outlet temperature would be likely above the saturation point. When the velocity is higher than the higher limit of this range, the cooling channel wall temperature cannot reach 10°C above the saturation point and therefore subcooled flow boiling is unlikely to occur. The subcooled flow boiling pressure drop along the cooling channel predicted based on correlations in the engineering literature is quite small (approximately 1443 Pa), which would result in low pumping power requirements.

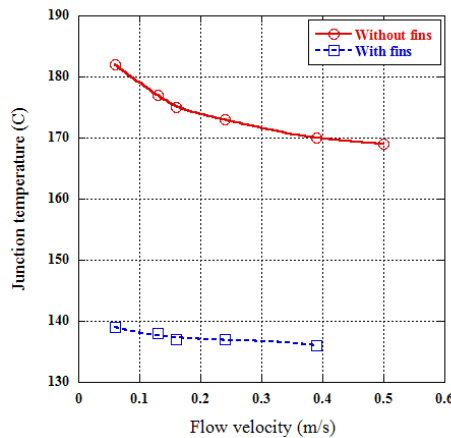


Figure VI-108: Coolant Flow Velocity Effects

Fluid Inlet Temperature Effects

A double-sided cooling system with a 7.5-W/mK TIM thermal conductivity for a 100-W/cm² heat flux on the IGBT and diode surfaces was also considered in the next simulations. Based on the results shown in Figure VI-109, the junction temperature can be controlled below 175°C without fins in the cooling channel and below 150°C with fins when using subcooled flow boiling. Without fins, the subcooled flow boiling dominates the cooling process. High coolant inlet temperatures cause strong subcooled flow boiling due to high subcooled flow boiling heat transfer coefficients caused by low liquid subcooling levels. Therefore, a higher coolant temperature results in a lower junction temperature. With fins in the cooling channels, convective heat transfer is also important. Consequently, a higher coolant temperature results in a higher junction temperature. In order to maintain subcooled flow boiling in the cooling channels, the fluid inlet temperature cannot be below 100°C with fins while the fluid inlet temperature cannot be below 90°C without fins because lower fluid inlet temperatures cause the channel wall temperature to be below the subcooled flow boiling range. Furthermore, according to the simulation results displayed in Figure VI-109, the coolant inlet temperature does not have significant effects on the junction temperature, especially for the non-finned cooling channel.

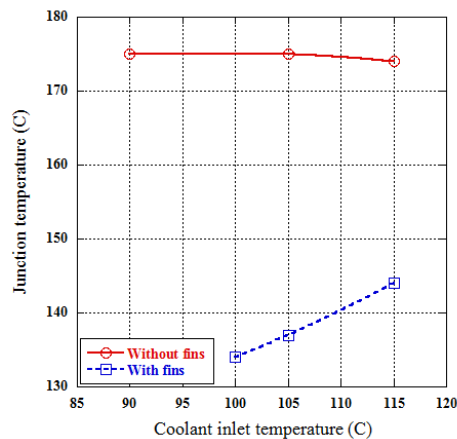


Figure VI-109: Fluid Inlet Temperature Effects

Heat Flux Effects

Figure VI-110 shows the semiconductor junction temperature versus the heat flux from the numerical simulations. The simulations were performed for a single-sided finned cooling system with a coolant inlet temperature of 105°C and a coolant flow velocity of 0.16 m/s. The 7.5-W/mK TIM thermal conductivity was applied. Referring to Figure VI-110, when the heat flux on the IGBT and diode surfaces is small, less than 30 W/cm², a single-phase flow occurs as indicated by the steep slope of the curve. Here, little to no subcooled flow boiling occurs. As the heat flux increases, subcooled flow boiling becomes stronger in the cooling channels and the slope of the curve is reduced in Figure VI-110. The junction temperature increases more gradually with subcooled flow boiling because of the increased heat transfer rates compared to a single-phase flow. Using subcooled flow boiling, the junction temperature can be controlled below 175°C with a heat flux on the IGBT and diode surfaces up to 125 W/cm², as shown in Figure VI-110. For a double-sided cooling system, the heat flux value would be doubled to 250 W/cm². This heat flux is a 25% increase over conventional single-phase cooling of HEV power electronics, and it is accomplished without a low-temperature radiator cooling system.

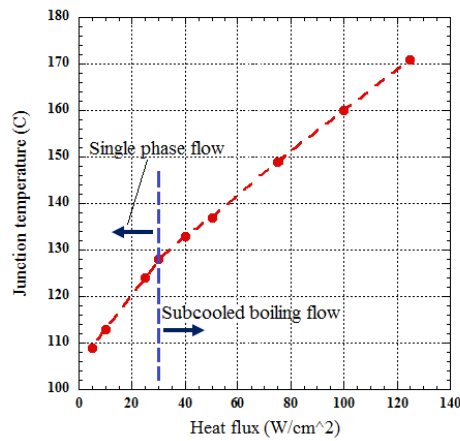
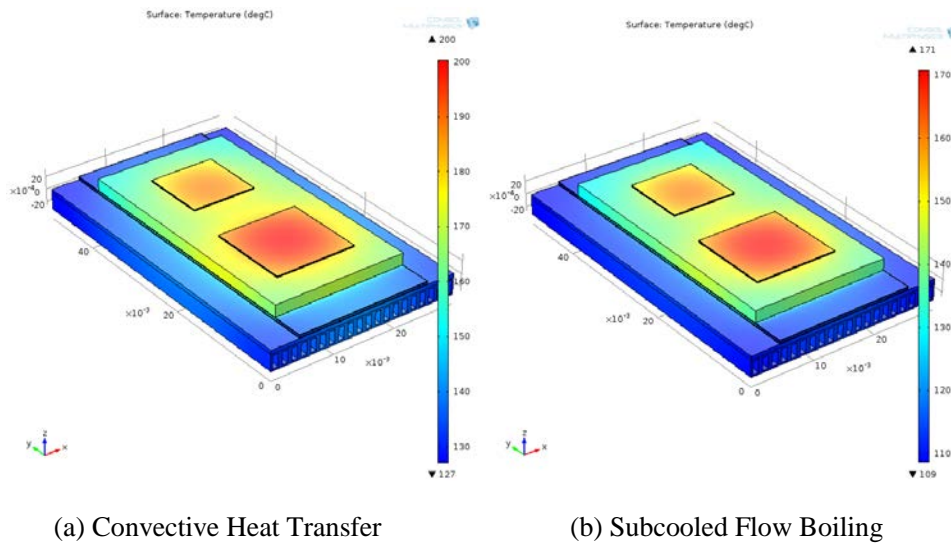


Figure VI-110: Heat Flux Effects

Figure VI-111 shows the temperature profiles through the power electronics for the high heat flux 250 W/cm² application (such as wideband-gap semiconductors) using subcooled flow boiling and convective single-phase cooling. The junction temperature can be maintained below 175°C using subcooled flow boiling combined with fins in a double-sided cooling system with a 7.5-W/mK TIM thermal conductivity, as shown in Figure VI-111 (b). Without subcooled flow boiling, the junction temperature would be 200°C, as shown in Figure VI-111 (a).



(a) Convective Heat Transfer

(b) Subcooled Flow Boiling

Figure VI-111: High Heat Flux Applications

Comparison of Convection and Subcooled Boiling

The comparison between single-phase convection and subcooled flow boiling for cooling power electronics in HEVs is illustrated in Table VI-8, where SS and DS indicate single-sided and double-sided, respectively. The TIM thermal conductivity is 7.5 W/mK in the simulations. Without fins (as indicated in column 1, Table VI-8), double-sided subcooled flow boiling can control the junction temperature below 175°C. With fins, subcooled flow boiling can increase the cooling rate by 25% (column 2, Table VI-8) compared to convection cooling or reduce the junction temperature (column 3, Table VI-8). By using subcooled flow boiling combined with fins, the double-sided subcooled flow boiling system can cool wideband-gap semiconductors with a heat flux up to 250 W/cm² (column 4, Table VI-8). It should be pointed out that all these are achieved for a coolant inlet temperature of 105°C without the second low-temperature radiator and the associated pumping system.

Table VI-8: Comparison of Convection and Subcooled Boiling

	Subcooled Flow Boiling				Convection	
Coolant Inlet Temperature (°C)	105	105	105	105	70	70
Total Heat Flux on IGBT and Diode Surfaces (W/cm ²)	100	125	100	250	127	100
Coolant Flow Velocity (m/s)	0.16	0.16	0.16	0.16	0.24	0.24
Fins in the Channel	No	Yes	Yes	Yes	Yes	Yes
Cooling System	DS	SS	SS	DS	DS	SS
Junction Temperature (°C)	175	175	160	175	150	175

Experimental Test System

Experimental Test Module Design and Fabrication

The experimental test module, shown in Figure VI-112, was designed and fabricated to investigate heat transfer characterizations of coolant subcooled boiling in practical power electronic cooling channels of HEVs. The experimental test module is based on the Toyota Prius cold plate as shown in Figure VI-112a (overview) and Figure VI-112b (channel details). To simulate the heat generated by the power electronic components, a heating wire was affixed to the experimental test module as shown in Figure VI-112d. The material, dimension, and arrangement of the heating wire were carefully chosen to generate uniform heat fluxes similar to the real power electronic cooling system. Thermocouples for measuring the wall temperatures and the in-stream fluid temperatures, a pressure transducer for measuring the system pressure, and a differential pressure transducer for measuring the pressure drop were installed into the experimental test module as shown in Figure VI-112e. The measurements from these sensors are used in the data reduction process to calculate the heat transfer coefficient. As shown in Figure VI-113, the completed experimental test module is attached to a structural frame, which enables the module to be tested on both top-heating and bottom-heating conditions to provide important design information for the double-sided cooling configuration. Through the cooling channel inlet and outlet ports, the experimental test module is connected into an experimental test loop that includes two preheaters for heating the coolant to a desired inlet temperature, a pressure subsystem for setting up the system pressure, and other necessary components such as the flowmeter and the heat exchanger.

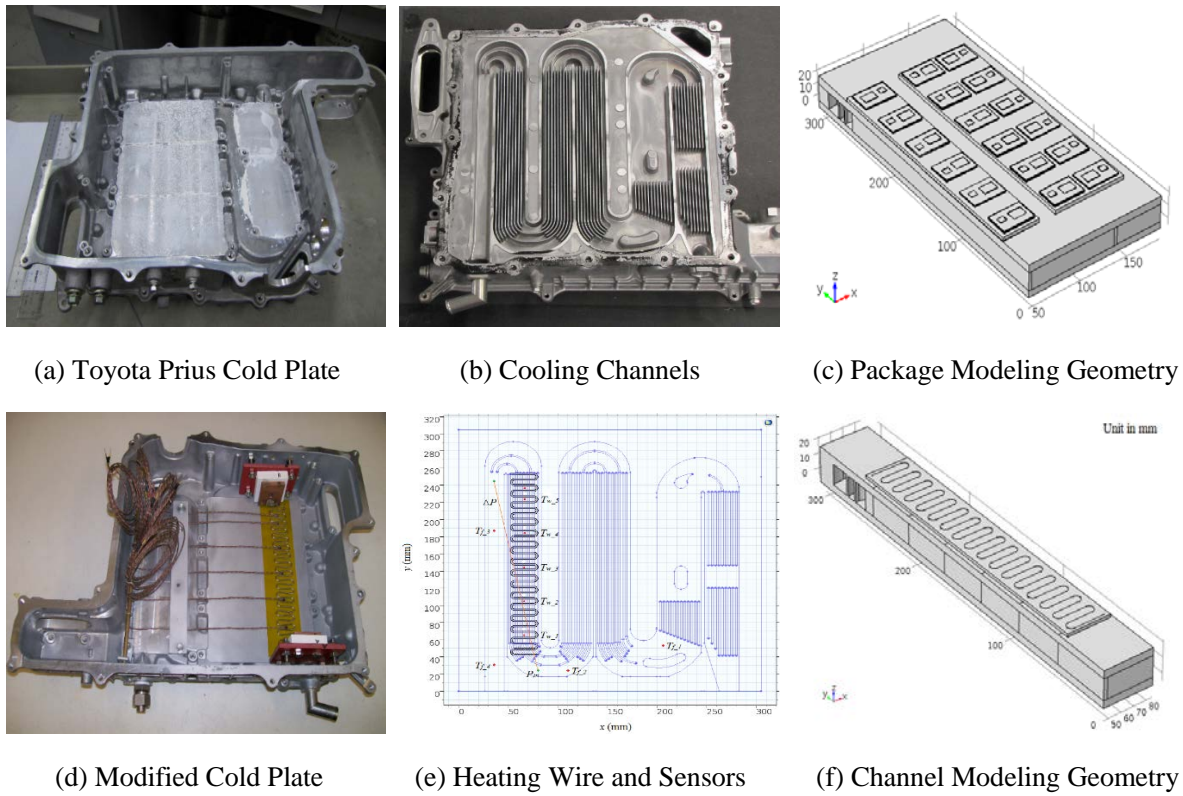


Figure VI-112: Experimental Test Module

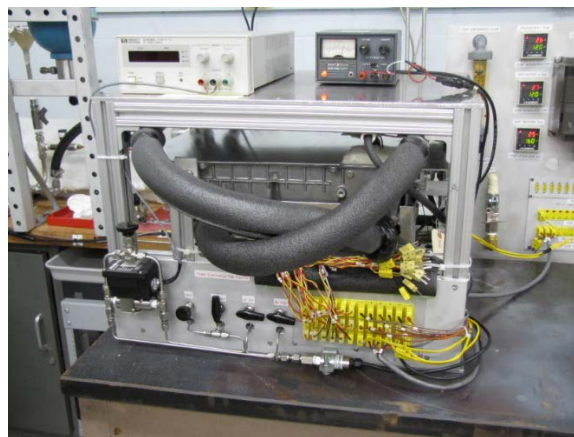


Figure VI-113: Experimental Test Module Overview

Experimental Test Module Characterizations

Two characterizations were performed to the experimental test module. The first is the heat transfer simulations of the cold plate package based on the package modeling geometry shown in Figure VI-112c. Figure VI-114 shows the heat transfer simulation results for single-phase convection. The simulation conditions are: the heat flux of 100 W/cm^2 , the coolant flow velocity of 0.16 m/s , the TIM of 1.5 W/mK , and the coolant inlet temperature of 70°C and 105°C , respectively. It can be seen from Figure VI-114a that for a coolant inlet temperature of 70°C , the junction temperature can be controlled below 175°C . However, when the coolant inlet temperature is increased to 105°C , the junction temperature rises to 183°C as shown in Figure VI-114b. Therefore, the single-phase flow will not work under this condition. Figure VI-115 shows the heat transfer simulation results for subcooled boiling. The simulation conditions are: the coolant flow velocity of 0.16 m/s , the TIM of 1.5 W/mK , the coolant inlet temperature of 105°C , and the heat flux of 100 W/cm^2 and

114 W/cm², respectively. It can be seen from Figure VI-115 that for a coolant inlet temperature of 105°C, the junction temperature can be controlled below 175°C for both heat flux levels. Therefore, with subcooled boiling, the heat flux of power electronics for this cold plate package can be increased to 114 W/cm² compared to the current technology.

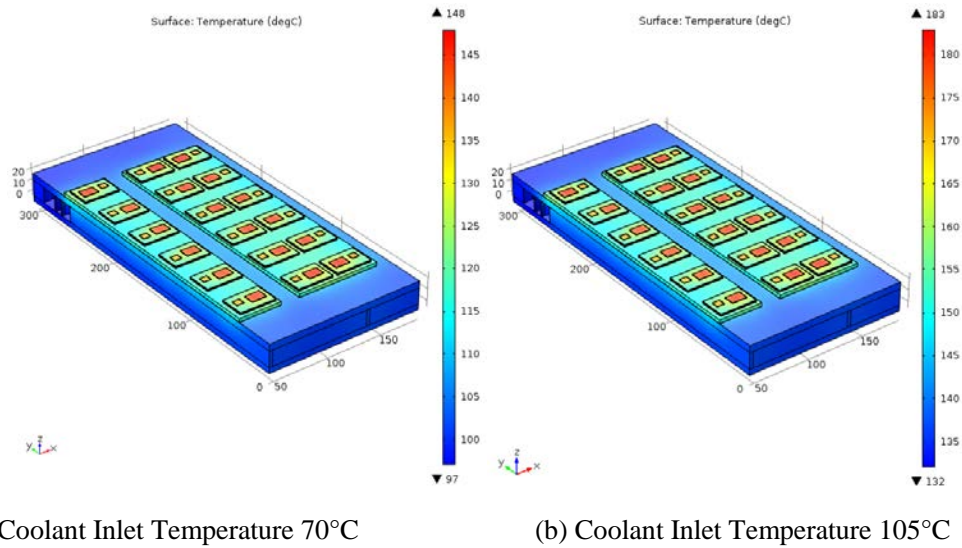


Figure VI-114: Convective Heat Transfer Simulation Results

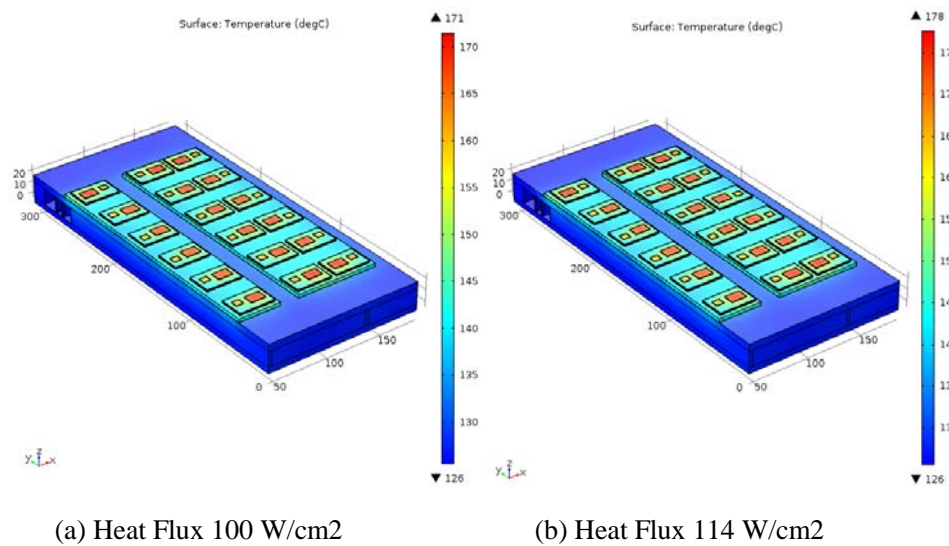


Figure VI-115: Subcooled Boiling Heat Transfer Simulation Results

The second is the heat loss calibrations of the experimental test module. The experimental test module is thermally insulated. However, because of the high thermal conductivity of the module material aluminum, the heat loss is not negligible. Therefore, heat loss tests were conducted by applying certain heating power to the experimental test module to bring its wall temperature to a selected level. The corresponding heat loss or the applied heating power was then correlated as a function of the driving temperature (the difference of the wall temperature and the ambient temperature). It can be seen from Figure VI-116 that the heat loss rate is linearly depending on the driving temperature and is well predicted by the correlation. The heat loss data are incorporated into the data reduction process for single-phase and boiling heat transfer tests.

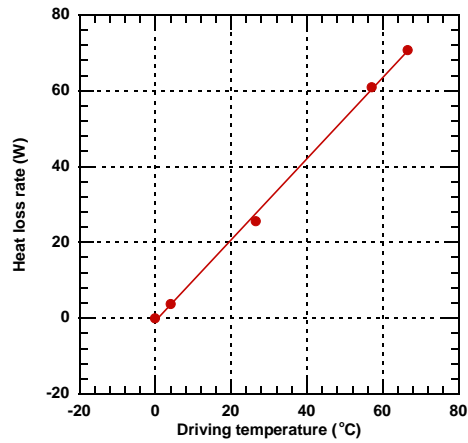


Figure VI-116: Heat Loss Calibration Results

Fin Effects on Subcooled Boiling

The experimental test module has finned multi-channels with the heat input from either the top or the bottom. Therefore, the overall heat transfer is complicated, especially for subcooled boiling heat transfer. During subcooled boiling, the boiling occurs on the inside surface of the heat input base and on certain fin surfaces as shown in Figure VI-117. To account for fin effects, energy balance analyses were conducted and formulae were worked out for calculating the boiling length of the fin surfaces and the boiling heat transfer coefficient. These results are incorporated into the data reduction process for boiling heat transfer tests. Figure VI-118 shows an example from simulations based on the channel modeling geometry in Figure VI-112f under the following conditions: the heat flux of 100 W/cm², the coolant inlet temperature of 105°C, and the coolant flow velocity of 0.16 m/s. It can be seen from Figure VI-118 that the wall temperature slightly increases with the subcooled boiling length of the fins due to the heat transfer improvement and the heat flux reduction from the larger effective area. However, the wall temperature difference is small.

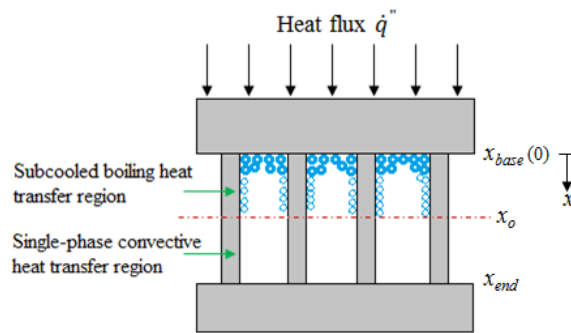


Figure VI-117: Fin Effect on Subcooled Boiling

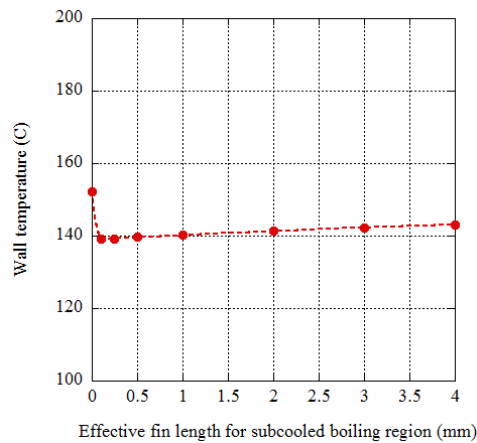


Figure VI-118: Wall Temperature as a Function of Subcooled Boiling Length

Conclusions

Use of subcooled flow boiling in the cooling channels to reduce the junction temperature of power electronics in HEVs is a novel cooling technology. Using subcooled flow boiling in the cooling channels can enhance the cooling capacity for vehicle power electronics while the coolant outlet temperature is still below the saturation point. Thus, there is no vapor in the rest of the cooling system. Based on the current numerical simulations, the subcooled flow boiling technology can (a) eliminate the second low-temperature cooling system currently used in HEVs by increasing the coolant inlet temperature to 105°C, thus reducing the weight and cost of HEVs and increasing the efficiency; (b) increase the cooling rate by 25% or reduce the junction temperature compared to convection cooling due to its improved heat transfer; (c) achieve HEV power electronics cooling and junction temperature control at low coolant flow velocities, thus reducing pressure drops and pumping power requirements; and (d) simplify the cooling system of HEV power electronics by integrating it into the main engine cooling system. The subcooled flow boiling system can also be used for cooling of high power-density electronics with a heat flux up to 250 W/cm² and for cooling of all-electric vehicle power electronics.

To investigate heat transfer characterizations of coolant subcooled boiling in practical power electronic cooling channels of HEVs, an experimental test module was designed and fabricated based on the Toyota Prius cold plate. The experimental test module was carefully characterized on heat transfer through numerical simulations and on heat losses through experimental tests. The fin effects on subcooled boiling heat transfer were also considered. These results from calculations and experiments are incorporated into further data reduction of single-phase and subcooled boiling heat transfer tests.

The future work will focus on (a) conducting subcooled flow boiling experiments and data analyses with a 50/50 EG/W mixture; (b) developing experimental data-based predictive correlations of the subcooled flow boiling heat transfer coefficients under the application conditions of cooling vehicle power electronics; and (c) refining simulation models and results of coolant subcooled flow boiling in cooling of vehicle power electronics based on the experimental heat transfer data.

VI.8.C. Products

Presentations/Publications/Patents

1. Weihuan Zhao, Wenhua Yu, David M. France, Dileep Singh, Roger K. Smith, Subcooled Boiling Heat Transfer for Thermal Control of Power Electronics in Hybrid Electric Vehicles, SAE 2015 Thermal Management Systems Symposium, September 29-October 1, 2015, Troy, Michigan, USA.
2. Weihuan Zhao, David M. France, Wenhua Yu, Dileep Singh, Subcooled Boiling Heat Transfer for Cooling of Power Electronics in Hybrid Electric Vehicles, ASME Journal of Electronic Packaging 137, July 2015, 031013, DOI: 10.1115/1.4030896.

3. David M. France, Wenhua Yu, Dileep Singh, Weihuan Zhao, System for Cooling Hybrid Vehicle Electronics, Method for Cooling Hybrid Vehicle Electronics, pending U.S. patent application, January 16, 2015.
4. Wenhua Yu, Weihuan Zhao, David M. France, Dileep Singh, Coolant Boiling for Thermal Control of Hybrid Electric Vehicle Power Electronics, SAE 2014 Thermal Management Systems Symposium, September 22-24, 2014, Denver, Colorado, USA.

VI.9. DC Fast Charging Study

Matthew Shirk, Principal Investigator

Idaho National Laboratory
P.O. Box 1625
Idaho Falls, ID 83401
Phone: (208) 526-7216; Fax: (208) 526-0828
E-mail: matthew.shirk@inl.gov

Lee Slezak, DOE Program Manager

Phone: (208) 586-2335
Email: Lee.slezak@ee.doe.gov

Start Date:

End Date:

VI.9.A. Abstract

Objectives

- Fast charging, though convenient, is understood to have an adverse effect on the life of a vehicle's battery. This project was designed to produce data to quantify the extent of degradation experienced by batteries in 2012 Nissan Leafs that were used exclusively with frequent fast charging when compared to the same vehicle exclusively using slow-charged AC Level 2 equipment.

Accomplishments

- As part of DOE's AVTA, four 2012 Nissan Leaf battery electric vehicles were instrumented with data loggers and operated over a fixed onroadonroad test cycle. Each vehicle was operated over the test route and charged twice daily. Two vehicles were charged exclusively by AC Level 2 EVSE, while two were exclusively charged by a 50-kW DCFC. The vehicles were performance tested on a closed test track when they were new and after they accumulated 50,000 miles. The traction battery packs were removed and laboratory tested when the vehicles were new and at 10,000-mile intervals throughout the onroad mile accumulation, which has been completed.
- To complement the onroad testing, two battery packs were removed from two additional 2012 Nissan Leafs and cycled in a constant-temperature laboratory environment using battery cycling equipment. Again, one was charged at the 50-kW DCFC rate, while the other was charged at the 3.3-kW AC Level 2 rate. Cycling of these packs still continues; however, at the time of this writing, over 36,000 miles of equivalent cycling had been performed, with a goal of reaching 50,000 miles of equivalent cycling.

Future Achievements

- The results of the onroad and laboratory testing will be analyzed together to determine the effects of varying ambient conditions on the batteries' degradation rates compared to those cycled and tested under constant laboratory temperature conditions. Related future work will test similar cells in the laboratory under a matrix of temperatures and charging conditions to further parse out the effects of fast charging on these batteries and to support development of testing procedures for investigating high-rate charging on other battery types.



VI.9.B. Technical Discussion

Background

Because driving range between charging is an obstacle to PEV adoption for many consumers, fast charging can play an important role in making PEVs practical for more drivers and for more trips. Fast charging, though convenient, is understood to have an adverse effect on the life of a vehicle's battery. The extent of the irreversible degradation is not well understood for PEV batteries. A real-world based quantification is useful to current and potential PEV owners. Data from this project, as input toward test method development, can help understand how well new energy storage technologies perform under fast-charge conditions and relative to current state-of-the-art. Future testing planned at various temperatures can further elucidate the value of battery thermal conditioning systems.

Introduction

This study quantifies the effects on a vehicle battery for a set of vehicles that are exclusively charged with DCFC and compares that vehicle to an identical set of vehicles that are exclusively charged using AC Level 2 EVSE. The vehicles used in this study are model year 2012 Nissan Leafs powered by lithium ion traction batteries and equipped with the optional CHAdeMO DCFC port. The battery pack on this vehicle is rated at 24 kW-hours and 66.2 Amp-hours; it is also rated to provide 73 miles of driving range per U.S. Environmental Protection Agency testing. The pack is constructed from 192 prismatic cells and packaged in 48 modules with each consisting of two sets of paralleled cells connected in series. The cell's active materials consist of an LMO with an LNO cathode and a graphite anode. The pack is located under the vehicle floor and is sealed. Heat is dissipated passively; there is no exchange of fluid through the pack.

Approach

To study the effects of fast charging on battery life and vehicle performance under a set of real-world conditions, four 2012 Nissan Leaf battery electric vehicles were commissioned to accumulate mileage through onroad operation in Phoenix, Arizona. Initial performance was gauged by a series of tests, beginning with baseline testing when the vehicles were new and at fixed intervals throughout the project. Two vehicles were used as the control group, which was restricted to AC Level 2 charging only. The other two vehicles were restricted to DCFC charging only. To isolate the differences in battery conditions due to charging effects, careful vehicle management during the mileage accumulation phases was necessary.

Several methods were designed to measure changes in battery and vehicle performance as the vehicles accumulated miles. These include, in order of increasingly controlled conditions, evaluation of data collected during onroad operation, track testing, and laboratory testing of the batteries.

The two additional packs that were cycled and performance tested in the laboratory were connected to 1,000-V/500-A battery pack cyclers. Data gathered from dynamometer testing were used to create a battery power trace, which was executed by the testers to discharge the packs identically. The fast charge packs were supplied up to 120 Amps of DC during charging, while the specific rate was controlled by the Nissan Leaf's battery management system. The slow charged pack was limited to 9 Amps of DC during charging and was also controlled by the Leaf's battery management system. The packs were operated in a large walk-in type of thermal chamber, which was fixed at 30°C.

Both the onroad packs and lab-cycled packs were charged and discharged twice daily. A thorough discussion of the executed testing methods can be found in "Effects of Electric Vehicle Fast Charging on Battery Life and Vehicle Performance," (Shirk and Wishart 2015).

Results

Following cycling of the batteries through onroad driving and charging and battery and vehicle testing, the collected data were analyzed to characterize the thermal conditions to which the batteries were subjected during driving and charging, with a focus on differences between the charging-type test groups. Next, battery

capacity and power capability fade were analyzed. Finally, the impacts this degradation had on range and acceleration are presented.

Distribution of battery power among the test vehicles, both onroad and in the laboratory showed minimal variation during driving events. This matched the intent of the project, where the differences were largely isolated to charging. The resulting thermal response of the batteries in the two test groups is shown in Figure VI-119.

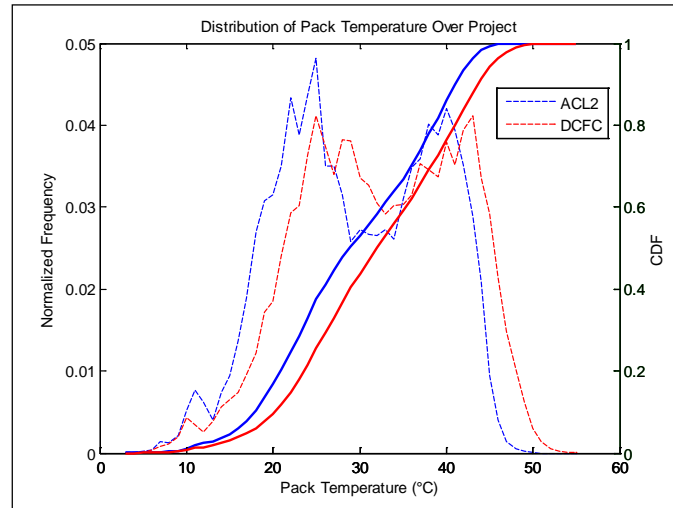


Figure VI-119: Distribution of battery pack temperature for each charge condition group. These data represent 50,000 miles of driving, charging, and parking over more than 500 days of the onroad study. The DCFC packs show a shift of a few degrees Celsius higher temperature than the two AC 2 charged packs.

INL

The energy capacity of the battery is the primary factor contributing to electric vehicle range. The capacity was tested every 10,000 miles. The capacity, as a percent of baseline, is shown in Figure VI-120. Significant capacity loss was observed in each group after 50,000 miles of operation; DCFC group did show more degradation; however, the additional fade was small relative to the AC Level 2 control group.

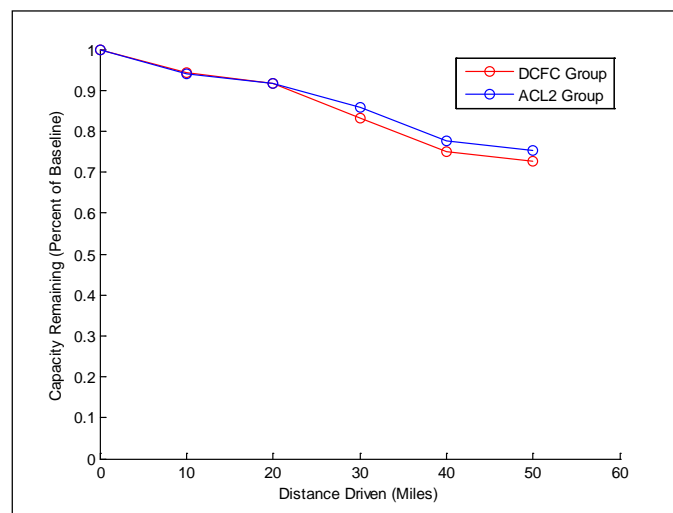


Figure VI-120: Battery capacity remaining, as a percent of baseline, THAT IS averaged among the onroad vehicles of each charge condition group.

INL

To directly measure range, constant speed range tests were carried out at three different speeds. These tests were performed starting with a full charge and ended when the vehicle could no longer maintain the target speed. The average ranges achieved by the DCFC and the AC Level 2-charged groups during track testing

after 50,000 miles are shown in Figure VI-121. The difference in range is more pronounced than the difference in battery capacity among the test groups. This is likely due to the vehicle control system limiting power in advance of battery depletion. Also, the battery management system was found to limit battery discharge to a higher-termination voltage than was used during laboratory capacity testing. The difference in 45-mph constant-speed range from baseline to 50,000 miles is shown in Figure VI-122.

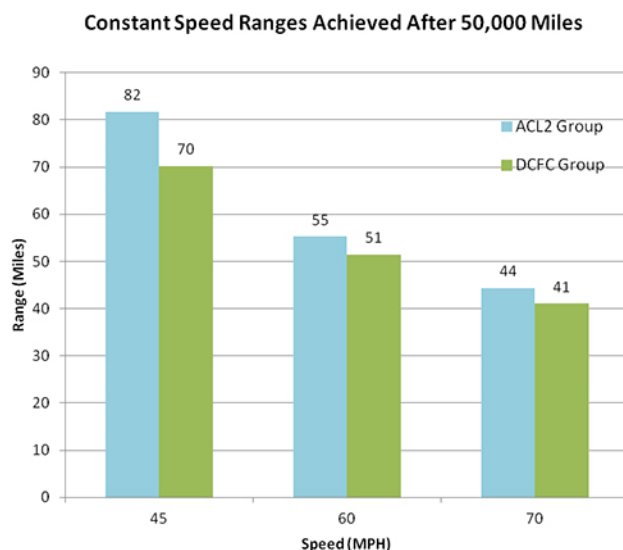


Figure VI-121: Constant-speed average range achieved at three different speeds for each test group after 50,000 miles of onroad operation.

INL

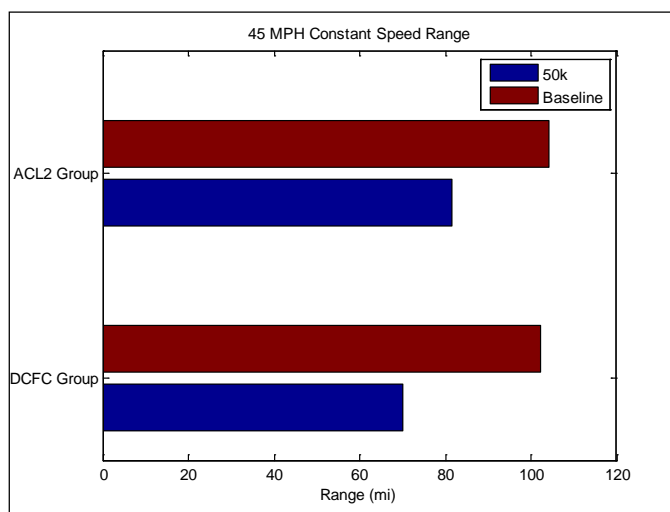


Figure VI-122: Constant-speed average range at 45 mph for each test group when new and after 50,000 miles of onroad operation.

INL

The range achieved during daily driving was also used as an indicator of battery capacity and health. The previous laboratory-based capacity and track-based range metrics were combined with the per-charge energy consumed during onroad operation, averaged over each testing interval, and are shown in Figure VI-123. The onroad based energy capacity discharged was less than either of the previously discussed capacity tests due to the need to keep residual energy in the battery for safety and practical considerations. Each vehicle returned to charge when the range remaining indicator on the dashboard displayed 5 miles. There are differences in the absolute energy capacity measurements among methods; however, the trends point to the same result. In

addition, the practical implications are most closely measured by the onroad performance, because consumers, though varied, will stop to charge prior to complete battery discharge.

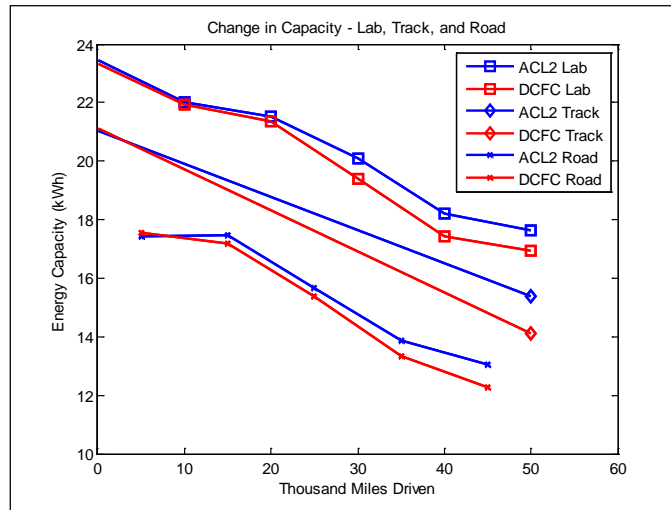


Figure VI-123: Battery capacity measured or inferred by three methods: (1) laboratory capacity testing, (2) track constant-speed range testing, and (3) onroad energy usage during daily driving.

INL

The rate of capacity fade varies by interval. Other than the first interval, the rate of capacity fade relates to the average ambient temperature during the interval. The first interval is an outlier due to a break-in period, where capacity loss was fastest. This is well illustrated by data obtained from the laboratory-cycled packs, which were held at a constant 30°C. Figure VI-124 shows that the initial energy fade begins steeply and approaches a nearly constant slope following approximately 10,000 miles of equivalent cycling.

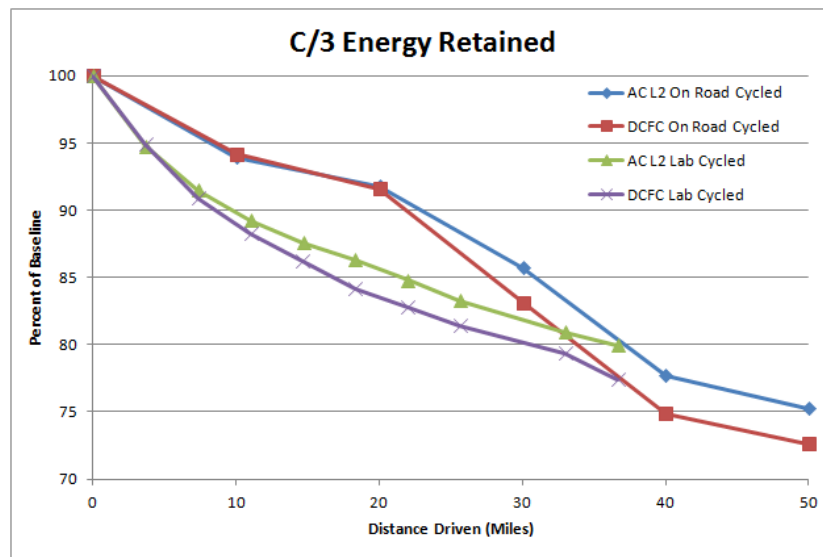


Figure VI-124: The percent of energy retained versus miles (or miles equivalent) driven or cycled is shown for the onroad and laboratory-cycled packs.

INL

Conclusions

The four battery electric vehicles driven in Phoenix, Arizona were faced with a hot climate and two were fast charged twice as often as recommended by their manufacturer. Despite these conditions, the vehicles were operated without failure for more than 50,000 miles. A greater loss in battery capacity was observed for the

DCFC vehicles; however, the difference compared to the AC Level 2-charged vehicles was small in comparison to the overall capacity loss. The vehicle operation was, as intended, verified to be very similar between the test groups; the largest difference in conditions noted was battery temperature during charging. Hotter ambient temperatures appear to have accelerated capacity loss for all vehicles in the study. The exact relationship remains to be seen, pending future study with various temperature conditions. Testing is currently underway for two packs, identical to those tested in this study, under constant temperature conditions and identical cycling in the laboratory. The results of that testing, combined with data from the onroad testing and cell testing at multiple temperatures, will serve to further answer the questions related to the rate of capacity, both in relation to time and temperature and will remove even small variations in conditions between the packs.

VI.9.C. Products

Presentations/Publications/Patents

1. Shirk, M. and Wishart, J., "Effects of Electric Vehicle Fast Charging on Battery Life and Vehicle Performance," SAE Technical Paper 2015-01-1190, 2015.
2. INL, "DC Fast Charge Effects of Battery Life and Vehicle Performance Study Fact Sheet," September 2015, http://avt.inl.gov/pdf/energystorage/DCFC_Study_FactSheet_EOT.pdf.
3. Shirk, M., "Effects of Electric Vehicle Fast Charging on Battery Life and Vehicle Performance," Paper presented at SAE World Congress 2015, COBO Center, Detroit Michigan, April 2015.

VI.10. Wireless and Conductive Charger Evaluation and Onroad 12-V Auxiliary Load Evaluation

James Francfort, Principal Investigator

Idaho National Laboratory
P.O. Box 1625
Idaho Falls, ID 83415-2209
Phone: (208) 526-6787
Email: James.francfort@inl.gov

Lee Slezak, DOE Program Manager

Phone: (208) 586-2335
Email: Lee.slezak@ee.doe.gov

Start Date: October 2013

End Date: Ongoing

VI.10.A. Abstract

Objectives

- Provide the U.S. Department of Energy (DOE) with independent and unbiased benchmark testing results by evaluating emerging technologies developed via DOE and industry investments
- Benchmark the efficiencies and safety of wireless power transfer (WPT) systems, conductive electric vehicle supply equipment (EVSE), and direct current fast chargers (DCFC)
- Benchmark the cyber security of charging systems
- Benchmark DCFC and Level 2 EVSE compatibility with new generations of plug-in electric vehicles (PEVs)
- Continue to provide testing results to other DOE programs, national laboratories, and several U.S. drive technical teams that Idaho National Laboratory (INL) staff are members of.

Accomplishments

- Completed initial vehicle-level testing for the Evatran PLUGLESS pre-production WPT system. Results were compared to previously published laboratory testing of the same Evatran pre-production WPT system in an effort to quantify the impact of the vehicle's steel chassis on electromagnetic field strength and system efficiency.
- Utilized the detailed test results from both the vehicle-level and laboratory open-air testing of the pre-production Evatran WPT system that supported improvements in design and efficiency for the forthcoming production Evatran WPT system.
- Provided significant support to Society of Automotive Engineers J2954 in their development of WPT codes and standards.
- Completed evaluation of the production PLUGLESS wireless charging system produced by Evatran. The evaluation was conducted for the system as integrated into a Chevy Volt and as a standalone system.
- Completed efficiency and functionality testing of the Eaton, Siemens, and Delta smart grid-capable EVSE, which are the final deliverable from Eaton, Siemens, and Delta for FOA-554 (i.e., development of smart grid-capable EVSE funded by the DOE Office of Electricity Delivery and Energy Reliability).
- Completed cyber security testing of the Eaton, Siemens, and Delta smart grid-capable EVSEs.

- Completed evaluation of the 12-V auxiliary loads from four vehicles each of four non-electrified vehicle models (i.e., 16 total vehicles). The results provide a real-world, 12-V auxiliary baseline to quantify future improvements in auxiliary load reduction technologies.
- Completed benchmark measurements of 15 individual auxiliary loads under steady-state conditions from four non-electrified vehicle models to quantify the individual impact of each load.

Future Achievements

- Continue identifying WPT, DCFC, and EVSE test partners and obtaining test systems
- Continue close coordination with the Society of Automotive Engineers J2954 committee
- Conduct charging compatibility/interoperability testing of DCFC, EVSE, wireless charging systems, and vehicles
- Continue evaluation of onroad, 12-V auxiliary loads of new vehicle models as coordinated with the Advanced Vehicle Testing Evaluation's (AVTE's) onroad evaluation and testing.



VI.10.B. Technical Discussion

Background

DOE's Advanced Vehicle Testing (AVTA) is part of DOE's Vehicle Technologies Office, which is within DOE's Office of Energy Efficiency and Renewable Energy. AVTA is the only DOE activity tasked by DOE to conduct field evaluations of vehicle technologies and fueling and charging infrastructure that use advanced technology systems and subsystems in light-duty vehicles to reduce petroleum consumption. A secondary benefit is reduction of exhaust emissions.

Most of these advanced technologies include use of electric drive propulsion systems and advanced energy storage systems. However, other vehicle technologies that employ advanced designs, control systems, or other technologies with production potential and significant petroleum reduction potential are also considered viable candidates for testing by AVTA.

Charging infrastructure for PEVs is also a study area of focus, because there is no singular successful business model that has been developed for public charging. In addition, there is much discussion within both the vehicle and charging infrastructure industries as to what the appropriate level of charging (kW) will be in the future and where that placement will occur (e.g., public, workplace, and/or residential). In support of this uncertainty, INL is testing the efficiencies, standby power, unit power during charging, and misalignment (for wireless power transfer) impacts on efficiency and electromagnetic field emissions.

AVTA's light-duty activities are conducted by INL for DOE. INL has responsibility for AVTA's technical execution, direction, management, and reporting, as well as data collection, analysis, and test reporting.

The current AVTA staff has 20+ years of experience testing grid-connected PEVs and PEV charging infrastructure. This experience includes significant use of DCFCs with various battery chemistries since the middle 1990s; this important legacy of experience is still available today. In addition, INL has significant experience performing cyber security testing for various federal agencies that are also being used for this project. During this reporting period, AVTA collected performance and use data from 17,000 Level 2 EVSE from the two largest providers of EVSE and several additional EVSE manufacturers.

Introduction

With the expanding introduction and use of grid-connected PEVs by fleets and individual taxpayers, development of both private and public PEV charging infrastructure (collectively known as conductive EVSE) continues. EVSE currently takes the form of Level 1 (110 Volt) and Level 2 (240 Volt) EVSE, which safely

supply alternating current (AC) electricity to the vehicle and the charger that resides on the vehicle. The third type of EVSE is the DCFC, which provides DC electricity to the vehicle and the power electronics equipment onboard the vehicle. For DCFCs, the charger is actually located off board the vehicle in the DCFC unit itself. AC Level 1 and 2 EVSE may either be in the form of smart EVSE, with functionalities such as revenue grade electricity meters, bidirectional communication capabilities, and other smart features, or “dumb” EVSE, which only provide electricity with minimal communication and metering capabilities. Regardless whether an EVSE is smart or less than optimally smart, its basic function is to safely transfer AC electricity from the consumers’ side of the electric utility meter to a PEV, which has an onboard vehicle battery charger and power electronics. By nature of its design, DCFCs are also at least somewhat smart units to ensure a minimal amount of communication between the DCFC charger and the vehicle’s battery control system.

Normally, the term EVSE will refer to AC Levels 1 or 2 and DCFC will be referred to by its acronym. It should be noted that most installed EVSE are AC Level 2 units, which provide significantly shorter charge times than AC Level 1.

Adding to the complexity of charging infrastructure selection and placement is the introduction of wireless charging systems, which transfer power without having the conductive connector of today’s EVSE and DCFCs (thus the term wireless power transfer or WPT). To support introduction of safe and efficient wireless charging systems, DOE and AVTA are conducting a series of activities to test and benchmark WPT systems. These activities include grants to support development of smart EVSE and wireless charging, as well as benchmarking the efficiencies of the different charging options and testing for vehicle-to-charging infrastructure compatibility. The activities discussed here detail the support activities being conducted by INL and some of the benchmarked results.

Vehicle auxiliary load data collection, analysis, and characterization were conducted on 16 non-electrified vehicles as part of the AVTA onroad vehicle evaluation. This auxiliary load characterization directly supports the U.S. automotive manufacturers in regards to potential off-cycle fuel economy credits for advanced technologies used to reduce energy consumption from vehicle auxiliary loads. A few examples of these advanced technologies are advanced alternators; heating, ventilating, and air conditioning systems; and lighting. The data collection and analysis details the auxiliary load during the onroad operation of 126,000 miles of 16 non-electrified vehicles (i.e., four Volkswagen Jetta TDI, four Honda Civic CNG, four Mazda 3 i-ELOOP, and four Chevrolet Cruze Diesel vehicles). Also, the analysis details the impacts of various real-world driving and ambient conditions on auxiliary loads.

In collaboration with Argonne National Laboratory, this study also evaluated the same four vehicle models (i.e., one of each model) over standardized drive cycles using a chassis dynamometer across a range of controlled ambient conditions. This was used to correlate and cross reference the onroad data collection across varying ambient conditions and temperatures.

Approach

INL has created a process for benchmarking wireless charging systems developed with DOE technology funding and with other wireless providers. Initial testing has been conducted and results from the first production system tests will be discussed in the next section. Of significant importance is the creation of non-disclosure agreements in order to support development of test procedures and sharing of protected proprietary information, while protecting release of the proprietary information.

INL has developed a testing regime for benchmarking AC Level 1 and AC Level 2 conductive EVSE efficiencies; this is being used to quantify grid-to-vehicle energy transfer efficiencies. This work is being leveraged to support benchmarking of the DOE Office of Electricity Delivery and Energy Reliability-developed smart grid EVSE. Testing was completed on three smart grid EVSEs, which that were produced by Eaton, Delta, and Siemens.

INL has completed the cyber security vulnerability assessment on the three smart grid EVSEs (i.e., Eaton, Delta, and Siemens). This is not an area that will receive significant disclosure due to the nature of the subject.

Much discussion has occurred regarding the efficiency of emerging wireless charging systems. For this reason, INL obtained, tested, and provided the first independent test results from the first production WPT system designed for light-duty electric vehicles (e.g., Chevy Volt and Nissan Leaf). The WPT system is the PLUGLESS wireless charger from Evatran. INL evaluated the WPT system installed on a Chevy Volt to determine interaction between the wireless charger and the vehicle and to quantify performance (e.g., efficiency and electromagnetic field strength). For comparison, the PLUGLESS system was also evaluated off board the vehicle in open-air test conditions.

The onroad evaluation of the 12-V auxiliary load of four vehicle models leveraged the onboard data acquisition system used by the AVTE evaluation, which records many signals and parameters, including vehicle speed, ambient temperature, 12-V battery voltage, and many more. Two current sensors were added to this data acquisition system to measure battery current and alternator output current. With these data, analysis was conducted to determine the 12-V auxiliary load during onroad driving over a wide range of conditions.

Benchmark testing of individual auxiliary loads was conducted by steady-state measurement, which enabled understanding of each load's contribution to the entire composite onroad load during normal onroad operation.

In accordance with AVTA's normal process, fact sheets and reports were used to document benchmarking procedures and results and the quantitative results were published, with the exception of cyber security findings.

Results

Electric Vehicle Supply Equipment Testing

Sixteen AC Level 1 and AC Level 2 EVSE have completed benchmark testing; the results are available at: <http://avt.inel.gov/evse.shtml>. A single fact sheet is published for each EVSE and the documented results include the following:

- Features
- Specifications
- Model tested
- Test conditions
- Test vehicle used
- Test results, including the following:
 - AC watt energy consumption prior to charge, during steady-state charge, and at post charge
 - Steady-state charge efficiency
 - Charge start and end profiles.

The three most recent EVSE tested were smart grid-enabled EVSE. These EVSE were produced by Eaton, Delta, and Siemens. The results were published in both a detailed technical document and a fact sheet. Cyber security vulnerability assessments were conducted on each of the three smart grid EVSE. These assessments investigated physical, communication, and software security. Because of the nature of the finding, no details can be provided without compromising the security of the EVSE tested.

Eaton Smart Grid Electric Vehicle Supply Equipment

The Eaton smart grid EVSE is an AC Level 2 commercial EVSE designed to charge two PEVs. Figure VI-125 shows a picture of the Eaton EVSE.



Figure VI-125: Eaton smart grid-enabled EVSE.

INL

EVSE testing was conducted in the laboratory for both the left and right J1772 plug (i.e., Plug 1 and Plug 2). Energy testing was done at four EVSE output power levels (i.e., 0.05 kW, 1.1 kW, 3.3 kW, and 6.2 kW), where each power level was tested for 10 minutes. EVSE standby power consumption also was tested to determine the amount of energy the EVSE uses while in a passive, non-charging state. Various power levels, such as AC Level 1 and AC Level 2, were chosen because they represent typical charge rates for a wide range of PEVs. The highest output power tested was limited to 6.2 kW, because of the 30-amp input continuous current limit. The nominal input voltage was 208 VAC.

Table VI-9 details EVSE efficiency while operating at various charge power test conditions. Table VI-10 details standby (i.e., not charging the vehicle) power consumption of EVSE in the various operational states. Note that State D is an operational state that is not compatible with this EVSE because State D requires a ventilation fan for operation per the operational codes and standards. The response of the Eaton EVSE to the requested State D is correct and expected.

Table VI-9: Eaton smart grid EVSE efficiency.

Test Condition	Average EVSE Efficiency (Output Power/Input Power)
50 watts	77.0%
1.1 kW	98.3%
3.3 kW	98.7%
6.2 kW	98.1%

Table VI-10: Eaton EVSE standby power (watts).

J1772 State	Left Plug	Right Plug
State B	11.9 watts	11.8 watts
State C	15.1 watts	15.1 watts
State D	NA	NA

Delta Smart Grid Electric Vehicle Supply Equipment

The Delta smart grid EVSE is an AC Level 2 residential EVSE designed to charge a PEV. Figure VI-126 shows a picture of the Delta EVSE.



Figure VI-126: Delta smart grid EVSE.

INL

EVSE testing was conducted in the laboratory for energy efficiency and standby power consumption. Energy efficiency testing was done at seven EVSE output power levels (i.e., 0.05 kW, 1.1 kW, 2.2 kW, 3.3 kW, 4.4 kW, 5.5 kW, and 6.2 kW), where each power level was tested for 10 minutes. EVSE standby power consumption also was tested to determine the amount of energy the EVSE uses while in a passive, non-charging state. Various power levels, such as AC Level 1 and AC Level 2, were chosen because they represent typical charge rates for a wide range of PEVs. The highest output power tested was limited to 6.2 kW, because of the 30-amp input continuous current limit. The nominal input voltage was 208 VAC.

Table VI-11 details the EVSE efficiency while operating at various charge power test conditions. Table VI-12 details standby (i.e., not charging the vehicle) power consumption of EVSE in various operational states.

Table VI-11. Delta smart grid EVSE efficiency.

Test Condition	Average EVSE Efficiency (Output Power/Input Power)
50 watts	90.8%
1.1 kW	99.2%
2.2 kW	99.1%
3.3 kW	99.1%
4.4 kW	98.7%
5.5 kW	98.5%
6.2 kW	98.3%

Table VI-12: Delta EVSE standby power (watts).

J1772 State	Delta EVSE Power Consumption
State A	3.98 watts
State B	4.15 watts
State C	5.18 watts
State D	5.21 watts

The EVSE's internal energy meter was tested during a 6.2- kW charge event over 10 minutes. The EVSE's output power was measured by a Hioki 3390 laboratory-grade power meter and an IQ 250 laboratory-grade watt-hour meter. These measurements were compared to the Delta EVSE's internal watt hour meter. After completion of the test, all three measurements were 1.02 kWh. Figure VI-127 shows a graph of the energy measurement through the test, ending with a total of 1.02 kWh after 10 minutes.

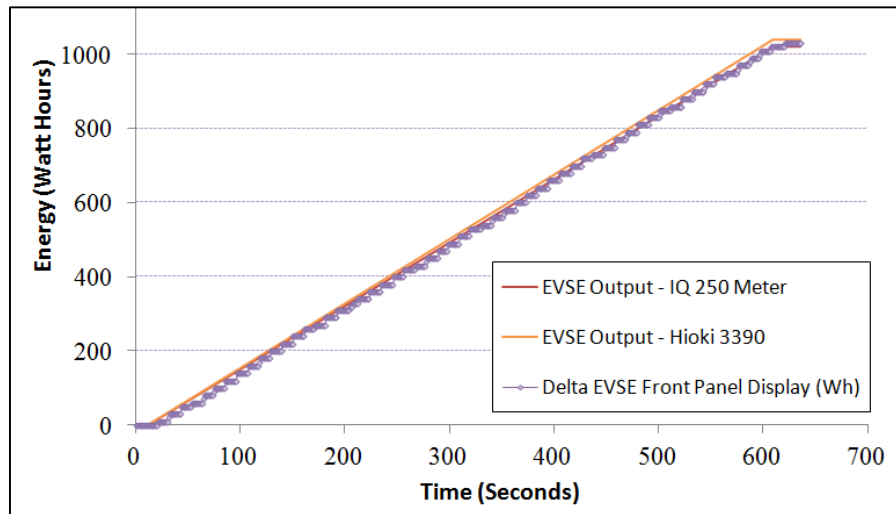


Figure VI-127: Delta smart grid EVSE energy meter test results.

INL

Siemens Smart Grid Electric Vehicle Supply Equipment

The Siemens smart grid EVSE is an AC Level 2 residential EVSE designed to charge a PEV. Figure VI-128 shows a picture of the Siemens EVSE.



Figure VI-128: Siemens smart grid EVSE.

INL

EVSE testing was conducted in the laboratory for energy efficiency and standby power consumption of the Siemens smart grid EVSE. Energy efficiency testing was done at seven EVSE output power levels (i.e., 0.05 kW, 1.1 kW, 2.2 kW, 3.3 kW, 4.4 kW, 5.5 kW, and 6.2 kW), where each power level was tested for 10 minutes. EVSE standby power consumption was also tested to determine the amount of energy the EVSE uses while in a passive, non-charging state. Various power levels, such as AC Level 1 and AC Level 2, were chosen because they represent typical charge rates for a wide range of PEVs. The highest output power tested was limited to 6.2 kW, because of the 30-amp input continuous current limit. The nominal input voltage was 208 VAC.

Table VI-13 details the EVSE's efficiency while operating at the various charge power test conditions. Table VI-14 details the standby (i.e., not charging the vehicle) power consumption of the EVSE in the various operational states. The EVSE's Wi-Fi module and LED status light indicator were both on during these measurements.

Table VI-13: Siemens smart grid EVSE efficiency.

Test Condition	Average EVSE Efficiency (Output Power/Input Power)
50 watts	84.3%
1.1 kW	99.3%
2.2 kW	99.4%
3.3 kW	99.3%
4.4 kW	99.1%
5.5 kW	99.0%
6.2 kW	98.9%

Table VI-14: Siemens EVSE standby power (watts).

J1772 State	Siemens EVSE Power Consumption
State A	3.49 watts
State B	5.44 watts
State C	8.28 watts
State D	5.17 watts

The EVSE's internal energy meter was tested during a 6.2-kW charge event over 10 minutes. The EVSE's output power was measured by a Hioki 3390 laboratory-grade power meter and an IQ 250 laboratory-grade watt-hour meter. These measurements were compared to the Siemens EVSE internal watt hour meter, which displayed the measurement on the user interface software application. After completion of the 30-minute charge event, the laboratory-grade instruments both measured 3.00 kWh but the Siemens EVSE watt meter display had increased from 0.21 kWh to 0.35 kWh (i.e., a 0.14 kWh difference). The Siemens watt hour meter measurement is significantly different from the laboratory-grade measurements. To ensure this difference is not due to communication latency, data acquisition was allowed to continue to run for an additional 60 minutes after the charge event was complete. At the end of this additional hour, both laboratory-grade instruments still measured 3.00 kWh, but the Siemens EVSE watt meter displayed 0.80 kWh. Figure VI-129 shows this EVSE energy meter test and the significant difference between the EVSE watt hour meter measurement and the laboratory-grade measurements.

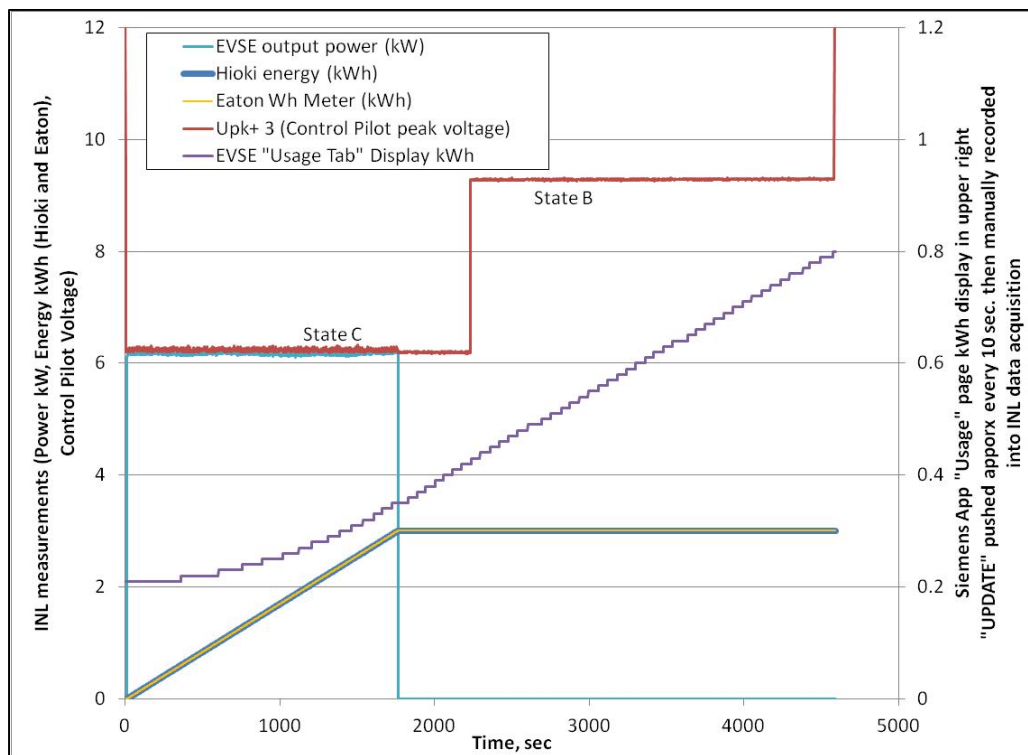


Figure VI-129: Siemens smart grid EVSE energy meter test results.

INL

Wireless Charger Testing

Vehicle testing and bench testing were completed on the production PLUGLESS wireless charger from Evatran. PLUGLESS was tested with a 2012 Chevy Volt (as shown in Figure VI-130) and bench tested using INL's non-metallic bench test setup (shown in Figure VI-131).

These tests evaluated the system efficiency, electromagnetic field emissions, and power quality at various power levels, coil misalignment, and coil gap.



Figure VI-130: Vehicle testing of the production Evatran PLUGLESS wireless charger on a 2012 Chevrolet Volt.

INL

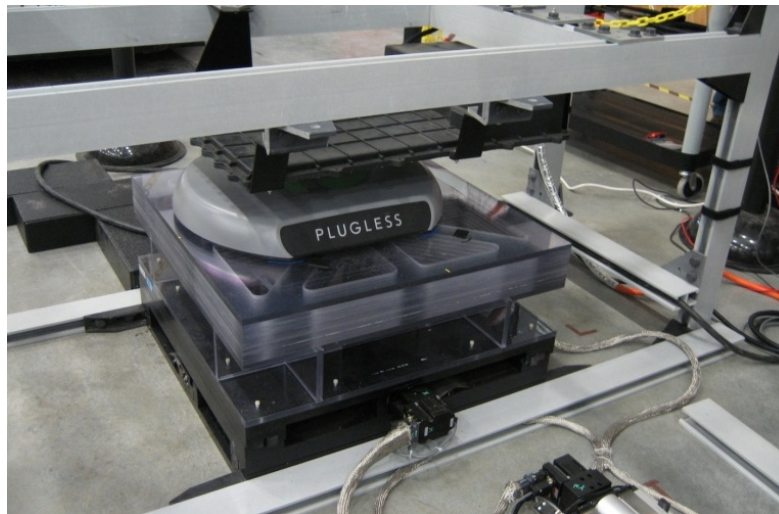


Figure VI-131: Bench testing of the production Evatran PLUGLESS wireless charger.

INL

The measured results of system efficiency, power quality, and electromagnetic field strength from testing of the production PLUGLESS charging system showed significant differences between bench testing and vehicle testing. This is due to interaction of the electromagnetic field with the steel chassis of the vehicle. This interaction is not present during bench testing, thus the difference in the results. Table VI-15 highlights test results from nominal conditions: aligned coils, 100-mm coil-to-coil gap, and 3.1-kW power transfer rate.

Table VI-15: Test results from the PLUGLESS wireless charger at nominal conditions.

Parameters	Bench Test	Vehicle Test
Efficiency at 100-mm gap	86.7 %	82.5 %
Gap with highest efficiency	71.5 mm	100.0 mm
Efficiency variation due to gap (71.5 to 109.5 mm)	0.6%	1.4%

Comparing the vehicle and bench test results in Figure VI-132 and Figure VI-133 shows the system efficiencies differ by 4 to 6% between the two test conditions. At nominal conditions, the system efficiency from vehicle testing is 82.5%, whereas standalone system efficiency is 86.7%. Additionally, bench testing shows the system efficiency is less variable with respect to change in coil gap showing a spread in efficiency of 0.6%. The vehicle test results show a 1.4% change in efficiency with respect to change in coil gap. Figure VI-133 also shows the for vehicle testing, a coil gap of 100 mm results in the highest efficiency when the coils are aligned. In contrast, Figure VI-132 shows that for the bench test results the 71.5-mm gap achieves the highest efficiency when the coils are aligned.

The vehicle test results in Figure VI-133 also show the non-symmetrical interaction of the vehicle chassis with the magnetic field of the PLUGLESS system with respect to coil alignment in the Y direction. The system efficiency results are roughly 0.3% lower in the positive misalignment direction (60 to 100 mm) when compared to efficiency with negative misalignment (-60 to -100 mm). The muffler and exhaust system in the vehicle are on the driver’s side of the vehicle (positive Y direction). When coil misalignment is in the positive Y direction, the primary coil is closer to the muffler and exhaust system. This results in more interaction between the magnetic field from wireless charging and the steel exhaust system.

The power quality of the PLUGLESS charging system was measured during both vehicle and bench test conditions. The power factor and the total harmonic distortion on the input current are consistent between the two test conditions and showed very little variation across the range of coil gap and misalignment. The nominal power quality test results are shown in Table VI-16.

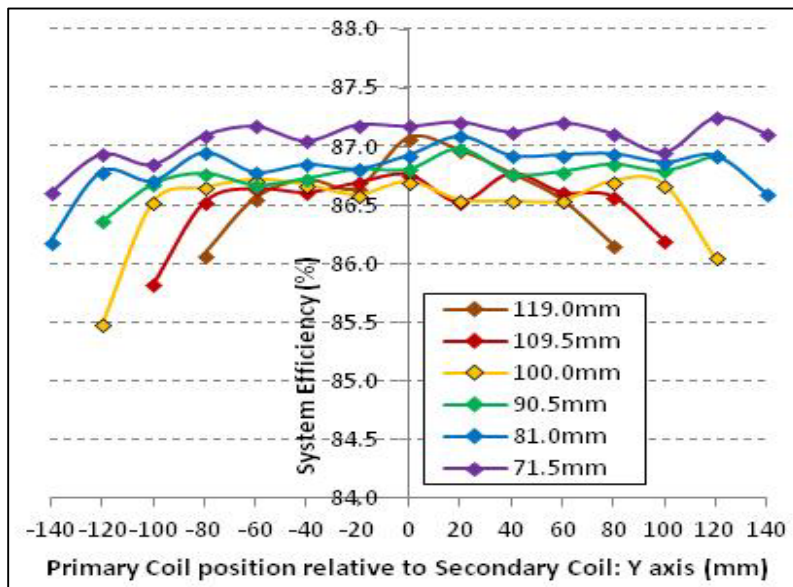


Figure VI-132: Bench test efficiency results of the production PLUGLESS wireless charger.

INL

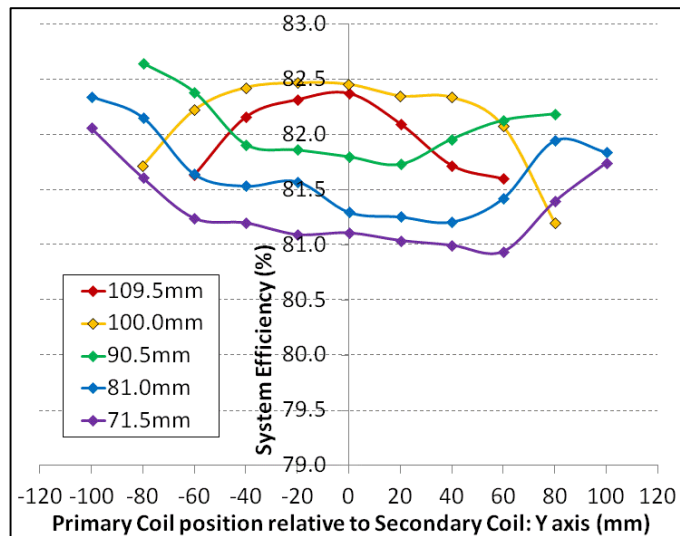


Figure VI-133: Vehicle test (i.e., Chevy Volt) efficiency results of the production PLUGLESS wireless charger.
INL

Table VI-16: Power quality test results from the PLUGLESS wireless charger.

Parameter	Bench Test	Vehicle Test
Power Factor	0.60	0.60
Total Harmonic Distortion Input Current	132%	134%

Electromagnetic field interaction with metallic objects and living entities is important to understand and quantify in order to verify that the field strength is below the industry safety limit. While the PLUGLESS system was operating under nominal conditions, the electromagnetic field was scanned across the plane perpendicular to the rear bumper of the vehicle. This would be representative of a person standing at the back of the vehicle while the vehicle is wirelessly charging. Figure VI-134 and Figure VI-135 show the electromagnetic field strength at the rear of the vehicle under nominal operating conditions for the vehicle test and the bench test.

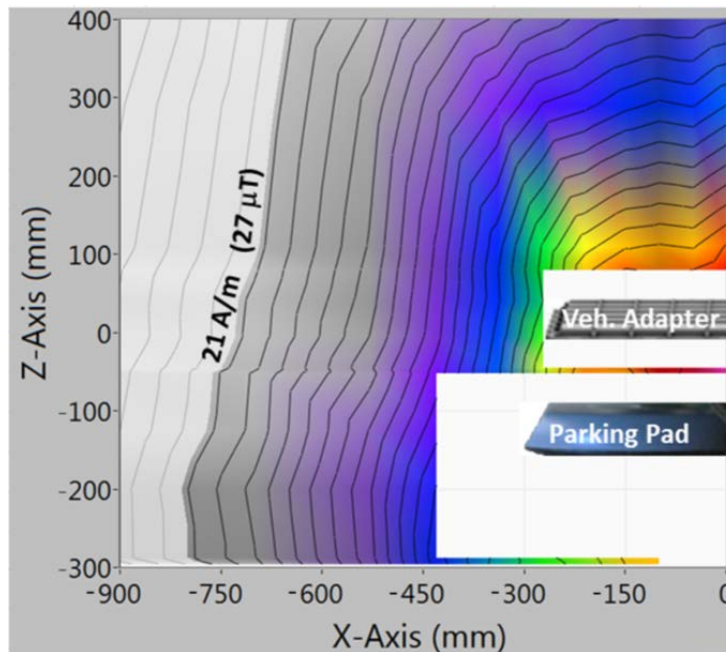


Figure VI-134: Bench test electromagnetic field scan results of the production PLUGLESS wireless charger.
INL

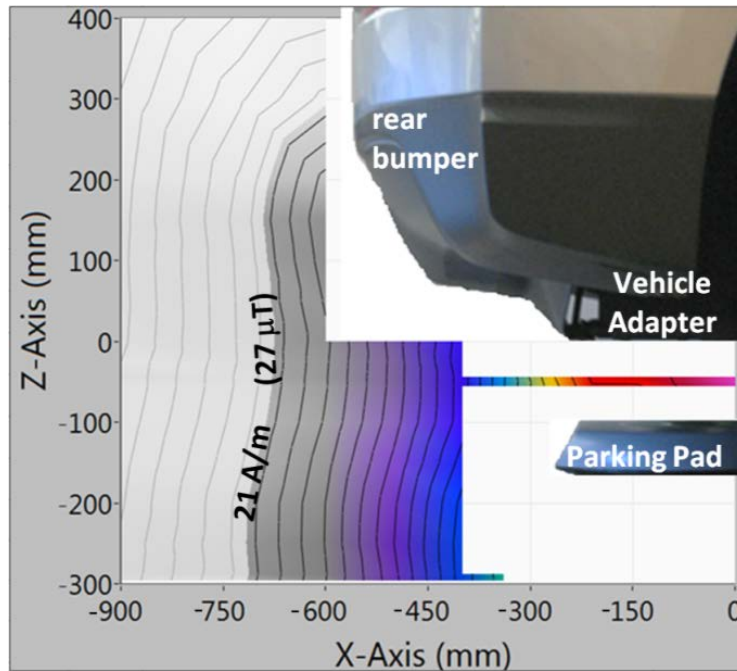


Figure VI-135: Vehicle test electromagnetic field scan results of the production PLUGLESS wireless charger.

INL

At nominal conditions (i.e., coils aligned, 100-mm gap, and 3.1-kW charge rate) the electromagnetic field strength was scanned at the rear of the vehicle. The test results again show interaction of the vehicle chassis with the PLUGLESS system. By closely comparing Figure VI-134 and Figure VI-135, the electromagnetic field strength between the coils is nearly the same for the two test conditions; however, the shape of the field from vehicle testing is contoured differently and attenuated when compared to the bench test results. This results in a small, but measurable, difference in magnetic field strength at the edge of the vehicle. For reference, the industry safety standard for electromagnetic field (International Commission for Non-Ionizing Radiation Protection) is highlighted in Figure VI-134 and Figure VI-135. The basic restriction limit for human exposure is 21 A/m (27 μ T).

Onroad Auxiliary Load Evaluation and Characterization

Vehicle 12-V auxiliary load data collection, analysis, and characterization were conducted on 16 non-electrified vehicles (i.e., four Volkswagen Jetta TDI, four Honda Civic CNG, four Mazda 3 i-ELOOP, and four Chevrolet Cruze Diesel vehicles) as part of the AVTA onroad vehicle evaluation. The evaluation encompassed two main activities: (1) characterization of individual loads and (2) evaluation of real-world, onroad auxiliary loads.

Auxiliary load characterization was conducted on individual vehicle accessories such as headlights, cabin fan, rear defroster, and so forth. The measurements were conducted at steady-state operation for each load. Figure VI-136 shows the results of several common auxiliary loads from the four vehicle models tested.

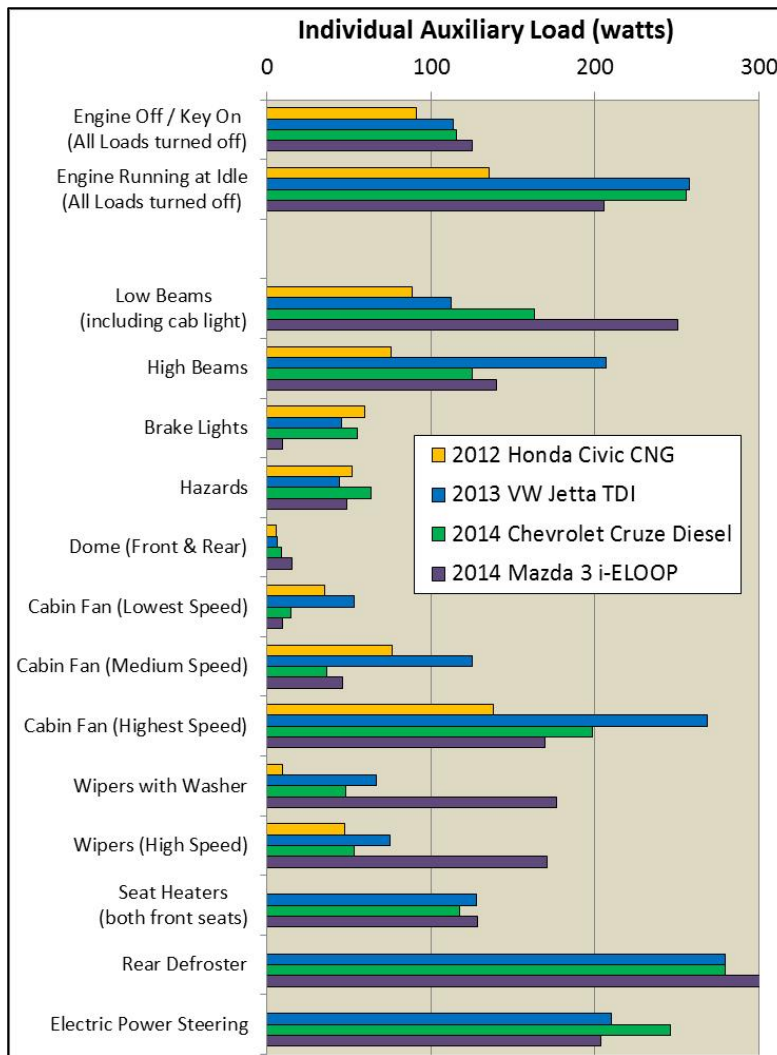


Figure VI-136: Individual auxiliary load characterization.

INL AVTE

As seen in Figure VI-136, there are two baseline conditions: (1) “Engine Off/Key On (All Loads Turned Off)” and (2) “Engine Running at Idle (All Loads Turned Off).” All individual auxiliary loads were in addition to a baseline condition, which resulted in the vehicle’s total auxiliary load. Note that the Civic CNG vehicles were not equipped with all of the evaluated accessories such as seat heater, rear defrost, or electric power steering.

Onroad data, which were collected from each of the 16 vehicles, were analyzed for auxiliary load. These data were collected on an ongoing basis for 12 months. Quarterly average auxiliary load by vehicle model is shown in Figure VI-137. Note the seasonal variation in auxiliary load. Seasonal temperature variation causes the driver to utilize differing accessories from season to season, which impacts the average auxiliary load.

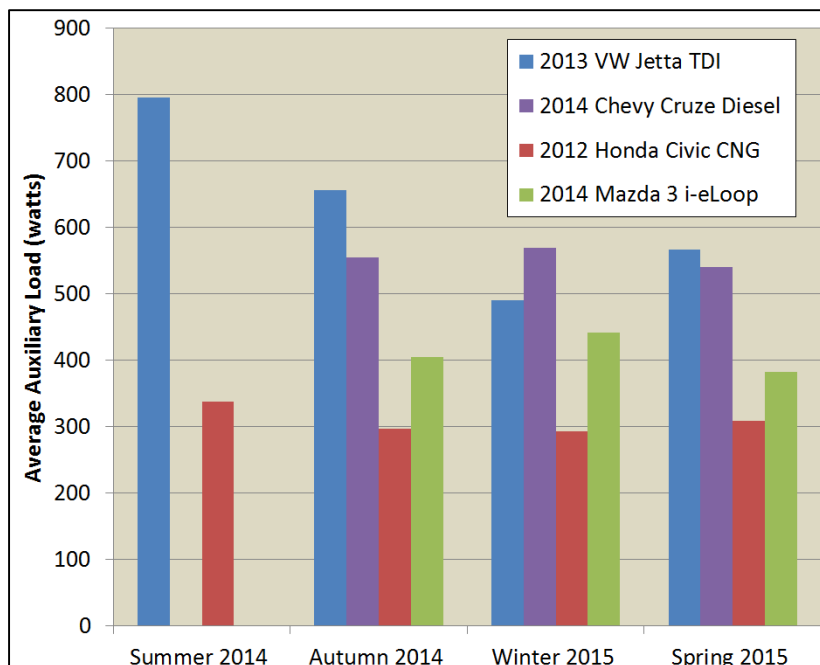


Figure VI-137: Quarterly average onroad vehicle auxiliary loads.

INL/AVTE

Closer examination of the impact of ambient temperature on auxiliary load shows a direct correlation (see Figure VI-138). The minimum average auxiliary load occurs at approximately 60°F ambient temperature due to minimal accessory utilization for cabin cooling or heating. In contrast, as the ambient temperature rises or falls, the driver utilizes more accessory heating or cooling, which increases auxiliary load. For the four Jetta TDI vehicles shown in Figure VI-138, the auxiliary load doubles from approximately 500 W to 1,000 W with the change in ambient temperature from 60°F to 110°F.

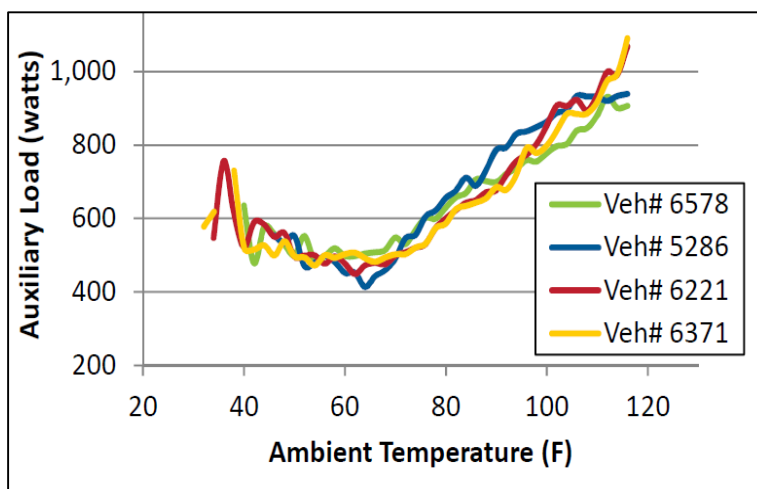


Figure VI-138: Ambient temperature impact on auxiliary loads (Jetta TDI).

INL/AVTE

Conclusions

INL will be testing additional wireless and conductive charging technologies with industry participation during the next 12 months. Industry, DOE, and INL are also conducting research into dynamic vehicle charging technologies that will use wireless power transfer technologies for possibly charging vehicles while they are driven on roadways.

Charging infrastructure is important to successful adoption of grid-connected vehicles; therefore, there are multiple key factors to successful integration of vehicles and charging infrastructure. This includes interoperability, safety, test methodology, and efficiency. Therefore, AVTA is working with industry to develop robust testing methodologies for evaluation of wireless and conductive charging systems.

Evaluation of the three smart grid EVSE completes evaluation of all EVSE from the FOA-554 final deliverables. The EVSE show that smart grid communications is an important aspect for EVSE to enable integration into the modern grid. Efficiency and cyber security are areas of continued importance.

In support of U.S. automotive manufacturers, information gathered by onroad data collection and analysis of the 12-V auxiliary load was a great success. The data serve as a baseline for quantifying future improvements in auxiliary load reduction technology. The results from this study directly support automotive manufacturers in regards to potential “off-cycle” fuel economy credits as part of the Corporate Average Fuel Economy regulations, where credit is provided for advanced technologies in which reduction of energy consumption from vehicle auxiliary loads can be demonstrated.

VI.10.C. Products

Presentations/Publications/Patents

1. Bennett et al., 2014, "Results from the Operational Testing of the Eaton Smart Grid Capable Electric Vehicle Supply Equipment (EVSE)," INL/LTD-14-33401, Idaho National Laboratory.
2. "Electric Vehicle Supply Equipment (EVSE) Test Report: Eaton Smart Grid Enabled EVSE," INL/EXT-11-23986, Idaho National Laboratory, http://avt.inel.gov/pdf/evse/EVSE_Eaton_Smart_Grid_Capable.pdf, March 2015.
3. Bennett et al., 2015, "Results from the Operational Testing of the Siemens Smart Grid Capable Electric Vehicle Supply Equipment (EVSE)," INL/LTD-15-35107, Idaho National Laboratory.
4. "Electric Vehicle Supply Equipment (EVSE) Test Report: Siemens Smart Grid Enabled EVSE," INL/EXT-11-23986, Idaho National Laboratory, http://avt.inel.gov/pdf/evse/EVSE_Siemens_Smart_Grid_Capable.pdf, June 2015.
5. Bennett et al., 2015, "Results from the Operational Testing of the Delta Smart Grid Capable Electric Vehicle Supply Equipment (EVSE)," INL/LTD-15-34461, Idaho National Laboratory.
6. "Electric Vehicle Supply Equipment (EVSE) Test Report: Delta Smart Grid Enabled EVSE," INL/EXT-11-23986, Idaho National Laboratory, http://avt.inel.gov/pdf/evse/EVSE_Delta_Smart_Grid_Capable_AC_Level2.pdf, July 2015.
7. "INL Wireless and Conductive Charging Testing," 2015 DOE Annual Merit Review, VSS096, Idaho National Laboratory, 2015.
8. "12-V Auxiliary Load Onroad Analysis," 2015 DOE Annual Merit Review, VSS168, Idaho National Laboratory, 2015.
9. "Auxiliary Loads: 2014 Mazda 3 i-ELOOP," INL/MIS-15-34255, <http://avt.inel.gov/pdf/ice/auxloadMazda3ProjectToDate.pdf>, July 2015.
10. "Auxiliary Loads: 2014 Chevrolet Cruze Diesel," INL/MIS-15-34255, <http://avt.inel.gov/pdf/ice/auxloadCruzeDieselProjectToDate.pdf>, July 2015.
11. "Auxiliary Loads: 2013 Volkswagen Jetta TDI," INL/MIS-15-34255, <http://avt.inel.gov/pdf/ice/auxloadJettaTDIProjectToDate.pdf>, July 2015.
12. "Auxiliary Loads: 2012 Honda Civic CNG," INL/MIS-15-34255, <http://avt.inel.gov/pdf/ice/auxloadCivicCNGProjectToDate.pdf>, July 2015.

VI.11. Wireless Power Transfer Grid Integration

Jeffrey Gonder, Principal Investigator

National Renewable Energy Laboratory (NREL)
15013 Denver West Parkway
Golden, CO 80401
Phone: (303) 275-4462; Fax: (303) 275-3765
E-mail: Jeff.Gonder@nrel.gov

David Anderson and Lee Slezak, DOE Program Managers

Phone: (202) 287-5688 (David Anderson)
E-mail: David.Anderson@ee.doe.gov
Phone: (202) 586-2335 (Lee Slezak)
E-mail: Lee.Slezak@ee.doe.gov

Start Date: 1/1/2014
End Date: 12/31/2015

VI.11.A. Abstract

Objectives

- Assess the impacts of multiple potential wireless power transfer (WPT) scenarios
 - Consider multiple vehicle classes/types, powertrain technologies, and WPT implementations (e.g., stationary charging vs. in-motion/roadway electrification)
- Analyze grid impacts for aggressive WPT vehicle penetration scenarios
 - Compare required growth to satisfy scenario demands with historic rates of load growth.

Accomplishments

- Completed detailed analysis of grid impacts from vehicle WPT scenarios by leveraging grid load and travel data for a specific metropolitan area (Atlanta, Georgia). Details are included in this report.
 - Considered electrification of high-capacity roads at multiple penetration rates of WPT-enabled vehicles
 - Based on historical rates of load growth, the analysis indicated that it should not be challenging to achieve the incremental growth rates required to keep pace with even aggressive roadway electrification scenarios.
- Completed incremental rollout analysis of roadway electrification scenarios for light-duty vehicles in urban areas and for heavy-duty trucks on substantial road grades
 - Presented and published analysis results in the Proceedings of the 3rd Conference on Electric Roads and Vehicles (CERV) in February 2015
- Completed analysis of quasi-static transit bus WPT scenarios, comparing costs and benefits of WPT-capable plug-in hybrid electric buses, hybrid electric buses, and conventional buses
 - Demonstrated that plug-in hybrid electric buses could achieve comparable lifetime costs as hybrid electric buses relative to conventional buses with roughly triple the fuel savings
 - Results to be presented and published at the 2015 IEEE Vehicle Power and Propulsion Conference.

Future Achievements

- Complete publication and presentation of results.



VI.11.B. Technical Discussion

Background

NREL has performed WPT analysis for several applications, including both in-motion roadway electrification and quasi-static charging at transit bus stops. Activities in fiscal year 2015 have included presenting and publishing results of incremental electric roadway deployment for light-duty vehicles on high-capacity roads in urban areas and for heavy-duty trucks while climbing substantial road grades during highway driving. Further activities include completing the quasi-static WPT transit bus analysis along with a publication on the results that will be presented at the IEEE Vehicle Power and Propulsion Conference in October 2015. Details on these activities can be found in the work products listed in the Presentations/Publications/Patents section. This report focuses on a grid impacts analysis of different light-duty vehicle roadway electrification scenarios.

Introduction

The electrified roadway grid impact analysis builds on NREL's incremental in-motion WPT rollout evaluation for urban areas [1]. That evaluation defined urban areas using the 2010 Census Combined Statistical Area (CSA) geographic boundaries to create delineations for analyzing road and travel distances within an analysis region and excluding travel outside that region. Datasets from NREL's Transportation Secure Data Center [2] were then paired with a specific CSA in multiple regions to investigate seven CSA regions. The following section details the approach used to conduct grid analysis on the Atlanta CSA which leverages and builds upon the work in [1].

Approach

Light-Duty Modeling Approach

Regional Travel Study: Hourly Travel

The Transportation Secure Data Center data for the Atlanta CSA comes from the Atlanta Regional Commission: 2011 Regional Travel Survey. In this survey, vehicle global positioning system (GPS) travel data were collected for a one-week period on a total of 1,422 vehicles from a 727-household subset of the study. The data were collected over the study period such that all vehicles were recorded for a full week, but not all vehicles were recorded in the same week. In this grid analysis, the travel data from all 1,422 vehicles is combined to provide an hourly travel distribution on the selected high-capacity roadways [3]. It is assumed that even though the recorded travel occurs on multiple weeks during the study, the combination of all vehicles provides a representative sample of a "typical" travel week. While six other CSAs were studied in the previous analysis, only the data from the Atlanta CSA are considered for the grid impacts analysis for two reasons: first, the collection of vehicle travel data took place over a consistent week period, and second, the initial survey was confined to households that reside in a single CSA. The hourly distribution of vehicle miles travelled (VMT) on the roadways selected for electrification by the initial analysis is included in Figure VI-139; note that these roadways are indicated in green on Figure VI-140.

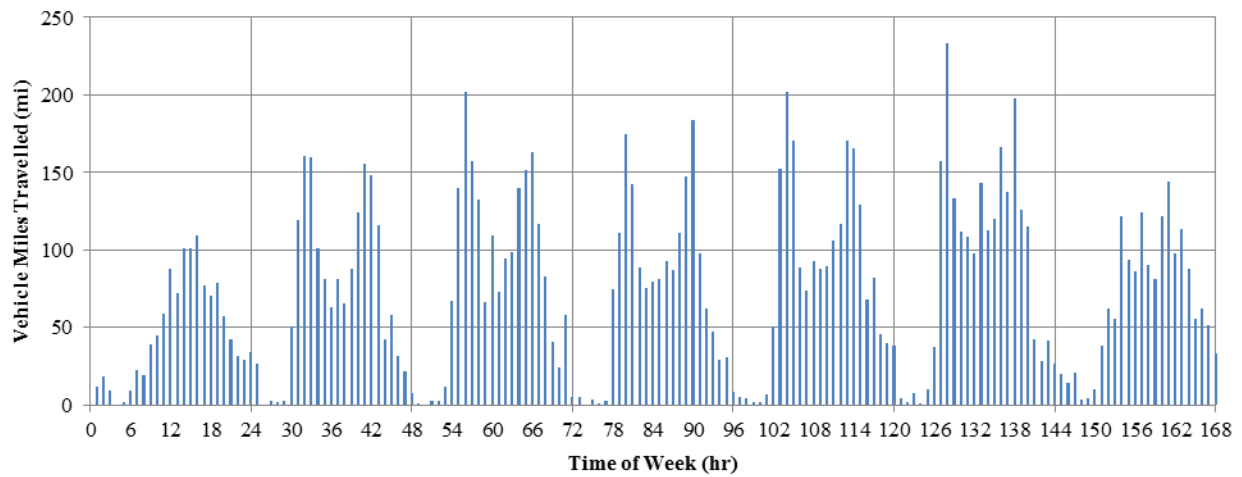


Figure VI-139: Hourly Distribution of Vehicle Miles Travelled on Selected Roadways for a "Typical" Week of Travel

Highway Performance Monitoring System: Total Roadway Travel

The travel survey data provide a distribution of travel miles at an hourly resolution throughout the week. In order to determine the hourly power use of the selected roadways, these segments were geospatially matched to the Federal Highway Administration's Highway Performance Monitoring System (HPMS) 2013 dataset. Figure VI-140 illustrates the results of this geospatial match with the road segments from the initial study shown in green and the newly selected HPMS segments shown in black. Note that the 2010 CSA boundary is identified with a dashed blue line and that the updated 2013 CSA boundary is defined in orange. The authors believe that the minor road and boundary changes between the different base map vintages do not meaningfully impact the high-level conclusions that can be drawn from this analysis.

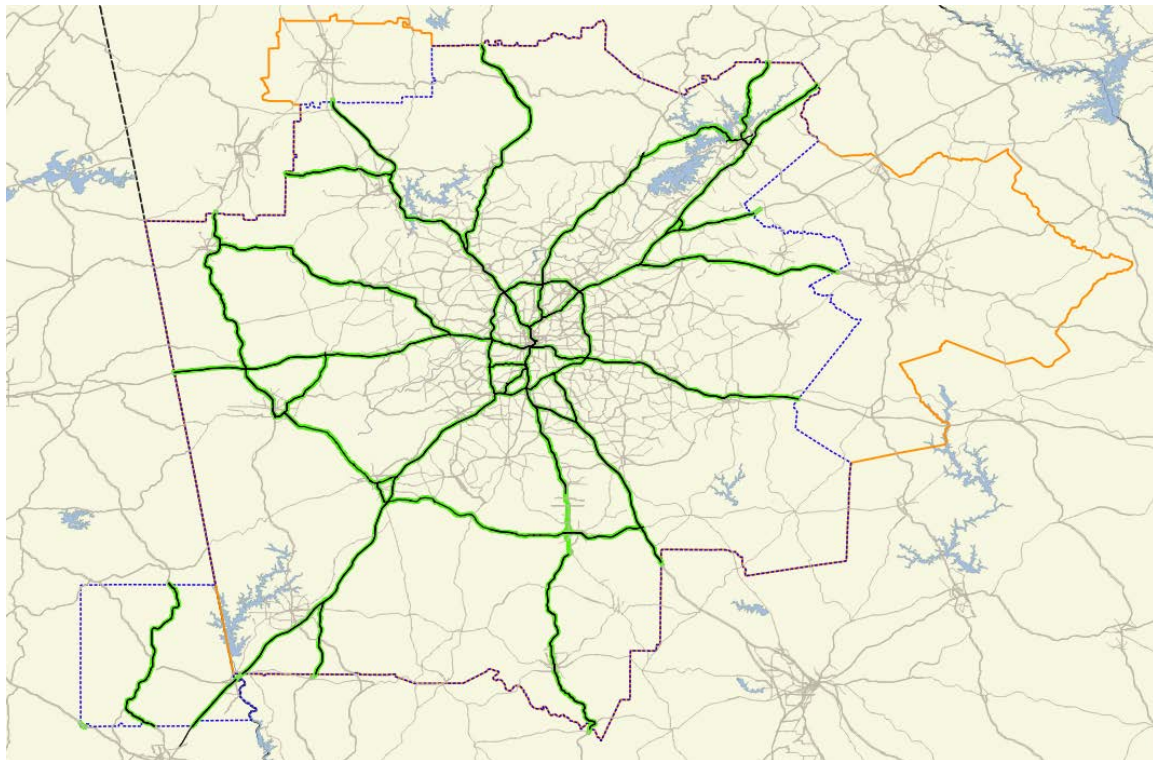


Figure VI-140: Comparison of Previous Analysis Roadway (Green) to Selected Roadway from 2013 HPMS (Black) with the 2010 Census CSA Boundary (blue Dashed) and 2013 CSA Boundary (Orange)

The HPMS dataset defines the annual average daily traffic flow, the length and functional class (FC) of each roadway, and many other road segment attributes. Daily VMT for any given segment can be calculated from the product of the segment length and the annual average daily traffic that traverses the segment. This calculation yields an estimated daily VMT of 59.3 million miles for the selected roadways, which include HPMS-defined FC 1, 2, and 3 segments (shown in black in Figure VI-140). As a sanity check, this same calculation was applied to travel on all Interstates (FC 1 roads) across the entire state of Georgia, which yielded a daily VMT estimate of 82.3 million miles. This result is indeed not far off from that suggested by the published annual VMT statistics for urban and rural interstate travel in Georgia [4].

This HPMS-derived estimation of VMT includes all traffic on the roadways selected for electrification. The Federal Highway Administration also reports annual vehicle travel disaggregated by roadway type and vehicle type [5]. For this light-duty focused analysis, the disaggregation was combined with the HPMS dataset to remove VMT attributed to heavy-duty vehicles. In [5], the distribution is defined by three categories: "interstate system," "other arterials," and "other." Each of these is further disaggregated into rural and urban sub-categories. To align these with the seven HPMS functional class categories (which also receive either a Census Urban Area Code or a rural area designation), NREL assumed the "interstate system" is defined as FC 1, the "other arterials" are FC 2 through FC 4, and the "other" roads are FC 5 through FC 7. Note that the removal of heavy-duty VMT is not meant to suggest that an electrified roadway system should or could only be designed separately for light-duty or heavy-duty vehicles. This analysis simply focuses on light-duty vehicles and leverages the light-duty Transportation Secure Data Center dataset to estimate hourly VMT distribution throughout a week.

Electrified Roadway Load

Total energy demand for the electrified roadway is calculated by multiplying the VMT results from the previous discussion by the energy consumption of individual vehicles on the roadway. NREL applied the following assumptions for calculating individual vehicle energy demands: 1) vehicles consume only the energy needed to traverse the distance of the electrified roadways (i.e., charge-neutral travel); 2) energy use per mile travelled is based on U.S. Environmental Protection Agency (EPA) combined city/highway consumption; and 3) the energy use is based on a vehicle representative of the average energy efficiency of the national light-duty fleet. Hourly power consumption, represented as an average power over the hour period, is calculated based on the temporal VMT distribution from the Atlanta Regional Commission survey's GPS-instrumented vehicles, and scaled so as to match the HPMS total average daily VMT.

Average energy efficiency of the national light-duty fleet is determined to be 24.3 mpg (4.12 gal/100 mi) by combining the production-weighted car and truck EPA fuel economy estimates and fleet proportions for 2014—i.e., 27.9 mpg (3.58 gal/100 mi) and 61.3% for cars, and 20.1 mpg (4.98 gal/100 mi) and 38.7% for trucks [6]. The 2014 Toyota RAV4 is used as a representative vehicle to compare fuel economy of a conventional vehicle to that of a similar electrified vehicle. The conventional 2014 RAV4 has an EPA city/highway combined fuel economy of 26 mpg (3.8 gal/100 mi) for the front-wheel drive automatic and 25 mpg (4.0 gal/100 mi) for the all-wheel drive automatic. The 44 kWh/100 mi (or 440 Wh/mi) EPA rating for the electric version of the RAV4 may therefore provide a reasonable basis from which to estimate the average per-mile efficiency of vehicles using the electrified roadway [7]. The EPA energy consumption is determined based on SAE J1634, which includes the conductive charging system efficiency. Given that electrified roadway charging is likely to have a lower efficiency than conductive charging, the estimated grid load is adjusted to 484 Wh per vehicle-mile based on [8] and [9]. Figure VI-141 provides the resulting hourly power use of the selected roadways for various assumed percentages of total light-duty VMT that are replaced by WPT-enabled vehicles.

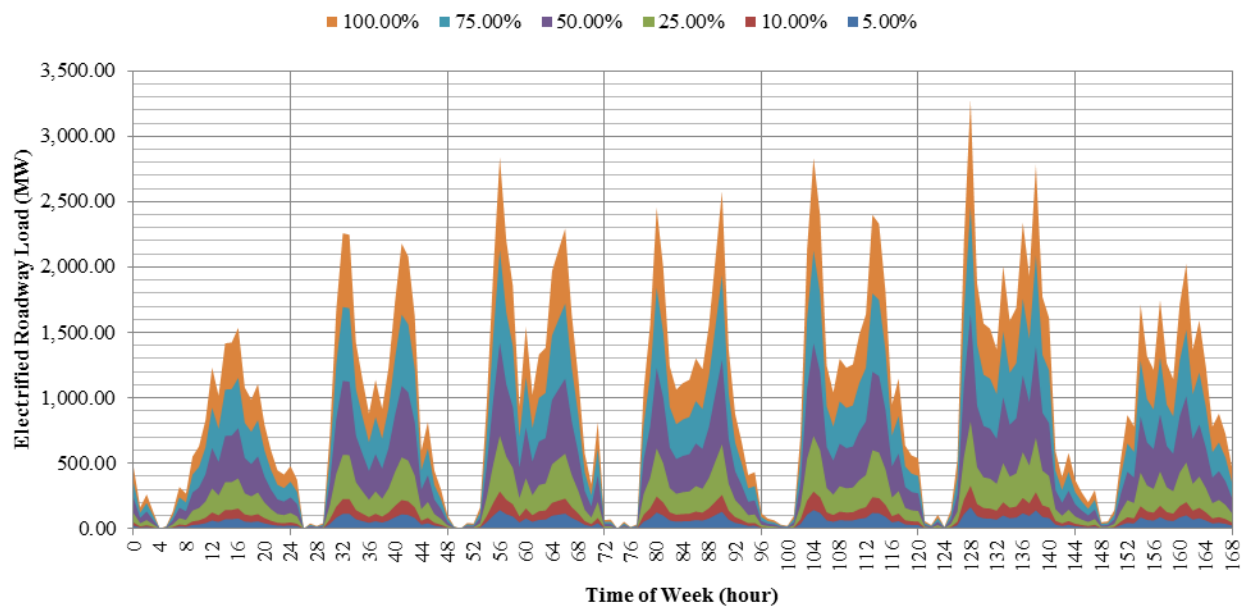


Figure VI-141: Electrified Roadway Grid Load for a "Typical" Week as a Percentage of Light-Duty VMT on the Designated Roads

Grid Load Modeling Approach

Grid load information for the eastern interconnect areas in this study has been provided from an Eastern Renewable Generation Integration Study (ERGIS) developed by NREL (forthcoming). For the ERGIS, historical hourly load data from 2006 were obtained and scaled to reach projected 2026 load levels, which required several steps. The 2006 hourly load profiles for each region were created by summing Ventyx Velocity Suite 2006 hourly profiles for the Ventyx transmission zones within each of the ERGIS sub-regions [10].

The first scale factor was calculated using 2006 to 2011 state retail load data [11]. For this process, the increase or decrease in load from 2006 to 2011 was found for each state in the U.S. Eastern Interconnect. The second scale factor was calculated using Energy Information Agency Annual Energy Outlook projected growth in retail electricity sales for each of the National Energy Modeling System Electricity Market Module (EMM) regions [12]. Scale factors for 2011 to 2026 were calculated as the projected 2026 load divided by the 2011 load for each EMM region.

To combine the two sets of scale factors, the state scale factors had to be aggregated to the EMM regions. This was done by mapping the states to the EMM regions and then calculating a load-weighted scale factor for each region. The two sets of scale factors were then compounded to get an aggregate for the entire 2006–2026 period for each EMM region. Hourly load information for the Atlanta region was then determined by identifying the load from nodes within the Atlanta 2013 CSA geospatial boundary identified by the orange line in Figure VI-140.

Results

Light-Duty Grid Impacts

Seasonal Results

Grid load information for the transmission nodes within the Atlanta 2013 CSA is averaged on an hourly level for each season to develop a seasonally averaged "typical" week of grid load. The electrified roadway load for the "typical" week is then added to each seasonal week to determine the combined load. The results are shown

for each season in Figure VI-142 through Figure VI-145. These figures identify six cases for a range of the total light-duty VMT, which are considered to understand the electrified vehicle rollout on the entire electrified roadway network.

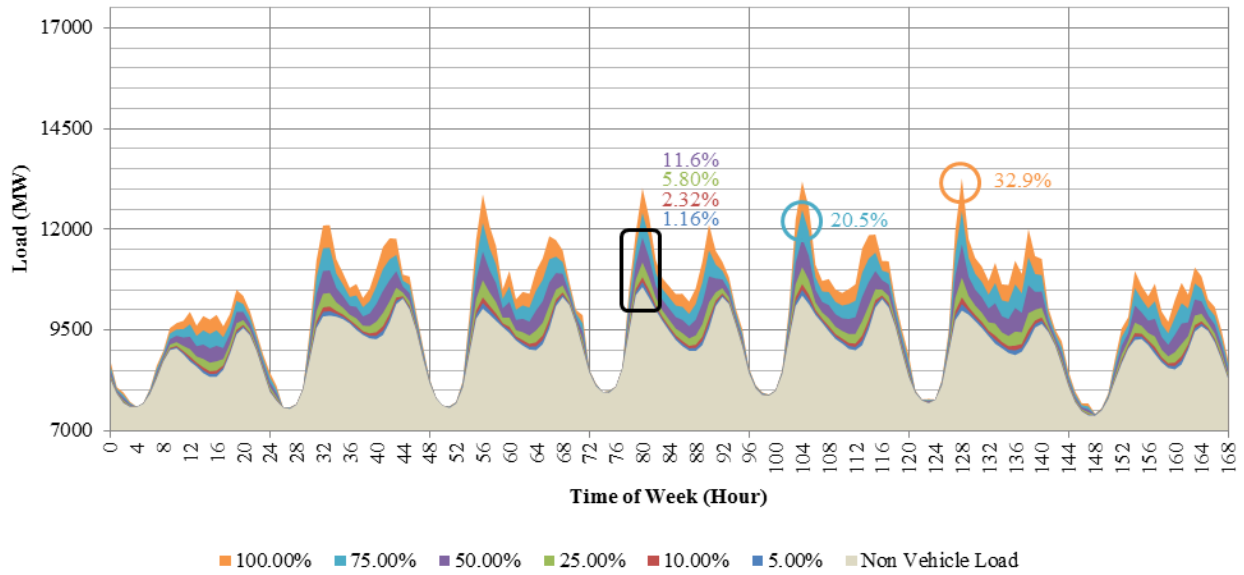


Figure VI-142: Electrified Roadway Scenarios Added to Typical Winter Grid Load. The numbers in colored text indicate the percent load growth over the baseline at the new seasonal average load peak resulting from each fractional VMT electrification scenario.

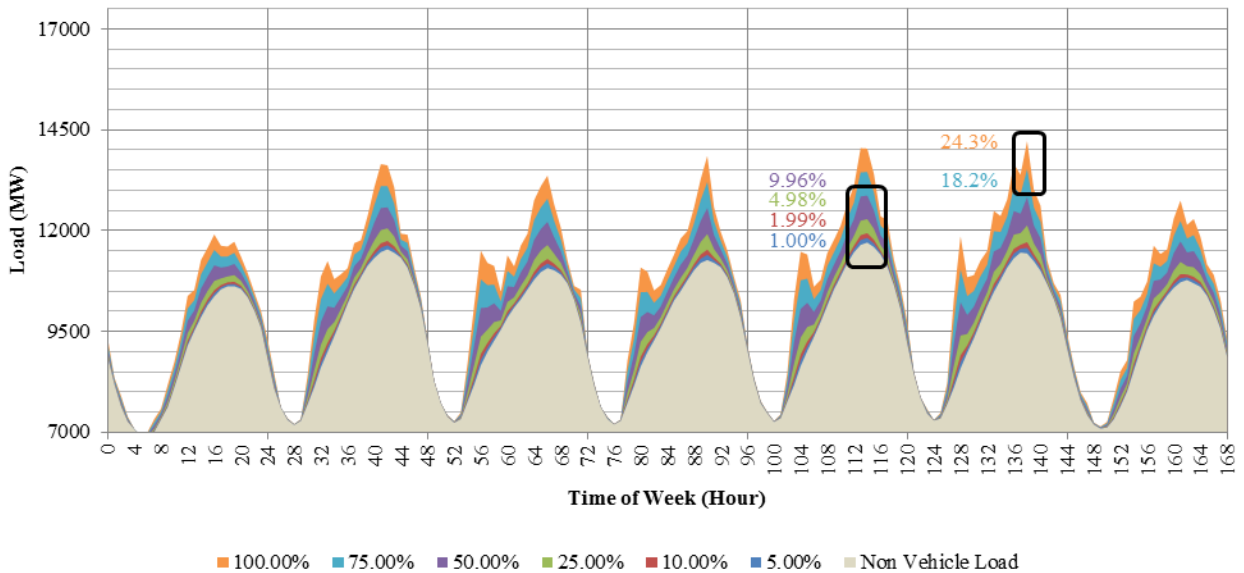


Figure VI-143: Electrified Roadway Scenarios Added to Typical Spring Grid Load. The numbers in colored text indicate the percent load growth over the baseline at the new seasonal average load peak resulting from each fractional VMT electrification scenario.

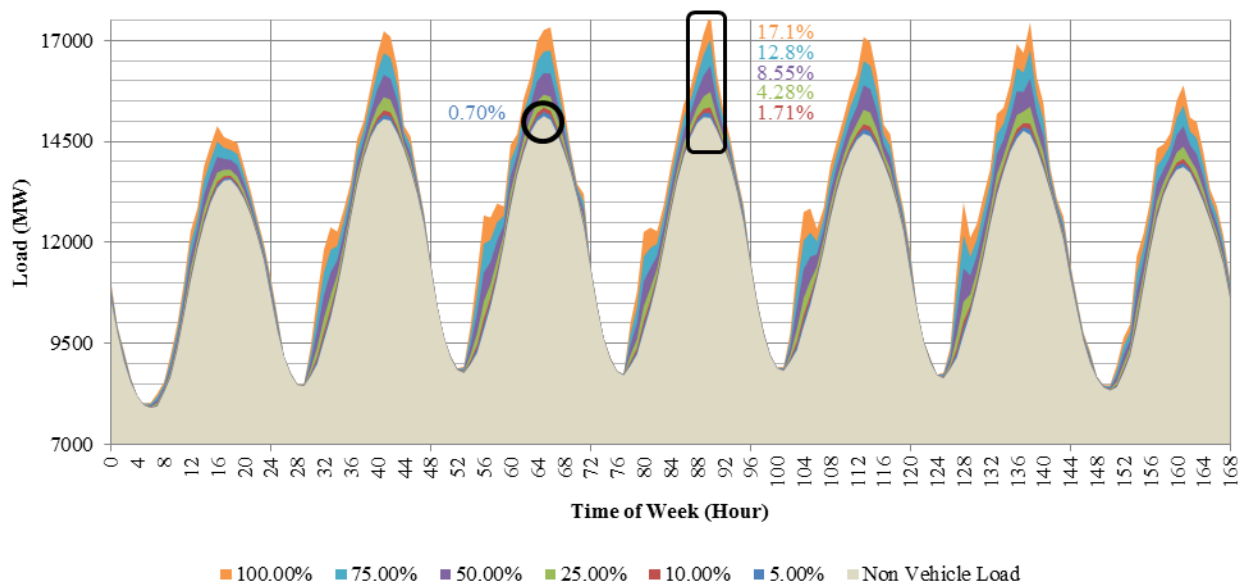


Figure VI-144: Electrified Roadway Scenarios Added to Typical Summer Grid Load. The numbers in colored text indicate the percent load growth over the baseline at the new seasonal average load peak resulting from each fractional VMT electrification scenario.

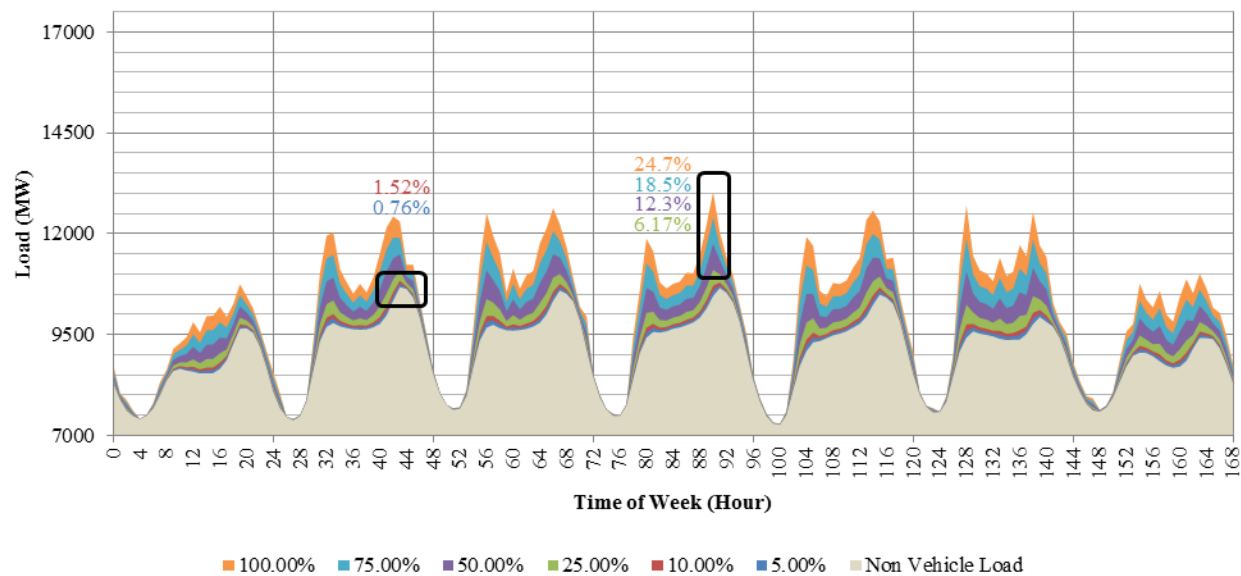


Figure VI-145: Electrified Roadway Scenarios Added to Typical Fall Grid Load. The numbers in colored text indicate the percent load growth over the baseline at the new seasonal average load peak resulting from each fractional VMT electrification scenario.

The seasonal average results show that the electrification of 5% of light-duty VMT results in a load growth between 0.70% and 1.16% for the peak load hour in the weekly average for each season. Similarly, the load growth for the electrification of 100% of light-duty VMT results in an increase between 17.1% and 32.9%. The magnitude of this load growth at the peak hour for the summer seasonal average load is between 107 MW and 2.60 GW for electrification of 5% and 100% light-duty VMT, respectively.

These results show that the effect this load growth would have on power generation requirements will vary by season as the overlap of grid peak load from non-vehicle load and peak travel periods change throughout the year. It should be noted that the seasonal impact of traffic flow could not be accounted for in this study given the available data for the Atlanta region. Further, additional vehicle load from daytime and nighttime static

charging of battery electric vehicles that may likely utilize these roads and be incentivized from its deployment have not been included in the total grid load. The illustrated scenarios instead reflect a case where the electrified vehicles utilize fuel for their remaining daily travel off of the electrified roadway (such as would be the case for WPT-enabled hybrid electric vehicles).

Load growth experienced for the 5% VMT electrification case in all seasonal average weeks is not enough to move the peak hour of weekly power from the hour in which it occurs for the non-vehicle load alone. For the higher-percent VMT electrification cases in which the traffic load was significant enough to move the hour in which the weekly peak load occurs, the new peak hours occur at either 08:00 or 18:00, corresponding to either the morning or early evening traffic peaks. This overlap exacerbates the midday trough in load that is seen in both the fall and winter seasonal average weeks where the morning and afternoon peaks in travel overlap with similar peaks in grid load. In the spring and summer the main overlap occurs with the early evening peak in both grid load and travel.

Highest Yearly Load Results

The peak hour of non-vehicle grid load for the Atlanta CSA occurs at 17:00 on Tuesday (or hour 65 for the week) of week 31 in July/August for the ERGIS 2026 dataset. This week also contains the second, third and fourth highest hourly loads, which occur on hours 137, 136, and 113, respectively, and is the highest week for total consumption throughout the year. Figure VI-146 shows the result of adding the "typical" week travel profile load to this highest load of the year week.

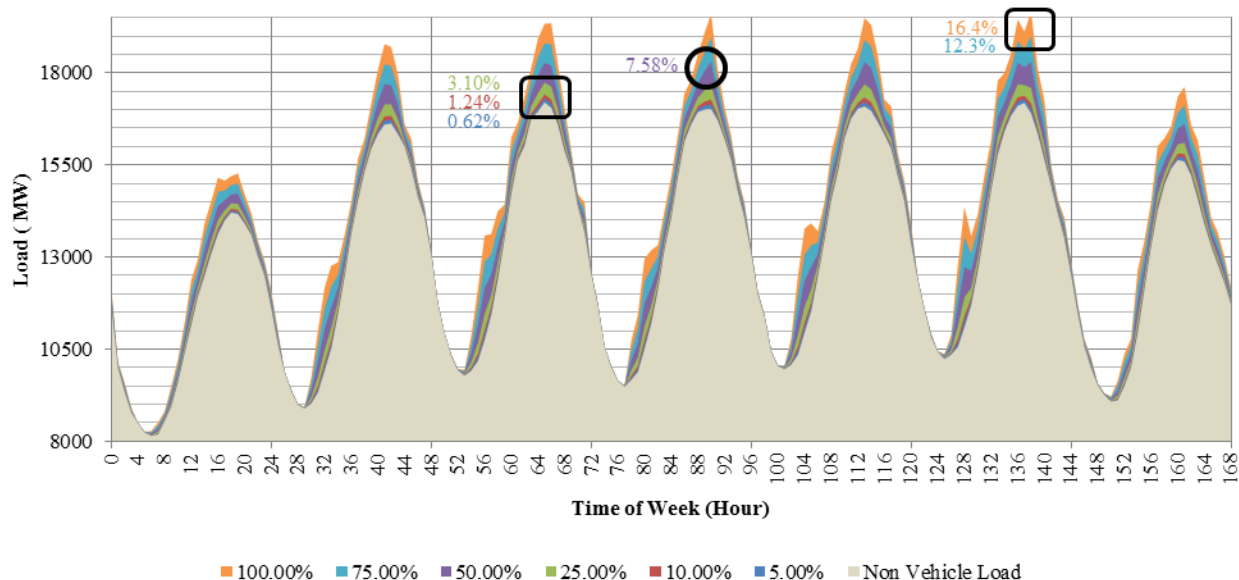


Figure VI-146: Electrified Roadway Scenarios Added to the Highest Yearly Grid Load Week. The numbers in colored text indicate the percent load growth over the baseline at the new seasonal average load peak resulting from each fractional VMT electrification scenario.

The highest yearly load results show that the electrification of 5% of light-duty VMT results in a load growth of 0.62% for the peak load hour in the week and similarly, the load growth for the electrification of 100% of light-duty VMT results in an increase of 16.4%. The magnitude of this load growth at the peak hour is between 107 MW and 2.78 GW for electrification of 5% and 100% of light-duty VMT, respectively.

These results are consistent with the peak hour trend seen in the summer seasonal average in which the new peak hour of load for the 50%, 75%, and 100% electrification of VMT cases occur in the early evenings at 18:00 when there is an overlap in evening peak traffic and non-vehicle grid load. For the 5%, 10%, and 25% of VMT electrification cases, the hour of peak grid load does not change in the highest yearly load week scenario. This is consistent for the 5% of VMT case in the summer seasonal average week scenario, but a change from that scenario for the 10% and 25% cases due to the greater amounts of load growth required to shift the peak hour in the highest load week relative to the average summer week scenario.

Electrified Roadway Adoption and Grid Impact

While 5% electrification of VMT is the lowest roadway electrification case examined in the preceding grid analysis, it should be noted that this assumption represents an aggressive penetration of WPT-enabled vehicles. Considering the historic example of hybrid electric vehicles, which have now been commercially available for over 15 years, recent data show them still accounting for less than 3% of new car sales [13]. In addition to the considerations of a technology's maturation rate and the pace at which it gains market share in new vehicle sales, the relative proportion it achieves in the entire fleet depends on the scrappage rate for legacy vehicles, which is predicted to be 6.56% for the light-duty fleet for 2020 to 2050 [14]. The difference between the baseline (non-vehicle load) and the 5% VMT electrification cases therefore represents a tremendous jump in vehicle technology adoption. The following discussion gives context for the corresponding increase in grid demand.

Figure VI-147 further illustrates the load growth for the 5% VMT electrification case relative to the highest load week of the year. The maximum percentage load increase for the week is slightly over 1% and corresponds to the weekday morning traffic peak. However, the overall peak load still occurs during the evening traffic peak, at which point the roadway electrification load adds less than 0.7% to the overall peak.

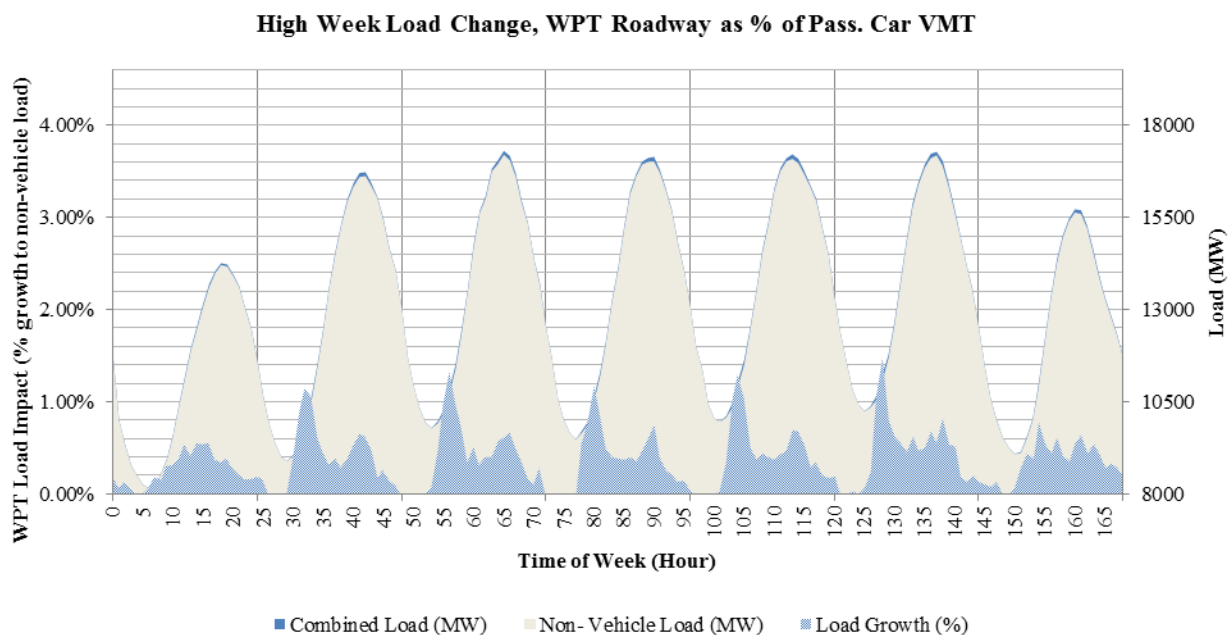


Figure VI-147: Absolute and Incremental Percentage Load Impacts from the 5% of Light-Duty VMT Electrified Roadway Scenario Added to the Baseline Highest Yearly Grid Load Week

The additional 0.62% of grid load from the electrified roadway at the peak hour can be compared to the historical level of grid load growth shown in Figure VI-148. This figure provides the annual load growth as calculated from both a linear fit and a polynomial fit to historical summer non-coincidental peak load for all interconnects of the grid. The long-term linear fit indicates annual growth rates between 1.6% and 2.5%, which exceeds the peak load growth that would be required to support the 5% VMT electrification scenario. What is more, the 7.7% single-year growth rate (from 2004 to 2005) shown in Figure VI-148 even exceeds the increased grid demand requirement from Figure VI-146 for the 50% VMT electrification case. The amount of load growth that electrified roadways present for peak hour energy consumption does not appear to be a significant challenge to generation capacity given the long period of time that it will likely take for vehicles capable of using this infrastructure to achieve substantial penetration levels into the vehicle fleet.

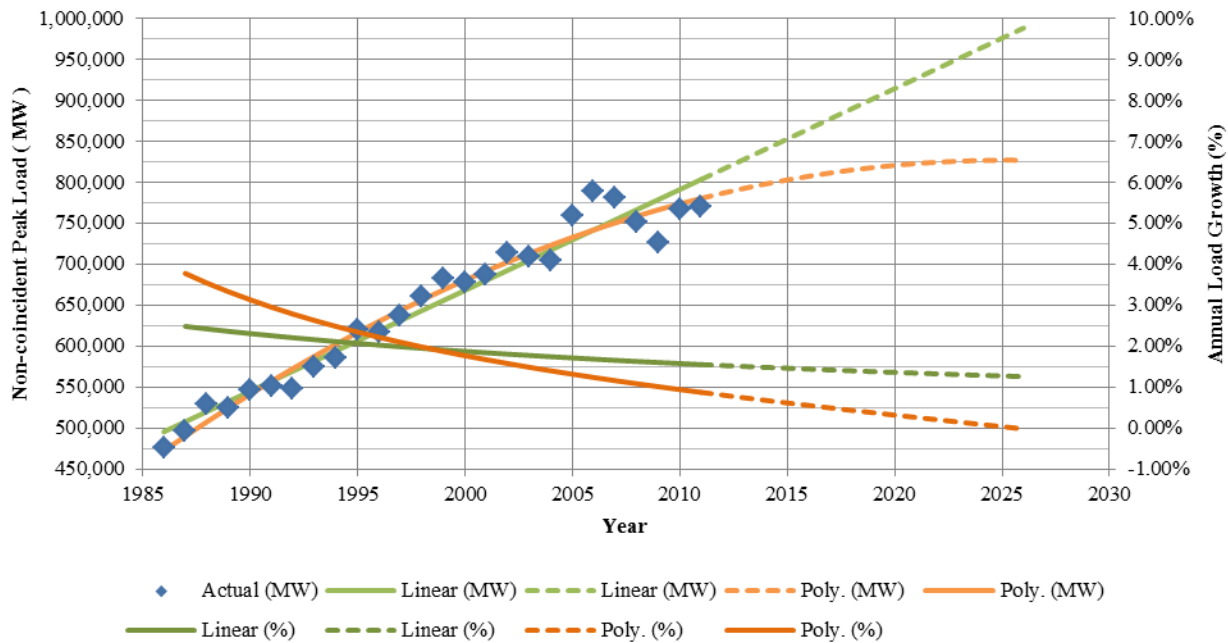


Figure VI-148: Historical Non-coincident Peak Load (All-Interconnects) with Linear and Polynomial Fits and Non-coincident Peak Load for the Summer Period for All Interconnection on the Grid from 1986 until 2011.

U.S. Energy Information Agency Annual Energy Review [15]

Conclusions

The grid impacts analysis presented builds on NREL's previous assessment of incremental electrified roadway rollout in an urban area. The analysis considered different fractional penetration levels of WPT-capable vehicles on electrified high-capacity roadways around the Atlanta area. The analysis assumed per-vehicle electric demands comparable to those that would be expected by a representative average vehicle in the light-duty fleet. Future work could consider sensitivity evaluation around the per-vehicle consumption value; however, such an evaluation should show little difference to the range of penetration rates that is considered here. The findings indicate that electrifying 5% of all VMT on high-capacity roads in the Atlanta area could increase peak grid demand by a little over 100 MW, which is a little less than a 1% load increase. Higher levels of VMT electrification obviously lead to higher levels of load growth, with a full 100% VMT electrification resulting in roughly 16% growth in grid load. Under the cases considered, the load growth during peak traffic periods does often coincide with existing periods of peak grid load. Future analysis could further determine to what degree this might present additional challenges to grid regulation based on the additional increase in grid load from road and vehicle electrification that would occur at other times of day. In particular, the exacerbation of the midday trough in load shown for the fall and winter seasonal average weeks could present additional challenges if considered in conjunction with higher penetrations of solar generation on the grid. When considering the overall magnitude of the load increases, however, the analysis suggests that the increase in demand due to roadway electrification would be small when compared with historic rates of load growth on the grid. For instance, while it would be expected to take many years to incrementally increase VMT electrification by 5% (leading to increased grid load on the order of 0.6%), historic trends show that grid load has commonly increased by over 2% in a single year.

VI.11.C. Products

Presentations/Publications/Patents

1. Wang, L., Gonder, J., Brooker, A., Burton, E., Konan, A. "Analyzing Future Potential of Targeted In-Motion Wireless Power Transfer for Line Haul Trucks." Proceedings of the 3rd Conference on Electric Roads and Vehicles (CERV), February 2015, Park City, UT. nrel.gov/docs/fy15osti/63457.pdf
2. Burton, E., Wang, L., Gonder, J., Brooker, A., Konan, A. "Fuel Savings Potential from Future In-Motion Wireless Power Transfer." Proceedings of the 3rd Conference on Electric Roads and Vehicles (CERV), February 2015, Park City, UT. nrel.gov/docs/fy15osti/63758.pdf
3. Meintz, A., Markel, T., Burton, E., Wang, L., Gonder, J., Brooker, A., Konan, A. "Implementation Scenarios for Electric Vehicle Roadway Wireless Power Transfer." Poster at the 2015 IEEE PELS Workshop on Emerging Technologies: Wireless Power (2015 WoW), June 2015, Daejeon, Korea.
4. Wang, L., Gonder, J., Burton, E., Brooker, A., Meintz, A., Konan, A. "A Cost Effectiveness Analysis of Quasi-Static Wireless Power Transfer for Plug-In Hybrid Electric Transit Buses." To be published at the 2015 IEEE Vehicle Power and Propulsion Conference (VPPC), October 2015, Montreal, Canada.

VI.11.D. References

1. Burton, E., Wang, L., Gonder, J., Brooker, A., Konan, A. "Fuel Savings Potential from Future In-Motion Wireless Power Transfer." Proceedings of the 3rd Conference on Electric Roads and Vehicles (CERV), February 2015, Park City, UT. nrel.gov/docs/fy15osti/63758.pdf.
2. "Transportation Secure Data Center." (2015). National Renewable Energy Laboratory. Accessed September 22, 2015: nrel.gov/tsdc.
3. Atlanta Regional Travel Commission, Regional Travel Survey: Final Report, November 2011.
4. Federal Highway Administration, Highway Statistics 2013: Annual Vehicle-Miles by Functional System. fhwa.dot.gov/policyinformation/statistics/2013/pdf/hm44.pdf.
5. Federal Highway Administration, Highway Statistics 2013: Distribution of Annual Vehicle Distance Traveled, by Vehicle Type fhwa.dot.gov/policyinformation/statistics/2013/vm4.cfm.
6. Environmental Protection Agency, "Trends Report: Light-Duty Automotive Technology, Carbon Dioxide Emissions, and Fuel Economy Trends: 1975 through 2014." EPA-420-R-12-023A, October 2014.
7. Retrieved on September 10, 2015. fueleconomy.gov/feg/Find.do?action=sbs&id=34425&id=34630&id=34633
8. Carlson, R. and Normann, B., "Test Results of the PLUGLESS™ Inductive Charging System from Evatran Group, Inc." SAE Int. J. Alt. Power. 3(1):2014, doi:10.4271/2014-01-1824.
9. Carlson, R. "Advanced Vehicle Testing Activity Benchmark Testing of the Chevrolet Volt Onboard Charger." Idaho National Laboratory, INL/EXT-12-25761, April 2012.
10. Ventyx Energy. (2013). Velocity Suite. Data Product. Boulder, CO: Ventyx Energy.
11. Energy Information Administration. (2015). "Retail Sales of Electricity by State by Sector by Provider (EIA-861)." April, 2005. Accessed: [date.] eia.gov/electricity/data/state/.
12. U.S. Energy Information Administration. (2011). "The Electricity Market Module of the National Energy Modeling System Model Documentation Report." Office of Integrated Analysis and Forecasting. July 2011. Accessed September 2015. eia.gov/forecasts/aeo/nems/documentation/electricity/pdf/m068%282011%29.pdf
13. Cobb, J. Jan. 6, 2015. "2014 December 2014 Dashboard." HybridCars. Accessed on 09/01/2015. hybridcars.com/december-2014-dashboard/
14. Environmental Protection Agency, "Fleet Characterization Data for MOBILE6: Development of Use of Age Distributions, Average Annual Mileage Accumulation Rates, and Projected Vehicle Counts for Use in MOBILE6." EPA420-R-01-047, September 2001.
15. U.S. Energy Information Agency. "Annual Energy Review, Table 8.12A." Accessed on September 2015. eia.gov/totalenergy/data/annual/showtext.cfm?t=ptb0812a

VI.12. INTEGRATE - Electric Vehicle Grid Integration R&D

Tony Markel, Principal Investigator

National Renewable Energy Laboratory
1617 Cole Boulevard
Golden, CO 80401
Phone: (303) 275-4478; Fax: (303) 275-4415
E-mail: tony.markel@nrel.gov

Lee Slezak, DOE Program Manager

Vehicle Systems
Phone: (202) 586-2335 (Lee Slezak)
E-mail: Lee.Slezak@ee.doe.gov

Start Date: 10/1/2014

End Date: 2/1/2016

VI.12.A. Abstract

Objectives

- The INTEGRATE (Integrated Network Testbed for Energy Grid Research and Technology) is a portfolio of projects to enable program technologies to form a system of devices that support future grid operations by enabling high penetration of renewable generation. Specific activities included,
 - Characterization of Devices and Systems for Grid Services
 - Evolution of System and Cyber Layer Communications and Controls
 - Holistic Assessment of Opportunities and Risks for Vehicle Assets in Future Grid Markets
 - A Multi-lab Requirements Study of EV Smart Grid Integration
- The efforts intend to enhance our system level knowledge, engage industry, and lead to system evaluation and demonstrations that provide guidance on policies and standards creation.

Accomplishments

- Energy System Integration Facility (ESIF) resources were used to characterize and test the performance of both a Mini-E electric sedan and a PG&E Utility truck both with export power functions.
- Multiple EVSE platforms were enabled varying communications architectures and control capabilities. Common interface software control tools were created that enable management of PEV charging that satisfy stakeholder expectations for drivers and building owners in high renewable generation scenarios.
- Building upon previous Energy Storage analysis efforts, simulation software was developed and applied to determine driver-specific opportunities for V2G functions that limit life impacts and maximize benefits
- Coordinated and developed a report from 6 national laboratories to guide DOE in planning EV smart grid research strategies in relation to the Grid Modernization Lab Consortium mission.

Future Achievements

- Share results with industry and engage toward further system evaluations and technology deployments that enable growth in PEV adoption.



VI.12.B. Technical Discussion

Background

Plug-in electric vehicles (PEVs) present an opportunity to provide a significant decrease in transportation fuel consumption and integrate with future clean grid operations. A new multi-program effort titled INTEGRATE was initiated to explore and develop the functionality of grid connected devices to become a coordinated resource. This project focused on the necessary steps, strategies and opportunities for PEVs to be a key component of this system. The work is a precursor to efforts planned to be conducted under the Grid Modernization Initiative.

Introduction

Integrated EVGI solutions have the potential to improve the marketability of electrified vehicles, resulting in expanded market share and long-term, national-level petroleum displacement. There is currently a lack of industry knowledge of the battery life and vehicle performance impacts of grid service applications. Additionally, the limited content and application of existing standards leaves an opening for the creation of open standards-based communications and infrastructure development that supports cross program (buildings, solar, wind, hydrogen, and transportation) systems integration for grid service market participation. Project research was conducted to identify barriers and explore solutions for the growth of electric vehicle grid integration.

Below are highlighted the DOE Grid Modernization objectives with some description of relevance to electric vehicles.

- 10% reduction in economic cost of power outages by 2025
 - Ability for a vehicle to be a “friendly” element of a microgrid
 - Export power function with grid-awareness
- 33% decrease in cost of reserve margins while maintaining reliability by 2025
 - Ability of a vehicle/driver to forecast demand, reserve, and flexibility
 - In aggregate, manage local variability of renewable generation
- 50% decrease in the net integration costs of distributed energy resources by 2025
 - Standardization, standardization, standardization
 - Accelerated testing and demonstrate

The work conducted for DOE in electric vehicle grid integration is relevant to industry in that the features and capabilities explored will enhance the plug-in electric vehicle (PEV) value proposition.

Approach

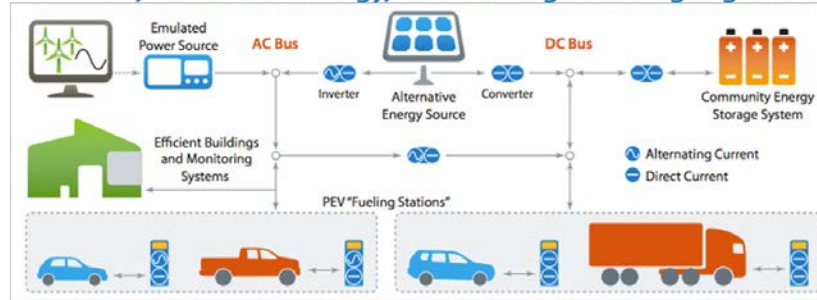
For electrified vehicles to benefit from integrated grid services capabilities, 3 key questions must be answered,

- What is the impact of vehicle-to-grid (V2G) power flow on the life/performance of a PEV battery?
- What are the communications, controls, and level of precision required to dynamically control PEV charging in response to grid conditions?
- What is the value proposition to all stakeholders (PEV owner, utility, automotive OEM, building owner, etc.) that will encourage PEVs to participate in the ancillary services market?

Figure VI-149 presents an architectural diagram and core topical research efforts that have been executed to address these questions.

Electric Vehicle Grid Integration at NREL

Vehicles, Renewable Energy, and Buildings Working Together



Developing Systems Integrated Applications



Vehicle-to-Grid Challenges



Figure VI-149: Approach to Conduct Research for Electric Vehicle Grid Integration

The research conducted under this project works to address key barriers to electric vehicle grid integration system adoption that include:

- Risk aversion of new technology
- Cost and value proposition for vehicles providing grid services
- Enabling technology related to Smart Charging Systems

Results

Characterization of Devices and Systems

During FY15, the NREL team had the opportunity to conduct grid interface testing on two vehicles with bi-directional power flow capability. These included a Mini-E sedan and a custom built PG&E utility truck.

The Mini-E was provided in partnership with the University of Delaware, NRG Energy, and Autoport. The vehicle is an all-electric vehicle with an AC grid interface capable of 19kW of power using an on-board charger/inverter technology. It is specifically tied to the grid through a Milbank EVSE. In addition to the power grid connection, the Milbank EVSE also provides for an internet connection. In this arrangement, both the EVSE and the vehicle have dedicated communications connections to an aggregation software system. This communications connection along with a hardware testing configuration in ESIF using a grid simulator allow the NREL engineers to complete characterization testing of this vehicle as it relates to IEEE 1547 for distributed energy resources interconnection with the grid. The initial tests completed highlighted the opportunity for vehicle software controls improvements. Changes were made by the vendor and further testing is planned.



Figure VI-150: Characterization of A Mini-E with Bi-directional Power Flow through Aggregation Software Tools was completed in ESIF

Similarly, in collaboration with Pacific Gas and Electric and Electric Drive Incorporated, NREL hosted a utility truck with export power systems capability for testing purposes. The vehicle represented a first generation implementation and the characterization and performance testing completed by NREL was used to guide the development of future interactions of this grid integrated electric vehicle. The vehicle is composed of a gasoline electric hybrid power train with integrated power electronics to provide up to 120kW of export power either in grid-tied or islanded modes. Figure VI-151 provides an image of the vehicle including its grid power connections while under test in NREL's ESIF thermal chamber.



Figure VI-151: Testing Power Interface Functions of PG&E Utility Truck with V2G capability was conducted at NREL's ESIF

NREL engineers and the product team resolved several implementation challenges during this research and in the end demonstrated the vehicle providing 120kW of export power as intended.

Communications and Control Architectures

In order for vehicles and other grid-tied devices to participate in the operations of the grid and potential provide some service function, there needs to be a functional communications interface between the devices and a system controller. The function, format, and implementation of these communications and control networks is still an open area. Ideally, open platforms that enable the interfacing of a diverse set of devices evolve. One such platform called Volttron has been supported by DOE and developed at PNNL. The interfaces to this system are still under development so in the meantime; existing systems have been evaluated and enhanced to provide core functionality.

Near the end of 2014, NREL completed the integration of a GE Wattstation into the NREL parking garage and enabled an interface between this station, the drivers that would use the station, and the NREL building energy management system. Figure VI-152 highlights the demonstration of this unit with DOE representatives and GE engineers. Software modules aggregated information such as driver energy needs and departure times, real-time and historical solar generation, and current net building loads on the grid. Controller software was

developed that generated a schedule for the charging of each individual vehicle such that it would jointly be aligned with solar generation, not impact building peak demand, and deliver on driver expectations.



Figure VI-152: NREL Demonstrates Interface between Vehicle and Building Energy Management Systems at NREL Parking Garage

The physical interface between the GE Wattstation and the controls software was achieved through a cellular network and a GE-managed cloud server. Although this is one implementation it is not the only solution.

NREL also partnered with Kitu Systems to evaluate an SEP 2.0 based communications and control architecture for EVSE management. Smart Energy Profile 2.0 (SEP2) is an international standard, IP-based application protocol specification providing Smart Grid services for home and business energy devices. The objective of these tests were to confirm functionality of the SEP software tools and enable future integration with a variety of devices in a home or business environment. The components of the system are depicted in Figure VI-153 and include a Utility server, a gateway device, and an enabled EVSE. Note that several communication media are used for this specific demonstration to make the connection between the NREL EVSE Management tools and the actual EVSEs. Software tools developed for the NREL Parking Garage demonstration were ported and leveraged to interface with 2 enabled EVSEs in this case. A functional demonstration was completed and it is expected that NREL team will continue to build on this platform for the integration of bi-directional and fast chargers in the future.

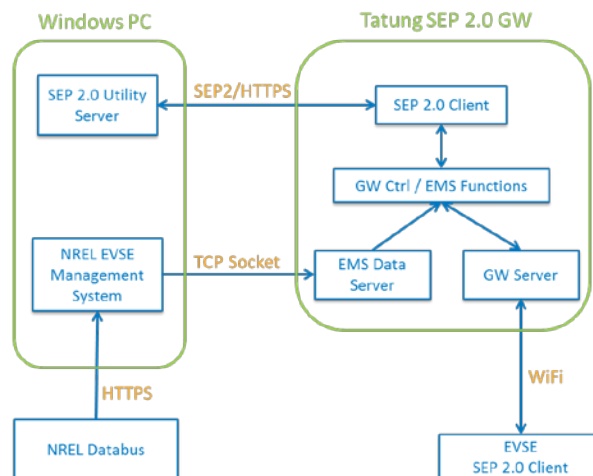


Figure VI-153: Testing Communications Architecture for PEV control

Future efforts in communication and control of EVSEs will incorporate Modbus protocols in addition to developing interface capabilities to the Volttron architecture.

Battery Life Implications of Electric Vehicle Grid Integration

In considering the applications of plug-in electric vehicles and their battery systems for grid integration, concerns are raised regarding the impacts of these functions on the long-term performance and life of the battery in addition to the short term range capabilities of the vehicle. It is important to understand that grid integration of PEVs does not necessitate export power or 2 way flow of power but can also simply incorporate scheduling and planning the charging events to achieve the lowest cost of operation and extension of the battery life.

NREL's Energy Storage research team with funding from DOE developed an extensive tool call BLAST-V for the financial and performance assessment of batteries for vehicle applications. The EVGI efforts leveraged the previous efforts and constructed specific extensions to the tool to consider grid service applications and the scheduling of charging relative to driver demands and utility rate structures, as depicted in Figure VI-154. This strategy enables to use of large data sets of travel profiles, validated models of battery life and climactic season profiles that capture thermal impacts to the battery system.

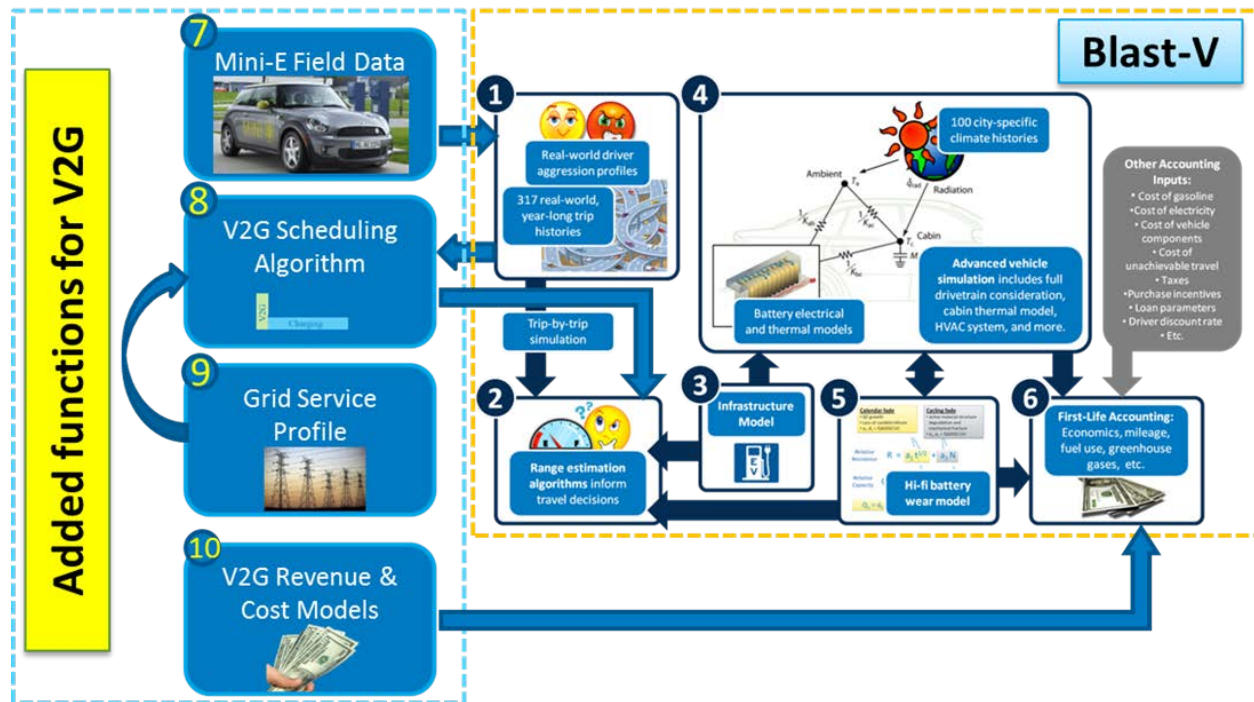


Figure VI-154: V2G Simulation Functions were built as an Extension to the BLAST-V tool

It was clear from previous analyses that the forecasted battery life times that result from a range of driving profiles suggest a broad range of scenarios in which at the end of vehicle life, there would be performance left in the battery and vice versa, in some cases the battery life would be shorter than a typical vehicle life and thus a second battery would be needed. In the analyses performed for EVGI efforts we worked to determine the most ideal use of EV Grid integration functions on a unique basis for each individual driving profile. In doing so, all drivers would optimize the use of the battery(ies) in relation to their own usage profile such that the battery and vehicle end of life coincide.

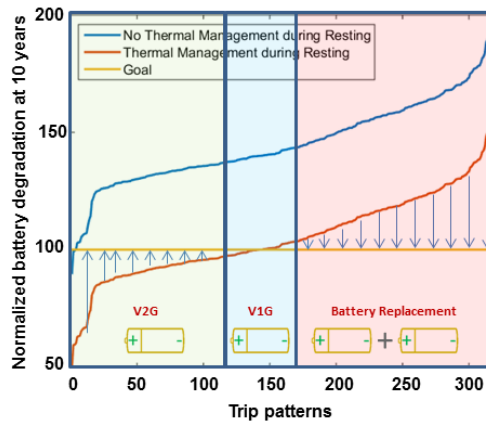


Figure VI-155: Simulations Show Opportunity to Provide V2G Functions can be Optimized Based on Driving Profile

Figure VI-155 summarizes the results from these battery life impacts assessments to highlight that about 20% of the vehicles would likely just employ V1G, or one-way charge scheduling simply to obtain lowest cost of energy since their battery life and vehicle life already coincide. In comparison, ~1/3 of the drivers would not utilize the battery with normal driving and would trade increased battery cycling for grid functions in exchange for grid value. Likewise, about 50% of the cases included a need to replace the battery anyway based solely on driving and thus would want to capitalize on the remaining unused capacity of a second battery for grid value too. All of these scenarios were compared both with and without grid-tied thermal management functions. The thermal environment of the battery system during non-operating times is quite influential and the grid connection can help mitigate those impacts.

The results of these studies have been compiled into 2 technical papers that are being prepared for publication. The tools offer opportunities for exploring a wide range of electric vehicle grid integration scenarios.

Holistic Systems Opportunities

When considering the opportunities for EV Grid integration it is important to take a holistic and coordinated systems perspective. EVGI researchers collaborated both with the Grid Operations and Markets experts and NREL and the Buildings Program engineers to develop relevant research reports.

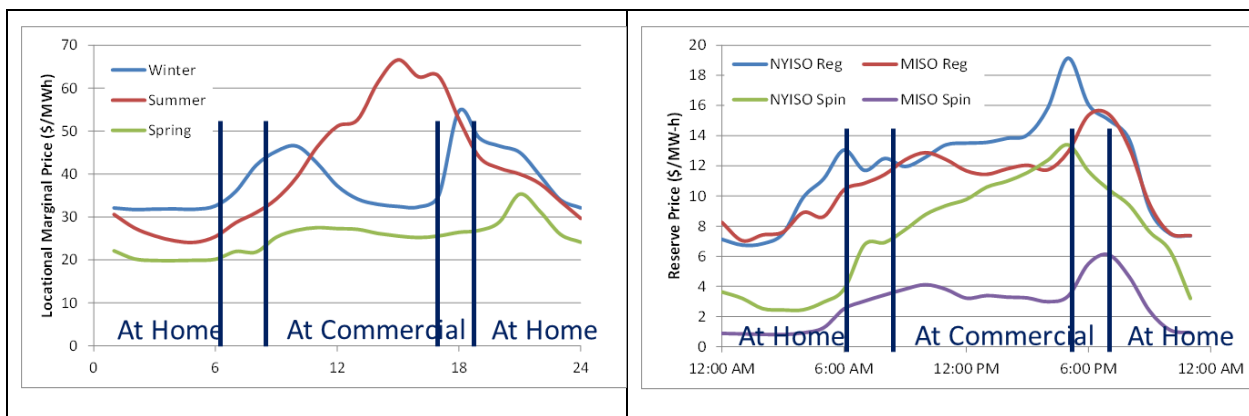


Figure VI-156: Daily and Seasonal Grid Variability will Impact PEV Value Proposition

A report entitled "Summary of Market Opportunities for Electric Vehicles and Dispatchable Load in Electrolyzers" was compiled. This report details the variability and accessibility of grid markets regionally. It summarizes the scale of resource procured from the variety of grid services in different markets. In Figure VI-156, we highlight how the Locational Marginal Price (left) and the Reserve Price vary with time, season, and region of the country. Overlaid on these charts are general periods of time and location of the vehicles. The take away is that vehicles need to be integrated with grid operations during daytime periods in which they are less likely to be in a home and necessitate both the use of public and workplace charging and the coordination

with a commercial meter and rate schedule. All of this adds complexity to the value proposition for vehicles to provide grid services.

In developing the report, the authors concluded the following,

- EV charge management should first be focused on minimizing or eliminating the capacity costs and optimized around energy cost
- The provision of ancillary services from EV charging has the potential to provide some additional value, but is small relative to avoiding capacity costs
- The unknown path forward on Distributed Energy Resource participation in markets makes assessment challenging and may differ by region

The EVGI team also supported the creation of a report initiated by the DOE Buildings program entitled "Challenges and Opportunities for Transactive Control of Electric Vehicle Supply Equipment." The report discusses proposed integration of electric vehicles and infrastructure as a component of building energy management systems that interact with grid expectations. Existing and needed standards activities are discussed along with use cases. Barriers identified in the report offer opportunities for government action and research to aid with industry growth.

Multi-lab Smart Grid Working Group

This year a collaborative working group with technical experts from 6 national laboratories was formed. NREL has led the group which includes Argonne National Lab, Idaho National Lab, Oak Ridge National Lab, Pacific Northwest National Lab, and Lawrence Berkeley National Lab. The group compiled and delivered a guidance document to DOE to highlight critical challenges to the growth of electric vehicle smart grid integration along with a summary of laboratory key capabilities that should be applied to these challenges. Content developed by the working group was also presented at key industry meetings including the U.S. Drive Grid Integration Tech Team and the EPRI Electric Vehicle Working Council. Industry has expressed support for the coordinated activities of the multi-lab team that has been formed.

In concluding the report the team highlighted three essential areas for further research and development including,

- Grid interactive vehicle systems simulation tools
- Hardware component development and testing including hardware in the loop
- Market structure evolution and utility engagement

Conclusions

It is clear that interest in vehicle grid integration opportunities is high and that significant work remains to make electric vehicle grid integration systems functional and economically viable with defined market opportunities. The research conducted so far is opening the door to a holistic system implementation and evaluation. Capabilities are continuing to grow in the Energy Systems Integration Facility at NREL and will start to offer insights. Some of these systems include, charge management hardware and software solutions, communications and control integrated with buildings and homes and software tools for scenario evaluation. Future systems will include, expanded bi-directional capabilities, fast charging and wireless power technologies to support the industry needs.

The collaboration between national laboratories in response to DOE Grid Modernization initiative objectives will support leveraging of capabilities and sharing of knowledge that should accelerate the removal of technical barriers. Future efforts will need to address some of the following key questions and concerns,

- How does the system of components and controls work to generate value in the future grid?
- What is the value opportunity, How big is it, What are the Regional differences, and What needs to happen to achieve functionality?
- How will specific grid integrated vehicle functions affect battery life?

- How to enable interactivity across multiple communications and controls structures and implementation environments?
- Local optimization of vehicle/driver behavior maybe driven by tariffs may not necessarily be a global optimal solution?
- How to make the use cases, implementation, and value stream simple and effective?

Presentations/Publications/Patents

1. Markel, T. "PEV Grid Integration Research - Vehicles, Buildings, and Renewables Working Together." Presented at IEEE Power and Energy Symposium Presentation (July 2015). NREL/PR-5400-64757.
2. Markel, T. "Multi-Lab EV Smart Grid Working Group Collaboration Status Update." Presented at EPRI Infrastructure Working Council. March 2015.
3. Markel, T. "Electric Vehicle Grid Integration." Presented at DOE VT Annual Merit Review presentation. June 2015.
4. "Challenges and Opportunities for Transactive Control of Electric Vehicle Supply Equipment." April 2015.
5. Jun, M. and Markel, T. "INTEGRATE – Electric Vehicle Communications and Control Applications Review." April 2015.
6. Markel, T.; et. al. "Multi-Lab EV Smart Grid Integration Requirements Study: Providing Guidance on Technology Development and Demonstration." NREL/TP-5400-63963. 2015.
7. Denholm P.; Eichman, J.; Markel, T.; Ma, O. "Summary of Market Opportunities for Electric Vehicles and Dispatchable Load in Electrolyzers." NREL/TP-6A20-64172. 2015.

VI.13. EVSE Data Collection

Melissa Lapsa, Principal Investigator, Group Leader, ORNL

Oak Ridge National Laboratory
1 Bethel Valley Road
Oak Ridge, Tennessee 37810
Phone: (865) 576-8620
E-mail: lapsamv@ornl.gov

David Anderson, DOE Program Manager

Vehicle and Systems Simulation and Testing
Phone: (202) 287-5688
E-mail: david.anderson@ee.doe.gov

Start Date: September 1, 2014

End Date: September 1, 2015

VI.13.A. Abstract

Objectives:

- Collect, analyze, and report Electric Vehicle (EV) charging data from the 25 solar-assisted Electric Vehicle Service Equipment (EVSEs) at ORNL.
- Collect, analyze, and report EV charging data from the 19 EVSEs at ORNL.
- Collect, analyze, and report EV charging data from ORNL and partner-installed solar-assisted EVSEs in Tennessee.
Collect, analyze, and report EV charging data from publicly-accessible EVSEs across Tennessee.

Accomplishments

- Throughout FY15, ORNL has collected data from all 44 EV charging stations on the ORNL campus and has summarized this data in the form of utilization charts and energy consumption information. This data set has allowed the tracking of station utilization, assistance with the possible new placement and/or the retention of existing stations, and tracking of the amount and cost of electricity consumed by EVs on campus.
- Likewise, ORNL has continued to track the utilization of solar-assisted stations across Tennessee to the extent data has remained available. The ownership of these stations has transferred from DOE to the site hosts, so maintenance and operation of the stations are no longer the responsibility of ORNL.
- ORNL has been successful in negotiating a contract with Car Charging Group Inc. (CCGI) for access to data from publicly-accessible EV charging stations across Tennessee on the CCGI network. This data covers 502 EVSEs at 263 unique locations for the period April 1, 2015, to September 30, 2015. To date, this data has allowed ORNL to calculate and chart the utilization of all these stations for the period April 1, 2015, to July 31, 2015.

Future Achievements (assuming extended funding for FY16)

- Continue tracking and analyzing all the data described above in order to advance the adoption of plug-in vehicles and enhance the user-charging process.
- Use the data described above to guide the installation of future EV charging stations and to maximize the benefits of existing charging stations.



VI.13.B. Technical Discussion

Background

Oak Ridge National Laboratory (ORNL), through funding from DOE's electric vehicle program, installed 44 electric vehicle charging stations on campus. These are comprised of 25 solar-assisted stations located on central campus, 18 non-solar stations (in groups of 2-4) distributed across campus near major office areas, and one high-voltage DC Fast Charger located near central campus. As of this writing, there are 41 plug-in vehicles on campus, 3 of which are fleet vehicles, with the balance being employee owned.

In addition, ORNL (through the DOE funding) and its statewide partners (via their own project matching funds) installed 100 solar-assisted charging stations across Tennessee. Finally, Ecotality (now CCGI) installed several hundred publicly-accessible EV charging stations across the state.

ORNL participates in a statewide group, Tennessee Electric Vehicle Advisory Council (TEVAC) where the data collected and analyzed by ORNL is shared and discussed. However, distribution of results based on the CCGI data is currently limited by a non-disclosure agreement between ORNL and CCGI.

Introduction

Under the DOE/ARRA-funded project described in the Background, data collection was begun in FY11 and continued through FY14. For FY15, a new data collection project was approved by DOE and, with this, data collection, analysis, and documentation has continued and been enhanced. This new project is the subject of this report.

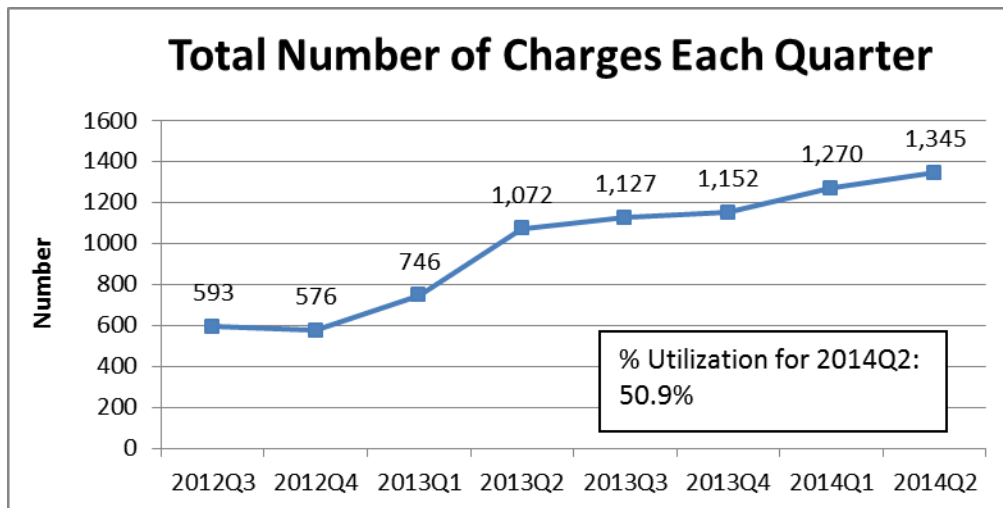
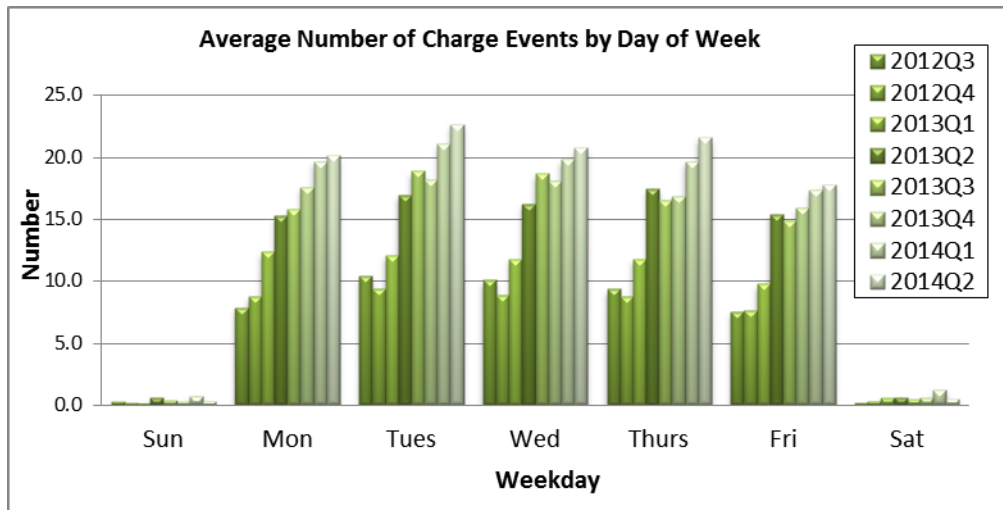
As referenced in the Background, there are now three potential sources of data - the 44 stations on the ORNL campus, the 100 solar-assisted stations statewide, and, under a new agreement with CCGI, all publicly-accessible stations in Tennessee currently on CCGI's Blink network. Data is being routinely collected and analyzed for the on-campus stations, but, since the original project has been completed and the off-site solar-assisted stations are now transferred to the site hosts, that data has not been available. However, given the agreement with CCGI, we are now able to analyze data from over 500 public stations in Tennessee.

Approach

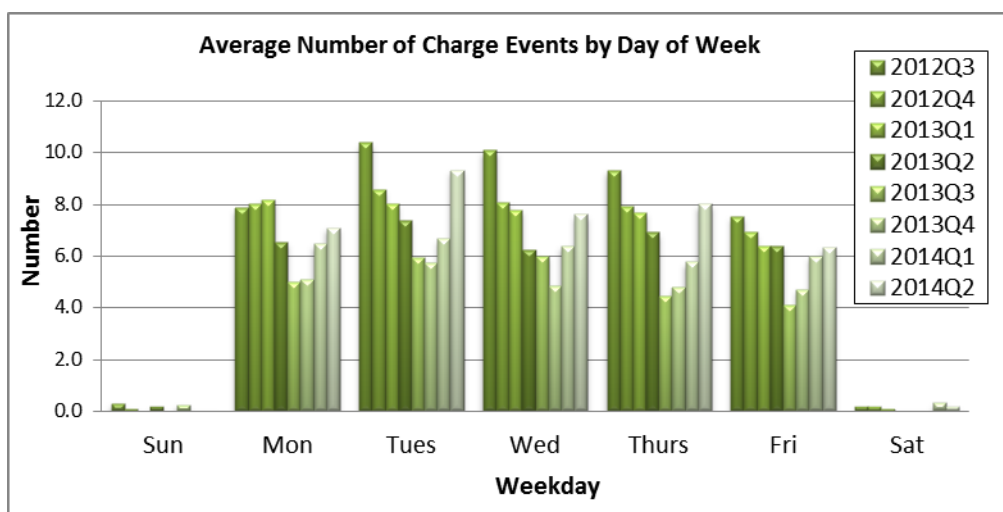
The major areas for tracking and analysis have been energy consumption, time of connect and disconnect by the drivers, duration of charge events, and the overall utilization of the stations. Therefore, data has been sorted by these areas of interest and has been presented in graphical summaries for analysis and decision making (Figure VI-157). Energy consumption and duration of charging are of interest for more insight into the state of the car's battery at the start of charging and the associated recharging patterns of drivers. Connect and disconnect times provide information on peak times of station use and, again, the recharging patterns of drivers at ORNL and in public settings (Figure VI-158). Utilization has been calculated as the ratio of actual charge events to the number of charge event opportunities per month per EVSE (one daily charging opportunity is assumed 5 days per week for 4 weeks each month). This has provided excellent insight to the actual use of the stations and will be (and to some degree has already been) beneficial for considering new stations on campus or elsewhere in the state (Figure VI-159).

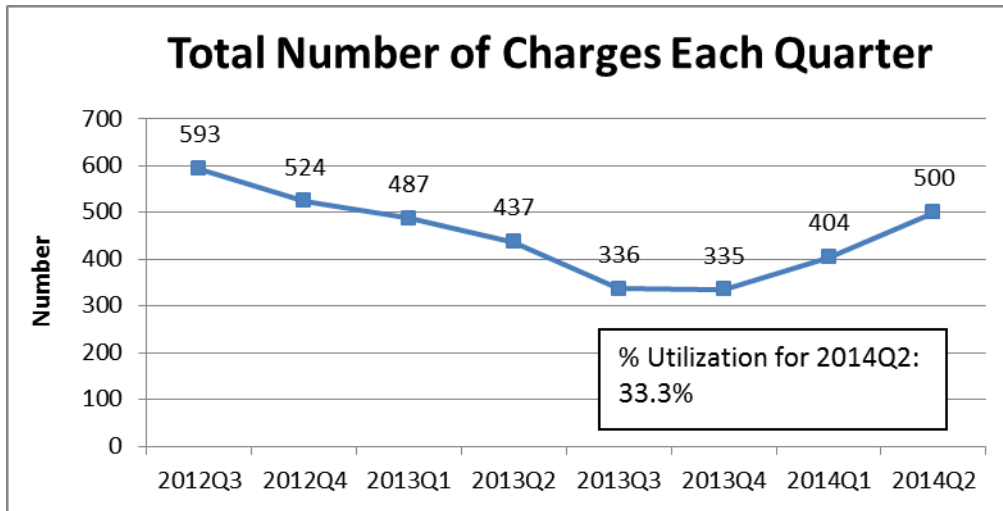
Results

Samples of the data are shown below (Figure VI-157).

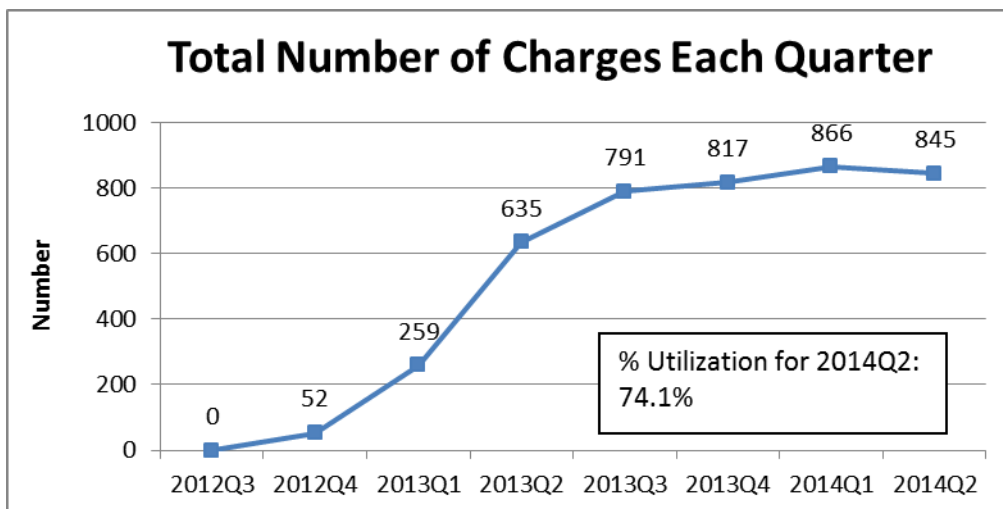
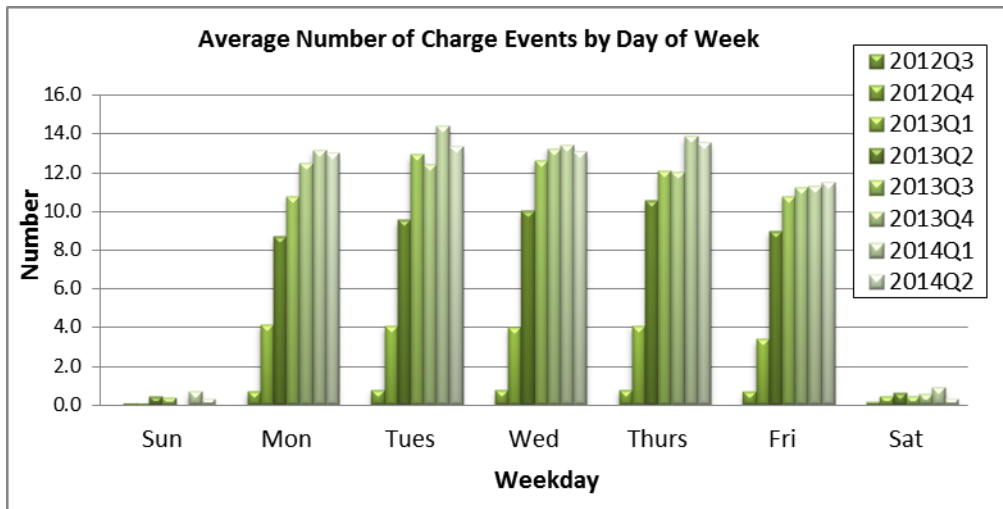


a) ORNL All Campus EVSEs





b) ORNL Solar-Assisted EVSEs



c) ORNL Non-Solar EVSEs

Figure VI-157: Sample summary pages of charge data.

ORNL Solar-Assisted Charging Infrastructure Summary Report

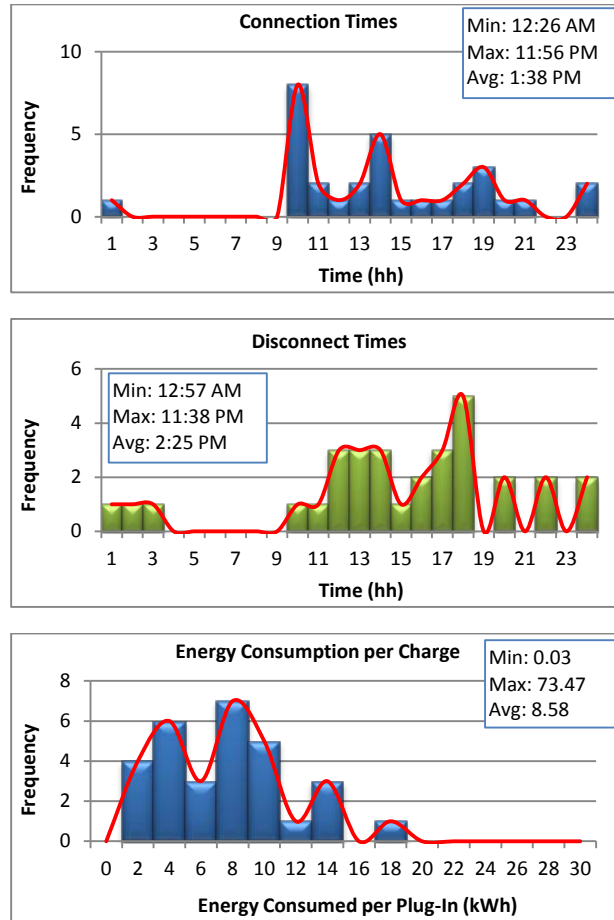


Figure VI-158: ORNL Solar-Assisted Charging Summary Report

July 2015 electric consumption data for all ORNL EVSEs:

Site	July 2015 total kWh
1520 - Interval Energy kWh	584.12
4007 - Interval Energy kWh	0.00
4015 - Interval Energy kWh	717.72
HFIR - Interval Energy kWh	261.79
NTRC - Interval Energy kWh	161.19
SNS - Interval Energy kWh	988.12
Non-Solar EVSEs Subtotal	2712.94
4008 Solar-Assisted Energy kWh	1772.71
Grand Total:	4485.6

There were 520 charge events (186 solar-assisted, 334 non-solar) for the month, not including those that appear in Blink with zero cumulative energy, which results in an average of 8.63 kWh/charge event.

Knoxville Market Square

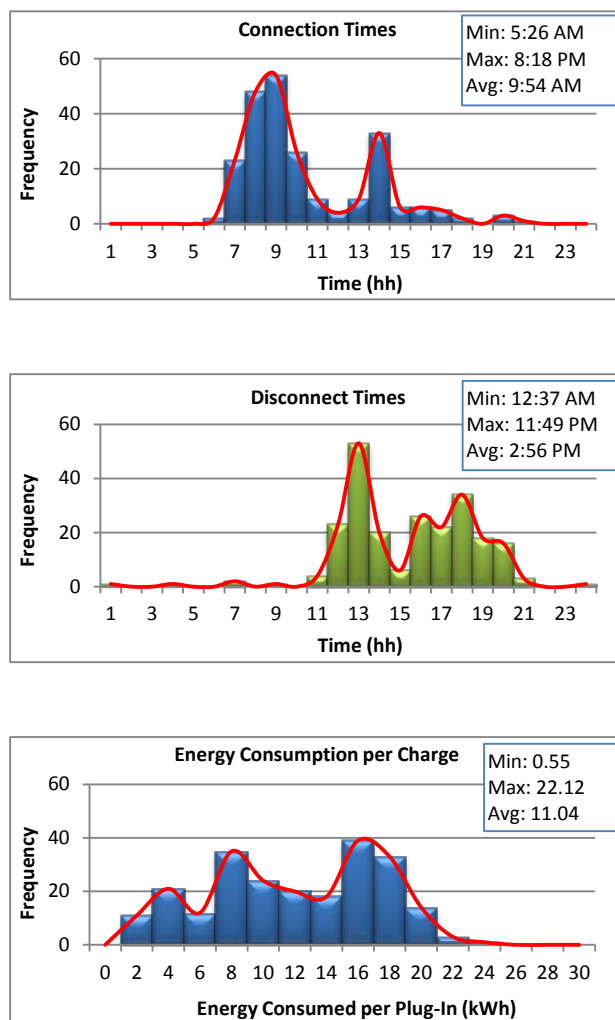


Figure VI-159: Knoxville Market Square Data

Conclusions

1. At ORNL, the distributed charging stations (located near major office areas) are more heavily utilized than the centrally-located stations, providing guidance on locating additional stations as the need arises. The data also guides the application of maintenance resources and has helped with identifying bottleneck locations and supporting changes necessary to relieve station availability problems.
2. Utilization of the statewide solar-assisted stations varies widely, with the highest demand being in workplace settings and at popular destination sites such as Market Square in Knoxville.
3. The statewide non-solar data from CCGI is the newest data set that covers a 4-month period in 2015. However, the data demonstrates that, while there are exceptions, utilization is relatively low across the system suggesting it can support a larger fleet of publicly-driven EVs. A large majority of these EVSEs are Level 2 charging stations.
4. Monthly power consumption for EVs charging at ORNL typically totals between 4000 and 5000 kWh, with 350-550 plug-ins monthly. At 3.25 miles per kWh (and using 4500 kWh), this equates to 14,625 miles of driving per month and, compared to a vehicle rated at 20 miles per gallon, this represents a fuel savings exceeding 700 gallons of gasoline each month.
5. For most of the ORNL-installed EV charging station sites, usage has increased rather steadily since they were first installed. This observation is apparent when examining data over several quarters, but

short-term variations can easily mask usage trends when only a few months are available. Data over a longer duration is therefore needed for the statewide data to draw additional conclusions about the usage trends.

VI.13.C. Products

No products were developed via the project

Presentations/Publications/Patents

1. There were no publications, presentations, or patents for this project in FY15

U.S. DEPARTMENT OF
ENERGY

Energy Efficiency &
Renewable Energy

For more information, visit: vehicles.energy.gov

DOE/EE-1304 • January 2016